

# **1,3-Bis(trifluoromethyl)benzene: A Versatile Building Block for the Synthesis of New Boron-Containing Conjugated Systems**

Dissertation zur Erlangung des naturwissenschaftlichen Doktorgrades

der Julius-Maximilians-Universität Würzburg

vorgelegt von

Florian Rauch

aus Würzburg

Würzburg 2020







Eingereicht bei der Fakultät für Chemie und Pharmazie am

---

Gutachter der schriftlichen Arbeit:

1. Gutachter: Prof. Dr. Dr. h.c. Todd B. Marder

2. Gutachter: Prof. Dr. Maik Finze

Püfer des öffentlichen Promotionskolloquiums

1. Prüfer: Prof. Dr. Dr. h.c. Todd B. Marder

2. Prüfer: Prof. Dr. Maik Finze

3. Prüfer:

Datum des öffentlichen Promotionskolloquiums

---

Doktorurkunde ausgehändigt am

---



*For everyone who made this work possible*



- I. Do not feel absolutely certain of anything.
- II. Do not think it worthwhile to proceed by concealing evidence, for the evidence is sure to come to light.
- III. Never try to discourage thinking for you are sure to succeed.
- IV. When you meet with opposition, even if it should be from your husband or your children, endeavor to overcome it by argument and not by authority, for a victory dependent upon authority is unreal and illusory.
- V. Have no respect for the authority of others, for there are always contrary authorities to be found.
- VI. Do not use power to suppress opinions you think pernicious, for if you do the opinions will suppress you.
- VII. Do not fear to be eccentric in opinion, for every opinion now accepted was once eccentric.
- VIII. Find more pleasure in intelligent dissent than in passive agreement, for, if you value intelligence as you should, the former implies a deeper agreement than the latter.
- IX. Be scrupulously truthful, even if the truth is inconvenient, for it is more inconvenient when you try to conceal it.
- X. Do not feel envious of the happiness of those who live in a fool's paradise, for only a fool will think that it is happiness.

Bertrand Russell

*"A Liberal Decalogue", The Autobiography of Bertrand Russell, Vol. 3: 1944-1969, p. 71-72*

Die Experimente zur vorliegenden Arbeit wurden in der Zeit von Januar 2016 bis Mai 2020 am Institut für Anorganische Chemie der Julius-Maximilians-Universität Würzburg unter der Aufsicht von Prof. Dr. Dr. h.c. Todd B. Marder durchgeführt.

**Acknowledgment**

I want to thank all the people that made this work possible.

First of all, I would like to thank **Prof. Dr. Dr. h.c. Todd B. Marder**. Dear Todd, I don't know how to thank you enough. You always made me feel welcome. When I joined your group, I was also adopted as a new member of the "**Marder family**". I am grateful for the enormous amount of scientific freedom you gave me, and the trust that entails. It was close to the end of the thesis, that I finally realized the method to your madness. You managed to trick me into becoming a better scientist and I will always be grateful for that. Thank you for showing me the world (through various conferences) and how nice it is to have friends all over the place. I have chosen Russell's decalogue for many reasons as the quote of this thesis, but especially, because you showed it to me, and it very much reminds me of you. I will always be proud to have worked with you. Thanks.

I would like to thank **Dr. Jörn Nitsch** (for discussions, for challenging my ideas, for teaching me about photophysics, spectroscopy, and quantum chemical calculations and motivating me) and **Dr. Ayush Narsaria** (for long discussions on the concept of TADF) and **Prof. Dr. Matthias Bickelhaupt** for our successful collaboration on our TADF paper. I am glad to have had this opportunity and I believe it elevated my work and gave me a broader perspective on the chemistry I was working on.

I would like to thank my in-house collaboration partners **Prof. Dr. Maik Finze**, **Dr. Ivo Krummenacher**, and **Prof. Dr. Holger Braunschweig**. I am grateful for your guidance and patient proof-reading of our joint publications. Thank you, Ivo, for countless cyclic voltammetry measurements and discussions.

I would like to thank all further collaboration partners from the labs of **Prof. Dr. Jean-François Halet**, **Prof. Dr. Frédéric Paul** and **Dr. Jacek Kubicki**. Thank you for giving me the opportunity to take part in your work. This has given me a new perspective and prepared me to formulate my own ideas in this thesis.

I would like to thank all of my students, without whom this work would not have been possible. Thank you, **Johannes Krebs**, **Peter Endres**, **Sonja Fuchs**, **Lukas Swoboda**, **Mario Guth**, **Marcel Härterich**, **Anna Lamprecht**, **Julian Günther** and **Christian Schmidle**. I had a lot of fun with all of you. I hope you learned a few things from me, because I definitely learned a lot from working with you guys. I wish you all the best. This thesis is your work as well.

I would like to thank all past, present and honorary members of the AK Marder.

## Acknowledgment

I would like to thank our senior researchers **Dr. Stephan Wagner** (for organizing pretty much everything in the institute and showing me how to deal with the strange world of academic bureaucracy), **Dr. Alexandra Friedrich** (for measuring and solving crystal-structures and proof-reading manuscripts. You have done so much for me and I am very grateful), and **Dr. Rüdiger Bertermann** (for keeping the NMR machines running and his patient explanations and execution of various NMR experiments).

I would like to thank **Dr. Stefanie Griesbeck** (for her help and guidance, for showing me how to deal with Todd and how to reign over the boron kingdom), **Dr. Julia Merz** (for her help and support, for all the good times during our travels together, and for bringing **Loki** into my life), **Jiang He** (for being a good friend and great lab partner, and for endless discussions on chemistry and life, with and without beer), **Sabine Lorenzen** (for taking me in as a member of Lab 105 and showing me the ropes, for her patience, guidance, help, and for taking care of the group), **Christof Mahler** (as the honorary member of Lab 105 for countless HRMS measurements and the occasional paint art), **Dr. Martin Eck** (for being an awesome guy, for showing me that chemistry can be fun, for introducing me to glove-box maintenance, and for countless discussions, with and without beer), **Matthias Ferger** (for our countless discussions on  $\text{BF}_3\text{K}$  salts and politics while smoking, and the great time during our travels to various conferences), **Laura Kuehn** (for help, discussions, and support), **Johannes Krebs** (for being the best, first student I could ever hope for, for countless discussions, for all the good times, and for taking over the TGIF lecture series), **Sarina Berger** (for countless discussions on  $\text{BF}_3\text{K}$  salts and for being so incredibly reliable. I hereby declare you the new queen of the boron kingdom and will abdicate my former title as king of the former. Have fun with it.), **Dr. Lei Ji** (for being the mentor I needed and a friend, for countless discussions, with and without beer), **Dr. Daniel Sieh** (for broadening my horizon in our discussions and measuring crystal structures. I believe you made me a better scientist and even better table football player), **Dr. Hashem Amini** (for encouraging me), **Florian Kerner** (for helping with glove-box maintenance and tips and tricks for crystallography), **Robert Ricker** (for his passionate care of the flash systems and discussions), **Jan Maier** (for teaching me the secrets of Gimp, taking pictures and somehow being the only one in the group with a similar fascination for strange TV shows), **Zhu Wu** (for discussions on photophysics and chemistry), **Mohamad Wawi** (for discussions on photophysics and chemistry), **Maria Eckhardt** (for keeping the Marder group running, sorting out travel expenses, contracts and everything else), **Dr. Carolin Sieck** (for welcoming me to the group, for helpful discussions and the great time in Leeds), **Charlotte Scheufler** (for teaching me about Sonogashira couplings), **Meltem Yildirim** (for discussions



and our sparkling wine parties), **Martin Stang** (for countless discussions and being a great lab partner), **Yaming Tian** (for helping with glove-box maintenance), **Dr. Xiaoning Guo** (for helpful discussions and proof-reading), **Dr. Andrea Deißberger** (for discussions and showing me the beautiful blue flame of perfluorinated grease), **Dr. Julia Schuster** (for her work on triarylboranes, that much of chapter 3 is based on, for countless discussions and our great time in Hong Kong together), **Dr. Amanda Nelson** (for proof reading my master's thesis, for being a great lab neighbor, and for a great time with her during her stays in Germany), **Yannik Reuß, Laura Wolz, Tamara Stawski, Celine Pfeuffer, Dominik Blümel** and **Marcel Müller** (for all the fun times in lab 105 and afterwards. I would like to thank Yannik in particular, for the productive time we had working together and the synthesis of precursors for this thesis).

I would like to thank all members of the inorganic institute. I can't remember how many interesting discussions about chemistry I had in the hallways of our institute. So many of the things presented in this work, be it synthetic or conceptual, were developed in discussion with members of all working groups of the institute. I think this is unique and should be preserved at all costs.

I especially would like to thank the technical staff of the inorganic institute, **Alfons Scherzer, Gertrud Wunderling, Sabine Timmroth, Liselotte Michels, Marie-Luise Schäfer** (thank you for running VT-NMR spectra for me), and **Berthold Fertig**, as well as the workshop team **Alois Ruf, Wolfgang Obert** (thank you for repairing our UV-Lamps and heat-guns), **Frank Förtsch, Michael Ramold, and Manfred Reinhart** (Thank you, Manni for helping me with various glove-box problems and your wordly wisdom).

I would like to thank the members of the AK Steffen, **Dr. Benjamin Hupp** (for being a companion in this madness, for hating Bon Jovi, for starting the TGIF lecture series with me, for our joint love of good and bad movies, for everything I am forgetting to mention, and for always motivating me to be better), **Prof. Dr. Andreas Steffen** (for introducing me to and teaching me about spectroscopy), and **Markus Gernet** (for discussions on photophysics and friendly suggestions for the snack-bar).

I would further like to thank all past and present members of the AK Braunschweig for discussions and fun times we had, especially **Dr. Lisa Mailänder** (for teaching me and preparing me for this thesis and for showing me what kind of chemist I want to be), **Dr. Katharina Ferkinghoff** (for patiently supervising me during my bachelor's thesis), **Torsten Thiess** (for our ongoing homoerotic tensions, our joint love for mountain biking, our joint hate for a lot of things (especially hippies), and all of the great times we had during our undergrad

## Acknowledgment

and PhD time. My grades would have been a lot worse, if we wouldn't have made a competition out of it. I love you), **Dr. Carsten Lenczyk** (for being a good friend, for his help and support for this work, for our joint love of music and movies, and for being one of the nicest people I know), **Dr. Jens Seufert** (for countless discussions about chemistry and pretty much everything else and for being a fellow nerd), **Felix Lindl** (for countless (!) discussions on chemistry), **Christian Saalfrank** (for all the fun times and our joint love for cooking), **Dr. Jonas Müssig** (for discussions (about applying Wade's rules), for our time in Hong Kong, and for our great times mountain biking), **Dr. Justin Wolf**, and **Dr. Thomas Kupfer** (for organizing the AC2 lab course. Thank you, Justin. You had a huge influence on the way I supervise students and look at synthesis).

I also would like to thank all the students I supervised in the AC2 for helping me to synthesize precursors for this thesis.

I would like to thank all members of the AK Finze for helpful discussions, especially **Raphael Wirthensohn** (for helpful discussions about chemistry and cuisine), **Dr. Tatjana Ribbeck** (for discussions and support), **Dr. Jan Sprenger** (for discussions on chemistry and our time mountain biking), and **Jarno Riefer** (for discussions and all the fun times).

I would like to thank the past and present members of the AK Müller-Buschbaum, especially **Thomas Schäfer** (for being a good friend and our great times during our undergraduate studies) and **Friedrich Mühlbach** (for countless discussions and our great times during our undergraduate studies and online shenanigans).

I would also like to thank the AK Radius for providing me with chemicals, especially **Prof. Dr. Udo Radius** for interesting discussions (and a great lecture during my undergraduate studies).

I would like to thank my family for their support. I can't imagine it being easy. Thank you for never losing faith in me. Thank you for inspiring me and thank you for keeping me grounded. Thank you for everything, I love you.

I would like to thank **Verena Borawski**. Thank you. Thank you for the TOC pictures. Thank you for keeping me motivated. Thank you for putting up with me. Thank you for being my partner in every conceivable way. I will never be able to describe just how much you mean to me. I love you and I admire you.

If you are looking through this acknowledgment section and are disappointed because you did not see yourself in there, I am very sorry. I am sure I missed some people. Let me fix this by thanking everyone I failed to mention even though they contributed to this work.

**List of Publications**

The publications listed below are partly reproduced in this dissertation with permission from Wiley-VCH. References [1] - [3] are published under a creative commons license (CC BY) and do not require a further permission statement from the publisher.

Publication	Position
<p>[1] A. Narsaria, F. Rauch, J. Krebs, P. Endres, A. Friedrich, I. Krummenacher, H. Braunschweig, M. Finze, J. Nitsch, F. M. Bickelhaupt, T. B. Marder, <i>Adv. Funct. Mater.</i> <b>2020</b>, DOI: 10.1002/adfm.202002064.</p>	Chapter 1
<p>[2] F. Rauch, S. Fuchs, A. Friedrich, D. Sieh, I. Krummenacher, H. Braunschweig, M. Finze, T. B. Marder, <i>Chem. Eur. J.</i> <b>2020</b>, DOI: 10.1002/chem.201905559.</p> <p>Furthermore, compounds in this chapter, as well as parts of their analytic data have been previously published in S. Fuchs, <b>2018</b>, ‘Investigation of trifluoromethylated polyannulated boron heterocycles’, master’s thesis, Julius-Maximilians-Universität, Würzburg, which was carried out under the supervision of Florian Rauch. These results were reproduced here for the sake of completeness. In this work further photophysical investigations and quantum chemical calculations, as well as a comprehensive interpretation of the results are reported.</p>	Chapter 2
<p>[3] F. Rauch, P. Endres, A. Friedrich, D. Sieh, M. Hähnel, I. Krummenacher, H. Braunschweig, M. Finze, L. Ji, T. B. Marder, <i>Chem. Eur. J.</i> <b>2020</b>, DOI: 10.1002/chem.202001985.</p> <p>Furthermore, compounds <b>BG1H</b> and <b>BG1Bpin</b> as well as their precursors and analytical data were previously reported in F. Rauch, <b>2015</b>, ‘Conjugated Borane Dendrimers’, master’s thesis, Julius-Maximilians-Universität. These results were included for the sake of completeness In this work further compounds, photophysical investigations and quantum chemical calculations are reported.</p>	Chapter 3
<p>[4] F. Rauch, J. Krebs, J. Günther, A. Friedrich, M. Hähnel, I. Krummenacher, H. Braunschweig, M. Finze, T. B. Marder, <i>submitted</i></p>	Chapter 4

**And in the following theses (under the supervision of Florian Rauch):**

P. Endres, **2017**, ‘Synthesis & characterization of conjugated borane dendrimers’, bachelor’s thesis, Julius-Maximilians-Universität, Würzburg.

L. Swoboda, **2018**, ‘Synthesis & Investigation of new, highly polarized B- $\pi$ -B-systems’, bachelor’s thesis, Julius-Maximilians-Universität, Würzburg.

S. Fuchs, **2018**, ‘Investigation of trifluoromethylated polyannulated boron heterocycles’, master’s thesis, Julius-Maximilians-Universität, Würzburg.

M. Guth, **2018**, ‘Investigation of  $\pi$ -bridged trifluoromethylated polyannulated boron heterocycles’, master’s thesis, Julius-Maximilians-Universität, Würzburg.

**Further publications:**

J. He, F. Rauch, A. Friedrich, D. Sieh, T. Ribbeck, I. Krummenacher, H. Braunschweig, M. Finze, T. B. Marder, *Chem. Eur. J.* **2019**, *25*, 13777-13784.

C. Lenczyk, D. K. Roy, J. Nitsch, K. Radacki, F. Rauch, R. D. Dewhurst, F. M. Bickelhaupt, T. B. Marder, H. Braunschweig, *Chem. Eur. J.* **2019**, *25*, 13566-13571.

S. Griesbeck, E. Michail, F. Rauch, H. Ogasawara, C. Wang, Y. Sato, R. M. Edkins, Z. Zhang, M. Taki, C. Lambert, S. Yamaguchi, T. B. Marder, *Chem. Eur. J.* **2019**, *25*, 13164-13175.

H. Belaidi, F. Rauch, Z. Zhang, C. Latouche, A. Boucekkine, T. B. Marder, J.-F. Halet, *ChemPhotoChem* **2020**, *4*, 173-180.

J. Kubicki, M. Lorenc, P. Cochelin, O. Mongin, A. Amar, A. Boucekkine, A. Gaje, M. G. Humphrey, M. Morshedi, S. Lorenzen, F. Rauch, C. Scheufler, T. B. Marder, F. Paul, *The Journal of Physical Chemistry C* **2020**, DOI: 10.1021/acs.jpcc.0c01532.

H. Amini, Ž. Ban, M. Ferger, S. Lorenzen, F. Rauch, A. Friedrich, I. Crnolatac, A. Kendel, S. Miljanic, I. Piantanida, T. B. Marder, *Chem. Eur. J.* **2020**, DOI: 10.1002/chem.201905328.

**List of Abbreviations**

A	acceptor
<i>a</i>	hyperfine coupling constant
Å	Ångström (1 Å = 10 <sup>-10</sup> m)
Abs	absorption
APCI	atmospheric-pressure chemical ionization
Ar	aryl
ASAP	atmospheric solids analysis probe
B <sub>2</sub> pin <sub>2</sub>	<i>bis</i> (pinacolato)diboron
Bf	dibenzoborole, borrafluorene
br	broad
Cbz	carbazolyl
COD	1,5-cyclooctadiene
CT	charge transfer
CV	cyclic voltammetry
D	donor
d	doublet
dba	dibenzylidene acetone
DF	delayed fluorescence
DFT	density functional theory
DMF	dimethylformamide
DMSO	dimethyl sulfoxide
dtbpy	4,4'- <i>di-tert</i> -butyl-2,2'-dipyridyl
Em	emission
eq.	equivalents
esd	estimated standard deviation
<i>f</i>	oscillator strength
<sup>F</sup> Bf	2,4,6,8-tetrakis(trifluoromethyl)-dibenzoboryl
<sup>F</sup> Mes	fluoromesityl, 2,4,6- <i>tris</i> (trifluoromethyl)phenyl
<sup>F</sup> Xyl	fluoroxylyl, 2,6- <i>bis</i> (trifluoromethyl)phenyl
<i>g</i> <sub>iso</sub>	anisotropic Landé factor
HOMO	highest occupied molecular orbital
<i>i</i>	<i>iso</i>
IC	internal conversion

## List of Abbreviations

ICT	intramolecular charge transfer
IRF	instrumental response function
ISC	inter system crossing
$J$	coupling constant
$k_r$	radiative decay rate
$k_{nr}$	non-radiative decay rate
LE	localized excitation
LUMO	lowest unoccupied molecular orbital
m	multiplet
MAS	magic-angle spinning
MeCN	acetonitrile
mes	mesityl, 2,4,6-trimethylphenyl
MS	mass spectrometry
MTBE	methyl <i>tert</i> -butyl ether
NIR	near-infrared
NMR	nuclear magnetic resonance
OFET	organic field-effect transistor
OLED	organic light emitting diode
OPV	organic photovoltaic cell
$p$	<i>para</i>
PAH	polycyclic aromatic hydrocarbons
PCM	polarizability continuum model
PF	prompt fluorescence
pin	pinacolato
q	quartet
rIC	reverse internal conversion
rISC	reverse inter system crossing
rt	room temperature
S	singlet (electronic state)
s	singlet (NMR spectra)
sPhos	2-dicyclohexylphosphino-2',6'-dimethoxybiphenyl
T	triplet (electronic state)
t	triplet (NMR spectra)
$t$	<i>tert</i>

TADF	thermally activated delayed fluorescence
TCSPC	time-correlated single-photon counting
TD-DFT	time-dependent density functional theory
Tip	2,4,6-triisopropylphenyl
THF	tetrahydrofuran
TICT	twisted intramolecular charge transfer
TLC	thin-layer chromatography
TMOP	2,4,6-trimethoxyphenyl
UV	ultraviolet
VC	vibronic coupling
Vis	visible
Xantphos	4,5-bis(diphenylphosphino)-9,9-dimethylxanthene
xPhos	2-dicyclohexylphosphino-2',4',6'-triisopropylbiphenyl

## List of Abbreviations



## Table of Contents

1 Computationally Guided Molecular Design to Minimize the LE/CT Gap in D- $\pi$ -A Fluorinated Triarylboranes for Efficient TADF via D and $\pi$ -Bridge Tuning.....	1
1.1 Introduction.....	1
1.2 Results and Discussion.....	5
1.2.1 In Silico Molecular Design.....	5
1.2.2 Synthesis.....	14
1.2.3 Crystal and Molecular Structures.....	16
1.2.4 Electrochemistry.....	19
1.2.5 Photophysical Properties.....	21
1.3 Conclusion.....	25
1.4 References.....	27
2 Highly Stable, Readily Reducible, Fluorescent, Trifluoromethylated 9-Borafluorenes.....	33
2.1 Introduction.....	33
2.2 Results and Discussion.....	36
2.2.1 Synthesis.....	36
2.2.2 Crystal and Molecular Structures.....	39
2.2.3 Electrochemistry.....	42
2.2.4 Photophysical Properties.....	46
2.2.5 DFT and TD-DFT Studies.....	51
2.3 Conclusion.....	56
2.4 References.....	58
3 An Iterative Divergent Approach to Conjugated Starburst Borane Dendrimers.....	65
3.1 Introduction.....	65
3.2 Results and Discussion.....	68
3.2.1 Synthesis.....	68
3.2.2 Crystal and Molecular Structures.....	72
3.2.3 Electrochemistry.....	75
3.2.4 Photophysical Properties.....	78
3.2.5 DFT and TD-DFT Studies.....	81
3.3 Conclusion.....	83
3.4 References.....	84

## Table of Contents

4 Electronically-driven Regioselective Iridium-Catalyzed C–H Borylation of Donor- $\pi$ -Acceptor Chromophores Containing Triarylboron Acceptors .....	89
4.1 Introduction .....	89
4.2 Results and Discussion .....	91
4.2.1 Synthesis .....	91
4.2.2 Crystal and Molecular Structures .....	92
4.2.3 Electrochemistry .....	94
4.2.4 Photophysical Properties .....	95
4.3 Conclusion .....	98
4.4 References .....	100
5 Summary/Zusammenfassung .....	105
5.1 Summary .....	105
5.1.1 Chapter 1 .....	105
5.1.2 Chapter 2 .....	109
5.1.3 Chapter 3 .....	113
5.1.4 Chapter 4 .....	116
5.2 Zusammenfassung .....	118
5.2.1 Kapitel 1 .....	118
5.2.2 Kapitel 2 .....	122
5.2.3 Kapitel 3 .....	126
5.2.4 Kapitel 4 .....	129
6 Experimental .....	131
6.1 General Experimental Details .....	131
6.2 Synthesis .....	134
6.2.1 Chapter 1 .....	134
6.2.2 Chapter 2 .....	150
6.2.3 Chapter 3 .....	160
6.2.4 Chapter 4 .....	169
6.3 Solid State Structures .....	172
6.3.1 Chapter 1 .....	172
6.3.2 Chapter 2 .....	181
6.3.3 Chapter 3 .....	192
6.3.4 Chapter 4 .....	197
6.4 Photophysical Data .....	202
6.4.1 Chapter 1 .....	202
6.4.2 Chapter 2 .....	205
6.4.3 Chapter 3 .....	208

6.5 Electrochemical Data .....	210
6.5.1 Chapter 1 .....	210
6.5.2 Chapter 2 .....	211
6.5.3 Chapter 3 .....	212
6.5.4 Chapter 4 .....	213
6.6 TD-DFT Calculations.....	215
6.6.1 Chapter 1 .....	215
6.6.2 Chapter 2 .....	231
6.6.3 Chapter 3 .....	236
6.6.4 Chapter 4 .....	254
7 References .....	257
8 Appendix .....	271
8.1 NMR Spectra.....	271
8.1.1 Chapter 1 .....	271
8.1.2 Chapter 2 .....	300
8.1.3 Chapter 3 .....	320
8.1.4 Chapter 4 .....	338
8.2 XYZ Coordinates .....	345
8.2.1 Chapter 1 .....	345
8.2.2 Chapter 2 .....	369
8.2.3 Chapter 3 .....	379
8.2.4 Chapter 4 .....	392
9 List of Compounds .....	393

## Table of Contents

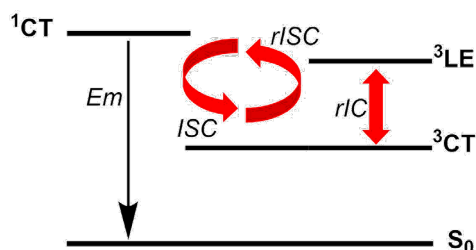
# 1 Computationally Guided Molecular Design to Minimize the LE/CT Gap in D- $\pi$ -A Fluorinated Triarylboranes for Efficient TADF via D and $\pi$ -Bridge Tuning

*The following section is slightly modified and reproduced from ref. [1] with permission from Wiley-VCH.*

## 1.1 Introduction

Achieving 100% internal quantum efficiency (IQE) in OLEDs<sup>[5]</sup> has been a challenging issue for several years. Spin-statistics dictate that electrons and holes recombine to generate 25% singlet and 75% triplet excitons.<sup>[6]</sup> Conventional fluorophores utilize only the singlet excitons leading to low IQE. Phosphorescent materials, on the other hand, are able to achieve, in theory, 100% IQE,<sup>[7-11]</sup> but require the involvement of expensive and less abundant heavy metal atoms essential for introducing large spin-orbit coupling to access rapid intersystem crossing.<sup>[11, 12]</sup> In 2012, Adachi and coworkers demonstrated that organic molecules can undergo an alternative mechanism known as thermally activated delayed fluorescence (TADF). In fact, TADF was first reported by Perrin in 1929,<sup>[13]</sup> and later investigated by others in the 20<sup>th</sup> century (so-called E-type fluorescence),<sup>[14, 15]</sup> such that organic TADF emitters can harvest both singlet and triplet excitons and thus, potentially, enhance the IQE to 100%.<sup>[16-23]</sup> TADF is a unimolecular process in which the triplet state is thermally up-converted via reverse intersystem crossing (rISC) back to the singlet state.<sup>[24-33]</sup> The efficiency of rISC determines the overall performance of the TADF process and is enabled by a small singlet-triplet energy splitting ( $\Delta E_{ST}$ ) such that the thermal energy at ambient temperature is sufficient to upconvert the triplet back to the singlet. In principle, a small  $\Delta E_{ST}$  can be achieved by spatially separating the highest occupied molecular orbital (HOMO) and lowest unoccupied molecular orbital (LUMO) in donor-acceptor (D-A) molecules, resulting in a small overlap of their wavefunctions and, thereby, a small exchange energy,  $K$  (in the Hartree-Fock approximation:  $\Delta E_{ST} = 2K$ ).<sup>[34-36]</sup> In the same way, twisted D-A molecules, in which the donor and acceptor orbitals are almost orthogonal, display small values for  $K$ . Another strategy is to enhance the spin-orbit coupling  $\langle T_1 | \hat{H}_{SO} | S_1 \rangle$  between pure spin states  $T_1$  and  $S_1$ , where  $\hat{H}_{SO} = \xi \hat{L} \cdot \hat{S}$  and  $\hat{L}$  and  $\hat{S}$  are total orbital and spin angular momentum, respectively, in order to increase the rate of the ISC and rISC processes.<sup>[37-40]</sup> However, generally, the spin-orbit coupling is very small in organic molecules (typically  $< 1 \text{ cm}^{-1}$ ),<sup>[41]</sup> in contrast to that in phosphors containing heavy metal atoms. To maximize the rISC efficiency, several researchers elucidated the crucial role of high-energy triplet (local-excited) states to

accelerate the rISC process. Based on carefully designed spectroscopic and quantum dynamics experiments, they elucidated an efficient dynamic two-step rISC mechanism (Scheme 1.1).<sup>[24, 41-48]</sup>



Scheme 1.1: Dynamic two-step TADF mechanism for a D-A molecule. Em: emission; ISC: intersystem crossing; rISC: reverse intersystem crossing; and rIC: reverse internal conversion.

First, local-excited and charge-transfer states ( $^3\text{LE}$  and  $^3\text{CT}$ ) are coupled via non-adiabatic coupling (reverse internal conversion: rIC), the strength of which depends on the size of the vibronic coupling (VC) and the corresponding energy gap (Equation 1.1).<sup>[45]</sup> Subsequently, a second order perturbation term couples  $^3\text{CT}$  and  $^1\text{CT}$  states mediated by the intermediate  $^3\text{LE}$  state (Equation 1.2).<sup>[45]</sup>

Equation 1.1:

$$k_{\text{rIC}} = \frac{2\pi}{\hbar} \left| \langle {}^3\psi_{\text{LE}} | \hat{H}_{\text{vib}} | {}^3\psi_{\text{CT}} \rangle \right|^2 \times \delta({}^3E_{\text{LE}} - {}^3E_{\text{CT}})$$

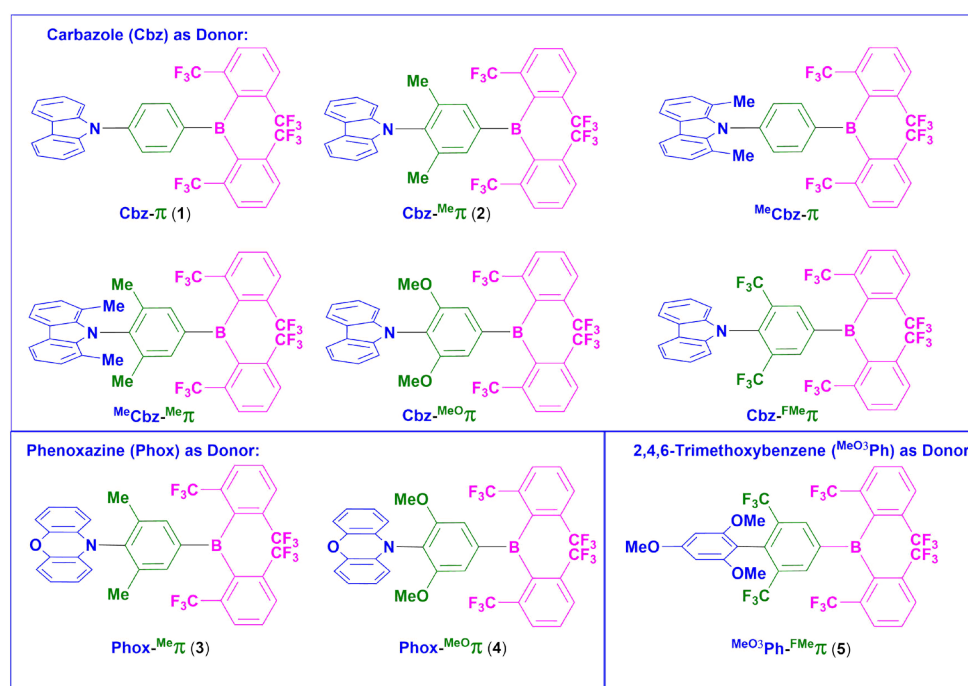
Equation 1.2:

$$k_{\text{rISC}} = \frac{2\pi}{\hbar} \left| \frac{\langle {}^1\psi_{\text{CT}} | \hat{H}_{\text{SOC}} | {}^3\psi_{\text{LE}} \rangle \langle {}^3\psi_{\text{LE}} | \hat{H}_{\text{vib}} | {}^3\psi_{\text{CT}} \rangle}{\delta({}^3E_{\text{LE}} - {}^3E_{\text{CT}})} \right|^2 \times \delta({}^3E_{\text{CT}} - {}^1E_{\text{CT}})$$

Thus, in order to design an efficient rISC process it is of paramount importance to decrease (at least) *two* gaps, the energy difference between  $^3\text{LE}$  and  $^1\text{CT}$  ( $\Delta E_{^1\text{CT}-^3\text{LE}}$ ), and  $^1\text{CT}$  and  $^3\text{CT}$  ( $\Delta E_{^1\text{CT}-^3\text{CT}}$ ), respectively,<sup>[36]</sup> instead of focusing only on the gap between  $S_1$  and  $T_1$ . In many cases, the lowest  $^1\text{CT}$  and  $^3\text{CT}$  states are described by the transition from a donor (D) to an acceptor (A) which, in the case of twisted molecules (large dihedral angle between the donor and acceptor moieties), lie close in energy leading to a small  $\Delta E_{^1\text{CT}-^3\text{CT}}$ .<sup>[49-53]</sup> One class of compounds that has successfully been employed for TADF is triarylboranes.<sup>[54-68]</sup> Three-coordinate boron can be used as an acceptor moiety due to the vacant  $p_z$  orbital perpendicular to its plane. Triarylboranes represent a well-researched acceptor class<sup>[69-80]</sup> and have been employed for a plethora of different applications such as linear<sup>[81-95]</sup> and non-linear<sup>[96-118]</sup> optics, sensors,<sup>[119-121]</sup> and OLEDs.<sup>[54, 122, 123]</sup> In all of these applications, it is important to note that, if

no explicit reactivity of the boron center towards nucleophiles is desired, electronic or steric protection is necessary. We and others have recently reported methodologies to enhance the accepting properties as well as the stability of boron by the introduction of *ortho*-trifluoromethylaryl moieties.<sup>[77, 91, 124-138]</sup> Increased stabilization can be partially attributed to a direct interaction between the electron pairs of the fluorine and the boron center, which is supported by short B-F distances in crystal structures.<sup>[91]</sup> In our experience, the trifluoromethyl groups also improve the volatility as well as the solubility of compounds, thereby improving their processability. The impact of trifluoromethyl substitution on carbazole for the development of deep blue TADF emitters has been demonstrated recently and investigated concerning their photostability. No direct correlation of the photostability with the employment of trifluoromethyl groups was observed.<sup>[139]</sup>

Herein, we report on a quantum-chemical exploration of structure-property relationships in a series of donor(D)- $\pi$ -bridge-acceptor(A) systems containing the B(FXyl)<sub>2</sub> (FXyl = 2,6-bis(trifluoromethyl)phenyl) acceptor group to design TADF emitters by selectively tuning the energy gap between the <sup>3</sup>LE (<sup>3</sup>LE<sub>D</sub>: LE state confined on D, <sup>3</sup>LE <sub>$\pi$</sub> : LE state confined on  $\pi$ -bridge) and the CT states, via functionalization of the donor (D) and the  $\pi$ -bridge (Scheme 1.2).



Scheme 1.2: Calculated D- $\pi$ -A systems with varying substituents on the donor (blue) and  $\pi$ -bridge (green), while the acceptor (magenta) is the same in all compounds. Compounds **Cbz- $\pi$  (1)**, **Cbz-Me $\pi$  (2)**, **Phox-Me $\pi$  (3)**, **Phox-MeO $\pi$  (4)**, and **MeO<sup>3</sup>Ph-FMe $\pi$  (5)** were synthesized and fully characterized and are numbered in the text (compounds without numbers are models used for computations).

## Chapter 1

To this end, we used *para*-phenylene ( $\pi = 1,4\text{-C}_6\text{H}_4$ ) as the  $\pi$ -bridge containing various substituents with varying electron-donating or -accepting strength in our computations. Subsequently, as a proof-of-concept, we experimentally corroborated our theoretical predictions. We demonstrate how the occurrence of a  ${}^3\text{LE}_\pi$  state provides an effective handle by which the CT and LE states can be independently tuned, and thus adjusting the energy gap between them. More importantly, we outline a novel and rational design strategy to generate an array of TADF emitters with exceptionally small energy gaps, and emission energies which span nearly the complete spectrum of visible light.



## 1.2 Results and Discussion

### 1.2.1 In Silico Molecular Design

In order to meet the required accuracy for the energy prediction of the charge transfer state, we used an optimally tuned range-separated functional (ZORA-LC-BLYP\*/TZ2P/COSMO, see Chapter 6.6.1 for detailed information) with a predetermined range separation parameter  $\gamma$  derived from the ionization potential of N and N+1 electron systems and benchmarked our protocol against available experimental data. A good linear relationship (correlation coefficient  $R^2 = 0.94$ , see Figure 6.55) and an excellent mean absolute deviation of 0.05 eV are achieved. Overall, our protocol can successfully predict the gaps in an unknown molecule D- $\pi$ -A except in cases where the assignment of the nature of the excited states as CT or LE becomes ill defined.<sup>[140, 141]</sup> All of the computed photophysical data for the compounds in Scheme 1.2 are listed in Table 1.1. To lay the foundation, we experimentally and theoretically investigated the structural and photophysical properties of 9-(4-(bis(2,6-bis(trifluoromethyl)phenyl)boryl)phenyl)-9*H*-carbazole, **Cbz- $\pi$**  (**1**, Scheme 1.2), which is composed of the moderately strong electron-donor carbazolyl (Cbz) and an unsubstituted phenylene ring connecting the carbazole nitrogen with the B(<sup>F</sup>Xyl)<sub>2</sub> acceptor. Photophysical measurements showed only prompt fluorescence ( $\tau_{\text{PF}} = 10.0$  ns in toluene) and revealed no delayed fluorescence or TADF behavior. The computed dihedral angles between the donor and the  $\pi$ -bridge, and between the  $\pi$ -bridge and the acceptor in the equilibrium ground state structure are 49° and 27°, respectively. From a single-crystal X-ray diffraction study, we found slightly smaller angles of 43.06(7)° and 17.83(10)°, respectively. Such small dihedral angles enable spatial delocalization of the frontier Kohn-Sham (KS) molecular orbitals, leading to a relatively large exchange energy  $K$  and thus a large  $\Delta E_{1_{\text{CT}}-3_{\text{CT}}}$  of 0.43 eV (Table 1.1). On the other hand,  $\Delta E_{1_{\text{CT}}-3_{\text{LE}}}$  is rather small (0.06 eV). However,  $\Delta E_{1_{\text{CT}}-3_{\text{CT}}}$  decreases to 0.13 eV upon gradually increasing the donor- and  $\pi$ -A dihedral angle to 90° (Figure 6.58), highlighting the importance of decoupling the donor and the acceptor via increased steric hindrance.<sup>[34-36]</sup>

## Chapter 1

Table 1.1: Calculated photophysical data for all compounds in Scheme 1.2. The table shows the vertical excitation energies (in eV and nm) with its corresponding oscillator strength ( $f$ ), charge transfer metrics ( $\Lambda$  and  $R_{\text{ch}}$  in Å), assignment of the excited states along with the MO composition (configuration interaction, CI) of the transition (in %) obtained from one-electron Tamm-Dancoff approximation-DFT (TDA-DFT) excitations, the computed S–T gaps and the emission energies ( $\Delta E(S_1)$  and  $\Delta E_{\text{VE}}(T_1)$ ) in eV and nm. Fields in bold represent the mapping of the FC- $T_n$  state corresponding to the relaxed  $T_1$  state according to the difference density plots.

Cpd.	State	State		Assign.	$f$	CI (%)	$\Lambda^a)$	$R_{\text{ch}}^b)$ [Å]	$\Delta E^{\text{CT-}}$ $^1\text{LE}$ [eV]	$\Delta E^{\text{CT-}}$ $^3\text{CT}$ [eV]	$\Delta E^{\text{CT-}}$ $^1\text{LE}$ [eV]
		[eV]	[nm]								
Cbz- $\pi$ (1)	FC-S <sub>1</sub>	3.42	363	<sup>1</sup> CT	0.512	H→L (84), H-3→L (4)	0.36	5.52			
	<b>FC-T<sub>1</sub></b>	<b>2.99</b>	<b>415</b>	<b><sup>3</sup>CT</b>	-	H→L (64), H-3→L (19)	<b>0.42</b>	<b>4.82</b>			
	FC-T <sub>2</sub>	3.48	356	<sup>3</sup> LE <sub>D</sub>	-	H-1→L+4 (60), H→L+5 (32)	0.63	1.66			
	FC-T <sub>3</sub>	3.54	350	<sup>3</sup> LE <sub>D</sub>	-	H-1→L+4 (61), H→L+5 (24)	0.62	2.38	0.06	0.43	0.49
	FC-T <sub>4</sub>	3.82	325	<sup>3</sup> LE <sub><math>\pi</math></sub>	-	H-4→L (64), H-5→L+5 (7)	0.51	1.77			
	FC-T <sub>5</sub>	3.89	319	<sup>3</sup> LE <sub>A</sub>	-	H-6→L (48), H-5→L+3 (15)	0.66	0.66			
	$\Delta E(S_1)$	3.19	389	-	-						
$\Delta E_{\text{VE}}(T_1)$	2.57	482	<b>FC-T<sub>1</sub></b>	-							
Cbz-Me $\pi$ (2)	FC-S <sub>1</sub>	3.56	348	<sup>1</sup> CT	0.075	H→L (85), H→L+5 (7)	0.18	6.35			
	<b>FC-T<sub>1</sub></b>	<b>3.32</b>	<b>373</b>	<b><sup>3</sup>CT</b>	-	H-5→L (47), H→L (33)	<b>0.36</b>	<b>5.01</b>			
	FC-T <sub>2</sub>	3.39	366	<sup>3</sup> LE <sub><math>\pi</math></sub>	-	H-2→L (83), H-2→L+5 (11)	0.43	2.51			
	FC-T <sub>3</sub>	3.44	360	<sup>3</sup> LE <sub>D</sub>	-	H→L+4 (81), H→L+5 (12)	0.62	0.82	0.17	0.24	0.07
	FC-T <sub>4</sub>	3.53	351	<sup>3</sup> LE <sub>D</sub>	-	H-1→L+4 (77), H-1→L+5 (10)	0.69	1.24			
	FC-T <sub>5</sub>	3.68	337	<sup>3</sup> CT	-	H→L (51), H-4→L (30)	0.30	5.52			
	$\Delta E(S_1)$	3.17	391	-	-						
$\Delta E_{\text{VE}}(T_1)$	2.65	468	<b>FC-T<sub>1</sub></b>	-							
Cbz-Me <sup>0</sup> $\pi$	FC-S <sub>1</sub>	3.44	360	<sup>1</sup> CT	0.175	H-2→L (55), H→L (37)	0.35	4.19			
	FC-T <sub>1</sub>	2.86	434	<sup>3</sup> LE <sub><math>\pi</math></sub>	-	H-2→L (77), H→L (7)	0.40	2.74			
	<b>FC-T<sub>2</sub></b>	<b>3.13</b>	<b>396</b>	<b><sup>3</sup>CT</b>	-	H→L (39), H-3→L (32)	<b>0.38</b>	<b>4.40</b>			
	FC-T <sub>3</sub>	3.50	354	<sup>3</sup> LE <sub>D</sub>	-	H→L+5 (61), H→L+4 (30)	0.61	2.15	0.58	0.31	0.27
	FC-T <sub>4</sub>	3.55	349	<sup>3</sup> LE <sub>D</sub>	-	H-1→L+5 (54), H-1→L+4 (32)	0.59	2.83			
	FC-T <sub>5</sub>	3.80	326	<sup>1</sup> CT	-	H→L (38), H-3→L (36)	0.39	4.20			
	$\Delta E(S_1)$	2.91	426	-	-						
$\Delta E_{\text{VE}}(T_1)$	2.61	475	<b>FC-T<sub>2</sub></b>	-							
MeCbz- $\pi$	FC-S <sub>1</sub>	3.27	379	<sup>1</sup> CT	0.122	H→L (85), H→L+4 (10)	0.19	6.42			
	<b>FC-T<sub>1</sub></b>	<b>3.13</b>	<b>396</b>	<b><sup>3</sup>CT</b>	-	H→L (68), H-3→L (15)	<b>0.26</b>	<b>5.68</b>			
	FC-T <sub>2</sub>	3.44	360	<sup>3</sup> LE <sub>D</sub>	-	H→L+5 (89)	0.68	0.07			
	FC-T <sub>3</sub>	3.54	350	<sup>3</sup> LE <sub>D</sub>	-	H-1→L+5 (74), H→L+7 (4)	0.72	1.02	0.17	0.14	0.31
	FC-T <sub>4</sub>	3.63	342	<sup>3</sup> LE <sub>D</sub>	-	H-3→L (57), H→L (17)	0.50	3.38			
	FC-T <sub>5</sub>	3.74	332	<sup>3</sup> LE <sub><math>\pi</math></sub>	-	H-5→L (67), H-1→L (13)	0.46	2.72			
	$\Delta E(S_1)$	2.74	452	-	-						
$\Delta E_{\text{VE}}(T_1)$	2.49	498	<b>FC-T<sub>1</sub></b>	-							

-Table 1.1 cont.-

Cpd.	State	State		Assign.	$f$	CI (%)	$\Lambda^a$	$R_{eh}^{b)}$ [Å]	$\Delta E_{CT}^{3LE}$ [eV]	$\Delta E_{CT}^{3CT}$ [eV]	$\Delta E_{CT}^{3LE}$ [eV]
		[eV]	[nm]								
MeCbz-Me $\pi$	FC-S <sub>1</sub>	3.23	384	<sup>1</sup> CT	0.012	H→L (87), H→L+4 (9)	0.12	6.54			
	<b>FC-T<sub>1</sub></b>	<b>3.20</b>	<b>388</b>	<sup>3</sup> CT	-	H→L (78), H→L+4 (8)	<b>0.27</b>	<b>5.20</b>			
	FC-T <sub>2</sub>	3.36	369	<sup>3</sup> LE $\pi$	-	H-3→L (49), H-2→L (36)	0.47	3.36			
	FC-T <sub>3</sub>	3.36	369	<sup>3</sup> LE <sub>D</sub>	-	H-4→L (71), H-4→L+4 (11)	0.35	4.63	0.13	0.03	0.16
	FC-T <sub>4</sub>	3.40	365	<sup>3</sup> LE <sub>D</sub>	-	H→L+5 (92)	0.65	0.13			
	FC-T <sub>5</sub>	3.54	350	<sup>3</sup> LE <sub>D</sub>	-	H-1→L+5 (82)	0.76	0.28			
	$\Delta E(S_1)$	2.71	457	-	-						
$\Delta E_{VE}(T_1)$	2.57	482	<b>FC-T<sub>1</sub></b>	-							
Phox-Me $\pi$ (3)	FC-S <sub>1</sub>	2.83	438	<sup>1</sup> CT	0.000	H→L (85), H→L+4 (10)	0.10	6.57			
	<b>FC-T<sub>1</sub></b>	<b>2.82</b>	<b>440</b>	<sup>3</sup> CT	-	H→L (85), H→L+4 (10)	<b>0.10</b>	<b>6.57</b>			
	FC-T <sub>2</sub>	3.06	405	<sup>3</sup> LE <sub>D</sub>	-	H→L+5 (89)	0.69	0.26			
	FC-T <sub>3</sub>	3.40	365	<sup>3</sup> LE $\pi$	-	H-2→L (83), H-2→L+4 (13)	0.43	2.61	0.23	0.01	0.24
	FC-T <sub>4</sub>	3.42	363	<sup>3</sup> LE $\pi$	-	H-3→L (78), H-3→L+4 (14)	0.58	2.40			
	FC-T <sub>5</sub>	3.49	355	<sup>3</sup> LE <sub>D</sub>	-	H→L+7 (92)	0.73	0.09			
	$\Delta E(S_1)$	2.15	577	-	-						
$\Delta E_{VE}(T_1)$	2.00	620	<b>FC-T<sub>1</sub></b>	-							
Phox-MeO $\pi$ (4)	FC-S <sub>1</sub>	2.76	449	<sup>1</sup> CT	0.070	H→L (88), H→L+4 (8)	0.17	6.49			
	<b>FC-T<sub>1</sub></b>	<b>2.67</b>	<b>464</b>	<sup>3</sup> CT	-	H→L (74), H-1→L (10)	<b>0.21</b>	<b>5.91</b>			
	FC-T <sub>2</sub>	2.80	443	<sup>3</sup> LE $\pi$	-	H-1→L (76), H→L (9)	0.39	3.29			
	FC-T <sub>3</sub>	3.10	400	<sup>3</sup> LE <sub>D</sub>	-	H→L+5 (92)	0.69	0.12	0.04	0.09	0.13
	FC-T <sub>4</sub>	3.37	368	<sup>3</sup> LE $\pi$	-	H-3→L (70), H-3→L+4 (12)	0.46	3.43			
	FC-T <sub>5</sub>	3.52	352	<sup>3</sup> LE <sub>D</sub>	-	H→L+7 (64), H→L+6 (24)	0.68	0.46			
	$\Delta E(S_1)$	2.02	614	-	-						
$\Delta E_{VE}(T_1)$	1.75	709	<b>FC-T<sub>1</sub></b>	-							
CBz-FMe $\pi$	FC-S <sub>1</sub>	3.03	409	<sup>1</sup> CT	0.000	H→L (80), H→L+2 (11)	0.10	6.48			
	<b>FC-T<sub>1</sub></b>	<b>3.02</b>	<b>411</b>	<sup>3</sup> CT	-	H→L (80), H→L+2 (12)	<b>0.11</b>	<b>6.48</b>			
	FC-T <sub>2</sub>	3.54	350	<sup>3</sup> CT	-	H-1→L (77), H-1→L+6 (9)	0.14	6.12			
	FC-T <sub>3</sub>	3.55	349	<sup>3</sup> LE <sub>D</sub>	-	H-1→L+6 (79), H-1→L (9)	0.70	0.83	0.52	0.01	0.53
	FC-T <sub>4</sub>	3.59	345	<sup>3</sup> LE <sub>D</sub>	-	H→L+6 (94)	0.68	0.33			
	FC-T <sub>5</sub>	3.66	339	<sup>3</sup> LE $\pi$	-	H-8→L (31), H-6→L (26), H-5→L (20)	0.68	0.12			
	$\Delta E(S_1)$	2.64	470	-	-						
$\Delta E_{VE}(T_1)$	2.35	528	<b>FC-T<sub>1</sub></b>	-							
MeO <sub>2</sub> Ph-FMe $\pi$ (5)	FC-S <sub>1</sub>	3.51	353	<sup>1</sup> CT	0.002	H-1→L (71), H-1→L+4 (9)	0.12	6.81			
	<b>FC-T<sub>1</sub></b>	<b>3.48</b>	<b>356</b>	<sup>3</sup> CT	-	H-1→L (64), H-1→L+4 (8)	<b>0.16</b>	<b>6.38</b>			
	FC-T <sub>2</sub>	3.53	351	<sup>3</sup> LE $\pi$	-	H-3→L (64), H-3→L+4 (7)	0.57	2.49			
	FC-T <sub>3</sub>	3.69	336	<sup>3</sup> CT	-	H→L (79), H→L+4 (7)	0.08	6.59	0.02	0.03	0.05
	FC-T <sub>4</sub>	3.84	323	<sup>3</sup> LE <sub>A</sub>	-	H-4→L (51), H-5→L+3 (11)	0.65	0.65			
	FC-T <sub>5</sub>	3.85	322	<sup>3</sup> LE <sub>A</sub>	-	H-5→L (48), H-4→L+3 (8)	0.66	0.82			
	$\Delta E(S_1)$	2.91	426	-	-						
$\Delta E_{VE}(T_1)$	2.46	504	<b>FC-T<sub>1</sub></b>	-							

a) Degree of spatial overlap between occupied and virtual orbitals involved in the excitation:  $\Lambda = \frac{\sum_{i,a} c_{ia}^2 \langle \varphi_a | r | \varphi_i \rangle}{\sum_{i,a} c_{ia}^2}$

b) Hole-electron distance:  $R_{eh} = \frac{\sum_{i,a} c_{ia}^2 \langle \varphi_a | r | \varphi_a \rangle - \langle \varphi_i | r | \varphi_i \rangle}{\sum_{i,a} c_{ia}^2}$

Of particular interest is the lowest localized triplet state ( ${}^3\text{LE}_\text{D}$ ) which is at 3.48 eV and is spatially confined on the Cbz donor in **Cbz- $\pi$**  (**1**), while the localized triplet state on the bridge ( ${}^3\text{LE}_\pi$ ) at 3.82 eV is rather high in energy and thus energetically forbidden to participate in the TADF process. We anticipated that inserting donor groups, such as methyl, at the 3- and 5-position on the phenylene bridge would increase the dihedral angle between D and  $\pi$ -A and simultaneously red-shift the  ${}^3\text{LE}_\pi$  energy such that the latter state becomes an integral part of the TADF mechanism. To achieve this, we modelled 9-(4-(bis(2,6-bis(trifluoromethyl)phenyl)boryl)-2,6-dimethylphenyl)-9*H*-carbazole (**Cbz- $\text{Me}\pi$** , **2**). Now, in contrast with the delocalized frontier KS molecular orbitals in **Cbz- $\pi$**  (**1**), the HOMO in **Cbz- $\text{Me}\pi$** , (**2**) is localized on the Cbz subunit, while the LUMO is localized more on the acceptor and is derived mostly from the empty  $p_z$  orbital on boron in  $\text{B}(\text{F}^\text{Xyl})_2$  (Figure 1.1).

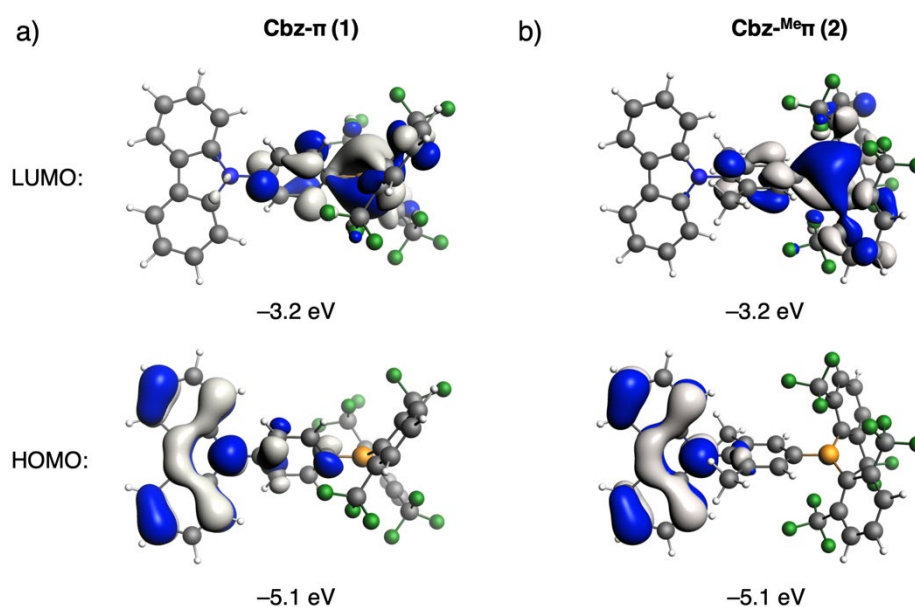


Figure 1.1: HOMO and LUMO of a) **Cbz- $\pi$**  (**1**); and b) **Cbz- $\text{Me}\pi$**  (**2**). Surface isovalue:  $\pm 0.03 [e a_0^{-3}]^{1/2}$ .

As predicted, the  $\Delta E_{1\text{CT}-3\text{CT}}$  becomes smaller (0.24 eV) owing to a small exchange energy  $K$  arising from a large dihedral angle ( $88^\circ$ ) between the D and the  $\pi$ -bridge. Indeed, experimentally, we found a dihedral angle of  $76.08(6)^\circ$  in the solid state for compound **Cbz- $\text{Me}\pi$**  (**2**). Moreover, the  ${}^3\text{LE}_\pi$  energy, which is essentially a  $\pi \rightarrow \pi^*$  transition on the phenylene bridge, is red-shifted from 3.82 eV in **Cbz- $\pi$**  (**1**) to 3.39 eV in **Cbz- $\text{Me}\pi$**  (**2**). As a result, the  ${}^3\text{LE}_\text{D}$  is replaced by  ${}^3\text{LE}_\pi$  as the lowest LE state, which results in a small  $\Delta E_{1\text{CT}-3\text{LE}}$  of 0.17 eV. This is a direct outcome of a decrease in the HOMO–LUMO gap of the bridge itself (4.8 eV in  $\text{Me}\pi\text{-H}_2$  vs. 5.1 eV in  $\pi\text{-H}_2$ , see Table 6.15) due to the mild positive inductive effect of the  $-\text{CH}_3$  substituents. Note that, in contrast with the  ${}^3\text{LE}_\text{D}$  state, the  ${}^3\text{LE}_\pi$  can, in principle, be tuned independently from the  ${}^1\text{CT}$  and  ${}^3\text{CT}$  states, i.e., by the modification of the bridge moiety.

Recently, Bickelhaupt and Lammertsma studied how the interplay of electronic properties of D,  $\pi$  or A fragments affect the electronic property of the overall D- $\pi$ -A molecule.<sup>[142]</sup> Subsequently, to simplify the picture and to link the changes in the different excited states with changes in the difference between the occupied and virtual orbital energies participating in the corresponding excitation, we need to consider two relevant HOMO–LUMO gaps: the HOMO–LUMO gap corresponding to the donor moiety (D-H) denoted as  $\Delta E_{\text{H-L}}^{\text{D}}$  and the HOMO–LUMO gap corresponding to the  $\pi$ -bridge denoted as  $\Delta E_{\text{H-L}}^{\pi}$ .

A smaller  $\Delta E_{\text{H-L}}^{\pi}$  results in a red-shifted  ${}^3\text{LE}_{\pi}$  or  $\pi \rightarrow \pi^*$  energy in  ${}^{\text{Me}}\pi\text{-H}_2$ , compared with that in  $\pi\text{-H}_2$ . Concomitantly, the energy gap  $\Delta E_{3\text{CT}-3\text{LE}}$ , which determines the extent of resonance between the triplet states, is smaller in **Cbz-Me $\pi$  (2)**, 0.07 eV in toluene) compared with that in **Cbz- $\pi$  (1)**, 0.37 eV). Thus, based on this simplified discussion, the former should have a much higher probability of showing TADF behavior than the latter. Indeed, we found experimentally that **Cbz-Me $\pi$  (2)** shows a delayed fluorescence lifetime of 13.6  $\mu\text{s}$  and an experimentally observed singlet–triplet gap in methylcyclohexane of 0.13 eV, in excellent agreement with the calculated  $\Delta E_{1\text{CT}-3\text{LE}}$  gap of 0.17 eV.

Further modelling of the bridge by replacing both methyl groups with methoxy substituents at the 2,6-positions of the phenylene bridge (Scheme 1.2) to generate 9-(4-(bis(2,6-bis(trifluoromethyl)-phenyl)boryl)-2,6-dimethoxyphenyl)-9*H*-carbazole (**Cbz-MeO $\pi$** ) leads to a further red-shifted  ${}^3\text{LE}_{\pi}$  state (3.39 eV in **Cbz-Me $\pi$**  to 2.86 eV in **Cbz-MeO $\pi$** ) as expected by the higher lying HOMO of the bridge fragment in **Cbz-MeO $\pi$**  compared to **Cbz-Me $\pi$  (2)**.

However, the introduction of two methoxy groups pushes the  ${}^3\text{LE}_{\pi}$  state below the  ${}^3\text{CT}$ . Such a large change in  ${}^3\text{LE}_{\pi}$  energy results in a large  $\Delta E_{1\text{CT}-3\text{LE}}$  of 0.58 eV, rendering the rISC process inefficient. So, the combination of D and  $\pi$ -bridge in **Cbz-Me $\pi$  (2)** and **Cbz-MeO $\pi$**  serves as an example of a match and a mismatch, respectively, of the TADF energy gaps. Interestingly, the CT energies are hardly affected for both **Cbz-Me $\pi$**  and **Cbz-MeO $\pi$**  (see Table 1.1).

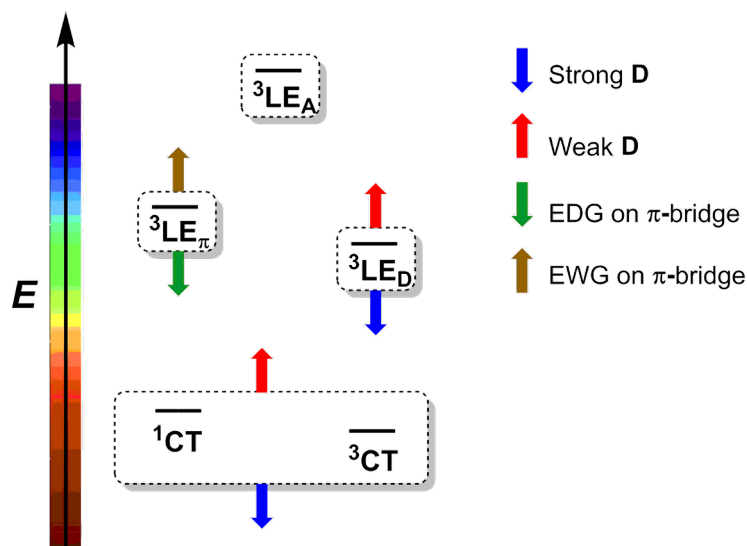
Another interesting example is the case of 10-(4-(bis(2,6-bis(trifluoromethyl)phenyl)boryl)-2,6-dimethylphenyl)-10*H*-phenoxazine (**Phox-Me $\pi$ , 3**, Scheme 1.2), in which the donor is transformed to phenoxazine (Phox) and the  $\pi$ -bridge is 2,6-dimethylphenylene. This has multiple effects on the excited states. Firstly, the large steric hindrance on the donor and  $\pi$ -A molecular planes [calculated: 89°, experimentally found in the solid state: 82.05(7)°] induced by hydrogens at the 1,9 positions of Phox and the methyl groups on the  ${}^{\text{Me}}\pi$ , results in a large spatial separation of the HOMO at the donor subunit and the LUMO at the acceptor subunit.

This leads to an expected extremely small  $\Delta E_{1\text{CT}-3\text{CT}}$  gap of 0.01 eV in **Phox-Me $\pi$  (3)**. Secondly, the introduction of Phox results in the decrease of the CT (both the lowest  $^1\text{CT}$  and  $^3\text{CT}$ ) energies from  $\sim 3.50$  eV in **Cbz-Me $\pi$  (2)** to  $\sim 2.80$  eV in **Phox-Me $\pi$  (3)**. Phox is a stronger electron donor than Cbz (HOMO =  $-4.3$  and  $-5.0$  eV for **Phox-H** and **Cbz-H**, respectively, see Table 6.15). Lastly, the lowest  $^3\text{LE}$  state is again switched from the bridge ( $^3\text{LE}_\pi$ ) in **Cbz-Me $\pi$  (2)** to the donor moiety ( $^3\text{LE}_\text{D}$ ) in **Phox-Me $\pi$  (3)**. This is due to a significantly stabilized  $^3\text{LE}_\text{D}$  in **Phox-Me $\pi$  (3)**: 3.06 eV) compared to that in **Cbz-Me $\pi$  (2)**: 3.44 eV), while the  $^3\text{LE}_\pi$  state is essentially unaffected. Again, this is directly related to the stronger electron-donating ability of Phox compared to Cbz, which leads to a higher HOMO energy and a smaller  $\Delta E_{\text{H-L}}^{\text{D}}$  of 2.9 eV in Phox-H compared to 3.3 eV in Cbz-H.

Therefore, despite a small  $\Delta E_{1\text{CT}-3\text{CT}}$  of 0.01 eV, the  $\Delta E_{1\text{CT}-3\text{LE}}$  is relatively large (0.23 eV) due to a strongly stabilized  $^1\text{CT}$  state. However, experimentally it was found that compound **Phox-Me $\pi$  (3)** shows TADF with a delayed fluorescence lifetime of 0.7  $\mu\text{s}$  and an experimentally observed singlet-triplet gap of 0.04 eV in toluene, which compares nicely with the calculated  $\Delta E_{1\text{CT}-3\text{CT}}$  of 0.01 eV.

To decrease the  $\Delta E_{1\text{CT}-3\text{LE}}$  gap in **Phox-Me $\pi$**  further, we need to stabilize the  $^3\text{LE}$  as well and, therefore, we replaced the methyl with methoxy groups on the  $\pi$ -bridge. As expected, 10-(4-(bis(2,6-bis(trifluoromethyl)phenyl)boryl)-2,6-dimethoxyphenyl)-10*H*-phenoxazine (**Phox-MeO $\pi$ , 4**) displays a significant stabilization of the  $^3\text{LE}_\pi$  state, compared with that of **Phox-Me $\pi$**  (2.80 eV vs. 3.40 eV). This enhanced stabilization proceeds with  $^3\text{LE}_\text{D}$  being replaced by  $^3\text{LE}_\pi$  as the lowest  $^3\text{LE}$  state. Consequently, the  $\Delta E_{1\text{CT}-3\text{LE}}$  drops to a mere 0.04 eV and **Phox-MeO $\pi$  (4)** exhibits ideal energy gaps for an efficient rISC process. The experimentally obtained singlet-triplet gap of 0.03 eV is in reasonable agreement with the corresponding calculated gap ( $\Delta E_{1\text{CT}-3\text{CT}}$ ) of 0.09 eV (vide infra).

Overall, we can summarize our findings thus far as follows: the nature and the energy of the lowest  $^3\text{LE}$  state involves an intricate interplay between the strength of the electron-donating substituent on the  $\pi$ -bridge and the strength of the electron donor (D), whereas, the energy of the CT state is a function of the strength of the donor (D) and the acceptor (A). It can be deduced that a combination of a strong donor (D) and a strong electron-donating substituent on the  $\pi$ -bridge or a weaker donor (D) and a weaker electron donating substituent, i.e. an electron-withdrawing group, on the  $\pi$ -bridge are required to achieve the desired TADF features (Scheme 1.3).



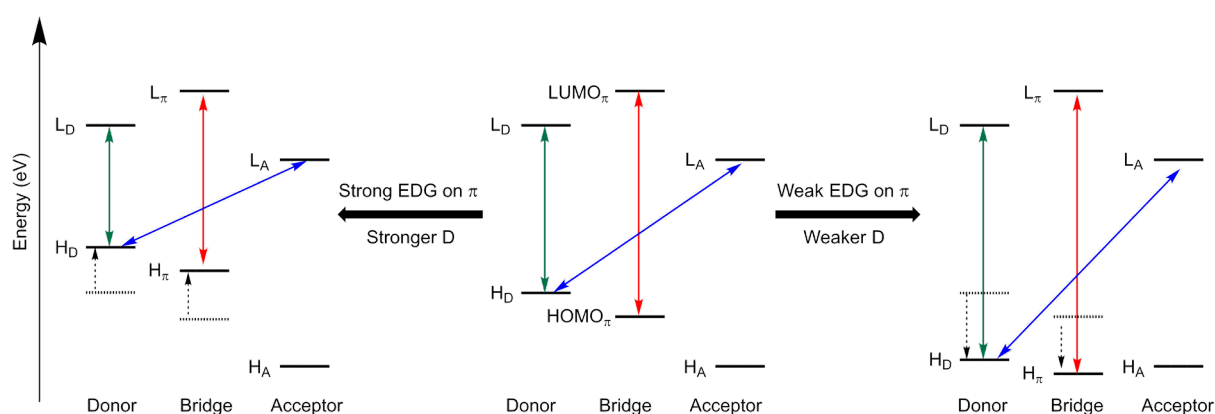
Scheme 1.3: Schematic illustration of the independent tuning of the local excited state on the  $\pi$ -bridge ( ${}^3\text{LE}_\pi$ ); the local excited state on the donor D ( ${}^3\text{LE}_D$ ) and the charge transfer from donor D to acceptor A in a D- $\pi$ -A molecule. The local excited state ( ${}^3\text{LE}_A$ ) on the acceptor is almost independent of the variation of the donor and bridge moieties. Tuning of the emission color is controlled by the energy of  ${}^1\text{CT}$ .

To generate more appropriate combinations, we computed the frontier molecular orbital energies (Table 6.15) and the HOMO–LUMO gaps of the various D-H and  $\pi$ -H<sub>2</sub> and used the data as a guideline for further calculations. Again, considering **Cbz- $\pi$**  (**1**) as the reference system, adding two methyl groups at the 1,8-positions (Scheme 1.2) to the Cbz donor to form <sup>Me</sup>Cbz raises the HOMO by 0.1 eV (Table 6.15). As a result, the CT energies (both the lowest  ${}^1\text{CT}$  and  ${}^3\text{CT}$ ) corresponding to both 9-(4-(bis(2,6-bis(trifluoromethyl)phenyl)boryl)phenyl)-1,8-dimethyl-9*H*-carbazole (<sup>Me</sup>**Cbz- $\pi$** ) and 9-(4-(bis(2,6-bis(trifluoromethyl)phenyl)boryl)-2,6-dimethylphenyl)-1,8-dimethyl-9*H*-carbazole (<sup>Me</sup>**Cbz-<sup>Me</sup> $\pi$** ) are slightly decreased, compared to those in the unsubstituted **Cbz- $\pi$**  (**1**). In contrast, the lowest LE state changes its nature from being confined on <sup>Me</sup>Cbz in the former ( ${}^3\text{LE}_D$ ) to <sup>Me</sup> $\pi$  in the latter ( ${}^3\text{LE}_\pi$ ). As a result, the high-lying  ${}^3\text{LE}_\pi$  at 3.74 eV in <sup>Me</sup>**Cbz- $\pi$**  drops to 3.36 eV in <sup>Me</sup>**Cbz-<sup>Me</sup> $\pi$**  leading to a small  $\Delta E_{{}^1\text{CT}-{}^3\text{LE}}$  of 0.13 eV. Therefore, both donors Cbz (explained above) and <sup>Me</sup>Cbz match with the bridge <sup>Me</sup> $\pi$  to exhibit small TADF energy gaps.

Finally, we analyzed the effect of adding two electron-withdrawing trifluoromethyl groups (–CF<sub>3</sub>) to the phenyl bridge to generate <sup>FMe</sup> $\pi$  (Scheme 1.2). To find a match with <sup>FMe</sup> $\pi$  as the bridge, we probed two different types of donors: (i) a moderately strong electron-donor Cbz to generate 9-(4-(bis(2,6-bis(trifluoromethyl)phenyl)boryl)-2,6-bis(trifluoromethyl)phenyl)-9*H*-carbazole (**Cbz-<sup>FMe</sup> $\pi$** ); and (ii) a moderately weak electron-donor such as 2,4,6-trimethoxybenzene (<sup>MeO</sup><sub>3</sub>Ph in Scheme 1.2) to generate 4'-(bis(2,6-bis(trifluoromethyl)phenyl)boryl)-2',6'-bis(trifluoromethyl)-[1,1'-biphenyl]-2,4,6-trimethoxy-benzene (<sup>MeO</sup><sub>3</sub>**Ph-<sup>FMe</sup> $\pi$**  (**5**)).

The bulky  $-\text{CF}_3$  group forces the D and  $\pi$ -A molecular planes to become nearly perpendicular ( $\sim 89^\circ$ ) in all cases, thereby decoupling the donor and the acceptor. As a result,  $\Delta E_{1\text{CT}-3\text{CT}}$  is, in general, quite small. The  $^3\text{LE}_\pi$  state, which is localized on  $^{\text{FMe}}\pi$  for both cases, is stabilized compared to the localized and higher lying  $^3\text{LE}_\pi$  state in phenylene (3.80 eV in phenylene-bridged *vs.*  $\sim 3.53$  and 3.66 eV in  $\text{MeO}_3\text{Ph-}^{\text{FMe}}\pi$  (**5**) and  $\text{Cbz-}^{\text{FMe}}\pi$ , respectively). This is due to a large negative inductive effect of  $-\text{CF}_3$  which strongly stabilizes the LUMO by 1.2 eV in  $^{\text{FMe}}\pi$ , compared to phenylene. Still, such a high-lying  $^3\text{LE}_\pi$  state would only match with a high-lying CT state emerging from a weak D. As predicted, in the case of the weak donor  $\text{MeO}_3\text{Ph}$ , the  $\Delta E_{1\text{CT}-3\text{LE}}$  and  $\Delta E_{3\text{CT}-3\text{LE}}$  reduce to  $\sim 0.05$  eV and  $\sim 0.06$  eV, respectively, while in the case of the moderately strong donor Cbz, the  $\Delta E_{1\text{CT}-3\text{LE}}$  and  $\Delta E_{3\text{CT}-3\text{LE}}$  gaps are 10 times larger ( $\sim 0.5$  eV). In the latter case, the CT states are much more stabilized than the  $^3\text{LE}_\pi$ , leading to a large  $\Delta E_{1\text{CT}-3\text{LE}}$ . Clearly,  $\text{MeO}_3\text{Ph}$ , has a lower energy HOMO (by 0.3 eV compared to Cbz). Thus, the larger energy gap between HOMO and LUMO increases the CT energies of the corresponding D- $\pi$ -A compounds. As a result,  $\text{MeO}_3\text{Ph-}^{\text{FMe}}\pi$  (**5**) displays a remarkably small  $\Delta E_{1\text{CT}-3\text{LE}}$  and, concomitantly, a small  $\Delta E_{3\text{CT}-3\text{LE}}$  as well.

Therefore, a combination of a weak donor with electron-withdrawing  $-\text{CF}_3$  substituents on the bridge in  $\text{MeO}_3\text{Ph-}^{\text{FMe}}\pi$  (**5**), a moderate donor with a moderate electron-donating substituent on the bridge in  $\text{Cbz-}^{\text{Me}}\pi$  (**2**) and a strong donor with a strong electron-donating substituent on the bridge in  $\text{Phox-}^{\text{MeO}}\pi$  (**4**) results in favorable TADF energy gaps; Scheme 1.4 summarizes this conclusion.



Scheme 1.4: Schematic illustration of the modulation of the HOMO–LUMO energy gap for the lowest CT states (blue), local-excited states at the donor (green) and at the bridge (red) via a combination of a strong donor–strong electron-donating group (EDG) on the bridge, or a weak donor–weak electron-donating group (i.e. an electron-withdrawing group) on the bridge. Here,  $H_D$  ( $L_D$ ),  $H_\pi$  ( $L_\pi$ ), and  $H_A$  ( $L_A$ ) denote the HOMO (LUMO) of donor, bridge and acceptor, respectively.

Additionally, the calculated delayed fluorescence energies in these three model systems range from deep blue (calc.: 391 nm, exp.: 460 nm) for  $\text{Cbz-}^{\text{Me}}\pi$  (**2**), to blue (calc.: 426 nm, exp.: 483

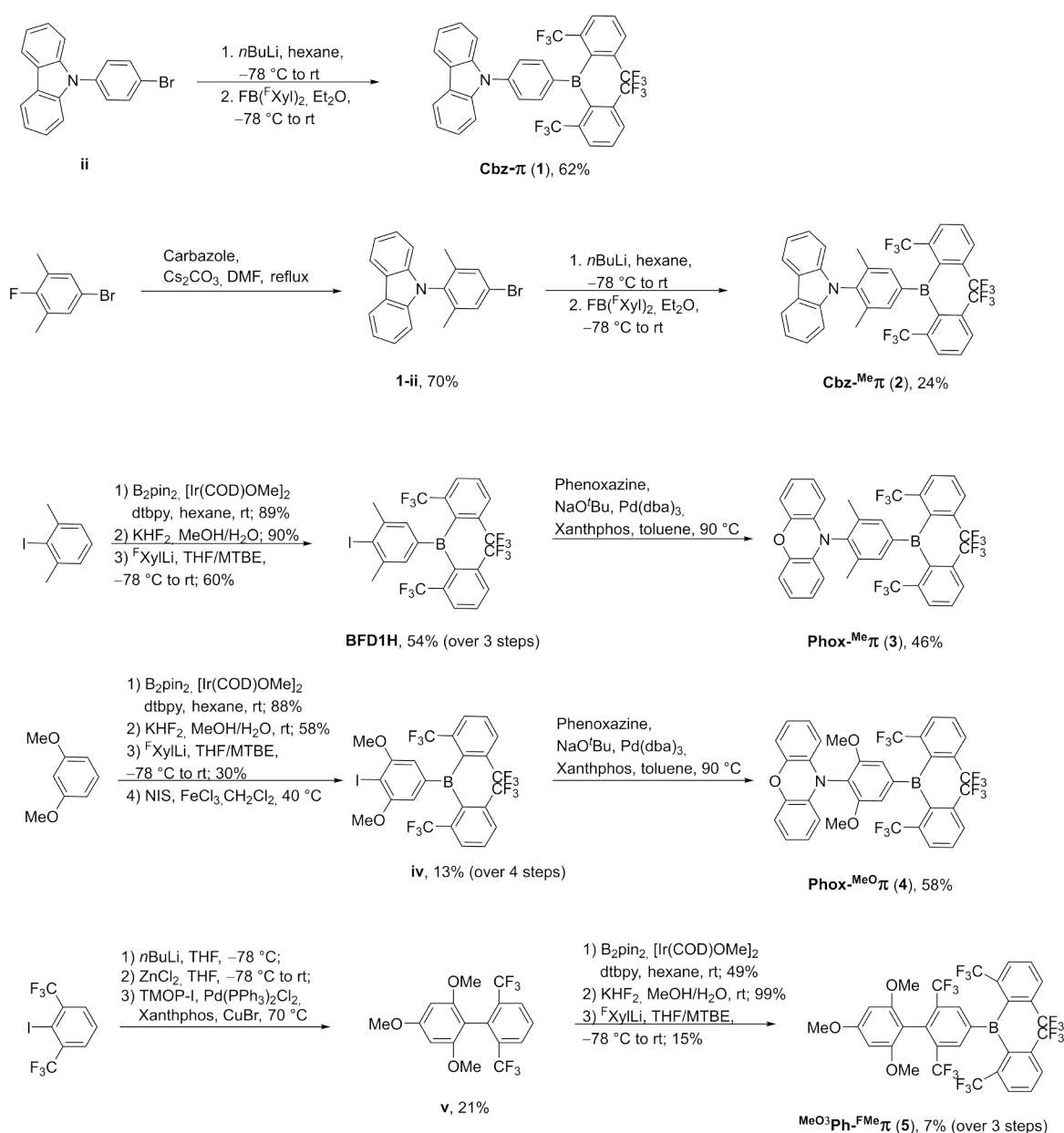


nm) for  $\text{MeO}_3\text{Ph-FMe}\pi$  (**5**) and red (calc.: 614 nm, exp.: 689 nm) for  $\text{Phox-MeO}\pi$  (**4**) (see  $\Delta E(S_1)$  in Table 1.1 for calculated and  $\lambda_{\text{em}}$  in Table 1.4 for the experimentally observed values, respectively).

After having characterized the excited state behavior of the model compounds in silico and having identified the potential TADF emitters, compounds **1-5** were synthesized, and all intermediates and resulting products were characterized by elemental analysis, single crystal X-ray diffraction,  $^1\text{H}$ ,  $^{13}\text{C}\{^1\text{H}\}$ ,  $^{11}\text{B}$  and  $^{19}\text{F}$  NMR spectroscopy, cyclic voltammetry and HRMS. The photophysical properties of compounds **1-5** in various solvents, polymeric films and in a frozen matrix were investigated in detail and the results are compared with the computationally obtained data.

## 1.2.2 Synthesis

The carbazole derivatives **Cbz- $\pi$**  (**1**) and **Cbz-Me $\pi$**  (**2**) were synthesized starting from the donor-bridge moiety (Scheme 1.5). The starting material **ii** was synthesized according to the literature<sup>[143]</sup> via an Ullman type amination. The methylated derivative **1-ii** was synthesized by nucleophilic *ipso*-substitution of fluorine in 5-bromo-2-fluoro-1,3-dimethylbenzene with carbazole. Both compounds were subsequently lithiated using *n*BuLi and reacted with bis(2,6-bis(trifluoromethyl)phenyl)fluoroborane to form **Cbz- $\pi$**  (**1**) and **Cbz-Me $\pi$**  (**2**), respectively.



Scheme 1.5: Synthesis of compounds **Cbz- $\pi$**  (**1**), **Cbz-Me $\pi$**  (**2**), **Phox-Me $\pi$**  (**3**), **Phox-MeO $\pi$**  (**4**), and **MeO<sub>3</sub>Ph-FMe $\pi$**  (**5**).

When attempting to synthesize **Phox-Me $\pi$**  (**3**) analogously to **Cbz-Me $\pi$**  (**2**), we encountered problems with the synthesis of the donor-bridge moiety. To circumvent this, an alternative route

was employed. To introduce the boron center, 2-iodo-1,3-dimethylbenzene was borylated using an iridium-catalyzed C–H borylation.<sup>[144, 145]</sup> This C–H borylation exhibits a high regioselectivity due to steric factors.<sup>[146]</sup> The boronate ester was then fluorinated using  $K[HF]_2$  to form the corresponding potassium aryltrifluoroborate salt. Aryltrifluoroborate salts are widely used as nucleophiles in Suzuki-Miyaura type cross-coupling reactions and are desirable intermediates due to their high stability.<sup>[147, 148]</sup> We and others have previously reported their application as convenient precursors to triarylboranes.<sup>[94, 132, 149-153]</sup> The potassium aryltrifluoroborate salt was reacted with 3 equivalents of (2,6-bis(trifluoromethyl)phenyl)lithium ( ${}^F\text{XylLi}$ ), prepared by the reaction of 2-iodo-1,3-bis(trifluoromethyl)benzene with  $n\text{BuLi}$ , to form the triarylborane **BFD1H** in 54% yield over three steps. Compared to the synthesis of **ii**, this approach is advantageous as it does not require expensive 5-bromo-2-fluoro-1,3-dimethylbenzene as the bridging moiety. In the last step, the phenoxazine donor moiety was introduced via a palladium-catalyzed Buchwald-Hartwig amination using  $\text{NaO}^t\text{Bu}$  as the base and Xantphos as the ligand. Compound **Phox-MeO $\pi$**  (**4**) was synthesized using the same basic approach. First, 1,3-dimethoxybenzene was regioselectively borylated, then fluorinated and reacted with  ${}^F\text{XylLi}$  to form the corresponding triarylborane. In order to introduce iodine, the triarylborane was reacted with NIS using  $\text{FeCl}_3$  as a Lewis acid to give **iv** in 13% yield over four steps. In this case, the iodination can be carried out at the triarylborane due to the electron rich and *ortho*-directing nature of the methoxy substituents. The donor moiety was introduced analogously to **Phox-Me $\pi$**  (**3**) in a palladium-catalyzed Buchwald-Hartwig amination. In the synthesis of **MeO<sub>3</sub>Ph-FMe $\pi$**  (**5**), the most problematic step is the coupling of 1,3,5-trimethoxybenzene with  ${}^F\text{XylLi}$ . For this reason, it was chosen as the first step. In a one-pot reaction,  ${}^F\text{XylLi}$  was prepared and converted to  $({}^F\text{Xyl})_2\text{Zn}$  which was then reacted with 2,4,6-trimethoxyiodobenzene in a palladium-catalyzed Negishi coupling reaction using Xantphos as the ligand with  $\text{CuBr}$  as an additive. Both the conversion to the organozinc compound and the copper salt are essential in this reaction. Then, **v** was borylated, fluorinated and reacted with  ${}^F\text{XylLi}$  to give **MeO<sub>3</sub>Ph-FMe $\pi$**  (**5**) in 7% yield over 3 steps.

Compounds **Cbz- $\pi$**  (**1**), **Cbz-Me $\pi$**  (**2**), **Phox-Me $\pi$**  (**3**), **Phox-MeO $\pi$**  (**4**), and **MeO<sub>3</sub>Ph-FMe $\pi$**  (**5**) were investigated by  ${}^1\text{H}$ ,  ${}^{11}\text{B}$ ,  ${}^{19}\text{F}$  and  ${}^{13}\text{C}$   $\{{}^1\text{H}\}$  NMR spectroscopy. For all compounds, a characteristic triplet and doublet corresponding to the  ${}^F\text{Xyl}$  backbone was observed in the  ${}^1\text{H}$  NMR spectra. The signals in the  ${}^{19}\text{F}$  NMR spectra corresponding to the *ortho*- $\text{CF}_3$  groups are broadened due to hindered rotation of the  ${}^F\text{Xyl}$  moieties. This has been previously observed and studied for other *ortho*- $\text{CF}_3$  substituted triarylboranes.<sup>[91, 131]</sup>

### 1.2.3 Crystal and Molecular Structures

Solid state structures of compounds **Cbz- $\pi$**  (1), **Cbz-Me $\pi$**  (2), **Phox-Me $\pi$**  (3), **Phox-MeO $\pi$**  (4), and **MeO<sub>2</sub>Ph-FMe $\pi$**  (5) determined by single-crystal X-ray diffraction are shown in Figure 1.2 and selected bond lengths and angles are listed in Table 1.2. The structures of the intermediates **BFD1H**, **iv**, **FB(FXyl)<sub>2</sub>** and **MeO $\pi$ -B(FXyl)<sub>2</sub>** along with their structural parameters can be found in Figure 6.6 - Figure 6.9 and Table 6.1.

Table 1.2: Selected bond lengths (Å) and angles (°) of **Cbz- $\pi$**  (1), **Cbz-Me $\pi$**  (2), **Phox-Me $\pi$**  (3), **Phox-MeO $\pi$**  (4), and **MeO<sub>2</sub>Ph-FMe $\pi$**  (5). Atomic numbering and the labels of the aryl rings R1, R2 and R3 are shown for compound **Cbz- $\pi$**  (1), in Figure 1.2 and are used for **Cbz-Me $\pi$**  (2), **Phox-Me $\pi$**  (3), **Phox-MeO $\pi$**  (4), and **MeO<sub>2</sub>Ph-FMe $\pi$**  (5) accordingly.

	<b>Cbz-<math>\pi</math></b> (1)	<b>Cbz-Me<math>\pi</math></b> (2)	<b>Phox-Me<math>\pi</math></b> (3)	<b>Phox-MeO<math>\pi</math></b> (4)	<b>MeO<sub>2</sub>Ph-FMe<math>\pi</math></b> (5)
B-C(R1)	1.557(2)	1.548(2)	1.553(3)	1.563(3)	1.568(4)
B-C(R2)	1.598(2)	1.603(2)	1.597(3)	1.598(3)	1.599(5)
B-C(R3)	1.606(2)	1.605(2)	1.599(3)	1.601(4)	1.601(5)
C(R1)-N/C <sup>a)</sup>	1.4168(18)	1.4296(17)	1.436(2)	1.421(3)	1.501(4)
C-N/C	1.4008(19)	1.3951(18)	1.401(2)	1.406(3)	1.388(4)
C-N/C	1.4055(18)	1.3937(19)	1.401(2)	1.411(3)	1.400(4)
C-C (R1, central):					
a	1.408(2)	1.4008(19)	1.400(2)	1.405(3)	1.397(4)
b	1.409(2)	1.4013(19)	1.399(2)	1.393(3)	1.394(4)
c	1.385(2)	1.3848(19)	1.389(2)	1.392(3)	1.390(4)
d	1.397(2)	1.3990(19)	1.395(2)	1.402(3)	1.403(4)
e	1.393(2)	1.4002(19)	1.389(2)	1.397(3)	1.402(4)
f	1.383(2)	1.3896(19)	1.400(2)	1.388(3)	1.393(4)
$\angle$ BC <sub>3</sub> -(N/C)C <sub>3</sub>	60.18(7)	44.83(7)	50.11(7)	55.51(11)	47.61(14)
$\angle$ BC <sub>3</sub> -R1 (central)	17.83(10)	31.25(6)	32.44(8)	34.16(12)	40.77(11)
$\angle$ B1C <sub>3</sub> -R2 (terminal)	67.13(6)	47.98(6)	54.07(6)	55.44(8)	59.87(11)
$\angle$ B1C <sub>3</sub> -R3 (terminal)	54.91(6)	53.04(6)	47.17(8)	43.51(9)	38.64(15)
$\angle$ NC <sub>3</sub> -R1 (central)	43.06(7)	76.08(6)	82.05(7)	89.55(8)	88.37(12)
$\angle$ N/C-moiety-R1 (central)	43.64(5)	76.36(4)	81.54(5)	88.37(5)	87.73(10)
Sum $\angle$ CBC	359.99(12)	359.99(12)	359.95(15)	360.0(2)	360.0(3)
Sum $\angle$ CNC/CCC	359.99(12)	357.01(11)	359.83(14)	356.31(18)	359.6(3)
Shortest B-F	2.708(2)	2.845(2)	2.747(3)	2.719(3)	2.705(4)
	2.933(2)	2.793(2)	2.845(6)	2.873(4)	2.898(4)
	2.516(2)	2.725(2)	2.844(2)	2.926(3)	2.713(4)
	2.853(2)	2.852(2)	2.836(2)	2.815(3)	2.918(4)

a) The ring-connecting bond is a C-C bond in compound **MeO<sub>2</sub>Ph-FMe $\pi$**  (5), while it is a C-N bond in compounds **Cbz- $\pi$**  (1), **Cbz-Me $\pi$**  (2), **Phox-Me $\pi$**  (3), and **Phox-MeO $\pi$**  (4).

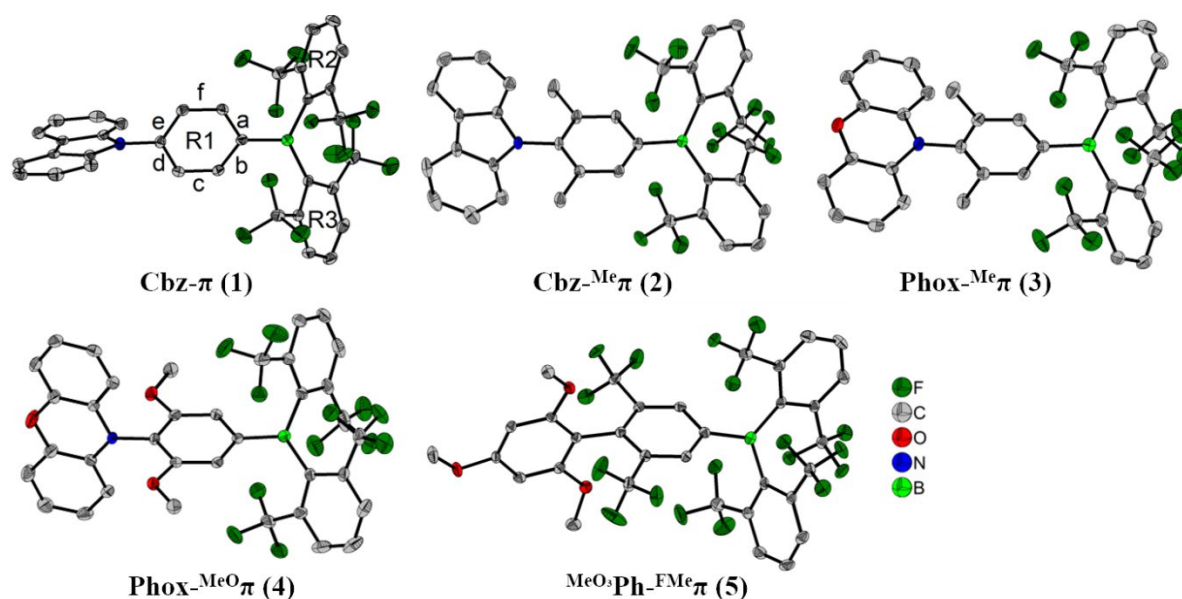


Figure 1.2: The solid-state molecular structures of **Cbz- $\pi$**  (**1**), **Cbz-<sup>Me</sup> $\pi$**  (**2**), **Phox-<sup>Me</sup> $\pi$**  (**3**), **Phox-<sup>MeO</sup> $\pi$**  (**4**), and **MeO<sub>3</sub>Ph-<sup>FMe</sup> $\pi$**  (**5**) determined by single-crystal X-ray diffraction at 100 K. All ellipsoids are drawn at the 50% probability level, and H atoms are omitted for clarity.

The acceptor moieties in compounds **Cbz- $\pi$**  (**1**), **Cbz-<sup>Me</sup> $\pi$**  (**2**), **Phox-<sup>Me</sup> $\pi$**  (**3**), **Phox-<sup>MeO</sup> $\pi$**  (**4**), and **MeO<sub>3</sub>Ph-<sup>FMe</sup> $\pi$**  (**5**) exhibit one shorter B–C bond to the bridge (R1) (1.548(2) - 1.568(4) Å) and two longer B–C bonds to the terminal <sup>F</sup>Xyl groups (1.597(3) - 1.606(2) Å) (Table 1.2). This can be partially attributed to the donor – acceptor nature of the compounds, which will shorten the B–C bond to R1, as well as the larger steric hinderance of the <sup>F</sup>Xyl moieties, which will elongate the B–C bonds to R2 and R3. An opposite behavior is observed for the nitrogen donor moieties in compounds **Cbz- $\pi$**  (**1**), **Cbz-<sup>Me</sup> $\pi$**  (**2**), **Phox-<sup>Me</sup> $\pi$**  (**3**), and **Phox-<sup>MeO</sup> $\pi$**  (**4**), which exhibit one longer C–N bond to R1 (1.417(2) - 1.436(2) Å) and two shorter C–N bonds (1.394(2) - 1.411(3) Å) to the terminal aryls of the donor moieties (Table 1.2). The same phenomenon is observable in compound **MeO<sub>3</sub>Ph-<sup>FMe</sup> $\pi$**  (**5**), in which the donor is connected to R1 via a C–C bond instead of a C–N bond, i.e., the C–C bond to R1 is longer than the aromatic C–C bonds of the donor moiety. For both the C–C and the C–N bonds, this is an expected behavior as the central carbon and nitrogen atoms are part of a heteroaryl or aryl moiety. The phenylene bridge between the donor and acceptor moieties of compound **Cbz- $\pi$**  (**1**) exhibits a quinoidal distortion, as the c and f bonds (Figure 1.2) are more than 0.008–0.026 Å shorter than the a, b, d, and e bonds (Table 1.2). This indicates a strongly polarized ground state of **1**. In the parent compound, 9-phenyl-9H-carbazole, no quinoidal distortion is present and C–N bond lengths are 1.420(5) and 1.427(4) Å, respectively, for two symmetrically non-equivalent molecules.<sup>[154]</sup> This is only slightly longer, within 1–2 standard deviations, if compared to **Cbz- $\pi$**  (**1**) (C–N = 1.417(2) Å). Compared to **Cbz- $\pi$**  (**1**), the C–N bond to R1 is elongated in

compound **Cbz-Me $\pi$  (2)** (C–N = 1.430(2) Å,  $\Delta$ C–N = 0.013 Å) which is likely due to the steric repulsion between the CH<sub>3</sub> groups on R1 and the carbazole donor moiety. However, in compound **Phox-Me $\pi$  (3)** no steric effect of the CH<sub>3</sub> groups on the C–N bond length is observed as the C–N bond of **Phox-Me $\pi$  (3)** (1.436(2) Å) is the same length as that of the parent compound 10-phenyl-10*H*-phenoxazine (1.435(3) Å) within one estimated standard deviation (esd).<sup>[155]</sup> Compounds **Cbz-Me $\pi$  (2)**, **Phox-Me $\pi$  (3)**, **Phox-MeO $\pi$  (4)**, and **MeO<sub>3</sub>Ph-FMe $\pi$  (5)** do not show a quinoidal distortion of the phenylene bridges within three esd's of the C–C bond lengths. This is attributed to the substitution with either CH<sub>3</sub>, MeO or CF<sub>3</sub> groups *ortho* to the donor moiety associated with an increase of the torsion angle between the donor moiety (NC<sub>3</sub> in **Cbz- $\pi$  (1)**, **Cbz-Me $\pi$  (2)**, **Phox-Me $\pi$  (3)**, and **Phox-MeO $\pi$  (4)**/CC<sub>3</sub> in **MeO<sub>3</sub>Ph-FMe $\pi$  (5)**) and R1. These torsion angles are 43.06(7)° (**Cbz- $\pi$  (1)**), 76.08(6)° (**Cbz-Me $\pi$  (2)**), 82.05(7)° (**Phox-Me $\pi$  (3)**), 89.55(8)° (**Phox-MeO $\pi$  (4)**) and 87.37(12)° (**MeO<sub>3</sub>Ph-FMe $\pi$  (5)**), respectively (Table 1.2). Groups on the *ortho*-positions were specifically introduced in order to increase the torsion angles and, hence, limit the orbital overlap between donor and acceptor, which is crucial for efficient TADF. The smallest torsion angle is observed for compound **Cbz- $\pi$  (1)** with the unsubstituted phenylene bridge. Due to steric repulsion between the *ortho*-substituted CH<sub>3</sub> groups and the carbazole donor moiety, the torsion angle is significantly increased in compound **Cbz-Me $\pi$  (2)**, however, to a slightly smaller extent than compared to the phenoxazine derivatives **Phox-Me $\pi$  (3)**, **Phox-MeO $\pi$  (4)** and the biphenyl derivative **MeO<sub>3</sub>Ph-FMe $\pi$  (5)**. This is attributed to the more extended sizes of the donor moieties of **Phox-Me $\pi$  (3)**, **Phox-MeO $\pi$  (4)**, and **MeO<sub>3</sub>Ph-FMe $\pi$  (5)** as well as the more extended MeO and CF<sub>3</sub> groups compared to CH<sub>3</sub>. Similarly to previously reported *ortho*-CF<sub>3</sub>-substituted triarylboranes,<sup>[91, 124, 131, 132]</sup> compounds **Cbz- $\pi$  (1)**, **Cbz-Me $\pi$  (2)**, **Phox-Me $\pi$  (3)**, **Phox-MeO $\pi$  (4)**, and **MeO<sub>3</sub>Ph-FMe $\pi$  (5)** exhibit four short B–F contacts (2.516(2) – 2.926(3) Å, Table 1.2) per B(<sup>F</sup>Xyl)<sub>2</sub> moiety, which are shorter than the sum of their van der Waals radii (3.39 Å).<sup>[156]</sup> This indicates a stabilizing effect of the *ortho*-CF<sub>3</sub> groups on the triarylborane.

### 1.2.4 Electrochemistry

Cyclic voltammograms of the D- $\pi$ -A compounds **Cbz- $\pi$**  (**1**), **Cbz-Me $\pi$**  (**2**), **Phox-Me $\pi$**  (**3**), **Phox-MeO $\pi$**  (**4**), and **MeO $_3$ Ph-FMe $\pi$**  (**5**) were recorded in order to determine their electronic properties (Figure 1.3 and Table 1.3). All compounds exhibit reversible reduction events corresponding to the B(FXyl) $_2$  acceptor moiety.

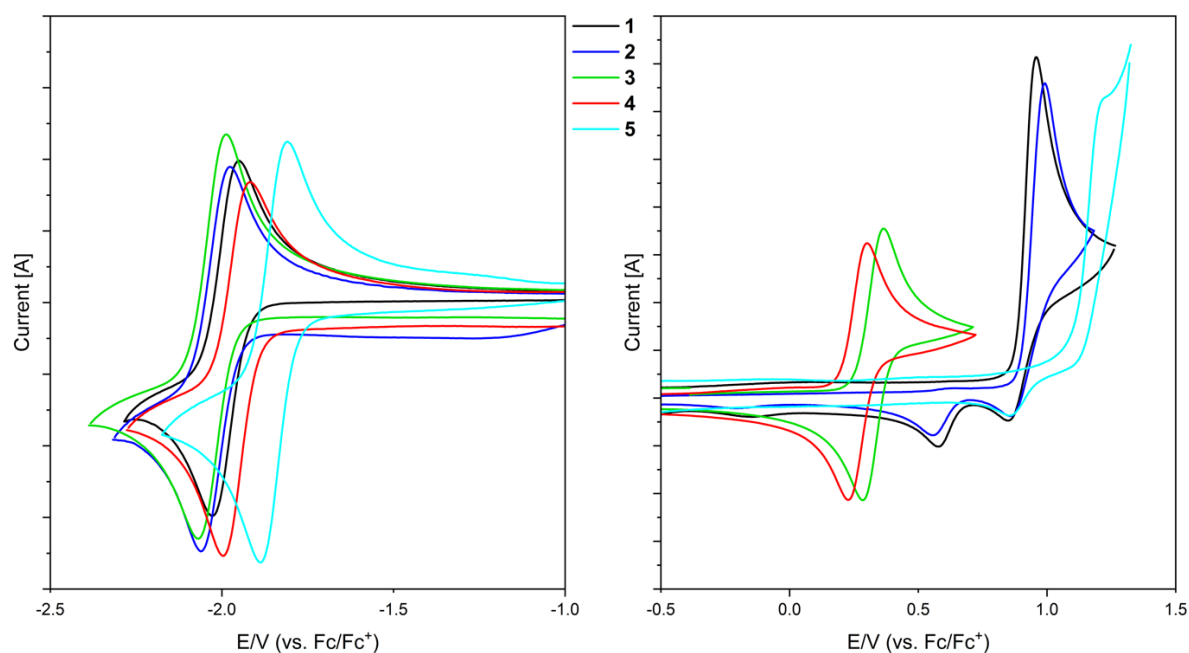


Figure 1.3: Cyclic voltammograms of **Cbz- $\pi$**  (**1**), **Cbz-Me $\pi$**  (**2**), **Phox-Me $\pi$**  (**3**), **Phox-MeO $\pi$**  (**4**), and **MeO $_3$ Ph-FMe $\pi$**  (**5**), reversible reductions (left) and oxidations (right). Potentials are given vs. ferrocene/ferrocenium (Fc/Fc $^+$ ).

Table 1.3: Reversible reduction and oxidation potentials of **Cbz- $\pi$**  (**1**), **Cbz-Me $\pi$**  (**2**), **Phox-Me $\pi$**  (**3**), **Phox-MeO $\pi$**  (**4**), and **MeO $_3$ Ph-FMe $\pi$**  (**5**).

Compound	$E_{1/2}$ vs. Fc/Fc $^+$ [V] <sup>a)</sup>		$E_{pa}$ vs. Fc/Fc $^+$ [V] <sup>a)</sup>	MO energies exp. [eV] <sup>b)</sup>	
	1 <sup>st</sup> reduction potential	1 <sup>st</sup> oxidation potential		HOMO	LUMO
<b>Cbz-<math>\pi</math></b> ( <b>1</b> )	-1.99		0.96	-6.20 <sup>c)</sup>	-3.27
<b>Cbz-Me<math>\pi</math></b> ( <b>2</b> )	-2.02		0.99	-6.27 <sup>c)</sup>	-3.24
<b>Phox-Me<math>\pi</math></b> ( <b>3</b> )	-2.03	0.33		-5.39	-3.23
<b>Phox-MeO<math>\pi</math></b> ( <b>4</b> )	-1.96	0.27		-5.33	-3.30
<b>MeO<math>_3</math>Ph-FMe<math>\pi</math></b> ( <b>5</b> )	-1.85		1.21	-6.45 <sup>c)</sup>	-3.40

a) Cyclic voltammograms were recorded in CH $_2$ Cl $_2$ /0.1 M [*n*Bu $_4$ N][PF $_6$ ] with a scan rate of 250 mVs $^{-1}$ .

b) Determined from the half wave potentials: HOMO =  $-(5.16 + E_{1/2,ox})$  eV, LUMO =  $-(5.16 + E_{1/2,red})$  eV.<sup>[157-159]</sup>

c) HOMO energies were estimated from  $E(\text{HOMO}) = E(\text{LUMO}) - E(\text{onset, abs})$  with onset, abs: **Cbz- $\pi$**  (**1**) = 423 nm (2.93 eV); **Cbz-Me $\pi$**  (**2**) = 409 nm (3.03 eV); **MeO $_3$ Ph-FMe $\pi$**  (**5**) = 407 nm (3.05 eV).

The reduction potentials of compounds **Cbz- $\pi$**  (**1**), **Cbz-Me $\pi$**  (**2**), **Phox-Me $\pi$**  (**3**), and **Phox-MeO $\pi$**  (**4**) are very similar ( $E_{1/2} \approx -2$  V vs. Fc/Fc $^+$ ). The xylyl bridged species **Cbz-Me $\pi$**  (**2**) and

**Phox-Me $\pi$**  (**3**) are shifted to slightly more negative potentials than **Cbz- $\pi$**  (**1**) and **Phox-MeO $\pi$**  (**4**). The reduction potential of **MeO<sub>3</sub>Ph-FMe $\pi$**  (**5**), however, is anodically shifted by about 150 mV. This is due to the CF<sub>3</sub> groups on the bridge that are positioned *meta* to the boron center and thus have a larger electron withdrawing effect than the ones in the *ortho*-positions at the terminal <sup>F</sup>Xyl moieties.<sup>[136]</sup> In our previous study on trifluoromethylarylboranes, we observed that exchanging mesityl for fluoromesityl leads to a cathodic shift of about 1 V

(Ph<sub>2</sub>NPhB(Mes)<sub>2</sub>: E<sub>1/2, red</sub> = -2.60 V vs Fc/Fc<sup>+</sup>; Ph<sub>2</sub>NPhB(<sup>F</sup>Mes)<sub>2</sub>: E<sub>1/2, red</sub> = -1.66 V vs Fc/Fc<sup>+</sup>).<sup>[131]</sup> Compounds **Cbz- $\pi$**  (**1**), **Cbz-Me $\pi$**  (**2**), **Phox-Me $\pi$**  (**3**), and **Phox-MeO $\pi$**  (**4**) are anodically shifted compared to the B(<sup>F</sup>Mes)<sub>2</sub> compound ( $\Delta E \approx 0.4$  V) and cathodically shifted compared to the BMes<sub>2</sub> compound ( $\Delta E \approx 0.6$  V). This also illustrates the stronger electron withdrawing effect of the CF<sub>3</sub> group in the *para*-position as compared to the ones in the *ortho*-positions. Only the phenoxazine derivatives **Phox-Me $\pi$**  (**3**) and **Phox-MeO $\pi$**  (**4**) exhibit reversible oxidation events corresponding to the donor moiety (E<sub>1/2</sub>  $\approx$  0.3 V vs Fc/Fc<sup>+</sup>). Compound **Phox-MeO $\pi$**  (**4**) is about 50 mV cathodically shifted compared to **Phox-Me $\pi$**  (**3**), which might be due to the electron donating nature of the OMe groups on the bridge. The carbazole derivatives **Cbz- $\pi$**  (**1**) and **Cbz-Me $\pi$**  (**2**) exhibit irreversible oxidation events characteristic of the carbazole moiety (E<sub>pa</sub>  $\approx$  1 V vs Fc/Fc<sup>+</sup>). The oxidation potential of compound **MeO<sub>3</sub>Ph-FMe $\pi$**  (**5**) is very close to the limit of the solvent window (E<sub>pa</sub> = 1.21 V vs Fc/Fc<sup>+</sup>). In comparison, the oxidation potential of 1,3,5-trimethoxybenzene is E<sub>1/2, ox</sub> = 1.5 V.<sup>[160]</sup>



## 1.2.5 Photophysical Properties

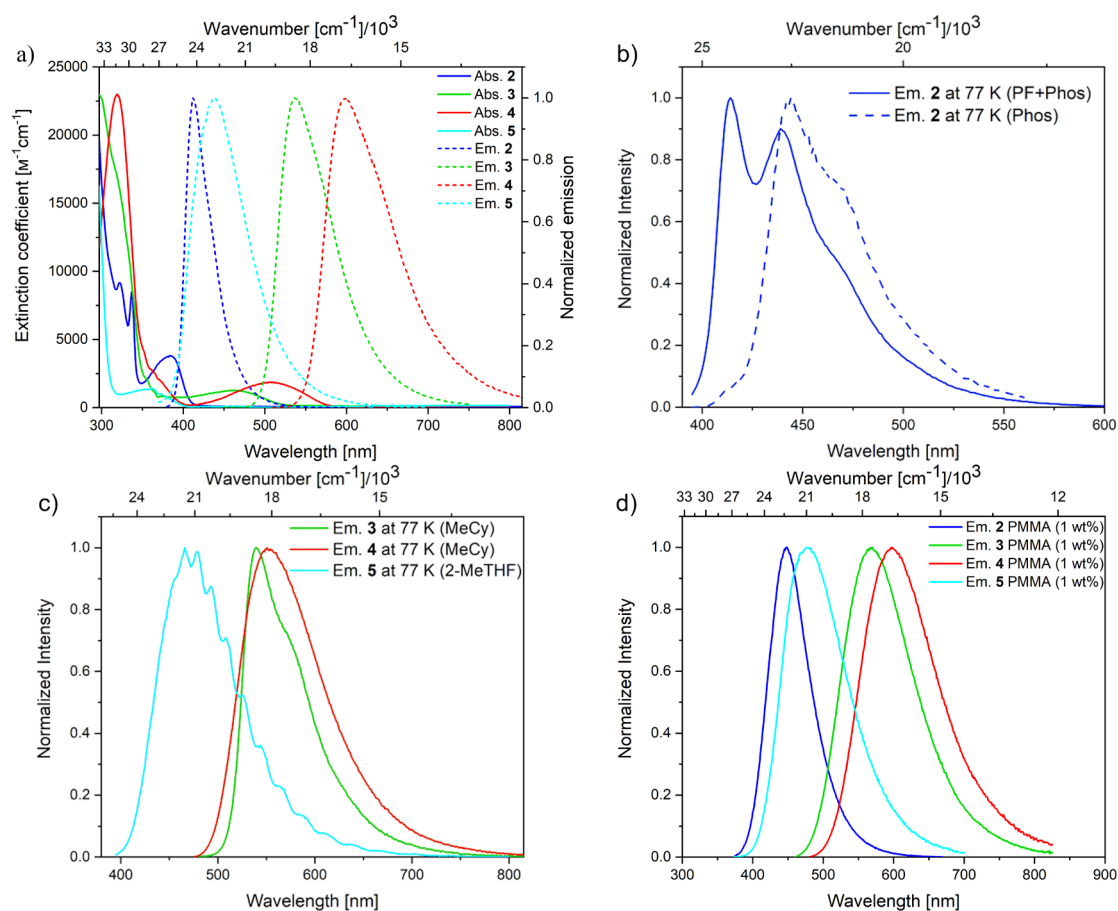


Figure 1.4: a) Absorption (solid line) and emission (dashed line) spectra of compounds **Cbz-Me $\pi$  (2)**, **Phox-Me $\pi$  (3)**, **Phox-MeO $\pi$  (4)**, and **MeO $_2$ Ph-FMe $\pi$  (5)** in degassed hexane. b) Overall emission spectrum (blue solid line) and time-gated spectrum (blue dashed line, >5 ms) of **Cbz-Me $\pi$  (2)** in a glassy matrix (MeCy = methylcyclohexane) at 77 K (PF = prompt fluorescence, Phos = phosphorescence). c) Emission spectra at 77 K of compounds **3**, **4**, and **5** in a glassy matrix (see Table 1.4). All concentrations are  $< 2 \times 10^{-5}$  mol/L. d) Emission spectra of compounds **2**, **3**, **4**, and **5** in 1 wt% PMMA films.

## Chapter 1

Table 1.4: Photophysical data for compounds **Cbz- $\pi$**  (1), **Cbz-Me $\pi$**  (2), **Phox-Me $\pi$**  (3), **Phox-MeO $\pi$**  (4), and **MeO $_2$ Ph-FMe $\pi$**  (5). Calculated gaps are shown in curly brackets.

	solvent	$\lambda_{\text{abs}}$ [nm]	$\epsilon$ [10 <sup>3</sup> M <sup>-1</sup> cm <sup>-1</sup> ]	$\lambda_{\text{em}}$ [nm]	Stokes shift [cm <sup>-1</sup> ]	$\tau_{PF}$ (%) [ns]	$\tau_{DF}$ (%) [ $\mu$ s]	$\Phi_{PL}$	$\Delta E_{ST}$ [eV]
1	hexane	400	17.7	423	1359	7.6 (100)	-	0.97	-
	toluene	398		470	3976	10.0 (100)	-	0.98	
	THF	387		524	6756	14.8 (100)	-	0.89	
2	hexane	384	3.8	412	1838	5.3 (97)	1.7 (3)	0.16	0.13 <sup>a)</sup> {0.17}
	toluene	380		460	4576	18.0 (62)	13.6 (38)	0.18	
	THF	370		515	7610	34.0 (21)	2.9 (79)	0.61	
	77 K <sup>b)</sup>	400		414 <sup>c)</sup>	1019	10.0 <sup>c)</sup>	- <sup>c)</sup>	-	
	PMMA <sup>d)</sup>	387		448	3518	10.3 (63)	8.4 (37)	0.55	
3	hexane	465	1.2	536	2849	40.0 (20)	1.4 (80)	0.79	0.04 <sup>e)</sup> {0.01}
	toluene	463		623	5547	38.1 (35)	0.7 (65)	0.26	
	THF	450		745	8799	- <sup>f)</sup>	- <sup>f)</sup>	- <sup>f)</sup>	
	77 K <sup>b)</sup>	480		540	2315	127.3 (30)	3.3 (70) <sup>g)</sup>	-	
	PMMA <sup>d)</sup>	443		568	4968	57.4 (41)	1.3 (59)	0.65	
4	hexane	506	1.8	600	3096	40.1 (43)	1.4 (57)	0.54	0.03 <sup>e)</sup> {0.09}
	toluene	508		689	5171	9.1 (90)	0.6 (10)	0.02	
	THF	480		778	7980	- <sup>f)</sup>	- <sup>f)</sup>	- <sup>f)</sup>	
	77 K <sup>b)</sup>	468		553	3284	55.4 (84)	2.6 (16)	-	
	PMMA <sup>d)</sup>	464		598	4829	37.0 (74)	1.6 (26)	0.40	
5	hexane	354	1.1	439	5470	13.8 (99)	0.4 (1)	0.13	0.03 <sup>h)</sup> {0.03}
	toluene	354		483	7545	34.7 (79)	29.3 (21)	0.42	
	THF	352		559	10520	22.5 (82)	1.2 (18)	0.12	
	77 K <sup>j)</sup>	361		469	6379	80.3 (59)	3.4 (41)	-	
	PMMA <sup>d)</sup>	355		477	7205	29.4 (58)	5.5 (42)	0.85	

a) Measured in 2-MeTHF and obtained from the onset of the fluorescence and phosphorescence spectra.

b) Measured in a methylcyclohexane glass matrix.

c) Phosphorescence with vibrational bands at 445 and 470 nm and  $\tau_{\text{Phos,av}} = 1.0$  s was observed.

d) Measured in a 1 wt% poly(methyl methacrylate) (PMMA) film.

e) Measured in toluene and obtained from an Arrhenius plot.

f) Too weak to measure.

g) Delayed component contains more than one lifetime, averaged lifetime ( $\tau_{DF,av}$ ) is used.

h) Measured in 2-MeTHF and obtained from an Arrhenius plot.

j) Measured in a 2-MeTHF glass matrix.

First, we studied the photophysical properties of **Cbz- $\pi$  (1)** in various solvents (Table 1.4 and Chapter 6.4.1 ). While the absorption is hardly affected by the polarity of the solvent, the emission maxima in hexane, toluene and THF are gradually red shifted from 423 to 470 and 524 nm, respectively. This agrees well with the calculated CT character of the lowest singlet excited state (Table 1.1). In agreement with the large calculated  $\Delta E_{3_{CT}-3_{LE}}$  and  $\Delta E_{1_{CT}-3_{CT}}$  gaps of 0.49 and 0.43 eV, respectively, we found only prompt fluorescence (PF) for compound **Cbz- $\pi$  (1)** with measured lifetimes between 7.6 and 14.8 ns. The quantum yields (QY) are near unity in hexane and toluene, indicating that the fluorescence is an efficient process. This demonstrates that bypassing of the intersystem crossing pathway leads to very effective organic fluorescent emitters. However, the introduction of two methyl groups at the 2,6-positions of the phenylene bridge to form **Cbz-Me $\pi$  (2)** increases the dihedral angle between the carbazole and the bridge to 76.08(6) $^\circ$  in **Cbz-Me $\pi$  (2)**, when compared to compound **Cbz- $\pi$  (1)** (43.06(7) $^\circ$ ). Therefore, we observe a decrease in the spatial overlap between the donor and acceptor orbitals *vide supra*;  $\Lambda$  drops from 0.36 for the lowest singlet transition in **Cbz- $\pi$  (1)** to 0.18 in **Cbz-Me $\pi$  (2)**, indicating a stronger CT character for **Cbz-Me $\pi$  (2)**. At the same time, the experimentally observed extinction coefficient in hexane is four times smaller for **Cbz-Me $\pi$  (2)** ( $3.8 \times 10^3 \text{ M}^{-1} \text{ cm}^{-1}$  vs.  $17.7 \times 10^3 \text{ M}^{-1} \text{ cm}^{-1}$ ). Interestingly, while the QY in hexane is only 16% and in toluene 18%, in the most polar solvent (THF), the QY is notably higher (61%). Both the absorption and the emission spectra are slightly blue shifted in all solvents (in hexane: 412 nm; Figure 1.4a) and a stronger solvatochromic effect is observed, when comparing the spectra and Stokes' shifts of compound **Cbz-Me $\pi$  (2)** with **Cbz- $\pi$  (1)**. As computationally predicted, **Cbz-Me $\pi$  (2)** displays both, a prompt and delayed component in the decay of the emission signal at room temperature. The lifetimes measured in toluene are 18.0 ns for the prompt fluorescence and 13.6  $\mu\text{s}$  for the delayed component, with relative percentages of 62% and 38%, respectively. The delayed fluorescence lifetime is several orders of magnitude shorter than one would expect for a pure phosphorescent emission of an organic molecule without any heavy atom (ms to s).<sup>[161]</sup> Interestingly, the highest relative percentage for the delayed fluorescence component to the emission decay is found in the most polar solvent (THF: 79%), in which the quantum yield is also the highest. We observe that the relative percentages of the prompt and the delayed component are strongly dependent on the polarity of the solvent. At 77 K, embedded in a glassy matrix (methylcyclohexane, MeCy), compound **Cbz-Me $\pi$  (2)** shows a structured emission with bands at 414, 445 and 470 nm (Figure 1.4c, blue line). The latter two bands correspond to a phosphorescent emission with an averaged lifetime of  $\tau_{\text{Phos,av}} = 1.0 \text{ s}$ , while the high energy band at 414 nm shows a much shorter lifetime of  $\tau_{\text{PF}} = 10.0 \text{ ns}$ . As these lifetimes are many orders of

magnitude different, we were able to measure a time-gated emission spectrum, recording the emission signal after a delay of 5 ms. The result is shown in Figure 1.4b (blue dashed line) and is the emission spectrum of the pure phosphorescent (Phos) component of the total emission, which is a mixture of the prompt fluorescence and the phosphorescence (PF+Phos). From these two spectra we were able to extract  $\Delta E_{1CT-3LE}$  (from the onset of prompt fluorescence and phosphorescence spectra), which has a value of 0.13 eV and is in good agreement with the calculated gap (0.17 eV). In a 1 wt% polymeric film (PMMA = poly(methylmethacrylate)), compound **Cbz-Me $\pi$**  (**2**) exhibits a structureless emission with a maximum at 448 nm (Figure 1.4d), and prompt and delayed lifetimes of  $\tau_{PF} = 10.3$  ns (63%) and  $\tau_{DF} = 8.4$   $\mu$ s (37%), respectively. The photoluminescence quantum yield of 55% indicates that the emission process is moderately efficient in a polymeric film.

Both compounds bearing a phenoxazine donor (**Phox-Me $\pi$**  (**3**) and **Phox-MeO $\pi$**  (**4**)) show a further red shift of the emission spectra: **Phox-Me $\pi$**  (**3**) and **Phox-MeO $\pi$**  (**4**) exhibit maxima of 623 and 689 nm in toluene, respectively. As the emission maxima are strongly solvent dependent, and these compounds display large Stokes' shifts and small extinction coefficients ( $1.2 \times 10^3$  M<sup>-1</sup> cm<sup>-1</sup> and  $1.8 \times 10^3$  M<sup>-1</sup> cm<sup>-1</sup>), the corresponding transitions have strong charge-transfer character. Both compounds show a prompt and a delayed component of the emission decay, but their relative contributions are again strongly solvent dependent. In toluene the lifetimes are 38.1 ns (35%) and 0.7  $\mu$ s (65%) for **Phox-Me $\pi$**  (**3**), while for **Phox-MeO $\pi$**  (**4**) the lifetimes are 9.1 ns (90%) and 0.6  $\mu$ s (10%). Thus, their delayed components are much shorter than that of **Cbz-Me $\pi$**  (**2**). The quantum yield of **Phox-Me $\pi$**  (**3**) in toluene is higher (26%) than that of **Cbz-Me $\pi$**  (**2**) (18%). However, for compound **Phox-MeO $\pi$**  (**4**), we found the opposite behavior, as the QY is much lower (2%) in toluene. In contrast to compound **Cbz-Me $\pi$**  (**2**), we found no sign of phosphorescence at 77 K. Instead, we observed a relative long-lived prompt fluorescence ( $\tau_{PF} = 127.3$  ns (**Phox-Me $\pi$**  (**3**)) and  $\tau_{PF} = 55.4$  ns (**Phox-MeO $\pi$**  (**4**))) and a second component of the decay, with values of  $\tau_{DF} = 3.3$   $\mu$ s (**Phox-Me $\pi$**  (**3**)) and  $\tau_{DF} = 2.6$   $\mu$ s (**Phox-MeO $\pi$**  (**4**))), which we assign to delayed fluorescence. In addition, we measured and plotted the relative components of the decays over a temperature range of 250 – 300 K and extracted from these Arrhenius plots the experimental values for  $\Delta E_{1CT-3CT}$  (Figure 6.27, Figure 6.28, and Figure 6.29). Both compounds have gaps of only 0.04 and 0.03 eV, for **Phox-Me $\pi$**  (**3**) and **Phox-MeO $\pi$**  (**4**), respectively, which agrees reasonably well with the calculated gaps (0.01 eV for **Phox-Me $\pi$**  (**3**) and 0.09 eV for **Phox-MeO $\pi$**  (**4**)). Such small gaps also explain why we did not observe phosphorescence, because, even at 77 K the reverse intersystem crossing process still takes place. The TADF process in a PMMA film is efficient, with high quantum yields for **Phox-Me $\pi$**

(**3**) (65%) to moderate for **Phox-MeO $\pi$**  (**4**) (40%), and emission maxima at 568 and 598 nm for **Phox-Me $\pi$**  (**3**) and **Phox-MeO $\pi$**  (**4**), respectively (Figure 1.4d). The lifetimes measured are  $\tau_{\text{PF}} = 57.4$  ns (41%) and  $\tau_{\text{DF}} = 1.3$   $\mu\text{s}$  (59%) for **Phox-Me $\pi$**  (**3**) and  $\tau_{\text{PF}} = 37.0$  ns (74%) and  $\tau_{\text{DF}} = 1.6$   $\mu\text{s}$  (26%) for **Phox-MeO $\pi$**  (**4**).

The combination of a weak donor (<sup>MeO<sub>3</sub></sup>Ph) with an electron-withdrawing group-containing bridge (<sup>FMe</sup>Ph) in compound **MeO<sub>3</sub>Ph-FMe $\pi$**  (**5**) gives rise to an emission maximum in toluene of 483 nm and lifetimes of  $\tau_{\text{PF}} = 34.7$  ns (79%) and  $\tau_{\text{DF}} = 29.3$   $\mu\text{s}$  (21%). Interestingly, compound **MeO<sub>3</sub>Ph-FMe $\pi$**  (**5**) has the highest quantum yield (42%) in toluene for all of our TADF emitters (**Cbz-Me $\pi$**  (**2**), **Phox-Me $\pi$**  (**3**), **Phox-MeO $\pi$**  (**4**), and **MeO<sub>3</sub>Ph-FMe $\pi$**  (**5**)) but has a lower QY in all other solvents. Compound **5** also displays the largest Stokes' shift (10520 cm<sup>-1</sup> in THF) of our compounds. In agreement with the calculated small gaps for **MeO<sub>3</sub>Ph-FMe $\pi$**  (**5**), there was no phosphorescence at 77 K, but an emission with a maximum at 469 nm with a pronounced vibrational fine structure was observed. The biexponential decay gives lifetimes of  $\tau_{\text{PF}} = 80.3$  ns (59%) and  $\tau_{\text{DF}} = 3.4$   $\mu\text{s}$  (41%). From an Arrhenius plot of the relative lifetimes, we obtained  $\Delta E_{1_{\text{CT}}-3_{\text{CT}}}$  of 0.03 eV for **MeO<sub>3</sub>Ph-FMe $\pi$**  (**5**), which is in excellent agreement with the calculated value of 0.03 eV. The quantum yield of 85% for **MeO<sub>3</sub>Ph-FMe $\pi$**  (**5**) in PMMA is the highest of the compounds. In combination with the lifetimes of  $\tau_{\text{PF}} = 29.4$  ns (58%) and  $\tau_{\text{DF}} = 5.5$   $\mu\text{s}$  (42%), **MeO<sub>3</sub>Ph-FMe $\pi$**  (**5**) is an excellent candidate for further testing in an OLED device.

### 1.3 Conclusion

We demonstrate how the computationally guided design of excited states leads to efficient TADF emitters. This is accomplished by the development of an accurate theoretical description of the local and charge-transfer states. A benchmark study shows an excellent agreement between experimentally observed singlet-triplet gaps and calculated values, as indicated by a small mean absolute deviation of 0.05 eV. However, it is important to note that our protocol is limited to cases in which CT and LE states are well defined and are not heavily mixed. The *in-silico* modifications of the donor and bridge moieties allowed us to derive a structure-property relationship, where the tuning of the intersystem crossing and reverse intersystem crossing processes can be achieved by modifying the energy of the local excited state at the bridge (<sup>3</sup>LE $\pi$ ). In contrast to the local-excited state at the donor (<sup>3</sup>LE<sub>D</sub>), the <sup>3</sup>LE $\pi$  can be tuned independently from the charge-transfer states. Thus, one strategy to minimize the relevant  $\Delta E_{1_{\text{CT}}-3_{\text{LE}}}$  and  $\Delta E_{3_{\text{CT}}-3_{\text{LE}}}$  gaps is to stabilize or destabilize the <sup>3</sup>LE $\pi$  state relative to the CT states, which can be achieved by the introduction of acceptor or donor substituents, respectively, at the  $\pi$ -bridge.

Furthermore, as a proof of concept, five computationally designed D- $\pi$ -A compounds were synthesized and fully characterized. While **Cbz- $\pi$**  (**1**) is a pure fluorescent emitter with a quantum yield of near unity, the decrease of the singlet-triplet gaps in **Cbz-Me $\pi$**  (**2**), **Phox-Me $\pi$**  (**3**), **Phox-MeO $\pi$**  (**4**), and **MeO<sub>3</sub>Ph-FMe $\pi$**  (**5**) switches on the delayed fluorescence pathway, exactly as quantum chemically predicted. An added benefit of this strategy is that the emission maxima of these systems can be fine-tuned and range from deep blue to red.

Depending on the polarity of the solvent, the relative contribution of the delayed fluorescence to the overall decay can be as high as 80%. The overall emission quantum yields in solution for **Cbz-Me $\pi$**  (**2**), **Phox-Me $\pi$**  (**3**), **Phox-MeO $\pi$**  (**4**), and **MeO<sub>3</sub>Ph-FMe $\pi$**  (**5**) are lower than that of the pure fluorescent emitter **Cbz- $\pi$**  (**1**), but increases in a polymer matrix up to 85% for **MeO<sub>3</sub>Ph-FMe $\pi$**  (**5**). Compound **MeO<sub>3</sub>Ph-FMe $\pi$**  (**5**) is an ideal candidate for further research on its application in an optimized light emitting device. However, while that is beyond the scope of this paper, we have demonstrated how the combination of computational methods with experimental data leads to new insights into the excited state properties of D- $\pi$ -A compounds and provides a rational strategy to manipulate them.

## 1.4 References

- [5] C. W. Tang, S. A. Vanslyke, *Appl. Phys. Lett.* **1987**, *51*, 913-915.
- [6] M. A. Baldo, D. F. O'Brien, M. E. Thompson, S. R. Forrest, *Phys. Rev. B: Condens. Matter Mater. Phys.* **1999**, *60*, 14422-14428.
- [7] M. A. Baldo, D. F. O'Brien, Y. You, A. Shoustikov, S. Sibley, M. E. Thompson, S. R. Forrest, *Nature* **1998**, *395*, 151-154.
- [8] M. A. Baldo, M. E. Thompson, S. R. Forrest, *Nature* **2000**, *403*, 750-753.
- [9] X. Gong, J. C. Ostrowski, G. C. Bazan, D. Moses, A. J. Heeger, *Appl. Phys. Lett.* **2002**, *81*, 3711-3713.
- [10] W. Y. Wong, C. L. Ho, *J. Mater. Chem.* **2009**, *19*, 4457-4482.
- [11] Y. Chi, P. T. Chou, *Chem. Soc. Rev.* **2010**, *39*, 638-655.
- [12] S. Y. Kim, W. I. Jeong, C. Mayr, Y. S. Park, K. H. Kim, J. H. Lee, C. K. Moon, W. Brütting, J. J. Kim, *Adv. Funct. Mater.* **2013**, *23*, 3896-3900.
- [13] F. Perrin, *Ann. Phys. (Paris)* **1929**, *12*, 169-275.
- [14] G. N. Lewis, D. Lipkin, *J. Am. Chem. Soc.* **1942**, *64*, 2801-2808.
- [15] C. A. Parker, C. G. Hatchard, *J. Chem. Soc. Faraday Trans.* **1961**, *57*, 1894-1904.
- [16] H. Uoyama, K. Goushi, K. Shizu, H. Nomura, C. Adachi, *Nature* **2012**, *492*, 234-238.
- [17] H. Tanaka, K. Shizu, H. Miyazaki, C. Adachi, *Chem. Commun.* **2012**, *48*, 11392-11394.
- [18] T. Nakagawa, S.-Y. Ku, K.-T. Wong, C. Adachi, *Chem. Commun.* **2012**, *48*, 9580-9582.
- [19] S. Youn Lee, T. Yasuda, H. Nomura, C. Adachi, *Appl. Phys. Lett.* **2012**, *101*, 093306.
- [20] K. Goushi, K. Yoshida, K. Sato, C. Adachi, *Nat. Photonics* **2012**, *6*, 253-258.
- [21] K. Goushi, C. Adachi, *Appl. Phys. Lett.* **2012**, *101*, 023306.
- [22] Q. Zhang, J. Li, K. Shizu, S. Huang, S. Hirata, H. Miyazaki, C. Adachi, *J. Am. Chem. Soc.* **2012**, *134*, 14706-14709.
- [23] G. Méhes, H. Nomura, Q. Zhang, T. Nakagawa, C. Adachi, *Angew. Chem. Int. Ed.* **2012**, *51*, 11311-11315; *Angew. Chem.* **2012**, *124*, 11473-11477.
- [24] X. K. Chen, S. F. Zhang, J. X. Fan, A. M. Ren, *J. Phys. Chem. C* **2015**, *119*, 9728-9733.
- [25] L. Bergmann, D. M. Zink, S. Brase, T. Baumann, D. Volz, *Top. Curr. Chem.* **2016**, *374*, 22.
- [26] M. Godumala, S. Choi, M. J. Cho, D. H. Choi, *J. Mater. Chem. C* **2016**, *4*, 11355-11381.
- [27] X. Cao, D. Zhang, S. Zhang, Y. Tao, W. Huang, *J. Mater. Chem. C* **2017**, *5*, 7699-7714.
- [28] Y. Im, M. Kim, Y. J. Cho, J.-A. Seo, K. S. Yook, J. Y. Lee, *Chem. Mater.* **2017**, *29*, 1946-1963.
- [29] Z. Yang, Z. Mao, Z. Xie, Y. Zhang, S. Liu, J. Zhao, J. Xu, Z. Chi, M. P. Aldred, *Chem. Soc. Rev.* **2017**, *46*, 915-1016.
- [30] Y. Olivier, J. C. Sancho-Garcia, L. Muccioli, G. D'Avino, D. Beljonne, *J. Phys. Chem. Lett.* **2018**, *9*, 6149-6163.
- [31] P. Xiao, T. Dong, J. Xie, D. Luo, J. Yuan, B. Liu, *Appl. Sci.* **2018**, *8*, 299.
- [32] J.-H. Lee, C.-H. Chen, P.-H. Lee, H.-Y. Lin, M.-k. Leung, T.-L. Chiu, C.-F. Lin, *J. Mater. Chem. C* **2019**, *7*, 5874-5888.
- [33] S. Jhulki, M. W. Cooper, S. Barlow, S. R. Marder, *Mater. Chem. Front.* **2019**, *3*, 1699-1721.
- [34] C. Adachi, *Jpn. J. Appl. Phys.* **2014**, *53*, 060101.
- [35] H. Kaji, H. Suzuki, T. Fukushima, K. Shizu, K. Suzuki, S. Kubo, T. Komino, H. Oiwa, F. Suzuki, A. Wakamiya, Y. Murata, C. Adachi, *Nat. Commun.* **2015**, *6*, 8476.
- [36] F. B. Dias, T. J. Penfold, A. P. Monkman, *Methods Appl. Fluores.* **2017**, *5*, 012001.
- [37] W. Zhang, J. Jin, Z. Huang, S. Zhuang, L. Wang, *Sci. Rep.* **2016**, *6*, 30178.
- [38] M. Einzinger, T. Zhu, P. de Silva, C. Belger, T. M. Swager, T. Van Voorhis, M. A. Baldo, *Adv. Mater.* **2017**, *29*, 1701987.

- [39] Y. Xiang, Y. Zhao, N. Xu, S. Gong, F. Ni, K. Wu, J. Luo, G. Xie, Z. H. Lu, C. Yang, *J. Mater. Chem. C* **2017**, *5*, 12204-12210.
- [40] L. Gan, K. Gao, X. Cai, D. Chen, S.-J. Su, *J. Phys. Chem. Lett.* **2018**, *9*, 4725-4731.
- [41] M. K. Etherington, J. Gibson, H. F. Higginbotham, T. J. Penfold, A. P. Monkman, *Nat. Commun.* **2016**, *7*, 13680.
- [42] B. T. Lim, S. Okajima, A. K. Chandra, E. C. Lim, *Chem. Phys. Lett.* **1981**, *79*, 22-27.
- [43] J. Tatchen, N. Gilka, C. M. Marian, *Phys. Chem. Chem. Phys.* **2007**, *9*, 5209-5221.
- [44] Z. E. X. Dance, S. M. Mickley, T. M. Wilson, A. B. Ricks, A. M. Scott, M. A. Ratner, M. R. Wasielewski, *J. Phys. Chem. A* **2008**, *112*, 4194-4201.
- [45] J. Gibson, A. P. Monkman, T. J. Penfold, *ChemPhysChem* **2016**, *17*, 2956-2961.
- [46] F. B. Dias, J. Santos, D. R. Graves, P. Data, R. S. Nobuyasu, M. A. Fox, A. S. Batsanov, T. Palmeira, M. N. Berberan-Santos, M. R. Bryce, A. P. Monkman, *Adv. Sci.* **2016**, *3*, 1600080.
- [47] X. K. Chen, D. Kim, J. L. Brédas, *Acc. Chem. Res.* **2018**, *51*, 2215-2224.
- [48] T. J. Penfold, E. Gindensperger, C. Daniel, C. M. Marian, *Chem. Rev.* **2018**, *118*, 6975-7025.
- [49] I. S. Park, H. Komiyama, T. Yasuda, *Chem. Sci.* **2017**, *8*, 953-960.
- [50] W. Huang, M. Einzinger, T. Zhu, H. S. Chae, S. Jeon, S.-G. Ihn, M. Sim, S. Kim, M. Su, G. Teverovskiy, T. Wu, T. Van Voorhis, T. M. Swager, M. A. Baldo, S. L. Buchwald, *Chem. Mater.* **2018**, *30*, 1462-1466.
- [51] J. R. Defrancisco, G. López-Espejo, J. L. Zafra, S. Yadav, R. E. Messersmith, C. J. Gómez-García, H. Ottosson, J. Casado, J. D. Tovar, *J. Phys. Chem. C* **2018**, *122*, 12148-12157.
- [52] G. A. Sommer, L. N. Mataranga-Popa, R. Czerwieniec, T. Hofbeck, H. H. H. Homeier, T. J. J. Müller, H. Yersin, *J. Phys. Chem. Lett.* **2018**, *9*, 3692-3697.
- [53] P. K. Samanta, D. Kim, V. Coropceanu, J.-L. Brédas, *J. Am. Chem. Soc.* **2017**, *139*, 4042-4051.
- [54] K. Suzuki, S. Kubo, K. Shizu, T. Fukushima, A. Wakamiya, Y. Murata, C. Adachi, H. Kaji, *Angew. Chem. Int. Ed.* **2015**, *54*, 15231-15235; *Angew. Chem.* **2015**, *127*, 15446-15450.
- [55] Y. Kitamoto, T. Namikawa, D. Ikemizu, Y. Miyata, T. Suzuki, H. Kita, T. Sato, S. Oi, *J. Mater. Chem. C* **2015**, *3*, 9122-9130.
- [56] M. Numata, T. Yasuda, C. Adachi, *Chem. Commun.* **2015**, *51*, 9443-9446.
- [57] T. Hatakeyama, K. Shiren, K. Nakajima, S. Nomura, S. Nakatsuka, K. Kinoshita, J. Ni, Y. Ono, T. Ikuta, *Adv. Mater.* **2016**, *28*, 2777-2781.
- [58] Y. Kitamoto, T. Namikawa, T. Suzuki, Y. Miyata, H. Kita, T. Sato, S. Oi, *Org. Electron.* **2016**, *34*, 208-217.
- [59] C. Tu, W. Liang, *ACS Omega* **2017**, *2*, 3098-3109.
- [60] Y.-J. Lien, T.-C. Lin, C.-C. Yang, Y.-C. Chiang, C.-H. Chang, S.-H. Liu, Y.-T. Chen, G.-H. Lee, P.-T. Chou, C.-W. Lu, Y. Chi, *ACS Appl. Mater. Interfaces* **2017**, *9*, 27090-27101.
- [61] Y. H. Lee, S. Park, J. Oh, J. W. Shin, J. Jung, S. Yoo, M. H. Lee, *ACS Appl. Mater. Interfaces* **2017**, *9*, 24035-24042.
- [62] C.-C. Tsai, W.-C. Huang, H.-Y. Chih, Y.-C. Hsh, C.-W. Liao, C.-H. Lin, Y.-X. Kang, C.-H. Chang, Y. J. Chang, C.-W. Lu, *Org. Electron.* **2018**, *63*, 166-174.
- [63] M.-Y. Zhang, Z.-Y. Li, B. Lu, Y. Wang, Y.-D. Ma, C.-H. Zhao, *Org. Lett.* **2018**, *20*, 6868-6871.
- [64] T.-L. Wu, M.-J. Huang, C.-C. Lin, P.-Y. Huang, T.-Y. Chou, R.-W. Chen-Cheng, H.-W. Lin, R.-S. Liu, C.-H. Cheng, *Nat. Photonics* **2018**, *12*, 235-240.
- [65] I. S. Park, K. Matsuo, N. Aizawa, T. Yasuda, *Adv. Funct. Mater.* **2018**, *28*, 1802031.
- [66] S.-Y. Li, Z.-B. Sun, C.-H. Zhao, *ACS Omega* **2018**, *3*, 12730-12736.



- [67] D.-G. Chen, T.-C. Lin, C.-L. Chen, Y.-T. Chen, Y.-A. Chen, G.-H. Lee, P.-T. Chou, C.-W. Liao, P.-C. Chiu, C.-H. Chang, Y.-J. Lien, Y. Chi, *ACS Appl. Mater. Interfaces* **2018**, *10*, 12886-12896.
- [68] M. Stanoppi, A. Lorbach, *Dalton Trans.* **2018**, *47*, 10394-10398.
- [69] C. D. Entwistle, T. B. Marder, *Angew. Chem. Int. Ed.* **2002**, *41*, 2927-2931; *Angew. Chem.* **2002**, *114*, 3051-3056.
- [70] C. D. Entwistle, T. B. Marder, *Chem. Mater.* **2004**, *16*, 4574-4585.
- [71] S. Yamaguchi, A. Wakamiya, *Pure Appl. Chem.* **2006**, *78*, 1413.
- [72] F. Jäkle, *Coord. Chem. Rev.* **2006**, *250*, 1107-1121.
- [73] M. Elbing, G. C. Bazan, *Angew. Chem. Int. Ed.* **2008**, *47*, 834-838; *Angew. Chem.* **2008**, *120*, 846-850.
- [74] Z. M. Hudson, S. Wang, *Acc. Chem. Res.* **2009**, *42*, 1584-1596.
- [75] C. R. Wade, A. E. J. Broomsgrove, S. Aldridge, F. P. Gabbaï, *Chem. Rev.* **2010**, *110*, 3958-3984.
- [76] Z. M. Hudson, S. Wang, *Dalton Trans.* **2011**, *40*, 7805-7816.
- [77] A. Wakamiya, S. Yamaguchi, *Bull. Chem. Soc. Jpn.* **2015**, *88*, 1357-1377.
- [78] L. Ji, S. Griesbeck, T. B. Marder, *Chem. Sci.* **2017**, *8*, 846-863.
- [79] S.-Y. Li, Z.-B. Sun, C.-H. Zhao, *Inorg. Chem.* **2017**, *56*, 8705-8717.
- [80] G. Turkoglu, M. E. Cinar, T. Ozturk, *Molecules* **2017**, *22*, 1522.
- [81] N. Matsumi, K. Naka, Y. Chujo, *J. Am. Chem. Soc.* **1998**, *120*, 5112-5113.
- [82] S. Yamaguchi, S. Akiyama, K. Tamao, *J. Am. Chem. Soc.* **2000**, *122*, 6335-6336.
- [83] W.-L. Jia, D. Song, S. Wang, *J. Org. Chem.* **2003**, *68*, 701-705.
- [84] A. Wakamiya, T. Ide, S. Yamaguchi, *J. Am. Chem. Soc.* **2005**, *127*, 14859-14866.
- [85] I. Yamaguchi, B.-J. Choi, T.-A. Koizumi, K. Kubota, T. Yamamoto, *Macromolecules* **2007**, *40*, 438-443.
- [86] U. Megerle, F. Selmaier, C. Lambert, E. Riedle, S. Lochbrunner, *Phys. Chem. Chem. Phys.* **2008**, *10*, 6245-6251.
- [87] A. Lorbach, M. Bolte, H. Li, H.-W. Lerner, M. C. Holthausen, F. Jäkle, M. Wagner, *Angew. Chem. Int. Ed.* **2009**, *48*, 4584-4588; *Angew. Chem.* **2009**, *121*, 4654-4658.
- [88] L. Weber, V. Werner, M. A. Fox, T. B. Marder, S. Schwedler, A. Brockhinke, H.-G. Stammler, B. Neumann, *Dalton Trans.* **2009**, 2823-2831.
- [89] L. Weber, D. Eickhoff, T. B. Marder, M. A. Fox, P. J. Low, A. D. Dwyer, D. J. Tozer, S. Schwedler, A. Brockhinke, H.-G. Stammler, B. Neumann, *Chem. Eur. J.* **2012**, *18*, 1369-1382.
- [90] C. Reus, S. Weidlich, M. Bolte, H.-W. Lerner, M. Wagner, *J. Am. Chem. Soc.* **2013**, *135*, 12892-12907.
- [91] X. Yin, J. Chen, R. A. Lalancette, T. B. Marder, F. Jäkle, *Angew. Chem. Int. Ed.* **2014**, *53*, 9761-9765; *Angew. Chem.* **2014**, *126*, 9919-9923.
- [92] Z. Zhang, R. M. Edkins, J. Nitsch, K. Fucke, A. Eichhorn, A. Steffen, Y. Wang, T. B. Marder, *Chem. Eur. J.* **2015**, *21*, 177-190.
- [93] J. Merz, J. Fink, A. Friedrich, I. Krummenacher, H. H. Al Mamari, S. Lorenzen, M. Haehnel, A. Eichhorn, M. Moos, M. Holzapfel, H. Braunschweig, C. Lambert, A. Steffen, L. Ji, T. B. Marder, *Chem. Eur. J.* **2017**, *23*, 13164-13180.
- [94] J. Merz, A. Steffen, J. Nitsch, J. Fink, C. B. Schürger, A. Friedrich, I. Krummenacher, H. Braunschweig, M. Moos, D. Mims, C. Lambert, T. B. Marder, *Chem. Sci.* **2019**, *10*, 7516-7534.
- [95] H. Belaidi, F. Rauch, Z. Zhang, C. Latouche, A. Boucekkine, T. B. Marder, J.-F. Halet, *ChemPhotoChem* **2020**, *4*, 173-180.
- [96] Z. Yuan, N. J. Taylor, T. B. Marder, I. D. Williams, S. K. Kurtz, L.-T. Cheng, *J. Chem. Soc., Chem. Commun.* **1990**, 1489-1492.
- [97] M. Lequan, R. M. Lequan, K. C. Ching, *J. Mater. Chem.* **1991**, *1*, 997-999.

- [98] M. Lequan, R. M. Lequan, K. C. Ching, M. Barzoukas, A. Fort, H. Lahoucine, G. Bravic, D. Chasseau, J. Gaultier, *J. Mater. Chem.* **1992**, *2*, 719-725.
- [99] M. Lequan, R. M. Lequan, K. Chane-Ching, A.-C. Callier, M. Barzoukas, A. Fort, *Adv. Mater. Optic. Electron.* **1992**, *1*, 243-247.
- [100] Z. Yuan, N. J. Taylor, Y. Sun, T. B. Marder, I. D. Williams, L.-T. Cheng, *J. Organomet. Chem.* **1993**, *449*, 27-37.
- [101] Z. Yuan, N. J. Taylor, R. Ramachandran, T. B. Marder, *Appl. Organomet. Chem.* **1996**, *10*, 305-316.
- [102] C. Branger, M. Lequan, R. M. Lequan, M. Barzoukas, A. Fort, *J. Mater. Chem.* **1996**, *6*, 555-558.
- [103] Z.-Q. Liu, Q. Fang, D. Wang, G. Xue, W.-T. Yu, Z.-S. Shao, M.-H. Jiang, *Chem. Commun.* **2002**, 2900-2901.
- [104] Z.-Q. Liu, Q. Fang, D. Wang, D.-X. Cao, G. Xue, W.-T. Yu, H. Lei, *Chem. Eur. J.* **2003**, *9*, 5074-5084.
- [105] Z.-Q. Liu, Q. Fang, D.-X. Cao, D. Wang, G.-B. Xu, *Org. Lett.* **2004**, *6*, 2933-2936.
- [106] M. Charlot, L. Porres, C. D. Entwistle, A. Beeby, T. B. Marder, M. Blanchard-Desce, *Phys. Chem. Chem. Phys.* **2005**, *7*, 600-606.
- [107] Z.-Q. Liu, M. Shi, F.-Y. Li, Q. Fang, Z.-H. Chen, T. Yi, C.-H. Huang, *Org. Lett.* **2005**, *7*, 5481-5484.
- [108] Z. Yuan, C. D. Entwistle, J. C. Collings, D. Albesa-Jové, A. S. Batsanov, J. A. K. Howard, N. J. Taylor, H. M. Kaiser, D. E. Kaufmann, S.-Y. Poon, W.-Y. Wong, C. Jardin, S. Fathallah, A. Boucekkine, J.-F. Halet, T. B. Marder, *Chem. Eur. J.* **2006**, *12*, 2758-2771.
- [109] C. D. Entwistle, J. C. Collings, A. Steffen, L.-O. Pålsson, A. Beeby, D. Albesa-Jove, J. M. Burke, A. S. Batsanov, J. A. K. Howard, J. A. Mosely, S.-Y. Poon, W.-Y. Wong, F. Ibersiene, S. Fathallah, A. Boucekkine, J.-F. Halet, T. B. Marder, *J. Mater. Chem.* **2009**, *19*, 7532-7544.
- [110] J. C. Collings, S.-Y. Poon, C. Le Droumaguet, M. Charlot, C. Katan, L.-O. Pålsson, A. Beeby, J. A. Mosely, H. M. Kaiser, D. Kaufmann, W.-Y. Wong, M. Blanchard-Desce, T. B. Marder, *Chem. Eur. J.* **2009**, *15*, 198-208.
- [111] L. Ji, Q. Fang, M.-S. Yuan, Z.-Q. Liu, Y.-X. Shen, H.-F. Chen, *Org. Lett.* **2010**, *12*, 5192-5195.
- [112] N. S. Makarov, S. Mukhopadhyay, K. Yesudas, J.-L. Brédas, J. W. Perry, A. Pron, M. Kivala, K. Müllen, *J. Phys. Chem. A* **2012**, *116*, 3781-3793.
- [113] L. Ji, R. M. Edkins, L. J. Sewell, A. Beeby, A. S. Batsanov, K. Fucke, M. Drafz, J. A. K. Howard, O. Moutounet, F. Ibersiene, A. Boucekkine, E. Furet, Z. Liu, J.-F. Halet, C. Katan, T. B. Marder, *Chem. Eur. J.* **2014**, *20*, 13618-13635.
- [114] P. Chen, A. S. Marshall, S. H. Chi, X. Yin, J. W. Perry, F. Jäkle, *Chem. Eur. J.* **2015**, *21*, 18237-18247.
- [115] S. Griesbeck, Z. Zhang, M. Gutmann, T. Lühmann, R. M. Edkins, G. Clermont, A. N. Lazar, M. Haehnel, K. Edkins, A. Eichhorn, M. Blanchard-Desce, L. Meinel, T. B. Marder, *Chem. Eur. J.* **2016**, *22*, 14701-14706.
- [116] S. Griesbeck, E. Michail, C. Wang, H. Ogasawara, S. Lorenzen, L. Gerstner, T. Zang, J. Nitsch, Y. Sato, R. Bertermann, M. Taki, C. Lambert, S. Yamaguchi, T. B. Marder, *Chem. Sci.* **2019**, *10*, 5405-5422.
- [117] S. Griesbeck, M. Ferger, C. Czernetzi, C. Wang, R. Bertermann, A. Friedrich, M. Haehnel, D. Sieh, M. Taki, S. Yamaguchi, T. B. Marder, *Chem. Eur. J.* **2019**, *25*, 7679-7688.
- [118] S. Griesbeck, E. Michail, F. Rauch, H. Ogasawara, C. Wang, Y. Sato, R. M. Edkins, Z. Zhang, M. Taki, C. Lambert, S. Yamaguchi, T. B. Marder, *Chem. Eur. J.* **2019**, *25*, 13164-13175.

- [119] S. Yamaguchi, S. Akiyama, K. Tamao, *J. Am. Chem. Soc.* **2001**, *123*, 11372-11375.
- [120] T. W. Hudnall, C.-W. Chiu, F. P. Gabbai, *Acc. Chem. Res.* **2009**, *42*, 388-397.
- [121] Ž. Ban, S. Griesbeck, S. Tomić, J. Nitsch, T. B. Marder, I. Piantanida, *Chem. Eur. J.* **2020**, *26*, 2195-2203.
- [122] Y. Shirota, *J. Mater. Chem.* **2000**, *10*, 1-25.
- [123] A. Wakamiya, K. Mori, S. Yamaguchi, *Angew. Chem. Int. Ed.* **2007**, *46*, 4273-4276; *Angew. Chem.* **2007**, *119*, 4351-4354.
- [124] S. Toyota, M. Asakura, M. Oki, F. Toda, *Bull. Chem. Soc. Jpn.* **2000**, *73*, 2357-2362.
- [125] S. M. Cornet, K. B. Dillon, C. D. Entwistle, M. A. Fox, A. E. Goeta, H. P. Goodwin, T. B. Marder, A. L. Thompson, *Dalton Trans.* **2003**, 4395-4405.
- [126] Z. Lu, Z. Cheng, Z. Chen, L. Weng, Z. H. Li, H. Wang, *Angew. Chem. Int. Ed.* **2011**, *50*, 12227-12231; *Angew. Chem.* **2011**, *123*, 12435-12439.
- [127] J. Wang, Y. Wang, T. Taniguchi, S. Yamaguchi, S. Irle, *J. Phys. Chem. A* **2012**, *116*, 1151-1158.
- [128] H. Ye, Z. Lu, D. You, Z. Chen, Z. H. Li, H. Wang, *Angew. Chem. Int. Ed.* **2012**, *51*, 12047-12050; *Angew. Chem.* **2012**, *124*, 12213-12216.
- [129] Z. Lu, Y. Wang, J. Liu, Y.-J. Lin, Z. H. Li, H. Wang, *Organometallics* **2013**, *32*, 6753-6758.
- [130] T. Taniguchi, J. Wang, S. Irle, S. Yamaguchi, *Dalton Trans.* **2013**, *42*, 620-624.
- [131] Z. Zhang, R. M. Edkins, J. Nitsch, K. Fucke, A. Steffen, L. E. Longobardi, D. W. Stephan, C. Lambert, T. B. Marder, *Chem. Sci.* **2015**, *6*, 308-321.
- [132] Z. Zhang, R. M. Edkins, M. Haehnel, M. Wehner, A. Eichhorn, L. Mailänder, M. Meier, J. Brand, F. Brede, K. Müller-Buschbaum, H. Braunschweig, T. B. Marder, *Chem. Sci.* **2015**, *6*, 5922-5927.
- [133] J. Zheng, Y.-J. Lin, H. Wang, *Dalton Trans.* **2016**, *45*, 6088-6093.
- [134] X. Yin, F. Guo, R. A. Lalancette, F. Jäkle, *Macromolecules* **2016**, *49*, 537-546.
- [135] D.-T. Yang, S. K. Møllerup, J.-B. Peng, X. Wang, Q.-S. Li, S. Wang, *J. Am. Chem. Soc.* **2016**, *138*, 11513-11516.
- [136] R. J. Blagg, E. J. Lawrence, K. Resner, V. S. Oganessian, T. J. Herrington, A. E. Ashley, G. G. Wildgoose, *Dalton Trans.* **2016**, *45*, 6023-6031.
- [137] Q. Yan, M. Yin, C. Chen, Y. Zhang, *J. Org. Chem.* **2018**, *83*, 9096-9102.
- [138] T. E. Stennett, P. Bissinger, S. Griesbeck, S. Ullrich, I. Krummenacher, M. Auth, A. Sperlich, M. Stolte, K. Radacki, C.-J. Yao, F. Würthner, A. Steffen, T. B. Marder, H. Braunschweig, *Angew. Chem. Int. Ed.* **2019**, *58*, 6449-6454. *Angew. Chem.* **2019**, *131*, 6516-6521.
- [139] M. Yokoyama, K. Inada, Y. Tsuchiya, H. Nakanotani, C. Adachi, *Chem. Commun.* **2018**, *54*, 8261-8264.
- [140] W. Li, Y. Pan, L. Yao, H. Liu, S. Zhang, C. Wang, F. Shen, P. Lu, B. Yang, Y. Ma, *Adv. Opt. Mater.* **2014**, *2*, 892-901.
- [141] Y. Jiang, Z. Hu, B. Zhou, C. Zhong, Z. Sun, H. Sun, *J. Phys. Chem. C* **2019**, *123*, 5616-5625.
- [142] A. K. Narsaria, J. Poater, C. Fonseca Guerra, A. W. Ehlers, K. Lammertsma, F. M. Bickelhaupt, *J. Comput. Chem.* **2018**, *39*, 2690-2696.
- [143] X.-H. Shan, B. Yang, H.-X. Zheng, J.-P. Qu, Y.-B. Kang, *Org. Lett.* **2018**, *20*, 7898-7901.
- [144] T. Ishiyama, J. Takagi, K. Ishida, N. Miyaura, N. R. Anastasi, J. F. Hartwig, *J. Am. Chem. Soc.* **2002**, *124*, 390-391.
- [145] E. C. Neeve, S. J. Geier, I. A. I. Mkhalid, S. A. Westcott, T. B. Marder, *Chem. Rev.* **2016**, *116*, 9091-9161.
- [146] J. M. Murphy, C. C. Tzschucke, J. F. Hartwig, *Org. Lett.* **2007**, *9*, 757-760.
- [147] A. J. J. Lennox, G. C. Lloyd-Jones, *Chem. Soc. Rev.* **2014**, *43*, 412-443.

- [148] G. A. Molander, *J. Org. Chem.* **2015**, *80*, 7837-7848.
- [149] K. Schickedanz, T. Trageser, M. Bolte, H.-W. Lerner, M. Wagner, *Chem. Commun.* **2015**, *51*, 15808-15810.
- [150] K. Schickedanz, J. Radtke, M. Bolte, H.-W. Lerner, M. Wagner, *J. Am. Chem. Soc.* **2017**, *139*, 2842-2851.
- [151] S. Konishi, T. Iwai, M. Sawamura, *Organometallics* **2018**, *37*, 1876-1883.
- [152] M. W. Drover, K. Nagata, J. C. Peters, *Chem. Commun.* **2018**, *54*, 7916-7919.
- [153] X. Jia, J. Nitsch, L. Ji, Z. Wu, A. Friedrich, F. Kerner, M. Moos, C. Lambert, T. B. Marder, *Chem. Eur. J.* **2019**, *25*, 10845-10857.
- [154] K. Zhang, Q. Sun, Z. Zhang, L. Tang, Z. Xie, Z. Chi, S. Xue, H. Zhang, W. Yang, *Chem. Commun.* **2018**, *54*, 5225-5228.
- [155] N. Liu, B. Wang, W. Chen, C. Liu, X. Wang, Y. Hu, *RSC Adv.* **2014**, *4*, 51133-51139.
- [156] M. Mantina, A. C. Chamberlin, R. Valero, C. J. Cramer, D. G. Truhlar, *J. Phys. Chem. A* **2009**, *113*, 5806-5812.
- [157] N. G. Connelly, W. E. Geiger, *Chem. Rev.* **1996**, *96*, 877-910.
- [158] D. Tsiplakides, D. Archonta, C. G. Vayenas, *Top. Catal.* **2007**, *44*, 469-479.
- [159] D. Reitzenstein, T. Quast, F. Kanal, M. Kullmann, S. Ruetzel, M. S. Hammer, C. Deibel, V. Dyakonov, T. Brixner, C. Lambert, *Chem. Mater.* **2010**, *22*, 6641-6655.
- [160] X. Cai, M. Sakamoto, M. Fujitsuka, T. Majima, *J. Phys. Chem. A* **2007**, *111*, 1788-1791.
- [161] B. Valeur, *Molecular Fluorescence*, Wiley-VCH, Weinheim, **2001**.

## 2 Highly Stable, Readily Reducible, Fluorescent, Trifluoromethylated 9-Borafluorenes

The following section is slightly modified and reproduced from ref. [2] with permission from Wiley-VCH.

### 2.1 Introduction

Boron-containing organic  $\pi$ -systems, especially triarylboranes<sup>[69-80, 162]</sup> and, more recently, boron-containing polyaromatics are of much current interest.<sup>[71, 77, 163-169]</sup> Three coordinate boron is isoelectronic with a carbonium ion, having an unoccupied p-orbital, making it inherently electron deficient and Lewis acidic. Thus, three-coordinate boranes can be employed as  $\pi$ -acceptors, single electron or electron pair acceptors. Such boranes have been used in linear<sup>[81-94, 116, 153, 170-173]</sup> and non-linear<sup>[96, 100, 101, 103, 104, 106, 108-110, 113-115, 118]</sup> optical materials, anion sensors,<sup>[75, 119, 120, 174]</sup> frustrated Lewis pairs (FLPs),<sup>[175-181]</sup> as well as in organic light emitting diodes (OLEDs).<sup>[54, 122, 123]</sup> There are numerous examples, both aromatic and antiaromatic, of boron-containing conjugated cyclic  $\pi$ -systems.<sup>[165, 169]</sup> The subclass of boroles is of special interest.<sup>[71, 132, 167, 182-196]</sup> They are isoelectronic with the antiaromatic cyclopentadiene cation, having  $4\pi$  electrons; however, the introduction of the boron vertex lowers the symmetry (Figure 2.1). This leads to a singlet ground state with a small HOMO-LUMO gap, resulting in the intense color of boroles, even though the molar extinction coefficient ( $\epsilon$ ) is quite small for their  $S_1 \leftarrow S_0$  transitions.

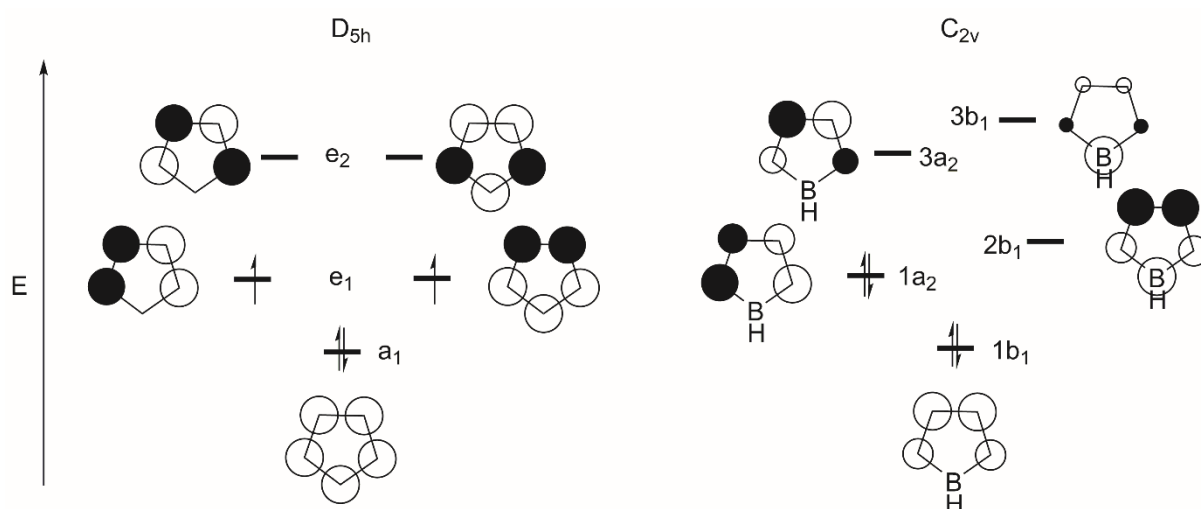


Figure 2.1: Frontier orbitals of the cyclopentadienyl cation (left) and borole (right).

Because of that, they are highly reactive towards nucleophiles and thereby unsuitable for many applications. Steric shielding, which works well for triarylboranes,<sup>[91, 197, 198]</sup> only stabilizes

boroles to a certain degree.<sup>[132, 199]</sup> Via benzannulation, the stability of boroles can be greatly increased,<sup>[200-203]</sup> but the anti-aromatic character is significantly decreased due to delocalization of  $\pi$  electron density over the biphenylene backbone. This leads to a stabilization of the HOMO as well as a destabilization of the LUMO resulting in a larger HOMO – LUMO gap and loss of the characteristic strong color of boroles. This also results in a lower Lewis acidity and, subsequently, significantly more stable systems.<sup>[165, 192]</sup> Detailed studies by Martin and co-workers demonstrate, however, that sterically less hindered derivatives, in particular, retain characteristic borole reactivity.<sup>[204-208]</sup> Compared with their triarylborane derivatives, borafluorenes are usually more Lewis acidic and exhibit more positive reduction potentials.<sup>[209]</sup> The stability of these systems can be further improved by sterically shielding<sup>[201, 202]</sup> or electronically saturating the boron center,<sup>[200]</sup> through direct n to p conjugation or indirect F–B interaction (Figure 2.2, left).

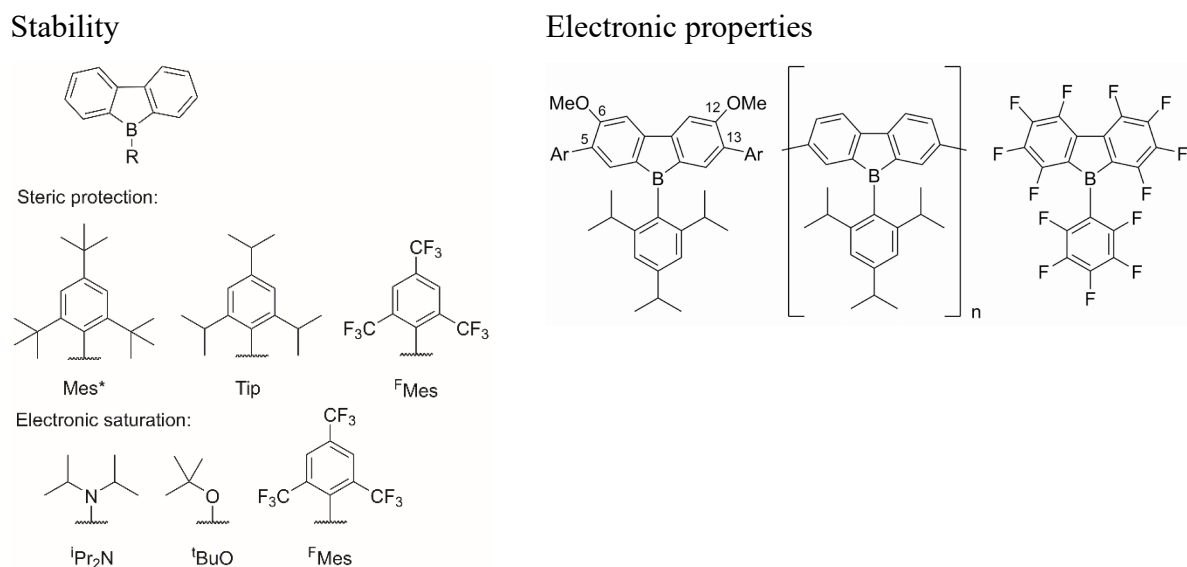


Figure 2.2: Selected examples of borafluorenes. A variety of *exo*-aryl substituents and the nature of their respective influence on the stability of the borafluorene (left).<sup>[201, 202]</sup> It is important to note, that *ortho*-trifluoromethyl substituted aryls provide both steric as well as electronic stabilization. Examples of the functionalization of the borafluorene backbone to tune the electronic properties (right).<sup>[200, 209-211]</sup>

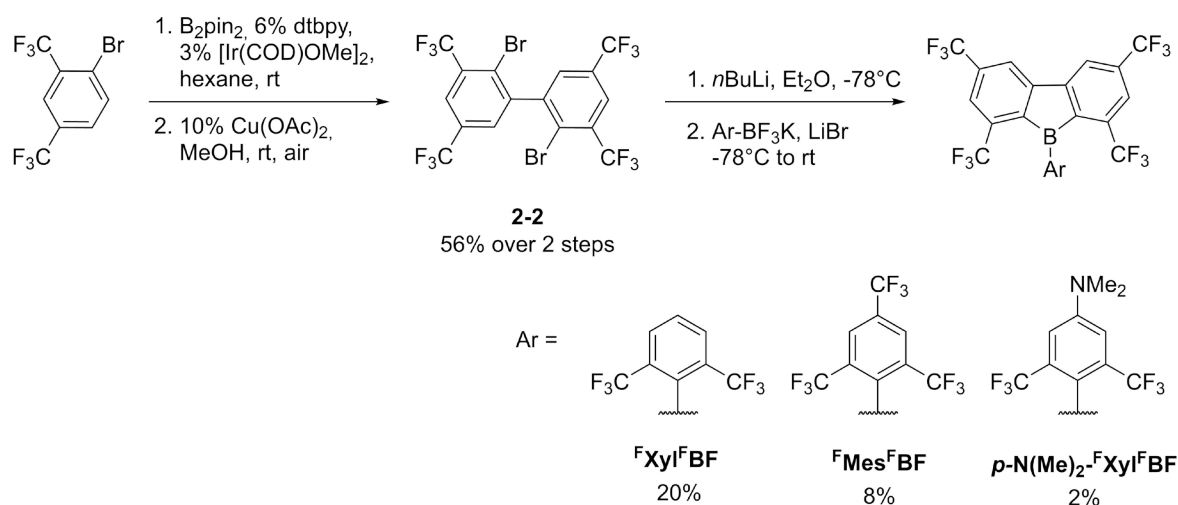
Yamaguchi and co-workers reported air and moisture stable borafluorene derivatives employing either Tip (2,4,6-tris(*triisopropyl*)phenyl) or the even bulkier Mes\* (2,4,6-tris(*tert-butyl*)phenyl) substituents.<sup>[200, 201]</sup> It was found that the Tip derivatives could be used as turn on type fluoride sensors, whereas the Mes\* compounds showed no reaction with fluoride. Recently, Rugar and co-workers have studied these effects in detail.<sup>[202]</sup> They found that while Tip-substituted derivatives still decompose slowly (<10% decomp. over 24 h) in wet solvents, the corresponding <sup>F</sup>Mes derivatives exhibit higher stability (5% decomp. over 24 h). Derivatives containing  $\pi$ -bonding moieties were found to be much more sensitive towards moisture (*i*PrN<sub>2</sub>:

50% decomp. over 1 h; <sup>t</sup>BuO: 10% decomp. over 1 h). *Ortho*-trifluoromethyl substituted aryls exhibit a strong stabilizing effect on boranes.<sup>[91, 124, 127, 131, 132, 134, 136]</sup> In addition to the steric effect, a direct interaction of the lone pairs of the fluorine atoms with the empty p orbital of the boron center is observed. This is supported by B–F distances which are much shorter than the sum of their van der Waals radii (3.39 Å)<sup>[156]</sup> in crystal structures. The electronic properties of borafluorenes can be easily tuned to fit different applications by the introduction of different substitution patterns on the biphenyl backbone (Figure 2.2, right). The introduction of methoxy groups at the 6 and 12 positions leads to a small hypsochromic shift of both the absorption and emission wavelength,<sup>[200]</sup> whereas elongation of the  $\pi$ -system with electron-rich conjugated systems attached at the 5 and 13 positions leads to a bathochromic shift of both the absorption and emission wavelength.<sup>[201]</sup> The photophysical properties of borafluorenes can also be modified by coordination of Lewis bases. Both Yamaguchi and co-workers and Rivard and co-workers observed turn-on fluorescence upon adduct formation.<sup>[200, 212]</sup> Wilson and Gillard and co-workers observed turn-off fluorescence of a borafluorenium cation upon coordination of a Lewis base at low temperature, resulting in thermochromism.<sup>[213]</sup> Piers and co-workers investigated the properties of a highly electron deficient perfluorinated borafluorene (Figure 2.2, right).<sup>[209, 210]</sup> While they only observed a reduction corresponding to the perfluoroaryls in the cyclic voltammogram, a reaction with the relatively mild reducing agent CoCp<sub>2</sub> (CoCp<sub>2</sub>/CoCp<sub>2</sub><sup>+</sup>: –1.3 vs Fc/Fc<sup>+</sup>) was observed, underlining the electron deficient nature of the compound. In competition experiments with the strong Lewis acid B(C<sub>6</sub>F<sub>5</sub>)<sub>3</sub>, preference towards the borafluorene derivative was observed, especially with sterically-demanding Lewis bases. The (sp<sup>2</sup>-C)–F bonds in this compound, however, are still reactive towards nucleophiles. In contrast, perfluoroalkyl groups are inert towards nucleophiles, provide a strong inductive electron withdrawing effect and have been previously employed in the synthesis of electron deficient triarylboranes.<sup>[136]</sup> To the best of our knowledge, there have been no photophysical studies of borafluorenes with electron deficient biphenyl backbones. We envisioned that judicious incorporation of trifluoromethyl groups both in the biphenyl core and at the *exo*-aryl moiety would provide a significant stability enhancement while retaining the low-lying LUMO typical of non-annulated boroles.

## 2.2 Results and Discussion

### 2.2.1 Synthesis

In order to maximize the stability of the trifluoromethylated borafluorenes (**F<sup>Bf</sup>**) we chose three different *meta*-fluoroxylylene (1,3-bis(trifluoromethyl)benzene) derivatives as the *exo*-aryl moieties. To examine the influence of the *exo*-aryl and, specifically, substituents at the *para*-position, we chose 2,6-bis(trifluoromethyl)phenyl (**F<sup>Xyl</sup>**), 2,4,6-tris(trifluoromethyl)phenyl (**F<sup>Mes</sup>**) and 4-(dimethylamino)-2,6-bis(trifluoromethyl)phenyl (***p*-NMe<sub>2</sub>-F<sup>Xyl</sup>**) groups (Scheme 2.1).



Scheme 2.1: Synthesis of **F<sup>Mes</sup>F<sup>Bf</sup>**, **F<sup>Xyl</sup>F<sup>Bf</sup>** and ***p*-NMe<sub>2</sub>-F<sup>Xyl</sup>F<sup>Bf</sup>**.

Biphenyl derivative **2-2** was synthesized via regioselective C–H borylation of 1-bromo-2,4-bis(trifluoromethyl)benzene<sup>[144, 214]</sup> *ortho* to the bromine and a subsequent copper-catalyzed oxidative homocoupling. For the last step, **2-2** was dilithiated and subsequently reacted with the appropriate Ar-BF<sub>3</sub>K salt. Attempts to synthesize the haloborafluorene with different BX<sub>3</sub> (X = F, Cl, Br) sources failed. Attempts to use aryl-boronates in place of the Ar-BF<sub>3</sub>K salt were also unsuccessful. The use of aryltrifluoroborate salts as boron source was previously reported by our group for the synthesis of boroles with enhanced stability,<sup>[132]</sup> and applied by others in the synthesis of boron PAHs<sup>[149, 150]</sup> and aryl-borates.<sup>[151, 152]</sup> Organic trifluoroborate salts are widely employed in cross-coupling reactions as they are readily accessible and very stable.<sup>[147, 148]</sup> During the synthesis we observed that adding LiBr greatly improves the reactivity of the Ar-BF<sub>3</sub>K salts. It is possible that a cation exchange reaction generates the more reactive Ar-BF<sub>3</sub>Li salt. The increased reactivity of the Ar-BF<sub>3</sub>Li salt is due to the thermodynamically favorable LiF-elimination. It is also possible that LiBr stabilizes the aryllithium species towards decomposition in ethereal solvents. This decomposition also explains the low isolated yields. It



is important to note that the corresponding *ortho*-trifluoromethylarylboron halides ( $X = \text{Cl}, \text{Br}$ ) are not stable due to halide exchange.<sup>[125]</sup> This might also explain why the synthesis of the haloborafluorenes was not possible. The compounds  $^{\text{F}}\text{Mes}^{\text{F}}\text{Bf}$ ,  $^{\text{F}}\text{Xyl}^{\text{F}}\text{Bf}$  and  $p\text{-NMe}_2\text{-}^{\text{F}}\text{Xyl}^{\text{F}}\text{Bf}$  were obtained after purification via sublimation and recrystallization. Both  $^{\text{F}}\text{Mes}^{\text{F}}\text{Bf}$  and  $^{\text{F}}\text{Xyl}^{\text{F}}\text{Bf}$  are bright green solids. In contrast,  $p\text{-NMe}_2\text{-}^{\text{F}}\text{Xyl}^{\text{F}}\text{Bf}$  is a red solid. All compounds exhibit  $^1\text{H}$  NMR and  $^{13}\text{C}\{^1\text{H}\}$  NMR signals consistent with their proposed structures. The  $^{11}\text{B}\{^1\text{H}\}$  NMR shifts for all three borafluorene derivatives are around 64 ppm and differ only slightly. The  $^{19}\text{F}\{^1\text{H}\}$  NMR spectra display singlets and septets, the latter with a  $J_{\text{FF}}$  coupling constant of 3 – 4 Hz. (Table 2.1)

Table 2.1:  $^{11}\text{B}\{^1\text{H}\}$  and  $^{19}\text{F}\{^1\text{H}\}$  NMR shifts of  $^{\text{F}}\text{Mes}^{\text{F}}\text{Bf}$ ,  $^{\text{F}}\text{Xyl}^{\text{F}}\text{Bf}$ , and  $p\text{-NMe}_2\text{-}^{\text{F}}\text{Xyl}^{\text{F}}\text{Bf}$  recorded in  $\text{C}_6\text{D}_6$ .

	$^{\text{F}}\text{Xyl}^{\text{F}}\text{Bf}$	$^{\text{F}}\text{Mes}^{\text{F}}\text{Bf}$	$p\text{-NMe}_2\text{-}^{\text{F}}\text{Xyl}^{\text{F}}\text{Bf}$
$^{11}\text{B}\{^1\text{H}\}$ NMR (ppm)	63.2	64.1	64.7
$^{19}\text{F}\{^1\text{H}\}$ NMR (ppm) singlet	-63.4	-62.0; -63.5	-63.4
$^{19}\text{F}\{^1\text{H}\}$ NMR (ppm) septets	-58.2 ( $J_{\text{FF}} = 4$ Hz)	-58.4 ( $J_{\text{FF}} = 4$ Hz)	-58.1 ( $J_{\text{FF}} = 4$ Hz)
	-59.6 ( $J_{\text{FF}} = 4$ Hz)	-59.6 ( $J_{\text{FF}} = 4$ Hz)	-59.5 ( $J_{\text{FF}} = 4$ Hz)

The singlets at ca.  $\delta = -63.5$  ppm correspond to the two freely rotating *para*- $\text{CF}_3$ -groups on the borafluorene core. For  $^{\text{F}}\text{Mes}^{\text{F}}\text{Bf}$ , another singlet corresponding to the *para*- $\text{CF}_3$ -group on the *exo*-aryl is observed. The  $\text{CF}_3$ -groups *ortho* to the boron center display a complex coupling pattern of two septets with small coupling constants ( $J_{\text{FF}} = 4$  Hz). This can be attributed to through-space F–F coupling as previously observed at low temperature (243 K) for  $(^{\text{F}}\text{Mes})_2\text{BAr}$  compounds.<sup>[131]</sup> The fact that the borafluorenes exhibit this phenomenon at room temperature is an indicator of the high rigidity of the systems.

All three compounds are stable in the solid-state and can be stored under ambient conditions without decomposition. In wet  $\text{CDCl}_3$  (1.5 eq.  $\text{H}_2\text{O}$ /borafluorene) at room temperature, no decomposition of either  $^{\text{F}}\text{Mes}^{\text{F}}\text{Bf}$  or  $^{\text{F}}\text{Xyl}^{\text{F}}\text{Bf}$  was observed over 4 d by NMR spectroscopy. This is surprising as for  $^{\text{F}}\text{MesBf}$  and  $\text{TipBf}$ , both less electron deficient compounds, decomposition rates of 5 and 10% respectively in wet solvents over 24 h were reported.<sup>[202]</sup> This indicates that the  $\text{CF}_3$ -groups *ortho* to the boron center on the borafluorene core have a stabilizing effect, likely due to steric shielding. However,  $p\text{-NMe}_2\text{-}^{\text{F}}\text{Xyl}^{\text{F}}\text{Bf}$  shows very rapid decomposition when exposed to wet solvents. It is likely that the dimethylamine moiety is protonated first, thereby further increasing the electrophilicity of the boron center and decreasing its stability towards nucleophilic attack. The reaction with  $\text{H}_2\text{O}$  leads to cleavage of one B–C bond of the borafluorene core, resulting in a BOH and CH moiety. The same reactivity

towards water and other E–H bonds (E = N, O, S) was previously observed by Martin and co-workers.<sup>[208]</sup> Likely due to less steric hinderance in their system, a second borafluorene reacts with the decomposition product to form a B–O–B motif. The product of the hydrolysis of *p*-NMe<sub>2</sub>-<sup>F</sup>Xyl<sup>F</sup>Bf was isolated and studied by X-ray diffraction (compound **D** in Figure 6.16). All three compounds are slightly soluble in non-polar solvents such as hexane or toluene and soluble in polar non-coordinating solvents such as CH<sub>2</sub>Cl<sub>2</sub> and THF. Dissolving <sup>F</sup>Mes<sup>F</sup>Bf in acetonitrile gives a colorless solution. Investigation of the solution via <sup>19</sup>F NMR spectroscopy revealed the formation of an acetonitrile adduct, which is consistent with previous studies by Martin and co-workers for less sterically hindered borafluorenes.<sup>[205]</sup> The *para*-CF<sub>3</sub>-groups, both on the borafluorene backbone as well as the *exo*-aryl moiety, are influenced only weakly by the coordination of acetonitrile, as both singlets in the <sup>19</sup>F NMR spectrum shift only slightly to lower field. The signals corresponding to the *ortho*-CF<sub>3</sub>-groups, however, change dramatically. Instead of two septets as observed for <sup>F</sup>Mes<sup>F</sup>Bf, one septet at –51.9 ppm (*J*<sub>FF</sub> = 10 Hz), one broad singlet at –56.2 ppm, and a quartet at –60.7 ppm (*J*<sub>FF</sub> = 10 Hz), are observed (Figure 2.3, middle).

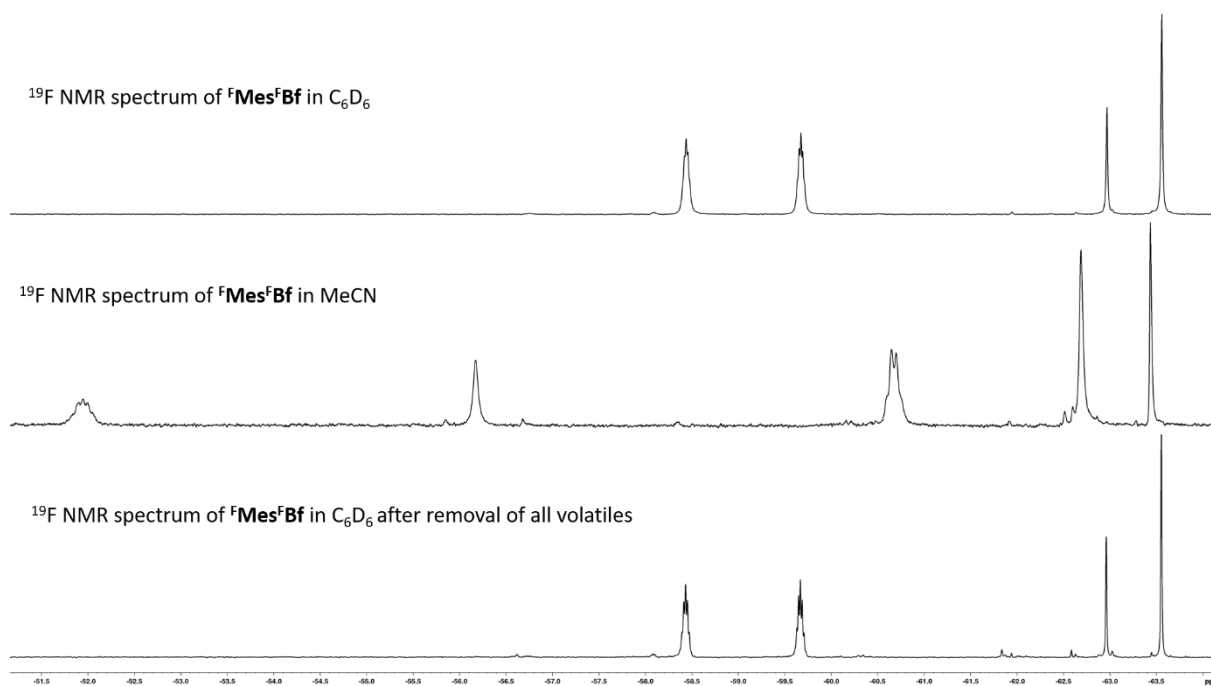


Figure 2.3: <sup>19</sup>F NMR spectra (188 MHz, 298 K) of <sup>F</sup>Mes<sup>F</sup>Bf in C<sub>6</sub>D<sub>6</sub> (top), in CH<sub>3</sub>CN (middle) and in C<sub>6</sub>D<sub>6</sub> after removal of all volatiles (bottom).

This suggests that only one *exo*-aryl trifluoromethyl moiety is coupling to the *ortho*-trifluoromethyl groups on the borafluorene backbone. After evaporation of the acetonitrile and dissolution in C<sub>6</sub>D<sub>6</sub>, only the borafluorene was observed via <sup>19</sup>F NMR spectroscopy. Thus, the formation of the adduct with acetonitrile is completely reversible.

## 2.2.2 Crystal and Molecular Structures

Single crystals of the three borafluorenes as well as the acetonitrile adduct of  ${}^{\text{F}}\text{Mes}^{\text{F}}\text{Bf}$  ( ${}^{\text{F}}\text{Mes}^{\text{F}}\text{Bf}\cdot\text{MeCN}$ ) suitable for X-ray studies were obtained (Figure 2.4) and selected bond lengths, angles, torsion angles and short B–F contacts are listed in Table 2.2. The single crystals of  ${}^{\text{F}}\text{Mes}^{\text{F}}\text{Bf}$  and  $p\text{-NMe}_2\text{-}{}^{\text{F}}\text{Xyl}^{\text{F}}\text{Bf}$  were obtained from a saturated hexane solution at  $-30\text{ }^{\circ}\text{C}$ , that of  ${}^{\text{F}}\text{Xyl}^{\text{F}}\text{Bf}$  was obtained by evaporation of a saturated DCM solution and that of  ${}^{\text{F}}\text{Mes}^{\text{F}}\text{Bf}\cdot\text{MeCN}$  was obtained from a saturated acetonitrile solution at  $-30\text{ }^{\circ}\text{C}$ .

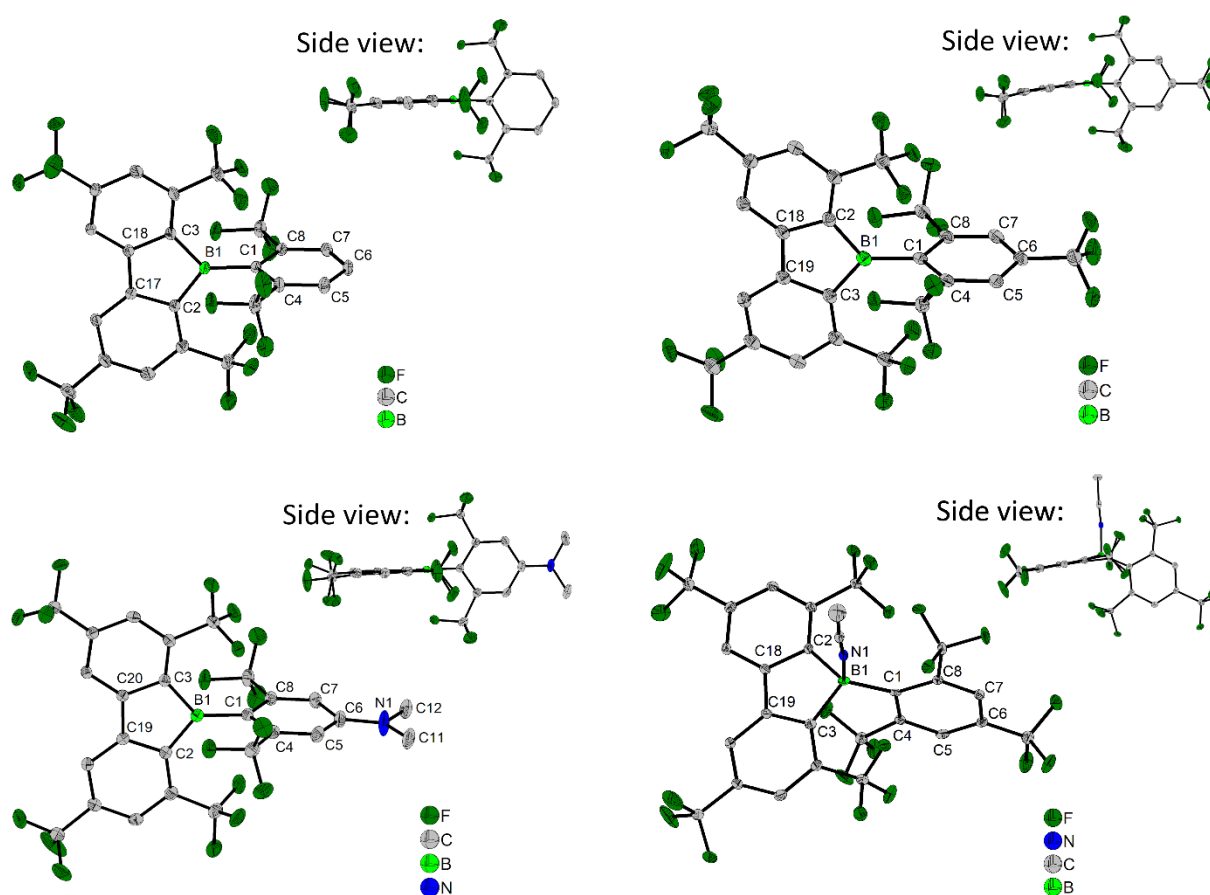


Figure 2.4: Molecular structures of  ${}^{\text{F}}\text{Mes}^{\text{F}}\text{Bf}$  (top left),  ${}^{\text{F}}\text{Xyl}^{\text{F}}\text{Bf}$  (top right),  $p\text{-NMe}_2\text{-}{}^{\text{F}}\text{Xyl}^{\text{F}}\text{Bf}$  (bottom left) and  ${}^{\text{F}}\text{Mes}^{\text{F}}\text{Bf}\cdot\text{MeCN}$  (bottom right) determined by single-crystal X-ray diffraction at 100 K. All ellipsoids are drawn at the 50% probability level, and H atoms and solvent molecules are omitted for clarity.

Table 2.2: Selected bond lengths [Å] and angles [°] in  ${}^{\text{F}}\text{Mes}^{\text{F}}\text{Bf}$ ,  ${}^{\text{F}}\text{Xyl}^{\text{F}}\text{Bf}$ ,  $p\text{-NMe}_2\text{-}{}^{\text{F}}\text{Xyl}^{\text{F}}\text{Bf}$  and  ${}^{\text{F}}\text{Mes}^{\text{F}}\text{Bf}\cdot\text{MeCN}$ . Atom labels for the respective molecular structures are shown in Figure 2.4.

	${}^{\text{F}}\text{Mes}^{\text{F}}\text{Bf}$	${}^{\text{F}}\text{Xyl}^{\text{F}}\text{Bf}$	$p\text{-NMe}_2\text{-}{}^{\text{F}}\text{Xyl}^{\text{F}}\text{Bf}$	${}^{\text{F}}\text{Mes}^{\text{F}}\text{Bf}\cdot\text{MeCN}$
B–C1	1.579(3)	1.570(2)	1.570(3)	1.652(3)
B–C2	1.581(3)	1.591(3)	1.595(3)	1.645(3)
B–C3	1.591(3)	1.591(3)	1.591(3)	1.645(3)
B–N				1.591(3)
C3–C19/C18/C20	1.408(3)	1.410(2)	1.409(2)	1.401(3)
C2–C18/C17/C19	1.410(2)	1.409(2)	1.408(2)	1.410(3)
C18/C17/C19–C19/C18/C20	1.481(3)	1.474(2)	1.482(2)	1.475(3)
$\angle \text{BC}_3\text{-Aryl}_{\text{exo}}$	89.32(7)	89.84(8)	89.27(6)	
$\angle \text{BC}_{12}\text{-Aryl}_{\text{exo}}$	89.43(6)	89.54(6)	88.69(5)	82.12(6)
Torsion of Ar <sub>exo</sub> out of borafluorene plane	171.28(16)	176.45(16)	178.83(17)	137.6(2)
$\angle \text{C1-B-C2-C18/C17/C19}$				
5-ring: $\angle \text{C2BC3}$	103.95(15)	103.07(13)	102.94(14)	99.74(18)
Sum $\angle \text{CBC}$	359.74(16)	359.90(15)	359.99(16)	338.43(18)
Sum $\angle \text{CNC}$			359.84(19)	
Shortest B–F contact(s)	2.392(3) 2.440(3)	2.379(2) 2.390(3)	2.366(2) 2.434(2)	2.853(3)

A comparison of the crystal structures of the three target compounds shows the following. While all three B–C bond distances are in a similar range for  ${}^{\text{F}}\text{Mes}^{\text{F}}\text{Bf}$  (1.579(3) - 1.591(3) Å), the B–C1<sub>exo</sub> distances to the  ${}^{\text{F}}\text{Xyl}$  groups of  ${}^{\text{F}}\text{Xyl}^{\text{F}}\text{Bf}$  and  $p\text{-NMe}_2\text{-}{}^{\text{F}}\text{Xyl}^{\text{F}}\text{Bf}$  (B–C = 1.570(3) Å) are slightly shorter than the respective B–C2 and B–C3 bonds (1.591(3) - 1.595(3) Å) within the borole moieties (Table 2.2). The boron atoms have a nearly ideal trigonal planar configuration with the sum of the C–B–C angles being 359.74(16) - 359.99(16)°. In all three compounds, the C2–B–C3 angle (102.94(14) - 103.95(15)°) within the borole moiety is much smaller than the other two C–B–C angles. The borole moiety shows similar bond lengths and angles in all three compounds. The angles increase from C–B–C to B–C–C (106.57(16) - 107.52(15)°) and to C–C–C (110.98(17) - 111.41(15)°). The C2–C and C3–C bond lengths (1.408(3) - 1.410(2) Å) are typical for aromatic bonds, while the C–C bond (1.474(2) - 1.482(2) Å) that is opposite to the boron atom has significant single-bond character. The interplanar angle between the borafluorene (BC<sub>12</sub>) and the *exo*-aryl substituent is close to 90° in all three compounds (88.69(5) - 89.54(6)°). This is due to the large steric demand of the CF<sub>3</sub> groups in the *ortho*-positions of both the *exo*-aryl moiety as well as the borafluorene core. In all three compounds, two B–F distances, each in the range of 2.366(2) - 2.440(3) Å, are observed, which are significantly shorter than the sum of the van der Waals radii for boron and fluorine (3.39 Å).<sup>[156]</sup> This was previously observed in boranes and boroles with *ortho*-CF<sub>3</sub> aryl

moieties.<sup>[91, 125, 132, 136, 215]</sup> As the two respective fluorine atoms are directly above and below the boron center, it is most likely that the lone pair electrons of these fluorine atoms interact with the empty p-orbital of the boron center. The torsion angle  $C_{endo}-C2_{endo}-B-C1_{exo}$  with the endo carbon atoms belonging to the borole moiety deviates slightly from  $180^\circ$  ( $171.28(16) - 178.83(17)^\circ$ ). This shows that the B–C1 bond to the *exocyclic* moiety is tilted slightly out of the borafluorene plane. The out-of-plane tilt increases from *p*-NMe<sub>2</sub>-<sup>F</sup>Xyl<sup>F</sup>Bf ( $1.17(17)^\circ$ ) to <sup>F</sup>Xyl<sup>F</sup>Bf ( $3.55(16)^\circ$ ) and <sup>F</sup>Mes<sup>F</sup>Bf ( $8.72(16)^\circ$ ). The magnitude of the tilt is related to the molecular packing, which is similar in all three crystal structures as the borafluorene moieties are arranged in pairs, which are related by inversion symmetry and form weak intermolecular  $\pi \cdots \pi$  interactions between the borafluorene backbones. The strongest  $\pi \cdots \pi$  interaction is observed in <sup>F</sup>Mes<sup>F</sup>Bf, which shows the smallest centroid-centroid distance, interplanar separation, and offset shift (Table 6.5). Hence, these pairs of molecules are closest in <sup>F</sup>Mes<sup>F</sup>Bf, and the *exocyclic* <sup>F</sup>Mes moiety is tilted out of the plane the most, away from the center of the pair in order to avoid close F $\cdots$ F contacts between the two molecules. In the crystal structure of the acetonitrile adduct of <sup>F</sup>Mes<sup>F</sup>Bf, as the hybridization at the boron is now sp<sup>3</sup> rather than sp<sup>2</sup>, all of the B–C bonds are elongated. The C2–B1–C3 angle of the borole ring ( $99.74(18)^\circ$ ) is decreased compared with <sup>F</sup>Mes<sup>F</sup>Bf ( $103.95(15)^\circ$ ). The torsion angle of the *exo*-aryl towards the borafluorene backbone is decreased ( $82.12(6)^\circ$ ) and the bending of the *exo*-aryl out of the plane of the borafluorene moiety ( $137.6(2)^\circ$ ) deviates significantly from  $180^\circ$ . In the adduct, there is only one short B–F contact (F3–B1 =  $2.853(3)$  Å) that is elongated compared to <sup>F</sup>Mes<sup>F</sup>Bf, but still shorter than the sum of the van der Waals radii. The B–N bond length is  $1.591(3)$  Å, which is significantly shorter than that in the acetonitrile adduct of B(C<sub>6</sub>F<sub>6</sub>)<sub>3</sub> ( $1.616(3)$  Å),<sup>[216]</sup> but similar to that in the previously reported MeCN adduct of **PhBf** (**PhBf**•MeCN) ( $1.598(4)$  Å).<sup>[205]</sup> The N≡C bond ( $1.129(3)$  Å) is also shorter than that in the acetonitrile adduct of B(C<sub>6</sub>F<sub>6</sub>)<sub>3</sub> ( $1.141(2)$  Å) and very similar to that in **PhBf**•MeCN ( $1.128(4)$  Å).

## 2.2.3 Electrochemistry

Cyclic voltammograms of the three borafluorenes were recorded in dichloromethane with  $[n\text{Bu}_4\text{N}][\text{PF}_6]$  as the electrolyte and a scan rate of  $250 \text{ mVs}^{-1}$  (Figure 2.5) in order to determine their reduction potentials.

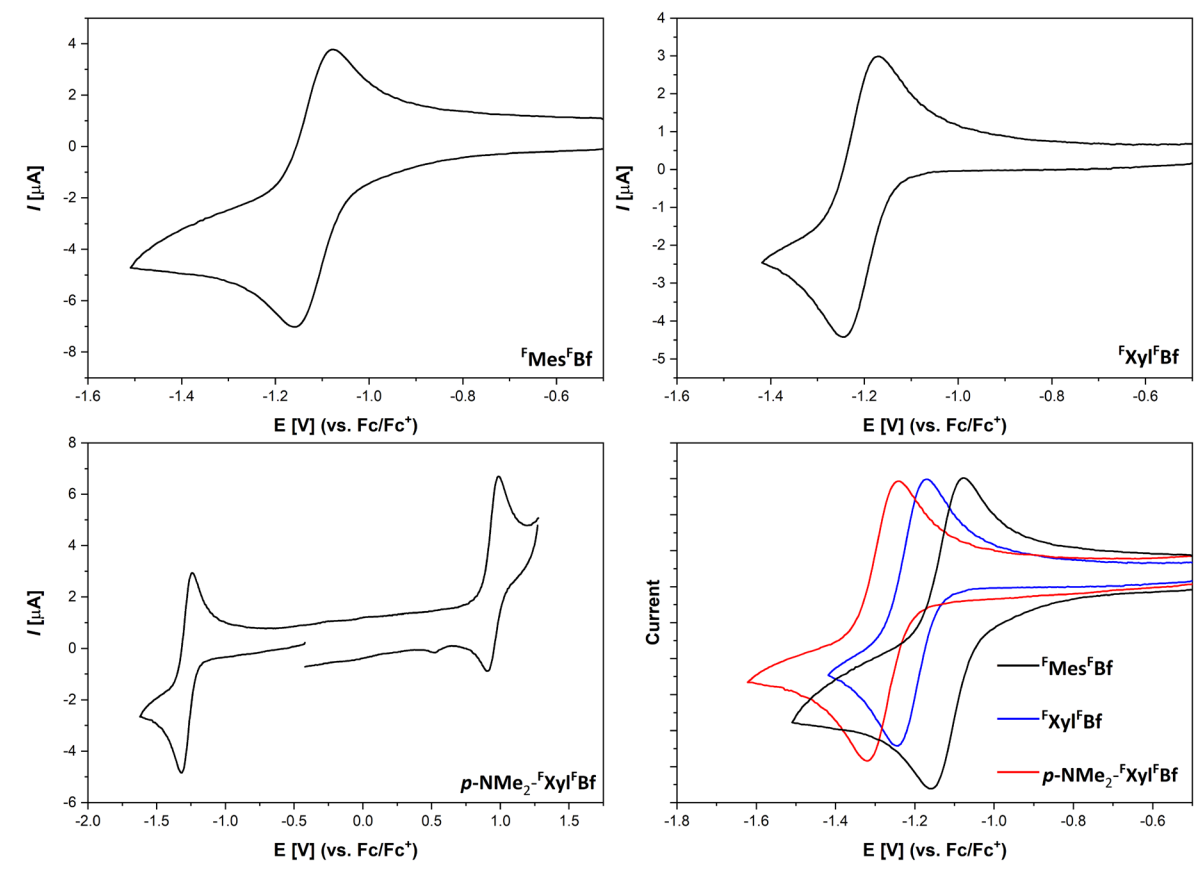
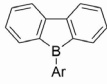
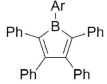
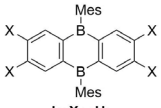
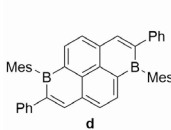
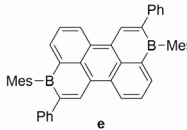


Figure 2.5: Cyclic voltammograms of the reversible redox events of  $\text{F}^{\text{Mes}}\text{F}^{\text{Bf}}$  (top left),  $\text{F}^{\text{Xyl}}\text{F}^{\text{Bf}}$  (top right) and  $p\text{-NMe}_2\text{-F}^{\text{Xyl}}\text{F}^{\text{Bf}}$  (bottom left). All samples are referenced against the  $\text{Fc}/\text{Fc}^+$  ion couple. For better comparison, the reduction waves are plotted together (bottom right;  $\text{F}^{\text{Mes}}\text{F}^{\text{Bf}}$  (black),  $\text{F}^{\text{Xyl}}\text{F}^{\text{Bf}}$  (blue),  $p\text{-NMe}_2\text{-F}^{\text{Xyl}}\text{F}^{\text{Bf}}$  (red)).

All measurements were referenced to the ferrocene/ferrocenium redox couple ( $\text{Fc}/\text{Fc}^+$ ). The most electron deficient borafluorene,  $\text{F}^{\text{Mes}}\text{F}^{\text{Bf}}$ , exhibits a reversible reduction at  $-1.13 \text{ V}$  and an irreversible reduction at  $-2.04 \text{ V}$ . For the slightly less electron deficient  $\text{F}^{\text{Xyl}}\text{F}^{\text{Bf}}$ , a reversible reduction at  $-1.21 \text{ V}$  and an irreversible reduction at  $-2.12 \text{ V}$  are observed. Interestingly,  $p\text{-NMe}_2\text{-F}^{\text{Xyl}}\text{F}^{\text{Bf}}$  shows a reversible reduction at  $-1.28 \text{ V}$ , an irreversible reduction at  $-2.15 \text{ V}$  and a partially reversible oxidation at  $0.95 \text{ V}$ .

Table 2.3: Tabulated 1<sup>st</sup> reduction potential values of various three-coordinate boron species.

compound	1 <sup>st</sup> reduction potential $E_{1/2}$ in [V] vs. $\text{Fc}/\text{Fc}^+$	compound	1 <sup>st</sup> reduction potential $E_{1/2}$ in [V] vs. $\text{Fc}/\text{Fc}^+$
<b>Borafluorenes</b>		<b>Free boroles</b>	
			
Mes* <b>Bf</b> : Ar = Mes*; Tip <b>Bf</b> : Ar = Tip; <sup>F</sup> Mes <b>Bf</b> : Ar = <sup>F</sup> Mes		PhBC <sub>4</sub> Ph <sub>4</sub> <sup>a</sup> : Ar = Ph; MesBC <sub>4</sub> Ph <sub>4</sub> <sup>a</sup> : Ar = Mes; <sup>F</sup> MesBC <sub>4</sub> Ph <sub>4</sub> <sup>a</sup> : Ar = <sup>F</sup> Mes	
<b>This work</b>			
<sup>F</sup> Mes <sup>F</sup> Bf <sup>a</sup>	-1.13	PhBC <sub>4</sub> Ph <sub>4</sub> <sup>a</sup>	-1.61 <sup>[217]</sup>
<sup>F</sup> Mes <sup>F</sup> Bf <sup>b</sup>	-1.21	MesBC <sub>4</sub> Ph <sub>4</sub> <sup>a</sup>	-1.69 <sup>[199, 217, 218]</sup>
<i>p</i> -NMe <sub>2</sub> - <sup>F</sup> Xyl <sup>F</sup> Bf <sup>b</sup>	-1.28	<sup>F</sup> MesBC <sub>4</sub> Ph <sub>4</sub> <sup>a</sup>	-1.52 <sup>[132]</sup>
Mes* <b>Bf</b> <sup>d</sup>	-2.28 <sup>[201]</sup>		
Tip <b>Bf</b> <sup>e</sup>	-2.14 <sup>[202]</sup>		
<sup>F</sup> Mes <b>Bf</b> <sup>e</sup>	-1.82 <sup>[202]</sup>		
<b>a</b> <sup>f</sup>	-1.98 <sup>[219]</sup>		
<b>Diboraanthracene</b>		<b>Boron PAHs</b>	
			
b: X = H; c: X = Cl			
<b>b</b> <sup>g</sup>	-1.84 <sup>[164]</sup>	<b>d</b> <sup>a</sup>	-1.15 <sup>[220]</sup>
<b>c</b> <sup>g</sup>	-1.38 <sup>[90]</sup>	<b>e</b> <sup>a</sup>	-1.07 <sup>[220]</sup>
<b>Triaryl boranes</b>			
<b>B</b> (Mes) <sub>3</sub> <sup>b</sup>	-2.73 <sup>[221]</sup>	<b>B</b> (3,5-(CF <sub>3</sub> ) <sub>2</sub> C <sub>6</sub> H <sub>3</sub> ) <sub>3</sub> <sup>c</sup>	-1.61 <sup>[136]</sup>
<b>B</b> (Mes) <sub>2</sub> (C <sub>6</sub> F <sub>5</sub> ) <sub>2</sub> <sup>b</sup>	-2.10 <sup>[221]</sup>	<b>B</b> (2,4-(CF <sub>3</sub> ) <sub>2</sub> C <sub>6</sub> H <sub>3</sub> ) <sub>3</sub> <sup>c</sup>	-1.79 <sup>[136]</sup>
<b>B</b> (Mes)(C <sub>6</sub> F <sub>5</sub> ) <sub>2</sub> <sup>b</sup>	-1.72 <sup>[221]</sup>	<b>B</b> (2,5-(CF <sub>3</sub> ) <sub>2</sub> C <sub>6</sub> H <sub>3</sub> ) <sub>3</sub> <sup>c</sup>	-1.85 <sup>[136]</sup>
<b>B</b> (C <sub>6</sub> F <sub>5</sub> ) <sub>3</sub> <sup>a</sup>	-1.97 <sup>[192]</sup>		
<sup>a</sup> Measured using a platinum electrode in CH <sub>2</sub> Cl <sub>2</sub> using [ <i>n</i> Bu <sub>4</sub> N][PF <sub>6</sub> ] as the electrolyte; <sup>b</sup> Measured using a platinum electrode in THF with [ <i>n</i> Bu <sub>4</sub> N][B(C <sub>6</sub> F <sub>5</sub> ) <sub>4</sub> ] as the electrolyte; <sup>c</sup> Measured using a glassy carbon electrode in CH <sub>2</sub> Cl <sub>2</sub> with [ <i>n</i> Bu <sub>4</sub> N][B(C <sub>6</sub> F <sub>5</sub> ) <sub>4</sub> ] as the electrolyte; <sup>d</sup> Measured using a glassy carbon electrode in THF with [ <i>n</i> Bu <sub>4</sub> N][ClO <sub>4</sub> ] as the electrolyte; <sup>e</sup> Measured using a glassy carbon electrode in CH <sub>2</sub> Cl <sub>2</sub> with [ <i>n</i> Bu <sub>4</sub> N][PF <sub>6</sub> ] as the electrolyte; <sup>f</sup> Measured using a glassy carbon electrode in THF with [ <i>n</i> Bu <sub>4</sub> N][PF <sub>6</sub> ] as the electrolyte; <sup>g</sup> Measured using a platinum electrode in THF with [ <i>n</i> Bu <sub>4</sub> N][PF <sub>6</sub> ] as the electrolyte.			

The three borafluorenes exhibit much higher reduction potentials (<sup>F</sup>Mes<sup>F</sup>Bf = -1.13 V; <sup>F</sup>Xyl<sup>F</sup>Bf = -1.21 V and *p*-NMe<sub>2</sub>-<sup>F</sup>Xyl<sup>F</sup>Bf = -1.28 V) than any of the previously reported borafluorenes and boroles or triarylboranes (Table 2.3). The substitution patterns of compounds <sup>F</sup>MesBC<sub>4</sub>Ph<sub>4</sub> ( $E_{1/2}$  = -1.52 V) and <sup>F</sup>MesBf ( $E_{1/2}$  = -1.82 eV) allows a direct comparison of the fluorinated borafluorene backbone (<sup>F</sup>Bf) with the unsubstituted borafluorene backbone (Bf) and the non-annulated borole.<sup>[202]</sup> The strong anodic shift of the <sup>F</sup>Mes<sup>F</sup>Bf as compared to <sup>F</sup>MesBC<sub>4</sub>Ph<sub>4</sub> and

**<sup>F</sup>MesBf** demonstrates the strong electron withdrawing effect of the CF<sub>3</sub>-groups on the borafluorene backbone. This is likely due to the planar geometry as well as the fact that the *ortho*-CF<sub>3</sub>-groups of the borafluorene backbone do not display B-F interactions, and thus do not increase electron density at the boron atom. The reduction potentials of the trifluoromethylated borafluorenes do not differ strongly from one another. This indicates that the *para*-substituent on the *exo*-cyclic aryl moiety does not have a significant influence on the electron accepting properties of these borafluorenes. This is best illustrated by the fact that the  $\pi$ -donating dimethylamino group only leads to a cathodic shift of 0.15 V compared to a trifluoromethyl group. This is likely due to the nearly perpendicular arrangement of the *exo*-aryl group with respect to the borafluorene backbone, that limits  $\pi$ -conjugation leaving only inductive effects of the *exo*-aryl moiety on the borafluorene core and the boron center. To investigate further the electronic properties of borafluorene **<sup>F</sup>Mes<sup>F</sup>Bf**, CoCp<sub>2</sub> was chosen as a reducing agent ( $E^{0'}(\text{CoCp}_2) = -1.3 \text{ V vs. Fc/Fc}^+$ ).<sup>[157]</sup> Thus, after addition of CoCp<sub>2</sub>, the yellowish THF solution of **<sup>F</sup>Mes<sup>F</sup>Bf** turned dark purple and an ESR measurement confirmed the presence of the borafluorene radical anion [**<sup>F</sup>Mes<sup>F</sup>Bf**]<sup>-</sup> (Figure 2.6).

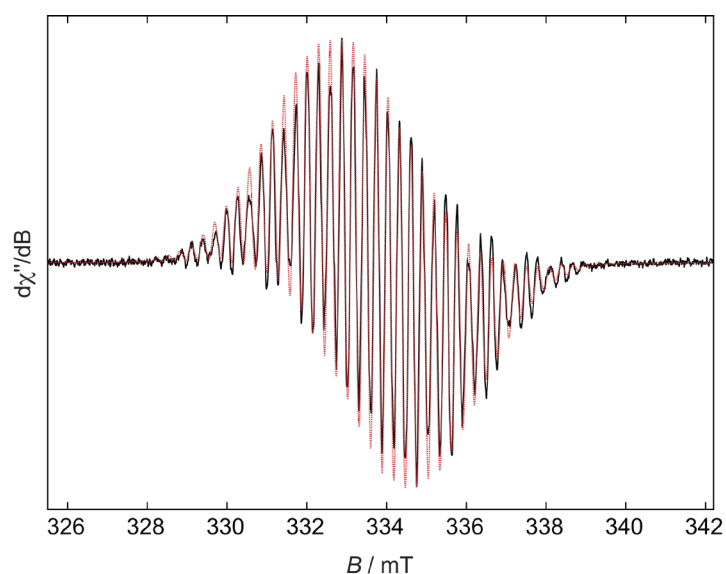


Figure 2.6: Experimental (black solid line) and simulated (red dashed line) continuous-wave X-band EPR spectra of [**<sup>F</sup>Mes<sup>F</sup>Bf**]<sup>-</sup> in a THF solution at room temperature.

A THF solution of the radical anion [**<sup>F</sup>Mes<sup>F</sup>Bf**]<sup>-</sup> shows a complex EPR signal centered at  $g_{\text{iso}} = 2.004$  consisting of hyperfine splittings to boron ( $a(^{11}\text{B}) = 3.3 \text{ G}$ ; cf. non-annulated borole derivatives ( $a(^{11}\text{B}) = 3.4 - 3.7 \text{ G}$ )<sup>[199, 222]</sup>), the CF<sub>3</sub> fluorines ( $a(^{19}\text{F}) = 11.3 \text{ G}$  and  $6.0 \text{ G}$ ) and the hydrogen atoms ( $a(^1\text{H}) = 6.1 \text{ G}$  and  $2.9 \text{ G}$ ) of the borafluorene core. The relatively small boron hyperfine coupling together with the relatively large proton and fluorine hyperfine couplings indicate significant spin delocalization onto the benzene rings, to a greater extent than in other



singly reduced borafluorenes.<sup>[201]</sup> Crystals of the radical anion suitable for X-ray diffraction were obtained by slow diffusion of pentane into a saturated THF solution (Figure 2.7).

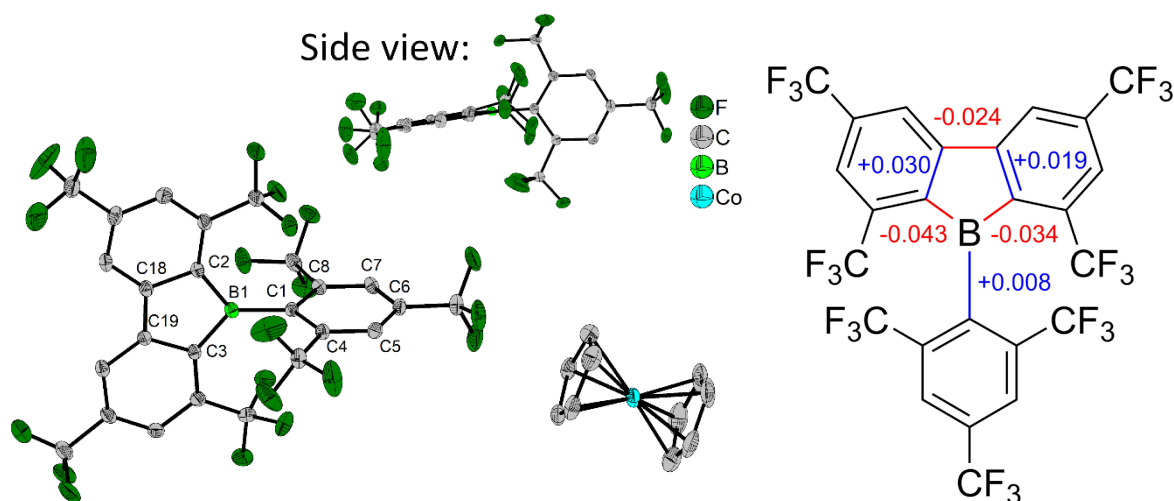


Figure 2.7: The solid-state molecular structure of  $[\text{FMeSFbf}][\text{CoCp}_2]$  determined by single-crystal X-ray diffraction at 100 K. All ellipsoids are drawn at the 50% probability level. H atoms and THF solvent molecules are omitted for clarity. Only half of the symmetrically non-equivalent molecules are shown. One of the  $\text{CF}_3$  groups on the borafluorene core is rotationally disordered and only the part with the higher occupancy (64%) is shown here (left). The relevant changes in bond lengths of  $[\text{FMeSFbf}]^-$  compared to the neutral starting material are shown at the right.

Upon reduction, a variety of changes in the structure are observed. As there are two independent molecules in the unit cell for the radical anion, both molecules are taken into account for comparison (Table 6.4). The negative charge is apparently localized on the borafluorene core, as the *exo*-aryl moiety is only slightly influenced, with almost all changes in bond length being within 3 esd's. While the B–C1 bond length is slightly increased ( $\Delta(\text{B–C1}) = +0.008$  and  $+0.015$  Å), both borafluorene B–C bonds (B–C2 and B–C3) are shortened ( $\Delta(\text{B–C2}) = -0.034$  and  $-0.025$  Å;  $\Delta(\text{B–C3}) = -0.043$  and  $-0.040$  Å). The neighboring borafluorene C–C bonds are elongated ( $\Delta(\text{C3–C19}) = +0.030$  and  $+0.027$  Å;  $\Delta(\text{C2–C18}) = +0.019$  and  $0.022$  Å) and the C–C bond connecting the two borafluorene aryls is shortened ( $\Delta(\text{C18–C19}) = -0.024$  Å). In summary, the bond lengths within the five-membered heterocycle equalize. This behavior was previously observed in the structures of borole radical anions and dianions.<sup>[199]</sup> The one-electron reduction also influences the shortest B–F distances which are elongated (mean  $\Delta(\text{B–F}) = +0.278$  Å).

### 2.2.4 Photophysical Properties

In order to obtain further insight into the electronic structure of the borafluorenes, absorption and emission spectra as well as quantum yields and excited state lifetimes were measured in hexane (Figure 2.8 and Table 2.4). Furthermore,  ${}^{\text{F}}\text{Mes}^{\text{F}}\text{Bf}$  was also studied in  $\text{CH}_2\text{Cl}_2$  and in the solid state. Solvatochromic studies of  $p\text{-NMe}_2\text{-}{}^{\text{F}}\text{Xyl}^{\text{F}}\text{Bf}$  could not be carried out, as no emission was detected in more polar solvents. This is most likely due to a further red shift of the emission, which in turn results in increased non-radiative decay processes and thus a much lower quantum yield.

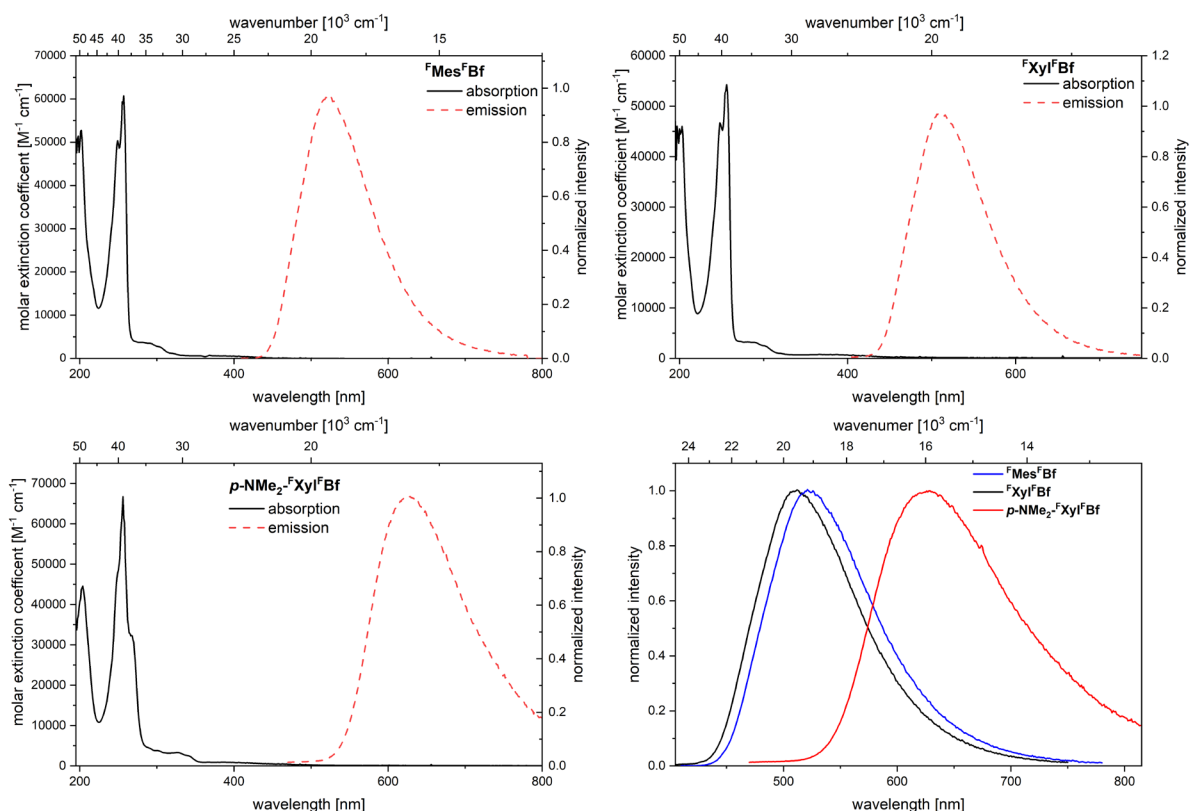


Figure 2.8: Absorption (black) and emission spectra (red) in hexane of  ${}^{\text{F}}\text{Mes}^{\text{F}}\text{Bf}$  (top left),  ${}^{\text{F}}\text{Xyl}^{\text{F}}\text{Bf}$  (top right) and  $p\text{-NMe}_2\text{-}{}^{\text{F}}\text{Xyl}^{\text{F}}\text{Bf}$  (bottom left). For comparison, the emission spectra are plotted together (bottom right;  ${}^{\text{F}}\text{Mes}^{\text{F}}\text{Bf}$  (black),  ${}^{\text{F}}\text{Xyl}^{\text{F}}\text{Bf}$  (blue),  $p\text{-NMe}_2\text{-}{}^{\text{F}}\text{Xyl}^{\text{F}}\text{Bf}$  (red)).

Table 2.4: Photophysical data for borafluorenes  ${}^{\text{F}}\text{Mes}^{\text{F}}\text{Bf}$ ,  ${}^{\text{F}}\text{Xyl}^{\text{F}}\text{Bf}$ , and  $p\text{-NMe}_2\text{-}{}^{\text{F}}\text{Xyl}^{\text{F}}\text{Bf}$ .

Compound	solvent	$\lambda_{\text{abs}}$ [nm] ( $\epsilon$ [ $10^3 \text{ M}^{-1} \text{ cm}^{-1}$ ]; $\log \epsilon$ )	$\lambda_{\text{em}}$ [nm] <sup>[a]</sup>	apparent Stokes shift ( $10^3 \text{ cm}^{-1}$ )	$\Phi_{\text{fl}}$	$\tau$ [ns] (rel%)	$\tau_0$ [ns]	$k_{\text{nr}}$ [ $10^7 \text{ s}^{-1}$ ] <sup>[b]</sup>	$k_{\text{r}}$ [ $10^7 \text{ s}^{-1}$ ] <sup>[c]</sup>
${}^{\text{F}}\text{Mes}^{\text{F}}\text{Bf}$	hexane	290 (2.9; 3.46),	521	5.8	0.37	224	605	0.3	0.2
		321 (0.8; 2.90),							
		400 (0.3; 2.48)							
	$\text{CH}_2\text{Cl}_2$	395	540	6.8	0.18	151	835	0.1	0.005
solid	405	527	6.0	0.06	173	2557	0.5	0.04	
${}^{\text{F}}\text{Xyl}^{\text{F}}\text{Bf}$	hexane	256 (54.2; 4.73),	510	6.3	0.30	249	820	0.3	0.1
		290 (2.9; 3.46),							
		386 (0.4; 2.60)							
$p\text{-NMe}_2\text{-}{}^{\text{F}}\text{Xyl}^{\text{F}}\text{Bf}$	hexane	268 (32.3; 4.51),	627	9.3	0.03	9.2 (64%),	-	-	-
		326 (2.7; 3.43),							
		396 (0.3; 2.48)							
						1626 (36%)			

[a] Excited at the respective  $\lambda_{\text{abs,max}}$  of the  $\text{S}_1 \leftarrow \text{S}_0$  transition. [b] The non-radiative rate constants were calculated from  $k_{\text{nr}} = (1 - \Phi_{\text{fl}})/\tau$ . [c] The radiative rate constants were calculated from  $k_{\text{r}} = \Phi_{\text{fl}}/\tau$ .

All borafluorenes exhibit very small extinction coefficients for their lowest energy absorption ( $\epsilon = 300 - 400 \text{ M}^{-1} \text{ cm}^{-1}$ ;  $\log \epsilon = 2.48 - 2.60$ ) which can be classified as weakly allowed transitions,<sup>[223]</sup> similar to those in previously reported boroles and borafluorenes. The lowest energy absorption of  ${}^{\text{F}}\text{Xyl}^{\text{F}}\text{Bf}$  ( $\lambda_{\text{abs,max}} = 386 \text{ nm}$ ) appears to be slightly hypsochromically shifted compared to  ${}^{\text{F}}\text{Mes}^{\text{F}}\text{Bf}$  ( $\lambda_{\text{abs,max}} = 400 \text{ nm}$ ) and  $p\text{-NMe}_2\text{-}{}^{\text{F}}\text{Xyl}^{\text{F}}\text{Bf}$  ( $\lambda_{\text{abs,max}} = 396 \text{ nm}$ ) but, due to the broad absorption bands, this is difficult to determine accurately. All three borafluorenes exhibit broad, structureless emission bands. The emission maximum of  $p\text{-NMe}_2\text{-}{}^{\text{F}}\text{Xyl}^{\text{F}}\text{Bf}$  is strongly bathochromically shifted ( $\lambda_{\text{em,max}} = 627 \text{ nm}$ ) compared to the two non-donor-substituted borafluorene derivatives ( ${}^{\text{F}}\text{Mes}^{\text{F}}\text{Bf}$ :  $\lambda_{\text{em,max}} = 521 \text{ nm}$ ;  ${}^{\text{F}}\text{Xyl}^{\text{F}}\text{Bf}$ :  $\lambda_{\text{em,max}} = 510 \text{ nm}$ ), which indicates that the emission arises from an intramolecular charge transfer (ICT) transition. The quantum yields of  ${}^{\text{F}}\text{Mes}^{\text{F}}\text{Bf}$  ( $\Phi_{\text{fl}} = 0.37$ ; hexane) and  ${}^{\text{F}}\text{Xyl}^{\text{F}}\text{Bf}$  ( $\Phi_{\text{fl}} = 0.30$ ; hexane) are higher than most of the reported borafluorenes (ca. 0.1). In contrast,  $p\text{-NMe}_2\text{-}{}^{\text{F}}\text{Xyl}^{\text{F}}\text{Bf}$  exhibits a very low quantum yield ( $\Phi_{\text{fl}} = 0.03$ ; hexane). To our surprise,  ${}^{\text{F}}\text{Mes}^{\text{F}}\text{Bf}$  and  ${}^{\text{F}}\text{Xyl}^{\text{F}}\text{Bf}$  exhibit very long fluorescent lifetimes in solution ( ${}^{\text{F}}\text{Mes}^{\text{F}}\text{Bf}$ :  $\tau = 224 \text{ ns}$  (hexane);  $\tau = 151 \text{ ns}$  ( $\text{CH}_2\text{Cl}_2$ );  ${}^{\text{F}}\text{Xyl}^{\text{F}}\text{Bf}$ :  $\tau = 249 \text{ ns}$  (hexane)) as well as in the solid state ( ${}^{\text{F}}\text{Mes}^{\text{F}}\text{Bf}$ :  $\tau = 173 \text{ ns}$ ). Similar fluorescence lifetimes (116 – 150 ns) of borafluorenes with

bulky exo-aryl moieties were previously observed by Rugar and co-workers.<sup>[203]</sup> This results in exceptionally long natural lifetimes,  $\tau_0$ , uncommon for organic molecules, for which fluorescence usually takes place on a ns timescale. There are, however, some exceptions such as pyrene.<sup>[93, 224, 225]</sup> This indicates a forbidden process. It is very interesting that even though the radiative rate constants are small for organic chromophores, the non-radiative rate constants are of the same order, resulting in moderate quantum yields. This is likely a result of the high rigidity of the systems. In contrast, ***p*-NMe<sub>2</sub>-<sup>F</sup>Xyl<sup>F</sup>Bf** exhibits two different radiative decay processes, a prompt ( $\tau = 9.2$  ns) and a delayed ( $\tau = 1.6$   $\mu$ s) one. This can be caused by different processes namely TTA (triplet-triplet annihilation)<sup>[226]</sup> or TADF (thermally activated delayed fluorescence).<sup>[54-68, 227]</sup> Due to the low concentrations ( $\leq 10^{-5}$  M) of the compound employed, the lack of dependence on the concentration and the temperature dependence of the lifetime, we can attribute the observed behavior to TADF. The mechanism for TADF is based on a reverse intersystem crossing process (rISC) between the lowest energy triplet state ( $T_1$ ) and excited singlet state ( $S_1$ ) of a molecule. In order for this to occur, the energy difference between  $S_1$  and  $T_1$  ( $\Delta E_{S-T}$ ) has to be sufficiently small. The most common structures to exhibit this phenomenon are twisted dipolar systems with spatially separated HOMO and LUMO such as D(donor)- $\pi$ -A(acceptor) compounds. This structural motif is also found in ***p*-NMe<sub>2</sub>-<sup>F</sup>Xyl<sup>F</sup>Bf**. The singlet-triplet gap ( $\Delta E_{S-T}$ ) can be easily determined experimentally if phosphorescence can be observed. However, for ***p*-NMe<sub>2</sub>-<sup>F</sup>Xyl<sup>F</sup>Bf**, even at 77 K in a frozen glass matrix of 2-MeTHF, no phosphorescence was observed. However,  $\Delta E_{S-T}$  can also be calculated once the rate constant of the rISC process ( $k_{rISC}$ ) is obtained, which is given by the Arrhenius Equation 2.1, or Equation 2.2 as derived by Dias *et al.*<sup>[36]</sup>

Equation 2.1:

$$k_{rISC} = A \exp\left(-\frac{\Delta E_{S-T}}{kT}\right)$$

Equation 2.2:

$$k_{rISC} = \frac{\Phi_{rISC}}{\tau_{DF}} \left( \frac{\Phi_{PF} + \Phi_{DF}}{\Phi_{PF}} \right)$$

with  $\Phi_{DF}$ ,  $\Phi_{PF}$  and  $\Phi_{rISC}$  being the quantum yields of the delayed and prompt fluorescence and the reverse intersystem crossing, respectively. As no phosphorescence was observed at 77 K, but delayed fluorescence was, it can be assumed that  $\Delta E_{S-T}$  is small and, as such, the rate of reverse intersystem crossing is very high, i.e.,  $\Phi_{rISC} = \frac{k_{rISC}}{k_{rISC} + k_{IC}^T + k_{PH}} \approx 1$  and, thus, Equation 2.2 can be modified to give Equation 2.3.

Equation 2.3:

$$k_{rISC} = \frac{1}{\tau_{DF}} \left( \frac{\Phi_{PF} + \Phi_{DF}}{\Phi_{PF}} \right) = \frac{1}{\tau_{DF}} \left( 1 + \frac{\Phi_{DF}}{\Phi_{PF}} \right) = \frac{1}{\tau_{DF}} + \frac{1}{\tau_{DF}} * \frac{\Phi_{DF}}{\Phi_{PF}}$$

The ratio  $\Phi_{DF}/\Phi_{PF}$  can be ascertained from time-resolved measurements via Equation 2.4,

Equation 2.4:

$$\frac{\Phi_{DF}}{\Phi_{PF}} = \frac{B_{DF}\tau_{DF}}{B_{PF}\tau_{DF}}$$

with  $B_{DF}$  and  $B_{PF}$  being the pre-exponential fitting parameters of the time-resolved fluorescence lifetime measurements. As such, Equation 2.1 can be written as Equation 2.5 where all parameters can be obtained from the time-resolved fluorescence decay.

Equation 2.5:

$$k_{rISC} = A \exp\left(-\frac{\Delta E_{S-T}}{kT}\right) = \frac{1}{\tau_{DF}} + \frac{1}{\tau_{DF}} \frac{A_{DF}\tau_{DF}}{A_{PF}\tau_{DF}}$$

Lifetimes were obtained at temperatures between 300 K and 230 K in methylcyclohexane. From the slope of a plot of  $\ln(k_{rISC})$  vs.  $1/T$  (Figure 2.9), we obtain  $\Delta E_{S-T} = 15$  meV, which is comparable to values previously reported for TADF emitters.<sup>[36]</sup>

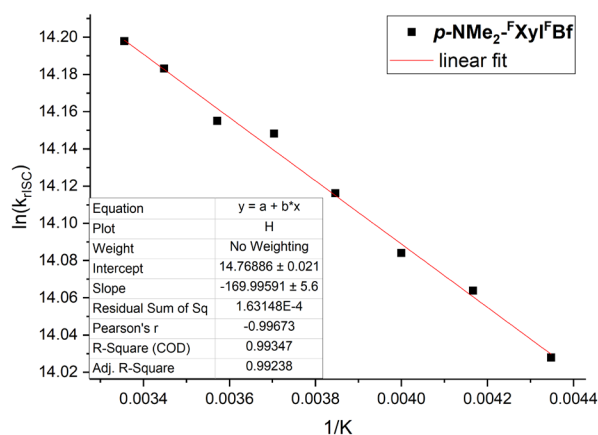


Figure 2.9: Arrhenius plot of  $\ln(k_{rISC})$  of  $p\text{-NMe}_2\text{-FXylF-Bf}$  (determined from temperature-dependent lifetime measurements) vs.  $1/T$ .

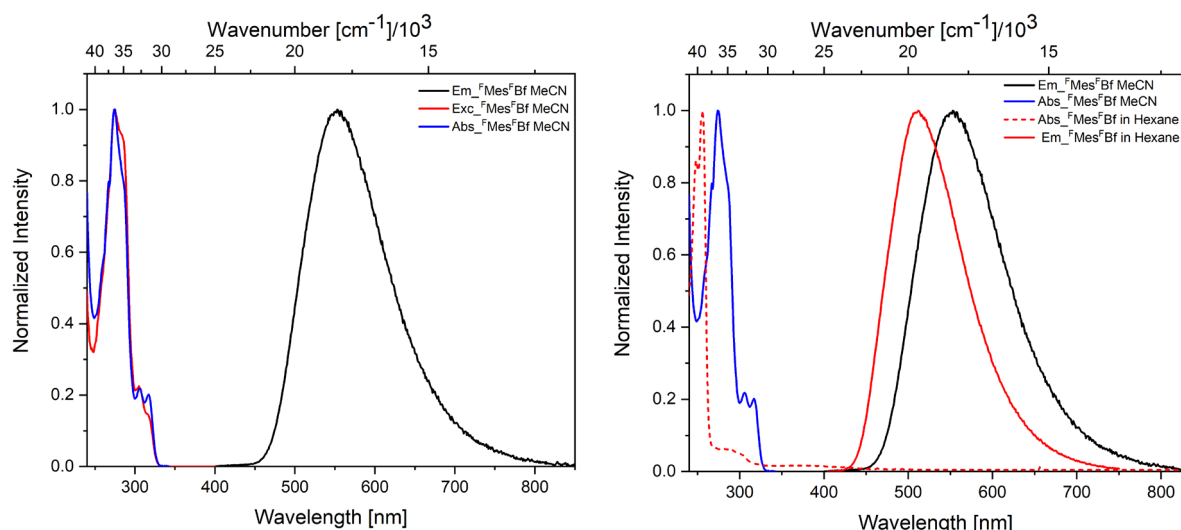


Figure 2.10: Absorption (blue), excitation (red) and emission (black) spectra of  ${}^{\text{F}}\text{Mes}^{\text{F}}\text{Bf}\cdot\text{MeCN}$  (left). Overlaid absorption spectra of  ${}^{\text{F}}\text{Mes}^{\text{F}}\text{Bf}\cdot\text{MeCN}$  in MeCN (Absorption: blue, Emission: black) and  ${}^{\text{F}}\text{Mes}^{\text{F}}\text{Bf}$  (Absorption: red dashed, Emission: red) (right).

Table 2.5: Photophysical data of  ${}^{\text{F}}\text{Mes}^{\text{F}}\text{Bf}\cdot\text{MeCN}$  in MeCN.

Compound	solvent	$\lambda_{\text{abs}}$ [nm]	$\lambda_{\text{em}}$ [nm] <sup>[a]</sup>	apparent	$\Phi_{\text{n}}$	$\tau$ [ns]	$\tau_0$ [ns]	$k_{\text{nr}}$ [ $10^7 \text{ s}^{-1}$ ] <sup>[b]</sup>	$k_{\text{r}}$ [ $10^7 \text{ s}^{-1}$ ] <sup>[c]</sup>
				Stokes shift ( $10^3 \text{ cm}^{-1}$ )					
${}^{\text{F}}\text{Mes}^{\text{F}}\text{Bf}\cdot\text{MeCN}$	MeCN	274, 306, 317	553	13.5	0.08	110	1375	0.8	0.07

[a] Excited at the respective  $\lambda_{\text{abs,max}}$  of the  $S_1 \leftarrow S_0$  transition. [b] The non-radiative rate constants were calculated from  $k_{\text{nr}} = (1 - \Phi_{\text{n}})/\tau$ . [c] The radiative rate constants were calculated from  $k_{\text{r}} = \Phi_{\text{n}}/\tau$ .

The acetonitrile adduct  ${}^{\text{F}}\text{Mes}^{\text{F}}\text{Bf}\cdot\text{MeCN}$  shows two weak absorption maxima at  $\lambda_{\text{abs}} = 317$  and 306 nm and a strong absorption maximum at  $\lambda_{\text{abs}} = 274$  nm (Figure 2.10, Table 2.5). Compared to  ${}^{\text{F}}\text{Mes}^{\text{F}}\text{Bf}$  no lower energy absorption could be observed. This is consistent with a population of the empty  $p_z$ -orbital on the boron center. The emission maximum of  ${}^{\text{F}}\text{Mes}^{\text{F}}\text{Bf}\cdot\text{MeCN}$  at  $\lambda_{\text{em}} = 553$  nm is slightly bathochromically shifted as compared to  ${}^{\text{F}}\text{Mes}^{\text{F}}\text{Bf}$  ( $\lambda_{\text{em}} = 521$  nm in hexane;  $\lambda_{\text{em}} = 540$  nm in  $\text{CH}_2\text{Cl}_2$ ). This is reminiscent of borafluorenes reported by Rugar and co-workers.<sup>[203]</sup> In their systems the *ortho*-methoxymethyl groups of the *exo*-aryl moieties coordinate to the boron center of the borafluorene, forming a four-coordinate species. However, upon photoexcitation, the boron oxygen bond is cleaved and thus the emission can be attributed to the three-coordinate borafluorene species resulting in a remarkable Stokes shift of up to  $16600 \text{ cm}^{-1}$ . This is likely similar to what is observable for  ${}^{\text{F}}\text{Mes}^{\text{F}}\text{Bf}\cdot\text{MeCN}$ . Upon photoexcitation, the acetonitrile dissociates and, as such, the resulting emission can be attributed to the three-coordinate borafluorene  ${}^{\text{F}}\text{Mes}^{\text{F}}\text{Bf}$  leading to a Stokes shift of  $13500 \text{ cm}^{-1}$ .

The observed emission lifetime is comparable to both Rugar's systems (116 – 132 ns) and the free borafluorenes in the present work (151 – 224 ns). Interestingly, only the excitation spectrum corresponding to  ${}^{\text{F}}\text{Mes}^{\text{F}}\text{Bf}\cdot\text{MeCN}$  was observed, which indicates that adduct formation, after the return to the ground state, must be very fast.

### 2.2.5 DFT and TD-DFT Studies

Using the crystal structures as the starting geometries, the ground state structures were optimized via DFT calculations at the B3LYP/6-31G+(d) level of theory. For  ${}^{\text{F}}\text{Mes}^{\text{F}}\text{Bf}$  and  ${}^{\text{F}}\text{Xyl}^{\text{F}}\text{Bf}$ , the optimized ground state structures exhibit  $C_s$  and  $C_{2v}$  symmetries, respectively. For  $p\text{-NMe}_2\text{-}{}^{\text{F}}\text{Xyl}^{\text{F}}\text{Bf}$ , optimization of the GS structure with  $C_{2v}$  symmetry did not lead to a global minimum but rather to a saddle point (1 imaginary frequency remained). However, as the  $C_1$  structure is very close to the  $C_{2v}$  symmetry one, in both geometry and energy, and exhibits almost the same transition dipole moments, the symmetry descriptors will be used as it simplifies the discussion. The optimized structures reproduce the geometries, bond lengths, angles, and shortest B–F contacts of the crystal structures reasonably well. However, as compared to the crystal structures, the optimized structures do not exhibit bending of the *exo*-aryl out of the plane of the borafluorene backbone. As this torsion arises from solid-state interactions, this is to be expected. The highest occupied molecular orbital (HOMO) and lowest unoccupied molecular orbital (LUMO) energies increase from  ${}^{\text{F}}\text{Mes}^{\text{F}}\text{Bf}$  to  ${}^{\text{F}}\text{Xyl}^{\text{F}}\text{Bf}$  to  $p\text{-NMe}_2\text{-}{}^{\text{F}}\text{Xyl}^{\text{F}}\text{Bf}$  (Figure 2.11 and Table 2.6). The calculated LUMO energies fit well with the LUMO energies estimated from the reduction potentials obtained via cyclic voltammetry. Due to the very broad nature of the lowest energy absorption band, the HOMO energies of  ${}^{\text{F}}\text{Mes}^{\text{F}}\text{Bf}$  and  ${}^{\text{F}}\text{Xyl}^{\text{F}}\text{Bf}$  were not calculated from the experimental data.

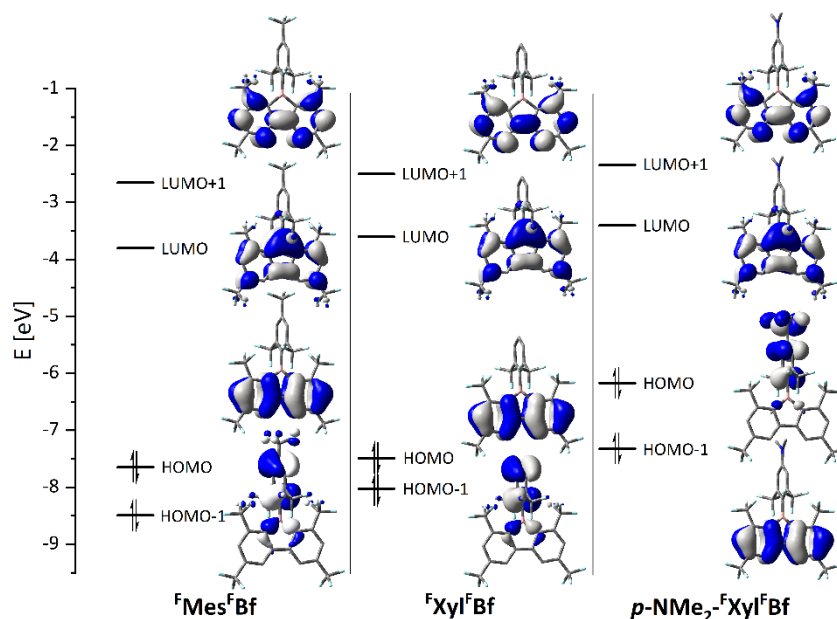


Figure 2.11: Frontier molecular orbitals of  $^{\text{F}}\text{Mes}^{\text{F}}\text{Bf}$  (left),  $^{\text{F}}\text{Xyl}^{\text{F}}\text{Bf}$  (middle), and  $p\text{-NMe}_2\text{-}^{\text{F}}\text{Xyl}^{\text{F}}\text{Bf}$  (right) calculated at the B3LYP/6-31+G(d) level.

Table 2.6: Frontier molecular p orbital energies [eV] and symmetries of  $^{\text{F}}\text{Mes}^{\text{F}}\text{Bf}$ ,  $^{\text{F}}\text{Xyl}^{\text{F}}\text{Bf}$ , and  $p\text{-NMe}_2\text{-}^{\text{F}}\text{Xyl}^{\text{F}}\text{Bf}$  calculated at the B3LYP/6-31+G(d) level.

Symmetry	$^{\text{F}}\text{Mes}^{\text{F}}\text{Bf}$		$^{\text{F}}\text{Xyl}^{\text{F}}\text{Bf}$		$p\text{-NMe}_2\text{-}^{\text{F}}\text{Xyl}^{\text{F}}\text{Bf}$		
	$C_s$		$C_{2v}$		$C_1$	$C_{2v}$	
	calc.	exp. <sup>[a]</sup>	calc.	exp. <sup>[a]</sup>	calc.	calc.	exp. <sup>[a]</sup>
<b>LUMO+1</b> [eV]	-2.66 ( $A^{**}$ )		-2.50 ( $B_1$ )		-2.34 ( $A_1$ )	-2.32 ( $B_1$ )	
<b>LUMO</b> [eV]	-3.80 ( $A^{**}$ )	-4.02	-3.60 ( $B_1$ )	-3.95	-3.41 ( $A_1$ )	-3.42 ( $B_1$ )	-3.88
<b>HOMO</b> [eV]	-7.65 ( $A^{**}$ )		-7.49 ( $A_2$ )		-6.17 ( $A_1$ )	-6.16 ( $B_2$ )	-6.11
<b>HOMO-1</b> [eV]	-8.49 ( $A^*$ )		-8.03 ( $B_2$ )		-7.32 ( $A_1$ )	-7.41 ( $A_2$ )	

<sup>a</sup> Determined from the half wave potentials: HOMO =  $-(5.16+E_{1/2,ox})$  eV, LUMO =  $-(5.16+E_{1/2,red})$  eV.<sup>[157-159]</sup>

The LUMOs are all localized on the borofluorene moieties with their largest components on boron, and the energies differ by only 0.2-0.4 eV. For  $^{\text{F}}\text{Mes}^{\text{F}}\text{Bf}$  and  $^{\text{F}}\text{Xyl}^{\text{F}}\text{Bf}$  the HOMOs are also localized on the borofluorene moieties with boron lying on a nodal plane and are energetically similar ( $\Delta E = 0.16$  eV). The HOMO of  $p\text{-NMe}_2\text{-}^{\text{F}}\text{Xyl}^{\text{F}}\text{Bf}$  is localized on the *exo*-aryl moiety and lies about 1.4 eV higher in energy than the HOMOs of  $^{\text{F}}\text{Mes}^{\text{F}}\text{Bf}$  and  $^{\text{F}}\text{Xyl}^{\text{F}}\text{Bf}$ . This is due to the electron donating effect of the *para*-dimethylamino-group that increases the energy of the *exo*-aryl fragment MO thereby raising it above the borofluorene-centered orbital which is now HOMO-1. For both  $^{\text{F}}\text{Mes}^{\text{F}}\text{Bf}$  and  $^{\text{F}}\text{Xyl}^{\text{F}}\text{Bf}$ , HOMO-1 is localized on the *exo*-aryl moiety; however, due to the *para*- $\text{CF}_3$ -group, the HOMO-1 of  $^{\text{F}}\text{Mes}^{\text{F}}\text{Bf}$  is about 0.5 eV lower in energy. Based on the optimized ground state structures the nucleus-independent chemical shift (NICS) values of the borofluorenes were calculated (Table 2.7).



Table 2.7: NICS(1)<sub>zz</sub> values of the borole moiety of <sup>F</sup>Mes<sup>F</sup>Bf, <sup>F</sup>Xyl<sup>F</sup>Bf, *p*-NMe<sub>2</sub>-<sup>F</sup>Xyl<sup>F</sup>Bf, and **TipBf** calculated at the B3LYP/6-311+G(d) level.

Compound	NICS(1) <sub>zz</sub>	
	Calc.	Lit.
<sup>F</sup> Mes <sup>F</sup> Bf	20.7	
<sup>F</sup> Xyl <sup>F</sup> Bf	20.2	
<i>p</i> -NMe <sub>2</sub> - <sup>F</sup> Xyl <sup>F</sup> Bf	20.0	
<b>TipBf</b>	24.3	24.5 <sup>[219]</sup>

It is apparent that the perfluoroalkylated borafluorenes exhibit lower NICS(1)<sub>zz</sub> values as compared to that of the borafluorene **TipBf** which does not contain CF<sub>3</sub>-groups. This suggests a higher degree of delocalization of the electron density over the borafluorene backbone in our compounds. Thus, the antiaromatic character is less than in non-trifluoromethylated borafluorenes. The optimized structures were then used for TD-DFT calculations to simulate the absorption spectra. Time-dependent DFT calculations on <sup>F</sup>Mes<sup>F</sup>Bf and <sup>F</sup>Xyl<sup>F</sup>Bf were carried out at the B3LYP/6-31+G(d) level of theory whereas for the donor substituted *p*-NMe<sub>2</sub>-<sup>F</sup>Xyl<sup>F</sup>Bf the Coulomb-attenuated functional CAM-B3LYP was employed using the same basis set (Table 2.8), as CAM-B3LYP is better suited to systems involving charge transfer.<sup>[228, 229]</sup> Furthermore, the optimized S<sub>1</sub>-state geometries of <sup>F</sup>Mes<sup>F</sup>Bf and <sup>F</sup>Xyl<sup>F</sup>Bf were obtained. In order to characterize the nature of the transition the overlap coefficients ( $\Lambda$ ) were determined.<sup>[228]</sup> The calculated lowest energy absorptions of the borafluorenes fit well with the experimental values. For all compounds, the lowest energy transitions are predominantly of HOMO to LUMO character.

Table 2.8: Lowest energy and highest oscillator strength absorptions and emissions of  ${}^F\text{Mes}^F\text{Bf}$  and  ${}^F\text{Xyl}^F\text{Bf}$  calculated at the B3LYP/6-31+G(d) level of theory and lowest energy absorptions of  $p\text{-NMe}_2\text{-}{}^F\text{Xyl}^F\text{Bf}$  calculated at the CAM-B3LYP/6-31+G(d) level of theory.

Compound	State	E [eV]	$\lambda$ [nm]	$\lambda_{\text{exp}}$ [nm]	$f$	Sym- metry	Major contributions	$\Lambda$
${}^F\text{Mes}^F\text{Bf}$ ( $C_s$ )	$S_1 \leftarrow S_0$	3.05	406	400	0.0005	A'	HOMO $\rightarrow$ LUMO (99%)	0.65
	$S_2 \leftarrow S_0$	3.90	318		0	A''	HOMO-1 $\rightarrow$ LUMO (99%)	0.25
	$S_7 \leftarrow S_0$	4.80	258	257	0.8333	A'	HOMO-2 $\rightarrow$ LUMO (24%), HOMO $\rightarrow$ LUMO+1 (70%)	0.73
	$S_1 \rightarrow S_0$	2.22	559	521	0.0038	A	H-SOMO $\leftarrow$ L-SOMO (99%)	
${}^F\text{Xyl}^F\text{Bf}$ ( $C_{2v}$ )	$S_1 \leftarrow S_0$	3.09	401	385	0.0006	$B_2$	HOMO $\rightarrow$ LUMO (99%)	0.66
	$S_2 \leftarrow S_0$	3.64	340		0	$A_2$	HOMO-1 $\rightarrow$ LUMO (99%)	0.23
	$S_6 \leftarrow S_0$	4.81	258	256	0.8413	$B_2$	HOMO-3 $\rightarrow$ LUMO (28%), HOMO $\rightarrow$ LUMO+1 (68%)	0.74
	$S_1 \rightarrow S_0$	2.34	531	510	0.0030	A	H-SOMO $\leftarrow$ L-SOMO (99%)	
$p\text{-NMe}_2\text{-}{}^F\text{Xyl}^F\text{Bf}$ ( $C_i$ )	$S_1 \leftarrow S_0$	3.25	382	396	0	A	HOMO $\rightarrow$ LUMO (92%)	0.15
	$S_2 \leftarrow S_0$	3.46	358	326	0.0006	A	HOMO-1 $\rightarrow$ LUMO (97%)	0.67
	$S_3 \leftarrow S_0$	4.25	292	270	0.0491	A	HOMO $\rightarrow$ L+2 (70%), HOMO $\rightarrow$ L+3 (24%)	0.49
	$S_8 \leftarrow S_0$	5.11	243	256	0.6022	A	HOMO $\rightarrow$ L+4 (86%)	0.71

For both  ${}^F\text{Mes}^F\text{Bf}$  and  ${}^F\text{Xyl}^F\text{Bf}$  these can be classified as locally excited (LE) transitions ( $\Lambda \approx 0.65$ ) as both HOMO and LUMO are localized on the borrafluorene backbone. This is surprising, as LE transitions usually exhibit high extinction coefficients and  ${}^F\text{Mes}^F\text{Bf}$  and  ${}^F\text{Xyl}^F\text{Bf}$  exhibit weakly allowed lowest energy absorptions. However, the calculated oscillator strengths of the  $S_1 \leftarrow S_0$  transitions of  ${}^F\text{Mes}^F\text{Bf}$  and  ${}^F\text{Xyl}^F\text{Bf}$  are also very small. From the symmetries of the frontier molecular orbitals it is possible to determine whether these transitions are forbidden by symmetry. The symmetries of the HOMOs of  ${}^F\text{Mes}^F\text{Bf}$  ( $C_s$ ) and  ${}^F\text{Xyl}^F\text{Bf}$  ( $C_{2v}$ ) are A'' and  $A_2$ , respectively, and the LUMO symmetries are A'' and  $B_1$ . Transitions are allowed by symmetry if the initial and final states multiplied by the x-, y-, and z-characters of the electronic dipole operator contain the totally symmetric irreducible representation ( $C_s$ : A' and  $C_{2v}$ :  $A_1$ ). For  ${}^F\text{Mes}^F\text{Bf}$  ( $C_s$ ), the lowest energy transition is forbidden in the z-direction, while x and y are allowed, making the transition an allowed transition. For  ${}^F\text{Xyl}^F\text{Bf}$  ( $C_{2v}$ ), the x- and z-directions are forbidden, while the y-direction is allowed, making the transition an allowed transition. However, for both molecules, the dipole moment is oriented along the z-axis, resulting in a very small transition dipole moment in the x- and y-directions, which results in very low oscillator strengths. So, the lowest energy transitions are allowed, but exhibit only small changes in dipole

moment resulting in weak absorptions. This can be, in part, attributed to the boron center, as its contribution to the LUMO gives the transition a  $\pi$ -n character. The  $S_2 \leftarrow S_0$  transitions, in both cases, are predominantly HOMO-1 to LUMO transitions. The HOMO-1 of  ${}^F\text{Mes}^F\text{Bf}$  and  ${}^F\text{Xyl}^F\text{Bf}$  are of  $A'$  and  $B_2$  symmetry, respectively, and, thus, are symmetry-forbidden. Both  ${}^F\text{Mes}^F\text{Bf}$  and  ${}^F\text{Xyl}^F\text{Bf}$ , exhibit large oscillator strengths for their  $S_7 \leftarrow S_0$  and  $S_6 \leftarrow S_0$  transitions, respectively. In both cases, these transitions have predominantly HOMO to LUMO+1 character. Both HOMO and LUMO+1 are delocalized over the borafluorene backbone without contributions from the boron center. The optimized  $S_1$  geometries of  ${}^F\text{Mes}^F\text{Bf}$  and  ${}^F\text{Xyl}^F\text{Bf}$  differ only slightly from their ground state structures (Figure 2.12).

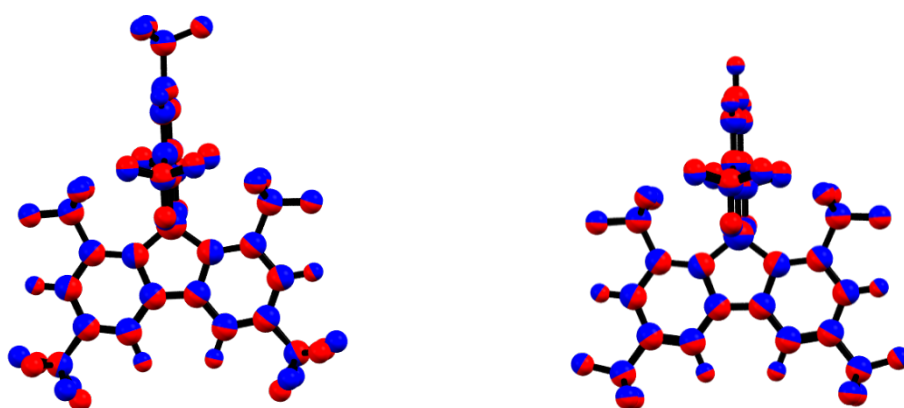


Figure 2.12: Overlap of the optimized ground state (blue) and  $S_1$  (red) geometries of  ${}^F\text{Mes}^F\text{Bf}$  (left) and  ${}^F\text{Xyl}^F\text{Bf}$  (right).

In comparison, in the  $S_1$  structure of  ${}^F\text{Mes}^F\text{Bf}$ , only the *para*- $\text{CF}_3$ -groups on the borafluorene backbone are rotated and in both  ${}^F\text{Mes}^F\text{Bf}$  and  ${}^F\text{Xyl}^F\text{Bf}$  the *ortho*- $\text{CF}_3$ -groups on the *exo*-aryl are slightly bent away from the boron center. The calculated emission maxima of  ${}^F\text{Mes}^F\text{Bf}$  and  ${}^F\text{Xyl}^F\text{Bf}$ , fit the experimental data in hexane and exhibit very low oscillator strengths. Even though the optimized structures do not exhibit a higher symmetry it can be assumed that a similar phenomenon as for the absorption takes place and is the reason for the observed long lifetimes. Interestingly, as previously discussed, the reasonably high quantum yields observed are due to extremely slow non-radiative decay processes.

The photophysical properties of *p*- $\text{NMe}_2$ - ${}^F\text{Xyl}^F\text{Bf}$  differ strongly from those of  ${}^F\text{Mes}^F\text{Bf}$  and  ${}^F\text{Xyl}^F\text{Bf}$ . This is, in part, because the nature of the lowest energy absorption has CT rather than LE character ( $\Lambda = 0.15$ ). This is not surprising, as *p*- $\text{NMe}_2$ - ${}^F\text{Xyl}^F\text{Bf}$  is a donor-acceptor system. The  $S_1 \leftarrow S_0$  transition of *p*- $\text{NMe}_2$ - ${}^F\text{Xyl}^F\text{Bf}$  exhibits an oscillator strength of 0. Using the optimized structure of  $C_{2v}$  symmetry as an approximation, it becomes apparent that this transition is symmetry forbidden and, furthermore, the overlap between HOMO and LUMO is minuscule due to the nearly perpendicular arrangement of the *exo*-aryl group with respect to

the borafluorene core. The HOMO is of B<sub>2</sub> symmetry and the LUMO has B<sub>1</sub> symmetry. This is the same as for the S<sub>2</sub>←S<sub>0</sub> transitions of <sup>F</sup>Mes<sup>F</sup>Bf and <sup>F</sup>Xyl<sup>F</sup>Bf, as the HOMO and HOMO-1 are inverted compared to those of *p*-NMe<sub>2</sub>-<sup>F</sup>Xyl<sup>F</sup>Bf. For *p*-NMe<sub>2</sub>-<sup>F</sup>Xyl<sup>F</sup>Bf, however, the S<sub>2</sub>←S<sub>0</sub> transition is allowed, but analogously to the <sup>F</sup>Mes<sup>F</sup>Bf and <sup>F</sup>Xyl<sup>F</sup>Bf cases, exhibits a very low oscillator strength. This explains the low extinction coefficient observed for the lowest energy absorption of *p*-NMe<sub>2</sub>-<sup>F</sup>Xyl<sup>F</sup>Bf. Furthermore, we optimized the S<sub>1</sub> structure of *p*-NMe<sub>2</sub>-<sup>F</sup>Xyl<sup>F</sup>Bf as well as its T<sub>1</sub> structure in order to calculate the S<sub>1</sub>-T<sub>1</sub> energy gap. Both optimizations were carried out using the PCM solvent correction model due to the charge transfer nature of the transitions and the high dipole moment of both S<sub>1</sub> and T<sub>1</sub>. Comparing the energies of both structures results in ΔE<sub>S-T</sub> = 423 meV which is almost 30 times higher than the experimentally determined gap. It is noteworthy that the experimental determination of the gap is highly flawed due to approximations as well as unpredictable solvent effects at lower temperature. However, this should still give a good estimate, but the calculations fail to match the experimental value at this level of theory, illustrating the difficulty of predicting phenomena such as TADF accurately.

## 2.3 Conclusion

Herein, we report the synthesis and properties of three trifluoromethylated borafluorenes <sup>F</sup>Mes<sup>F</sup>Bf, <sup>F</sup>Xyl<sup>F</sup>Bf, and *p*-NMe<sub>2</sub>-<sup>F</sup>Xyl<sup>F</sup>Bf. The copper-catalyzed homocoupling of boronate esters provides a convenient route to 2,2'-dibromobiphenyl derivatives, which can be lithiated and then reacted with stable and accessible aryl-BF<sub>3</sub>K salts for the synthesis of borafluorenes. All of the borafluorenes exhibit a rigid geometry with the *exo*-aryl group lying perpendicular to the borafluorene plane. All three borafluorenes exhibit exceptionally positively shifted reduction potentials, emphasizing the electron withdrawing nature of the CF<sub>3</sub>-groups. This allowed us to use a mild reducing agent (CoCp<sub>2</sub> E<sup>0</sup> = -1.3 eV vs. Fc/Fc<sup>+</sup>) to reduce the most anodically shifted borafluorene <sup>F</sup>Mes<sup>F</sup>Bf. The resulting radical anion of <sup>F</sup>Mes<sup>F</sup>Bf exhibits a strong delocalization of the additional electron over the borafluorene backbone as evidenced by EPR spectroscopy and its solid-state structure. The trifluoromethylated borafluorenes exhibit unusually long excited state lifetimes and weakly allowed lowest energy transitions. For <sup>F</sup>Mes<sup>F</sup>Bf and <sup>F</sup>Xyl<sup>F</sup>Bf, this is the result of the transitions being forbidden in the z-direction which coincides with the dipole moment and the transition dipole moment being negligible in the x- and y-directions. The same is apparently true for their emissions, as both compounds exhibit fluorescence lifetimes of τ > 200 ns in hexane. Even with small oscillator strengths, the two compounds exhibit fluorescence quantum yields of 0.37 and 0.30, respectively, as their

rigidity results in exceptionally slow non-radiative decay. In contrast, the twisted donor-acceptor system *p*-NMe<sub>2</sub>-<sup>F</sup>Xyl<sup>F</sup>Bf has a symmetry-forbidden lowest energy transition and exhibits TADF, with a singlet-triplet energy gap  $\Delta E_{S-T}$  experimentally determined to be only 15 meV. <sup>F</sup>Mes<sup>F</sup>Bf and <sup>F</sup>Xyl<sup>F</sup>Bf are highly stable towards hydrolysis, which makes them interesting potential building blocks for organic materials.

## 2.4 References

- [36] F. B. Dias, T. J. Penfold, A. P. Monkman, *Methods Appl. Fluores.* **2017**, *5*, 012001.
- [54] K. Suzuki, S. Kubo, K. Shizu, T. Fukushima, A. Wakamiya, Y. Murata, C. Adachi, H. Kaji, *Angew. Chem. Int. Ed.* **2015**, *54*, 15231-15235; *Angew. Chem.* **2015**, *127*, 15446-15450.
- [55] Y. Kitamoto, T. Namikawa, D. Ikemizu, Y. Miyata, T. Suzuki, H. Kita, T. Sato, S. Oi, *J. Mater. Chem. C* **2015**, *3*, 9122-9130.
- [56] M. Numata, T. Yasuda, C. Adachi, *Chem. Commun.* **2015**, *51*, 9443-9446.
- [57] T. Hatakeyama, K. Shiren, K. Nakajima, S. Nomura, S. Nakatsuka, K. Kinoshita, J. Ni, Y. Ono, T. Ikuta, *Adv. Mater.* **2016**, *28*, 2777-2781.
- [58] Y. Kitamoto, T. Namikawa, T. Suzuki, Y. Miyata, H. Kita, T. Sato, S. Oi, *Org. Electron.* **2016**, *34*, 208-217.
- [59] C. Tu, W. Liang, *ACS Omega* **2017**, *2*, 3098-3109.
- [60] Y.-J. Lien, T.-C. Lin, C.-C. Yang, Y.-C. Chiang, C.-H. Chang, S.-H. Liu, Y.-T. Chen, G.-H. Lee, P.-T. Chou, C.-W. Lu, Y. Chi, *ACS Appl. Mater. Interfaces* **2017**, *9*, 27090-27101.
- [61] Y. H. Lee, S. Park, J. Oh, J. W. Shin, J. Jung, S. Yoo, M. H. Lee, *ACS Appl. Mater. Interfaces* **2017**, *9*, 24035-24042.
- [62] C.-C. Tsai, W.-C. Huang, H.-Y. Chih, Y.-C. Hsh, C.-W. Liao, C.-H. Lin, Y.-X. Kang, C.-H. Chang, Y. J. Chang, C.-W. Lu, *Org. Electron.* **2018**, *63*, 166-174.
- [63] M.-Y. Zhang, Z.-Y. Li, B. Lu, Y. Wang, Y.-D. Ma, C.-H. Zhao, *Org. Lett.* **2018**, *20*, 6868-6871.
- [64] T.-L. Wu, M.-J. Huang, C.-C. Lin, P.-Y. Huang, T.-Y. Chou, R.-W. Chen-Cheng, H.-W. Lin, R.-S. Liu, C.-H. Cheng, *Nat. Photonics* **2018**, *12*, 235-240.
- [65] I. S. Park, K. Matsuo, N. Aizawa, T. Yasuda, *Adv. Funct. Mater.* **2018**, *28*, 1802031.
- [66] S.-Y. Li, Z.-B. Sun, C.-H. Zhao, *ACS Omega* **2018**, *3*, 12730-12736.
- [67] D.-G. Chen, T.-C. Lin, C.-L. Chen, Y.-T. Chen, Y.-A. Chen, G.-H. Lee, P.-T. Chou, C.-W. Liao, P.-C. Chiu, C.-H. Chang, Y.-J. Lien, Y. Chi, *ACS Appl. Mater. Interfaces* **2018**, *10*, 12886-12896.
- [68] M. Stanoppi, A. Lorbach, *Dalton Trans.* **2018**, *47*, 10394-10398.
- [69] C. D. Entwistle, T. B. Marder, *Angew. Chem. Int. Ed.* **2002**, *41*, 2927-2931; *Angew. Chem.* **2002**, *114*, 3051-3056.
- [70] C. D. Entwistle, T. B. Marder, *Chem. Mater.* **2004**, *16*, 4574-4585.
- [71] S. Yamaguchi, A. Wakamiya, *Pure Appl. Chem.* **2006**, *78*, 1413.
- [72] F. Jäkle, *Coord. Chem. Rev.* **2006**, *250*, 1107-1121.
- [73] M. Elbing, G. C. Bazan, *Angew. Chem. Int. Ed.* **2008**, *47*, 834-838; *Angew. Chem.* **2008**, *120*, 846-850.
- [74] Z. M. Hudson, S. Wang, *Acc. Chem. Res.* **2009**, *42*, 1584-1596.
- [75] C. R. Wade, A. E. J. Broomsgrrove, S. Aldridge, F. P. Gabbaï, *Chem. Rev.* **2010**, *110*, 3958-3984.
- [76] Z. M. Hudson, S. Wang, *Dalton Trans.* **2011**, *40*, 7805-7816.
- [77] A. Wakamiya, S. Yamaguchi, *Bull. Chem. Soc. Jpn.* **2015**, *88*, 1357-1377.
- [78] L. Ji, S. Griesbeck, T. B. Marder, *Chem. Sci.* **2017**, *8*, 846-863.
- [79] S.-Y. Li, Z.-B. Sun, C.-H. Zhao, *Inorg. Chem.* **2017**, *56*, 8705-8717.
- [80] G. Turkoglu, M. E. Cinar, T. Ozturk, *Molecules* **2017**, *22*, 1522.
- [81] N. Matsumi, K. Naka, Y. Chujo, *J. Am. Chem. Soc.* **1998**, *120*, 5112-5113.
- [82] S. Yamaguchi, S. Akiyama, K. Tamao, *J. Am. Chem. Soc.* **2000**, *122*, 6335-6336.
- [83] W.-L. Jia, D. Song, S. Wang, *J. Org. Chem.* **2003**, *68*, 701-705.
- [84] A. Wakamiya, T. Ide, S. Yamaguchi, *J. Am. Chem. Soc.* **2005**, *127*, 14859-14866.

- [85] I. Yamaguchi, B.-J. Choi, T.-A. Koizumi, K. Kubota, T. Yamamoto, *Macromolecules* **2007**, *40*, 438-443.
- [86] U. Megerle, F. Selmaier, C. Lambert, E. Riedle, S. Lochbrunner, *Phys. Chem. Chem. Phys.* **2008**, *10*, 6245-6251.
- [87] A. Lorbach, M. Bolte, H. Li, H.-W. Lerner, M. C. Holthausen, F. Jäkle, M. Wagner, *Angew. Chem. Int. Ed.* **2009**, *48*, 4584-4588; *Angew. Chem.* **2009**, *121*, 4654-4658.
- [88] L. Weber, V. Werner, M. A. Fox, T. B. Marder, S. Schwedler, A. Brockhinke, H.-G. Stammler, B. Neumann, *Dalton Trans.* **2009**, 2823-2831.
- [89] L. Weber, D. Eickhoff, T. B. Marder, M. A. Fox, P. J. Low, A. D. Dwyer, D. J. Tozer, S. Schwedler, A. Brockhinke, H.-G. Stammler, B. Neumann, *Chem. Eur. J.* **2012**, *18*, 1369-1382.
- [90] C. Reus, S. Weidlich, M. Bolte, H.-W. Lerner, M. Wagner, *J. Am. Chem. Soc.* **2013**, *135*, 12892-12907.
- [91] X. Yin, J. Chen, R. A. Lalancette, T. B. Marder, F. Jäkle, *Angew. Chem. Int. Ed.* **2014**, *53*, 9761-9765; *Angew. Chem.* **2014**, *126*, 9919-9923.
- [92] Z. Zhang, R. M. Edkins, J. Nitsch, K. Fucke, A. Eichhorn, A. Steffen, Y. Wang, T. B. Marder, *Chem. Eur. J.* **2015**, *21*, 177-190.
- [93] J. Merz, J. Fink, A. Friedrich, I. Krummenacher, H. H. Al Mamari, S. Lorenzen, M. Haehnel, A. Eichhorn, M. Moos, M. Holzappel, H. Braunschweig, C. Lambert, A. Steffen, L. Ji, T. B. Marder, *Chem. Eur. J.* **2017**, *23*, 13164-13180.
- [94] J. Merz, A. Steffen, J. Nitsch, J. Fink, C. B. Schürger, A. Friedrich, I. Krummenacher, H. Braunschweig, M. Moos, D. Mims, C. Lambert, T. B. Marder, *Chem. Sci.* **2019**, *10*, 7516-7534.
- [96] Z. Yuan, N. J. Taylor, T. B. Marder, I. D. Williams, S. K. Kurtz, L.-T. Cheng, *J. Chem. Soc., Chem. Commun.* **1990**, 1489-1492.
- [100] Z. Yuan, N. J. Taylor, Y. Sun, T. B. Marder, I. D. Williams, L.-T. Cheng, *J. Organomet. Chem.* **1993**, *449*, 27-37.
- [101] Z. Yuan, N. J. Taylor, R. Ramachandran, T. B. Marder, *Appl. Organomet. Chem.* **1996**, *10*, 305-316.
- [103] Z.-Q. Liu, Q. Fang, D. Wang, G. Xue, W.-T. Yu, Z.-S. Shao, M.-H. Jiang, *Chem. Commun.* **2002**, 2900-2901.
- [104] Z.-Q. Liu, Q. Fang, D. Wang, D.-X. Cao, G. Xue, W.-T. Yu, H. Lei, *Chem. Eur. J.* **2003**, *9*, 5074-5084.
- [106] M. Charlot, L. Porres, C. D. Entwistle, A. Beeby, T. B. Marder, M. Blanchard-Desce, *Phys. Chem. Chem. Phys.* **2005**, *7*, 600-606.
- [108] Z. Yuan, C. D. Entwistle, J. C. Collings, D. Albesa-Jové, A. S. Batsanov, J. A. K. Howard, N. J. Taylor, H. M. Kaiser, D. E. Kaufmann, S.-Y. Poon, W.-Y. Wong, C. Jardin, S. Fathallah, A. Boucekkine, J.-F. Halet, T. B. Marder, *Chem. Eur. J.* **2006**, *12*, 2758-2771.
- [109] C. D. Entwistle, J. C. Collings, A. Steffen, L.-O. Pålsson, A. Beeby, D. Albesa-Jové, J. M. Burke, A. S. Batsanov, J. A. K. Howard, J. A. Mosely, S.-Y. Poon, W.-Y. Wong, F. Ibersiene, S. Fathallah, A. Boucekkine, J.-F. Halet, T. B. Marder, *J. Mater. Chem.* **2009**, *19*, 7532-7544.
- [110] J. C. Collings, S.-Y. Poon, C. Le Droumaguet, M. Charlot, C. Katan, L.-O. Pålsson, A. Beeby, J. A. Mosely, H. M. Kaiser, D. Kaufmann, W.-Y. Wong, M. Blanchard-Desce, T. B. Marder, *Chem. Eur. J.* **2009**, *15*, 198-208.
- [113] L. Ji, R. M. Edkins, L. J. Sewell, A. Beeby, A. S. Batsanov, K. Fucke, M. Drafz, J. A. K. Howard, O. Moutounet, F. Ibersiene, A. Boucekkine, E. Furet, Z. Liu, J.-F. Halet, C. Katan, T. B. Marder, *Chem. Eur. J.* **2014**, *20*, 13618-13635.
- [114] P. Chen, A. S. Marshall, S. H. Chi, X. Yin, J. W. Perry, F. Jäkle, *Chem. Eur. J.* **2015**, *21*, 18237-18247.

- [115] S. Griesbeck, Z. Zhang, M. Gutmann, T. Lühmann, R. M. Edkins, G. Clermont, A. N. Lazar, M. Haehnel, K. Edkins, A. Eichhorn, M. Blanchard-Desce, L. Meinel, T. B. Marder, *Chem. Eur. J.* **2016**, *22*, 14701-14706.
- [116] S. Griesbeck, E. Michail, C. Wang, H. Ogasawara, S. Lorenzen, L. Gerstner, T. Zang, J. Nitsch, Y. Sato, R. Bertermann, M. Taki, C. Lambert, S. Yamaguchi, T. B. Marder, *Chem. Sci.* **2019**, *10*, 5405-5422.
- [118] S. Griesbeck, E. Michail, F. Rauch, H. Ogasawara, C. Wang, Y. Sato, R. M. Edkins, Z. Zhang, M. Taki, C. Lambert, S. Yamaguchi, T. B. Marder, *Chem. Eur. J.* **2019**, *25*, 13164-13175.
- [119] S. Yamaguchi, S. Akiyama, K. Tamao, *J. Am. Chem. Soc.* **2001**, *123*, 11372-11375.
- [120] T. W. Hudnall, C.-W. Chiu, F. P. Gabbaï, *Acc. Chem. Res.* **2009**, *42*, 388-397.
- [122] Y. Shirota, *J. Mater. Chem.* **2000**, *10*, 1-25.
- [123] A. Wakamiya, K. Mori, S. Yamaguchi, *Angew. Chem. Int. Ed.* **2007**, *46*, 4273-4276; *Angew. Chem.* **2007**, *119*, 4351-4354.
- [124] S. Toyota, M. Asakura, M. Oki, F. Toda, *Bull. Chem. Soc. Jpn.* **2000**, *73*, 2357-2362.
- [125] S. M. Cornet, K. B. Dillon, C. D. Entwistle, M. A. Fox, A. E. Goeta, H. P. Goodwin, T. B. Marder, A. L. Thompson, *Dalton Trans.* **2003**, 4395-4405.
- [127] J. Wang, Y. Wang, T. Taniguchi, S. Yamaguchi, S. Irle, *J. Phys. Chem. A* **2012**, *116*, 1151-1158.
- [131] Z. Zhang, R. M. Edkins, J. Nitsch, K. Fucke, A. Steffen, L. E. Longobardi, D. W. Stephan, C. Lambert, T. B. Marder, *Chem. Sci.* **2015**, *6*, 308-321.
- [132] Z. Zhang, R. M. Edkins, M. Haehnel, M. Wehner, A. Eichhorn, L. Mailänder, M. Meier, J. Brand, F. Brede, K. Müller-Buschbaum, H. Braunschweig, T. B. Marder, *Chem. Sci.* **2015**, *6*, 5922-5927.
- [134] X. Yin, F. Guo, R. A. Lalancette, F. Jäkle, *Macromolecules* **2016**, *49*, 537-546.
- [136] R. J. Blagg, E. J. Lawrence, K. Resner, V. S. Oganessian, T. J. Herrington, A. E. Ashley, G. G. Wildgoose, *Dalton Trans.* **2016**, *45*, 6023-6031.
- [144] T. Ishiyama, J. Takagi, K. Ishida, N. Miyaura, N. R. Anastasi, J. F. Hartwig, *J. Am. Chem. Soc.* **2002**, *124*, 390-391.
- [147] A. J. J. Lennox, G. C. Lloyd-Jones, *Chem. Soc. Rev.* **2014**, *43*, 412-443.
- [148] G. A. Molander, *J. Org. Chem.* **2015**, *80*, 7837-7848.
- [149] K. Schickedanz, T. Trageser, M. Bolte, H.-W. Lerner, M. Wagner, *Chem. Commun.* **2015**, *51*, 15808-15810.
- [150] K. Schickedanz, J. Radtke, M. Bolte, H.-W. Lerner, M. Wagner, *J. Am. Chem. Soc.* **2017**, *139*, 2842-2851.
- [151] S. Konishi, T. Iwai, M. Sawamura, *Organometallics* **2018**, *37*, 1876-1883.
- [152] M. W. Drover, K. Nagata, J. C. Peters, *Chem. Commun.* **2018**, *54*, 7916-7919.
- [153] X. Jia, J. Nitsch, L. Ji, Z. Wu, A. Friedrich, F. Kerner, M. Moos, C. Lambert, T. B. Marder, *Chem. Eur. J.* **2019**, *25*, 10845-10857.
- [156] M. Mantina, A. C. Chamberlin, R. Valero, C. J. Cramer, D. G. Truhlar, *J. Phys. Chem. A* **2009**, *113*, 5806-5812.
- [157] N. G. Connelly, W. E. Geiger, *Chem. Rev.* **1996**, *96*, 877-910.
- [158] D. Tsiplakides, D. Archonta, C. G. Vayenas, *Top. Catal.* **2007**, *44*, 469-479.
- [159] D. Reitzenstein, T. Quast, F. Kanal, M. Kullmann, S. Ruetzel, M. S. Hammer, C. Deibel, V. Dyakonov, T. Brixner, C. Lambert, *Chem. Mater.* **2010**, *22*, 6641-6655.
- [162] R. Stahl, C. Lambert, C. Kaiser, R. Wortmann, R. Jakober, *Chem. Eur. J.* **2006**, *12*, 2358-2370.
- [163] C. Dou, S. Saito, K. Matsuo, I. Hisaki, S. Yamaguchi, *Angew. Chem. Int. Ed.* **2012**, *51*, 12206-12210; *Angew. Chem.* **2012**, *124*, 12372-12376.
- [164] C. Hoffend, M. Diefenbach, E. Januszewski, M. Bolte, H. W. Lerner, M. C. Holthausen, M. Wagner, *Dalton Trans.* **2013**, *42*, 13826-13837.



- [165] A. Escande, M. J. Ingleson, *Chem. Commun.* **2015**, 51, 6257-6274.
- [166] V. M. Hertz, N. Ando, M. Hirai, M. Bolte, H.-W. Lerner, S. Yamaguchi, M. Wagner, *Organometallics* **2016**, 36, 2512-2519.
- [167] B. Su, R. Kinjo, *Synthesis* **2017**, 49, 2985-3034.
- [168] E. von Grotthuss, A. John, T. Kaese, M. Wagner, *Asian J. Org. Chem.* **2018**, 7, 37-53.
- [169] Y. Su, R. Kinjo, *Chem. Soc. Rev.* **2019**, 48, 3613-3659.
- [170] Z. Zhou, A. Wakamiya, T. Kushida, S. Yamaguchi, *J. Am. Chem. Soc.* **2012**, 134, 4529-4532.
- [171] J. Yoshino, Y. Nakamura, S. Kunitomo, N. Hayashi, H. Higuchi, *Tetrahedron Lett.* **2013**, 54, 2817-2820.
- [172] A. Ito, K. Kawanishi, E. Sakuda, N. Kitamura, *Chem. Eur. J.* **2014**, 20, 3940-3953.
- [173] J. He, F. Rauch, A. Friedrich, D. Sieh, T. Ribbeck, I. Krummenacher, H. Braunschweig, M. Finze, T. B. Marder, *Chem. Eur. J.* **2019**, 25, 13777-13784.
- [174] K. Parab, K. Venkatasubbaiah, F. Jäkle, *J. Am. Chem. Soc.* **2006**, 128, 12879-12885.
- [175] G. C. Welch, R. R. S. Juan, J. D. Masuda, D. W. Stephan, *Science* **2006**, 314, 1124-1126.
- [176] G. C. Welch, D. W. Stephan, *J. Am. Chem. Soc.* **2007**, 129, 1880-1881.
- [177] S. J. Geier, D. W. Stephan, *J. Am. Chem. Soc.* **2009**, 131, 3476-3477.
- [178] D. W. Stephan, G. Erker, *Angew. Chem. Int. Ed.* **2010**, 49, 46-76; *Angew. Chem.* **2010**, 122, 50-81.
- [179] D. W. Stephan, G. Erker, *Chem. Sci.* **2014**, 5, 2625-2641.
- [180] D. W. Stephan, *J. Am. Chem. Soc.* **2015**, 137, 10018-10032.
- [181] D. W. Stephan, G. Erker, *Angew. Chem. Int. Ed.* **2015**, 54, 6400-6441; *Angew. Chem.* **2015**, 127, 6498-6541.
- [182] J. J. Eisch, N. K. Hota, S. Kozima, *J. Am. Chem. Soc.* **1969**, 91, 4575-4577.
- [183] J. J. Eisch, J. E. Galle, S. Kozima, *J. Am. Chem. Soc.* **1986**, 108, 379-385.
- [184] S. Kim, K.-H. Song, S. O. Kang, J. Ko, *Chem. Commun.* **2004**, 68-69.
- [185] H. Braunschweig, I. Fernández, G. Frenking, T. Kupfer, *Angew. Chem. Int. Ed.* **2008**, 47, 1951-1954; *Angew. Chem.* **2008**, 120, 1977-1980.
- [186] C. Fan, W. E. Piers, M. Parvez, *Angew. Chem. Int. Ed.* **2009**, 48, 2955-2958.
- [187] J. Koehler, S. Lindenmeier, I. Fischer, H. Braunschweig, T. Kupfer, D. Gamon, C.-W. Chiu, *J. Raman Spectrosc.* **2010**, 41, 636-641.
- [188] A. Steffen, R. M. Ward, W. D. Jones, T. B. Marder, *Coord. Chem. Rev.* **2010**, 254, 1950-1976.
- [189] H. Braunschweig, T. Kupfer, *Chem. Commun.* **2011**, 47, 10903-10914.
- [190] H. Braunschweig, C.-W. Chiu, D. Gamon, M. Kaupp, I. Krummenacher, T. Kupfer, R. Müller, K. Radacki, *Chem. Eur. J.* **2012**, 18, 11732-11746.
- [191] T. Araki, A. Fukazawa, S. Yamaguchi, *Angew. Chem. Int. Ed.* **2012**, 51, 5484-5487; *Angew. Chem.* **2012**, 124, 5580-5583.
- [192] H. Braunschweig, I. Krummenacher, J. Wahler, *Adv. Organomet. Chem.* **2013**, 61, 1-53.
- [193] H. Braunschweig, C. Hörl, L. Mailänder, K. Radacki, J. Wahler, *Chem. Eur. J.* **2014**, 20, 9858-9861.
- [194] J. H. Barnard, S. Yruegas, K. Huang, C. D. Martin, *Chem. Commun.* **2016**, 52, 9985-9991.
- [195] W. Zhang, B. Zhang, D. Yu, G. He, *Sci. Bull.* **2017**, 62, 899-900.
- [196] M. Meier, L. Ji, J. Nitsch, I. Krummenacher, A. Deissenberger, D. Auerhammer, M. Schäfer, T. B. Marder, H. Braunschweig, *Chem. Eur. J.* **2019**, 25, 4707-4712.
- [197] H. C. Brown, V. H. Dodson, *J. Am. Chem. Soc.* **1957**, 79, 2302-2306.
- [198] P. J. Grisdale, J. L. R. Williams, M. E. Glogowski, B. E. Babb, *J. Org. Chem.* **1971**, 36, 544-549.

- [199] H. Braunschweig, V. Dyakonov, J. O. C. Jimenez-Halla, K. Kraft, I. Krummenacher, K. Radacki, A. Sperlich, J. Wahler, *Angew. Chem. Int. Ed.* **2012**, *51*, 2977-2980; *Angew. Chem.* **2012**, *124*, 3031-3034.
- [200] S. Yamaguchi, T. Shirasaka, S. Akiyama, K. Tamao, *J. Am. Chem. Soc.* **2002**, *124*, 8816-8817.
- [201] A. Wakamiya, K. Mishima, K. Ekawa, S. Yamaguchi, *Chem. Commun.* **2008**, 579-581.
- [202] M. F. Smith, S. J. Cassidy, I. A. Adams, M. Vasiliu, D. L. Gerlach, D. A. Dixon, P. A. Rugar, *Organometallics* **2016**, *35*, 3182-3191.
- [203] S. J. Cassidy, I. Brettell-Adams, L. E. McNamara, M. F. Smith, M. Bautista, H. Cao, M. Vasiliu, D. L. Gerlach, F. Qu, N. I. Hammer, D. A. Dixon, P. A. Rugar, *Organometallics* **2018**, *37*, 3732-3741.
- [204] S. Yruegas, J. J. Martinez, C. D. Martin, *Chem. Commun.* **2018**, *54*, 6808-6811.
- [205] K. R. Bluer, L. E. Laperriere, A. Pujol, S. Yruegas, V. A. K. Adiraju, C. D. Martin, *Organometallics* **2018**, *37*, 2917-2927.
- [206] S. Yruegas, J. H. Barnard, K. Al-Furaiji, J. L. Dutton, D. J. D. Wilson, C. D. Martin, *Organometallics* **2018**, *37*, 1515-1518.
- [207] T. A. Bartholome, K. R. Bluer, C. D. Martin, *Dalton Trans.* **2019**, *48*, 6319-6322.
- [208] L. E. Laperriere, S. Yruegas, C. D. Martin, *Tetrahedron* **2019**, *75*, 937-943.
- [209] P. A. Chase, P. E. Romero, W. E. Piers, M. Parvez, B. O. Patrick, *Can. J. Chem.* **2005**, *83*, 2098-2105.
- [210] P. A. Chase, W. E. Piers, B. O. Patrick, *J. Am. Chem. Soc.* **2000**, *122*, 12911-12912.
- [211] I. A. Adams, P. A. Rugar, *Macromol. Rapid Commun.* **2015**, *36*, 1336-1340.
- [212] C. J. Berger, G. He, C. Merten, R. McDonald, M. J. Ferguson, E. Rivard, *Inorg. Chem.* **2014**, *53*, 1475-1486.
- [213] W. Yang, K. E. Krantz, L. A. Freeman, D. A. Dickie, A. Molino, A. Kaur, D. J. D. Wilson, R. J. Gilliard Jr., *Chem. Eur. J.* **2019**, *25*, 12512-12516.
- [214] I. A. I. Mkhaliid, J. H. Barnard, T. B. Marder, J. M. Murphy, J. F. Hartwig, *Chem. Rev.* **2010**, *110*, 890-931.
- [215] R. J. Blagg, T. R. Simmons, G. R. Hatton, J. M. Courtney, E. L. Bennett, E. J. Lawrence, G. G. Wildgoose, *Dalton Trans.* **2016**, *45*, 6032-6043.
- [216] H. Jacobsen, H. Berke, S. Döring, G. Kehr, G. Erker, R. Fröhlich, O. Meyer, *Organometallics* **1999**, *18*, 1724-1735.
- [217] H. Braunschweig, I. Krummenacher, *Electrochemical Behavior and Redox Chemistry of Boroles*, in *Organic Redox Systems* John Wiley & Sons, Inc., Hoboken, NJ, **2015**, pp. 503-522.
- [218] P. Bissinger, H. Braunschweig, A. Damme, C. Hörl, I. Krummenacher, T. Kupfer, *Angew. Chem. Int. Ed.* **2015**, *54*, 359-362; *Angew. Chem.* **2015**, *127*, 366-369.
- [219] A. Iida, S. Yamaguchi, *J. Am. Chem. Soc.* **2011**, *133*, 6952-6955.
- [220] J. M. Farrell, C. Mützel, D. Bialas, M. Rudolf, K. Menekse, A.-M. Krause, M. Stolte, F. Würthner, *J. Am. Chem. Soc.* **2019**, *141*, 9096-9104.
- [221] S. A. Cummings, M. Iimura, C. J. Harlan, R. J. Kwaan, I. V. Trieu, J. R. Norton, B. M. Bridgewater, F. Jäkle, A. Sundararaman, M. Tilset, *Organometallics* **2006**, *25*, 1565-1568.
- [222] H. Braunschweig, F. Breher, C.-W. Chiu, D. Gamon, D. Nied, K. Radacki, *Angew. Chem. Int. Ed.* **2010**, *49*, 8975-8978; *Angew. Chem.* **2010**, *122*, 9159-9162.
- [223] K. M. M. Josef, *Lichtabsorption und Photochemie organischer Moleküle*, VCH, Weinheim; New York, **1989**.
- [224] A. G. Crawford, A. D. Dwyer, Z. Liu, A. Steffen, A. Beeby, L.-O. Pålsson, D. J. Tozer, T. B. Marder, *J. Am. Chem. Soc.* **2011**, *133*, 13349-13362.
- [225] T. M. Figueira-Duarte, K. Müllen, *Chem. Rev.* **2011**, *111*, 7260-7314.

- [226] M. K. Manna, S. Shokri, G. P. Wiederrecht, D. J. Gosztola, A. J.-L. Ayitou, *Chem. Commun.* **2018**, 54, 5809-5818.
- [227] Y. Liu, C. Li, Z. Ren, S. Yan, M. R. Bryce, *Nat. Rev. Mater.* **2018**, 3, 18020.
- [228] M. J. G. Peach, P. Benfield, T. Helgaker, D. J. Tozer, *J. Chem. Phys.* **2008**, 128, 044118.
- [229] T. Yanai, D. P. Tew, N. C. Handy, *Chem. Phys. Lett.* **2004**, 393, 51-57.

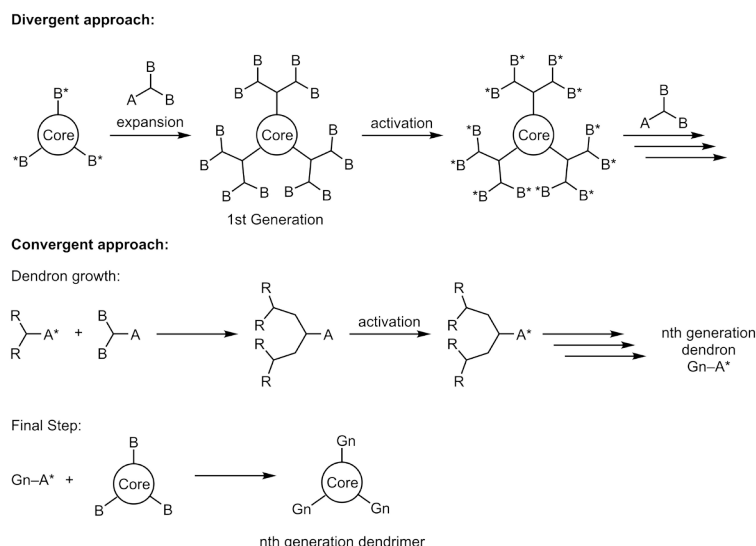


## 3 An Iterative Divergent Approach to Conjugated Starburst Borane Dendrimers

*The following section is slightly modified and reproduced from ref. [3] with permission from Wiley-VCH.*

### 3.1 Introduction

Three-coordinate boranes have attracted considerable interest due to their inherent and interesting properties.<sup>[69-73, 75-80, 230, 231]</sup> Three-coordinate boron is isoelectronic with a carbonium ion, and has an empty p-orbital which is located on the boron center. Thus, boranes can be employed as Lewis acids or electron acceptors. Therefore, a plethora of different potential applications have been investigated, including linear<sup>[81-94, 116, 153, 170-173, 232]</sup> and non-linear<sup>[96, 100, 101, 103, 104, 106, 108-110, 113-115, 118]</sup> optics, bioimaging,<sup>[115-118, 233]</sup> sensors,<sup>[75, 119, 120, 174]</sup> frustrated Lewis pairs (FLP),<sup>[175-181]</sup> and organic light emitting diodes (OLEDs).<sup>[54, 122, 123]</sup> Dendrimers represent a class of macromolecules which, as opposed to linear and hyperbranched polymers, can be isolated as monodisperse compounds. As such, dendrimers provide potential alternatives to polymers in areas where monodispersity is essential, and they have been studied extensively for applications in a wide variety of fields.<sup>[234-246]</sup> Due to their attachment to a focal point, dendrimers usually adopt a spherical structure, especially at higher generations. Thus, their chemistry and properties are often dominated by their outermost layer. This is not the case for conjugated dendrimers, as the goal is to generate large systems with a high degree of  $\pi$ -electron delocalization. These systems show promising properties for application such as charge transport<sup>[247-251]</sup> or emitter materials<sup>[252-259]</sup> in OLEDs, or as electron-acceptor or -donor materials in organic solar cells.<sup>[260-262]</sup> There are generally two approaches to dendrimer synthesis, namely – convergent and divergent (Scheme 3.1).



Scheme 3.1: General approaches to dendrimer synthesis. A, B and A\* and B\* indicate different end groups. Gn indicates the generation of the dendrimers.

In the convergent approach, the dendrimer is built up concentrically from the focal point or core moiety, adding one generation at a time. The drawback of this method is that the number of active centers needed for the expansion, increases exponentially with each generation. This also increases the probability of defects. In the convergent approach, the dendrons are synthesized up to a desired generation, and then attached to the focal point in the last step. The drawback of this strategy is the last step, which needs to be highly efficient in order to warrant the effort of first synthesizing the dendrons. However, the probability of defects is lower using this approach. There are several examples of boron-containing dendrimers.<sup>[82, 263-269]</sup> However, the majority are dendrimers with a boron-functionalized periphery. The number of conjugated dendrimers reported which contain boron is limited (Figure 3.1).<sup>[82, 111, 268, 269]</sup>

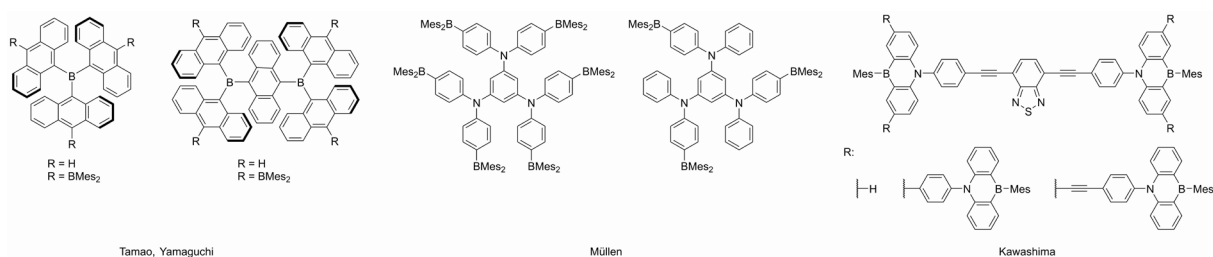
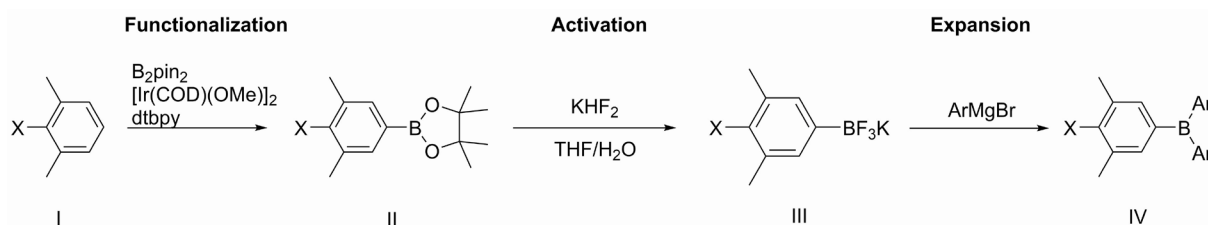


Figure 3.1: Examples of previously synthesized conjugated borane dendrimers.<sup>[82, 268, 269]</sup>

The first example, reported by Tamao, Yamaguchi, and co-workers, was synthesized by a convergent approach (Figure 3.1, left).<sup>[82]</sup> Tri-9-anthrylborane was used as the core and expanded with dimesitylborane (BMes<sub>2</sub>). The dendrimers show a red shift of their absorption bands as well as a rise of their molar extinction coefficients and an anodic shift of their first reduction potentials with increasing dendrimer size, indicating good conjugation throughout the

system. The reduction events can be attributed to reduction of the boron centers. The boron-containing dendrimers reported by Müllen and co-workers contain an electron-rich arylamine core with BMe<sub>2</sub> moieties as the outer periphery (Figure 3.1, middle).<sup>[268]</sup> Changing the ratio of boron and nitrogen changes the excited state properties of those dendrimers. In a third example, reported by Kawashima and co-workers, azaborinines were used as the branching points of the dendrons.<sup>[269]</sup> However, due to a perpendicular arrangement of the azaborinine centers with respect to each other and to the focal point, conjugation seems to be limited, and the dendrimers show very similar properties to the dendrons themselves.

Based on these systems, and our own expertise, we designed a new iterative, divergent methodology for the synthesis of conjugated starburst borane dendrimers (Scheme 3.2).



Scheme 3.2: Divergent approach for the synthesis of conjugated starburst borane dendrimers.

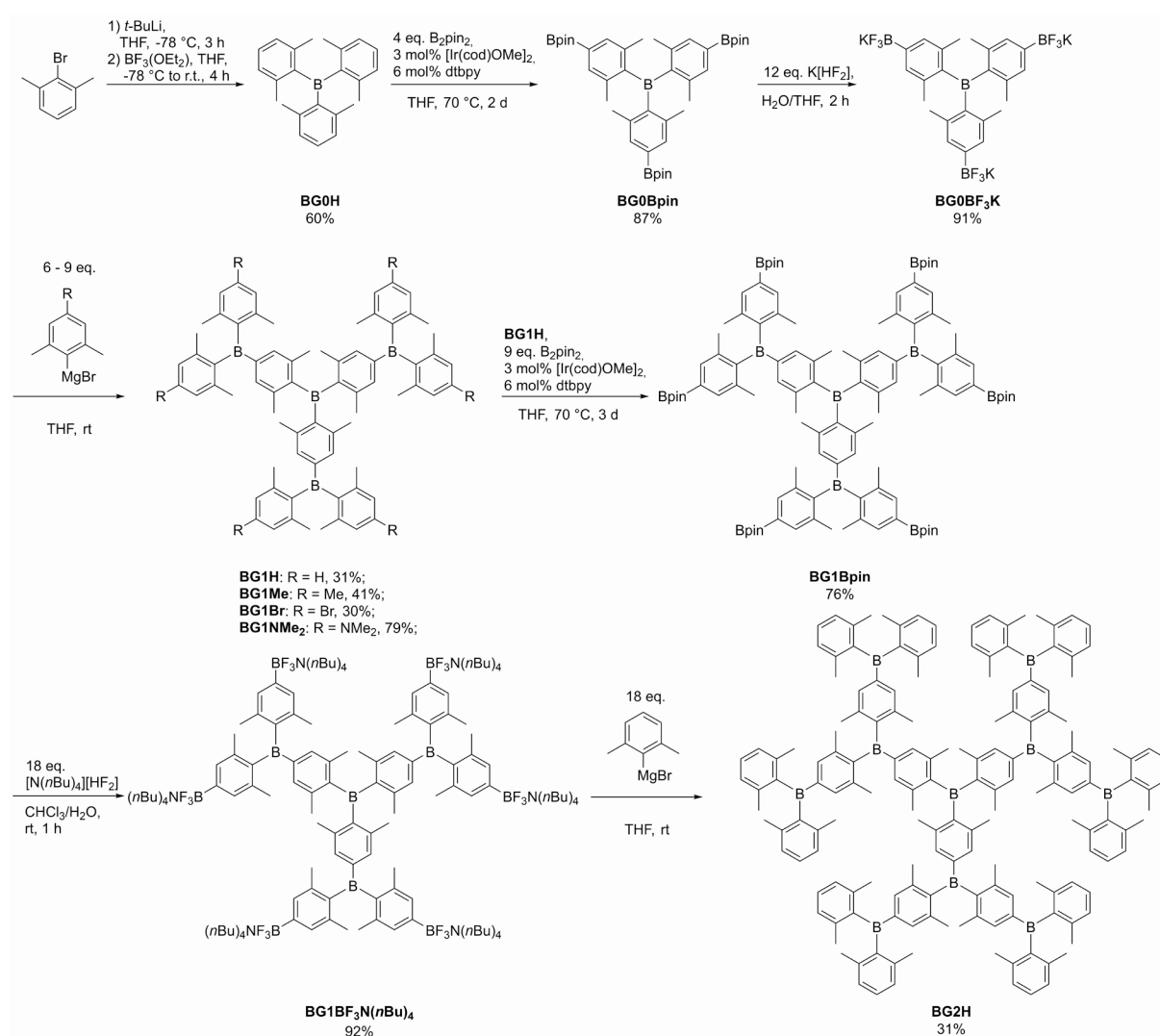
Our method consists of three steps: functionalization, activation and expansion. Tris(2,6-dimethylphenyl)borane (**BG0H**) was chosen as the core moiety, as it exhibits a very high degree of stability due to the steric protection of the boron center by six *ortho*-methyl groups. In the first step (functionalization), the xylene moieties were regioselectively borylated *para* to the boron center via iridium-catalyzed C–H borylation.<sup>[144, 270]</sup> This catalytic system has been studied extensively and is highly efficient and regioselective for sterically-demanding aromatic substrates. This is also a particularly convenient approach, as the boron in the center of the dendrimer needs to be sterically protected in order to achieve stability towards nucleophiles (hydrolysis). In the second step (activation), the arylboronate ester was converted to the corresponding potassium trifluoroborate salt with K[HF<sub>2</sub>]. This transformation is also generally very efficient. Aryltrifluoroborate salts are highly stable compounds and are widely used in cross-coupling reactions.<sup>[147, 148]</sup> Despite their high stability and anionic charge, we and others have found that [aryl-BF<sub>3</sub>]K salts can be employed as convenient electrophiles for the synthesis of triarylboranates.<sup>[1, 2, 93, 94, 132, 149-153, 232]</sup> Thus, in the third step (expansion), all boron centers are arylated using the 2,6-dimethylphenyl (Xyl) Grignard reagent. It is important to note that this method was designed to be generally applicable to 2,6-functionalized phenyl groups. Herein we present the results of this study.

## 3.2 Results and Discussion

### 3.2.1 Synthesis

The nomenclature for the dendrimers was chosen as follows: **BG** denotes dendrimers, **BD** denotes dendrons, the subsequent number denotes the generation, and the last character(s) denote the substituent *para* to the boron center on the outermost layer.

The divergent synthesis is depicted in Scheme 3.3. All compounds were fully characterized by 1D and 2D NMR spectroscopy, high resolution mass spectrometry and, when possible, by X-ray crystallography.



Scheme 3.3: Divergent synthesis of conjugated borane dendrimers **BG1H**, **BG1Me**, **BG1Br**, **BG1NMe<sub>2</sub>**, **BG1Bpin**, **BG1BF<sub>3</sub>N(*n*Bu)<sub>4</sub>**, and **BG2H**.

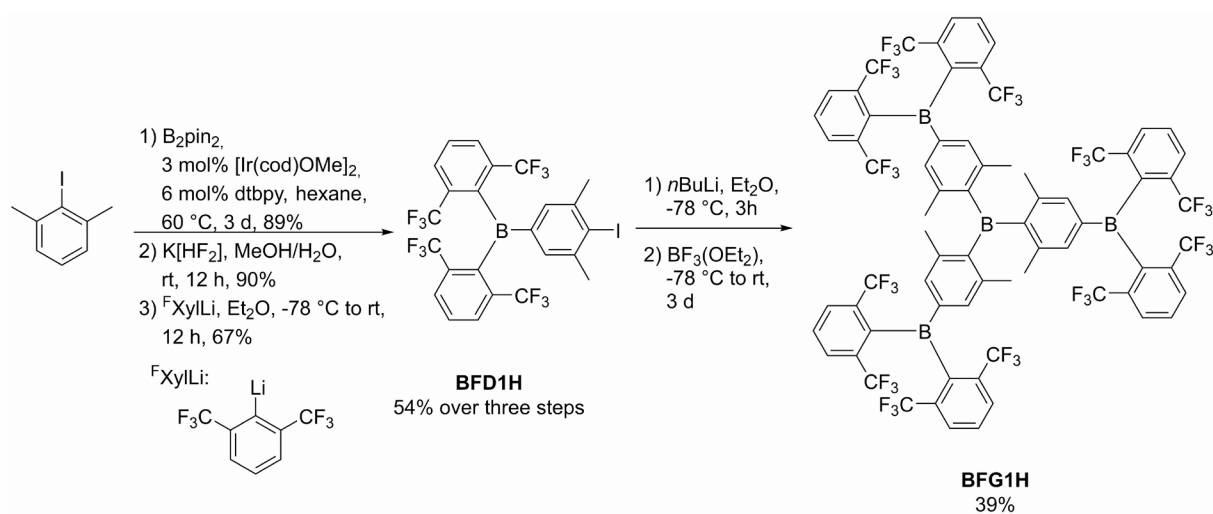
The core moiety **BG0H** was synthesized according to a literature procedure and was isolated in a good yield.<sup>[172]</sup> **BG0H** was subsequently borylated with [Ir(COD)OMe]<sub>2</sub> (COD = cyclooctadiene) as the catalyst precursor, di-*tert*-butylbipyridine (dtbpy) as the ligand,



bis(pinacolato)diboron ( $B_2pin_2$ ) as the boron source, and THF as the solvent. Then, **BG0Bpin** was fluorinated using  $K[HF]_2$  in THF/ $H_2O$  to form the activated core moiety **BG0BF<sub>3</sub>K**. Both **BG0Bpin** and **BG0BF<sub>3</sub>K** were isolated in very good yields on a multi-gram scale with a very simple work-up. However, it was apparent that the solubility of **BG0BF<sub>3</sub>K** in polar organic solvents is quite low. As **BG0BF<sub>3</sub>K** is only slightly soluble in THF, a suspension was reacted with an excess of 2,6-dimethylphenylmagnesium bromide (9 eq. instead of 6 eq.), and **BG1H** was isolated in 31% yield. Yields of arylation reactions of the aryl- $BF_3K$  salts were found to be strongly dependent on the substituents on the aryl moiety, as electron withdrawing substituents increase the stability of the trifluoroborate salts whereas electron donating substituents decrease their stability.<sup>[232]</sup> It is likely that both the low solubility, as well as the electron withdrawing nature of the boron substituents are responsible for the modest yield. In order to test the functional group tolerance and the influence of the substituent *para* to the boron center on the outermost layer, we also synthesized the 1<sup>st</sup> generation derivatives **BG1Me**, **BG1Br**, and **BG1NMe<sub>2</sub>** with methyl, bromide, and dimethylamino substituents, respectively. The syntheses were analogous to that used for the preparation of **BG1H**, but the respective Grignard reagents were employed. The dendrimers **BG1Me**, **BG1Br**, and **BG1NMe<sub>2</sub>** were isolated in moderate to good yields. **BG1H** was purified without the use of column chromatography simply by precipitation from  $CHCl_3$  with EtOH. This procedure did not work as well for **BG1Me**, **BG1Br**, and **BG1NMe<sub>2</sub>**; therefore, those products were purified by column chromatography. To synthesize the 2<sup>nd</sup> generation dendrimer, **BG1H** was borylated analogously to **BG0H**, and **BG1Bpin** was isolated in a very good yield. However, **BG1Bpin** is almost insoluble in most polar or non-polar organic solvents, with  $CHCl_3$  being the exception. This became problematic for the activation step, and several attempts to synthesize **BG1BF<sub>3</sub>K** in various solvent mixtures (THF/ $H_2O$ , MeOH/ $H_2O$ ,  $CHCl_3$ / $H_2O$ , and toluene/ $H_2O$ ), or with the addition of a crown ether (18-C-6) or phase transfer catalysts ( $[N(nBu)_4]Cl$ ,  $[N(nBu)_4]Br$ ,  $[N(nBu)_4]OH$ ), were unsuccessful. Finally, exchange of the cation of the fluorination agent from potassium to tetrabutylammonium, allowed the isolation of **BG1BF<sub>3</sub>N(nBu)<sub>4</sub>** in a very good yield. **BG1BF<sub>3</sub>N(nBu)<sub>4</sub>** is very soluble in a variety of polar organic solvents (especially  $CH_2Cl_2$ ) and almost insoluble in water. However, it was unclear what influence the exchange of the cation would have on the expansion step. We have previously proposed that exchanging potassium for lithium increases the reactivity due to the thermodynamically more favorable formation of LiF compared to KF.<sup>[2]</sup> **BG1BF<sub>3</sub>N(nBu)<sub>4</sub>** was reacted with an excess of 2,6-dimethylphenylmagnesium bromide (18 eq. instead of 12 eq.) in THF. It is important to note that **BG1BF<sub>3</sub>N(nBu)<sub>4</sub>** does not dissolve very well in THF and forms a viscous oil. However,

upon addition of the Grignard reagent, a clear solution formed. After purification by column chromatography, **BG2H** was isolated in a moderate yield, which can be attributed to the fact that **BG2H** decomposes slowly on silica gel. Unfortunately, we have not yet found a better procedure to obtain pure **BG2H**.

All compounds discussed herein exhibit high apparent symmetry in solution as observed by  $^1\text{H}$  and  $^{13}\text{C}$  NMR spectroscopy. Only one set of resonances for each of the chemically equivalent protons and carbon atoms was observed. No  $^{11}\text{B}$  NMR signals corresponding to the three-coordinate boron center were observed for most dendrimers in solution, due to the quadrupole moment of boron and, thus, inherent signal broadening combined with their low solubilities. As **BG0BF<sub>3</sub>K**, **BG1H**, and **BG1Bpin** were synthesized in larger quantities, solid-state  $^{11}\text{B}$  NMR spectra were recorded (Figure 8.101, Figure 8.104 and Figure 8.108 in the Appendix). While we struggled with the synthesis of **BG1BF<sub>3</sub>N(*n*Bu)<sub>4</sub>** and **BG2H**, we searched for ways to increase the solubility of the precursors. Having previously worked with 2,6-bis(trifluoromethyl)phenyl ( $^{\text{F}}\text{Xyl}$ )-substituted triarylboranes<sup>[1, 2]</sup> which show significantly improved solubility compared to their xylyl analogues, we decided to exchange the methyl groups on the periphery of **BG1H** with trifluoromethyl groups. Initial attempts to achieve this using the above methodology failed, as the  $^{\text{F}}\text{Xyl}$  Grignard reagent is very unreactive, and is also unstable at higher temperatures. Using  $^{\text{F}}\text{XylLi}$  was also unsuccessful, as the reaction is very slow, and  $^{\text{F}}\text{XylLi}$  decomposes in THF at room temperature. Instead, we decided to synthesize **BFG1H** via a convergent approach using the dendron **BFD1H** that we had previously reported for the synthesis of borane-containing TADF materials (Scheme 3.4).<sup>[1]</sup>



Scheme 3.4: Convergent synthesis of conjugated borane dendrimer **BFG1H**.

Thus, **BFD1H** was synthesized according to our previously published procedure (**BFD1H** in Chapter 1 Computationally Guided Molecular Design to Minimize the LE/CT Gap in D- $\pi$ -A Fluorinated Triarylboranes for Efficient TADF via D and  $\pi$ -Bridge Tuning). Before preparing **BFD1H**, we had also synthesized a derivative with a bromide instead of iodide, but its lithiation was unsuccessful. Upon addition of either *n*BuLi or *t*BuLi at  $-78$  °C the reaction changed from colorless to deep green, and upon slight warming, became dark brown. This might be due to radical intermediates formed in the bromine/lithium exchange, whereas the iodine/lithium exchange does not involve radical intermediates.<sup>[271, 272]</sup> We assume that a radical species is formed which is thermally unstable.

In contrast, **BFD1H** was successfully lithiated using *n*BuLi and then reacted with  $\text{BF}_3 \cdot \text{OEt}_2$  to give **BFG1H** in a moderate yield after purification by column chromatography. As expected **BFG1H** is qualitatively more soluble in non-polar and polar solvents than **BG1H**. **BFG1H** also exhibits apparent  $C_3$  symmetry in solution as observed by NMR spectroscopy. Two broad singlets are observed in the  $^{19}\text{F}$  NMR spectrum, their linewidth indicative of a hindered rotation process, as previously observed for similar boranes with *ortho*-trifluoromethyl groups.<sup>[131]</sup> The solid-state  $^{11}\text{B}$  NMR spectrum of **BFG1H** shows three distinct boron signals with  $^{11}\text{B}$  NMR shifts of  $\delta = 77.4, 71.0$  and  $69.6$  ppm, which integrate to approximately 1:3:3, respectively, indicative of possible geometrical isomers in the solid-state (see below).

### 3.2.2 Crystal and Molecular Structures

Single crystals suitable for X-ray diffraction were obtained via slow liquid-liquid diffusion, by layering saturated solutions of the dendrimer in  $\text{CHCl}_3$  (**BG1Bpin**) or  $\text{CH}_2\text{Cl}_2$  (**BG1NMe<sub>2</sub>** and **BFG1H**) with ethanol (**BG1Bpin** and **BG1NMe<sub>2</sub>**) or hexane (**BFG1H**). The molecular structures are shown in Figure 3.2 and selected bond lengths and angles are listed in Table 3.1.

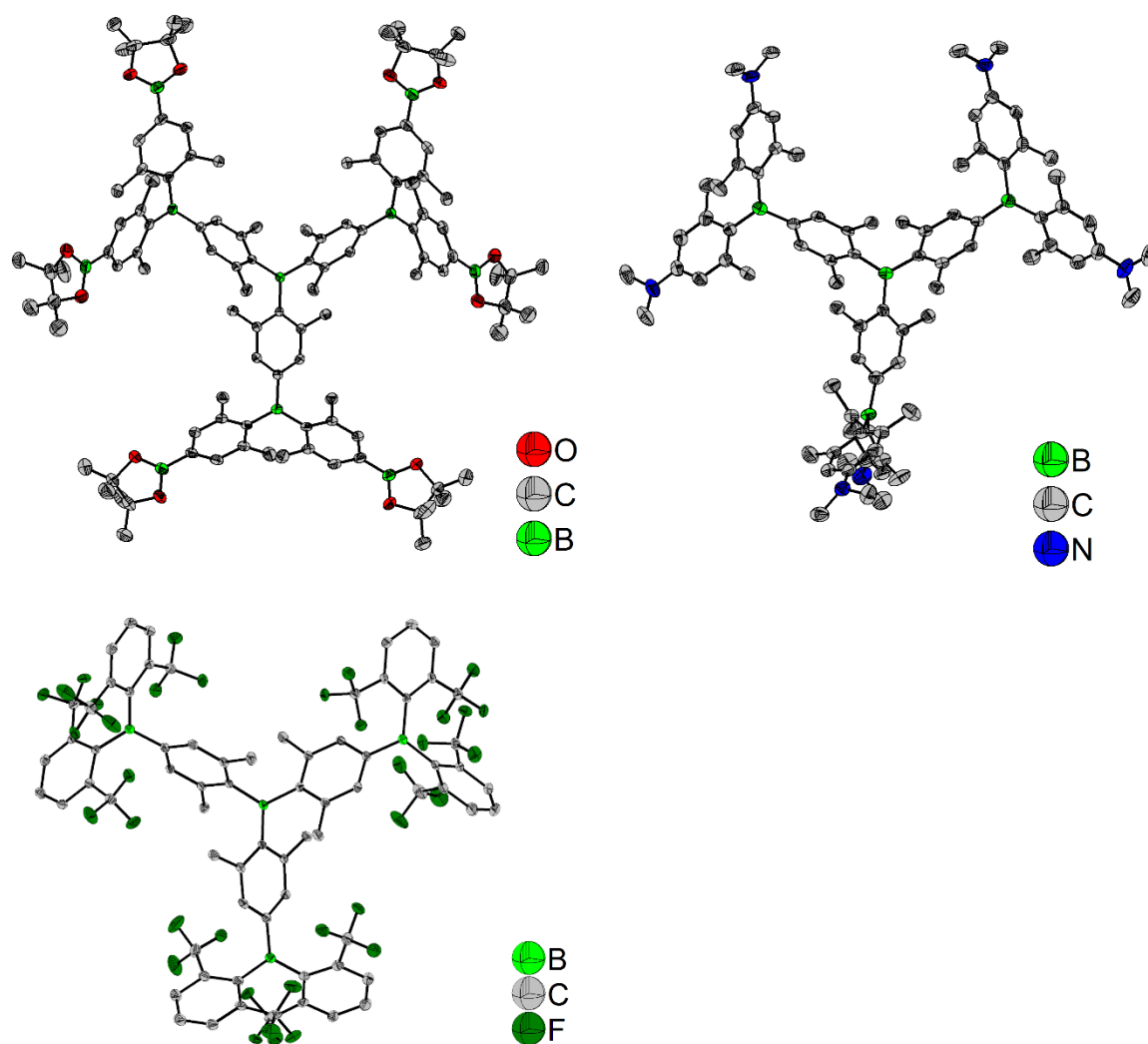


Figure 3.2: Molecular structures of **BG1Bpin** (top left), **BG1NMe<sub>2</sub>** (top right) and **BFG1H** (bottom left) determined by single-crystal X-ray diffraction at 100 K. All ellipsoids are drawn at the 50% probability level, and H atoms and solvent molecules are omitted for clarity. For **BG1Bpin**, the Bpin moieties are slightly disordered and only the major part (94%) is shown. The molecule has 3-fold and 2-fold rotation symmetries. For **BFG1H**, one of the bis(2,6-bis(trifluoromethyl)phenyl)boryl ( $\text{B}^{\text{FXYl}}_2$ ) groups is disordered and only the major part (69%) is shown.

Table 3.1: Selected angles [°], bond lengths and distances [Å] of **BG1Bpin**, **BFG1H**, and **BG1NMe<sub>2</sub>**.

	<b>BG1Bpin</b>		<b>BFG1H</b>		<b>BG1NMe<sub>2</sub></b>					
	Angle [°]	B–C bond length [Å]	Angle [°] / distance [Å]	B–C bond length / distance [Å]	Angle [°]	B–C bond length [Å]	C–N bond length [Å]			
∠ BC <sub>3</sub> -Ar and B–C bond length inner layer	50.95(8) 3x	1.576(3) 3x	50.00(6)	1.585(2)	54.31(14)	1.579(7)				
			46.96(6)	1.576(2)	48.88(15)	1.584(7)				
			47.36(6)	1.581(2)	45.06(14)	1.572(7)				
∠ BC <sub>3</sub> -Ar and B–C or C–N bond length outer layer	23.45(12) 3x	1.566(4) 3x	34.64(6)	1.559(2)	44.39(15)	1.571(7)	1.381(6)			
			53.75(7) 6x	1.577(2) 6x	55.50(6)	1.608(2)	44.92(15)	1.567(7)	1.388(6)	
				61.07(6)	1.602(2)	50.33(15)	1.563(7)	1.401(6)		
				40.40(6)	1.558(2)	42.0(2)	1.576(7)	1.393(6)		
				44.42(6)	1.604(2)	50.4(2)	1.562(8)	1.379(6)		
				57.62(6)	1.604(2)	46.8(2)	1.547(8)	1.387(14)/ 1.446(16)		
				22.94(19)/ 28.6(4)	1.555(2)/ 1.554(3)	37.67(14)	1.578(7)			
				59.07(16)/ 57.9(4)	1.607(2)/ 1.607(2)	50.93(15)	1.569(7)			
				44.90(19)/ 45.1(4)	1.609(2)/ 1.608(2)	51.19(16)	1.561(7)			
				Sum ∠ CBC inner	360.000(1)	359.97(12)		360.0(4)		
				Sum ∠ CBC outer	360.0(2) 3x	359.99(12) 360.00(12) 360.0(4)/ 360.0(9)		359.9(4) 360.0(5) 360.0(4)		
Sum ∠ CNC				359.0(4) 359.7(5) 350.4(5) 354.5(5) 357.2(4) 360.0(14)/ 354.3(13)						
shortest B···F contacts		2.935(2) 2.954(2) 2.925(2) 2.871(2) 2.770(18)/ 2.70(4) 2.804(14)/ 2.70(3)	2.584(2) 2.688(2) 2.818(2) 2.729(2) 2.850(9)/ 2.89(2) 2.928(13)/ 2.82(3)							

The borylated 1<sup>st</sup> generation dendrimer **BG1Bpin** molecule exhibits  $D_3$  symmetry in the solid state. In contrast, the central boron atoms of the molecules of **BFG1H** and **BG1NMe<sub>2</sub>** occupy general positions in the crystal structure and, hence, those compounds do not exhibit any symmetry in the solid state. The B–C (1.547(8) – 1.609(2) Å) and C–N (1.379(6) – 1.446(16) Å) bond lengths are in the expected range (B–C<sub>ar</sub>: 1.556 Å, C<sub>ar</sub>–N: 1.390 Å)<sup>[273]</sup> and comparable to those of other triarylboranes.<sup>[101, 115, 117, 274]</sup> Due to steric hindrance, in **BG1Bpin** the B–C bonds to aryl rings with *ortho*-methyl groups (1.576(3) – 1.577(2) Å) are slightly longer than the B–C bonds to aryls without *ortho*-methyl groups (1.566(4) Å). Similarly, in **BFG1H**, the B–C bonds to aryls with *ortho*-trifluoromethyl groups (1.602(2) – 1.609(2) Å) are longer than the B–C bonds to the inner aryls without methyl groups in the near vicinity (1.554(3) – 1.559(2) Å). This is analogous to previously reported *ortho*-trifluoromethylaryl-substituted triarylboranes.<sup>[1, 91, 124, 131, 132]</sup> In contrast, the NMe<sub>2</sub> groups on the outer aryl rings of **BG1NMe<sub>2</sub>** have an opposite effect on the B–C bond distances, so that the B–C bonds to the inner aryl rings

(1.571(7) – 1.578(7) Å) are slightly longer than the B–C bonds to the outer NMe<sub>2</sub>-bearing aryl rings with *ortho*-methyl groups (1.547(8) – 1.569(7) Å). We previously observed a similar shortening of the respective B–C bond in the presence of a strong electron-donating NMe<sub>2</sub> group, which indicates a degree of polarization in the ground state.<sup>[2, 115]</sup> The boron atoms have a nearly ideal trigonal planar configuration, with the sum of the C–B–C angles being between 359.97(12) and 360.0(9)°. In **BG1NMe<sub>2</sub>**, the sum of the C–N–C angles around the nitrogen atoms varies from 350.4(5) to 360.0(5)°. In all of these compounds, we observe an effect of aryl *ortho*-methylation on the torsion angles of the aryl moieties with respect to the BC<sub>3</sub> plane.<sup>[101, 115, 117, 274]</sup> Due to steric repulsion, the torsion angles are significantly increased in *ortho*-methylated aryls (45.06(14) – 54.31(14)°) compared to non-methylated aryls (22.94(19) – 44.39(15)°). In **BFG1H**, several B··F distances in the range 2.584(2)–2.954(2) Å are observed, which are significantly shorter than the sum of the van der Waals radii for boron and fluorine (3.39 Å).<sup>[156]</sup> This was previously observed in boranes with *ortho*-CF<sub>3</sub> aryl moieties.<sup>[91, 124, 131, 132]</sup> As the respective fluorine atoms are directly above and below the boron center, it is most likely that the lone pair electrons of these fluorine atoms interact with the empty p<sub>z</sub>-orbital of the boron center, which results in a stabilizing effect of the *ortho*-CF<sub>3</sub> groups on the triarylborane. The packing of our molecules in their crystal structures is determined by their bulk. Due to the large torsion angles between the aryl moieties and the BC<sub>3</sub> planes, there are no π··π stacking interactions present between the molecules. The crystal structure of **BG1Bpin** contains strongly disordered ethanol solvent molecules and, hence, there is no obvious direct interaction between the molecules of the main compound themselves. The crystal structure of **BFG1H** mainly exhibits H··F, H··H, and F··F contacts, while in **BG1NMe<sub>2</sub>**, H··H contacts dominate, and weak interactions are observed involving a disordered dichloromethane solvent molecule of low-occupation.

### 3.2.3 Electrochemistry

Cyclic voltammograms of the six borane dendrimers were recorded in THF with  $[n\text{Bu}_4\text{N}][\text{PF}_6]$  as the electrolyte and a scan rate of  $250 \text{ mVs}^{-1}$  (Figure 3.3) in order to determine their reduction potentials, which are referenced to the ferrocene/ferrocenium redox couple ( $\text{Fc}/\text{Fc}^+$ ).

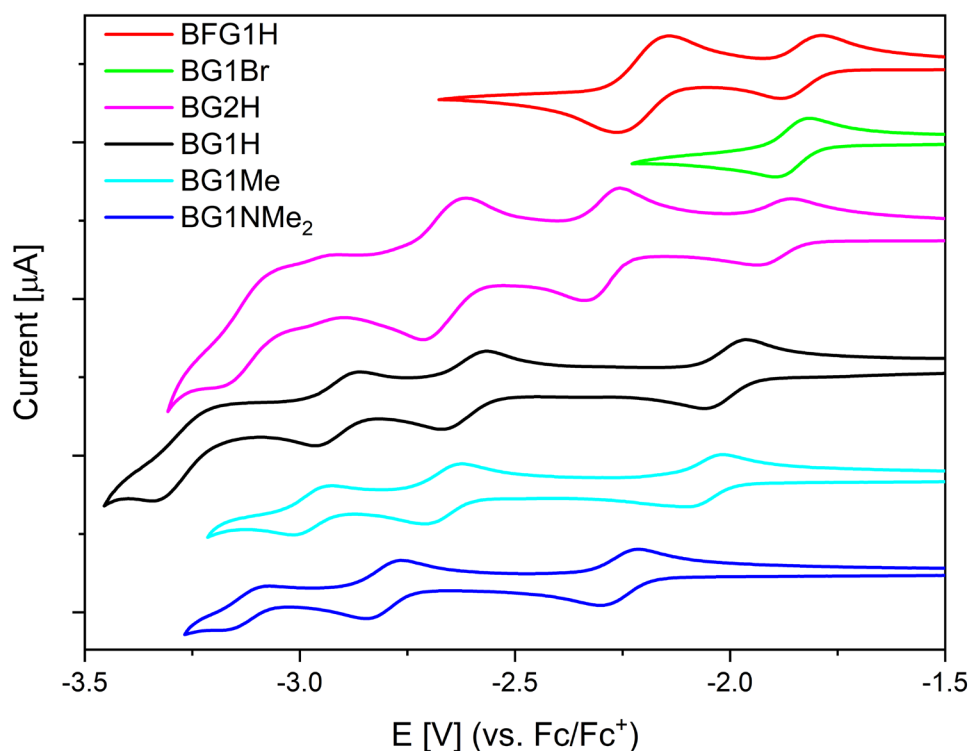


Figure 3.3: Cyclic voltammograms of **BG1H** (black), **BG1Me** (cyan), **BG1NMe<sub>2</sub>** (blue), **BG1Br** (green), **BFG1H** (red) and **BG2H** (magenta) in THF ordered by decreasing first reduction potential. All samples are referenced against the  $\text{Fc}/\text{Fc}^+$  redox couple.

Table 3.2: Reduction potentials of **BG1H**, **BG1Me**, **BG1NMe<sub>2</sub>**, **BG1Br**, **BFG1H** and **BG2H** ordered by decreasing first reduction potential, referenced vs. the  $\text{Fc}/\text{Fc}^+$  redox couple.

Compound	E vs. $\text{Fc}/\text{Fc}^+$ [V]			
	$E_{1/2}$ (red 1)	$E_{1/2}$ (red 2)	$E_{1/2}$ (red 3)	$E_{p,c}$ (red 4)
<b>BFG1H</b>	-1.83	-2.19	-2.98 (irr) <sup>a)</sup>	N.D.
<b>BG1Br</b>	-1.89	-2.56 (irr) <sup>a)</sup>	N.D.	N.D.
<b>BG2H</b>	-1.90	-2.30	-2.66	-3.19 (irr) <sup>b)</sup>
<b>BG1H</b>	-2.01	-2.62	-2.91	-3.34 (irr) <sup>b)</sup>
<b>BG1Me</b>	-2.05	-2.62	-2.96	N.D.
<b>BG1NMe<sub>2</sub></b>	-2.24	-2.79	-3.11	N.D.

a)  $E_{p,c}$  is given for irreversible reduction potentials. b) Too close to the solvent window to determine accurately whether it is reversible. Multiple potential sweeps of all reductions showed no loss in intensity, indicating reversibility.

Compared to  $\text{BMes}_3$  ( $E_{1/2} = 2.8$  V (calculated from measurements vs SCE with  $\text{Fc}/\text{Fc}^+ = 0.4$  V vs. SCE))<sup>[275]</sup> all conjugated borane dendrimers exhibit anodically shifted first reduction potentials, showcasing the electron withdrawing nature of the triarylborane moieties.<sup>[274]</sup> For the parent compound **BG1H**, three distinct reversible reduction waves were observed. The fourth reduction is too close to the solvent window, and thus, whether or not it is reversible or irreversible cannot be determined accurately. However, almost no decrease in intensity was observed when repeatedly cycling through all four reductions. This indicates that the fourth reduction is also reversible. The difference between the first and second reduction wave is 610 mV and the difference between the 2<sup>nd</sup> and 3<sup>rd</sup> is 290 mV. According to Kaim and Schulz, the difference between equivalent redox centers can be used as an indicator for the conjugation of the system as, in a well conjugated system, the reduction potentials are dependent on each other.<sup>[275-277]</sup> They observed a peak splitting of 690 mV for 1,4-bis(dimesitylboryl)benzene and 250 mV for 4,4'-bis(dimesitylboryl)-1,1'-biphenyl.<sup>[276]</sup> Similarly, we previously observed a peak splitting of 280 mV for 2,7-bis(dimesitylborane)pyrene<sup>[278]</sup> and 380 mV for 2,5,8,11-tetrakis(dimesitylborane)perylene.<sup>[94]</sup> It is important to note that, in our systems, not all boron centers are equivalent. The central boron atom can be expected to exhibit a lower reduction potential compared to that of the boron centers of the outer periphery. Assuming that the 1<sup>st</sup> reduction event corresponds to the central boron center, and the consecutive reductions correspond to the outer periphery, the peak splitting between the 2<sup>nd</sup> and 3<sup>rd</sup> reductions should provide a more accurate description of the conjugation. The peak splitting for **BG1Me** ( $\Delta E(1^{\text{st}}/2^{\text{nd}}) = 570$  mV;  $\Delta E(2^{\text{nd}}/3^{\text{rd}}) = 340$  mV) and **BG1NMe<sub>2</sub>** ( $\Delta E(1^{\text{st}}/2^{\text{nd}}) = 550$  mV;  $\Delta E(2^{\text{nd}}/3^{\text{rd}}) = 320$  mV) is similar to that of **BG1H**. However, for **BFG1H** ( $\Delta E(1^{\text{st}}/2^{\text{nd}}) = 360$  mV), due to the electron withdrawing <sup>F</sup>Xyl moieties, it can be assumed that the first and second reductions correspond to the peripheral boron centers and, as such, the separation can indeed be regarded as a measure of the communication between the boron centers. Functionalization at the *para*-position of the outer aryl layer has a large influence on the reduction potentials. Electron donating substituents (Me and NMe<sub>2</sub>) shift the reduction potential cathodically, while electron withdrawing substituents (Br) shift the reduction potential anodically. Three reversible reduction events were observed for both **BG1Me** and **BG1NMe<sub>2</sub>**. The fourth reduction is shifted beyond the limit of the solvent. In contrast, **BG1Br** exhibits only one reversible reduction. At more negative potentials, only irreversible events occur (Figure 6.48). The reason for this is not clear, but one possibility would be activation of the C–Br bonds. The electron withdrawing <sup>F</sup>Xyl groups in **BFG1H** also shift the reduction potential anodically. Analogously to **BG1Br**, only irreversible reductions occur at more negative potentials (Figure 6.49).



Interestingly, the first reduction potential of **BFG1H** is only slightly anodically shifted compared to that of **BG1Br** ( $\Delta E_{1/2} = 60$  mV). This illustrates the importance of the position of the electron withdrawing groups. The effect of the substitution pattern of trifluoromethyl groups on the reduction potential of triarylboranes was previously studied by Wildgoose and co-workers.<sup>[136]</sup> The second reduction wave of **BFG1H** exhibits much higher intensity compared to the first one (integration of 1:2). This is most likely due to two coincidental one electron reductions, indicating a smaller conjugation of the system compared to that in the non-trifluoromethylated derivatives. This is also observed for the reduction waves of **BG2H**. The first and 4<sup>th</sup> reductions exhibit a much lower intensity than the 2<sup>nd</sup> and 3<sup>rd</sup> reductions (integration of 1:2:3). Assuming that the 2<sup>nd</sup> and 3<sup>rd</sup> reduction waves correspond to two and three coincidental one electron reductions, respectively, it should be possible to reversibly reduce **BG2H** seven times. This is a potentially interesting property for accumulators.<sup>[279]</sup>

### 3.2.4 Photophysical Properties

The photophysical data of conjugated dendrimers **BG1H**, **BG1Bpin**, **BG1Me**, **BG1NMe<sub>2</sub>**, **BG1Br**, **BFG1H**, and **BG2H** were determined in CHCl<sub>3</sub> due to the high solubility of all compounds in that solvent (Figure 4 and 5 and Table 3.3). The photophysical properties of **BG1H** and **BG1NMe<sub>2</sub>** were also recorded in THF or toluene, respectively, in order to observe possible solvent polarity dependence. To compare the properties of the dendrimers accurately with those of the core moiety **BG0H**, photophysical properties of **BG0H** were also investigated.

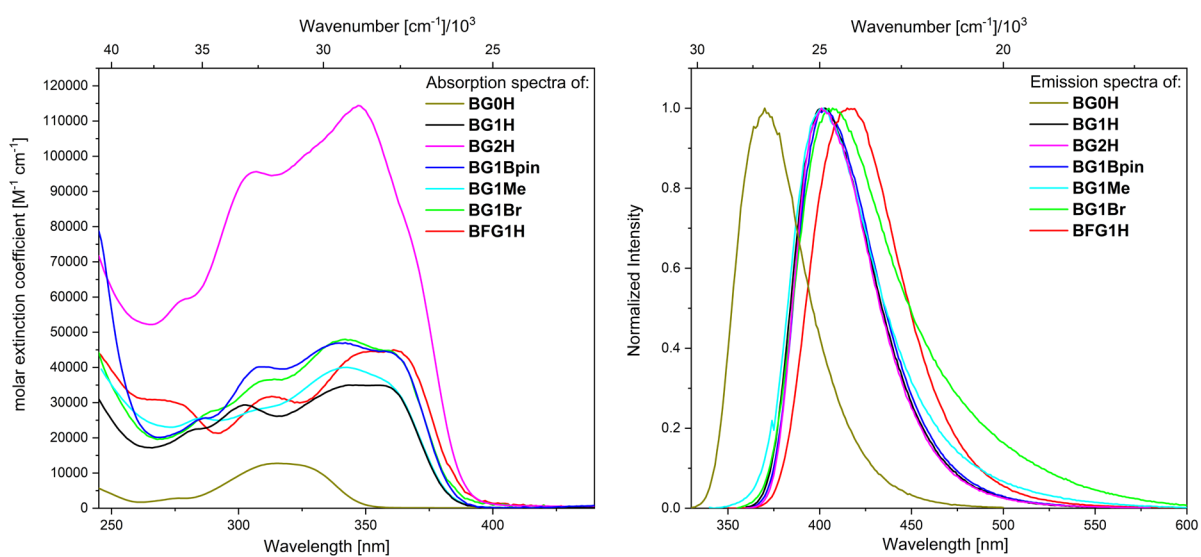


Figure 3.4: Absorption (left) and emission (right) spectra of **BG0H** (gold), **BG1H** (black), **BG2H** (magenta), **BG1Bpin** (blue), **BG1Br** (green), **BFG1H** (red), and **BG1Me** (cyan).

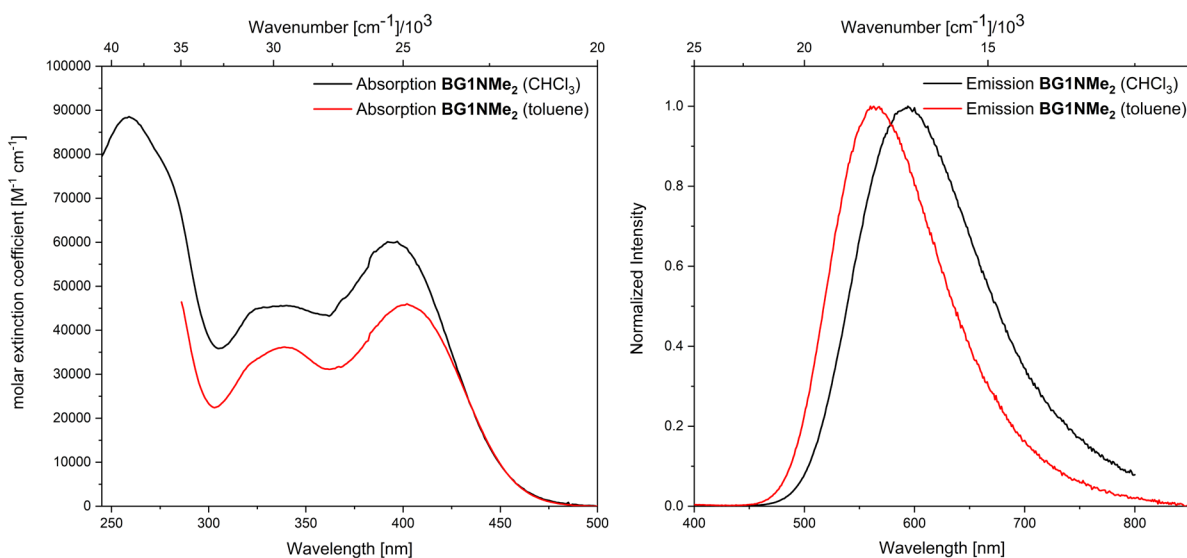


Figure 3.5: Absorption (left) and emission (right) spectra of **BG1NMe<sub>2</sub>** in CHCl<sub>3</sub> (black) and toluene (red)

Table 3.3: Photophysical properties of conjugated borane dendrimers **BG1H**, **BG1Bpin**, **BG1Me**, **BG1NMe<sub>2</sub>**, **BG1Br**, **BFG1H**, and **BG2H**, and the core moiety **BG0H**.

Compound	Solvent	$\lambda_{\text{max}}$	$\epsilon$	$\lambda_{\text{max}}$	Apparent	$\tau_{\text{f}}$ [ns]	$\tau_0$ [ns] <sup>a)</sup>	$\Phi_{\text{f}}$	$k_{\text{r}}$ [10 <sup>9</sup> s <sup>-1</sup> ] c)	$k_{\text{nr}}$ [10 <sup>9</sup> s <sup>-1</sup> ] b)
		(abs.) [nm]	10 <sup>3</sup> [M <sup>-1</sup> cm <sup>-1</sup> ]; (log $\epsilon$ )	(em.) [nm]	Stokes Shift [cm <sup>-1</sup> ]					
<b>BG0H</b>	CHCl <sub>3</sub>	315	13 (4.11)	370	4700	1.6	22.9	0.07	0.04	0.6
<b>BG1H</b>	CHCl <sub>3</sub>	346	35 (4.54)	403	4100	2.5	14.7	0.17	0.07	0.3
	THF	344	35 (4.54)	403	4300	2.7	15.0	0.18	0.07	0.3
<b>BG1Bpin</b>	CHCl <sub>3</sub>	342	47 (4.67)	403	4400	2.4	11.4	0.21	0.09	0.3
<b>BG1Me</b>	CHCl <sub>3</sub>	343	40 (4.60)	402	4300	2.0	22.2	0.09	0.05	0.5
<b>BG1NMe<sub>2</sub></b>	toluene	402	46 (4.66)	560	7000	d)	d)	d)	d)	d)
	CHCl <sub>3</sub>	390	60 (4.78)	593	8800	d)	d)	d)	d)	d)
<b>BG1Br</b>	CHCl <sub>3</sub>	340	48 (4.68)	407	4800	1.0 <sup>e)</sup>	16.7	0.06	0.06	0.9
<b>BFG1H</b>	CHCl <sub>3</sub>	361	45 (4.65)	416	3700	4.6	35.4	0.13	0.03	0.2
<b>BG2H</b>	CHCl <sub>3</sub>	347	114 (5.06)	401	3900	2.1	21.0	0.10	0.05	0.4

a) Calculated from  $\tau_{\text{f}}/\Phi_{\text{f}}$ ; b) The non-radiative rate constants were calculated from  $k_{\text{nr}} = (1-\Phi_{\text{f}})/\tau_{\text{f}}$ ; c) The radiative rate constants were calculated from  $k_{\text{r}} = \Phi_{\text{f}}/\tau_{\text{f}}$ ; d) not photostable; e) calculated average of three lifetimes: 0.7 (76%), 1.8 (18%), 9.8 (6%).

Compared to the core moiety **BG0H** ( $\lambda_{\text{abs, max}} = 315$  nm,  $\lambda_{\text{em, max}} = 370$  nm), all dendrimers exhibit a bathochromically shifted lowest energy absorption and emission (**BG1H**, **BG1Bpin**, **BG1Me**, **BG1Br** and **BG2H**:  $\lambda_{\text{abs, max}} \approx 345$  nm,  $\lambda_{\text{em, max}} \approx 405$  nm; **BFG1H**:  $\lambda_{\text{abs, max}} = 361$  nm,  $\lambda_{\text{em, max}} = 416$  nm; **BG1NMe<sub>2</sub>**:  $\lambda_{\text{abs, max}} = 390$  nm,  $\lambda_{\text{em, max}} = 593$  nm). This shows that the conjugated system has been enlarged as compared to the core moiety; however, the electronic parameters of the different substituents also need to be considered. The observed absorption and emission spectra of **BG1H**, **BG1Bpin**, **BG1Me**, **BG1Br**, and even **BG2H**, are very similar. Thus, in contrast to what was observed for the electrochemical properties, expanding or functionalizing the 1<sup>st</sup> generation dendrimer at the *para*-position of the outer layer, with electron withdrawing substituents or weakly donating substituents, influences the energy of the absorption and emission only slightly. This also indicates that the nature of excitations and emissions are very similar. In analogous systems, such as those of Tamao, Yamaguchi, and coworkers,<sup>[82]</sup> the transitions were classified as  $\pi$ - $\pi^*$  transitions. This is also likely the case for our dendrimers. However, it can be assumed that there is also a large  $\pi$ -p<sub>z</sub> contribution due to the empty p<sub>z</sub>-orbital localized on the boron centers. In addition to the bathochromic shift, extension of the systems from the core moiety **BG0H** to **BG1H**, increases the molar extinction coefficient ( $\epsilon(\text{BG0H}) = 13 \times 10^3$  [M<sup>-1</sup> cm<sup>-1</sup>],  $\epsilon(\text{BG1H}) = 35 \times 10^3$  [M<sup>-1</sup> cm<sup>-1</sup>]). Functionalization at the *para*-position of the outer layer slightly increases the molar extinction coefficient ( $\epsilon(\text{BG1Bpin}) = 47 \times 10^3$  [M<sup>-1</sup> cm<sup>-1</sup>],  $\epsilon(\text{BG1Me}) = 40 \times 10^3$  [M<sup>-1</sup> cm<sup>-1</sup>],  $\epsilon(\text{BG1Br}) = 48 \times 10^3$  [M<sup>-1</sup> cm<sup>-1</sup>]), while expanding the system by one more generation greatly increases the molar extinction coefficient (**BG2H** =  $114 \times 10^3$  [M<sup>-1</sup> cm<sup>-1</sup>]). Comparison of the extinction coefficients

of **BG0H**, **BG1H**, and **BG2H**, shows an almost linear increase with the number of triarylborane subunits. Combined with the fact that no further red-shift is observed from **BG1H** to **BG2H**, this indicates that the maximum conjugation is reached at the first generation for these systems. Thus, the 2<sup>nd</sup> generation dendrimer **BG2H** consists of 2.5 localized, conjugated 1<sup>st</sup> generation subunits that only weakly interact with each other. This phenomenon is of potential application for a photonic antenna.<sup>[247]</sup> Exchanging the xylyl moieties at the outer periphery with <sup>F</sup>Xyl groups slightly red shifts the absorption and emission and increases the molar extinction coefficient slightly compared to **BG1H** ( $\epsilon(\text{BFG1H}) = 45 \times 10^3 \text{ [M}^{-1} \text{ cm}^{-1}\text{]}$ ). This small bathochromic shift is due to the electron-withdrawing nature of the <sup>F</sup>Xyl moiety. It is surprising that no analogous bathochromic shift was observed for **BG1Br**, as the electrochemical measurements indicate a very similar electron withdrawing effect for **BFG1H**. Adding a *para*-NMe<sub>2</sub> group, which is a strong  $\pi$ -donor, drastically shifts both absorption and emission bathochromically, and increases the molar extinction coefficient of the lowest energy absorption compared to that of **BG1H** ( $\epsilon(\text{BG1NMe}_2, \text{CHCl}_3) = 60 \times 10^3 \text{ [M}^{-1} \text{ cm}^{-1}\text{]}$ ). Furthermore, a bathochromic shift of the emission with increasing solvent polarity was observed for **BG1NMe<sub>2</sub>** ( $\lambda_{\text{em, max}}(\text{toluene}) = 560 \text{ nm}$ ;  $\lambda_{\text{em, max}}(\text{CHCl}_3) = 593 \text{ nm}$ ), but it was only fairly small. This indicates that the nature of the transition is significantly changed by the introduction of a strong  $\pi$ -donor, most likely from a local excitation (LE) to an intramolecular charge transfer (ICT). The small bathochromic shift of about  $1000 \text{ cm}^{-1}$  can be attributed to the radial structure of the dendrimers. As such, the change in dipole moment and the subsequent dependence of the emission on solvent polarity can only occur due to symmetry breaking.<sup>[118, 162, 172]</sup> All compounds, except **BG1Br**, exhibit mono-exponential radiative decays of their excited states. Fluorescent lifetimes  $\tau_f$  of all of the conjugated borane dendrimers are ca. 2 ns, with **BG1Br** exhibiting a shorter lifetime  $\tau_f = 1 \text{ ns}$  (average over three lifetimes) and **BFG1H** exhibiting a slightly longer lifetime  $\tau_f = 4.6 \text{ ns}$ . We did not measure the lifetime of **BG1NMe<sub>2</sub>** as partial photodecomposition was observed during the measurements (faster in CHCl<sub>3</sub> than in toluene). The quantum yields of all compounds are modest ( $\Phi_f \approx 0.1$ ), which can be attributed to their fast non-radiative decay rates. This is likely due to the large number of degrees of freedom the systems have because of their size and flexibility.

### 3.2.5 DFT and TD-DFT Studies

DFT and TD-DFT calculations were carried out to gain further insight into the electronic and photophysical properties of the conjugated borane dendrimers. Due to the large size of the systems, and their apparent high symmetry observed in solution by NMR spectroscopy, all dendrimers were calculated with  $C_3$  symmetry (**BG1H**, **BG1Me**, **BG1Br**, and **BFG1H**) or  $D_3$  symmetry (**BG2H**), in order to reduce the cost of the calculations. The HOMO and LUMO energies are plotted in Figure 3.6 and listed in Table 3.4.

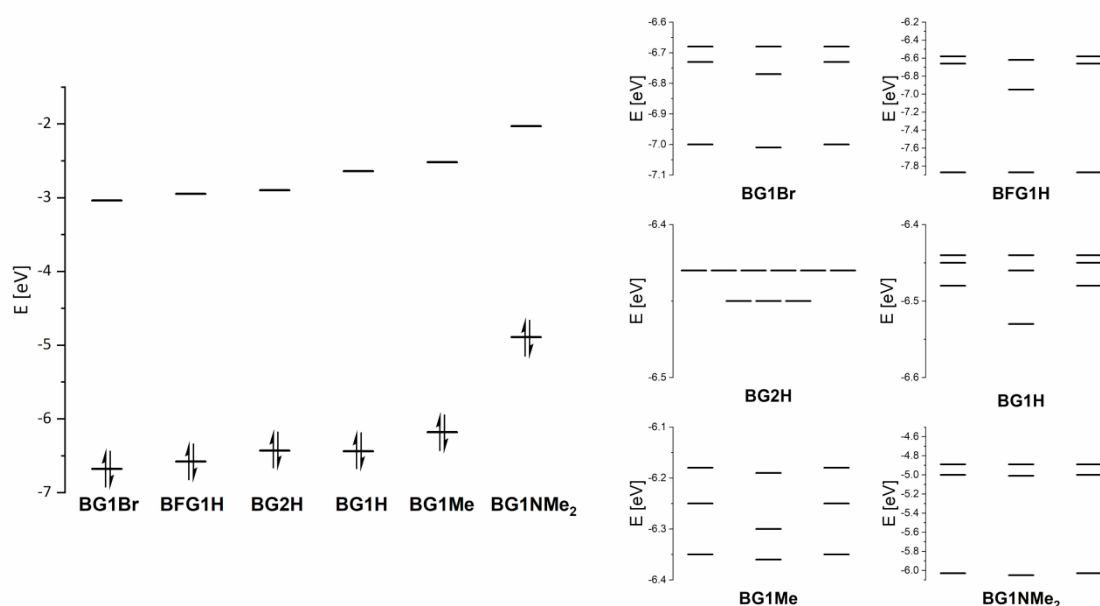


Figure 3.6: Calculated HOMO and LUMO energies of the conjugated borane dendrimers **BG1Br**, **BFG1H**, **BG2H**, **BG1H**, **BG1Me**, and **BG1NMe<sub>2</sub>** (left) and energy diagrams depicting HOMO to HOMO–8 (right), calculated at the B3LYP/6-31+G(d) level of theory.

Table 3.4: Calculated and experimentally determined HOMO and LUMO energies of conjugated borane dendrimers **BG1Br**, **BFG1H**, **BG2H**, **BG1H**, **BG1Me**, and **BG1NMe<sub>2</sub>**, calculated at the B3LYP/6-31+G(d) level of theory.

	<b>BG1Br</b>		<b>BFG1H</b>		<b>BG2H</b>		<b>BG1H</b>		<b>BG1Me</b>		<b>BG1NMe<sub>2</sub></b>	
	calc.	exp. <sup>a)</sup>	calc.	exp. <sup>a)</sup>	calc.	exp. <sup>a)</sup>	calc.	exp. <sup>a)</sup>	calc.	exp. <sup>a)</sup>	calc.	exp. <sup>a)</sup>
<b>LUMO</b>	-3.04	-3.27	-2.95	-3.33	-2.90	-3.26	-2.64	-3.15	-2.52	-3.11	-2.03	-2.92
<b>HOMO</b>	-6.68	-6.49	-6.58	-6.41	-6.43	-6.40	-6.44	-6.36	-6.18	-6.32	-4.89	-5.50

<sup>a</sup> Determined from the half wave potentials: LUMO =  $-(5.16 + E_{1/2, \text{red}}) \text{ eV}$ ; <sup>[157-159]</sup> HOMO =  $E(\text{HOMO}) + E(\text{onset Abs.})$ .

At the B3LYP/6-31+G(d) level of theory, the calculated LUMO energy levels rise from **BG1Br** < **BFG2H** < **BG2H** < **BG1H** < **BG1Me** < **BG1NMe<sub>2</sub>**. The calculated HOMO energies show almost the same trend, except that the order of **BG1H** and **BG2H** is switched. The experimental HOMO and LUMO energies also show the same trend; however, the order of **BG1Br** and **BFG1H** is switched for the LUMO energies. The calculations describe the trends in HOMO

and LUMO energies of the conjugated borane dendrimers rather well, accounting for the fact that all calculations were carried out using symmetry. TD-DFT calculations were carried out in order to gain more insight into the photophysical properties of the dendrimers. The lowest energy transitions  $S_1 \leftarrow S_0$  and  $S_2 \leftarrow S_0$  are degenerate for all dendrimers, due to the symmetry used in the calculations. The natural transition orbitals (NTOs) for the  $S_1 \leftarrow S_0$  and  $S_2 \leftarrow S_0$  transitions of all dendrimers are depicted in Figure 3.7.

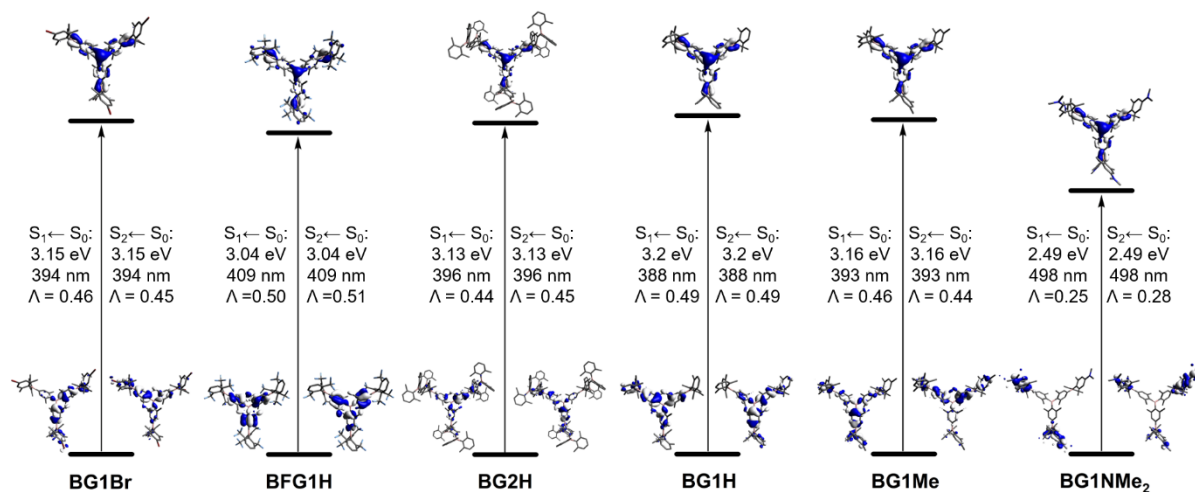


Figure 3.7: NTOs of the  $S_1 \leftarrow S_0$  and  $S_2 \leftarrow S_0$  transitions of the conjugated borane dendrimers **BG1Br**, **BFG1H**, and **BG2H**, **BG1H**, **BG1Me**, and **BG1NMe<sub>2</sub>**.

For **BG1Br**, **BFG1H**, **BG2H**, **BG1H**, and **BG1Me**, the  $S_1 \leftarrow S_0$  and  $S_2 \leftarrow S_0$  transitions correspond to  $\pi(\text{xylene})\text{-}p_z(\text{boron})$  transitions. The outer xylene moieties have a smaller contribution than the inner xylene moieties. In all cases, the virtual NTOs correspond to the LUMO of the respective dendrimer, which are mainly localized on the four boron centers of the core and the 1<sup>st</sup> generation. This is also the case for **BG2H**, illustrating the limited conjugation of the 2<sup>nd</sup> generation dendrimer, and it explains the similarity of its absorption and emission spectra to those of the 1<sup>st</sup> generation dendrimers. For **BG1NMe<sub>2</sub>**, the  $S_1 \leftarrow S_0$  and  $S_2 \leftarrow S_0$  transitions can be classified as charge transfer (CT) transitions from the 4-dimethylaminoxylene moieties of the outer layer to the four boron centers. This is also supported by the small orbital overlap coefficients ( $0 \leq \Lambda \leq 1$ , where  $\Lambda = 0$  corresponds to no overlap and  $\Lambda = 1$  corresponds to complete overlap),<sup>[228]</sup> that are significantly lower ( $\Lambda = 0.25$  and  $0.28$ ) than those of the other dendrimers ( $\Lambda \approx 0.5$ ). The specific orbitals contributing to the transitions vary, depending on the substitution patterns of the outer periphery of the dendrimers.

### 3.3 Conclusion

We have designed and applied a new divergent strategy for the synthesis of conjugated borane dendrimers **BG1Br**, **BG1H**, **BG1Me**, **BG1NMe<sub>2</sub>**, and **BG2H**. The three step divergent approach, consisting of: 1) functionalization, via iridium-catalyzed C–H borylation; 2) activation, via fluorination of the boronate ester generated with K[HF<sub>2</sub>] or [N(*n*Bu)<sub>4</sub>][HF<sub>2</sub>]; 3) expansion, via reaction of the trifluoroborate salts with an aryl Grignard reagent, works as designed up until the 1<sup>st</sup> generation. After the 1<sup>st</sup> generation, solubility issues forced us to modify the synthesis slightly. The 2<sup>nd</sup> generation dendrimer **BG2H** was synthesized after exchanging the cation of the fluorination step from potassium to tetra-*n*-butylammonium, in order to improve the solubility in organic solvents. Substrate tolerance is mainly limited by the reactivity of the aryl Grignard reagent. Additionally, we synthesized **BFG1H** by a convergent approach. All dendrimers were investigated via cyclic voltammetry, UV-Vis absorption and emission spectroscopy, and by DFT and TD-DFT calculations, in order to gain more insight into their electrochemical and photophysical properties. All dendrimers, except **BG1Br**, exhibit multiple, distinct and reversible reductions, that can be easily modified via the substitution pattern of the outer periphery of the dendrimers. As such, they might have potential application as molecular accumulators.<sup>[279]</sup> In contrast to the electrochemical properties, the photophysical properties of the dendrimers are not strongly influenced by the substitution pattern of the outer periphery. Only strong donor moieties significantly altered the nature of the excitation and emission of the dendrimers. While conjugation within the systems does not increase after the 1<sup>st</sup> generation, the molar extinction coefficient does, which is of possible interest for the design of a photonic antenna.<sup>[247]</sup>

### 3.4 References

- [1] A. Narsaria, F. Rauch, J. Krebs, P. Endres, A. Friedrich, I. Krummenacher, H. Braunschweig, M. Finze, J. Nitsch, F. M. Bickelhaupt, T. B. Marder, *Adv. Funct. Mater.* **2020**, 10.1002/adfm.202002064.
- [2] F. Rauch, S. Fuchs, A. Friedrich, D. Sieh, I. Krummenacher, H. Braunschweig, M. Finze, T. B. Marder, *Chem. Eur. J.* **2020**, 10.1002/chem.201905559.
- [54] K. Suzuki, S. Kubo, K. Shizu, T. Fukushima, A. Wakamiya, Y. Murata, C. Adachi, H. Kaji, *Angew. Chem. Int. Ed.* **2015**, *54*, 15231-15235; *Angew. Chem.* **2015**, *127*, 15446-15450.
- [69] C. D. Entwistle, T. B. Marder, *Angew. Chem. Int. Ed.* **2002**, *41*, 2927-2931; *Angew. Chem.* **2002**, *114*, 3051-3056.
- [70] C. D. Entwistle, T. B. Marder, *Chem. Mater.* **2004**, *16*, 4574-4585.
- [71] S. Yamaguchi, A. Wakamiya, *Pure Appl. Chem.* **2006**, *78*, 1413.
- [72] F. Jäkle, *Coord. Chem. Rev.* **2006**, *250*, 1107-1121.
- [73] M. Elbing, G. C. Bazan, *Angew. Chem. Int. Ed.* **2008**, *47*, 834-838; *Angew. Chem.* **2008**, *120*, 846-850.
- [75] C. R. Wade, A. E. J. Broomsgrove, S. Aldridge, F. P. Gabbaï, *Chem. Rev.* **2010**, *110*, 3958-3984.
- [76] Z. M. Hudson, S. Wang, *Dalton Trans.* **2011**, *40*, 7805-7816.
- [77] A. Wakamiya, S. Yamaguchi, *Bull. Chem. Soc. Jpn.* **2015**, *88*, 1357-1377.
- [78] L. Ji, S. Griesbeck, T. B. Marder, *Chem. Sci.* **2017**, *8*, 846-863.
- [79] S.-Y. Li, Z.-B. Sun, C.-H. Zhao, *Inorg. Chem.* **2017**, *56*, 8705-8717.
- [80] G. Turkoglu, M. E. Cinar, T. Ozturk, *Molecules* **2017**, *22*, 1522.
- [81] N. Matsumi, K. Naka, Y. Chujo, *J. Am. Chem. Soc.* **1998**, *120*, 5112-5113.
- [82] S. Yamaguchi, S. Akiyama, K. Tamao, *J. Am. Chem. Soc.* **2000**, *122*, 6335-6336.
- [83] W.-L. Jia, D. Song, S. Wang, *J. Org. Chem.* **2003**, *68*, 701-705.
- [84] A. Wakamiya, T. Ide, S. Yamaguchi, *J. Am. Chem. Soc.* **2005**, *127*, 14859-14866.
- [85] I. Yamaguchi, B.-J. Choi, T.-A. Koizumi, K. Kubota, T. Yamamoto, *Macromolecules* **2007**, *40*, 438-443.
- [86] U. Megerle, F. Selmaier, C. Lambert, E. Riedle, S. Lochbrunner, *Phys. Chem. Chem. Phys.* **2008**, *10*, 6245-6251.
- [87] A. Lorbach, M. Bolte, H. Li, H.-W. Lerner, M. C. Holthausen, F. Jäkle, M. Wagner, *Angew. Chem. Int. Ed.* **2009**, *48*, 4584-4588; *Angew. Chem.* **2009**, *121*, 4654-4658.
- [88] L. Weber, V. Werner, M. A. Fox, T. B. Marder, S. Schwedler, A. Brockhinke, H.-G. Stammler, B. Neumann, *Dalton Trans.* **2009**, 2823-2831.
- [89] L. Weber, D. Eickhoff, T. B. Marder, M. A. Fox, P. J. Low, A. D. Dwyer, D. J. Tozer, S. Schwedler, A. Brockhinke, H.-G. Stammler, B. Neumann, *Chem. Eur. J.* **2012**, *18*, 1369-1382.
- [90] C. Reus, S. Weidlich, M. Bolte, H.-W. Lerner, M. Wagner, *J. Am. Chem. Soc.* **2013**, *135*, 12892-12907.
- [91] X. Yin, J. Chen, R. A. Lalancette, T. B. Marder, F. Jäkle, *Angew. Chem. Int. Ed.* **2014**, *53*, 9761-9765; *Angew. Chem.* **2014**, *126*, 9919-9923.
- [92] Z. Zhang, R. M. Edkins, J. Nitsch, K. Fucke, A. Eichhorn, A. Steffen, Y. Wang, T. B. Marder, *Chem. Eur. J.* **2015**, *21*, 177-190.
- [93] J. Merz, J. Fink, A. Friedrich, I. Krummenacher, H. H. Al Mamari, S. Lorenzen, M. Haehnel, A. Eichhorn, M. Moos, M. Holzapfel, H. Braunschweig, C. Lambert, A. Steffen, L. Ji, T. B. Marder, *Chem. Eur. J.* **2017**, *23*, 13164-13180.
- [94] J. Merz, A. Steffen, J. Nitsch, J. Fink, C. B. Schürger, A. Friedrich, I. Krummenacher, H. Braunschweig, M. Moos, D. Mims, C. Lambert, T. B. Marder, *Chem. Sci.* **2019**, *10*, 7516-7534.



- [96] Z. Yuan, N. J. Taylor, T. B. Marder, I. D. Williams, S. K. Kurtz, L.-T. Cheng, *J. Chem. Soc., Chem. Commun.* **1990**, 1489-1492.
- [100] Z. Yuan, N. J. Taylor, Y. Sun, T. B. Marder, I. D. Williams, L.-T. Cheng, *J. Organomet. Chem.* **1993**, *449*, 27-37.
- [101] Z. Yuan, N. J. Taylor, R. Ramachandran, T. B. Marder, *Appl. Organomet. Chem.* **1996**, *10*, 305-316.
- [103] Z.-Q. Liu, Q. Fang, D. Wang, G. Xue, W.-T. Yu, Z.-S. Shao, M.-H. Jiang, *Chem. Commun.* **2002**, 2900-2901.
- [104] Z.-Q. Liu, Q. Fang, D. Wang, D.-X. Cao, G. Xue, W.-T. Yu, H. Lei, *Chem. Eur. J.* **2003**, *9*, 5074-5084.
- [106] M. Charlot, L. Porres, C. D. Entwistle, A. Beeby, T. B. Marder, M. Blanchard-Desce, *Phys. Chem. Chem. Phys.* **2005**, *7*, 600-606.
- [108] Z. Yuan, C. D. Entwistle, J. C. Collings, D. Albesa-Jové, A. S. Batsanov, J. A. K. Howard, N. J. Taylor, H. M. Kaiser, D. E. Kaufmann, S.-Y. Poon, W.-Y. Wong, C. Jardin, S. Fathallah, A. Boucekkine, J.-F. Halet, T. B. Marder, *Chem. Eur. J.* **2006**, *12*, 2758-2771.
- [109] C. D. Entwistle, J. C. Collings, A. Steffen, L.-O. Pålsson, A. Beeby, D. Albesa-Jove, J. M. Burke, A. S. Batsanov, J. A. K. Howard, J. A. Mosely, S.-Y. Poon, W.-Y. Wong, F. Ibersiene, S. Fathallah, A. Boucekkine, J.-F. Halet, T. B. Marder, *J. Mater. Chem.* **2009**, *19*, 7532-7544.
- [110] J. C. Collings, S.-Y. Poon, C. Le Droumaguet, M. Charlot, C. Katan, L.-O. Pålsson, A. Beeby, J. A. Mosely, H. M. Kaiser, D. Kaufmann, W.-Y. Wong, M. Blanchard-Desce, T. B. Marder, *Chem. Eur. J.* **2009**, *15*, 198-208.
- [111] L. Ji, Q. Fang, M.-S. Yuan, Z.-Q. Liu, Y.-X. Shen, H.-F. Chen, *Org. Lett.* **2010**, *12*, 5192-5195.
- [113] L. Ji, R. M. Edkins, L. J. Sewell, A. Beeby, A. S. Batsanov, K. Fucke, M. Drafz, J. A. K. Howard, O. Moutounet, F. Ibersiene, A. Boucekkine, E. Furet, Z. Liu, J.-F. Halet, C. Katan, T. B. Marder, *Chem. Eur. J.* **2014**, *20*, 13618-13635.
- [114] P. Chen, A. S. Marshall, S. H. Chi, X. Yin, J. W. Perry, F. Jäkle, *Chem. Eur. J.* **2015**, *21*, 18237-18247.
- [115] S. Griesbeck, Z. Zhang, M. Gutmann, T. Lühmann, R. M. Edkins, G. Clermont, A. N. Lazar, M. Haehnel, K. Edkins, A. Eichhorn, M. Blanchard-Desce, L. Meinel, T. B. Marder, *Chem. Eur. J.* **2016**, *22*, 14701-14706.
- [116] S. Griesbeck, E. Michail, C. Wang, H. Ogasawara, S. Lorenzen, L. Gerstner, T. Zang, J. Nitsch, Y. Sato, R. Bertermann, M. Taki, C. Lambert, S. Yamaguchi, T. B. Marder, *Chem. Sci.* **2019**, *10*, 5405-5422.
- [117] S. Griesbeck, M. Ferger, C. Czernetzi, C. Wang, R. Bertermann, A. Friedrich, M. Haehnel, D. Sieh, M. Taki, S. Yamaguchi, T. B. Marder, *Chem. Eur. J.* **2019**, *25*, 7679-7688.
- [118] S. Griesbeck, E. Michail, F. Rauch, H. Ogasawara, C. Wang, Y. Sato, R. M. Edkins, Z. Zhang, M. Taki, C. Lambert, S. Yamaguchi, T. B. Marder, *Chem. Eur. J.* **2019**, *25*, 13164-13175.
- [119] S. Yamaguchi, S. Akiyama, K. Tamao, *J. Am. Chem. Soc.* **2001**, *123*, 11372-11375.
- [120] T. W. Hudnall, C.-W. Chiu, F. P. Gabbaï, *Acc. Chem. Res.* **2009**, *42*, 388-397.
- [122] Y. Shirota, *J. Mater. Chem.* **2000**, *10*, 1-25.
- [123] A. Wakamiya, K. Mori, S. Yamaguchi, *Angew. Chem. Int. Ed.* **2007**, *46*, 4273-4276; *Angew. Chem.* **2007**, *119*, 4351-4354.
- [124] S. Toyota, M. Asakura, M. Oki, F. Toda, *Bull. Chem. Soc. Jpn.* **2000**, *73*, 2357-2362.
- [131] Z. Zhang, R. M. Edkins, J. Nitsch, K. Fucke, A. Steffen, L. E. Longobardi, D. W. Stephan, C. Lambert, T. B. Marder, *Chem. Sci.* **2015**, *6*, 308-321.

- [132] Z. Zhang, R. M. Edkins, M. Haehnel, M. Wehner, A. Eichhorn, L. Mailänder, M. Meier, J. Brand, F. Brede, K. Müller-Buschbaum, H. Braunschweig, T. B. Marder, *Chem. Sci.* **2015**, *6*, 5922-5927.
- [136] R. J. Blagg, E. J. Lawrence, K. Resner, V. S. Oganessian, T. J. Herrington, A. E. Ashley, G. G. Wildgoose, *Dalton Trans.* **2016**, *45*, 6023-6031.
- [144] T. Ishiyama, J. Takagi, K. Ishida, N. Miyaura, N. R. Anastasi, J. F. Hartwig, *J. Am. Chem. Soc.* **2002**, *124*, 390-391.
- [147] A. J. J. Lennox, G. C. Lloyd-Jones, *Chem. Soc. Rev.* **2014**, *43*, 412-443.
- [148] G. A. Molander, *J. Org. Chem.* **2015**, *80*, 7837-7848.
- [149] K. Schickedanz, T. Trageser, M. Bolte, H.-W. Lerner, M. Wagner, *Chem. Commun.* **2015**, *51*, 15808-15810.
- [150] K. Schickedanz, J. Radtke, M. Bolte, H.-W. Lerner, M. Wagner, *J. Am. Chem. Soc.* **2017**, *139*, 2842-2851.
- [151] S. Konishi, T. Iwai, M. Sawamura, *Organometallics* **2018**, *37*, 1876-1883.
- [152] M. W. Drover, K. Nagata, J. C. Peters, *Chem. Commun.* **2018**, *54*, 7916-7919.
- [153] X. Jia, J. Nitsch, L. Ji, Z. Wu, A. Friedrich, F. Kerner, M. Moos, C. Lambert, T. B. Marder, *Chem. Eur. J.* **2019**, *25*, 10845-10857.
- [156] M. Mantina, A. C. Chamberlin, R. Valero, C. J. Cramer, D. G. Truhlar, *J. Phys. Chem. A* **2009**, *113*, 5806-5812.
- [157] N. G. Connelly, W. E. Geiger, *Chem. Rev.* **1996**, *96*, 877-910.
- [158] D. Tsiplakides, D. Archonta, C. G. Vayenas, *Top. Catal.* **2007**, *44*, 469-479.
- [159] D. Reitzenstein, T. Quast, F. Kanal, M. Kullmann, S. Ruetzel, M. S. Hammer, C. Deibel, V. Dyakonov, T. Brixner, C. Lambert, *Chem. Mater.* **2010**, *22*, 6641-6655.
- [162] R. Stahl, C. Lambert, C. Kaiser, R. Wortmann, R. Jakober, *Chem. Eur. J.* **2006**, *12*, 2358-2370.
- [170] Z. Zhou, A. Wakamiya, T. Kushida, S. Yamaguchi, *J. Am. Chem. Soc.* **2012**, *134*, 4529-4532.
- [171] J. Yoshino, Y. Nakamura, S. Kunitomo, N. Hayashi, H. Higuchi, *Tetrahedron Lett.* **2013**, *54*, 2817-2820.
- [172] A. Ito, K. Kawanishi, E. Sakuda, N. Kitamura, *Chem. Eur. J.* **2014**, *20*, 3940-3953.
- [173] J. He, F. Rauch, A. Friedrich, D. Sieh, T. Ribbeck, I. Krummenacher, H. Braunschweig, M. Finze, T. B. Marder, *Chem. Eur. J.* **2019**, *25*, 13777-13784.
- [174] K. Parab, K. Venkatasubbaiah, F. Jäkle, *J. Am. Chem. Soc.* **2006**, *128*, 12879-12885.
- [175] G. C. Welch, R. R. S. Juan, J. D. Masuda, D. W. Stephan, *Science* **2006**, *314*, 1124-1126.
- [176] G. C. Welch, D. W. Stephan, *J. Am. Chem. Soc.* **2007**, *129*, 1880-1881.
- [177] S. J. Geier, D. W. Stephan, *J. Am. Chem. Soc.* **2009**, *131*, 3476-3477.
- [178] D. W. Stephan, G. Erker, *Angew. Chem. Int. Ed.* **2010**, *49*, 46-76; *Angew. Chem.* **2010**, *122*, 50-81.
- [179] D. W. Stephan, G. Erker, *Chem. Sci.* **2014**, *5*, 2625-2641.
- [180] D. W. Stephan, *J. Am. Chem. Soc.* **2015**, *137*, 10018-10032.
- [181] D. W. Stephan, G. Erker, *Angew. Chem. Int. Ed.* **2015**, *54*, 6400-6441; *Angew. Chem.* **2015**, *127*, 6498-6541.
- [228] M. J. G. Peach, P. Benfield, T. Helgaker, D. J. Tozer, *J. Chem. Phys.* **2008**, *128*, 044118.
- [230] F. Jäkle, *Chem. Rev.* **2010**, *110*, 3985-4022.
- [231] S. M. Berger, M. Ferger, T. B. Marder, **2020**, manuscript in preparation.
- [232] M. Ferger, S. M. Berger, F. Rauch, M. Schönitz, J. Rühle, J. Krebs, A. Friedrich, T. B. Marder, **2020**, manuscript in preparation.
- [233] J. Liu, S. Zhang, J. Zhu, X. Liu, G. Yang, X. Zhang, *Anal. Bioanal. Chem.* **2019**, *411*, 5223-5231.

- [234] D. A. Tomalia, H. Baker, J. Dewald, M. Hall, G. Kallos, S. Martin, J. Roeck, J. Ryder, P. Smith, *Polym. J.* **1985**, *17*, 117-132.
- [235] A. W. Bosman, H. M. Janssen, E. W. Meijer, *Chem. Rev.* **1999**, *99*, 1665-1688.
- [236] J.-P. Majoral, A.-M. Caminade, *Chem. Rev.* **1999**, *99*, 845-880.
- [237] D. Astruc, F. Chardac, *Chem. Rev.* **2001**, *101*, 2991-3024.
- [238] G. M. Dykes, *J. Chem. Technol. Biotechnol.* **2001**, *76*, 903-918.
- [239] S. M. Grayson, J. M. J. Fréchet, *Chem. Rev.* **2001**, *101*, 3819-3868.
- [240] A. D'Emanuele, D. Attwood, *Adv. Drug Delivery Rev.* **2005**, *57*, 2147-2162.
- [241] D. Astruc, C. Ornelas, J. Ruiz, *Acc. Chem. Res.* **2008**, *41*, 841-856.
- [242] E. de Jesús, J. C. Flores, *Ind. Eng. Chem. Res.* **2008**, *47*, 7968-7981.
- [243] D. Astruc, E. Boisselier, C. Ornelas, *Chem. Rev.* **2010**, *110*, 1857-1959.
- [244] R. Hourani, A. Kakkar, *Macromol. Rapid Commun.* **2010**, *31*, 947-974.
- [245] A. Sellinger, T. Zhou, Conjugated Dendrimers, in *Encyclopedia of Polymeric Nanomaterials* Springer, Berlin, **2015**, pp. 412-427.
- [246] A. R. Menjoge, R. M. Kannan, D. A. Tomalia, *Drug Discov. Today* **2010**, *15*, 171-185.
- [247] R. Kopelman, M. Shortreed, Z.-Y. Shi, W. Tan, Z. Xu, J. S. Moore, A. Bar-Haim, J. Klafter, *Phys. Rev. Lett.* **1997**, *78*, 1239-1242.
- [248] Y. Shirota, Y. Kuwabara, H. Inada, T. Wakimoto, H. Nakada, Y. Yonemoto, S. Kawami, K. Imai, *Appl. Phys. Lett.* **1994**, *65*, 807-809.
- [249] J. Bettenhausen, M. Greczmiel, M. Jandke, P. Stroehriegl, *Synth. Met.* **1997**, *91*, 223-228.
- [250] J. M. Lupton, I. D. W. Samuel, R. Beavington, M. J. Frampton, P. L. Burn, H. Bäessler, *Phys. Rev. B* **2001**, *63*, 155206.
- [251] J. Ding, B. Zhang, J. Lü, Z. Xie, L. Wang, X. Jing, F. Wang, *Adv. Mater.* **2009**, *21*, 4983-4986.
- [252] J.-L. Wang, Y. Zhou, Y. Li, J. Pei, *J. Org. Chem.* **2009**, *74*, 7449-7456.
- [253] J.-L. Wang, Z.-M. Tang, Q. Xiao, Y. Ma, J. Pei, *Org. Lett.* **2008**, *10*, 4271-4274.
- [254] T. Shimamoto, K. Miyanari, A. Fujii, I. Akai, M. Kimura, *Phys. Status Solidi C* **2011**, *8*, 58-61.
- [255] M. Halim, I. D. W. Samuel, J. N. G. Pillow, P. L. Burn, *Synth. Met.* **1999**, *102*, 1113-1114.
- [256] S.-C. Lo, G. J. Richards, J. P. J. Markham, E. B. Namdas, S. Sharma, P. L. Burn, I. D. W. Samuel, *Adv. Funct. Mater.* **2005**, *15*, 1451-1458.
- [257] T. D. Anthopoulos, M. J. Frampton, E. B. Namdas, P. L. Burn, I. D. W. Samuel, *Adv. Mater.* **2004**, *16*, 557-560.
- [258] J. C. Ribierre, A. Ruseckas, I. D. W. Samuel, H. S. Barcena, P. L. Burn, *J. Chem. Phys.* **2008**, *128*, 204703.
- [259] S.-C. Lo, N. A. H. Male, J. P. J. Markham, S. W. Magennis, P. L. Burn, O. V. Salata, I. D. W. Samuel, *Adv. Mater.* **2002**, *14*, 975-979.
- [260] N. Kopidakis, W. J. Mitchell, J. v. d. Lagemaat, D. S. Ginley, G. Rumbles, S. E. Shaheen, W. L. Rance, *Appl. Phys. Lett.* **2006**, *89*, 103524.
- [261] C.-Q. Ma, M. Fonrodona, M. C. Schikora, M. M. Wienk, R. A. J. Janssen, P. Bäuerle, *Adv. Funct. Mater.* **2008**, *18*, 3323-3331.
- [262] C.-Q. Ma, E. Mena-Osteritz, T. Debaerdemaeker, M. M. Wienk, R. A. J. Janssen, P. Bäuerle, *Angew. Chem. Int. Ed.* **2007**, *46*, 1679-1683; *Angew. Chem.* **2007**, *119*, 1709-1713.
- [263] G. Wu, R. F. Barth, W. Yang, M. Chatterjee, W. Tjarks, M. J. Ciesielski, R. A. Fenstermaker, *Bioconjugate Chem.* **2004**, *15*, 185-194.
- [264] R. Roesler, B. J. N. Har, W. E. Piers, *Organometallics* **2002**, *21*, 4300-4302.
- [265] B. Qualmann, M. M. Kessels, H.-J. Musiol, W. D. Sierralta, P. W. Jungblut, L. Moroder, *Angew. Chem. Int. Ed.* **1996**, *35*, 909-911; *Angew. Chem.* **1996**, *108*, 970-973.

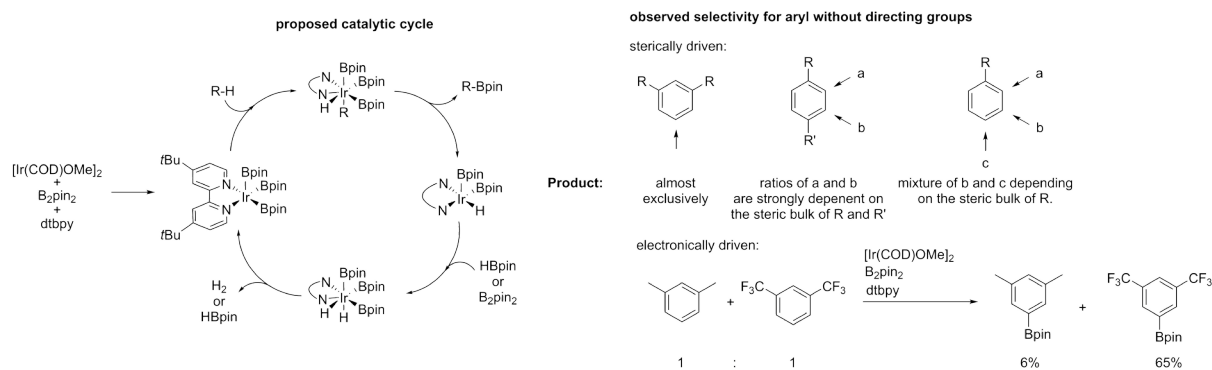
- [266] D. Armspach, M. Cattalini, E. C. Constable, C. E. Housecroft, D. Phillips, *Chem. Commun.* **1996**, 1823-1824.
- [267] H. Nemoto, J. Cai, Y. Yamamoto, *J. Chem. Soc., Chem. Commun.* **1994**, 577-578.
- [268] A. Proñ, M. Baumgarten, K. Müllen, *Org. Lett.* **2010**, *12*, 4236-4239.
- [269] T. Agou, T. Kojima, J. Kobayashi, T. Kawashima, *Org. Lett.* **2009**, *11*, 3534-3537.
- [270] I. A. I. Mkhaliid, J. H. Barnard, T. B. Marder, J. M. Murphy, J. F. Hartwig, *Chem. Rev.* **2010**, *110*, 890-931.
- [271] T. L. Rathman, W. F. Bailey, *Org. Process Res. Dev.* **2009**, *13*, 144-151.
- [272] W. F. Bailey, J. J. Patricia, *J. Organomet. Chem.* **1988**, *352*, 1-46.
- [273] F. H. Allen, O. Kennard, D. G. Watson, L. Brammer, A. G. Orpen, R. Taylor, *J. Chem. Soc., Perkin Trans. 2* **1987**, S1-S19.
- [274] K. Okada, T. Sugawa, M. Oda, *J. Chem. Soc., Chem. Commun.* **1992**, 74-75.
- [275] W. Kaim, A. Schulz, *Angew. Chem. Int. Ed.* **1984**, *23*, 615-616.
- [276] A. Schulz, W. Kaim, *Chem. Ber.* **1989**, *122*, 1863-1868.
- [277] R. F. Winter, *Organometallics* **2014**, *33*, 4517-4536.
- [278] L. Ji, R. M. Edkins, A. Lorbach, I. Krummenacher, C. Brückner, A. Eichhorn, H. Braunschweig, B. Engels, P. J. Low, T. B. Marder, *J. Am. Chem. Soc.* **2015**, *137*, 6750-6753.
- [279] A. B. Buades, V. Sanchez Arderiu, D. Olid-Britos, C. Viñas, R. Sillanpää, M. Haukka, X. Fontrodona, M. Paradinas, C. Ocal, F. Teixidor, *J. Am. Chem. Soc.* **2018**, *140*, 2957-2970.

## 4 Electronically-driven Regioselective Iridium-Catalyzed C–H Borylation of Donor- $\pi$ -Acceptor Chromophores Containing Triarylboron Acceptors

The following section is slightly modified and reproduced from ref. [4].

### 4.1 Introduction

In recent decades, three-coordinate boron containing conjugated systems such as triarylboranes have been of high academic interest.<sup>[69-73, 75-80, 165, 168, 230, 231]</sup> The relevance of boron in these systems is due to the empty  $p_z$ -orbital on boron that can act as an electron acceptor (A) in conjugated systems. Based on this, potential applications of three-coordinate boron have been investigated, such as for linear<sup>[1, 81-94, 116, 153, 170-173, 232]</sup> and non-linear<sup>[96, 100, 101, 103, 104, 106, 108-110, 113-115, 118]</sup> optics, bioimaging,<sup>[115-118, 233]</sup> sensors,<sup>[75, 119, 120, 174]</sup> frustrated Lewis pairs (FLPs),<sup>[175-181]</sup> and organic light emitting diodes (OLEDs).<sup>[54, 122, 123]</sup> The drawback of the employment of three-coordinate boron in conjugated systems, however, is their inherent reactivity towards nucleophiles, such as water, due to the empty  $p_z$ -orbital. This can be avoided by using bulky substituents or by fixing the boron center in a rigid scaffold.<sup>[166, 170, 197, 201]</sup> Only recently the use of *ortho*-trifluoromethylated aryls in triarylboranes has been established as a strategy to improve acceptor strength as well as stability.<sup>[1, 2, 77, 91, 92, 124-127, 131, 132, 134, 135, 137, 138, 202, 280]</sup> The improved acceptor strength can be attributed to the electron withdrawing nature of the trifluoromethyl groups, while the increase in stability is due to steric shielding of the boron center and its empty  $p_z$ -orbital, as well as a direct interaction of the fluorine lone pairs with the empty  $p_z$ -orbital on boron. The introduction of boron into organic systems can be efficiently carried out via a metalation/borylation strategy with different metal stabilized organic nucleophiles such as organolithium<sup>[281-283]</sup> or Grignard reagents<sup>[197, 284]</sup> with boron halides or alkoxides.<sup>[231, 285]</sup> Furthermore, boron can also be introduced via transition metal catalyzed C–X<sup>[286, 287]</sup> or C–H<sup>[144, 214, 288]</sup> activation.<sup>[145, 289]</sup> One of the most widely used and efficient catalytic systems is the iridium catalyzed C–H borylation using [Ir(COD)OMe]<sub>2</sub> (COD = 1,5-cyclooctadiene) as the precatalytic species, bis(pinacolato)diboron (B<sub>2</sub>pin<sub>2</sub>) as the boron source and 4,4'-*di**tert*butyl-2,2'-bipyridin (dtbpy) as the ligand (Scheme 4.1).<sup>[144, 145, 214, 290-295]</sup>



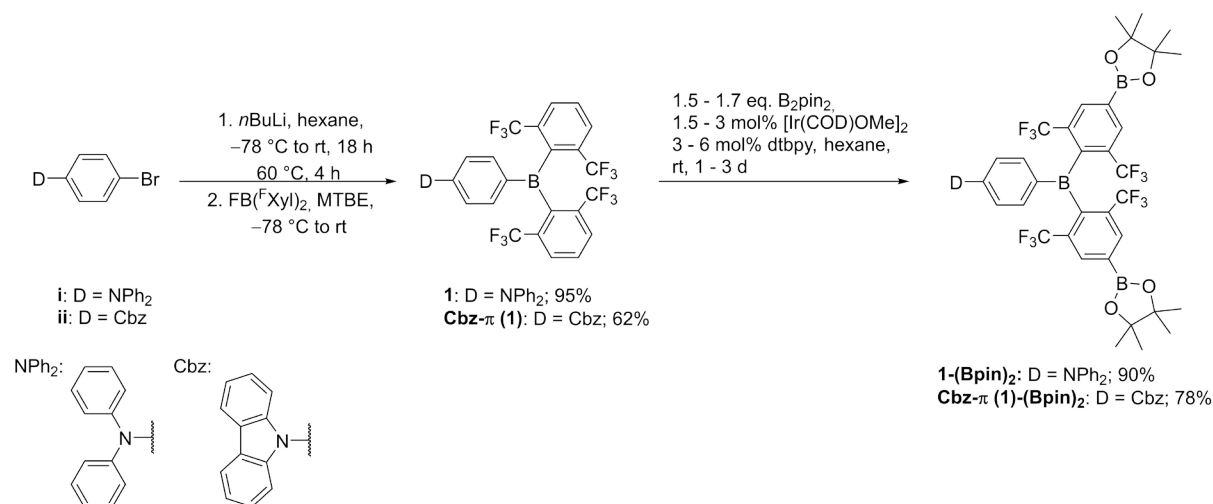
Scheme 4.1: Proposed mechanism for the iridium catalyzed C–H borylation (left).<sup>[289, 296]</sup> Sterically and electronically driven selectivity of the C–H borylation of arenes without directing groups (right).<sup>[144, 214, 289, 291, 296, 297]</sup>

This catalytic system has been thoroughly investigated and exhibits a high regioselectivity due to sterically bulky nature of the proposed catalytically active species.<sup>[93, 144, 291, 298-307]</sup> Additionally, the regioselectivity can also be influenced by functional groups<sup>[292, 293, 295, 308, 309]</sup> or via modification of the ligand.<sup>[310-313]</sup> The relevance of the iridium catalyzed C–H borylation is due to the use of boronate esters and boronic acids in Suzuki-Miyaura cross-coupling<sup>[147, 314-316]</sup> as well as the possibility of functional group transformations.<sup>[146, 285, 289, 297, 314, 317-322]</sup> In addition to the steric influence on the regioselectivity, there is also an electronic component.<sup>[323]</sup> A high electronically directed regioselectivity was observed for the borylation of quinolines<sup>[324]</sup> and the borylation of hetero-aryls.<sup>[325-328]</sup> Furthermore, in a competitive borylation experiment of a 1:1 mixture of *m*-xylene and 1,3-bis(trifluoromethyl)phenyl, only 6% borylation of *m*-xylene and 65% borylation of 1,3-bis(trifluoromethyl)phenyl were observed.<sup>[296]</sup> This illustrated the electronic favorization of electron deficient aryls or more acidic C–H bonds.

We have previously investigated donor- $\pi$ -acceptor (D- $\pi$ -A) systems with *bis*(2,6-*bis*(trifluoromethyl)phenyl)boryl ( $\text{B}(\text{FXYl})_2$ ) as the acceptor group.<sup>[1]</sup> In order to fine tune the acceptor properties we wanted to look for a regioselective methodology to functionalize the acceptor in D- $\pi$ -A systems, exclusively. Based on previous results we decided to use the iridium catalyzed C–H borylation and found the system to exhibit a surprisingly high electronically driven regioselectivity for our systems.

## 4.2 Results and Discussion

### 4.2.1 Synthesis



Scheme 4.2: Synthesis of **1**, Cbz- $\pi$  (**1**),<sup>[1]</sup> **1**-(Bpin)<sub>2</sub>, and Cbz- $\pi$  (**1**)-(Bpin)<sub>2</sub>.

Compound **1** was synthesized analogously to our previously published methodology for donor- $\pi$ -acceptor (D- $\pi$ -A) compound Cbz- $\pi$  (**1**) (Scheme 4.2).<sup>[1]</sup> The brominated donor-bridge moiety (**i** and **ii**) was lithiated using *n*-BuLi in hexane. Afterwards, bis(2,6-bis(trifluoromethyl)phenyl)fluoroborane (FB(<sup>F</sup>Xyl)<sub>2</sub>) was added in methyl *tert*-butyl ether (MTBE). We found, that the solvent mixture is important. When Et<sub>2</sub>O is used for the lithiation, the lithiation is much faster, but the reaction with FB(<sup>F</sup>Xyl)<sub>2</sub> is strongly inhibited. The amount of coordinating solvents, even weakly coordinating ones, has a strong influence on the yield and duration of the reaction. We assume that the solvent coordinates to the fluoroborane, thereby reducing the reactivity towards nucleophiles. After purification via column chromatography, compounds **1** and Cbz- $\pi$  (**1**)<sup>[1]</sup> were isolated in excellent yields. The iridium catalyzed C-H borylation was conducted in hexane at room temperature with 1.5 to 1.7 equivalents of B<sub>2</sub>pin<sub>2</sub> and a catalyst loading of 1.5 to 3 mol% and 3 to 6 mol% ligand. The mixture of catalyst, B<sub>2</sub>pin<sub>2</sub>, and ligand was stirred in hexane for 10 min before adding the D- $\pi$ -A compounds **1** and **2**, in order to form the catalytically active species before adding the substrate. The reaction was closely monitored via <sup>1</sup>H NMR spectroscopy, and only **1**-(Bpin)/Cbz- $\pi$  (**1**)-(Bpin), **1**-(Bpin)<sub>2</sub>/Cbz- $\pi$  (**1**)-(Bpin)<sub>2</sub> or unreacted **1**/Cbz- $\pi$  (**1**) were detected. This high degree of regioselectivity was surprising to us, as no borylation at the sterically less encumbered arylamino moieties could be observed. Note that the selectivity is clearly electronic in nature, as the two arenes have similar steric properties, at least at their *para*-positions. However, when the amount of B<sub>2</sub>pin<sub>2</sub> is increased to 2.2 equivalents, borylation at the donor

moieties can be observed via  $^1\text{H}$  NMR spectroscopy. Residual, small amounts of mono-borylated D- $\pi$ -A can be removed by washing with methanol and recrystallization. No column chromatography was needed, which is beneficial, as aryl-boronates can be very difficult to purify by column chromatography due to their strong interaction with the solid phase. All compounds exhibit  $^1\text{H}$ ,  $^{11}\text{B}$ ,  $^{19}\text{F}$  and  $^{13}\text{C}$  NMR spectra in accordance with their structures. The  $^{19}\text{F}$  NMR spectra exhibit strong signal broadening, indicative of a hindered rotation about the B–C bonds, as previously observed for similar boranes with *ortho*-trifluoromethyl groups.<sup>[1, 2, 131]</sup>

#### 4.2.2 Crystal and Molecular Structures

Crystals suitable for X-ray diffraction analysis of **1** and **1-(Bpin)<sub>2</sub>** were obtained from a saturated hexane solution or from a saturated  $\text{CH}_2\text{Cl}_2$  solution that was layered with hexane, respectively. The molecular structures are depicted in Figure 4.1 and selected bond lengths, distances and angles are listed in Table 4.1. The molecular structure of **Cbz- $\pi$ (1)-(Bpin)<sub>2</sub>** was obtained via single-crystal X-ray diffraction (Figure 6.25). Although the quality of the data does not allow a detailed discussion of the structural parameters, it does provide proof of the connectivity, confirming that borylation took place at the electron-poor arene rings.

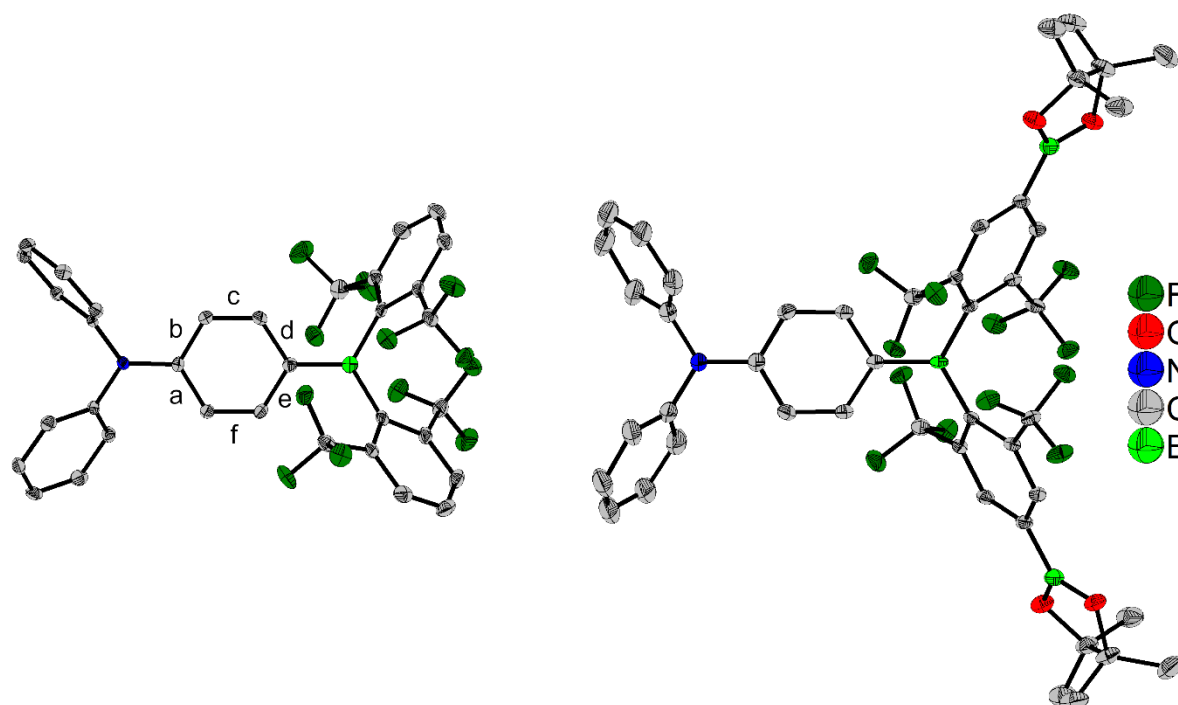


Figure 4.1: The solid-state molecular structure of **1** (left) and **1-(Bpin)<sub>2</sub>** (right) determined by single-crystal X-ray diffraction at 100 K. All ellipsoids are drawn at the 50% probability level. H atoms and solvent molecules are omitted for clarity. For **1-(Bpin)<sub>2</sub>**, the diphenylamino group ( $\text{NPh}_2$ ) is disordered by twofold rotational symmetry and only one part (50%) is shown here.



Table 4.1: Selected bond lengths, distances (Å) and angles (°) of **1** and **1-(Bpin)<sub>2</sub>**.

	<b>1</b>	<b>1-(Bpin)<sub>2</sub></b>
B–C (triarylborane, internal)	1.525(3)	1.531(5)
B–C (triarylborane, terminal)	1.611(3) 1.617(3)	1.606(3) 2x
C–N (internal)	1.395(3)	1.395(4)
C–N (terminal)	1.433(3) 1.440(3)	1.436(12) 1.430(12)
Sum ∠ CBC	360.0(2)	360.00(14)
Sum ∠ CNC	358.50(17)	359.1(7)
C–C (phenylene bridge):		
a	1.405(3)	1.407(3)
b	1.402(3)	= a
c	1.373(3)	1.374(3)
d	1.414(3)	1.408(3)
e	1.408(3)	= d
f	1.374(3)	= c
∠ BC <sub>3</sub> -NC <sub>3</sub>	37.27(9)	15.2(2)
∠ BC <sub>3</sub> -phenylene (central)	20.55(18)	23.31(11)
∠ BC <sub>3</sub> - <sup>F</sup> Xyl (terminal)	53.51(9)	51.45(7) 2x
∠ BC <sub>3</sub> - <sup>F</sup> Xyl (terminal)	52.78(8)	
∠ NC <sub>3</sub> -phenylene (central)	16.71(8)	8.2(2)
∠ NC <sub>3</sub> -phenyl (terminal)	41.86(9)	69.9(3)
∠ NC <sub>3</sub> -phenyl (terminal)	60.10(8)	71.3(3)
Shortest B...F contacts	2.769(3) 2.797(3) 2.861(3) 2.876(3)	2.822(2) 2.855(3)

The triarylboron and -nitrogen centers in **1** and **1-(Bpin)<sub>2</sub>** exhibit trigonal planar geometries with the sum of the angles around the centers of  $\approx 360^\circ$ . Compounds **1** and **1-(Bpin)<sub>2</sub>** exhibit two longer B–C bonds (1.606(3) – 1.617(3) Å) towards the terminal <sup>F</sup>Xyl moieties and one shorter B–C bond (1.525(3) and 1.531(3) Å) towards the phenylene bridge. This can be mainly attributed to the steric demand of the <sup>F</sup>Xyl *ortho*-trifluoromethyl groups. Due to the steric hinderance the <sup>F</sup>Xyl moieties also exhibit a larger torsion angles (51.45(7) – 53.51(9)°) with respect to the BC<sub>3</sub> plane than the phenylene bridge (20.55(18) and 23.31(11)°). The C–N bond lengths of **1** and **1-(Bpin)<sub>2</sub>** show a similar behavior and exhibit two longer bonds (1.430(12) – 1.440(3) Å) to the terminal phenyl moieties and one shorter bond (1.395(3) and 1.395(4) Å) to the phenylene bridge. As the steric demand of all three substituents at the N atom is equal, this can be attributed to a polarized ground state, which is well known for D- $\pi$ -A systems.<sup>[2, 115]</sup> This is further supported by the larger torsion angles of the terminal phenyl groups with respect to the NC<sub>3</sub> plane (41.86(9) – 71.3(3)°), compared to those of the phenylene bridge (16.71(8) and 8.2(2)°). The polarized ground state also results in a quinoidal distortion of the phenylene

spacer, as the c and f bonds in **1** and **1-(Bpin)<sub>2</sub>** (Figure 4.1, Table 4.1) (1.373(3) – 1.374(3) Å) are significantly shorter than the a, b, d, and e bonds (1.402(3) – 1.414(3) Å). Similar to previously reported triarylboranes bearing *ortho*-trifluoromethyl groups,<sup>[91, 124, 131, 132]</sup> the molecular structures of **1** and **1-(Bpin)<sub>2</sub>** show B...F contacts (2.769(3) – 2.876(3) Å), which are shorter than the sum of their van der Waals radii (3.39 Å),<sup>[156]</sup> indicating a stabilizing interaction between the lone pairs of the CF<sub>3</sub> fluorine atoms and the empty p<sub>z</sub>-orbital of the boron center.

### 4.2.3 Electrochemistry

Cyclic voltammograms of **1**, **1-(Bpin)<sub>2</sub>**, and **Cbz-π (1)-(Bpin)<sub>2</sub>** were recorded in CH<sub>2</sub>Cl<sub>2</sub> with [(*n*Bu)<sub>4</sub>N][PF<sub>6</sub>] as the electrolyte and a scan rate of 250 mVs<sup>-1</sup> (Figure 4.2) in order to determine their reduction and oxidation potentials, which are referenced to the ferrocene/ferrocenium redox couple (Fc/Fc<sup>+</sup>) and listed in Table 4.2. For comparison, our previously reported D-π-A systems **Cbz-π (I)**,<sup>[1]</sup> 4-(dimesitylboryl)-N,N-diphenylaniline (**I**),<sup>[131]</sup> and 4-(bis(2,4,6-tris(trifluoromethyl)phenyl)boryl)-N,N-diphenylaniline (**II**)<sup>[131]</sup> are also listed in Table 4.2.

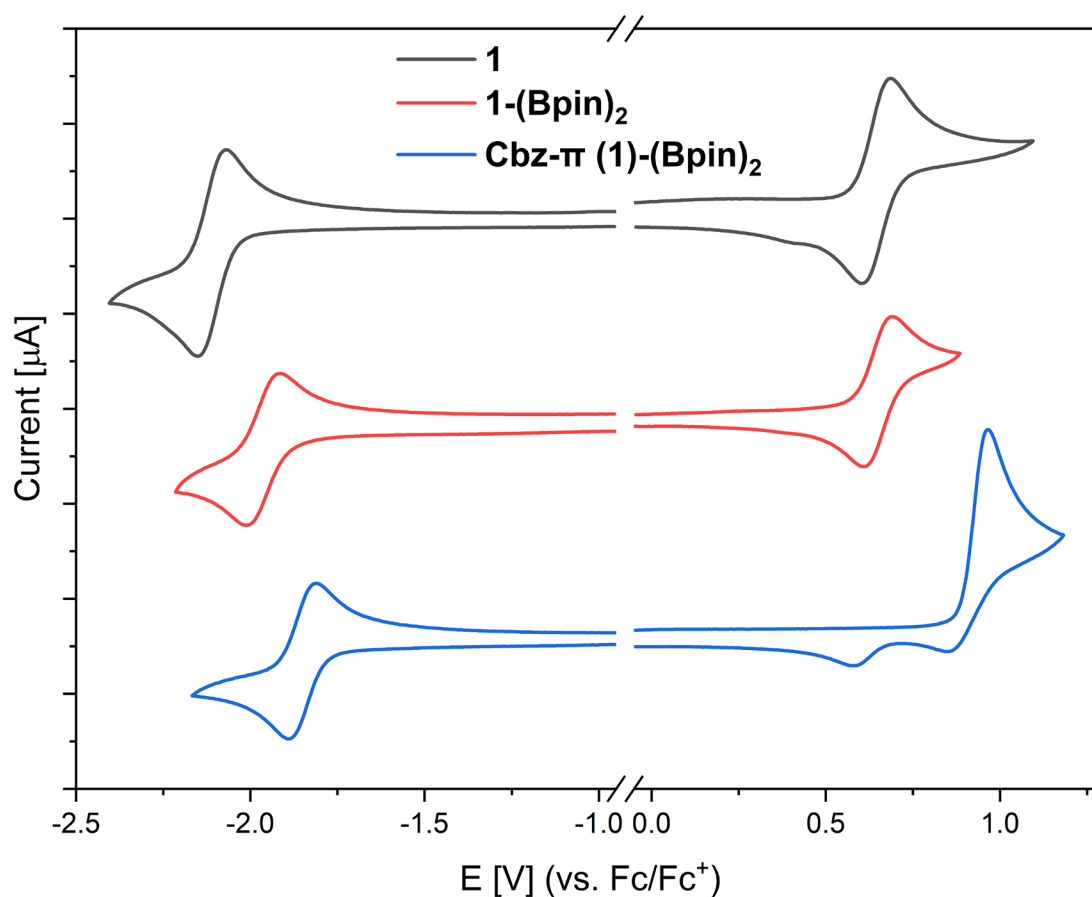


Figure 4.2: Cyclic voltammograms of **1**, **1-(Bpin)<sub>2</sub>**, and **Cbz-π (1)-(Bpin)<sub>2</sub>** in CH<sub>2</sub>Cl<sub>2</sub>. All samples are referenced to the Fc/Fc<sup>+</sup> redox couple.

Table 4.2: Reduction potentials of **1**, **1-(Bpin)<sub>2</sub>**, **Cbz- $\pi$  (1)**, **Cbz- $\pi$  (1)-(Bpin)<sub>2</sub>**, **I**, and **II** referenced to the Fc/Fc<sup>+</sup> redox couple.

Compound	<i>E</i> <sub>1/2</sub> vs. Fc/Fc <sup>+</sup> [V]	
	red	ox
<b>1</b>	-2.11	0.64
<b>1-(Bpin)<sub>2</sub></b>	-1.97	0.65
<b>Cbz-<math>\pi</math> (1)</b> <sup>[1]</sup>	-1.96	0.96 (irr) <sup>a)</sup>
<b>Cbz-<math>\pi</math> (1)-(Bpin)<sub>2</sub></b>	-1.86	0.96 (irr) <sup>a)</sup>
<b>I</b> <sup>[131]</sup>	-2.60	0.39
<b>II</b> <sup>[131]</sup>	-1.66	0.72

a) for irreversible oxidation events *E*<sub>p,a</sub> is given

Compounds **1** (*E*<sub>1/2, red</sub> = -2.11 V; *E*<sub>1/2, ox</sub> = 0.64 V) and **1-(Bpin)<sub>2</sub>** (*E*<sub>1/2, red</sub> = -1.97 V; *E*<sub>1/2, ox</sub> = 0.65 V) both exhibit reversible reduction and oxidation waves, that can be attributed to the triarylboron and nitrogen centers, respectively. **Cbz- $\pi$  (1)-(Bpin)<sub>2</sub>** (*E*<sub>1/2, red</sub> = -1.86 V; *E*<sub>p,a, ox</sub> = 0.96 V) exhibits a reversible reduction corresponding to the triarylboron center and an irreversible oxidation characteristic of the carbazolyl moiety, analogous to what was previously observed for **Cbz- $\pi$  (1)** (*E*<sub>1/2, red</sub> = -1.96 V; *E*<sub>p,a, ox</sub> = 0.96 V).<sup>[1]</sup> The reduction potentials of **1** is 150 mV cathodically shifted compared to **Cbz- $\pi$  (1)**, indicating that diphenylamine is a stronger donor than carbazolyl.<sup>[329, 330]</sup> The introduction of a Bpin group *para* to the boron on the <sup>F</sup>Xyl moieties shifts the reduction potentials anodically by 140 and 100 mV, respectively for **1** and **Cbz- $\pi$  (1)**. This indicates the electron-withdrawing nature of the boronate ester moieties. This is in line with our previously published comprehensive comparison of different boron based acceptor groups.<sup>[331]</sup> The reduction potential of **1** is anodically shifted by 490 mV compared to its mesityl analogue (**I**), and cathodically shifted by 450 mV compared to its fluoromesityl analogue (**II**).<sup>[131]</sup> This indicates the stronger electron withdrawing effect of the trifluoromethyl group *para* to the boron center as compared to the *ortho*-trifluoromethyl groups.<sup>[136]</sup>

#### 4.2.4 Photophysical Properties

The photophysical properties of **1** (Figure 4.3, Table 4.3) and **1-(Bpin)<sub>2</sub>** (Figure 4.4, Table 4.3) were examined in solvents of increasing polarity. Additionally, the photophysical properties of **Cbz- $\pi$  (1)-(Bpin)<sub>2</sub>** were also examined in hexane (Figure 4.5, Table 4.3).

## Chapter 4

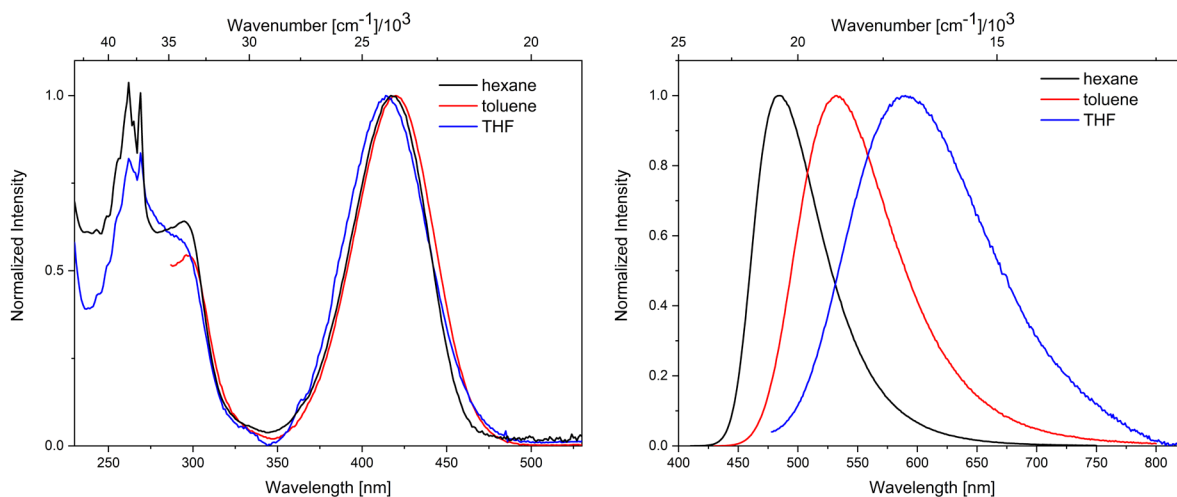


Figure 4.3: Normalized absorption (left) and emission (right) spectra of **1** in hexane (black), toluene (red), and THF (blue).

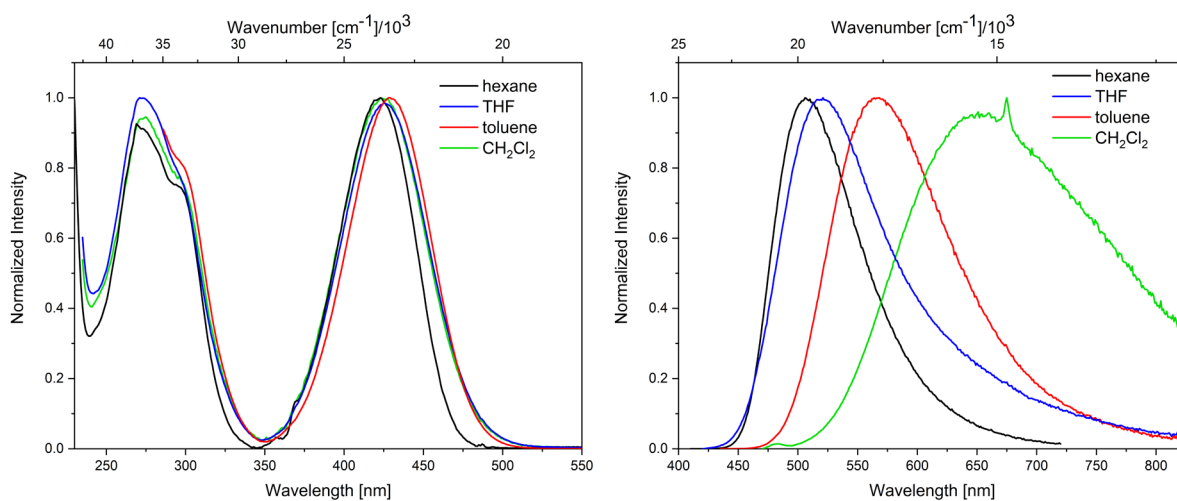


Figure 4.4: Normalized absorption (left) and emission (right) spectra of **1-(Bpin)<sub>2</sub>** in hexane (black), toluene (red), THF (blue) and  $\text{CH}_2\text{Cl}_2$  (green).

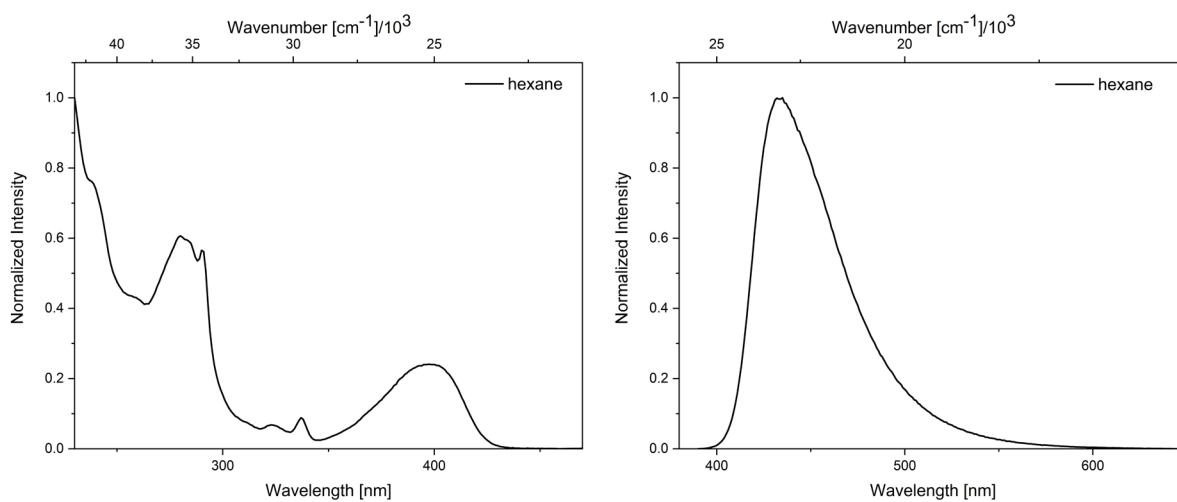


Figure 4.5: Normalized absorption (left) and emission (right) spectra of **2-Bpin<sub>2</sub>** in hexane.

Table 4.3: Photophysical properties of **1**, **1-(Bpin)<sub>2</sub>**, and **2-(Bpin)<sub>2</sub>**.

Compound	Solvent	$\lambda_{\text{max}}$ (abs.) [nm]	$\epsilon$ [M <sup>-1</sup> cm <sup>-1</sup> ]	$\lambda_{\text{max}}$ (em.) [nm]	Apparent Stokes Shift [cm <sup>-1</sup> ]	$\tau_{\text{f}}$ [ns]	$\tau_0$ [ns] <sup>a)</sup>	$\Phi_{\text{f}}$
<b>1</b>	hexane	418	35000	484	3400	10.3	10.5	0.98
	toluene	420		532	5000	9.9	11.1	0.89
	THF	414		590	7200	2.4 <sup>b)</sup>	30.0	0.08
<b>1-(Bpin)<sub>2</sub></b>	hexane	423	13000	506	3900	8.8	13.8	0.64
	toluene	428		566	5700	4.7	18.8	0.25
	THF	426		520	4200	7.2	36.0	0.20
	CH <sub>2</sub> Cl <sub>2</sub>	424		650	8200	N.D.	N.D.	N.D.
<b>Cbz-<math>\pi</math> (1)- (Bpin)<sub>2</sub></b>	hexane	398		433	2000	8.9	10.0	0.89

a) Calculated from  $\tau_{\text{f}} / \Phi_{\text{f}}$ ; b) calculated average of two lifetimes: 1.7 ns (90%), 8.6 ns (10%).

Compound **1** exhibits a broad, structureless lowest energy absorptions at  $\lambda_{\text{max, abs}} = 418, 420,$  and 414 nm in hexane, toluene and THF, respectively. No obvious shift of the absorption spectra as a function of solvent polarity is observed, indicating only a weakly polarized ground state. TD-DFT calculations on **1** at the CAM-B3LYP/6-31+G(d) level of theory suggest that the  $S_1 \leftarrow S_0$  transition can be attributed to a HOMO to LUMO transition. The HOMO is localized on the donor and  $\pi$ -bridge, and the LUMO is mainly localized on the acceptor. As such, the transition can be classified as a charge transfer (CT) transition. Similar observations were made for our previously reported D- $\pi$ -A systems with B(<sup>F</sup>Xyl)<sub>2</sub>, B(<sup>F</sup>Mes)<sub>2</sub> or BMes<sub>2</sub> as the acceptor.<sup>[1, 92, 95, 131]</sup> In accordance with a CT transition, the emission maximum of **1** shifts bathochromically with increasing solvent polarity ( $\lambda_{\text{max, em}} = 484, 532,$  and 590 nm in hexane, toluene and THF, respectively). This is expected for dipolar D- $\pi$ -A systems, due to the stabilization of the excited state in solvents of higher polarity. In comparison to our previously investigated analogues of **1** with BMes<sub>2</sub> (**I**) and B(<sup>F</sup>Mes)<sub>2</sub> (**II**), both absorption and emission of compound **1** are bathochromically shifted compared to **I** ( $\lambda_{\text{max, abs}} = 377, 380, 378$  nm;  $\lambda_{\text{max, em}} = 410, 437, 462$  nm in hexane, toluene and THF, respectively) and hypsochromically shifted compared to **II** ( $\lambda_{\text{max, abs}} = 444, 448, 441$  nm;  $\lambda_{\text{max, em}} = 563, 638, 743$  nm in hexane, toluene and THF, respectively). This supports the results from the cyclovoltammetry measurements, in that B(<sup>F</sup>Xyl)<sub>2</sub> is right in the middle between BMes<sub>2</sub> and B(<sup>F</sup>Mes)<sub>2</sub> in terms of acceptor strength. The lowest energy absorption maxima of **1-(Bpin)<sub>2</sub>** are slightly red-shifted compared to **1** ( $\lambda_{\text{max, abs}} = 423, 428, 426,$  and 424 nm in hexane, toluene, THF and CH<sub>2</sub>Cl<sub>2</sub>, respectively). The emission maxima of **1-(Bpin)<sub>2</sub>** in hexane ( $\lambda_{\text{max, em}} = 506$  nm) and toluene ( $\lambda_{\text{max, em}} = 566$  nm) are also red-shifted compared to **1** and also exhibit a bathochromic shift with increasing solvent

polarity. In THF, however, the emission maximum ( $\lambda_{\text{max, em}} = 520 \text{ nm}$ ) of **1-(Bpin)<sub>2</sub>** is blue-shifted compared to those of **1** and **1-(Bpin)<sub>2</sub>** in toluene. This is unexpected, as THF due to the higher polarity of THF a further bathochromic shift is to be expected. We suspect that this is due to the coordination of THF to the boron centers of the boronate ester moieties, as a result of which the Bpin moieties change from being weak acceptors to weak donors, decreasing the acceptor strength of the  $\text{B}(\text{FXYl})_2$  moiety, resulting in a hypsochromic shift. This is further supported by the strongly red-shifted and very weak emission of **1-Bpin<sub>2</sub>** in  $\text{CH}_2\text{Cl}_2$ , a non-coordinating polar solvent. Hence, the lowest energy transitions of **1-Bpin<sub>2</sub>** can also be classified as CT transitions. Compared to **1-(Bpin)<sub>2</sub>**, **Cbz- $\pi$  (1)-(Bpin)<sub>2</sub>** exhibits blue-shifted lowest energy absorption ( $\lambda_{\text{max, abs}} = 398 \text{ nm}$ ) and emission ( $\lambda_{\text{max, em}} = 433 \text{ nm}$ ) maxima in hexane. This can be attributed to carbazolyl being a weaker donor than diphenylamine, resulting in a weaker charge transfer (CT).<sup>[329, 330]</sup> Similarly, the previously reported lowest energy absorption ( $\lambda_{\text{max, abs}} = 400, 398, \text{ and } 387 \text{ nm}$ ) and emission ( $\lambda_{\text{max, em}} = 423, 470, \text{ and } 524 \text{ nm}$ ) maxima of **Cbz- $\pi$  (1)**<sup>[1]</sup> are also blue shifted compared to those of **1** in hexane, toluene, and THF, respectively. The quantum yield of **1** in hexane is close to unity, which is similar to that previously observed for **2**. Similar to **2**, the quantum yield of **1** in toluene is still high, but unlike **2**, the quantum yield of **1** drops drastically in THF. This could be due to the energy gap law, as internal conversion processes become more effective, as the energy gap between the excited and ground state becomes smaller, which we previously observed for similar systems.<sup>[92, 131]</sup> The quantum yields of **1-(Bpin)<sub>2</sub>** and **Cbz- $\pi$  (1)-(Bpin)<sub>2</sub>** in hexane are lower than those of their respective unborylated parent compounds **1** and **2**. The same was observed for **1-(Bpin)<sub>2</sub>** in toluene. Interestingly, the quantum yield of **1-(Bpin)<sub>2</sub>** is higher in THF than that of **1**. This is likely a result of the blue-shifted emission maximum of **1-(Bpin)<sub>2</sub>** as compared with **1**.

### 4.3 Conclusion

While looking for a methodology in order to post-functionalize D- $\pi$ -A systems, we found a surprisingly high electronically-driven regioselectivity for an iridium-catalyzed C-H borylation using  $[\text{Ir}(\text{COD})\text{OMe}]_2$  as the precatalytic species,  $\text{B}_2\text{pin}_2$  as the boron source and dtbpy as the ligand in hexane.<sup>[144, 145, 214, 290-295]</sup> We believe that, due to the versatility of boronate esters for C-C coupling or functional group transformations, this provides a good handle for post-functionalization of D- $\pi$ -A systems in order to fine tune the electronic properties as suggested by the literature.<sup>[146, 147, 285, 289, 297, 314-322]</sup> This is especially useful in light of our recent TADF paper, that illustrates the importance of the relative energy levels of donor,  $\pi$ -bridge and acceptor moiety.<sup>[1]</sup> The investigation of the electrochemical properties show that  $\text{B}(\text{FXYl})_2$  is a

stronger acceptor than  $\text{BMes}_2$  and a weaker acceptor than  $\text{B}(\text{FMe}_s)_2$ , and provides the possibility of further functionalization due to the unsubstituted *para*-position. This is also supported by the photophysical data of **1**, **1-(Bpin)<sub>2</sub>**, and **Cbz- $\pi$  (1)-(Bpin)<sub>2</sub>**. The borylated derivatives are slightly red shifted compared to their parent compounds, indicating an electron withdrawing effect of the Bpin moieties. The compounds show CT transitions with bathochromic shifts of the emission with increasing solvent polarity. A surprising exception is **1-(Bpin)<sub>2</sub>**, which exhibits a hypsochromic shift of the emission when increasing the solvent polarity from toluene to THF. This is attributed to a coordination of THF to the boron centers of the boronate ester groups and a subsequent weakening of its acceptor strength.

## 4.4 References

- [1] A. Narsaria, F. Rauch, J. Krebs, P. Endres, A. Friedrich, I. Krummenacher, H. Braunschweig, M. Finze, J. Nitsch, F. M. Bickelhaupt, T. B. Marder, *Adv. Funct. Mater.* **2020**, 10.1002/adfm.202002064.
- [2] F. Rauch, S. Fuchs, A. Friedrich, D. Sieh, I. Krummenacher, H. Braunschweig, M. Finze, T. B. Marder, *Chem. Eur. J.* **2020**, 10.1002/chem.201905559.
- [54] K. Suzuki, S. Kubo, K. Shizu, T. Fukushima, A. Wakamiya, Y. Murata, C. Adachi, H. Kaji, *Angew. Chem. Int. Ed.* **2015**, *54*, 15231-15235; *Angew. Chem.* **2015**, *127*, 15446-15450.
- [69] C. D. Entwistle, T. B. Marder, *Angew. Chem. Int. Ed.* **2002**, *41*, 2927-2931; *Angew. Chem.* **2002**, *114*, 3051-3056.
- [70] C. D. Entwistle, T. B. Marder, *Chem. Mater.* **2004**, *16*, 4574-4585.
- [71] S. Yamaguchi, A. Wakamiya, *Pure Appl. Chem.* **2006**, *78*, 1413.
- [72] F. Jäkle, *Coord. Chem. Rev.* **2006**, *250*, 1107-1121.
- [73] M. Elbing, G. C. Bazan, *Angew. Chem. Int. Ed.* **2008**, *47*, 834-838; *Angew. Chem.* **2008**, *120*, 846-850.
- [75] C. R. Wade, A. E. J. Broomsgrove, S. Aldridge, F. P. Gabbaï, *Chem. Rev.* **2010**, *110*, 3958-3984.
- [76] Z. M. Hudson, S. Wang, *Dalton Trans.* **2011**, *40*, 7805-7816.
- [77] A. Wakamiya, S. Yamaguchi, *Bull. Chem. Soc. Jpn.* **2015**, *88*, 1357-1377.
- [78] L. Ji, S. Griesbeck, T. B. Marder, *Chem. Sci.* **2017**, *8*, 846-863.
- [79] S.-Y. Li, Z.-B. Sun, C.-H. Zhao, *Inorg. Chem.* **2017**, *56*, 8705-8717.
- [80] G. Turkoglu, M. E. Cinar, T. Ozturk, *Molecules* **2017**, *22*, 1522.
- [81] N. Matsumi, K. Naka, Y. Chujo, *J. Am. Chem. Soc.* **1998**, *120*, 5112-5113.
- [82] S. Yamaguchi, S. Akiyama, K. Tamao, *J. Am. Chem. Soc.* **2000**, *122*, 6335-6336.
- [83] W.-L. Jia, D. Song, S. Wang, *J. Org. Chem.* **2003**, *68*, 701-705.
- [84] A. Wakamiya, T. Ide, S. Yamaguchi, *J. Am. Chem. Soc.* **2005**, *127*, 14859-14866.
- [85] I. Yamaguchi, B.-J. Choi, T.-A. Koizumi, K. Kubota, T. Yamamoto, *Macromolecules* **2007**, *40*, 438-443.
- [86] U. Megerle, F. Selmaier, C. Lambert, E. Riedle, S. Lochbrunner, *Phys. Chem. Chem. Phys.* **2008**, *10*, 6245-6251.
- [87] A. Lorbach, M. Bolte, H. Li, H.-W. Lerner, M. C. Holthausen, F. Jäkle, M. Wagner, *Angew. Chem. Int. Ed.* **2009**, *48*, 4584-4588; *Angew. Chem.* **2009**, *121*, 4654-4658.
- [88] L. Weber, V. Werner, M. A. Fox, T. B. Marder, S. Schwedler, A. Brockhinke, H.-G. Stammler, B. Neumann, *Dalton Trans.* **2009**, 2823-2831.
- [89] L. Weber, D. Eickhoff, T. B. Marder, M. A. Fox, P. J. Low, A. D. Dwyer, D. J. Tozer, S. Schwedler, A. Brockhinke, H.-G. Stammler, B. Neumann, *Chem. Eur. J.* **2012**, *18*, 1369-1382.
- [90] C. Reus, S. Weidlich, M. Bolte, H.-W. Lerner, M. Wagner, *J. Am. Chem. Soc.* **2013**, *135*, 12892-12907.
- [91] X. Yin, J. Chen, R. A. Lalancette, T. B. Marder, F. Jäkle, *Angew. Chem. Int. Ed.* **2014**, *53*, 9761-9765; *Angew. Chem.* **2014**, *126*, 9919-9923.
- [92] Z. Zhang, R. M. Edkins, J. Nitsch, K. Fucke, A. Eichhorn, A. Steffen, Y. Wang, T. B. Marder, *Chem. Eur. J.* **2015**, *21*, 177-190.
- [93] J. Merz, J. Fink, A. Friedrich, I. Krummenacher, H. H. Al Mamari, S. Lorenzen, M. Haehnel, A. Eichhorn, M. Moos, M. Holzapfel, H. Braunschweig, C. Lambert, A. Steffen, L. Ji, T. B. Marder, *Chem. Eur. J.* **2017**, *23*, 13164-13180.
- [94] J. Merz, A. Steffen, J. Nitsch, J. Fink, C. B. Schürger, A. Friedrich, I. Krummenacher, H. Braunschweig, M. Moos, D. Mims, C. Lambert, T. B. Marder, *Chem. Sci.* **2019**, *10*, 7516-7534.



- [95] H. Belaidi, F. Rauch, Z. Zhang, C. Latouche, A. Boucekkine, T. B. Marder, J.-F. Halet, *ChemPhotoChem* **2020**, *4*, 173-180.
- [96] Z. Yuan, N. J. Taylor, T. B. Marder, I. D. Williams, S. K. Kurtz, L.-T. Cheng, *J. Chem. Soc., Chem. Commun.* **1990**, 1489-1492.
- [100] Z. Yuan, N. J. Taylor, Y. Sun, T. B. Marder, I. D. Williams, L.-T. Cheng, *J. Organomet. Chem.* **1993**, *449*, 27-37.
- [101] Z. Yuan, N. J. Taylor, R. Ramachandran, T. B. Marder, *Appl. Organomet. Chem.* **1996**, *10*, 305-316.
- [103] Z.-Q. Liu, Q. Fang, D. Wang, G. Xue, W.-T. Yu, Z.-S. Shao, M.-H. Jiang, *Chem. Commun.* **2002**, 2900-2901.
- [104] Z.-Q. Liu, Q. Fang, D. Wang, D.-X. Cao, G. Xue, W.-T. Yu, H. Lei, *Chem. Eur. J.* **2003**, *9*, 5074-5084.
- [106] M. Charlot, L. Porres, C. D. Entwistle, A. Beeby, T. B. Marder, M. Blanchard-Desce, *Phys. Chem. Chem. Phys.* **2005**, *7*, 600-606.
- [108] Z. Yuan, C. D. Entwistle, J. C. Collings, D. Albesa-Jové, A. S. Batsanov, J. A. K. Howard, N. J. Taylor, H. M. Kaiser, D. E. Kaufmann, S.-Y. Poon, W.-Y. Wong, C. Jardin, S. Fathallah, A. Boucekkine, J.-F. Halet, T. B. Marder, *Chem. Eur. J.* **2006**, *12*, 2758-2771.
- [109] C. D. Entwistle, J. C. Collings, A. Steffen, L.-O. Pålsson, A. Beeby, D. Albesa-Jove, J. M. Burke, A. S. Batsanov, J. A. K. Howard, J. A. Mosely, S.-Y. Poon, W.-Y. Wong, F. Ibersiene, S. Fathallah, A. Boucekkine, J.-F. Halet, T. B. Marder, *J. Mater. Chem.* **2009**, *19*, 7532-7544.
- [110] J. C. Collings, S.-Y. Poon, C. Le Droumaguet, M. Charlot, C. Katan, L.-O. Pålsson, A. Beeby, J. A. Mosely, H. M. Kaiser, D. Kaufmann, W.-Y. Wong, M. Blanchard-Desce, T. B. Marder, *Chem. Eur. J.* **2009**, *15*, 198-208.
- [113] L. Ji, R. M. Edkins, L. J. Sewell, A. Beeby, A. S. Batsanov, K. Fucke, M. Drafz, J. A. K. Howard, O. Moutounet, F. Ibersiene, A. Boucekkine, E. Furet, Z. Liu, J.-F. Halet, C. Katan, T. B. Marder, *Chem. Eur. J.* **2014**, *20*, 13618-13635.
- [114] P. Chen, A. S. Marshall, S. H. Chi, X. Yin, J. W. Perry, F. Jäkle, *Chem. Eur. J.* **2015**, *21*, 18237-18247.
- [115] S. Griesbeck, Z. Zhang, M. Gutmann, T. Lühmann, R. M. Edkins, G. Clermont, A. N. Lazar, M. Haehnel, K. Edkins, A. Eichhorn, M. Blanchard-Desce, L. Meinel, T. B. Marder, *Chem. Eur. J.* **2016**, *22*, 14701-14706.
- [116] S. Griesbeck, E. Michail, C. Wang, H. Ogasawara, S. Lorenzen, L. Gerstner, T. Zang, J. Nitsch, Y. Sato, R. Bertermann, M. Taki, C. Lambert, S. Yamaguchi, T. B. Marder, *Chem. Sci.* **2019**, *10*, 5405-5422.
- [117] S. Griesbeck, M. Ferger, C. Czernetzi, C. Wang, R. Bertermann, A. Friedrich, M. Haehnel, D. Sieh, M. Taki, S. Yamaguchi, T. B. Marder, *Chem. Eur. J.* **2019**, *25*, 7679-7688.
- [118] S. Griesbeck, E. Michail, F. Rauch, H. Ogasawara, C. Wang, Y. Sato, R. M. Edkins, Z. Zhang, M. Taki, C. Lambert, S. Yamaguchi, T. B. Marder, *Chem. Eur. J.* **2019**, *25*, 13164-13175.
- [119] S. Yamaguchi, S. Akiyama, K. Tamao, *J. Am. Chem. Soc.* **2001**, *123*, 11372-11375.
- [120] T. W. Hudnall, C.-W. Chiu, F. P. Gabbaï, *Acc. Chem. Res.* **2009**, *42*, 388-397.
- [122] Y. Shirota, *J. Mater. Chem.* **2000**, *10*, 1-25.
- [123] A. Wakamiya, K. Mori, S. Yamaguchi, *Angew. Chem. Int. Ed.* **2007**, *46*, 4273-4276; *Angew. Chem.* **2007**, *119*, 4351-4354.
- [124] S. Toyota, M. Asakura, M. Oki, F. Toda, *Bull. Chem. Soc. Jpn.* **2000**, *73*, 2357-2362.
- [125] S. M. Cornet, K. B. Dillon, C. D. Entwistle, M. A. Fox, A. E. Goeta, H. P. Goodwin, T. B. Marder, A. L. Thompson, *Dalton Trans.* **2003**, 4395-4405.

- [126] Z. Lu, Z. Cheng, Z. Chen, L. Weng, Z. H. Li, H. Wang, *Angew. Chem. Int. Ed.* **2011**, *50*, 12227-12231; *Angew. Chem.* **2011**, *123*, 12435-12439.
- [127] J. Wang, Y. Wang, T. Taniguchi, S. Yamaguchi, S. Irle, *J. Phys. Chem. A* **2012**, *116*, 1151-1158.
- [131] Z. Zhang, R. M. Edkins, J. Nitsch, K. Fucke, A. Steffen, L. E. Longobardi, D. W. Stephan, C. Lambert, T. B. Marder, *Chem. Sci.* **2015**, *6*, 308-321.
- [132] Z. Zhang, R. M. Edkins, M. Haehnel, M. Wehner, A. Eichhorn, L. Mailänder, M. Meier, J. Brand, F. Brede, K. Müller-Buschbaum, H. Braunschweig, T. B. Marder, *Chem. Sci.* **2015**, *6*, 5922-5927.
- [134] X. Yin, F. Guo, R. A. Lalancette, F. Jäkle, *Macromolecules* **2016**, *49*, 537-546.
- [135] D.-T. Yang, S. K. Møllerup, J.-B. Peng, X. Wang, Q.-S. Li, S. Wang, *J. Am. Chem. Soc.* **2016**, *138*, 11513-11516.
- [136] R. J. Blagg, E. J. Lawrence, K. Resner, V. S. Oganessian, T. J. Herrington, A. E. Ashley, G. G. Wildgoose, *Dalton Trans.* **2016**, *45*, 6023-6031.
- [137] Q. Yan, M. Yin, C. Chen, Y. Zhang, *J. Org. Chem.* **2018**, *83*, 9096-9102.
- [138] T. E. Stennett, P. Bissinger, S. Griesbeck, S. Ullrich, I. Krummenacher, M. Auth, A. Sperlich, M. Stolte, K. Radacki, C.-J. Yao, F. Würthner, A. Steffen, T. B. Marder, H. Braunschweig, *Angew. Chem. Int. Ed.* **2019**, *58*, 6449-6454. *Angew. Chem.* **2019**, *131*, 6516-6521.
- [144] T. Ishiyama, J. Takagi, K. Ishida, N. Miyaura, N. R. Anastasi, J. F. Hartwig, *J. Am. Chem. Soc.* **2002**, *124*, 390-391.
- [145] E. C. Neeve, S. J. Geier, I. A. I. Mkhallid, S. A. Westcott, T. B. Marder, *Chem. Rev.* **2016**, *116*, 9091-9161.
- [146] J. M. Murphy, C. C. Tzschucke, J. F. Hartwig, *Org. Lett.* **2007**, *9*, 757-760.
- [147] A. J. J. Lennox, G. C. Lloyd-Jones, *Chem. Soc. Rev.* **2014**, *43*, 412-443.
- [153] X. Jia, J. Nitsch, L. Ji, Z. Wu, A. Friedrich, F. Kerner, M. Moos, C. Lambert, T. B. Marder, *Chem. Eur. J.* **2019**, *25*, 10845-10857.
- [156] M. Mantina, A. C. Chamberlin, R. Valero, C. J. Cramer, D. G. Truhlar, *J. Phys. Chem. A* **2009**, *113*, 5806-5812.
- [165] A. Escande, M. J. Ingleson, *Chem. Commun.* **2015**, *51*, 6257-6274.
- [166] V. M. Hertz, N. Ando, M. Hirai, M. Bolte, H.-W. Lerner, S. Yamaguchi, M. Wagner, *Organometallics* **2016**, *36*, 2512-2519.
- [168] E. von Grotthuss, A. John, T. Kaese, M. Wagner, *Asian J. Org. Chem.* **2018**, *7*, 37-53.
- [170] Z. Zhou, A. Wakamiya, T. Kushida, S. Yamaguchi, *J. Am. Chem. Soc.* **2012**, *134*, 4529-4532.
- [171] J. Yoshino, Y. Nakamura, S. Kunitomo, N. Hayashi, H. Higuchi, *Tetrahedron Lett.* **2013**, *54*, 2817-2820.
- [172] A. Ito, K. Kawanishi, E. Sakuda, N. Kitamura, *Chem. Eur. J.* **2014**, *20*, 3940-3953.
- [173] J. He, F. Rauch, A. Friedrich, D. Sieh, T. Ribbeck, I. Krummenacher, H. Braunschweig, M. Finze, T. B. Marder, *Chem. Eur. J.* **2019**, *25*, 13777-13784.
- [174] K. Parab, K. Venkatasubbaiah, F. Jäkle, *J. Am. Chem. Soc.* **2006**, *128*, 12879-12885.
- [175] G. C. Welch, R. R. S. Juan, J. D. Masuda, D. W. Stephan, *Science* **2006**, *314*, 1124-1126.
- [176] G. C. Welch, D. W. Stephan, *J. Am. Chem. Soc.* **2007**, *129*, 1880-1881.
- [177] S. J. Geier, D. W. Stephan, *J. Am. Chem. Soc.* **2009**, *131*, 3476-3477.
- [178] D. W. Stephan, G. Erker, *Angew. Chem. Int. Ed.* **2010**, *49*, 46-76; *Angew. Chem.* **2010**, *122*, 50-81.
- [179] D. W. Stephan, G. Erker, *Chem. Sci.* **2014**, *5*, 2625-2641.
- [180] D. W. Stephan, *J. Am. Chem. Soc.* **2015**, *137*, 10018-10032.
- [181] D. W. Stephan, G. Erker, *Angew. Chem. Int. Ed.* **2015**, *54*, 6400-6441; *Angew. Chem.* **2015**, *127*, 6498-6541.

- [197] H. C. Brown, V. H. Dodson, *J. Am. Chem. Soc.* **1957**, *79*, 2302-2306.
- [201] A. Wakamiya, K. Mishima, K. Ekawa, S. Yamaguchi, *Chem. Commun.* **2008**, 579-581.
- [202] M. F. Smith, S. J. Cassidy, I. A. Adams, M. Vasiliu, D. L. Gerlach, D. A. Dixon, P. A. Rupar, *Organometallics* **2016**, *35*, 3182-3191.
- [214] I. A. I. Mkhaliid, J. H. Barnard, T. B. Marder, J. M. Murphy, J. F. Hartwig, *Chem. Rev.* **2010**, *110*, 890-931.
- [230] F. Jäkle, *Chem. Rev.* **2010**, *110*, 3985-4022.
- [231] S. M. Berger, M. Ferger, T. B. Marder, **2020**, manuscript in preparation.
- [232] M. Ferger, S. M. Berger, F. Rauch, M. Schönitz, J. Rühle, J. Krebs, A. Friedrich, T. B. Marder, **2020**, manuscript in preparation.
- [233] J. Liu, S. Zhang, J. Zhu, X. Liu, G. Yang, X. Zhang, *Anal. Bioanal. Chem.* **2019**, *411*, 5223-5231.
- [280] J. Li, C. G. Daniliuc, G. Kehr, G. Erker, *Angew. Chem. Int. Ed.* **2019**, *58*, 6737-6741; *Angew. Chem.* **2019**, *58*, 6737-6741.
- [281] G. Wittig, W. Herwig, *Chem. Ber.* **1955**, *88*, 962-976.
- [282] G. Wittig, G. Keicher, A. Rückert, P. Raff, *Liebigs Ann. Chem.* **1949**, *563*, 110-126.
- [283] J. C. Doty, B. Babb, P. J. Grisdale, M. Glogowski, J. L. R. Williams, *J. Organomet. Chem.* **1972**, *38*, 229-236.
- [284] R. T. Hawkins, W. J. Lennarz, H. R. Snyder, *J. Am. Chem. Soc.* **1960**, *82*, 3053-3059.
- [285] *Boronic Acids: Preparation and Applications in Organic Synthesis, Medicine and Materials*, 2nd, D. G. Hall, Wiley-VCH, Weinheim, **2011**.
- [286] T. Ishiyama, M. Murata, N. Miyaura, *J. Org. Chem.* **1995**, *60*, 7508-7510.
- [287] W. K. Chow, O. Y. Yuen, P. Y. Choy, C. M. So, C. P. Lau, W. T. Wong, F. Y. Kwong, *RSC Adv.* **2013**, *3*, 12518-12539.
- [288] T. Ishiyama, K. Ishida, J. Takagi, N. Miyaura, *Chem. Lett.* **2001**, *30*, 1082-1083.
- [289] J. F. Hartwig, *Acc. Chem. Res.* **2012**, *45*, 864-873.
- [290] J. Y. Cho, M. K. Tse, D. Holmes, R. E. Maleczka, Jr., M. R. Smith, 3rd, *Science* **2002**, *295*, 305-308.
- [291] J. F. Hartwig, *Chem. Soc. Rev.* **2011**, *40*, 1992-2002.
- [292] P. C. Roosen, V. A. Kallepalli, B. Chattopadhyay, D. A. Singleton, R. E. Maleczka, Jr., M. R. Smith, 3rd, *J. Am. Chem. Soc.* **2012**, *134*, 11350-11353.
- [293] A. J. Roering, L. V. A. Hale, P. A. Squier, M. A. Ringgold, E. R. Wiederspan, T. B. Clark, *Org. Lett.* **2012**, *14*, 3558-3561.
- [294] A. G. Crawford, Z. Liu, I. A. I. Mkhaliid, M.-H. Thibault, N. Schwarz, G. Alcaraz, A. Steffen, J. C. Collings, A. S. Batsanov, J. A. K. Howard, T. B. Marder, *Chem. Eur. J.* **2012**, *18*, 5022-5035.
- [295] A. Ros, R. Fernandez, J. M. Lassaletta, *Chem. Soc. Rev.* **2014**, *43*, 3229-3243.
- [296] T. M. Boller, J. M. Murphy, M. Hapke, T. Ishiyama, N. Miyaura, J. F. Hartwig, *J. Am. Chem. Soc.* **2005**, *127*, 14263-14278.
- [297] J. M. Murphy, X. Liao, J. F. Hartwig, *J. Am. Chem. Soc.* **2007**, *129*, 15434-15435.
- [298] T. Ishiyama, J. Takagi, J. F. Hartwig, N. Miyaura, *Angew. Chem. Int. Ed.* **2002**, *41*, 3056-3058; *Angew. Chem.* **2002**, *114*, 3182-3184.
- [299] G. A. Chotana, M. A. Rak, M. R. Smith, *J. Am. Chem. Soc.* **2005**, *127*, 10539-10544.
- [300] D. N. Coventry, A. S. Batsanov, A. E. Goeta, J. A. K. Howard, T. B. Marder, R. N. Perutz, *Chem. Commun.* **2005**, 2172-2174.
- [301] T. E. Hurst, T. K. Macklin, M. Becker, E. Hartmann, W. Kügel, J.-C. Parisienne-La Salle, A. S. Batsanov, T. B. Marder, V. Snieckus, *Chem. Eur. J.* **2010**, *16*, 8155-8161.
- [302] Z. Liu, Y. Wang, Y. Chen, J. Liu, Q. Fang, C. Kleeberg, T. B. Marder, *J. Org. Chem.* **2012**, *77*, 7124-7128.

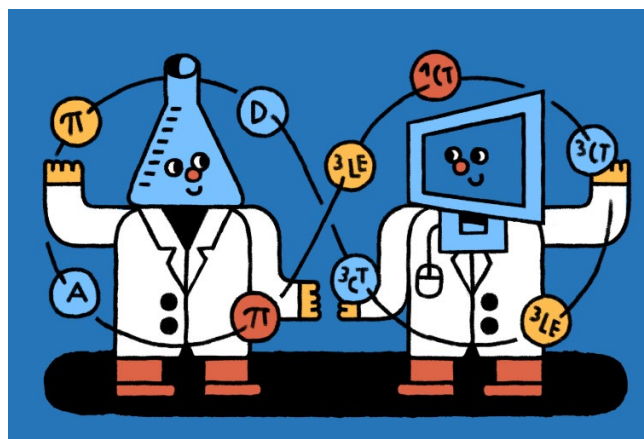
- [303] S. M. Preshlock, B. Ghaffari, P. E. Maligres, S. W. Krska, R. E. Maleczka, Jr., M. R. Smith, 3rd, *J. Am. Chem. Soc.* **2013**, *135*, 7572-7582.
- [304] L. Ji, A. Lorbach, R. M. Edkins, T. B. Marder, *J. Org. Chem.* **2015**, *80*, 5658-5665.
- [305] L. Ji, K. Fucke, S. K. Bose, T. B. Marder, *J. Org. Chem.* **2015**, *80*, 661-665.
- [306] L. Ji, I. Krummenacher, A. Friedrich, A. Lorbach, M. Haehnel, K. Edkins, H. Braunschweig, T. B. Marder, *J. Org. Chem.* **2018**, *83*, 3599-3606.
- [307] Y. Kuroda, Y. Nakao, *Chem. Lett.* **2019**, *48*, 1092-1100.
- [308] S. Paul, G. A. Chotana, D. Holmes, R. C. Reichle, R. E. Maleczka, Jr., M. R. Smith, 3rd, *J. Am. Chem. Soc.* **2006**, *128*, 15552-15553.
- [309] S. Konishi, S. Kawamorita, T. Iwai, P. G. Steel, T. B. Marder, M. Sawamura, *Chem. Asian J.* **2014**, *9*, 434-438.
- [310] Y. Kuninobu, H. Ida, M. Nishi, M. Kanai, *Nat. Chem.* **2015**, *7*, 712-717.
- [311] H. J. Davis, M. T. Mihai, R. J. Phipps, *J. Am. Chem. Soc.* **2016**, *138*, 12759-12762.
- [312] R. Bisht, B. Chattopadhyay, *J. Am. Chem. Soc.* **2016**, *138*, 84-87.
- [313] L. Yang, K. Semba, Y. Nakao, *Angew. Chem. Int. Ed.* **2017**, *56*, 4853-4857; *Angew. Chem.* **2017**, *129*, 4931-4935.
- [314] N. Miyaura, A. Suzuki, *Chem. Rev.* **1995**, *95*, 2457-2483.
- [315] A. Suzuki, *Heterocycles* **2010**, *80*, 15-43.
- [316] A. Suzuki, *Angew. Chem., Int. Ed.* **2011**, *50*, 6722-6737; *Angew. Chem.* **2011**, *123*, 6854-6869.
- [317] G. K. S. Prakash, C. Panja, T. Mathew, V. Surampudi, N. A. Petasis, G. A. Olah, *Org. Lett.* **2004**, *6*, 2205-2207.
- [318] C. C. Tzschucke, J. M. Murphy, J. F. Hartwig, *Org. Lett.* **2007**, *9*, 761-764.
- [319] C. W. Liskey, X. Liao, J. F. Hartwig, *J. Am. Chem. Soc.* **2010**, *132*, 11389-11391.
- [320] P. Novák, A. Lishchynskiy, V. V. Grushin, *Angew. Chem. Int. Ed.* **2012**, *51*, 7767-7770; *Angew. Chem.* **2012**, *124*, 7887-7890.
- [321] P. J. Moon, H. M. Halperin, R. J. Lundgren, *Angew. Chem. Int. Ed.* **2016**, *55*, 1894-1898; *Angew. Chem.* **2016**, *128*, 1926-1930.
- [322] A. Gevorgyan, K. H. Hopmann, A. Bayer, *Chem. Eur. J.* **2020**, *26*, 6064-6069.
- [323] B. A. Vanchura, 2nd, S. M. Preshlock, P. C. Roosen, V. A. Kallepalli, R. J. Staples, R. E. Maleczka, Jr., D. A. Singleton, M. R. Smith, 3rd, *Chem. Commun.* **2010**, *46*, 7724-7726.
- [324] H. Tajuddin, P. Harrisson, B. Bitterlich, J. C. Collings, N. Sim, A. S. Batsanov, M. S. Cheung, S. Kawamorita, A. C. Maxwell, L. Shukla, J. Morris, Z. Lin, T. B. Marder, P. G. Steel, *Chem. Sci.* **2012**, *3*, 3505-3515.
- [325] J. Takagi, K. Sato, J. F. Hartwig, T. Ishiyama, N. Miyaura, *Tetrahedron Lett.* **2002**, *43*, 5649-5651.
- [326] T. Ishiyama, J. Takagi, Y. Yonekawa, J. F. Hartwig, N. Miyaura, *Adv. Synth. Catal.* **2003**, *345*, 1103-1106.
- [327] S. A. Sadler, H. Tajuddin, I. A. I. Mkhallid, A. S. Batsanov, D. Albesa-Jove, M. S. Cheung, A. C. Maxwell, L. Shukla, B. Roberts, D. C. Blakemore, Z. Lin, T. B. Marder, P. G. Steel, *Org. Biomol. Chem.* **2014**, *12*, 7318-7327.
- [328] S. A. Sadler, A. C. Hones, B. Roberts, D. Blakemore, T. B. Marder, P. G. Steel, *J. Org. Chem.* **2015**, *80*, 5308-5314.
- [329] X.-M. Wang, Y.-F. Zhou, W.-T. Yu, C. Wang, Q. Fang, M.-H. Jiang, H. Lei, H.-Z. Wang, *J. Mater. Chem.* **2000**, *10*, 2698-2703.
- [330] O. Kwon, S. Barlow, S. A. Odom, L. Beverina, N. J. Thompson, E. Zojer, J.-L. Brédas, S. R. Marder, *J. Phys. Chem. A* **2005**, *109*, 9346-9352.
- [331] L. Weber, V. Werner, M. A. Fox, T. B. Marder, S. Schwedler, A. Brockhinke, H.-G. Stammler, B. Neumann, *Dalton Trans.* **2009**, 1339-1351.

## 5 Summary/Zusammenfassung

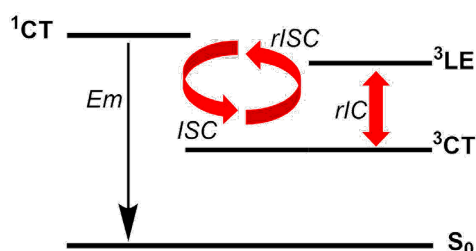
The summaries are, in part, modified reproductions of the corresponding publications of Chapters 1 - 4 with the permission of Wiley-VCH.<sup>[1-4]</sup>

### 5.1 Summary

#### 5.1.1 Chapter 1



Thermally activated delayed fluorescence (TADF) materials provide a strategy to improve external quantum efficiencies of organic light emitting diodes (OLEDs). Because of spin-statistics, 25% singlet and 75% triplet excitons are generated in an electronic device. Conventional organic emitters cannot harvest the triplet excitons, due to low spin orbit coupling, and exhibit low external quantum efficiencies. TADF materials have to be designed in such a way, that the energy gap between the lowest singlet and triplet states ( $\Delta E_{S-T}$ ) is sufficiently small to allow reverse intersystem crossing (rISC) in organic systems (Scheme 5.1).

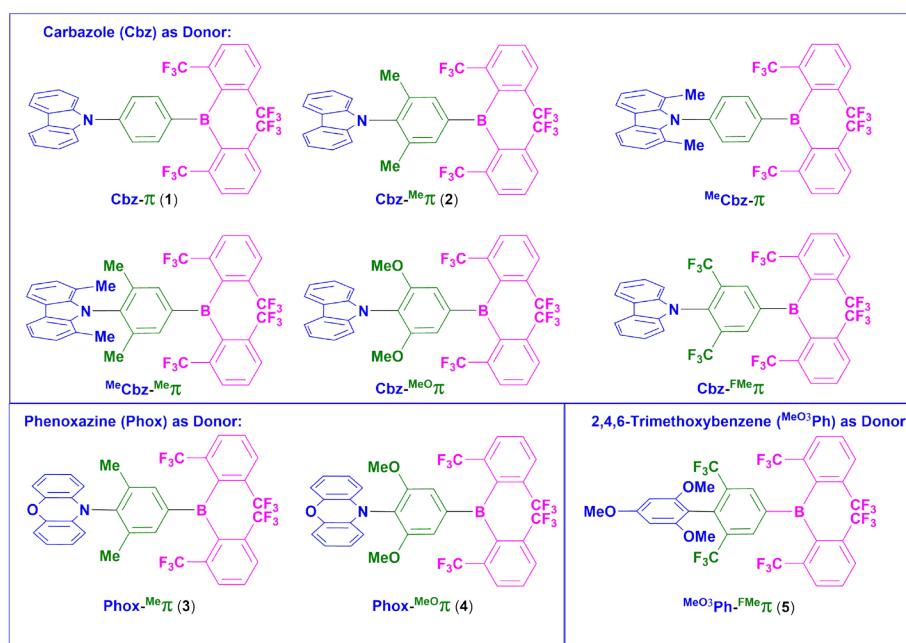


Scheme 5.1: Dynamic two-step TADF mechanism for a D-A molecule. Em: emission; ISC: intersystem crossing; rISC: reverse intersystem crossing; and rIC: reverse internal conversion.

An established structure property relationship for the generation of TADF materials is the spatial separation of HOMO and LUMO via an orthogonal arrangement of donor and acceptor in donor- $\pi$ -acceptor (D- $\pi$ -A) compounds. This is achieved by increasing the steric bulk of the

$\pi$ -bridge. However, this is not always the most efficient method and electronic parameters have to be considered.

In a combined experimental and theoretical study, a computational protocol to predict the excited states in D- $\pi$ -A compounds containing the B(<sup>F</sup>Xyl)<sub>2</sub> (<sup>F</sup>Xyl = 2,6-bis(trifluoromethyl)phenyl) acceptor group for the design of new TADF emitters is presented. To this end, the effect of different donor and  $\pi$ -bridge moieties on the energy gaps between local and charge-transfer singlet and triplet states was examined (Scheme 5.2).



Scheme 5.2: Calculated D- $\pi$ -A systems with varying substituents on the donor (blue) and  $\pi$ -bridge (green), while the acceptor (magenta) is the same in all compounds. Compounds **Cbz- $\pi$  (1)**, **Cbz-Me $\pi$  (2)**, **Phox-Me $\pi$  (3)**, **Phox-MeO $\pi$  (4)**, and **MeO<sub>3</sub>Ph-FMe $\pi$  (5)** were synthesized and fully characterized.

To prove the computationally aided design concept, the D- $\pi$ -B(<sup>F</sup>Xyl)<sub>2</sub> compounds **Cbz- $\pi$  (1)**, **Cbz-Me $\pi$  (2)**, **Phox-Me $\pi$  (3)**, **Phox-MeO $\pi$  (4)**, and **MeO<sub>3</sub>Ph-FMe $\pi$  (5)** were synthesized and fully characterized. The photophysical properties of these compounds in various solvents, polymeric film and in a frozen matrix were investigated in detail and show excellent agreement with the computationally obtained data (Figure 5.1).

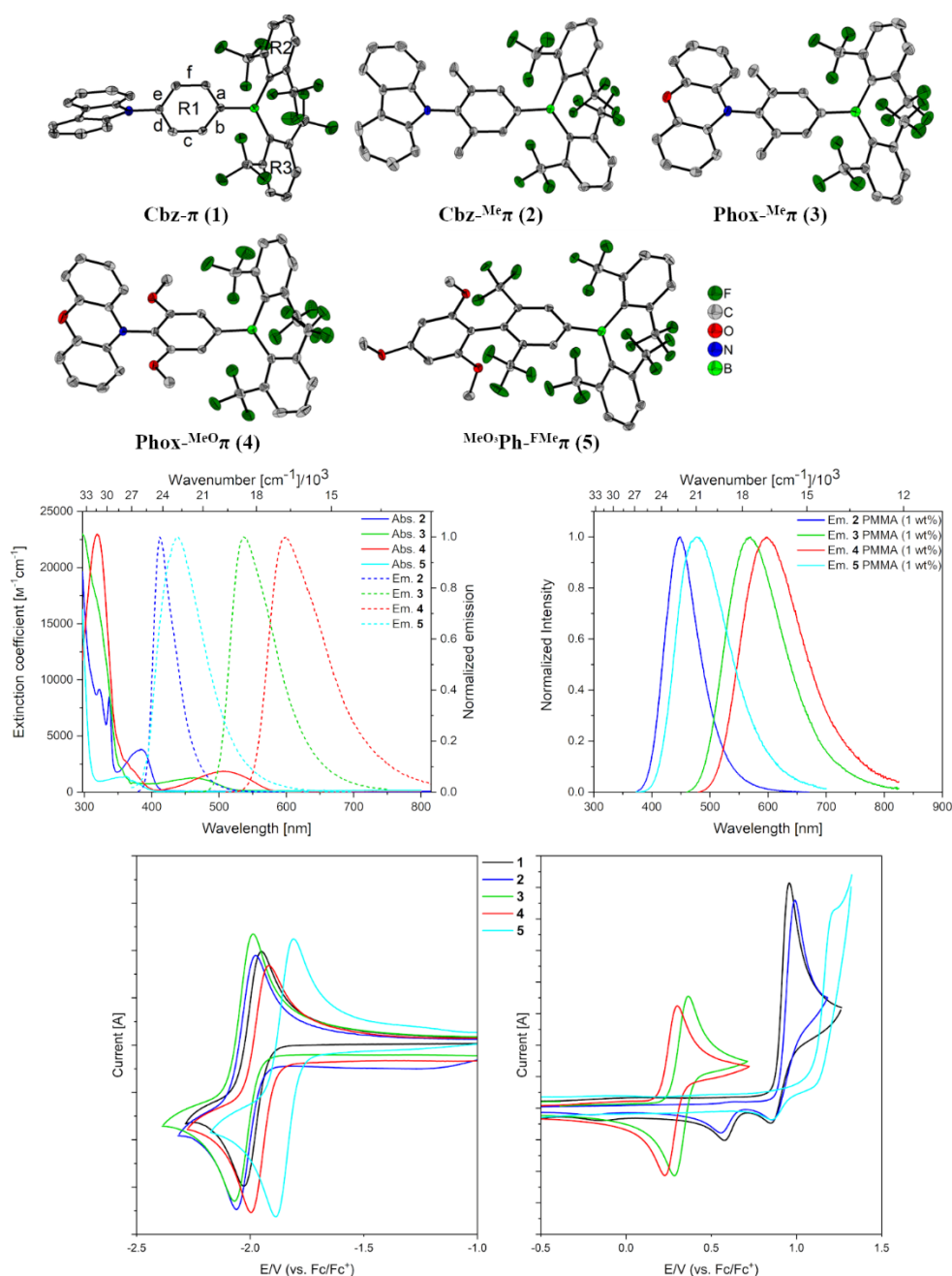
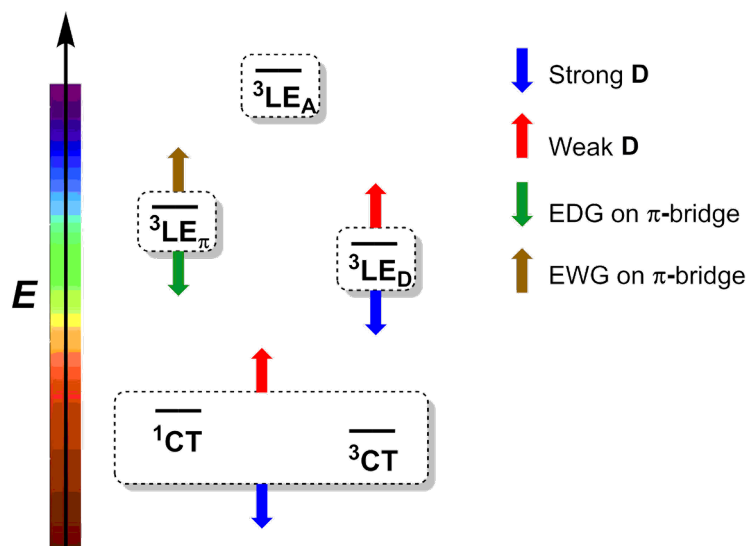


Figure 5.1: Molecular structures of **Cbz- $\pi$  (1)**, **Cbz-Me $\pi$  (2)**, **Phox-Me $\pi$  (3)**, **Phox-MeO $\pi$  (4)**, and **MeO<sub>2</sub>Ph-FMe $\pi$  (5)** as determined by X-ray diffraction (top). Absorption and emission spectra of **Cbz- $\pi$  (1)**, **Cbz-Me $\pi$  (2)**, **Phox-Me $\pi$  (3)**, **Phox-MeO $\pi$  (4)**, and **MeO<sub>2</sub>Ph-FMe $\pi$  (5)** in hexane (middle, left). Normalized emission spectra of **Cbz- $\pi$  (1)**, **Cbz-Me $\pi$  (2)**, **Phox-Me $\pi$  (3)**, **Phox-MeO $\pi$  (4)**, and **MeO<sub>2</sub>Ph-FMe $\pi$  (5)** in PMMA film (1 wt%) (middle, right). Cyclic voltammograms of **Cbz- $\pi$  (1)**, **Cbz-Me $\pi$  (2)**, **Phox-Me $\pi$  (3)**, **Phox-MeO $\pi$  (4)**, and **MeO<sub>2</sub>Ph-FMe $\pi$  (5)** (bottom).

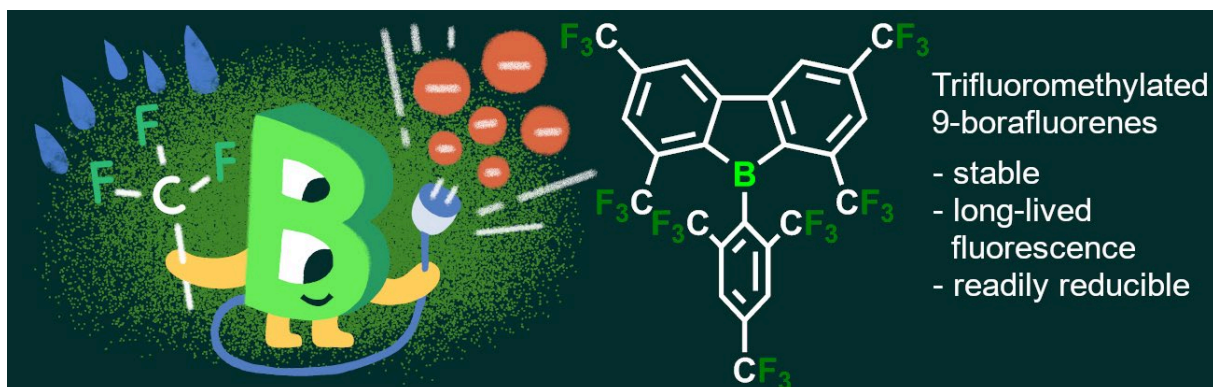
A simple structure-property relationship based on the molecular fragment orbitals of the donor and the  $\pi$ -bridge which minimize the relevant singlet-triplet gaps to achieve efficient TADF emitters is presented (Scheme 5.3).



Scheme 5.3: Schematic illustration of the independent tuning of the local excited state on the  $\pi$ -bridge ( ${}^3\text{LE}_\pi$ ); the local excited state on the donor D ( ${}^3\text{LE}_\text{D}$ ) and the charge transfer from donor D to acceptor A in a D- $\pi$ -A molecule. The local excited state ( ${}^3\text{LE}_\text{A}$ ) on the acceptor is almost independent of the variation of the donor and bridge moieties. Tuning of the emission color is controlled by the energy of  ${}^1\text{CT}$ .



## 5.1.2 Chapter 2



Three-coordinate boron is widely used as an acceptor in conjugated materials. In recent years the employment of trifluoromethylated aryls was shown to improve the acceptor properties of such boranes. Astonishingly, the use of *ortho*-trifluoromethylated aryls in boron containing systems also improves the stability of those systems in regard to their inherent reactivity towards nucleophiles. Borafluorenes are stronger acceptors than their non-annulated triarylborane derivatives. In previous studies, the effect of trifluoromethylated aryls as the *exo*-aryl moieties in borafluorenes, as well as the effect of fluorination on the backbone, were examined. As the latter suffers from a very low stability, systems using trifluoromethyl groups, both on the *exo*-aryl as well as the borafluorene backbone were designed in order to maximize both the stability as well as the acceptor strength.

Three different perfluoroalkylated borafluorenes were prepared and their electronic and photophysical properties were investigated. The systems have four trifluoromethyl moieties on the borafluorene moiety as well as two trifluoromethyl groups at the *ortho* positions of their *exo*-aryl moieties. They differ with regard to the *para*-substituents on their *exo*-aryl moieties, being a proton ( ${}^{\text{F}}\text{Xyl}^{\text{F}}\text{Bf}$ ), a trifluoromethyl group ( ${}^{\text{F}}\text{Mes}^{\text{F}}\text{Bf}$ ) or a dimethylamino group ( $p\text{-NMe}_2\text{-}{}^{\text{F}}\text{Xyl}^{\text{F}}\text{Bf}$ ), respectively (Figure 5.2). Furthermore, an acetonitrile adduct of  ${}^{\text{F}}\text{Mes}^{\text{F}}\text{Bf}$  was obtained and characterized.

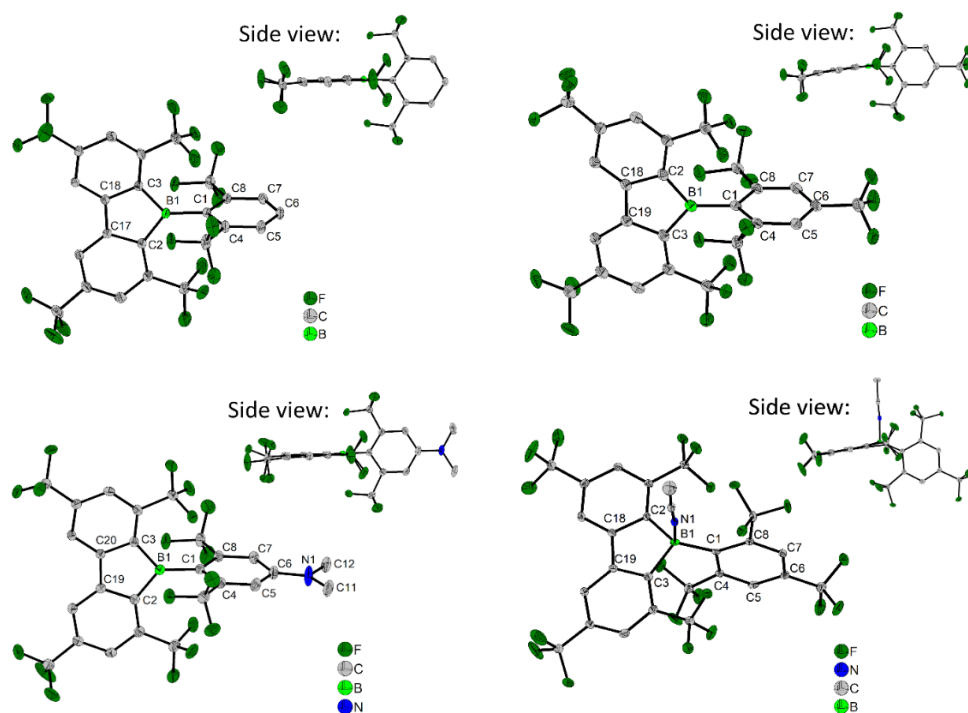


Figure 5.2: Molecular structures of  $^{\text{F}}\text{Mes}^{\text{F}}\text{Bf}$  (top left),  $^{\text{F}}\text{Xyl}^{\text{F}}\text{Bf}$  (top right),  $p\text{-NMe}_2\text{-}^{\text{F}}\text{Xyl}^{\text{F}}\text{Bf}$  (bottom left) and  $^{\text{F}}\text{Mes}^{\text{F}}\text{Bf}\cdot\text{MeCN}$  (bottom right) determined by single-crystal X-ray diffraction at 100 K. All ellipsoids are drawn at the 50% probability level, and H atoms and solvent molecules are omitted for clarity.

All derivatives exhibit extraordinarily low reduction potentials, comparable to those of perylenediimides (Figure 5.3).

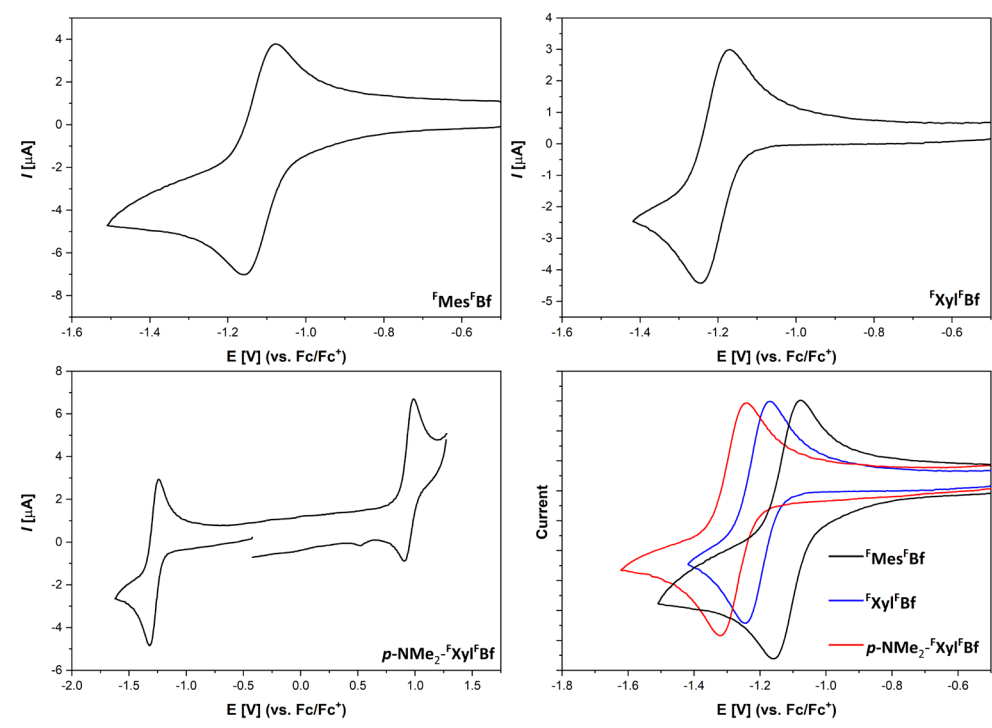


Figure 5.3: Cyclic voltammograms of the reversible redox events of  $^{\text{F}}\text{Mes}^{\text{F}}\text{Bf}$  (top left),  $^{\text{F}}\text{Xyl}^{\text{F}}\text{Bf}$  (top right) and  $p\text{-NMe}_2\text{-}^{\text{F}}\text{Xyl}^{\text{F}}\text{Bf}$  (bottom left). All samples are referenced against the  $\text{Fc}/\text{Fc}^+$  ion couple. For better comparison, the reduction waves are plotted together (bottom right;  $^{\text{F}}\text{Mes}^{\text{F}}\text{Bf}$  (black),  $^{\text{F}}\text{Xyl}^{\text{F}}\text{Bf}$  (blue),  $p\text{-NMe}_2\text{-}^{\text{F}}\text{Xyl}^{\text{F}}\text{Bf}$  (red)).

The most electron deficient derivative  ${}^{\text{F}}\text{Mes}^{\text{F}}\text{Bf}$  was also chemically reduced and its radical anion isolated and characterized (Figure 5.4 and Figure 5.5).

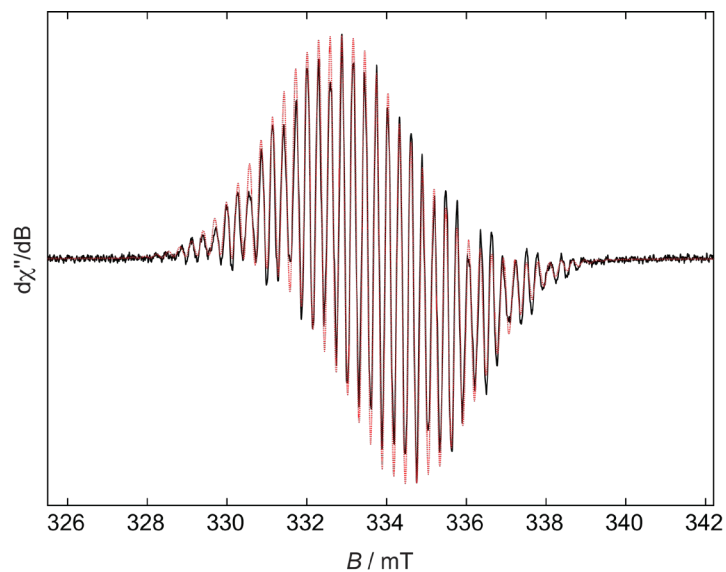


Figure 5.4: Experimental (black solid line) and simulated (red dashed line) continuous-wave X-band EPR spectra of  $[\text{FMeSFbf}]^{-}$  in a THF solution at room temperature.

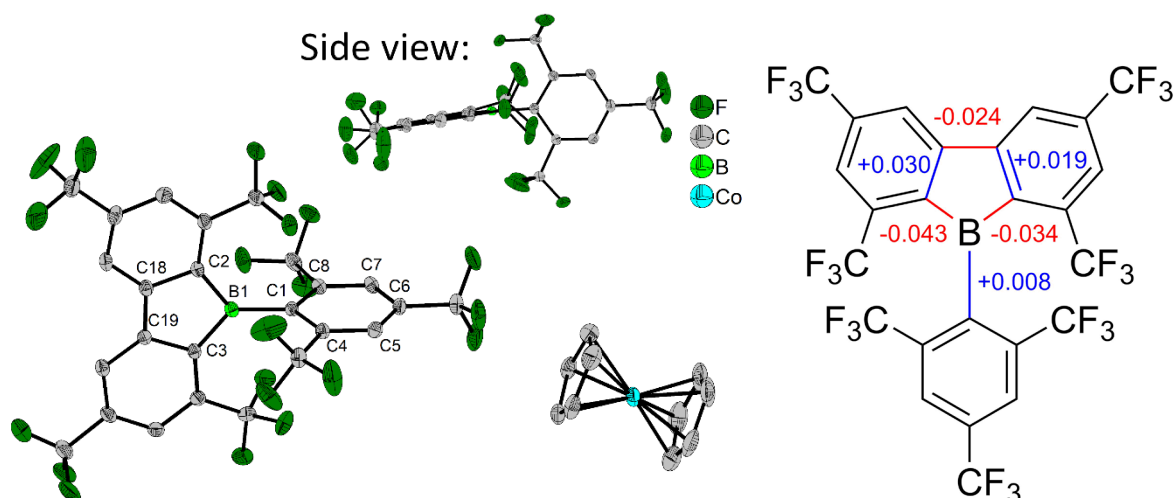


Figure 5.5: The solid-state molecular structure of  $[\text{FMeSFbf}][\text{CoCp}_2]$  determined by single-crystal X-ray diffraction at 100 K. All ellipsoids are drawn at the 50% probability level. H atoms and THF solvent molecules are omitted for clarity. Only half of the symmetrically non-equivalent molecules are shown. One of the  $\text{CF}_3$  groups on the borafuorene core is rotationally disordered and only the part with the higher occupancy (64%) is shown here (left). The relevant changes in bond lengths of  $[\text{FMeSFbf}]^{-}$  compared to the neutral starting material are shown at the right.

Furthermore, the photophysical properties of all compounds were investigated (Figure 5.6). All compounds exhibit weakly allowed lowest energy absorptions and very long fluorescent lifetimes of ca. 250 ns up to 1.6  $\mu\text{s}$ ; however, the underlying mechanisms differ.

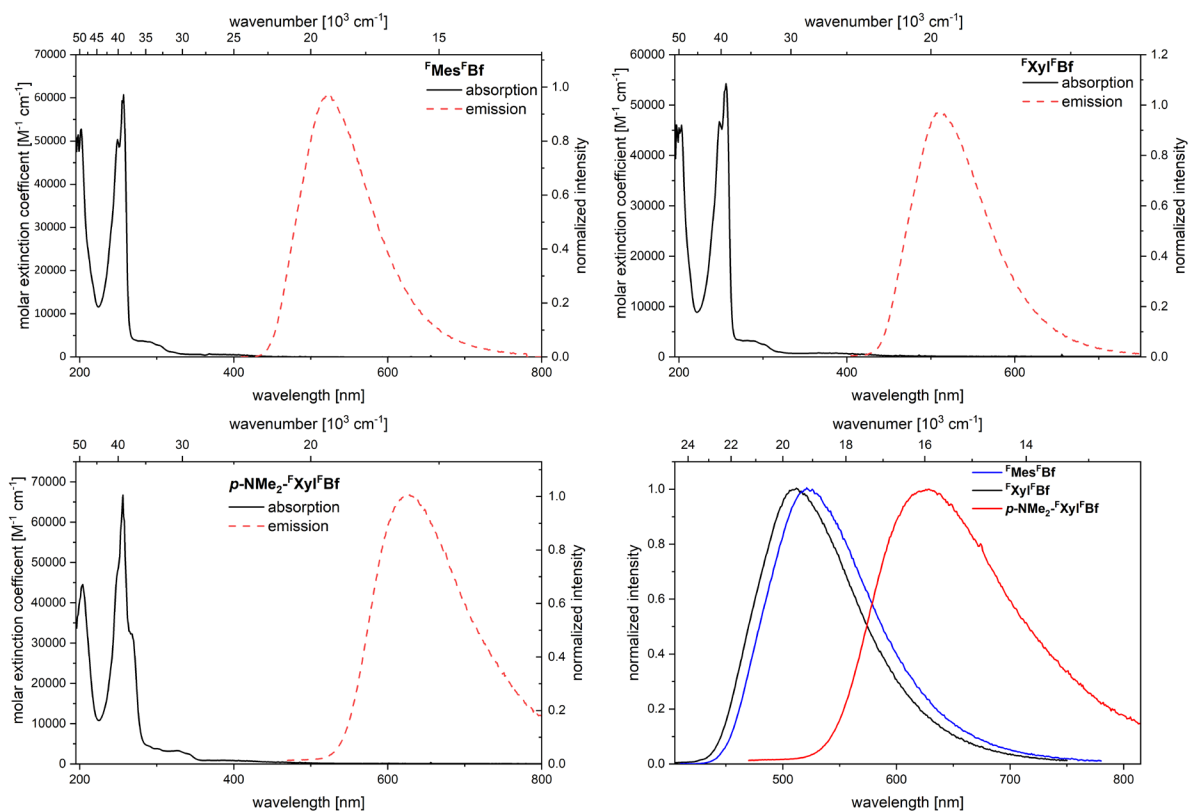
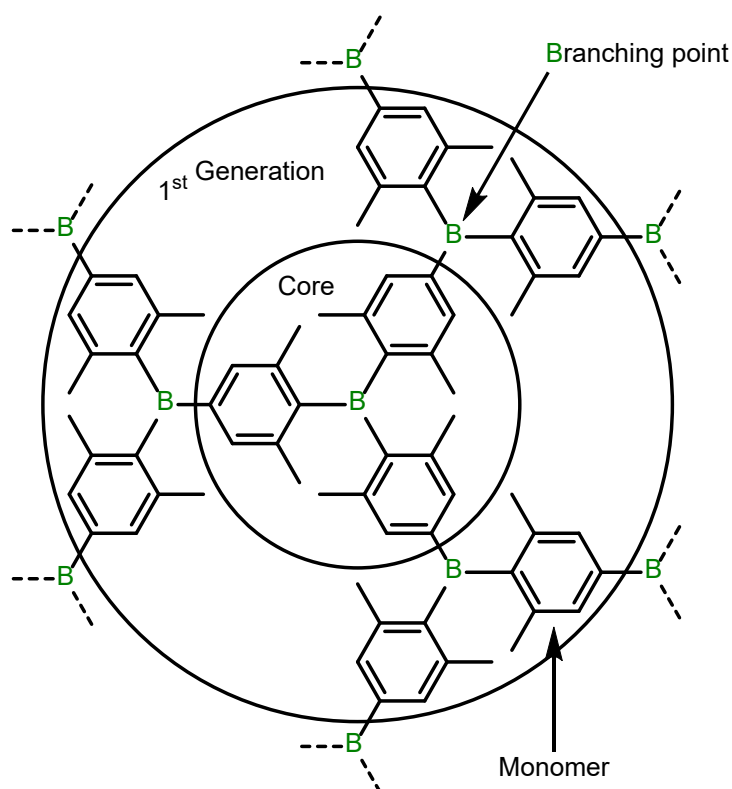


Figure 5.6: Absorption (black) and emission spectra (red) in hexane of  ${}^F\text{Mes}^F\text{Bf}$  (top left),  ${}^F\text{Xyl}^F\text{Bf}$  (top right) and  $p\text{-NMe}_2\text{-}{}^F\text{Xyl}^F\text{Bf}$  (bottom left). For comparison, the emission spectra are plotted together (bottom right;  ${}^F\text{Mes}^F\text{Bf}$  (black),  ${}^F\text{Xyl}^F\text{Bf}$  (blue),  $p\text{-NMe}_2\text{-}{}^F\text{Xyl}^F\text{Bf}$  (red)).

The donor substituted derivative  $p\text{-NMe}_2\text{-}{}^F\text{Xyl}^F\text{Bf}$  exhibits thermally activated delayed fluorescence from a charge transfer (CT) state, while the  ${}^F\text{Mes}^F\text{Bf}$  and  ${}^F\text{Xyl}^F\text{Bf}$  boron difluorides exhibit only weakly allowed locally excited (LE) transitions due to their symmetry and low transition dipole moments, as suggested by DFT and TD-DFT calculations.

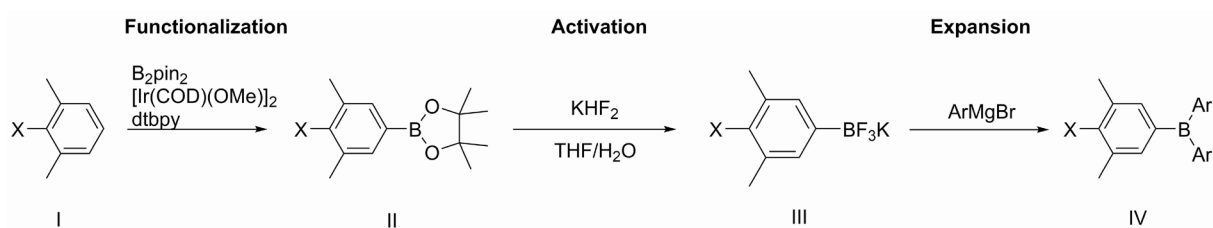
## 5.1.3 Chapter 3



Conjugated dendrimers find wide application in various fields, such as charge transport/storage or emitter materials in organic solar cells or OLEDs. Previous studies on boron containing conjugated dendrimers are scarce and mostly employ a convergent synthesis approach, lacking a simple, generally applicable synthetic access.

A new divergent approach was designed and conjugated triarylborane dendrimers were synthesized up to the 2<sup>nd</sup> generation. The synthetic strategy consists of three steps (Scheme 5.4):

- 1) functionalization, via iridium catalyzed C–H borylation;
- 2) activation, via fluorination of the generated boronate ester with  $\text{K}[\text{HF}_2]$  or  $[\text{N}(\text{nBu})_4][\text{HF}_2]$ ; and
- 3) expansion, via reaction of the trifluoroborate salts with aryl Grignard reagents.



Scheme 5.4: Divergent approach for the synthesis of conjugated starburst borane dendrimers.

The concept was also shown to be viable for a convergent approach. All but one of the conjugated borane dendrimers exhibit multiple, distinct and reversible reduction potentials, making them potentially interesting materials for applications in molecular accumulators (Figure 5.7).

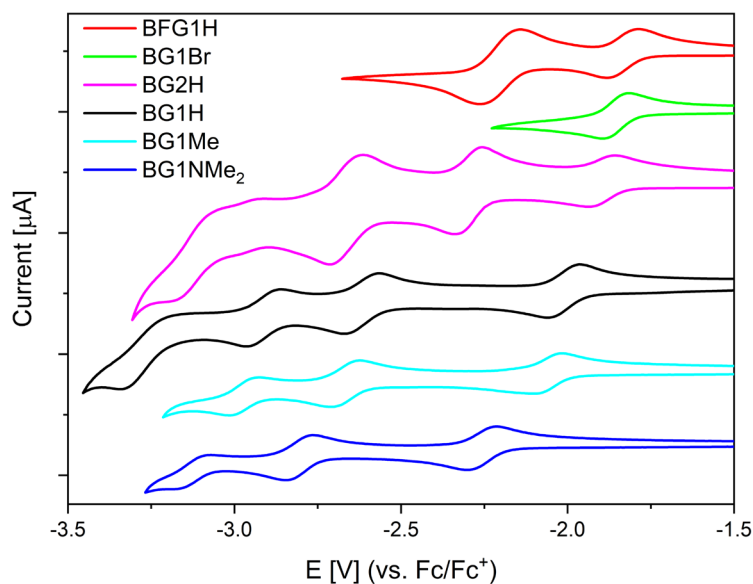


Figure 5.7: Cyclic voltammograms of **BG1H** (black), **BG1Me** (cyan), **BG1NMe<sub>2</sub>** (blue), **BG1Br** (green), **BFG1H** (red) and **BG2H** (magenta) in THF ordered by decreasing first reduction potential. All samples are referenced against the  $\text{Fc}/\text{Fc}^+$  redox couple.

Based on their photophysical properties, the 1<sup>st</sup> generation dendrimers exhibit good conjugation over the whole system. The conjugation does not further increase upon expansion to the 2<sup>nd</sup> generation, but the molar extinction coefficients increase linearly with the number of triarylborane sub-units, suggesting a potential application as photonic antennas (Figure 5.8).

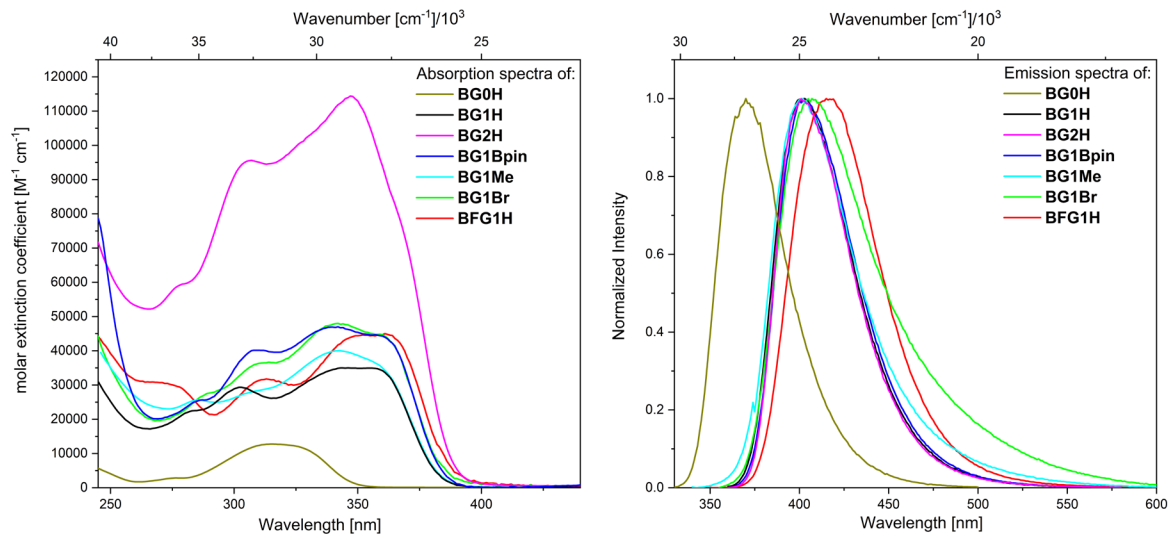
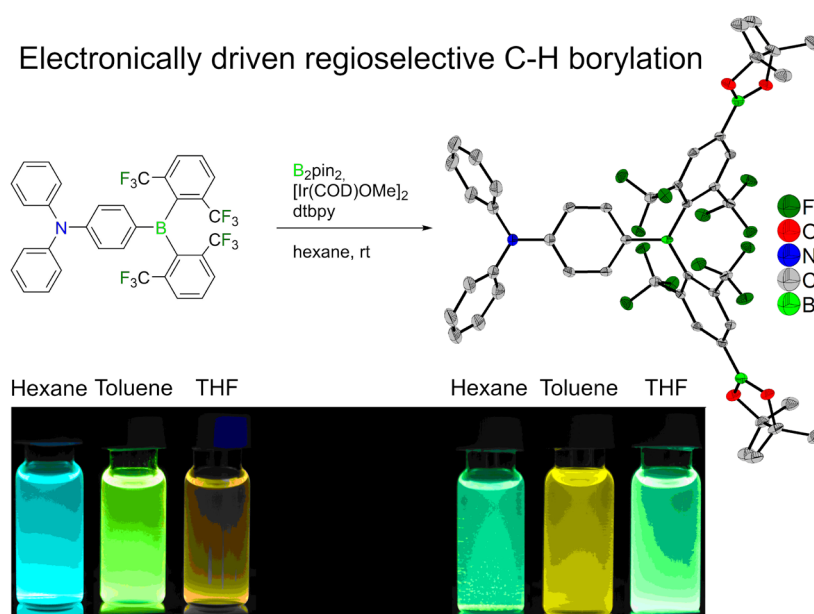
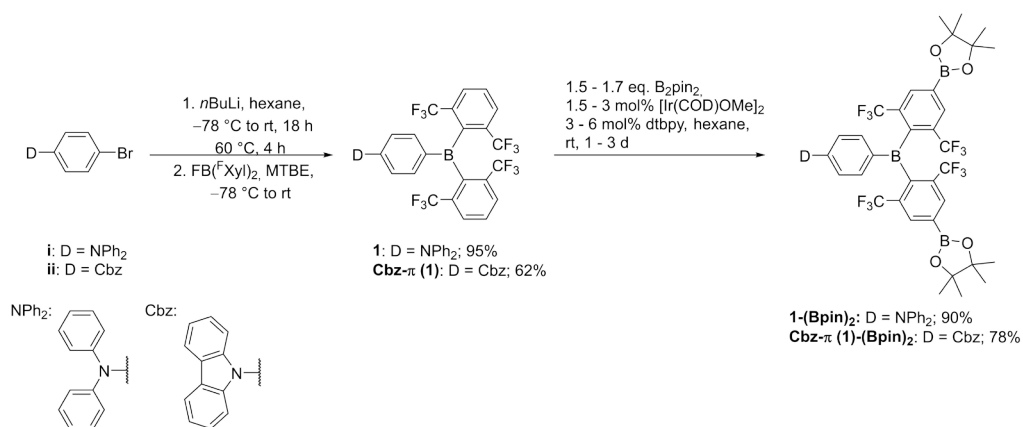


Figure 5.8: Absorption (left) and emission (right) spectra of **BG0H** (gold), **BG1H** (black), **BG2H** (magenta) **BG1Bpin** (blue), **BG1Br** (green), **BFG1H** (red), and **BG1Me** (cyan).

## 5.1.4 Chapter 4



A surprisingly high electronically-driven regioselectivity for the iridium-catalyzed C–H borylation using  $[\text{Ir}(\text{COD})\text{OMe}]_2$  (COD = 1,5-cyclooctadiene) as the precatalytic species, bis(pinacolato)diboron ( $\text{B}_2\text{pin}_2$ ) as the boron source and 4,4'-*di-tert*butyl-2,2'-bipyridin (dtbpy) as the ligand of D- $\pi$ -A systems with diphenylamino (**1**) or carbazolyl (**2**) moieties as the donor, bis(2,6-bis(trifluoromethyl)phenyl)boryl ( $\text{B}^{\text{FXYL}}_2$ ) as the acceptor, and 1,4-phenylene as the  $\pi$ -bridge was observed (Scheme 5.5).



Scheme 5.5: Synthesis of **1**, Cbz- $\pi$  (**1**), **1-(Bpin)<sub>2</sub>**, and Cbz- $\pi$  (**1**)-(Bpin)<sub>2</sub>.

Under these conditions, borylation was observed only at the sterically least encumbered *para*-positions of the acceptor groups. As boronate esters are versatile building blocks for organic synthesis (C–C coupling, functional group transformations), the C–H borylation represents a simple potential method for post-functionalization by which electronic or other properties of D- $\pi$ -A systems can be fine-tuned for specific applications. The photophysical and



electrochemical properties of the borylated (**1-(Bpin)<sub>2</sub>**) and unborylated (**1**) diphenylamino-substituted D- $\pi$ -A systems were investigated. Interestingly, the borylated derivative exhibits coordination of THF to the boronate ester moieties, influencing the photophysical properties and exemplifying the non-innocence of boronate esters (Figure 5.9).

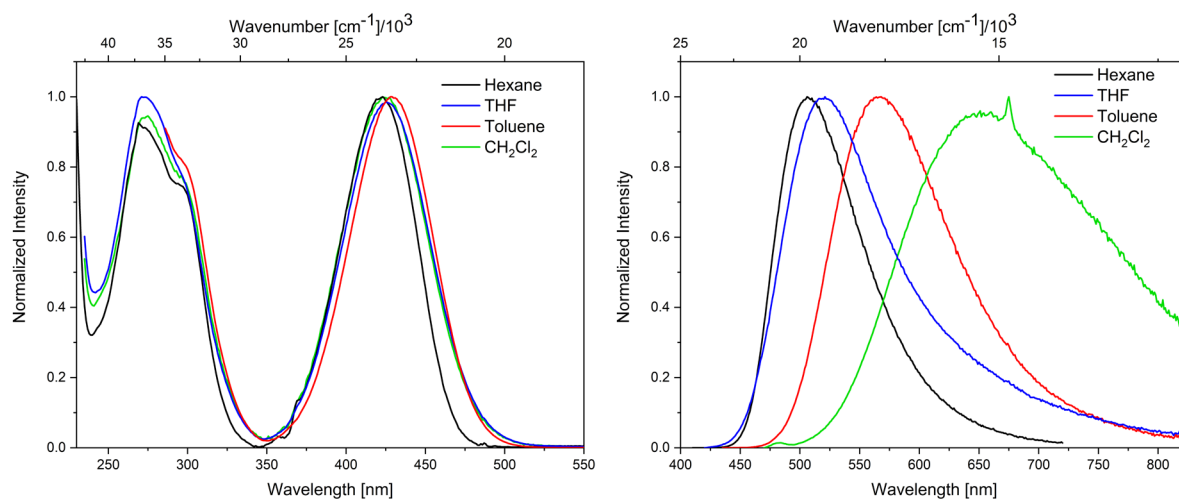
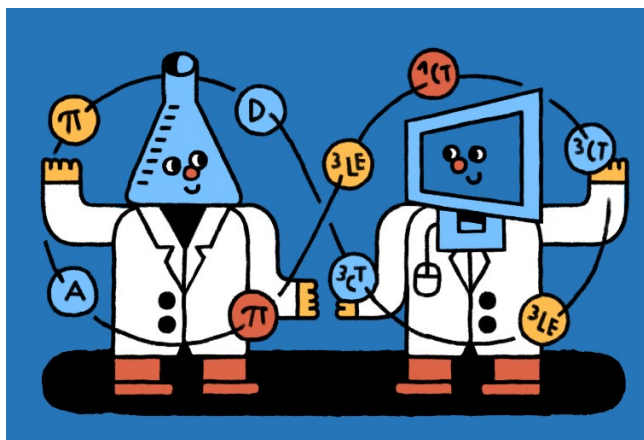


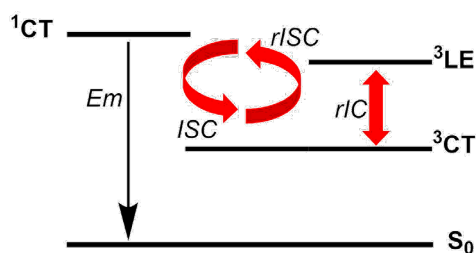
Figure 5.9: Normalized absorption (left) and emission (right) spectra of **1-(Bpin)<sub>2</sub>** in hexane (black), toluene (red), THF (blue) and CH<sub>2</sub>Cl<sub>2</sub> (green).

## 5.2 Zusammenfassung

### 5.2.1 Kapitel 1



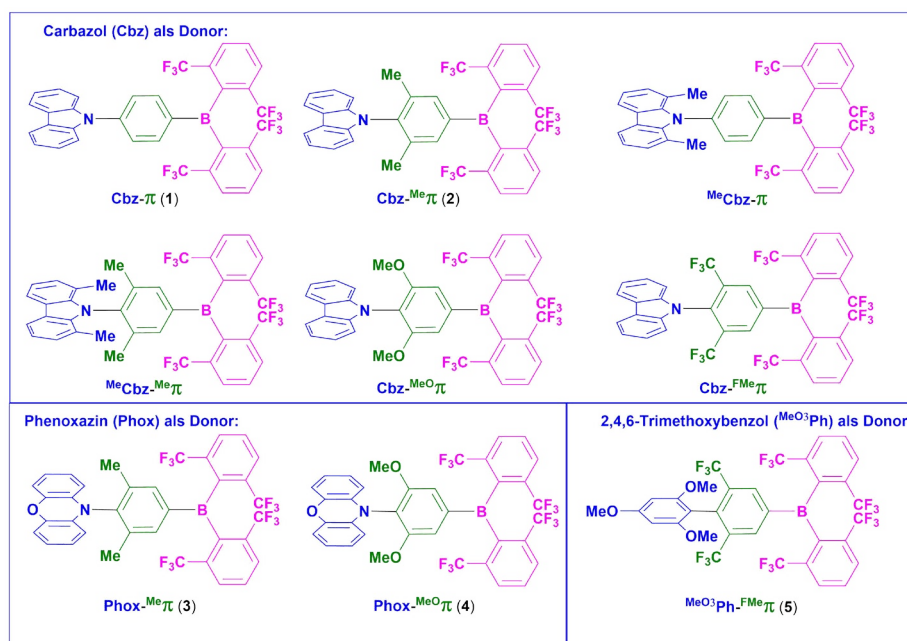
Materialien mit thermisch aktivierter verzögerter Fluoreszenz (TADF) eröffnen einen Weg zur Verbesserung der externen Quanteneffizienz von organischen Leuchtdioden (OLEDs). Aufgrund der Spin-Statistik werden in einem elektronischen Bauelement 25% Singulett- und 75% Triplett-Exzitonen erzeugt. Konventionelle organische Emittoren können Triplett-Exzitonen aufgrund ihrer geringen Spin-Bahnkopplung nicht nutzen und weisen niedrige externe Quanteneffizienzen auf. TADF-Materialien müssen so entworfen werden, dass die Energielücke zwischen dem niedrigsten Singulett- und dem niedrigsten Triplett-Zustand ( $\Delta E_{S-T}$ ) ausreichend klein ist, um Rück-Interkombination (rISC) in organischen Systemen zu ermöglichen (Schema 5.1).



Schema 5.1: Dynamischer zweistufiger TADF-Mechanismus für ein D-A-Molekül. Em: Emission; ISC: Interkombination; rISC: Rück-Interkombination; und rIC: umgekehrte interne Konversion.

Eine etablierte Struktur-Eigenschafts-Beziehung für die Erzeugung von TADF-Materialien ist die räumliche Trennung von HOMO und LUMO über eine orthogonale Anordnung von Donor und Akzeptor in Donor- $\pi$ -Akzeptor-Verbindungen (D- $\pi$ -A). Dies wird durch eine Vergrößerung des sterischen Anspruchs der  $\pi$ -Brücke erreicht. Dies ist jedoch nicht immer die effizienteste Methode und elektronische Parameter müssen berücksichtigt werden.

In einer kombinierten experimentellen und theoretischen Studie wird ein Berechnungsprotokoll zur Vorhersage der angeregten Zustände in D- $\pi$ -A-Verbindungen, die die Akzeptorgruppe B(FXyl)<sub>2</sub> (FXyl = 2,6-Bis(trifluoromethyl)phenyl) enthalten, für das Design neuer TADF-Emitter vorgestellt. Zu diesem Zweck wurde die Wirkung verschiedener Donor- und  $\pi$ -Brückeneinheiten auf die Energielücken zwischen lokalen und ladungsübertragenden Singulett- und Triplett-Zuständen untersucht (Schema 5.2).



Schema 5.2: Berechnete D- $\pi$ -A-Systeme mit unterschiedlichen Substituenten an Donor (blau) und  $\pi$ -Brücke (grün), während der Akzeptor (magenta) in allen Verbindungen gleich ist. Die Verbindungen **Cbz- $\pi$  (1)**, **Cbz-Me $\pi$  (2)**, **Phox-Me $\pi$  (3)**, **Phox-MeO $\pi$  (4)** und **MeO<sub>3</sub>Ph-FMe $\pi$  (5)** wurden synthetisiert und vollständig charakterisiert.

Um das durch quantenchemische Rechnungen gestützte Designkonzept zu beweisen, wurden die D- $\pi$ -B(FXyl)<sub>2</sub>-Verbindungen **Cbz- $\pi$  (1)**, **Cbz-Me $\pi$  (2)**, **Phox-Me $\pi$  (3)**, **Phox-MeO $\pi$  (4)** und **MeO<sub>3</sub>Ph-FMe $\pi$  (5)** synthetisiert und vollständig charakterisiert. Die photophysikalischen Eigenschaften dieser Verbindungen in verschiedenen Lösungsmitteln, im Polymerfilm und in einer gefrorenen Glas-Matrix wurden im Detail untersucht und zeigen eine ausgezeichnete Übereinstimmung mit den berechneten Daten (Abbildung 5.1).

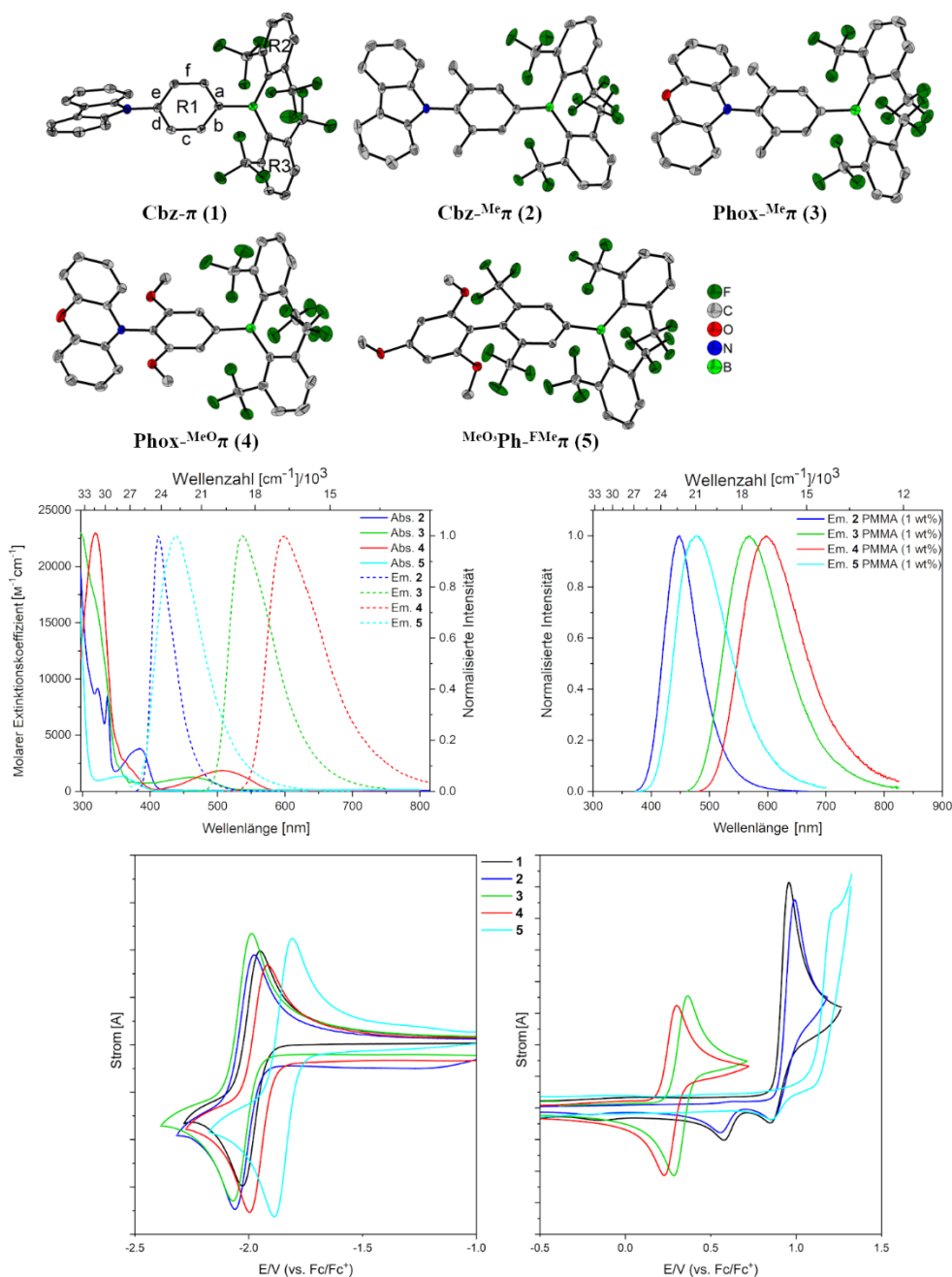
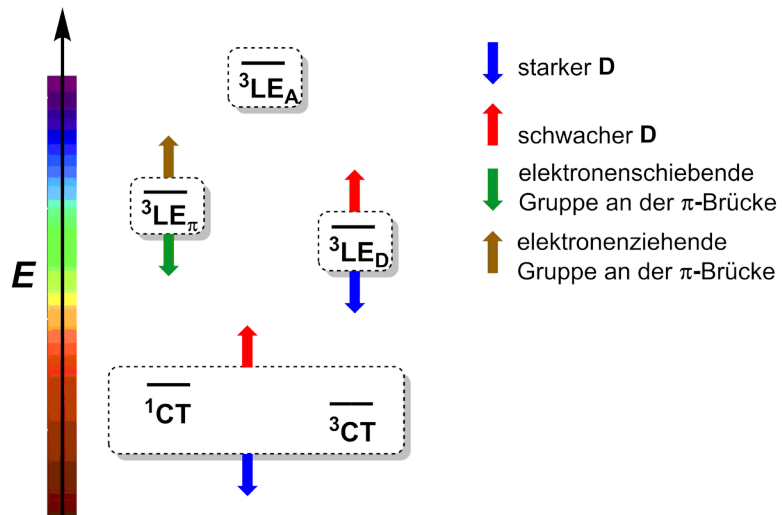


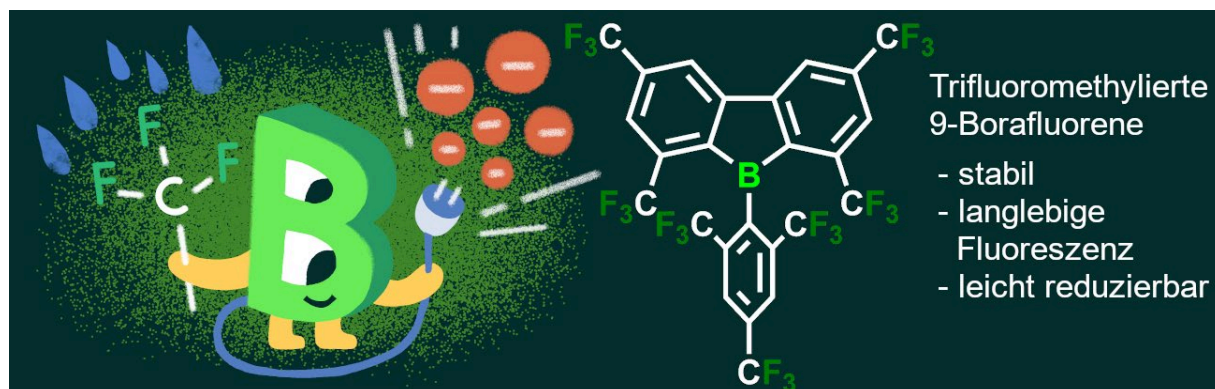
Abbildung 5.1: Molekülstrukturen von **Cbz- $\pi$  (1)**, **Cbz- $^{Me}\pi$  (2)**, **Phox- $^{Me}\pi$  (3)**, **Phox- $^{MeO}\pi$  (4)** und  **$^{MeO_3}Ph$ - $^{FMe}\pi$  (5)**, bestimmt durch Röntgenbeugung (oben). Absorptions- und Emissionsspektren von **Cbz- $\pi$  (1)**, **Cbz- $^{Me}\pi$  (2)**, **Phox- $^{Me}\pi$  (3)**, **Phox- $^{MeO}\pi$  (4)** und  **$^{MeO_3}Ph$ - $^{FMe}\pi$  (5)** in Hexan (Mitte, links). Normalisierte Emissionsspektren von **Cbz- $\pi$  (1)**, **Cbz- $^{Me}\pi$  (2)**, **Phox- $^{Me}\pi$  (3)**, **Phox- $^{MeO}\pi$  (4)** und  **$^{MeO_3}Ph$ - $^{FMe}\pi$  (5)** in PMMA-Filmen (1 Gew.-%) (Mitte, rechts). Zyklische Voltammogramme von **Cbz- $\pi$  (1)**, **Cbz- $^{Me}\pi$  (2)**, **Phox- $^{Me}\pi$  (3)**, **Phox- $^{MeO}\pi$  (4)** und  **$^{MeO_3}Ph$ - $^{FMe}\pi$  (5)** (unten).

Eine einfache Struktur-Eigenschafts-Beziehung wird vorgestellt, die auf den molekularen Fragment-Orbitalen des Donors und der  $\pi$ -Brücke basiert, welche die relevanten Singulett-Triplett-Lücken minimieren, um effiziente TADF-Emitter zu erhalten (Schema 5.3).



Schema 5.3: Schematische Darstellung der unabhängigen Abstimmung des lokal angeregten Zustands auf der  $\pi$ -Brücke ( $\overline{^3LE_\pi}$ ); des lokal angeregten Zustands auf dem Donor D ( $\overline{^3LE_D}$ ) und des Ladungstransfers von Donor D zu Akzeptor A in einem D- $\pi$ -A-Molekül. Der lokal angeregte Zustand ( $\overline{^3LE_A}$ ) auf dem Akzeptor ist nahezu unabhängig von der Variation der Donor- und Brückeneinheiten. Die Abstimmung der Emissionsfarbe wird durch die Energie des  $\overline{^1CT}$  gesteuert.

## 5.2.2 Kaptiel 2



Dreifach koordiniertes Bor ist als Akzeptor in konjugierten Materialien weit verbreitet. In den letzten Jahren hat sich gezeigt, dass der Einsatz trifluoromethylierter Aromaten die Akzeptoreigenschaften solcher Borane verbessert. Erstaunlicherweise verbessert die Verwendung von *ortho*-trifluormethylierten Aromaten in borhaltigen Systemen auch die Stabilität dieser Systeme hinsichtlich ihrer inhärenten Reaktivität gegenüber Nukleophilen. Borafluorene sind von Natur aus stärkere Akzeptoren als ihre nicht benzannulierten Triarylboran-Derivate. In frühere Studien wurde bereits die Wirkung trifluormethylierter Aryle als *exo*-Aryl-Einheiten in Borfluororenen sowie die Auswirkung der Fluorierung auf das Rückgrat untersucht. Da letztere unter einer sehr geringen Stabilität leiden, wurden Systeme mit Trifluoromethylgruppen sowohl auf dem *exo*-Aromaten- als auch auf dem Borafluoren-Gerüst entwickelt, um sowohl die Stabilität als auch die Akzeptorstärke zu maximieren.

Es wurden drei verschiedene perfluoralkylierte Borfluorene hergestellt und ihre elektronischen und photophysikalischen Eigenschaften untersucht. Die Systeme haben vier Trifluoromethylgruppen am Borafluoren-Gerüst sowie zwei Trifluoromethylgruppen an den *ortho*-Positionen ihrer *exo*-Aromaten. Sie unterscheiden sich in Bezug auf die *para*-Substituenten an ihren *exo*-Aromaten, die jeweils ein Proton ( ${}^{\text{F}}\text{Xyl}^{\text{F}}\text{Bf}$ ), eine Trifluormethylgruppe ( ${}^{\text{F}}\text{Mes}^{\text{F}}\text{Bf}$ ) oder eine Dimethylaminogruppe ( $p\text{-NMe}_2\text{-}{}^{\text{F}}\text{Xyl}^{\text{F}}\text{Bf}$ ) sind (Abbildung 5.2). Des Weiteren wurde ein Acetonitril Addukt von  ${}^{\text{F}}\text{Mes}^{\text{F}}\text{Bf}$  isoliert und charakterisiert.

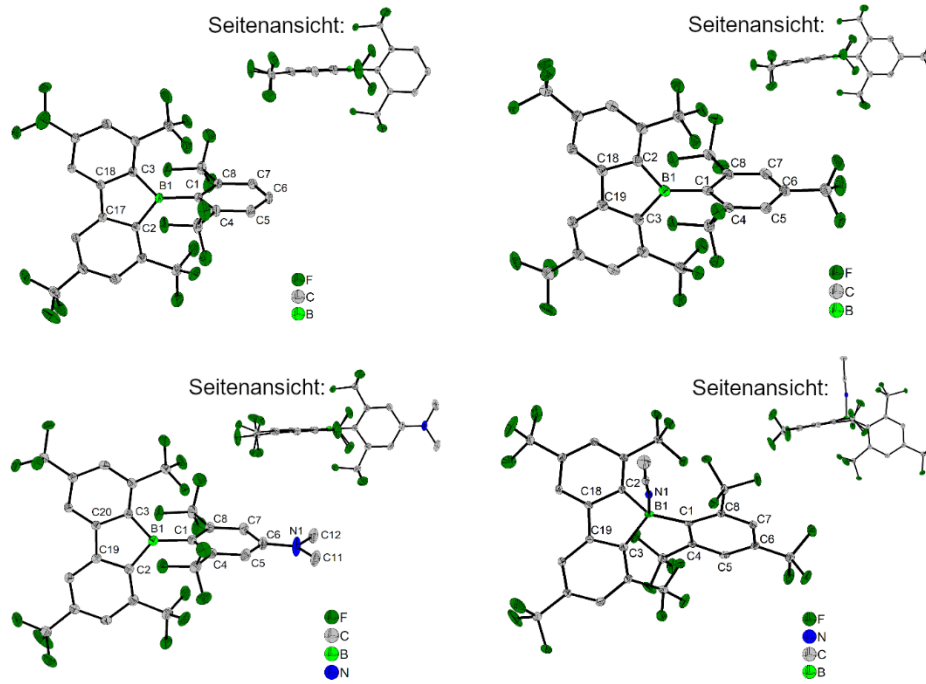


Abbildung 5.2: Molekülstrukturen von  $\text{FMe}_5\text{Bf}$  (oben links),  $\text{FXylBf}$  (oben rechts),  $p\text{-NMe}_2\text{-FXylBf}$  (unten links) und  $\text{FMe}_5\text{Bf}\cdot\text{MeCN}$  (unten rechts), bestimmt durch Einkristall-Röntgenbeugung bei 100 K. Alle Ellipsoide sind mit einer Wahrscheinlichkeit von 50% gezeichnet, wobei H-Atome und Lösungsmittelmoleküle zur besseren Übersichtlichkeit ausgeblendet wurden.

Alle Derivate weisen außergewöhnlich niedrige Reduktionspotenziale auf, die mit denen von Perylendiimiden vergleichbar sind (Abbildung 5.3).

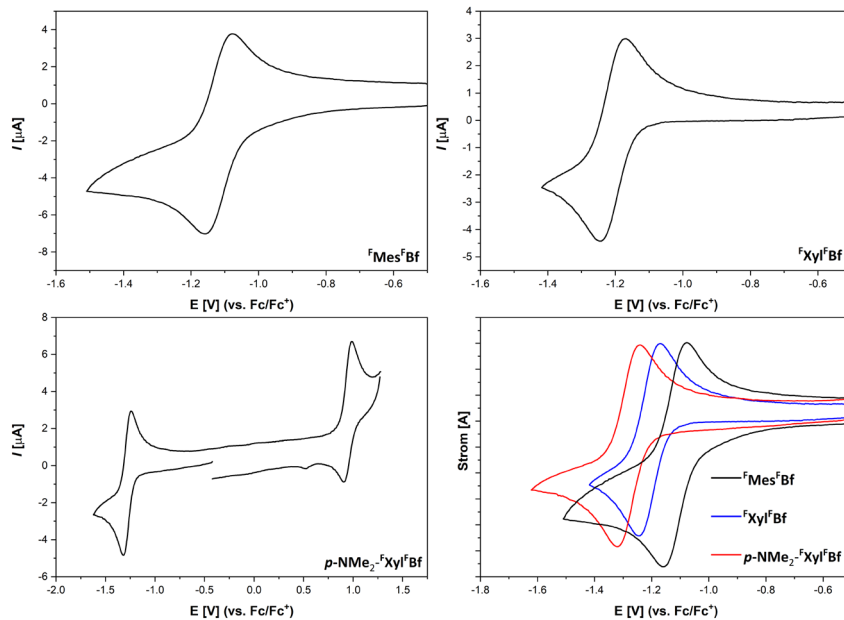


Abbildung 5.3: Zyklische Voltammogramme der reversiblen Redox-Ereignisse von  $\text{FMe}_5\text{Bf}$  (oben links),  $\text{FXylBf}$  (oben rechts) und  $p\text{-NMe}_2\text{-FXylBf}$  (unten links). Alle Proben wurden gegen das  $\text{Fc}/\text{Fc}^+$ -Ionenpaar referenziert. Zum besseren Vergleich sind die Reduktionswellen zusammen aufgetragen (unten rechts;  $\text{FMe}_5\text{Bf}$  (schwarz),  $\text{FXylBf}$  (blau),  $p\text{-NMe}_2\text{-FXylBf}$  (rot)).



Das elektronenärmste Derivat  ${}^{\text{F}}\text{Mes}^{\text{F}}\text{Bf}$  wurde ebenfalls chemisch reduziert und das korrespondierende radikalische Anion isoliert und charakterisiert (Abbildung 5.4 und Abbildung 5.5).

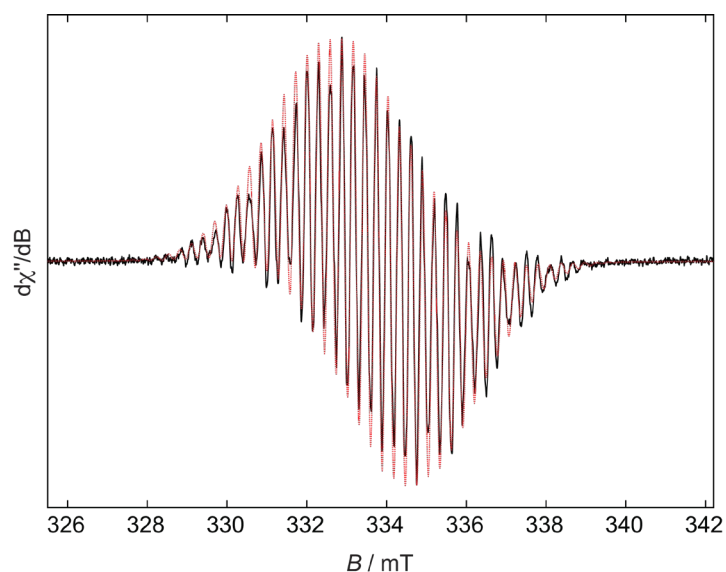


Abbildung 5.4: Experimentelle (schwarze durchgezogene Linie) und simulierte (rot gestrichelte Linie) continuous wave-X-Band-EPR-Spektren von  $[\text{FMeSFb}]^{\bullet-}$  in einer THF-Lösung bei Raumtemperatur.

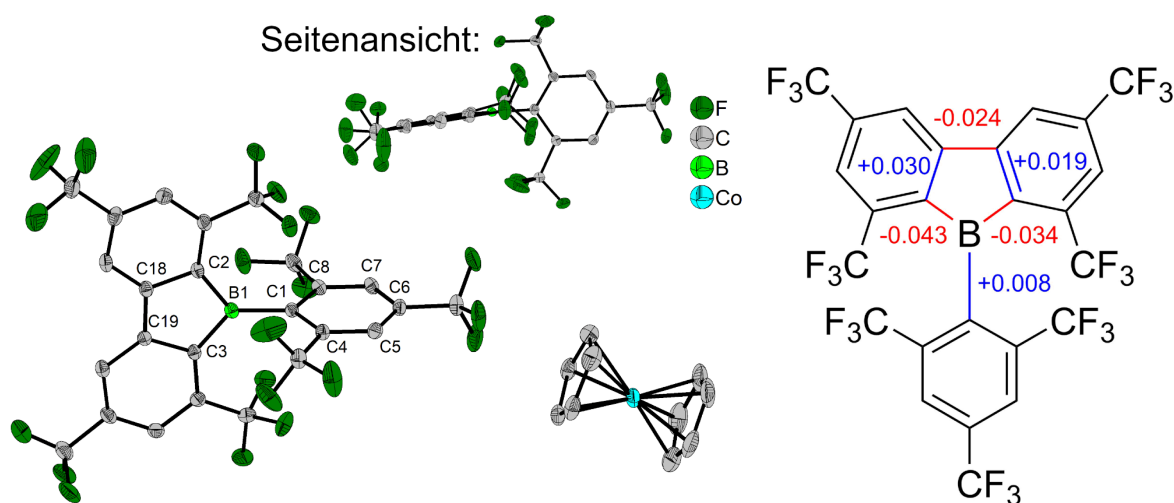


Abbildung 5.5: Molekularstruktur von  $[\text{FMeSFb}][\text{CoCp}_2]$ , bestimmt durch Einkristall-Röntgenbeugung bei 100 K. Alle Ellipsoide sind mit einer Wahrscheinlichkeit von 50% gezeichnet. H-Atome und THF-Lösungsmittelmoleküle wurden zur besseren Übersichtlichkeit ausgeblendet. Nur die Hälfte der symmetrisch nicht-äquivalenten Moleküle ist dargestellt. Eine der  $\text{CF}_3$ -Gruppen auf dem Borfluoren-Kern ist fehlgeordnet und nur der Teil mit der höheren Belegung (64%) ist hier dargestellt (links). Rechts sind die relevanten Änderungen der Bindungslängen von  $[\text{FMeSFb}]^{\bullet-}$  im Vergleich zum neutralen Ausgangsmaterial dargestellt.

Eigenschaften aller Verbindungen untersucht (Abbildung 5.6). Alle Verbindungen weisen schwach erlaubte niederenergetischste Absorptionsmaxima, sowie sehr lange Fluoreszenzlebensdauern von ca. 250 ns bis zu 1,6  $\mu\text{s}$  auf; die zugrunde liegenden Mechanismen, unterscheiden sich jedoch.



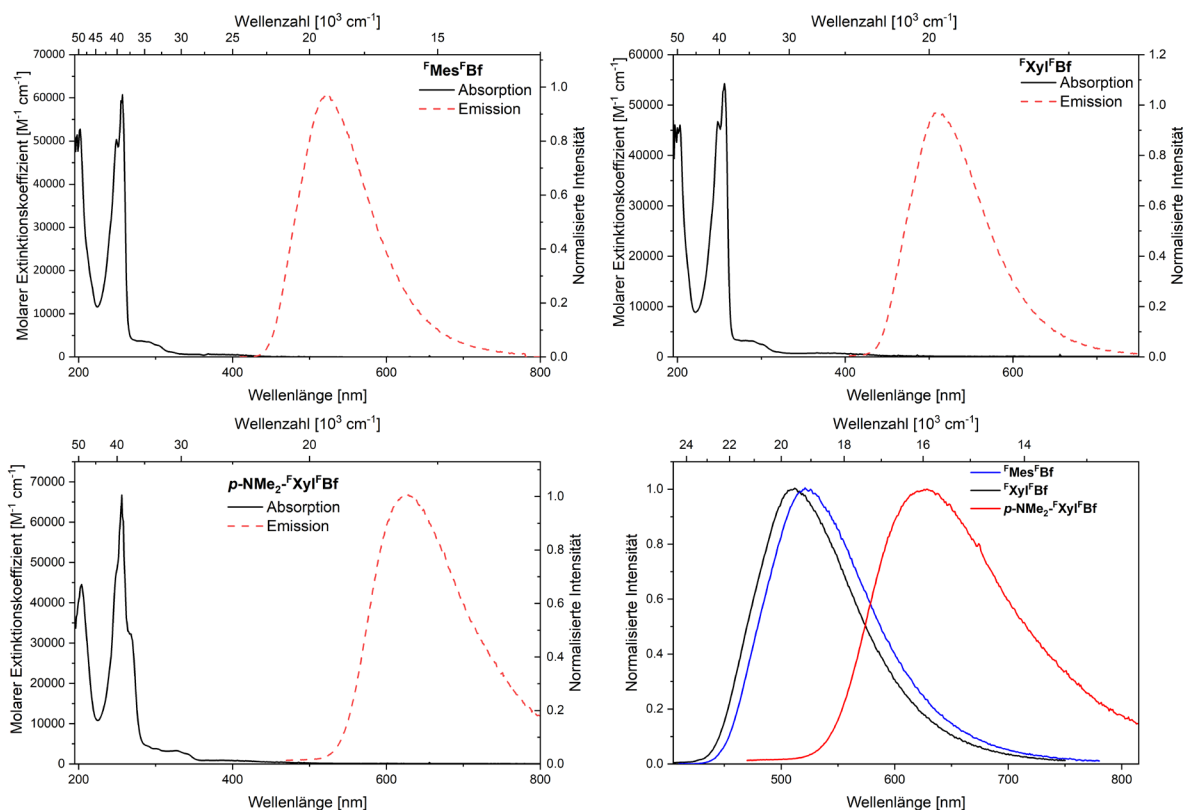
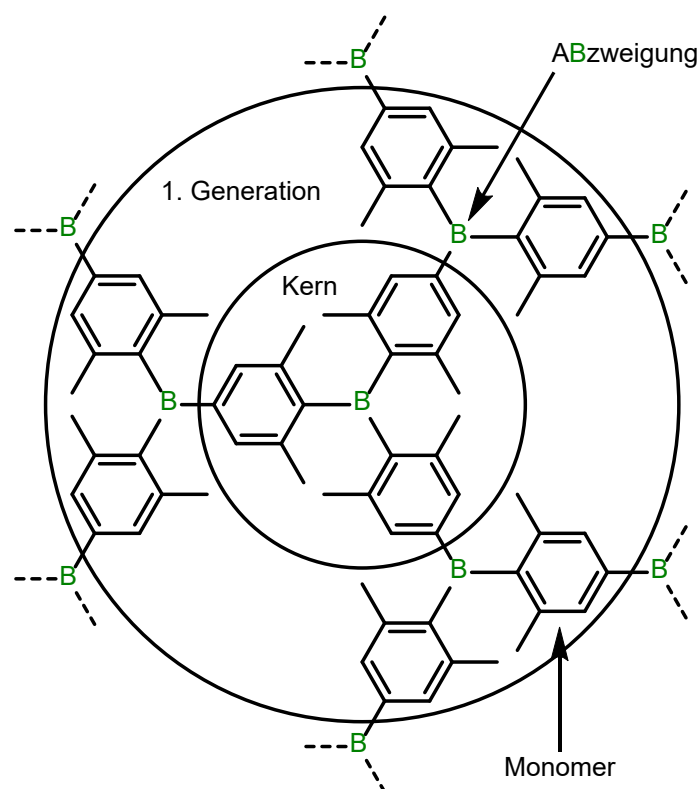


Abbildung 5.6: Absorptions- (schwarz) und Emissionsspektren (rot) in Hexan von  ${}^F\text{Mes}^F\text{Bf}$  (oben links),  ${}^F\text{Xyl}^F\text{Bf}$  (oben rechts) und  $p\text{-NMe}_2\text{-}{}^F\text{Xyl}^F\text{Bf}$  (unten links). Zum Vergleich werden die Emissionsspektren zusammen aufgetragen (unten rechts;  ${}^F\text{Mes}^F\text{Bf}$  (Schwarz),  ${}^F\text{Xyl}^F\text{Bf}$  (Blau),  $p\text{-NMe}_2\text{-}{}^F\text{Xyl}^F\text{Bf}$  (Rot)).

Das donorsubstituierte Derivat  $p\text{-NMe}_2\text{-}{}^F\text{Xyl}^F\text{Bf}$  zeigt thermisch aktivierte verzögerte Fluoreszenz aus einem Ladungstransfer-(CT)-Zustand, während die Borfluorene  ${}^F\text{Mes}^F\text{Bf}$  und  ${}^F\text{Xyl}^F\text{Bf}$  aufgrund ihrer Symmetrie und niedriger Übergangsdipolmomente nur schwach erlaubte lokal angeregte (LE-)Übergänge aufweisen, wie aus DFT- und TD-DFT-Berechnungen hervorgeht.

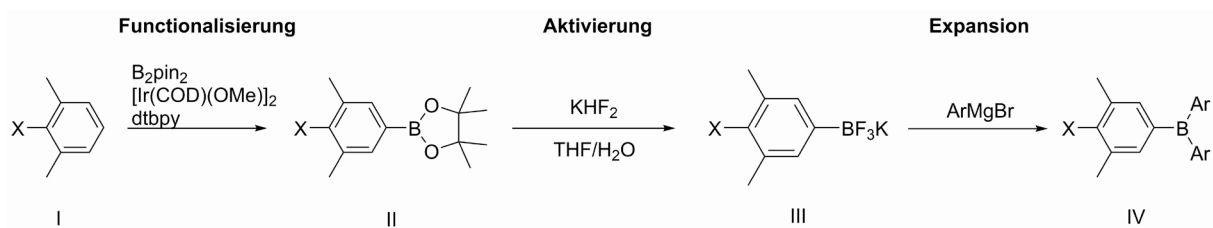
## 5.2.3 Kapitel 3



Konjugierte Dendrimere finden breite Anwendung in verschiedenen Bereichen, wie z.B. als Ladungstransport/-speicher- oder Emittiermaterialien in organischen Solarzellen oder OLEDs. Bisherige Studien über borhaltige konjugierte Dendrimere sind rar gesät und verwenden meist einen konvergenten Syntheseansatz, dem ein einfacher, allgemein anwendbarer synthetischer Zugang fehlt.

Ein neuer divergenter Ansatz wurde entwickelt und konjugierte Triarylboran-Dendrimere wurden bis einschließlich zur zweiten Generation synthetisiert. Die Synthesestrategie besteht aus drei Schritten (Schema 5.4):

- 1) Funktionalisierung durch Iridium-katalysierte C-H-Borylierung;
- 2) Aktivierung durch Fluorierung des erzeugten Boronatesers mit  $K[HF_2]$  oder  $[N(nBu)_4][HF_2]$ ; und
- 3) Expansion durch Reaktion der Trifluorboratsalze mit Aryl-Grignard-Reagenzien.



Schema 5.4: Divergender Ansatz für die Synthese von konjugierten Starburst-Boran-Dendrimeren.

Das Konzept erwies sich auch auf einen konvergenten Ansatz übertragbar. Bis auf eine Ausnahme weisen alle konjugierten Boran-Dendrimere mehrere, isolierte und reversible Reduktionsprozesse auf, was sie zu potenziell interessanten Materialien für die Anwendung in molekularen Akkumulatoren macht (Abbildung 5.7).

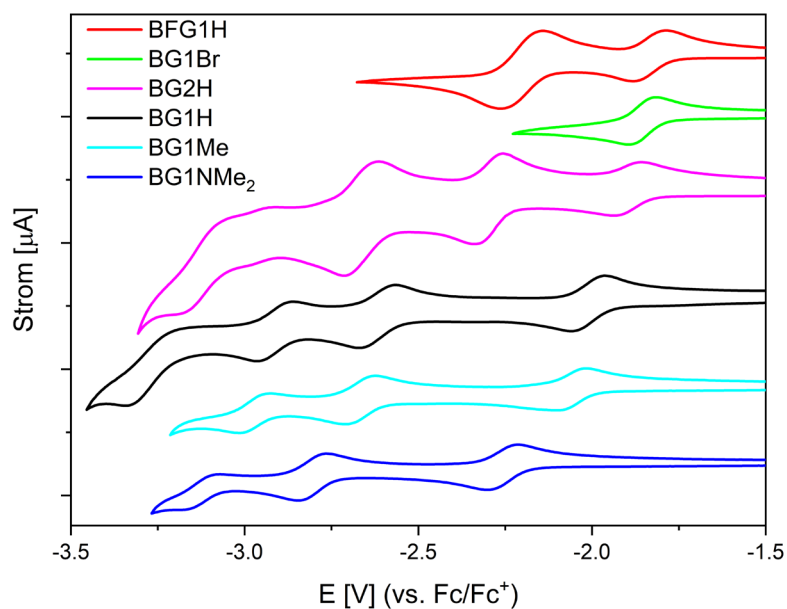


Abbildung 5.7: Zyklische Voltammogramme von **BG1H** (schwarz), **BG1Me** (cyan), **BG1NMe<sub>2</sub>** (blau), **BG1Br** (grün), **BFG1H** (rot) und **BG2H** (magenta) in THF geordnet nach abnehmendem ersten Reduktionspotential. Alle Proben werden gegen das Fc/Fc<sup>+</sup>-Redoxpaar referenziert.

Basierend auf ihren photophysikalischen Eigenschaften zeigen die Dendrimere der 1. Generation eine gute Konjugation über das gesamte System. Bei der Erweiterung der Systeme zur zweiten Generation nimmt die Konjugation nicht weiter zu. Allerdings steigen die molaren Extinktionskoeffizienten linear mit der Anzahl der Triarylboran-Untereinheiten, was auf eine Möglichkeit für die Anwendung als photonische Antennen hindeutet (Abbildung 5.8).

## Summary/Zusammenfassung

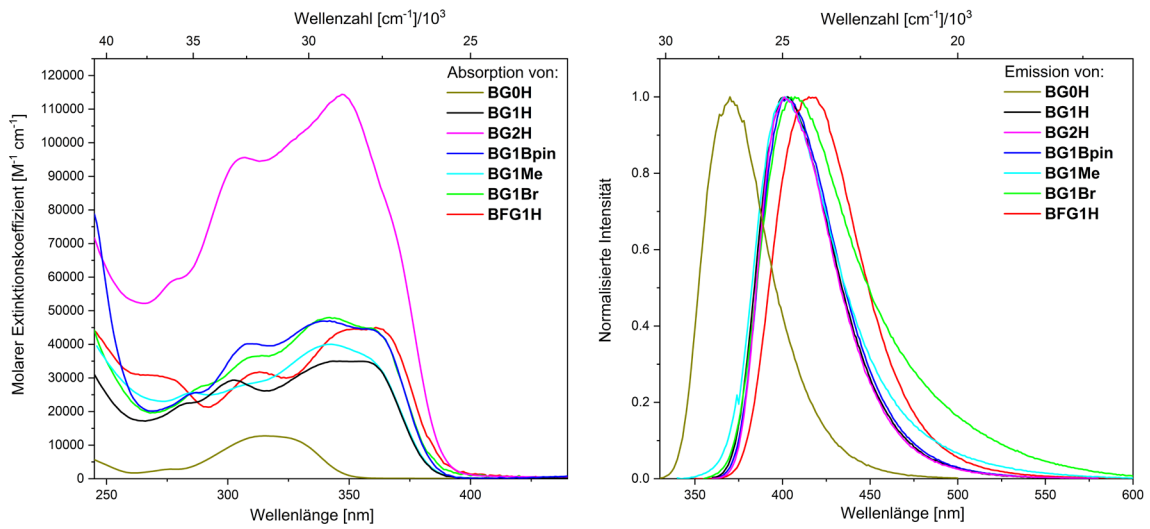
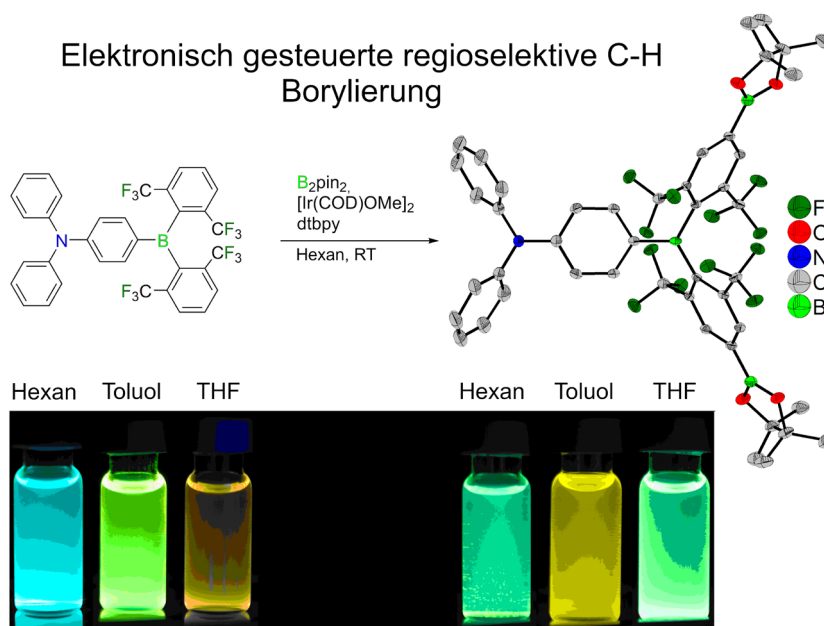
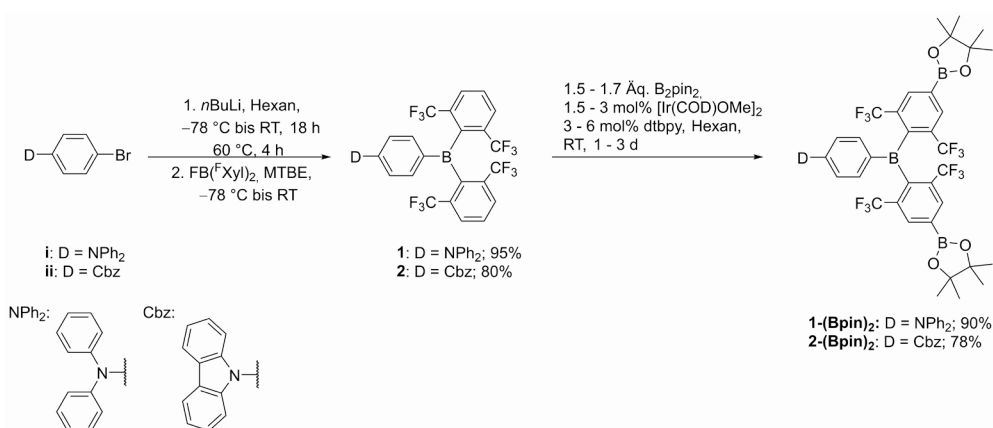


Abbildung 5.8: Absorptions- (links) und Emissionsspektren (rechts) von **BG0H** (Gold), **BG1H** (schwarz), **BG2H** (magenta), **BG1Bpin** (blau), **BG1Br** (grün), **BFG1H** (rot) und **BG1Me** (cyan).

## 5.2.4 Kapitel 4



Es wurde eine überraschend hohe, elektronisch gesteuerte Regioselektivität für die Iridium-katalysierte C-H-Borylierung mit  $[\text{Ir}(\text{COD})\text{OMe}]_2$  (COD = 1,5-Cyclooctadien) als präkatalytische Spezies, Bis(pinacolato)diboran ( $\text{B}_2\text{pin}_2$ ) als Borquelle und 4,4'-Di-*tert*-butyl-2,2'-bipyridin (dtbpy) als Ligand von D- $\pi$ -A-Systemen mit Diphenylamin (**1**) oder Carbazolyl (**Cbz- $\pi$  (1)**) als Donoren, Bis(2,6-bis(trifluoromethyl)phenyl)boryl ( $\text{B}(\text{F}^{\text{Xyl}})_2$ ) als Akzeptor und 1,4-Phenylen als  $\pi$ -Brücke beobachtet (Schema 5.5).



Schema 5.5: Synthese von **1**, **Cbz- $\pi$  (1)**, **1-( $\text{Bpin}$ )<sub>2</sub>** und **Cbz- $\pi$  (1)-( $\text{Bpin}$ )<sub>2</sub>**.

Unter diesen Bedingungen wurde die Borylierung nur an den sterisch am wenigsten gehinderten *para*-Positionen der Akzeptorgruppen beobachtet. Da Boronatester vielseitige Bausteine für die organische Synthese sind (C-C-Kupplung, funktionelle Gruppentransformationen), stellt die C-H-Borylierung eine einfache, potentielle Methode zur Funktionalisierung dar, mit der elektronische oder andere Eigenschaften von D- $\pi$ -A-Systemen für spezifische Anwendungen

fein abgestimmt werden können. Die photophysikalischen und elektrochemischen Eigenschaften der borylierten (**1-(Bpin)<sub>2</sub>**) und unborylierten (**1**) diphenylaminosubstituierten D- $\pi$ -A-Systeme wurden untersucht. Interessanterweise weist das borylierte Derivat eine Koordination von THF an die Boronatester-Einheiten auf, was die photophysikalischen Eigenschaften beeinflusst und die Nicht-Unschuld der Boronatester veranschaulicht (Abbildung 5.7).

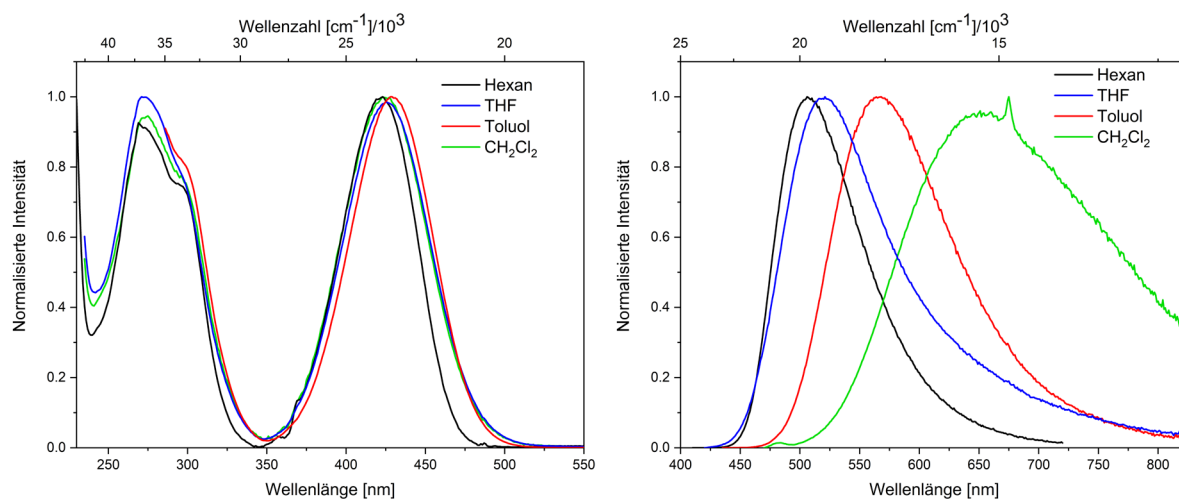


Abbildung 5.9: Normierte Absorptions- (links) und Emissionsspektren (rechts) von **1-(Bpin)<sub>2</sub>** in Hexan (schwarz), Toluol (rot), THF (blau) und CH<sub>2</sub>Cl<sub>2</sub> (grün).

## 6 Experimental

### 6.1 General Experimental Details

Unless otherwise noted, the following conditions apply.

All syntheses were carried out using standard Schlenk and glovebox techniques under an argon atmosphere. The solvents were dried using a solvent purification system (SPS) from Innovative Technology Inc. and were degassed and stored over molecular sieves under argon. Deuterated solvents ( $\text{CD}_2\text{Cl}_2$ ,  $\text{CDCl}_3$ ,  $\text{C}_6\text{D}_6$ , acetone- $d_6$ , and DMSO- $d_6$ ) used for NMR spectroscopy were purchased from Eurisotop, Sigma Aldrich or deuterio.  $\text{C}_6\text{D}_6$  was dried over molecular sieves and stored under an argon atmosphere before use. Trimethyl borate was purchased from Sigma Aldrich and distilled before use. Boron trifluoride diethyl etherate was purchased from Merck Millipore. *n*-Butyllithium (2.5 M solution in hexane) and 4-bromo-N,N-diphenylaniline (**i**) were purchased from Acros Organics and used as received. The compounds 1-bromo-bis-2,4-(trifluoromethyl)benzene and 3,5-bis-trifluoromethylaniline were purchased from Fluorochem and used as received. Tris-1,3,5-trifluoromethylbenzene was purchased from Fluorochem, distilled and degassed before use.  $\text{B}_2\text{pin}_2$  was kindly provided by AllylChem Co. Ltd. (Dalian, China).  $\text{CoCp}_2$  was kindly provided by Prof. Dr. Udo Radius. Bis-1,3-trifluoromethylbenzene was purchased from ABCR, distilled and degassed before use.  $[\text{Ir}(\text{COD})(\text{OMe})]_2$  was prepared according to a literature procedure.<sup>[147]</sup> The compounds 9-(4-bromophenyl)-9*H*-carbazole (**ii**)<sup>[143]</sup> 2-(3,5-dimethoxyphenyl)-4,4,5,5-tetramethyl-1,3,2-dioxaborolane,<sup>[151]</sup> and potassium(3,5-dimethoxyphenyl)trifluoroborate<sup>[152]</sup> were synthesized according to literature procedures. All other starting materials were purchased from commercial sources and were used without further purification.

**Column chromatography** was performed on silica gel 60 (40-63  $\mu\text{m}$ ) (purchased from VWR), or basic alumina 90 active (purchased from Merck), and automated flash chromatography was performed on silica gel (Biotage SNAP cartridge KP-Sil 10 g or KP-Sil 100 g), obtained from Biotage, using a Biotage® Isolera Four Flash system. Solvents were generally removed using a rotary evaporator *in vacuo* at a maximum temperature of 55 °C.

**NMR spectra** were recorded on a Bruker Avance 200 (operating at  $^1\text{H}$ : 199.9 MHz,  $^{11}\text{B}\{^1\text{H}\}$ : 64.1 MHz,  $^{19}\text{F}\{^1\text{H}\}$ : 188.1 MHz), a Bruker Avance Nanobay HDIII (operating at  $^1\text{H}$ : 400 MHz,  $^{11}\text{B}\{^1\text{H}\}$ : 128 MHz,  $^{19}\text{F}\{^1\text{H}\}$ : 377 MHz) or a Bruker Avance 500 FT NMR spectrometer

## Experimental

(operating at  $^1\text{H}$ : 500 MHz,  $^{11}\text{B}\{^1\text{H}\}$ : 160 MHz,  $^{13}\text{C}\{^1\text{H}\}$ : 126 MHz,  $^{19}\text{F}\{^1\text{H}\}$ : 471 MHz). Chemical shifts ( $\delta$ ) are given in ppm and are referenced to external  $\text{BF}_3\cdot\text{Et}_2\text{O}$  ( $^{11}\text{B}\{^1\text{H}\}$ ) and  $\text{CFC}_3$  ( $^{19}\text{F}\{^1\text{H}\}$ ).  $^1\text{H}$  NMR spectra were referenced via residual proton resonances of  $\text{CDCl}_3$  (7.26 ppm),  $\text{CD}_2\text{Cl}_2$  (5.32 ppm), acetone- $d_6$  (2.05 ppm),  $\text{C}_6\text{D}_6$  (7.16 ppm), or DMSO- $d_6$  (2.50).<sup>[149]</sup>  $^{13}\text{C}\{^1\text{H}\}$  spectra were referenced to  $\text{CDCl}_3$  (77.16 ppm),  $\text{CD}_2\text{Cl}_2$  (53.84 ppm), acetone- $d_6$  (29.84 ppm),  $\text{C}_6\text{D}_6$  (128.06 ppm) or DMSO- $d_6$  (39.52).<sup>[150]</sup>

**Solid-state magic angle spinning (MAS) NMR spectra** were recorded using a Bruker DSX-400 solid state spectrometer ( $^{11}\text{B}$ : 128.3 MHz,  $^{13}\text{C}$ : 100.6 MHz,  $^{19}\text{F}$ : 376.5 MHz, rotor 4 mm OD).

**GCMS** analyses were performed on an Agilent Technologies GCMS system (GC 7890A, EI-MS 5975C).

**HRMS** were recorded using a Thermo Scientific Exactive Plus Orbitrap MS system with either an Atmospheric Sample Analysis Probe (ASAP) or by Electro-Spray Ionization (ESI).

**Elemental analyses** were performed on an Elementar vario MICRO cube elemental analyzer.

**Photophysical measurements:** All measurements were performed in standard quartz cuvettes (1 cm x 1 cm cross-section). UV-visible absorption spectra were recorded using an Agilent 8453 diode array UV-visible spectrophotometer.

**The extinction coefficients** of all compounds were calculated from 6 independently prepared samples in hexane.

**The emission spectra** were recorded using an Edinburgh Instruments FLSP920 spectrometer equipped with a double monochromator for both excitation and emission, operating in right-angle geometry mode, and all spectra were fully corrected for the spectral response of the instrument. All solutions used for photophysical measurements had a concentration lower than  $2 \times 10^{-5}$  M to minimize inner filter effects during fluorescence measurements.

**The fluorescence quantum yields** were measured using a calibrated integrating sphere (inner diameter: 150 mm) from Edinburgh Instruments combined with the FLSP920 spectrometer described above. For solution-state and solid-state measurements, the longest-wavelength absorption maximum of the compound in the respective solvent was chosen as the excitation wavelength.

**Fluorescence lifetimes** were recorded using the time-correlated single-photon counting (TCSPC) method using the same FLSP920 spectrometer described above. Solutions were



excited with a picosecond pulsed diode laser at emission maxima of 320 nm (**BG1H** and **BG1Bpin**) 376.6 nm (**Cbz- $\pi$**  (1), **Cbz-Me $\pi$**  (2), **MeO<sub>3</sub>Ph-FMe $\pi$**  (5), **FMe<sup>F</sup>Bf**, **FXyl<sup>F</sup>Bf**, ***p*-NMe<sub>2</sub>-F<sup>F</sup>Xyl<sup>F</sup>Bf**, **BG1Me**, **BG1Br**, **BG1CF<sub>3</sub>H**, **BG1NMe<sub>2</sub>**, **1**, **1-(Bpin)<sub>2</sub>**, and **2-(Bpin)<sub>2</sub>**), 472.6 nm (**Phox-Me $\pi$**  (3)) and 508.8 nm (**Phox-MeO $\pi$**  (4)). The full width at half maximum (FWHM) of the laser pulses were ca. 70–200 ps, while the instrument response function (IRF) had a FWHM of ca. 1.0 ns, measured from the scatter of a Ludox solution at the excitation wavelength. Decays were recorded to at least 10000 counts in the peak channel with a record length of at least 1000 channels. The band pass of the monochromator was adjusted to give a signal count rate of <10 kHz. Iterative reconvolution of the IRF with one decay function and non-linear least-squares analysis were used to analyze the data. The quality of the fit was judged by the calculated value of the reduced  $\chi^2$  and visual inspection of the weighted residuals.

**The time-gated emission spectrum** of **Cbz-Me $\pi$**  (2) at 77 K was recorded with a 5 ms delay after opening the shutter to the excitation source. Due to the large difference in lifetime of the prompt fluorescence and the phosphorescence (a factor of  $10^8$ ), it was possible to record the phosphorescence spectrum without the fluorescence signal. Spectra were background corrected for the dark noise and spectral sensitivity of the spectrometer.

**Electrochemical measurements:** Cyclic voltammetry experiments were conducted in an argon-filled glovebox using a Gamry Instruments Reference 600 potentiostat. A standard three-electrode cell configuration was employed using a platinum disk working electrode, a platinum wire counter electrode, and a silver wire reference electrode separated by a Vycor frit, serving as the reference electrode. The redox potentials are referenced to the ferrocene/ferrocenium ([Fc/Fc<sup>+</sup>]) redox couple by using decamethylferrocene ([Cp\*<sub>2</sub>Fe];  $E_{1/2} = -0.532$  V in CH<sub>2</sub>Cl<sub>2</sub>) as an internal standard. Tetra-*n*-butylammonium hexafluorophosphate ([*n*Bu<sub>4</sub>N][PF<sub>6</sub>]) was employed as the supporting electrolyte. Compensation for resistive losses (*iR* drop) was employed for all measurements.

**EPR measurements** at X-band (9.37 GHz) were carried out at room temperature using a Bruker ELEXSYS E580 CW EPR spectrometer. CW EPR spectra were measured using 1 mW microwave power and 0.5 G field modulation at 100 kHz, with a conversion time of 20 ms. The spectral simulations were performed using MATLAB 8.6 and the EasySpin 5.2.11 toolbox.<sup>[332]</sup>

## 6.2 Synthesis

### 6.2.1 Chapter 1

#### 6.2.1.1 2-iodo-1,3-bis(trifluoromethyl)benzene (FXyII)

The synthesis reported herein is an optimization of the conditions reported by Schlosser and co-workers.<sup>[333]</sup> The synthetic conditions were optimized in terms of batch size, yield as well as cost efficiency.

A solution of MeLi in Et<sub>2</sub>O (1.6 M solution in Et<sub>2</sub>O, 80 mmol, 50 mL) was added dropwise to a solution of KO<sup>t</sup>Bu (17.95 g, 160 mmol) in THF (250 mL) at -78 °C. After addition, the solution was stirred at -78 °C for 30 min. Then 1,3-bis(trifluoromethyl)benzene (12.3 mL, 80.0 mmol) was added dropwise and the dark purple reaction was stirred for 3 h at -78 °C. Then, iodine (20.3 g, 80 mmol) was rapidly added as a solid. The reaction was stirred overnight and slowly warmed to ambient temperature. Afterwards, the reaction was diluted with 200 mL of pentane and filtered through a silica plug (pentane/silica, 5 cm). All volatiles were removed under reduced pressure to give a brown oil. The crude product was sublimed (2 x 10<sup>-2</sup> mbar, 30 to 80 °C) to give 2-iodo-1,3-bis(trifluoromethyl)benzene as a colorless solid (18.7 g, 63.6 mmol, 69%).

<sup>1</sup>H NMR (200 MHz, 298 K, CDCl<sub>3</sub>): δ = 7.82 (d, <sup>3</sup>J = 8 Hz, 2H), 7.58 (t, <sup>3</sup>J = 8 Hz, 1H) ppm;

<sup>19</sup>F NMR (188.1 MHz, 298 K, CDCl<sub>3</sub>): δ = -61.9 ppm;

**Elem. Anal. Calc.** (%) for C<sub>8</sub>H<sub>3</sub>F<sub>6</sub>I: C 28.26, H 0.89; found: C 28.57, H 0.87;

The data fit those previously reported.<sup>[333]</sup>

**6.2.1.2 Bis(2,6-bis(trifluoromethyl)phenyl)fluoroborane (FB(FXyl)<sub>2</sub>)**

A solution of *n*BuLi (7.7 mL, 2.3 M in hexane, 17.7 mmol) was added dropwise to a solution of 2-iodo-1,3-bis(trifluoromethyl)benzene (5.00 g, 14.7 mmol) in MTBE (30 mL) at  $-78$  °C. The reaction was warmed to ambient temperature and stirred for 2 h. After cooling to  $-78$  °C, BF<sub>3</sub>•OEt<sub>2</sub> (0.89 mL, 7.1 mmol) was added dropwise and the reaction was warmed to ambient temperature overnight. All volatiles were removed *in vacuo* and the remaining solid was extracted with hexane (4 x 40 mL). The solution was concentrated *in vacuo*. After crystallization at  $-30$  °C and removal of the residual solvent, bis(2,6-bis(trifluoromethyl)phenyl)fluoroborane was obtained as colorless crystals (1.75 g, 3.84 mmol, 52%).

**<sup>1</sup>H NMR** (200 MHz, 298 K, CDCl<sub>3</sub>):  $\delta$  = 7.34 (d, <sup>3</sup>*J* = 8 Hz, 2H), 6.76 (t, <sup>3</sup>*J* = 8 Hz, 1H) ppm;

**<sup>11</sup>B NMR** (64.1 MHz, 298 K, CDCl<sub>3</sub>):  $\delta$  = 47.5 ppm;

**<sup>19</sup>F NMR** (188.1 MHz, 298 K, CDCl<sub>3</sub>):  $\delta$  =  $-56.7$  (d, *J*<sub>F-F</sub> = 14 Hz) ppm;

The data fit those previously reported.<sup>[125]</sup>

## Experimental

### 6.2.1.3 9-(4-(bis(2,6-bis(trifluoromethyl)phenyl)boryl)phenyl)carbazole (Cbz- $\pi$ (1))

A solution of *n*BuLi in hexane (1.30 mL, 2.3 M, 3.0 mmol) was added dropwise to a suspension of 9-(4-bromophenyl)-9*H*-carbazole (950 mg, 2.95 mmol) in hexane (60 mL) at  $-78$  °C. The reaction was slowly warmed to ambient temperature and stirred overnight. The reaction was cooled to  $-78$  °C and a solution of bis-(2,6-bis(trifluoromethyl)phenyl)-fluoroborane (1.12 g, 2.46 mmol) in Et<sub>2</sub>O (40 mL) was added dropwise. The reaction was slowly warmed to ambient temperature and stirred overnight. All volatiles were removed *in vacuo*. The product was then purified by column chromatography (hexane/CH<sub>2</sub>Cl<sub>2</sub> (2:1)) and recrystallized from hexane to give 9-(4-(bis(2,6-bis(trifluoromethyl)phenyl)boryl)phenyl)-9*H*-carbazole as light blue crystals (1.04 g, 1.53 mmol, 62 %).

<sup>1</sup>H NMR (500 MHz, 298 K, CDCl<sub>3</sub>):  $\delta$  = 8.02 (m, 2H), 7.51 (d, <sup>3</sup>*J* = 8 Hz, 4H), 7.47 – 7.49 (m, 2H), 7.20 – 7.29 (m, 8H), 6.85 (t, <sup>3</sup>*J* = 8 Hz, 2H) ppm;

<sup>13</sup>C{<sup>1</sup>H} NMR (126 MHz, 298 K, CDCl<sub>3</sub>):  $\delta$  = 145.0 (C<sub>q</sub>, 1C), 142.2 (C<sub>q</sub>, 1C), 140.8 (C<sub>q</sub>, 2C), 139.2 (C<sub>q</sub>, 2C), 138.5 (CH, 2C), 135.9 (C<sub>q</sub>, 4C), 130.8 (CH, 2C), 130.2 (CH, 4C), 126.6 (CH, 2C), 125.5 (CH, 2C), 124.6 (C<sub>q</sub>, 4C, q, <sup>1</sup>*J*<sub>CF</sub> = 274 Hz), 124.4 (C<sub>q</sub>, 2C), 120.9 (CH, 2C), 120.7 (CH, 2C), 110.2 (CH, 2C) ppm;

<sup>11</sup>B{<sup>1</sup>H} NMR (160 MHz, 298 K, CDCl<sub>3</sub>):  $\delta$  = 72.9 ppm;

<sup>19</sup>F{<sup>1</sup>H} NMR (470 MHz, CDCl<sub>3</sub>):  $\delta$  =  $-52.8$  ppm;

**Elem. Anal. Calc.** (%) for C<sub>34</sub>H<sub>18</sub>BF<sub>12</sub>N: C 60.12, H 2.67, N 2.06; found: C 60.67, H 2.65, N 2.21;

**HRMS** (APCI, pos): Calc.: 680.1413 [m/z]; found: m/z = 680.1403 [MH<sup>+</sup>].

**6.2.1.4 9-(4-bromo-2,6-dimethylphenyl)carbazole (1-ii)**

Carbazole (1.01 g, 6.0 mmol) and Cs<sub>2</sub>CO<sub>3</sub> (10.5 g, 32 mmol) were suspended in 30 mL of dry and degassed DMF. The suspension was stirred for 15 min at ambient temperature before 5-bromo-2-fluoro-1,3-dimethylbenzene (2.43 g, 12 mmol) was added. The reaction was heated to reflux overnight. Then water was added and the reaction was extracted with ethyl acetate (3 x 70 mL). The organic phase was dried of MgSO<sub>4</sub> and all volatiles were removed *in vacuo*. The resulting light yellow solid was recrystallized from hexane to give 9-(4-bromo-2,6-dimethylphenyl)-9H-carbazole as an off-white solid in 71% yield (1.49 g, 4.26 mmol)

**<sup>1</sup>H NMR** (500 MHz, 298 K, CDCl<sub>3</sub>):  $\delta$  = 7.99 (m, 2H), 7.26 (s, 2H, overlaps with CDCl<sub>3</sub> residual proton signal) 7.21 (m, 2H), 7.11 (m, 2H), 6.75 (m, 2H), 1.66 (m, 6H) ppm;

**<sup>13</sup>C{<sup>1</sup>H} NMR** (126 MHz, 298 K, CDCl<sub>3</sub>):  $\delta$  = 140.5 (C<sub>q</sub>, 2C), 140.2 (C<sub>q</sub>, 2C), 133.9 (C<sub>q</sub>, 1C), 131.7 (CH, 2C), 126.3 (CH, 2C), 123.2 (C<sub>q</sub>, 2C), 122.6 (C<sub>q</sub>, 1C), 120.7 (CH, 2C), 119.8 (CH, 2C), 109.4 (CH, 2C), 17.5 (CH<sub>3</sub>, 2C) ppm;

**HRMS** (APCI, neg): Calc.: 350.0373 [m/z]; found: m/z = 350.0379 [M<sup>-</sup>].

## Experimental

### 6.2.1.5 9-(4-(bis(2,6-bis(trifluoromethyl)phenyl)boryl)-2,6-dimethylphenyl)carbazole (Cbz-Me $\pi$ (2))

A solution of 9-(4-bromo-2,6-dimethylphenyl)-9H-carbazole (350 mg, 1 mmol) in 20 mL of hexane was cooled to  $-78\text{ }^{\circ}\text{C}$  and *n*BuLi (1.6 M, 1.1 mmol, 0.69 mL) was added. The reaction was warmed to ambient temperature and stirred overnight. Then the reaction was cooled to  $-78\text{ }^{\circ}\text{C}$  again and a solution of bis(2,6-bis(trifluoromethyl)phenyl)fluoroborane (456 mg, 1 mmol) in 20 mL of hexane was added. The reaction was warmed to ambient temperature and stirred for 2 d. Then, 2 mL of methanol were added, all volatiles removed *in vacuo*, and the residue was purified by column chromatography (hexane/CH<sub>2</sub>Cl<sub>2</sub>, silica) to give 9-(4-(bis(2,6-bis(trifluoromethyl)phenyl)boryl)-2,6-dimethylphenyl)-9H-carbazole as a light green solid (170 mg, 0.24 mmol, 24%).

<sup>1</sup>H NMR (500 MHz, CDCl<sub>3</sub>):  $\delta$  = 8.20 – 8.17 (m, 2H), 8.01 (d, 4H, <sup>3</sup>*J* = 8 Hz), 7.79 (t, 2H, <sup>3</sup>*J* = 8 Hz), 7.42 – 7.38 (m, 2H), 7.30 – 7.26 (m, 2H), 7.08 (s, 2H), 6.88 (dt, 2H, *J*<sub>1</sub> = 8 Hz, *J*<sub>2</sub> = 1 Hz), 1.78 (s, 6H) ppm.

<sup>13</sup>C{<sup>1</sup>H} NMR (126 MHz, CDCl<sub>3</sub>):  $\delta$  = 140.1 (C<sub>q</sub>, 2C), 139.0 (C<sub>q</sub>, 1C), 138.6 (CH, 1C), 137.1 (C<sub>q</sub>, 1C), 136.8 (CH, 2C), 130.7 (CH, 2C), 130.2 (CH, 4C), 126.3 (CH, 2C), 124.7 (C<sub>q</sub>, 4C, q, <sup>1</sup>*J*<sub>CF</sub> = 275 Hz), 123.1 (C<sub>q</sub>, 1C), 120.6 (CH, 2C), 119.7 (CH, 2C), 109.5 (CH, 2C), 17.5 (CH<sub>3</sub>, 2C) ppm.

<sup>11</sup>B{<sup>1</sup>H} NMR (160 MHz, 298 K, CDCl<sub>3</sub>):  $\delta$  = 70.6 ppm.

<sup>19</sup>F{<sup>1</sup>H} NMR (471 MHz, 298 K, CDCl<sub>3</sub>):  $\delta$  =  $-53.40$  ppm.

**Elem. Anal. Calc.** (%) for C<sub>36</sub>H<sub>22</sub>BF<sub>12</sub>N: C 61.13, H 3.13, N 1.98; found: C 61.38, H 2.97, N 1.64

**HRMS** (ASAP, pos): Calc.: 708.1726 [m/z]; found: m/z = 708.1711 [MH<sup>+</sup>].

**6.2.1.6 2-(4-iodo-3,5-dimethylphenyl)-4,4,5,5-tetramethyl-1,3,2-dioxaborolane**

A solution of B<sub>2</sub>pin<sub>2</sub> (4.03 g, 15.9 mmol), [Ir(COD)OMe]<sub>2</sub> (0.21 g, 0.32 mmol) (COD = 1,5-cyclooctadiene) and 4,4'-di-*tert*butyl-2,2'-bipyridine (dtbpy) (0.18 g, 0.67 mmol) in hexane (30 mL) was stirred for 10 min at r.t. Then, 2-iodo-1,3-dimethylbenzene (2.46 g, 10.60 mmol) was added and the reaction was stirred for 3 d at 60 °C. The reaction was filtered through a silica plug and washed with hexane (200 mL) and the product eluted with a CH<sub>2</sub>Cl<sub>2</sub>:hexane mixture (200 mL, 1:9). All volatiles were removed *in vacuo*, to give 2-(4-iodo-3,5-dimethylphenyl)-4,4,5,5-tetramethyl-1,3,2-dioxaborolane as a white solid (3.38 g, 9.43 mmol, 89%).

**<sup>1</sup>H NMR** (500 Hz, 298 K, CDCl<sub>3</sub>): δ = 7.46 – 7.44 (m, 2H), 2.49 – 2.45 (m 6H), 1.34 (s, 12H) ppm;

**<sup>11</sup>B{<sup>1</sup>H} NMR** (160 Hz, 298 K, CDCl<sub>3</sub>): δ = 31.2 ppm;

**<sup>13</sup>C{<sup>1</sup>H} NMR** (126 Hz, 298 K, CDCl<sub>3</sub>): δ = 141.6 (C<sub>q</sub>, 2C), 132.9 (CH, 2C), 113.0 (C<sub>q</sub>, 1C), 83.9 (C<sub>q</sub>, 2C), 29.5 (CH<sub>3</sub>, 2C), 24.9 (CH<sub>3</sub>, 4C) ppm;

**HRMS** (ASAP pos): calc.: 359.0674 [m/z]; found: m/z = 359.0668 [MH<sup>+</sup>].

## Experimental

### 6.2.1.7 Potassium(4-iodo-3,5-dimethylphenyl)trifluoroborate

To a solution of 2-(4-iodo-3,5-dimethylphenyl)-4,4,5,5-tetramethyl-1,3,2-dioxaborolane (3.70 g, 10.3 mmol) in THF (30 mL), a saturated solution of  $K[HF]_2$  (3.63 g, 46.5 mmol, 4.5 eq.) in water was added. The reaction was stirred over night at ambient temperature. All volatiles were removed *in vacuo* and the remaining solid was extracted with acetone (3 x 50 mL). The solvent was removed *in vacuo* and the crude product was recrystallized from ethanol to give potassium(4-iodo-3,5-dimethylphenyl)trifluoroborate as a white solid (3.14 g, 9.29 mmol, 90%).

$^1H$  NMR (500 Hz, 298 K, acetone- $d_6$ ):  $\delta$  = 7.20 (s, 2H), 2.36 – 2.35 (m, 6H) ppm;

$^{11}B\{^1H\}$  NMR (160 Hz, 298 K, acetone- $d_6$ ):  $\delta$  = 3.3 (q,  $^1J_{BF}$  = 51 Hz) ppm;

$^{19}F\{^1H\}$  NMR (471.6 Hz, 298 K, acetone- $d_6$ ):  $\delta$  = -142.82 ppm;

$^{13}C\{^1H\}$  NMR (126 Hz, 298 K, acetone- $d_6$ ):  $\delta$  = 138.6 ( $C_q$ , 2C), 131.3 (CH, 2C, q,  $^3J_{CF}$  = 2 Hz), 104.2 ( $C_q$ , 1C), 28.9 ( $CH_3$ , 2C) ppm;

HRMS (ESI neg): calc.: 298.9710 [m/z]; found: m/z = 298.9723 [ $M^-$ ].



**6.2.1.8 Bis(2,6-bis(trifluoromethyl)phenyl)(4-iodo-3,5-dimethylphenyl)borane (BFD1H)**

To a solution of 2-iodo-1,3-bis(trifluoromethyl)benzene (3.37 g, 9.89 mmol) in MTBE (40 mL) a solution of *n*BuLi (1.6 M in hexane, 8.27 mL, 13.2 mmol) was slowly added at  $-78\text{ }^{\circ}\text{C}$  and the mixture was stirred for 30 min. The reaction was warmed to ambient temperature. and stirred for 2 h. The reaction mixture was added to a suspension of potassium(4-iodo-3,5-dimethylphenyl)trifluoroborate (1.52 g, 4.50 mmol) in THF (20 mL) at  $-78\text{ }^{\circ}\text{C}$  and then stirred overnight. The reaction was quenched with MeOH (1 mL) and all volatiles were removed *in vacuo*. The residue was dissolved in hexane and filtered through a plug of silica (silica/hexane). The solvent was evaporated to give bis(2,6-bis(trifluoromethyl)phenyl)(4-iodo-3,5-dimethylphenyl)borane as a light yellow solid (2.01 g, 3.02 mmol, 67% yield).

**$^1\text{H}$  NMR** (500 Hz, 298 K,  $\text{CDCl}_3$ ):  $\delta = 7.94$  (d, 4H,  $^3J = 8$  Hz), 7.75 (t, 2H,  $^3J = 8$  Hz), 6.82 (s, 2H), 2.40 (s, 6H) ppm;

**$^{11}\text{B}\{^1\text{H}\}$  NMR** (160 Hz, 298 K,  $\text{CDCl}_3$ ):  $\delta = 69.5$  ppm;

**$^{19}\text{F}\{^1\text{H}\}$  NMR** (471.6 Hz, 298 K,  $\text{CDCl}_3$ ):  $\delta = -53.15$  ppm;

**$^{13}\text{C}\{^1\text{H}\}$  NMR** (126 Hz, 298 K,  $\text{CDCl}_3$ ):  $\delta = 140.9$  ( $\text{C}_q$ , 2C), 134.4 (CH, 4C), 130.5 (CH, 2C), 130.1 (CH, 2C), 123.9 ( $\text{CF}_3$ , 4C, q,  $^1J_{\text{CF}} = 274$  Hz), 115.8 ( $\text{C}_q$ , 2C), 29.7 ( $\text{CH}_3$ , 2C) ppm;

**HRMS** (ASAP neg): calc.: 668.0036 [m/z]; found: m/z = 668.0048 [ $\text{M}^-$ ].

## Experimental

### 6.2.1.9 10-(4-(bis(2,6-bis(trifluoromethyl)phenyl)boryl)-2,6-dimethylphenyl) phenoxazine (Phox-Me $\pi$ (3))

A suspension of bis(2,6-bis(trifluoromethyl)phenyl)(4-iodo-3,5-dimethylphenyl)borane (400 mg, 0.6 mmol), phenoxazine (148 mg, 0.8 mmol), NaO<sup>t</sup>Bu (88 mg, 0.92 mmol), Pd(dba)<sub>3</sub>\*CHCl<sub>3</sub> (12 mg, 0.01 mmol) and Xantphos (8 mg, 0.01 mmol) in toluene was heated to 90 °C for 18 h. Afterwards, all volatiles were removed *in vacuo* and the product mixture was purified by column chromatography (CH<sub>2</sub>Cl<sub>2</sub>/hexane). The product was recrystallized from hexane to give 10-(4-(bis(2,6-bis(trifluoromethyl)phenyl)boryl)-2,6-dimethylphenyl)-10H-phenoxazine as a yellow solid (201 mg, 0.27 mmol, 46%).

<sup>1</sup>H NMR (500 Hz, 298 K, C<sub>6</sub>D<sub>6</sub>):  $\delta$  = 7.49 (d, 4 H, <sup>3</sup>J = 8 Hz), 7.21 (s, 2 H), 6.83 (t, 2 H, <sup>3</sup>J = 8 Hz), 6.78 – 6.67 (m, 2 H), 6.54 – 6.38 (m, 4 H), 5.99 – 5.85 (m, 2 H), 1.98 (s, 6 H) ppm;

<sup>11</sup>B{<sup>1</sup>H} NMR (160 Hz, 298 K, C<sub>6</sub>D<sub>6</sub>):  $\delta$  = 71.2 ppm;

<sup>19</sup>F{<sup>1</sup>H} NMR (471.6 Hz, 298 K, C<sub>6</sub>D<sub>6</sub>):  $\delta$  = -52.75 ppm;

<sup>13</sup>C{<sup>1</sup>H} NMR (126 Hz, 298 K, C<sub>6</sub>D<sub>6</sub>):  $\delta$  = 147.1 (C<sub>q</sub>, 1C), 144.4 (C<sub>q</sub>, 2C), 139.8 (C<sub>q</sub>, 2C), 139.2 (C<sub>q</sub>, 2C), 138.5 (C<sub>q</sub>, 2C), 138.3 (CH, 4C), 132.3 (C<sub>q</sub>, 2C), 130.9 (CH, 2C), 130.2 (CH, 4C), 124.6 (C<sub>q</sub>, 4C, q, <sup>1</sup>J<sub>CF</sub> = 273 Hz), 124.3 (CH, 2C), 121.9 (CH, 2C), 116.1 (CH, 2C), 111.8 (CH, 2C), 17.5 (CH<sub>3</sub>, 2C) ppm;

HRMS (APCI neg): calc.: 723.1597 [m/z]; found: m/z = 723.1617 [M<sup>-</sup>];

Elem. Anal. Calc. (%) for: C 59.78, H 3.07, N 1.94; found: C 60.12, H 3.04, N 2.12.

**6.2.1.10 Bis(2,6-bis(trifluoromethyl)phenyl)(3,5-dimethoxyphenyl)borane (iv')**

To a solution of 2-iodo-1,3-bis(trifluoromethyl)benzene (1.36 g, 4.0 mmol) in MTBE (20 mL) a solution of *n*BuLi (1.6 M in hexane, 2.75 mL, 4.4 mmol) was added at  $-78\text{ }^{\circ}\text{C}$  and the mixture was stirred for 30 min. The reaction was warmed to ambient temperature and stirred for 2 h. The reaction was cooled to  $-78\text{ }^{\circ}\text{C}$  again and potassium(3,5-dimethoxyphenyl)trifluoroborate (488 mg, 2.0 mmol) was added as a solid. The suspension was slowly warmed to ambient temperature and stirred overnight. All volatiles were removed *in vacuo* and the resulting solid extracted with hexane (3 x 80 mL). The solvent was evaporated and the crude product purified by column chromatography (pentane/ $\text{CH}_2\text{Cl}_2$ ) to give bis(2,6-bis(trifluoromethyl)phenyl)(3,5-dimethoxyphenyl)borane as a light green solid (350 mg, 0.61 mmol, 30 %)

**$^1\text{H}$  NMR** (500 Hz, 298 K,  $\text{CDCl}_3$ ):  $\delta = 7.48$  (d, 4H,  $^3J = 8$  Hz), 7.98 (t, 2H,  $^3J = 8$  Hz), 6.67 (d, 2H,  $^4J = 2.3$  Hz), 6.65 (t, 1H,  $^4J = 2$  Hz), 3.20 (s, 6H) ppm;

**$^{11}\text{B}\{^1\text{H}\}$  NMR** (160 Hz, 298 K,  $\text{CDCl}_3$ ):  $\delta = 70.4$  ppm;

**$^{19}\text{F}\{^1\text{H}\}$  NMR** (471.6 Hz, 298 K,  $\text{CDCl}_3$ ):  $\delta = -52.96$  ppm;

**$^{13}\text{C}\{^1\text{H}\}$  NMR** (126 Hz, 298 K,  $\text{CDCl}_3$ ):  $\delta = 160.6$  ( $\text{C}_q$ , 2C), 148.4 ( $\text{C}_q$ , 1C), 139.1 ( $\text{C}_q$ , 2C), 136.1 ( $\text{C}_q$ , 4C), 130.7 (CH, 2C), 130.1 (CH, 4C), 124.7 ( $\text{C}_q$ , 4C, q,  $^1J_{\text{CF}} = 280$  Hz) 115.2 (CH, 2C), 105.7 (CH, 1C), 54.7 ( $\text{CH}_3$ , 2C) ppm;

**HRMS** (APCI neg): calc.: 574.0979 [m/z]; found: m/z = 574.0979 [ $\text{M}^-$ ];

**Elem. Anal. Calc.** (%) for  $\text{C}_{24}\text{H}_{15}\text{BF}_{12}\text{O}_2$ : C 50.21, H 2.63; found: C 50.53, H 2.67.

## Experimental

### 6.2.1.11 Bis(2,6-bis(trifluoromethyl)phenyl)(4-iodo-3,5-dimethoxyphenyl)borane (iv)

To a solution of bis(2,6-bis(trifluoromethyl)phenyl)(3,5-dimethoxyphenyl)borane (350 mg, 0.61 mmol) and *N*-iodosuccinimide (150 mg, 0.67 mmol) in CH<sub>2</sub>Cl<sub>2</sub> (20 mL), FeCl<sub>3</sub> (10 mg, 0.06 mmol) was added. The reaction was heated to 40 °C for 18 h. Additional *N*-iodosuccinimide (60 mg, 0.27 mmol) was added and the reaction was stirred at ambient temperature for 24 h. The reaction was quenched with 10 mL of a saturated Na<sub>2</sub>S<sub>2</sub>O<sub>3(aq)</sub> solution and extracted with Et<sub>2</sub>O (3 x 50 mL). The organic phases were dried over sodium sulfate and all volatiles were removed *in vacuo* to give the crude product. Pure bis(2,6-bis(trifluoromethyl)phenyl)(4-iodo-3,5-dimethoxyphenyl)borane was obtained by recrystallization from hexane (360 mg, 0.51 mmol, 84%).

<sup>1</sup>H NMR (500 Hz, 298 K, CDCl<sub>3</sub>): δ = 7.47 (d, 4H, <sup>3</sup>J = 8 Hz), 6.83 (t, 2H, <sup>3</sup>J = 8 Hz), 6.43 (s, 2H), 3.17 (s, 6H) ppm;

<sup>11</sup>B{<sup>1</sup>H} NMR (160 Hz, 298 K, CDCl<sub>3</sub>): δ = 70.0 ppm;

<sup>19</sup>F{<sup>1</sup>H} NMR (471.6 Hz, 298 K, CDCl<sub>3</sub>): δ = -52.92 ppm;

<sup>13</sup>C{<sup>1</sup>H} NMR (126 Hz, 298 K, CDCl<sub>3</sub>): δ = 159.3 (C<sub>q</sub>, 2C), 147.3 (C<sub>q</sub>, 1C), 138.4 (C<sub>q</sub>, 2C), 136.1 (C<sub>q</sub>, 4C), 130.5 (CH, 2C), 129.9 (CH, 4C), 124.2 (C<sub>q</sub>, 4C, q, <sup>1</sup>J<sub>CF</sub> = 276 Hz) 111.7 (CH, 2C), 86.9 (CH, 1C), 55.4 (CH<sub>3</sub>, 2C) ppm;

HRMS (APCI neg): calc.: 699.9945 [m/z]; found: m/z = 699.9952 [M<sup>-</sup>]

### 6.2.1.12 10-(4-(bis(2,6-bis(trifluoromethyl)phenyl)boryl)-2,6-dimethoxyphenyl)phenoxazine (Phox-MeO $\pi$ (4))

A suspension of bis(2,6-bis(trifluoromethyl)phenyl)(4-iodo-3,5-dimethoxyphenyl)borane (360 mg, 0.5 mmol), phenoxazine (122 mg, 0.67 mmol), NaO<sup>t</sup>Bu (73 mg, 0.76 mmol), Pd(dba)<sub>3</sub>\*CHCl<sub>3</sub> (12 mg, 0.01 mmol) and Xantphos (8 mg, 0.01 mmol) in toluene was heated to 90 °C for 3 d. Afterwards, all volatiles were removed *in vacuo* and the crude product was purified by column chromatography (CH<sub>2</sub>Cl<sub>2</sub>/pentane). The product was recrystallized from hexane to give 10-(4-(bis(2,6-bis(trifluoromethyl)phenyl)boryl)-2,6-dimethoxyphenyl)-10H-phenoxazine as a red solid (220 mg, 0.29 mmol, 58%).

**<sup>1</sup>H NMR** (500 Hz, 298 K, CDCl<sub>3</sub>):  $\delta$  = 7.50 (d, 4H, <sup>3</sup>J = 8 Hz), 6.84 (t, 2H, <sup>3</sup>J = 8 Hz), 6.72 (dd, 2 H,  $J_1$  = 1 Hz,  $J_2$  = 8 Hz), 6.68 (s, 2H) 6.58 (td, 2 H,  $J_1$  = 2 Hz,  $J_2$  = 8 Hz), 6.46 (td, 2 H,  $J_1$  = 2 Hz,  $J_2$  = 8 Hz), 6.27 (dd, 2 H,  $J_1$  = 1 Hz,  $J_2$  = 8 Hz), 3.03(s, 6H) ppm;

**<sup>11</sup>B{<sup>1</sup>H} NMR** (160 Hz, 298 K, CDCl<sub>3</sub>):  $\delta$  = 71.0 ppm;

**<sup>19</sup>F{<sup>1</sup>H} NMR** (471.6 Hz, 298 K, CDCl<sub>3</sub>):  $\delta$  = -52.81 ppm;

**<sup>13</sup>C{<sup>1</sup>H} NMR** (126 Hz, 298 K, CDCl<sub>3</sub>):  $\delta$  = 158.3 (C<sub>q</sub>, 2C), 148.0 (C<sub>q</sub>, 1C), 145.0 (C<sub>q</sub>, 2C), 138.9 (C<sub>q</sub>, 2C), 136.0 (C<sub>q</sub>, 4C), 133.6 (CH, 2C), 131.0 (CH, 4C), 124.7 (C<sub>q</sub>, 4C, q, <sup>1</sup>J<sub>CF</sub> = 280 Hz), 130.3 (CH, 2C), 123.9 (CH, 2C), 121.6 (C<sub>q</sub>, 2C), 116.0 (CH, 2C), 119.6 (CH, 1C), 113.7 (CH, 2C), 112.6 (CH, 2C), 55.3 (CH, 2C) ppm;

**HRMS** (APCI pos): calc.: 755.1496 [m/z]; found: m/z = 755.1478 [MH<sup>+</sup>];

**Elem. Anal. Calc.** (%) for C<sub>36</sub>H<sub>22</sub>BF<sub>12</sub>NO<sub>3</sub>: C 57.24, H 2.94, N 1.85; found: C 58.03, H 2.92, N 2.24.

## Experimental

### 6.2.1.13 2,4,6-trimethoxy-2',6'-bis(trifluoromethyl)-1,1'-biphenyl

To a solution of 2-iodo-1,3-bis(trifluoromethyl)benzene (1.0 g, 2.94 mmol) in THF (10 mL), *n*BuLi (2.5 M in hexane, 1.24 mL, 3.09 mmol) was added at  $-78\text{ }^{\circ}\text{C}$ . The reaction was slowly warmed to ambient temperature over 3 h. Then,  $\text{ZnCl}_2$  (0.42 g, 3.09 mmol) was added and the reaction was stirred for 1 h at ambient temperature. Then, 2-iodo-1,3,5-trimethoxybenzene (0.86 g, 2.93 mmol)  $\text{Pd}(\text{PPh}_3)_2\text{Cl}_2$  (0.21 g, 0.29 mmol), Xantphos (0.17 g, 0.29 mmol) and CuBr (0.42 g, 2.94 mmol) were added and the reaction was heated to  $70\text{ }^{\circ}\text{C}$  for 12 h. The reaction was poured into water and extracted with  $\text{Et}_2\text{O}$  (3 x 50 mL). The solvent was removed *in vacuo* and 2,4,6-trimethoxy-2',6'-bis(trifluoromethyl)-1,1'-biphenyl was purified by column chromatography (hexane/ $\text{CH}_2\text{Cl}_2$ ). Yield: 240 mg, 0.63 mmol, 21%.

$^1\text{H NMR}$  (500 Hz, 298 K,  $\text{CDCl}_3$ ):  $\delta = 7.93$  (*d*, 2H,  $^3J = 8$  Hz), 7.55 (*t*, 1H,  $^3J = 8$  Hz), 6.17 (*s*, 2H), 3.86 (*s*, 3H), 3.66 (*s*, 6H) ppm;

$^{19}\text{F}\{^1\text{H}\}$  NMR (471.6 Hz, 298 K,  $\text{CDCl}_3$ ):  $\delta = -61.89$  ppm;

$^{13}\text{C}\{^1\text{H}\}$  NMR (126 Hz, 298 K,  $\text{CDCl}_3$ ):  $\delta = 162.3$  ( $\text{C}_q$ , 2C), 159.2 ( $\text{C}_q$ , 1C), 134.4 ( $\text{C}_q$ , m, 1C), 132.4 ( $\text{C}_q$ , 2C, q,  $^2J_{\text{CF}} = 30$  Hz), 129.4 (CH, 2C, q,  $^3J_{\text{CF}} = 5$  Hz), 127.6 (CH, 1C), 123.5 ( $\text{C}_q$ , 2C, q,  $^1J_{\text{CF}} = 274$  Hz), 104.9 ( $\text{C}_q$ , 1C), 90.1 (CH, 2C), 55.7 ( $\text{CH}_3$ , 2C), 55.4 ( $\text{CH}_3$ , 2C) ppm;

HRMS (ASAP pos): calc.: 382.0953 [m/z]; found: m/z = 382.0946 [ $\text{MH}^+$ ].

**6.2.1.14 4,4,5,5-tetramethyl-2-(2',4',6'-trimethoxy-2,6-bis(trifluoromethyl)-[1,1'-biphenyl]-4-yl)-1,3,2-dioxaborolane**

A solution of B<sub>2</sub>pin<sub>2</sub> (133 mg, 0.52 mmol), [Ir(COD)OMe]<sub>2</sub> (11 mg, 0.016 mmol) and dtbpy (9 mg, 0.032 mmol) in hexane (20 mL) was stirred for 10 min at ambient temperature. Then, 2,4,6-trimethoxy-2',6'-bis(trifluoromethyl)-1,1'-biphenyl (200 mg, 0.52 mmol) was added and the reaction was stirred over night at ambient temperature. The reaction was filtered through a silica plug and washed with hexane (100 mL) and the product was eluted with a CH<sub>2</sub>Cl<sub>2</sub>/pentane mixture (200 mL, 3:7). All volatiles were removed *in vacuo*, to give 4,4,5,5-tetramethyl-2-(2',4',6'-trimethoxy-2,6-bis(trifluoromethyl)-[1,1'-biphenyl]-4-yl)-1,3,2-dioxaborolane as a white solid (130 mg, 0.26 mmol, 49%).

**<sup>1</sup>H NMR** (500 Hz, 298 K, CDCl<sub>3</sub>): δ = 8.34 (s, 2H), 6.16 (s, 2H), 3.86 (s, 3H), 3.64 (s, 6H), 1.37 (s, 12H) ppm;

**<sup>11</sup>B{<sup>1</sup>H} NMR** (160 Hz, 298 K, CDCl<sub>3</sub>): δ = 30.5 ppm;

**<sup>19</sup>F{<sup>1</sup>H} NMR** (471.6 Hz, 298 K, CDCl<sub>3</sub>): δ = 61.68 ppm;

**<sup>13</sup>C{<sup>1</sup>H} NMR** (126 Hz, 298 K, CDCl<sub>3</sub>): δ = 162.3 (C<sub>q</sub>, 2C), 159.1 (C<sub>q</sub>, 1C), 137.1 (C<sub>q</sub>, 1C, sept., <sup>3</sup>J<sub>CF</sub> = 2 Hz), 135.4 (CH, 2C, q, <sup>3</sup>J<sub>CF</sub> = 6 Hz), 131.9 (C<sub>q</sub>, 2C, q, <sup>2</sup>J<sub>CF</sub> = 29 Hz), 128.9 (C<sub>q</sub>, 1C), 123.7 (C<sub>q</sub>, 2C, q, <sup>1</sup>J<sub>CF</sub> = 275 Hz), 105.0 (C<sub>q</sub>, 1C), 90.1 (CH, 2C), 84.7 (C<sub>q</sub>, 2C), 55.7 (CH<sub>3</sub>, 2C), 55.4 (CH<sub>3</sub>, 1C), 25.0 (CH<sub>3</sub>, 4C) ppm;

**HRMS** (ASAP pos): calc.: 507.1772 [m/z]; found: m/z = 507.1768 [MH<sup>+</sup>].

## Experimental

### 6.2.1.15 Potassium(2',4',6'-trimethoxy-2,6-bis(trifluoromethyl)-[1,1'-biphenyl]-4-yl)trifluoroborate

To a solution of 4,4,5,5-tetramethyl-2-(2',4',6'-trimethoxy-2,6-bis(trifluoromethyl)-[1,1'-biphenyl]-4-yl)-1,3,2-dioxaborolane (127 mg, 0.25 mmol) in THF a saturated solution of  $K[HF]_2$  (88 mg, 1.13 mmol, 4.5 eq.) in water was added. The reaction was stirred for 45 min at ambient temperature. All volatiles were removed *in vacuo* and the remaining solid extracted with acetone (3 x 15 mL). The solvent was removed *in vacuo* and the crude product was washed with pentane (2 x 30 mL) to give potassium(2',4',6'-trimethoxy-2,6-bis(trifluoromethyl)-[1,1'-biphenyl]-4-yl)trifluoroborate as a white solid (121 mg, 0.25 mmol, 99%).

$^1H$  NMR (500 Hz, 298 K, acetone- $d_6$ ):  $\delta$  = 8.08 (s, 2H), 6.24 (s, 2H), 3.85 (s, 3H), 3.62 (s, 6H) ppm;

$^{11}B\{^1H\}$  NMR (160 Hz, 298 K, acetone- $d_6$ ):  $\delta$  = 2.8 ppm;

$^{19}F\{^1H\}$  NMR (471.6 Hz, 298 K, acetone- $d_6$ ):  $\delta$  = -61.10, -144.06 ppm;

$^{13}C\{^1H\}$  NMR (126 Hz, 298 K, acetone- $d_6$ ):  $\delta$  = 162.9 ( $C_q$ , 2C), 160.2 ( $C_q$ , 1C), 133.1 (CH, 2C), 131.1 ( $C_q$ , 2C), 130.3 ( $C_q$ , 2C, q,  $^2J_{CF}$  = 28 Hz), 125.6 ( $C_q$ , 2C, q,  $^1J_{CF}$  = 274 Hz), 106.7 ( $C_q$ , 1C), 90.7 (CH, 2C), 55.7 (CH<sub>3</sub>, 2C), 55.5 (CH<sub>3</sub>, 1C) ppm;

HRMS (ESI neg): calc.: 447.0820 [m/z]; found: m/z = 447.0814 [ $M^+$ ].



### 6.2.1.16 Bis(2,6-bis(trifluoromethyl)phenyl)(2',4',6'-trimethoxy-2,6-bis(trifluoromethyl)-[1,1'-biphenyl]-4-yl)borane ( $^{\text{MeO}_3\text{Ph-FMe}}\pi$ (5))

To a solution of 2-iodo-1,3-bis(trifluoromethyl)benzene (210 mg, 0.61 mmol) in Et<sub>2</sub>O (10 mL) a solution of *n*BuLi (2.5 M in hexane, 0.27 mL, 0.68 mmol) was added at  $-78$  °C and the mixture was stirred for 30 min. The reaction was then warmed to ambient temperature and stirred for 2 h. The reaction was then cooled to  $-78$  °C and potassium(2',4',6'-trimethoxy-2,6-bis(trifluoromethyl)-[1,1'-biphenyl]-4-yl)trifluoroborate (100 mg, 0.21 mmol) was added as a solid. The suspension was slowly warmed to ambient temperature and stirred for 2 d. All volatiles were removed *in vacuo* and the resulting solid was extracted with hexane (3 x 20 mL). The solvent was evaporated and the crude product was purified by column chromatography (hexane/CH<sub>2</sub>Cl<sub>2</sub>) to give bis(2,6-bis(trifluoromethyl)phenyl)(2',4',6'-trimethoxy-2,6-bis(trifluoromethyl)-[1,1'-biphenyl]-4-yl)borane as a light blue solid (25 mg, 0.03 mmol, 15%).

**<sup>1</sup>H NMR** (500 Hz, 298 K, C<sub>6</sub>D<sub>6</sub>):  $\delta$  = 8.17 (s, 2H), 7.39 (d, 4H, <sup>3</sup>*J* = 8 Hz), 6.72 (t, 2H, <sup>3</sup>*J* = 8 Hz), 6.09 (s, 2H), 3.31 (s, 3H), 3.26 (s, 6H) ppm;

**<sup>11</sup>B{<sup>1</sup>H} NMR** (160 Hz, 298 K, C<sub>6</sub>D<sub>6</sub>):  $\delta$  = 71.0 ppm;

**<sup>19</sup>F{<sup>1</sup>H} NMR** (471.6 Hz, 298 K, C<sub>6</sub>D<sub>6</sub>):  $\delta$  =  $-52.83$  (br),  $-61.63$  (s) ppm;

**<sup>13</sup>C{<sup>1</sup>H} NMR** (126 Hz, 298 K, C<sub>6</sub>D<sub>6</sub>):  $\delta$  = 163.2 (C<sub>q</sub>, 2C), 159.5 (C<sub>q</sub>, 1C), 145.2 (C<sub>q</sub>, 2C), 140.4 (C<sub>q</sub>, 1C), 137.6 (C<sub>q</sub>, 1C), 136.8 (CH, 2C, q, <sup>3</sup>*J*<sub>CF</sub> = 5 Hz), 135.8 (C<sub>q</sub>, 4C, q, <sup>2</sup>*J*<sub>CF</sub> = 31 Hz), 132.6 (C<sub>q</sub>, 2C, q, <sup>2</sup>*J*<sub>CF</sub> = 30 Hz), 131.5 (CH, 2C), 130.3 (CH, 4C, q, <sup>3</sup>*J*<sub>CF</sub> = 5 Hz), 124.4 (C<sub>q</sub>, 4C, q, <sup>1</sup>*J*<sub>CF</sub> = 275 Hz), 124.4 (C<sub>q</sub>, 2C, q, <sup>1</sup>*J*<sub>CF</sub> = 272 Hz), 104.8 (C<sub>q</sub>, 1C), 90.5 (CH, 2C), 55.3 (CH<sub>3</sub>, 2C), 54.7 (CH<sub>3</sub>, 1C) ppm;

**HRMS** (ASAP neg): calc.: 816.1145 [m/z]; found: m/z = 816.1153 [M<sup>-</sup>].

## Experimental

### 6.2.2 Chapter 2

#### 6.2.2.1 2-(2-Bromo-3,5-bis(trifluoromethyl)phenyl)-4,4,5,5-tetramethyl-1,3,2-dioxaborolane (2-1)

B<sub>2</sub>pin<sub>2</sub> (3.9 g, 15.4 mmol), 4,4'-di-tert-butyl-2,2'-bipyridine (247 mg, 0.9 mmol) and [Ir(COD)OMe]<sub>2</sub> (305 mg, 0.46 mmol) were dissolved in hexane and stirred for 10 min, then 1-bromo-2,4-bis(trifluoromethyl)benzene (4.5 g, 2.6 mL, 15.4 mmol) was added dropwise. The suspension was stirred for 12 h and afterwards filtered through a silica plug with hexane as the eluent. The solvent was removed under reduced pressure to obtain 2-(2-bromo-3,5-bis(trifluoromethyl)phenyl)-4,4,5,5-tetramethyl-1,3,2-dioxaborolane (4.54 g, 10.8 mmol) as a white solid in 70% yield.

**<sup>1</sup>H NMR** (500 MHz, 298 K, CDCl<sub>3</sub>): δ(ppm) = 7.93 (m, 2 H), 1.41 (s, 12 H)

**<sup>11</sup>B{<sup>1</sup>H} NMR** (64.1 MHz, 298 K, CDCl<sub>3</sub>): δ(ppm) = 30.5

**<sup>19</sup>F{<sup>1</sup>H} NMR** (188.1 MHz, 298 K, CDCl<sub>3</sub>): δ(ppm) = -62.8 (s, 3 F), -63.0 (s, 3 F)

**<sup>13</sup>C{<sup>1</sup>H} NMR** (126 MHz, 298 K, CDCl<sub>3</sub>): δ(ppm) = 138.0 (br, 1C, C<sub>q</sub>), 135.4 (q, <sup>3</sup>J<sub>CF</sub> = 4 Hz, 1C, CH), 131.5 (q, <sup>2</sup>J<sub>CF</sub> = 32 Hz, 1C, C<sub>q</sub>), 129.4 (q, <sup>2</sup>J<sub>CF</sub> = 34 Hz, 1C, C<sub>q</sub>), 129.4 (br, 1C, CH), 126.5 (m, 1C, CH), 123.4 (q, <sup>1</sup>J<sub>CF</sub> = 271 Hz, 1C, CF<sub>3</sub>), 122.6 (q, <sup>1</sup>J<sub>CF</sub> = 274 Hz, 1C, CF<sub>3</sub>), 85.4 (s, 2C, C<sub>q</sub>), 24.9 (s, 4C, CH<sub>3</sub>)

**HRMS** (APCI<sup>+</sup>): *m/z* calculated for [C<sub>14</sub>H<sub>15</sub>B<sub>1</sub>Br<sub>1</sub>F<sub>6</sub>O<sub>2</sub>]<sup>+</sup> 419.0247, found 419.0245 [M]<sup>+</sup> (|Δ| = 0.4 ppm)

**6.2.2.2 2,2'-Dibromo-3,3',5,5'-tetrakis(trifluoromethyl)-1,1'-biphenyl (2-2)**

The compound 2-(2-bromo-3,5-bis(trifluoromethyl)phenyl)-4,4,5,5-tetramethyl-1,3,2-dioxaborolane (0.875 g, 2.08 mmol) and Cu(OAc)<sub>2</sub> (0.075 g, 0.41 mmol) were dissolved in 200 mL of methanol open to air and the reaction was stirred for 12 h at room temperature. All volatiles were removed under reduced pressure and the resulting solid was dissolved in hexane and filtered through a silica plug using hexane as the eluent. The volatiles were removed under reduced pressure and compound **2-2** was obtained as a white solid (0.49 g, 0.83 mmol) in 80% yield.

**<sup>1</sup>H NMR** (500 MHz, 298 K, C<sub>6</sub>D<sub>6</sub>): δ(ppm) = 7.79 (d, 2 H, <sup>4</sup>J = 2 Hz), 6.85 (d, 2 H, <sup>4</sup>J = 2 Hz)

**<sup>13</sup>C{<sup>1</sup>H} NMR** (126 MHz, 298 K, C<sub>6</sub>D<sub>6</sub>): δ(ppm) = 144.2 (2C), 132.6 (q, <sup>2</sup>J<sub>CF</sub> = 32 Hz, 2C), 130.5 (q, <sup>3</sup>J<sub>CF</sub> = 1 Hz, 2C), 130.5 (q, <sup>2</sup>J<sub>CF</sub> = 34 Hz, 2C), 126.2 (m, 2C), 125.3 (m, 2C), 123.3, (q, <sup>1</sup>J<sub>CF</sub> = 273 Hz, 2C), 122.7 (q, <sup>1</sup>J<sub>CF</sub> = 274 Hz, 2C)

**<sup>19</sup>F{<sup>1</sup>H} NMR** (471.6 MHz, 298 K, C<sub>6</sub>D<sub>6</sub>): δ(ppm) = -62.5 (s, 6 F), -62.9 (s, 6 F)

**HRMS** (APCI<sup>+</sup>): *m/z* calculated for [C<sub>16</sub>H<sub>4</sub>Br<sub>2</sub>F<sub>12</sub>]<sup>+</sup> 504.9279, found 504.9276 [M]<sup>+</sup> (Δ = 0.1 ppm)

## Experimental

### 6.2.2.3 9-(2,4,6-Tris(trifluoromethyl)phenyl)-2,4,6,8-tetrakis(trifluoromethyl)-dibenzoborole (<sup>F</sup>Mes<sup>F</sup>Bf)

In a Schlenk tube compound **2.2** (1.00 g, 1.71 mmol) was dissolved in 30 mL of diethylether. A 2.5 M *n*BuLi solution in hexane (1.4 mL, 3.50 mmol) was added dropwise at -78 °C and the mixture was stirred for 45 min. Meanwhile, <sup>F</sup>Mes-BF<sub>3</sub>K (0.66 g, 1.71 mmol) and LiBr (0.15 g, 1.72 mmol) were suspended in 10 mL of diethylether and stirred for 45 min. Then, the suspension was added dropwise to the lithiated compound **2.2** and the reaction was slowly warmed to room temperature overnight. After addition of a few drops of *iso*-propanol, the solvent was removed under reduced pressure. The resulting solid was purified via sublimation (180 °C, 5 x 10<sup>-2</sup> mbar) and washed with hexane to obtain compound <sup>F</sup>Mes<sup>F</sup>Bf (0.25 g, 0.35 mmol) as a bright green solid in 20% yield. Single crystals of compound <sup>F</sup>Mes<sup>F</sup>Bf were obtained by recrystallization from hexane.

<sup>1</sup>H NMR (500 MHz, 298 K, C<sub>6</sub>D<sub>6</sub>): δ(ppm) = 7.93 (s, 2 H), 7.43 (s, 2 H), 7.11 (s, 2 H)

<sup>11</sup>B{<sup>1</sup>H} NMR (160 MHz, 298 K, C<sub>6</sub>D<sub>6</sub>): δ(ppm) = 64.1 (br)

<sup>13</sup>C{<sup>1</sup>H} NMR (126 MHz, 298 K, CDCl<sub>3</sub>): δ(ppm) = 152.9 (2C, C<sub>q</sub>), 139.9 (br, 2C, C<sub>q</sub>), 137.7 (q, <sup>2</sup>J<sub>CF</sub> = 33 Hz, 2C, C<sub>q</sub>), 136.3 (q, <sup>2</sup>J<sub>CF</sub> = 33 Hz, 2C, C<sub>q</sub>), 134.0 (q, <sup>2</sup>J<sub>CF</sub> = 33 Hz, 2C, C<sub>q</sub>), 133.4 (q, <sup>2</sup>J<sub>CF</sub> = 35 Hz, 1C, C<sub>q</sub>), 126.0 (2C, CH) 124.1 (q, <sup>1</sup>J<sub>CF</sub> = 274 Hz, 2C, CF<sub>3</sub>), 122.7 (q, <sup>1</sup>J<sub>CF</sub> = 278 Hz, 2C, CF<sub>3</sub>), 122.6 (q, <sup>1</sup>J<sub>CF</sub> = 273 Hz, 1C, CF<sub>3</sub>), 122.4 (q, <sup>1</sup>J<sub>CF</sub> = 274 Hz, 2C, CF<sub>3</sub>) 124.2 (m, 2C, CH), 120.4 (m, 2C, CH)

<sup>19</sup>F{<sup>1</sup>H} NMR (471 MHz, 298 K, C<sub>6</sub>D<sub>6</sub>): δ(ppm) = -58.4 (sept, 6 F, J<sub>FF</sub> = 4 Hz), -59.6 (sept, 6 F, J<sub>FF</sub> = 4 Hz), -62.0 (s, 3 F), -63.5 (s, 6 F)

<sup>19</sup>F{<sup>1</sup>H} NMR (471 MHz, 298 K, CDCl<sub>3</sub>): δ(ppm) = -58.6 (sept, 6 F, J<sub>FF</sub> = 4 Hz), -59.6 (sept, 6 F, J<sub>FF</sub> = 4 Hz), -63.1 (s, 3 F), -64.0 (s, 6 F)

HRMS (APCI<sup>-</sup>): *m/z* calculated for [C<sub>25</sub>H<sub>6</sub>B<sub>1</sub>F<sub>21</sub>]<sup>-</sup> 716.0233, found 716.0245 [M]<sup>-</sup> (Δ = 1.6 ppm)

#### 6.2.2.4 9-(2,6-Bis(trifluoromethyl)phenyl)-2,4,6,8-tetrakis(trifluoromethyl)-dibenzoborole (<sup>F</sup>Xyl<sup>F</sup>Bf)

In a Schlenk tube, compound **2.2** (1.00 g, 1.71 mmol) was dissolved in 30 mL of diethylether. A 2.5 M *n*BuLi solution in hexane (1.40 mL, 3.51 mmol) was added dropwise at  $-78\text{ }^{\circ}\text{C}$  and the reaction mixture was stirred for 30 min. Meanwhile, <sup>F</sup>Xyl-BF<sub>3</sub>K (0.55 g, 1.71 mmol) and LiBr (1.71 mmol, 0.15 g) were suspended in 10 mL of diethylether and stirred for 30 min. Then the suspension was added dropwise to the lithiated compound **2.2** and the reaction was slowly warmed to room temperature overnight. After addition of a few drops of *iso*-propanol, the solvent was removed under reduced pressure. The resulting solid was purified via sublimation ( $170\text{ }^{\circ}\text{C}$ ,  $5 \times 10^{-2}$  mbar) and recrystallization from hexane to obtain <sup>F</sup>Xyl<sup>F</sup>Bf (91 mg, 139 μmol) as a bright green solid in 8% yield. Single crystals of compound <sup>F</sup>Xyl<sup>F</sup>Bf for X-ray diffraction were obtained by crystallization from dichloromethane.

<sup>1</sup>H NMR (500 MHz, 298 K, C<sub>6</sub>D<sub>6</sub>):  $\delta(\text{ppm}) = 7.49$  (s, 2 H), 7.31 (d, 2 H,  $J_{\text{HH}} = 8$  Hz), 7.16 (s under solvent signal, 2 H) 6.85 (t, 2 H,  $J_{\text{HH}} = 8$  Hz)

<sup>11</sup>B{<sup>1</sup>H} NMR (160 MHz, 298 K, C<sub>6</sub>D<sub>6</sub>):  $\delta(\text{ppm}) = 63.2$  (br)

<sup>13</sup>C{<sup>1</sup>H} NMR (126 MHz, 298 K, C<sub>6</sub>D<sub>6</sub>):  $\delta(\text{ppm}) = 152.7$  (2C), 140.5 (2C), 136.8 (q,  $^2J_{\text{CF}} = 33$  Hz, 2C), 136.0 (q,  $^2J_{\text{CF}} = 33$  Hz, 2C), 132.7 (q,  $^2J_{\text{CF}} = 33$  Hz, 2C), 130.4, 129.1 (m, 2C), 125.6 (q,  $^1J_{\text{CF}} = 274$  Hz, 2C), 123.9 (m, 2C), 123.2 (q,  $^1J_{\text{CF}} = 273$  Hz, 2C), 122.8 (q,  $^1J_{\text{CF}} = 274$  Hz, 2C), 120.5 (m, 2C)

<sup>19</sup>F{<sup>1</sup>H} NMR (471 MHz, 298 K, C<sub>6</sub>D<sub>6</sub>):  $\delta(\text{ppm}) = -58.2$  (sept, 6 F,  $J_{\text{FF}} = 3$  Hz)  $-59.6$  (sept, 6 F,  $J_{\text{FF}} = 4$  Hz),  $-63.4$  (s, 6 F)

HRMS (APCI<sup>-</sup>):  $m/z$  calculated for [C<sub>24</sub>H<sub>7</sub>B<sub>1</sub>F<sub>18</sub>]<sup>-</sup> 648.0348, found 648.0336 [M]<sup>-</sup> ( $|\Delta| = 1.8$  ppm)

## Experimental

### 6.2.2.5 9-(4-(Dimethylamino)-2,6-bis(trifluoromethyl)phenyl)-2,4,6,8-tetrakis(trifluoromethyl)-dibenzoborole (*p*-NMe<sub>2</sub>-<sup>F</sup>Xyl<sup>F</sup>Bf)

Compound **2.2** (1.00 g, 1.71 mmol) was dissolved in 30 mL of diethylether and a 2.5 M *n*BuLi solution in hexane (1.40 mL, 3.51 mmol) was added dropwise at  $-78\text{ }^{\circ}\text{C}$  and the reaction mixture was stirred for 45 min. Meanwhile, *p*-NMe<sub>2</sub>-<sup>F</sup>Xyl-BF<sub>3</sub>K (0.61 g, 1.71 mmol) and LiBr (0.15 g, 1.71 mmol) were suspended in 10 mL of diethylether and stirred. Then, the suspension was added dropwise to the lithiated compound **2.2** and the reaction was slowly warmed to room temperature overnight. After addition of a few drops *iso*-propanol, the solvent was removed under reduced pressure. The resulting solid was purified via sublimation ( $200\text{ }^{\circ}\text{C}$ ,  $5 \times 10^{-2}$  mbar) and washed with hexane to obtain *p*-NMe<sub>2</sub>-<sup>F</sup>Xyl<sup>F</sup>Bf (25 mg, 36.2 mmol) as a red solid in 2% yield. Crystals of compound *p*-NMe<sub>2</sub>-<sup>F</sup>Xyl<sup>F</sup>Bf suitable for X-ray diffraction were obtained by crystallization from hexane at  $-30\text{ }^{\circ}\text{C}$ .

<sup>1</sup>H NMR (500 MHz, 298 K, C<sub>6</sub>D<sub>6</sub>):  $\delta(\text{ppm}) = 7.57$  (s, 2 H),  $7.22$  (s, 2 H),  $6.95$  (s, 2 H),  $2.10$  (s, 6 H)

<sup>11</sup>B{<sup>1</sup>H} NMR (160 MHz, 298 K, C<sub>6</sub>D<sub>6</sub>):  $\delta(\text{ppm}) = 64.7$  (br)

<sup>13</sup>C{<sup>19</sup>F} NMR (126 MHz, 298 K, C<sub>6</sub>D<sub>6</sub>):  $\delta(\text{ppm}) = 152.7$  (d, <sup>2</sup>*J*<sub>CH</sub> = 3 Hz, 2C)  $150.9$  (br, 2C),  $141.3$  (br, 2C),  $136.4$  (2C),  $136.1$  (2C),  $133.9$  (2C),  $129.0$  (2C),  $126.12$  (m, 2C),  $123.8$  (dd, <sup>1</sup>*J*<sub>CH</sub> = 167 Hz, <sup>2</sup>*J*<sub>CH</sub> = 6 Hz, 2C),  $123.3$  (t, <sup>2</sup>*J*<sub>CH</sub> = 4 Hz),  $123.1$  (d, <sup>2</sup>*J*<sub>CH</sub> = 4 Hz, 2C),  $120.4$  (dd, <sup>1</sup>*J*<sub>CH</sub> = 164 Hz, <sup>2</sup>*J*<sub>CH</sub> = 6 Hz, 2C),  $117.93$  (br, 2C),  $111.2$  (dd, <sup>1</sup>*J*<sub>CH</sub> = 160 Hz, <sup>2</sup>*J*<sub>CH</sub> = 5 Hz, 2C),  $38.87$  (m, 2C)

<sup>19</sup>F{<sup>1</sup>H} NMR (471 MHz, 298 K, C<sub>6</sub>D<sub>6</sub>):  $\delta(\text{ppm}) = -58.1$  (sept, 6 F, *J*<sub>FF</sub> = 3 Hz),  $-59.5$  (sept, 6 F, *J*<sub>FF</sub> = 4 Hz),  $-63.4$  (s, 6 F)

HRMS (APCI<sup>-</sup>): *m/z* calculated for [C<sub>26</sub>H<sub>12</sub>B<sub>1</sub>F<sub>18</sub>N]<sup>-</sup> 691.0781, found 691.0792 [M]<sup>-</sup> ( $|\Delta| = 1.6$  ppm)

### 6.2.2.6 Potassium (2,4,6-tris(trifluoromethyl)phenyl)trifluoroborate

2,4,6-tris(trifluoromethyl)benzene (4.50 g, 2.97 mL, 16.0 mmol) was dissolved in 70 mL of diethylether and then a 2.5 M *n*BuLi solution in hexane (7.02 mL, 17.6 mmol) was added dropwise at  $-78\text{ }^{\circ}\text{C}$  and the mixture was allowed to warm slowly to room temperature over 8 h. Afterwards, the reaction was cooled to  $-78\text{ }^{\circ}\text{C}$ , B(OMe)<sub>3</sub> (4.97 g, 5.39 mL, 47.9 mmol) was added dropwise and the reaction was slowly warmed to room temperature overnight. Then, the suspension was filtered, and the solvent was removed under reduced pressure. The resulting solid was dissolved in 200 mL of methanol, while K[HF]<sub>2</sub> (3.31 g, 42.4 mmol) was dissolved in 25 mL of H<sub>2</sub>O. The aqueous solution was added dropwise, and the reaction mixture was stirred overnight. The solvents were removed under reduced pressure and the remaining solid was suspended in hexane and filtered. The product was extracted with acetone and filtered. The solvent was removed from the filtrate under reduced pressure to give potassium (2,4,6-tris(trifluoromethyl)phenyl)trifluoroborate (4.9 g, 12.6 mmol) as a white solid in 79% yield.

<sup>1</sup>H NMR (500 MHz, 298 K, acetone-*d*<sub>6</sub>):  $\delta(\text{ppm}) = 8.05$  (s, 2 H)

<sup>11</sup>B{<sup>1</sup>H} NMR (160 MHz, 298 K, acetone-*d*<sub>6</sub>):  $\delta(\text{ppm}) = 1.9$  (q,  $J_{\text{BF}} = 44$  Hz)

<sup>13</sup>C{<sup>1</sup>H} NMR (126 MHz, 298 K, acetone-*d*<sub>6</sub>):  $\delta(\text{ppm}) = 155.1$  (br), 137.7 (q,  $^2J_{\text{CF}} = 32$  Hz, 2C), 127.7 (q,  $J_{\text{CF}} = 33$  Hz), 125.0 (br, 2C), 124.5 (q,  $J_{\text{CF}} = 274$  Hz, 2C) 123.7 (q,  $J_{\text{CF}} = 271$  Hz).

<sup>19</sup>F{<sup>1</sup>H} NMR (471 MHz, 298 K, acetone-*d*<sub>6</sub>):  $\delta(\text{ppm}) = -57.9$  (q, 6 F  $J_{\text{FF}} = 14$  Hz),  $-63.5$  (s, 3 F),  $-136.4$  (m, 3 F)

HRMS (ESI<sup>-</sup>):  $m/z$  calculated for [C<sub>9</sub>H<sub>2</sub>B<sub>1</sub>F<sub>12</sub>]<sup>-</sup>: 349.0063, found 349.0062 [M]<sup>-</sup> ( $|\Delta| = 0.3$  ppm)

## Experimental

### 6.2.2.7 Potassium (2,6-bis(trifluoromethyl)phenyl)trifluoroborate

The compound 2-iodo-1,3-bis(trifluoromethyl)benzene (3.05 g, 8.97 mmol) was dissolved in 50 mL of MeO<sup>t</sup>Bu (MTBE). A 2.5 M *n*BuLi solution in hexane (3.77 mL, 9.23 mmol) was added dropwise at  $-78\text{ }^{\circ}\text{C}$  and the reaction mixture was stirred for 45 min. Then, B(OMe)<sub>3</sub> (2.02 mL, 17.9 mmol) was added dropwise to the lithiated species and the reaction was slowly warmed to room temperature overnight. Afterwards, the suspension was filtered and the solvent was removed from the filtrate under reduced pressure to give dimethyl(2,6-bis(trifluoromethyl)phenyl)boronate. The remaining solid was dissolved in 80 mL of MeOH, while K[HF]<sub>2</sub> (2.3 g, 30 mmol) was dissolved in 10 mL of H<sub>2</sub>O. The aqueous solution was added dropwise, and the methanol-water solution was stirred for 12 h. The solvents were removed from the mixture under reduced pressure and the resulting solid was suspended in hexane and filtered. The product was extracted with acetone and filtered. The solvent was removed from the filtrate under reduced pressure to give potassium (2,6-bis(trifluoromethyl)phenyl)trifluoroborate (2.8 g, 8.8 mmol) as a white solid in 89% yield.

**<sup>1</sup>H NMR** (200 MHz, 298 K, DMSO-*d*<sub>6</sub>):  $\delta(\text{ppm}) = 7.75$  (d, 2 H,  $J_{\text{HH}} = 8$  Hz), 7.43 (t, 1 H,  $J_{\text{HH}} = 8$  Hz)

**<sup>11</sup>B{<sup>1</sup>H} NMR** (64 MHz, 298 K, DMSO-*d*<sub>6</sub>):  $\delta(\text{ppm}) = 1.9$  (q,  $J_{\text{BF}} = 45$  Hz)

**<sup>19</sup>F{<sup>1</sup>H} NMR** (188 MHz, 298 K, DMSO-*d*<sub>6</sub>):  $\delta(\text{ppm}) = -55.6$  (q, 6 F,  $J_{\text{FF}} = 14$  Hz),  $-133.2$  (m, 3 F)

**<sup>13</sup>C{<sup>1</sup>H} NMR** (126 MHz, 298 K, DMSO-*d*<sub>6</sub>):  $\delta(\text{ppm}) = 134.5$  (q, 2 C,  $^2J_{\text{CF}} = 31$  Hz), 128.6 (q, 2 C,  $^3J_{\text{CF}} = 6$  Hz), 126.0 (1 C), 125.6 (q, 2 C,  $^1J_{\text{CF}} = 275$  Hz).

**HRMS** (ESI<sup>-</sup>):  $m/z$  calculated for [C<sub>8</sub>H<sub>3</sub>B<sub>1</sub>F<sub>9</sub>]<sup>-</sup>: 281.0186, found 281.0189 [M]<sup>-</sup> ( $|\Delta| = 3.55$  ppm)

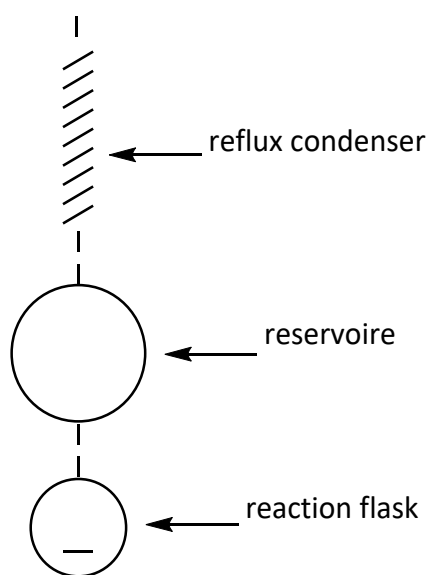


### 6.2.2.8 N,N-Dimethyl-3,5-bis(trifluoromethyl)aniline

In a 250 mL flask with a solvent reservoir (typically used for column chromatography) and a condenser attached to it, 3,5-bis(trifluoromethyl)aniline (10.0 g, 43.6 mmol) was stirred at 0 °C. Formic acid (16.5 mL, 437 mmol) was added slowly and the reaction mixture was warmed to room temperature. Then, formaldehyde (30.1 mL, 818 mmol) was added, and the reaction mixture was heated to reflux. During the reaction the crude product sublimes as a white solid in the reservoir. The sublimed product was dissolved in 100 mL of Et<sub>2</sub>O and washed with 3 x 50 mL of water. The organic phase was dried over magnesium sulfate and filtered. After removal of all volatiles under reduced pressure, N,N-dimethyl-3,5-bis(trifluoromethyl)aniline (9.1 g, 35.4 mmol) was obtained as a white solid in 81% yield.

The analytical data match those previously reported.<sup>[334]</sup>

Experimental setup:



## Experimental

### 6.2.2.9 4-Bromo-*N,N*-dimethyl-3,5-bis(trifluoromethyl)aniline

*N,N*-dimethyl-3,5-bis(trifluoromethyl)aniline (3.0 g, 11.7 mmol) was dissolved in 150 mL of acetonitrile and *N*-bromosuccinimide (2.28 g, 12.8 mmol) was added over 10 min. The yellow solution was stirred for 20 min, then an excess of saturated sodium thiosulfate solution was added to obtain a colorless solution. Afterwards, 200 mL of Et<sub>2</sub>O were added and the solution was washed with 3 x 50 mL of brine. The organic phase was dried over sodium sulfate and filtered. All volatiles were removed under reduced pressure, and the resulting solid was recrystallized from hexane and dried *in vacuo*. The product 4-bromo-*N,N*-dimethyl-3,5-bis(trifluoromethyl)aniline was obtained as white solid (3.1 g, 9.22 mmol) in 79% yield.

**<sup>1</sup>H NMR** (500 MHz, 298 K, CDCl<sub>3</sub>): δ(ppm) = 7.11 (s, 2 H), 3.06 (s, 6 H)

**<sup>13</sup>C{<sup>1</sup>H} NMR** (126 MHz, 298 K, CDCl<sub>3</sub>): δ(ppm) = 148.7 (1C, C<sub>q</sub>), 132.9 (q, *J*<sub>CF</sub> = 30 Hz, 2C, C<sub>q</sub>), 123.1 (q, *J*<sub>CF</sub> = 274 Hz, 2C, CF<sub>3</sub>), 113.6 (q, *J*<sub>CF</sub> = 6 Hz, 2C, CH), 101.7 (m, 1C, C<sub>q</sub>), 40.3 (2C, CH<sub>3</sub>)

**<sup>19</sup>F{<sup>1</sup>H} NMR** (471 MHz, 298 K, CDCl<sub>3</sub>): δ(ppm) = -62.1 (s, 6 F)

**HRMS** (ASAP<sup>+</sup>): *m/z* calculated for [C<sub>10</sub>H<sub>9</sub>Br<sub>1</sub>F<sub>6</sub>]<sup>+</sup>: 335.9817, found 335.9810 [M]<sup>+</sup> (|Δ| = 3.42 ppm)

**6.2.2.10 Potassium (4-(dimethylamino)-2,6-bis(trifluoromethyl)phenyl)trifluoroborate**

The compound 4-bromo-*N,N*-dimethyl-3,5-bis(trifluoromethyl)aniline (2.5 g, 7.4 mmol) was dissolved in 50 mL of diethylether, a 2.5 M *n*BuLi solution in hexane (3.12 mL, 7.80 mmol) was added dropwise at  $-78$  °C, and the mixture was stirred for 45 min. Then, B(OMe)<sub>3</sub> (1.7 mL, 15 mmol) was added dropwise and the reaction was slowly warmed to room temperatures overnight. Afterwards, the suspension was filtered, and the solvent was removed from the filtrate under reduced pressure to give dimethyl(4-(dimethylamino)-2,6-bis(trifluoromethyl)phenyl)boronate. This was dissolved in 80 mL of methanol, while K[HF]<sub>2</sub> (1.84 g, 23.6 mmol) was dissolved in 10 mL of H<sub>2</sub>O. The aqueous solution was added dropwise, and the methanol-water solution was stirred 12 h. The solvents were removed under reduced pressure and the resulting solid was washed with hexane and filtered and then extracted with acetone and filtered. The solvent was removed under reduced pressure to give potassium (4-(dimethylamino)-2,6-bis(trifluoromethyl)phenyl)trifluoroborate) (1.3 g, 3.6 mmol) as a white solid in 49% yield.

**<sup>1</sup>H NMR** (500 MHz, 298 K, acetone-*d*<sub>6</sub>):  $\delta$ (ppm) = 7.11 (s, 2 H), 2.97 (s, 6 H)

**<sup>11</sup>B{<sup>1</sup>H} NMR** (160 MHz, 298 K, acetone-*d*<sub>6</sub>):  $\delta$ (ppm) = 2.5 (q,  $J_{BF} = 49$  Hz)

**<sup>13</sup>C{<sup>1</sup>H} NMR** (126 MHz, 298 K, acetone-*d*<sub>6</sub>):  $\delta$ (ppm) = 151.0 (1C, C<sub>q</sub>) 149.0 (1C, C<sub>q</sub>), 136.9 (m, 2C, C<sub>q</sub>), 126.6 (q,  $J_{CF} = 274$  Hz, 2C, CF<sub>3</sub>), 113.2 (q,  $J_{CF} = 7$  Hz, 2C, CH), 40.4 (2C, CH<sub>3</sub>)

**<sup>19</sup>F{<sup>1</sup>H} NMR** (471 MHz, 298 K, acetone-*d*<sub>6</sub>):  $\delta$ (ppm) =  $-57.3$  (q, 6 F,  $J_{FF} = 14$  Hz),  $-135.1$  (m, 3 F)

**HRMS** (ESI<sup>-</sup>):  $m/z$  calculated for [C<sub>10</sub>H<sub>8</sub>B<sub>1</sub>F<sub>9</sub>N<sub>1</sub>]<sup>-</sup> 324.0612, found 324.0611 [M]<sup>-</sup> ( $|\Delta| = 0.3$  ppm)

### 6.2.3 Chapter 3

#### 6.2.3.1 Tris(2,6-dimethyl-4-(4,4,5,5-tetramethyl-1,3,2-dioxaborolan-2-yl)phenyl)borane (BG0Bpin)

Tris(2,6-dimethylphenyl)borane (4.0 g, 12.3 mmol), B<sub>2</sub>pin<sub>2</sub> (13.7 g, 49.0 mmol), [Ir(COD)(OMe)]<sub>2</sub> (243.8 mg, 0.37 mmol) and dtbpy (197 mg, 0.74 mmol) were dissolved in THF (120 mL) and stirred at 70 °C for 3 d. The solvent was removed under reduced pressure and the residue dissolved in a hexane/CH<sub>2</sub>Cl<sub>2</sub> mixture (1:1, 150 mL) and filtered through a plug (silica: hexane/CH<sub>2</sub>Cl<sub>2</sub>). The solvent was removed under reduced pressure and the remaining residue washed with methanol. Tris(2,6-dimethyl-4-(4,4,5,5-tetramethyl-1,3,2-dioxaborolan-2-yl)phenyl)borane was isolated as a white solid in 87% yield (7.58 g, 10.7 mmol).

<sup>1</sup>H NMR (300 MHz, CDCl<sub>3</sub>): δ (ppm) = 7.36 (s, 6H), 2.02 (s, 18H), 1.37 (s, 36H).

<sup>11</sup>B NMR (128 MHz, CDCl<sub>3</sub>): δ (ppm) = 84.0 (br), 31.5 (br).

<sup>13</sup>C{<sup>1</sup>H} NMR (75 MHz, CDCl<sub>3</sub>): δ (ppm) = 149.8 (C<sub>q</sub>, 3C), 139.7(C<sub>q</sub>, 6C), 133.9 (CH, 6C), 129.9 (C<sub>q</sub>, 3C), 83.9 (C<sub>q</sub>, 6C), 25.1 (CH<sub>3</sub>, 6C), 25.0 (CH<sub>3</sub>, 6C), 22.9 (CH<sub>3</sub>, 6C).

HRMS (APCI neg): calc.: 704.4768 [m/z]; found: 704.4778 [M<sup>-</sup>]

Elemental analysis calcd. [%] for C<sub>42</sub>H<sub>60</sub>B<sub>4</sub>: C 71.64, H 8.59; found: C 71.20 H 8.69.

**6.2.3.2 Tris(2,6-dimethyl-4-(trifluoroborate)phenyl)borane, tripotassium salt (BG0BF<sub>3</sub>K)**

To a solution of tris(2,6-dimethyl-4-(4,4,5,5-tetramethyl-1,3,2-dioxaborolan-2-yl)phenyl)borane (2.18 g, 3.1 mmol) in THF (60 mL), a solution of K[HF<sub>2</sub>] (2.90 g, 37.1 mmol) in water (7 mL) was added and stirred for 1 h. The precipitate was isolated by filtration and washed with THF (4 x 10 mL) and an acetone/water mixture (1:9, 50 mL), successively. Tris(2,6-dimethyl-4-(trifluoroboryl)phenyl)borane, tripotassium salt was obtained as a white solid in 91% yield (1.81 g).

**<sup>1</sup>H NMR** (200 MHz, 298 K, DMSO-d<sub>6</sub>):  $\delta$  (ppm) = 6.82 (s, 6H), 1.86 (s, 12H).

**<sup>11</sup>B NMR** (95 MHz, 298 K, DMSO-d<sub>6</sub>):  $\delta$  (ppm) = 3.3 (s, br).

**<sup>11</sup>B NMR** (128 MHz, 298 K, D<sub>2</sub>O):  $\delta$  (ppm) = 82.3 (br), 3.9 (br).

**<sup>19</sup>F NMR** (188 MHz, 298 K, DMSO-d<sub>6</sub>):  $\delta$  (ppm) = -138.9 (br).

**<sup>13</sup>C{<sup>1</sup>H} NMR** (101 MHz, 298 K, D<sub>2</sub>O):  $\delta$  (ppm) = 146.5 (C<sub>q</sub>, 3C), 139.9 (C<sub>q</sub>, 6C), 130.0 (CH, 6C), 22.0 (CH<sub>3</sub>, 6C).

**<sup>13</sup>C-SS NMR** (249 MHz, 298 K):  $\delta$  (ppm) = 146.4, 139.5, 130.8, 22.6.

**<sup>11</sup>B-SS NMR** (128 MHz, 298 K):  $\delta$  (ppm) = 78.5 ( $\eta_Q = 0.1$ ), 4.9 ( $\eta_Q = 0.35$ ).

**<sup>19</sup>F-SS NMR** (377 MHz, 298 K):  $\delta$  (ppm) = -141.1.

**HRMS** (ESI neg): calc.: 175.7374 [m/z]; found: 175.7365 [M<sup>3-</sup> - 3 K<sup>+</sup>]

## Experimental

### 6.2.3.3 Tris(4-(bis(2,6-dimethylphenyl)boryl)-2,6-dimethylphenyl)borane (BG1H)

To a suspension of tris(2,6-dimethyl-4-(trifluoroborate)phenyl)borane, tripotassium salt (1.0 g, 1.6 mmol) in THF (50 mL), a solution of (2,6-dimethylphenyl)magnesium bromide in THF (13 mL, 1.1 M, 10.2 mmol) was added. The reaction was stirred for 18 h at ambient temperature. The excess Grignard reagent was quenched with water (10 mL), then the solvent was removed under reduced pressure. The remaining solid was dissolved in refluxing chloroform precipitated with cold ethanol. **BG1H** was obtained by filtration as a white solid in 31% yield (504 mg, 0.5 mmol).

$^1\text{H NMR}$  (500 MHz, 298 K,  $\text{CDCl}_3$ )  $\delta$  (ppm) = 7.17 (t,  $J$  = 8 Hz, 6H), 7.05 (s, 6H), 6.97 (d,  $J$  = 8 Hz, 12H), 2.04 (s, 36H), 1.99 (s, 18H).

$^{11}\text{B-SS NMR}$  (128 MHz), 298 K  $\delta$  (ppm) = 78.2 ( $\eta_{\text{Q}}$  = 0.0), 75.0 ( $\eta_{\text{Q}}$  = 0.0).

$^{11}\text{B NMR}$  (160 MHz, 298 K,  $\text{CDCl}_3$ ):  $\delta$  (ppm) = 83.4 (br.).

$^{13}\text{C}\{^1\text{H}\}$  NMR (126 MHz, 298 K,  $\text{CDCl}_3$ ):  $\delta$  (ppm) = 150.6 ( $\text{C}_q$ , 3C), 147.7 ( $\text{C}_q$ , 3C), 144.9 ( $\text{C}_q$ , 6C), 140.8 ( $\text{C}_q$ , 6C), 139.9 ( $\text{C}_q$ , 6C), 135.2 (CH, 6C), 129.0 (CH, 6C), 127.4 (CH, 12C), 23.7 ( $\text{CH}_3$ , 6C), 23.1 ( $\text{CH}_3$ , 12C).

**MALDI-TOF**  $m/z$  = 986.367 [ $\text{M}^-$ ]

**Elemental analysis** calcd. [%] for  $\text{C}_{72}\text{H}_{78}\text{B}_4$ : C 87.65, H 7.97; found: C 87.15, H 8.11.

#### 6.2.3.4 Tris(4-(bis(2,6-dimethyl-4-(4,4,5,5-tetramethyl-1,3,2-dioxaborolan-2-yl)phenyl)boryl)-2,6-dimethylphenyl)borane (BG1Bpin)

**BG1H** (300 mg, 0.3 mmol), B<sub>2</sub>pin<sub>2</sub> (926 mg, 3.7 mmol), [Ir(COD)(OMe)]<sub>2</sub> (36 mg, 0.4 mmol) and dtbpy (30 mg, 0.7 mmol) were suspended in THF (50 mL) and stirred at 70 °C for 2 d. The reaction was filtrated and the remaining solid was washed with hexane (2 x 10 mL) and MeOH (2 x 10 mL), then dissolved in hot chloroform and precipitated with cold ethanol. **BG1Bpin** was isolated by filtration as a white solid in 76% yield (400 mg, 0.23 mmol).

<sup>1</sup>H NMR (500 MHz, 298 K, CDCl<sub>3</sub>): δ (ppm) = 7.41 (s, 12H), 6.99 (s, 6H), 2.04 (s, 36H), 1.93 (s, 18H), 1.35 (s, 74H).

<sup>11</sup>B-SS NMR (128.3 MHz, 298 K): δ (ppm) = 80.3 ( $\eta_Q = 0.0$ ), 74.4 ( $\eta_Q = 0.0$ ), 31.1 ( $\eta_Q = 0.67$ ).

<sup>13</sup>C{<sup>1</sup>H} NMR (126 MHz, 298 K, CDCl<sub>3</sub>): δ (ppm) = 150.7 (C<sub>q</sub>, 3C), 148.2 (C<sub>q</sub>, 6C), 147.1 (C<sub>q</sub>, 3C), 140.1 (C<sub>q</sub>, 12C), 139.9 (C<sub>q</sub>, 6C), 135.2 (CH, 6C), 133.4 (C<sub>q</sub>, 12C), 129.2 (C<sub>q</sub>, 6C), 83.8 (C<sub>q</sub>, 12C), 25.1 (CH<sub>3</sub>, 24C), 23.5 (CH<sub>3</sub>, 6C), 23.0 (CH<sub>3</sub>, 12C).

Elemental analysis calcd. [%] for C<sub>108</sub>H<sub>144</sub>B<sub>10</sub>O<sub>12</sub>: C 74.45, H 8.33; found: C 73.93, H 8.59.

#### 6.2.3.5 Tris(4-(dimesitylboryl)-2,6-dimethylphenyl)borane (BG1Me)

To a suspension of tris(2,6-dimethyl-4-(trifluoroborate)phenyl)borane, tripotassium salt (100 mg, 0.16 mmol) in THF (80 mL), a solution of mesitylmagnesium bromide in THF (1.4 mL, 1 M, 1.4 mmol) was added. The reaction was stirred for 18 h at ambient temperature and the excess Grignard reagent quenched with MeOH (1 mL). All volatiles were removed under reduced pressure. The remaining solid was washed with 50 mL of hexane, water (3 x 10 mL) and acetone (3 x 10 mL) to give **BG1Me** as a white solid in 41% yield (68 mg, 0.06 mmol).

<sup>1</sup>H-NMR (500 Hz, 298 K, CDCl<sub>3</sub>): δ (ppm) = 7.03 (s, 6H), 6.79 (s, 12H), 2.29 (s, 18H), 1.99 (s, 36H), 1.97 (s, 18H).

<sup>11</sup>B NMR (160 Hz, 298 K, CDCl<sub>3</sub>): δ (ppm) = N.D.

<sup>13</sup>C{<sup>1</sup>H} NMR (126 Hz, 298 K, CDCl<sub>3</sub>): δ (ppm) = 150.4 (C<sub>q</sub>, 3C), 148.2 (C<sub>q</sub>, 3C), 142.1 (C<sub>q</sub>, 6C), 141.0 (C<sub>q</sub>, 12C), 139.8 (C<sub>q</sub>, 6C), 138.6 (C<sub>q</sub>, 6C), 134.2 (CH, 6C), 128.1 (CH, 12C), 23.5 (CH<sub>3</sub>, 6C), 23.1 (CH<sub>3</sub>, 12C); 21.4 (CH<sub>3</sub>, 6C).

HRMS (APCI pos): calc.: 1071.7488 [m/z]; found: 1071.7478 [MH<sup>+</sup>]

## Experimental

### 6.2.3.6 Tris(4-(bis(4-bromo-2,6-dimethylphenyl)boryl)-2,6-dimethylphenyl)-borane (BG1Br)

A solution of 5-bromo-2-iodo-1,3-dimethylbenzene (5.60 mmol, 1.74 g) in THF (20 mL) was cooled to  $-15\text{ }^{\circ}\text{C}$  and a solution of *isopropylmagnesium chloride lithium chloride complex* in THF (5.54 mmol, 0.8 M, 6.93 mL) was slowly added. The reaction mixture was stirred for 1.5 h at  $-15\text{ }^{\circ}\text{C}$  and 1 h at ambient temperature. A suspension of tris(2,6-dimethyl-4-(trifluoroboryl)phenyl)borane, tripotassium salt (0.47 mmol, 0.30 g) in THF (75 mL) was added and the yellow suspension was stirred for 4 d at ambient temperature. The excess Grignard reagent was quenched with MeOH (3 mL) and all volatiles were removed under reduced pressure. The remaining solid was washed with water (3 x 20 mL) and hexane (3 x 20 mL). The yellow solid was extracted with chloroform (120 mL). The solution was concentrated and layered with ethanol. The crystallized white solid was further purified by column chromatography (hexane/ $\text{CH}_2\text{Cl}_2$ ) to give **BG1Br** as a white solid in 30% yield (0.14 mmol, 206 mg).

$^1\text{H NMR}$  (500 Hz, 298 K,  $\text{CDCl}_3$ ):  $\delta$  (ppm) = 7.16 (s, 12H), 7.00 (s, 6H), 2.00 (s, 36H), 1.98 (s, 18H).

$^{11}\text{B NMR}$  (160 Hz, 298 K,  $\text{CDCl}_3$ ):  $\delta$  (ppm) = N.D.

$^{13}\text{C}\{^1\text{H}\}$  NMR (126 Hz, 298 K,  $\text{CDCl}_3$ ):  $\delta$  (ppm) = 150.9 ( $\text{C}_q$ , 3C), 146.9 ( $\text{C}_q$ , 3C), 143.0 ( $\text{C}_q$ , 6C), 142.9 ( $\text{C}_q$ , 12C), 140.1 ( $\text{C}_q$ , 12C), 135.2 (CH, 6C), 130.4 (CH, 12C), 123.7 ( $\text{C}_q$ , 6C), 23.3 ( $\text{CH}_3$ , 6C), 22.9 ( $\text{CH}_3$ , 12C).

HRMS (APCI neg): calc.: 1460.1051 [m/z]; found: 1460.1090 [M $^-$ ]



**6.2.3.7 4,4',4'',4''',4''''-((Boranetriyltris(3,5-dimethylbenzene-4,1-diyl))tris-(boranetriyl))hexakis(N,N,3,5-tetramethylaniline) (BG1NMe<sub>2</sub>)**

In a three-necked flask with reflux condenser and dropping funnel, magnesium turnings (4.45 mmol, 0.11 g) were covered with THF. Then, a few drops of a solution of 4-bromo-N,N,3,5-tetramethylaniline (4.37 mmol, 1.00 g) in THF (20 mL) were added. The reaction mixture was heated until the reaction started and the rest of the solution was then added dropwise. The reaction mixture was heated at reflux for 1 h and then cooled to rt. The Grignard reagent was slowly added to a white suspension of tris(2,6-dimethyl-4-(trifluoroboryl)phenyl)borane, tripotassium salt (0.36 mmol, 0.23 g) in THF (50 mL). The orange reaction mixture was stirred for 3 days at ambient temperature and then all volatiles were removed under reduced pressure. The green solid was slurried in a 1:1 CH<sub>2</sub>Cl<sub>2</sub>/hexane solution and filtered and all volatiles removed under reduced pressure. The remaining solid was purified by column chromatography (hexane/CH<sub>2</sub>Cl<sub>2</sub> with 1% Et<sub>3</sub>N as an additive). The product was dissolved in 10 mL of CH<sub>2</sub>Cl<sub>2</sub> and precipitated with ethanol to give **BG1NMe<sub>2</sub>** as a yellow solid in 79% yield (0.28 mmol, 354 mg).

**<sup>1</sup>H NMR** (500 Hz, 298 K, CDCl<sub>3</sub>):  $\delta$  (ppm) = 7.06 (s, 6H), 6.36 (s, 12H), 2.97 (s, 36H), 2.00 (s, 18H), 1.98 (s, 36H).

**<sup>11</sup>B NMR** (160 Hz, 298 K, CDCl<sub>3</sub>):  $\delta$  (ppm) = N.D.

**<sup>13</sup>C{<sup>1</sup>H} NMR** (126 Hz, 298 K, CDCl<sub>3</sub>):  $\delta$  (ppm) = 150.9 (C<sub>q</sub>, 6C), 150.2 (C<sub>q</sub>, 3C), 149.6 (C<sub>q</sub>, 6C), 143.0 (C<sub>q</sub>, 12C), 139.5 (C<sub>q</sub>, 6C), 138.7 (C<sub>q</sub>, 6C), 134.6 (CH, 6C), 111.4 (CH, 12C), 40.3 (CH<sub>3</sub>, 12C), 24.4 (CH<sub>3</sub>, 6C), 23.1 (CH<sub>3</sub>, 12C).

**HRMS** (APCI neg): calc.: 1244.9013 [m/z]; found: 1244.9023 [M<sup>-</sup>]

## Experimental

### 6.2.3.8 Tris(4-(bis(2,6-bis(trifluoromethyl)phenyl)boryl)-2,6-dimethylphenyl)-borane (BFG1H)

A solution of **BFD1H** (1.50 mmol, 1.00 g) in diethyl ether (25 mL) was cooled to  $-78\text{ }^{\circ}\text{C}$ . Then *n*BuLi (1.65 mmol, 1.6 M, 1.10 mL) was added dropwise and the reaction stirred for 3 h at  $-78\text{ }^{\circ}\text{C}$ . Then  $\text{BF}_3(\text{OEt}_2)$  (0.50 mmol, 0.06 mL) in diethyl ether (12 mL) was slowly added and the solution slowly warmed to ambient temperature. The reaction was stirred for 3 days at ambient temperature and then quenched with MeOH (2 mL). All volatiles were removed under reduced pressure. The remaining solid was extracted with hexane and toluene. The solvent was evaporated under reduced pressure and the product was purified by column chromatography (hexane/ $\text{CH}_2\text{Cl}_2$ ), to give **BFG1H** as a white solid in 39% yield (0.2 mmol, 319 mg).

$^1\text{H NMR}$  (500 Hz, 298 K,  $\text{CDCl}_3$ ):  $\delta$  (ppm) = 8.01 (d,  $^3J = 8\text{ Hz}$ , 12H), 7.96 (t, 6H,  $^3J = 8\text{ Hz}$ ), 6.71 (s, 6H), 1.90 (s, 18H).

$^{11}\text{B SS NMR}$  (128.3 MHz):  $\delta$  (ppm) = 77.4 ( $\eta_{\text{Q}} = 0.0$ ), 71.0 ( $\eta_{\text{Q}} = 0.16$ ), 69.6 ( $\eta_{\text{Q}} = 0.13$ ).

$^{13}\text{C}\{^1\text{H}\}$  NMR (126 Hz, 298 K,  $\text{CDCl}_3$ ):  $\delta$  (ppm) = 151.0 ( $\text{C}_{\text{q}}$ , 3C), 147.6 ( $\text{C}_{\text{q}}$ , 3C), 139.1 ( $\text{C}_{\text{q}}$ , 6C), 139.0 ( $\text{C}_{\text{q}}$ , 6C), 136.1 (CH, 6C), 130.2 (CH, 12C), 130.0 (CH, br, 6C, assignment by HSQC), 124.0 ( $\text{CF}_3$ , 12C,  $^1J_{\text{CF}} = 275\text{ Hz}$ ); 22.5 ( $\text{CH}_3$ , 6C).

$^{19}\text{F NMR}$  (471.6 Hz, 298 K,  $\text{CDCl}_3$ ):  $\delta$  (ppm) =  $-50.46$  (br.), 55.50 (br.).

**HRMS** (APCI neg): calc.: 1633.3115 [m/z]; found: 1633.3105 [ $\text{M}^-$ ]

### 6.2.3.9 Tris(4-(bis(2,6-dimethyl-4-(trifluoroborate)phenyl)boryl)-2,6-dimethylphenyl)borane, hexa(tetra-butylammonium) salt (BG1BF<sub>3</sub>N(*n*Bu)<sub>4</sub>)

To a suspension of **BG1Bpin** (0.12 mmol, 206 mg) in CHCl<sub>3</sub> (50 mL), a solution of [N(*n*Bu<sub>4</sub>)]HF<sub>2</sub> (2.13 mmol, 599 mg) was added. Shortly after addition the residual solid dissolved. The reaction was stirred for 1 h. Then all volatiles were removed *in vacuo*. The resulting oil was washed with water (3 x 30 mL) to give the tris(4-(bis(2,6-dimethyl-4-(trifluoroborate)phenyl)boryl)-2,6-dimethylphenyl)borane,hexa(tetra-butylammonium) salt as light yellow solid in 92% yield (0.11 mmol, 310 mg).

<sup>1</sup>H NMR (500 Hz, 298 K, CD<sub>2</sub>Cl<sub>2</sub>): δ (ppm) = 7.06 (s, 12H), 7.01 (s, 6H), 3.13 – 3.04 (m, 48H), 2.01 – 1.96 (m, 54H), 1.60 – 1.48 (m, 48H), 1.35 (sex., <sup>3</sup>J = 7 Hz, 48H), 0.95 (t, <sup>3</sup>J = 7 Hz, 72H).

<sup>11</sup>B NMR (160 Hz, 298 K, CD<sub>2</sub>Cl<sub>2</sub>): δ (ppm) = 2.8 (br.).

<sup>13</sup>C{<sup>1</sup>H NMR (126 Hz, 298 K, CD<sub>2</sub>Cl<sub>2</sub>): δ (ppm) = 149.9 (C<sub>q</sub>, 3C), 149.9 (C<sub>q</sub>, 3C), 143.0 (C<sub>q</sub>, 6C), 139.7 (C<sub>q</sub>, 6C), 138.7 (C<sub>q</sub>, 12C), 134.8 (CH, 6C), 131.2 (CH, 12C), 75.1 (CH<sub>2</sub>, 24C), 24.1 (CH<sub>2</sub>, 24C), 23.8 (CH<sub>3</sub>, 12C), 23.2 (CH<sub>3</sub>, 6C), 20.0 (CH<sub>2</sub>, 24C), 13.7 (CH<sub>3</sub>, 24C).

<sup>19</sup>F NMR (471.6 Hz, 298 K, CD<sub>2</sub>Cl<sub>2</sub>): δ (ppm) = -141.19 (s, br.).

**HRMS** (ESI neg): calc.: 325.9852 [m/z]; found: 325.9847 [M<sup>-5</sup>(N(*n*Bu<sub>4</sub>))]

calc.: 468.0525 [m/z]; found: 468.0517 [M<sup>-4</sup>(N(*n*Bu<sub>4</sub>))<sub>2</sub>]

calc.: 704.8314 [m/z]; found: 704.8314 [M<sup>-3</sup>(N(*n*Bu<sub>4</sub>))<sub>3</sub>]

**Elemental analysis** calcd. [%] for C<sub>168</sub>H<sub>300</sub>B<sub>10</sub>F<sub>18</sub>N<sub>6</sub>: C 70.69; H 10.59; N 2.94; found: C 70.94, H 10.15, N 2.63.

## Experimental

### 6.2.3.10 Tris(4-(bis(4-(bis(2,6-dimethylphenyl)boryl)-2,6-dimethylphenyl)boryl)-2,6-dimethylphenyl)borane (BG2H)

To a suspension of **BG1BF<sub>3</sub>N(*n*Bu)<sub>4</sub>** (0.04 mmol, 100 mg) in THF (40 mL), a solution of mesitylmagnesium bromide in THF (0.8 mL, 0.8 M, 0.64 mmol) was added. The reaction was stirred for 2 d at ambient temperature. Then the excess Grignard reagent was quenched with aqueous Et<sub>2</sub>O (5 mL) and all volatiles were removed *in vacuo*. The resulting solid was extracted with toluene (3 x 20 mL). The solvent was removed under reduced pressure and the raw product purified by column chromatography (hexane:CH<sub>2</sub>Cl<sub>2</sub>) to give **BG2H** as a white solid in 31% yield (0.01 mmol, 25 mg).

**<sup>1</sup>H NMR** (500 Hz, 298 K, CD<sub>2</sub>Cl<sub>2</sub>):  $\delta$  (ppm) = 7.17 (t, <sup>3</sup>*J* = 8 Hz, 12H), 7.09 (s, 12H), 7.05 (s, 6H), 6.98 (d, <sup>3</sup>*J* = 8 Hz, 24H), 2.05 (s, 72H), 2.01 (s, 36H), 1.98 (s, 18H).

**<sup>11</sup>B NMR** (160 Hz, 298 K, CD<sub>2</sub>Cl<sub>2</sub>):  $\delta$  (ppm) = N.D.

**<sup>13</sup>C{<sup>1</sup>H} NMR** (126 Hz, 298 K, CD<sub>2</sub>Cl<sub>2</sub>):  $\delta$  (ppm) = 151.1 (C<sub>q</sub>, 3C), 149.5 (C<sub>q</sub>, 6C), 147.2 (C<sub>q</sub>, 3C), 147.0 (C<sub>q</sub>, 6C), 145.2 (C<sub>q</sub>, 12C), 141.1 (C<sub>q</sub>, 24C), 140.5 (C<sub>q</sub>, 6C), 140.3 (C<sub>q</sub>, 12C), 135.6 (CH, 6C), 135.0 (CH, 12C), 129.2 (CH, 12C), 127.6 (CH, 24C), 23.6 (CH<sub>3</sub>, 24C), 23.2 (CH<sub>3</sub>, 12C), 23.1 (CH<sub>3</sub>, 6C).

**HRMS** (APCI neg): calc.: 2307.5129 [m/z]; found: 2307.5156 [M<sup>-</sup>]

**Elemental analysis** calcd. [%] for C<sub>174</sub>H<sub>194</sub>B<sub>10</sub>: C 87.31, H 8.17; found: C 86.43, H 8.28.

## 6.2.4 Chapter 4

### 6.2.4.1 4-(Bis(2,6-bis(trifluoromethyl)phenyl)boryl)-*N,N*-diphenylaniline (1)

To a solution of 4-bromo-*N,N*-diphenylaniline (510 mg, 1.57 mmol) in hexane (20 mL) *n*BuLi (0.70 mL, 2.3 M, 1.61 mmol) was added dropwise at  $-78\text{ }^{\circ}\text{C}$ . The reaction was slowly warmed to ambient temperature and stirred overnight. The solution was further heated to  $60\text{ }^{\circ}\text{C}$  for 4 h. The suspension was cooled to  $-78\text{ }^{\circ}\text{C}$  and a solution of bis(2,6-bis(trifluoromethyl)phenyl)fluoroborane (600 mg, 1.31 mmol) in MTBE (5 mL) was added dropwise. The reaction was warmed to room temperature and stirred for 12 h. All volatiles were removed *in vacuo*. The residue was dissolved in hexane and filtered over a short silica plug. The product was eluted with Et<sub>2</sub>O and purified by column chromatography (silica, hexane/CH<sub>2</sub>Cl<sub>2</sub> (9:1)). Recrystallization from hexane gave 4-(bis(2,6-bis(trifluoromethyl)phenyl)boryl)-*N,N*-diphenylaniline (1) as bright greenish-yellow crystals in 95% yield (852 mg, 1.25 mmol).

**<sup>1</sup>H NMR (400 MHz, CDCl<sub>3</sub>):**  $\delta$ (ppm) = 7.93 (d, <sup>3</sup>*J* = 8 Hz, 4H), 7.69 (t, <sup>3</sup>*J* = 8 Hz, 2H), 7.35 – 7.28 (m, 4H), 7.20 – 7.05 (m, 6H), 7.01 (d, <sup>3</sup>*J* = 9 Hz, 2H), 6.87 (d, <sup>3</sup>*J* = 9 Hz, 2H).

**<sup>13</sup>C{<sup>1</sup>H} NMR (126 MHz, CDCl<sub>3</sub>):**  $\delta$ (ppm) = 152.1 (C<sub>q</sub>, 1C), 146.7 (C<sub>q</sub>, 2C), 139.9 (C<sub>q</sub>, 4C), 139.6 (C<sub>q</sub>, 2C), 138.7 (CH, 2C), 129.9 (CH, 2C), 129.6 (CH, 4C), 126.1 (CH, 4C), 124.6 (CH, 2C), 124.1 (C<sub>q</sub>, q, *J*<sub>CF</sub> = 273 Hz, 4C), 118.7 (CH, 2C).

**<sup>11</sup>B NMR (128 MHz, CD<sub>2</sub>Cl<sub>2</sub>):**  $\delta$ (ppm) = 72.0 (s, br).

**<sup>19</sup>F NMR (377 MHz, CD<sub>2</sub>Cl<sub>2</sub>):**  $\delta$ (ppm) =  $-56.12$  (s, br), 51.06 (s, br).

**Elem. Anal.:** Calc. (%) for C<sub>34</sub>H<sub>20</sub>BF<sub>12</sub>N: C 59.94, H 2.96, N 2.06; found: C 59.95, H 3.02, N 2.29.

**HRMS (APCI pos):** calc.: 682.1570 [m/z]; found: 682.1564 [MH<sup>+</sup>]

## Experimental

### 6.2.4.2 4-(Bis(4-(4,4,5,5-tetramethyl-1,3,2-dioxaborolan-2-yl)-2,6-bis(trifluoromethyl)phenyl)boryl)-N,N-diphenylaniline (**1-(Bpin)<sub>2</sub>**)

A solution of B<sub>2</sub>pin<sub>2</sub> (56 mg, 220 μmol), [Ir(COD)(OMe)]<sub>2</sub> (1.5 mg, 2.20 μmol), and dtbpy (1.26 mg, 4.40 μmol) in hexane (40 mL) was stirred for 10 min at room temperature. Then, 4-(bis(2,6-bis(trifluoromethyl)phenyl)boryl)-N,N-diphenylaniline (100 mg, 147 μmol) was added and the reaction was stirred at room temperature for 72 h. All volatiles were removed *in vacuo* and the residue was washed with MeOH (3 x 30 mL). The product was extracted with Et<sub>2</sub>O and all volatiles were removed *in vacuo* to give 4-(bis(4-(4,4,5,5-tetramethyl-1,3,2-dioxaborolan-2-yl)-2,6-bis(trifluoromethyl)phenyl)boryl)-N,N-diphenylaniline (**1-(Bpin)<sub>2</sub>**) as bright greenish-yellow crystals in 90% yield (123 mg, 132 μmol).

**<sup>1</sup>H NMR (500 MHz, C<sub>6</sub>D<sub>6</sub>):** δ(ppm) = 8.72 (s, 4H), 6.97 – 7.04 (m, 10H), 6.82 – 6.85 (m, 4H), 1.07 (s, 24H).

**<sup>1</sup>H NMR (400 MHz, CD<sub>2</sub>Cl<sub>2</sub>):** δ(ppm) = 8.28 (s, 4H), 7.34 – 7.28 (m, 4 H), 7.17 – 7.09 (m, 6H), 6.97 – 6.93 (m, 2H), 6.84 – 6.80 (m, 2H), 1.37 (s, 24 H).

**<sup>13</sup>C{<sup>1</sup>H} NMR (126 MHz, C<sub>6</sub>D<sub>6</sub>):** δ(ppm) = 152.6 (C<sub>q</sub>, 1C), 146.9 (C<sub>q</sub>, 2C), 143.2 (C<sub>q</sub>, 2C), 139.8 (CH, 1C), 139.4 (CH, 2C), 136.0 (CH, br, 4C, assigned by HSQC), 131.9 (C<sub>q</sub>, 4C), 129.8 (CH, 4C), 126.6 (CH, 4C), 125.0 (C<sub>q</sub>, q, <sup>1</sup>J<sub>CF</sub> = 273 Hz, 4 C) 124.8 (CH, 2C), 118.8 (CH, 2C), 84.8 (C<sub>q</sub>, 4C), 24.5 (CH<sub>3</sub>, 8C).

**<sup>11</sup>B NMR (128 MHz, CD<sub>2</sub>Cl<sub>2</sub>):** δ(ppm) = 68.9 (s, br.), 30.6 (s, br.).

**<sup>19</sup>F NMR (377 MHz, CD<sub>2</sub>Cl<sub>2</sub>):** δ(ppm) = –50.96 (s, br.), –56.12(s, br.).

**Elem. Anal.:** Calc. (%) for C<sub>46</sub>H<sub>42</sub>B<sub>3</sub>F<sub>12</sub>NO<sub>4</sub>: C 59.20, H 4.54, N 1.50; found: C 59.54, H 4.68, N 1.55.

### 6.2.4.3 9-(4-(Bis(4-(4,4,5,5-tetramethyl-1,3,2-dioxaborolan-2-yl)-2,6-bis(trifluoromethyl)phenyl)boryl)phenyl)-9H-carbazole (Cbz- $\pi$ (1)-(Bpin)<sub>2</sub>)

A solution of B<sub>2</sub>pin<sub>2</sub> (656 mg, 2.58 mmol), [Ir(COD)(OMe)]<sub>2</sub> (30.2 mg, 45.6  $\mu$ mol), and dtbpy (26.1 mg, 91.2  $\mu$ mol, 0.06 eq.) in hexane (40 mL) was stirred for 10 min at room temperature. Then 9-(4-(bis(2,6-bis(trifluoromethyl)phenyl)boryl)phenyl)-9H-carbazole (**2**) (1.03 g, 1.52 mmol) was added and the reaction was stirred at room temperature for 1 d. After removing all volatiles *in vacuo* the residue was washed on a silica plug with hexane (500 mL), then the plug was extracted with hexane/Et<sub>2</sub>O (9:1). After removing all volatiles *in vacuo*, the product was recrystallized from hexane to give 9-(4-(bis(4-(4,4,5,5-tetramethyl-1,3,2-dioxaborolan-2-yl)-2,6-bis(trifluoromethyl)phenyl)boryl)phenyl)-9H-carbazole (Cbz- $\pi$  (1)-(Bpin)<sub>2</sub>) as colorless blue-greenish fluorescent crystals in 78 % yield (1.11 g, 1.19 mmol).

**<sup>1</sup>H NMR (500 MHz, C<sub>6</sub>D<sub>6</sub>):**  $\delta$ (ppm) = 8.74 (s, 4H), 8.03 – 8.00 (m, 2H), 7.49 – 7.45 (m, 2H), 7.30 – 7.26 (m, 4H), 7.24 – 7.18 (m, 4H), 1.07 (s, 24H).

**<sup>13</sup>C{<sup>1</sup>H} NMR (126 MHz, C<sub>6</sub>D<sub>6</sub>):**  $\delta$ (ppm) = 145.0 (C<sub>q</sub>, 1C), 142.2 (C<sub>q</sub>, 1C), 142.0 (C<sub>q</sub>, 2C), 140.8 (C<sub>q</sub>, 2C), 138.6 (CH, 2C), 136.4 (CH, 4C), 132.8 (C<sub>q</sub>, 2C), 126.6 (CH, 2C), 125.5 (CH, 2C), 124.8 (C<sub>q</sub>, q, <sup>1</sup>J<sub>CF</sub> = 247 Hz), 124.4 (C<sub>q</sub>, 2C), 120.9 (CH, 2C), 120.7 (CH, 2C), 110.3 (CH, 2C), 84.9 (C<sub>q</sub>, 4C), 24.8 (CH<sub>3</sub>, 8C).

**<sup>11</sup>B NMR (160 MHz, C<sub>6</sub>D<sub>6</sub>):**  $\delta$ (ppm) = 31.9 (s, br.).

**<sup>19</sup>F NMR (471 MHz, C<sub>6</sub>D<sub>6</sub>):**  $\delta$ (ppm) = –52.8 (s, br.).

**Elem. Anal.:** Calc. (%) for C<sub>46</sub>H<sub>40</sub>B<sub>3</sub>F<sub>12</sub>NO<sub>4</sub>: C 59.33, H 4.33, N 1.50; found: C 59.67, H 4.40, N 1.55.

## 6.3 Solid State Structures

### 6.3.1 Chapter 1

Single crystals suitable for X-ray diffraction were selected, coated in perfluoropolyether oil, and mounted on MiTeGen sample holders. Diffraction data were collected on Bruker X8 Apex II 4-circle diffractometers with CCD area detectors using MoK $\alpha$  radiation monochromated by graphite (**2**, **FB(FXyl)<sub>2</sub>**, **iv'**, **iv**, **5**) or multi-layer focusing mirrors (**3**, **4**), or on a Bruker D8 Quest diffractometer with a CMOS area detector and multi-layer mirror monochromated MoK $\alpha$  radiation (**BFD1H**). The crystals were cooled using an Oxford Cryostreams or Bruker Kryostream low-temperature device. Data were collected at 100 K. The images were processed and corrected for Lorentz-polarization effects and absorption as implemented in the Bruker software packages. The structures were solved using the intrinsic phasing method (SHELXT)<sup>[335]</sup> and Fourier expansion technique. All non-hydrogen atoms were refined in anisotropic approximation, with hydrogen atoms 'riding' in idealized positions, by full-matrix least squares against  $F^2$  of all data, using SHELXL<sup>[336]</sup> software and the SHELXLE graphical user interface.<sup>[337]</sup> Diamond<sup>[338]</sup> software was used for graphical representation. Other structural information was extracted using Mercury<sup>[339]</sup> and OLEX2<sup>[340]</sup> software. Crystal data and experimental details are listed in Table 6.1; full structural information has been deposited with Cambridge Crystallographic Data Centre. CCDC-1949269 (**Cbz- $\pi$  (1)**), 1949270 (**Cbz-Me $\pi$  (2)**), 1949271 (**Phox-Me $\pi$  (3)**), 1949272 (**Phox-MeO $\pi$  (4)**), 1949273 (**MeO<sub>3</sub>Ph-FMe $\pi$  (5)**), 1949275 (**BFD1H**), 1949277 (**iv'**), 1949276 (**iv**) and 1949274 (**FB(FXyl)<sub>2</sub>**)



Table 6.1: Single-crystal X-ray diffraction data and structure refinements of **Cbz- $\pi$**  (1), **Cbz-Me $\pi$**  (2), **Phox-Me $\pi$**  (3), **Phox-MeO $\pi$**  (4), **MeO $\cdot$ Ph-FMe $\pi$**  (5), **FB(FXyl) $_2$** , **BFD1H**, **iv'** and **iv**.

Data	<b>Cbz-<math>\pi</math></b> (1)	<b>Cbz-Me<math>\pi</math></b> (2)	<b>Phox-Me<math>\pi</math></b> (3)
CCDC number	1949269	1949270	1949271
Empirical formula	C <sub>34</sub> H <sub>18</sub> BF <sub>12</sub> N <sub>3</sub>	C <sub>36</sub> H <sub>22</sub> BF <sub>12</sub> N	C <sub>36</sub> H <sub>22</sub> BF <sub>12</sub> NO
Formula weight / g·mol <sup>-1</sup>	679.30	707.35	723.35
<i>T</i> / K	100(2)	100(2)	100(2)
$\lambda$ / Å, radiation	MoK $\alpha$ , 0.71073	MoK $\alpha$ , 0.71073	MoK $\alpha$ , 0.71073
Crystal size / mm <sup>3</sup>	0.15×0.30×0.30	0.14×0.40×0.67	0.23×0.36×0.41
Crystal color, habit	colorless block	colorless plate	yellow block
$\mu$ / mm <sup>-1</sup>	0.146	0.140	0.141
Crystal system	Triclinic	Monoclinic	Monoclinic
Space group	<i>P</i> $\bar{1}$	<i>P</i> 2 <sub>1</sub> / <i>c</i>	<i>P</i> 2 <sub>1</sub> / <i>c</i>
<i>a</i> / Å	8.897(6)	8.903(4)	10.190(5)
<i>b</i> / Å	13.114(4)	7.855(3)	17.215(9)
<i>c</i> / Å	13.376(6)	43.996(18)	18.029(9)
$\alpha$ / °	104.185(18)	90	90
$\beta$ / °	106.14(3)	95.273(14)	96.36(2)
$\gamma$ / °	95.50(3)	90	90
Volume / Å <sup>3</sup>	1430.7(12)	3064(2)	3143(3)
<i>Z</i>	2	4	4
$\rho_{calc}$ / g·cm <sup>-3</sup>	1.577	1.534	1.529
<i>F</i> (000)	684	1432	1464
$\theta$ range / °	1.627 – 26.876	2.297 – 28.374	1.640 – 26.119
Reflections collected	18113	47352	30980
Unique reflections	6169	7632	6243
Parameters / restraints	433 / 0	453 / 0	462 / 0
GooF on <i>F</i> <sup>2</sup>	1.027	1.030	1.017
R <sub>1</sub> [ <i>I</i> > 2 $\sigma$ ( <i>I</i> )]	0.0336	0.0400	0.0380
wR <sup>2</sup> (all data)	0.0817	0.1018	0.0866
Max. / min. residual electron density / e·Å <sup>-3</sup>	0.327 / -0.259	0.358 / -0.334	0.261 / -0.194

-Table 6.1 cont.-

Data	<b>Phox-MeO<math>\pi</math> (4)</b>	<b>MeO<sub>3</sub>Ph-FMe<math>\pi</math> (5)</b>	<b>FB(FXyl)<sub>2</sub></b>
CCDC number	1949272	1949273	1949274
Empirical formula	C <sub>36</sub> H <sub>22</sub> BF <sub>12</sub> NO <sub>3</sub>	C <sub>33</sub> H <sub>19</sub> BF <sub>18</sub> O <sub>3</sub>	C <sub>16</sub> H <sub>6</sub> BF <sub>13</sub>
Formula weight / g·mol <sup>-1</sup>	755.35	816.29	456.02
<i>T</i> / K	100(2)	100(2)	100(2)
$\lambda$ / Å, radiation	MoK $\alpha$ , 0.71073	MoK $\alpha$ , 0.71073	MoK $\alpha$ , 0.71073
Crystal size / mm <sup>3</sup>	0.12×0.20×0.38	0.09×0.25×0.43	0.11×0.32×0.48
Crystal color, habit	orange plate	colorless plate	colorless plate
$\mu$ / mm <sup>-1</sup>	0.147	0.176	0.207
Crystal system	Monoclinic	Orthorhombic	Monoclinic
Space group	<i>P2<sub>1</sub>/c</i>	<i>Pca2<sub>1</sub></i>	<i>P2<sub>1</sub>/n</i>
<i>a</i> / Å	9.372(4)	31.798(14)	12.932(4)
<i>b</i> / Å	17.270(7)	12.137(4)	9.272(6)
<i>c</i> / Å	19.717(7)	8.395(4)	15.166(7)
$\alpha$ / °	90	90	90
$\beta$ / °	95.729(14)	90	113.26(2)
$\gamma$ / °	90	90	90
Volume / Å <sup>3</sup>	3175(2)	3240(2)	1670.7(14)
<i>Z</i>	4	4	4
$\rho_{calc}$ / g·cm <sup>-3</sup>	1.580	1.674	1.813
<i>F</i> (000)	1528	1632	896
$\theta$ range / °	1.571 – 26.874	2.111 – 26.789	2.656 – 26.021
Reflections collected	29146	40159	9349
Unique reflections	6764	6901	3288
Parameters / restraints	480 / 0	499 / 1	386 / 229
GooF on <i>F</i> <sup>2</sup>	1.028	1.022	1.021
R <sub>1</sub> [ <i>I</i> >2 $\sigma$ ( <i>I</i> )]	0.0497	0.0350	0.0333
wR <sup>2</sup> (all data)	0.1243	0.0773	0.0840
Max. / min. residual electron density / e·Å <sup>-3</sup>	0.480 / -0.260	0.275 / -0.228	0.218 / -0.269

-Table 6.1 cont.-

Data	<b>BFD1H</b>	<b>iv'</b>	<b>iv</b>
CCDC number	1949275	1949277	1949276
Empirical formula	C <sub>24</sub> H <sub>14</sub> BF <sub>12</sub> I	C <sub>24</sub> H <sub>15</sub> BF <sub>12</sub> O <sub>2</sub>	C <sub>24</sub> H <sub>14</sub> BF <sub>12</sub> IO <sub>2</sub>
Formula weight / g·mol <sup>-1</sup>	668.06	574.17	700.06
<i>T</i> / K	100(2)	100(2)	100(2)
$\lambda$ / Å, radiation	MoK $\alpha$ , 0.71073	MoK $\alpha$ , 0.71073	MoK $\alpha$ , 0.71073
Crystal size / mm <sup>3</sup>	0.52×0.55×0.58	0.19×0.29×0.42	0.20×0.37×0.37
Crystal color, habit	yellow block	colorless plate	yellow block
$\mu$ / mm <sup>-1</sup>	1.471	0.170	1.418
Crystal system	Monoclinic	Monoclinic	Orthorhombic
Space group	<i>P</i> 2 <sub>1</sub> / <i>c</i>	<i>P</i> 2 <sub>1</sub> / <i>n</i>	<i>Pbca</i>
<i>a</i> / Å	7.999(5)	8.598(3)	14.928(7)
<i>b</i> / Å	13.770(8)	20.097(11)	9.307(3)
<i>c</i> / Å	21.6673(13)	13.285(7)	35.349(13)
$\alpha$ / °	90	90	90
$\beta$ / °	100.16(2)	93.38(3)	90
$\gamma$ / °	90	90	90
Volume / Å <sup>3</sup>	2349.1(19)	2291.6(19)	4912(3)
<i>Z</i>	4	4	8
$\rho_{\text{calc}}$ / g·cm <sup>-3</sup>	1.889	1.664	1.893
<i>F</i> (000)	1296	1152	2720
$\theta$ range / °	1.760 – 30.707	1.840 – 28.321	2.642 – 30.574
Reflections collected	36626	41544	154227
Unique reflections	7292	5660	7539
Parameters / restraints	345 / 0	354 / 0	363 / 0
GooF on <i>F</i> <sup>2</sup>	1.047	1.026	1.122
R <sub>1</sub> [ <i>I</i> > 2 $\sigma$ ( <i>I</i> )]	0.0325	0.0341	0.0302
wR <sup>2</sup> (all data)	0.0797	0.0870	0.0753
Max. / min. residual electron density / e·Å <sup>-3</sup>	1.973 / -1.581	0.330 / -0.309	0.573 / -1.079

## Experimental

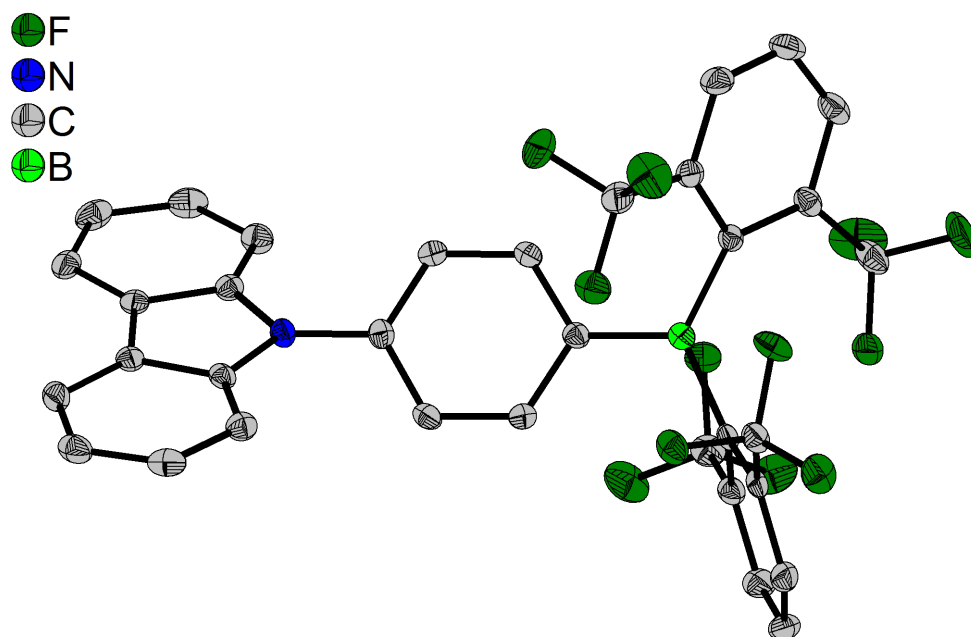


Figure 6.1: The solid-state molecular structure of **Cbz- $\pi$**  (**1**) determined by single-crystal X-ray diffraction at 100 K. All ellipsoids are drawn at the 50% probability level, and H atoms are omitted for clarity.

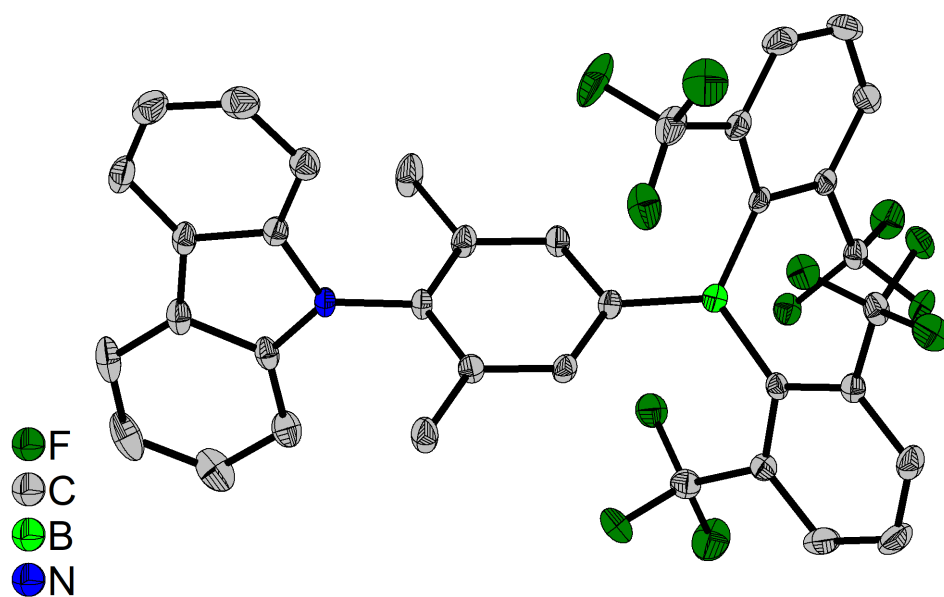


Figure 6.2: The solid-state molecular structure of **Cbz-Me $\pi$**  (**2**) determined by single-crystal X-ray diffraction at 100 K. All ellipsoids are drawn at the 50% probability level, and H atoms are omitted for clarity.

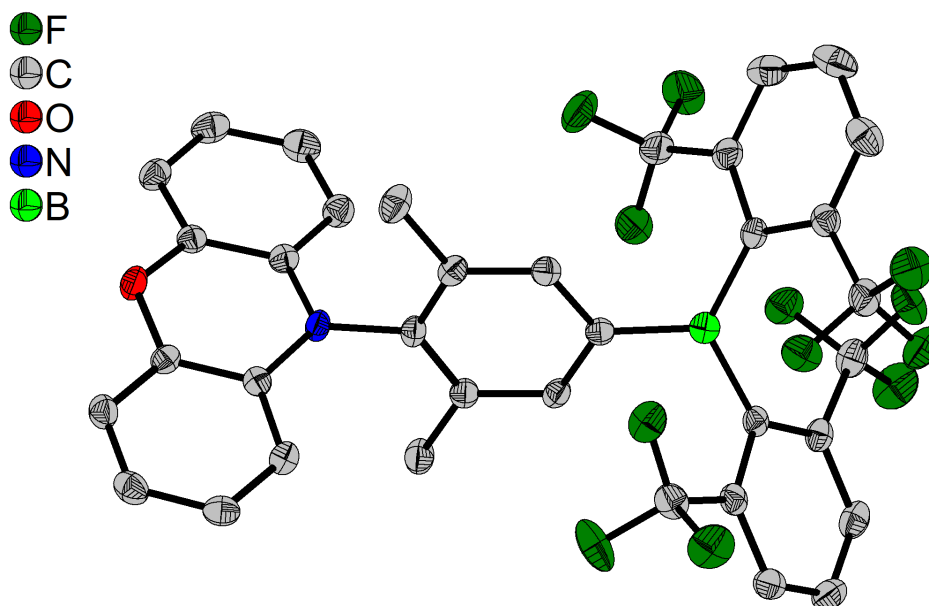


Figure 6.3: The solid-state molecular structure of **Phox-Me $\pi$  (3)** determined by single-crystal X-ray diffraction at 100 K. All ellipsoids are drawn at the 50% probability level, and H atoms are omitted for clarity.

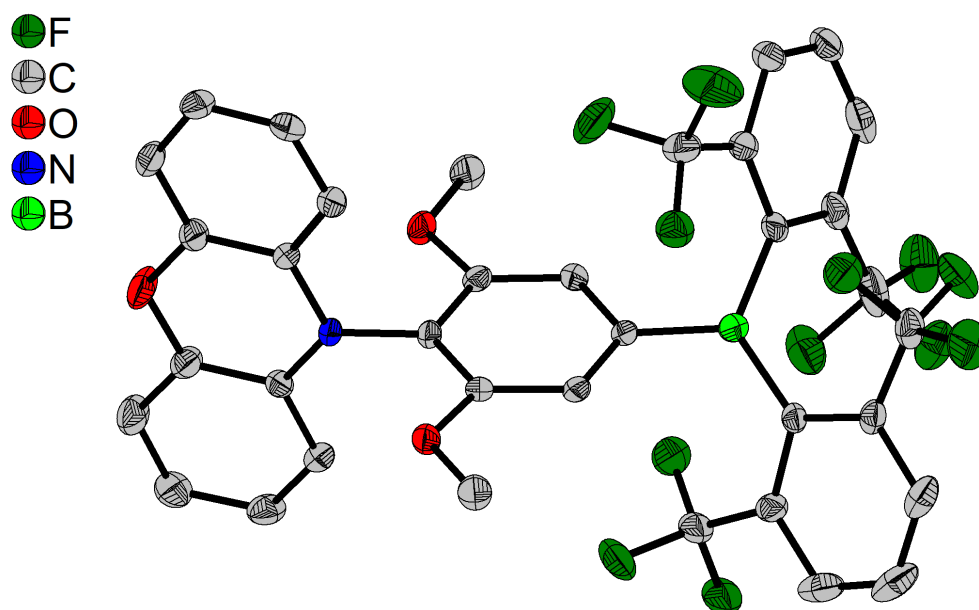


Figure 6.4: The solid-state molecular structure of **Phox-MeO $\pi$  (4)** determined by single-crystal X-ray diffraction at 100 K. All ellipsoids are drawn at the 50% probability level, and H atoms are omitted for clarity.

## Experimental

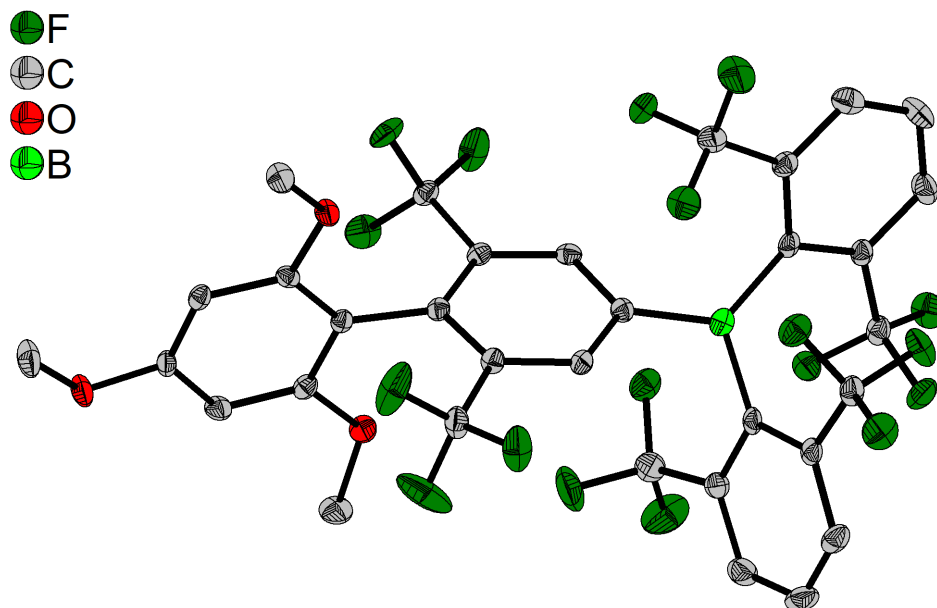


Figure 6.5: The solid-state molecular structure of MeO<sub>3</sub>Ph-FMe $\pi$  (5) determined by single-crystal X-ray diffraction at 100 K. All ellipsoids are drawn at the 50% probability level, and H atoms are omitted for clarity.

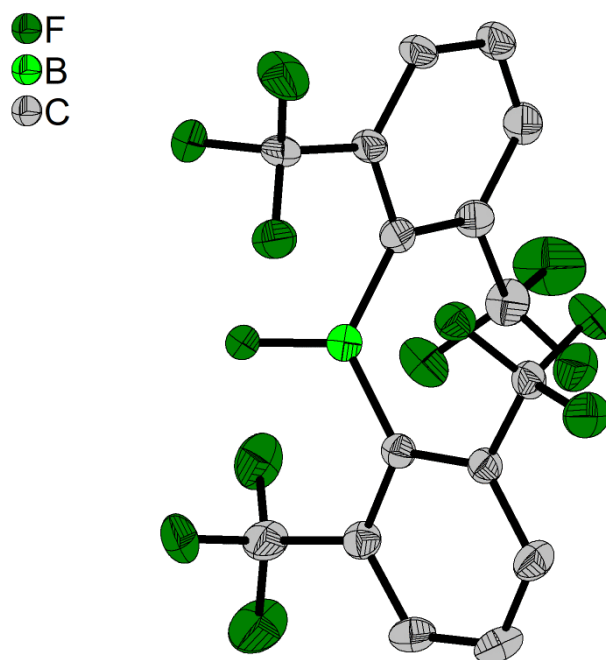


Figure 6.6: The solid-state molecular structure of FB(FXyl)<sub>2</sub> determined by single-crystal X-ray diffraction at 100 K. All ellipsoids are drawn at the 50% probability level, and H atoms are omitted for clarity. One of the xylyl groups is disordered. Only the part with 80% occupancy is shown.

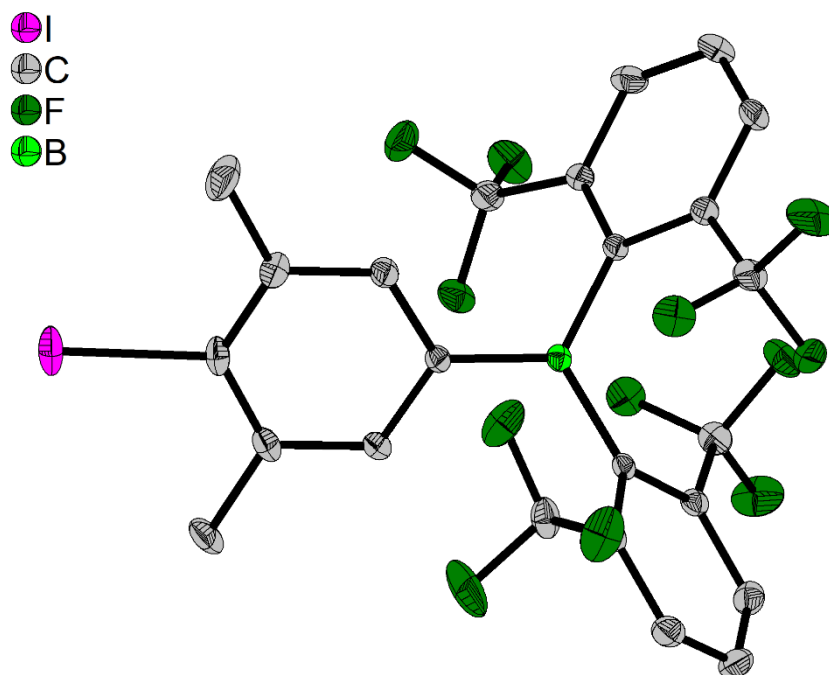


Figure 6.7: The solid-state molecular structure of **BFD1H** determined by single-crystal X-ray diffraction at 100 K. All ellipsoids are drawn at the 50% probability level, and H atoms are omitted for clarity.

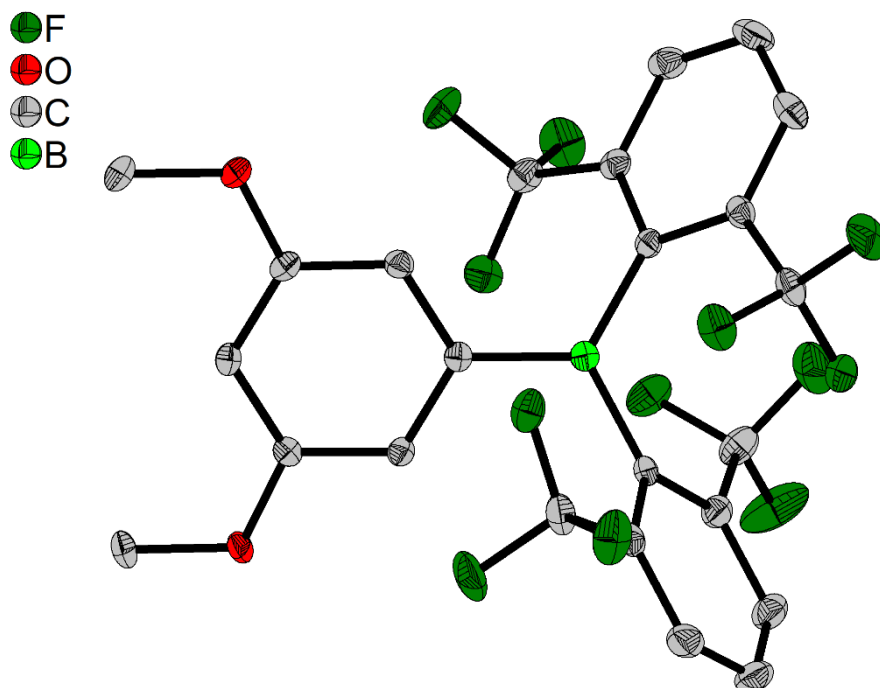


Figure 6.8: The solid-state molecular structure of **iv'** determined by single-crystal X-ray diffraction at 100 K. All ellipsoids are drawn at the 50% probability level, and H atoms are omitted for clarity.

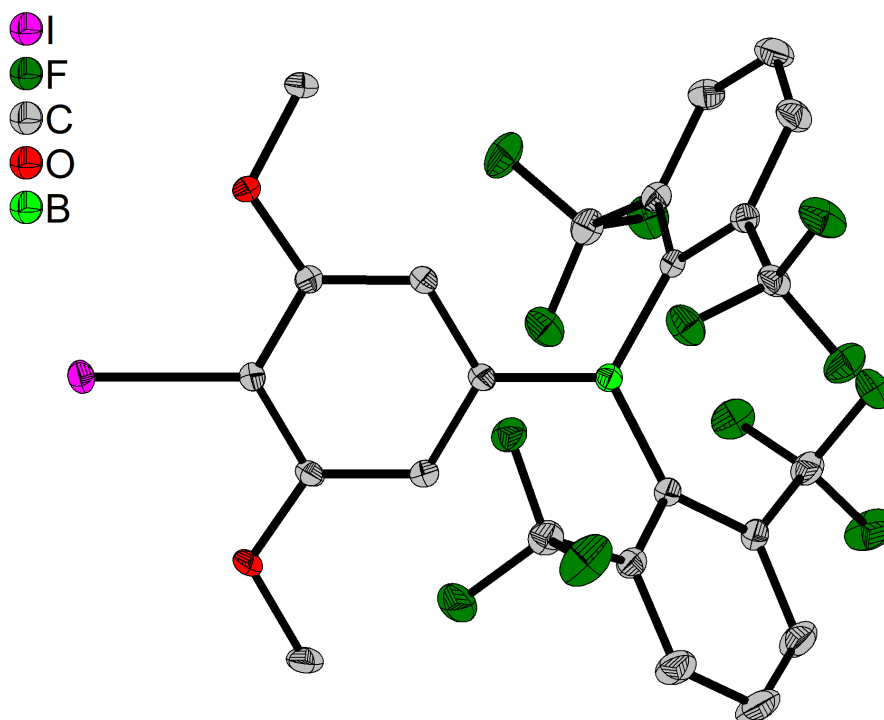


Figure 6.9: The solid-state molecular structure of **iv** determined by single-crystal X-ray diffraction at 100 K. All ellipsoids are drawn at the 50% probability level, and H atoms are omitted for clarity.

Table 6.2: Aryl $\cdots$ aryl ( $\pi\cdots\pi$ ) distances [ $\text{\AA}$ ] in crystals of **Cbz- $\pi$**  (**1**) at 100 K: centroid-centroid distance, interplanar separation, and offset shift.

Aryl $\cdots$ Aryl	Centroid-centroid distance	Interplanar separation	Offset shift
<b>Phen<math>\cdots</math>Phen</b>	3.712(2)	3.447(2)	1.378(4)



### 6.3.2 Chapter 2

Single crystals suitable for X-ray diffraction were selected, coated in perfluoropolyether oil, and mounted on MiTeGen sample holders. Diffraction data were collected on Bruker X8 Apex II 4-circle diffractometers with CCD area detectors using Mo-K $\alpha$  radiation monochromated by graphite (**<sup>F</sup>Mes<sup>F</sup>Bf•MeCN**, **<sup>F</sup>XylBF<sub>3</sub>K**, **2-1**) or multi-layer focusing mirrors (**<sup>F</sup>Mes<sup>F</sup>Bf**, **<sup>F</sup>Xyl<sup>F</sup>Bf**, ***p*-NMe<sub>2</sub>-<sup>F</sup>Xyl<sup>F</sup>Bf**, [**<sup>F</sup>Mes<sup>F</sup>Bf**]<sup>-</sup>, ***p*-NMe<sub>2</sub>-<sup>F</sup>Xyl<sup>F</sup>Bf•HF**, **D** and **2-2**). The crystals were cooled using an Oxford Cryostreams low-temperature device. Data were collected at 100 K. The images were processed and corrected for Lorentz-polarization effects and absorption as implemented in the Bruker software packages. The structures were solved using the intrinsic phasing method (SHELXT)<sup>[335]</sup> and Fourier expansion technique. All non-hydrogen atoms were refined in anisotropic approximation, with hydrogen atoms ‘riding’ in idealized positions, by full-matrix least squares against  $F^2$  of all data, using SHELXL<sup>[336]</sup> software and the SHELXLE graphical user interface.<sup>[337]</sup> The crystal of **<sup>F</sup>Mes<sup>F</sup>Bf•MeCN** was a pseudo-merohedral twin with domains rotated by 179.9° around real axis [100]. The twin fraction was refined to 14%. Diamond<sup>[338]</sup> software was used for graphical representation. Other structural information was extracted using OLEX2<sup>[340]</sup> software. Crystal data and experimental details are listed in Table 6.3; full structural information has been deposited with Cambridge Crystallographic Data Centre. CCDC-1940986 (**<sup>F</sup>Mes<sup>F</sup>Bf**), 1940987 (**<sup>F</sup>Xyl<sup>F</sup>Bf**), 1940988 (***p*-NMe<sub>2</sub>-<sup>F</sup>Xyl<sup>F</sup>Bf**), 1940989 (**<sup>F</sup>Mes<sup>F</sup>Bf•MeCN**), 1940990 ([**<sup>F</sup>Mes<sup>F</sup>Bf**]<sup>-</sup>), 1940991 (***p*-NMe<sub>2</sub>-<sup>F</sup>Xyl<sup>F</sup>Bf•HF**), 1940992 (**D**), 1949706 (**<sup>F</sup>XylBF<sub>3</sub>K**), 1949707 (**1**), and 1949708 (**2**).

## Experimental

Table 6.3: Single-crystal X-ray diffraction data collection and structure refinement parameters for  ${}^{\text{F}}\text{Mes}^{\text{F}}\text{Bf}$ ,  ${}^{\text{F}}\text{Xyl}^{\text{F}}\text{Bf}$ ,  $p\text{-NMe}_2\text{-}{}^{\text{F}}\text{Xyl}^{\text{F}}\text{Bf}$ ,  ${}^{\text{F}}\text{Mes}^{\text{F}}\text{Bf}\cdot\text{MeCN}$ ,  $[{}^{\text{F}}\text{Mes}^{\text{F}}\text{Bf}]^{-}$ ,  $p\text{-NMe}_2\text{-}{}^{\text{F}}\text{Xyl}^{\text{F}}\text{Bf}\cdot\text{HF}$ , **D**,  ${}^{\text{F}}\text{Xyl}^{\text{F}}\text{BF}_3\text{K}$ , **2.1** and **2.2**.

Data	${}^{\text{F}}\text{Mes}^{\text{F}}\text{Bf}$	${}^{\text{F}}\text{Xyl}^{\text{F}}\text{Bf}$	$p\text{-NMe}_2\text{-}{}^{\text{F}}\text{Xyl}^{\text{F}}\text{Bf}$
CCDC number	1940986	1940987	1940988
Empirical formula	$\text{C}_{25}\text{H}_6\text{BF}_{21}$ , $0.5(\text{C}_6\text{H}_6)$	$\text{C}_{24}\text{H}_7\text{BF}_{18}$	$\text{C}_{26}\text{H}_{12}\text{BF}_{18}\text{N}$
Formula weight / $\text{g}\cdot\text{mol}^{-1}$	755.16	648.11	691.18
$T / \text{K}$	100(2)	100(2)	100(2)
$\lambda / \text{\AA}$ , radiation	MoK $\alpha$ , 0.71073	MoK $\alpha$ , 0.71073	MoK $\alpha$ , 0.71073
Crystal size / $\text{mm}^3$	0.14 $\times$ 0.23 $\times$ 0.26	0.15 $\times$ 0.19 $\times$ 0.36	0.07 $\times$ 0.24 $\times$ 0.33
Crystal color, habit	colorless block	colorless block	orange plate
$\mu / \text{mm}^{-1}$	0.212	0.207	0.198
Crystal system	Monoclinic	Triclinic	Monoclinic
Space group	$C2/c$	$P\bar{1}$	$P2_1/c$
$a / \text{\AA}$	21.958(12)	8.803(5)	14.222(6)
$b / \text{\AA}$	10.228(6)	11.967(6)	21.197(11)
$c / \text{\AA}$	25.424(14)	12.163(5)	8.482(4)
$\alpha / ^\circ$	90	66.411(16)	90
$\beta / ^\circ$	110.60(3)	88.132(9)	94.355(13)
$\gamma / ^\circ$	90	85.47(2)	90
Volume / $\text{\AA}^3$	5345(5)	1170.5(10)	2550(2)
$Z$	8	2	4
$\rho_{\text{calc}} / \text{g}\cdot\text{cm}^{-3}$	1.877	1.839	1.801
$F(000)$	2968	636	1368
$\theta$ range / $^\circ$	1.711 – 26.022	1.827 – 29.999	1.728 – 26.828
Reflections collected	22615	60818	30438
Unique reflections	5257	6785	5446
Parameters / restraints	451 / 0	388 / 0	417 / 0
Goof on $F^2$	1.051	1.050	1.034
$R_1 [I > 2\sigma(I)]$	0.0350	0.0497	0.0386
$wR^2$ (all data)	0.0902	0.1123	0.0892
Max. / min. residual electron density / $\text{e}\cdot\text{\AA}^{-3}$	0.347 / –0.227	0.469 / –0.306	0.407 / –0.340

-Table 6.3 cont.-

Data	${}^{\text{F}}\text{Mes}^{\text{F}}\text{Bf}\cdot\text{MeCN}$	$[\text{F}^{\text{Mes}}\text{F}^{\text{Bf}}]^{-}$	$p\text{-NMe}_2\text{-F}^{\text{Xyl}}\text{F}^{\text{Bf}}\cdot\text{HF}$
CCDC number	1940989	1940990	1940991
Empirical formula	$\text{C}_{27}\text{H}_9\text{BF}_{21}\text{N}$	$\text{C}_{25}\text{H}_6\text{BF}_{21}$ , $\text{C}_{10}\text{H}_{10}\text{Co}$ , $\text{C}_4\text{H}_8\text{O}$	$\text{C}_{26}\text{H}_{13}\text{BF}_{19}\text{N}$ , $2(\text{C}_6\text{H}_6)$
Formula weight / $\text{g}\cdot\text{mol}^{-1}$	757.16	977.32	867.40
$T / \text{K}$	100(2)	100(2)	100(2)
$\lambda / \text{\AA}$ , radiation	MoK $\alpha$ , 0.71073	MoK $\alpha$ , 0.71073	MoK $\alpha$ , 0.71073
Crystal size / $\text{mm}^3$	0.20×0.35×0.41	0.31×0.36×0.37	0.64×0.09×0.08
Crystal color, habit	colorless block	black block	colorless needle
$\mu / \text{mm}^{-1}$	0.216	0.595	0.161
Crystal system	Monoclinic	Triclinic	Monoclinic
Space group	$P2_1/n$	$P\bar{1}$	$P2_1/n$
$a / \text{\AA}$	9.496(5)	11.832(2)	14.243(10)
$b / \text{\AA}$	12.874(3)	18.769(8)	15.061(12)
$c / \text{\AA}$	21.574(6)	20.035(4)	17.978(16)
$\alpha / ^\circ$	90	108.553(15)	90
$\beta / ^\circ$	93.218(18)	103.243(16)	110.26(3)
$\gamma / ^\circ$	90	107.35(2)	90
Volume / $\text{\AA}^3$	2633.4(16)	3759(2)	3618(5)
$Z$	4	4	4
$\rho_{\text{calc}} / \text{g}\cdot\text{cm}^{-3}$	1.910	1.727	1.592
$F(000)$	1488	1945	1744
$\theta$ range / $^\circ$	1.466 – 26.888	1.830 – 28.426	1.583 – 26.449
Reflections collected	23439	94726	33520
Unique reflections	5756	18824	7422
Parameters / restraints	453 / 0	1237 / 126	565 / 186
GooF on $F^2$	1.059	1.019	0.978
$R_1 [I > 2\sigma(I)]$	0.0424	0.0547	0.0557
$wR^2$ (all data)	0.1089	0.1487	0.1349
Max. / min. residual electron density / $\text{e}\cdot\text{\AA}^{-3}$	0.454 / -0.354	1.786 / -0.594	0.311 / -0.367

## Experimental

-Table 6.3 cont.-

Data	<b>D</b>	<b><sup>F</sup>XyIBF<sub>3</sub>K</b>	<b>2.1</b>	<b>2.2</b>
CCDC number	1940992	1949706	1949707	1949708
Empirical formula	C <sub>26</sub> H <sub>14</sub> BF <sub>18</sub> NO, 0.5(C <sub>6</sub> H <sub>14</sub> )	C <sub>8</sub> H <sub>3</sub> BF <sub>9</sub> K	C <sub>14</sub> H <sub>14</sub> BBrF <sub>6</sub> O <sub>2</sub>	C <sub>16</sub> H <sub>4</sub> Br <sub>2</sub> F <sub>12</sub>
Formula weight / g·mol <sup>-1</sup>	752.28	320.01	418.97	584.01
<i>T</i> / K	100(2)	100(2)	100(2)	100(2)
$\lambda$ / Å, radiation	MoK $\alpha$ , 0.71073	MoK $\alpha$ , 0.71073	MoK $\alpha$ , 0.71073	MoK $\alpha$ , 0.71073
Crystal size / mm <sup>3</sup>	0.52×0.39×0.28	0.40×0.40×0.08	0.36×0.33×0.18	0.44×0.12×0.08
Crystal color, habit	colorless block	colorless plate	colorless block	colorless needle
$\mu$ / mm <sup>-1</sup>	0.179	0.590	2.596	4.872
Crystal system	Monoclinic	Orthorhombic	Monoclinic	Monoclinic
Space group	<i>P</i> 2 <sub>1</sub> / <i>n</i>	<i>Pbca</i>	<i>P</i> 2 <sub>1</sub> / <i>c</i>	<i>C</i> 2/ <i>c</i>
<i>a</i> / Å	17.913(7)	8.813(14)	10.281(4)	22.316(8)
<i>b</i> / Å	9.135(3)	9.512(13)	21.199(10)	13.744(5)
<i>c</i> / Å	18.163(6)	26.11(4)	15.659(8)	5.760(3)
$\alpha$ / °	90	90	90	90
$\beta$ / °	92.026(16)	90	107.681(14)	104.795(11)
$\gamma$ / °	90	90	90	90
Volume / Å <sup>3</sup>	2970.2(18)	2189(6)	3252(3)	1708.1(12)
<i>Z</i>	4	8	8	4
$\rho_{calc}$ / g·cm <sup>-3</sup>	1.682	1.942	1.712	2.271
<i>F</i> (000)	1508	1248	1664	1112
$\theta$ range / °	2.244 – 27.575	1.560 – 26.717	1.921 – 26.022	1.757 – 30.507
Reflections collected	54695	16096	34308	15357
Unique reflections	6859	2299	6406	2618
Parameters / restraints	457 / 1	172 / 0	613 / 438	136 / 0
GooF on <i>F</i> <sup>2</sup>	1.027	1.041	1.023	1.010
R <sub>1</sub> [ <i>I</i> >2 $\sigma$ ( <i>I</i> )]	0.0384	0.0310	0.0569	0.0318
wR <sup>2</sup> (all data)	0.0984	0.0716	0.1416	0.0817
Max. / min. residual electron density / e·Å <sup>-3</sup>	0.655 / -0.497	0.390 / -0.265	1.364 / -0.959	1.192 / -0.420

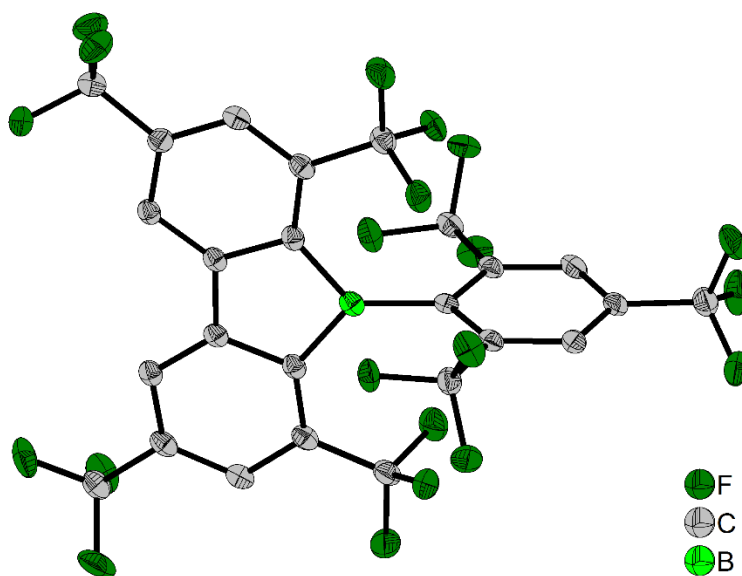


Figure 6.10: The solid-state molecular structure of  $^{\text{F}}\text{Mes}^{\text{F}}\text{Bf}$  determined by single-crystal X-ray diffraction at 100 K. All ellipsoids are drawn at the 50% probability level. H atoms and the solvent molecule (benzene) are omitted for clarity.

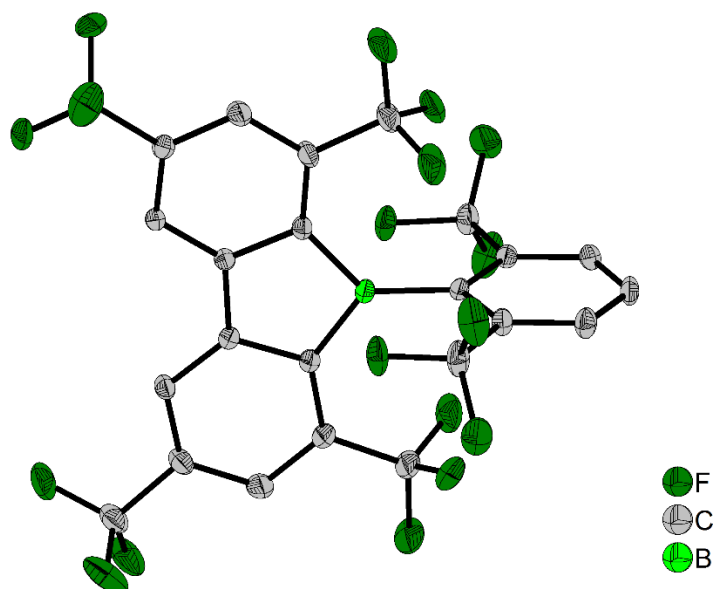


Figure 6.11: The solid-state molecular structure of  $^{\text{F}}\text{Xyl}^{\text{F}}\text{Bf}$  determined by single-crystal X-ray diffraction at 100 K. All ellipsoids are drawn at the 50% probability level, and H atoms are omitted for clarity.

## Experimental

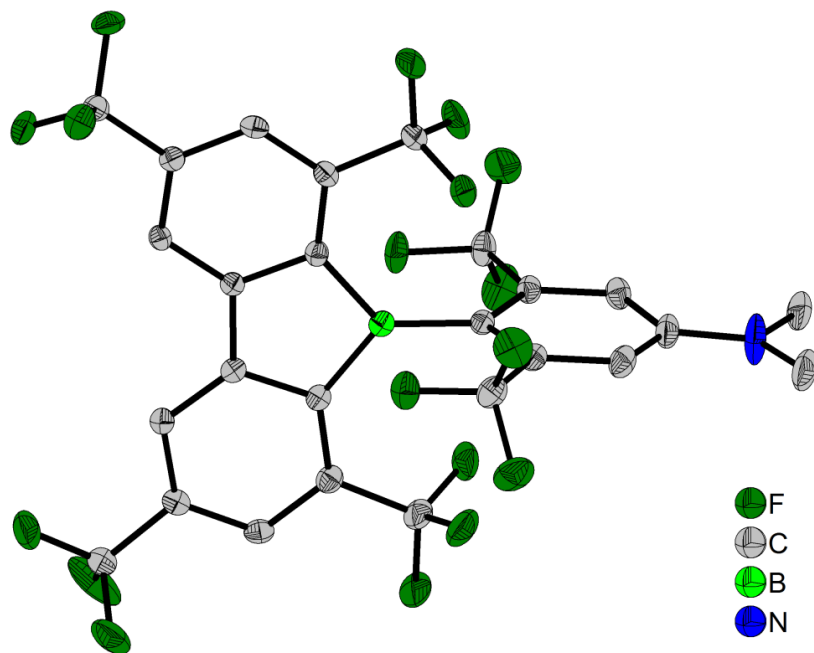


Figure 6.12: The solid-state molecular structure of *p*-NMe<sub>2</sub>-<sup>F</sup>Xyl<sup>F</sup>Bf determined by single-crystal X-ray diffraction at 100 K. All ellipsoids are drawn at the 50% probability level, and H atoms are omitted for clarity.

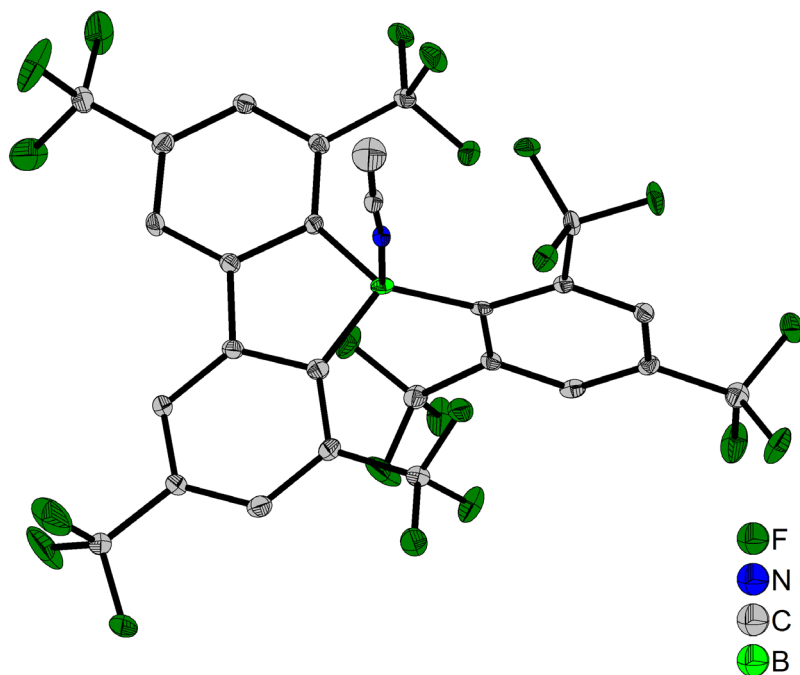


Figure 6.13: The solid-state molecular structure of <sup>F</sup>Mes<sup>F</sup>Bf•MeCN determined by single-crystal X-ray diffraction at 100 K. All ellipsoids are drawn at the 50% probability level, and H atoms are omitted for clarity.

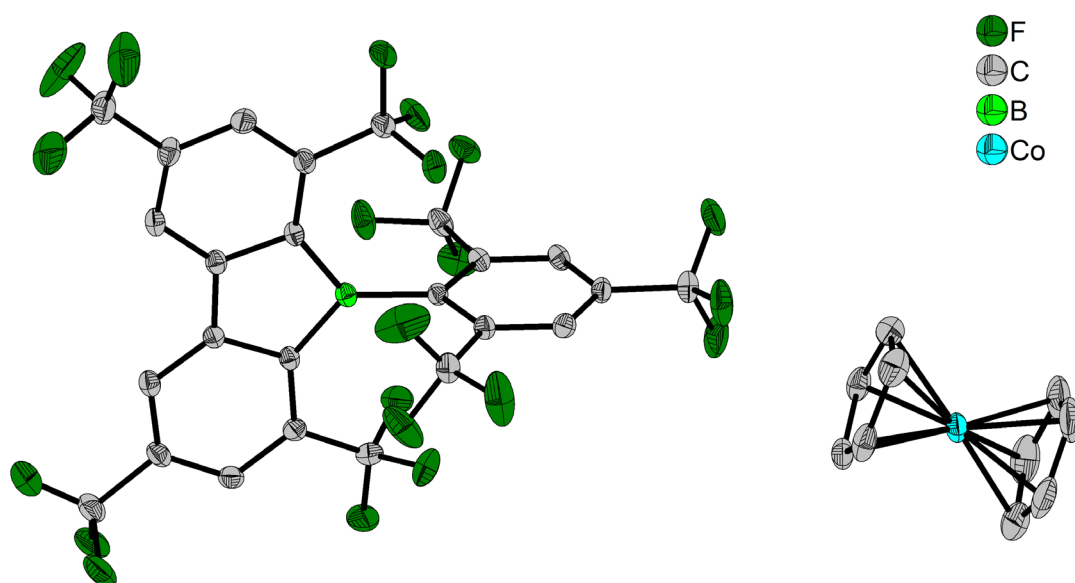


Figure 6.14: The solid-state molecular structure of  $[\text{Mes}^{\text{F}}\text{Bf}]^-$  determined by single-crystal X-ray diffraction at 100 K. All ellipsoids are drawn at the 50% probability level. H atoms and THF solvent molecules are omitted for clarity. Only half of the symmetrically non-equivalent molecules are shown. One of the  $\text{CF}_3$  groups is rotationally disordered and only the part with the higher occupancy (64%) is shown here.

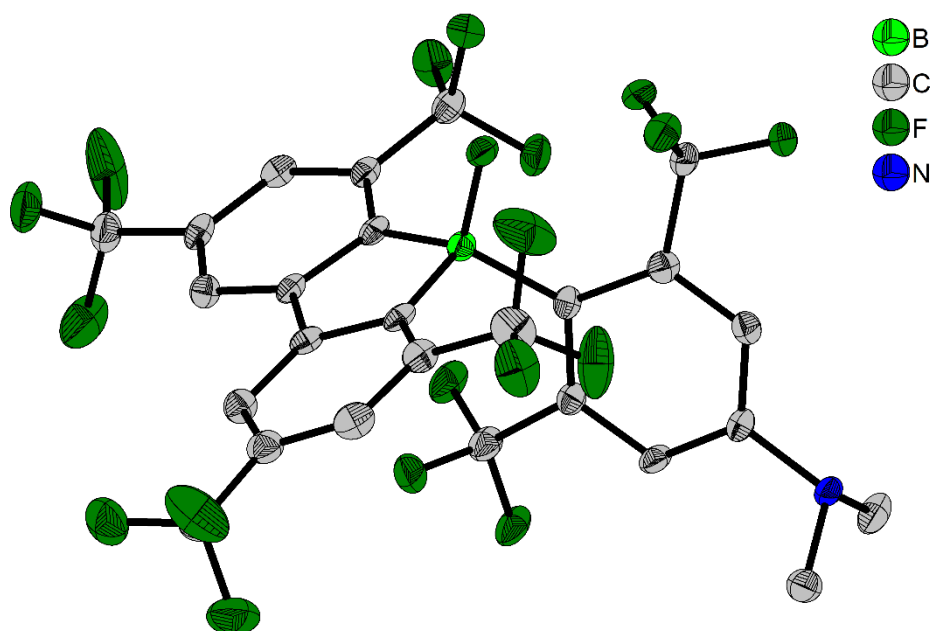


Figure 6.15: The solid-state molecular structure of  $p\text{-NMe}_2\text{-}^{\text{F}}\text{Xyl}^{\text{F}}\text{Bf}\cdot\text{HF}$  determined by single-crystal X-ray diffraction at 100 K. All ellipsoids are drawn at the 50% probability level. H atoms and benzene solvent molecules are omitted for clarity.

## Experimental

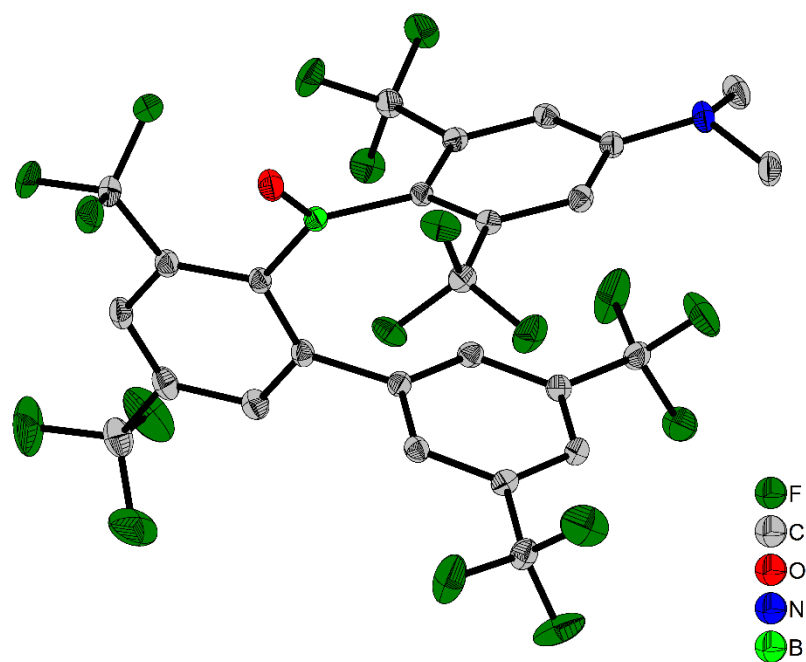


Figure 6.16: The solid-state molecular structure of compound **D** determined by single-crystal X-ray diffraction at 100 K. All ellipsoids are drawn at the 50% probability level. H atoms and the solvent molecule (hexane) are omitted for clarity.

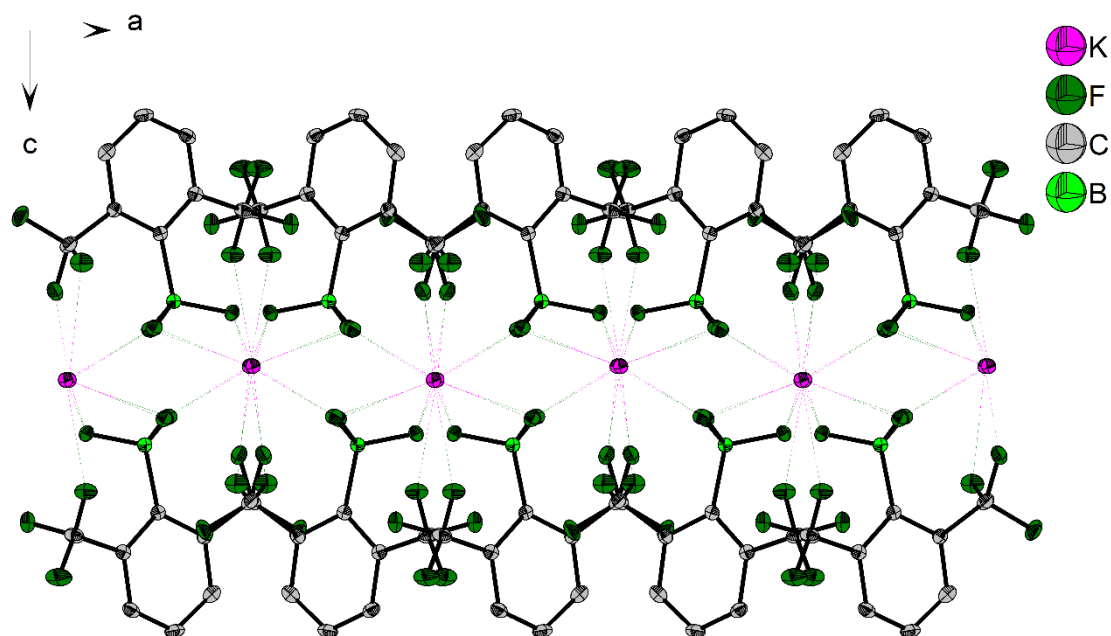


Figure 6.17: Projection of part of the crystal structure of  $\text{F}^x\text{ylBF}_3\text{K}$  along the  $b$  axis shows the connectivity in a layer-like unit which further extends in  $a$  and  $b$  directions. Layers are arranged along the  $c$  axis. The structure was determined by single-crystal X-ray diffraction at 100 K. All ellipsoids are drawn at the 50% probability level. H atoms are omitted for clarity.



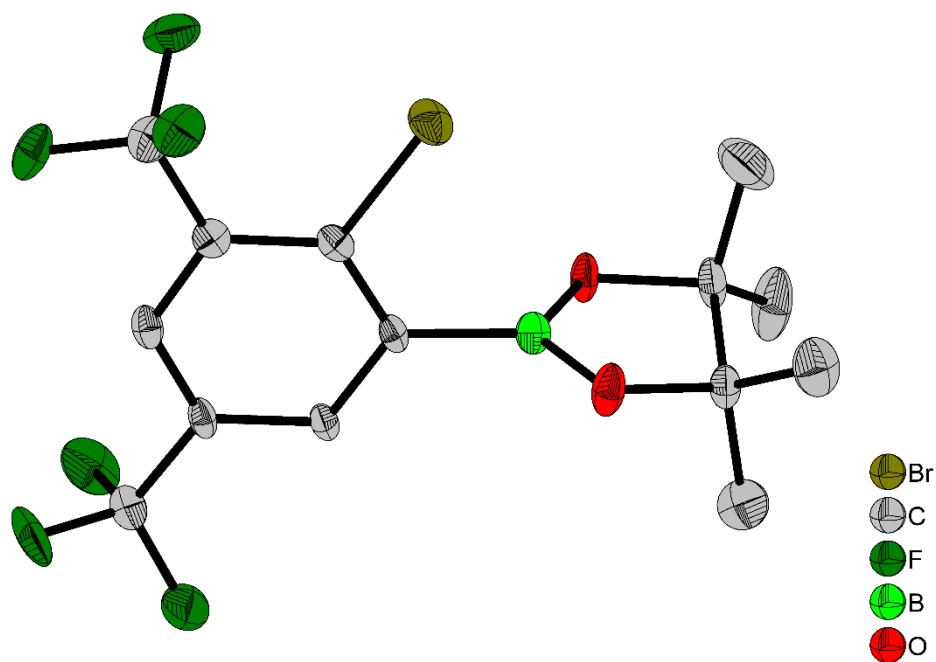


Figure 6.18: The solid-state molecular structure of compound **2.1** determined by single-crystal X-ray diffraction at 100 K. All ellipsoids are drawn at the 50% probability level. H atoms are omitted for clarity. Only one of two symmetrically non-equivalent molecules is shown. Part of this molecule is disordered and only the part with the higher occupancy (87%) is shown.

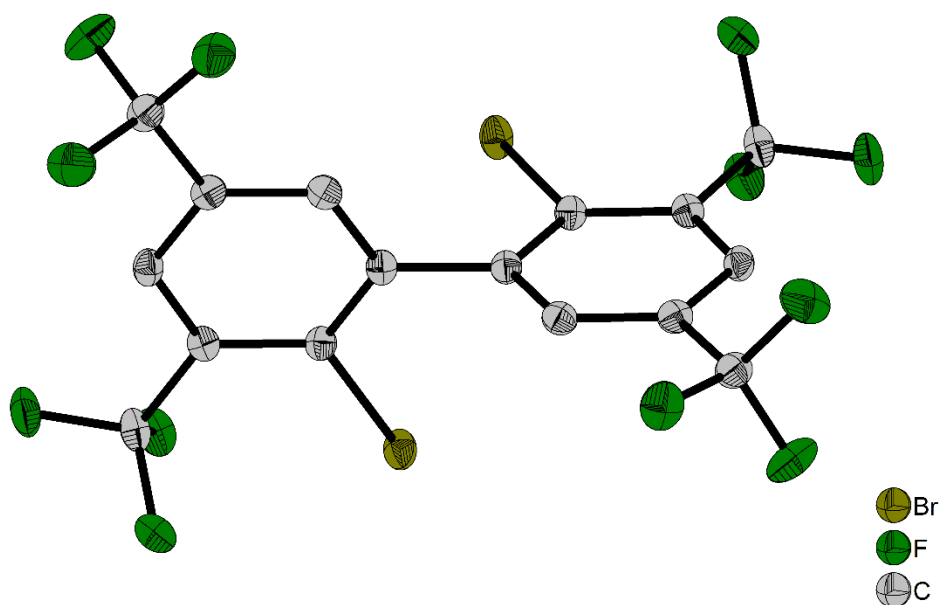


Figure 6.19: The solid-state molecular structure of compound **2.2** determined by single-crystal X-ray diffraction at 100 K. All ellipsoids are drawn at the 50% probability level. H atoms are omitted for clarity.

## Experimental

Table 6.4: Selected bond lengths [Å] and angles [°] of <sup>F</sup>Mes<sup>F</sup>Bf, <sup>F</sup>Xyl<sup>F</sup>Bf, *p*-NMe<sub>2</sub>-<sup>F</sup>Xyl<sup>F</sup>Bf, <sup>F</sup>Mes<sup>F</sup>Bf•MeCN, and [<sup>F</sup>Mes<sup>F</sup>Bf]<sup>-a</sup>

	<sup>F</sup> Mes <sup>F</sup> Bf	<sup>F</sup> Xyl <sup>F</sup> Bf	<i>p</i> -NMe <sub>2</sub> - <sup>F</sup> Xyl <sup>F</sup> Bf	<sup>F</sup> Mes <sup>F</sup> Bf• MeCN	[ <sup>F</sup> Mes <sup>F</sup> Bf] <sup>-a</sup>	
					Molecule 1	Molecule 2
B–C1	1.579(3)	1.570(2)	1.570(3)	1.652(3)	1.587(4)	1.594(4)
B–C2	1.581(3)	1.591(3)	1.595(3)	1.645(3)	1.547(4)	1.556(4)
B–C3	1.591(3)	1.591(3)	1.591(3)	1.645(3)	1.548(4)	1.551(4)
B–N				1.591(3)		
C3–C19/C18/C20	1.408(3)	1.410(2)	1.409(2)	1.401(3)	1.438(3)	1.432(3)
C2–C18/C17/19	1.410(2)	1.409(2)	1.408(2)	1.410(3)	1.429(3)	1.432(3)
C18/C17/C19–C19/C18/C20	1.481(3)	1.474(2)	1.482(2)	1.475(3)	1.457(3)	1.457(3)
<i>exo</i> -aryl:						
C1–C4	1.405(3)	1.400(2)	1.400(2)	1.419(3)	1.404(3)	1.405(3)
C1–C8	1.402(3)	1.401(2)	1.398(3)	1.428(3)	1.414(3)	1.417(3)
C4–C5	1.385(3)	1.390(2)	1.381(3)	1.399(3)	1.392(3)	1.389(4)
C8–C7	1.387(3)	1.387(2)	1.385(3)	1.383(3)	1.382(3)	1.382(3)
C5–C6	1.384(3)	1.380(3)	1.400(3)	1.372(3)	1.380(4)	1.380(4)
C7–C6	1.384(3)	1.380(3)	1.400(3)	1.373(3)	1.384(4)	1.384(4)
C6–N			1.373(3)			
C11–N			1.441(3)			
C12–N			1.431(3)			
∠ BC <sub>3</sub> -Aryl <sub>exo</sub>	89.32(7)	89.84(8)	89.27(6)		88.38(10)	89.87(10)
∠ BC <sub>12</sub> - Aryl <sub>exo</sub>	89.43(6)	89.54(6)	88.69(5)	82.12(6)	88.02(7)	88.71(7)
Torsion of Ar <sub>exo</sub> out of plane ∠ C1–B–C2–C18/C17/C19	171.28(16)	176.45(16)	178.83(17)	137.6(2)	173.2(2)	179.6(2)
5-ring:						
∠ C2BC3	103.95(15)	103.07(13)	102.94(14)	99.74(18)	104.3(2)	104.1(2)
∠ BC2C	107.01(16)	107.41(15)	107.46(15)	107.83(19)	107.8(2)	107.6(2)
∠ C2CC	110.98(17)	111.01(15)	111.01(15)	111.82(19)	110.3(2)	110.3(2)
∠ C3CC	111.41(15)	111.31(14)	111.05(15)	111.60(19)	110.0(2)	110.2(2)
∠ BC3C	106.57(16)	107.20(14)	107.52(15)	108.46(19)	107.5(2)	107.7(2)
Sum ∠ CBC	359.74(16)	359.90(15)	359.99(16)	338.43(18)	359.8(2)	360.0(2)
Sum ∠ CNC			359.84(19)			
Shortest B–F contact(s)	2.392(3) 2.440(3)	2.379(2) 2.390(3)	2.366(2) 2.434(2)	2.853(3)	2.637(4)	2.615(4) 2.886(3)

<sup>a</sup>Two independent molecules are present in the unit cell. Hence, values are given for both molecules.

Table 6.5: Aryl⋯aryl ( $\pi$ ⋯ $\pi$ ) distances [ $\text{\AA}$ ] in crystals of  $^{\text{F}}\text{Mes}^{\text{F}}\text{Bf}$ ,  $^{\text{F}}\text{Xyl}^{\text{F}}\text{Bf}$ , and  $p\text{-NMe}_2\text{-}^{\text{F}}\text{Xyl}^{\text{F}}\text{Bf}$  at 100 K: centroid-centroid distance, interplanar separation, and offset shift.

Aryl⋯Aryl	Centroid-centroid distance	Interplanar separation	Offset shift <sup>[a]</sup>
<b>Compound <math>^{\text{F}}\text{Mes}^{\text{F}}\text{Bf}</math></b>			
dibenzoborole⋯dibenzoborole	3.8028(18)	3.469(2)	1.557(3)
<b>Compound <math>^{\text{F}}\text{Xyl}^{\text{F}}\text{Bf}</math></b>			
dibenzoborole⋯dibenzoborole	4.011(2)	3.565(2)	1.838(2)
<b>Compound <math>p\text{-NMe}_2\text{-}^{\text{F}}\text{Xyl}^{\text{F}}\text{Bf}</math></b>			
dibenzoborole⋯dibenzoborole	4.0116(15)	3.5655(18)	1.839(3)

<sup>[a]</sup> The offset shift, also called inter-centroid shift, is the distance within a plane of an aryl ring between the centroid of the respective aryl ring and the intersection point with the normal to the plane through the centroid of the other aryl ring.

### 6.3.3 Chapter 3

**Single** crystals suitable for X-ray diffraction were selected, coated in perfluoropolyether oil, and mounted on MiTeGen sample holders. Diffraction data were collected on Bruker X8 Apex II 4-circle diffractometers with CCD area detectors using Mo- $K_{\alpha}$  radiation monochromated by graphite (**BFG1H**) or multi-layer focusing mirrors (**BG1BPin** and **BG1NMe<sub>2</sub>**). The crystals were cooled using an open flow N<sub>2</sub> Oxford Cryostream or Bruker Cryoflex II low-temperature device. Data were collected at 100 K. The images were processed and corrected for Lorentz-polarization effects and absorption as implemented in the Bruker software packages. The structures were solved using the intrinsic phasing method (SHELXT)<sup>[335]</sup> and Fourier expansion technique. All non-hydrogen atoms were refined in anisotropic approximation, with hydrogen atoms ‘riding’ in idealized positions, by full-matrix least squares against  $F^2$  of all data, using SHELXL<sup>[336]</sup> software and the SHELXLE graphical user interface.<sup>[337]</sup> The unit cell of **BG1BPin** contains six disordered ethanol solvent molecules, which have been treated as a diffuse contribution to the overall scattering without specific atom positions by SQUEEZE/PLATON.<sup>[341]</sup> In **BG1NMe<sub>2</sub>**, one of the voids of the crystal structure is fully occupied by a dichloromethane solvent molecule, while another void is nearly empty being only partly occupied by disordered dichloromethane molecules. Fractions of 0.085 and 0.069 were refined for these disordered parts resulting in an overall fraction of only 0.154 molecules in this void. Diamond<sup>[338]</sup> software was used for graphical representation. Other structural information was extracted using OLEX2<sup>[340]</sup> software. Crystal data and experimental details are listed in Table 6.6; full structural information has been deposited with Cambridge Crystallographic Data Centre. CCDC-1990178 (**BG1Bpin**), 1990179 (**BG1NMe<sub>2</sub>**), and 1990180 (**BFG1H**).

Table 6.6: Single-crystal X-ray diffraction data and structure refinements of **BG1Bpin**, **BG1NMe<sub>2</sub>**, and **BFG1H**.

Data	<b>BG1Bpin</b>	<b>BG1NMe<sub>2</sub></b>	<b>BFG1H</b>
CCDC number	1990178	1990179	1990180
Empirical formula	C <sub>108</sub> H <sub>144</sub> B <sub>10</sub> O <sub>12</sub>	C <sub>84</sub> H <sub>108</sub> B <sub>4</sub> N <sub>6</sub> , 1.154(CH <sub>2</sub> Cl <sub>2</sub> )	C <sub>72</sub> H <sub>42</sub> B <sub>4</sub> F <sub>36</sub>
Formula weight (g·mol <sup>-1</sup> )	1742.32	1342.95	1634.29
Temperature (K)	100(2)	100(2)	100(2)
Radiation, λ (Å)	Mo-K <sub>α</sub> , 0.71073	Mo-K <sub>α</sub> , 0.71073	Mo-K <sub>α</sub> , 0.71073
Crystal size (mm <sup>3</sup> )	0.21×0.20×0.15	0.46×0.41×0.12	0.65×0.45×0.37
Crystal color, habit	Colorless block	Yellow plate	Colorless block
Crystal system	Trigonal	Monoclinic	Triclinic
Space group	<i>P</i> $\bar{3}$ 1 <i>c</i>	<i>P</i> 2 <sub>1</sub> / <i>c</i>	<i>P</i> $\bar{1}$
<i>a</i> (Å)	22.484(6)	15.1535(15)	8.807(3)
<i>b</i> (Å)	22.484(6)	27.079(3)	16.050(6)
<i>c</i> (Å)	13.358(5)	20.2435(19)	25.018(8)
α (°)	90	90	106.517(10)
β (°)	90	109.323(3)	97.039(11)
γ (°)	120	90	91.027(6)
Volume (Å <sup>3</sup> )	5848(4)	7838.9(13)	3359(2)
<i>Z</i>	2	4	2
ρ <sub>cal</sub> (g·cm <sup>-3</sup> )	0.989	1.138	1.616
μ (mm <sup>-1</sup> )	0.061	0.141	0.163
<i>F</i> (000)	1876	2890	1636
θ range (°)	1.811 – 25.032	1.424 – 24.886	1.774 – 30.999
Reflections collected	33242	43194	148305
Unique reflections	3459	13515	21404
Min. / max. transmission	0.6978/0.7453	0.6762/0.7451	0.7072/0.7463
Parameters / restraints	224 / 18	990 / 126	1241 / 441
GooF on <i>F</i> <sup>2</sup>	1.082	1.027	1.009
R1 [ <i>I</i> > 2σ( <i>I</i> )]	0.0561	0.0902	0.0430
wR <sup>2</sup> (all data)	0.1733	0.2767	0.1080
Max. / min. residual electron density (e·Å <sup>-3</sup> )	0.456 / -0.222	0.598 / -0.929	0.435 / -0.374

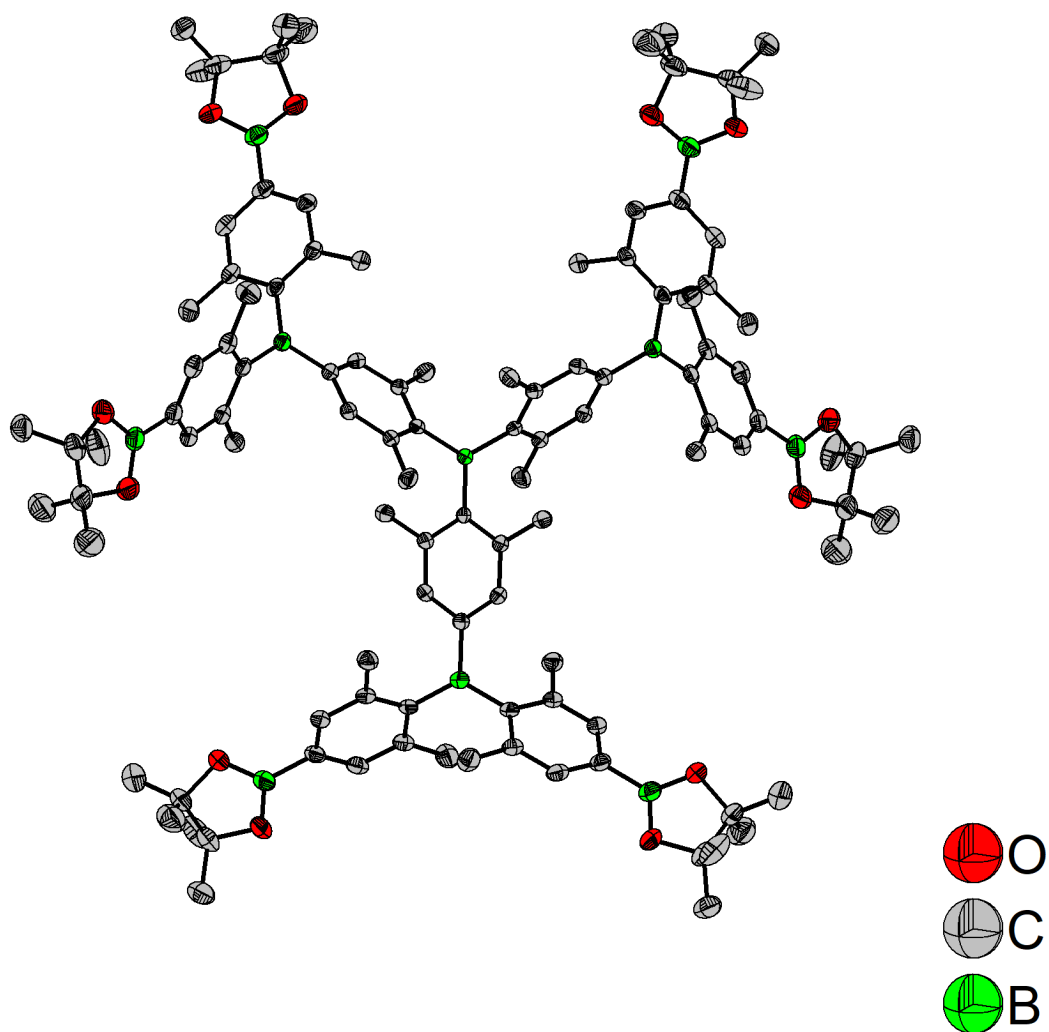


Figure 6.20: The solid-state molecular structure of **BG1Bpin** determined by single-crystal X-ray diffraction at 100 K. All ellipsoids are drawn at the 50% probability level. H atoms are omitted for clarity. The Bpin moieties are slightly disordered and only the major part (94%) is shown here. The molecule has 3-fold and 2-fold rotational symmetries.

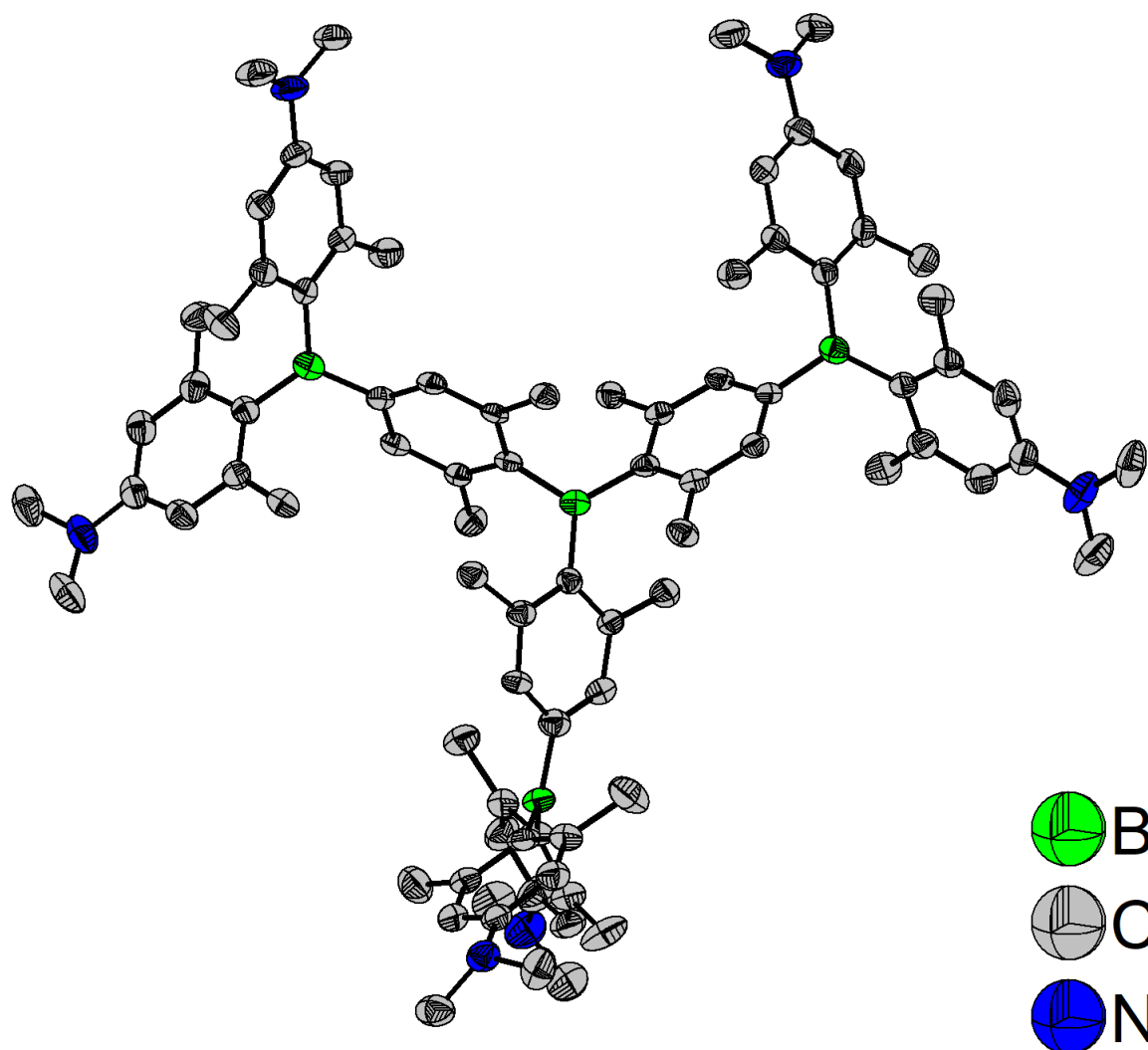


Figure 6.21: The solid-state molecular structure of **BG1NMe<sub>2</sub>** determined by single-crystal X-ray diffraction at 100 K. All ellipsoids are drawn at the 50% probability level. H atoms and CH<sub>2</sub>Cl<sub>2</sub> solvent molecules are omitted for clarity. One of the NMe<sub>2</sub> moieties is equally disordered and only one part is shown here.

## Experimental

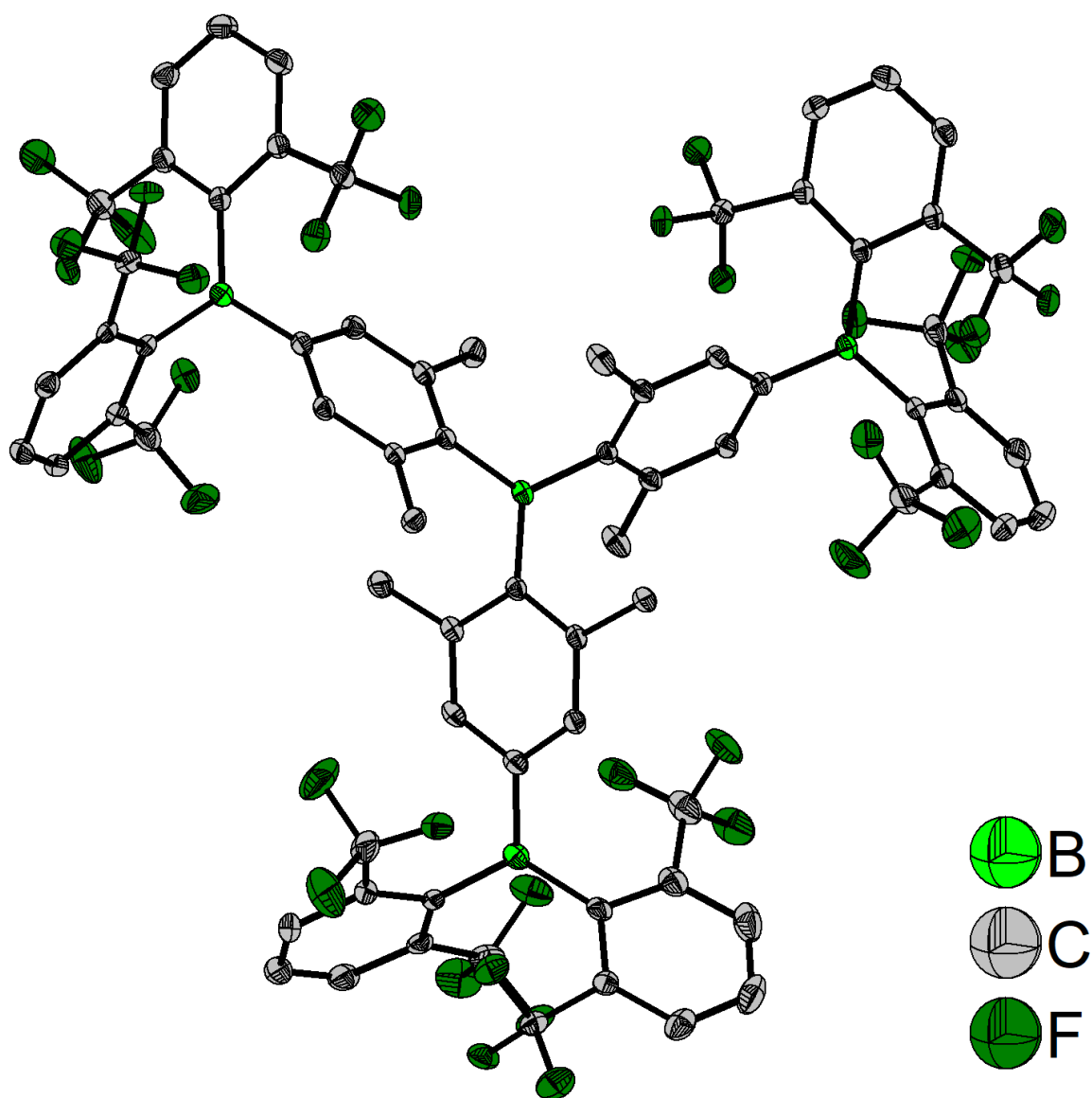


Figure 6.22: The solid-state molecular structure of **BFG1H** determined by single-crystal X-ray diffraction at 100 K. All ellipsoids are drawn at the 50% probability level. H atoms are omitted for clarity. One of the bis(2,6-bis(trifluoromethyl)phenyl)boryl ( $B(FXyl)_2$ ) groups is disordered and only the major part (69%) is shown here.



### 6.3.4 Chapter 4

Single-crystals suitable for X-ray diffraction were selected, coated in perfluoropolyether oil, and mounted on MiTeGen sample holders. Diffraction data were collected on Bruker X8 Apex II 4-circle diffractometers with CCD area detectors using Mo-K $\alpha$  radiation monochromated by graphite (**1**) or multi-layer focusing mirrors (**1-(Bpin)<sub>2</sub>**). Diffraction data of **Cbz- $\pi$  (1)-(Bpin)<sub>2</sub>** were collected on a Rigaku Oxford Diffraction XtaLAB Synergy diffractometer with a semiconductor HPA-detector (HyPix-6000) and multi-layer mirror monochromated Cu-K $\alpha$  radiation. The crystals were cooled using an open flow N<sub>2</sub> Oxford Cryostream or a Bruker Kryoflex II low-temperature device. Data were collected at 100 K. The images were processed and corrected for Lorentz-polarization effects and absorption as implemented in the Bruker software packages. The structures were solved using the intrinsic phasing method (SHELXT)<sup>[335]</sup> and Fourier expansion technique. All non-hydrogen atoms were refined in anisotropic approximation, with hydrogen atoms ‘riding’ in idealized positions, by full-matrix least squares against  $F^2$  of all data, using SHELXL<sup>[336]</sup> software and the SHELXLE graphical user interface.<sup>[337]</sup> The single-crystal of **Cbz- $\pi$  (1)-(Bpin)<sub>2</sub>** was a very thin long needle with long reflections spanning several frames. This led to partly too high reflection intensities from data reduction, which is a result of overlap with other reflections’ tails. Though residual values are high, the structure solution can be considered as a proof of the conformation of the molecule. Diamond<sup>[338]</sup> software was used for graphical representation. Other structural information was extracted using OLEX2<sup>[340]</sup> software. Crystal data and experimental details are listed in Table 6.7; full structural information has been deposited with the Cambridge Crystallographic Data Centre: CCDC-1999432 (**1**), 1999433 (**1-(Bpin)<sub>2</sub>**) and 2003436 (**Cbz- $\pi$  (1)-(Bpin)<sub>2</sub>**).

## Experimental

Table 6.7: Single-crystal X-ray diffraction data and structure refinements of **1**, **1-(Bpin)<sub>2</sub>** and **Cbz- $\pi$  (1)-(Bpin)<sub>2</sub>**.

Data	<b>1</b>	<b>1-(Bpin)<sub>2</sub></b>
CCDC number	1999432	1999433
Empirical formula	C <sub>34</sub> H <sub>20</sub> BF <sub>12</sub> N	C <sub>46</sub> H <sub>42</sub> B <sub>3</sub> F <sub>12</sub> NO <sub>4</sub>
Formula weight (g·mol <sup>-1</sup> )	681.32	933.23
Temperature (K)	100(2)	100(2)
Radiation, $\lambda$ (Å)	Mo-K $\alpha$ , 0.71073	Mo-K $\alpha$ , 0.71073
Crystal size (mm <sup>3</sup> )	0.45×0.40×0.05	0.35×0.25×0.08
Crystal color, habit	yellow plate	yellow plate
Crystal system	Monoclinic	Monoclinic
Space group	<i>P2<sub>1</sub>/n</i>	<i>C2/c</i>
<i>a</i> (Å)	8.756(4)	26.351(9)
<i>b</i> (Å)	35.52(3)	14.031(5)
<i>c</i> (Å)	9.607(4)	13.994(5)
$\alpha$ (°)	90	90
$\beta$ (°)	101.430(12)	121.024(18)
$\gamma$ (°)	90	90
Volume (Å <sup>3</sup> )	2929(3)	4434(3)
<i>Z</i>	4	4
$\rho_{\text{cal}}$ (g·cm <sup>-3</sup> )	1.545	1.398
$\mu$ (mm <sup>-1</sup> )	0.143	0.121
<i>F</i> (000)	1376	1920
$\theta$ range (°)	2.441 – 25.999	1.709 – 26.000
Reflections collected	19617	20936
Unique reflections	5747	4377
Min. / max. transmission	0.6246/0.7454	0.6778/0.7454
Parameters / restraints	433 / 0	363 / 151
GooF on <i>F</i> <sup>2</sup>	1.037	1.022
R1 [ <i>I</i> >2 $\sigma$ ( <i>I</i> )]	0.0439	0.0486
<i>w</i> R <sup>2</sup> (all data)	0.1033	0.1437
Max. / min. residual electron density (e·Å <sup>-3</sup> )	0.248 / -0.293	0.560 / -0.278

-Table 6.7 cont.-

Data	<b>Cbz-<math>\pi</math> (1)-(Bpin)<sub>2</sub></b>
CCDC number	2003436
Empirical formula	C <sub>46</sub> H <sub>40</sub> B <sub>3</sub> F <sub>12</sub> NO <sub>4</sub>
Formula weight (g·mol <sup>-1</sup> )	931.22
Temperature (K)	100(2)
Radiation, $\lambda$ (Å)	Cu-K $\alpha$ 1.54184
Crystal size (mm <sup>3</sup> )	0.57×0.06×0.04
Crystal color, habit	colorless needle
Crystal system	Monoclinic
Space group	<i>P2<sub>1</sub>/n</i>
<i>a</i> (Å)	19.3861(10)
<i>b</i> (Å)	10.3578(2)
<i>c</i> (Å)	24.2273(10)
<i>a</i> (°)	90
<i>b</i> (°)	107.664(5)
<i>g</i> (°)	90
Volume (Å <sup>3</sup> )	4635.4(4)
<i>Z</i>	4
$\rho_{\text{cal}}$ (g·cm <sup>-3</sup> )	1.334
$\mu$ (mm <sup>-1</sup> )	1.005
<i>F</i> (000)	1912
$\theta$ range (°)	2.570 – 67.079
Reflections collected	29926
Unique reflections	8166
Min. / max. transmission	0.511/1.000
Parameters / restraints	669 / 168
GooF on <i>F</i> <sup>2</sup>	1.078
R <sub>1</sub> [ <i>I</i> >2 $\sigma$ ( <i>I</i> )]	0.0965
wR <sup>2</sup> (all data)	0.2683
Max. / min. residual electron density (e·Å <sup>-3</sup> )	0.419 / -0.361

## Experimental

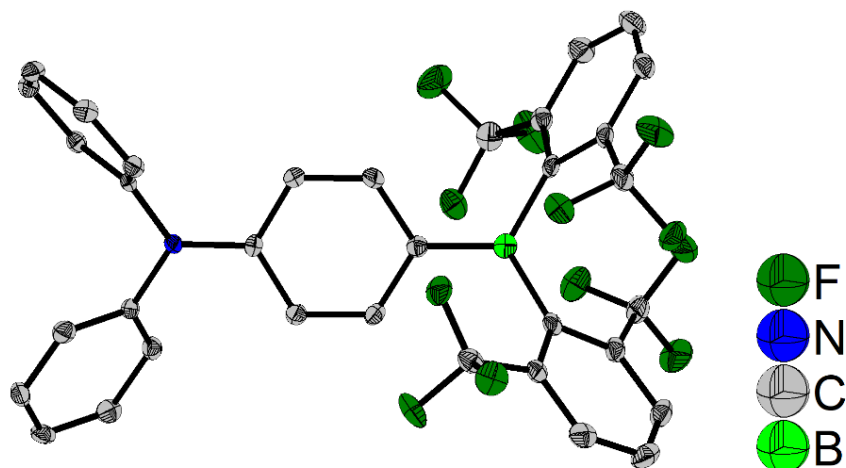


Figure 6.23: The solid-state molecular structure of **1** determined by single-crystal X-ray diffraction at 100 K. All ellipsoids are drawn at the 50% probability level. H atoms and solvent molecules are omitted for clarity.

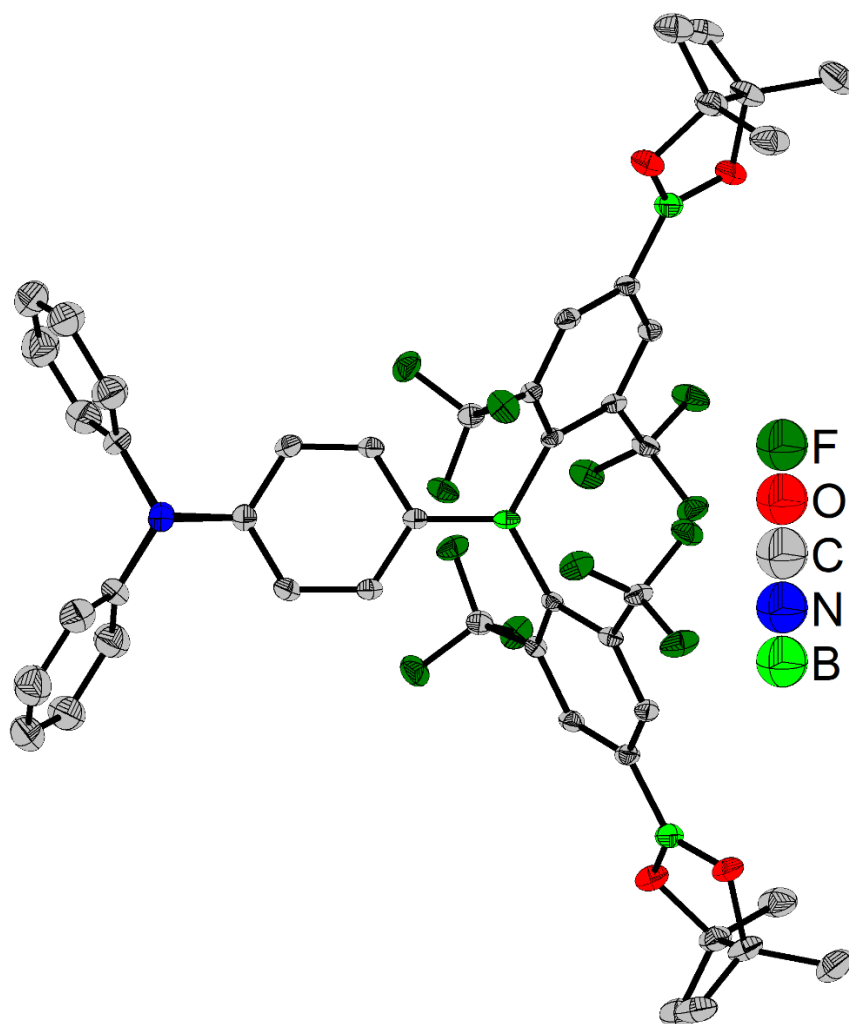


Figure 6.24: The solid-state molecular structure of **1-(Bpin)<sub>2</sub>** determined by single-crystal X-ray diffraction at 100 K. All ellipsoids are drawn at the 50% probability level. H atoms are omitted for clarity. The diphenylamino group (NPh<sub>2</sub>) is disordered by twofold rotational symmetry and only one part (50%) is shown here.

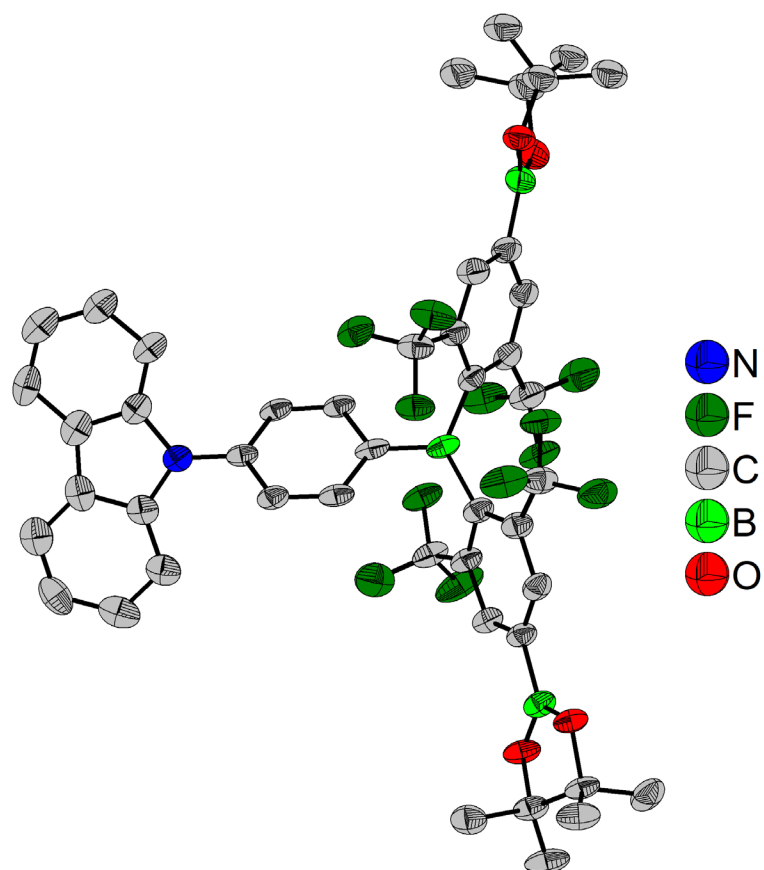


Figure 6.25: The solid-state molecular structure of **Cbz- $\pi$  (1)-(Bpin)<sub>2</sub>** determined by single-crystal X-ray diffraction at 100 K. All ellipsoids are drawn at the 50% probability level. H atoms are omitted for clarity. One of the Bpin groups is disordered and only the major part (71%) is shown here.

## 6.4 Photophysical Data

### 6.4.1 Chapter 1

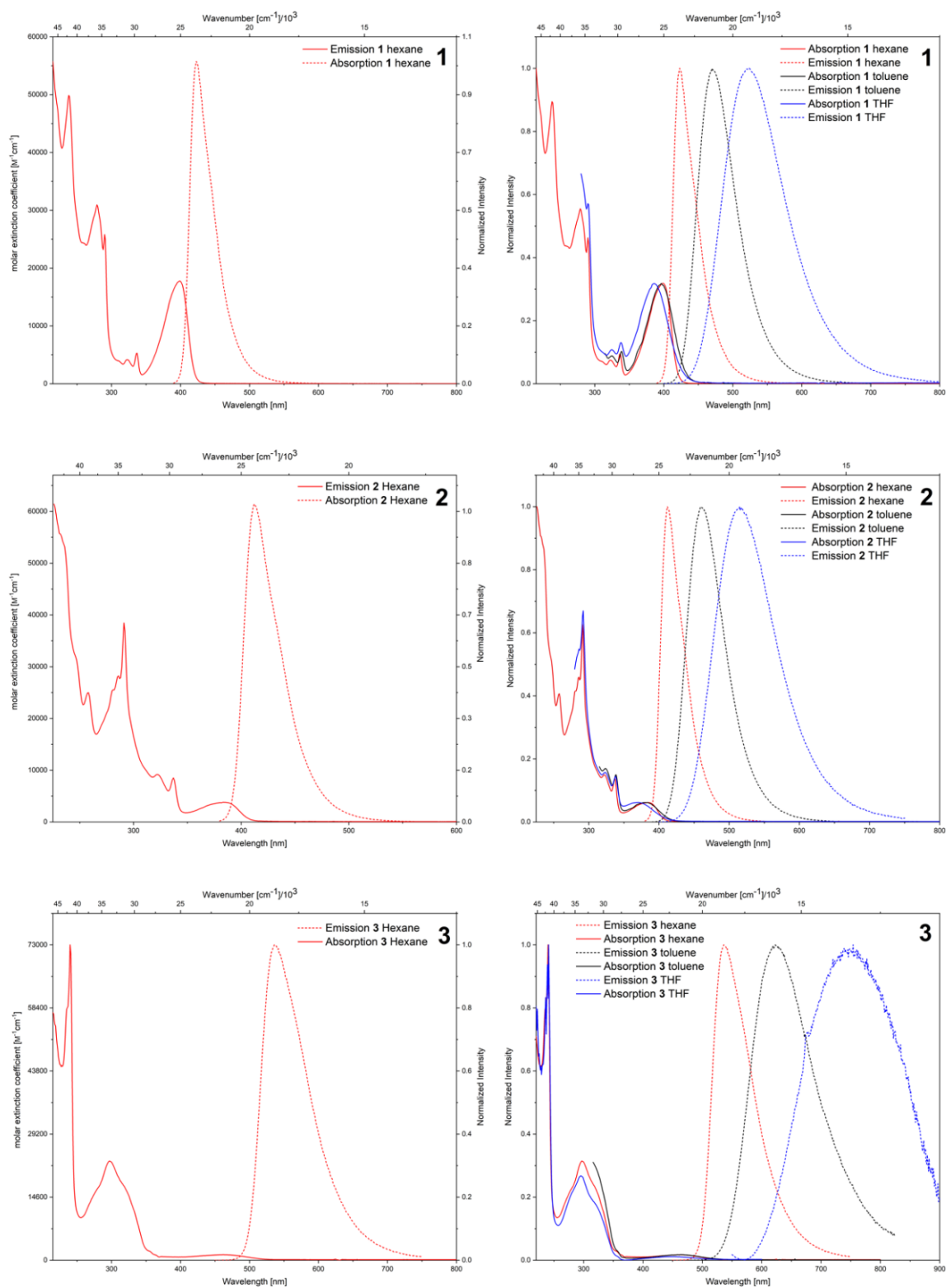


Figure 6.26: Absorption and emission spectra of **Cbz- $\pi$  (1)** (1<sup>st</sup> row; left: hexane with extinction coefficient; right: normalized spectra in hexane, toluene and THF), **Cbz-Me $\pi$  (2)** (2<sup>nd</sup> row; left: hexane with extinction coefficient; right: normalized spectra in hexane, toluene and THF), **Phox-Me $\pi$  (3)** (3<sup>rd</sup> row; left: hexane with extinction coefficient; right: normalized spectra in hexane, toluene and THF).

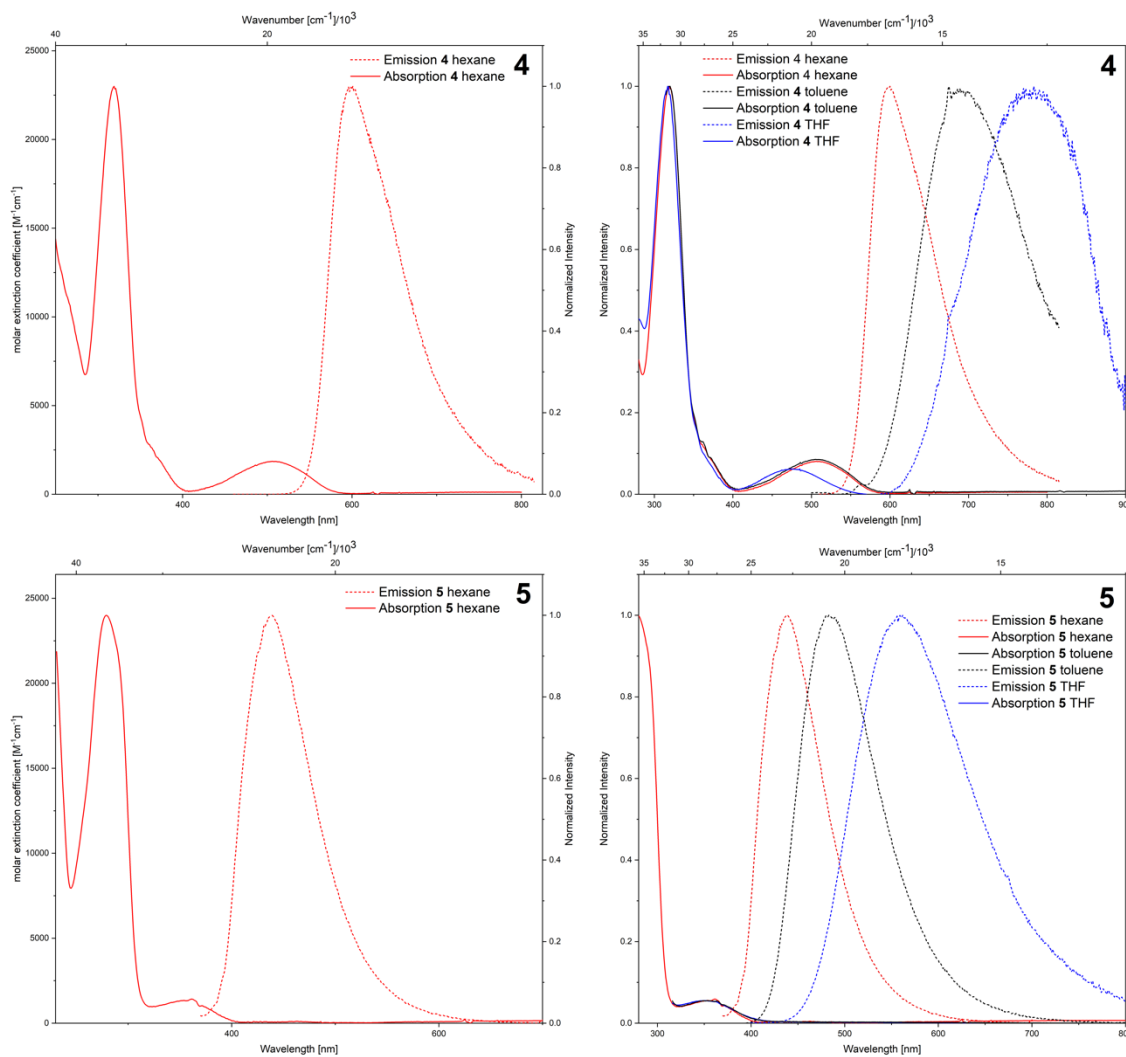


Figure 6.26 cont.: Absorption and emission spectra of **Phox-MeOπ (4)** (1<sup>st</sup> row; left: hexane with extinction coefficient; right: normalized spectra in hexane, toluene and THF) and **MeO<sub>3</sub>Ph-FMeπ (5)** (2<sup>nd</sup> row; left: hexane with extinction coefficient; right: normalized spectra in hexane, toluene and THF).

## Experimental

Linear fit results of plotting  $\ln\left(\frac{B_{DF}\tau_{DF}}{B_{PF}\tau_{PF}}\right)$  vs.  $1/K$

Table 6.8: Energy gaps obtained from the fits.

Compound	Solvent	S-T gap [eV]
<b>Phox-Me<math>\pi</math> (3)</b>	toluene	0.043
<b>Phox-MeO<math>\pi</math> (4)</b>	toluene	0.030
<b>MeO<sub>3</sub>Ph-FMe<math>\pi</math> (5)</b>	2-MeTHF	0.034

Table 6.9: Linear fit results of plotting  $\ln\left(\frac{B_{DF}\tau_{DF}}{B_{PF}\tau_{PF}}\right)$  vs.  $1/K$ .

Compound	Solvent	Intercept		Slope		Statistics	
		Value	Standard Error	Value	Standard Error	Adj. Square	R-Square
<b>Phox-Me<math>\pi</math> (3)</b>	toluene	2.20893	0.00946	-496.36761	2.5967	0.99975	
<b>Phox-MeO<math>\pi</math> (4)</b>	toluene	-1.04653	0.02534	-346.68245	6.9631	0.99718	
<b>MeO<sub>3</sub>Ph-FMe<math>\pi</math> (5)</b>	2-MeTHF	0.27125	0.1051	-396.48542	20.29432	0.96698	

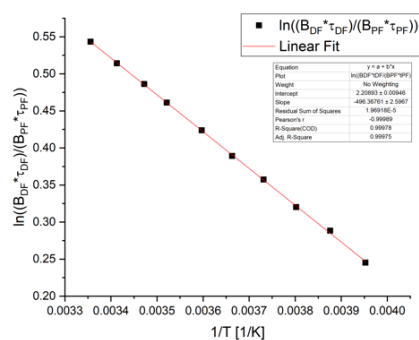


Figure 6.27: Linear fit of **Phox-Me $\pi$  (3)**.

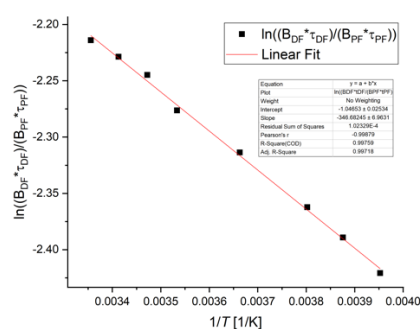


Figure 6.28: Linear fit of **Phox-MeO $\pi$  (4)**.

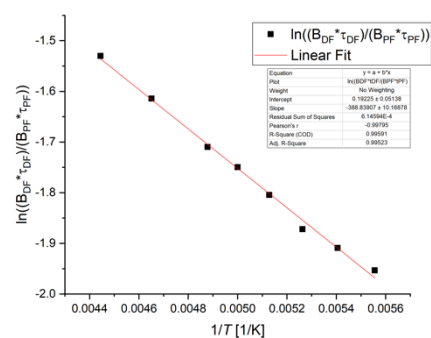
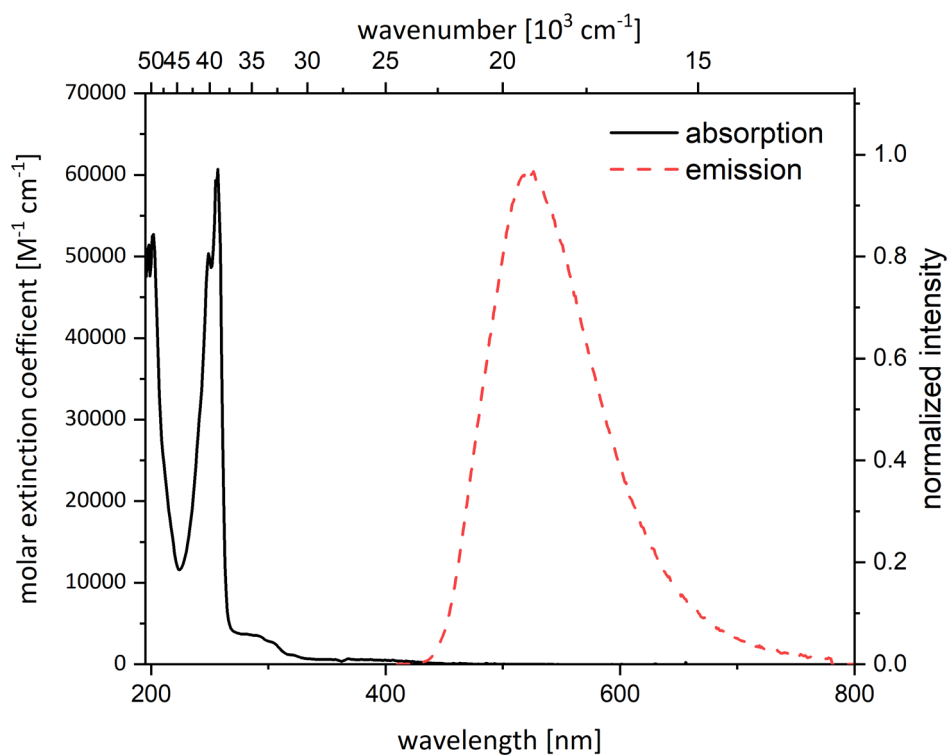
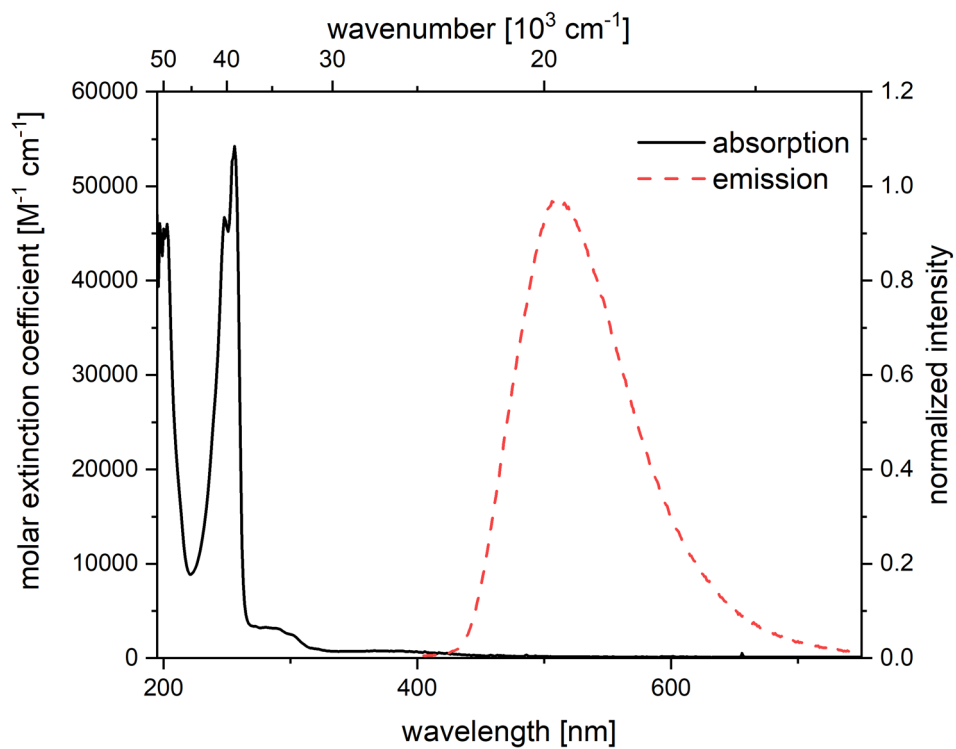


Figure 6.29: Linear fit of **MeO<sub>3</sub>Ph-FMe $\pi$  (5)**.



## 6.4.2 Chapter 2

Figure 6.30: Absorption and emission spectra of  ${}^F\text{MeSBf}$  in hexane.Figure 6.31: Absorption and emission spectra of  ${}^F\text{XylBf}$  in hexane.

## Experimental

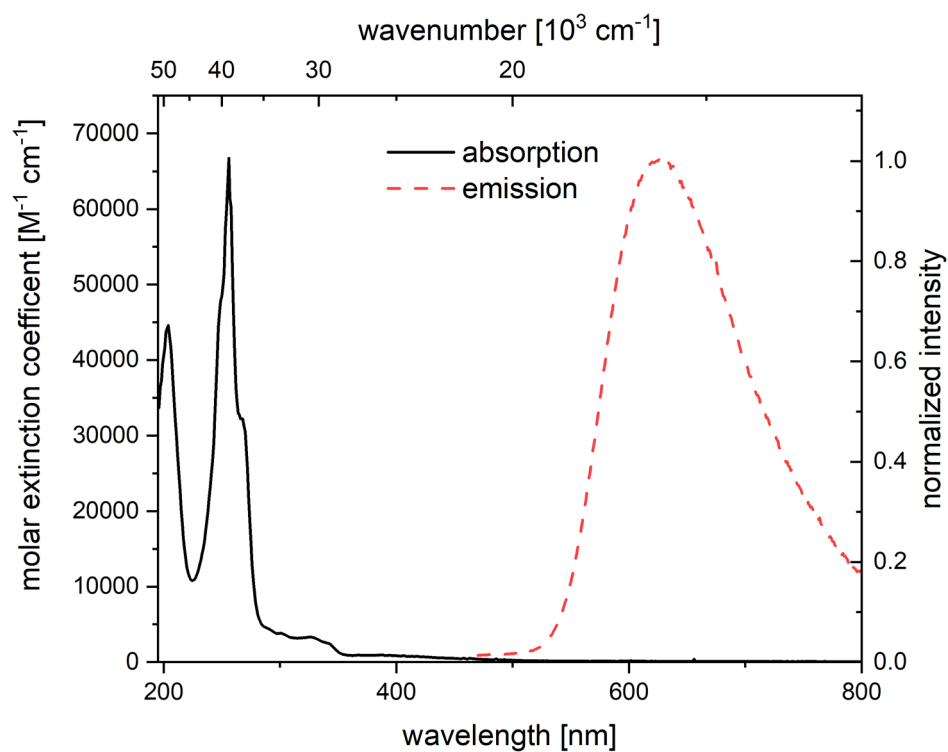


Figure 6.32: Absorption and emission spectra of  $p\text{-NMe}_2\text{-}^{\text{F}}\text{Xyl}^{\text{F}}\text{Bf}$  in hexane.

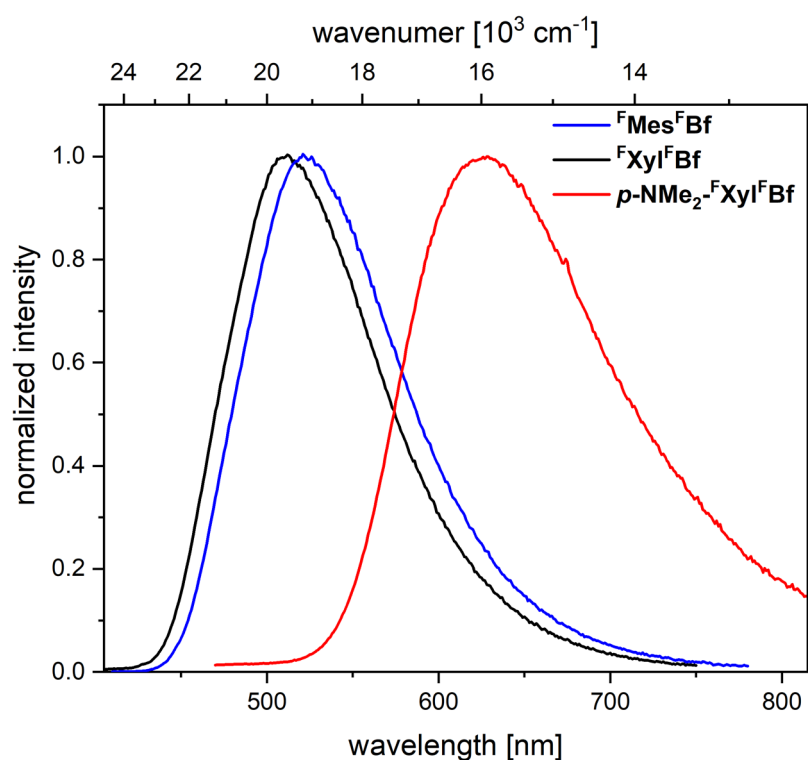


Figure 6.33: Emission spectra of  $^{\text{F}}\text{Mes}^{\text{F}}\text{Bf}$ ,  $^{\text{F}}\text{Xyl}^{\text{F}}\text{Bf}$  and  $p\text{-NMe}_2\text{-}^{\text{F}}\text{Xyl}^{\text{F}}\text{Bf}$ .

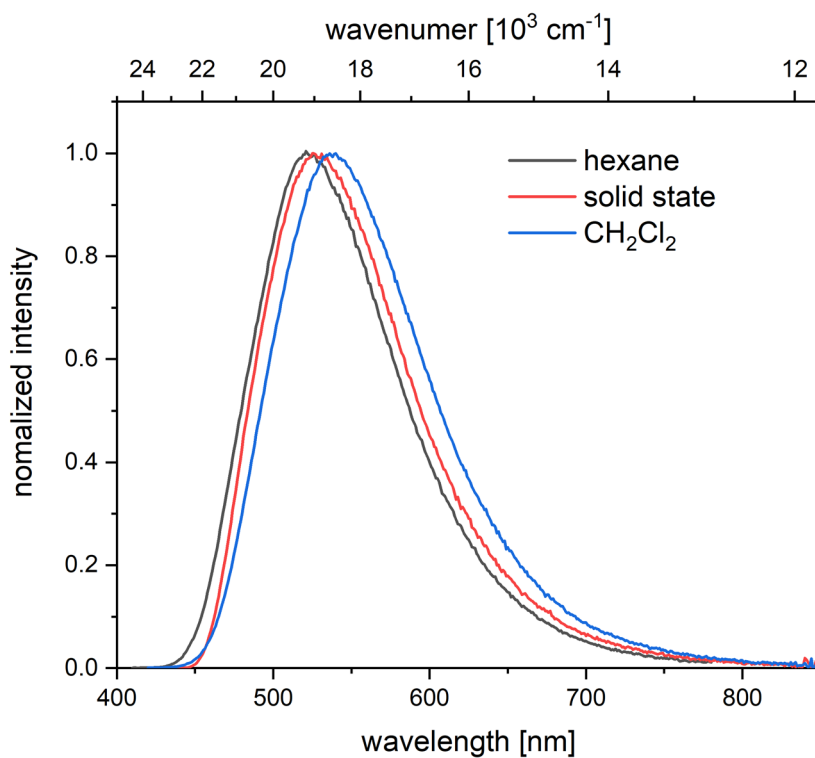


Figure 6.34: Environment dependent emission spectra of  ${}^{\text{F}}\text{MeS}^{\text{F}}\text{Bf}$ .

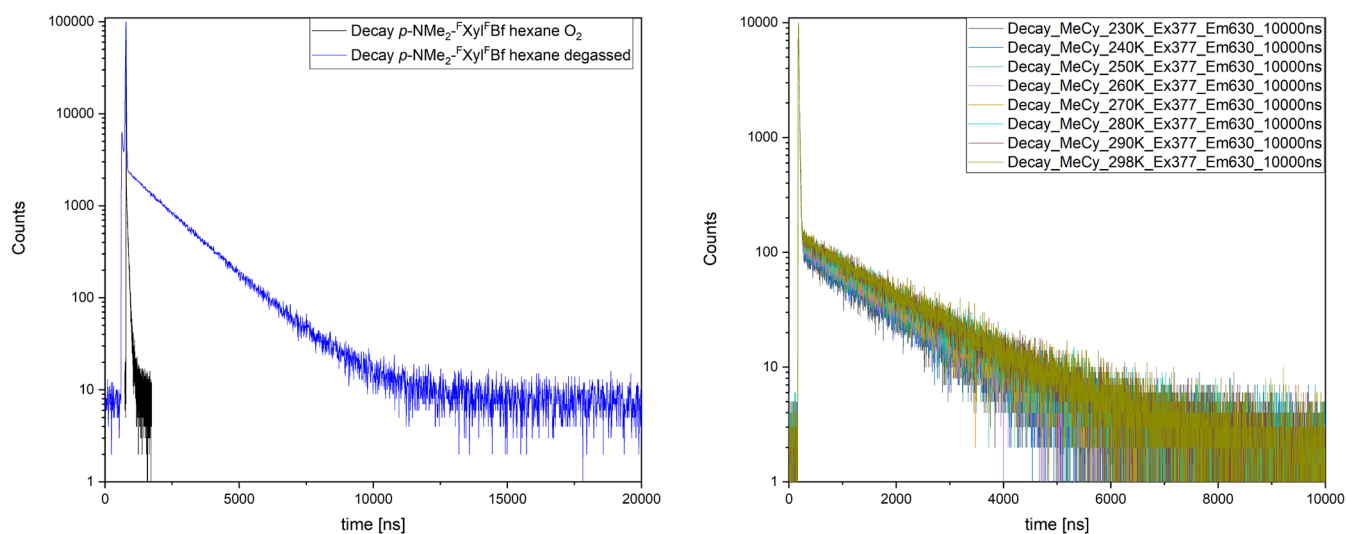


Figure 6.35 Lifetime measurements of  $p\text{-NMe}_2\text{-}^{\text{F}}\text{Xyl}^{\text{F}}\text{Bf}$  in hexane (left) degassed (blue) and after bubbling oxygen through the sample (black). Temperature-dependent lifetime measurements of  $p\text{-NMe}_2\text{-}^{\text{F}}\text{Xyl}^{\text{F}}\text{Bf}$  in methylcyclohexane (right) between 298 K and 230 K.

### 6.4.3 Chapter 3

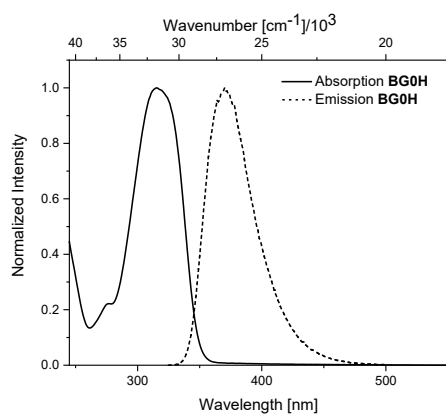


Figure 6.36: Absorption and emission spectra of **BG0H** in  $\text{CHCl}_3$ .

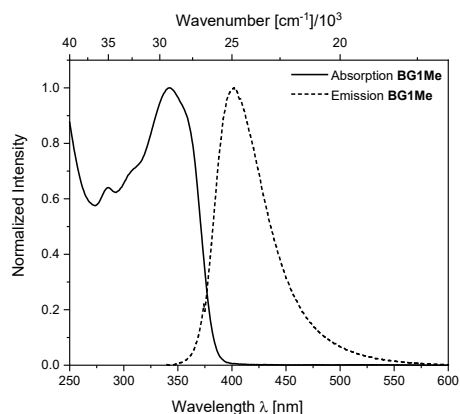


Figure 6.39: Absorption and emission spectra of **BG1Me** in  $\text{CHCl}_3$ .

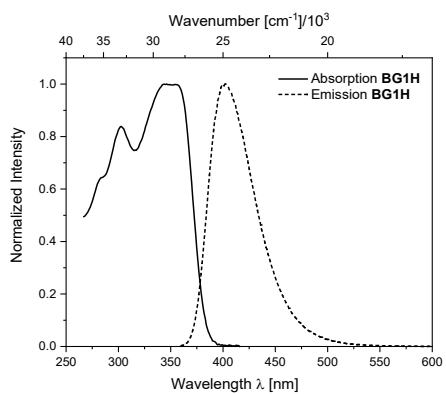


Figure 6.37: Absorption and emission spectra of **BG1H** in  $\text{CHCl}_3$ .

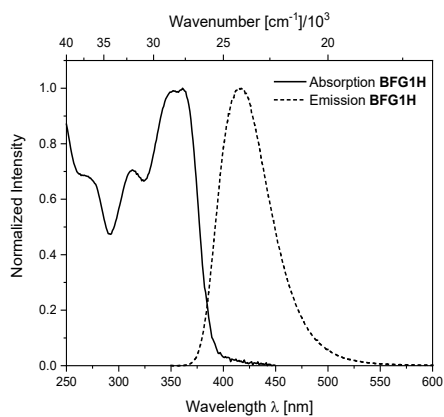


Figure 6.40: Absorption and emission spectra of **BFG1H** in  $\text{CHCl}_3$ .

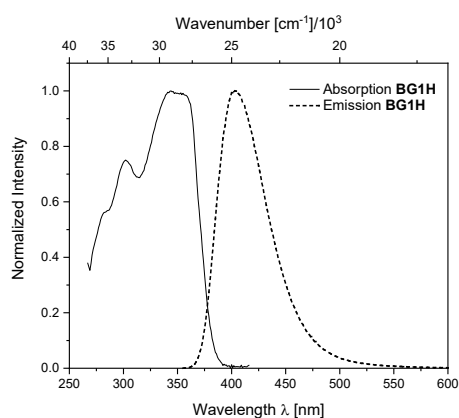


Figure 6.38: Absorption and emission spectra of **BG1H** in THF.

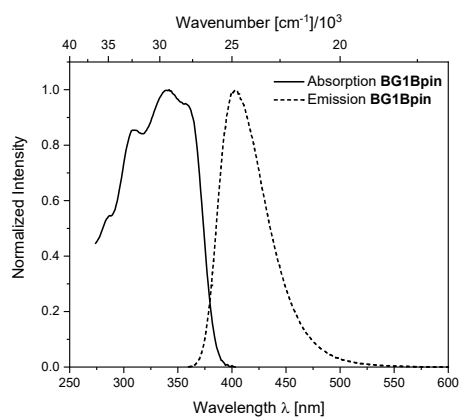


Figure 6.41: Absorption and emission spectra of **BG1Bpin** in  $\text{CHCl}_3$ .

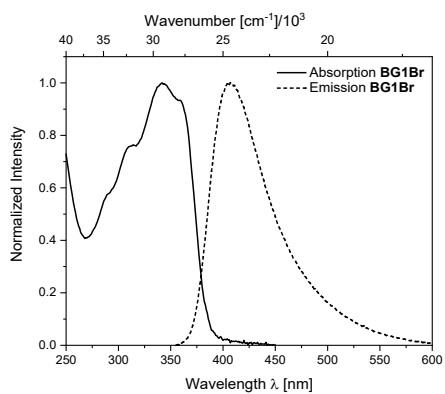


Figure 6.42: Absorption and emission spectra of **BG1Br** in  $\text{CHCl}_3$ .

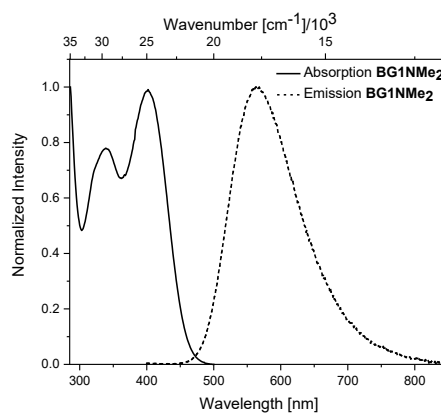


Figure 6.44: Absorption and emission spectra of **BG1NMe<sub>2</sub>** in toluene.

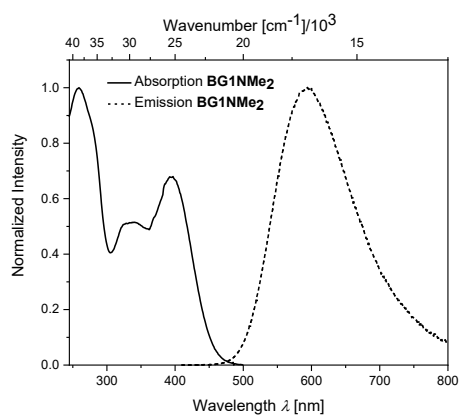


Figure 6.43: Absorption and emission spectra of **BG1NMe<sub>2</sub>** in  $\text{CHCl}_3$ .

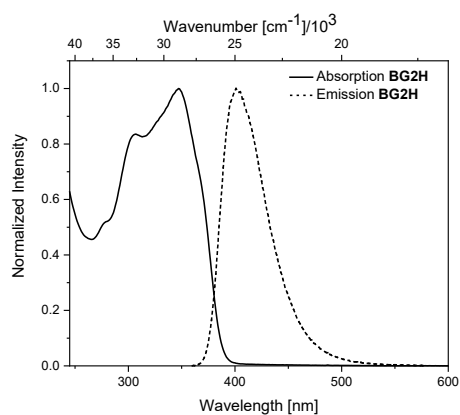


Figure 6.45: Absorption and emission spectra of **BG2H** in  $\text{CHCl}_3$ .

## 6.5 Electrochemical Data

## 6.5.1 Chapter 1

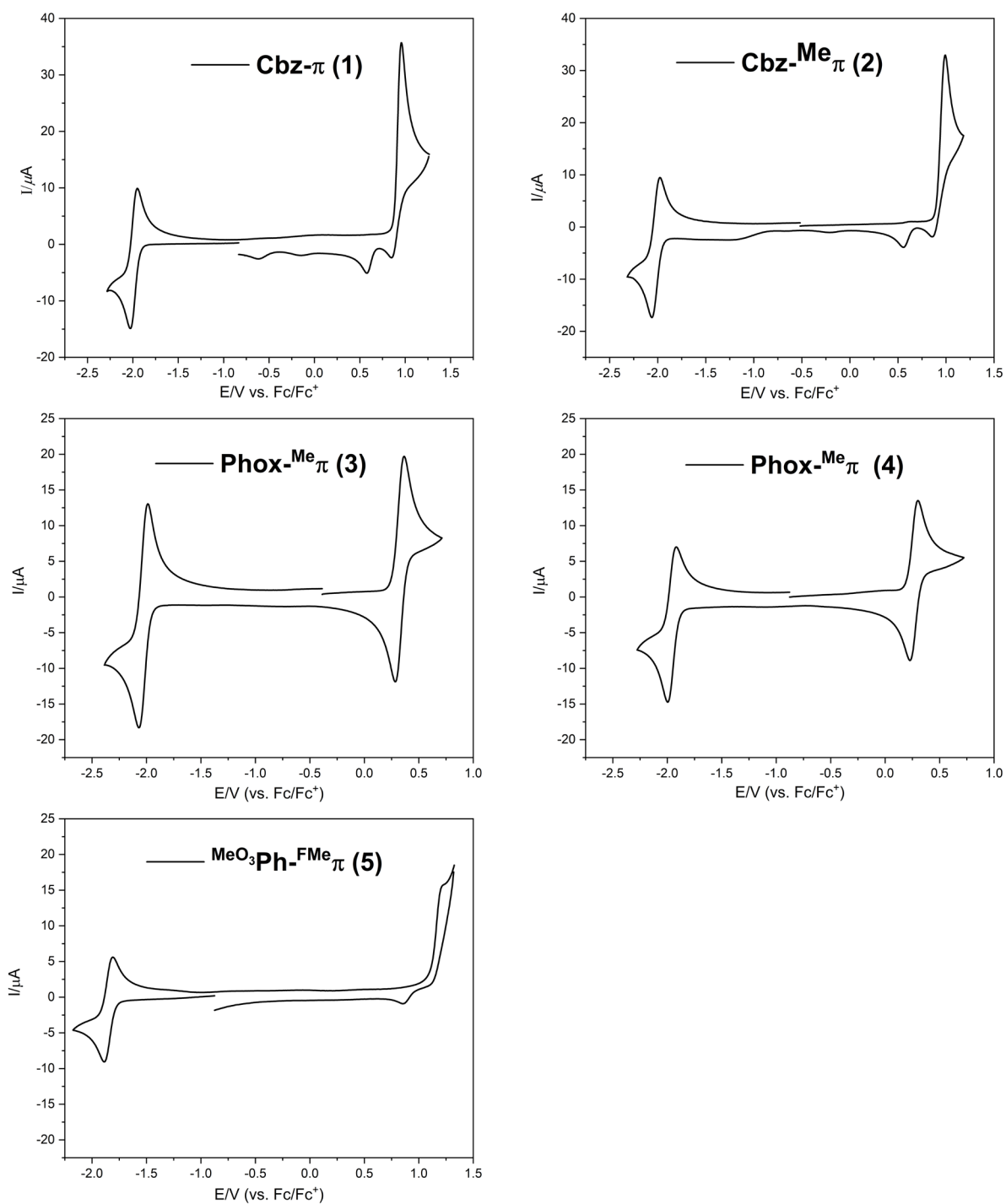


Figure 6.46: Cyclic voltammograms of  $\text{Cbz}-\pi$  (1),  $\text{Cbz-Me}_\pi$  (2),  $\text{Phox-Me}_\pi$  (3),  $\text{Phox-MeO}_\pi$  (4), and  $\text{MeO}_3\text{Ph-FMe}_\pi$  (5). The cyclic voltammograms were measured in dichloromethane with  $[\text{nBu}_4\text{N}][\text{PF}_6]$  as the electrolyte with a scan rate of  $250 \text{ mVs}^{-1}$ . All measurements were referenced to the  $\text{Fc}/\text{Fc}^+$  ion couple.

## 6.5.2 Chapter 2

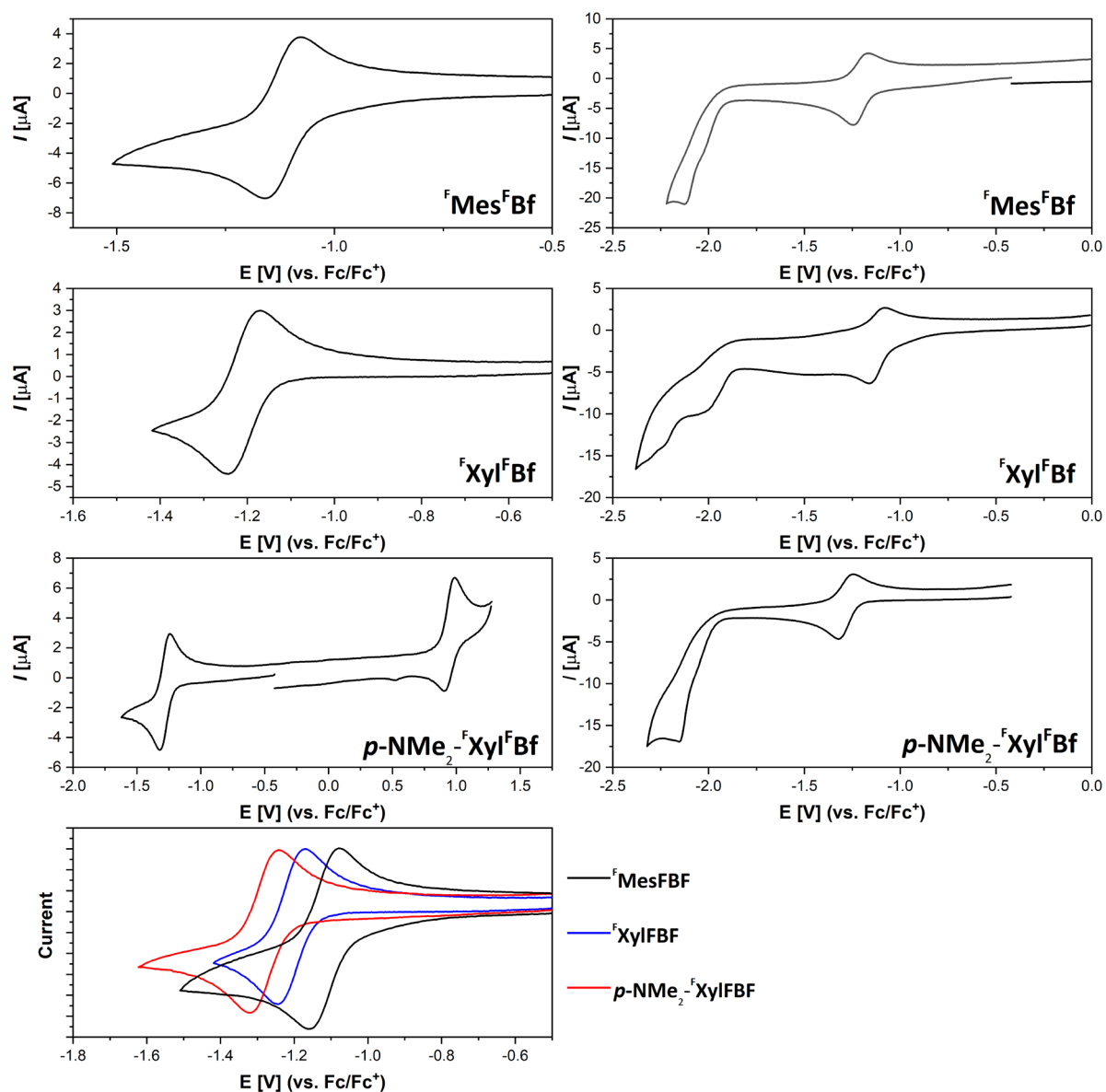


Figure 6.47: Cyclic voltammograms of the reversible and irreversible redox events of  ${}^{\text{F}}\text{Mes}^{\text{F}}\text{Bf}$  (top),  ${}^{\text{F}}\text{Xyl}^{\text{F}}\text{Bf}$  (2<sup>nd</sup> row) and  $p\text{-NMe}_2\text{-}{}^{\text{F}}\text{Xyl}^{\text{F}}\text{Bf}$  (3<sup>rd</sup> row). For comparison, the reduction waves are plotted together (bottom;  ${}^{\text{F}}\text{Mes}^{\text{F}}\text{Bf}$  (black),  ${}^{\text{F}}\text{Xyl}^{\text{F}}\text{Bf}$  (blue),  $p\text{-NMe}_2\text{-}{}^{\text{F}}\text{Xyl}^{\text{F}}\text{Bf}$  (red)). The cyclovoltammogramms were measured in  $\text{CH}_2\text{Cl}_2$  with  $[(n\text{Bu})_4\text{N}][\text{PF}_6]$  as the electrolyte with a scan rate of  $250\text{ mVs}^{-1}$ . All measurements are referenced to the  $\text{Fc}/\text{Fc}^+$  ion couple.

Table 6.10: Reversible and irreversible reduction and oxidation potentials of  ${}^{\text{F}}\text{Mes}^{\text{F}}\text{Bf}$ ,  ${}^{\text{F}}\text{Xyl}^{\text{F}}\text{Bf}$ , and  $p\text{-NMe}_2\text{-}{}^{\text{F}}\text{Xyl}^{\text{F}}\text{Bf}$ .

compound	1 <sup>st</sup> reduction potential	2 <sup>nd</sup> reduction potential	1 <sup>st</sup> oxidation potential $E_{1/2}$
	$E_{1/2}$ in [V] vs. $\text{Fc}/\text{Fc}^+$	$E_{\text{pc}}$ in [V] vs. $\text{Fc}/\text{Fc}^+$	in [V] vs. $\text{Fc}/\text{Fc}^+$
${}^{\text{F}}\text{Mes}^{\text{F}}\text{Bf}^{\text{a}}$	-1.13	-2.04	-
${}^{\text{F}}\text{Xyl}^{\text{F}}\text{Bf}^{\text{a}}$	-1.21	-2.12	-
$p\text{-NMe}_2\text{-}{}^{\text{F}}\text{Xyl}^{\text{F}}\text{Bf}^{\text{a}}$	-1.28	-2.15	0.95 (partially reversible)

## 6.5.3 Chapter 3

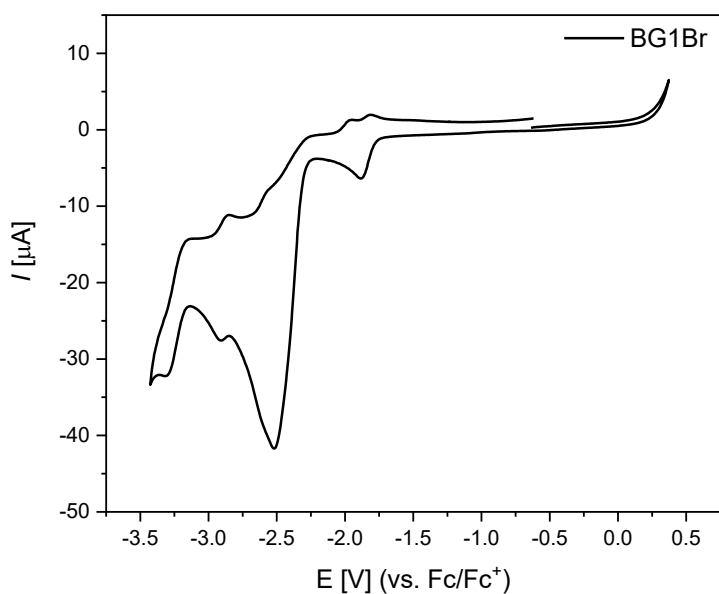


Figure 6.48: Cyclic voltammogram of **BG1Br** in THF with  $[n\text{Bu}_4\text{N}][\text{PF}_6]$  as the electrolyte and a scan rate of  $250 \text{ mVs}^{-1}$  referenced vs. the  $\text{Fc}/\text{Fc}^+$  redox couple, including irreversible reduction waves.

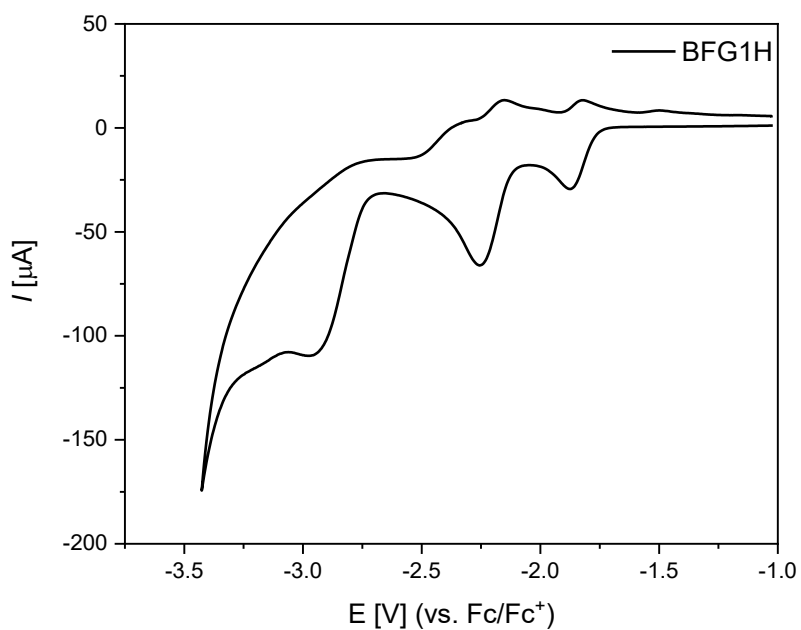


Figure 6.49: Cyclic voltammogram of **BFG1H** in THF with  $[n\text{Bu}_4\text{N}][\text{PF}_6]$  as the electrolyte and a scan rate of  $250 \text{ mVs}^{-1}$  referenced vs. the  $\text{Fc}/\text{Fc}^+$  redox couple, including irreversible reduction waves.



## 6.5.4 Chapter 4

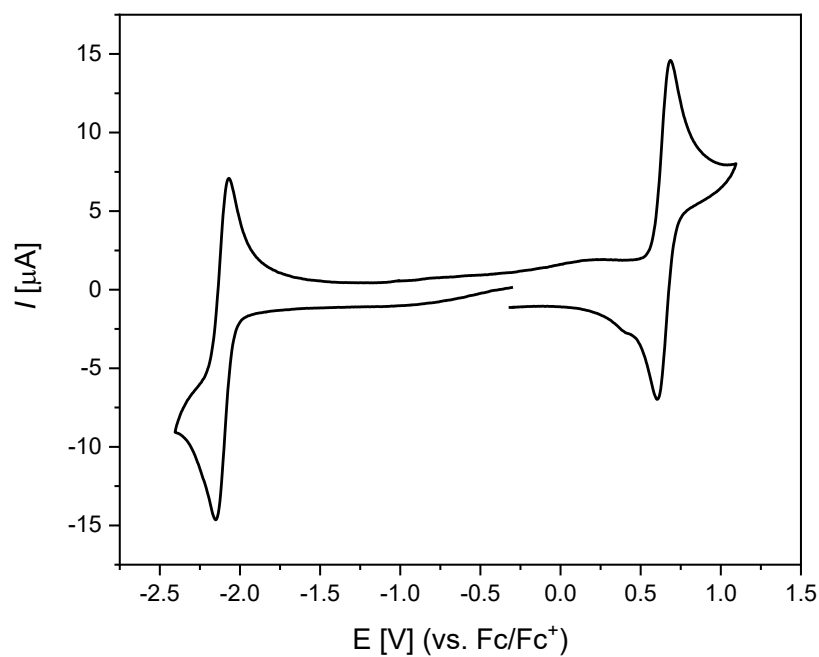


Figure 6.50: Cyclic voltammogram of **1** in  $\text{CH}_2\text{Cl}_2$  with  $[\text{nBu}_4\text{N}][\text{PF}_6]$  as the electrolyte and a scan rate of  $250 \text{ mVs}^{-1}$  referenced vs. the  $\text{Fc}/\text{Fc}^+$  redox couple.

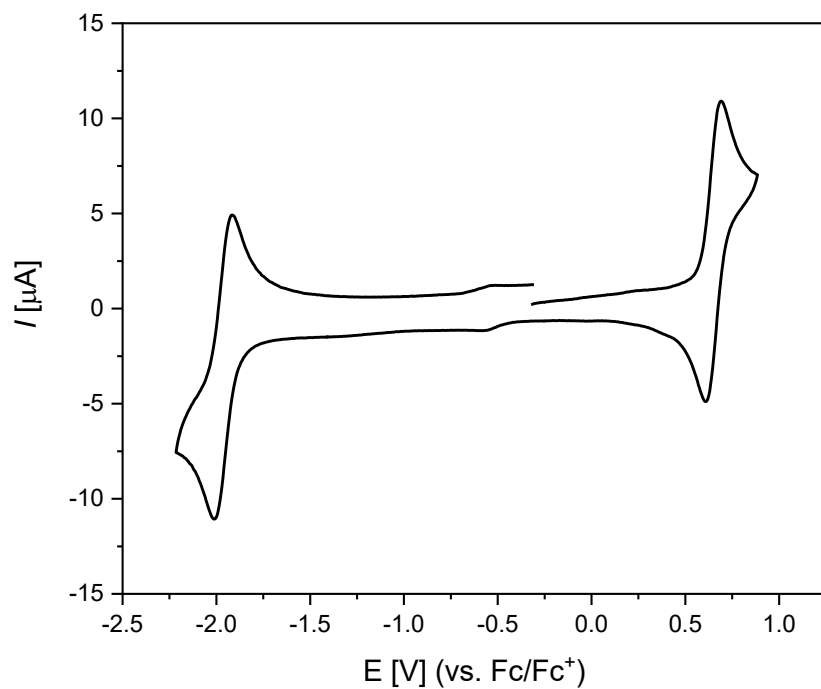


Figure 6.51: Cyclic voltammogram of **1-(Bpin)<sub>2</sub>** in  $\text{CH}_2\text{Cl}_2$  with  $[\text{nBu}_4\text{N}][\text{PF}_6]$  as the electrolyte and a scan rate of  $250 \text{ mVs}^{-1}$  referenced vs. the  $\text{Fc}/\text{Fc}^+$  redox couple.

## Experimental

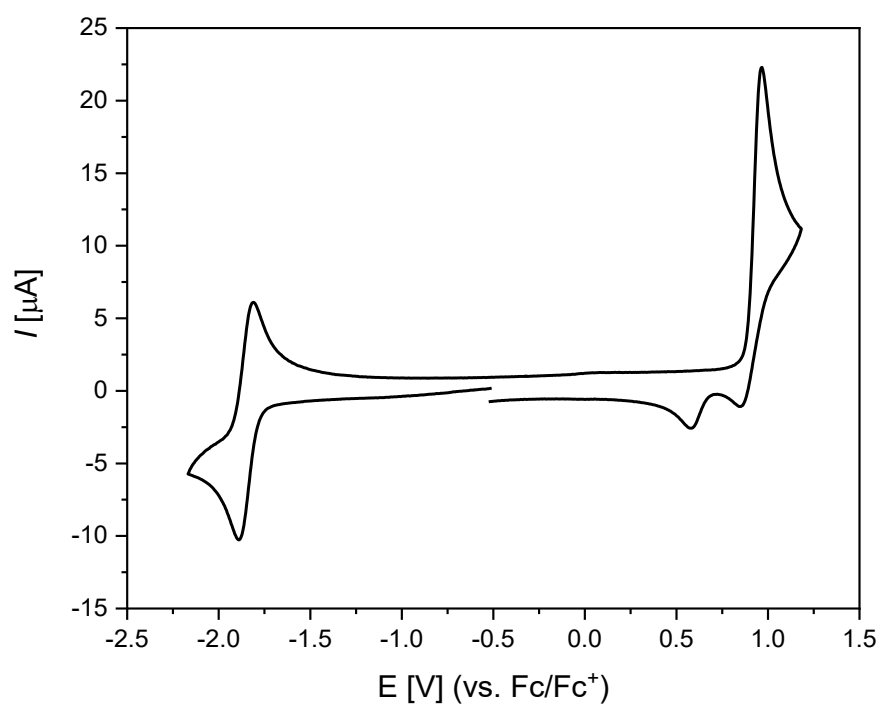


Figure 6.52: Cyclic voltammogram of **2-(Bpin)<sub>2</sub>** in CH<sub>2</sub>Cl<sub>2</sub> with [nBu<sub>4</sub>N][PF<sub>6</sub>] as the electrolyte and a scan rate of 250 mVs<sup>-1</sup> referenced vs. the Fc/Fc<sup>+</sup> redox couple.

## 6.6 TD-DFT Calculations

### 6.6.1 Chapter 1

#### 6.6.1.1 Methodology & Computational Details

All calculations were performed using the Amsterdam Density Functional (ADF) 2018 quantum chemistry package developed by SCM.<sup>[342-344]</sup> Electronic ground-state geometry optimizations were performed with the dispersion corrected BLYP-D3(BJ)<sup>[345-350]</sup> functional in combination with the TZ2P basis set and small frozen core approximation, i.e. the 1s electrons for second period were kept frozen.

Relativistic effects were accounted for using the scalar zeroth-order regular approximation (ZORA).<sup>[351]</sup> In order to account for solvation effects, the calculations were conducted with the COSMO formalism in toluene ( $\epsilon = 2.38$ ), except for the benchmark systems **B4–B8** which were optimized in their respective media. Geometries were verified by analytical frequency calculations to be (local) minima.<sup>[352-354]</sup> The optimal  $\gamma$  value in a range-separated (RS) functional, in our case LC-BLYP, was determined by the Janak's theorem<sup>[355-357]</sup> (Equation 6.1) by minimizing the  $J(\gamma)$  function.<sup>[358-362]</sup>

Equation 6.1:

$$J(\gamma) = \sqrt{\sum_{i=0}^1 [\epsilon_H(N+i) + IP(N+i)]}$$

This scheme is well-known to provide accurate values for CT states.<sup>[361, 363, 364]</sup> Calculations to find the optimal  $\gamma$  value (tuning calculations) were performed in the gas phase in combination with the TZ2P functional on the BLYP-D3(BJ) optimized ground state geometries. We used PLAMS<sup>[344]</sup> as implemented in ADF and the open-source python library QMFlows<sup>[365]</sup> to automate the job submission and handling procedure. The vertical or Franck-Condon excitation energies (FC-S<sub>n</sub> and FC-T<sub>n</sub>) were calculated using the optimally tuned LC-BLYP\* functional (where \* denotes the tuned LC-BLYP functional) in combination with the TZ2P basis set and without a frozen core within the Tamm-Dancoff approximation (TDA). This approximation has been extensively tested. It saves computational time and avoids triplet instability issues.<sup>[364, 366, 367]</sup> We also performed Natural Transition Orbital (NTO)<sup>[368]</sup> analyses as some of the excited states exhibit heavily mixed electronic configurations. Moreover, NTO allows for qualitative characterization of the excited states as local excited (LE<sub>D</sub>: localized triplet exciton on the

## Experimental

donor,  $LE_{\pi}$ : localized triplet exciton on the  $\pi$ -bridge, or  $LE_A$ : localized triplet exciton on the acceptor) and charge transfer (CT). Furthermore, metrics such as Tozers index ( $\Lambda$ )<sup>[228, 369]</sup> (Equation 6.2) in conjunction with the hole–electron distance descriptor ( $R_{eh}$ )<sup>[370]</sup> (Equation 6.3) were also employed to quantify the nature of excited states. It has to be noted that excited states involved in TADF processes are sometimes a mixture of CT/LE and not “pure” LE or CT.<sup>[53, 371]</sup> However, in order to characterize the different excited states, and to ensure a fair comparison between them, we assign, although not strictly,  $\Lambda > 0.5$  and  $R_{eh} < 2.0 \text{ \AA}$  as LE and the opposite as CT.

Equation 6.2:

$$\Lambda = \frac{\sum_{i,a} c_{i,a}^2 \langle |\varphi_a| | |\varphi_i| \rangle}{\sum_{i,a} c_{i,a}^2}$$

Equation 6.3:

$$R_{eh} = \frac{\sum_{i,a} c_{i,a}^2 |\langle \varphi_a | r | \varphi_a \rangle - \langle \varphi_i | r | \varphi_i \rangle|}{\sum_{i,a} c_{i,a}^2}$$

In the equations above,  $\varphi_a$  and  $\varphi_i$  represents the occupied and unoccupied one-electron wavefunction respectively,  $|\langle \varphi_a | r | \varphi_a \rangle|$  represents the norm of the one-electron wavefunction centroid and  $c_{i,a}$  represents the weight of the one-electron excitation. As TADF is an emission process, and there are multiple close-lying triplet excited states involved in the TADF mechanism which might lead to state crossing, it is crucial to determine which vertically excited FC- $T_n$  (where  $n$  can be  $> 1$ ) state relaxes to the adiabatic  $T_1$  state. For this reason, we plotted the electron difference density profile ( $\Delta\rho = \rho_{T_1}(T_1) - \rho_{S_0}(T_1)$ ) which qualitatively maps the nature of the relaxed  $T_1$  to the corresponding FC- $T_n$  state;  $\rho_{T_1}(T_1)$  and  $\rho_{S_0}(T_1)$  is computed using UKS and RKS, respectively, at the LC-BLYP\*/TZ2P/COSMO level of theory without a frozen core approximation.

Except for **B1** and **Cbz-Ph** to some extent and especially **B7** where there is mixture of  $^3CT$  and  $^3LE$ , we found that the relaxed  $T_1$  state is essentially a  $^3CT$  state. Similar situations, in which the  $^3CT$  state is lower in energy than the  $^3LE$  state, have been observed previously.<sup>[372]</sup> We also evaluated the  $S_0 \leftarrow T_1$  emission energy (Figure 6.53), denoted as  $\Delta E_{VE}(T_1)$ , as well as the  $S_0 \leftarrow S_1$  emission energy, denoted as  $\Delta E(S_1)$ . As stated in the manuscript, the excited states in the TADF mechanism are in dynamic equilibrium with each other which in turn is intricately dependent on the corresponding energy gaps. Therefore, we report three energy gaps (differences in vertical excitation energies obtained from TDA-LC-BLYP\*) in this study:

$\Delta E_{1\text{CT}-3\text{CT}}$ ,  $\Delta E_{1\text{CT}-3\text{LE}}$ , and  $\Delta E_{3\text{LE}-3\text{CT}}$ . Here,  $^3\text{CT}$  denotes the FC- $T_n$  corresponding to the relaxed  $T_1$  state and  $^3\text{LE}$  denotes the lowest FC- $T_n$  with predominant LE character. An important aspect which is often overlooked when benchmarking S-T gaps is the actual measurement method involved to extract the experimental gaps. The gap can be extracted in two ways, first from fitting the integrated delayed fluorescence (DF) emission or its lifetime as a function of temperature which yields the activation energy ( $\Delta E_a^{\text{TADF}}$ ), and second, from the difference between the onset of fluorescence and phosphorescence signals at low temperature which is defined as the optical gap ( $\Delta E_{\text{opt}}^{\text{TADF}}$ ).<sup>[373-375]</sup>

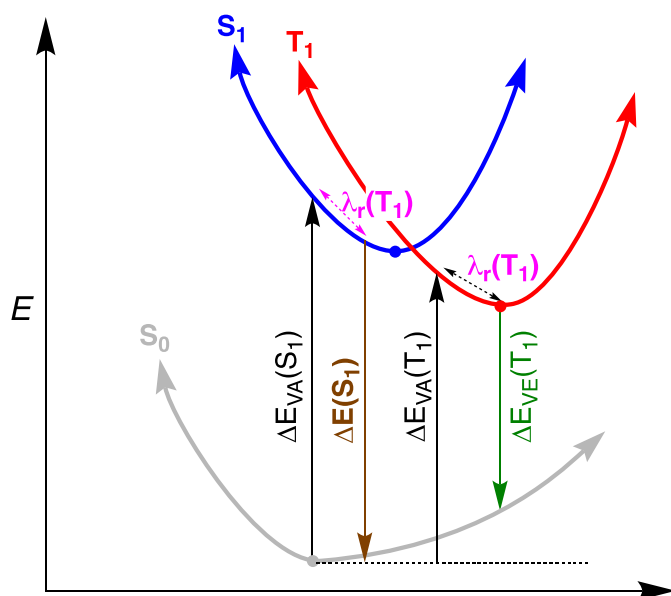


Figure 6.53: Jablonski diagram depicting the protocol used to compute the emission energies:  $\Delta E(S_1)$  in brown; and  $\Delta E_{VE}(T_1)$  in green. The geometrical reorganization energy  $\lambda_r(T_1)$  is depicted in pink and the vertical Franck-Condon absorption energies,  $\Delta E_{VA}(S_1)$  and  $\Delta E_{VA}(T_1)$ , are depicted in black. The bold dots depict the minima of the corresponding electronic states. The geometrical reorganization energy  $\lambda_r(T_1)$  is determined by the energy difference between the relaxed  $T_1$  and the corresponding FC- $T_n$  state. The  $S_0 \leftarrow S_1$  emission energy ( $\Delta E(S_1)$ ) was approximated by subtracting  $\lambda_r(T_1)$  from FC- $S_1$ , i.e. by assuming that the reorganization energies for singlet and triplet (both CT states) are same.

We benchmarked our protocol using a set of eight known boron-based D- $\pi$ -A compounds (**B1–B8**, see Figure 6.54).<sup>[54, 56, 58]</sup> For this purpose, we compared the experimental singlet–triplet (S-T) gaps with our computed  $\Delta E_{ST}$ . The experimentally measured gap depends on the type of measurement performed and thus it is highly crucial to benchmark against the correct gap.<sup>[373]</sup> As such, the gap obtained from  $\Delta E_a^{\text{TADF}}$  correspond to  $\Delta E_{1\text{CT}-3\text{CT}}$ , while the optical gap corresponds to  $\Delta E_{1\text{CT}-3\text{LE}}$ .

Overall, our protocol can successfully predict the three gaps in an unknown molecule D- $\pi$ -A except in cases where the assignment of the nature of the excited states as CT or LE becomes ill defined *vide infra*.<sup>[140, 141]</sup>

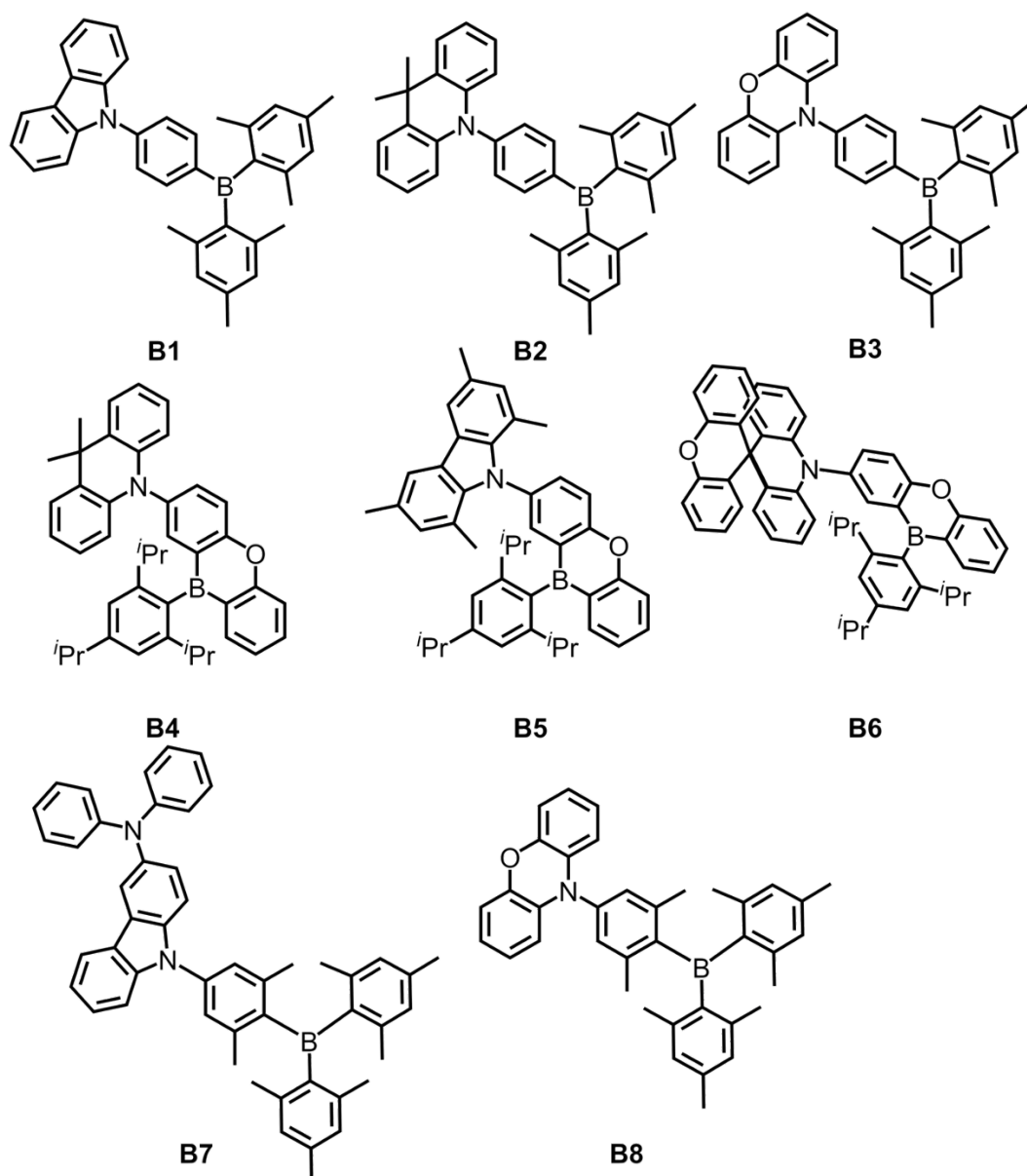


Figure 6.54: Structures of the molecules **B1** – **B8**<sup>[54, 56, 58]</sup> used in our benchmark study. **B1** – **B4** was measured in frozen toluene, **B4**–**B6** in poly(propylene)fumarate (PPF), **B7** in bis[2-(diphenylphosphino)phenyl] ether oxide (DPEPO) and **B8** in 4,4'-bis(*N*-carbazolyl)-1,1'-biphenyl (CBP).

### 6.6.1.2 Modeling Solvent/Matrix Effects

We benchmarked our method using a set of eight known boron-based D– $\pi$ -A compounds (**B1**–**B8**, Figure 6.54).<sup>[54, 56, 58]</sup> For this purpose, we compared the experimental singlet-triplet (S–T) gaps measured in toluene at 77 K or at lower temperatures with our estimated  $\Delta E_{S-T}$  computed in toluene. However, the gaps in **B4**–**B8** were measured in amorphous thin-film matrices. As the matrix, poly(propylene)fumarate (PPF) was used in the cases of **B4**–**B6**, bis[2-(diphenylphosphino)phenyl] ether oxide (DPEPO) in the case of **B7**, and 4,4'-bis(*N*-carbazolyl)-1,1'-biphenyl (CBP) in the case of **B8**. Therefore, to mimic the environment of the

amorphous films we calculated its static dielectric constant  $\epsilon$  using the Clausius-Mossotti relation<sup>[376, 377]</sup> (Equation 6.4).

Equation 6.4:

$$\frac{\epsilon - 1}{\epsilon + 2} = \frac{4\pi\alpha}{3V}$$

where  $V$  is the surface volume obtained from the continuum solvation model (COSMO)<sup>[378-380]</sup> calculation using atomic radii and  $\alpha$  term denotes the isotropic component of the molecular polarizability obtained from the response calculation.<sup>[381]</sup> We calculated these parameters with the range-separated (RS) CAMY-B3LYP functional<sup>[382]</sup> using the TZ2P Slater-type basis set.<sup>[383]</sup>

Table 6.11: Calculated permittivity using Equation 6.4 of the amorphous thin films used to measure the S–T gap in the selected benchmark molecules (**B4–B8**).

Thin film	Volume ( $V$ in bohr <sup>3</sup> )	Polarizability ( $\alpha$ in bohr <sup>3</sup> )	$\epsilon$
PPF	3930.18	456.80	3.75
DPEPO	3983.89	466.76	3.88
CBP	3375.52	449.56	4.78

### 6.6.1.3 Ground State (S<sub>0</sub>) Optimization

Electronic ground-state geometry optimizations were performed with the dispersion corrected BLYP-D3(BJ) functional<sup>[347, 348, 350, 384-387]</sup> in combination with the TZ2P basis set and small frozen core approximation (i.e. the 1s electrons for second period were kept frozen) using restricted Kohn-Sham (RKS). Relativistic effects were accounted for using the scalar zeroth-order regular approximation (ZORA).<sup>[388-390]</sup> In order to account for the solvation effects, all calculations were conducted with the COSMO formalism in toluene ( $\epsilon = 2.38$ ). Due to the different environment for **B4–B8**, as mentioned above, all the optimizations for these systems were done using their respective permittivity as described in Table 6.11. All optimized structures were verified by analytical frequency calculations to be (local) minima.<sup>[352-354]</sup>

### 6.6.1.4 Optimal $\gamma$ Parameter in RS Functionals

A range-separated (RS) functional, in our case ZORA-LC-BLYP, separates the exchange term into two components: short-range component which is described by DFT exchange and the long-range component which is described by the Hartree-Fock (HF) exchange, based on the

## Experimental

interelectronic parameter  $r_{12}$  and a switching function. In ADF, the switching function is based on the Yukawa potential  $\exp(-\gamma r_{12})$ ,<sup>[382]</sup> where  $\gamma$  represents the inverse of the inter-electronic distance  $r_{12}$  at which the exchange term switches from DFT-like to HF-like exact exchange as described by Equation 6.5 (in our case  $\alpha = 0$  and  $\beta = 1$ ). According to exact Kohn-Sham and generalized Kohn-Sham theory, the negative HOMO energy  $-\varepsilon_H(N)$  for an  $N$ -electron system should be equal to the vertical ionization potential  $IP(N)$ .<sup>[355-357, 391]</sup> Most of the DFT functionals give a large difference between the two quantities, and therefore, the optimally tuned version tries to minimize this difference. The formalism of the  $N$ -electron system can be extended to an  $N+1$  electron system to provide a better estimation of the HOMO–LUMO gap as described by Equation 6.6. The optimal  $\gamma$  for a particular molecule is obtained by minimizing the  $J(\gamma)$  function.<sup>[358-362]</sup> This approach has been applied to all the benchmark and model systems as they are known to provide accurate values for the gap.<sup>[361, 363, 364]</sup> All tuning calculations have been performed in the gas phase in combination with the TZ2P functional on the BLYP-D3(BJ) optimized ground state geometries. We used PLAMS as implemented in ADF2018 and the open-source python library QMFlows to automate the job submission and handling procedure and to obtain the optimal  $\gamma$  for each molecule (Table 6.12).

Equation 6.5:

$$\frac{1}{r_{12}} = \frac{1 - [\alpha + \beta (1 - \exp(-\gamma r_{12}))]}{r_{12}} + \frac{\alpha + \beta (1 - \exp(-\gamma r_{12}))}{r_{12}}$$

Equation 6.6:

$$J(\gamma) = \sqrt{\sum_{i=0}^1 [\varepsilon_H(N+i) + IP(N+i)]}$$

Table 6.12: Self-consistently tuned  $\gamma$  (in  $a_0^{-1}$ ) for the benchmark molecules with ZORA-LC-BLYP\*/TZ2P/COSMO (toluene) level of theory.

Benchmark molecule	Optimum $\gamma$
<b>B1</b>	0.28
<b>B2</b>	0.26
<b>B3</b>	0.28
<b>B4</b>	0.28
<b>B5</b>	0.26
<b>B6</b>	0.26
<b>B7</b>	0.26
<b>B8</b>	0.28



### 6.6.1.5 Excited State Calculations

Vertical or Franck-Condon excitation energies (FC- $S_n$  and FC- $T_n$ ) were calculated using the optimally tuned LC-BLYP\* functional (where \* denotes the tuned LC-BLYP functional) in combination with the TZ2P basis set within the Tamm-Dancoff approximation (TDA). This approximation was employed as it saves computational time and avoids triplet instability issues.<sup>[364, 366, 367]</sup> We did not use a frozen core approximation, in other words, all the electrons were correlated. To account for the solvation effect, we used the non-equilibrium solvation model described in COSMO with toluene as the condensed phase (see Modeling Solvent section). Non-equilibrium solvation is necessary to account for the slow relaxation of the solvent nuclei compared to its electrons. For this purpose, only the optical part of the dielectric constant (dynamic dielectric constant) is considered in the TDA calculations, which in the case of toluene, corresponds to a value of 2.24. For **B4–B8** we used a fixed dynamic dielectric constant of 2.0 as the change in the excitation energies is negligible with change in the dynamic dielectric constant parameter.<sup>[392]</sup>

### 6.6.1.6 Phosphorescence Emission Energy

To obtain the relaxed ground triplet state ( $T_1$ ) we employed unrestricted Kohn-Sham (UKS) at the LC-BLYP\*/TZ2P level of theory with no frozen core approximation. Again, these calculations were performed using the equilibrium COSMO solvation model with toluene as the solvent except for **B4–B8**, which were computed at their respective permittivity noted in Table 6.11. We also performed single point energy calculations using RKS at the optimized  $T_1$  geometry to estimate the  $S_0 \leftarrow T_1$  vertical emission energy  $\Delta E_{VE}(T_1)$ . The difference between the energies obtained from the latter calculation and the relaxed  $T_1$  state provides  $\Delta E_{VE}(T_1)$ , the phosphorescence emission energy maximum. To comment on the nature of the relaxed  $T_1$  excited state, we plotted electron difference density profile ( $\Delta\rho = \rho_{T_1}(T_1) - \rho_{S_0}(T_1)$ ) which is essential to map the relaxed  $T_1$  qualitatively to the corresponding FC- $T_n$  state (Figure 6.59 and Figure 6.60). We found, in all cases, that the relaxed  $T_1$  state is essentially a  ${}^3CT$  state (except for **B7** in the benchmark systems). A similar situation has been observed previously in other systems in which the  ${}^3CT$  state is lower in energy than the  ${}^3LE$  state.<sup>[372]</sup>

### 6.6.1.7 Fluorescence Emission Energy

The geometrical reorganization energy  $\lambda_r(T_1)$ , or the  $T_1$  relaxation energy, is determined by the energy difference between the LC-BLYP\* relaxed  $T_1$  state and the corresponding FC- $T_n$  state. This leads to correct local minima for computing accurate  $\lambda_r(T_1)$ . To see how much the change in geometry changes the optimal  $\gamma$  we again performed the self-consistent tuning of the  $\gamma$  parameter on some test cases. We found that the change in the optimal  $\gamma$  value is negligible and so is the change in vertical excitation energies. The  $S_0 \leftarrow S_1$  emission energy ( $\Delta E(S_1)$ ) was approximated as the difference between the FC- $S_1$  and the  $\lambda_r(T_1)$ . This protocol of estimating the fluorescence emission energy involves approximations. First, we assume that the relaxation of CT states, or a mixture thereof, is larger than the LE state due to the electron and hole occupying different regions in space leading to more reorganization of the electron density upon relaxation, which is generally the case. Moreover, the transitions to  $^3CT$  corresponding to the relaxed  $T_1$  and  $^1CT$  are composed mostly of the same pair of MOs, e.g., HOMO  $\rightarrow$  LUMO (Table 6.13, except for **B7**). Second, the  $\Delta E(S_1)$  computed from the above-mentioned formalism is blue-shifted as it does not correspond to the true vertical emission energy maximum, but resembles the adiabatic energy or the onset of fluorescence emission ( $\Delta E^{0-0}(S_1)$ ) without the zero-point vibrational energy (ZPVE) correction term. Figure 6.53 describes the approximations and the formalism used to approximate the fluorescence emission energy ( $\Delta E(S_1)$ ). As it is not the vertical emission energy, we refrain from calling it so, and thus named it  $\Delta E(S_1)$ .

### 6.6.1.8 LE/CT Gaps

The mechanism of TADF might involve several higher excited states which have small energy gaps between them resulting in a dynamic equilibrium with each other.<sup>[24, 41, 45-47, 393, 394]</sup> As a result, the kinetics of the individual steps involved in the reverse intersystem crossing (rISC) depends intricately on the energy gaps between these excited states. Therefore, we benchmarked and report three gaps (differences in vertical excitation energies obtained from TDA-LC-BLYP\*) in this study:  $\Delta E_{1CT-3CT}$ ,  $\Delta E_{1CT-3LE}$ , and  $\Delta E_{3LE-3CT}$ . Here  $^3CT$  denotes the FC- $T_n$  corresponding to the relaxed  $T_1$  state and  $^3LE$  denotes the lowest FC- $T_n$  with predominant LE character. An important aspect which is often overlooked when benchmarking the S-T gaps is the actual method of measurement involved to extract the experimental gaps. Thus, the gap can be extracted in two ways, first from fitting the integrated delayed fluorescence (DF) emission as a function of temperature which gives the activation energy ( $\Delta E_a^{TADF}$ ), and second,

from the difference between the onset of fluorescence and phosphorescence signals which is defined as the optical gap. Recently, Gibson and Penfold reported how non-adiabatic coupling derived from the involvement of an intermediate triplet state can reduce the activation energy in the rISC process and can give rise to two different energy gaps corresponding to the optical gap and the activation energy.<sup>[373-375]</sup> For this reason, the experimentally measured gap can change depending on the type of measurement performed and so it becomes highly crucial to benchmark the correct gap. As such, the gap obtained from the activation energy measurements correspond to  $\Delta E_{1_{CT}-3_{CT}}$ , while the optical gap corresponds to  $\Delta E_{1_{CT}-3_{LE}}$ . Compound **B8** serves as the perfect example to demonstrate the effect of comparing the correct computed gap with the experimental S-T gap. In this case, Kaji and coworkers<sup>[54]</sup> measured the gap using the activation energy obtained from the Arrhenius plot, so,  $\Delta E_{1_{CT}-3_{CT}}$  corresponds to the measured gap resulting in an error of 0.06 eV, while comparing  $\Delta E_{1_{CT}-3_{LE}}$  results in an error of 0.22 eV. The third gap  $\Delta E_{3_{LE}-3_{CT}}$  determines the strength of the non-adiabatic coupling between the triplet states involved in the reverse internal conversion (rIC). Smaller  $\Delta E_{3_{CT}-3_{LE}}$  facilitates faster  $k_{rISC}$ .<sup>[45, 374]</sup>

## Experimental

Table 6.13: Calculated photophysical data for **B1-B8**. The table shows the vertical excitation energies (in eV and nm) with its corresponding, charge transfer metrics ( $\Lambda$  and  $R_{ch}$  in Å), assignment of the excited states along with the MO composition (configuration interaction, CI) of the transition (in %), the computed S–T gaps and the emission energies ( $\Delta E(S_1)$  and  $\Delta E_{VE}(T_1)$ ) in eV and nm. Experimental values in curly brackets. Fields in bold represents the mapping of the FC- $T_n$  state corresponding to the relaxed  $T_1$  state according to the difference density plots.

Cpd.	State	Energy		Assign.	CI (%)	$\Lambda^a)$	$R_{ch}^b)$ [Å]	$\Delta E_{CT \rightarrow LE}$ [eV]	$\Delta E_{CT \rightarrow CT}$ [eV]	$\Delta E_{CT-}$ [eV]
		[eV]	[nm]							
<b>B1</b>	<b>FC-<math>T_1</math></b>	<b>3.21</b>	<b>386</b>	$^3CT/^3LE_{\pi}$	<b>H<math>\rightarrow</math>L (57), H-7<math>\rightarrow</math>L (17)</b>	<b>0.47</b>	<b>3.71</b>	0.36 {0.46}	0.46	0.10
	FC- $T_2$	3.31	375	$^3LE_A/^3CT$	H-2 $\rightarrow$ L (81)	0.52	2.02			
	FC- $T_3$	3.45	359	$^3LE_A$	H-3 $\rightarrow$ L(60)	0.57	1.01			
	FC- $T_4$	3.45	359	$^3LE_D$	H $\rightarrow$ L+1 (88)	0.62	1.29			
	FC- $T_5$	3.54	350	$^3LE_D$	H-1 $\rightarrow$ L+1(85)	0.76	0.02			
	FC- $S_1$	3.67	338	$^1CT$	H $\rightarrow$ L (70), H-3 $\rightarrow$ L (17)	0.42	3.87			
	$\Delta E(S_1)$	3.37 {3.13}	368 {398}	-						
$\Delta E_{VE}(T_1)$	2.65 {2.81}	468 {442}	$^3CT/^3LE_{\pi}$							
<b>B2</b>	<b>FC-<math>T_1</math></b>	<b>3.20</b>	<b>388</b>	$^3CT$	<b>H<math>\rightarrow</math>L (84)</b>	<b>0.14</b>	<b>5.82</b>	0.04 {0.04}	0.01	0.05
	FC- $S_1$	3.21	386	$^1CT$	H $\rightarrow$ L (87)	0.13	6.04			
	FC- $T_2$	3.25	382	$^3LE_A$	H-1 $\rightarrow$ L(84)	0.52	1.85			
	FC- $T_3$	3.35	370	$^3LE_A$	H-2 $\rightarrow$ L(77)	0.57	1.35			
	FC- $T_4$	3.44	360	$^3LE_D$	H $\rightarrow$ L+4(65)	0.60	1.27			
	FC- $T_5$	3.57	347	$^3LE_D$	H $\rightarrow$ L+3(90),	0.65	0.08			
	$\Delta E(S_1)$	2.70 {2.66}	459 {466}	-						
$\Delta E_{VE}(T_1)$	2.45 {2.66}	506 {466}	$^3CT$							
<b>B3</b>	FC- $T_1$	3.07	404	$^3LE_D$	H $\rightarrow$ L+2 (40), H $\rightarrow$ L+1 (33)	0.51	2.75	0.05 {0.03}	0.02	0.03
	<b>FC-<math>T_2</math></b>	<b>3.10</b>	<b>400</b>	$^3CT$	<b>H<math>\rightarrow</math>L (79)</b>	<b>0.19</b>	<b>5.64</b>			
	FC- $S_1$	3.12	397	$^1CT$	H $\rightarrow$ L(85)	0.17	5.88			
	FC- $T_3$	3.27	379	$^3LE_A$	H-1 $\rightarrow$ L(83)	0.51	1.92			
	FC- $T_4$	3.37	368	$^3LE_A$	H-2 $\rightarrow$ L(70)	0.54	0.73			
	FC- $T_5$	3.46	358	$^3LE_D$	H $\rightarrow$ L+6(32), H $\rightarrow$ L+1(26)	0.5	2.86			
	$\Delta E(S_1)$	2.48 {2.49}	500 {498}	-						
$\Delta E_{VE}(T_1)$	2.25 {2.45}	551 {506}	$^3CT$							
<b>B4</b>	FC- $T_1$	3.27	379	$^3LE_{\pi}$	H-3 $\rightarrow$ L (81)	0.63	0.81	0.03 {0.10}	0.02	0.01
	<b>FC-<math>T_2</math></b>	<b>3.28</b>	<b>378</b>	$^3CT$	<b>H<math>\rightarrow</math>L (74)</b>	<b>0.23</b>	<b>5.04</b>			
	FC- $S_1$	3.30	376	$^1CT$	H $\rightarrow$ L(85)	0.17	5.66			
	FC- $T_3$	3.48	356	$^3LE_D$	H $\rightarrow$ L+4(56), H $\rightarrow$ L+2(23)	0.54	2.23			
	FC- $T_4$	3.61	343	$^3LE_D$	H $\rightarrow$ L+3(91)	0.65	0.18			
	FC- $T_5$	3.76	330	$^3LE_{\pi}$	H-6 $\rightarrow$ L(51), H-7 $\rightarrow$ L(20)	0.59	1.16			
	$\Delta E(S_1)$	2.85 {2.97}	435 {417}	-						
$\Delta E_{VE}(T_1)$	2.64 {2.87}	470 {432}	$^3CT$							

-Table 6.13 cont.-

B5	FC-T <sub>1</sub>	3.23	384	<sup>3</sup> LE <sub>A</sub>	H-4→L (89)	0.67	0.62	0.19 {0.12}	0.03	0.16
	FC-T <sub>2</sub>	3.27	379	<sup>3</sup> LE <sub>D</sub>	H→L+1 (90)	0.67	0.26			
	<b>FC-T<sub>3</sub></b>	<b>3.39</b>	<b>366</b>	<sup>3</sup> CT	<b>H→L(78)</b>	<b>0.21</b>	<b>5.76</b>			
	FC-T <sub>4</sub>	3.50	354	<sup>3</sup> LE <sub>A</sub>	H-1→L+1(81)	0.72	0.56			
	FC-S <sub>1</sub>	3.42	363	<sup>1</sup> CT	H→L(87)	0.16	6.24			
	FC-T <sub>5</sub>	3.72	333	<sup>3</sup> LE <sub>A</sub>	H-2→L(88),	0.24	3.7			
	ΔE(S <sub>1</sub> )	2.96 {3.11}	419 {399}							
ΔE <sub>VE</sub> (T <sub>1</sub> )	2.72 {2.99}	456 {415}	<sup>3</sup> CT							
B6	FC-T <sub>1</sub>	3.24	383	<sup>3</sup> LE <sub>A</sub>	H-3→L (87)	0.62	1.62	0.08 {0.06}	0.02	0.06
	<b>FC-T<sub>2</sub></b>	<b>3.30</b>	<b>376</b>	<sup>3</sup> CT	<b>H→L(79)</b>	<b>0.17</b>	<b>5.4</b>			
	FC-S <sub>1</sub>	3.32	373	<sup>1</sup> CT	H→L (86)	0.15	5.71			
	FC-T <sub>3</sub>	3.43	362	<sup>3</sup> LE <sub>D</sub>	H→L+1(64)	0.48	0.55			
	FC-T <sub>4</sub>	3.6	344	<sup>3</sup> LE <sub>D</sub>	H→L+4(91)	0.65	0.42			
	FC-T <sub>5</sub>	3.73	332	<sup>3</sup> CT	H-2→L(92)	0.21	3.9			
	ΔE(S <sub>1</sub> )	2.93 {3.01}	423 {412}							
ΔE <sub>VE</sub> (T <sub>1</sub> )	2.68 {2.95}	463 {420}	<sup>3</sup> CT							
B7	FC-T <sub>1</sub>	3.00	413	<sup>3</sup> LE <sub>D</sub>	H→L+1 (82)	0.56	2.25	0.48	0.36 {0.06}	0.12
	<b>FC-T<sub>2</sub></b>	<b>3.12</b>	<b>397</b>	<sup>3</sup> LE <sub>π</sub> / <sup>3</sup> CT	<b>H-1→L (29), H-4→L (25), H→L (16)</b>	<b>0.42</b>	<b>4.28</b>			
	FC-T <sub>3</sub>	3.14	395	<sup>3</sup> LE <sub>A</sub>	H-3→L(86)	0.57	1.42			
	FC-T <sub>4</sub>	3.30	376	<sup>3</sup> LE <sub>D</sub>	H→L+3(75)	0.58	1.73			
	FC-T <sub>5</sub>	3.35	370	<sup>3</sup> LE <sub>A</sub>	H-4→L(43)	0.56	1.18			
	FC-T <sub>6</sub>	3.43	362		H→L(8)	0.63	0.94			
	FC-S <sub>1</sub>	3.46	358	<sup>1</sup> LE <sub>D</sub>	H-2→L+1(24), H-2→L+6(22)	0.56	2.51			
	FC-S <sub>2</sub>	3.48	356	<sup>1</sup> LE <sub>D</sub> / <sup>1</sup> CT	H→L+1(86)	0.35	5.73			
	ΔE(S <sub>1</sub> )	3.09 {2.60}	401 {477}							
ΔE <sub>VE</sub> (T <sub>1</sub> )	2.44	508	<sup>3</sup> LE <sub>π</sub> / <sup>3</sup> CT							
B8	FC-T <sub>1</sub>	3.03	409	<sup>3</sup> LE <sub>D</sub>	H→L+1 (66), H→L+3 (25)	0.61	1.27	0.34	0.01 {0.07}	0.33
	FC-T <sub>2</sub>	3.15	394	<sup>3</sup> LE <sub>A</sub>	H-1→L (86)	0.57	1.32			
	FC-T <sub>3</sub>	3.26	380	<sup>3</sup> LE <sub>A</sub>	H-2→L(83)	0.63	0.61			
	<b>FC-T<sub>4</sub></b>	<b>3.36</b>	<b>369</b>	<sup>3</sup> CT	<b>H→L(76)</b>	<b>0.12</b>	<b>6.42</b>			
	FC-S <sub>1</sub>	3.37	368	<sup>1</sup> CT	H→L(80)	0.1	6.66			
	FC-T <sub>5</sub>	3.45	359	<sup>3</sup> LE <sub>D</sub>	H→L+3(48), H→L+1(12)	0.5	2.81			
	ΔE(S <sub>1</sub> )	2.51 {2.43}	494 {509}							
	ΔE <sub>VE</sub> (T <sub>1</sub> )	2.26	549	<sup>3</sup> CT						

a) Degree of spatial overlap between occupied and virtual orbitals involved in the excitation:  $\Lambda = \frac{\sum_{i,a} c_{i,a}^2 \langle \psi_a | \psi_i \rangle}{\sum_{i,a} c_{i,a}^2}$

b) Hole-electron distance:  $R_{eh} = \frac{\sum_{i,a} c_{i,a}^2 |\langle \psi_a | r | \psi_i \rangle - \langle \psi_i | r | \psi_a \rangle|}{\sum_{i,a} c_{i,a}^2}$

## Experimental

Table 6.14: Statistical parameters (signed error, mean deviation, and mean absolute deviation, all in eV) based on benchmarking the S–T gap and emission energies for all of the benchmark molecules. Left: including compound **B7**; right: without **B7**.

Molecule	$\Delta\Delta E_{S-T}$	$\Delta\Delta E(S_1)$	$\Delta\Delta E_{VE}(T_1)$
<b>B1</b>	-0.10	0.24	-0.16
<b>B2</b>	0.00	0.04	-0.21
<b>B3</b>	0.02	-0.01	-0.20
<b>B4</b>	-0.07	-0.12	-0.23
<b>B5</b>	0.07	-0.15	-0.27
<b>B6</b>	0.02	-0.08	-0.27
<b>B7</b>	0.30	0.49	–
<b>B8</b>	-0.06	0.08	–
MD	-0.02	0.00	-0.22
MAD	0.05	0.10	0.22

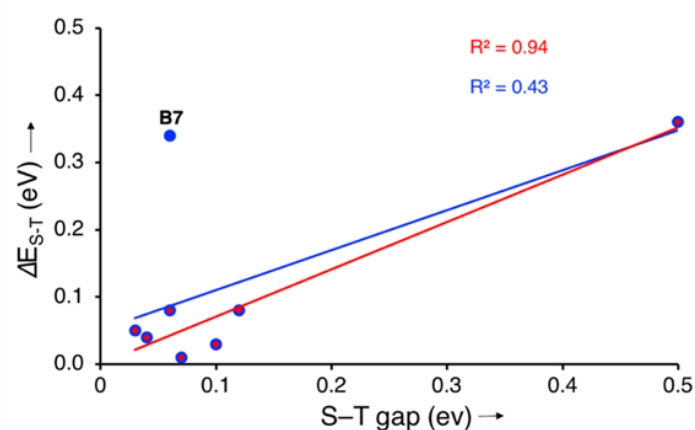


Figure 6.55: Correlation between the experimentally obtained S–T gap and the computed gap  $\Delta E_{S-T}$ . Linear fit in blue fits all molecules in the benchmark test set while the linear fit in red excludes **B7**.

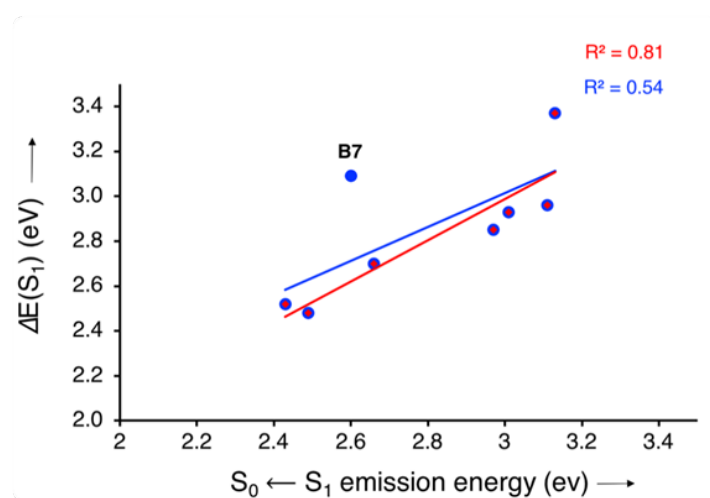


Figure 6.56: Correlation between the experimentally obtained  $S_0 \leftarrow S_1$  emission energy and the computed fluorescence emission energy  $\Delta E(S_1)$ . Linear fit in blue fits all molecules in the benchmark test set while the linear fit in red excludes **B7**.

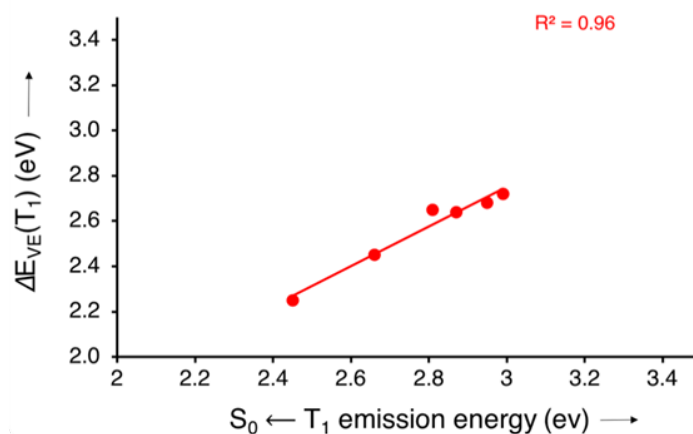


Figure 6.57: Correlation between the experimentally obtained  $S_0 \leftarrow T_1$  emission energy and the computed phosphorescence emission energy  $\Delta E_{VE}(T_1)$ .

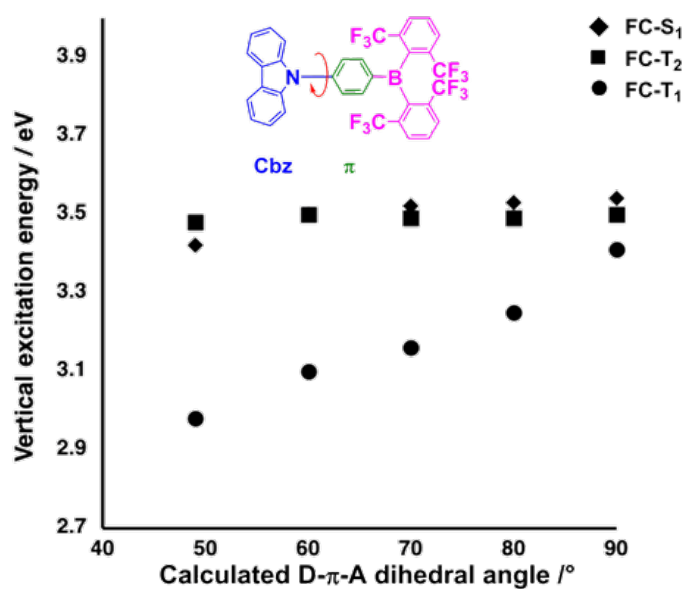


Figure 6.58: Modulation of calculated excited state energy levels upon increase in the torsional angle in intervals of  $10^\circ$  between the donor (Cbz) and the  $\pi$ -bridge-acceptor (1,4- $C_6H_4$ -B( $F^Xyl$ ) $_2$ ) in **Cbz- $\pi$**  (**1**).

Table 6.15: Frontier molecular orbital energies and HOMO–LUMO gaps of the various donors and bridges used in the model systems computed at the BLYP-D3(BJ)/TZ2P/COSMO (toluene) level.

Donor	HOMO [eV]	LUMO [eV]	$\Delta E_{H-L}^D$ [eV]
MeO <sub>2</sub> Ph-H	-5.2	-0.6	4.6
Cbz-H	-5.0	-1.8	3.2
MeCbz-H	-4.9	-1.6	3.3
Phox-H	-4.3	-1.4	2.9
$\pi$ -Bridge			$\Delta E_{H-L}^\pi$ [eV]
<sup>FM</sup> e $\pi$ -H <sub>2</sub>	-7.2	-2.4	4.8
$\pi$ -H <sub>2</sub>	-6.3	-1.2	5.1
<sup>Me</sup> e $\pi$ -H <sub>2</sub>	-5.8	-1.0	4.8
<sup>MeO</sup> e $\pi$ -H <sub>2</sub>	-5.1	-0.9	4.2

### 6.6.1.9 Discussion

The optimal  $\gamma$  values for all benchmark molecules fall in a very small window between 0.26-0.28  $a_0^{-1}$  (Table 6.12). This would mean that the interelectronic distance where the DFT exchange at short-range changes to HF exact exchange at long-range is very similar in these systems. Table 6.14 lists the performance of our formalism to compute the S–T gap and the emission energies based on statistical parameters such as the mean deviation (MD) and mean absolute deviation (MAD). Our results show excellent accuracy to predict the S–T gap with an MD of 0.02 eV and an MAD of 0.08 eV. The maximum error is found for **B7** (0.30 eV). This large error stems from the difficulty in assigning the correct  $^3\text{CT}$  state which relaxes to  $T_1$  resulting from a heavy mixing between  $^3\text{LE}$  and  $^3\text{CT}$ . In this case, the excited states are either heavily mixed together with no predominant pair of MOs involved in the transition, or the assignment of the transition based on  $\Lambda$  and  $R_{\text{eh}}$  parameters is inconclusive. We selected FC-S<sub>2</sub> as the state with higher CT character and the state which relaxes to relaxed S<sub>1</sub> state due to favorable  $\Lambda$  and  $R_{\text{eh}}$  parameters ( $\Lambda = 0.345$  vs. 0.555 and  $R_{\text{eh}} = 5.73 \text{ \AA}$  vs 2.51  $\text{\AA}$ ) as well as close-lying energies (0.02 eV), compared to FC-S<sub>1</sub>, albeit the assignment is not strictly  $^1\text{CT}$ . Considering the composition of the transitions based on MOs, FC-T<sub>2</sub> is composed of a heavy mixture of MOs which are similar to that of FC-S<sub>2</sub> and contains a small component from HOMO  $\rightarrow$  LUMO (33% and 16% in case of FC-S<sub>2</sub> and FC-T<sub>2</sub>, respectively) indicating a small CT nature in both states. However, the MO composition of the transition to FC-T<sub>5</sub> also has a small HOMO  $\rightarrow$  LUMO component (7%), but the charge transfer metrics are unfavorable compared to FC-T<sub>2</sub>. Mapping the difference density profile of the relaxed  $T_1$  state (Figure 6.59: Mapping difference density profiles ( $\Delta\rho$ ) plotted at isovalue =  $\pm 0.002 [e a_0^{-3}]^{1/2}$  (hole density in blue and the electron density in red) with the NTO of the corresponding FC-T<sub>n</sub> state plotted at isovalue =  $\pm 0.05 [e a_0^{-3}]^{1/2}$  for all the benchmark systems.) provides the closest match to the NTO derived from FC-T<sub>2</sub> state, thereby indicating FC-T<sub>2</sub> might be the relaxed  $T_1$  state. We also considered higher FC-T<sub>n</sub> states where  $n > 5$ , but, all of them were predominantly  $^3\text{LE}$  in nature. Therefore, we assumed FC-S<sub>2</sub> and FC-T<sub>2</sub> to be the relaxed  $^1\text{CT}$  and  $^3\text{CT}$  state, respectively. As expected, removing **B7** from our test set gave an excellent linear relationship (correlation coefficient  $R^2 = 0.94$ ) and an excellent MAD of 0.05 eV. So, overall, our protocol can successfully predict the gap in unknown molecules, except in cases in which the transitions are composed of heavily mixing of MOs, and assigning the nature of the transition becomes problematic.



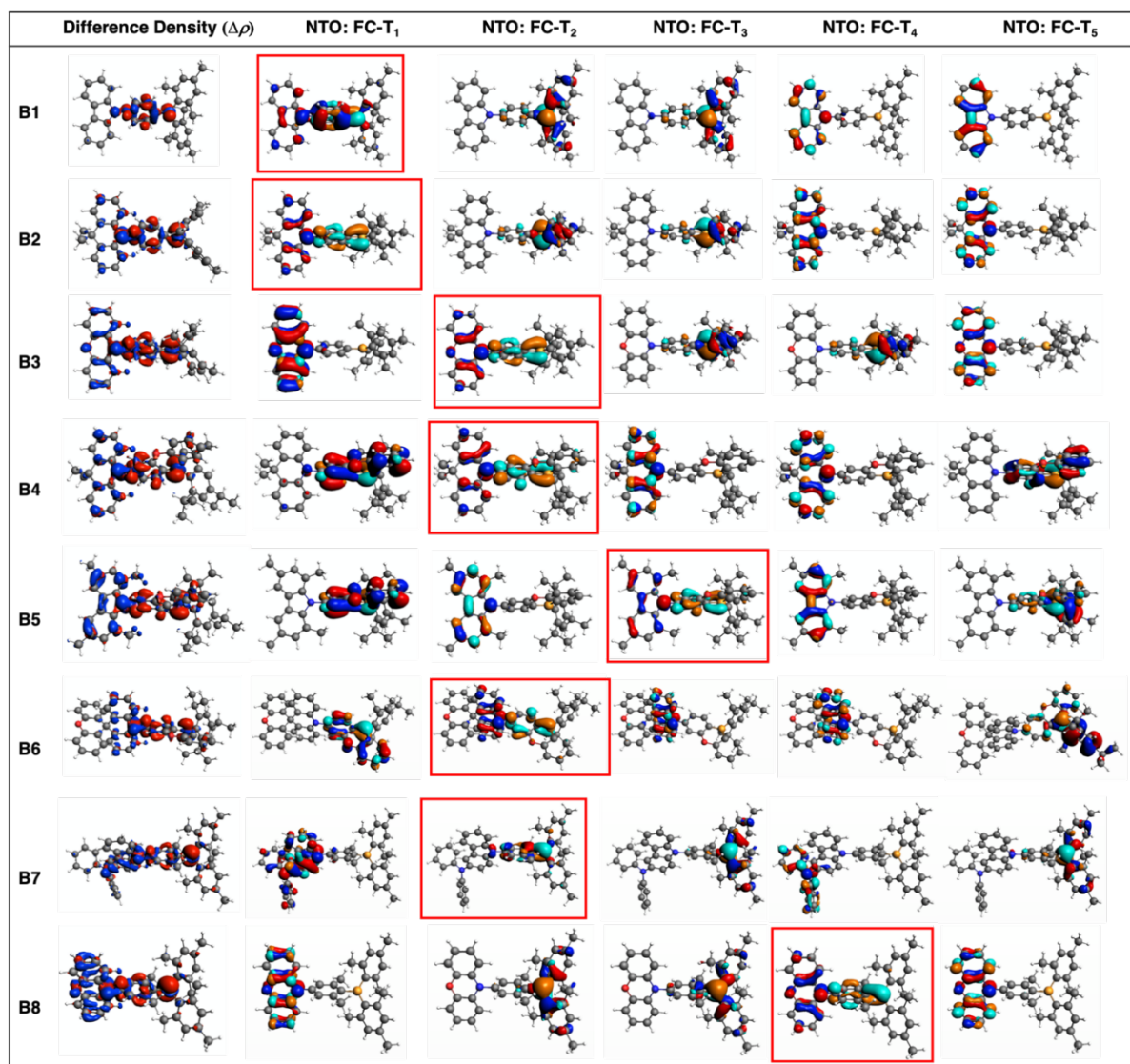


Figure 6.59: Mapping difference density profiles ( $\Delta\rho$ ) plotted at isovalue =  $\pm 0.002 [e a_0^{-3}]^{1/2}$  (hole density in blue and the electron density in red) with the NTO of the corresponding FC-T<sub>n</sub> state plotted at isovalue =  $\pm 0.05 [e a_0^{-3}]^{1/2}$  for all the benchmark systems.

Due to the approximations involved,  $\Delta E(S_1)$  exhibits a larger variation in errors with MD and MAD of 0.10 eV and 0.15 eV, respectively. The small deviation is a result of the cancellation of errors emerging mostly from a large overestimation for **B7** (0.47 eV) and consistent small underestimation for **B4**, **B5** and **B6** ( $\approx -0.12$  eV). Poor performance of our protocol to estimate the fluorescence energy of **B7** is again due to ambiguous assignment of the FC-S<sub>2</sub> as the relaxed S<sub>1</sub> state, details of which are mentioned above. Therefore, our approximation of equating  $\lambda_r(T_1)$  and  $\lambda_r(S_1)$  is very poor in this case, which is reflected in a large error in predicting the fluorescence energy maximum. Interestingly, **B2** and **B3** show a very small deviation which might be due to cancellation of errors. For example, if  $\lambda_r(T_1)$  is larger than the true  $\lambda_r(S_1)$ , a cancellation of red-shift, and blue-shift originating from the emission energy resembling more  $\Delta E^{0-0}(S_1)$ , can occur which might, fortunately, lead to better estimation of the fluorescence

## Experimental

energy maximum. On the other hand, if  $\lambda_r(T_1)$  is smaller than the true  $\lambda_r(S_1)$ , then the blue-shift adds up and might lead to more error-prone results as for **B1** or **B7**. But, fortunately, barring **B7**, the errors are quite small with MAD of 0.10 eV, which means our approximations work very well for the rest of the molecules. However, the correlation between  $\Delta E(S_1)$  and the experimental emission energy is very poor ( $R^2 = 0.53$ ) but, when **B7** is removed from our test set, the correlation increases to  $R^2 = 0.81$  (see Figure 6.56). This stems from irregular estimations of the emission energy. As a result, our methodology for predicting the fluorescence energy maximum should be used carefully for benchmarking purposes, but it can definitely provide a good prediction of the color of the prompt or the delayed emission.

Statistically speaking, all of the computed  $\Delta E_{VE}(T_1)$  are underestimated, leading to an MD and an MAD of 0.22 eV (Table 6.14). The underestimation might be the result of using the optimal  $\gamma$  value calculated from ground state geometry to optimize the  $T_1$  state. However, an excellent correlation of 0.96 (Figure 6.57) suggests that the error is systematic and, hence, can be corrected. Correcting the raw  $\Delta E_{VE}(T_1)$  by the MAD, reduces the resulting unsigned error from 0.220 eV to 0.003 eV. Overall, our methodology can predict the phosphorescence emission energy maximum of an unknown model system belonging to a similar class of benchmark systems with an unsigned error of 0.22 eV.

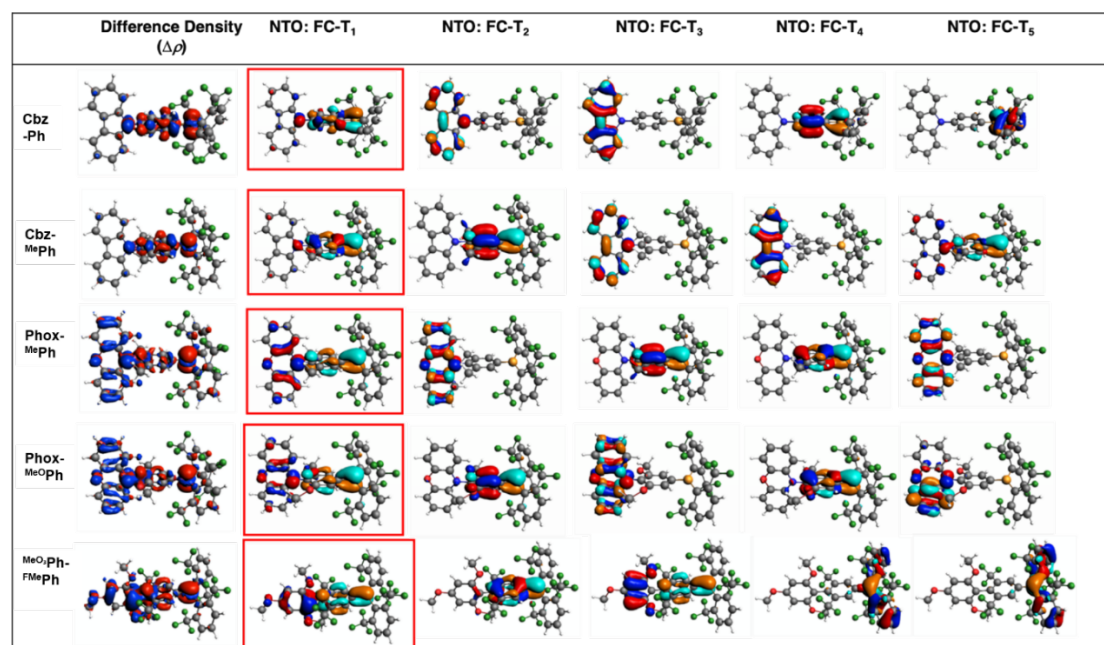


Figure 6.60: Mapping difference density profiles ( $\Delta\rho$ ) plotted at isovalue =  $\pm 0.002 [e a_0^{-3}]^{1/2}$  (hole density in blue and the electron density in red) with the NTO of the corresponding FC- $T_n$  state plotted at isovalue =  $\pm 0.05 [e a_0^{-3}]^{1/2}$  for the synthesized model systems.

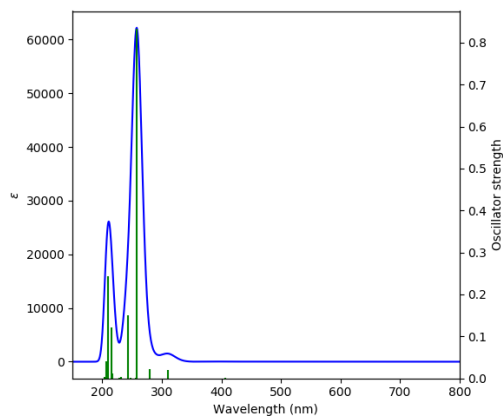
## 6.6.2 Chapter 2

All calculations (DFT and TD-DFT) were carried out with the Gaussian 09 (9.E.01)<sup>[395]</sup> program package and were performed on a parallel cluster system. GaussView (6.0.16) and multiwfn<sup>[396]</sup> were used to visualize the results, to measure calculated structural parameters, and to plot orbital surfaces (isovalue:  $\pm 0.030 [e a_0^{-3}]^{1/2}$ ). The ground-state geometries were optimized using the B3LYP functional<sup>[397]</sup> in combination with the 6-31+G(d) basis set.<sup>[398, 399]</sup> The D3 dispersion correction of Grimme and coworkers was used.<sup>[349]</sup> The polarizable continuum model (PCM) was used to include solvent effects for the ground state structures. The ultrafine integration grid and symmetry constraints were used for all molecules. Frequency calculation were performed on the optimized structures to confirm them to be local minima showing no negative (imaginary) frequencies. Based on these optimized structures, the lowest-energy vertical transitions (gas-phase and solvent correction using the polarizable continuum model) were calculated (singlets, 25 states) by TD-DFT, using the Coulomb attenuated functional CAM-B3LYP<sup>[229]</sup> as well as B3LYP. The CAM-B3LYP has been shown to more accurately describe ICT systems in comparison to B3LYP.<sup>[228]</sup> The optimized ground-state geometries were used as starting coordinates for TD-DFT geometry optimizations. The  $S_1$  states of  ${}^F\text{Mes}{}^F\text{Bf}$  and  ${}^F\text{Xyl}{}^F\text{Bf}$  were optimized using eight excited states with the B3LYP functional in combination with the 6-31+G(d) basis set and D3 dispersion correction and no symmetry constraints. The  $S_1$  state of  $p\text{-NMe}_2\text{-}{}^F\text{Xyl}{}^F\text{Bf}$  was optimized using eight states with the CAM-B3LYP functional in combination with the 6-31+G(d) basis set and D3 dispersion correction and no symmetry constraints.

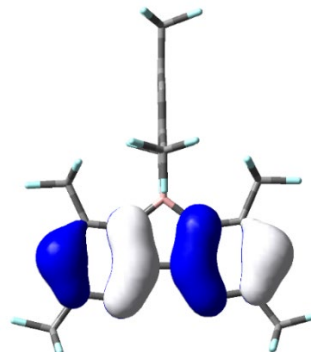
## Experimental

### 6.6.2.1 <sup>F</sup>Mes<sup>F</sup>Bf

#### Calculated absorption spectrum

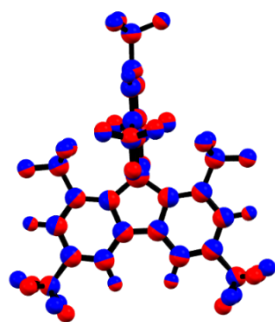


#### Orbitals relevant to the S<sub>1</sub>←S<sub>0</sub> transition

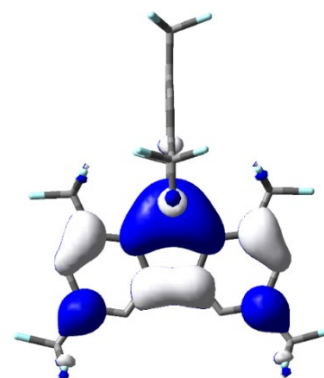


**HOMO: -7.65 eV**

#### TD-DFT B3LYP/6-31+G(d), gas phase



**Overlap S<sub>0</sub>(blue)-S<sub>1</sub>(red)**



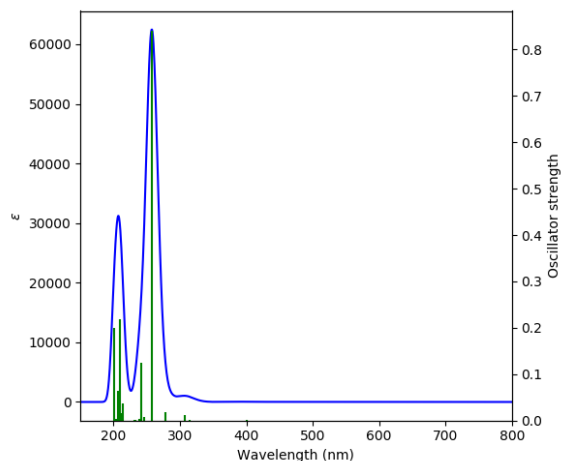
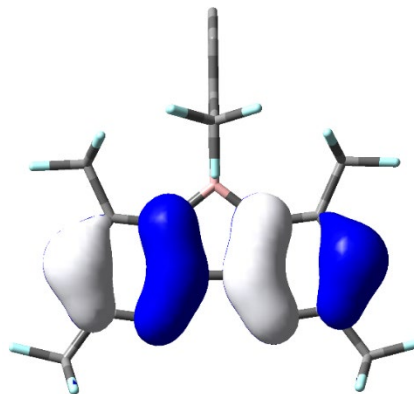
**LUMO: -3.80 eV**

Table 6.16: Lowest energy singlet electronic transition of <sup>F</sup>Mes<sup>F</sup>Bf (TD-DFT B3LYP/6-31+G(d), gas phase).

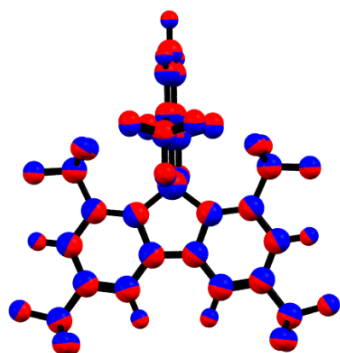
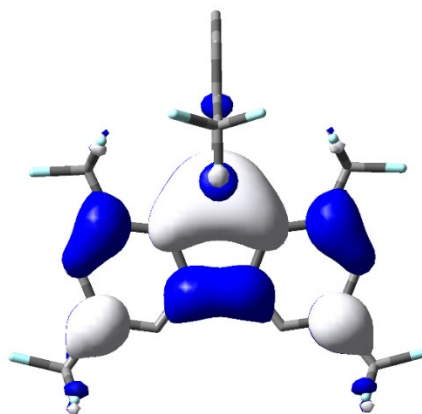
State	E [eV]	λ [nm]	<i>f</i>	Symmetry	Major contributions	Λ
1	3.05	406.32	0.0005	A'	HOMO->LUMO (99%)	0.65
2	3.90	317.96	0	A''	H-1->LUMO (99%)	0.25
3	4.00	309.72	0.0206	A'	H-2->LUMO (73%), HOMO->L+1 (25%)	0.70
4	4.18	296.91	0	A'	H-3->LUMO (97%)	0.26
5	4.44	279.17	0.0217	A'	H-4->LUMO (80%), HOMO->L+4 (12%)	0.77
6	4.80	258.23	0	A''	HOMO->L+3 (100%)	0.10
7	4.80	258.17	0.8333	A'	H-2->LUMO (24%), HOMO->L+1 (70%)	0.73
8	4.85	255.73	0.0005	A'	HOMO->L+2 (99%)	0.07

6.6.2.2 <sup>F</sup>Xyl<sup>F</sup>Bf

## Calculated absorption spectrum

Orbitals relevant to the  $S_1 \leftarrow S_0$  transitionHOMO:  $-7.49$  eV

## TD-DFT B3LYP/6-31+G(d), gas phase

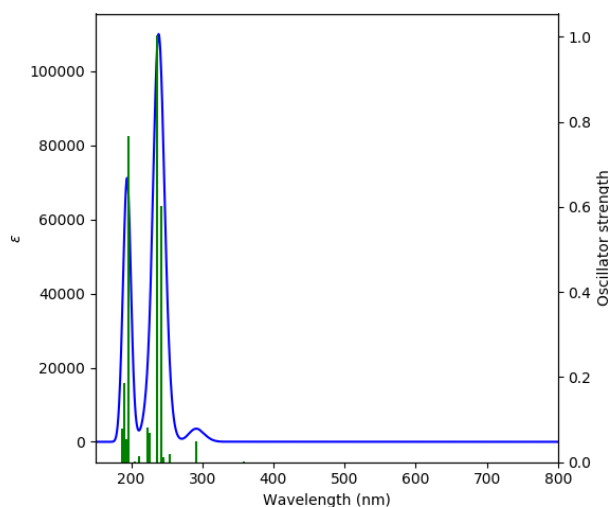
Overlap  $S_0$ (blue)- $S_1$ (red)LUMO:  $-3.60$  eVTable 6.17: Lowest energy singlet electronic transition of <sup>F</sup>Xyl<sup>F</sup>Bf (TD-DFT B3LYP/6-31+G(d), gas phase).

State	E [eV]	$\lambda$ [nm]	$f$	Symmetry	Major contributions	$\Lambda$
1	3.09	400.88	0.0006	B <sub>2</sub>	HOMO→LUMO (99%)	0.66
2	3.64	340.31	0	A <sub>2</sub>	H-1→LUMO (99%)	0.23
3	3.94	314.98	0.0021	B <sub>2</sub>	H-2→LUMO (98%)	0.22
4	4.04	306.75	0.0122	B <sub>2</sub>	H-3→LUMO (70%), HOMO→L+1 (26%)	0.71
5	4.47	277.65	0.0182	A <sub>1</sub>	H-4→LUMO (79%), HOMO→L+3 (13%)	0.77
6	4.81	257.99	0.8413	B <sub>2</sub>	H-3→LUMO (28%), HOMO→L+1 (68%)	0.74
7	4.94	250.76	0	A <sub>2</sub>	H-1→L+1 (99%)	0.11
8	5.03	246.48	0.0083	A <sub>1</sub>	H-5→LUMO (31%), HOMO→L+2 (23%), HOMO→L+3 (36%)	0.60

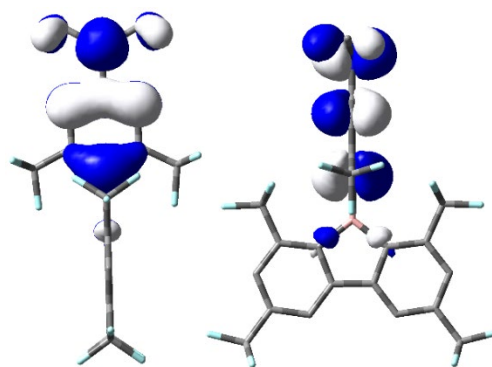
## Experimental

### 6.6.2.3 $p$ -NMe<sub>2</sub>-<sup>F</sup>Xyl<sup>F</sup>Bf

#### Calculated absorption spectrum

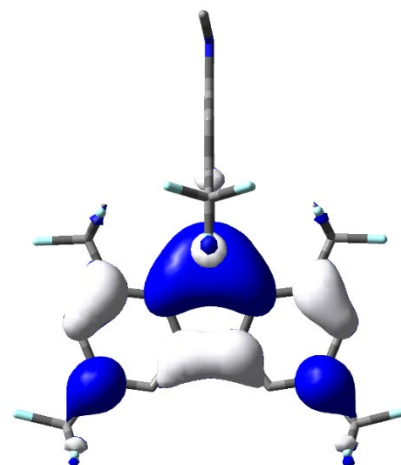


#### Orbitals relevant to the S<sub>1</sub>←S<sub>0</sub> transition



**HOMO: -6.17 eV (B3LYP); -7.53 eV (CAM-B3LYP)**

#### TD-DFT CAM-B3LYP/6-31+G(d), gas phase



**LUMO: -3.41 eV (B3LYP); -2.25 eV (CAM-B3LYP)**

Table 6.18: Lowest energy singlet electronic transition of  $p$ -NMe<sub>2</sub>-<sup>F</sup>Xyl<sup>F</sup>Bf (C<sub>1</sub>) (TD-DFT CAM-B3LYP/6-31+G(d), gas phase).

State	E [eV]	$\lambda$ [nm]	$f$	Symmetry	Major contributions	$\Lambda$
1	3.25	382.07	0	A	HOMO→LUMO (92%)	0.15
2	3.46	358.41	0.0006	A	H-1→LUMO (97%)	0.67
3	4.25	291.56	0.0491	A	HOMO→L+2 (70%), HOMO→L+3 (24%)	0.49
4	4.46	277.94	0	A	H-3→LUMO (49%), H-1→L+1 (41%)	0.71
5	4.84	256.21	0	A	HOMO→L+1 (97%)	0.06
6	4.88	254.09	0.0188	A	H-4→LUMO (53%), H-1→L+3 (18%)	0.71
7	5.04	245.93	0.0127	A	H-2→LUMO (95%)	0.20
8	5.11	242.61	0.6022	A	HOMO→L+4 (86%)	0.71

Table 6.19: Lowest energy singlet electronic transition of *p*-NMe<sub>2</sub>-<sup>F</sup>Xyl<sup>F</sup>Bf (C<sub>2v</sub>) (TD-DFT CAM-B3LYP/6-31+G(d), gas phase).

State	E [eV]	$\lambda$ [nm]	<i>f</i>	Symmetry	Major contributions	$\Lambda$
1	3.22	385.34	0	A <sub>2</sub>	HOMO->LUMO (92%)	0.15
2	3.46	358.29	0.0006	B <sub>2</sub>	H-1->LUMO (97%)	0.67
3	4.23	292.76	0.0507	B <sub>1</sub>	HOMO->L+2 (65%), HOMO->L+3 (29%)	0.48
4	4.46	277.90	0	B <sub>2</sub>	H-3->LUMO (49%), H-1->L+1 (41%)	0.71
5	4.81	257.74	0	A <sub>2</sub>	HOMO->L+1 (97%)	0.06
6	4.88	254.06	0.0182	A <sub>1</sub>	H-4->LUMO (53%), H-1->L+3 (16%)	0.70
7	5.04	246.06	0.0124	B <sub>2</sub>	H-2->LUMO (95%)	0.20
8	5.12	242.09	0.6312	A <sub>1</sub>	HOMO->L+4 (86%)	0.72

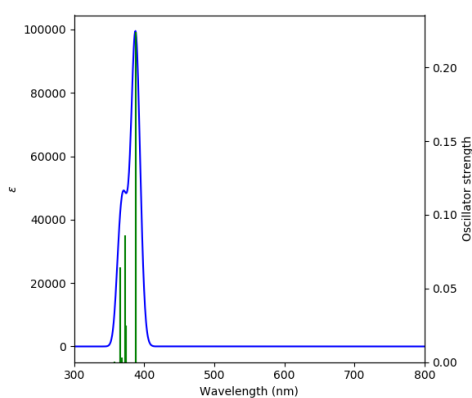
### 6.6.3 Chapter 3

All calculations (DFT and TD-DFT) were carried out with the Gaussian 09 (9.E.01)<sup>[395]</sup> program package and were performed on a parallel cluster system. GaussView (6.0.16), Avogadro (1.2.0)<sup>[400]</sup> and multiwfn<sup>[396]</sup> were used to visualize the results, to measure calculated structural parameters, and to plot orbital surfaces (isovalue:  $\pm 0.030 [e a_0^{-3}]^{1/2}$ ). The ground-state geometries were optimized using the B3LYP functional<sup>[397]</sup> in combination with the 6-31G basis set.<sup>[398, 399]</sup> The ultrafine integration grid and symmetry constraints were used for all molecules. Frequency calculations were performed on the optimized structures to confirm them to be local minima showing no negative (imaginary) frequencies. Based on these optimized structures, the lowest-energy vertical transitions (gas-phase and solvent correction using the polarizable continuum model) were calculated (singlets, at least 12 states) by TD-DFT, using the B3LYP functional in combination with the 6-31G+(d) basis set.



## 6.6.3.1 BG1H

## Calculated absorption spectrum



## TD-DFT B3LYP/6-31+G(d), gas phase

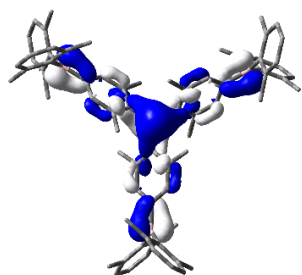
Orbital	Energy [eV]	Symmetry
L+4	-0.55	E
L+3	-1.26	A
L+2	-2.03	E
L+1	-2.03	E
LUMO	-2.64	A
HOMO	-6.44	E
H-1	-6.44	E
H-2	-6.44	A
H-3	-6.45	E
H-4	-6.45	E

Table 6.20: Lowest energy singlet electronic transition of **BG1H** (TD-DFT B3LYP/6-31+G(d), gas phase).

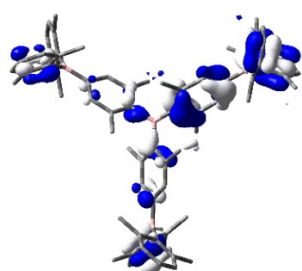
State	E [eV]	$\lambda$ [nm]	$f$	Symmetry	Major contributions	$\Lambda$
1	3.20	387.54	0.2242	E	H-7->LUMO (43%), H-6->LUMO (20%)	0.49
2	3.20	387.54	0.2242	E	H-7->LUMO (20%), H-6->LUMO (43%)	0.49
3	3.32	373.22	0.0248	E	H-6->LUMO (16%), H-4->LUMO (62%)	0.42
4	3.32	373.22	0.0249	E	H-7->LUMO (16%), H-3->LUMO (62%)	0.41
5	3.32	373.08	0.0861	A	H-5->LUMO (83%)	0.36
6	3.36	368.67	0	A	H-2->LUMO (88%)	0.25
7	3.37	368.30	0.0013	A	H-12->LUMO (71%), H-8->LUMO (25%)	0.48
8	3.37	368.26	0.0033	E	HOMO->LUMO (78%)	0.33
9	3.37	368.26	0.0033	E	H-1->LUMO (78%)	0.32
10	3.39	365.41	0.0645	E	H-14->LUMO (73%), H-9->LUMO (15%)	0.49
11	3.39	365.41	0.0645	E	H-13->LUMO (73%), H-10->LUMO (15%)	0.46
12	3.47	357.00	0.0003	E	H-14->LUMO (14%), H-9->LUMO (74%)	0.33

Experimental

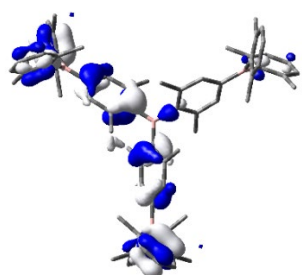
**Orbitals relevant to the  
 $S_1 \leftarrow S_0$  and  $S_2 \leftarrow S_0$   
transition**



**LUMO: -2.637 eV**

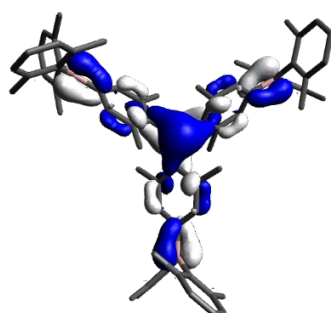


**HOMO-6: -6.484 eV**

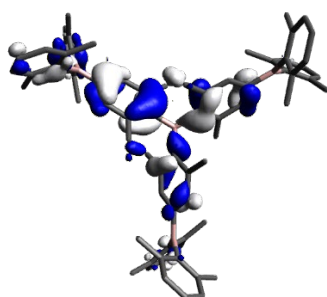


**HOMO-7: -6.484 eV**

**NTOs of the  $S_1 \leftarrow S_0$   
transition**

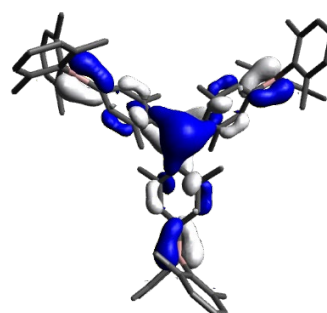


**virtual**

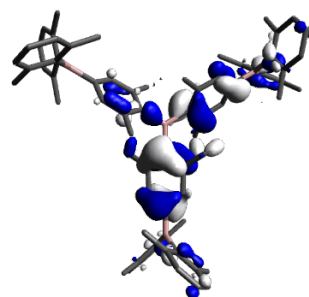


**occupied**

**NTOs of the  $S_2 \leftarrow S_0$   
transition**



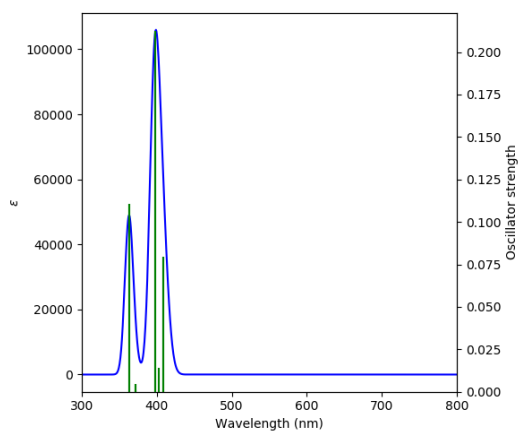
**virtual**



**occupied**

## 6.6.3.2 BFG1H

## Calculated absorption spectrum



## TD-DFT B3LYP/6-31+G(d), gas phase

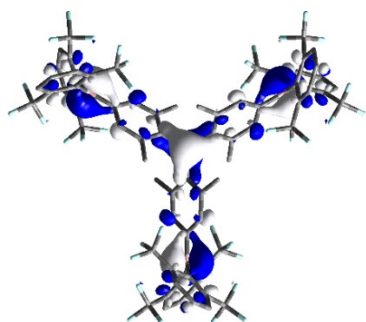
Orbital	Energy [eV]	Symmetry
L+4	-1.86	A
L+3	-1.96	A
L+2	-2.74	E
L+1	-2.74	E
LUMO	-2.95	A
HOMO	-6.58	E
H-1	-6.58	E
H-2	-6.62	A
H-3	-6.66	E
H-4	-6.66	E

Table 6.21: Lowest energy singlet electronic transition of **BFG1H** (TD-DFT B3LYP/6-31+G(d), gas phase).

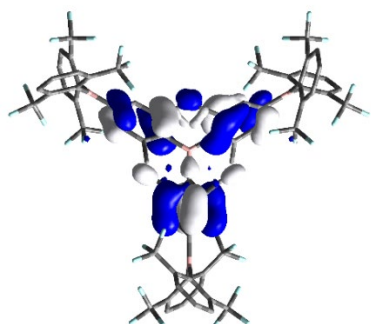
State	E [eV]	$\lambda$ [nm]	$f$	Symmetry	Major contributions	$\Lambda$
1	3.04	408.50	0.0794	E	HOMO->LUMO (89%)	0.50
2	3.04	408.50	0.0794	E	H-1->LUMO (89%)	0.51
3	3.08	402.38	0.0139	A	H-2->LUMO (81%)	0.41
4	3.12	397.39	0.2126	E	H-4->LUMO (85%)	0.51
5	3.12	397.39	0.2126	E	H-3->LUMO (85%)	0.52
6	3.34	371.35	0.0048	E	H-4->LUMO (11%), H-2->L+2 (29%), H-1->L+1 (23%), HOMO->L+2 (23%)	0.38
7	3.34	371.35	0.0048	E	H-3->LUMO (11%), H-2->L+1 (29%), H-1->L+2 (23%), HOMO->L+1 (23%)	0.38
8	3.34	371.20	0.0011	A	H-2->LUMO (16%), H-1->L+1 (31%), HOMO->L+2 (31%)	0.38
9	3.42	362.99	0.1108	A	H-4->L+2 (27%), H-3->L+1 (27%), H-2->L+2 (14%), H-1->L+1 (12%), HOMO->L+2 (12%)	0.36
10	3.42	362.99	0.1108	A	H-4->L+1 (27%), H-3->L+2 (27%), H-2->L+1 (14%), H-1->L+2 (12%), HOMO->L+1 (12%)	0.39
11	3.42	362.56	0	A	H-1->L+2 (40%), HOMO->L+1 (40%)	0.39
12	3.48	356.23	0	A	H-4->L+2 (38%), H-3->L+1 (38%), H-1->L+1 (11%), HOMO->L+2 (11%)	0.36

Experimental

Orbitals relevant to the  $S_1 \leftarrow S_0$  transition

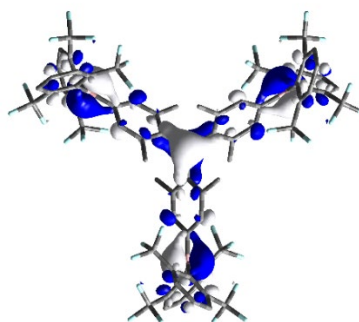


LUMO: -2.953 eV

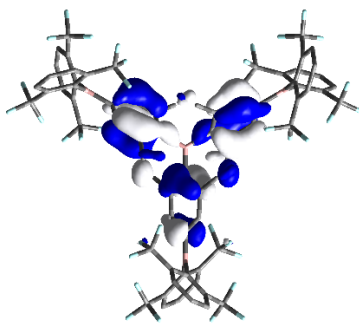


HOMO: -6.577 eV

Orbitals relevant to the  $S_2 \leftarrow S_0$  transition



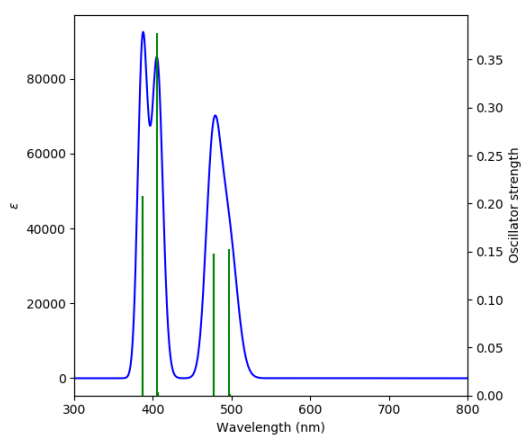
LUMO: -2.953 eV



HOMO-1: -6.577 eV

6.6.3.3 BG1NMe<sub>2</sub>

## Calculated absorption spectrum



## TD-DFT B3LYP/6-31+G(d), gas phase

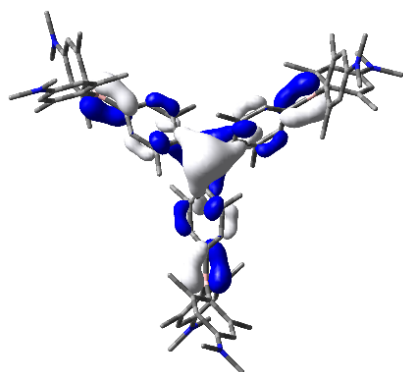
Orbital	Energy [eV]	Symmetry
L+4	-0.09	A
L+3	-0.66	A
L+2	-1.37	E
L+1	-1.37	E
LUMO	-2.03	A
HOMO	-4.89	E
H-1	-4.89	E
H-2	-4.89	A
H-3	-5.00	E
H-4	-5.00	E

Table 6.22: Lowest energy singlet electronic transition of BG1NMe<sub>2</sub> (TD-DFT B3LYP/6-31+G(d), gas phase).

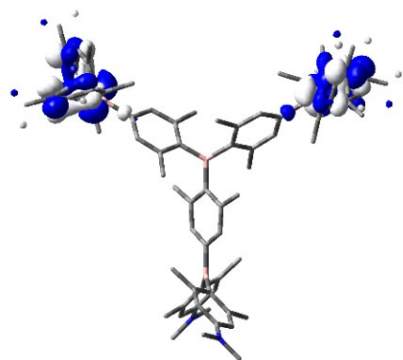
State	E [eV]	$\lambda$ [nm]	$f$	Symmetry	Major contributions	$\Lambda$
1	2.49	497.95	0.0016	E	H-1->LUMO (96%)	0.25
2	2.49	497.95	0.0016	E	HOMO->LUMO (96%)	0.28
3	2.49	497.29	0.1525	A	H-2->LUMO (96%)	0.30
4	2.60	477.41	0.1482	E	H-4->LUMO (94%)	0.31
5	2.60	477.41	0.1482	E	H-3->LUMO (94%)	0.34
6	2.65	468.61	0	A	H-5->LUMO (98%)	0.37
7	3.05	406.01	0.0034	E	H-2->L+1 (46%), H-1->L+2 (23%), HOMO->L+1 (23%)	0.32
8	3.05	406.01	0.0034	E	H-2->L+2 (46%), H-1->L+1 (23%), HOMO->L+2 (23%)	0.43
9	3.06	405.47	0.3778	A	H-1->L+1 (46%), HOMO->L+2 (46%)	0.44
10	3.20	387.12	0.2080	E	H-5->L+1 (39%), H-4->L+2 (24%), H-3->L+1 (24%)	0.40
11	3.20	387.12	0.2080	E	H-5->L+2 (39%), H-4->L+1 (24%), H-3->L+2 (24%)	0.51
12	3.23	384.11	0	A	H-4->L+1 (46%), H-3->L+2 (46%)	0.52

Experimental

Orbitals relevant to the  $S_1 \leftarrow S_0$  transition

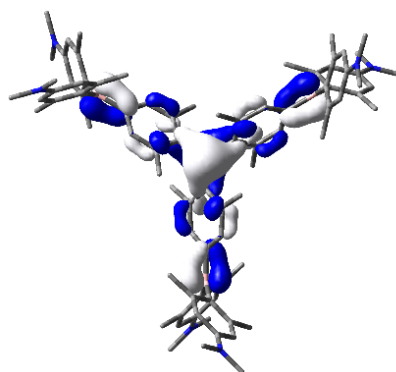


LUMO: -2.028 eV

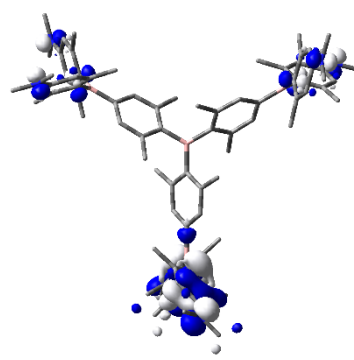


HOMO-1: -4.893 eV

Orbitals relevant to the  $S_2 \leftarrow S_0$  transition



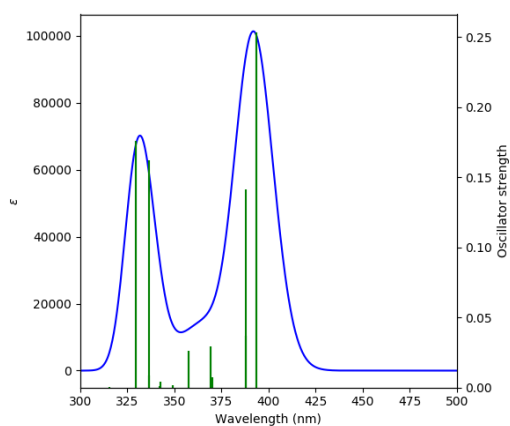
LUMO: -2.028 eV



HOMO: -4.893 eV

## 6.6.3.4 BG1Br

## Calculated absorption spectrum



## TD-DFT B3LYP/6-31+G(d), gas phase

Orbital	Energy [eV]	Symmetry
L+4	-1.00	E
L+3	-1.70	A
L+2	-2.47	E
L+1	-2.47	E
LUMO	-3.04	A
HOMO	-6.68	E
H-1	-6.68	E
H-2	-6.68	A
H-3	-6.73	E
H-4	-6.73	E

Table 6.23: Lowest energy singlet electronic transition of **BG1Br** (TD-DFT CAM-B3LYP/6-31+G(d), gas phase).

State	E [eV]	$\lambda$ [nm]	$f$	Symmetry	Major contributions	$\Lambda$
1	3.15	393.71	0.2535	E	H-6->LUMO (11%), H-4->LUMO (13%), H-3->LUMO (53%)	0.46
2	3.15	393.71	0.2535	E	H-7->LUMO (11%), H-4->LUMO (53%), H-3->LUMO (13%)	0.45
3	3.20	387.95	0.0371	E	H-1->LUMO (13%), HOMO->LUMO (67%)	0.33
4	3.20	387.95	0.0371	E	H-1->LUMO (67%), HOMO->LUMO (13%)	0.32
5	3.20	387.75	0.1415	A	H-2->LUMO (87%)	0.34
6	3.33	372.25	0	A	H-5->LUMO (92%)	0.41
7	3.35	370.04	0.0072	A	H-8->LUMO (92%)	0.52
8	3.36	369.20	0.0294	E	H-10->LUMO (25%), H-7->LUMO (37%), H-6->LUMO (14%)	0.53
9	3.36	369.20	0.0294	E	H-11->LUMO (25%), H-7->LUMO (14%), H-6->LUMO (37%)	0.53
10	3.47	357.60	0.0264	E	H-16->LUMO (25%), H-12->LUMO (25%), H-11->LUMO (12%), H-6->LUMO (12%), H-3->LUMO (10%)	0.54
11	3.47	357.60	0.0264	E	H-15->LUMO (25%), H-13->LUMO (25%), H-10->LUMO (12%), H-7->LUMO (12%), H-4->LUMO (10%)	0.53
12	3.54	350.15	0	A	H-9->LUMO (88%)	0.28
13	3.55	348.98	0.0014	E	H-13->LUMO (13%), H-10->LUMO (40%), H-6->LUMO (12%)	0.49
14	3.55	348.98	0.0014	E	H-12->LUMO (13%), H-11->LUMO (40%), H-7->LUMO (12%)	0.49
15	3.62	342.35	0.0042	E	H-15->LUMO (39%), H-13->LUMO (42%)	0.56

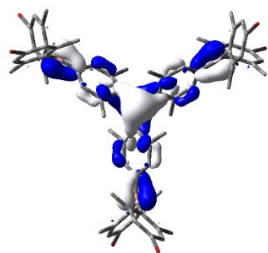
## Experimental

-Table 6.23 cont.-

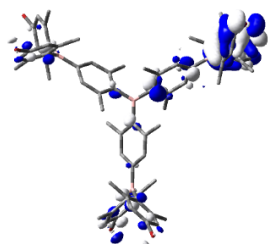
State	E [eV]	$\lambda$ [nm]	$f$	Symmetry	Major contributions	$\Lambda$
16	3.62	342.35	0.0042	E	H-16->LUMO (39%), H-12->LUMO (42%)	0.57
17	3.62	342.18	0.0011	A	H-14->LUMO (84%)	0.38
18	3.69	336.46	0.0085	E	H-2->L+1 (26%), H-2->L+2 (15%), H-1->LUMO (12%), H-1->L+1 (18%), HOMO->L+2 (18%)	0.40
19	3.69	336.46	0.0085	E	H-2->L+1 (15%), H-2->L+2 (26%), H-1->L+2 (18%), HOMO->LUMO (12%), HOMO->L+1 (18%)	0.41
20	3.69	336.36	0.1621	A	H-2->LUMO (13%), H-1->L+1 (21%), H-1->L+2 (21%), HOMO->L+1 (21%), HOMO->L+2 (21%)	0.39
21	3.74	331.60	0	A	H-17->LUMO (36%), H-4->L+1 (13%), H-4->L+2 (15%), H-3->L+1 (15%), H-3->L+2 (13%)	0.57
22	3.76	329.63	0.1757	A	H-5->L+1 (16%), H-5->L+2 (11%), H-4->L+1 (10%), H- 4->L+2 (18%), H-3->L+1 (18%), H-3->L+2 (10%)	0.48
23	3.76	329.63	0.1757	A	H-5->L+1 (11%), H-5->L+2 (16%), H-4->L+1 (18%), H- 4->L+2 (10%), H-3->L+1 (10%), H-3->L+2 (18%)	0.48
24	3.84	323.15	0	A	H-17->LUMO (55%)	0.63
25	3.93	315.26	0.0002	A	H-4->L+1 (19%), H-4->L+2 (16%), H-3->L+1 (16%), H- 3->L+2 (19%)	0.49



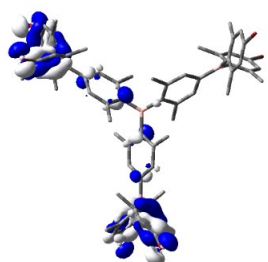
**Orbitals relevant to the  
 $S_1 \leftarrow S_0$  and  $S_2 \leftarrow S_0$   
transition**



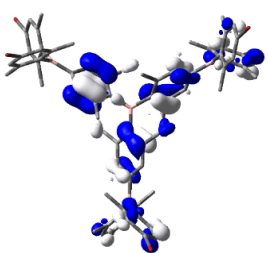
**LUMO: -3.036 eV**



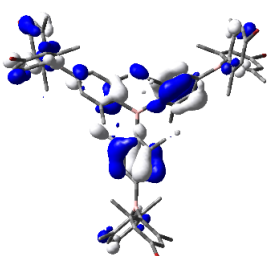
**HOMO-3: -6.732 eV**



**HOMO-4: -6.732 eV**

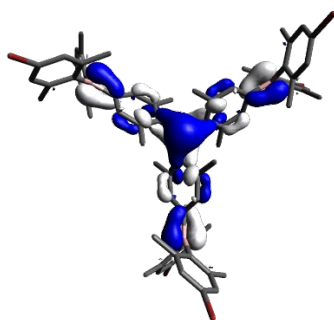


**HOMO-6: -6.999 eV**

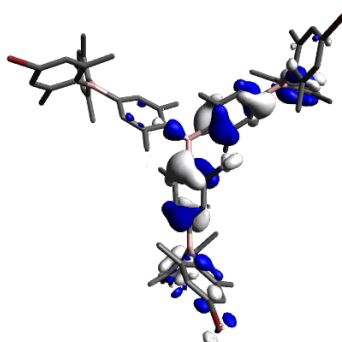


**HOMO-7: -6.999 eV**

**NTOs of the  $S_1 \leftarrow S_0$   
transition**

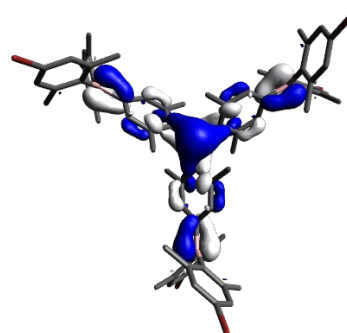


**virtual**

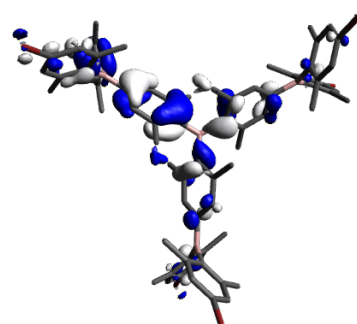


**occupied**

**NTOs of the  $S_2 \leftarrow S_0$   
transition**



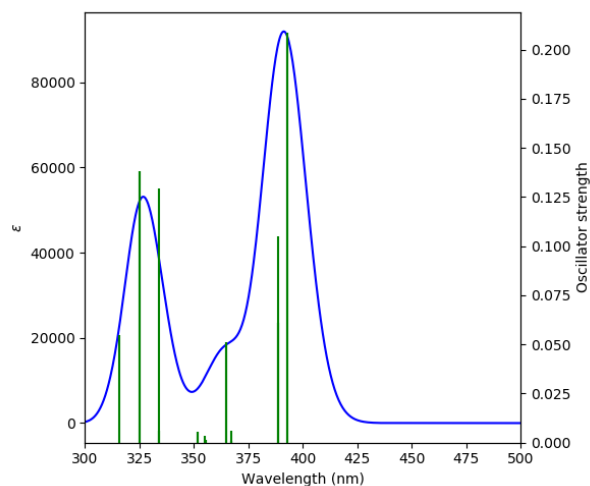
**virtual**



**occupied**

## 6.6.3.5 BG1Me

## Calculated absorption spectrum



Orbital	Energy [eV]	Symmetry
L+4	-0.44	E
L+3	-1.14	A
L+2	-1.90	E
L+1	-1.90	E
LUMO	-2.52	A
HOMO	-6.18	E
H-1	-6.18	E
H-2	-6.19	A
H-3	-6.25	E
H-4	-6.25	E

## TD-DFT B3LYP/6-31+G(d), gas phase

Table 6.24: Lowest energy singlet electronic transition of **BG1Me** (TD-DFT CAM-B3LYP/6-31+G(d), gas phase).

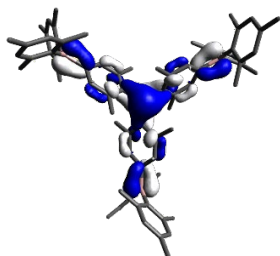
State	E [eV]	$\lambda$ [nm]	$f$	Symmetry	Major contributions	$\Lambda$
1	3.16	392.77	0.2088	E	H-3->LUMO (61%), H-1->LUMO (16%)	0.46
2	3.16	392.77	0.2088	E	H-4->LUMO (61%), HOMO->LUMO (16%)	0.44
3	3.19	388.91	0.1052	A	H-2->LUMO (87%)	0.36
4	3.19	388.88	0.0608	E	H-4->LUMO (14%), HOMO->LUMO (71%)	0.36
5	3.19	388.88	0.0608	E	H-3->LUMO (14%), H-1->LUMO (71%)	0.33
6	3.33	371.95	0	A	H-5->LUMO (90%)	0.41
7	3.38	367.32	0.0059	A	H-14->LUMO (70%), H-9->LUMO (26%)	0.47
8	3.38	367.23	0.0011	E	H-13->LUMO (38%), H-7->LUMO (38%)	0.42
9	3.38	367.23	0.0011	E	H-12->LUMO (38%), H-6->LUMO (38%)	0.44
10	3.40	364.73	0.0512	E	H-15->LUMO (12%), H-13->LUMO (28%), H-11->LUMO (10%), H-7->LUMO (44%)	0.42
11	3.40	364.73	0.0512	E	H-16->LUMO (12%), H-12->LUMO (28%), H-10->LUMO (10%), H-6->LUMO (44%)	0.43
12	3.42	362.40	0.0	A	H-8->LUMO (91%)	0.34
13	3.49	355.68	0.0012	E	H-13->LUMO (17%), H-11->LUMO (72%)	0.35
14	3.49	355.68	0.0012	E	H-12->LUMO (17%), H-10->LUMO (72%)	0.33
15	3.49	355.18	0.0036	A	H-14->LUMO (26%), H-9->LUMO (65%)	0.39
16	3.52	351.86	0.0056	E	H-16->LUMO (75%)	0.63
17	3.52	351.86	0.0056	E	H-15->LUMO (75%)	0.60

-Table 6.24 cont.-

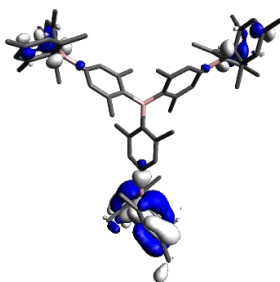
State	E [eV]	$\lambda$ [nm]	$f$	Symmetry	Major contributions	$\Lambda$
18	3.71	334.03	0.006	E	H-2->L+1 (41%), H-1->LUMO (12%), H-1->L+2 (21%), HOMO->L+1 (21%)	0.36
19	3.71	334.03	0.006	E	H-2->L+2 (41%), H-1->L+1 (21%), HOMO->LUMO (12%), HOMO->L+2 (21%)	0.47
20	3.71	333.96	0.1293	A	H-2->LUMO (12%), H-1->L+1 (41%), HOMO->L+2 (41%)	0.48
21	3.77	329.03	0	A	H-17->LUMO (46%), H-4->L+1 (23%), H-3->L+2 (23%)	0.67
22	3.81	325.26	0.1383	E	H-5->L+2 (29%), H-4->L+1 (27%), H-3->L+2 (27%)	0.56
23	3.81	325.26	0.1384	E	H-5->L+1 (29%), H-4->L+2 (27%), H-3->L+1 (27%)	0.43
24	3.87	320.75	0	A	H-17->LUMO (36%), H-4->L+1 (18%), H-3->L+2 (18%)	0.61
25	3.92	315.95	0.0546	E	H-8->L+1 (37%), H-7->L+2 (23%), H-6->L+1 (23%)	0.34

Experimental

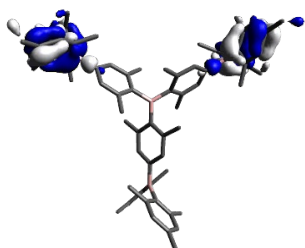
**Orbitals relevant to  
the  $S_1 \leftarrow S_0$  and  $S_2 \leftarrow S_0$   
transition**



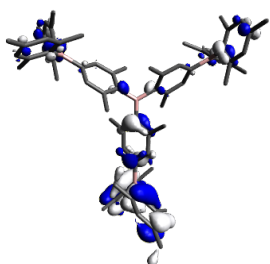
**LUMO: -2.520 eV**



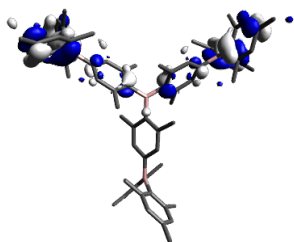
**HOMO: -6.183 eV**



**HOMO-1: -6.183 eV**

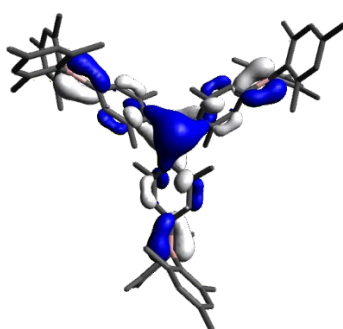


**HOMO-3: -6.251 eV**

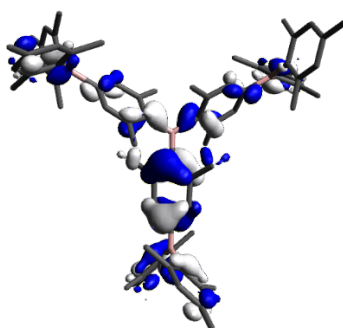


**HOMO-4: -6.251 eV**

**NTOs of the  $S_1 \leftarrow S_0$   
transition**

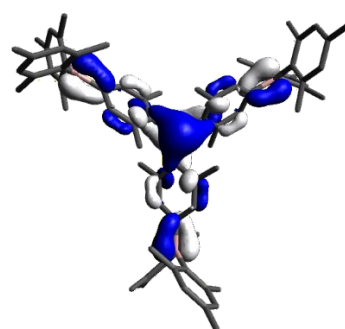


**virtual**

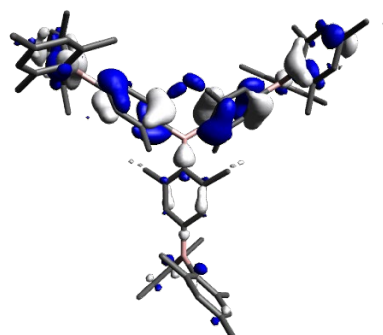


**occupied**

**NTOs of the  $S_2 \leftarrow S_0$   
transition**



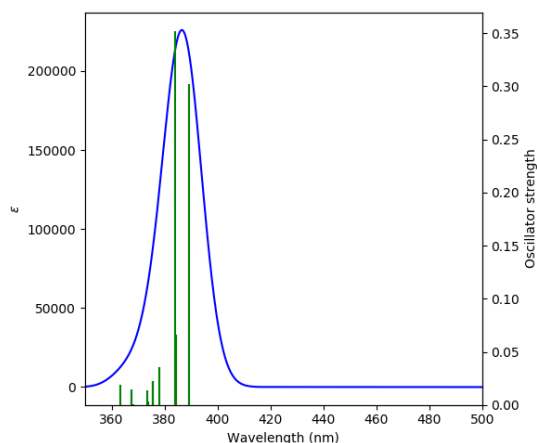
**virtual**



**occupied**

## 6.6.3.6 BG2H

## Calculated absorption spectrum



Orbital	Energy [eV]	Symmetry
L+4	-1.72	E
L+3	-1.78	A2
L+2	-2.21	E
L+1	-2.21	E
LUMO	-2.63	A2
HOMO	-6.21	E
H-1	-6.21	E
H-2	-6.21	E
H-3	-6.21	E
H-4	-6.21	A1

## TD-DFT B3LYP/6-31G, gas phase

Table 6.25: Lowest energy singlet electronic transition of **BG2H** (TD-DFT B3LYP/6-31G, gas phase).

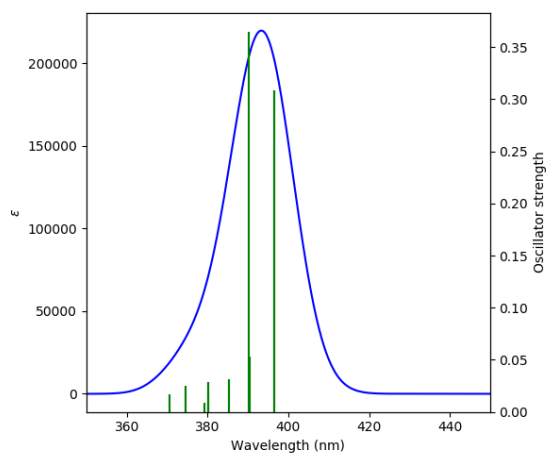
State	E [eV]	$\lambda$ [nm]	$f$	Symmetry	Major contributions	$\Lambda$
1	3.18	389.41	0.3024	E	H-31->LUMO (33%), H-15->LUMO (37%)	0.43
2	3.18	389.41	0.3024	E	H-30->LUMO (33%), H-16->LUMO (37%)	0.41
3	3.23	384.23	0.0660	E	H-12->LUMO (53%)	0.31
4	3.23	384.23	0.0660	E	H-13->LUMO (53%)	0.28
5	3.23	384.01	0.3522	A2	H-14->LUMO (60%), H-4->LUMO (10%)	0.32
6	3.27	379.10	0	A1	H-26->LUMO (27%), H-17->LUMO (11%), H-8->LUMO (22%), H-5->LUMO (23%)	0.23
7	3.28	378.08	0.0354	E	H-25->LUMO (26%), H-7->LUMO (24%), HOMO->LUMO (16%)	0.21
8	3.28	378.08	0.0354	E	H-24->LUMO (26%), H-6->LUMO (24%), H-1->LUMO (16%)	0.19
9	3.30	375.48	0.0228	A2	H-9->LUMO (81%)	0.19
10	3.30	375.45	0.0228	E	H-11->LUMO (81%)	0.16
11	3.30	375.45	0.0228	E	H-10->LUMO (81%)	0.17
12	3.31	374.18	0	A1	H-8->LUMO (67%)	0.18
13	3.32	373.91	0.0030	E	H-25->LUMO (10%), H-7->LUMO (45%), H-6->LUMO (14%)	0.17
14	3.32	373.91	0.0030	E	H-24->LUMO (10%), H-7->LUMO (14%), H-6->LUMO (45%)	0.16
15	3.32	373.44	0.0013	E	H-3->LUMO (74%)	0.14
16	3.32	373.44	0.0013	E	H-2->LUMO (74%)	0.15
17	3.32	373.42	0.0140	A2	H-4->LUMO (82%)	0.16

## Experimental

-Table 6.25 cont.-

State	E [eV]	$\lambda$ [nm]	$f$	Symmetry	Major contributions	$\Lambda$
18	3.32	373.40	0	A1	H-26->LUMO (17%), H-17->LUMO (12%), H-5->LUMO (60%)	0.19
19	3.32	373.40	0	E	H-25->LUMO (16%), HOMO->LUMO (54%)	0.20
20	3.32	373.40	0	E	H-24->LUMO (16%), H-1->LUMO (54%)	0.18
21	3.37	368.11	0.0003	A2	H-36->LUMO (15%), H-27->LUMO (46%), H-20->LUMO (27%)	0.34
22	3.37	367.37	0.0147	E	H-38->LUMO (10%), H-28->LUMO (36%), H-21->LUMO (35%)	0.29
23	3.37	367.37	0.0145	E	H-37->LUMO (10%), H-29->LUMO (37%), H-22->LUMO (35%)	0.30
24	3.38	367.27	0	A1	H-26->LUMO (14%), H-23->LUMO (68%)	0.31
25	3.41	363.27	0.0191	E	H-38->LUMO (34%), H-31->LUMO (11%), H-21->LUMO (27%), H-19->LUMO (10%)	0.35

## Calculated absorption spectrum



## Orbital

## Energy

[eV]

L+4	-2.02
L+3	-2.07
L+2	-2.49
L+1	-2.49
LUMO	-2.89
HOMO	-6.43
H-1	-6.43
H-2	-6.43
H-3	-6.43
H-4	-6.43

## TD-DFT B3LYP/6-31+G(d), gas phase

Table6.26: Lowest energy singlet electronic transition of **BG2H** (TD-DFT B3LYP/6-31+G(d), gas phase).

State	E [eV]	$\lambda$ [nm]	$f$	Major contributions	$\Lambda$
1	3.13	396.44	0.3082	H-30->LUMO (36%), H-16->LUMO (36%)	0.44
2	3.13	396.44	0.3082	H-31->LUMO (36%), H-15->LUMO (36%)	0.45
3	3.18	390.43	0.0532	H-12->LUMO (60%)	0.33
4	3.18	390.43	0.0531	H-13->LUMO (60%)	0.29
5	3.18	390.10	0.3649	H-14->LUMO (63%)	0.34
6	3.21	386.14	0	H-26->LUMO (36%), H-17->LUMO (17%), H-8->LUMO (24%)	0.28
7	3.22	385.27	0.0316	H-24->LUMO (48%), H-7->LUMO (23%)	0.25
8	3.22	385.27	0.0316	H-25->LUMO (48%), H-6->LUMO (23%)	0.29
9	3.26	380.21	0.0185	H-9->LUMO (78%)	0.20
10	3.26	380.14	0.0288	H-10->LUMO (80%)	0.19
11	3.26	380.14	0.0288	H-11->LUMO (80%)	0.16
12	3.27	379.55	0	H-8->LUMO (25%), H-5->LUMO (61%)	0.14
13	3.27	379.48	0.0002	H-7->LUMO (25%), H-4->LUMO (60%)	0.12
14	3.27	379.48	0.0002	H-6->LUMO (25%), H-3->LUMO (61%)	0.13
15	3.27	379.26	0.0010	H-2->LUMO (87%)	0.11
16	3.27	379.26	0.0010	H-1->LUMO (87%)	0.13
17	3.27	379.25	0.0089	HOMO->LUMO (87%)	0.14

## Experimental

-Table6.26 cont.-

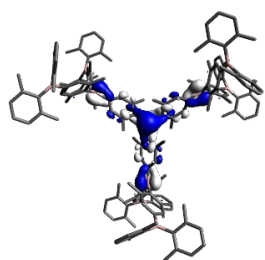
State	E [eV]	$\lambda$ [nm]	$f$	Major contributions	$\Lambda$
18	3.27	379.12	0	H-26->LUMO (12%), H-17->LUMO (11%), H-8->LUMO (35%), H-5->LUMO (27%)	0.20
19	3.27	379.11	0.0001	H-25->LUMO (12%), H-6->LUMO (34%), H-3->LUMO (29%)	0.20
20	3.27	379.11	0.0001	H-24->LUMO (12%), H-7->LUMO (34%), H-4->LUMO (29%)	0.17
21	3.30	375.66	0.0001	H-35->LUMO (27%), H-27->LUMO (46%), H-20->LUMO (14%)	0.39
22	3.31	374.64	0.0247	H-38->LUMO (20%), H-28->LUMO (44%), H-21->LUMO (19%)	0.36
23	3.31	374.64	0.0246	H-37->LUMO (20%), H-29->LUMO (44%), H-22->LUMO (19%)	0.33
24	3.32	373.72	0	H-26->LUMO (16%), H-23->LUMO (61%)	0.33
25	3.35	370.53	0.0171	H-38->LUMO (39%), H-30->LUMO (13%), H-21->LUMO (23%)	0.40



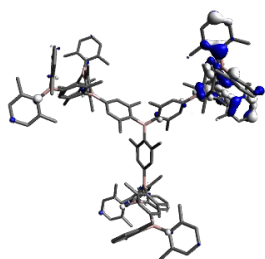
**Orbitals relevant to  
the  $S_1 \leftarrow S_0$  and  $S_2 \leftarrow S_0$   
transition**

**NTOs of the  $S_1 \leftarrow S_0$  transition**

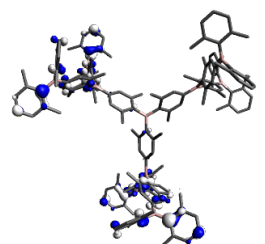
**NTOs of the  $S_2 \leftarrow S_0$  transition**



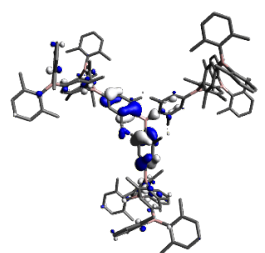
**LUMO: -2.629 eV**



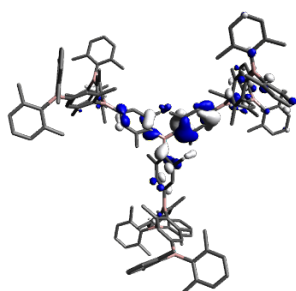
**HOMO-15: -6.302 eV**



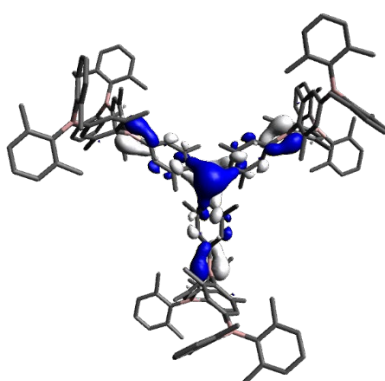
**HOMO-16: -6.302 eV**



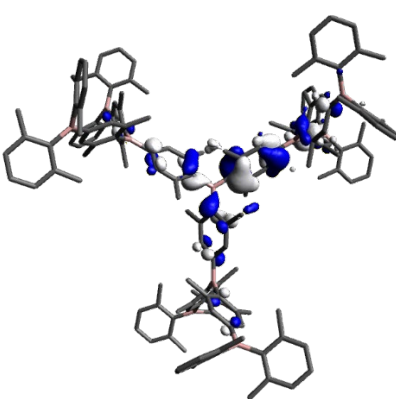
**HOMO-30: -6.542 eV**



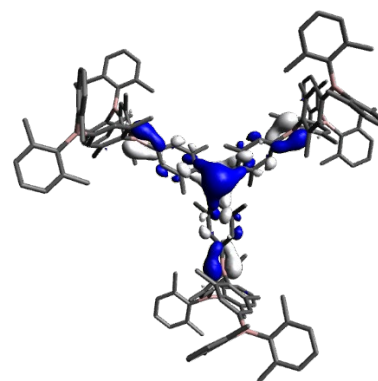
**HOMO-31: -6.542 eV**



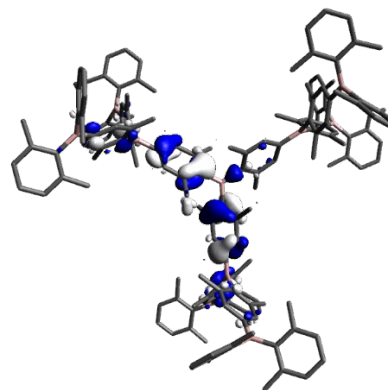
**virtual**



**occupied**



**virtual**

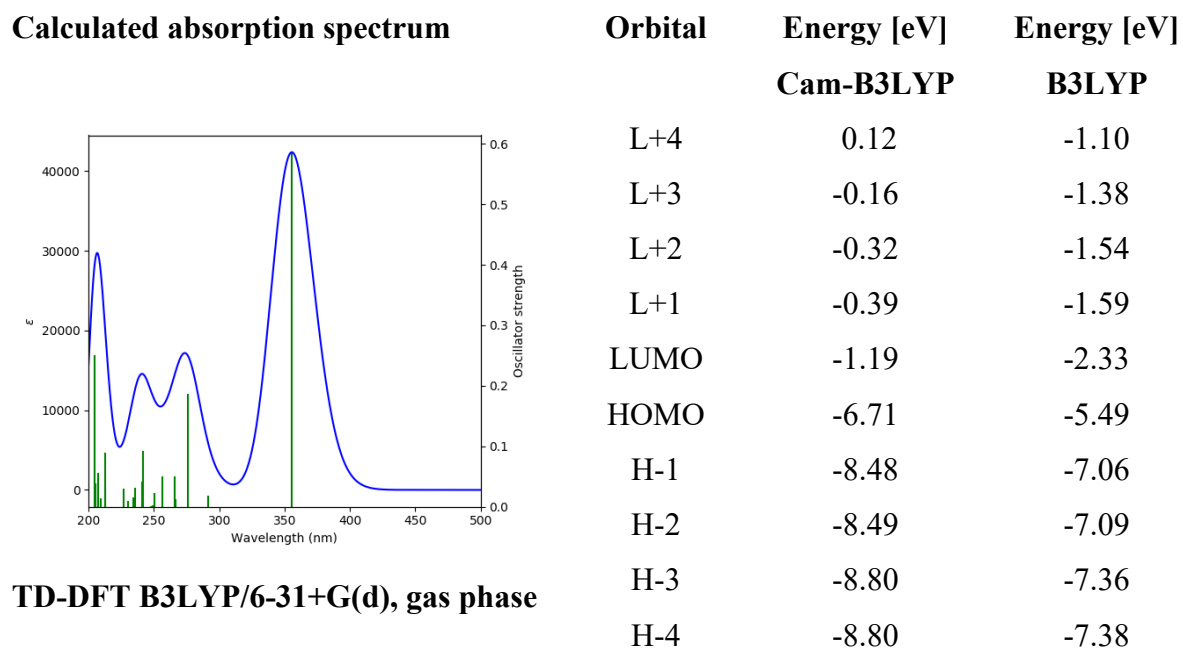


**occupied**

#### 6.6.4 Chapter 4

All calculations (DFT and TD-DFT) were carried out with the Gaussian 09 (9.E.01)<sup>[395]</sup> program package and were performed on a parallel cluster system. GaussView (6.0.16), Avogadro<sup>[400]</sup> and multiwfn<sup>[396]</sup> were used to visualize the results, to measure calculated structural parameters, and to plot orbital surfaces (isovalue:  $\pm 0.030 [e a_0^{-3}]^{1/2}$ ). The ground-state geometries were optimized using the B3LYP functional<sup>[397]</sup> in combination with the 6-31+G(d) basis set.<sup>[398, 399]</sup> The D3 dispersion correction of Grimme and coworkers was used.<sup>[349]</sup> The ultrafine integration grid and symmetry constraints were used for all molecules. Frequency calculation were performed on the optimized structure to confirm that it was a local minimum showing no negative (imaginary) frequencies. Based on the optimized structure, the lowest-energy vertical transitions (gas-phase and solvent correction using the polarizable continuum model) were calculated (singlets, 25 states) by TD-DFT, using the Coulomb attenuated functional CAM-B3LYP.<sup>[229]</sup> The CAM-B3LYP has been shown to describe ICT systems more accurately than B3LYP.<sup>[228]</sup>

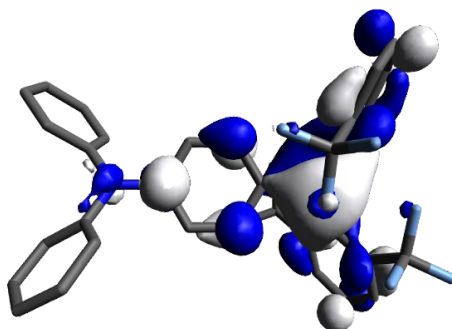
## 6.6.4.1 1

Table 6.27: Lowest energy singlet electronic transition of **1** (TD-DFT B3LYP/6-31+G(d), gas phase).

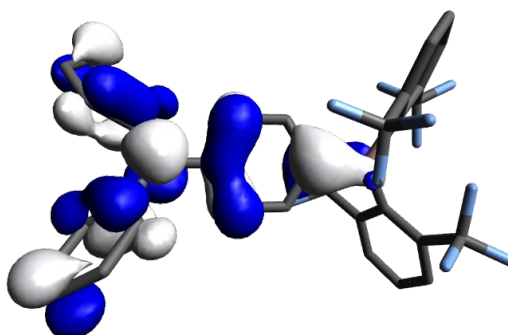
State	E [eV]	$\lambda$ [nm]	$f$	Major contributions	$\Lambda$
1	3.49	355.54	0.5849	HOMO->LUMO (85%)	0.44
2	4.25	291.69	0.0178	HOMO->L+1 (14%), HOMO->L+5 (65%)	0.50
3	4.49	276.15	0.1867	HOMO->L+6 (91%)	0.58
4	4.65	266.55	0.0129	H-4->LUMO (13%), H-1->LUMO (30%), HOMO->L+5 (19%), HOMO->L+13 (13%)	0.44
5	4.67	265.69	0.0508	HOMO->L+4 (67%)	0.49
6	4.84	256.18	0.0497	H-1->LUMO (16%), HOMO->L+1 (57%), HOMO->L+3 (12%)	0.25
7	4.95	250.42	0.0232	HOMO->L+10 (40%), HOMO->L+11 (23%)	0.41
8	4.97	249.36	0.0027	HOMO->L+2 (74%)	0.18
9	5.01	247.56	0.0015	HOMO->L+3 (74%)	0.19
10	5.13	241.47	0.0927	H-6->LUMO (49%)	0.63
11	5.15	240.95	0.0412	H-8->LUMO (23%), H-7->L+1 (12%), H-6->LUMO (32%), H- 6->L+2 (10%)	0.60
12	5.15	240.75	0.0044	H-9->LUMO (27%), H-8->L+3 (10%), H-7->L+2 (18%), H-6- >L+1 (15%)	0.61
13	5.26	235.76	0.0315	H-7->LUMO (52%), H-3->LUMO (16%)	0.58
14	5.29	234.29	0.0153	HOMO->L+13 (33%)	0.43
15	5.39	230.23	0.0091	HOMO->L+7 (30%), HOMO->L+9 (38%)	0.28
16	5.46	227.10	0.0301	H-7->LUMO (33%), H-3->LUMO (26%), H-2->LUMO (21%)	0.51

-Table 6.27 cont.-

State	E [eV]	$\lambda$ [nm]	$f$	Major contributions	$\Lambda$
17	5.61	220.92	0.0001	HOMO->L+12 (65%)	0.46
18	5.81	213.57	0	HOMO->L+10 (35%), HOMO->L+11 (41%)	0.39
19	5.82	212.97	0.0309	H-4->LUMO (24%), H-2->L+6 (16%), HOMO->L+13 (10%)	0.53
20	5.83	212.57	0.0894	H-3->LUMO (16%), H-2->LUMO (32%), HOMO->L+11 (18%)	0.43
21	5.91	209.66	0.0147	HOMO->L+7 (11%), HOMO->L+9 (22%), HOMO->L+15 (46%)	0.29
22	5.93	209.01	0.0002	HOMO->L+8 (11%), HOMO->L+14 (31%), HOMO->L+17 (23%), HOMO->L+18 (15%)	0.29
23	5.98	207.21	0.0555	H-11->LUMO (13%), H-8->LUMO (19%), H-7->L+1 (15%)	0.63
24	6.03	205.49	0.0382	H-5->LUMO (20%), H-4->LUMO (23%), H-2->L+6 (11%)	0.41
25	6.05	204.83	0.2513	H-9->LUMO (36%), H-6->L+1 (12%), H-1->L+1 (19%)	0.52

Orbitals relevant to the  $S_1 \leftarrow S_0$ 

LUMO: -1.19 eV



HOMO: -6.71 eV

## 7 References

- [1] A. Narsaria, F. Rauch, J. Krebs, P. Endres, A. Friedrich, I. Krummenacher, H. Braunschweig, M. Finze, J. Nitsch, F. M. Bickelhaupt, T. B. Marder, *Adv. Funct. Mater.* **2020**, DOI: 10.1002/adfm.202002064.
- [2] F. Rauch, S. Fuchs, A. Friedrich, D. Sieh, I. Krummenacher, H. Braunschweig, M. Finze, T. B. Marder, *Chem. Eur. J.* **2020**, DOI: 10.1002/chem.201905559.
- [3] F. Rauch, P. Endres, A. Friedrich, D. Sieh, M. Hähnel, I. Krummenacher, H. Braunschweig, M. Finze, L. Ji, T. B. Marder, *Chem. Eur. J.* **2020**, DOI: 10.1002/chem.202001985.
- [4] F. Rauch, J. Krebs, J. Günther, A. Friedrich, M. Hähnel, I. Krummenacher, H. Braunschweig, M. Finze, T. B. Marder, **2020**, *submitted*.
- [5] C. W. Tang, S. A. Vanslyke, *Appl. Phys. Lett.* **1987**, *51*, 913-915.
- [6] M. A. Baldo, D. F. O'Brien, M. E. Thompson, S. R. Forrest, *Phys. Rev. B: Condens. Matter Mater. Phys.* **1999**, *60*, 14422-14428.
- [7] M. A. Baldo, D. F. O'Brien, Y. You, A. Shoustikov, S. Sibley, M. E. Thompson, S. R. Forrest, *Nature* **1998**, *395*, 151-154.
- [8] M. A. Baldo, M. E. Thompson, S. R. Forrest, *Nature* **2000**, *403*, 750-753.
- [9] X. Gong, J. C. Ostrowski, G. C. Bazan, D. Moses, A. J. Heeger, *Appl. Phys. Lett.* **2002**, *81*, 3711-3713.
- [10] W. Y. Wong, C. L. Ho, *J. Mater. Chem.* **2009**, *19*, 4457-4482.
- [11] Y. Chi, P. T. Chou, *Chem. Soc. Rev.* **2010**, *39*, 638-655.
- [12] S. Y. Kim, W. I. Jeong, C. Mayr, Y. S. Park, K. H. Kim, J. H. Lee, C. K. Moon, W. Brütting, J. J. Kim, *Adv. Funct. Mater.* **2013**, *23*, 3896-3900.
- [13] F. Perrin, *Ann. Phys. (Paris)* **1929**, *12*, 169-275.
- [14] G. N. Lewis, D. Lipkin, *J. Am. Chem. Soc.* **1942**, *64*, 2801-2808.
- [15] C. A. Parker, C. G. Hatchard, *J. Chem. Soc. Faraday Trans.* **1961**, *57*, 1894-1904.
- [16] H. Uoyama, K. Goushi, K. Shizu, H. Nomura, C. Adachi, *Nature* **2012**, *492*, 234-238.
- [17] H. Tanaka, K. Shizu, H. Miyazaki, C. Adachi, *Chem. Commun.* **2012**, *48*, 11392-11394.
- [18] T. Nakagawa, S.-Y. Ku, K.-T. Wong, C. Adachi, *Chem. Commun.* **2012**, *48*, 9580-9582.
- [19] S. Youn Lee, T. Yasuda, H. Nomura, C. Adachi, *Appl. Phys. Lett.* **2012**, *101*, 093306.
- [20] K. Goushi, K. Yoshida, K. Sato, C. Adachi, *Nat. Photonics* **2012**, *6*, 253-258.
- [21] K. Goushi, C. Adachi, *Appl. Phys. Lett.* **2012**, *101*, 023306.
- [22] Q. Zhang, J. Li, K. Shizu, S. Huang, S. Hirata, H. Miyazaki, C. Adachi, *J. Am. Chem. Soc.* **2012**, *134*, 14706-14709.
- [23] G. Méhes, H. Nomura, Q. Zhang, T. Nakagawa, C. Adachi, *Angew. Chem. Int. Ed.* **2012**, *51*, 11311-11315; *Angew. Chem.* **2012**, *124*, 11473-11477.
- [24] X. K. Chen, S. F. Zhang, J. X. Fan, A. M. Ren, *J. Phys. Chem. C* **2015**, *119*, 9728-9733.
- [25] L. Bergmann, D. M. Zink, S. Brase, T. Baumann, D. Volz, *Top. Curr. Chem.* **2016**, *374*, 22.
- [26] M. Godumala, S. Choi, M. J. Cho, D. H. Choi, *J. Mater. Chem. C* **2016**, *4*, 11355-11381.
- [27] X. Cao, D. Zhang, S. Zhang, Y. Tao, W. Huang, *J. Mater. Chem. C* **2017**, *5*, 7699-7714.
- [28] Y. Im, M. Kim, Y. J. Cho, J.-A. Seo, K. S. Yook, J. Y. Lee, *Chem. Mater.* **2017**, *29*, 1946-1963.
- [29] Z. Yang, Z. Mao, Z. Xie, Y. Zhang, S. Liu, J. Zhao, J. Xu, Z. Chi, M. P. Aldred, *Chem. Soc. Rev.* **2017**, *46*, 915-1016.
- [30] Y. Olivier, J. C. Sancho-Garcia, L. Muccioli, G. D'Avino, D. Beljonne, *J. Phys. Chem. Lett.* **2018**, *9*, 6149-6163.
- [31] P. Xiao, T. Dong, J. Xie, D. Luo, J. Yuan, B. Liu, *Appl. Sci.* **2018**, *8*, 299.

## References

- [32] J.-H. Lee, C.-H. Chen, P.-H. Lee, H.-Y. Lin, M.-k. Leung, T.-L. Chiu, C.-F. Lin, *J. Mater. Chem. C* **2019**, *7*, 5874-5888.
- [33] S. Jhulki, M. W. Cooper, S. Barlow, S. R. Marder, *Mater. Chem. Front.* **2019**, *3*, 1699-1721.
- [34] C. Adachi, *Jpn. J. Appl. Phys.* **2014**, *53*, 060101.
- [35] H. Kaji, H. Suzuki, T. Fukushima, K. Shizu, K. Suzuki, S. Kubo, T. Komino, H. Oiwa, F. Suzuki, A. Wakamiya, Y. Murata, C. Adachi, *Nat. Commun.* **2015**, *6*, 8476.
- [36] F. B. Dias, T. J. Penfold, A. P. Monkman, *Methods Appl. Fluores.* **2017**, *5*, 012001.
- [37] W. Zhang, J. Jin, Z. Huang, S. Zhuang, L. Wang, *Sci. Rep.* **2016**, *6*, 30178.
- [38] M. Einzinger, T. Zhu, P. de Silva, C. Belger, T. M. Swager, T. Van Voorhis, M. A. Baldo, *Adv. Mater.* **2017**, *29*, 1701987.
- [39] Y. Xiang, Y. Zhao, N. Xu, S. Gong, F. Ni, K. Wu, J. Luo, G. Xie, Z. H. Lu, C. Yang, *J. Mater. Chem. C* **2017**, *5*, 12204-12210.
- [40] L. Gan, K. Gao, X. Cai, D. Chen, S.-J. Su, *J. Phys. Chem. Lett.* **2018**, *9*, 4725-4731.
- [41] M. K. Etherington, J. Gibson, H. F. Higginbotham, T. J. Penfold, A. P. Monkman, *Nat. Commun.* **2016**, *7*, 13680.
- [42] B. T. Lim, S. Okajima, A. K. Chandra, E. C. Lim, *Chem. Phys. Lett.* **1981**, *79*, 22-27.
- [43] J. Tatchen, N. Gilka, C. M. Marian, *Phys. Chem. Chem. Phys.* **2007**, *9*, 5209-5221.
- [44] Z. E. X. Dance, S. M. Mickley, T. M. Wilson, A. B. Ricks, A. M. Scott, M. A. Ratner, M. R. Wasielewski, *J. Phys. Chem. A* **2008**, *112*, 4194-4201.
- [45] J. Gibson, A. P. Monkman, T. J. Penfold, *ChemPhysChem* **2016**, *17*, 2956-2961.
- [46] F. B. Dias, J. Santos, D. R. Graves, P. Data, R. S. Nobuyasu, M. A. Fox, A. S. Batsanov, T. Palmeira, M. N. Berberan-Santos, M. R. Bryce, A. P. Monkman, *Adv. Sci.* **2016**, *3*, 1600080.
- [47] X. K. Chen, D. Kim, J. L. Brédas, *Acc. Chem. Res.* **2018**, *51*, 2215-2224.
- [48] T. J. Penfold, E. Gindensperger, C. Daniel, C. M. Marian, *Chem. Rev.* **2018**, *118*, 6975-7025.
- [49] I. S. Park, H. Komiyama, T. Yasuda, *Chem. Sci.* **2017**, *8*, 953-960.
- [50] W. Huang, M. Einzinger, T. Zhu, H. S. Chae, S. Jeon, S.-G. Ihn, M. Sim, S. Kim, M. Su, G. Teverovskiy, T. Wu, T. Van Voorhis, T. M. Swager, M. A. Baldo, S. L. Buchwald, *Chem. Mater.* **2018**, *30*, 1462-1466.
- [51] J. R. Defrancisco, G. López-Espejo, J. L. Zafra, S. Yadav, R. E. Messersmith, C. J. Gómez-García, H. Ottosson, J. Casado, J. D. Tovar, *J. Phys. Chem. C* **2018**, *122*, 12148-12157.
- [52] G. A. Sommer, L. N. Mataranga-Popa, R. Czerwieńiec, T. Hofbeck, H. H. H. Homeier, T. J. J. Müller, H. Yersin, *J. Phys. Chem. Lett.* **2018**, *9*, 3692-3697.
- [53] P. K. Samanta, D. Kim, V. Coropceanu, J.-L. Brédas, *J. Am. Chem. Soc.* **2017**, *139*, 4042-4051.
- [54] K. Suzuki, S. Kubo, K. Shizu, T. Fukushima, A. Wakamiya, Y. Murata, C. Adachi, H. Kaji, *Angew. Chem. Int. Ed.* **2015**, *54*, 15231-15235; *Angew. Chem.* **2015**, *127*, 15446-15450.
- [55] Y. Kitamoto, T. Namikawa, D. Ikemizu, Y. Miyata, T. Suzuki, H. Kita, T. Sato, S. Oi, *J. Mater. Chem. C* **2015**, *3*, 9122-9130.
- [56] M. Numata, T. Yasuda, C. Adachi, *Chem. Commun.* **2015**, *51*, 9443-9446.
- [57] T. Hatakeyama, K. Shiren, K. Nakajima, S. Nomura, S. Nakatsuka, K. Kinoshita, J. Ni, Y. Ono, T. Ikuta, *Adv. Mater.* **2016**, *28*, 2777-2781.
- [58] Y. Kitamoto, T. Namikawa, T. Suzuki, Y. Miyata, H. Kita, T. Sato, S. Oi, *Org. Electron.* **2016**, *34*, 208-217.
- [59] C. Tu, W. Liang, *ACS Omega* **2017**, *2*, 3098-3109.

- [60] Y.-J. Lien, T.-C. Lin, C.-C. Yang, Y.-C. Chiang, C.-H. Chang, S.-H. Liu, Y.-T. Chen, G.-H. Lee, P.-T. Chou, C.-W. Lu, Y. Chi, *ACS Appl. Mater. Interfaces* **2017**, *9*, 27090-27101.
- [61] Y. H. Lee, S. Park, J. Oh, J. W. Shin, J. Jung, S. Yoo, M. H. Lee, *ACS Appl. Mater. Interfaces* **2017**, *9*, 24035-24042.
- [62] C.-C. Tsai, W.-C. Huang, H.-Y. Chih, Y.-C. Hsh, C.-W. Liao, C.-H. Lin, Y.-X. Kang, C.-H. Chang, Y. J. Chang, C.-W. Lu, *Org. Electron.* **2018**, *63*, 166-174.
- [63] M.-Y. Zhang, Z.-Y. Li, B. Lu, Y. Wang, Y.-D. Ma, C.-H. Zhao, *Org. Lett.* **2018**, *20*, 6868-6871.
- [64] T.-L. Wu, M.-J. Huang, C.-C. Lin, P.-Y. Huang, T.-Y. Chou, R.-W. Chen-Cheng, H.-W. Lin, R.-S. Liu, C.-H. Cheng, *Nat. Photonics* **2018**, *12*, 235-240.
- [65] I. S. Park, K. Matsuo, N. Aizawa, T. Yasuda, *Adv. Funct. Mater.* **2018**, *28*, 1802031.
- [66] S.-Y. Li, Z.-B. Sun, C.-H. Zhao, *ACS Omega* **2018**, *3*, 12730-12736.
- [67] D.-G. Chen, T.-C. Lin, C.-L. Chen, Y.-T. Chen, Y.-A. Chen, G.-H. Lee, P.-T. Chou, C.-W. Liao, P.-C. Chiu, C.-H. Chang, Y.-J. Lien, Y. Chi, *ACS Appl. Mater. Interfaces* **2018**, *10*, 12886-12896.
- [68] M. Stanoppi, A. Lorbach, *Dalton Trans.* **2018**, *47*, 10394-10398.
- [69] C. D. Entwistle, T. B. Marder, *Angew. Chem. Int. Ed.* **2002**, *41*, 2927-2931; *Angew. Chem.* **2002**, *114*, 3051-3056.
- [70] C. D. Entwistle, T. B. Marder, *Chem. Mater.* **2004**, *16*, 4574-4585.
- [71] S. Yamaguchi, A. Wakamiya, *Pure Appl. Chem.* **2006**, *78*, 1413.
- [72] F. Jäkle, *Coord. Chem. Rev.* **2006**, *250*, 1107-1121.
- [73] M. Elbing, G. C. Bazan, *Angew. Chem. Int. Ed.* **2008**, *47*, 834-838; *Angew. Chem.* **2008**, *120*, 846-850.
- [74] Z. M. Hudson, S. Wang, *Acc. Chem. Res.* **2009**, *42*, 1584-1596.
- [75] C. R. Wade, A. E. J. Broomsgrove, S. Aldridge, F. P. Gabbaï, *Chem. Rev.* **2010**, *110*, 3958-3984.
- [76] Z. M. Hudson, S. Wang, *Dalton Trans.* **2011**, *40*, 7805-7816.
- [77] A. Wakamiya, S. Yamaguchi, *Bull. Chem. Soc. Jpn.* **2015**, *88*, 1357-1377.
- [78] L. Ji, S. Griesbeck, T. B. Marder, *Chem. Sci.* **2017**, *8*, 846-863.
- [79] S.-Y. Li, Z.-B. Sun, C.-H. Zhao, *Inorg. Chem.* **2017**, *56*, 8705-8717.
- [80] G. Turkoglu, M. E. Cinar, T. Ozturk, *Molecules* **2017**, *22*, 1522.
- [81] N. Matsumi, K. Naka, Y. Chujo, *J. Am. Chem. Soc.* **1998**, *120*, 5112-5113.
- [82] S. Yamaguchi, S. Akiyama, K. Tamao, *J. Am. Chem. Soc.* **2000**, *122*, 6335-6336.
- [83] W.-L. Jia, D. Song, S. Wang, *J. Org. Chem.* **2003**, *68*, 701-705.
- [84] A. Wakamiya, T. Ide, S. Yamaguchi, *J. Am. Chem. Soc.* **2005**, *127*, 14859-14866.
- [85] I. Yamaguchi, B.-J. Choi, T.-A. Koizumi, K. Kubota, T. Yamamoto, *Macromolecules* **2007**, *40*, 438-443.
- [86] U. Megerle, F. Selmaier, C. Lambert, E. Riedle, S. Lochbrunner, *Phys. Chem. Chem. Phys.* **2008**, *10*, 6245-6251.
- [87] A. Lorbach, M. Bolte, H. Li, H.-W. Lerner, M. C. Holthausen, F. Jäkle, M. Wagner, *Angew. Chem. Int. Ed.* **2009**, *48*, 4584-4588; *Angew. Chem.* **2009**, *121*, 4654-4658.
- [88] L. Weber, V. Werner, M. A. Fox, T. B. Marder, S. Schwedler, A. Brockhinke, H.-G. Stammler, B. Neumann, *Dalton Trans.* **2009**, 2823-2831.
- [89] L. Weber, D. Eickhoff, T. B. Marder, M. A. Fox, P. J. Low, A. D. Dwyer, D. J. Tozer, S. Schwedler, A. Brockhinke, H.-G. Stammler, B. Neumann, *Chem. Eur. J.* **2012**, *18*, 1369-1382.
- [90] C. Reus, S. Weidlich, M. Bolte, H.-W. Lerner, M. Wagner, *J. Am. Chem. Soc.* **2013**, *135*, 12892-12907.
- [91] X. Yin, J. Chen, R. A. Lalancette, T. B. Marder, F. Jäkle, *Angew. Chem. Int. Ed.* **2014**, *53*, 9761-9765; *Angew. Chem.* **2014**, *126*, 9919-9923.

## References

- [92] Z. Zhang, R. M. Edkins, J. Nitsch, K. Fucke, A. Eichhorn, A. Steffen, Y. Wang, T. B. Marder, *Chem. Eur. J.* **2015**, *21*, 177-190.
- [93] J. Merz, J. Fink, A. Friedrich, I. Krummenacher, H. H. Al Mamari, S. Lorenzen, M. Haehnel, A. Eichhorn, M. Moos, M. Holzapfel, H. Braunschweig, C. Lambert, A. Steffen, L. Ji, T. B. Marder, *Chem. Eur. J.* **2017**, *23*, 13164-13180.
- [94] J. Merz, A. Steffen, J. Nitsch, J. Fink, C. B. Schürger, A. Friedrich, I. Krummenacher, H. Braunschweig, M. Moos, D. Mims, C. Lambert, T. B. Marder, *Chem. Sci.* **2019**, *10*, 7516-7534.
- [95] H. Belaidi, F. Rauch, Z. Zhang, C. Latouche, A. Boucekkine, T. B. Marder, J.-F. Halet, *ChemPhotoChem* **2020**, *4*, 173-180.
- [96] Z. Yuan, N. J. Taylor, T. B. Marder, I. D. Williams, S. K. Kurtz, L.-T. Cheng, *J. Chem. Soc., Chem. Commun.* **1990**, 1489-1492.
- [97] M. Lequan, R. M. Lequan, K. C. Ching, *J. Mater. Chem.* **1991**, *1*, 997-999.
- [98] M. Lequan, R. M. Lequan, K. C. Ching, M. Barzoukas, A. Fort, H. Lahoucine, G. Bravic, D. Chasseau, J. Gaultier, *J. Mater. Chem.* **1992**, *2*, 719-725.
- [99] M. Lequan, R. M. Lequan, K. Chane-Ching, A.-C. Callier, M. Barzoukas, A. Fort, *Adv. Mater. Optic. Electron.* **1992**, *1*, 243-247.
- [100] Z. Yuan, N. J. Taylor, Y. Sun, T. B. Marder, I. D. Williams, L.-T. Cheng, *J. Organomet. Chem.* **1993**, *449*, 27-37.
- [101] Z. Yuan, N. J. Taylor, R. Ramachandran, T. B. Marder, *Appl. Organomet. Chem.* **1996**, *10*, 305-316.
- [102] C. Branger, M. Lequan, R. M. Lequan, M. Barzoukas, A. Fort, *J. Mater. Chem.* **1996**, *6*, 555-558.
- [103] Z.-Q. Liu, Q. Fang, D. Wang, G. Xue, W.-T. Yu, Z.-S. Shao, M.-H. Jiang, *Chem. Commun.* **2002**, 2900-2901.
- [104] Z.-Q. Liu, Q. Fang, D. Wang, D.-X. Cao, G. Xue, W.-T. Yu, H. Lei, *Chem. Eur. J.* **2003**, *9*, 5074-5084.
- [105] Z.-Q. Liu, Q. Fang, D.-X. Cao, D. Wang, G.-B. Xu, *Org. Lett.* **2004**, *6*, 2933-2936.
- [106] M. Charlot, L. Porres, C. D. Entwistle, A. Beeby, T. B. Marder, M. Blanchard-Desce, *Phys. Chem. Chem. Phys.* **2005**, *7*, 600-606.
- [107] Z.-Q. Liu, M. Shi, F.-Y. Li, Q. Fang, Z.-H. Chen, T. Yi, C.-H. Huang, *Org. Lett.* **2005**, *7*, 5481-5484.
- [108] Z. Yuan, C. D. Entwistle, J. C. Collings, D. Albesa-Jové, A. S. Batsanov, J. A. K. Howard, N. J. Taylor, H. M. Kaiser, D. E. Kaufmann, S.-Y. Poon, W.-Y. Wong, C. Jardin, S. Fathallah, A. Boucekkine, J.-F. Halet, T. B. Marder, *Chem. Eur. J.* **2006**, *12*, 2758-2771.
- [109] C. D. Entwistle, J. C. Collings, A. Steffen, L.-O. Pålsson, A. Beeby, D. Albesa-Jove, J. M. Burke, A. S. Batsanov, J. A. K. Howard, J. A. Mosely, S.-Y. Poon, W.-Y. Wong, F. Ibersiene, S. Fathallah, A. Boucekkine, J.-F. Halet, T. B. Marder, *J. Mater. Chem.* **2009**, *19*, 7532-7544.
- [110] J. C. Collings, S.-Y. Poon, C. Le Droumaguet, M. Charlot, C. Katan, L.-O. Pålsson, A. Beeby, J. A. Mosely, H. M. Kaiser, D. Kaufmann, W.-Y. Wong, M. Blanchard-Desce, T. B. Marder, *Chem. Eur. J.* **2009**, *15*, 198-208.
- [111] L. Ji, Q. Fang, M.-S. Yuan, Z.-Q. Liu, Y.-X. Shen, H.-F. Chen, *Org. Lett.* **2010**, *12*, 5192-5195.
- [112] N. S. Makarov, S. Mukhopadhyay, K. Yesudas, J.-L. Brédas, J. W. Perry, A. Pron, M. Kivala, K. Müllen, *J. Phys. Chem. A* **2012**, *116*, 3781-3793.
- [113] L. Ji, R. M. Edkins, L. J. Sewell, A. Beeby, A. S. Batsanov, K. Fucke, M. Drafz, J. A. K. Howard, O. Moutounet, F. Ibersiene, A. Boucekkine, E. Furet, Z. Liu, J.-F. Halet, C. Katan, T. B. Marder, *Chem. Eur. J.* **2014**, *20*, 13618-13635.



- [114] P. Chen, A. S. Marshall, S. H. Chi, X. Yin, J. W. Perry, F. Jäkle, *Chem. Eur. J.* **2015**, *21*, 18237-18247.
- [115] S. Griesbeck, Z. Zhang, M. Gutmann, T. Lühmann, R. M. Edkins, G. Clermont, A. N. Lazar, M. Haehnel, K. Edkins, A. Eichhorn, M. Blanchard-Desce, L. Meinel, T. B. Marder, *Chem. Eur. J.* **2016**, *22*, 14701-14706.
- [116] S. Griesbeck, E. Michail, C. Wang, H. Ogasawara, S. Lorenzen, L. Gerstner, T. Zang, J. Nitsch, Y. Sato, R. Bertermann, M. Taki, C. Lambert, S. Yamaguchi, T. B. Marder, *Chem. Sci.* **2019**, *10*, 5405-5422.
- [117] S. Griesbeck, M. Ferger, C. Czernetzi, C. Wang, R. Bertermann, A. Friedrich, M. Haehnel, D. Sieh, M. Taki, S. Yamaguchi, T. B. Marder, *Chem. Eur. J.* **2019**, *25*, 7679-7688.
- [118] S. Griesbeck, E. Michail, F. Rauch, H. Ogasawara, C. Wang, Y. Sato, R. M. Edkins, Z. Zhang, M. Taki, C. Lambert, S. Yamaguchi, T. B. Marder, *Chem. Eur. J.* **2019**, *25*, 13164-13175.
- [119] S. Yamaguchi, S. Akiyama, K. Tamao, *J. Am. Chem. Soc.* **2001**, *123*, 11372-11375.
- [120] T. W. Hudnall, C.-W. Chiu, F. P. Gabbaï, *Acc. Chem. Res.* **2009**, *42*, 388-397.
- [121] Ž. Ban, S. Griesbeck, S. Tomić, J. Nitsch, T. B. Marder, I. Piantanida, *Chem. Eur. J.* **2020**, *26*, 2195-2203.
- [122] Y. Shirota, *J. Mater. Chem.* **2000**, *10*, 1-25.
- [123] A. Wakamiya, K. Mori, S. Yamaguchi, *Angew. Chem. Int. Ed.* **2007**, *46*, 4273-4276; *Angew. Chem.* **2007**, *119*, 4351-4354.
- [124] S. Toyota, M. Asakura, M. Oki, F. Toda, *Bull. Chem. Soc. Jpn.* **2000**, *73*, 2357-2362.
- [125] S. M. Cornet, K. B. Dillon, C. D. Entwistle, M. A. Fox, A. E. Goeta, H. P. Goodwin, T. B. Marder, A. L. Thompson, *Dalton Trans.* **2003**, 4395-4405.
- [126] Z. Lu, Z. Cheng, Z. Chen, L. Weng, Z. H. Li, H. Wang, *Angew. Chem. Int. Ed.* **2011**, *50*, 12227-12231; *Angew. Chem.* **2011**, *123*, 12435-12439.
- [127] J. Wang, Y. Wang, T. Taniguchi, S. Yamaguchi, S. Irle, *J. Phys. Chem. A* **2012**, *116*, 1151-1158.
- [128] H. Ye, Z. Lu, D. You, Z. Chen, Z. H. Li, H. Wang, *Angew. Chem. Int. Ed.* **2012**, *51*, 12047-12050; *Angew. Chem.* **2012**, *124*, 12213-12216.
- [129] Z. Lu, Y. Wang, J. Liu, Y.-J. Lin, Z. H. Li, H. Wang, *Organometallics* **2013**, *32*, 6753-6758.
- [130] T. Taniguchi, J. Wang, S. Irle, S. Yamaguchi, *Dalton Trans.* **2013**, *42*, 620-624.
- [131] Z. Zhang, R. M. Edkins, J. Nitsch, K. Fucke, A. Steffen, L. E. Longobardi, D. W. Stephan, C. Lambert, T. B. Marder, *Chem. Sci.* **2015**, *6*, 308-321.
- [132] Z. Zhang, R. M. Edkins, M. Haehnel, M. Wehner, A. Eichhorn, L. Mailänder, M. Meier, J. Brand, F. Brede, K. Müller-Buschbaum, H. Braunschweig, T. B. Marder, *Chem. Sci.* **2015**, *6*, 5922-5927.
- [133] J. Zheng, Y.-J. Lin, H. Wang, *Dalton Trans.* **2016**, *45*, 6088-6093.
- [134] X. Yin, F. Guo, R. A. Lalancette, F. Jäkle, *Macromolecules* **2016**, *49*, 537-546.
- [135] D.-T. Yang, S. K. Møllerup, J.-B. Peng, X. Wang, Q.-S. Li, S. Wang, *J. Am. Chem. Soc.* **2016**, *138*, 11513-11516.
- [136] R. J. Blagg, E. J. Lawrence, K. Resner, V. S. Oganessian, T. J. Herrington, A. E. Ashley, G. G. Wildgoose, *Dalton Trans.* **2016**, *45*, 6023-6031.
- [137] Q. Yan, M. Yin, C. Chen, Y. Zhang, *J. Org. Chem.* **2018**, *83*, 9096-9102.
- [138] T. E. Stennett, P. Bissinger, S. Griesbeck, S. Ullrich, I. Krummenacher, M. Auth, A. Sperlich, M. Stolte, K. Radacki, C.-J. Yao, F. Würthner, A. Steffen, T. B. Marder, H. Braunschweig, *Angew. Chem. Int. Ed.* **2019**, *58*, 6449-6454. *Angew. Chem.* **2019**, *131*, 6516-6521.
- [139] M. Yokoyama, K. Inada, Y. Tsuchiya, H. Nakanotani, C. Adachi, *Chem. Commun.* **2018**, *54*, 8261-8264.

## References

- [140] W. Li, Y. Pan, L. Yao, H. Liu, S. Zhang, C. Wang, F. Shen, P. Lu, B. Yang, Y. Ma, *Adv. Opt. Mater.* **2014**, *2*, 892-901.
- [141] Y. Jiang, Z. Hu, B. Zhou, C. Zhong, Z. Sun, H. Sun, *J. Phys. Chem. C* **2019**, *123*, 5616-5625.
- [142] A. K. Narsaria, J. Poater, C. Fonseca Guerra, A. W. Ehlers, K. Lammertsma, F. M. Bickelhaupt, *J. Comput. Chem.* **2018**, *39*, 2690-2696.
- [143] X.-H. Shan, B. Yang, H.-X. Zheng, J.-P. Qu, Y.-B. Kang, *Org. Lett.* **2018**, *20*, 7898-7901.
- [144] T. Ishiyama, J. Takagi, K. Ishida, N. Miyaura, N. R. Anastasi, J. F. Hartwig, *J. Am. Chem. Soc.* **2002**, *124*, 390-391.
- [145] E. C. Neeve, S. J. Geier, I. A. I. Mkhaliid, S. A. Westcott, T. B. Marder, *Chem. Rev.* **2016**, *116*, 9091-9161.
- [146] J. M. Murphy, C. C. Tzschucke, J. F. Hartwig, *Org. Lett.* **2007**, *9*, 757-760.
- [147] A. J. J. Lennox, G. C. Lloyd-Jones, *Chem. Soc. Rev.* **2014**, *43*, 412-443.
- [148] G. A. Molander, *J. Org. Chem.* **2015**, *80*, 7837-7848.
- [149] K. Schickedanz, T. Trageser, M. Bolte, H.-W. Lerner, M. Wagner, *Chem. Commun.* **2015**, *51*, 15808-15810.
- [150] K. Schickedanz, J. Radtke, M. Bolte, H.-W. Lerner, M. Wagner, *J. Am. Chem. Soc.* **2017**, *139*, 2842-2851.
- [151] S. Konishi, T. Iwai, M. Sawamura, *Organometallics* **2018**, *37*, 1876-1883.
- [152] M. W. Drover, K. Nagata, J. C. Peters, *Chem. Commun.* **2018**, *54*, 7916-7919.
- [153] X. Jia, J. Nitsch, L. Ji, Z. Wu, A. Friedrich, F. Kerner, M. Moos, C. Lambert, T. B. Marder, *Chem. Eur. J.* **2019**, *25*, 10845-10857.
- [154] K. Zhang, Q. Sun, Z. Zhang, L. Tang, Z. Xie, Z. Chi, S. Xue, H. Zhang, W. Yang, *Chem. Commun.* **2018**, *54*, 5225-5228.
- [155] N. Liu, B. Wang, W. Chen, C. Liu, X. Wang, Y. Hu, *RSC Adv.* **2014**, *4*, 51133-51139.
- [156] M. Mantina, A. C. Chamberlin, R. Valero, C. J. Cramer, D. G. Truhlar, *J. Phys. Chem. A* **2009**, *113*, 5806-5812.
- [157] N. G. Connelly, W. E. Geiger, *Chem. Rev.* **1996**, *96*, 877-910.
- [158] D. Tsiplakides, D. Archonta, C. G. Vayenas, *Top. Catal.* **2007**, *44*, 469-479.
- [159] D. Reitzenstein, T. Quast, F. Kanal, M. Kullmann, S. Ruetzel, M. S. Hammer, C. Deibel, V. Dyakonov, T. Brixner, C. Lambert, *Chem. Mater.* **2010**, *22*, 6641-6655.
- [160] X. Cai, M. Sakamoto, M. Fujitsuka, T. Majima, *J. Phys. Chem. A* **2007**, *111*, 1788-1791.
- [161] B. Valeur, *Molecular Fluorescence*, Wiley-VCH, Weinheim, **2001**.
- [162] R. Stahl, C. Lambert, C. Kaiser, R. Wortmann, R. Jakober, *Chem. Eur. J.* **2006**, *12*, 2358-2370.
- [163] C. Dou, S. Saito, K. Matsuo, I. Hisaki, S. Yamaguchi, *Angew. Chem. Int. Ed.* **2012**, *51*, 12206-12210; *Angew. Chem.* **2012**, *124*, 12372-12376.
- [164] C. Hoffend, M. Diefenbach, E. Januszewski, M. Bolte, H. W. Lerner, M. C. Holthausen, M. Wagner, *Dalton Trans.* **2013**, *42*, 13826-13837.
- [165] A. Escande, M. J. Ingleson, *Chem. Commun.* **2015**, *51*, 6257-6274.
- [166] V. M. Hertz, N. Ando, M. Hirai, M. Bolte, H.-W. Lerner, S. Yamaguchi, M. Wagner, *Organometallics* **2016**, *36*, 2512-2519.
- [167] B. Su, R. Kinjo, *Synthesis* **2017**, *49*, 2985-3034.
- [168] E. von Grotthuss, A. John, T. Kaese, M. Wagner, *Asian J. Org. Chem.* **2018**, *7*, 37-53.
- [169] Y. Su, R. Kinjo, *Chem. Soc. Rev.* **2019**, *48*, 3613-3659.
- [170] Z. Zhou, A. Wakamiya, T. Kushida, S. Yamaguchi, *J. Am. Chem. Soc.* **2012**, *134*, 4529-4532.
- [171] J. Yoshino, Y. Nakamura, S. Kunitomo, N. Hayashi, H. Higuchi, *Tetrahedron Lett.* **2013**, *54*, 2817-2820.
- [172] A. Ito, K. Kawanishi, E. Sakuda, N. Kitamura, *Chem. Eur. J.* **2014**, *20*, 3940-3953.

- [173] J. He, F. Rauch, A. Friedrich, D. Sieh, T. Ribbeck, I. Krummenacher, H. Braunschweig, M. Finze, T. B. Marder, *Chem. Eur. J.* **2019**, *25*, 13777-13784.
- [174] K. Parab, K. Venkatasubbaiah, F. Jäkle, *J. Am. Chem. Soc.* **2006**, *128*, 12879-12885.
- [175] G. C. Welch, R. R. S. Juan, J. D. Masuda, D. W. Stephan, *Science* **2006**, *314*, 1124-1126.
- [176] G. C. Welch, D. W. Stephan, *J. Am. Chem. Soc.* **2007**, *129*, 1880-1881.
- [177] S. J. Geier, D. W. Stephan, *J. Am. Chem. Soc.* **2009**, *131*, 3476-3477.
- [178] D. W. Stephan, G. Erker, *Angew. Chem. Int. Ed.* **2010**, *49*, 46-76; *Angew. Chem.* **2010**, *122*, 50-81.
- [179] D. W. Stephan, G. Erker, *Chem. Sci.* **2014**, *5*, 2625-2641.
- [180] D. W. Stephan, *J. Am. Chem. Soc.* **2015**, *137*, 10018-10032.
- [181] D. W. Stephan, G. Erker, *Angew. Chem. Int. Ed.* **2015**, *54*, 6400-6441; *Angew. Chem.* **2015**, *127*, 6498-6541.
- [182] J. J. Eisch, N. K. Hota, S. Kozima, *J. Am. Chem. Soc.* **1969**, *91*, 4575-4577.
- [183] J. J. Eisch, J. E. Galle, S. Kozima, *J. Am. Chem. Soc.* **1986**, *108*, 379-385.
- [184] S. Kim, K.-H. Song, S. O. Kang, J. Ko, *Chem. Commun.* **2004**, 68-69.
- [185] H. Braunschweig, I. Fernández, G. Frenking, T. Kupfer, *Angew. Chem. Int. Ed.* **2008**, *47*, 1951-1954; *Angew. Chem.* **2008**, *120*, 1977-1980.
- [186] C. Fan, W. E. Piers, M. Parvez, *Angew. Chem. Int. Ed.* **2009**, *48*, 2955-2958.
- [187] J. Koehler, S. Lindenmeier, I. Fischer, H. Braunschweig, T. Kupfer, D. Gamon, C.-W. Chiu, *J. Raman Spectrosc.* **2010**, *41*, 636-641.
- [188] A. Steffen, R. M. Ward, W. D. Jones, T. B. Marder, *Coord. Chem. Rev.* **2010**, *254*, 1950-1976.
- [189] H. Braunschweig, T. Kupfer, *Chem. Commun.* **2011**, *47*, 10903-10914.
- [190] H. Braunschweig, C.-W. Chiu, D. Gamon, M. Kaupp, I. Krummenacher, T. Kupfer, R. Müller, K. Radacki, *Chem. Eur. J.* **2012**, *18*, 11732-11746.
- [191] T. Araki, A. Fukazawa, S. Yamaguchi, *Angew. Chem. Int. Ed.* **2012**, *51*, 5484-5487; *Angew. Chem.* **2012**, *124*, 5580-5583.
- [192] H. Braunschweig, I. Krummenacher, J. Wahler, *Adv. Organomet. Chem.* **2013**, *61*, 1-53.
- [193] H. Braunschweig, C. Hörl, L. Mailänder, K. Radacki, J. Wahler, *Chem. Eur. J.* **2014**, *20*, 9858-9861.
- [194] J. H. Barnard, S. Yruegas, K. Huang, C. D. Martin, *Chem. Commun.* **2016**, *52*, 9985-9991.
- [195] W. Zhang, B. Zhang, D. Yu, G. He, *Sci. Bull.* **2017**, *62*, 899-900.
- [196] M. Meier, L. Ji, J. Nitsch, I. Krummenacher, A. Deissenberger, D. Auerhammer, M. Schäfer, T. B. Marder, H. Braunschweig, *Chem. Eur. J.* **2019**, *25*, 4707-4712.
- [197] H. C. Brown, V. H. Dodson, *J. Am. Chem. Soc.* **1957**, *79*, 2302-2306.
- [198] P. J. Grisdale, J. L. R. Williams, M. E. Glogowski, B. E. Babb, *J. Org. Chem.* **1971**, *36*, 544-549.
- [199] H. Braunschweig, V. Dyakonov, J. O. C. Jimenez-Halla, K. Kraft, I. Krummenacher, K. Radacki, A. Sperlich, J. Wahler, *Angew. Chem. Int. Ed.* **2012**, *51*, 2977-2980; *Angew. Chem.* **2012**, *124*, 3031-3034.
- [200] S. Yamaguchi, T. Shirasaka, S. Akiyama, K. Tamao, *J. Am. Chem. Soc.* **2002**, *124*, 8816-8817.
- [201] A. Wakamiya, K. Mishima, K. Ekawa, S. Yamaguchi, *Chem. Commun.* **2008**, 579-581.
- [202] M. F. Smith, S. J. Cassidy, I. A. Adams, M. Vasiliu, D. L. Gerlach, D. A. Dixon, P. A. Rugar, *Organometallics* **2016**, *35*, 3182-3191.
- [203] S. J. Cassidy, I. Brettell-Adams, L. E. McNamara, M. F. Smith, M. Bautista, H. Cao, M. Vasiliu, D. L. Gerlach, F. Qu, N. I. Hammer, D. A. Dixon, P. A. Rugar, *Organometallics* **2018**, *37*, 3732-3741.

## References

- [204] S. Yruegas, J. J. Martinez, C. D. Martin, *Chem. Commun.* **2018**, *54*, 6808-6811.
- [205] K. R. Bluer, L. E. Laperriere, A. Pujol, S. Yruegas, V. A. K. Adiraju, C. D. Martin, *Organometallics* **2018**, *37*, 2917-2927.
- [206] S. Yruegas, J. H. Barnard, K. Al-Furaiji, J. L. Dutton, D. J. D. Wilson, C. D. Martin, *Organometallics* **2018**, *37*, 1515-1518.
- [207] T. A. Bartholome, K. R. Bluer, C. D. Martin, *Dalton Trans.* **2019**, *48*, 6319-6322.
- [208] L. E. Laperriere, S. Yruegas, C. D. Martin, *Tetrahedron* **2019**, *75*, 937-943.
- [209] P. A. Chase, P. E. Romero, W. E. Piers, M. Parvez, B. O. Patrick, *Can. J. Chem.* **2005**, *83*, 2098-2105.
- [210] P. A. Chase, W. E. Piers, B. O. Patrick, *J. Am. Chem. Soc.* **2000**, *122*, 12911-12912.
- [211] I. A. Adams, P. A. Rugar, *Macromol. Rapid Commun.* **2015**, *36*, 1336-1340.
- [212] C. J. Berger, G. He, C. Merten, R. McDonald, M. J. Ferguson, E. Rivard, *Inorg. Chem.* **2014**, *53*, 1475-1486.
- [213] W. Yang, K. E. Krantz, L. A. Freeman, D. A. Dickie, A. Molino, A. Kaur, D. J. D. Wilson, R. J. Gilliard Jr., *Chem. Eur. J.* **2019**, *25*, 12512-12516.
- [214] I. A. I. Mkhallid, J. H. Barnard, T. B. Marder, J. M. Murphy, J. F. Hartwig, *Chem. Rev.* **2010**, *110*, 890-931.
- [215] R. J. Blagg, T. R. Simmons, G. R. Hatton, J. M. Courtney, E. L. Bennett, E. J. Lawrence, G. G. Wildgoose, *Dalton Trans.* **2016**, *45*, 6032-6043.
- [216] H. Jacobsen, H. Berke, S. Döring, G. Kehr, G. Erker, R. Fröhlich, O. Meyer, *Organometallics* **1999**, *18*, 1724-1735.
- [217] H. Braunschweig, I. Krummenacher, *Electrochemical Behavior and Redox Chemistry of Boroles*, in *Organic Redox Systems*, John Wiley & Sons, Inc., Hoboken, NJ, **2015**, pp. 503-522.
- [218] P. Bissinger, H. Braunschweig, A. Damme, C. Hörl, I. Krummenacher, T. Kupfer, *Angew. Chem. Int. Ed.* **2015**, *54*, 359-362; *Angew. Chem.* **2015**, *127*, 366-369.
- [219] A. Iida, S. Yamaguchi, *J. Am. Chem. Soc.* **2011**, *133*, 6952-6955.
- [220] J. M. Farrell, C. Mützel, D. Bialas, M. Rudolf, K. Menekse, A.-M. Krause, M. Stolte, F. Würthner, *J. Am. Chem. Soc.* **2019**, *141*, 9096-9104.
- [221] S. A. Cummings, M. Iimura, C. J. Harlan, R. J. Kwaan, I. V. Trieu, J. R. Norton, B. M. Bridgewater, F. Jäkle, A. Sundararaman, M. Tilset, *Organometallics* **2006**, *25*, 1565-1568.
- [222] H. Braunschweig, F. Breher, C.-W. Chiu, D. Gamon, D. Nied, K. Radacki, *Angew. Chem. Int. Ed.* **2010**, *49*, 8975-8978; *Angew. Chem.* **2010**, *122*, 9159-9162.
- [223] K. M. M. Josef, *Lichtabsorption und Photochemie organischer Moleküle*, VCH, Weinheim; New York, **1989**.
- [224] A. G. Crawford, A. D. Dwyer, Z. Liu, A. Steffen, A. Beeby, L.-O. Pålsson, D. J. Tozer, T. B. Marder, *J. Am. Chem. Soc.* **2011**, *133*, 13349-13362.
- [225] T. M. Figueira-Duarte, K. Müllen, *Chem. Rev.* **2011**, *111*, 7260-7314.
- [226] M. K. Manna, S. Shokri, G. P. Wiederrecht, D. J. Gosztola, A. J.-L. Aytou, *Chem. Commun.* **2018**, *54*, 5809-5818.
- [227] Y. Liu, C. Li, Z. Ren, S. Yan, M. R. Bryce, *Nat. Rev. Mater.* **2018**, *3*, 18020.
- [228] M. J. G. Peach, P. Benfield, T. Helgaker, D. J. Tozer, *J. Chem. Phys.* **2008**, *128*, 044118.
- [229] T. Yanai, D. P. Tew, N. C. Handy, *Chem. Phys. Lett.* **2004**, *393*, 51-57.
- [230] F. Jäkle, *Chem. Rev.* **2010**, *110*, 3985-4022.
- [231] S. M. Berger, M. Ferger, T. B. Marder, **2020**, manuscript in preparation.
- [232] M. Ferger, S. M. Berger, F. Rauch, M. Schönitz, J. Rühle, J. Krebs, A. Friedrich, T. B. Marder, **2020**, manuscript in preparation.
- [233] J. Liu, S. Zhang, J. Zhu, X. Liu, G. Yang, X. Zhang, *Anal. Bioanal. Chem.* **2019**, *411*, 5223-5231.

- [234] D. A. Tomalia, H. Baker, J. Dewald, M. Hall, G. Kallos, S. Martin, J. Roeck, J. Ryder, P. Smith, *Polym. J.* **1985**, *17*, 117-132.
- [235] A. W. Bosman, H. M. Janssen, E. W. Meijer, *Chem. Rev.* **1999**, *99*, 1665-1688.
- [236] J.-P. Majoral, A.-M. Caminade, *Chem. Rev.* **1999**, *99*, 845-880.
- [237] D. Astruc, F. Chardac, *Chem. Rev.* **2001**, *101*, 2991-3024.
- [238] G. M. Dykes, *J. Chem. Technol. Biotechnol.* **2001**, *76*, 903-918.
- [239] S. M. Grayson, J. M. J. Fréchet, *Chem. Rev.* **2001**, *101*, 3819-3868.
- [240] A. D'Emanuele, D. Attwood, *Adv. Drug Delivery Rev.* **2005**, *57*, 2147-2162.
- [241] D. Astruc, C. Ornelas, J. Ruiz, *Acc. Chem. Res.* **2008**, *41*, 841-856.
- [242] E. de Jesús, J. C. Flores, *Ind. Eng. Chem. Res.* **2008**, *47*, 7968-7981.
- [243] D. Astruc, E. Boisselier, C. Ornelas, *Chem. Rev.* **2010**, *110*, 1857-1959.
- [244] R. Hourani, A. Kakkar, *Macromol. Rapid Commun.* **2010**, *31*, 947-974.
- [245] A. Sellinger, T. Zhou, Conjugated Dendrimers, in *Encyclopedia of Polymeric Nanomaterials*, Springer, Berlin, **2015**, pp. 412-427.
- [246] A. R. Menjoge, R. M. Kannan, D. A. Tomalia, *Drug Discov. Today* **2010**, *15*, 171-185.
- [247] R. Kopelman, M. Shortreed, Z.-Y. Shi, W. Tan, Z. Xu, J. S. Moore, A. Bar-Haim, J. Klafter, *Phys. Rev. Lett.* **1997**, *78*, 1239-1242.
- [248] Y. Shirota, Y. Kuwabara, H. Inada, T. Wakimoto, H. Nakada, Y. Yonemoto, S. Kawami, K. Imai, *Appl. Phys. Lett.* **1994**, *65*, 807-809.
- [249] J. Bettenhausen, M. Greczmiel, M. Jandke, P. Stroehriegl, *Synth. Met.* **1997**, *91*, 223-228.
- [250] J. M. Lupton, I. D. W. Samuel, R. Beavington, M. J. Frampton, P. L. Burn, H. Bäessler, *Phys. Rev. B* **2001**, *63*, 155206.
- [251] J. Ding, B. Zhang, J. Lü, Z. Xie, L. Wang, X. Jing, F. Wang, *Adv. Mater.* **2009**, *21*, 4983-4986.
- [252] J.-L. Wang, Y. Zhou, Y. Li, J. Pei, *J. Org. Chem.* **2009**, *74*, 7449-7456.
- [253] J.-L. Wang, Z.-M. Tang, Q. Xiao, Y. Ma, J. Pei, *Org. Lett.* **2008**, *10*, 4271-4274.
- [254] T. Shimamoto, K. Miyanari, A. Fujii, I. Akai, M. Kimura, *Phys. Status Solidi C* **2011**, *8*, 58-61.
- [255] M. Halim, I. D. W. Samuel, J. N. G. Pillow, P. L. Burn, *Synth. Met.* **1999**, *102*, 1113-1114.
- [256] S.-C. Lo, G. J. Richards, J. P. J. Markham, E. B. Namdas, S. Sharma, P. L. Burn, I. D. W. Samuel, *Adv. Funct. Mater.* **2005**, *15*, 1451-1458.
- [257] T. D. Anthopoulos, M. J. Frampton, E. B. Namdas, P. L. Burn, I. D. W. Samuel, *Adv. Mater.* **2004**, *16*, 557-560.
- [258] J. C. Ribierre, A. Ruseckas, I. D. W. Samuel, H. S. Barcena, P. L. Burn, *J. Chem. Phys.* **2008**, *128*, 204703.
- [259] S.-C. Lo, N. A. H. Male, J. P. J. Markham, S. W. Magennis, P. L. Burn, O. V. Salata, I. D. W. Samuel, *Adv. Mater.* **2002**, *14*, 975-979.
- [260] N. Kopidakis, W. J. Mitchell, J. v. d. Lagemaat, D. S. Ginley, G. Rumbles, S. E. Shaheen, W. L. Rance, *Appl. Phys. Lett.* **2006**, *89*, 103524.
- [261] C.-Q. Ma, M. Fonrodona, M. C. Schikora, M. M. Wienk, R. A. J. Janssen, P. Bäuerle, *Adv. Funct. Mater.* **2008**, *18*, 3323-3331.
- [262] C.-Q. Ma, E. Mena-Osteritz, T. Debaerdemaeker, M. M. Wienk, R. A. J. Janssen, P. Bäuerle, *Angew. Chem. Int. Ed.* **2007**, *46*, 1679-1683; *Angew. Chem.* **2007**, *119*, 1709-1713.
- [263] G. Wu, R. F. Barth, W. Yang, M. Chatterjee, W. Tjarks, M. J. Ciesielski, R. A. Fenstermaker, *Bioconjugate Chem.* **2004**, *15*, 185-194.
- [264] R. Roesler, B. J. N. Har, W. E. Piers, *Organometallics* **2002**, *21*, 4300-4302.
- [265] B. Qualmann, M. M. Kessels, H.-J. Musiol, W. D. Sierralta, P. W. Jungblut, L. Moroder, *Angew. Chem. Int. Ed.* **1996**, *35*, 909-911; *Angew. Chem.* **1996**, *108*, 970-973.

## References

- [266] D. Armspach, M. Cattalini, E. C. Constable, C. E. Housecroft, D. Phillips, *Chem. Commun.* **1996**, 1823-1824.
- [267] H. Nemoto, J. Cai, Y. Yamamoto, *J. Chem. Soc., Chem. Commun.* **1994**, 577-578.
- [268] A. Proñ, M. Baumgarten, K. Müllen, *Org. Lett.* **2010**, *12*, 4236-4239.
- [269] T. Agou, T. Kojima, J. Kobayashi, T. Kawashima, *Org. Lett.* **2009**, *11*, 3534-3537.
- [270] I. A. I. Mkhaliid, J. H. Barnard, T. B. Marder, J. M. Murphy, J. F. Hartwig, *Chem. Rev.* **2010**, *110*, 890-931.
- [271] T. L. Rathman, W. F. Bailey, *Org. Process Res. Dev.* **2009**, *13*, 144-151.
- [272] W. F. Bailey, J. J. Patricia, *J. Organomet. Chem.* **1988**, *352*, 1-46.
- [273] F. H. Allen, O. Kennard, D. G. Watson, L. Brammer, A. G. Orpen, R. Taylor, *J. Chem. Soc., Perkin Trans. 2* **1987**, S1-S19.
- [274] K. Okada, T. Sugawa, M. Oda, *J. Chem. Soc., Chem. Commun.* **1992**, 74-75.
- [275] W. Kaim, A. Schulz, *Angew. Chem. Int. Ed.* **1984**, *23*, 615-616.
- [276] A. Schulz, W. Kaim, *Chem. Ber.* **1989**, *122*, 1863-1868.
- [277] R. F. Winter, *Organometallics* **2014**, *33*, 4517-4536.
- [278] L. Ji, R. M. Edkins, A. Lorbach, I. Krummenacher, C. Brückner, A. Eichhorn, H. Braunschweig, B. Engels, P. J. Low, T. B. Marder, *J. Am. Chem. Soc.* **2015**, *137*, 6750-6753.
- [279] A. B. Buades, V. Sanchez Arderiu, D. Olid-Britos, C. Viñas, R. Sillanpää, M. Haukka, X. Fontrodona, M. Paradinas, C. Ocal, F. Teixidor, *J. Am. Chem. Soc.* **2018**, *140*, 2957-2970.
- [280] J. Li, C. G. Daniliuc, G. Kehr, G. Erker, *Angew. Chem. Int. Ed.* **2019**, *58*, 6737-6741; *Angew. Chem.* **2019**, *58*, 6737-6741.
- [281] G. Wittig, W. Herwig, *Chem. Ber.* **1955**, *88*, 962-976.
- [282] G. Wittig, G. Keicher, A. Rückert, P. Raff, *Liebigs Ann. Chem.* **1949**, *563*, 110-126.
- [283] J. C. Doty, B. Babb, P. J. Grisdale, M. Glogowski, J. L. R. Williams, *J. Organomet. Chem.* **1972**, *38*, 229-236.
- [284] R. T. Hawkins, W. J. Lennarz, H. R. Snyder, *J. Am. Chem. Soc.* **1960**, *82*, 3053-3059.
- [285] *Boronic Acids: Preparation and Applications in Organic Synthesis, Medicine and Materials*, 2<sup>nd</sup> ed., (Editor: D. G. Hall), Wiley-VCH, Weinheim, **2011**.
- [286] T. Ishiyama, M. Murata, N. Miyaura, *J. Org. Chem.* **1995**, *60*, 7508-7510.
- [287] W. K. Chow, O. Y. Yuen, P. Y. Choy, C. M. So, C. P. Lau, W. T. Wong, F. Y. Kwong, *RSC Adv.* **2013**, *3*, 12518-12539.
- [288] T. Ishiyama, K. Ishida, J. Takagi, N. Miyaura, *Chem. Lett.* **2001**, *30*, 1082-1083.
- [289] J. F. Hartwig, *Acc. Chem. Res.* **2012**, *45*, 864-873.
- [290] J. Y. Cho, M. K. Tse, D. Holmes, R. E. Maleczka, Jr., M. R. Smith, 3<sup>rd</sup>, *Science* **2002**, *295*, 305-308.
- [291] J. F. Hartwig, *Chem. Soc. Rev.* **2011**, *40*, 1992-2002.
- [292] P. C. Roosen, V. A. Kallepalli, B. Chattopadhyay, D. A. Singleton, R. E. Maleczka, Jr., M. R. Smith, 3<sup>rd</sup>, *J. Am. Chem. Soc.* **2012**, *134*, 11350-11353.
- [293] A. J. Roering, L. V. A. Hale, P. A. Squier, M. A. Ringgold, E. R. Wiederspan, T. B. Clark, *Org. Lett.* **2012**, *14*, 3558-3561.
- [294] A. G. Crawford, Z. Liu, I. A. I. Mkhaliid, M.-H. Thibault, N. Schwarz, G. Alcaraz, A. Steffen, J. C. Collings, A. S. Batsanov, J. A. K. Howard, T. B. Marder, *Chem. Eur. J.* **2012**, *18*, 5022-5035.
- [295] A. Ros, R. Fernandez, J. M. Lassaletta, *Chem. Soc. Rev.* **2014**, *43*, 3229-3243.
- [296] T. M. Boller, J. M. Murphy, M. Hapke, T. Ishiyama, N. Miyaura, J. F. Hartwig, *J. Am. Chem. Soc.* **2005**, *127*, 14263-14278.
- [297] J. M. Murphy, X. Liao, J. F. Hartwig, *J. Am. Chem. Soc.* **2007**, *129*, 15434-15435.
- [298] T. Ishiyama, J. Takagi, J. F. Hartwig, N. Miyaura, *Angew. Chem. Int. Ed.* **2002**, *41*, 3056-3058; *Angew. Chem.* **2002**, *114*, 3182-3184.

- [299] G. A. Chotana, M. A. Rak, M. R. Smith, *J. Am. Chem. Soc.* **2005**, *127*, 10539-10544.
- [300] D. N. Coventry, A. S. Batsanov, A. E. Goeta, J. A. K. Howard, T. B. Marder, R. N. Perutz, *Chem. Commun.* **2005**, 2172-2174.
- [301] T. E. Hurst, T. K. Macklin, M. Becker, E. Hartmann, W. Kügel, J.-C. Parisienne-La Salle, A. S. Batsanov, T. B. Marder, V. Snieckus, *Chem. Eur. J.* **2010**, *16*, 8155-8161.
- [302] Z. Liu, Y. Wang, Y. Chen, J. Liu, Q. Fang, C. Kleeberg, T. B. Marder, *J. Org. Chem.* **2012**, *77*, 7124-7128.
- [303] S. M. Preshlock, B. Ghaffari, P. E. Maligres, S. W. Krska, R. E. Maleczka, Jr., M. R. Smith, 3rd, *J. Am. Chem. Soc.* **2013**, *135*, 7572-7582.
- [304] L. Ji, A. Lorbach, R. M. Edkins, T. B. Marder, *J. Org. Chem.* **2015**, *80*, 5658-5665.
- [305] L. Ji, K. Fucke, S. K. Bose, T. B. Marder, *J. Org. Chem.* **2015**, *80*, 661-665.
- [306] L. Ji, I. Krummenacher, A. Friedrich, A. Lorbach, M. Haehnel, K. Edkins, H. Braunschweig, T. B. Marder, *J. Org. Chem.* **2018**, *83*, 3599-3606.
- [307] Y. Kuroda, Y. Nakao, *Chem. Lett.* **2019**, *48*, 1092-1100.
- [308] S. Paul, G. A. Chotana, D. Holmes, R. C. Reichle, R. E. Maleczka, Jr., M. R. Smith, 3rd, *J. Am. Chem. Soc.* **2006**, *128*, 15552-15553.
- [309] S. Konishi, S. Kawamorita, T. Iwai, P. G. Steel, T. B. Marder, M. Sawamura, *Chem. Asian J.* **2014**, *9*, 434-438.
- [310] Y. Kuninobu, H. Ida, M. Nishi, M. Kanai, *Nat. Chem.* **2015**, *7*, 712-717.
- [311] H. J. Davis, M. T. Mihai, R. J. Phipps, *J. Am. Chem. Soc.* **2016**, *138*, 12759-12762.
- [312] R. Bisht, B. Chattopadhyay, *J. Am. Chem. Soc.* **2016**, *138*, 84-87.
- [313] L. Yang, K. Semba, Y. Nakao, *Angew. Chem. Int. Ed.* **2017**, *56*, 4853-4857; *Angew. Chem.* **2017**, *129*, 4931-4935.
- [314] N. Miyaura, A. Suzuki, *Chem. Rev.* **1995**, *95*, 2457-2483.
- [315] A. Suzuki, *Heterocycles* **2010**, *80*, 15-43.
- [316] A. Suzuki, *Angew. Chem., Int. Ed.* **2011**, *50*, 6722-6737; *Angew. Chem.* **2011**, *123*, 6854-6869.
- [317] G. K. S. Prakash, C. Panja, T. Mathew, V. Surampudi, N. A. Petasis, G. A. Olah, *Org. Lett.* **2004**, *6*, 2205-2207.
- [318] C. C. Tzschucke, J. M. Murphy, J. F. Hartwig, *Org. Lett.* **2007**, *9*, 761-764.
- [319] C. W. Liskey, X. Liao, J. F. Hartwig, *J. Am. Chem. Soc.* **2010**, *132*, 11389-11391.
- [320] P. Novák, A. Lishchynskiy, V. V. Grushin, *Angew. Chem. Int. Ed.* **2012**, *51*, 7767-7770; *Angew. Chem.* **2012**, *124*, 7887-7890.
- [321] P. J. Moon, H. M. Halperin, R. J. Lundgren, *Angew. Chem. Int. Ed.* **2016**, *55*, 1894-1898; *Angew. Chem.* **2016**, *128*, 1926-1930.
- [322] A. Gevorgyan, K. H. Hopmann, A. Bayer, *Chem. Eur. J.* **2020**, *26*, 6064-6069.
- [323] B. A. Vanchura, 2nd, S. M. Preshlock, P. C. Roosen, V. A. Kallepalli, R. J. Staples, R. E. Maleczka, Jr., D. A. Singleton, M. R. Smith, 3rd, *Chem. Commun.* **2010**, *46*, 7724-7726.
- [324] H. Tajuddin, P. Harisson, B. Bitterlich, J. C. Collings, N. Sim, A. S. Batsanov, M. S. Cheung, S. Kawamorita, A. C. Maxwell, L. Shukla, J. Morris, Z. Lin, T. B. Marder, P. G. Steel, *Chem. Sci.* **2012**, *3*, 3505-3515.
- [325] J. Takagi, K. Sato, J. F. Hartwig, T. Ishiyama, N. Miyaura, *Tetrahedron Lett.* **2002**, *43*, 5649-5651.
- [326] T. Ishiyama, J. Takagi, Y. Yonekawa, J. F. Hartwig, N. Miyaura, *Adv. Synth. Catal.* **2003**, *345*, 1103-1106.
- [327] S. A. Sadler, H. Tajuddin, I. A. I. Mkhallid, A. S. Batsanov, D. Albresa-Jove, M. S. Cheung, A. C. Maxwell, L. Shukla, B. Roberts, D. C. Blakemore, Z. Lin, T. B. Marder, P. G. Steel, *Org. Biomol. Chem.* **2014**, *12*, 7318-7327.

## References

- [328] S. A. Sadler, A. C. Hones, B. Roberts, D. Blakemore, T. B. Marder, P. G. Steel, *J. Org. Chem.* **2015**, *80*, 5308-5314.
- [329] X.-M. Wang, Y.-F. Zhou, W.-T. Yu, C. Wang, Q. Fang, M.-H. Jiang, H. Lei, H.-Z. Wang, *J. Mater. Chem.* **2000**, *10*, 2698-2703.
- [330] O. Kwon, S. Barlow, S. A. Odom, L. Beverina, N. J. Thompson, E. Zojer, J.-L. Brédas, S. R. Marder, *J. Phys. Chem. A* **2005**, *109*, 9346-9352.
- [331] L. Weber, V. Werner, M. A. Fox, T. B. Marder, S. Schwedler, A. Brockhinke, H.-G. Stammer, B. Neumann, *Dalton Trans.* **2009**, 1339-1351.
- [332] S. Stoll, A. Schweiger, *J. Magn. Reson.* **2006**, *178*, 42-55.
- [333] M. Schlosser, F. Mongin, J. Porwisiak, W. Dmowski, H. H. Büker, N. M. M. Nibbering, *Chem. Eur. J.* **1998**, *4*, 1281-1286.
- [334] D. E. Grocock, T. K. Jones, G. Hallas, J. D. Hepworth, *J. Chem. Soc. C* **1971**, 3305-3308.
- [335] G. M. Sheldrick, *Acta Crystallogr. A* **2015**, *71*, 3-8.
- [336] G. M. Sheldrick, *Acta Crystallogr. A* **2008**, *64*, 112-122.
- [337] C. B. Hübschle, G. M. Sheldrick, B. Dittrich, *J. Appl. Crystallogr.* **2011**, *44*, 1281-1284.
- [338] Diamond, 4.6.0, K. Brandenburg, Crystal Impact H. Putz & K. Brandenburg GbR, Bonn (Germany), **2017**.
- [339] C. F. Macrae, I. J. Bruno, J. A. Chisholm, P. R. Edgington, P. McCabe, E. Pidcock, L. Rodriguez-Monge, R. Taylor, J. van de Streek, P. A. Wood, *J. Appl. Crystallogr.* **2008**, *41*, 466-470.
- [340] O. V. Dolomanov, L. J. Bourhis, R. J. Gildea, J. A. K. Howard, H. Puschmann, *J. Appl. Crystallogr.* **2009**, *42*, 339-341.
- [341] A. Spek, *Acta Crystallogr. C* **2015**, *71*, 9-18.
- [342] C. Fonseca Guerra, J. G. Snijders, G. Te Velde, E. J. Baerends, *Theor. Chem. Acc.* **1998**, *99*, 391-403.
- [343] G. te Velde, F. M. Bickelhaupt, E. J. Baerends, C. Fonseca Guerra, S. J. A. van Gisbergen, J. G. Snijders, T. Ziegler, *J. Comput. Chem.* **2001**, *22*, 931-967.
- [344] ADF2018, E. J. Baerends, T. Ziegler, A. J. Atkins, J. Autschbach, O. Baseggio, D. Bashford, A. Bérces, F. M. Bickelhaupt, C. Bo, P. M. Boerrigter, L. Cavallo, C. Daul, D. P. Chong, D. V. Chulhai, L. Deng, R. M. Dickson, J. M. Dieterich, D. E. Ellis, M. van Faassen, L. Fan, T. H. Fischer, C. Fonseca Guerra, M. Franchini, A. Ghysels, A. Giammona, S. J. A. van Gisbergen, A. Goez, A. W. Götz, J. A. Groeneveld, O. V. Gritsenko, M. Grüning, S. Gusarov, F. E. Harris, P. van den Hoek, Z. Hu, C. R. Jacob, H. Jacobsen, L. Jensen, L. Joubert, J. W. Kaminski, G. van Kessel, C. König, F. Kootstra, A. Kovalenko, M. V. Krykunov, E. van Lenthe, D. A. McCormack, A. Michalak, M. Mitoraj, S. M. Morton, J. Neugebauer, V. P. Nicu, L. Noodleman, V. P. Osinga, S. Patchkovskii, M. Pavanello, C. A. Peeples, P. H. T. Philipsen, D. Post, C. C. Pye, H. Ramanantoanina, P. Ramos, W. Ravenek, J. I. Rodríguez, P. Ros, R. Rüger, P. R. T. Schipper, D. Schlüns, H. van Schoot, G. Schreckenbach, J. S. Seldenthuis, M. Seth, J. G. Snijders, M. Solà, M. Stener, M. Swart, D. Swerhone, V. Tognetti, G. te Velde, P. Vernooijs, L. Versluis, L. Visscher, O. Visser, F. Wang, T. A. Wesolowski, E. M. van Wezenbeek, G. Wiesenekker, S. K. Wolff, T. K. Woo, A. L. Yakovlev, ADF2018, SCM, Theoretical Chemistry, Vrije Universiteit, <http://www.scm.com>, Amsterdam, The Netherlands, **2018**.
- [345] J. P. Perdew, *Phys. Rev. B* **1986**, *33*, 8822-8824.
- [346] J. P. Perdew, *Phys. Rev. B* **1986**, *34*, 7406-7406.
- [347] A. D. Becke, *Phys. Rev. A* **1988**, *38*, 3098-3100.
- [348] B. G. Johnson, P. M. W. Gill, J. A. Pople, *J. Chem. Phys.* **1993**, *98*, 5612-5626.
- [349] S. Grimme, *Chem. Eur. J.* **2004**, *10*, 3423-3429.
- [350] S. Grimme, S. Ehrlich, L. Goerigk, *J. Comput. Chem.* **2011**, *32*, 1456-1465.



- [351] A. Rosa, E. J. Baerends, S. J. A. Van Gisbergen, E. Van Lenthe, J. A. Groeneveld, J. G. Snijders, *J. Am. Chem. Soc.* **1999**, *121*, 10356-10365.
- [352] A. Bérces, R. M. Dickson, L. Fan, H. Jacobsen, D. Swerhone, T. Ziegler, *Comput. Phys. Commun.* **1997**, *100*, 247-262.
- [353] H. Jacobsen, A. Bérces, D. P. Swerhone, T. Ziegler, *Comput. Phys. Commun.* **1997**, *100*, 263-276.
- [354] S. K. Wolff, *Int. J. Quantum Chem.* **2005**, *104*, 645-659.
- [355] J. F. Janak, *Phys. Rev. B* **1978**, *18*, 7165-7168.
- [356] J. P. Perdew, M. Levy, *Phys. Rev. Lett.* **1983**, *51*, 1884-1887.
- [357] L. Kleinman, *Phys. Rev. B: Condens. Matter Mater. Phys.* **1997**, *56*, 16029-16030.
- [358] R. Baer, E. Livshits, U. Salzner, *Annu. Rev. Phys. Chem.* **2010**, *61*, 85-109.
- [359] L. Kronik, T. Stein, S. Refaely-Abramson, R. Baer, *J. Chem. Theory Comput.* **2012**, *8*, 1515-1531.
- [360] H. Sun, J. Autschbach, *ChemPhysChem* **2013**, *14*, 2450-2461.
- [361] T. J. Penfold, *J. Phys. Chem. C* **2015**, *119*, 13535-13544.
- [362] H. Sun, S. Zhang, C. Zhong, Z. Sun, *J. Comput. Chem.* **2016**, *37*, 684-693.
- [363] T. Körzdörfer, J.-L. Brédas, *Acc. Chem. Res.* **2014**, *47*, 3284-3291.
- [364] H. Sun, C. Zhong, J. L. Brédas, *J. Chem. Theory Comput.* **2015**, *11*, 3851-3858.
- [365] F. Zapata, L. Ridder, J. Hidding, C. R. Jacob, I. Infante, L. Visscher, *J. Chem. Inf. Model.* **2019**, *59*, 3191-3197.
- [366] S. Hirata, M. Head-Gordon, *Chem. Phys. Lett.* **1999**, *314*, 291-299.
- [367] A. Chantzis, A. D. Laurent, C. Adamo, D. Jacquemin, *J. Chem. Theory Comput.* **2013**, *9*, 4517-4525.
- [368] R. L. Martin, *J. Chem. Phys.* **2003**, *118*, 4775-4777.
- [369] M. J. G. Peach, D. J. Tozer, *J. Phys. Chem. A* **2012**, *116*, 9783-9789.
- [370] C. A. Guido, P. Cortona, B. Mennucci, C. Adamo, *J. Chem. Theory Comput.* **2013**, *9*, 3118-3126.
- [371] Y. Olivier, B. Yurash, L. Muccioli, G. D'Avino, O. Mikhnenko, J. C. Sancho-García, C. Adachi, T.-Q. Nguyen, D. Beljonne, *Phys. Rev. Mater.* **2017**, *1*, 075602.
- [372] S. Huang, Q. Zhang, Y. Shiota, T. Nakagawa, K. Kuwabara, K. Yoshizawa, C. Adachi, *J. Chem. Theory Comput.* **2013**, *9*, 3872-3877.
- [373] F. B. Dias, K. N. Bourdakos, V. Jankus, K. C. Moss, K. T. Kamtekar, V. Bhalla, J. Santos, M. R. Bryce, A. P. Monkman, *Adv. Mater.* **2013**, *25*, 3707-3714.
- [374] J. Gibson, T. J. Penfold, *Phys. Chem. Chem. Phys.* **2017**, *19*, 8428-8434.
- [375] P. L. Dos Santos, M. K. Etherington, A. P. Monkman, *J. Mater. Chem. C* **2018**, *6*, 4842-4853.
- [376] P. V. Rysselberghe, *J. Phys. Chem.* **1931**, *36*, 1152-1155.
- [377] P. K. Nayak, N. Periasamy, *Org. Electron.* **2009**, *10*, 532-535.
- [378] C. C. Pye, T. Ziegler, *Theor. Chem. Acc.* **1999**, *101*, 396-408.
- [379] A. Klamt, G. Schüürmann, *J. Chem. Soc., Perkin Trans. 2* **1993**, *53*, 799-805.
- [380] A. Klamt, *J. Phys. Chem.* **1995**, *99*, 2224-2235.
- [381] S. J. A. Van Gisbergen, J. G. Snijders, E. J. Baerends, *J. Chem. Phys.* **1998**, *109*, 10644-10656.
- [382] M. Seth, T. Ziegler, *J. Chem. Theory Comput.* **2012**, *8*, 901-907.
- [383] E. Van Lenthe, E. J. Baerends, *J. Comput. Chem.* **2003**, *24*, 1142-1156.
- [384] J. C. Slater, *Quantum Theory of Molecules and Solids*, 4<sup>th</sup> ed., (Editor: McGraw-Hill), New York, **1974**.
- [385] A. D. Becke, *J. Chem. Phys.* **1986**, *84*, 4524-4529.
- [386] T. V. Russo, R. L. Martin, P. J. Hay, *J. Chem. Phys.* **1994**, *101*, 7729-7737.
- [387] C. Lee, W. Yang, R. G. Parr, *Phys. Rev. B* **1988**, *37*, 785-789.
- [388] E. v. Lenthe, E. J. Baerends, J. G. Snijders, *J. Chem. Phys.* **1993**, *99*, 4597-4610.

## References

- [389] E. v. Lenthe, E. J. Baerends, J. G. Snijders, *J. Chem. Phys.* **1994**, *101*, 9783-9792.
- [390] E. v. Lenthe, J. G. Snijders, E. J. Baerends, *J. Chem. Phys.* **1996**, *105*, 6505-6516.
- [391] L. Kleinman, *Phys. Rev. B: Condens. Matter Mater. Phys.* **1997**, *56*, 12042-12045.
- [392] Z. Hu, B. Zhou, Z. Sun, H. Sun, *J. Comput. Chem.* **2017**, *38*, 569-575.
- [393] C. M. Marian, *J. Phys. Chem. C* **2016**, *120*, 3715-3721.
- [394] T. Hosokai, H. Matsuzaki, H. Nakanotani, K. Tokumaru, T. Tsutsui, A. Furube, K. Nasu, H. Nomura, M. Yahiro, C. Adachi, *Sci. Adv.* **2017**, *3*, e1603282.
- [395] Gaussian 09 Revision E.01, M. J. Frisch, G. W. Trucks, H. B. Schlegel, G. E. Scuseria, M. A. Robb, J. R. Cheeseman, G. Scalmani, V. Barone, B. Mennucci, G. A. Petersson, H. Nakatsuji, M. Caricato, X. Li, H. P. Hratchian, A. F. Izmaylov, J. Bloino, G. Zheng, J. L. Sonnenberg, M. Hada, M. Ehara, K. Toyota, R. Fukuda, J. Hasegawa, M. Ishida, T. Nakajima, Y. Honda, O. Kitao, H. Nakai, T. Vreven, J. A. Montgomery, J. E. Peralta, F. Ogliaro, M. Bearpark, J. J. Heyd, E. Brothers, K. N. Kudin, V. N. Staroverov, R. Kobayashi, J. Normand, K. Raghavachari, A. Rendell, J. C. Burant, S. S. Iyengar, J. Tomasi, M. Cossi, N. Rega, J. M. Millam, M. Klene, J. E. Knox, J. B. Cross, V. Bakken, C. Adamo, J. Jaramillo, R. Gomperts, R. E. Stratmann, O. Yazyev, A. J. Austin, R. Cammi, C. Pomelli, J. W. Ochterski, R. L. Martin, K. Morokuma, V. G. Zakrzewski, G. A. Voth, P. Salvador, J. J. Dannenberg, S. Dapprich, A. D. Daniels, Farkas, J. B. Foresman, J. V. Ortiz, J. Cioslowski, D. J. Fox, Gaussian Inc., Wallingford CT, **2016**.
- [396] T. Lu, F. Chen, *J. Comput. Chem.* **2012**, *33*, 580-592.
- [397] C. Lee, W. Yang, R. G. Parr, *Phys. Rev. B: Condens. Matter Mater. Phys.* **1988**, *37*, 785-789.
- [398] G. A. Petersson, M. A. Al-Laham, *J. Chem. Phys.* **1991**, *94*, 6081-6090.
- [399] G. A. Petersson, A. Bennett, T. G. Tensfeldt, M. A. Al-Laham, W. A. Shirley, J. Mantzaris, *J. Chem. Phys.* **1988**, *89*, 2193-2218.
- [400] M. D. Hanwell, D. E. Curtis, D. C. Lonie, T. Vandermeersch, E. Zurek, G. R. Hutchison, *J. Cheminformatics* **2012**, *4*, 17.

## 8 Appendix

### 8.1 NMR Spectra

#### 8.1.1 Chapter 1

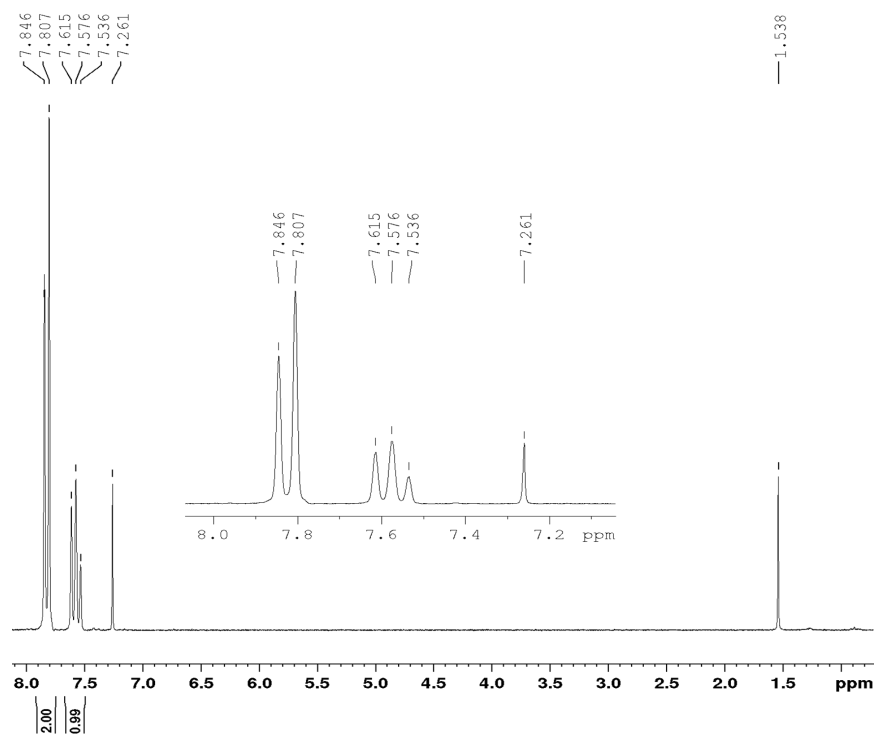


Figure 8.1:  $^1\text{H}$  NMR spectrum (200 MHz, 298 K,  $\text{CDCl}_3$ ) of 2-iodo-1,3-bis(trifluoromethyl)benzene.

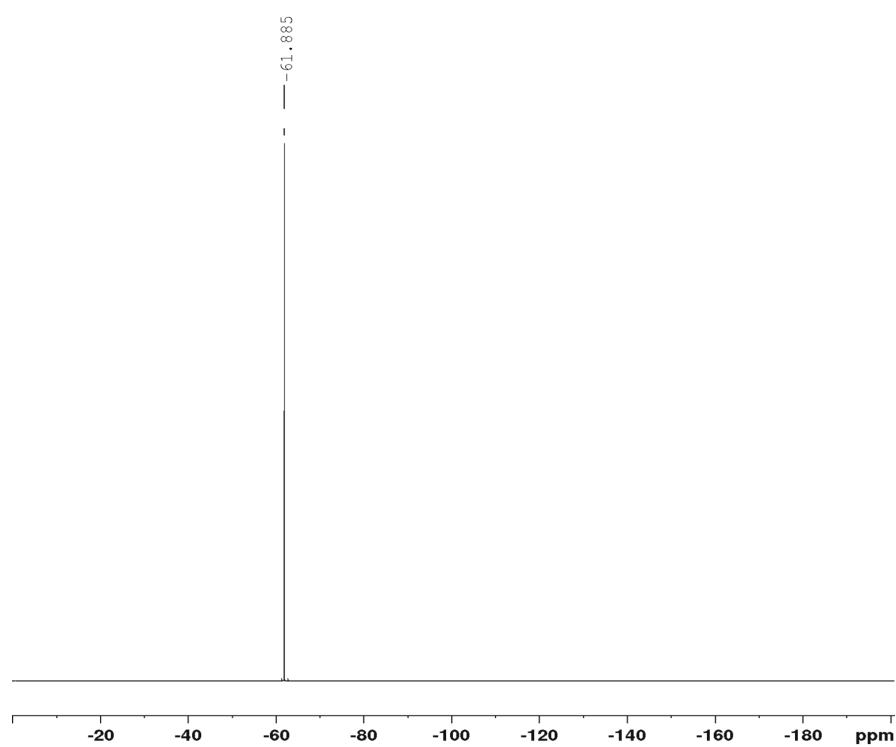


Figure 8.2:  $^{19}\text{F}$  NMR spectrum (188 MHz, 298 K,  $\text{CDCl}_3$ ) of 2-iodo-1,3-bis(trifluoromethyl)benzene.

## Appendix

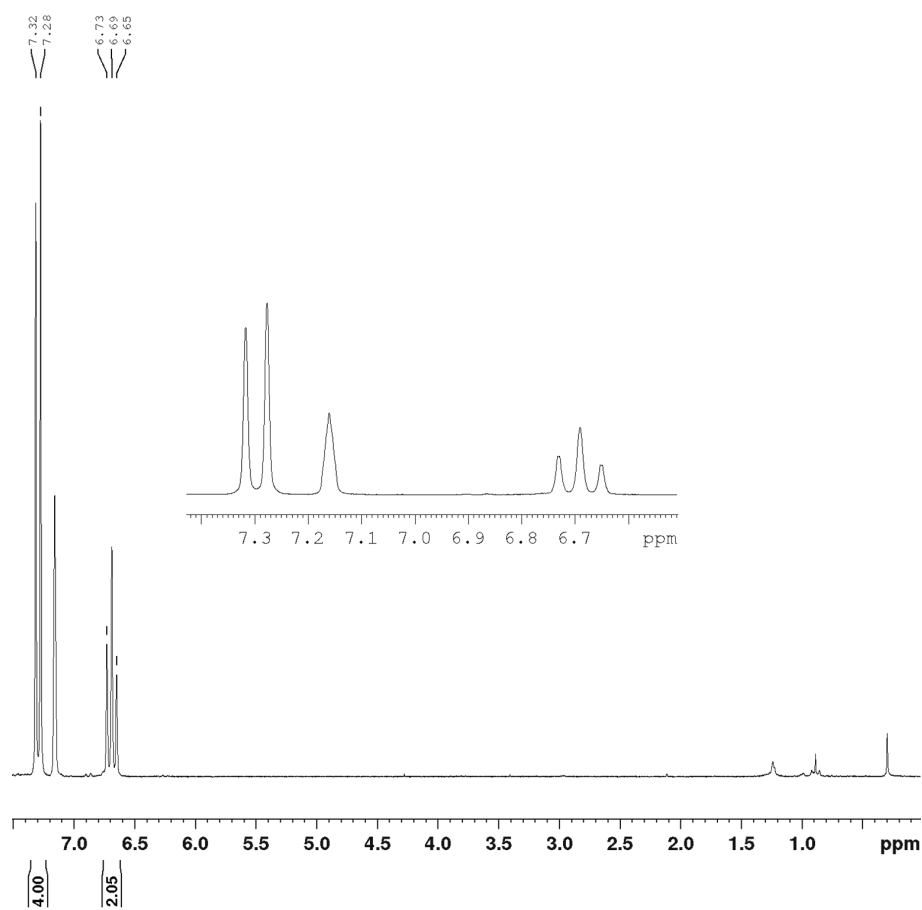


Figure 8.3:  $^1\text{H}$  NMR spectrum (200 MHz, 298 K,  $\text{C}_6\text{D}_6$ ) of  $\text{FB}(\text{FXyl})_2$ .

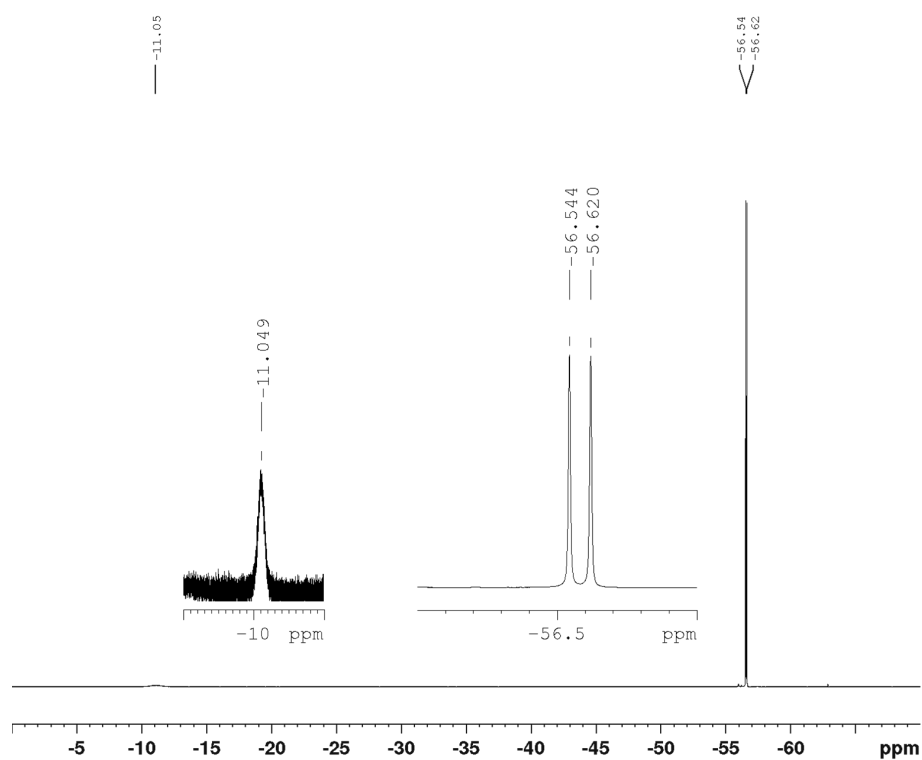
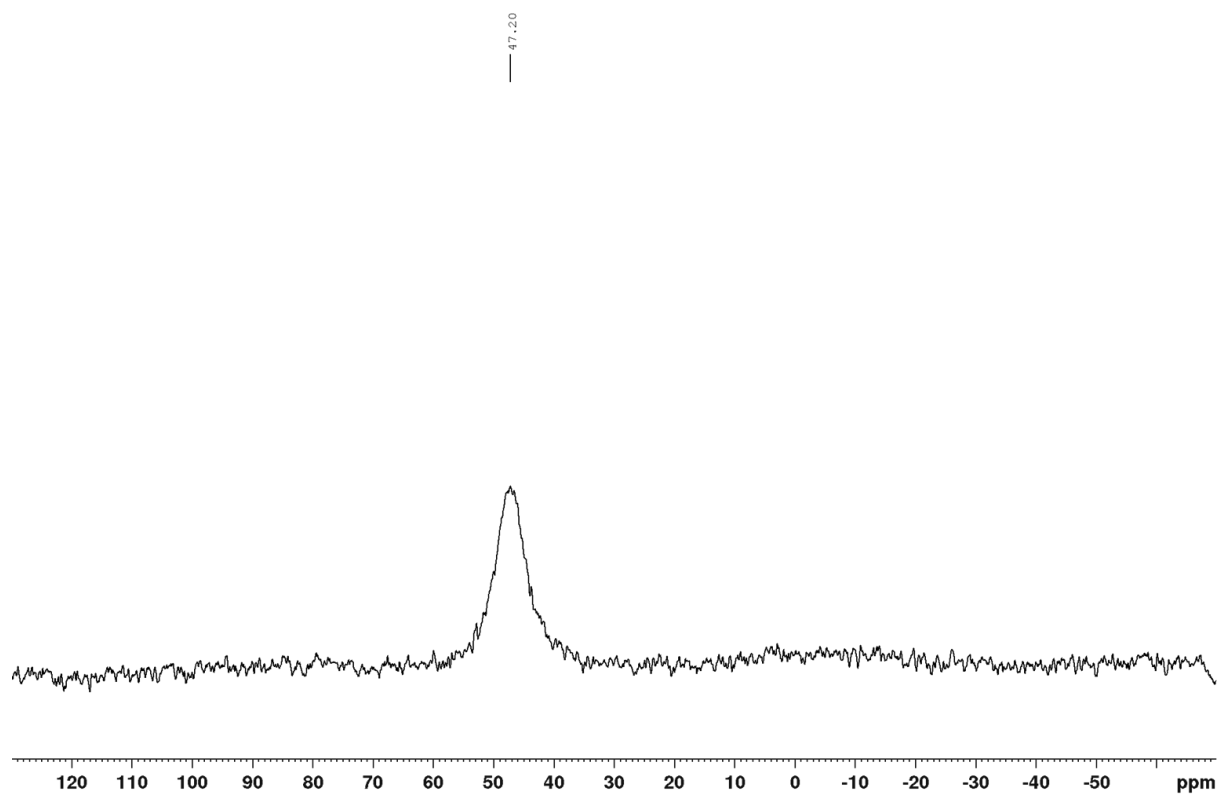
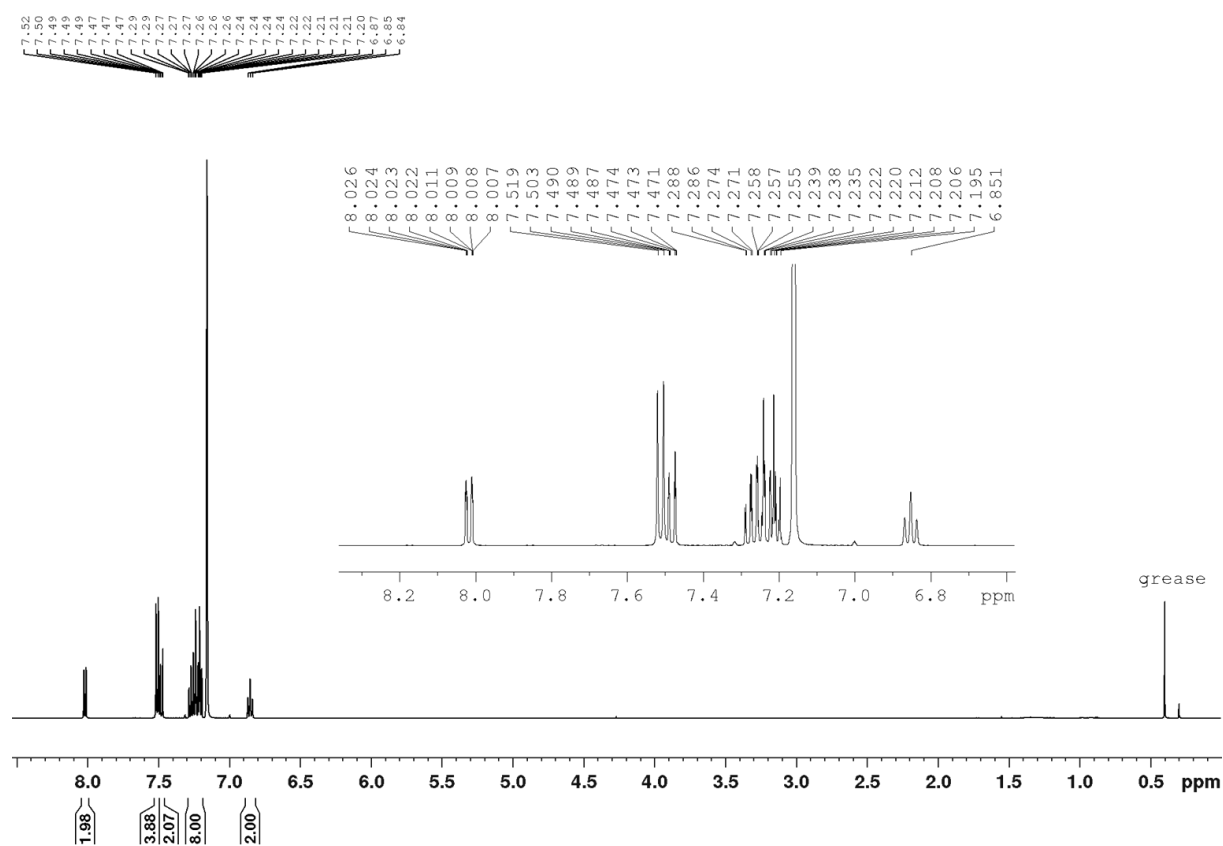


Figure 8.4:  $^{19}\text{F}$  NMR spectrum (188 MHz, 298 K,  $\text{C}_6\text{D}_6$ ) of  $\text{FB}(\text{FXyl})_2$ .

Figure 8.5:  $^{11}\text{B}$  NMR spectrum (64 MHz, 298 K,  $\text{C}_6\text{D}_6$ ) of  $\text{FB}(\text{FXyl})_2$ .Figure 8.6:  $^1\text{H}$  NMR spectrum (500 MHz, 298 K,  $\text{C}_6\text{D}_6$ ) of compound  $\text{Cbz-}\pi$  (**1**).

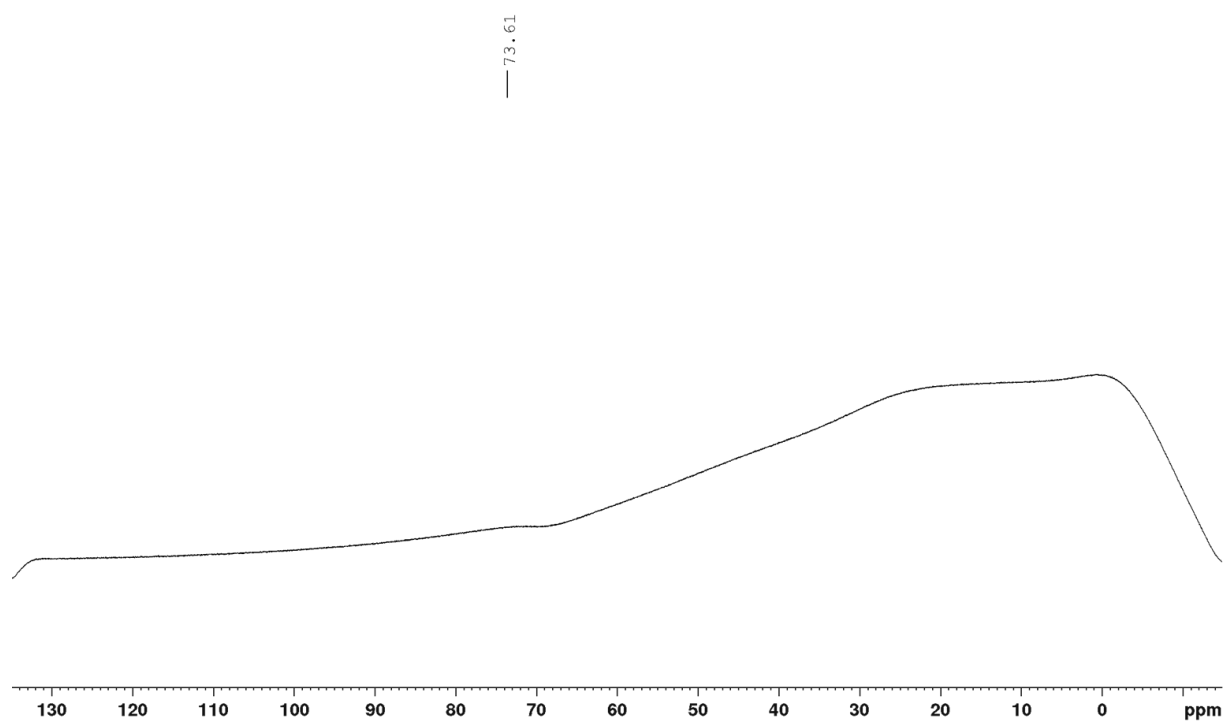


Figure 8.7:  $^{11}\text{B}\{^1\text{H}\}$  NMR spectrum (160 MHz, 298 K,  $\text{C}_6\text{D}_6$ ) of compound **Cbz- $\pi$  (1)**.

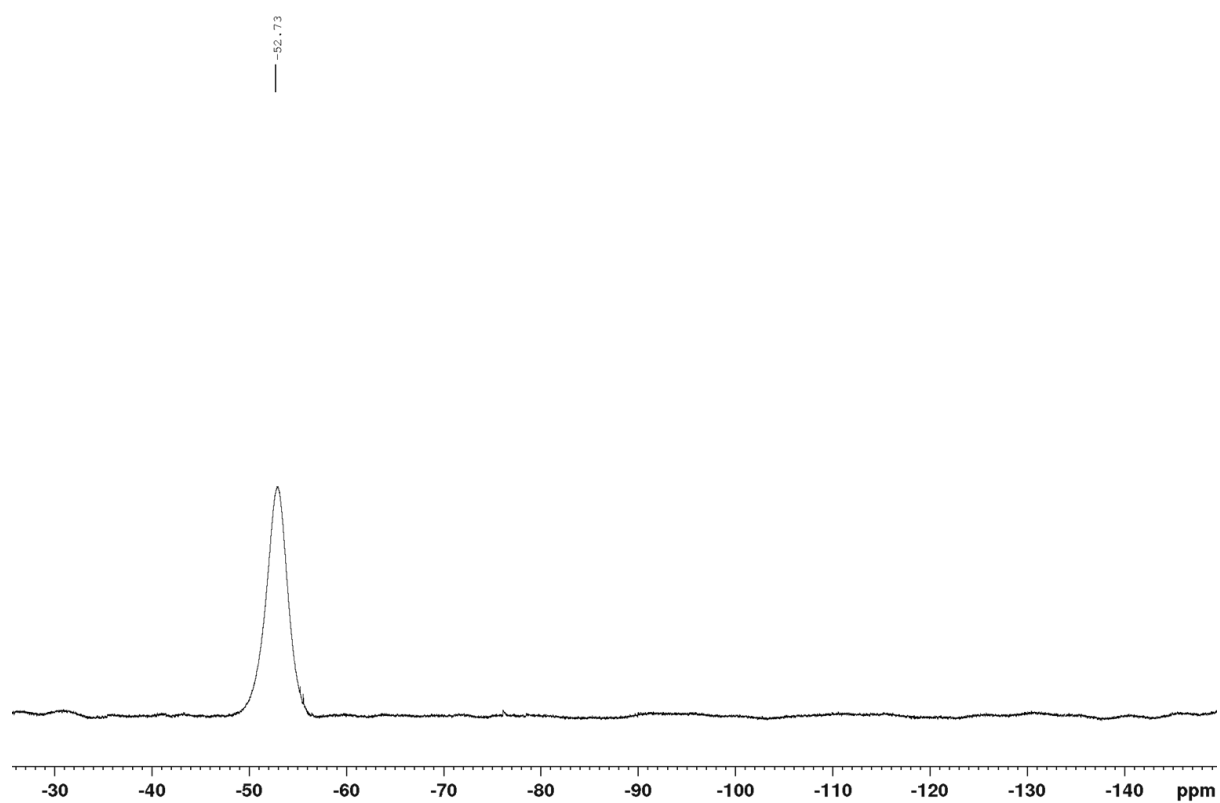
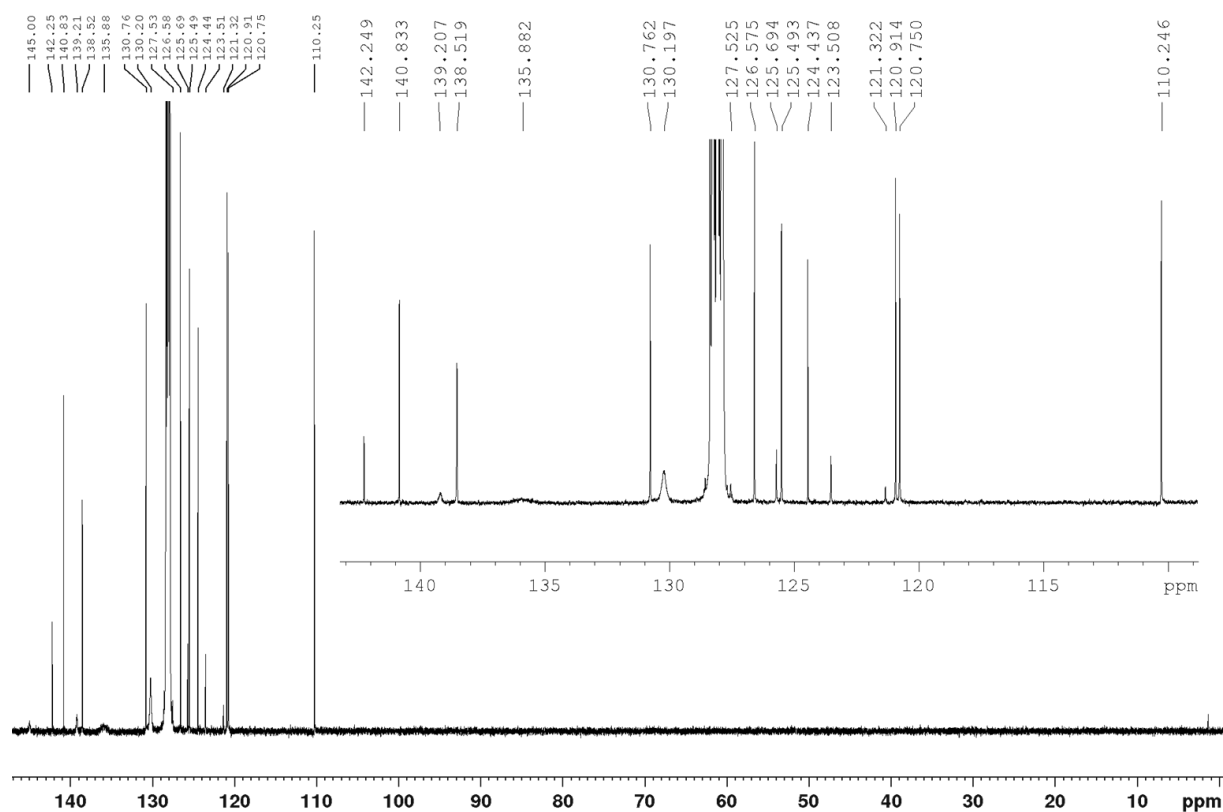
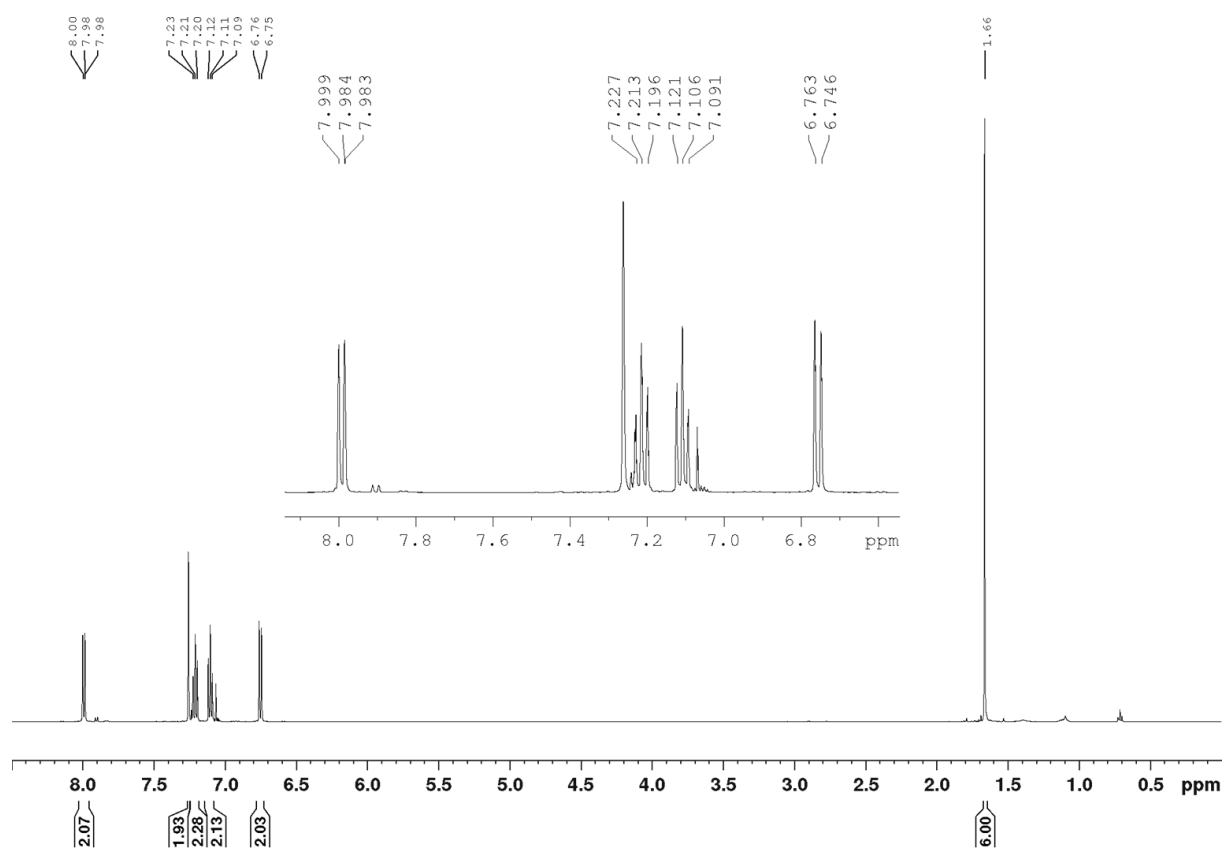


Figure 8.8:  $^{19}\text{F}\{^1\text{H}\}$  NMR spectrum (471 MHz, 298 K,  $\text{C}_6\text{D}_6$ ) of compound **Cbz- $\pi$  (1)**.

Figure 8.9:  $^{13}\text{C}\{^1\text{H}\}$  NMR spectrum (126 MHz, 298 K,  $\text{C}_6\text{D}_6$ ) of compound **Cbz- $\pi$  (1)**.Figure 8.10:  $^1\text{H}$  NMR spectrum (500 MHz, 298 K,  $\text{CDCl}_3$ ) of **9-(4-bromo-2,6-dimethylphenyl)carbazole (1-ii)**.

## Appendix

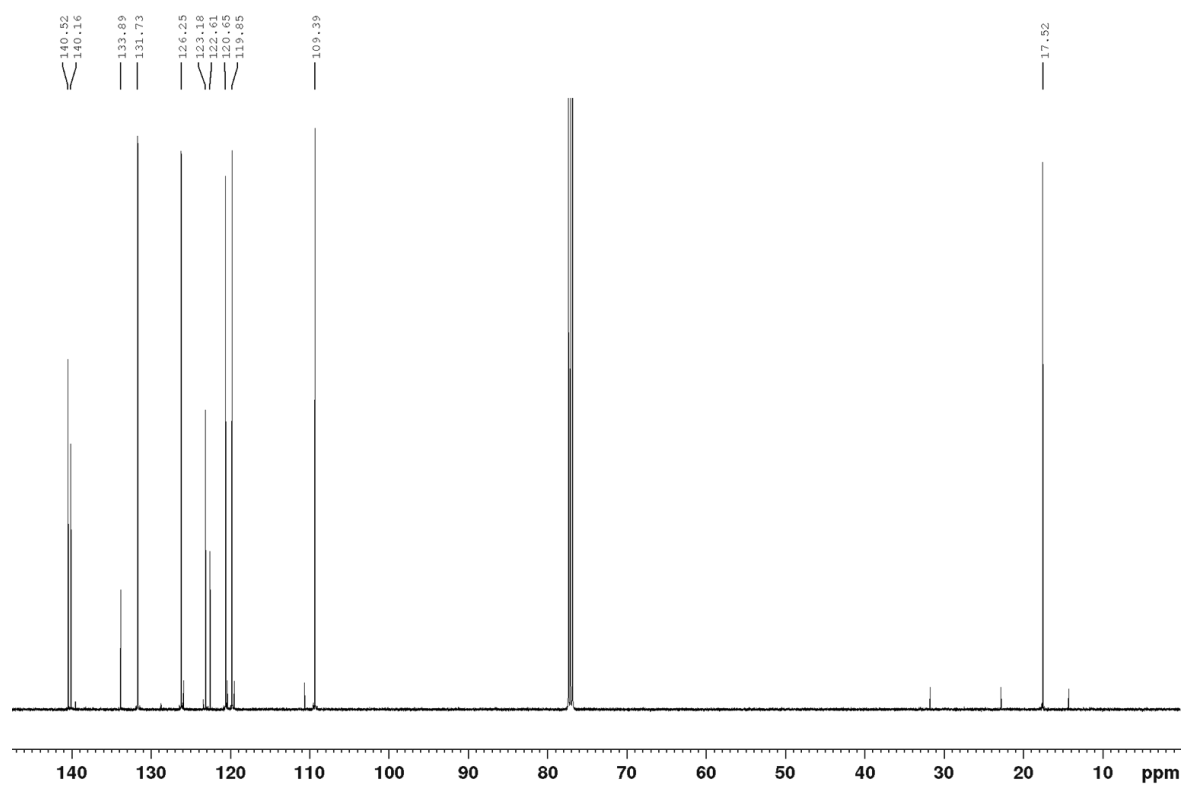


Figure 8.11:  $^{13}\text{C}\{^1\text{H}\}$  NMR spectrum (126 MHz, 298 K,  $\text{CDCl}_3$ ) of **9-(4-bromo-2,6-dimethylphenyl)carbazole (1-ii)**.

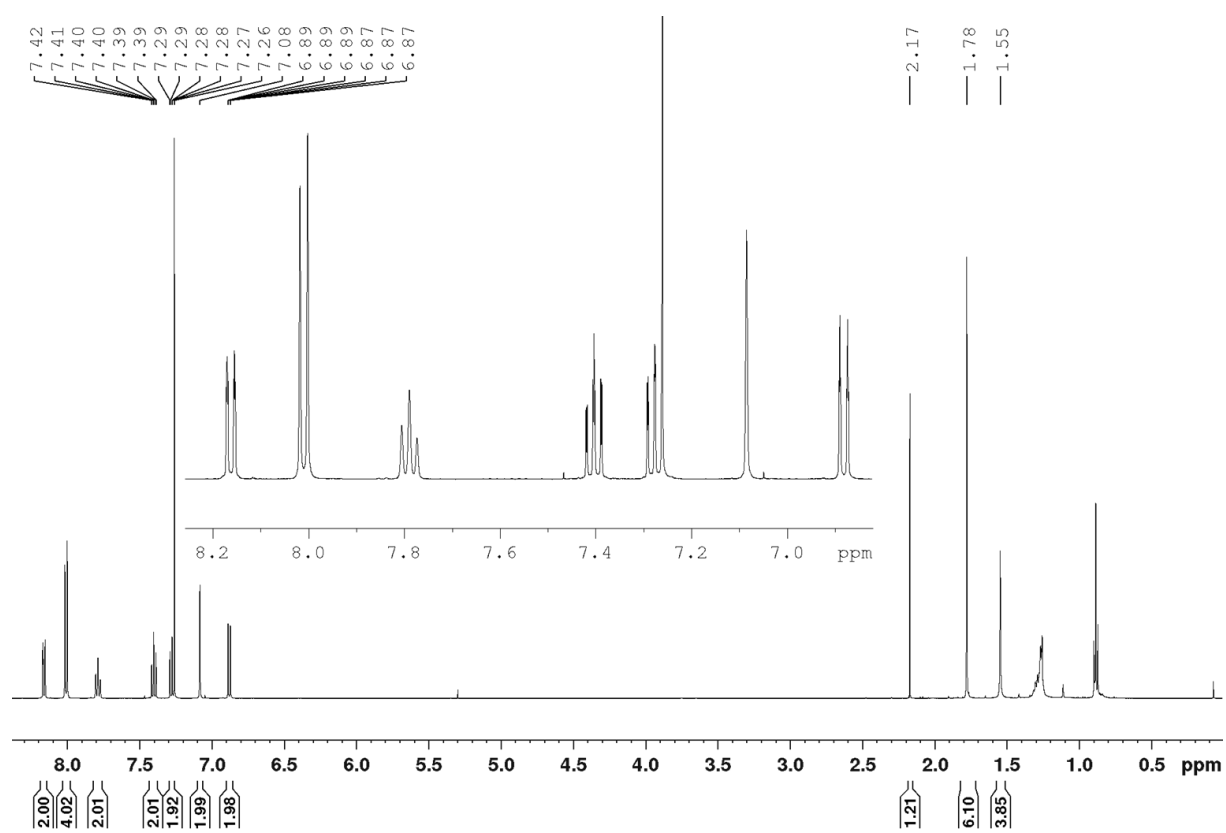


Figure 8.12:  $^1\text{H}$  NMR spectrum (500 MHz, 298 K,  $\text{CDCl}_3$ ) of compound **Cbz-Me $\pi$  (2)**.



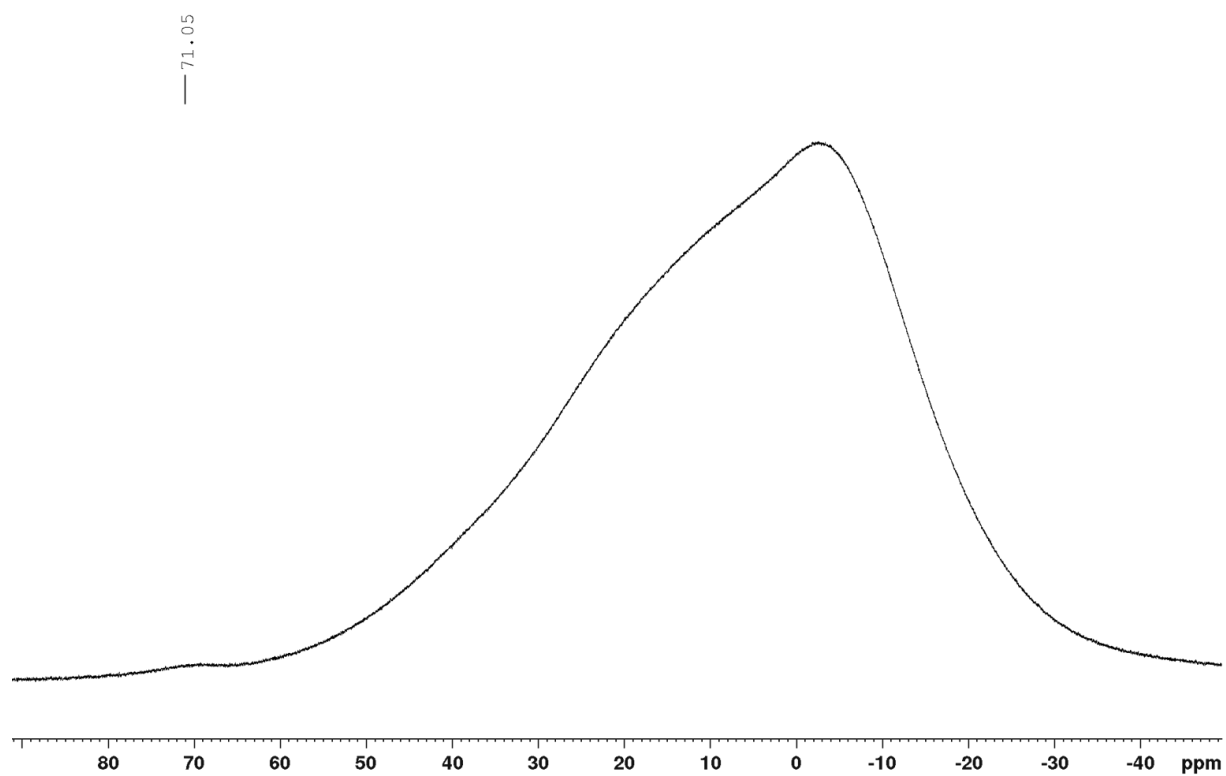


Figure 8.13:  $^{11}\text{B}\{^1\text{H}\}$  NMR spectrum (160 MHz, 298 K,  $\text{CDCl}_3$ ) of compound  $\text{Cbz-Me}\pi$  (**2**).

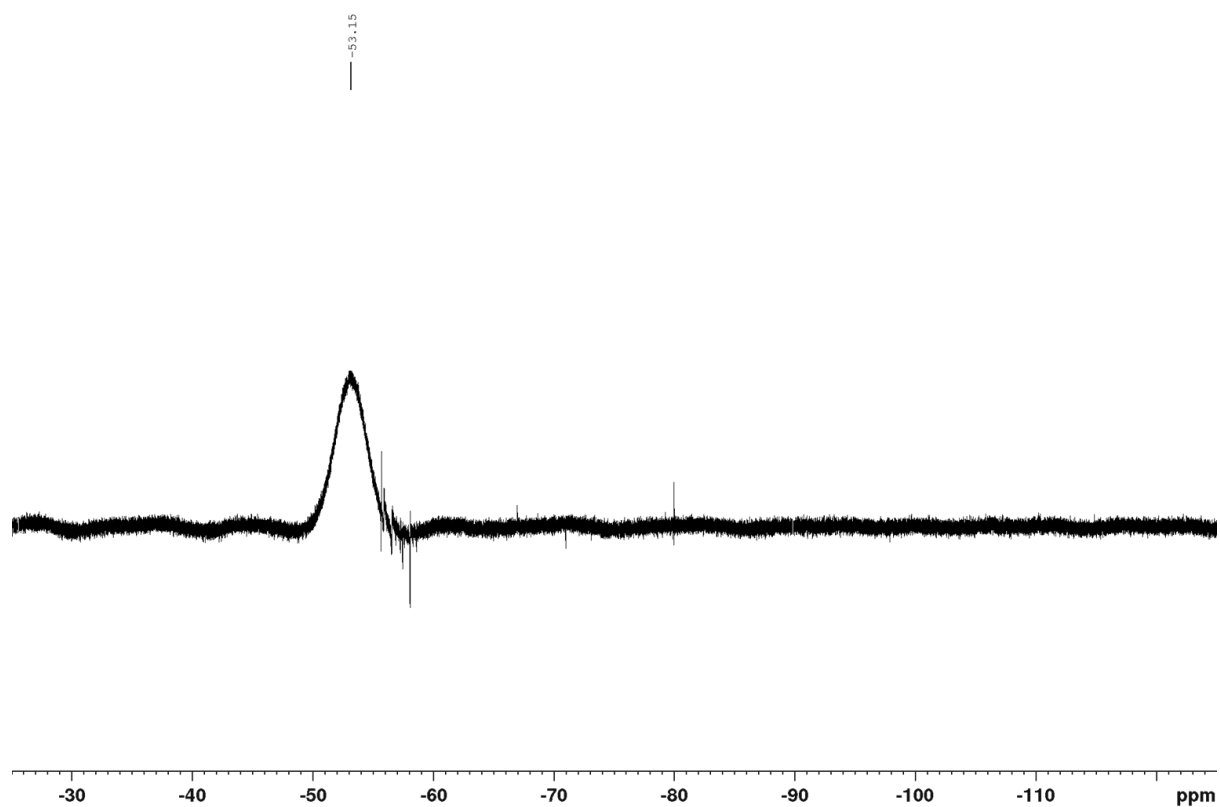


Figure 8.14:  $^{19}\text{F}\{^1\text{H}\}$  NMR spectrum (471 MHz, 298 K,  $\text{CDCl}_3$ ) of compound  $\text{Cbz-Me}\pi$  (**2**).

## Appendix

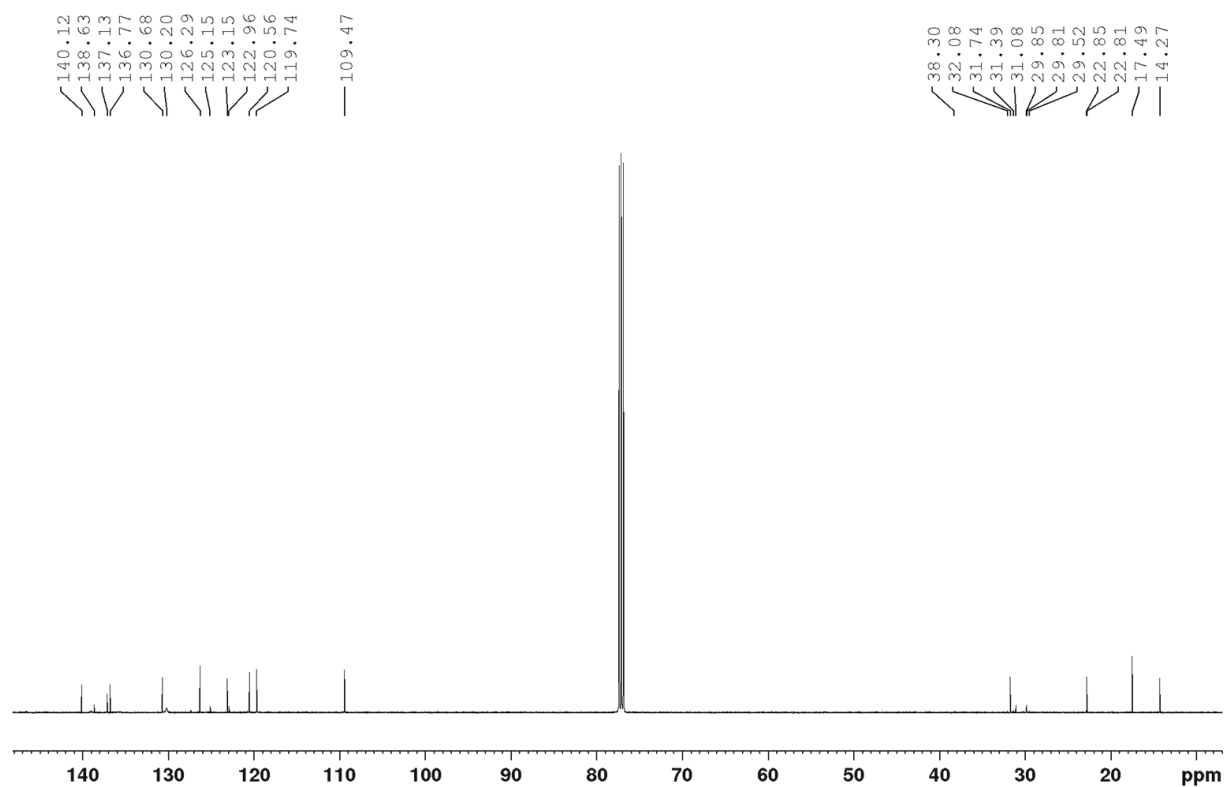


Figure 8.15:  $^{13}\text{C}\{^1\text{H}\}$  NMR spectrum (126 MHz, 298 K,  $\text{CDCl}_3$ ) of compound **Cbz-Me $\pi$  (2)**.

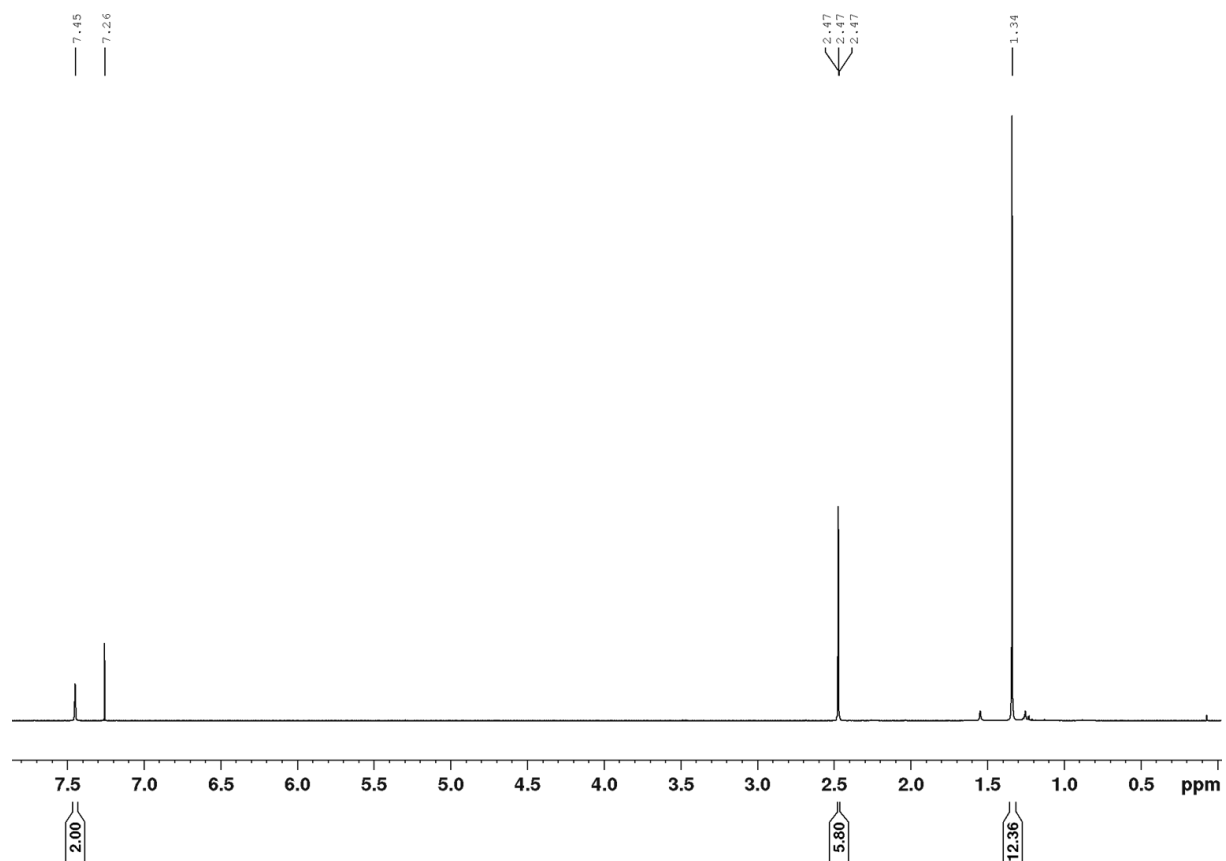


Figure 8.16:  $^1\text{H}$  NMR spectrum (500 MHz, 298 K,  $\text{CDCl}_3$ ) of **2-(4-iodo-3,5-dimethylphenyl)-4,4,5,5-tetramethyl-1,3,2-dioxaborolane**.

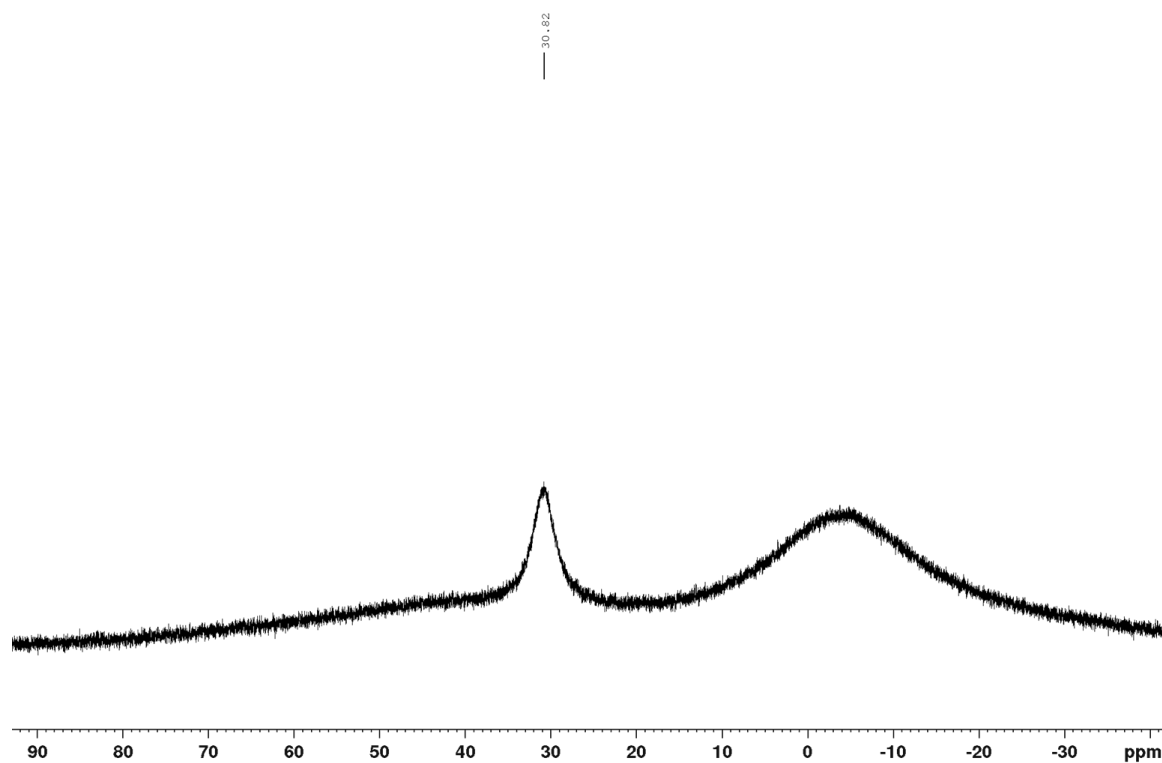


Figure 8.17:  $^{11}\text{B}\{^1\text{H}\}$  NMR spectrum (160 MHz, 298 K,  $\text{CDCl}_3$ ) of 2-(4-iodo-3,5-dimethylphenyl)-4,4,5,5-tetramethyl-1,3,2-dioxaborolane.

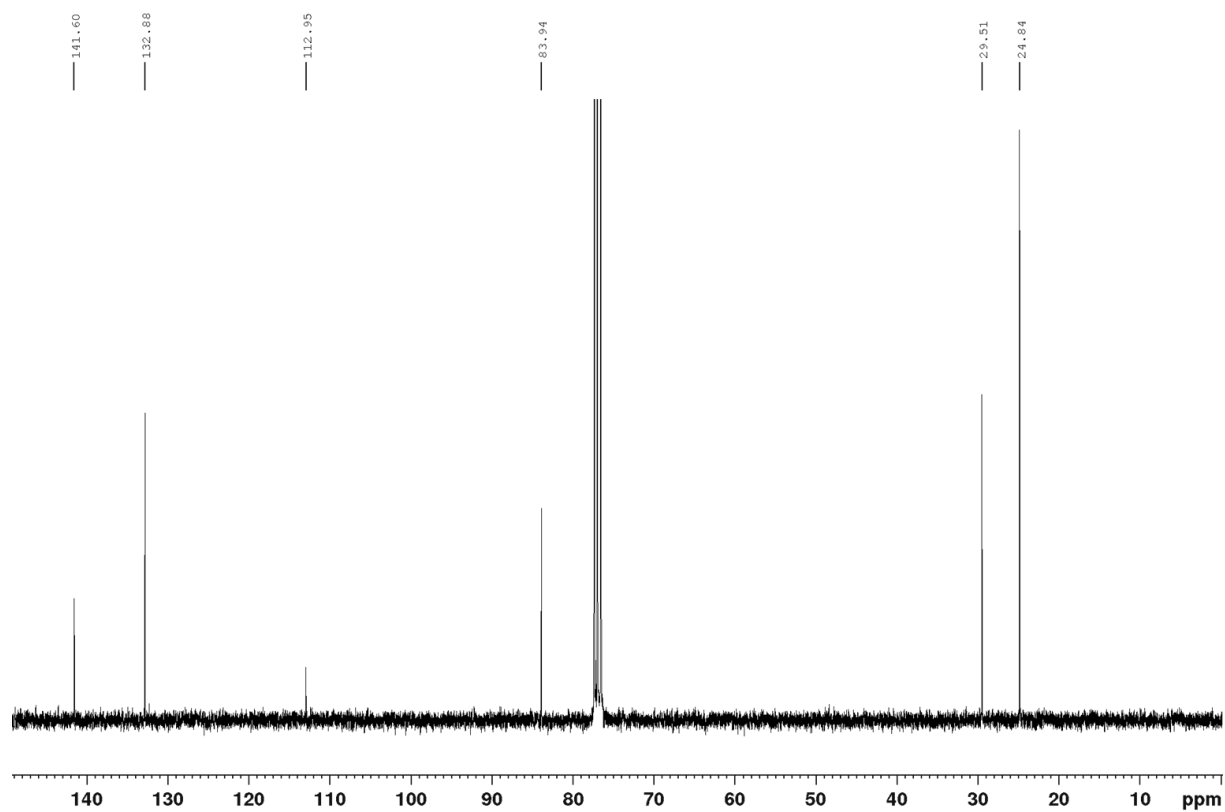


Figure 8.18:  $^{13}\text{C}\{^1\text{H}\}$  NMR spectrum (126 MHz, 298 K,  $\text{CDCl}_3$ ) of 2-(4-iodo-3,5-dimethylphenyl)-4,4,5,5-tetramethyl-1,3,2-dioxaborolane.

## Appendix

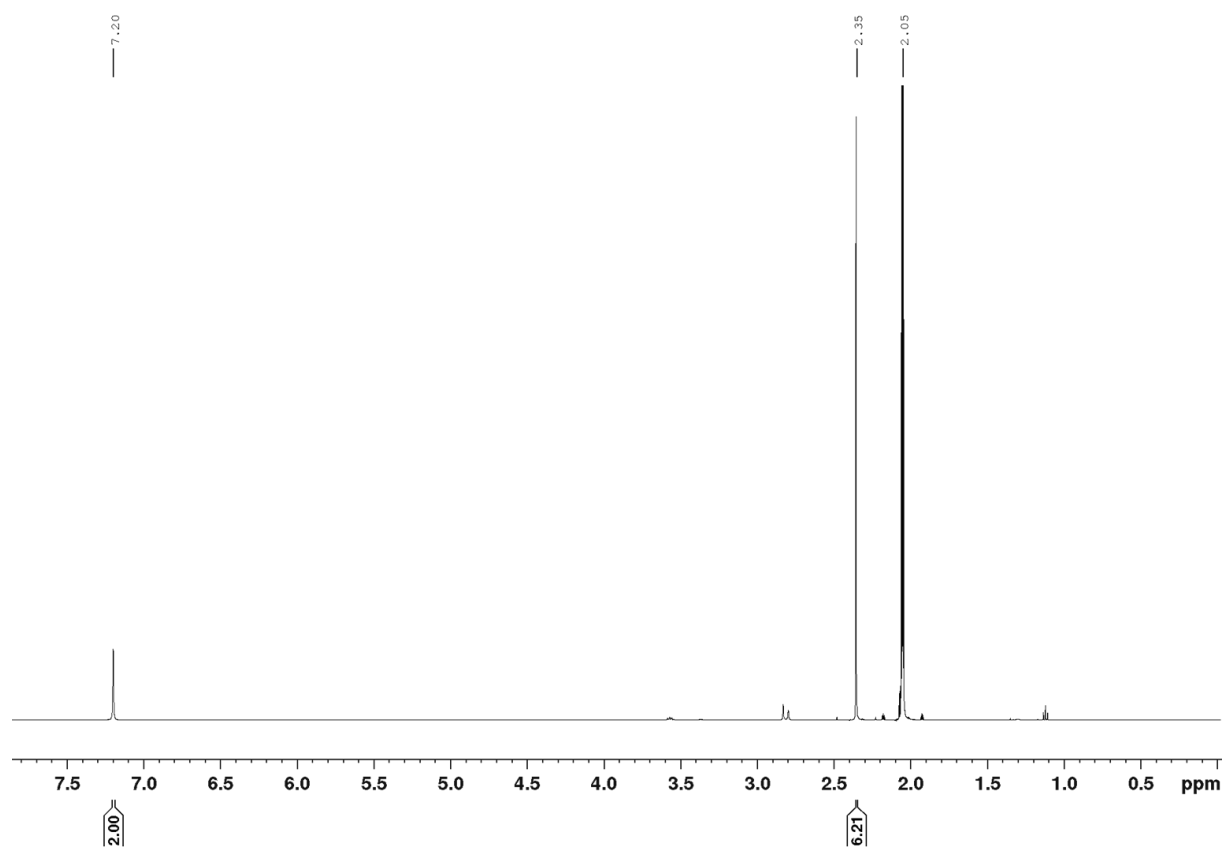


Figure 8.19:  $^1\text{H}$  NMR spectrum (500 MHz, 298 K, acetone- $\text{d}_6$ ) of **potassium(4-iodo-3,5-dimethylphenyl)trifluoroborate**.

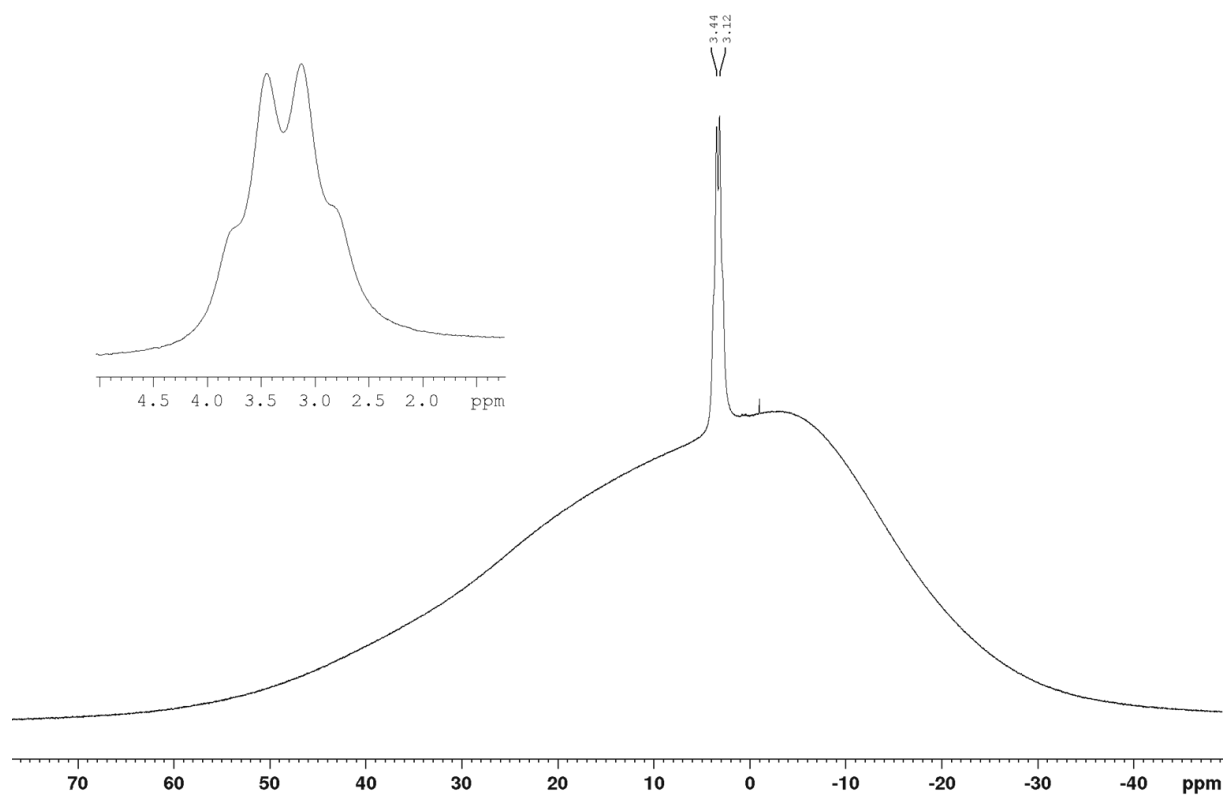


Figure 8.20:  $^{11}\text{B}\{^1\text{H}\}$  NMR spectrum (160 MHz, 298 K, acetone- $\text{d}_6$ ) of **potassium(4-iodo-3,5-dimethylphenyl)trifluoroborate**.

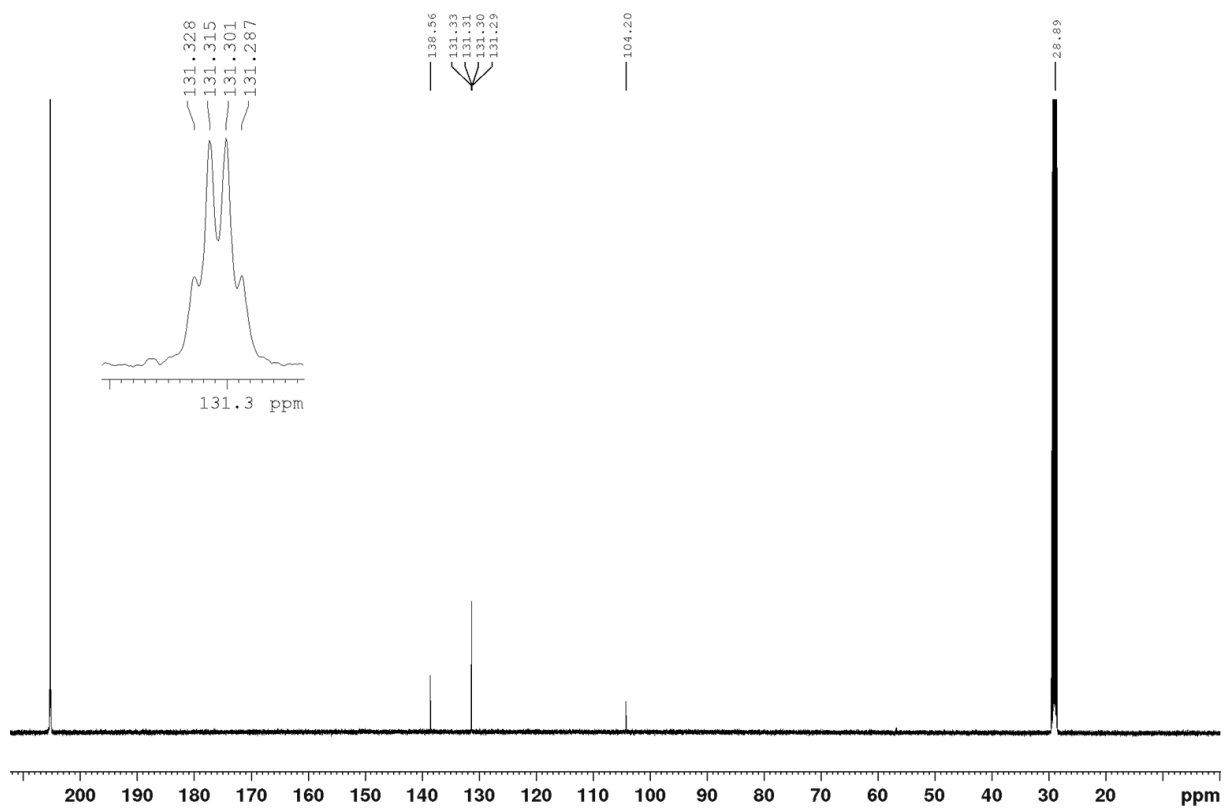


Figure 8.21:  $^{13}\text{C}\{^1\text{H}\}$  NMR spectrum (126 MHz, 298 K, acetone- $d_6$ ) of **potassium(4-iodo-3,5-dimethylphenyl)trifluoroborate**.

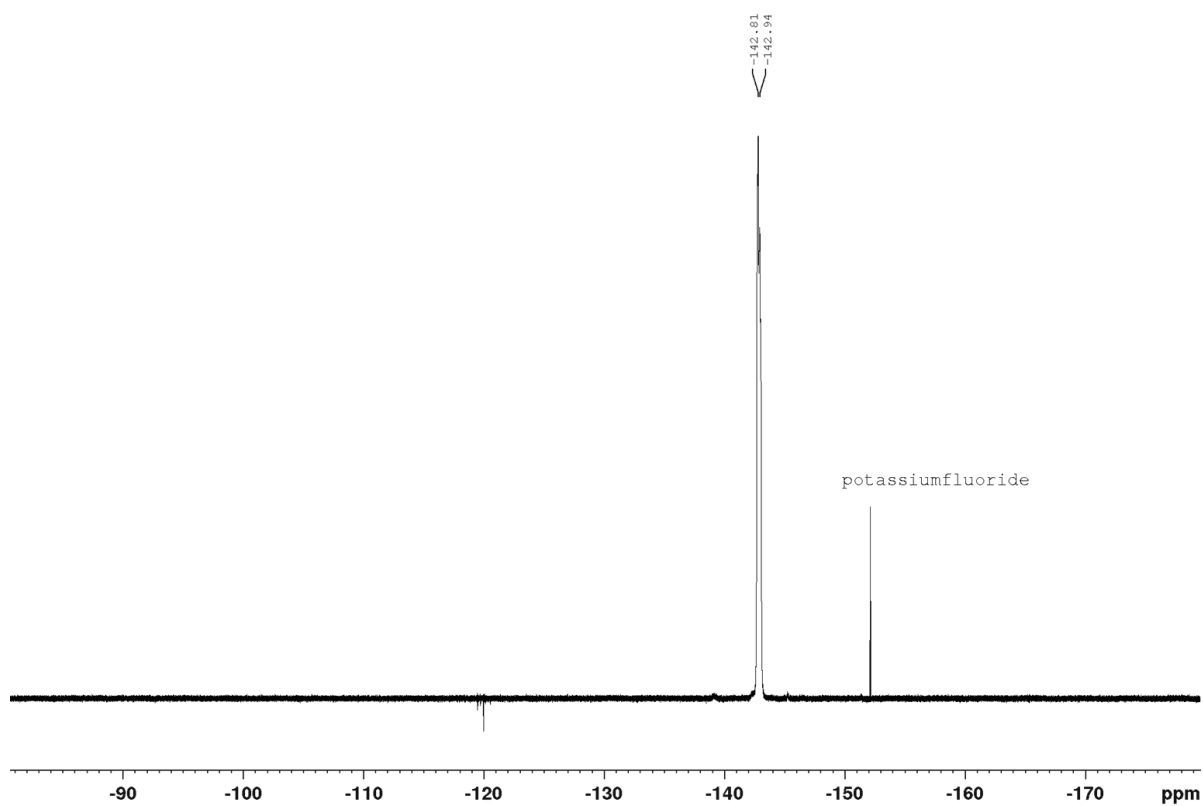


Figure 8.22:  $^{19}\text{F}\{^1\text{H}\}$  NMR spectrum (471 MHz, 298 K, acetone- $d_6$ ) of **potassium(4-iodo-3,5-dimethylphenyl)trifluoroborate**.

## Appendix

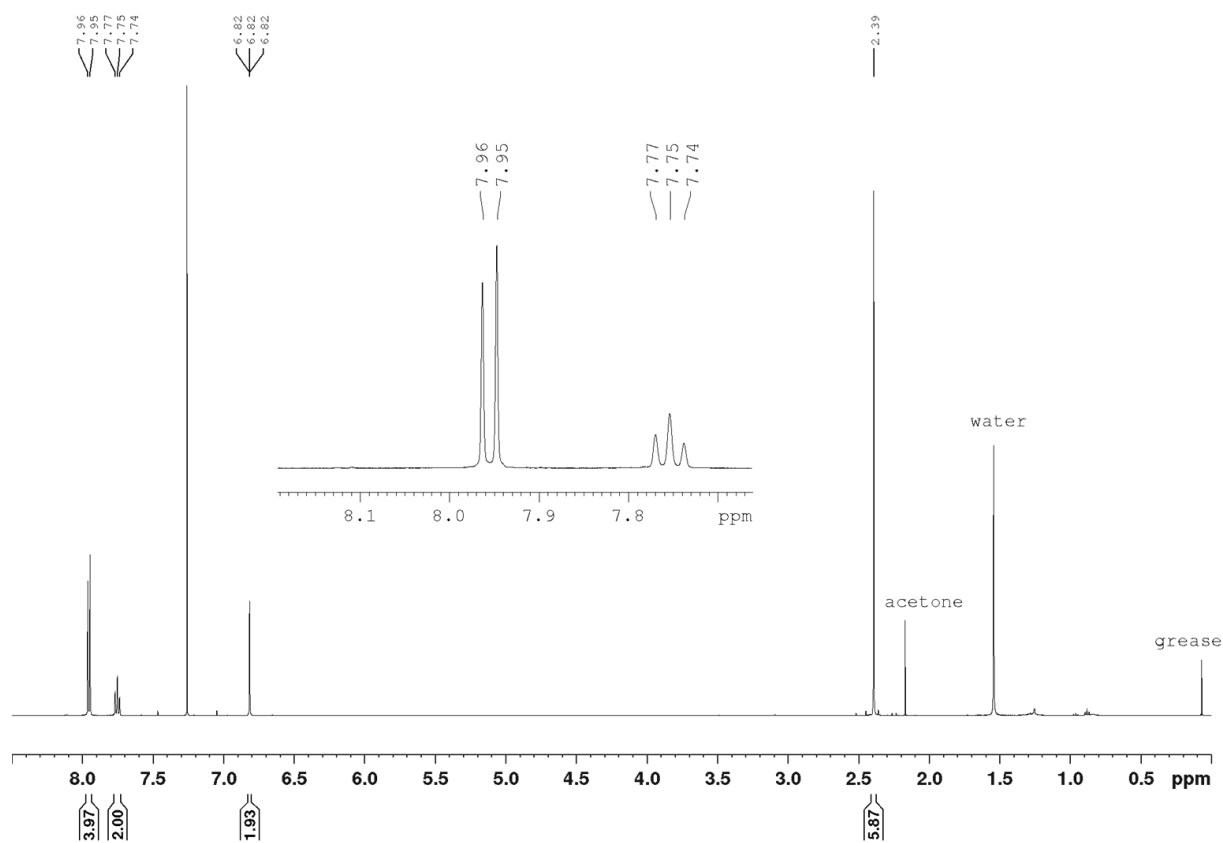


Figure 8.23:  $^1\text{H}$  NMR spectrum (500 MHz, 298 K,  $\text{CDCl}_3$ ) of compound **BFD1H**.

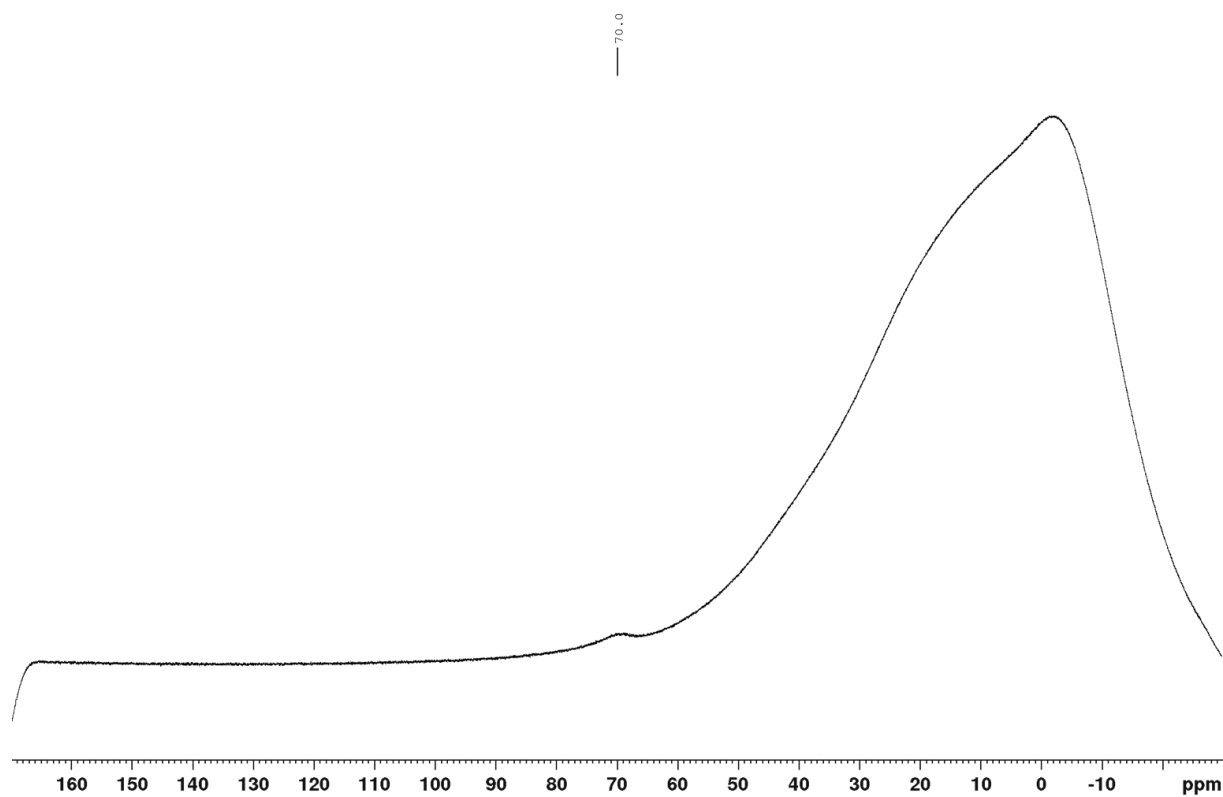


Figure 8.24:  $^{11}\text{B}\{^1\text{H}\}$  NMR spectrum (160 MHz, 298 K,  $\text{CDCl}_3$ ) of compound **BFD1H**.

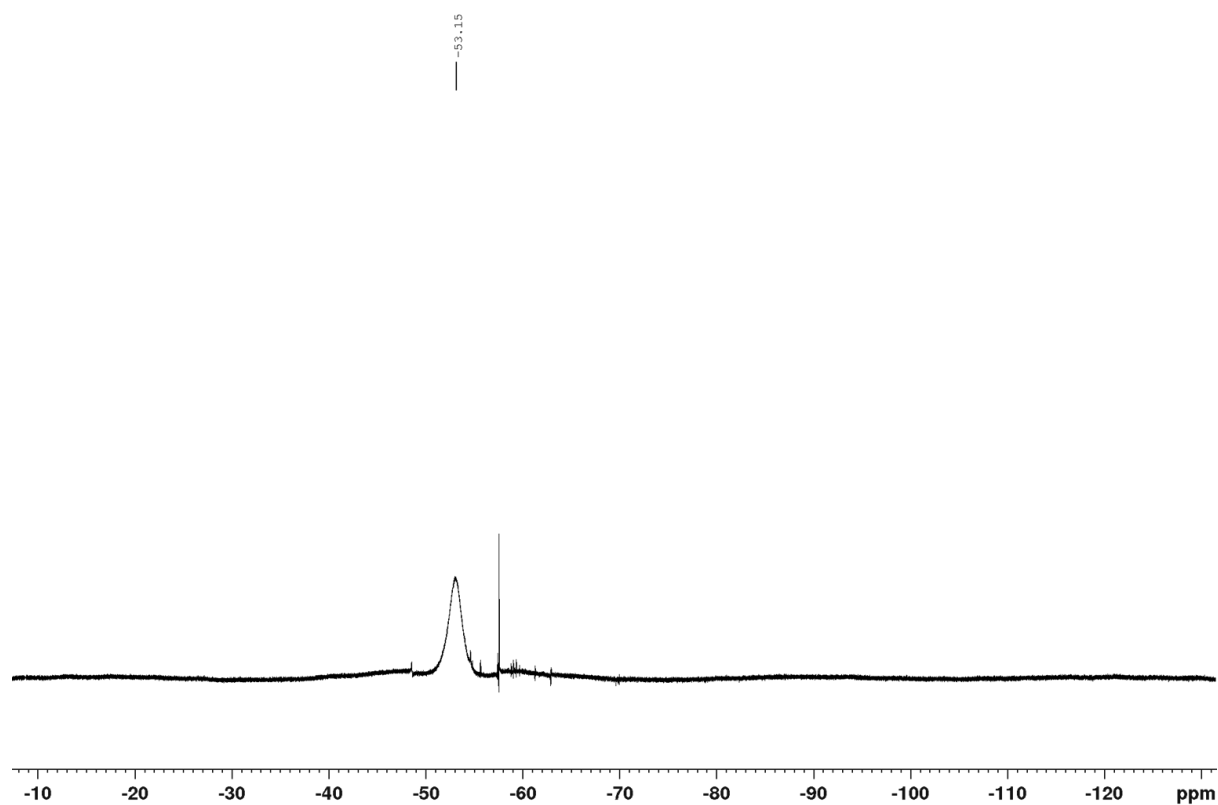


Figure 8.25:  $^{19}\text{F}\{^1\text{H}\}$  NMR spectrum (471 MHz, 298 K,  $\text{CDCl}_3$ ) of compound **BFD1H**.

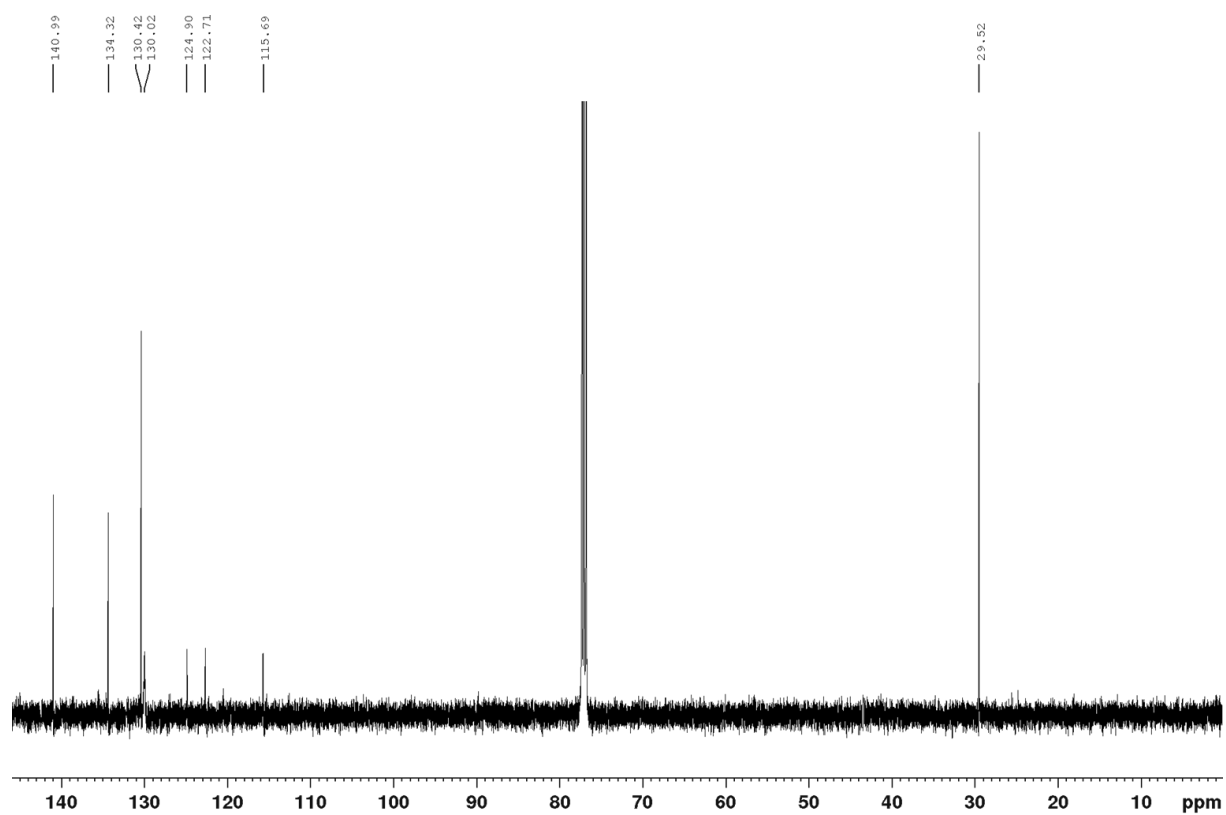


Figure 8.26:  $^{13}\text{C}\{^1\text{H}\}$  NMR spectrum (126 MHz, 298 K,  $\text{CDCl}_3$ ) of compound **BFD1H**.

## Appendix

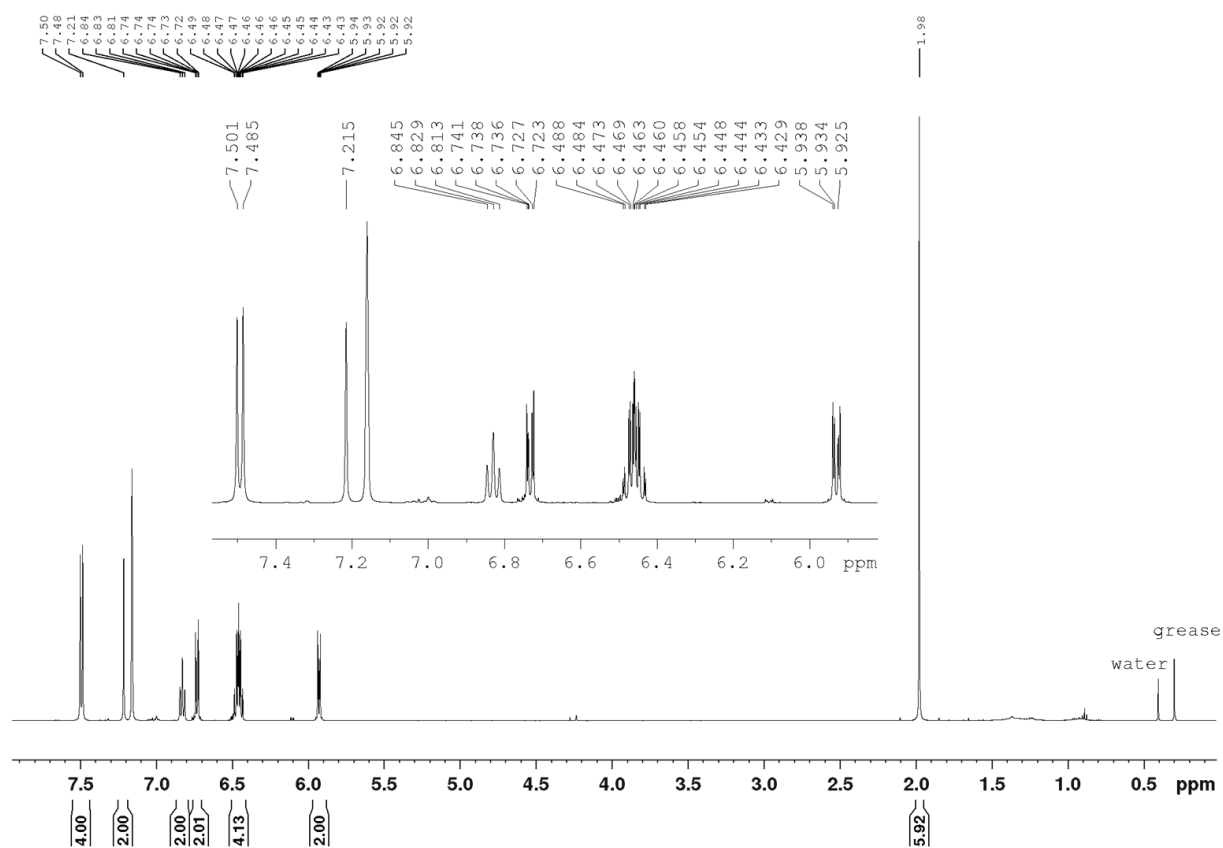


Figure 8.27: <sup>1</sup>H NMR spectrum (500 MHz, 298 K, C<sub>6</sub>D<sub>6</sub>) of compound **Phox-Me $\pi$  (3)**.

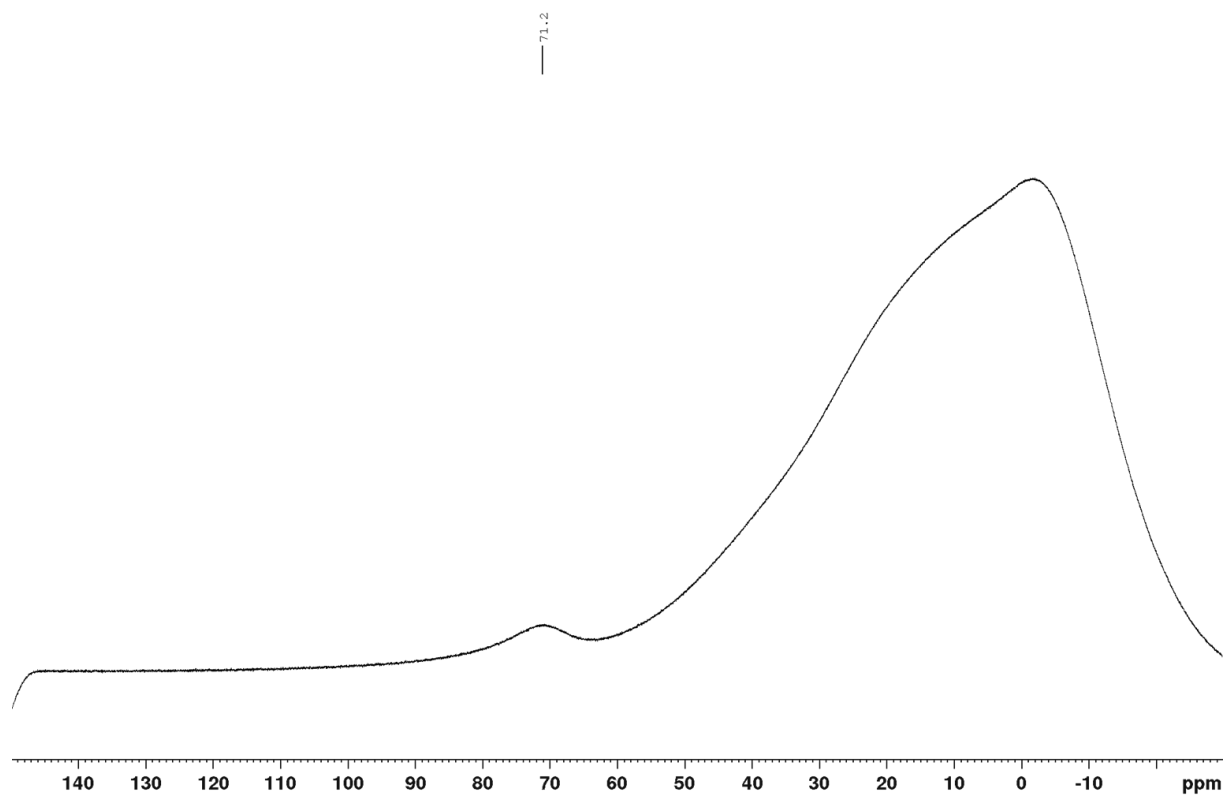


Figure 8.28: <sup>11</sup>B{<sup>1</sup>H} NMR spectrum (160 MHz, 298 K, C<sub>6</sub>D<sub>6</sub>) of compound **Phox-Me $\pi$  (3)**.



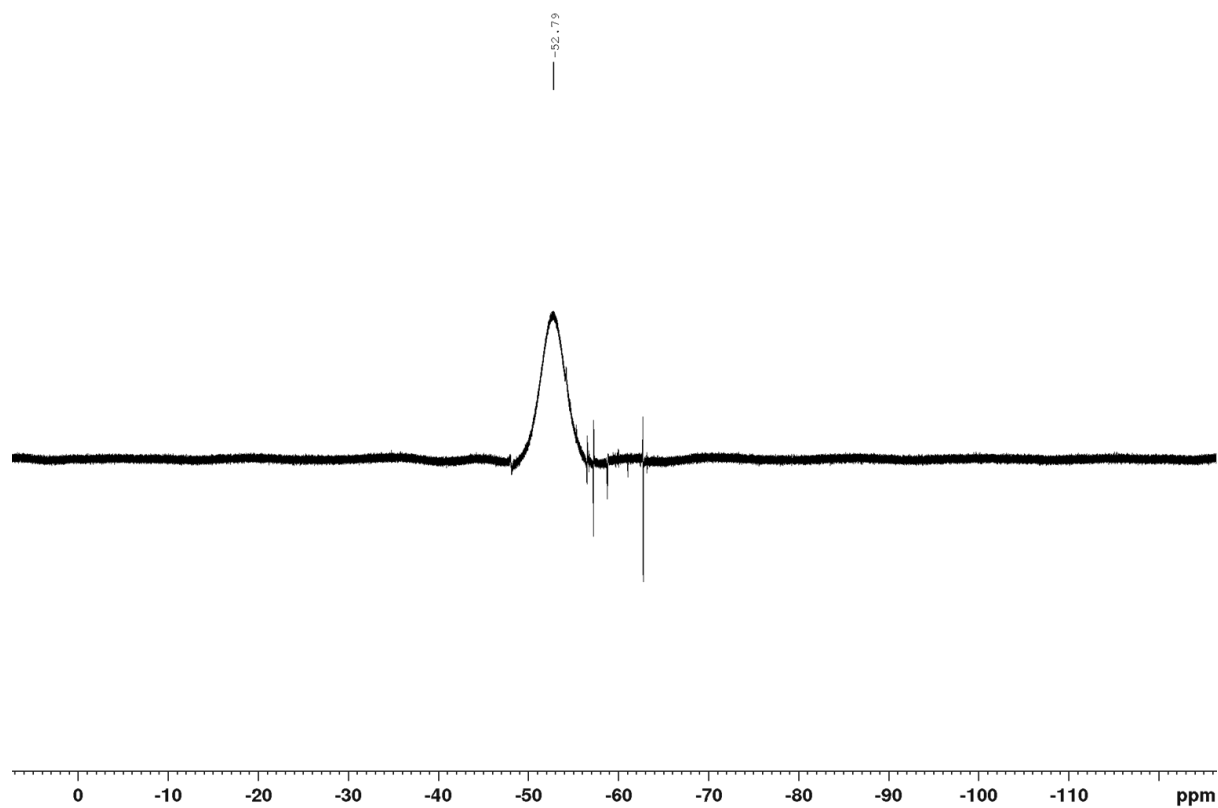


Figure 8.29:  $^{19}\text{F}\{^1\text{H}\}$  NMR spectrum (471 MHz, 298 K,  $\text{C}_6\text{D}_6$ ) of compound **Phox-Me $\pi$  (3)**.

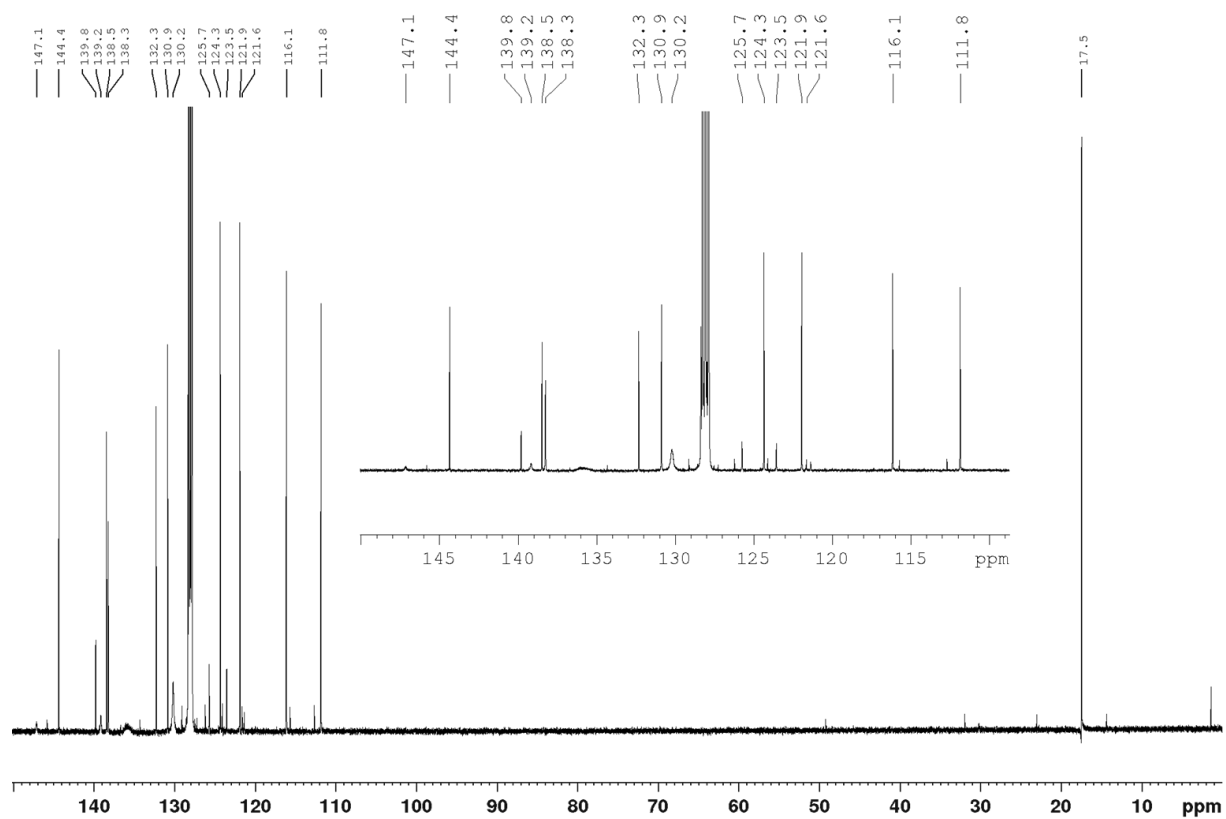


Figure 8.30:  $^{13}\text{C}\{^1\text{H}\}$  NMR spectrum (126 MHz, 298 K,  $\text{C}_6\text{D}_6$ ) of compound **Phox-Me $\pi$  (3)**.

## Appendix

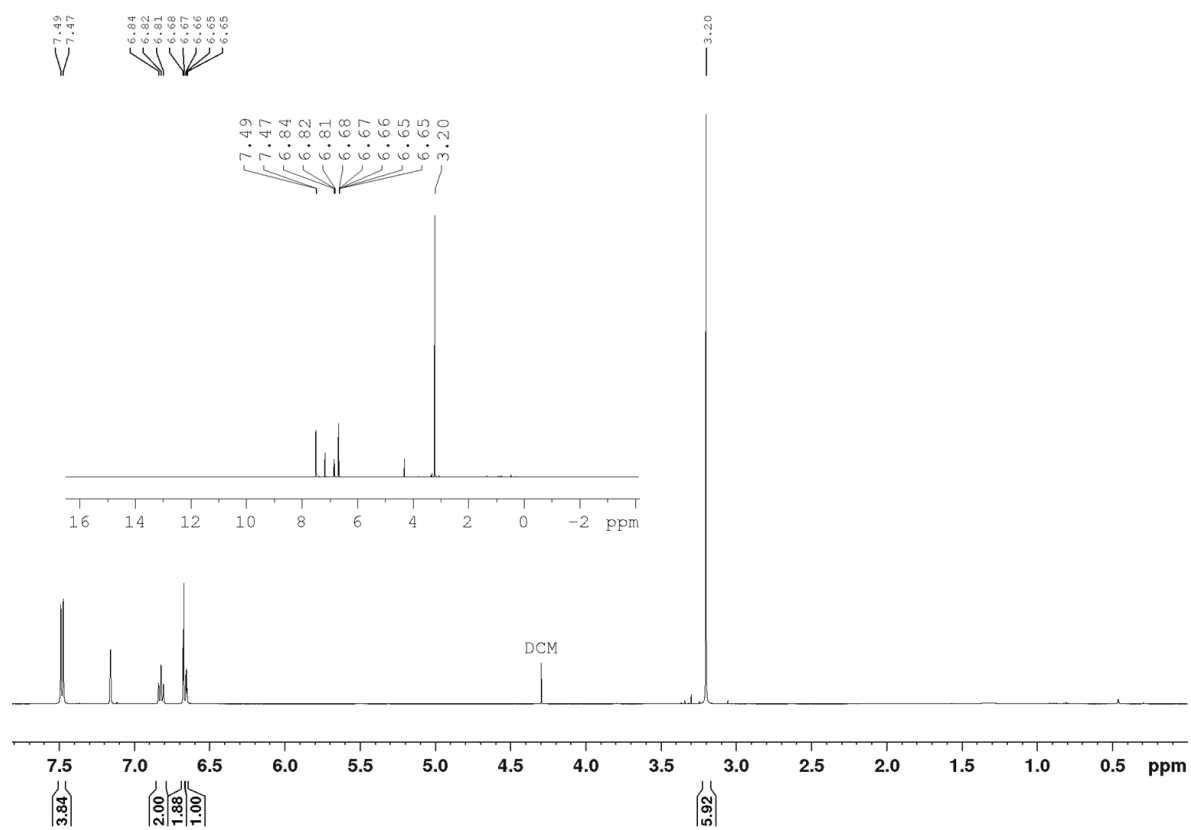


Figure 8.31:  $^1\text{H}$  NMR spectrum (500 MHz, 298 K,  $\text{C}_6\text{D}_6$ ) of compound **iv'**.

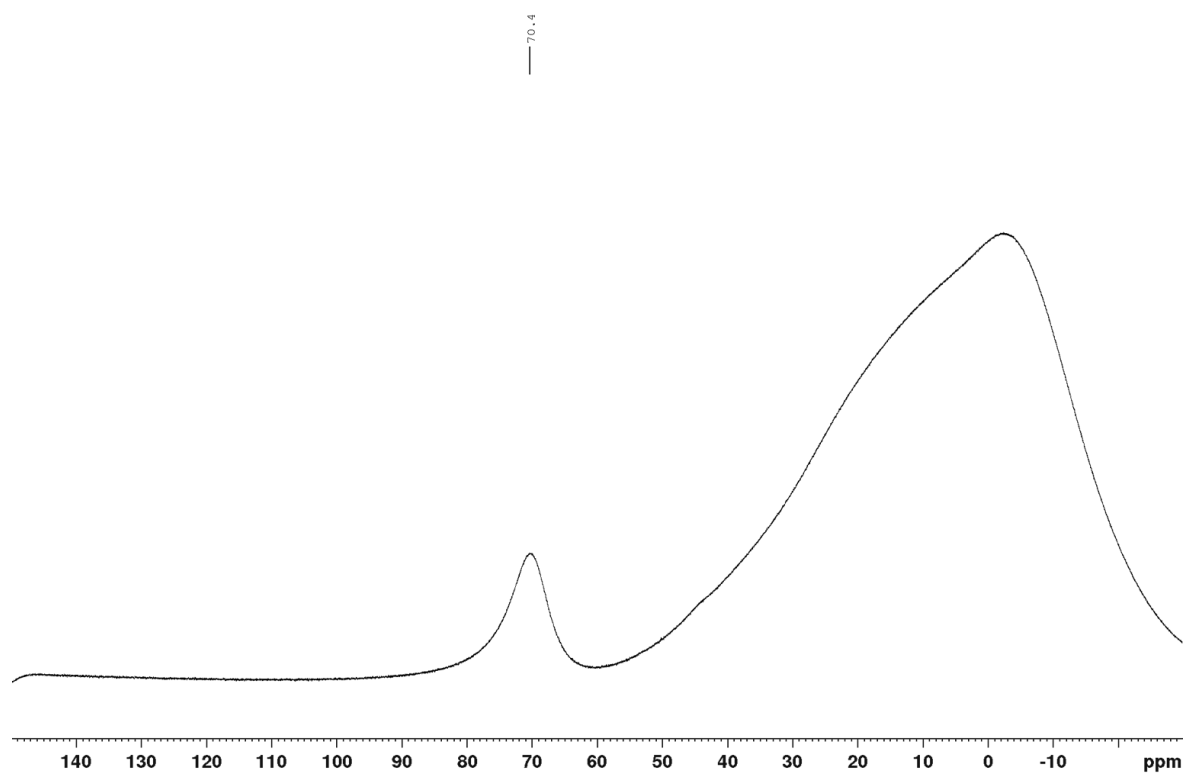


Figure 8.32:  $^{11}\text{B}\{^1\text{H}\}$  NMR spectrum (160 MHz, 298 K,  $\text{C}_6\text{D}_6$ ) of compound **iv'**.

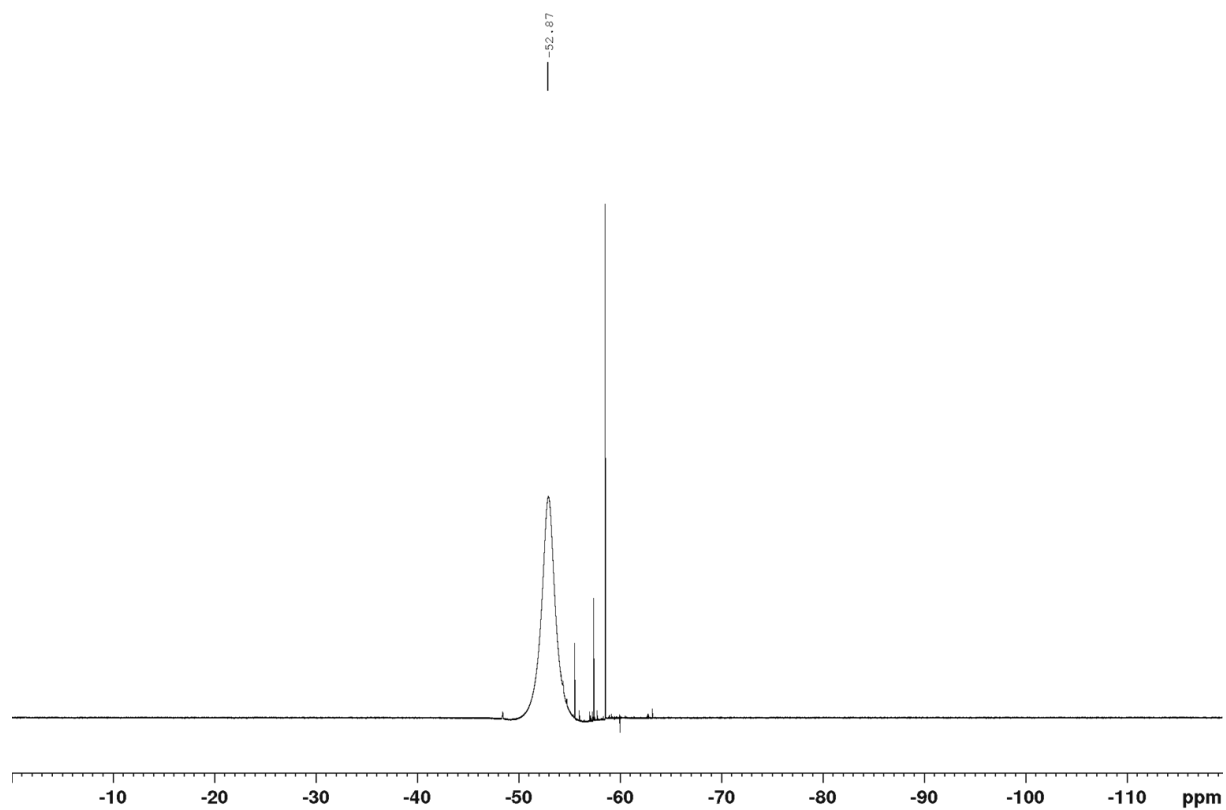


Figure 8.33:  $^{19}\text{F}\{^1\text{H}\}$  NMR spectrum (471 MHz, 298 K,  $\text{C}_6\text{D}_6$ ) of compound **iv'**.

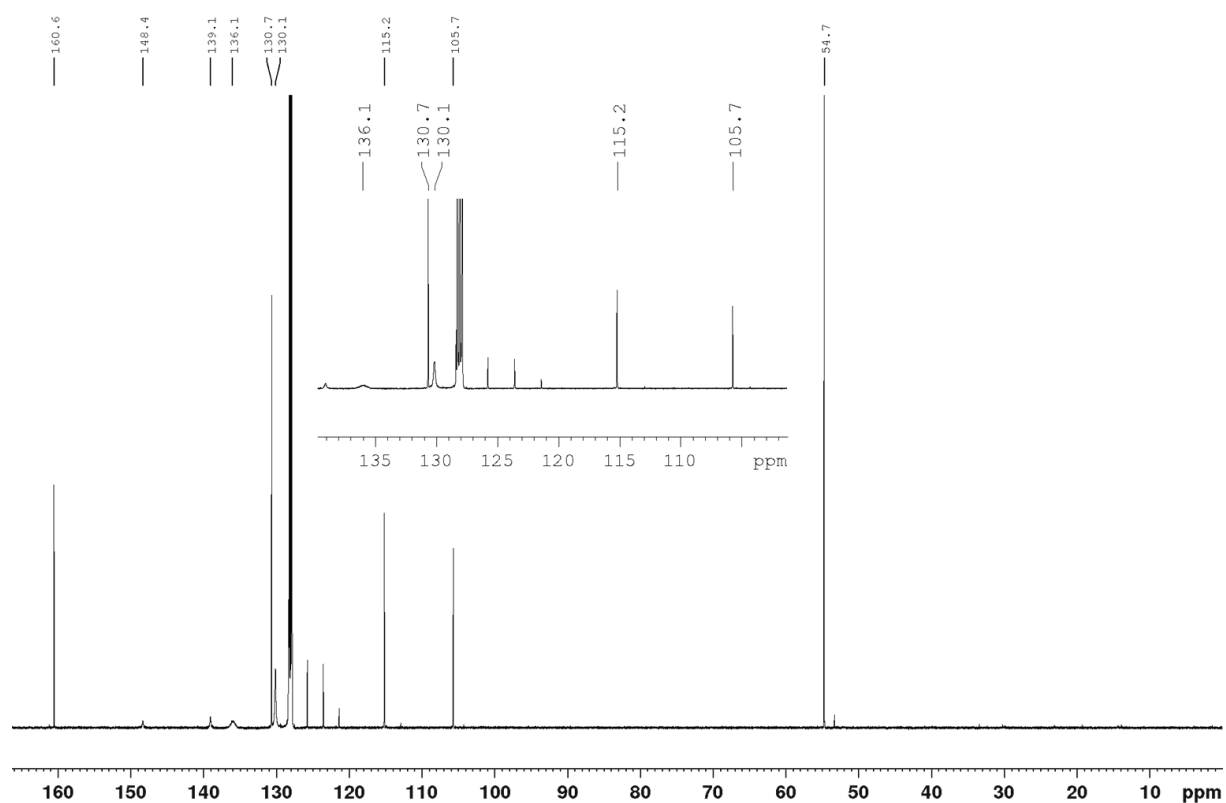


Figure 8.34:  $^{13}\text{C}\{^1\text{H}\}$  NMR spectrum (126 MHz, 298 K,  $\text{C}_6\text{D}_6$ ) of compound **iv'**.

## Appendix

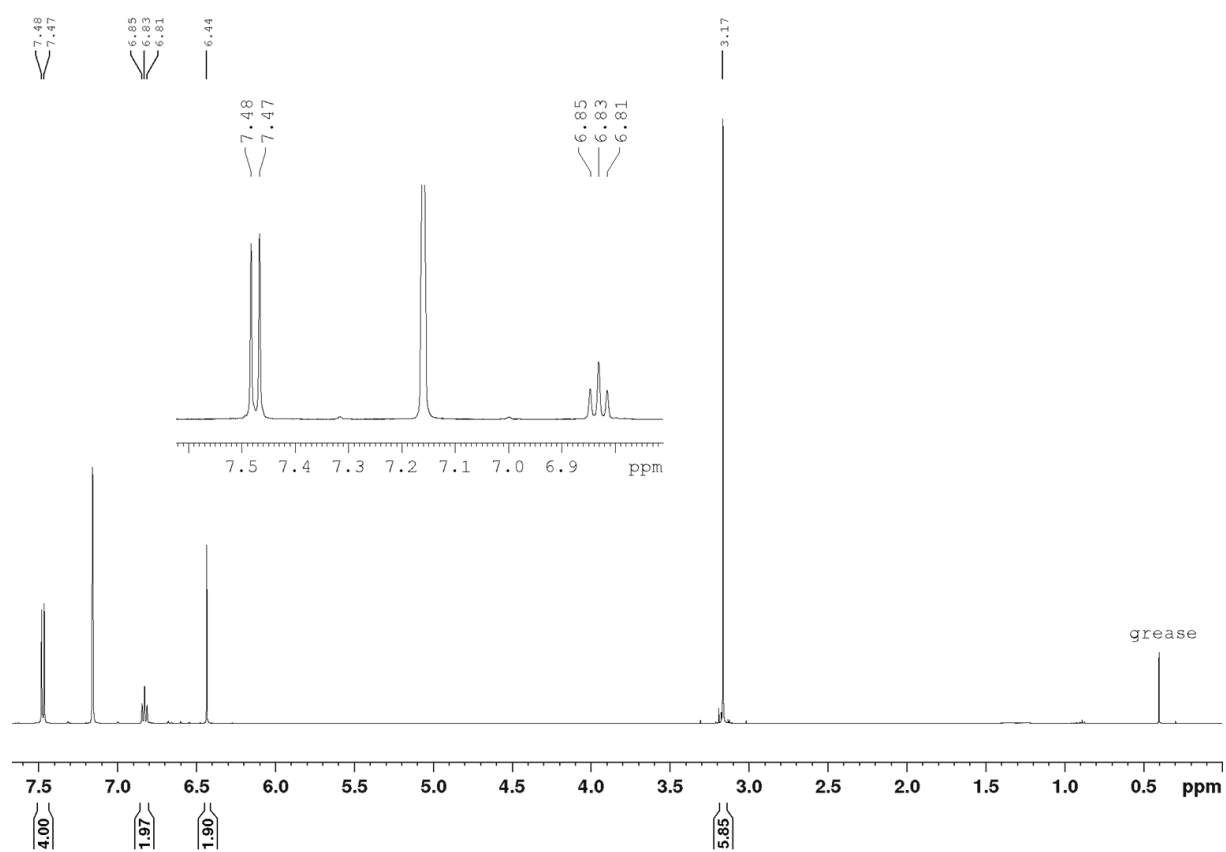


Figure 8.35:  $^1\text{H}$  NMR spectrum (500 MHz, 298 K,  $\text{C}_6\text{D}_6$ ) of compound **iv**.

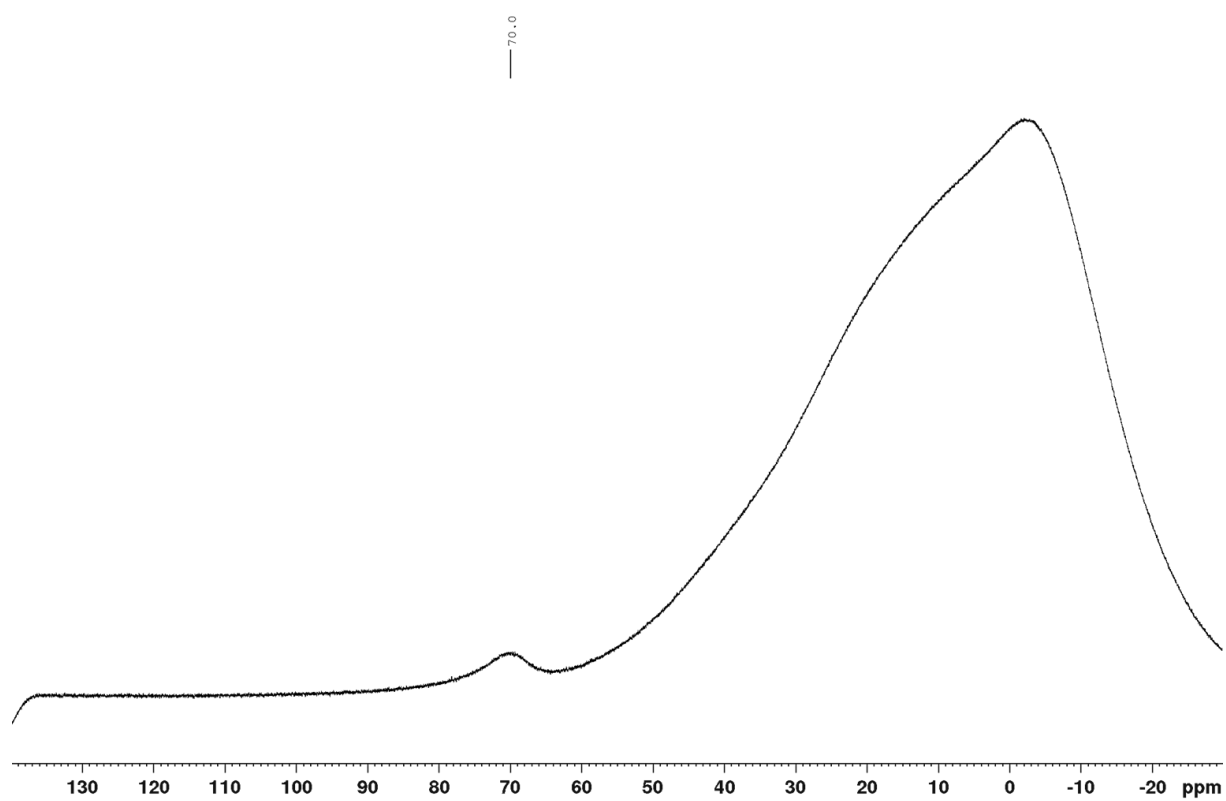


Figure 8.36:  $^{11}\text{B}\{^1\text{H}\}$  NMR spectrum (160 MHz, 298 K,  $\text{C}_6\text{D}_6$ ) of compound **iv**.

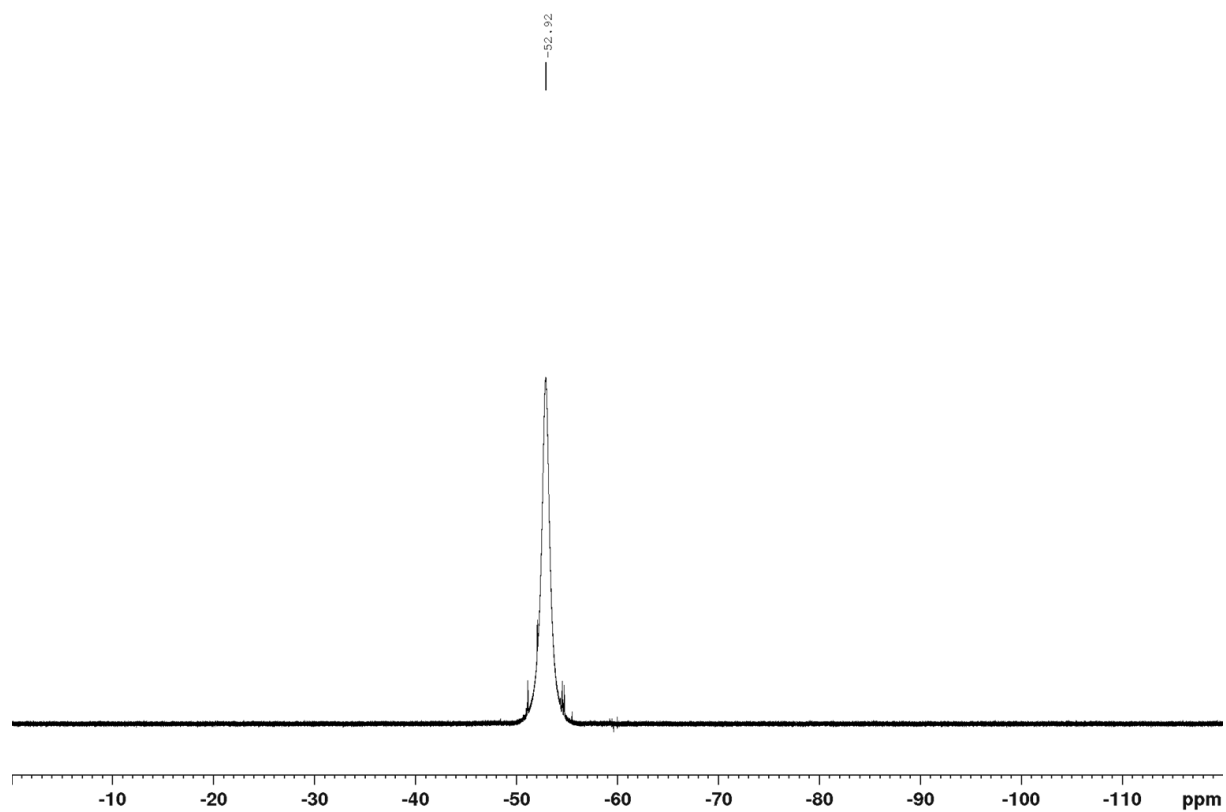


Figure 8.37:  $^{19}\text{F}\{^1\text{H}\}$  NMR spectrum (471 MHz, 298 K,  $\text{C}_6\text{D}_6$ ) of compound **iv**.

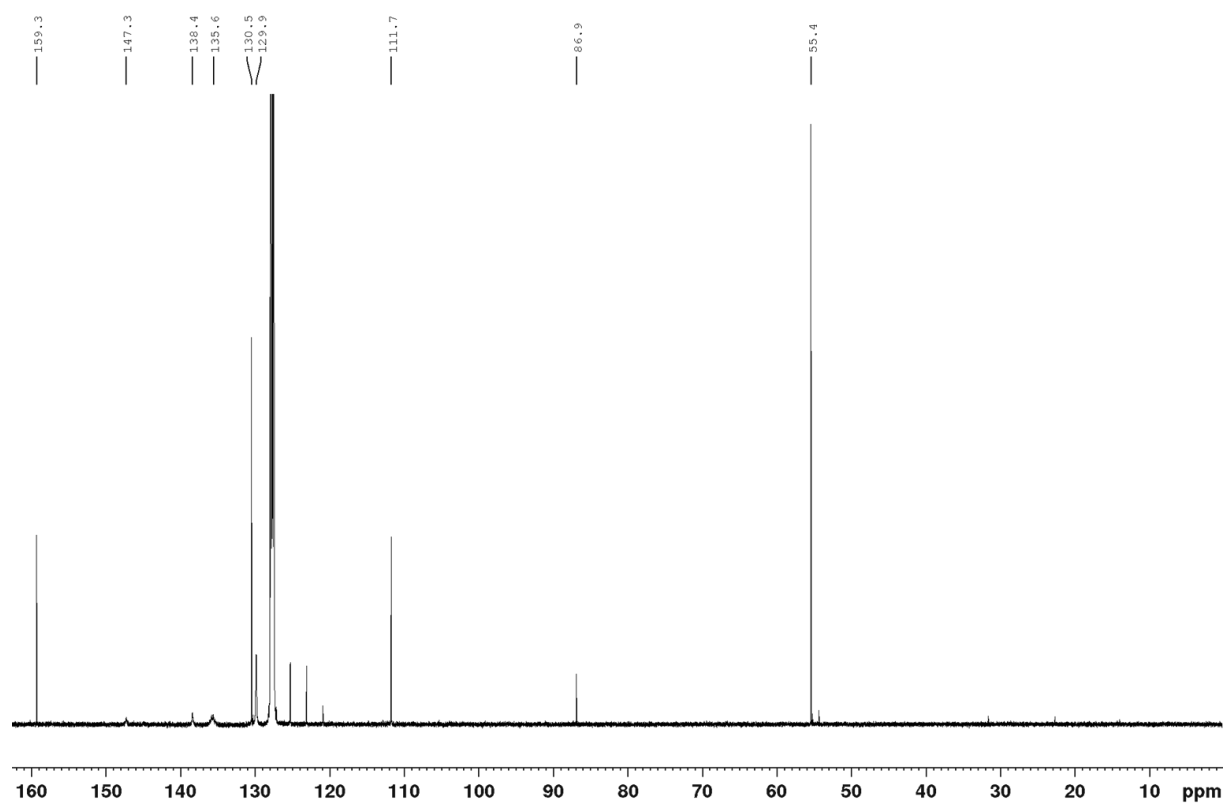


Figure 8.38:  $^{13}\text{C}\{^1\text{H}\}$  NMR spectrum (126 MHz, 298 K,  $\text{C}_6\text{D}_6$ ) of compound **iv**.

## Appendix

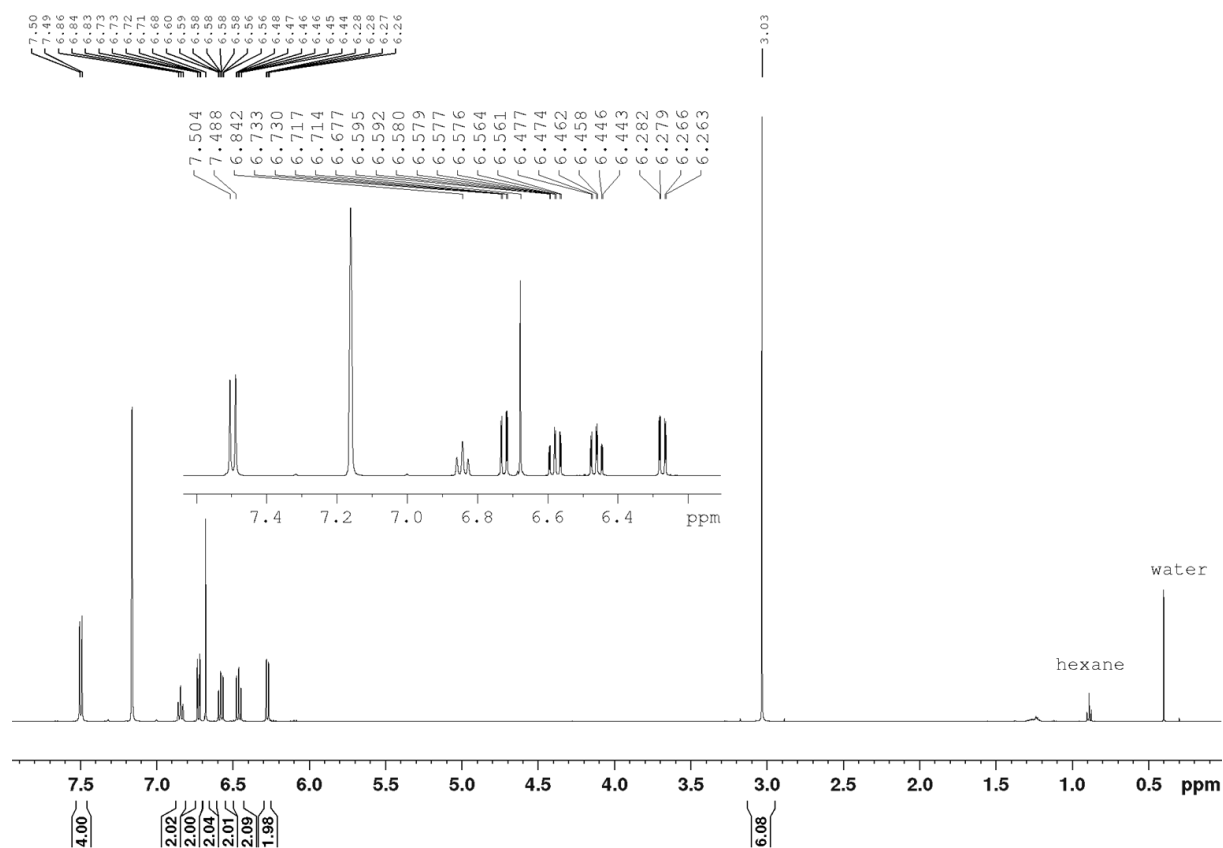


Figure 8.39:  $^1\text{H}$  NMR spectrum (500 MHz, 298 K,  $\text{C}_6\text{D}_6$ ) of compound **Phox-MeO $\pi$  (4)**.

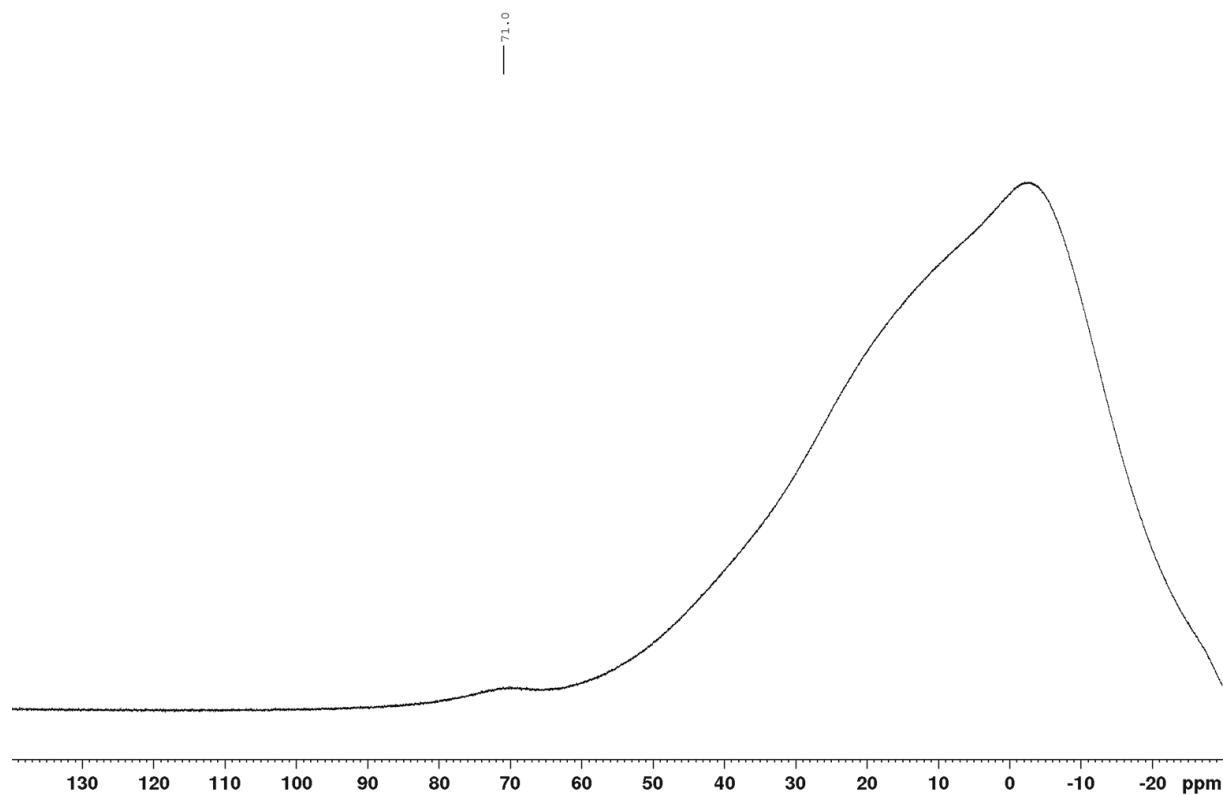


Figure 8.40:  $^{11}\text{B}\{^1\text{H}\}$  NMR spectrum (160 MHz, 298 K,  $\text{C}_6\text{D}_6$ ) of compound **Phox-MeO $\pi$  (4)**.

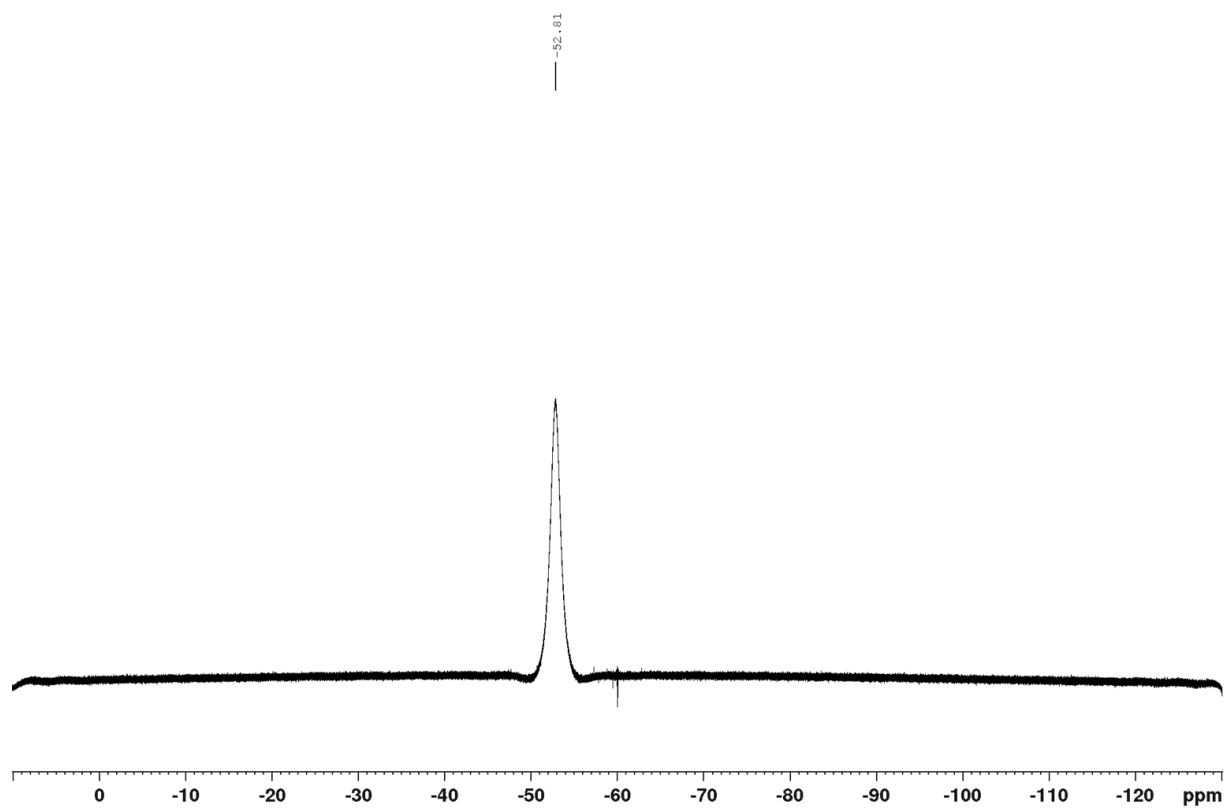


Figure 8.41:  $^{19}\text{F}\{^1\text{H}\}$  NMR spectrum (471 MHz, 298 K,  $\text{C}_6\text{D}_6$ ) of compound **Phox-MeO $\pi$  (4)**.

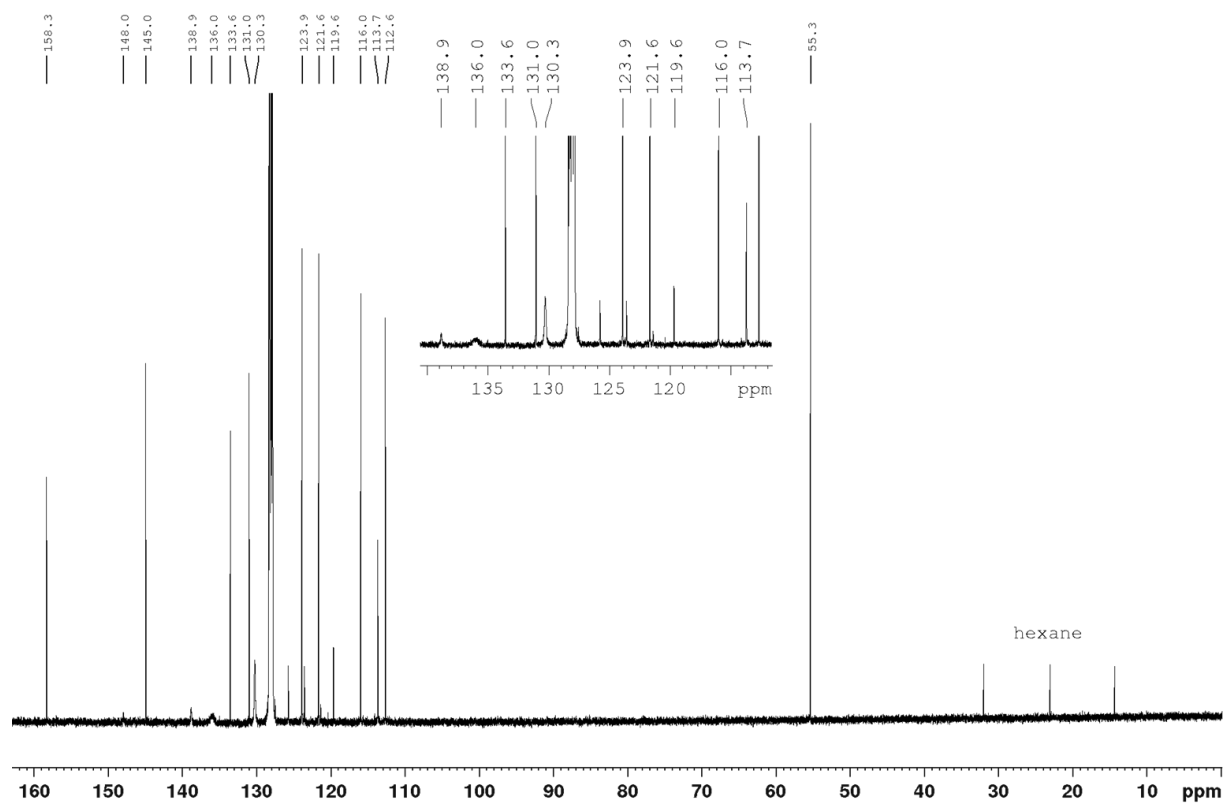


Figure 8.42:  $^{13}\text{C}\{^1\text{H}\}$  NMR spectrum (126 MHz, 298 K,  $\text{C}_6\text{D}_6$ ) of compound **Phox-MeO $\pi$  (4)**.

## Appendix

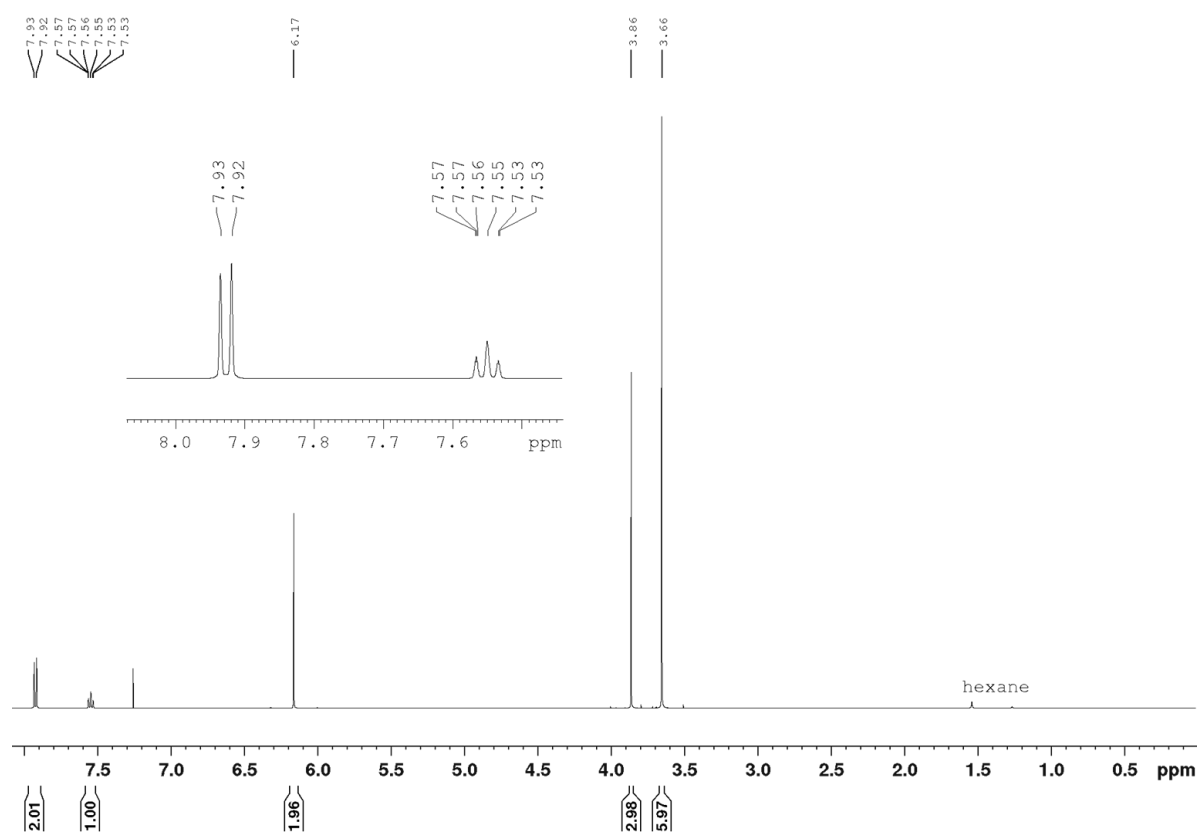


Figure 8.43:  $^1\text{H}$  NMR spectrum (500 MHz, 298 K,  $\text{CDCl}_3$ ) of **2,4,6-trimethoxy-2,6-bis(trifluoromethyl)-1,1'-biphenyl**.

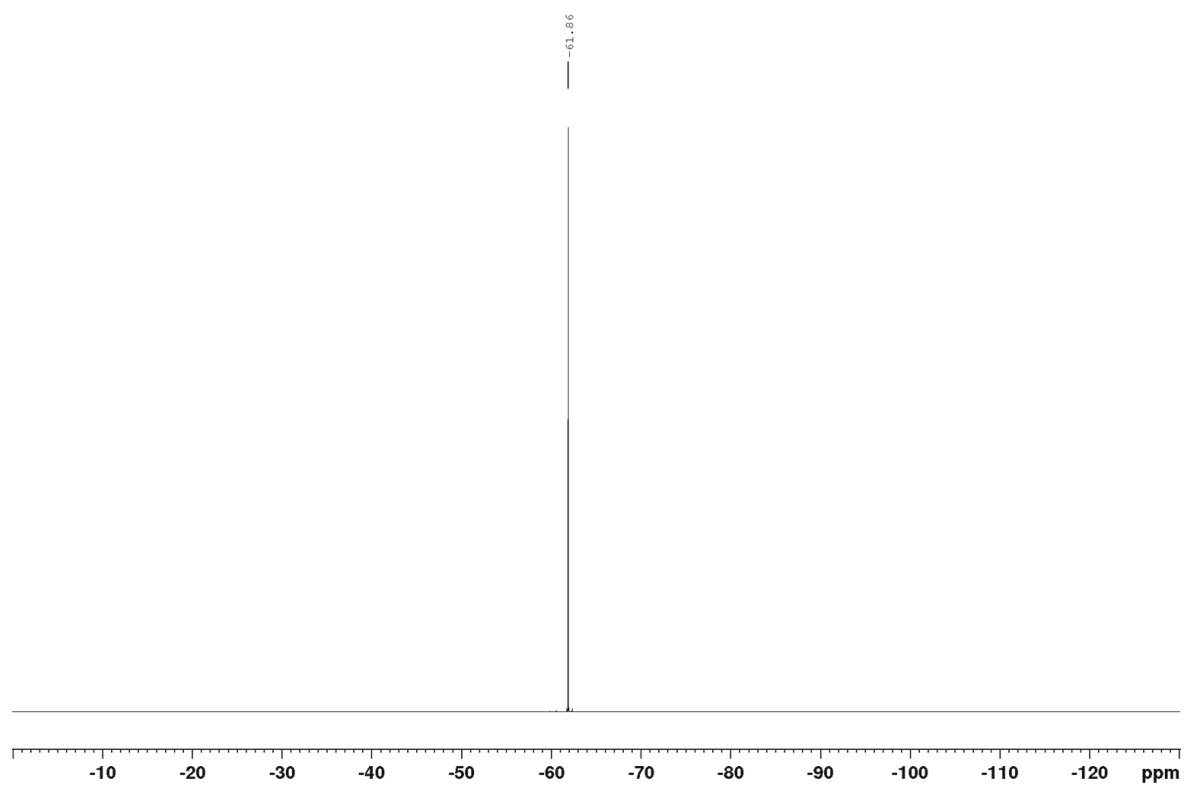


Figure 8.44:  $^{19}\text{F}\{^1\text{H}\}$  NMR spectrum (471 MHz, 298 K,  $\text{CDCl}_3$ ) of **2,4,6-trimethoxy-2,6-bis(trifluoromethyl)-1,1'-biphenyl**.



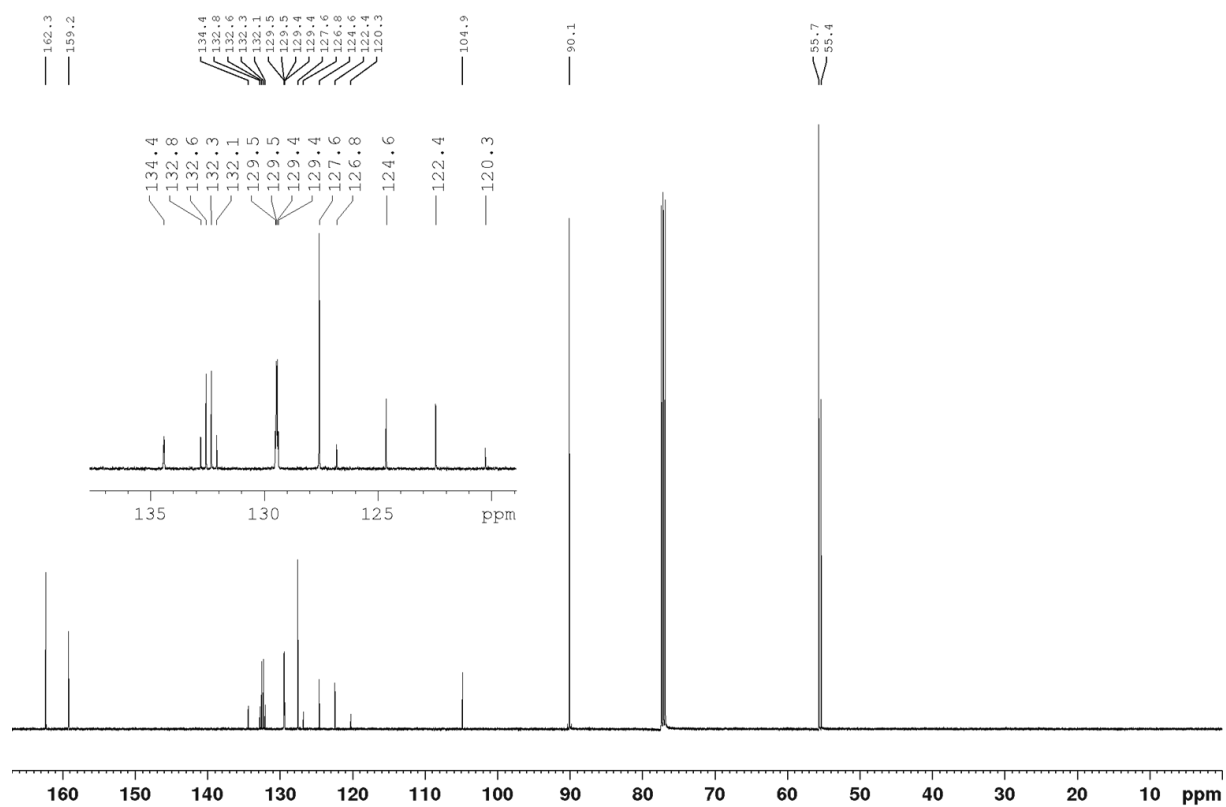


Figure 8.45:  $^{13}\text{C}\{^1\text{H}\}$  NMR spectrum (126 MHz, 298 K,  $\text{CDCl}_3$ ) of **2,4,6-trimethoxy-2,6-bis(trifluoromethyl)-1,1'-biphenyl**.

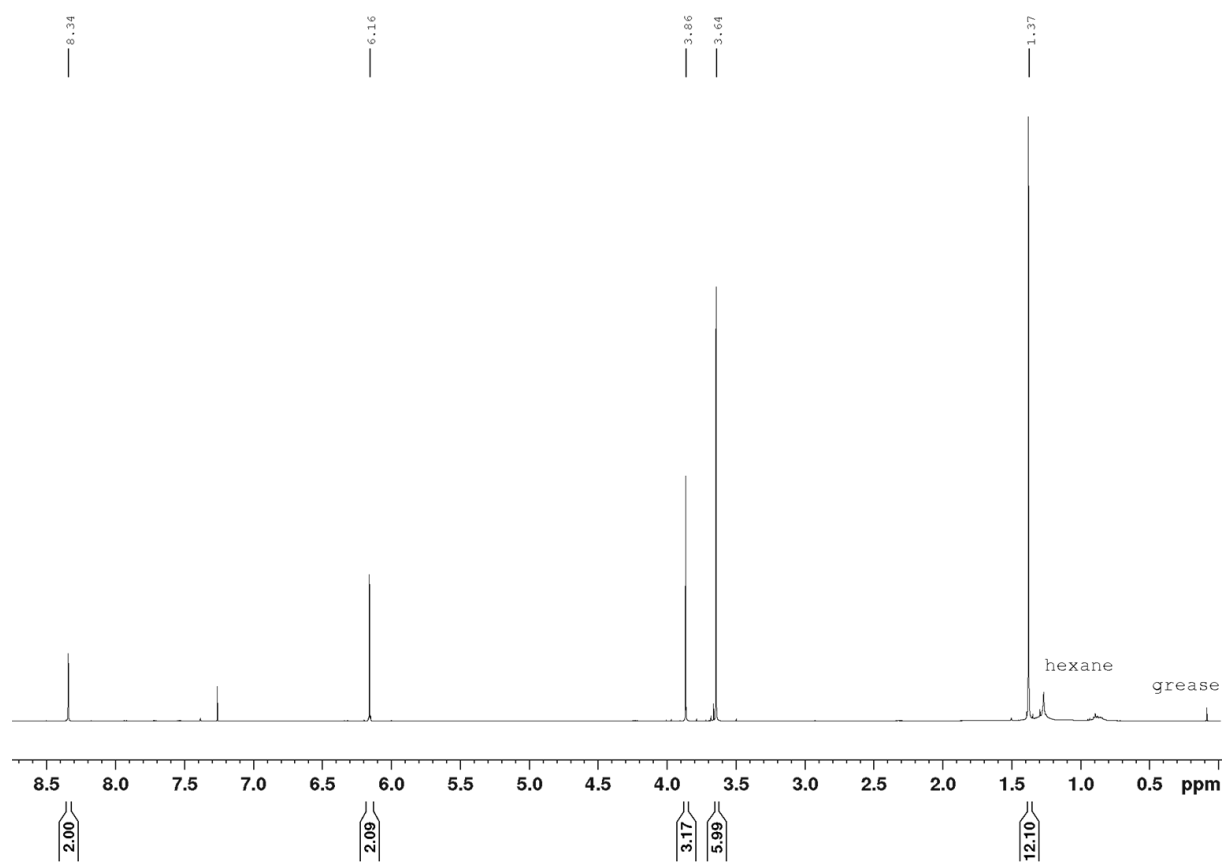


Figure 8.46:  $^1\text{H}$  NMR spectrum (500 MHz, 298 K,  $\text{CDCl}_3$ ) of **4,4,5,5-tetramethyl-2-(2',4',6'-trimethoxy-2,6-bis(trifluoromethyl)-[1,1'-biphenyl]-4-yl)-1,3,2-dioxaborolane**.

# Appendix

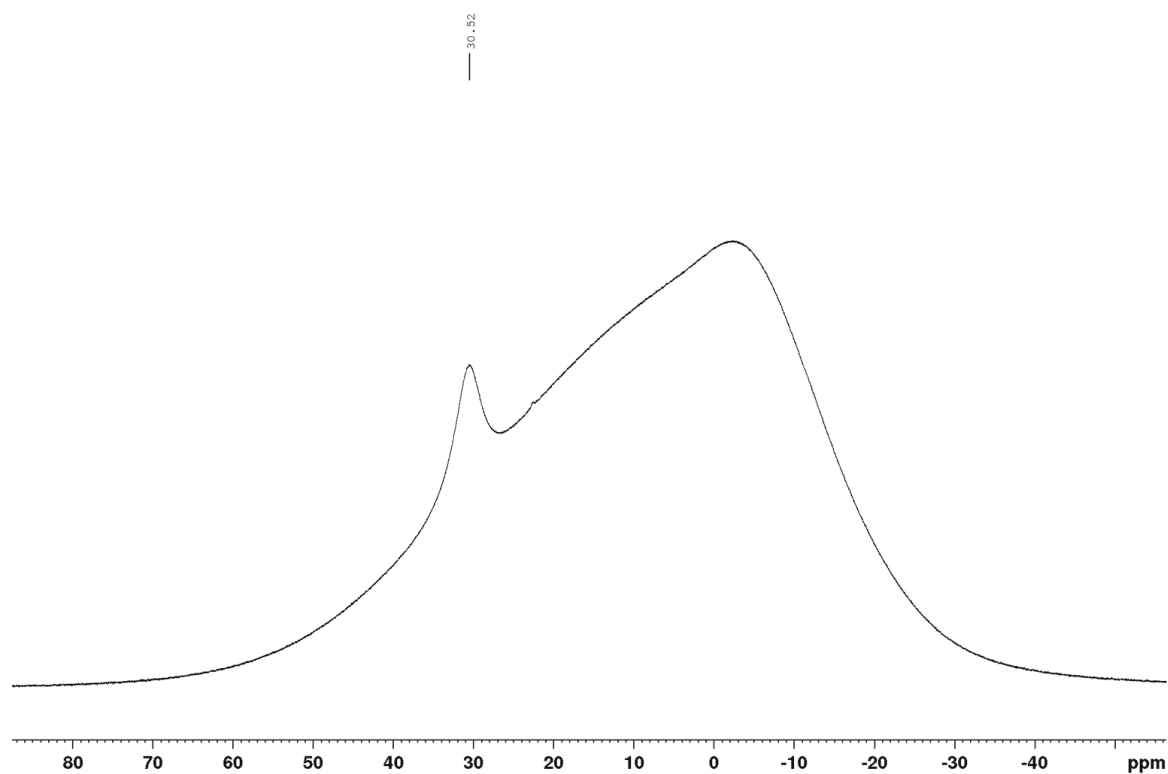


Figure 8.47:  $^{11}\text{B}\{^1\text{H}\}$  NMR spectrum (160 MHz, 298 K,  $\text{CDCl}_3$ ) of 4,4,5,5-tetramethyl-2-(2',4',6'-trimethoxy-2,6-bis(trifluoromethyl)-[1,1'-biphenyl]-4-yl)-1,3,2-dioxaborolane.

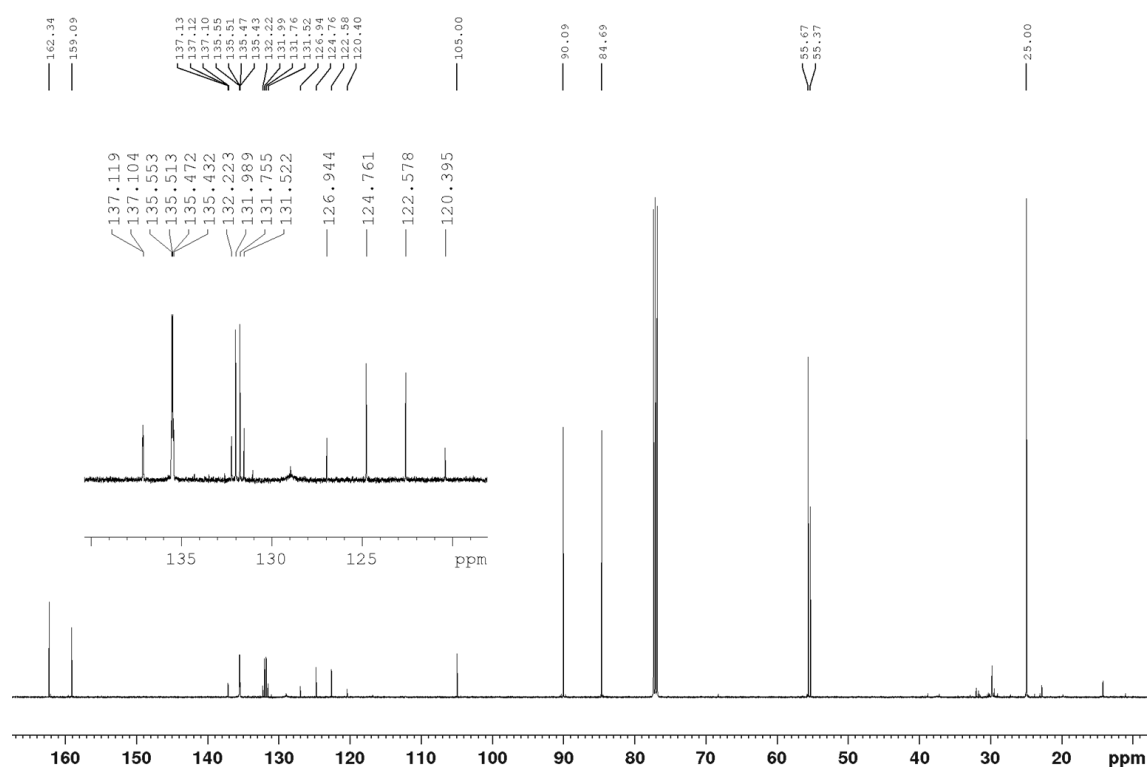


Figure 8.48:  $^{13}\text{C}\{^1\text{H}\}$  NMR spectrum (126 MHz, 298 K,  $\text{CDCl}_3$ ) of 4,4,5,5-tetramethyl-2-(2',4',6'-trimethoxy-2,6-bis(trifluoromethyl)-[1,1'-biphenyl]-4-yl)-1,3,2-dioxaborolane.

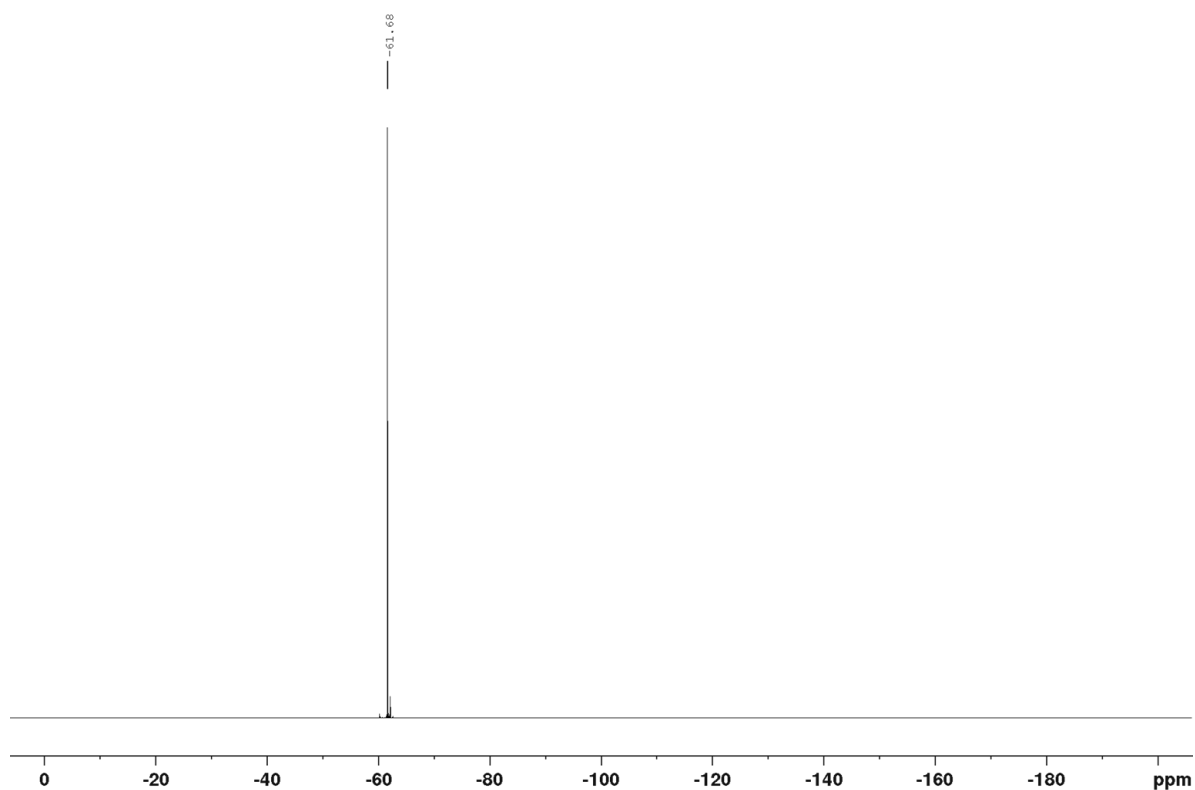


Figure 8.49:  $^{19}\text{F}\{^1\text{H}\}$  NMR spectrum (471 MHz, 298 K,  $\text{CDCl}_3$ ) of **4,4,5,5-tetramethyl-2-(2',4',6'-trimethoxy-2,6-bis(trifluoromethyl)-[1,1'-biphenyl]-4-yl)-1,3,2-dioxaborolane**.

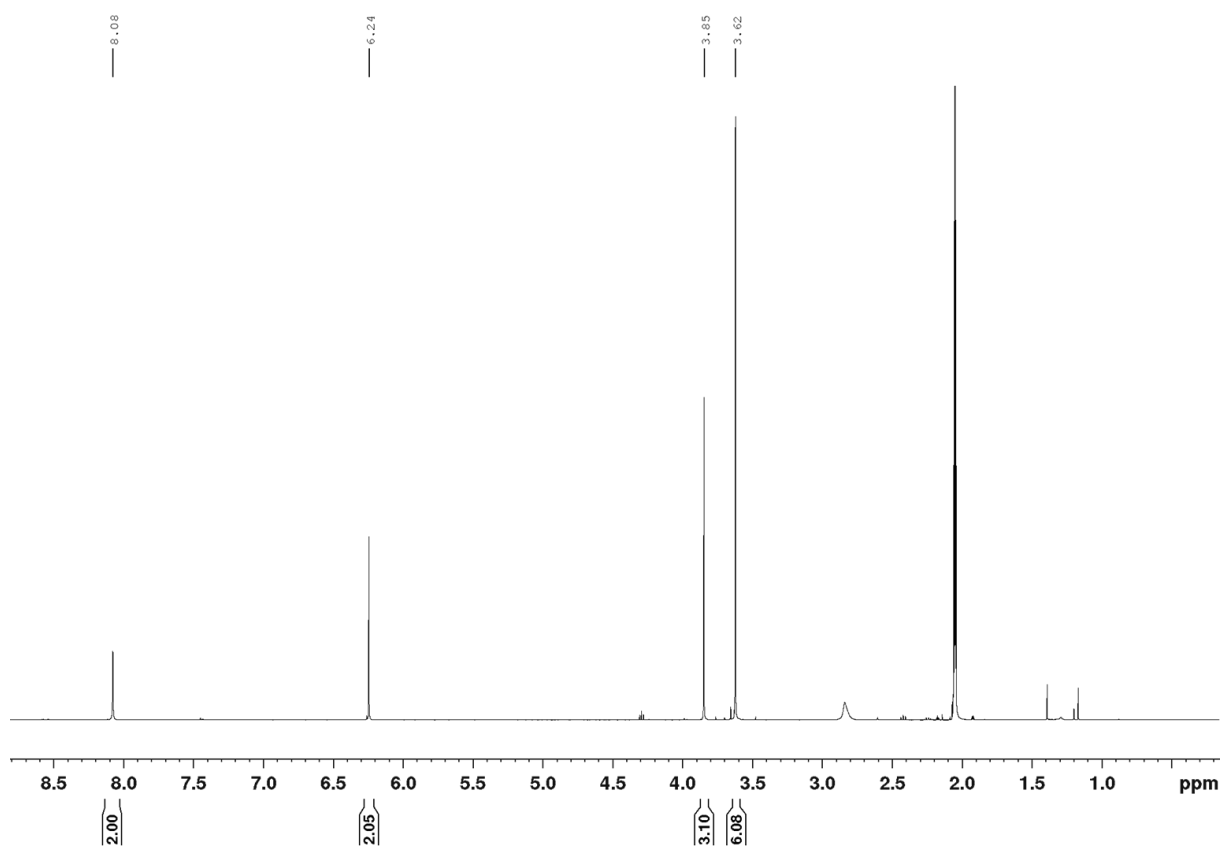


Figure 8.50:  $^1\text{H}$  NMR spectrum (500 MHz, 298 K,  $\text{acetone-d}_6$ ) of **potassium(2',4',6'-trimethoxy-2,6-bis(trifluoromethyl)-[1,1'-biphenyl]-4-yl)trifluoroborate**.

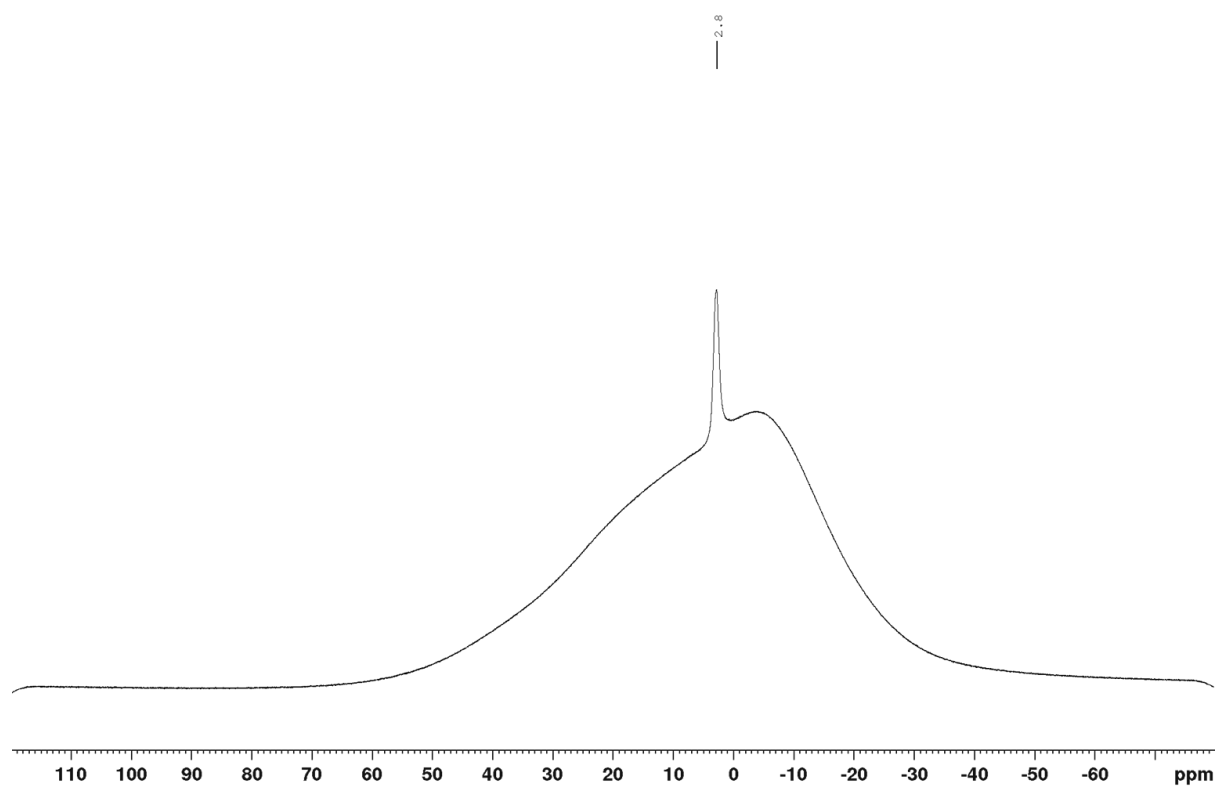


Figure 8.51:  $^{11}\text{B}\{^1\text{H}\}$  NMR spectrum (160 MHz, 298 K, acetone- $\text{d}_6$ ) of potassium(2',4',6'-trimethoxy-2,6-bis(trifluoromethyl)-[1,1'-biphenyl]-4-yl)trifluoroborate.

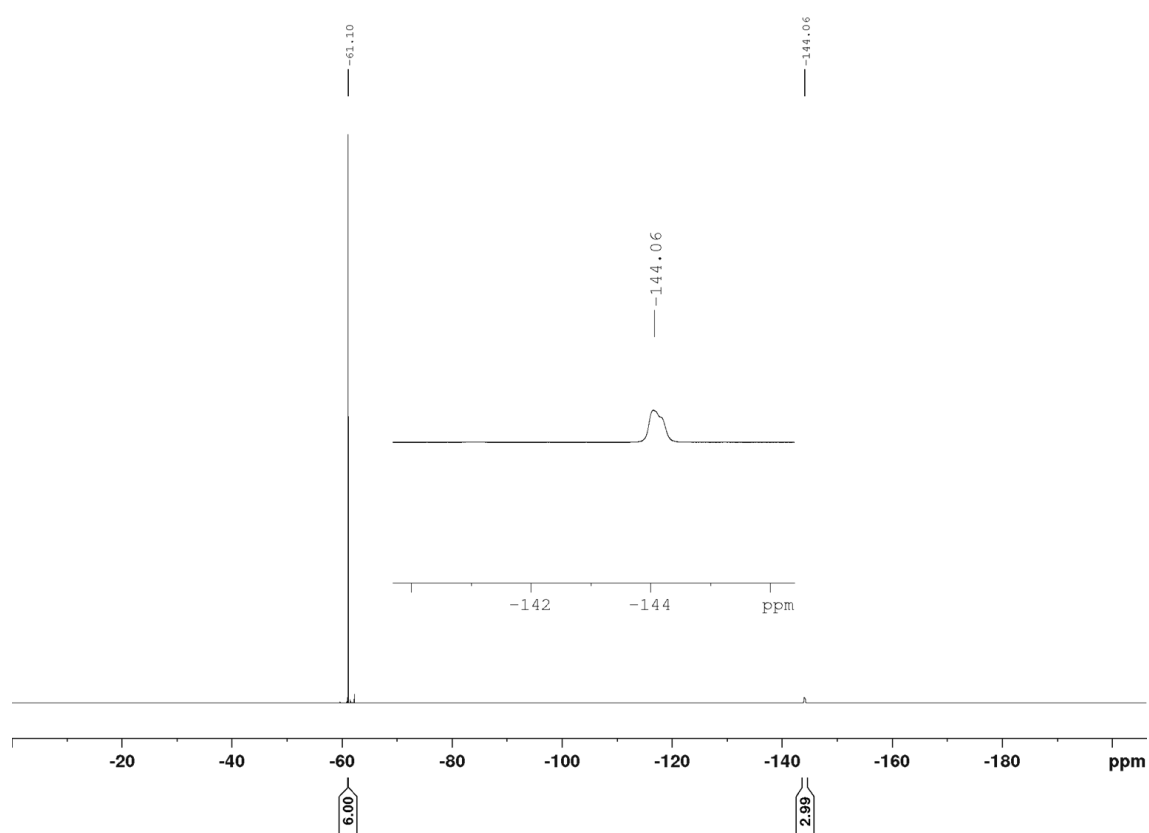


Figure 8.52:  $^{19}\text{F}\{^1\text{H}\}$  NMR spectrum (471 MHz, 298 K, acetone- $\text{d}_6$ ) of potassium(2',4',6'-trimethoxy-2,6-bis(trifluoromethyl)-[1,1'-biphenyl]-4-yl)trifluoroborate.

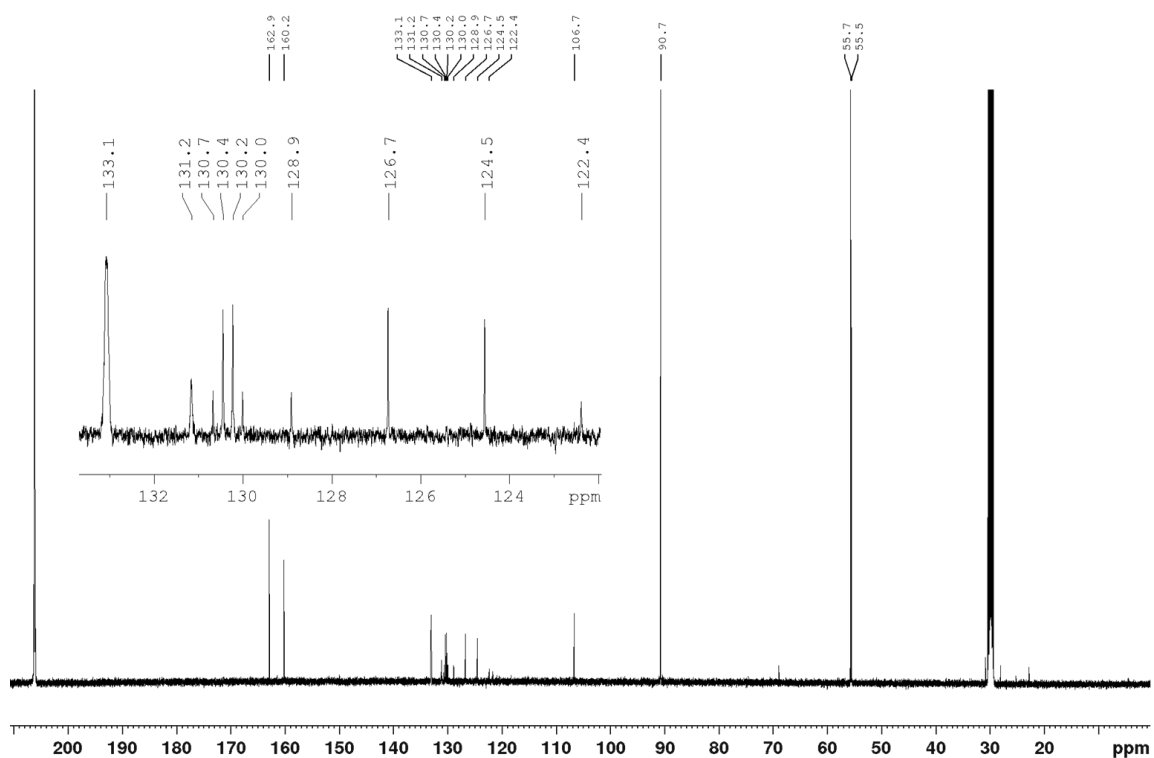


Figure 8.53:  $^{13}\text{C}\{^1\text{H}\}$  NMR spectrum (126 MHz, 298 K, acetone- $d_6$ ) of potassium(2',4',6'-trimethoxy-2,6-bis(trifluoromethyl)-[1,1'-biphenyl]-4-yl)trifluoroborate.

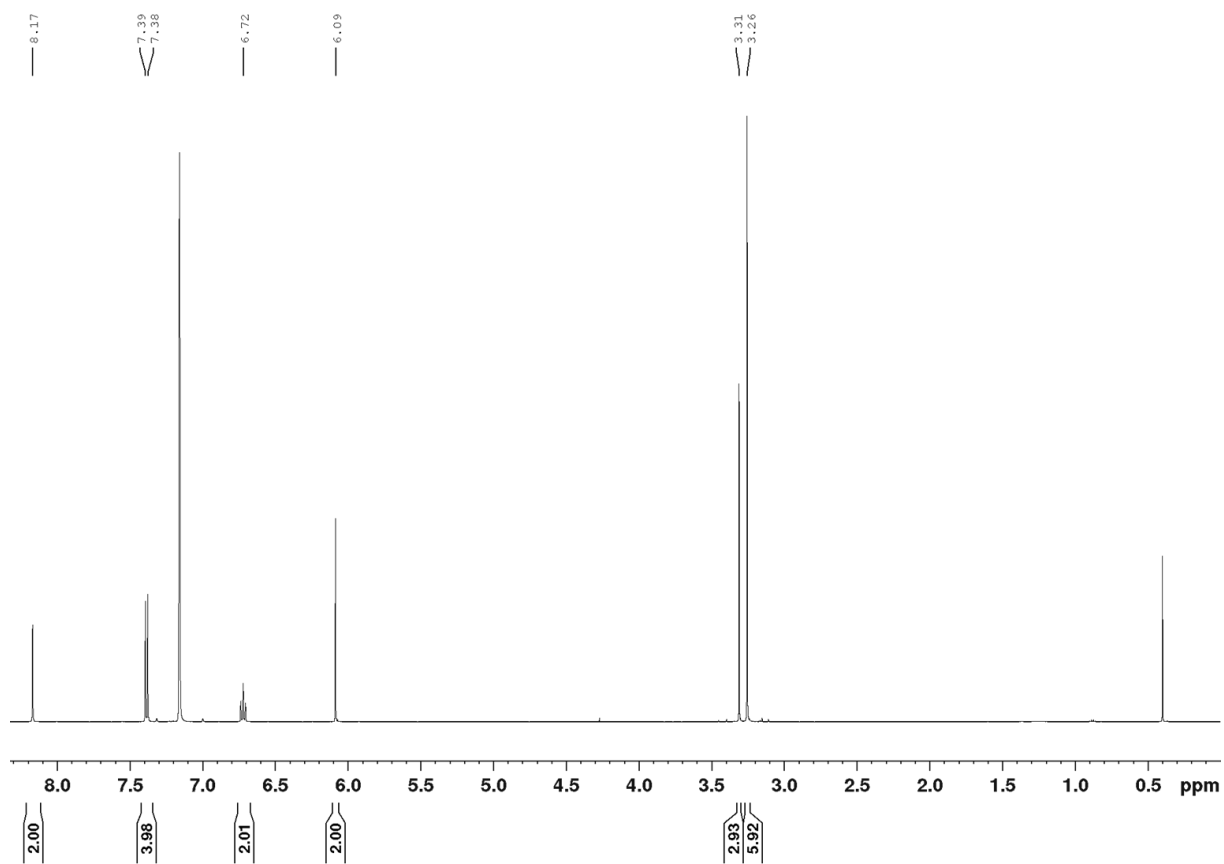


Figure 8.54:  $^1\text{H}$  NMR spectrum (500 MHz, 298 K,  $\text{C}_6\text{D}_6$ ) of compound  $\text{MeO}_3\text{Ph-FMe}\pi$  (5).

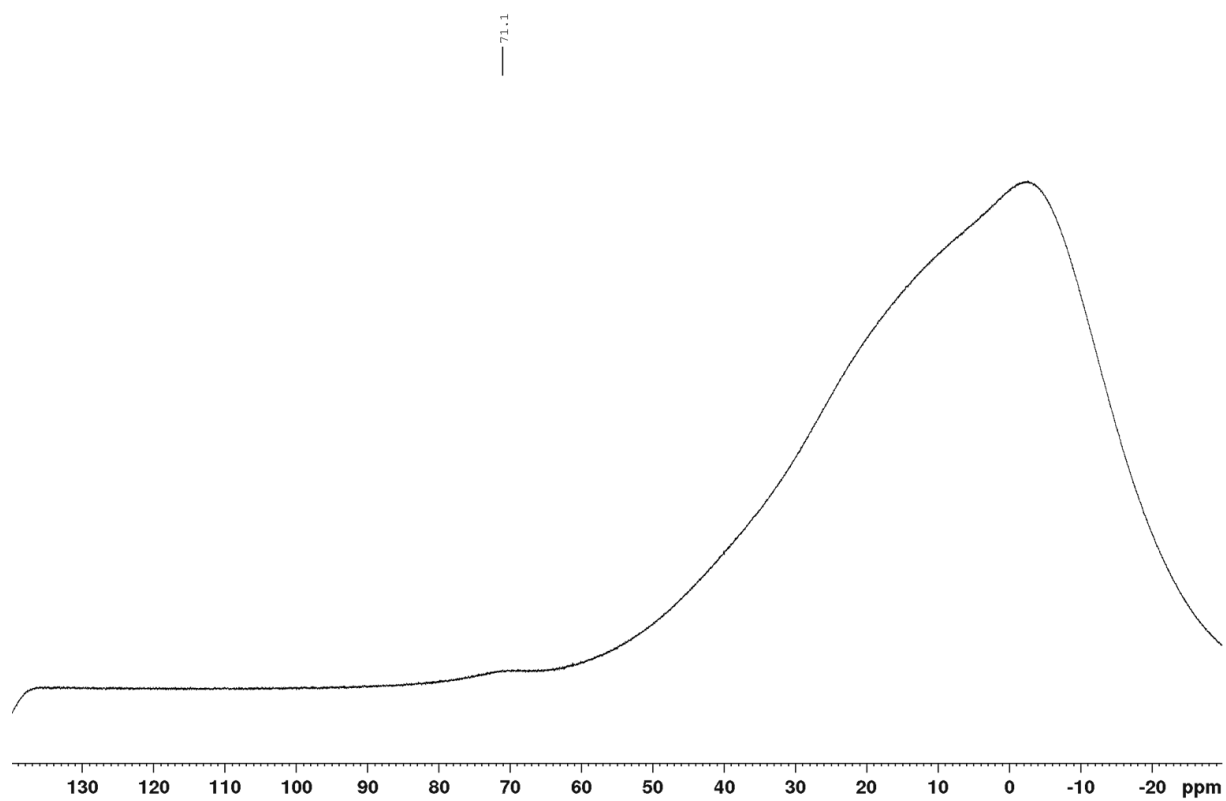


Figure 8.55:  $^{11}\text{B}\{^1\text{H}\}$  NMR spectrum (160 MHz, 298 K,  $\text{C}_6\text{D}_6$ ) of compound  $\text{MeO}_2\text{Ph-FMe}_2\pi$  (**5**).

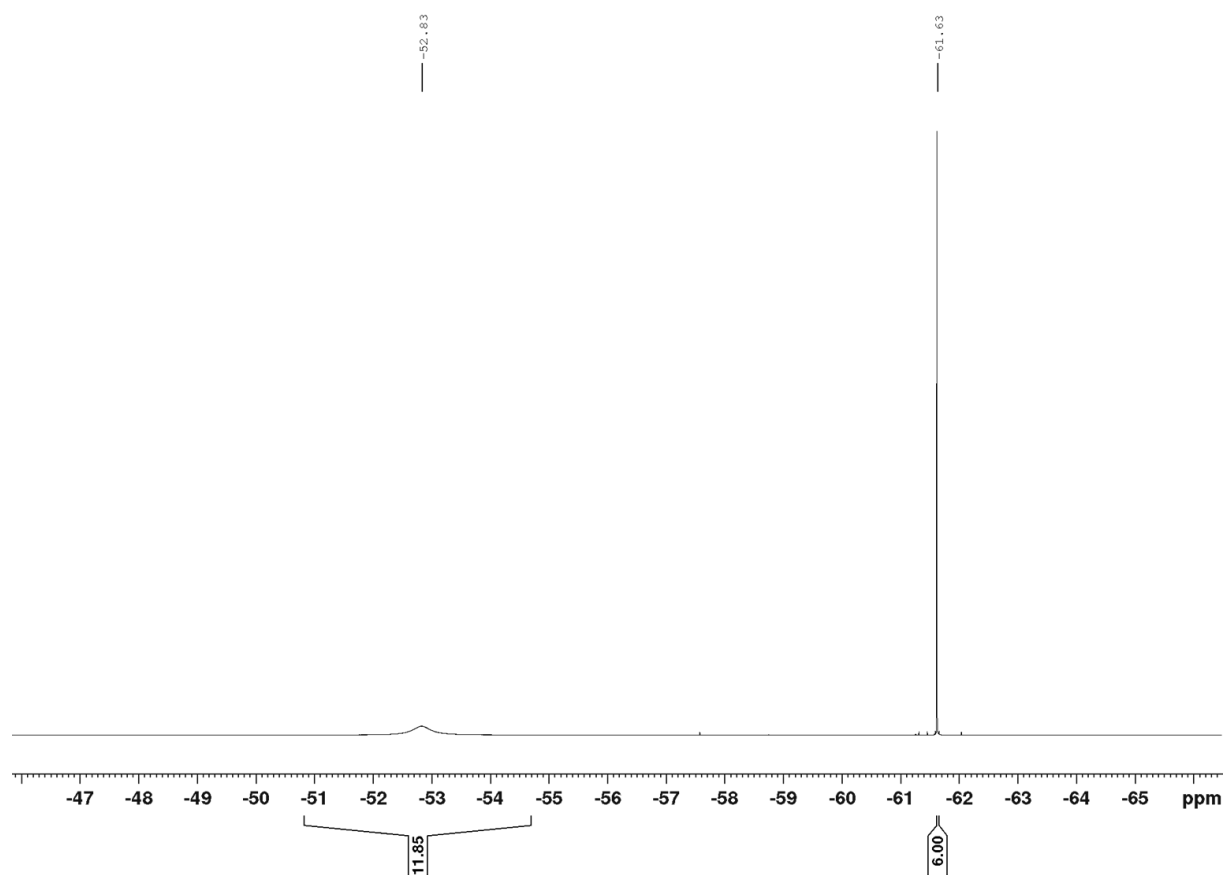


Figure 8.56:  $^{19}\text{F}\{^1\text{H}\}$  NMR spectrum (471 MHz, 298 K,  $\text{C}_6\text{D}_6$ ) of compound  $\text{MeO}_2\text{Ph-FMe}_2\pi$  (**5**).

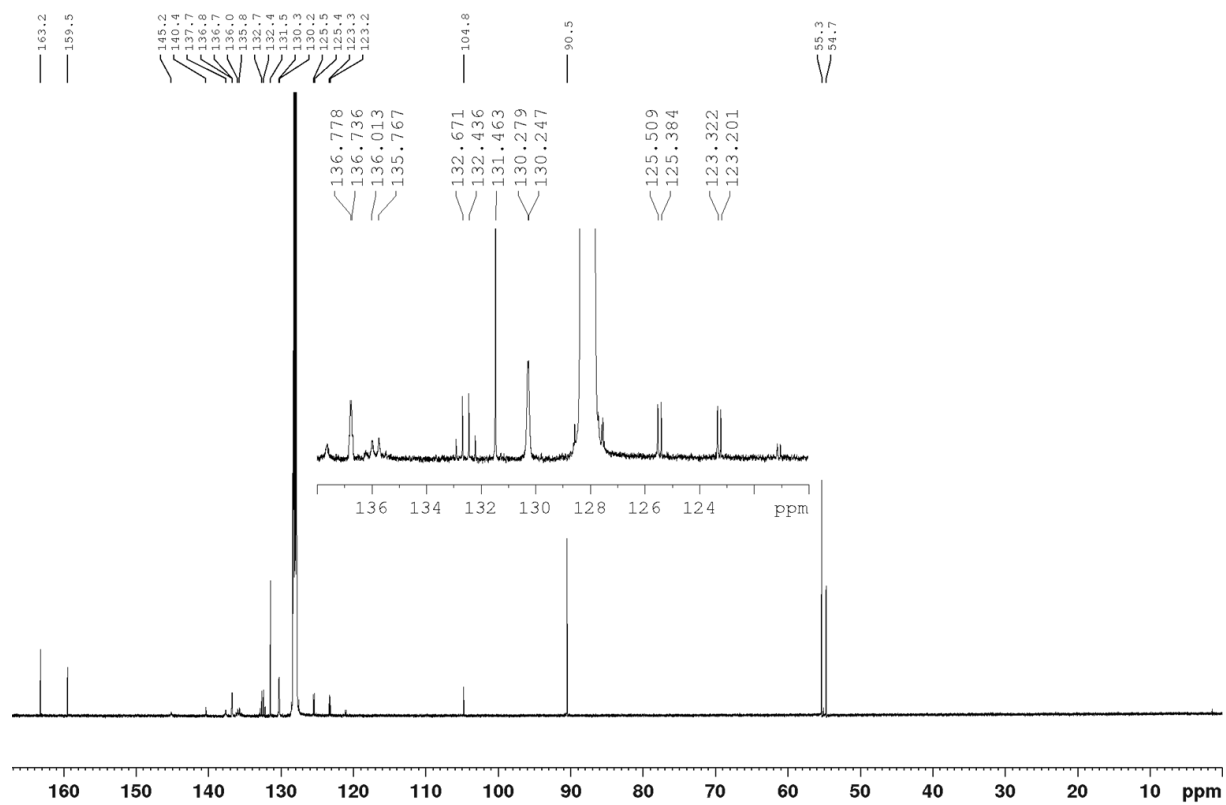


Figure 8.57:  $^{13}\text{C}\{^1\text{H}\}$  NMR spectrum (126 MHz, 298 K,  $\text{C}_6\text{D}_6$ ) of compound  $\text{MeO}_3\text{Ph}^{\text{FMe}}\pi$  (**5**).

## 8.1.2 Chapter 2

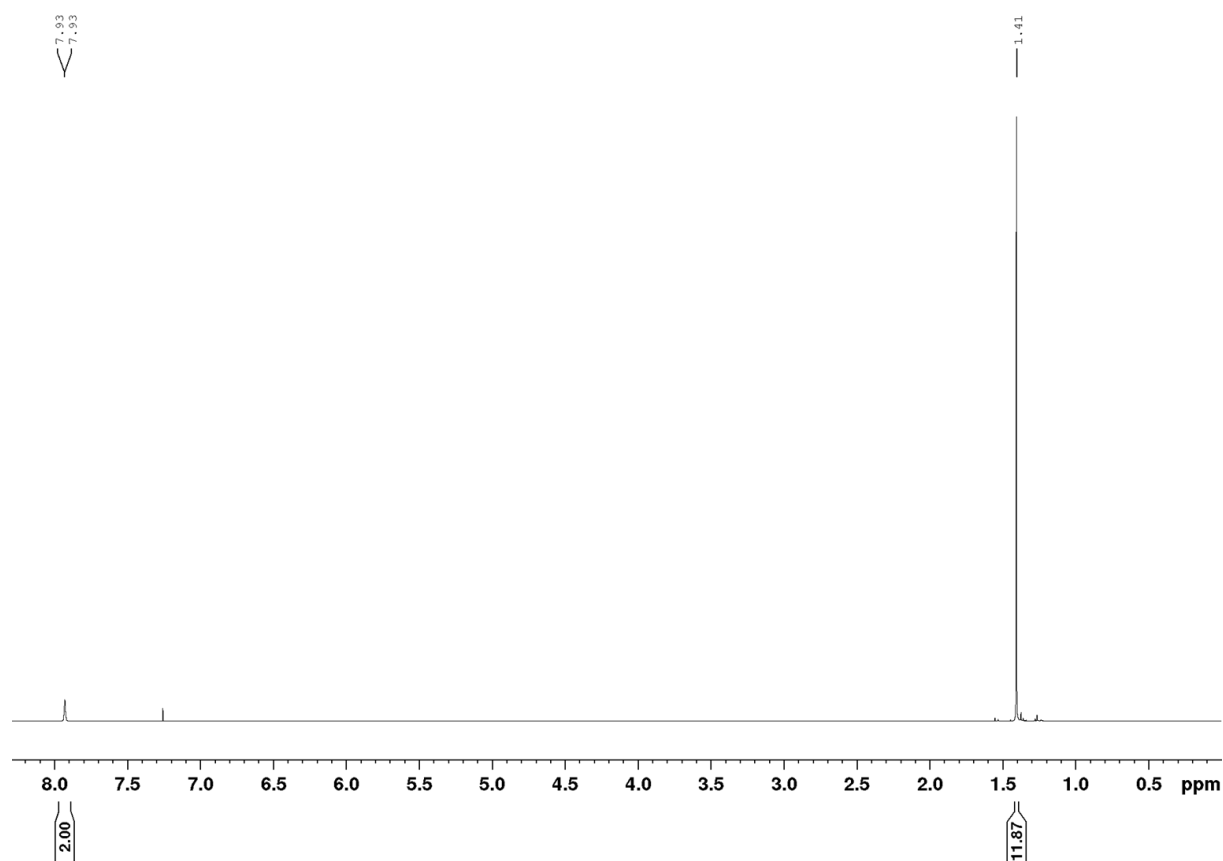


Figure 8.58:  $^1\text{H}$  NMR spectrum (500 MHz, 298 K,  $\text{CDCl}_3$ ) of 2-(2-bromo-3,5-bis(trifluoromethyl)phenyl)-4,4,5,5-tetramethyl-1,3,2-dioxaborolane (2-1).

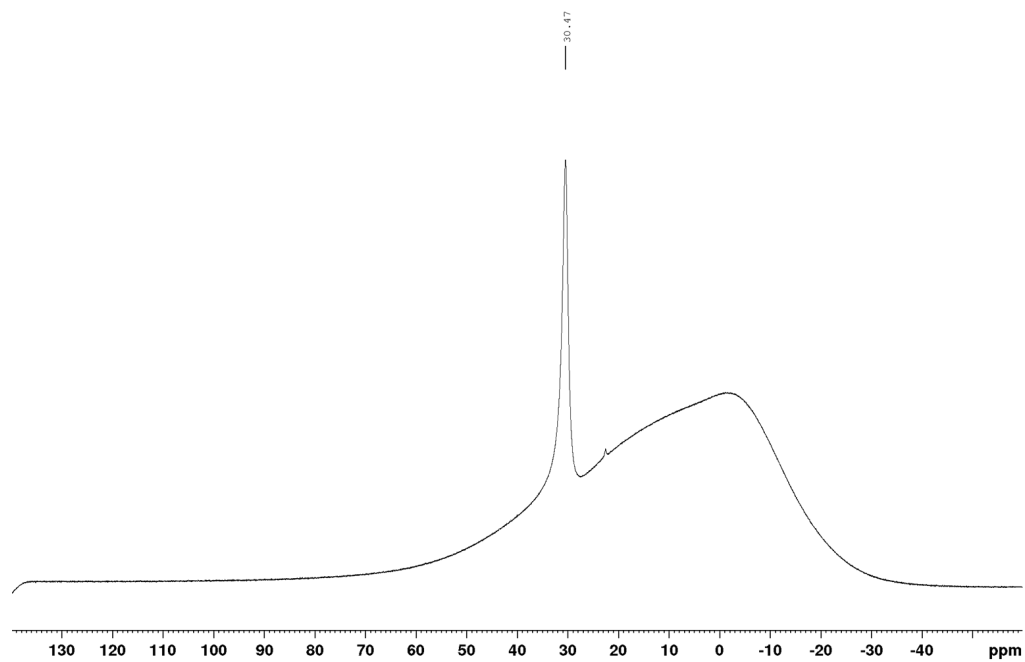


Figure 8.59:  $^{11}\text{B}\{^1\text{H}\}$  NMR spectrum (160 MHz, 298 K,  $\text{CDCl}_3$ ) of 2-(2-bromo-3,5-bis(trifluoromethyl)phenyl)-4,4,5,5-tetramethyl-1,3,2-dioxaborolane (2-1).



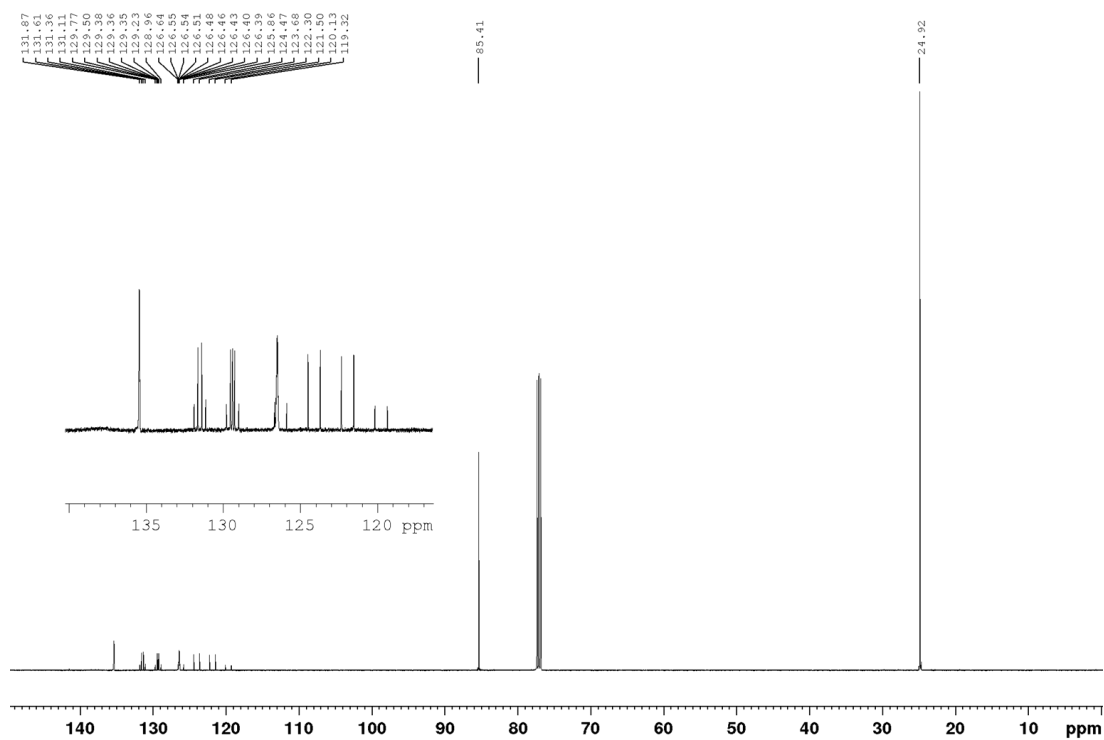


Figure 8.60:  $^{13}\text{C}\{^1\text{H}\}$  NMR spectrum (126 MHz, 298 K,  $\text{CDCl}_3$ ) of 2-(2-bromo-3,5-bis(trifluoromethyl)phenyl)-4,4,5,5-tetramethyl-1,3,2-dioxaborolane (2-1).

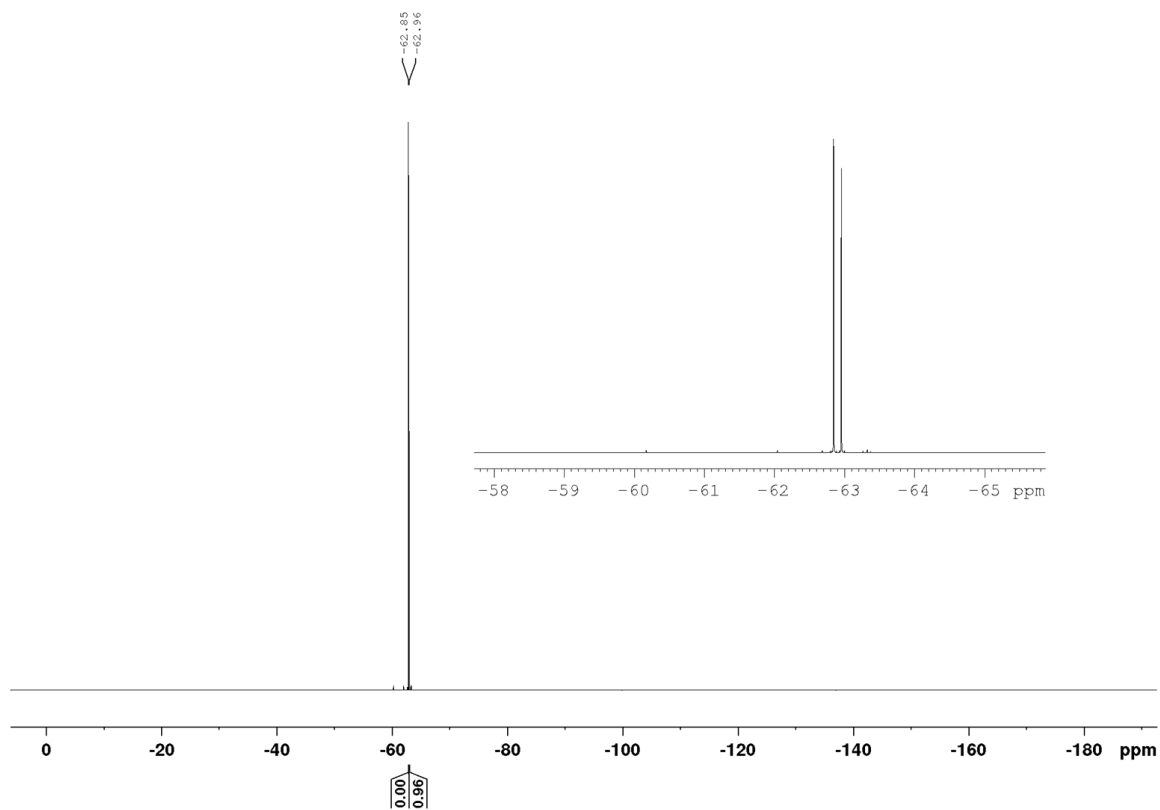


Figure 8.61:  $^{19}\text{F}\{^1\text{H}\}$  NMR spectrum (471 MHz, 298 K,  $\text{CDCl}_3$ ) of 2-(2-bromo-3,5-bis(trifluoromethyl)phenyl)-4,4,5,5-tetramethyl-1,3,2-dioxaborolane (2-1).

# Appendix

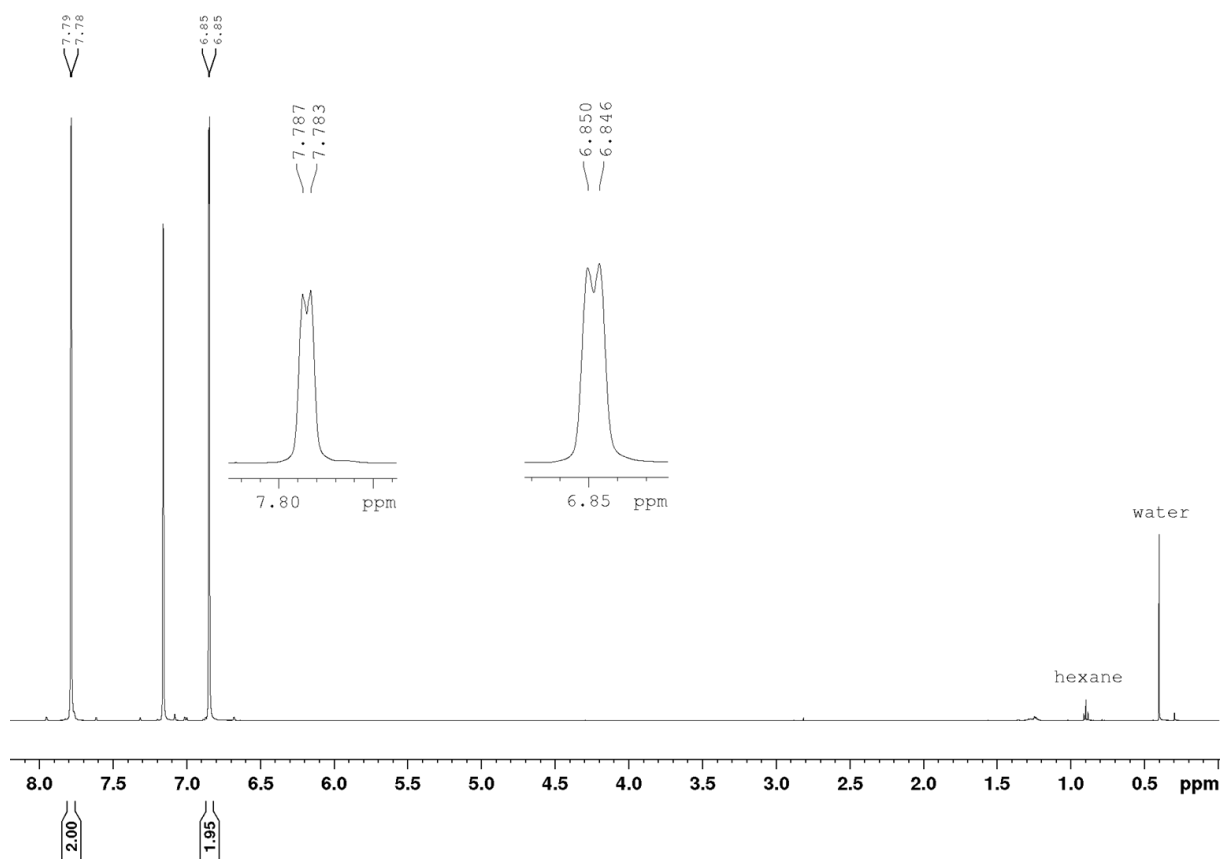


Figure 8.62:  $^1\text{H}$  NMR spectrum (500 MHz, 298 K,  $\text{C}_6\text{D}_6$ ) of **2,2'-dibromo-3,3',5,5'-tetrakis(trifluoromethyl)-1,1'-biphenyl (2-2)**.

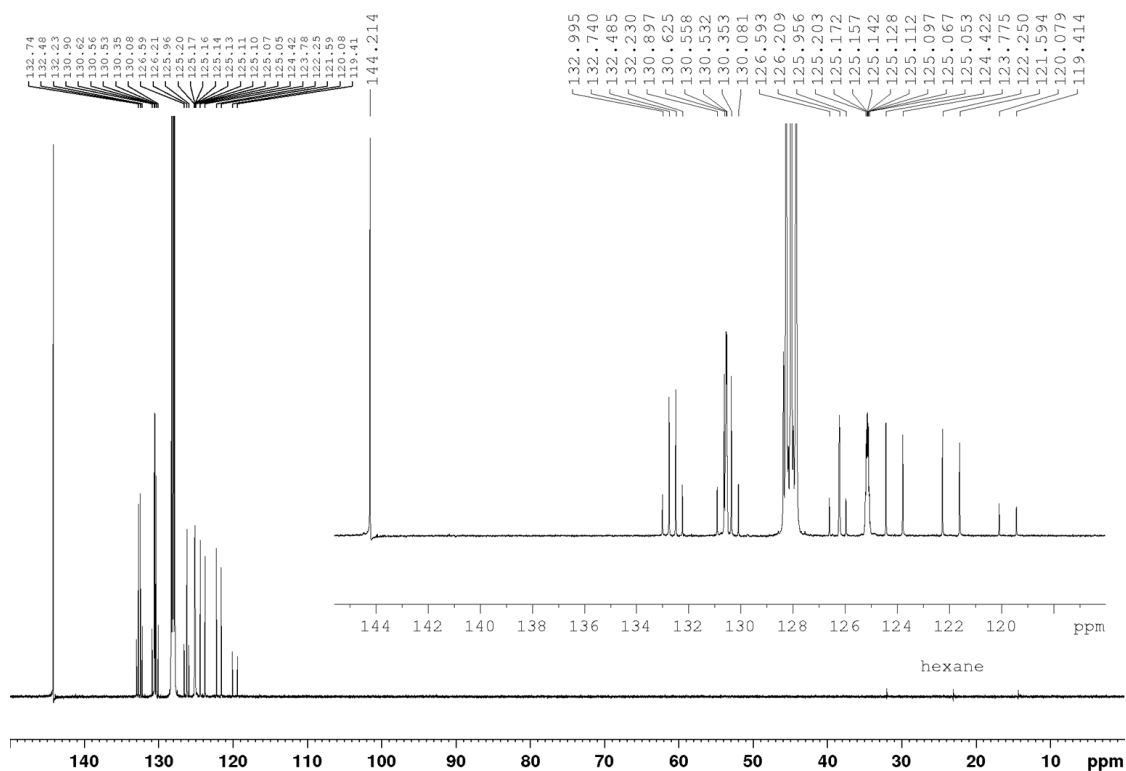


Figure 8.63:  $^{13}\text{C}\{^1\text{H}\}$  NMR spectrum (126 MHz, 298 K,  $\text{C}_6\text{D}_6$ ) of **2,2'-dibromo-3,3',5,5'-tetrakis(trifluoromethyl)-1,1'-biphenyl (2-2)**.

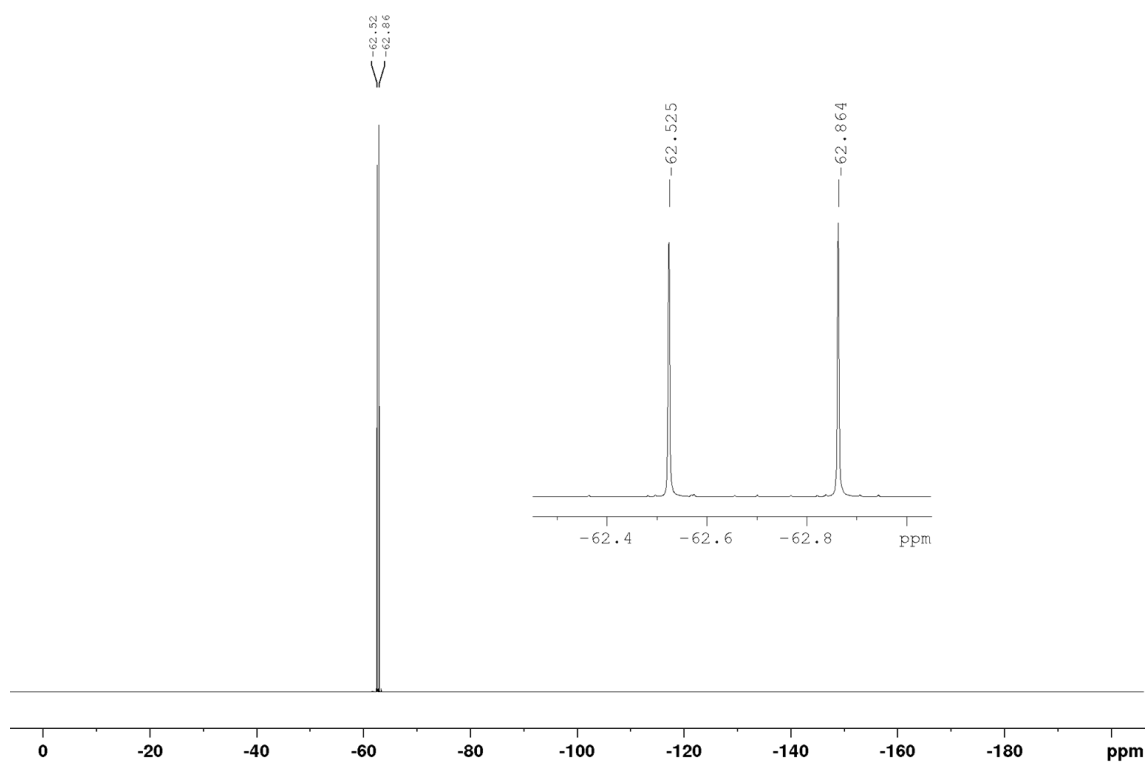


Figure 8.64:  $^{19}\text{F}\{^1\text{H}\}$  NMR spectrum (471 MHz, 298 K,  $\text{C}_6\text{D}_6$ ) of **2,2'-dibromo-3,3',5,5'-tetrakis(trifluoromethyl)-1,1'-biphenyl (2-2)**.

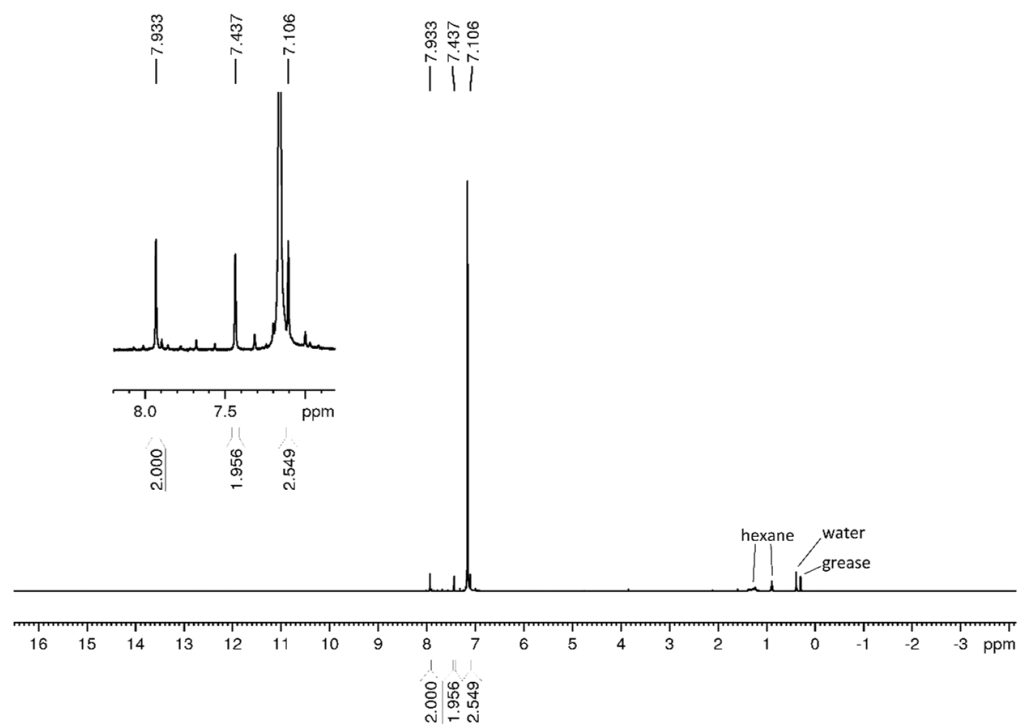


Figure 8.65:  $^1\text{H}$  NMR spectrum (500 MHz, 298 K,  $\text{C}_6\text{D}_6$ ) of  **$^{\text{F}}\text{Mes}^{\text{F}}\text{Bf}$** .

# Appendix

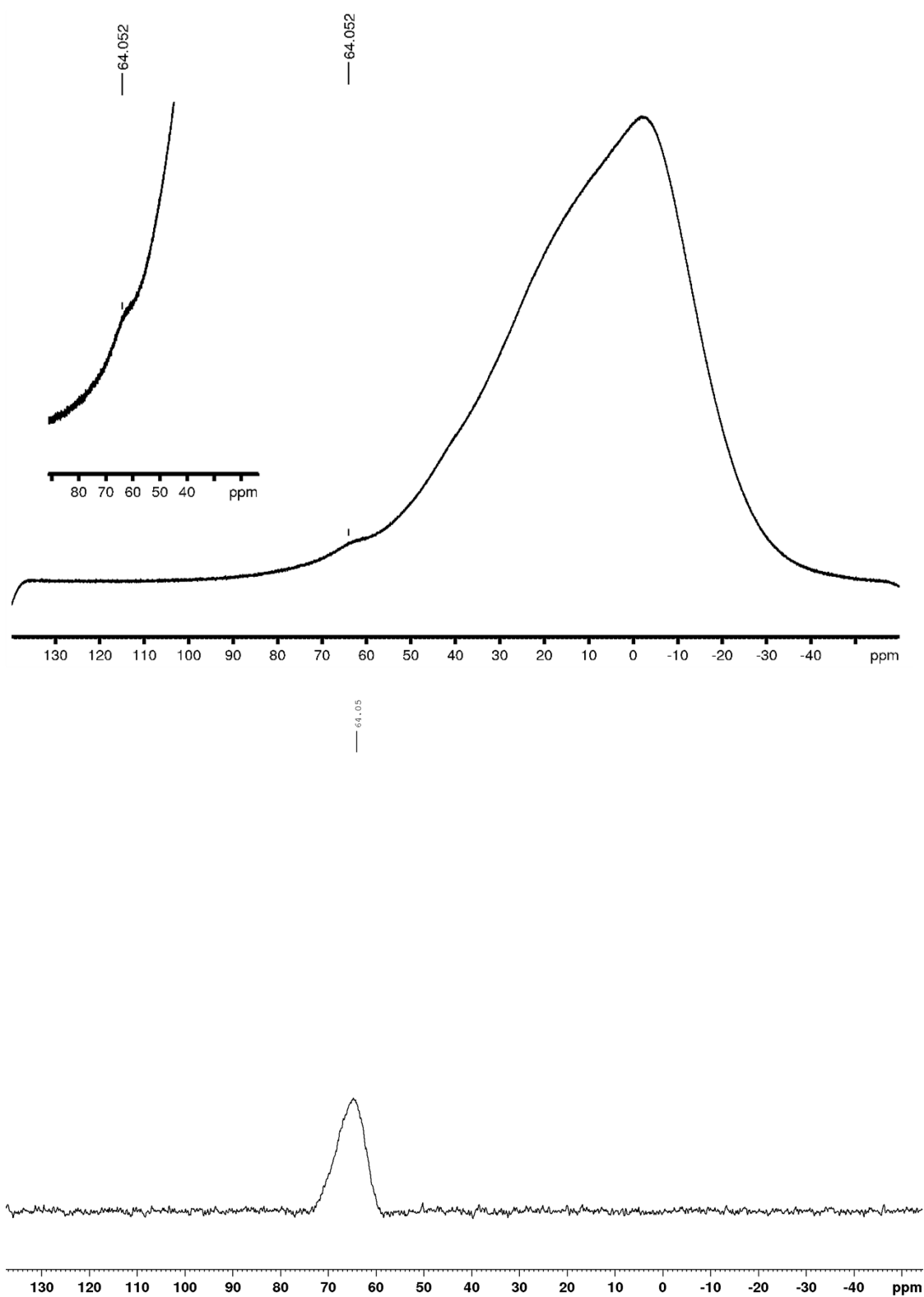


Figure 8.66:  $^{11}\text{B}\{^1\text{H}\}$  NMR spectrum (160 MHz, 298 K,  $\text{C}_6\text{D}_6$ ) of  $^{\text{F}}\text{MeS}^{\text{F}}\text{Bf}$  (top) and baseline corrected spectrum (bottom).

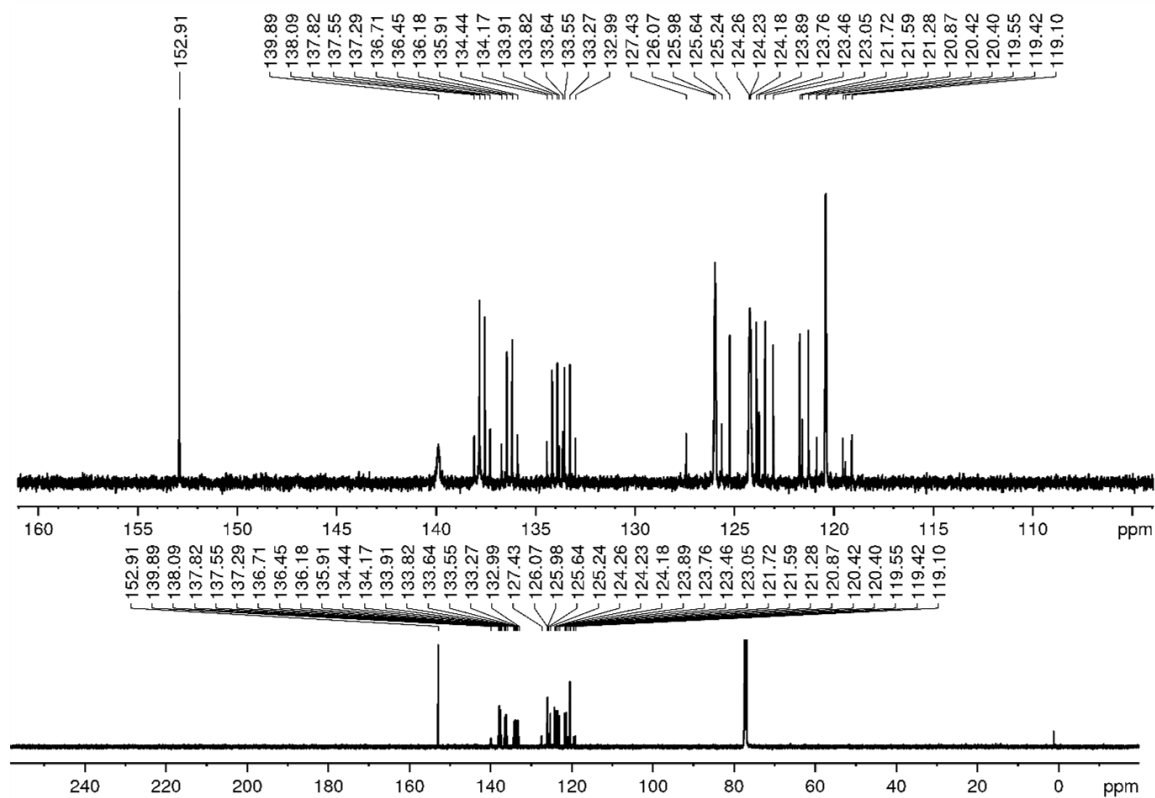


Figure 8.67:  $^{13}\text{C}\{^1\text{H}\}$  NMR spectrum (126 MHz, 298 K,  $\text{CDCl}_3$ ) of  $^{\text{F}}\text{MeS}^{\text{F}}\text{Bf}$ .

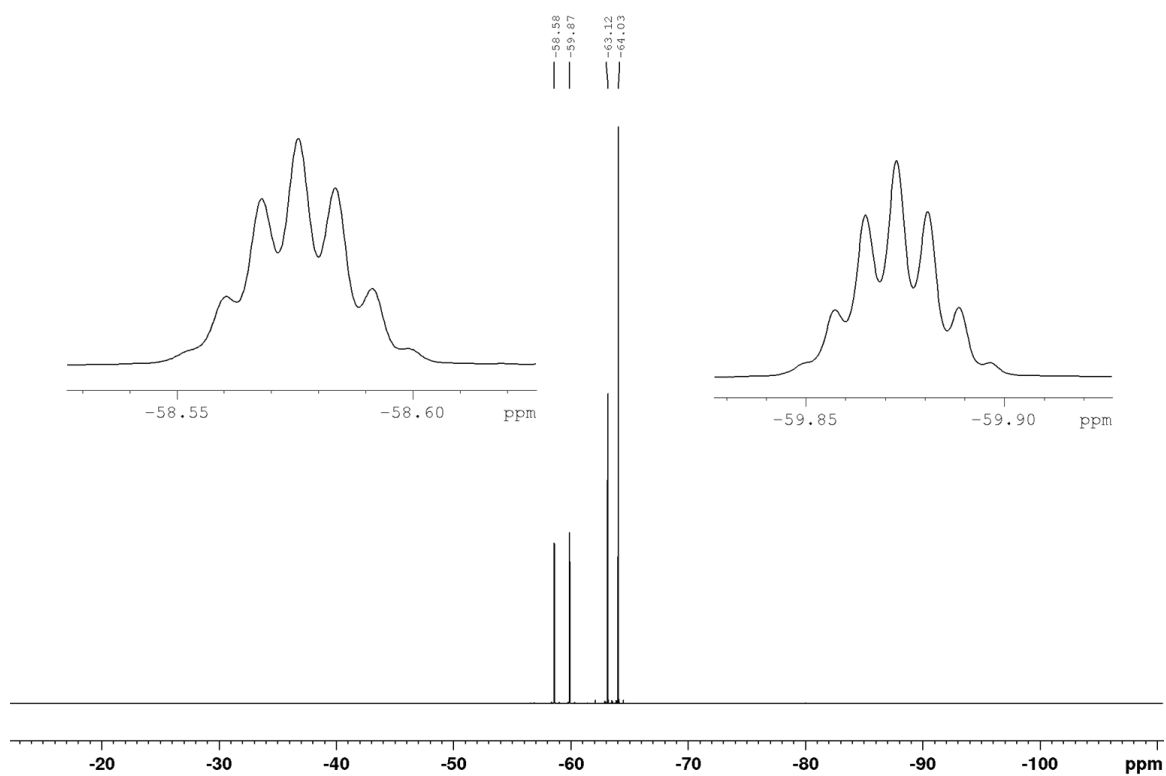


Figure 8.68:  $^{19}\text{F}\{^1\text{H}\}$  NMR spectrum (471 MHz, 298 K,  $\text{CDCl}_3$ ) of  $^{\text{F}}\text{MeS}^{\text{F}}\text{Bf}$ .

# Appendix

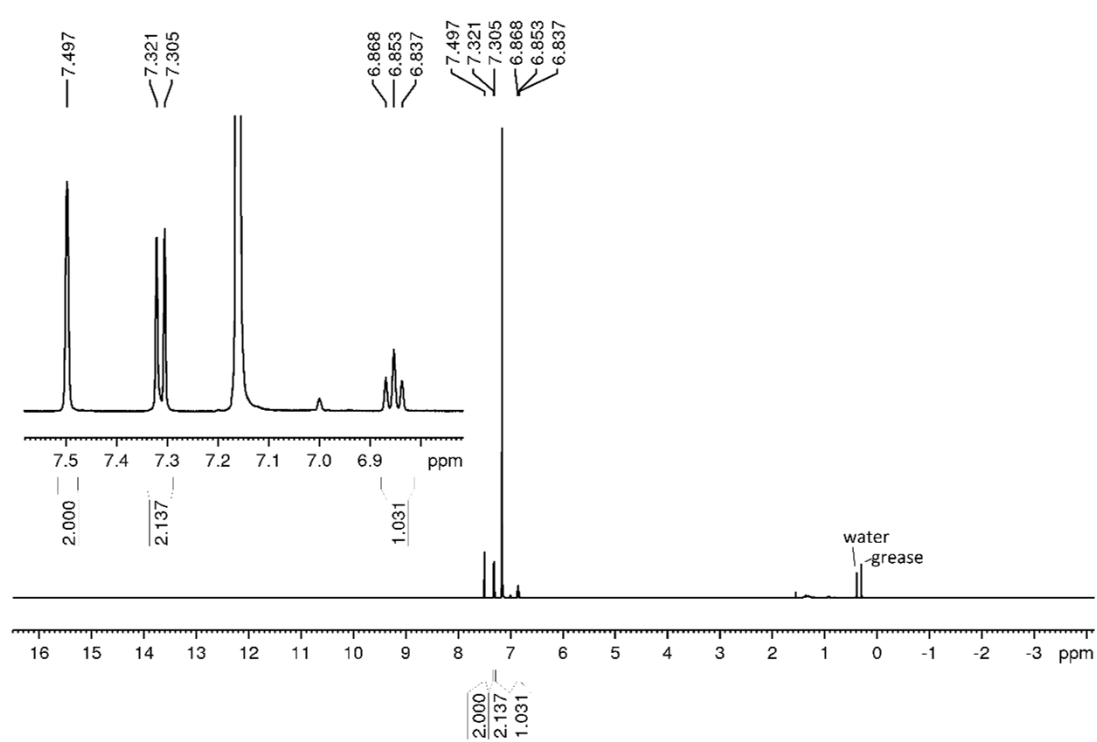


Figure 8.69:  $^1\text{H}$  NMR spectrum (500 MHz, 298 K,  $\text{C}_6\text{D}_6$ ) of  $\text{F}^x\text{ylF}^b\text{f}$ .

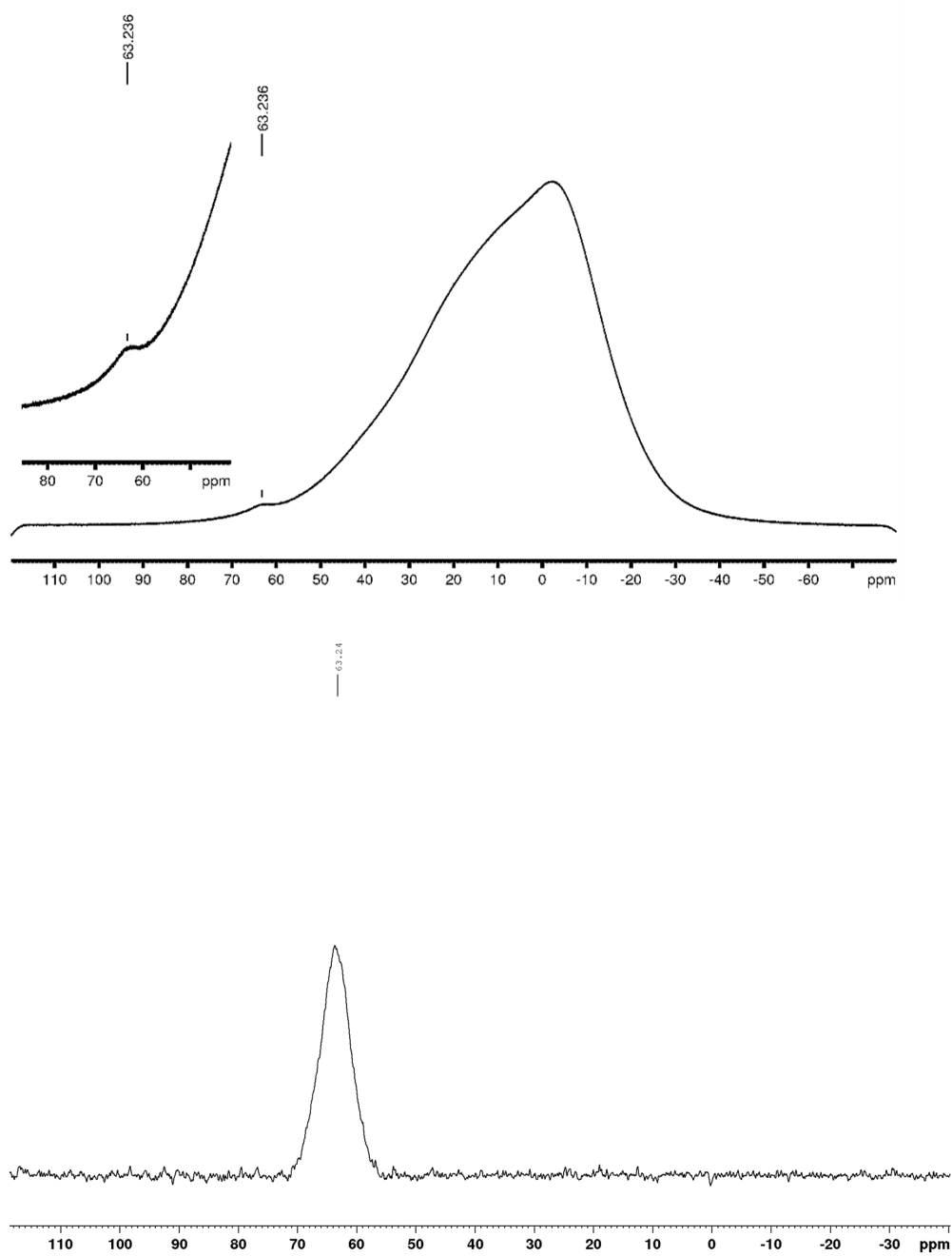


Figure 8.70:  $^{11}\text{B}\{^1\text{H}\}$  NMR spectrum (160 MHz, 298 K,  $\text{C}_6\text{D}_6$ ) of  $\text{F}^{\text{xyl}}\text{I}^{\text{F}}\text{Bf}$  (top) and baseline corrected spectrum (bottom).

# Appendix

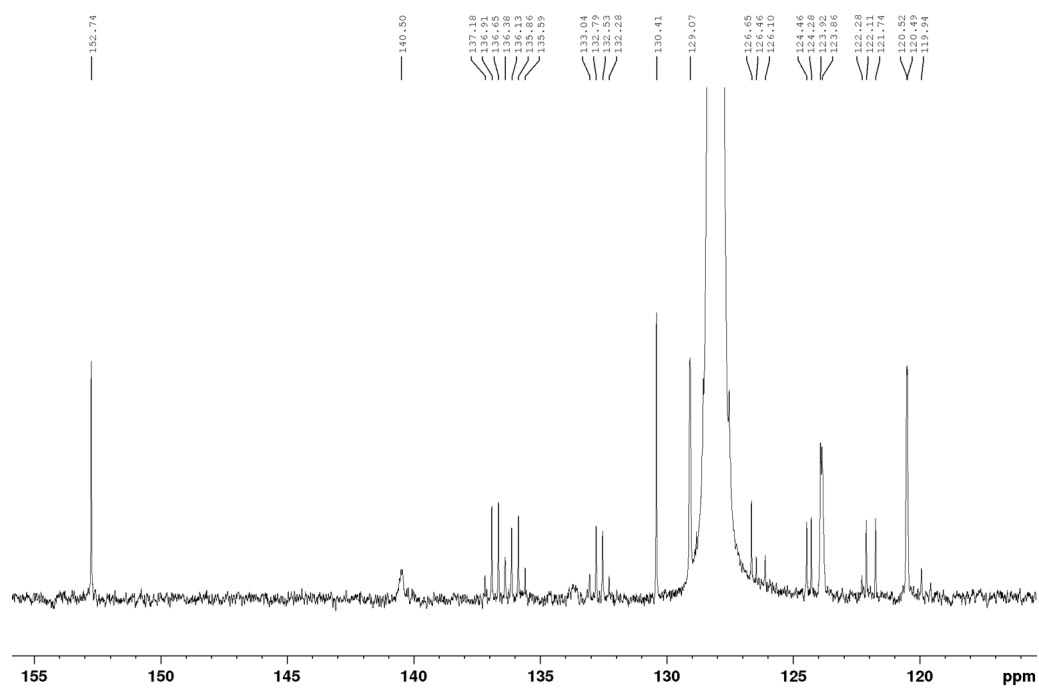


Figure 8.71:  $^{13}\text{C}\{^1\text{H}\}$  NMR spectrum (126 MHz, 298 K,  $\text{C}_6\text{D}_6$ ) of  $^{\text{F}}\text{Xyl}^{\text{F}}\text{Bf}$ .

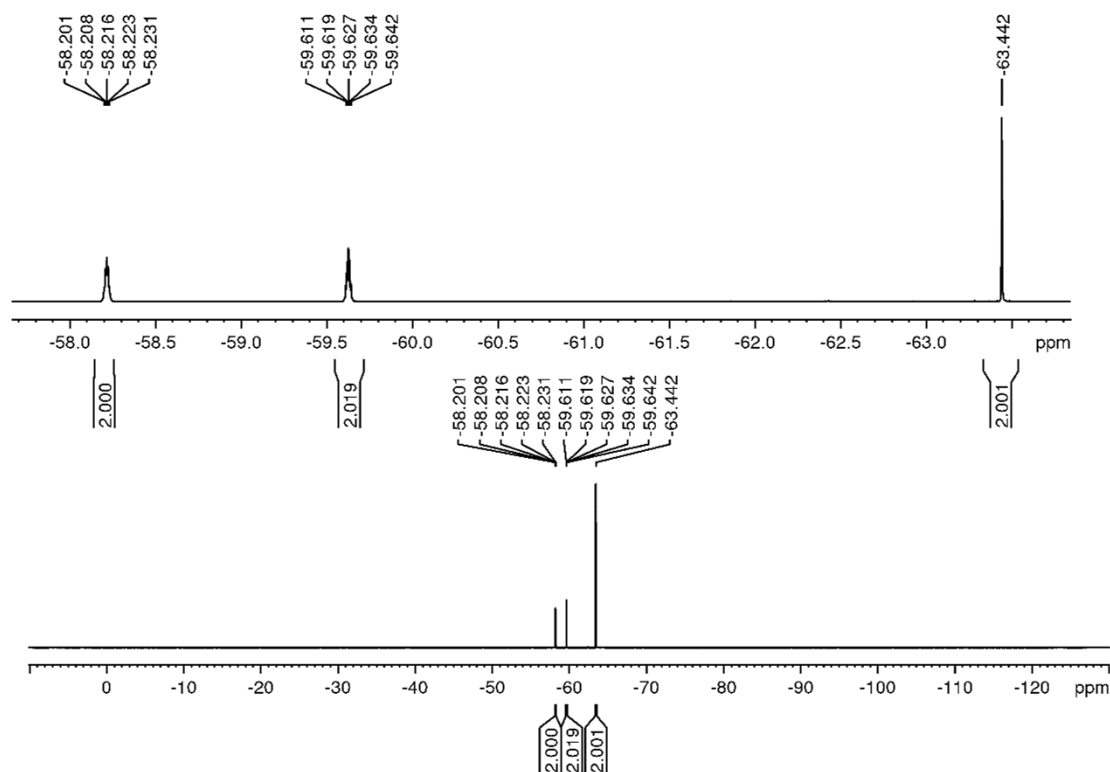


Figure 8.72:  $^{19}\text{F}\{^1\text{H}\}$  NMR spectrum (471 MHz, 298 K,  $\text{C}_6\text{D}_6$ ) of  $^{\text{F}}\text{Xyl}^{\text{F}}\text{Bf}$ .



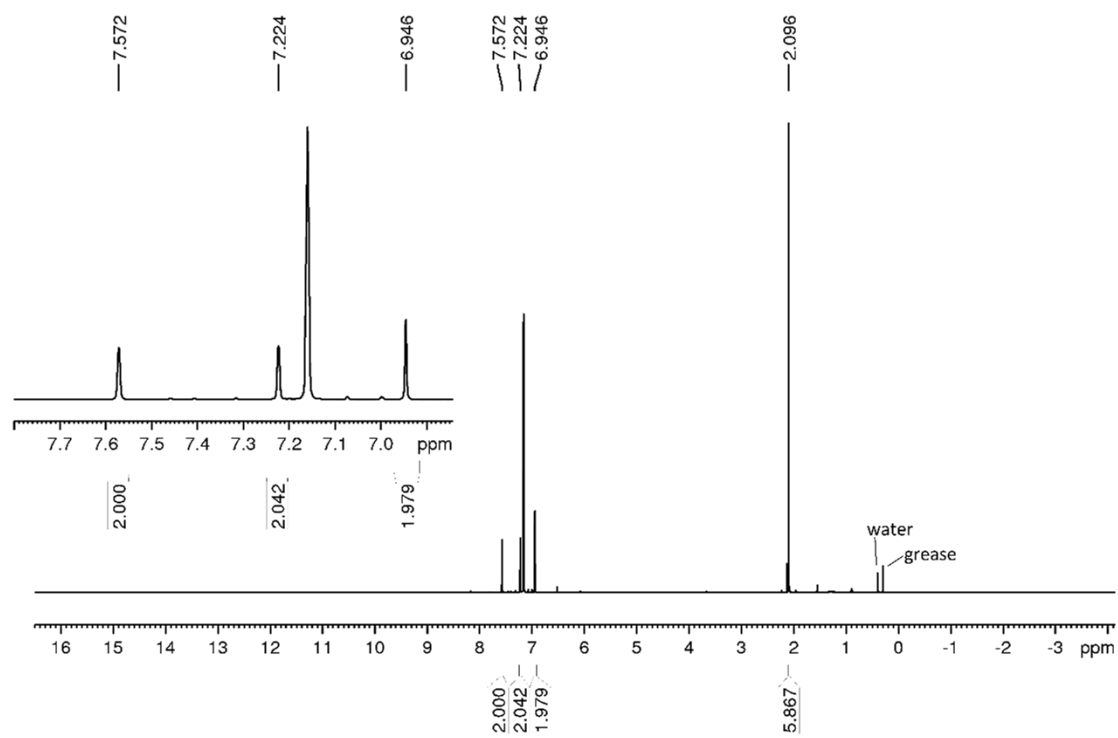


Figure 8.73:  $^1\text{H}$  NMR spectrum (500 MHz, 298 K,  $\text{C}_6\text{D}_6$ ) of  $p\text{-NMe}_2\text{-}^{\text{F}}\text{Xyl}^{\text{F}}\text{Bf}$ .

# Appendix

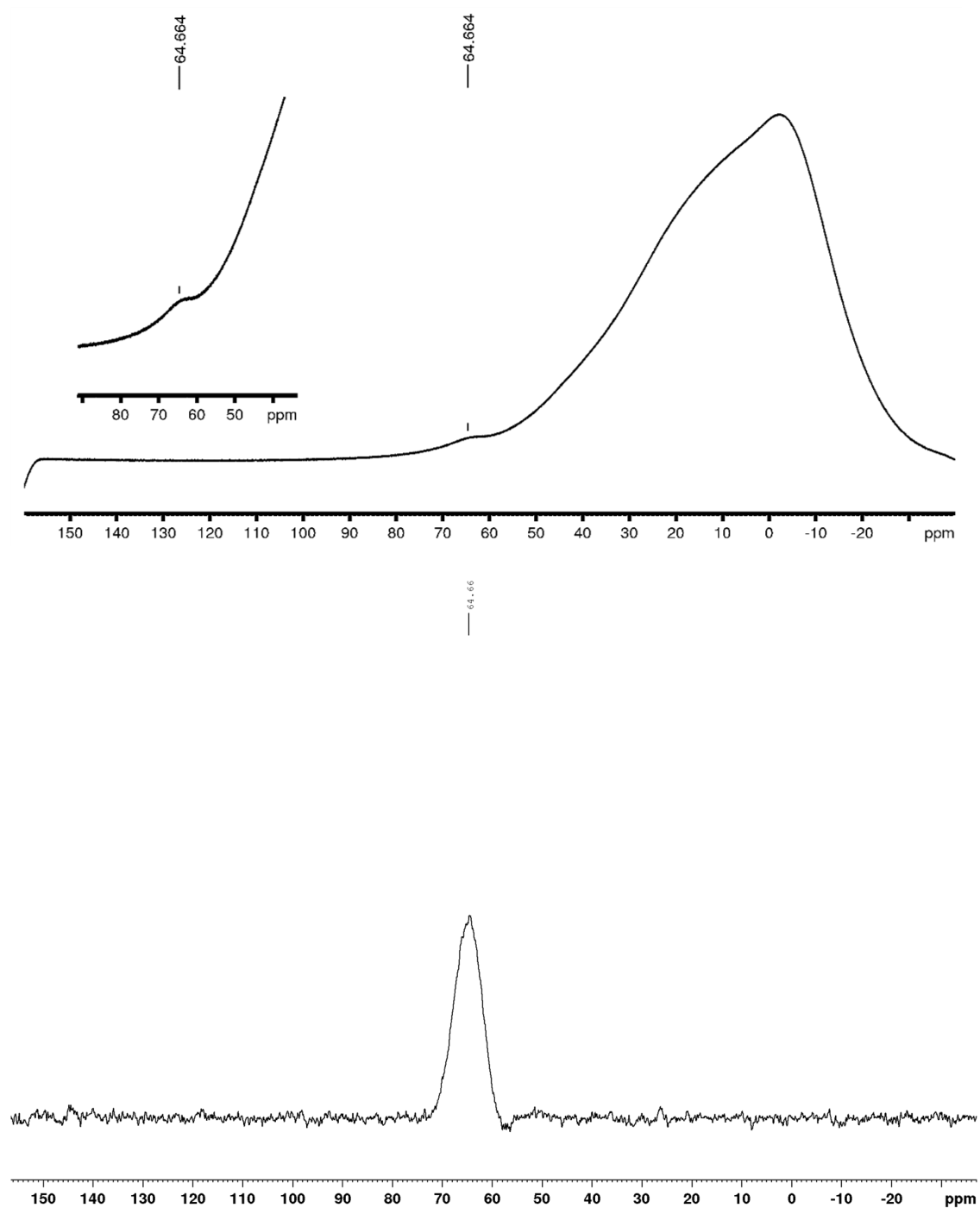


Figure 8.74:  $^{11}\text{B}\{^1\text{H}\}$  NMR spectrum (160 MHz, 298 K,  $\text{C}_6\text{D}_6$ ) of  $p\text{-NMe}_2\text{-}^{\text{F}}\text{Xyl}^{\text{F}}\text{Bf}$  (top) and baseline corrected spectrum (bottom).

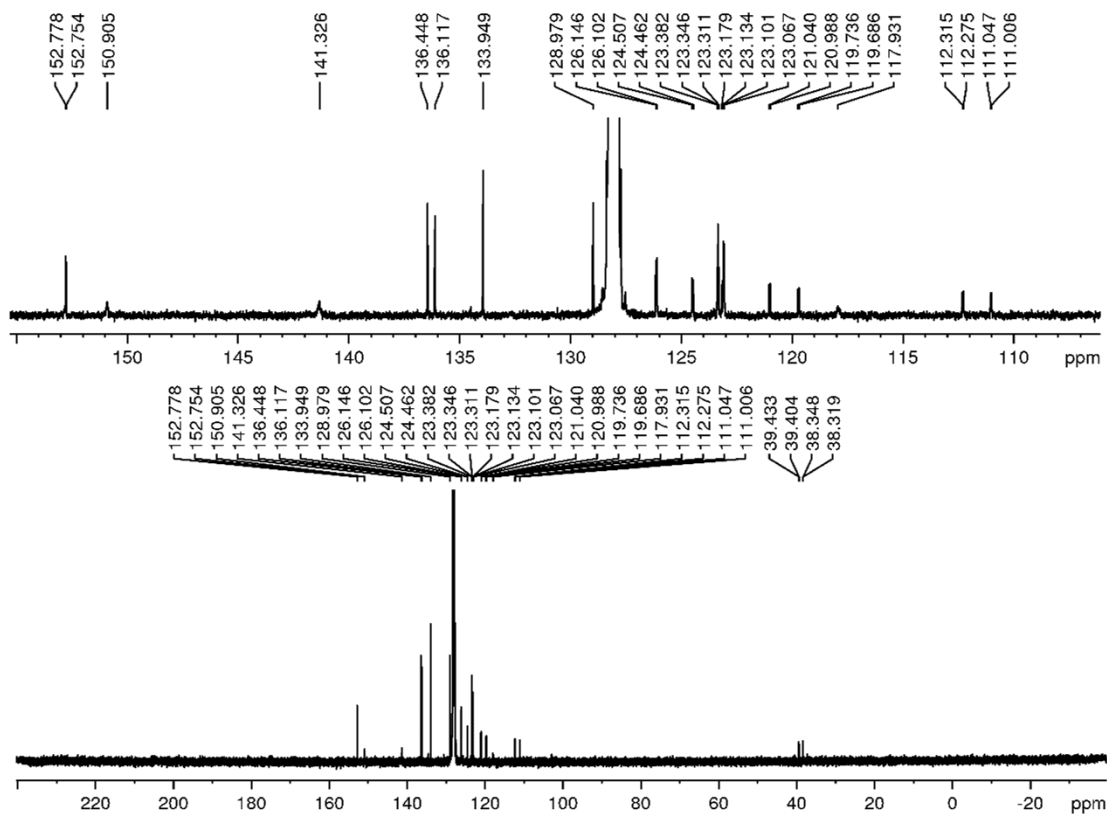


Figure 8.75:  $^{13}\text{C}\{^{19}\text{F}\}$  NMR spectrum (126 MHz, 298 K,  $\text{C}_6\text{D}_6$ ) of  $p\text{-NMe}_2\text{-}^{\text{F}}\text{Xyl}^{\text{F}}\text{Bf}$ .

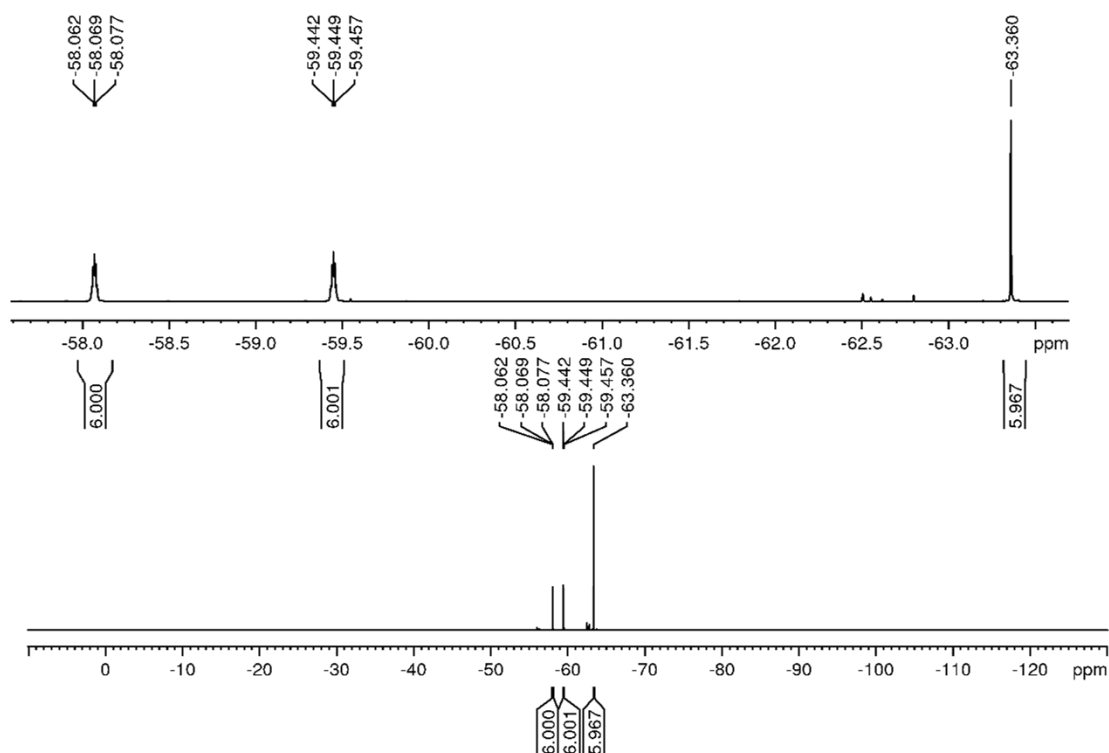


Figure 8.76:  $^{19}\text{F}\{^1\text{H}\}$  NMR spectrum (471 MHz, 298 K,  $\text{C}_6\text{D}_6$ ) of  $p\text{-NMe}_2\text{-}^{\text{F}}\text{Xyl}^{\text{F}}\text{Bf}$ .

## Appendix

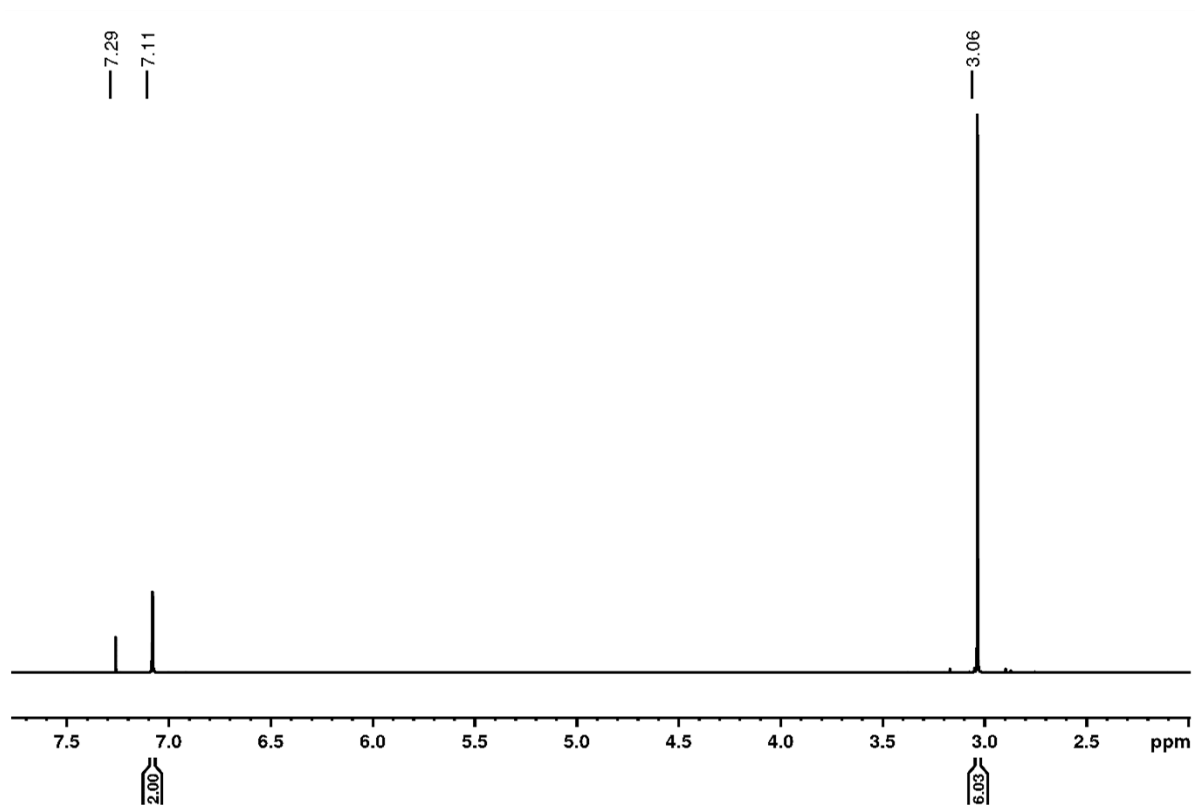


Figure 8.77:  $^1\text{H}$  NMR spectrum (500 MHz, 298 K,  $\text{CDCl}_3$ ) of 4-(dimethylamino)-2,6-bis(trifluoromethyl)phenylbromide.

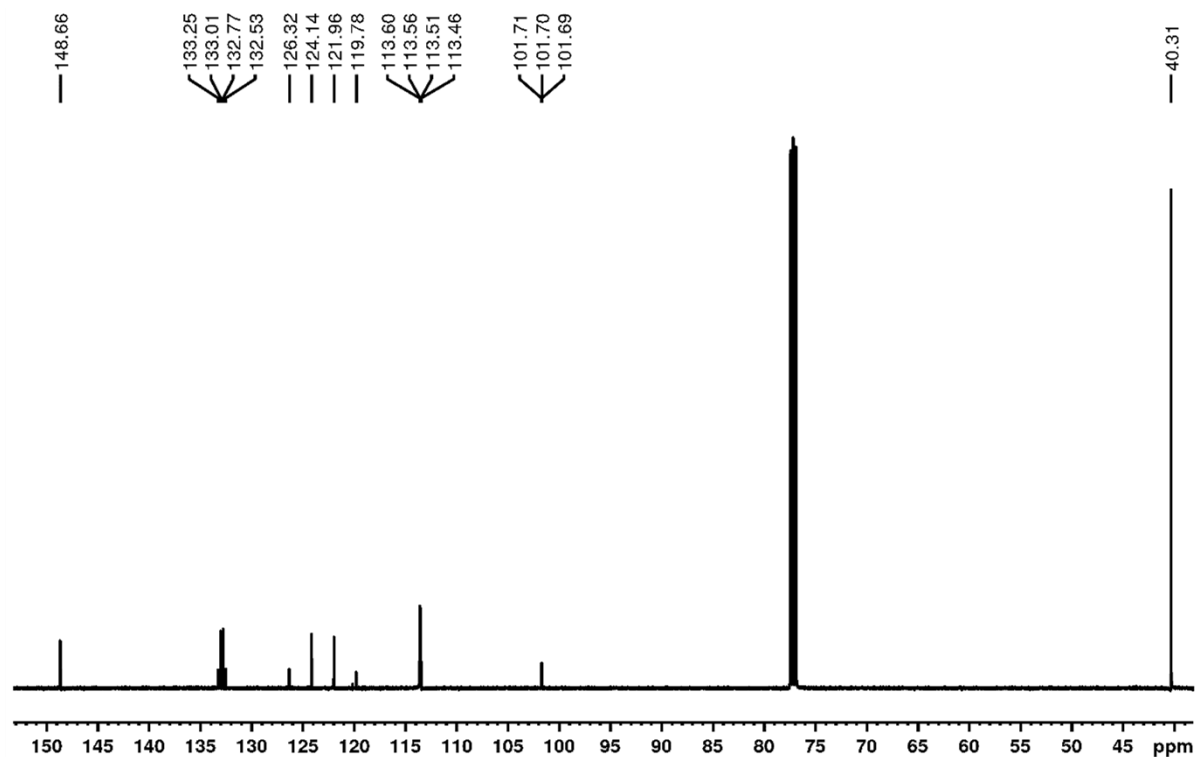


Figure 8.78:  $^{13}\text{C}\{^1\text{H}\}$  NMR spectrum (126 MHz, 298 K,  $\text{CDCl}_3$ ) of 4-(dimethylamino)-2,6-bis(trifluoromethyl)phenylbromide.

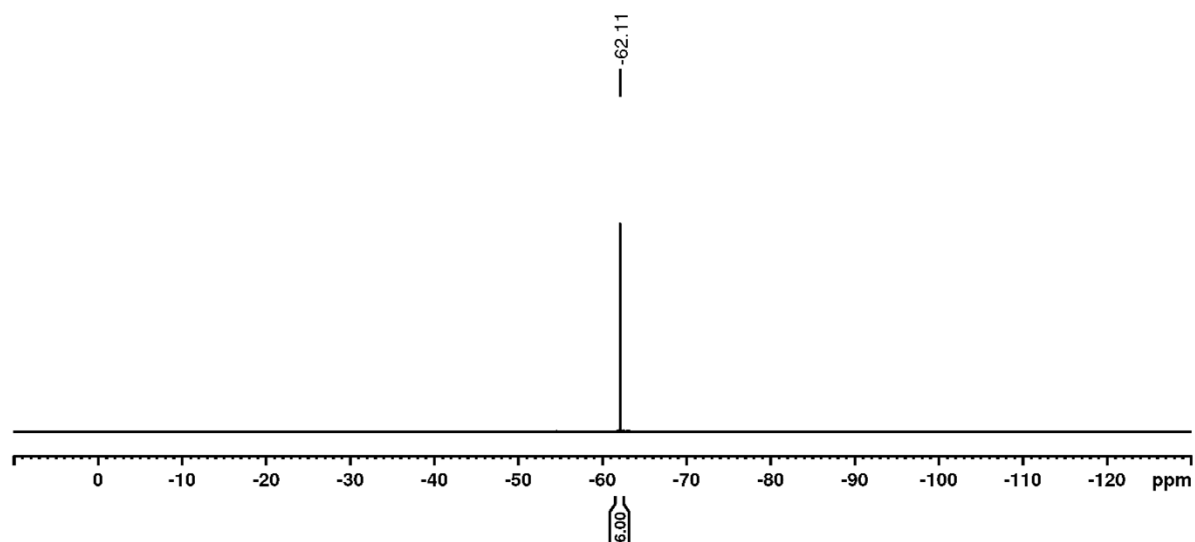


Figure 8.79:  $^{19}\text{F}\{^1\text{H}\}$  NMR spectrum (471 MHz, 298 K,  $\text{CDCl}_3$ ) of 4-(dimethylamino)-2,6-bis(trifluoromethyl)phenylbromide.

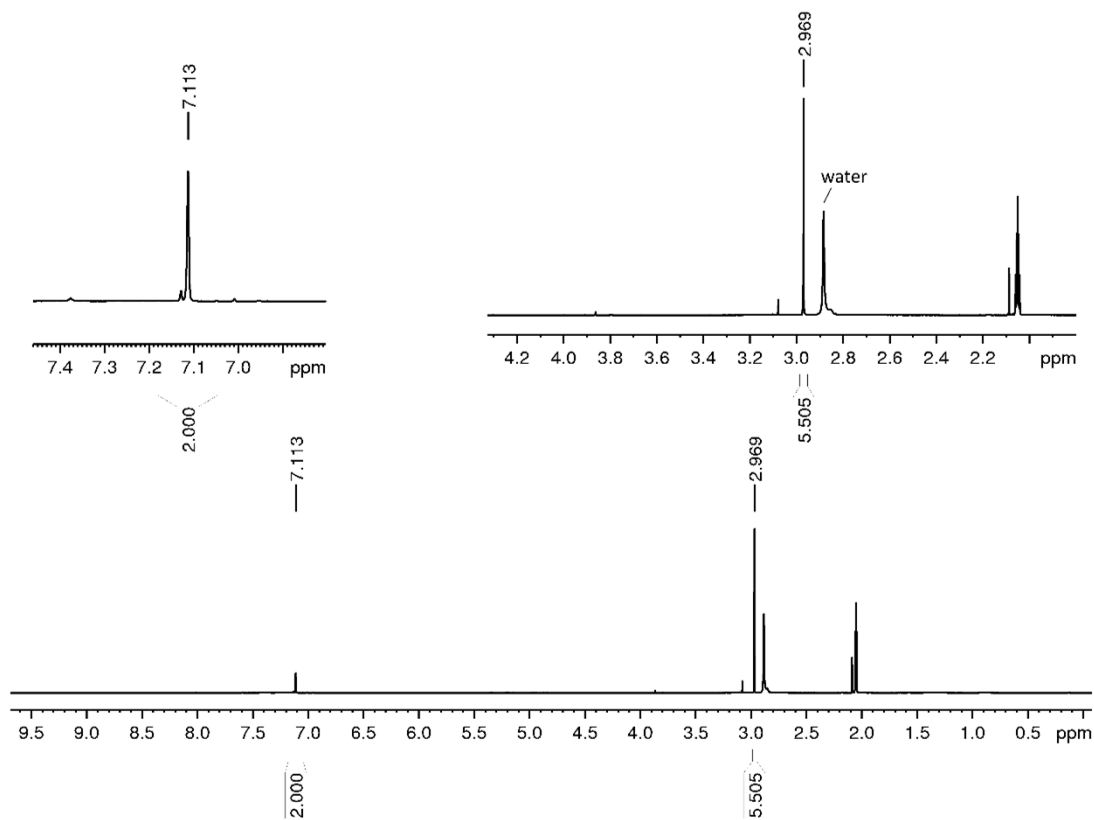


Figure 8.80:  $^1\text{H}$  NMR spectrum (500 MHz, 298 K,  $\text{acetone-}d_6$ ) of potassium 4-(dimethylamino)-2,6-bis(trifluoromethyl)phenyltrifluoroborate.

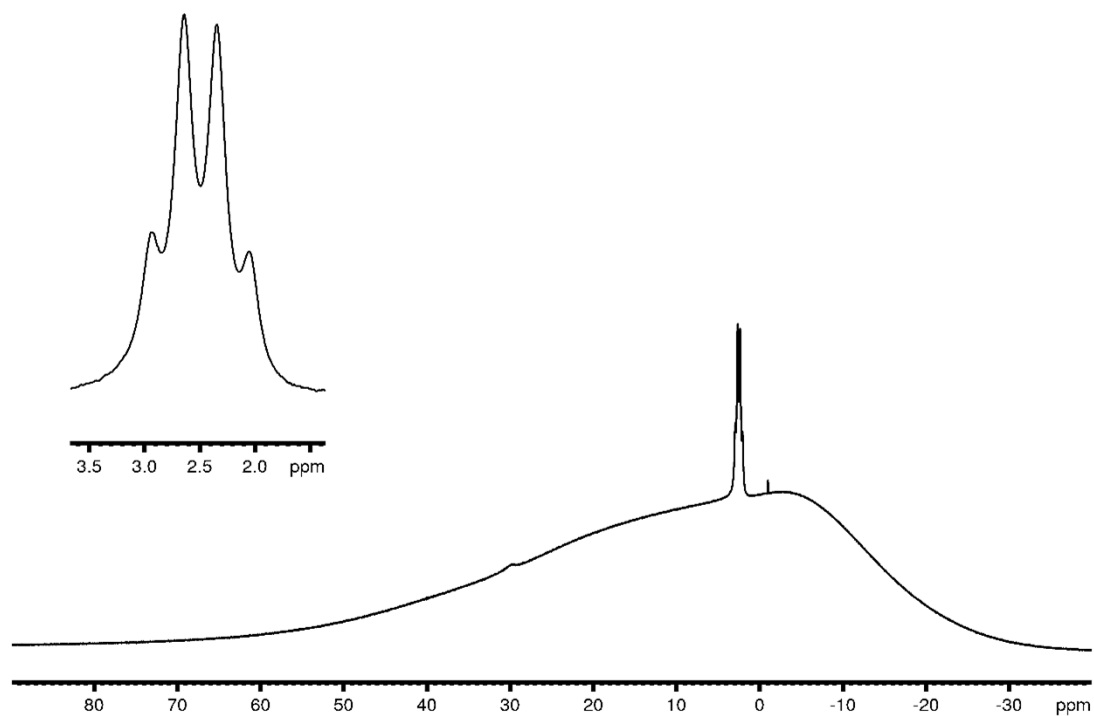


Figure 8.81:  $^{11}\text{B}\{^1\text{H}\}$  NMR spectrum (160 MHz, 298 K, acetone- $d_6$ ) of potassium (4-(dimethylamino)-2,6-bis(trifluoromethyl)phenyl)trifluoroborate.

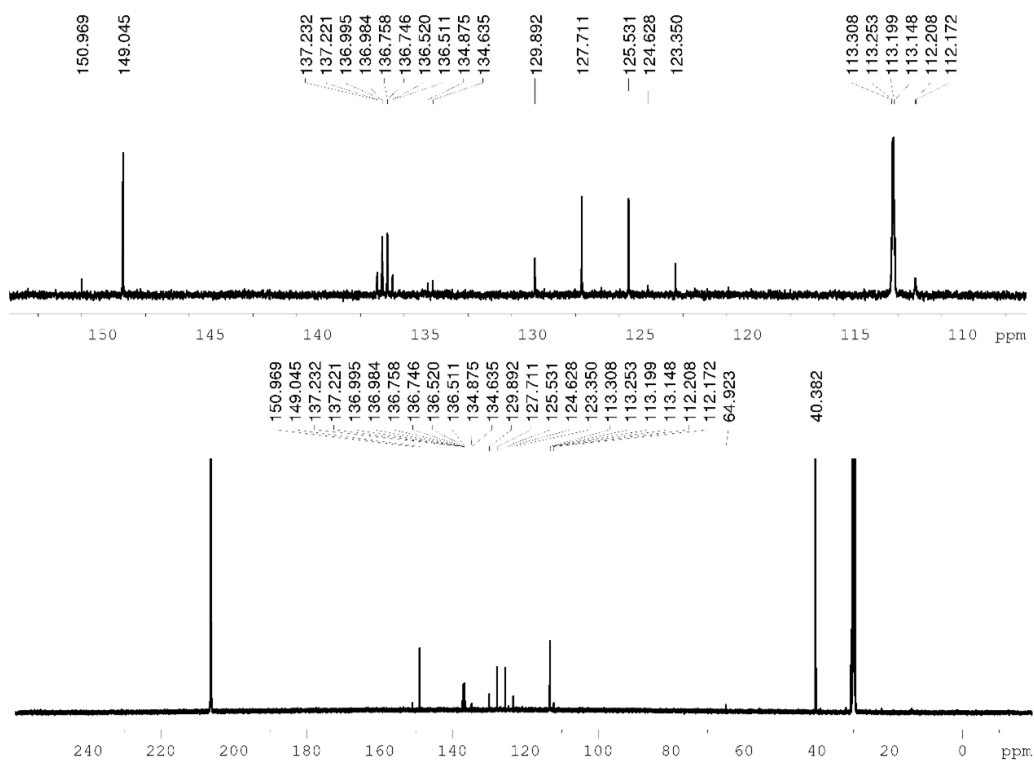


Figure 8.82:  $^{13}\text{C}\{^1\text{H}\}$  NMR spectrum (126 MHz, 298 K, acetone- $d_6$ ) of potassium (4-(dimethylamino)-2,6-bis(trifluoromethyl)phenyl)trifluoroborate.

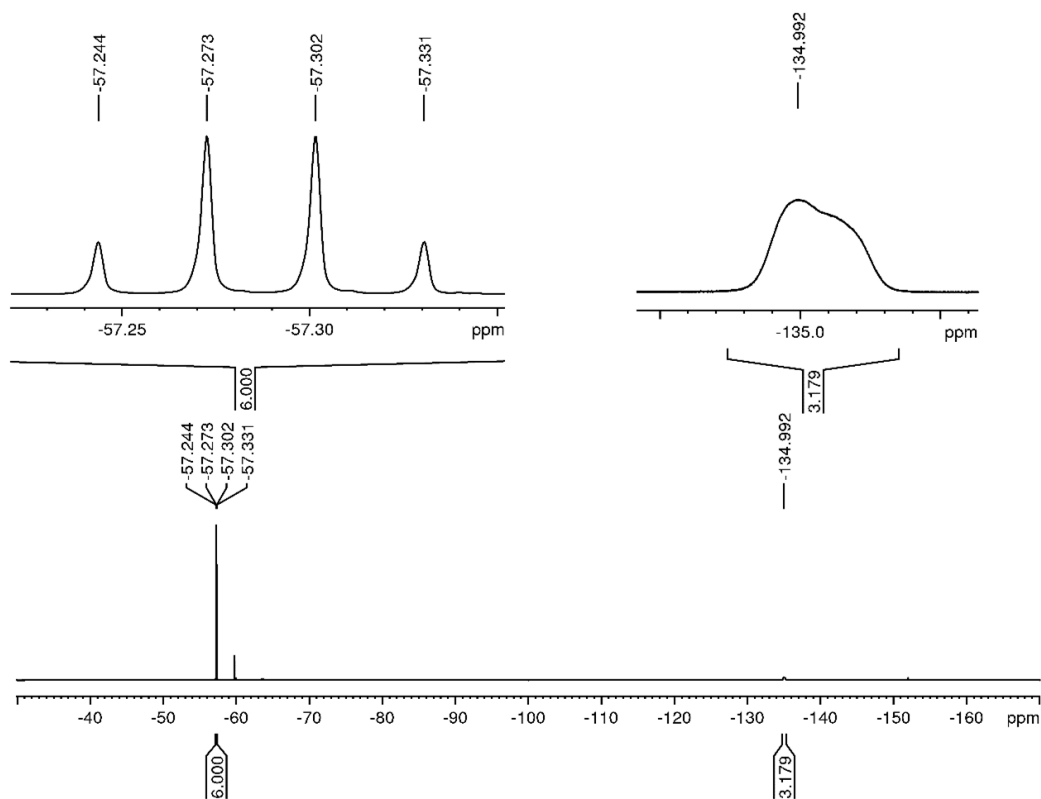


Figure 8.83:  $^{19}\text{F}\{^1\text{H}\}$  NMR spectrum (471 MHz, 298 K, acetone- $d_6$ ) of **potassium (4-(dimethylamino)-2,6-bis(trifluoromethyl)phenyl)trifluoroborate**.

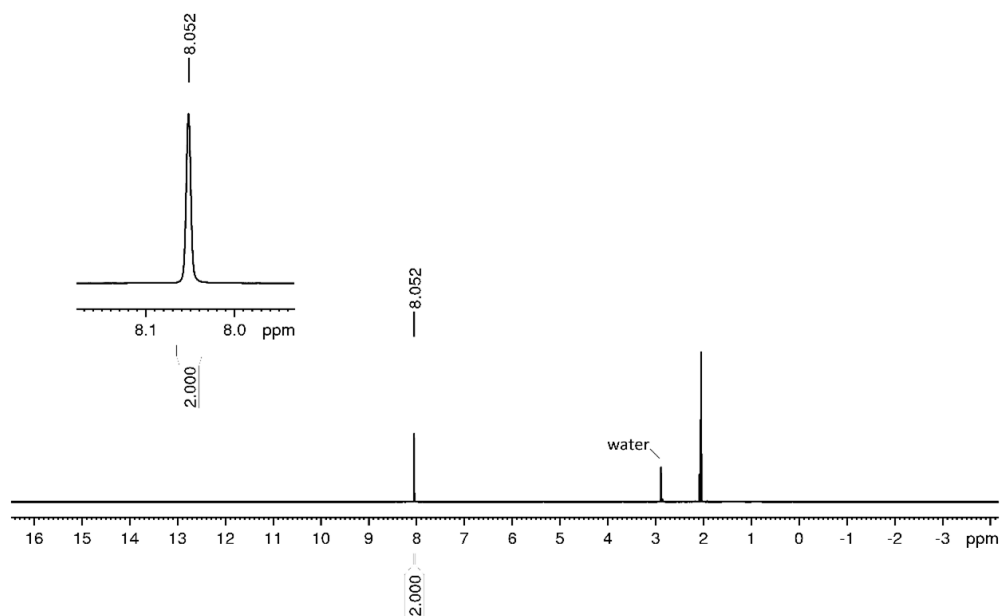


Figure 8.84:  $^1\text{H}$  NMR spectrum (500 MHz, 298 K, acetone- $d_6$ ) of **potassium (2,4,6-tris(trifluoromethyl)phenyl)trifluoroborate**.

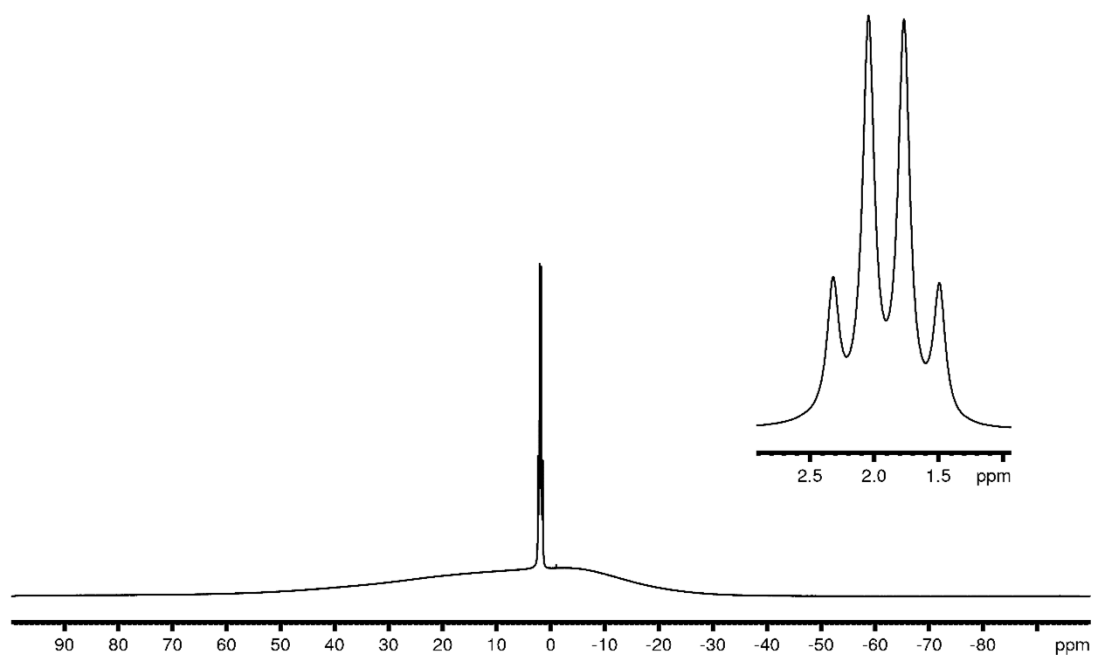


Figure 8.85:  $^{11}\text{B}\{^1\text{H}\}$  NMR spectrum (160 MHz, 298 K, acetone- $d_6$ ) of potassium (2,4,6-tris(trifluoromethyl)phenyl)trifluoroborate.

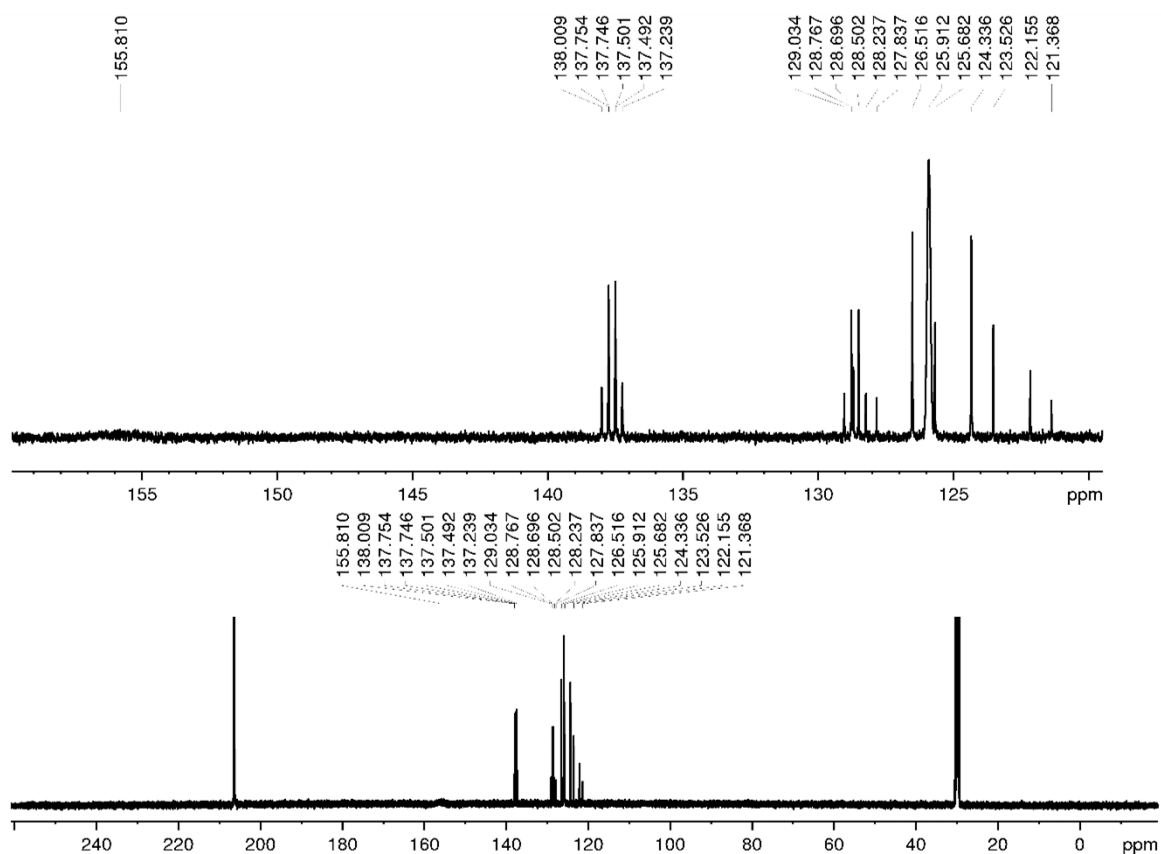


Figure 8.86:  $^{13}\text{C}\{^1\text{H}\}$  NMR spectrum (126 MHz, 298 K, acetone- $d_6$ ) of potassium (2,4,6-tris(trifluoromethyl)phenyl)trifluoroborate.



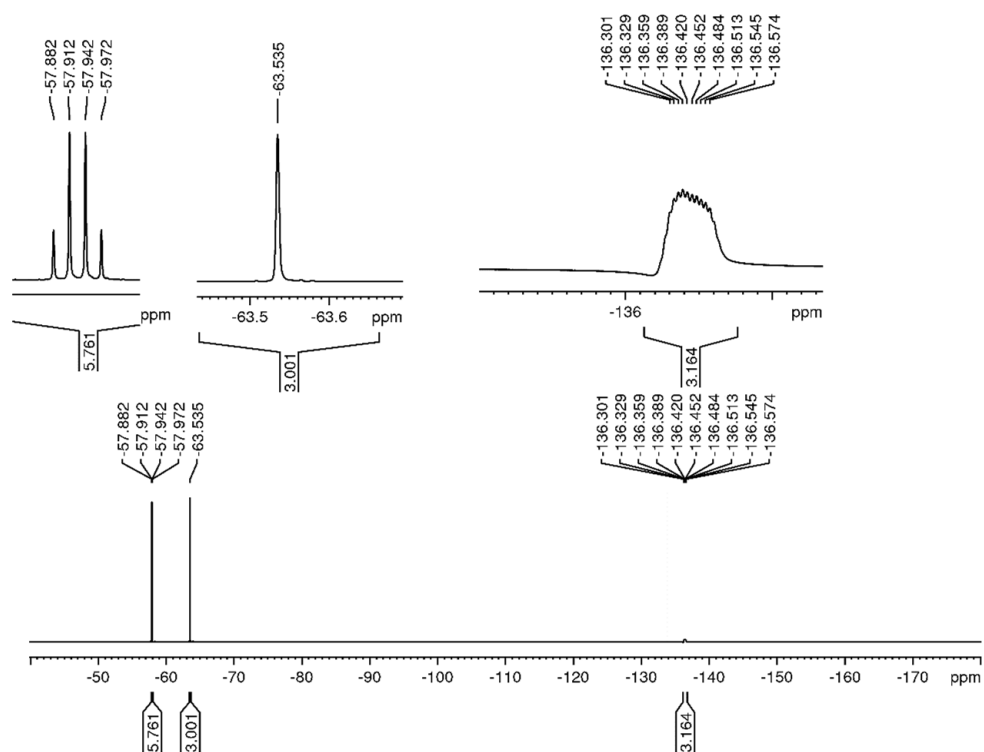


Figure 8.87:  $^{19}\text{F}\{^1\text{H}\}$  NMR spectrum (471 MHz, 298 K, acetone- $d_6$ ) of potassium (2,4,6-tris(trifluoromethyl)phenyl)trifluoroborate.

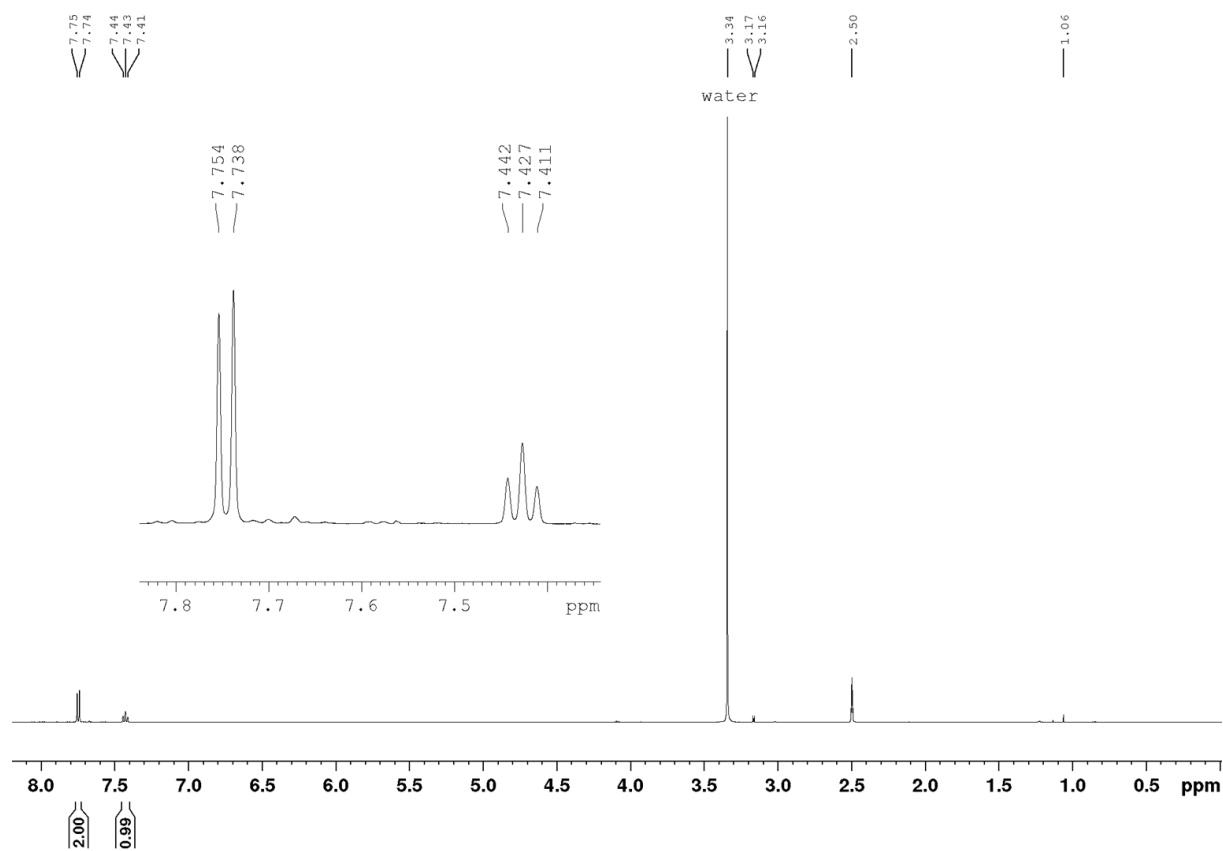


Figure 8.88:  $^1\text{H}$  NMR spectrum (500 MHz, 298 K, DMSO- $d_6$ ) of potassium (2,6-bis(trifluoromethyl)phenyl)trifluoroborate.

# Appendix

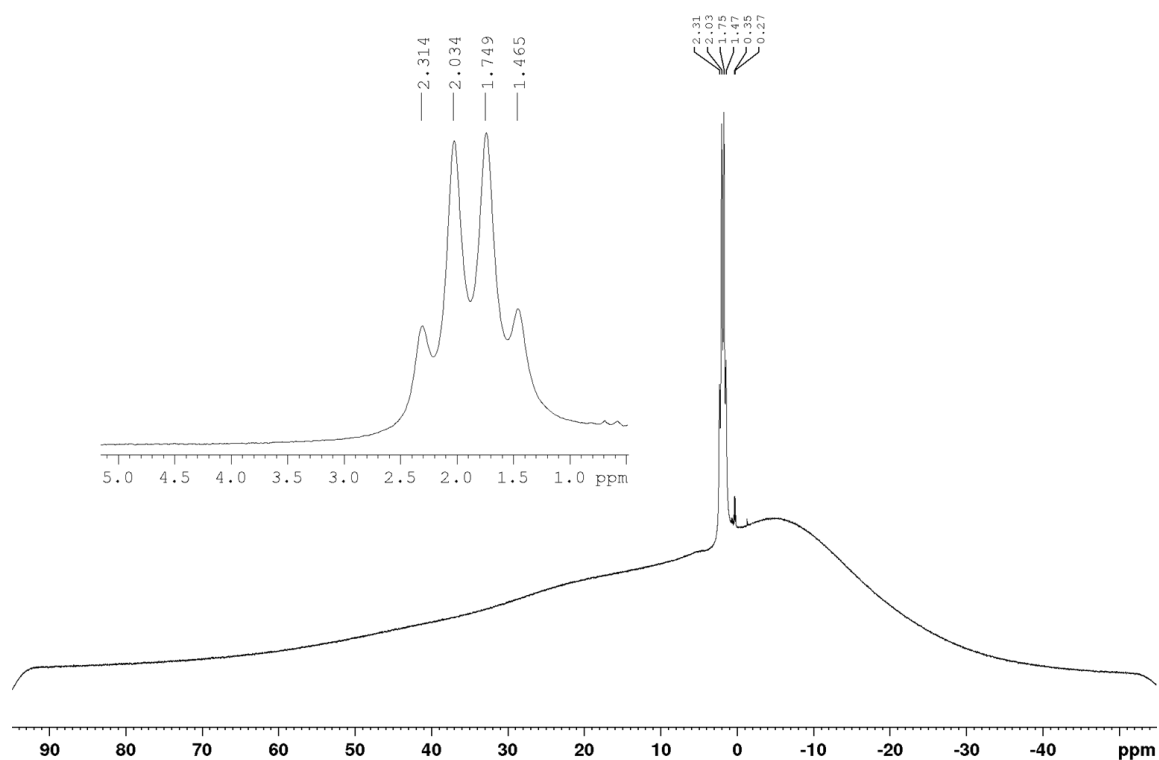


Figure 8.89:  $^{11}\text{B}\{^1\text{H}\}$  NMR spectrum (160 MHz, 298 K,  $\text{DMSO-}d_6$ ) of potassium (2,6-bis(trifluoromethyl)phenyl)trifluoroborate.

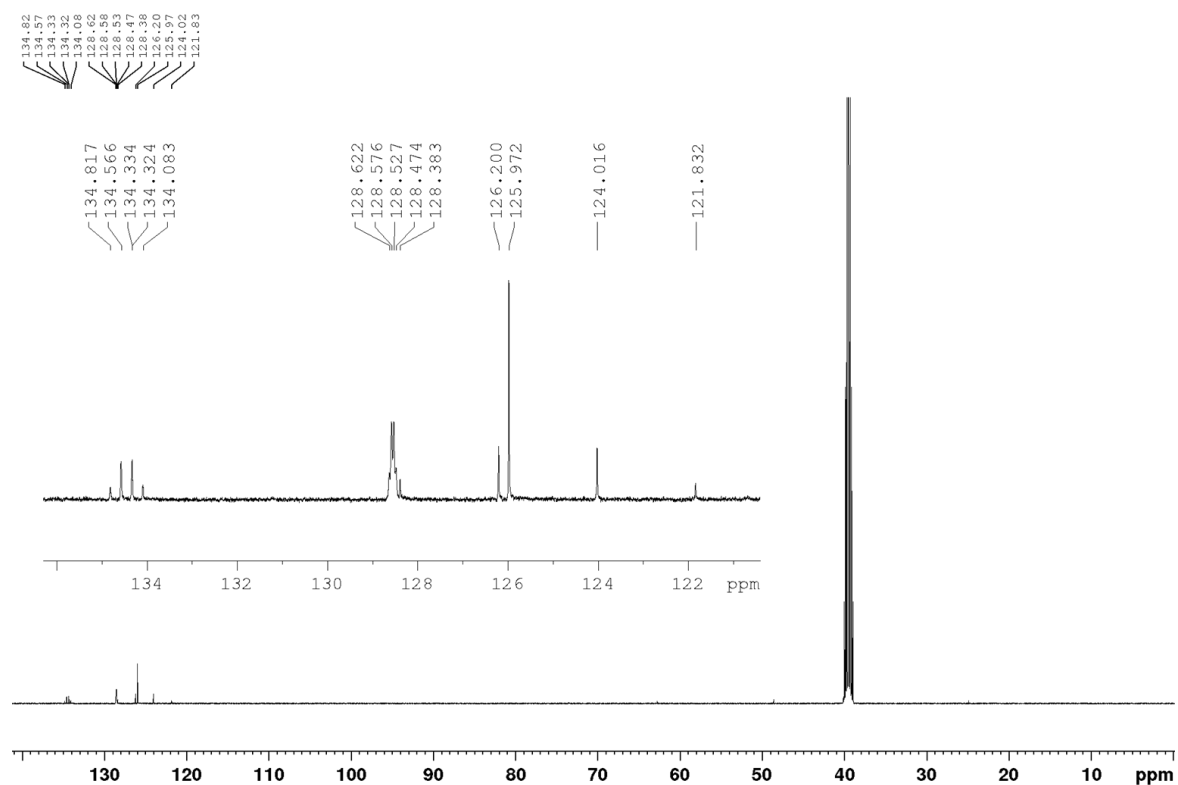


Figure 8.90:  $^{13}\text{C}\{^1\text{H}\}$  NMR spectrum (126 MHz, 298 K,  $\text{DMSO-}d_6$ ) of potassium (2,6-bis(trifluoromethyl)phenyl)trifluoroborate.

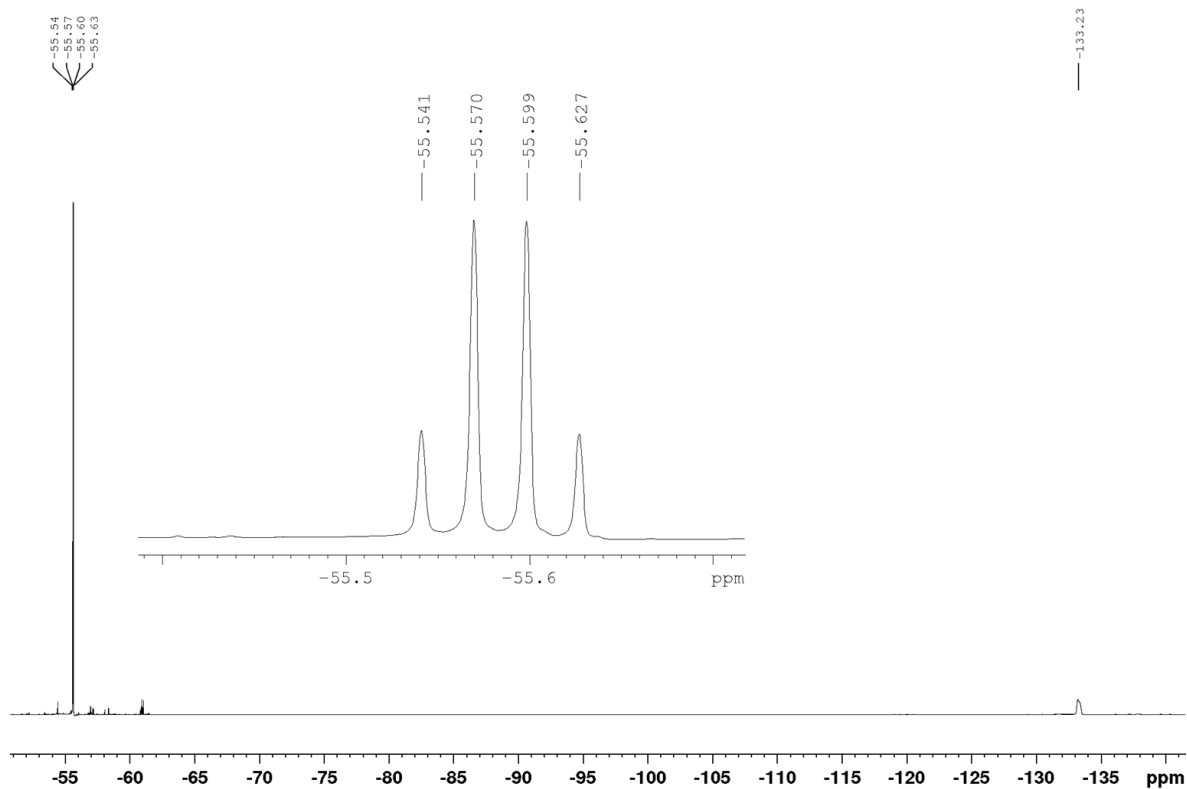


Figure 8.91:  $^{19}\text{F}\{^1\text{H}\}$  NMR spectrum (471 MHz, 298 K, DMSO- $d_6$ ) of **potassium (2,6-bis(trifluoromethyl)phenyl)trifluoroborate**.

## 8.1.3 Chapter 3

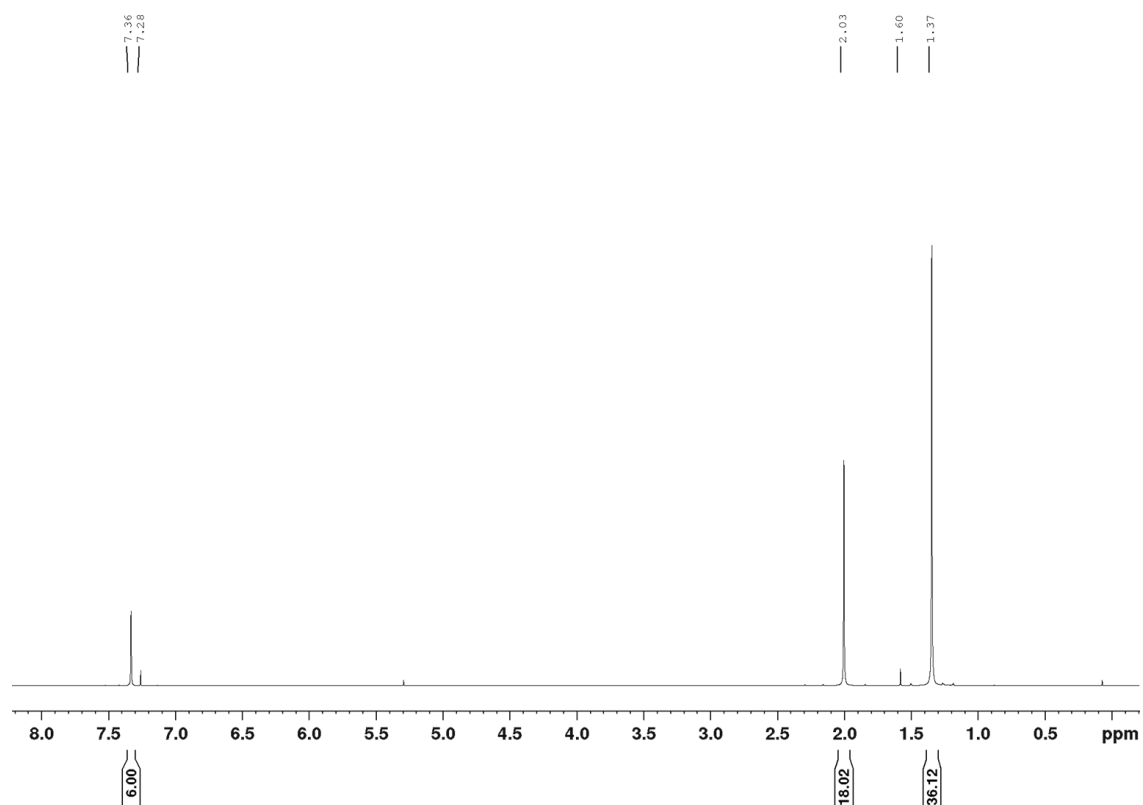


Figure 8.92:  $^1\text{H}$  NMR spectrum (400 MHz, 298 K,  $\text{CDCl}_3$ ) of tris(2,6-dimethyl-4-(4,4,5,5-tetramethyl-1,3,2-dioxaborolan-2-yl)phenyl)borane.

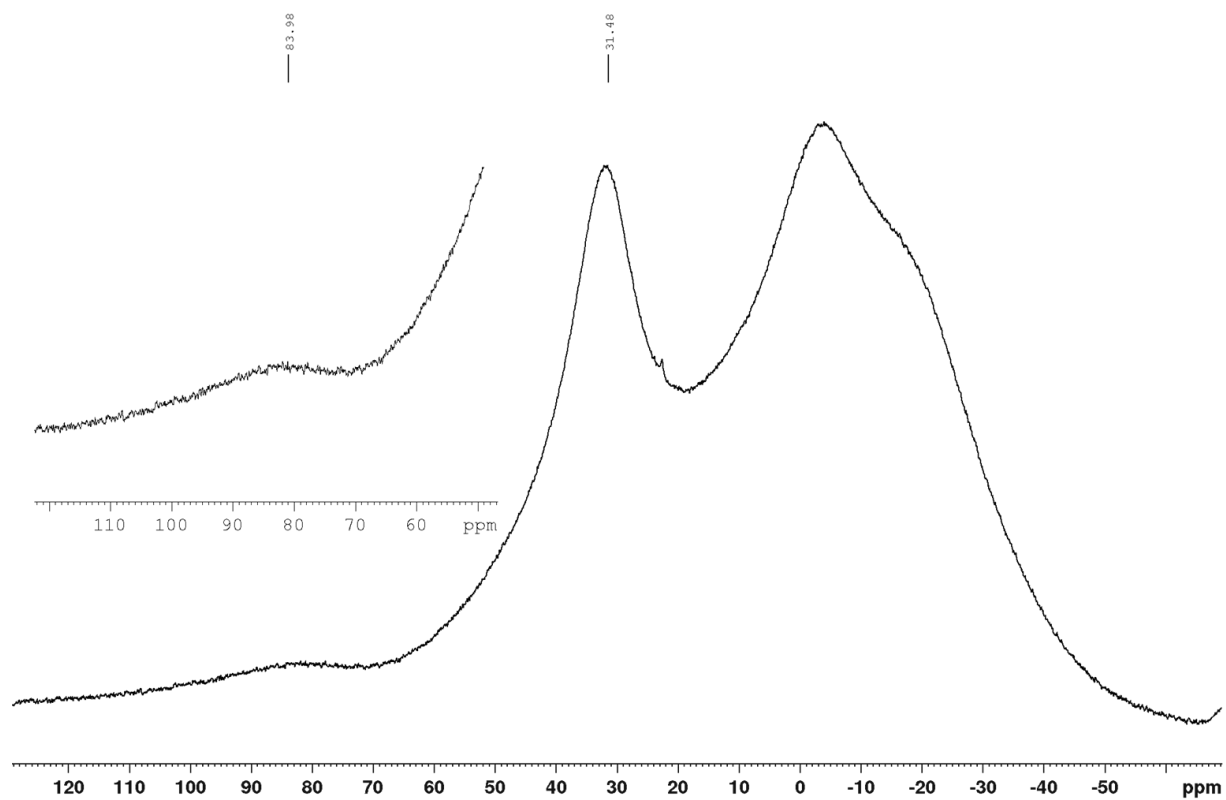


Figure 8.93:  $^{11}\text{B}$  NMR spectrum (128 MHz, 298 K,  $\text{CDCl}_3$ ) of tris(2,6-dimethyl-4-(4,4,5,5-tetramethyl-1,3,2-dioxaborolan-2-yl)phenyl)borane.

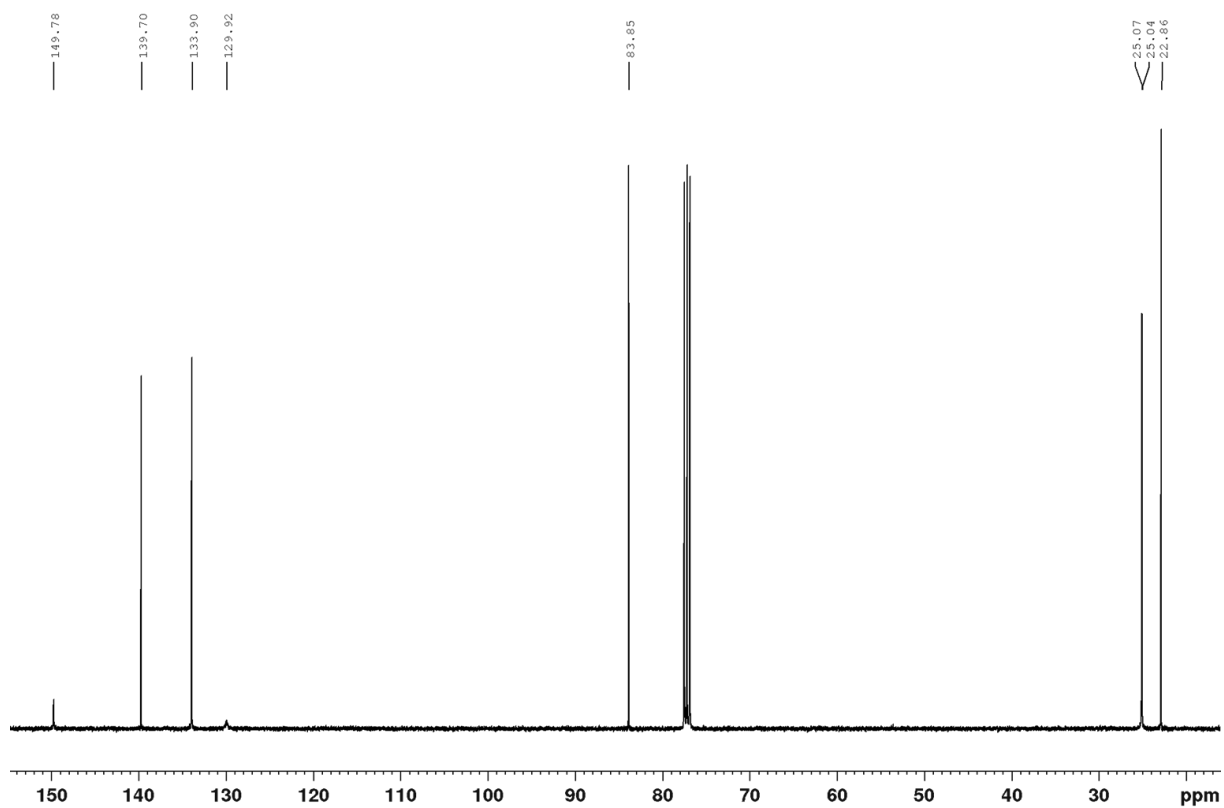


Figure 8.94:  $^{13}\text{C}\{^1\text{H}\}$  NMR spectrum (101 MHz, 298 K,  $\text{CDCl}_3$ ) of **tris(2,6-dimethyl-4-(4,4,5,5-tetramethyl-1,3,2-dioxaborolan-2-yl)phenyl)borane**.

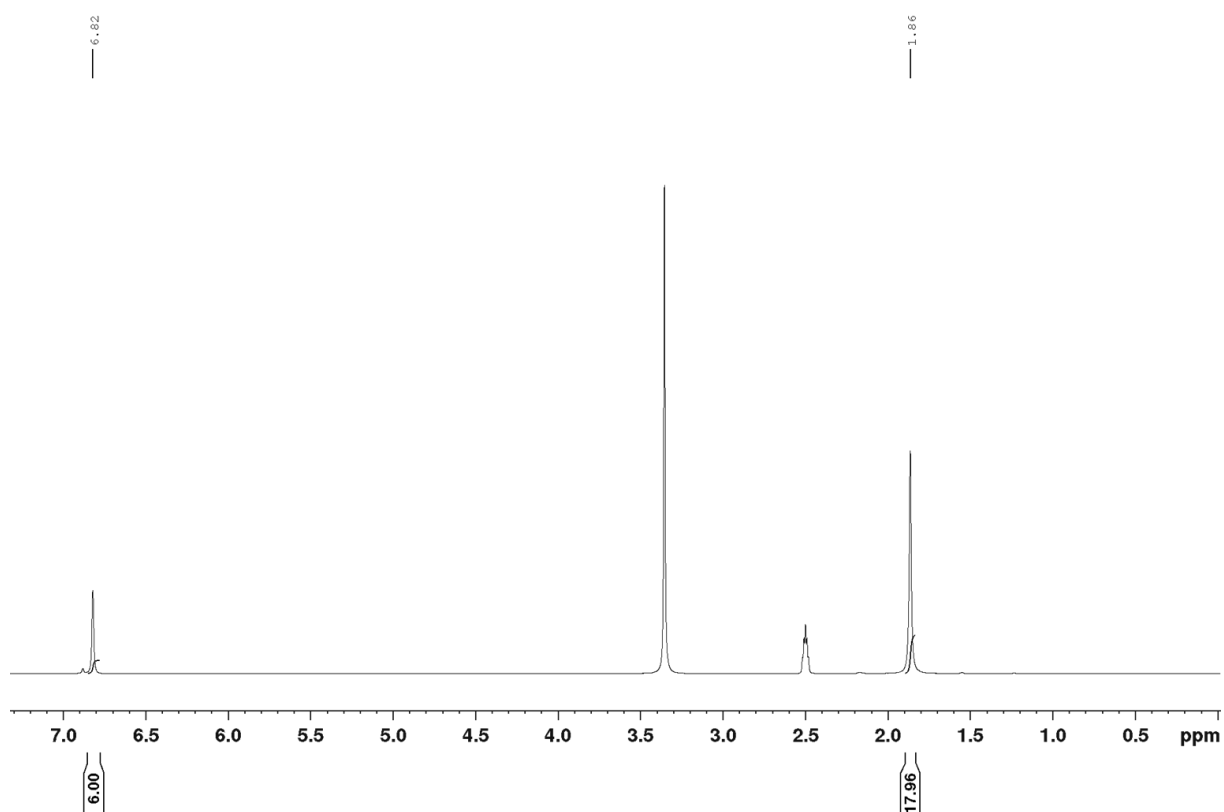


Figure 8.95:  $^1\text{H}$  NMR spectrum (200 MHz, 298 K,  $\text{DMSO-d}_6$ ) of **tris(2,6-dimethyl-4-(trifluoroboryl)phenyl)borane, tripotassium salt**.

## Appendix

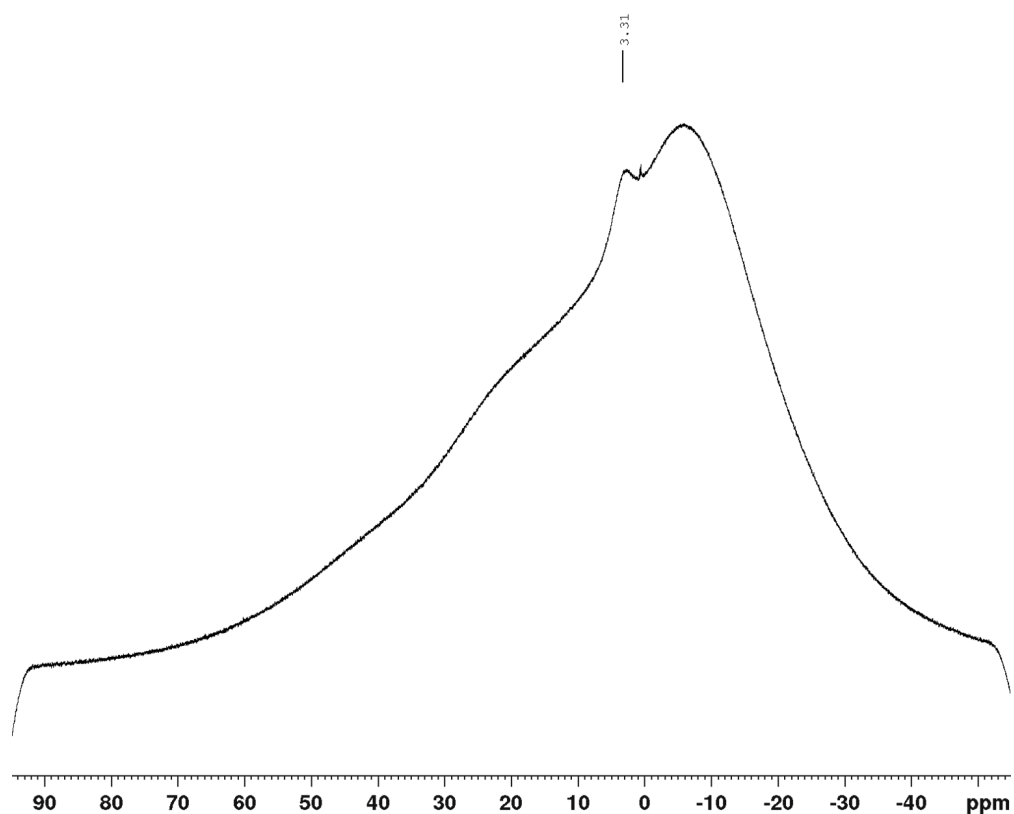


Figure 8.96:  $^{11}\text{B}$  NMR spectrum (95 MHz, 298 K,  $\text{DMSO-d}_6$ ) of **tris(2,6-dimethyl-4-(trifluoroboryl)phenyl)borane, tripotassium salt**.

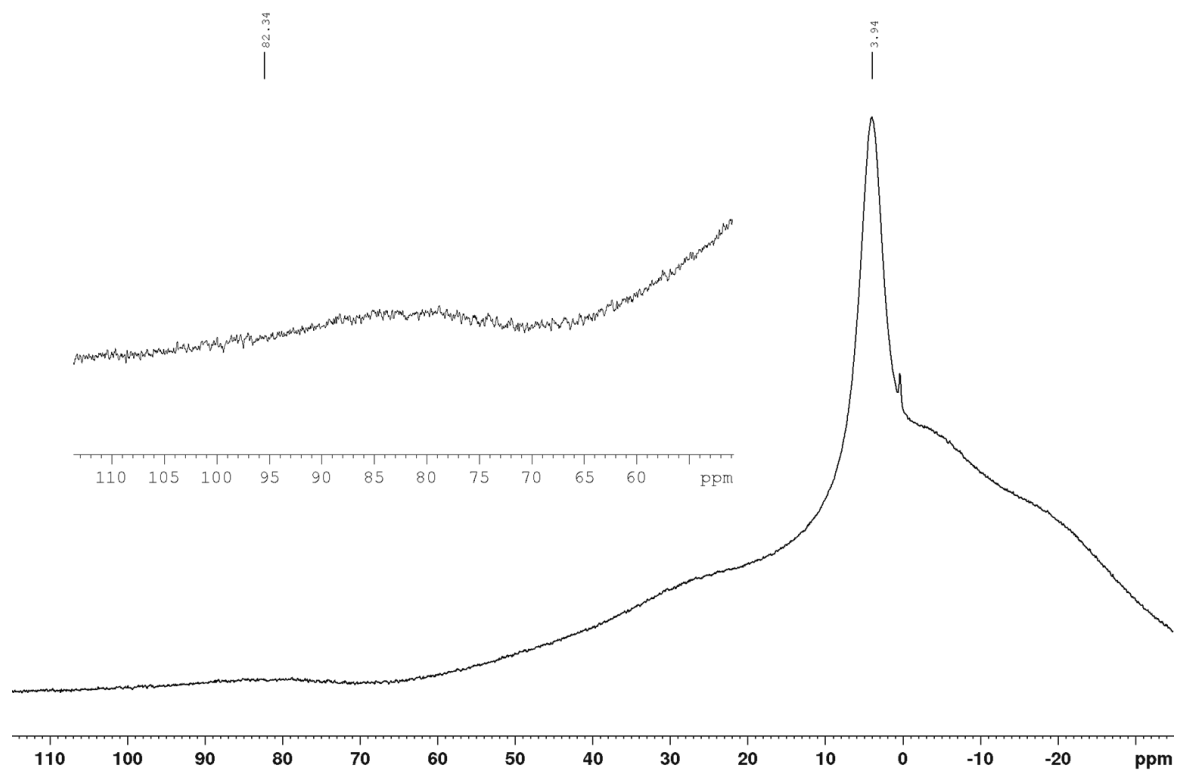


Figure 8.97:  $^{11}\text{B}$  NMR spectrum (128 MHz, 298 K,  $\text{D}_2\text{O}$ ) of **tris(2,6-dimethyl-4-(trifluoroboryl)phenyl)borane, tripotassium salt**.

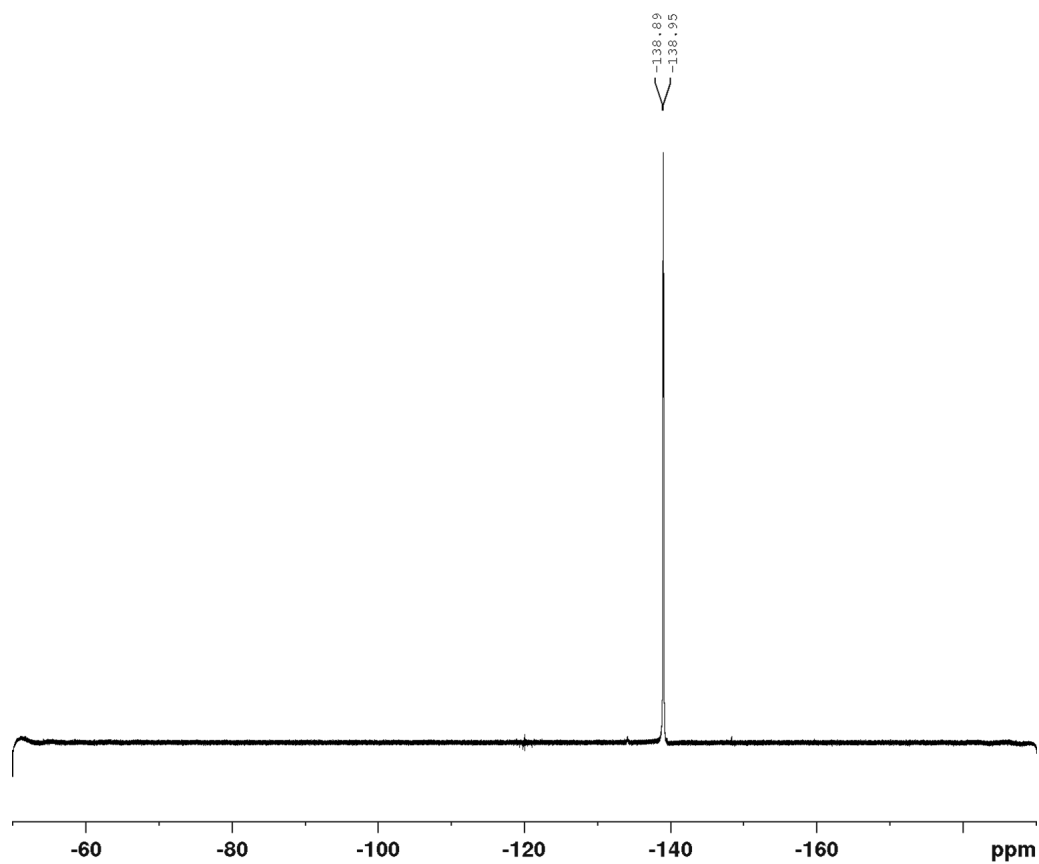


Figure 8.98:  $^{19}\text{F}$  NMR spectrum (471 MHz, 298 K,  $\text{DMSO-d}_6$ ) of **tris(2,6-dimethyl-4-(trifluoroboryl)phenyl)borane, tripotassium salt**.

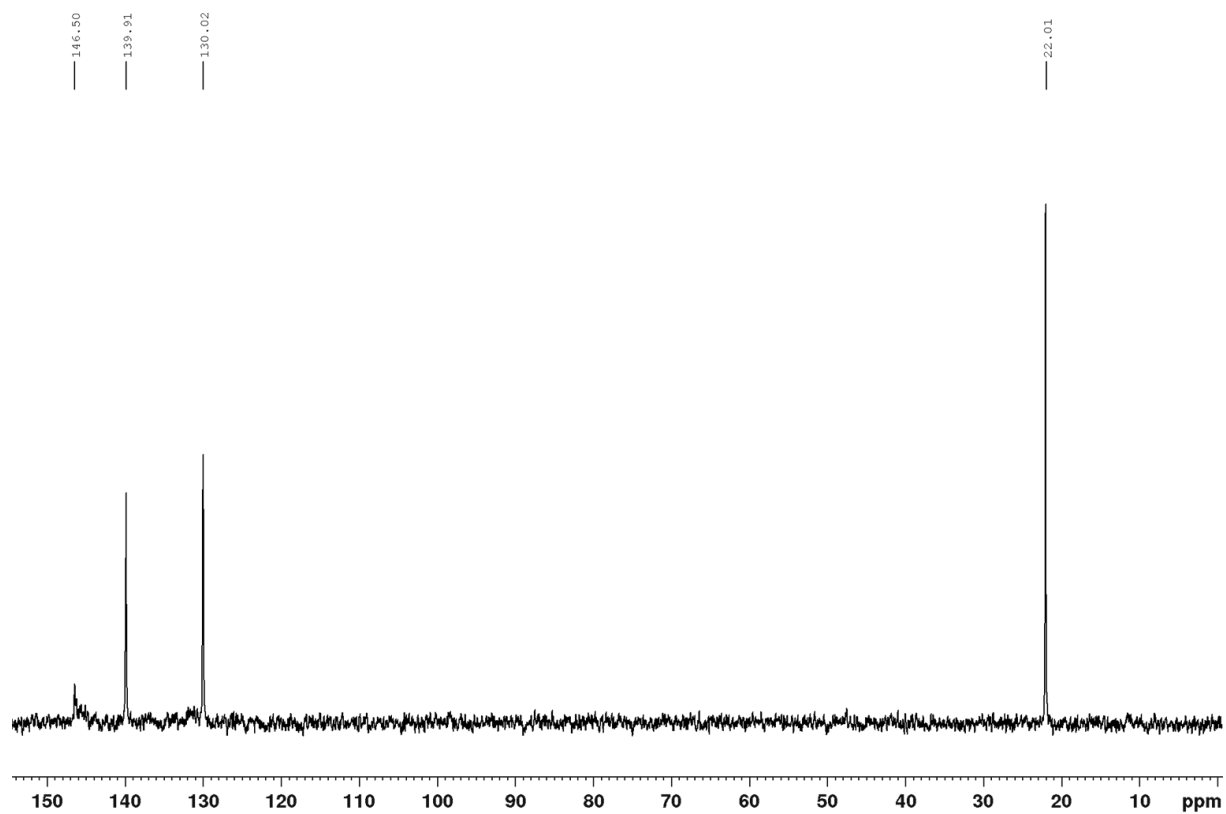


Figure 8.99:  $^{13}\text{C}\{^1\text{H}\}$  NMR spectrum (101 MHz, 298 K,  $\text{D}_2\text{O}$ ) of **tris(2,6-dimethyl-4-(trifluoroboryl)phenyl)borane, tripotassium salt**.

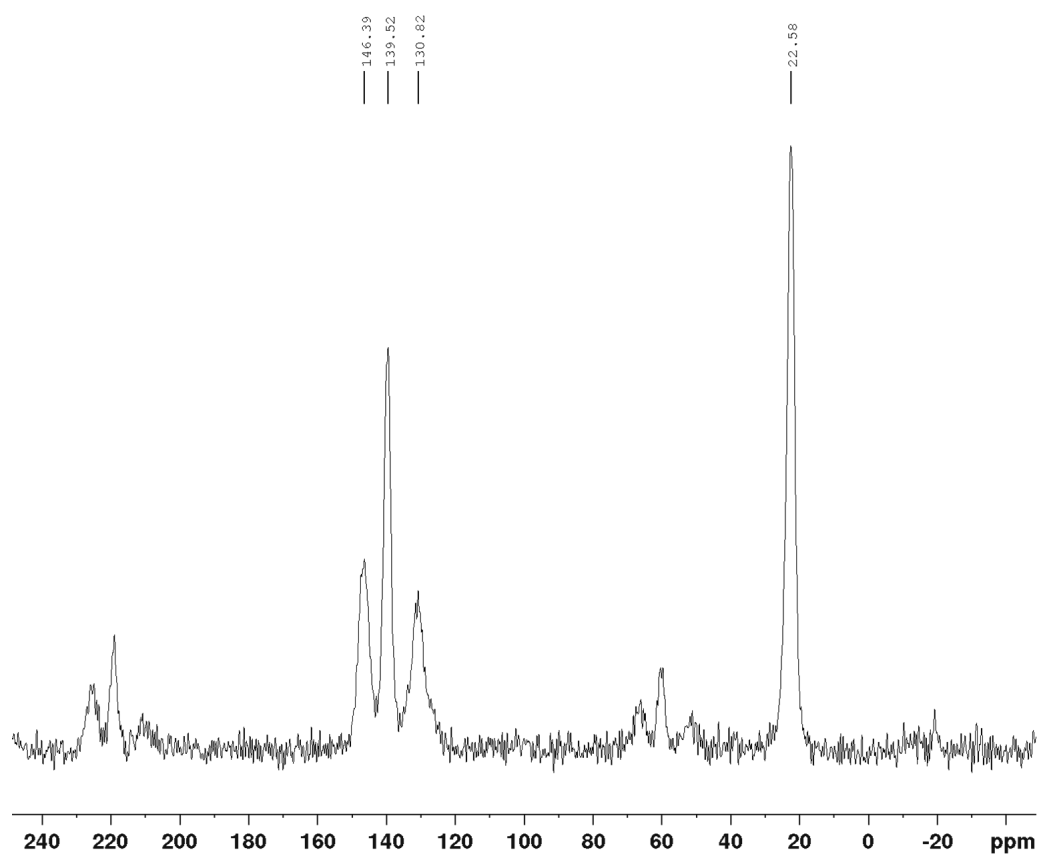


Figure 8.100:  $^{13}\text{C}$ -SS NMR spectrum (248.8 MHz, 298 K) of **tris(2,6-dimethyl-4-(trifluoroboryl)phenyl)borane, tripotassium salt**.

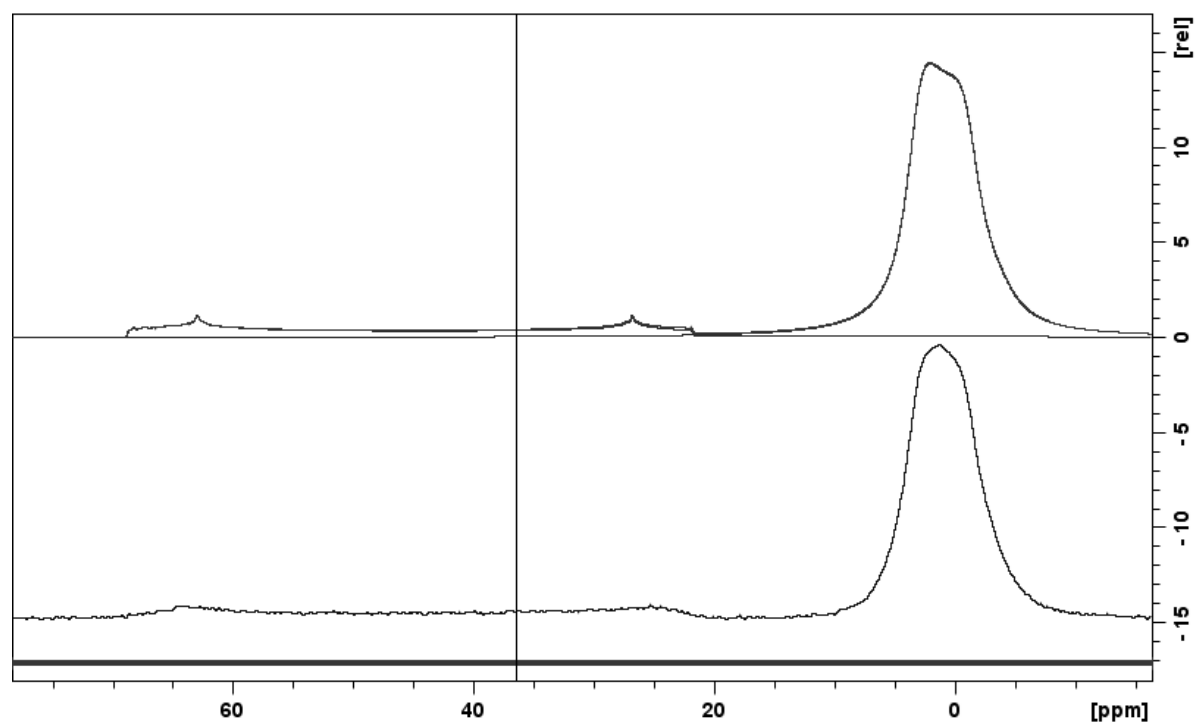


Figure 8.101:  $^{11}\text{B}$ -SS NMR spectrum (128.3 MHz, 298 K) of **tris(2,6-dimethyl-4-(trifluoroboryl)phenyl)borane, tripotassium salt** (bottom). Simulated spectrum (top).



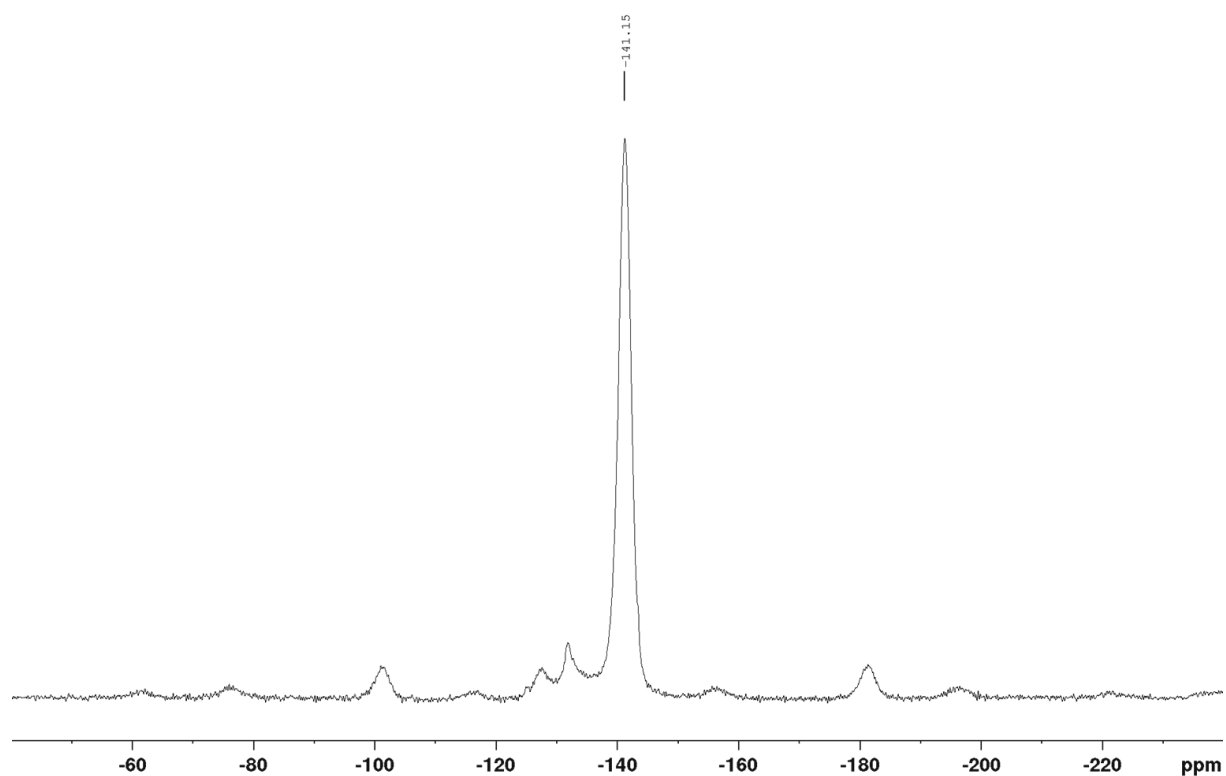


Figure 8.102:  $^{19}\text{F}$ -SS NMR spectrum (376.5 MHz, 298 K) of **tris(2,6-dimethyl-4-(trifluoroboryl)phenyl)borane, tripotassium salt**.

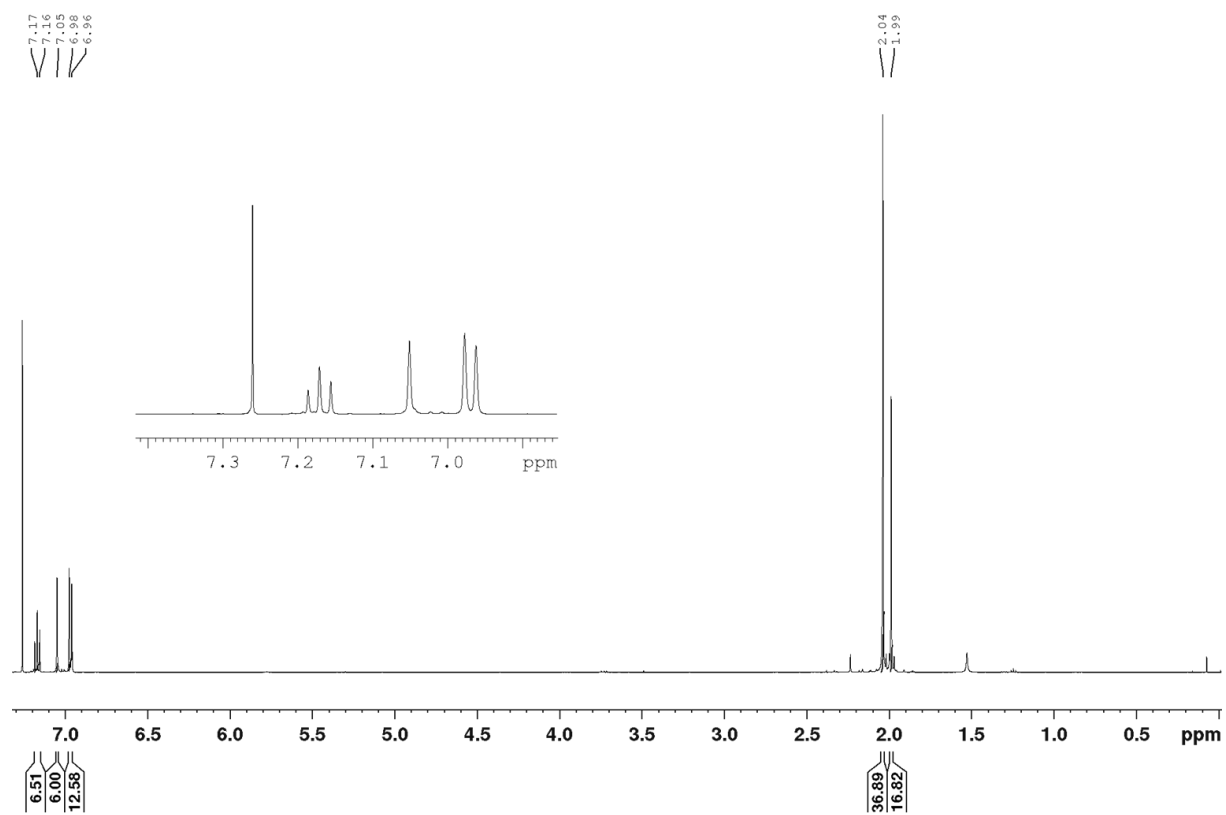


Figure 8.103:  $^1\text{H}$  NMR spectrum (500 MHz, 298 K,  $\text{CDCl}_3$ ) of **BG1H**.

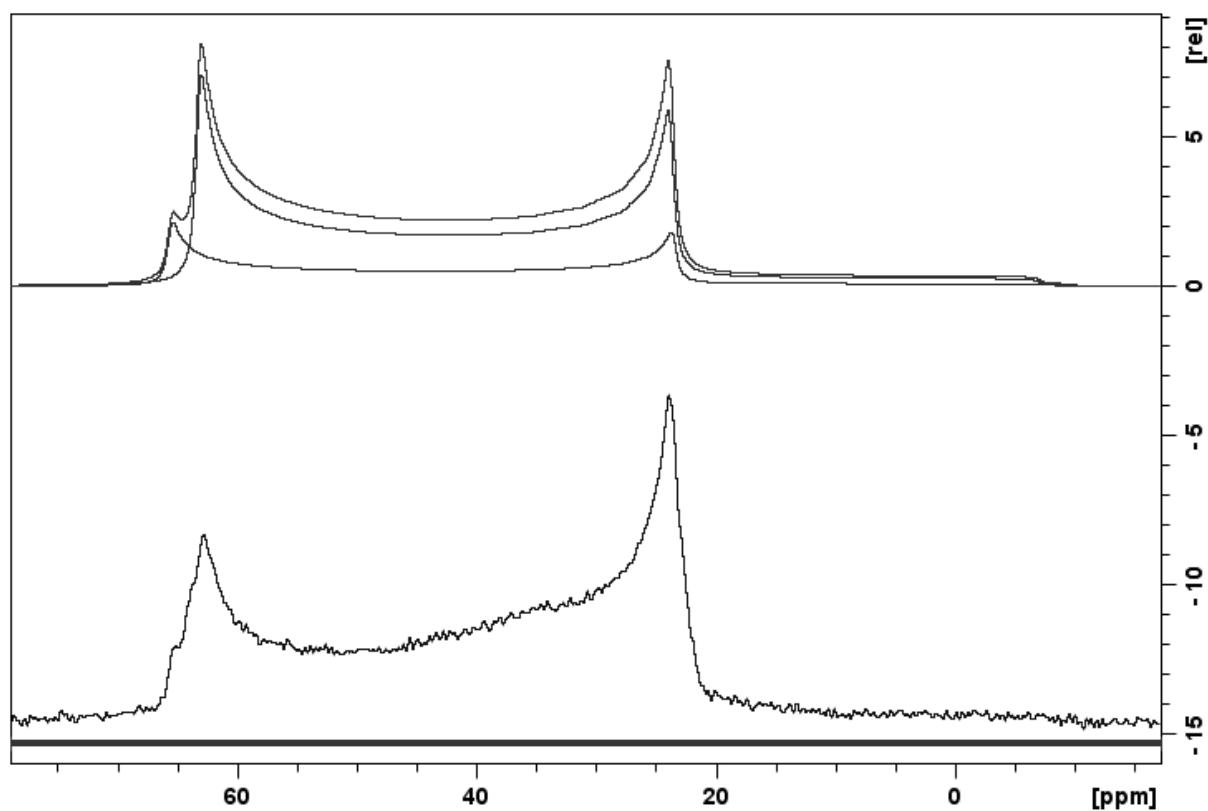


Figure 8.104:  $^{11}\text{B}$ -SS NMR spectrum (128.3 MHz, 298 K) of **BG1H** (bottom). Simulated spectrum (top).

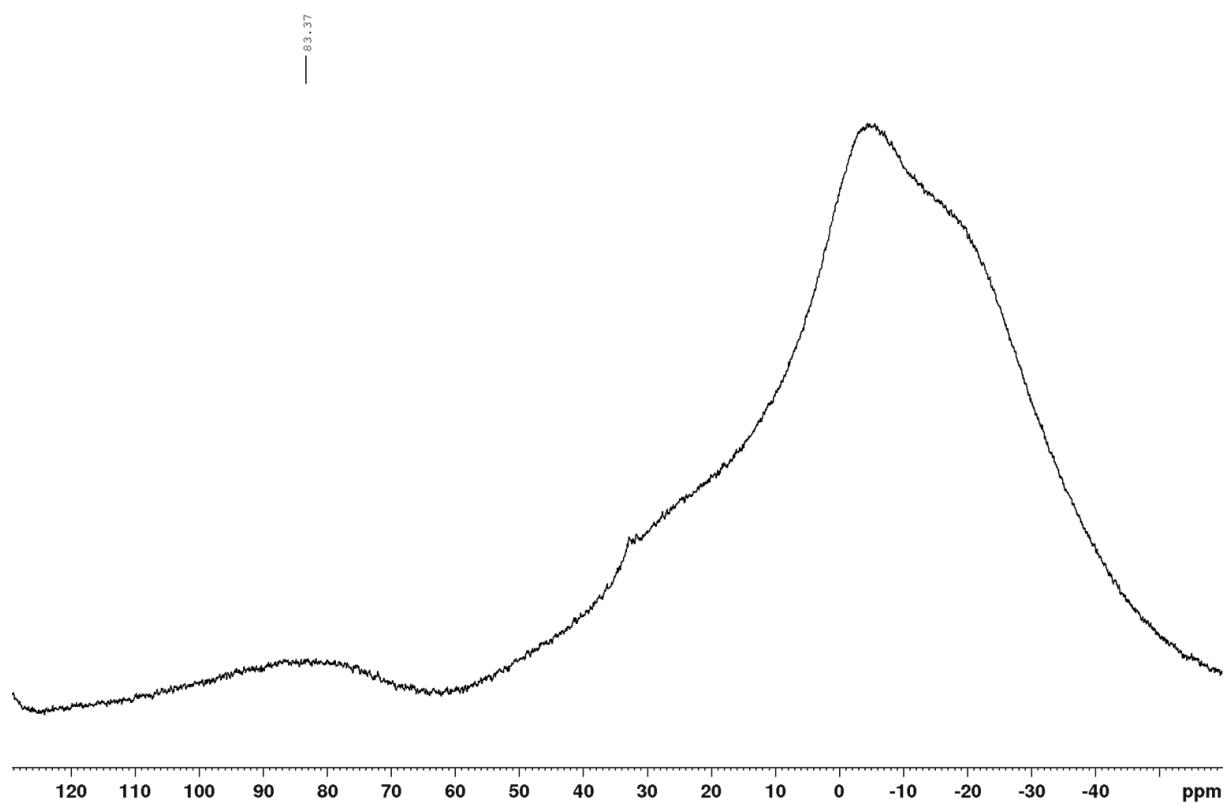
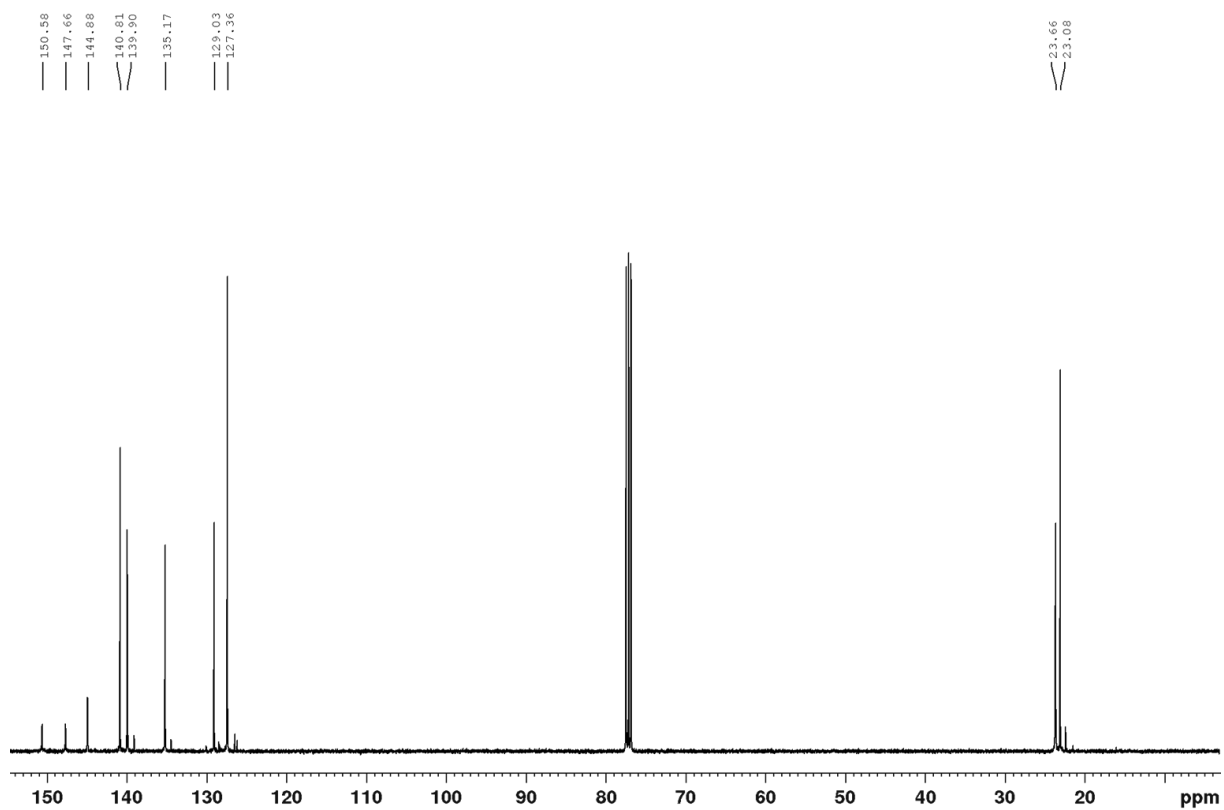
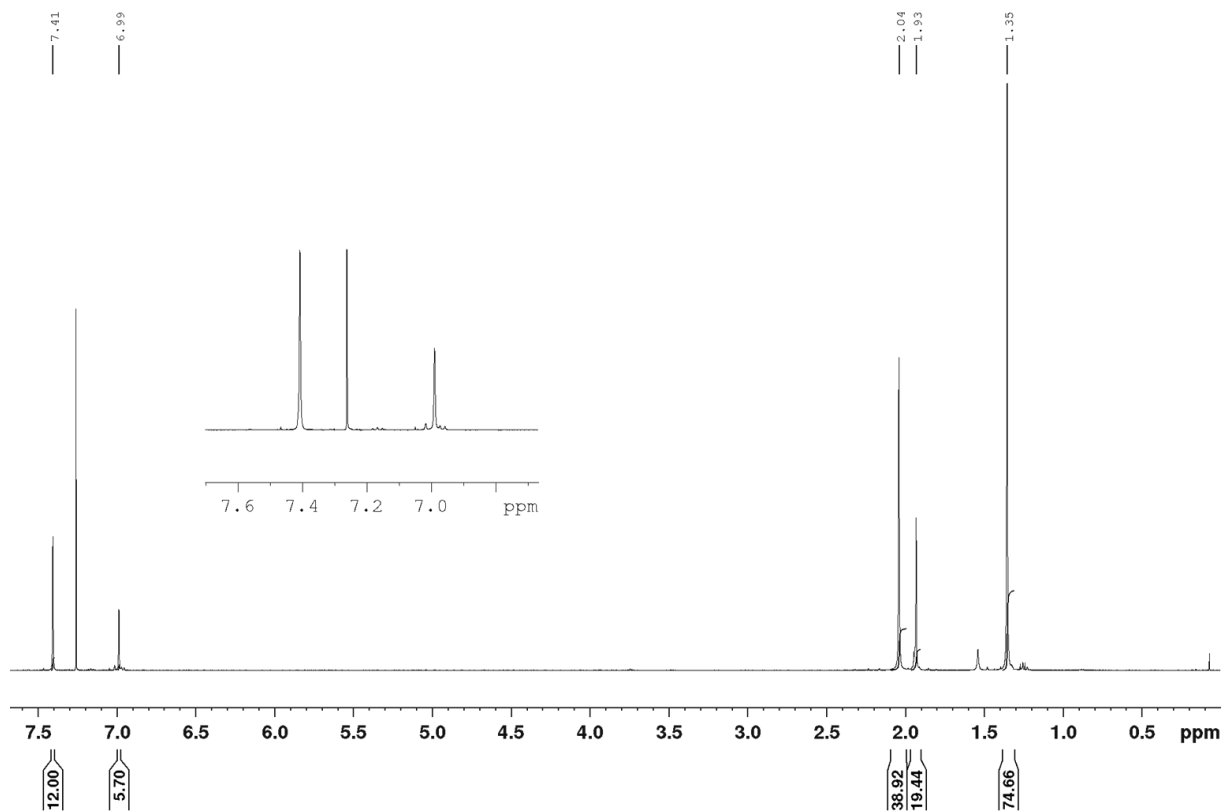


Figure 8.105:  $^{11}\text{B}$  NMR spectrum (128 MHz, 298 K,  $\text{CDCl}_3$ ) of **BG1H**.

Figure 8.106:  $^{13}\text{C}\{^1\text{H}\}$  NMR spectrum (126 MHz, 298 K,  $\text{CDCl}_3$ ) of **BG1H**.Figure 8.107:  $^1\text{H}$  NMR spectrum (500 MHz, 298 K,  $\text{CDCl}_3$ ) of **BG1Bpin**.

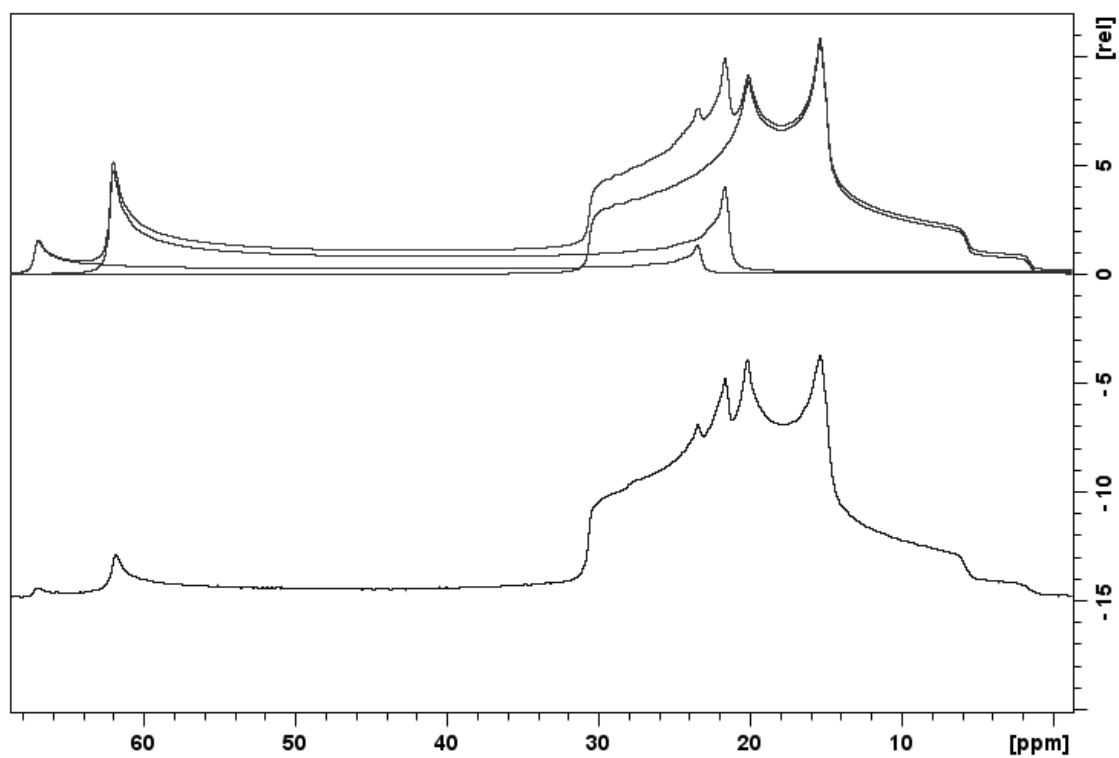


Figure 8.108:  $^{11}\text{B}$ -SS NMR spectrum (128.3 MHz, 298 K) of **BG1Bpin** (bottom). Simulated spectrum (top)

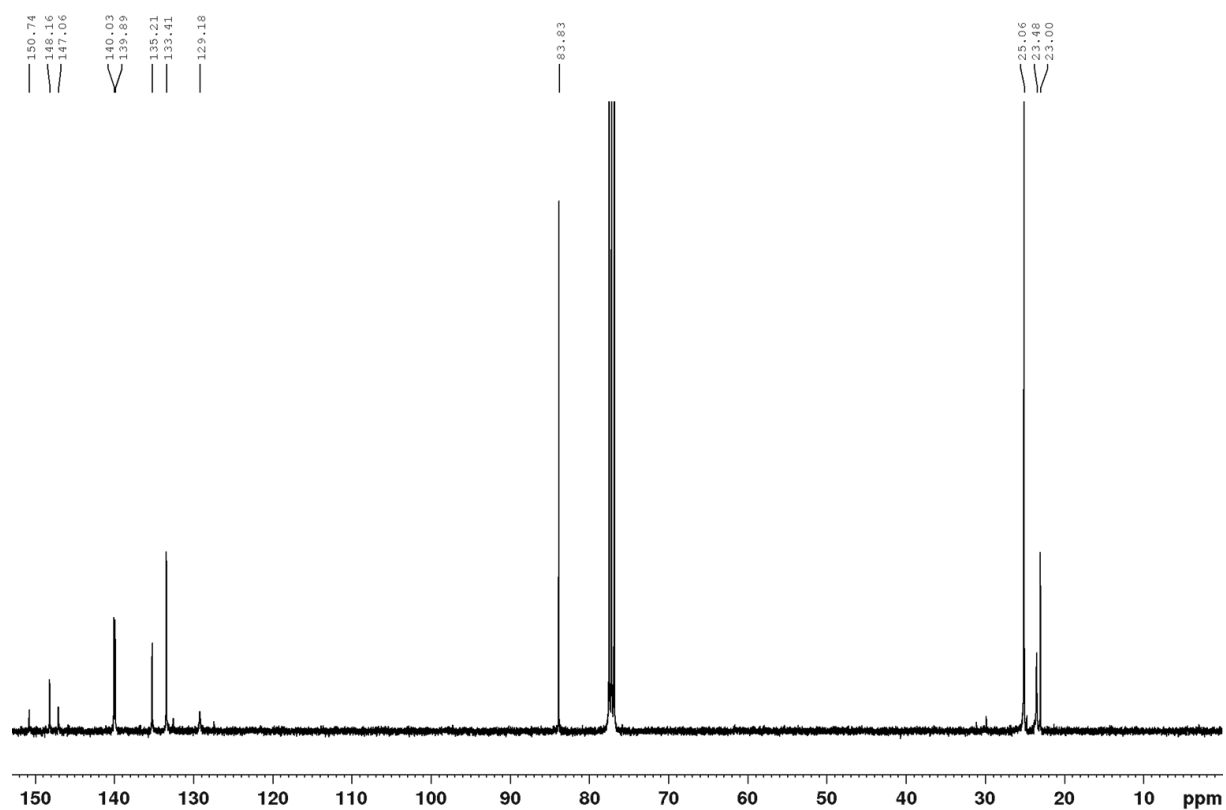
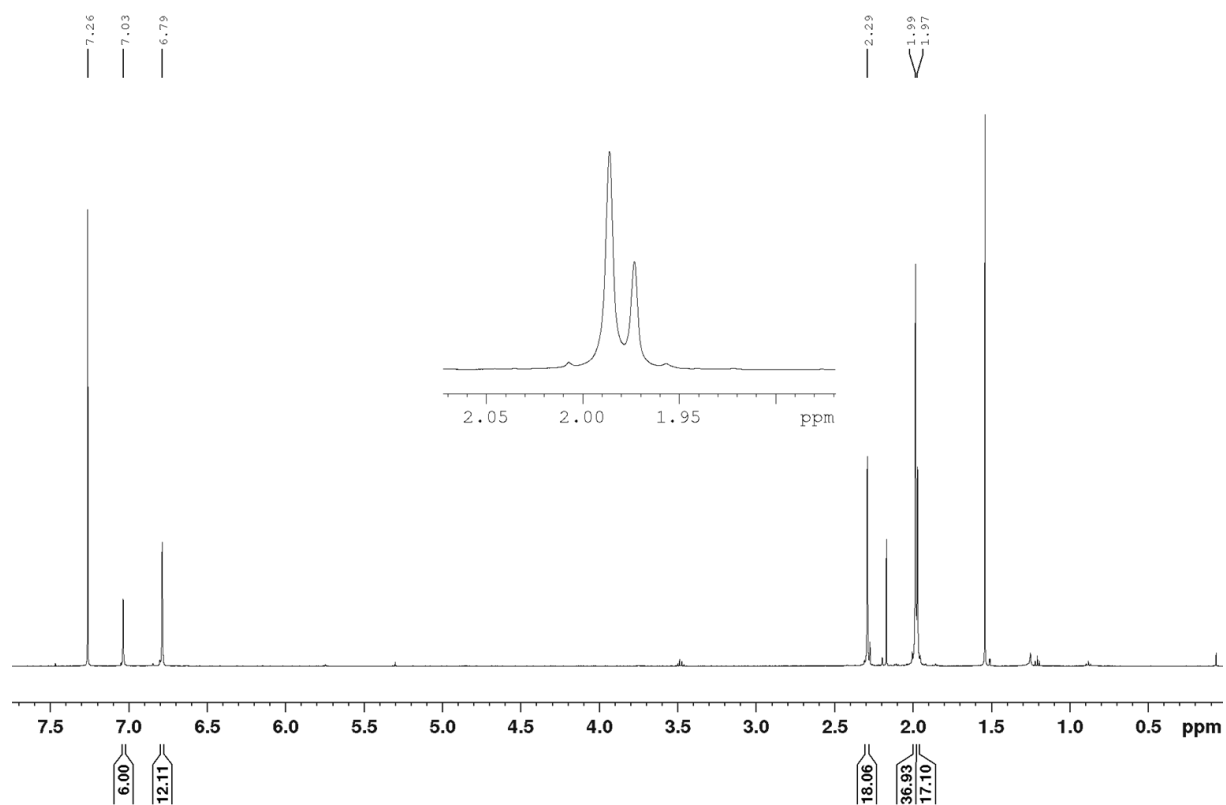
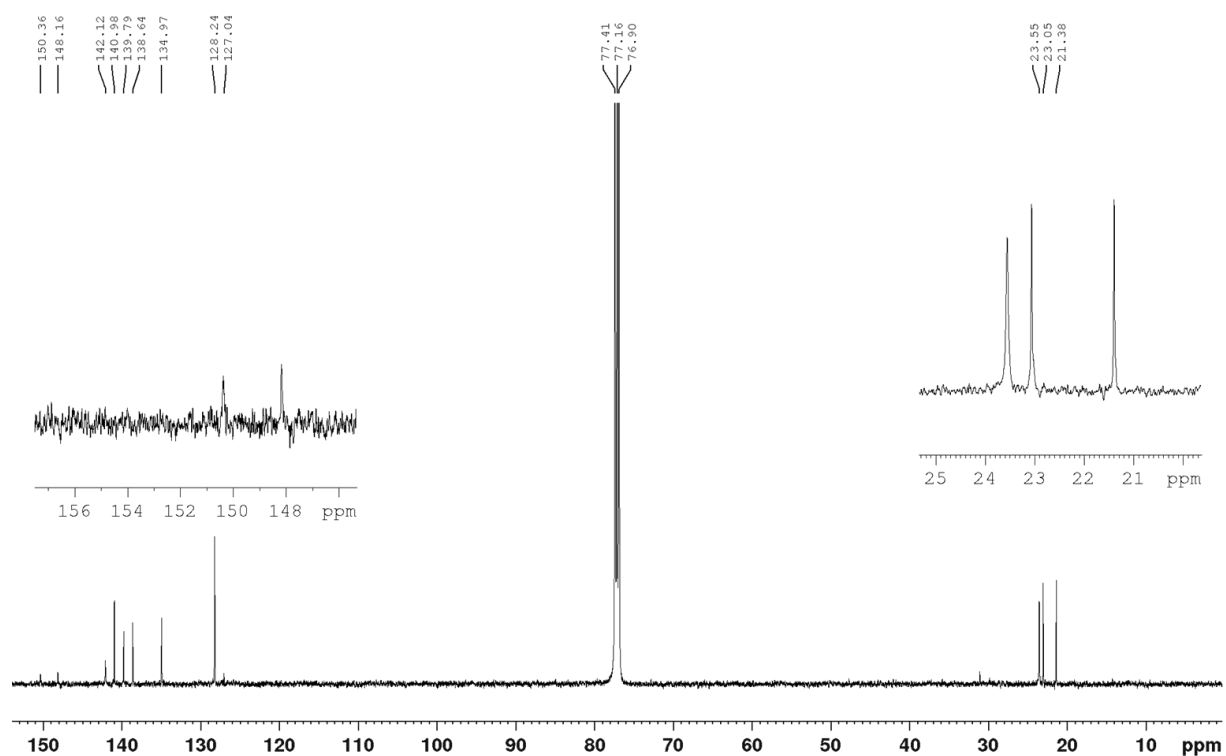


Figure 8.109:  $^{13}\text{C}\{^1\text{H}\}$  NMR spectrum (126 MHz, 298 K,  $\text{CDCl}_3$ ) of **BG1Bpin**.

Figure 8.110:  $^1\text{H}$  NMR spectrum (500 MHz, 298 K,  $\text{CDCl}_3$ ) of **BG1Me**.Figure 8.111:  $^{13}\text{C}\{^1\text{H}\}$  NMR spectrum (126 MHz, 298 K,  $\text{CDCl}_3$ ) of **BG1Me**.

# Appendix

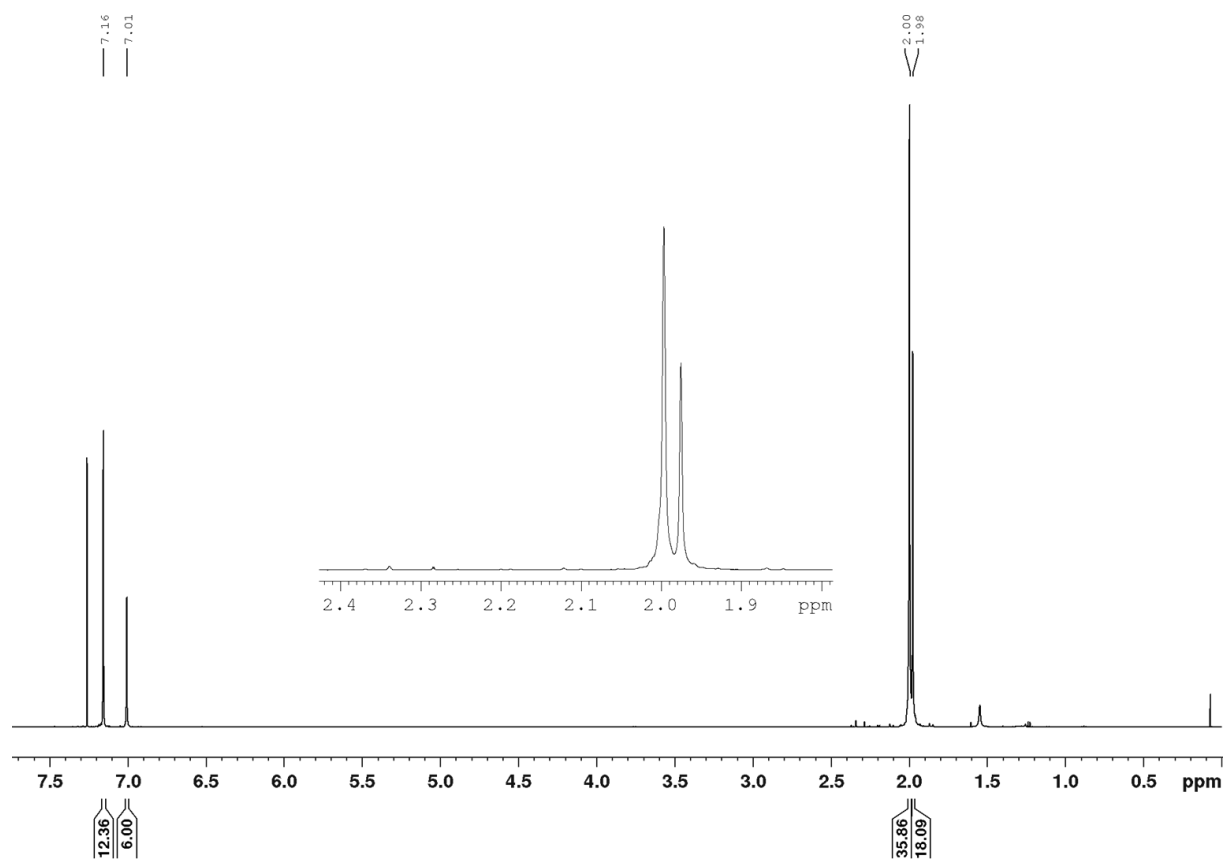


Figure 8.112:  $^1\text{H}$  NMR spectrum (500 MHz, 298 K,  $\text{CDCl}_3$ ) of **BG1Br**.

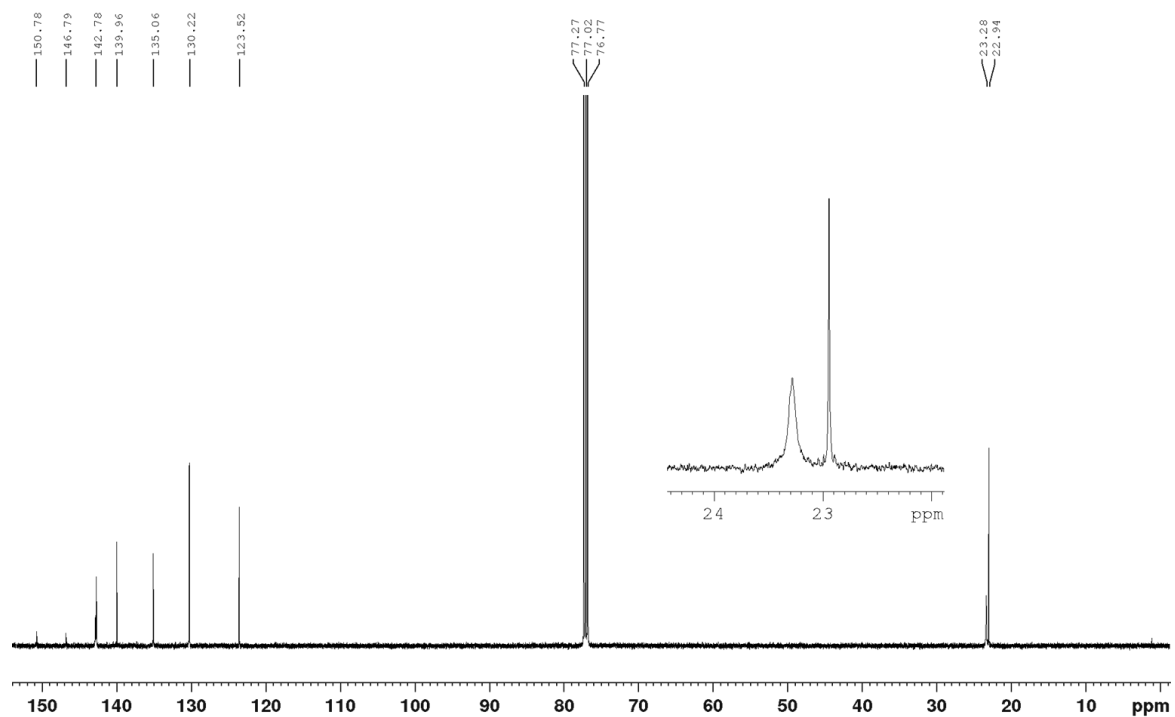
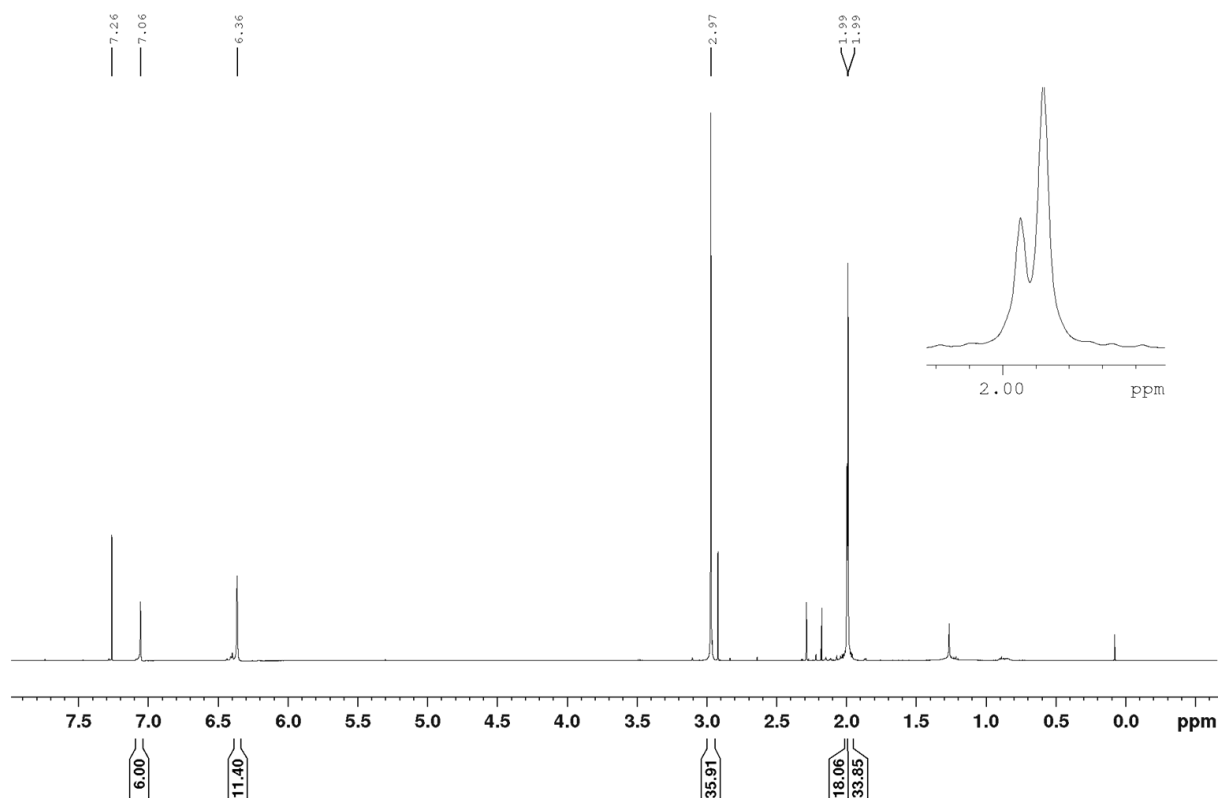
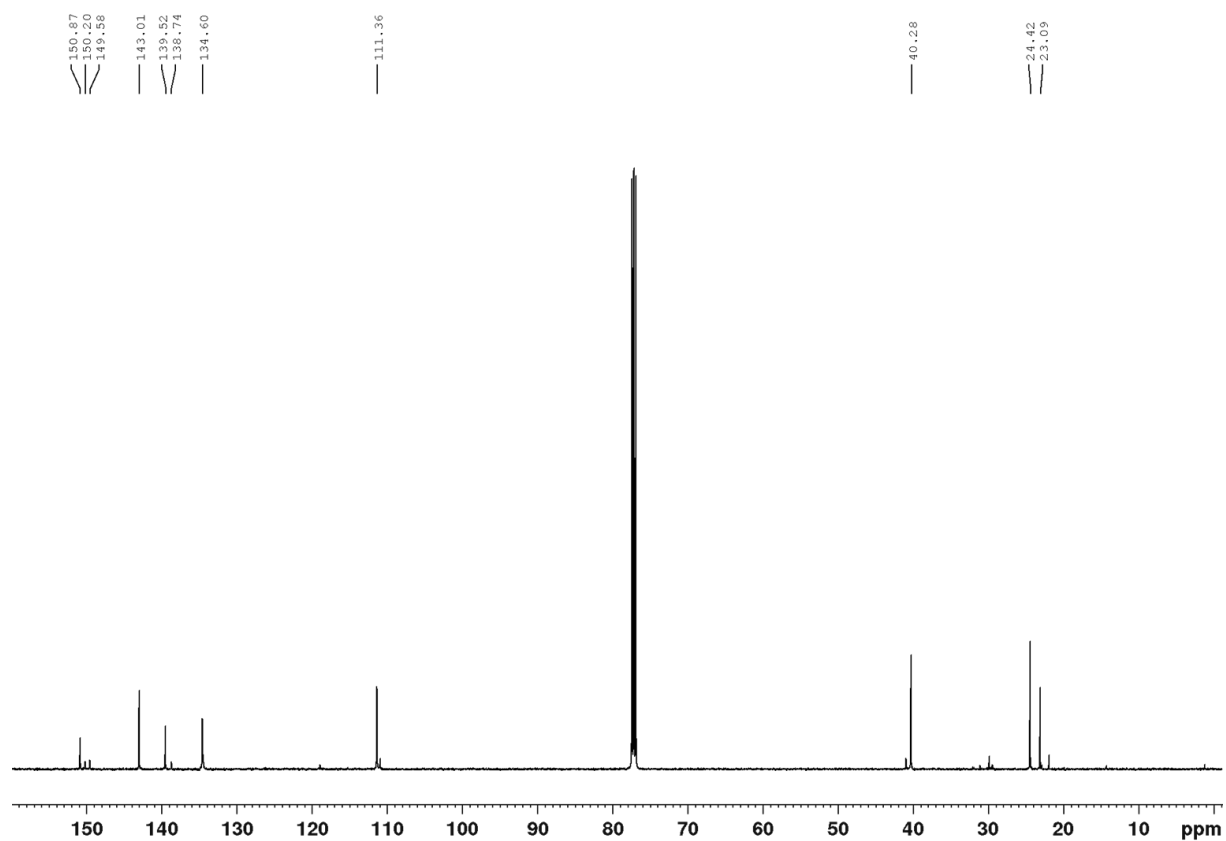


Figure 8.113:  $^{13}\text{C}\{^1\text{H}\}$  NMR spectrum (126 MHz, 298 K,  $\text{CDCl}_3$ ) of **BG1Br**.

Figure 8.114:  $^1\text{H}$  NMR spectrum (500 MHz, 298 K,  $\text{CDCl}_3$ ) of **BG1NMe<sub>2</sub>**.Figure 8.115:  $^{13}\text{C}\{^1\text{H}\}$  NMR spectrum (126 MHz, 298 K,  $\text{CDCl}_3$ ) of **BG1NMe<sub>2</sub>**.

# Appendix

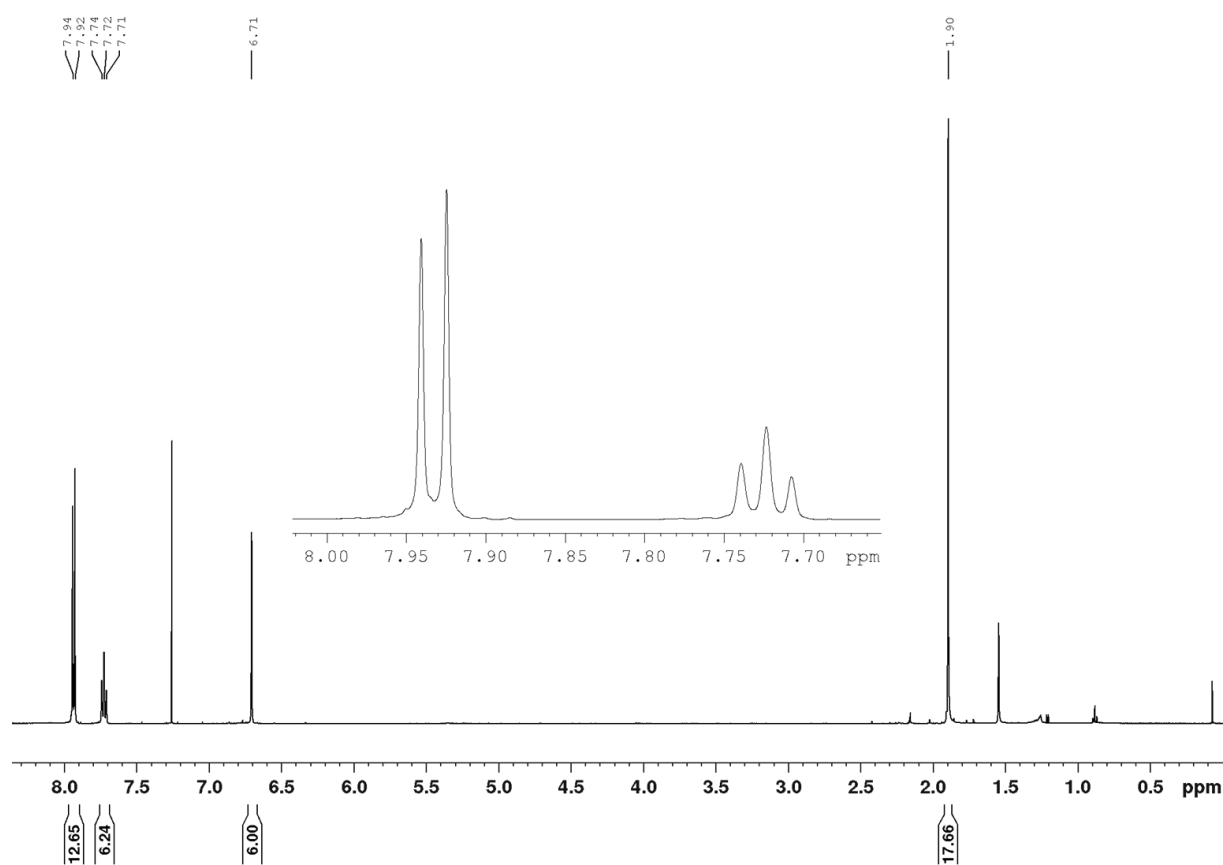


Figure 8.116:  $^1\text{H}$  NMR spectrum (500 MHz, 298 K,  $\text{CDCl}_3$ ) of **BFG1H**.

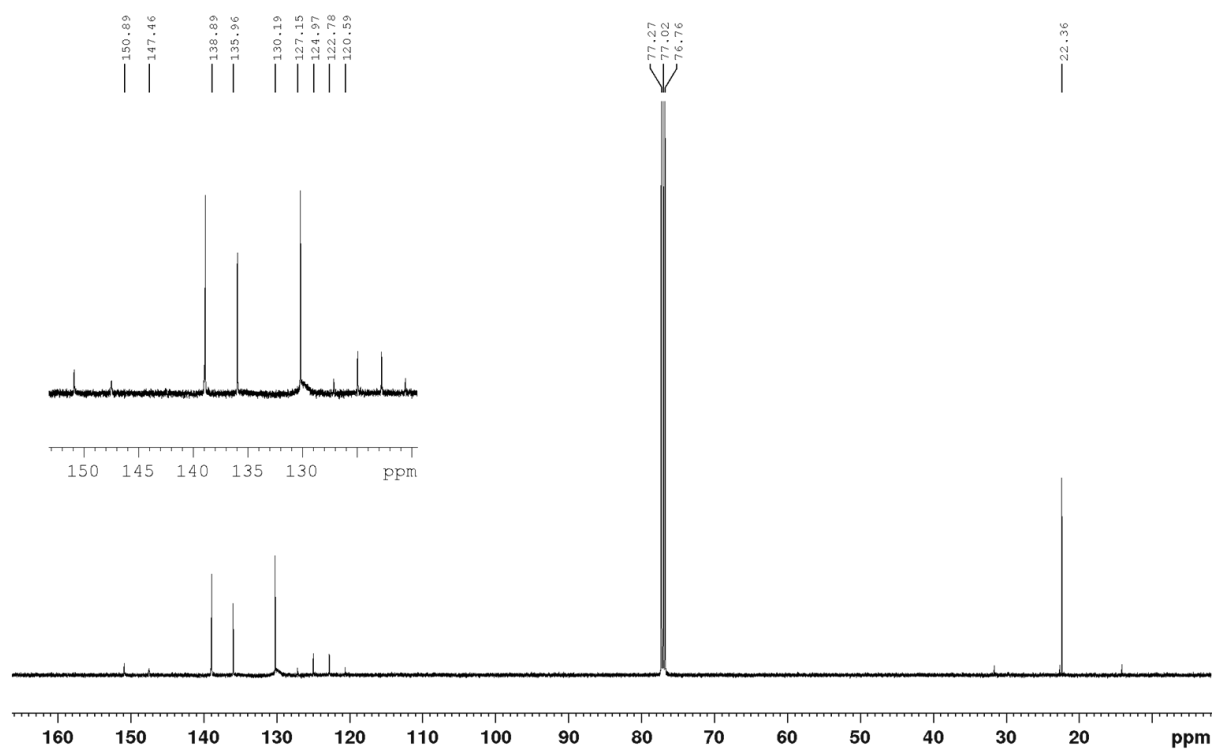


Figure 8.117:  $^{13}\text{C}\{^1\text{H}\}$  NMR spectrum (126 MHz, 298 K,  $\text{CDCl}_3$ ) of **BFG1H**.



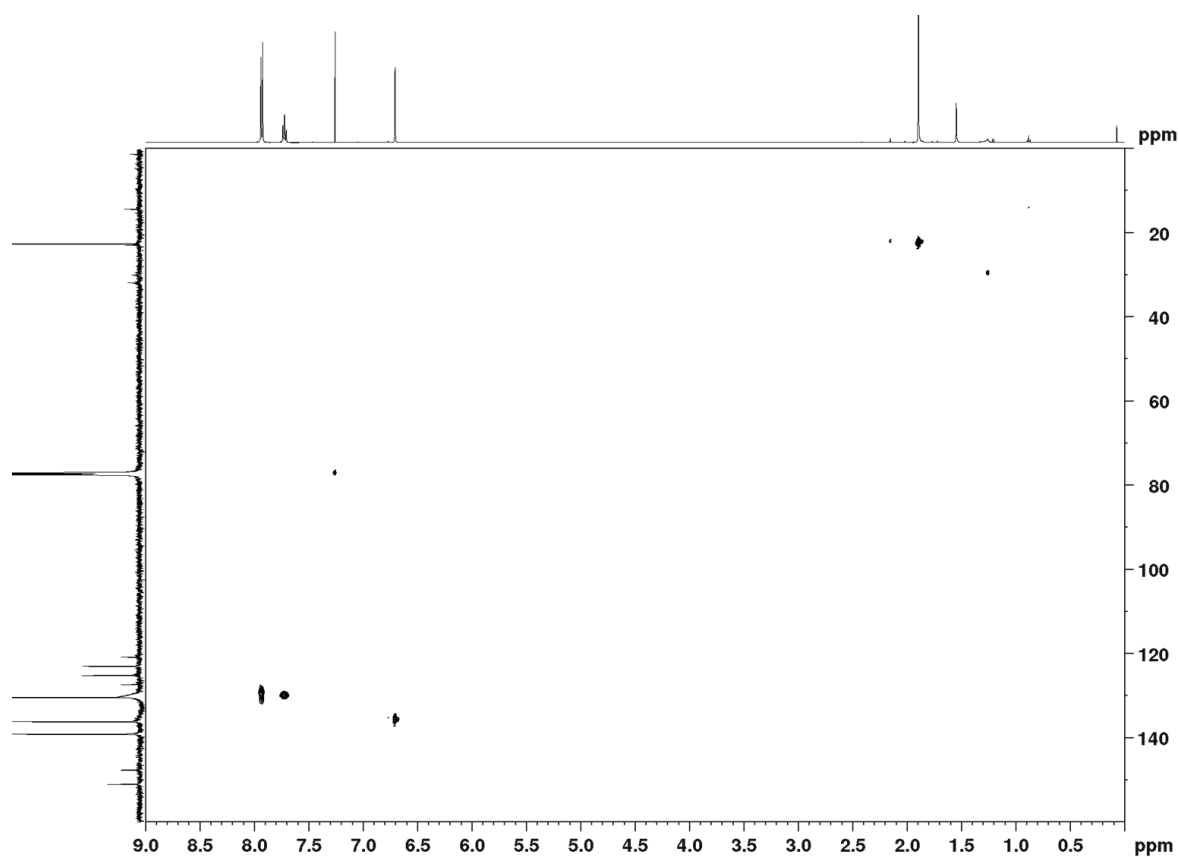


Figure 8.118: HSQC NMR spectrum ( $^{13}\text{C}\{^1\text{H}\}$  126 MHz,  $^1\text{H}$  500 MHz, 298 K,  $\text{CDCl}_3$ ) of **BFG1H**.

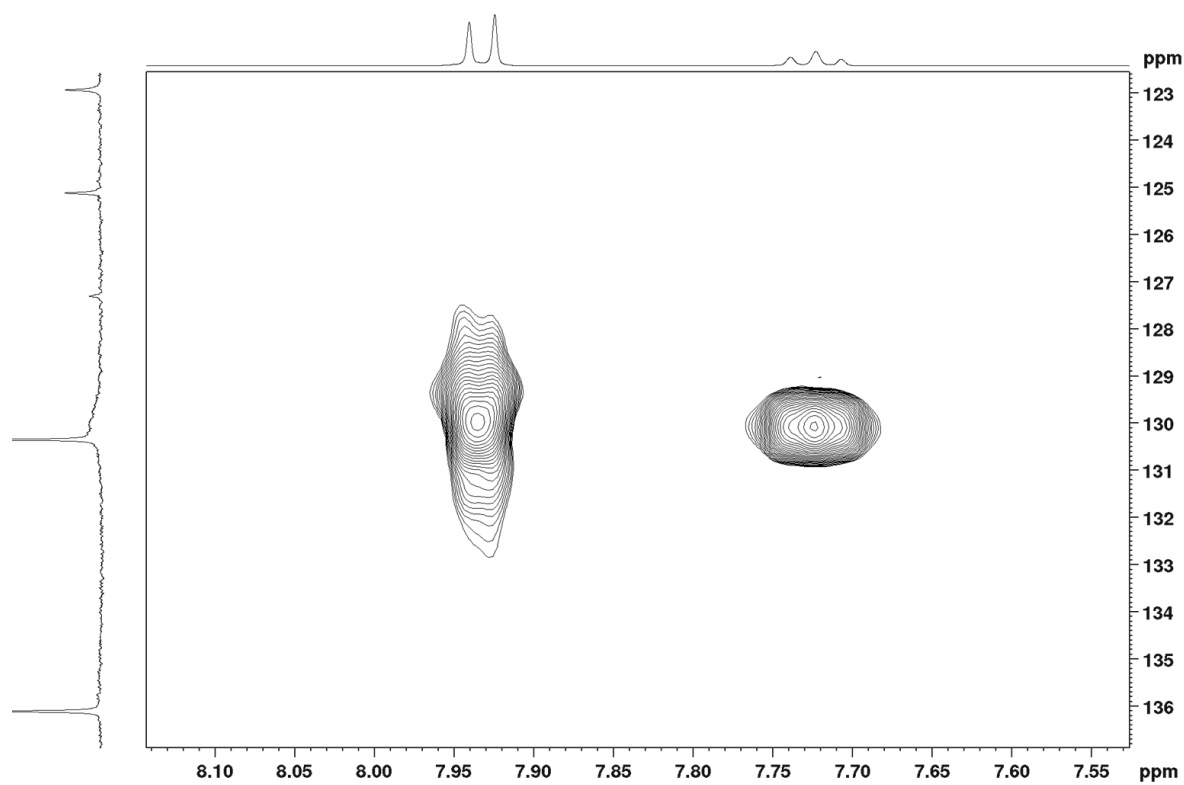


Figure 8.119: HSQC NMR spectrum ( $^{13}\text{C}\{^1\text{H}\}$  126 MHz,  $^1\text{H}$  500 MHz, 298 K,  $\text{CDCl}_3$ ) of **BFG1H**.

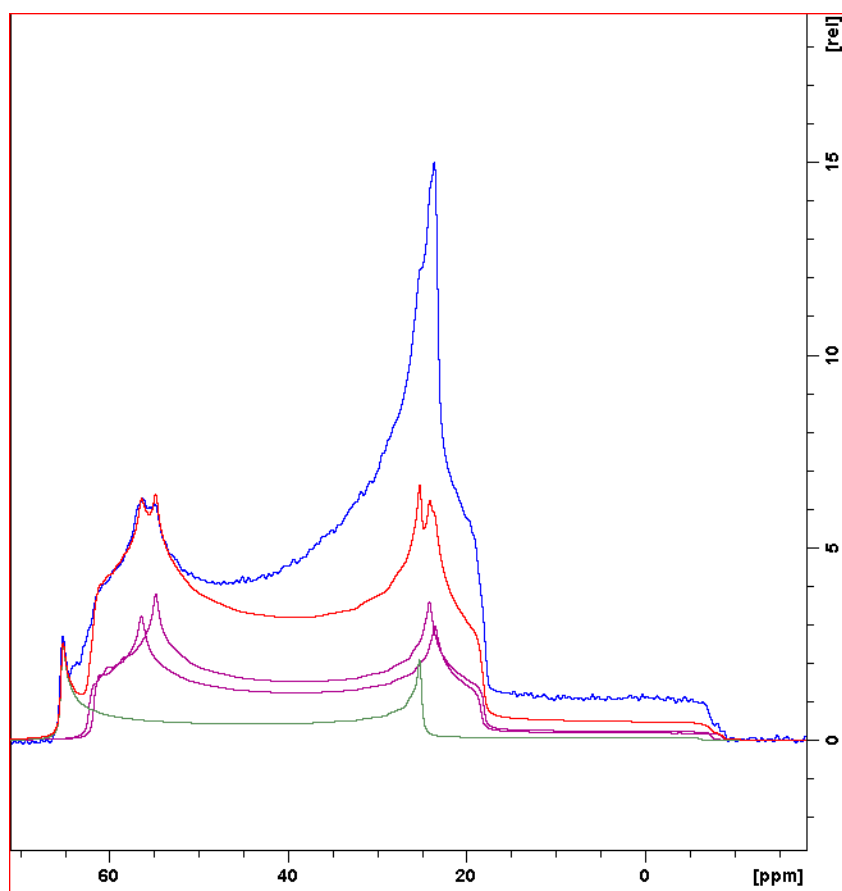


Figure 8.120:  $^{11}\text{B}$  SS NMR spectrum (128.3 MHz, 298 K) of **BFG1H**. Measured spectrum (blue), simulated spectra combined (red), simulated spectra of individual boron centres (green and purple).

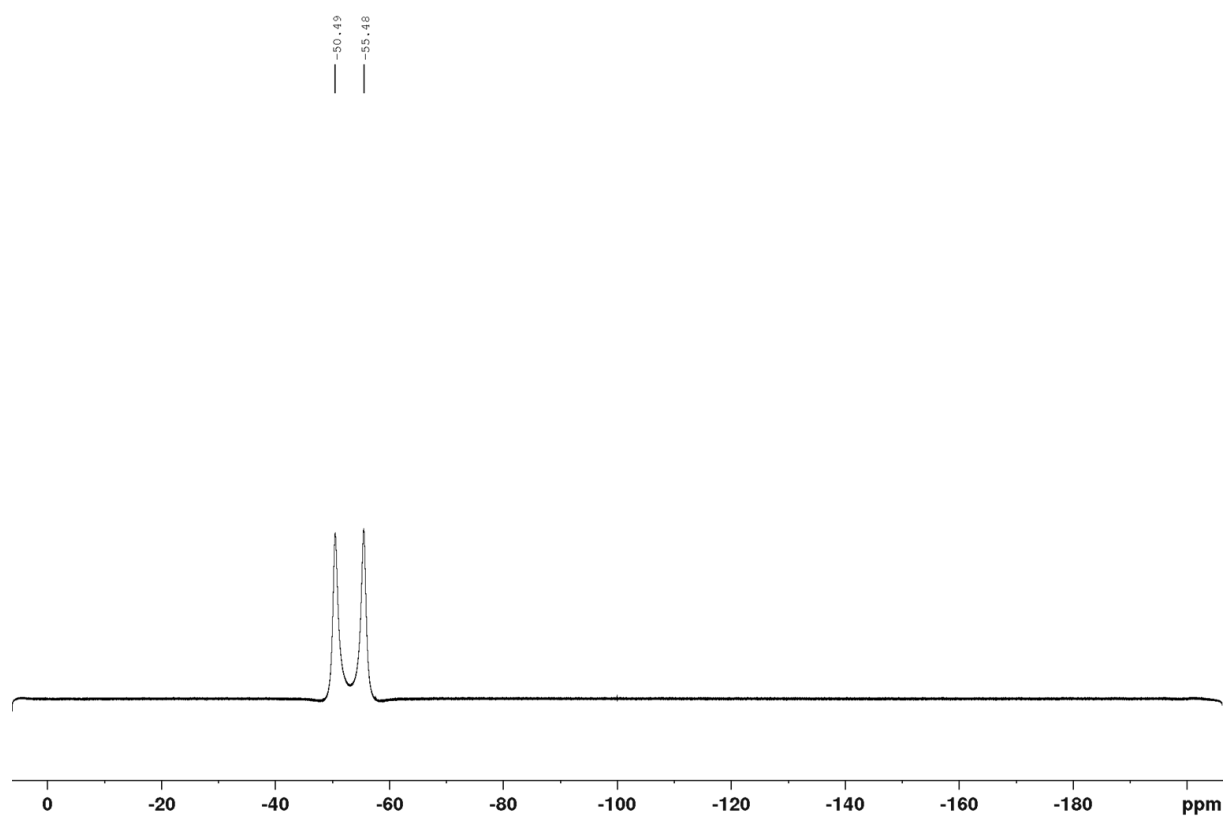
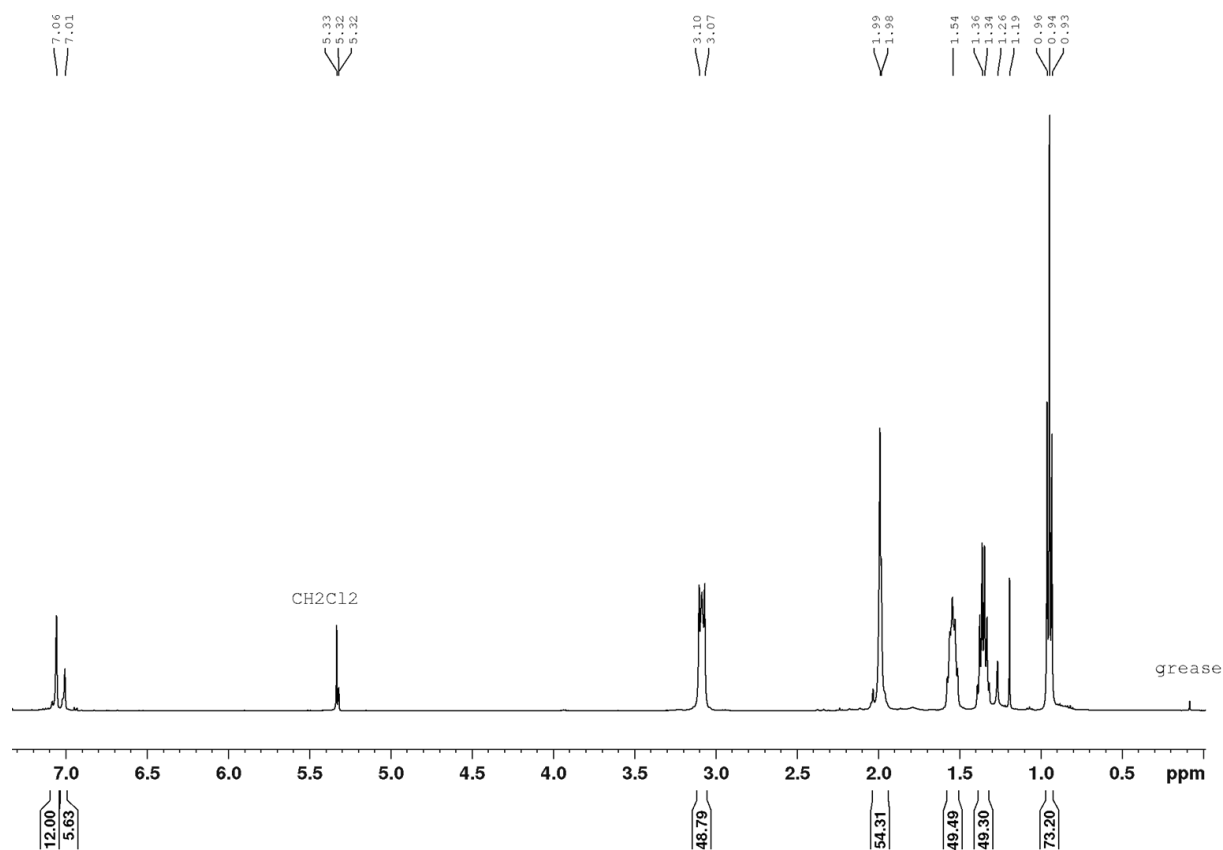
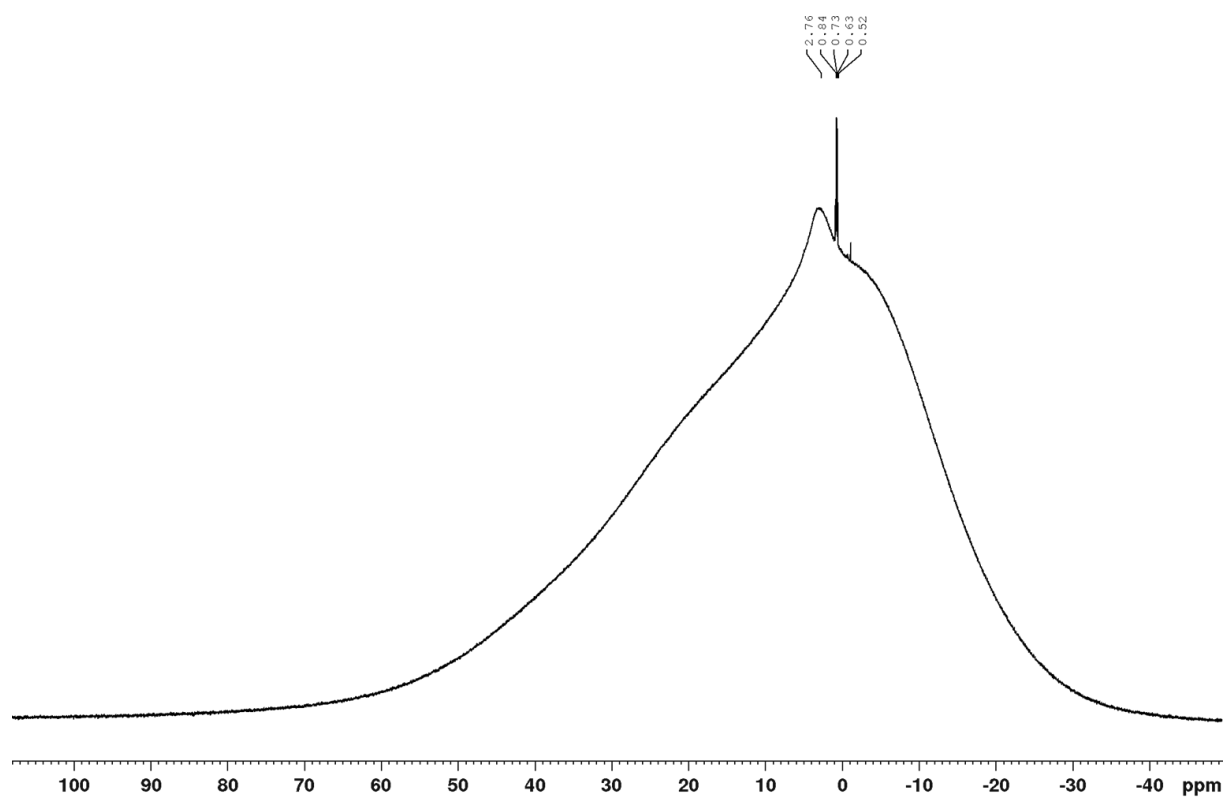
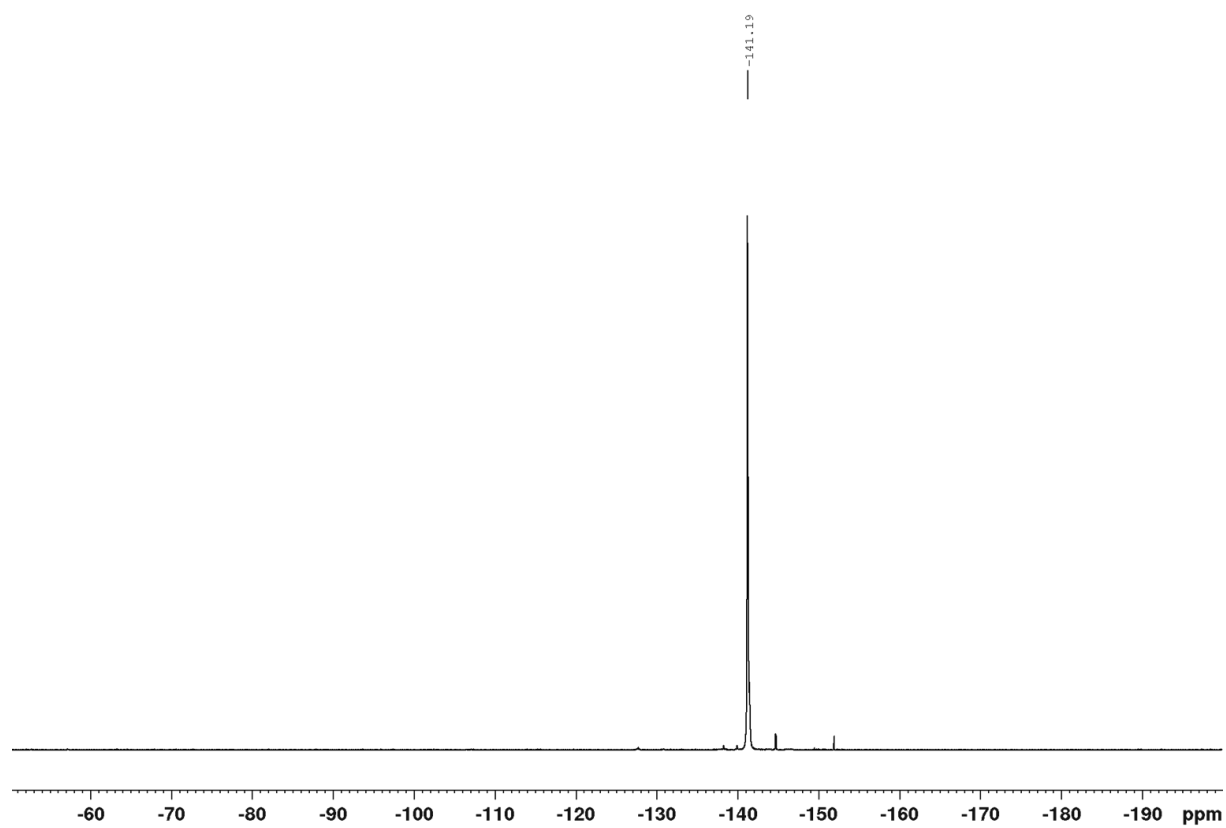
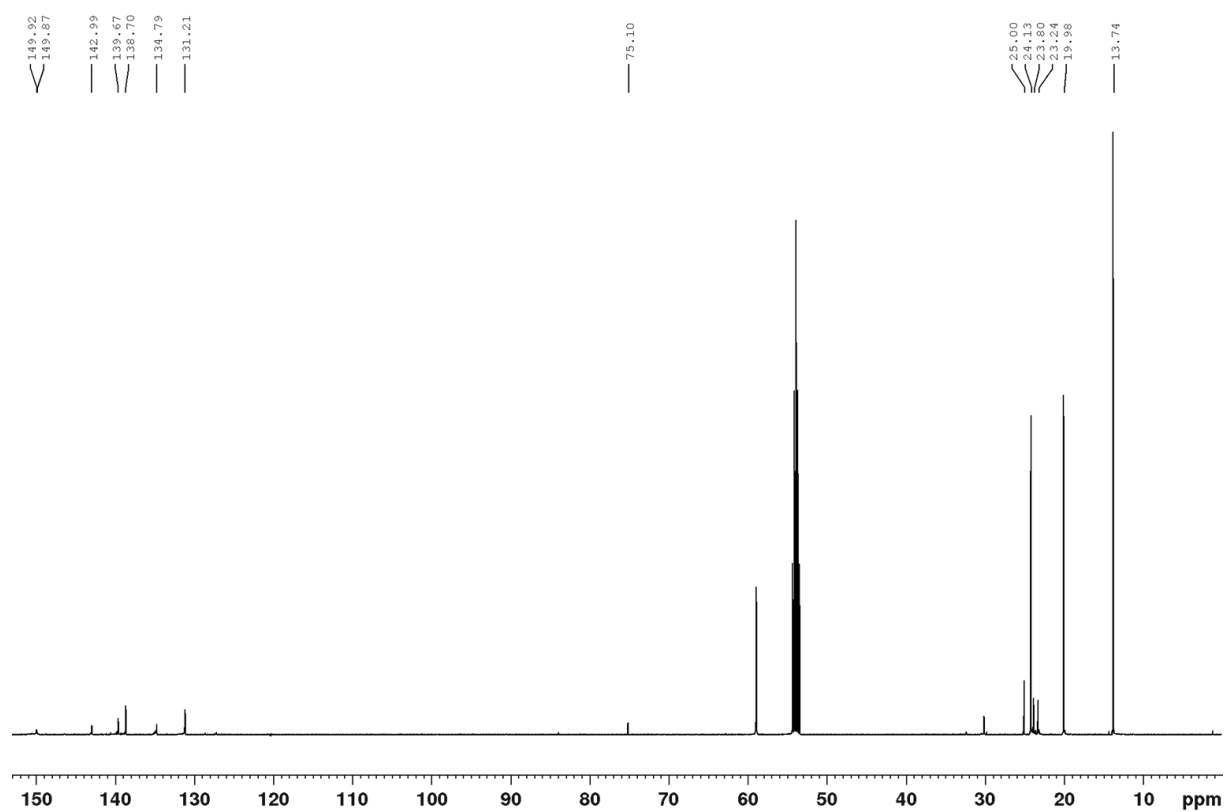
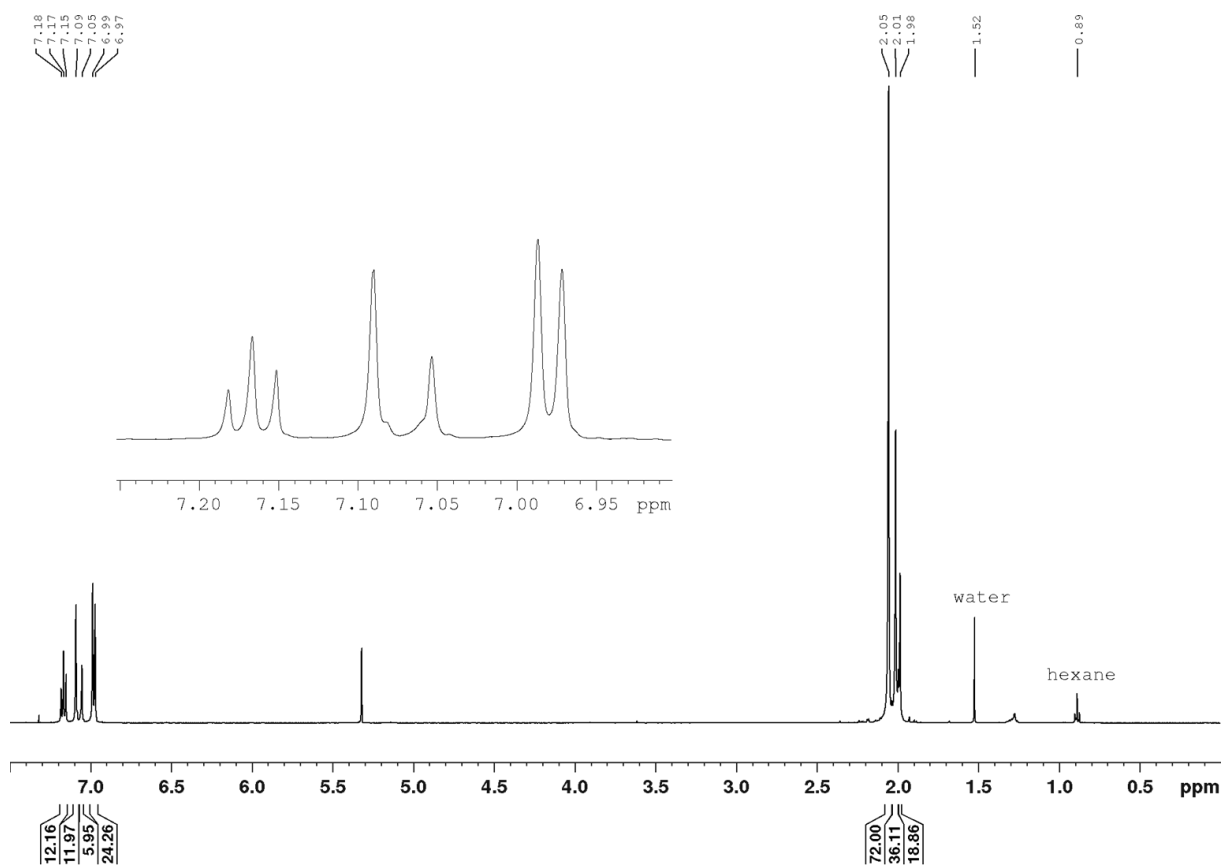
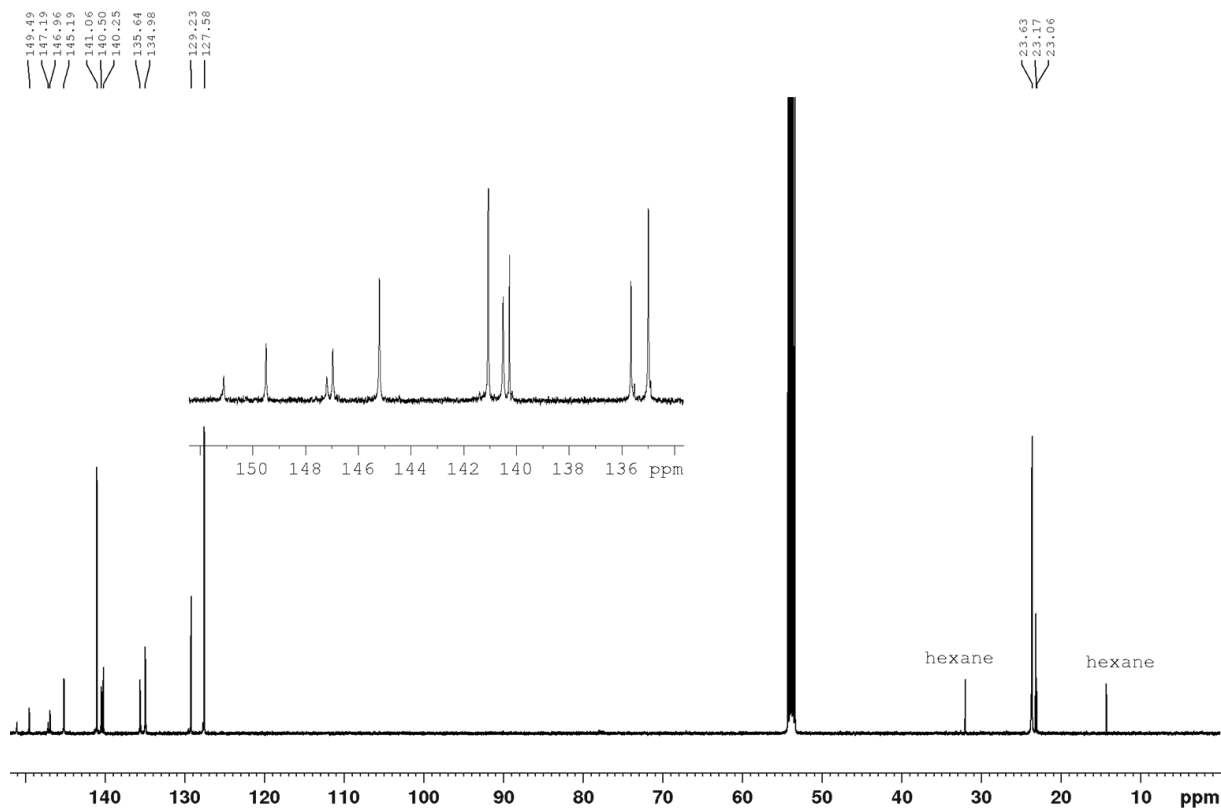


Figure 8.121:  $^{19}\text{F}$  NMR spectrum (471 MHz, 298 K,  $\text{CDCl}_3$ ) of **BFG1H**.

Figure 8.122: <sup>1</sup>H NMR spectrum (500 MHz, 298 K, CD<sub>2</sub>Cl<sub>2</sub>) of **BG1BF<sub>3</sub>N(*n*Bu)<sub>4</sub>**.Figure 8.123: <sup>11</sup>B NMR spectrum (128 MHz, 298 K, CD<sub>2</sub>Cl<sub>2</sub>) of **BG1BF<sub>3</sub>N(*n*Bu)<sub>4</sub>**.

Figure 8.124:  $^{19}\text{F}$  NMR spectrum (471 MHz, 298 K,  $\text{CD}_2\text{Cl}_2$ ) of  $\text{BG1BF}_3\text{N}(\text{nBu})_4$ .Figure 8.125:  $^{13}\text{C}\{^1\text{H}\}$  NMR spectrum (126 MHz, 298 K,  $\text{CD}_2\text{Cl}_2$ ) of  $\text{BG1BF}_3\text{N}(\text{nBu})_4$ .

Figure 8.126:  $^1\text{H}$  NMR spectrum (500 MHz, 298 K,  $\text{CD}_2\text{Cl}_2$ ) of **BG2H**.Figure 8.127:  $^{13}\text{C}\{^1\text{H}\}$  NMR spectrum (126 MHz, 298 K,  $\text{CD}_2\text{Cl}_2$ ) of **BG2H**.

## 8.1.4 Chapter 4

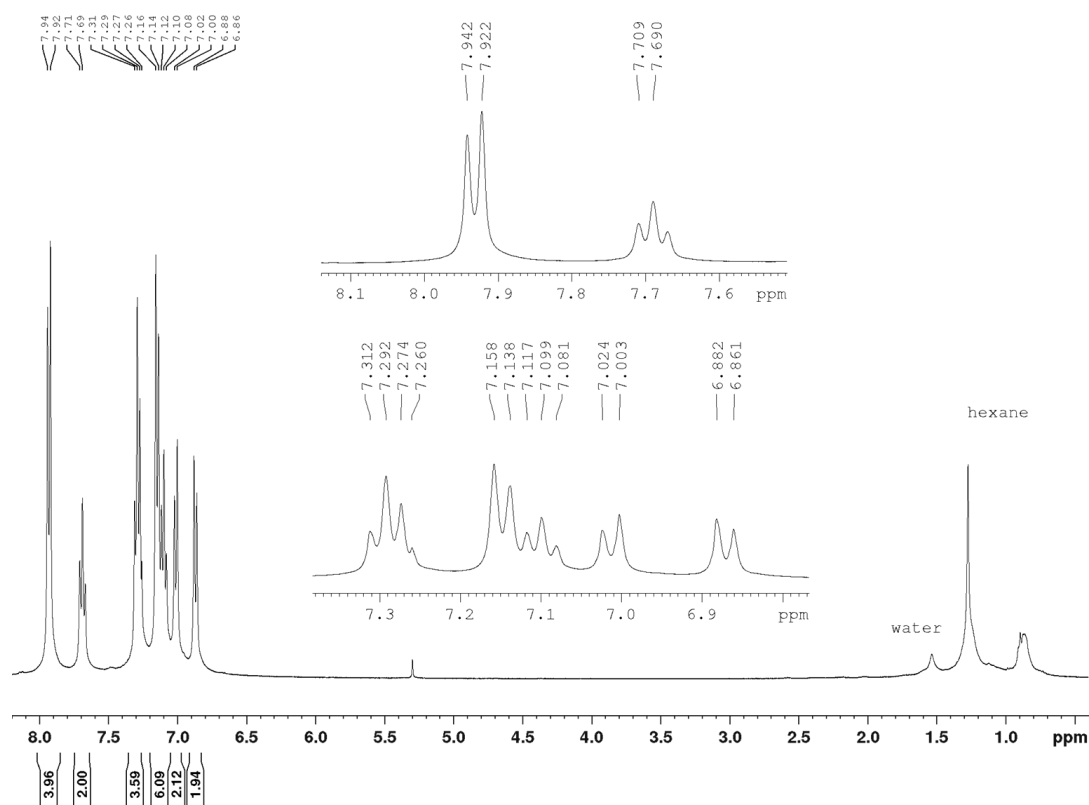


Figure 8.128: <sup>1</sup>H NMR spectrum (400 MHz, 298 K, CDCl<sub>3</sub>) of 4-(bis(2,6-bis(trifluoromethyl)phenyl)boryl)-*N,N*-diphenylaniline (1).

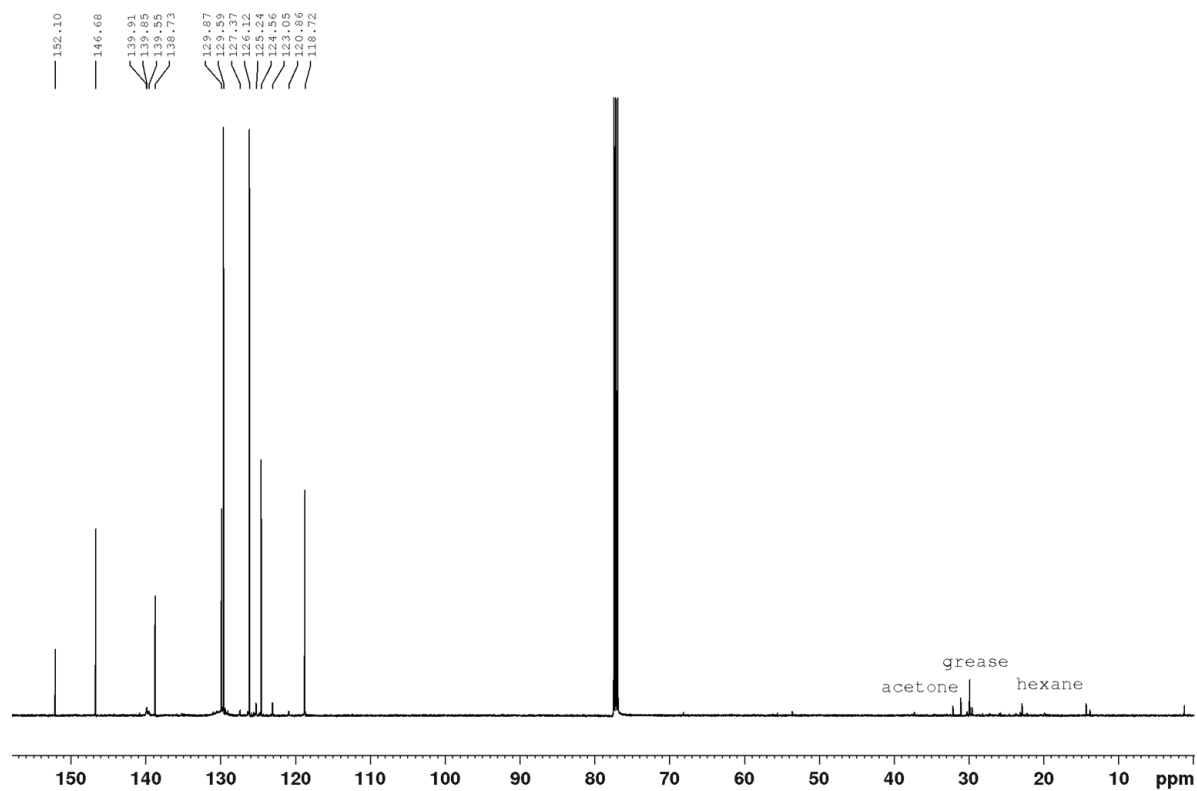


Figure 8.129: <sup>13</sup>C {<sup>1</sup>H} NMR spectrum (126 MHz, 298 K, CDCl<sub>3</sub>) of 4-(bis(2,6-bis(trifluoromethyl)phenyl)boryl)-*N,N*-diphenylaniline (1).

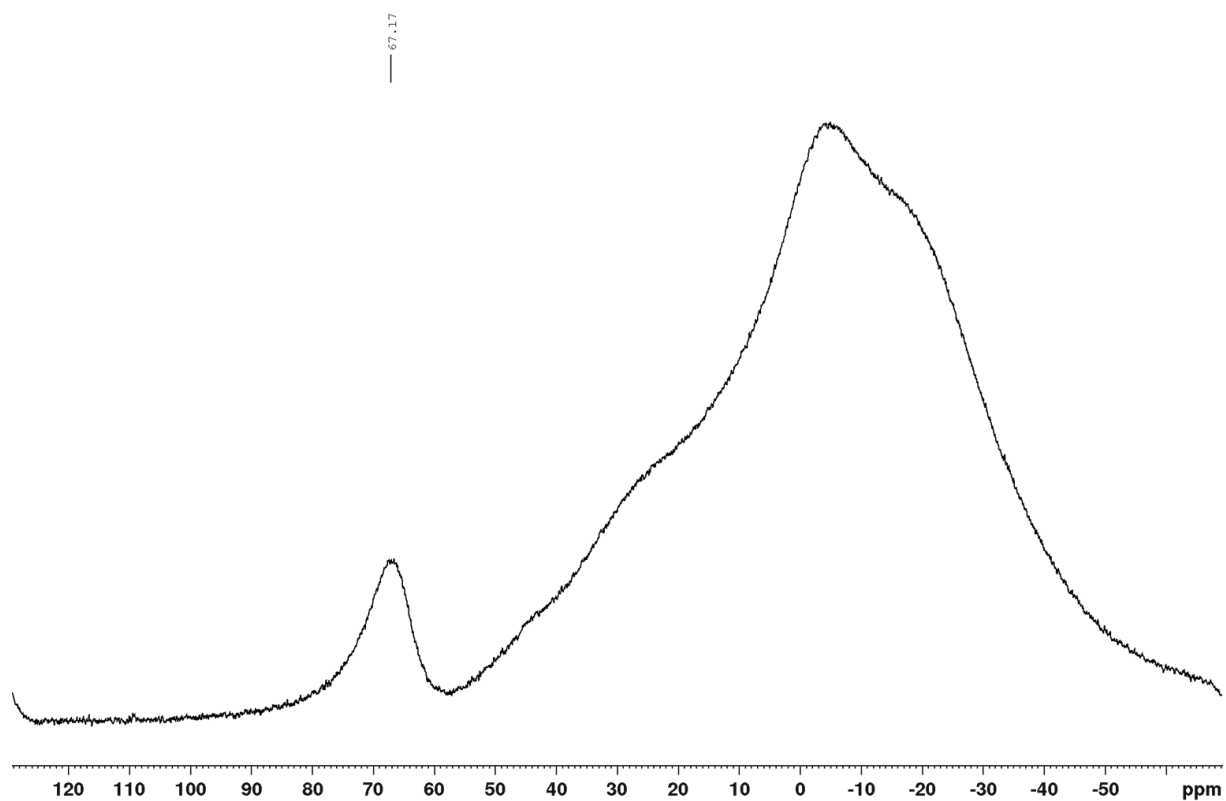


Figure 8.130:  $^{11}\text{B}$  NMR spectrum (128 MHz, 298 K,  $\text{CD}_2\text{Cl}_2$ ) of **4-(bis(2,6-bis(trifluoromethyl)phenyl)boryl)-*N,N*-diphenylaniline (1)**.

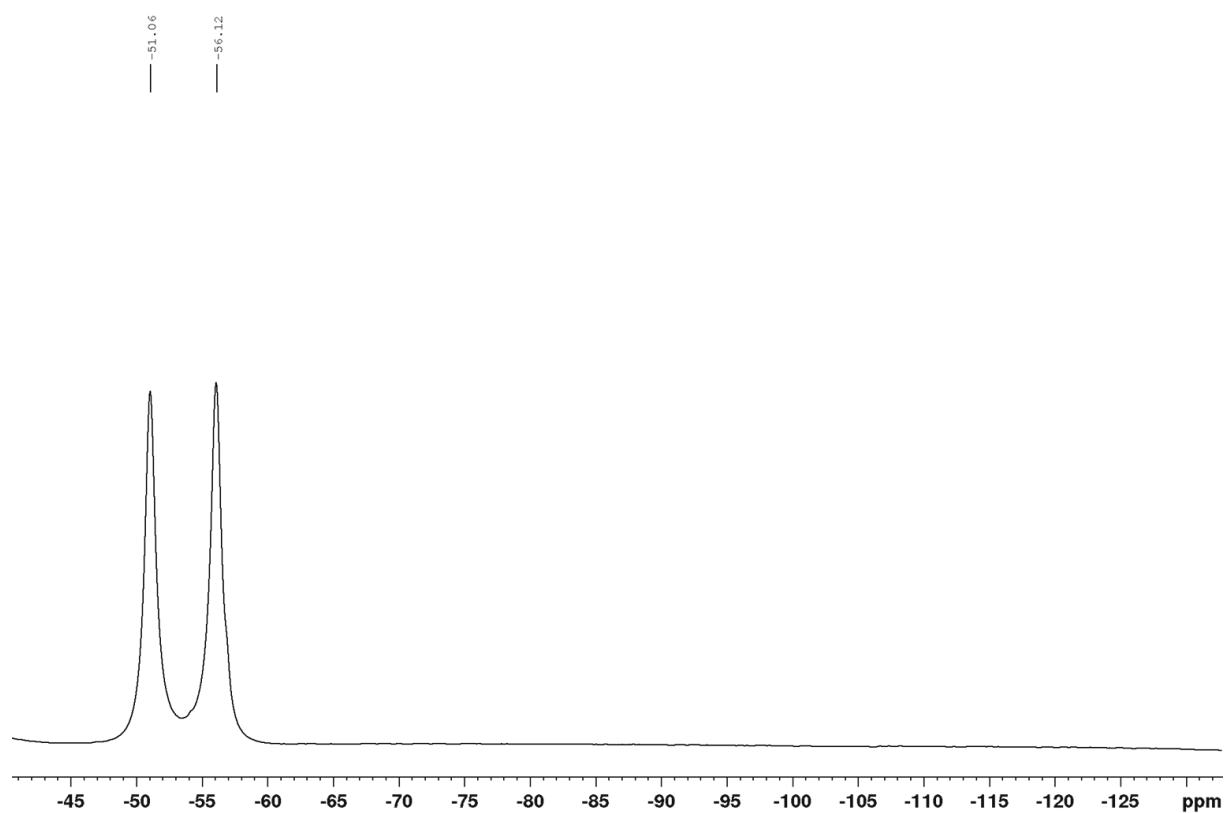


Figure 8.131:  $^{19}\text{F}$  NMR spectrum (377 MHz, 298 K,  $\text{CD}_2\text{Cl}_2$ ) of **4-(bis(2,6-bis(trifluoromethyl)phenyl)boryl)-*N,N*-diphenylaniline (1)**.

## Appendix

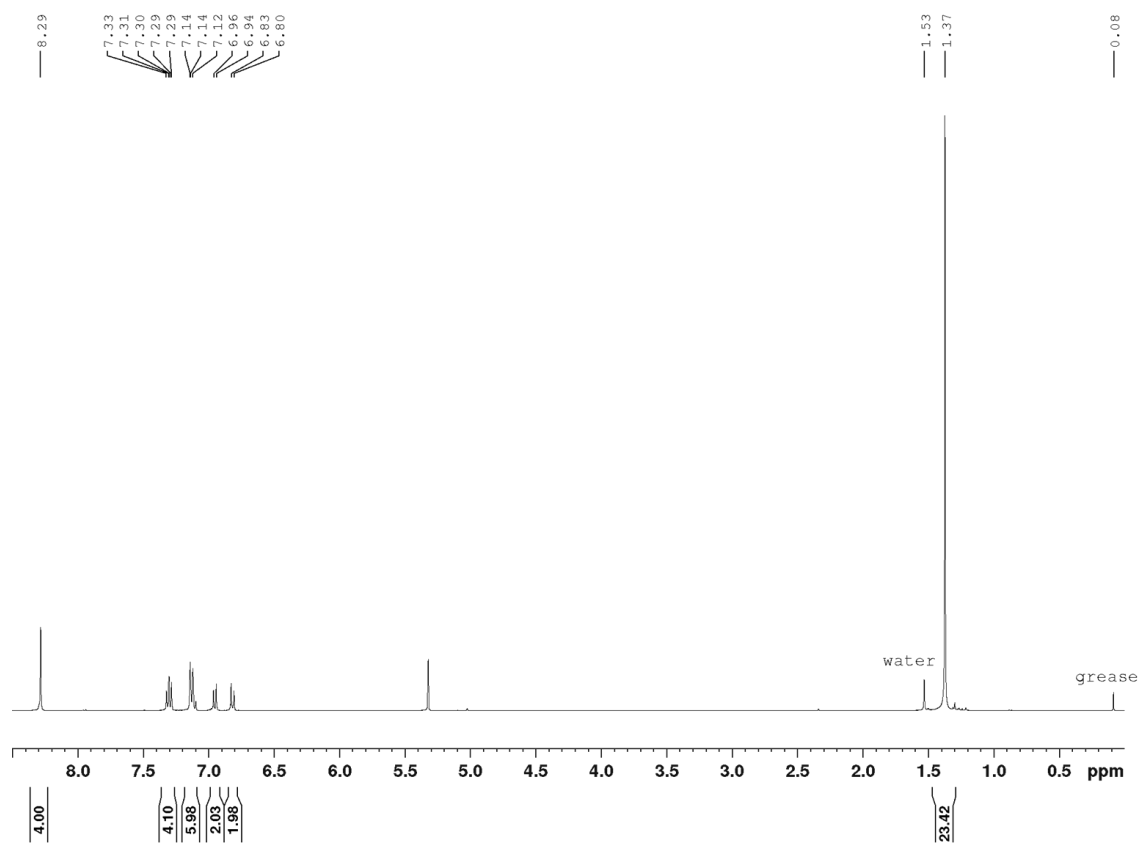


Figure 8.132: <sup>1</sup>H NMR spectrum (400 MHz, 298 K, CD<sub>2</sub>Cl<sub>2</sub>) of 4-(bis(4-(4,4,5,5-tetramethyl-1,3,2-dioxaborolan-2-yl)-2,6-bis(trifluoromethyl)phenyl)boryl)-N,N-diphenylaniline (1-(Bpin)<sub>2</sub>).

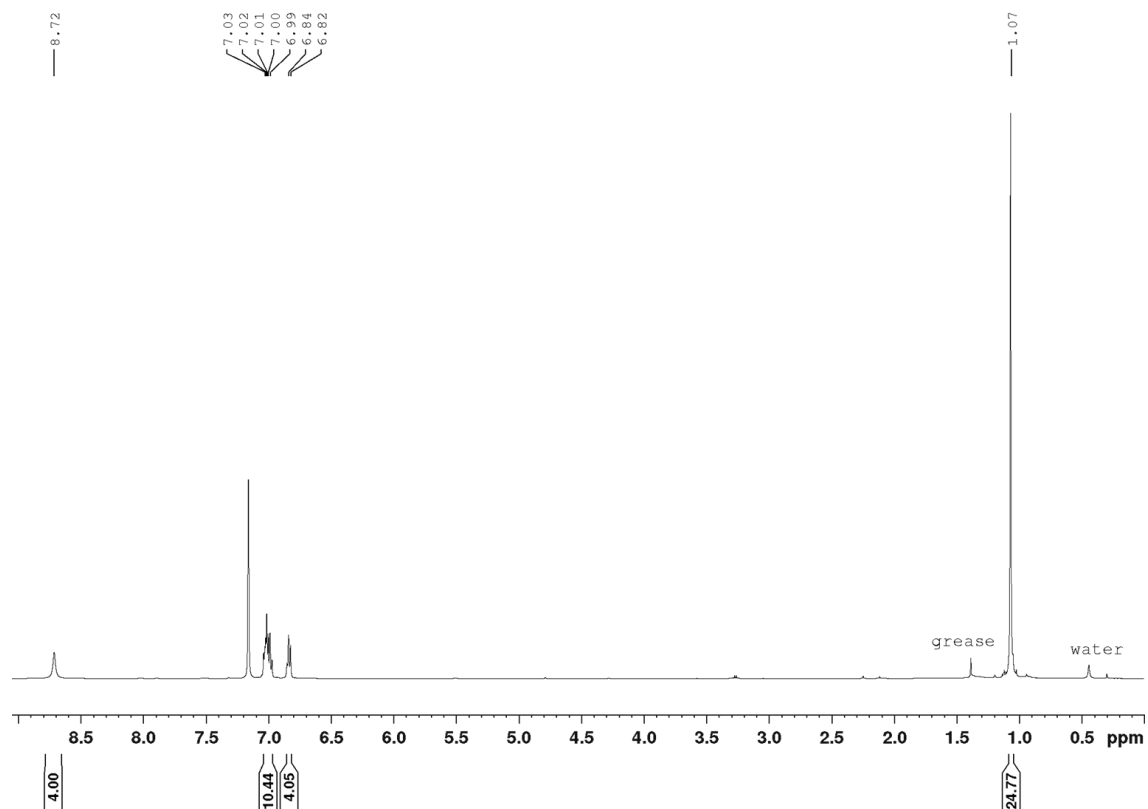


Figure 8.133: <sup>1</sup>H NMR spectrum (500 MHz, 298 K, C<sub>6</sub>D<sub>6</sub>) of 4-(bis(4-(4,4,5,5-tetramethyl-1,3,2-dioxaborolan-2-yl)-2,6-bis(trifluoromethyl)phenyl)boryl)-N,N-diphenylaniline (1-(Bpin)<sub>2</sub>).



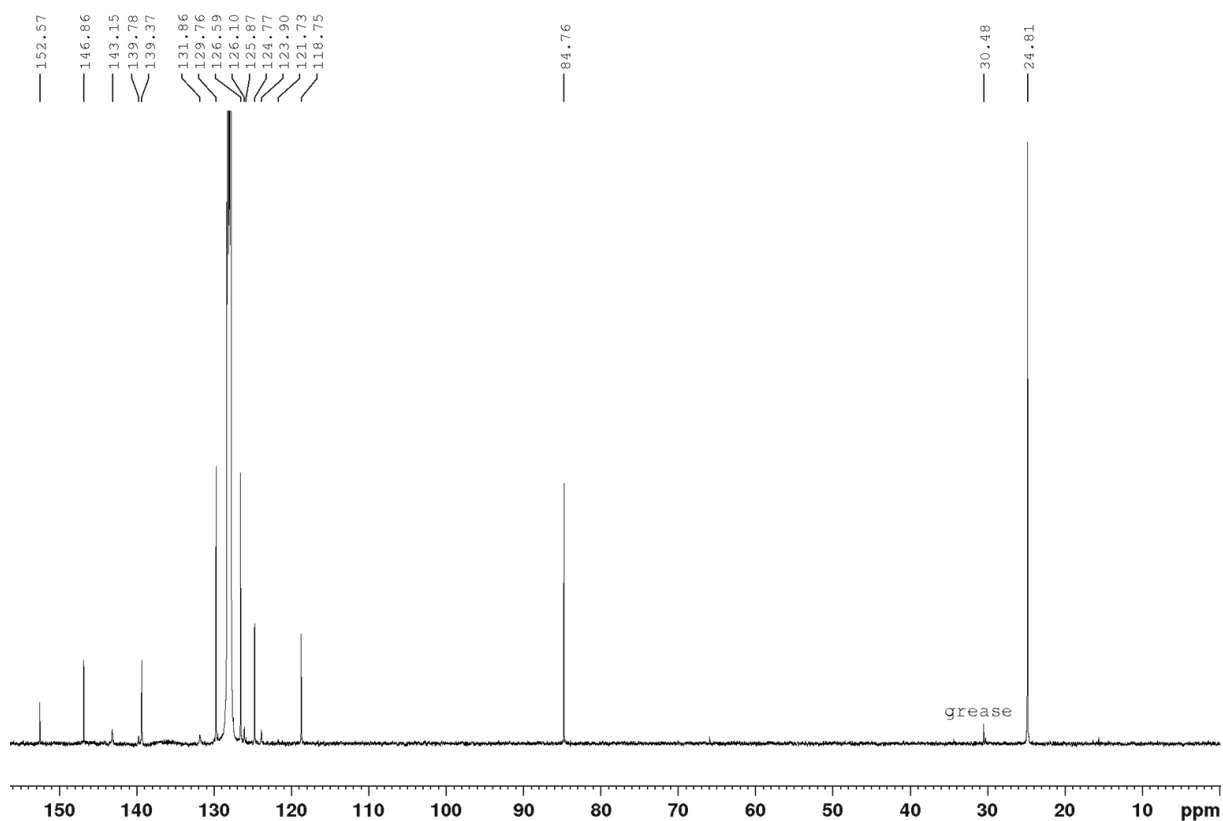


Figure 8.134:  $^{13}\text{C}\{^1\text{H}\}$  NMR spectrum (126 MHz, 298 K,  $\text{CDCl}_3$ ) of 4-(bis(4-(4,4,5,5-tetramethyl-1,3,2-dioxaborolan-2-yl)-2,6-bis(trifluoromethyl)phenyl)boryl)-N,N-diphenylaniline (1-(Bpin) $_2$ ).

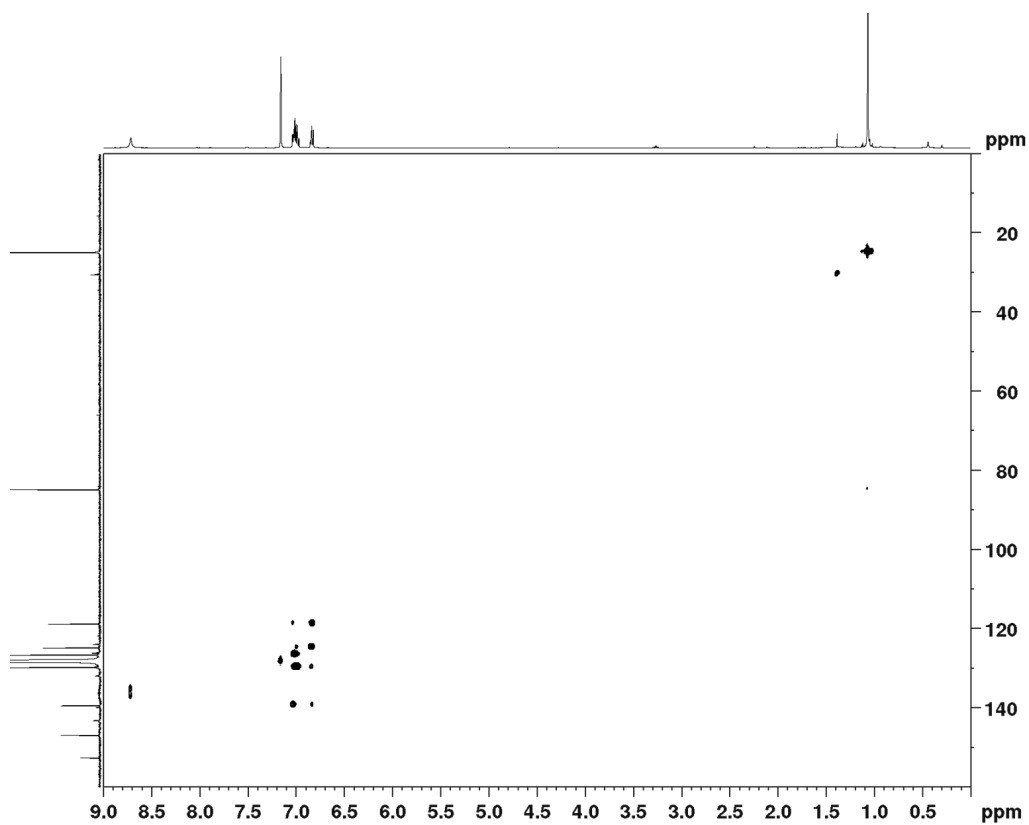


Figure 8.135: HSQC NMR spectrum ( $^{13}\text{C}\{^1\text{H}\}$  126 MHz,  $^1\text{H}$  500 MHz, 298 K,  $\text{CDCl}_3$ ) of 4-(bis(4-(4,4,5,5-tetramethyl-1,3,2-dioxaborolan-2-yl)-2,6-bis(trifluoromethyl)phenyl)boryl)-N,N-diphenylaniline (1-(Bpin) $_2$ ).

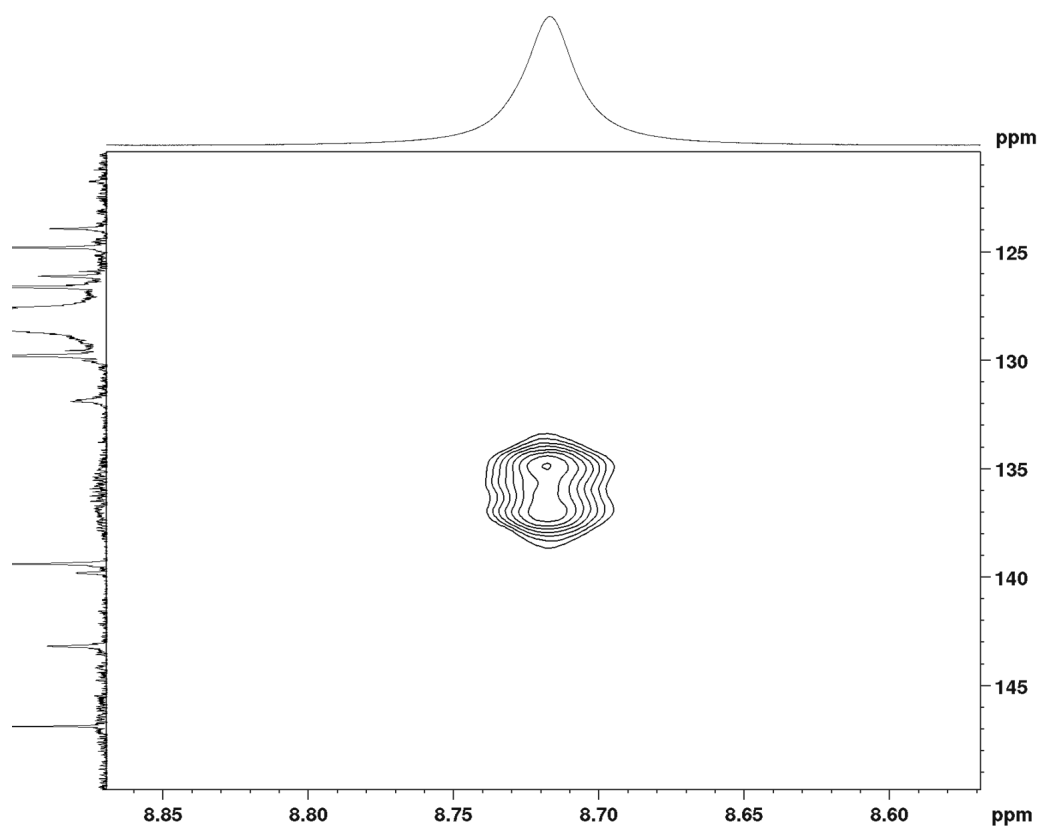


Figure 8.136: HSQC NMR spectrum ( $^{13}\text{C}\{^1\text{H}\}$  126 MHz,  $^1\text{H}$  500 MHz, 298 K,  $\text{CDCl}_3$ ) of 4-(bis(4-(4,4,5,5-tetramethyl-1,3,2-dioxaborolan-2-yl)-2,6-bis(trifluoromethyl)phenyl)boryl)-N,N-diphenylaniline (1-(Bpin) $_2$ ).

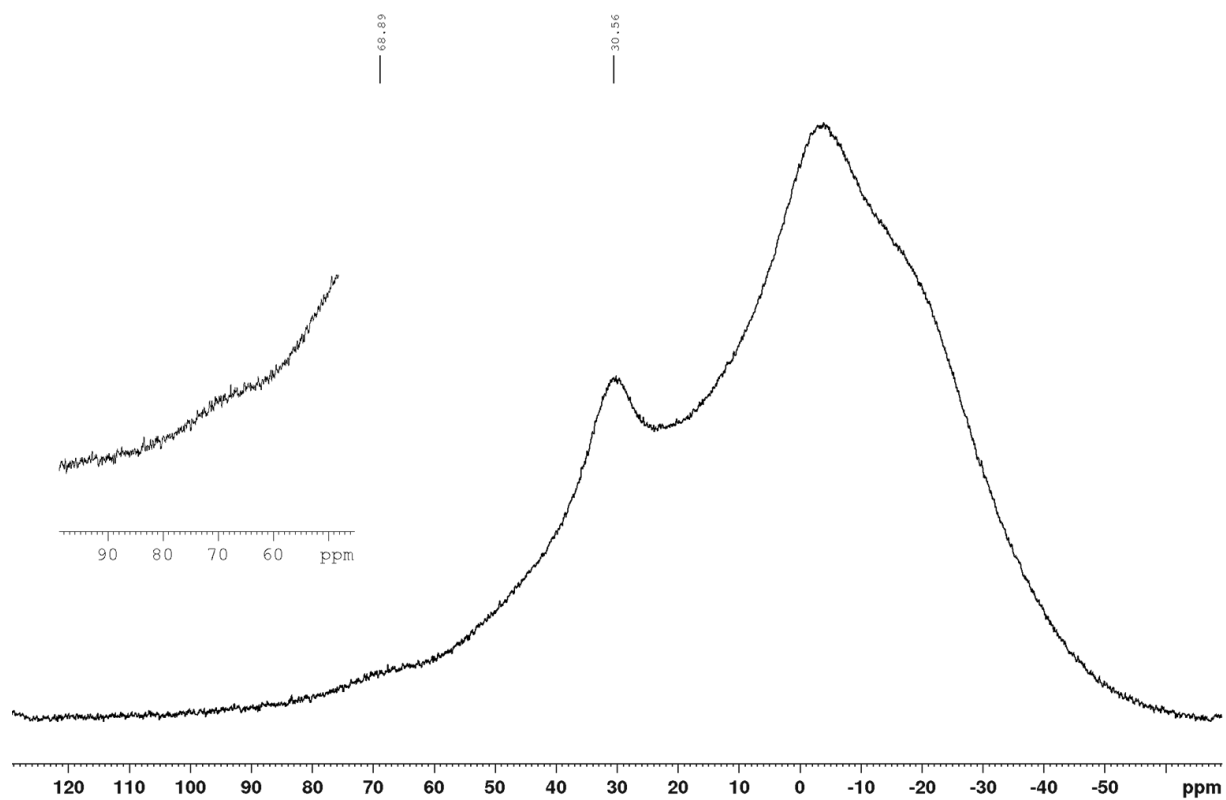


Figure 8.137:  $^{11}\text{B}$  NMR spectrum (128 MHz, 298 K,  $\text{CD}_2\text{Cl}_2$ ) of 4-(bis(4-(4,4,5,5-tetramethyl-1,3,2-dioxaborolan-2-yl)-2,6-bis(trifluoromethyl)phenyl)boryl)-N,N-diphenylaniline (1-(Bpin) $_2$ ).

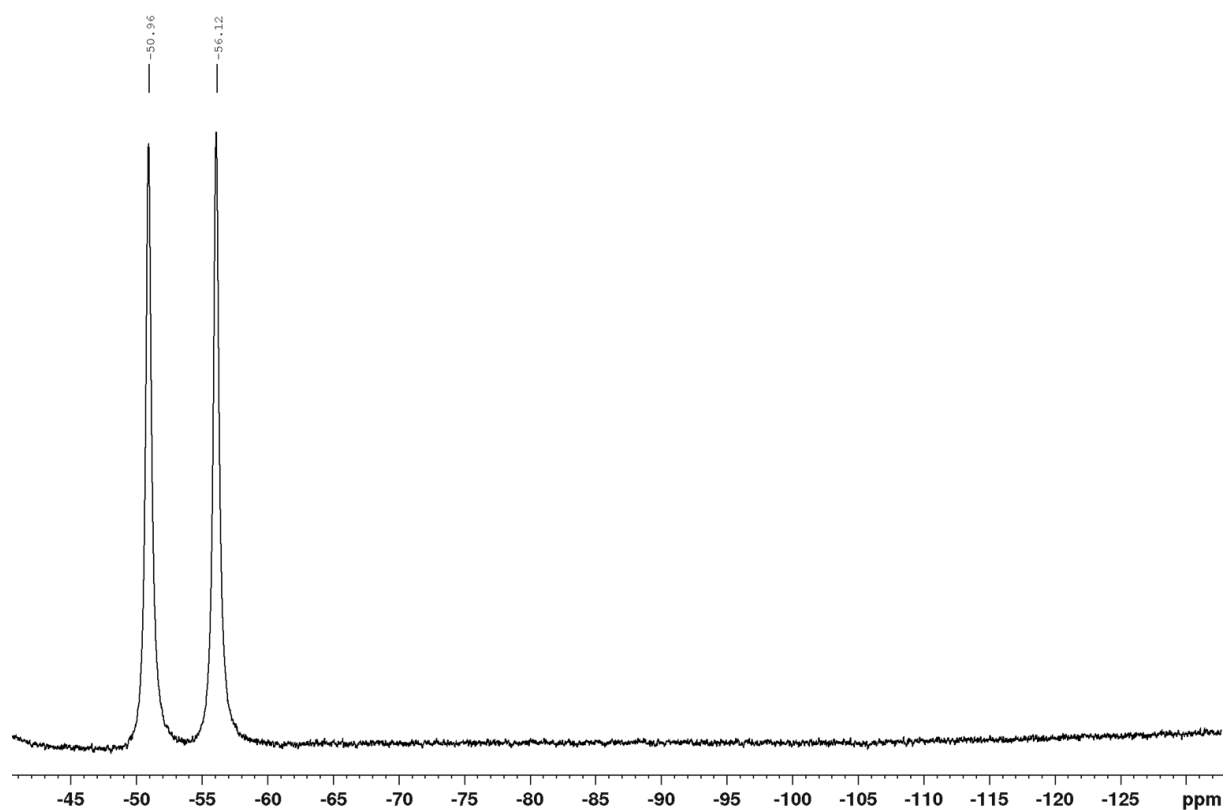


Figure 8.138:  $^{19}\text{F}$  NMR spectrum (377 MHz, 298 K,  $\text{CD}_2\text{Cl}_2$ ) of 4-(bis(4-(4,4,5,5-tetramethyl-1,3,2-dioxaborolan-2-yl)-2,6-bis(trifluoromethyl)phenyl)boryl)-N,N-diphenylaniline (1-(Bpin) $_2$ ).

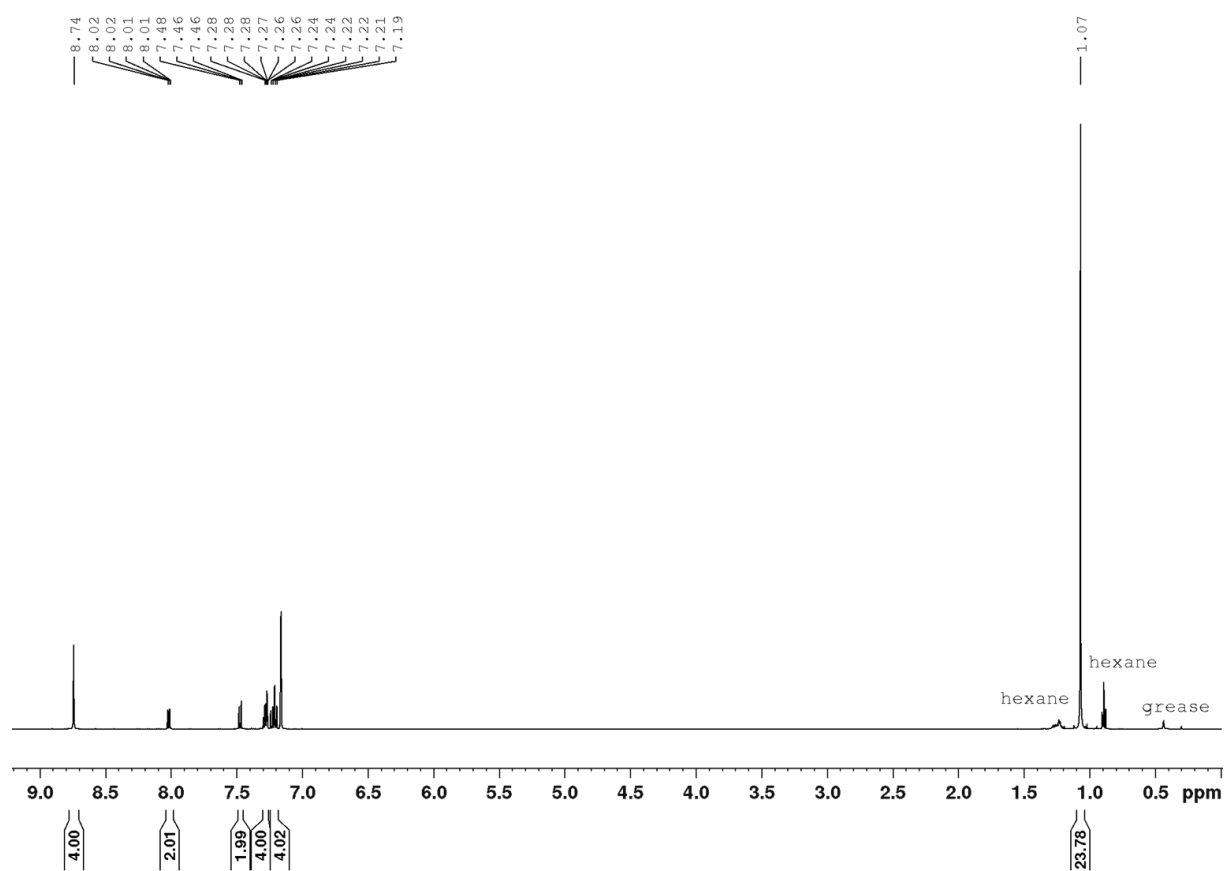


Figure 8.139:  $^1\text{H}$  NMR spectrum (500 MHz, 298 K,  $\text{C}_6\text{D}_6$ ) of 9-(4-(bis(4-(4,4,5,5-tetramethyl-1,3,2-dioxaborolan-2-yl)-2,6-bis(trifluoromethyl)phenyl)boryl)phenyl)-9H-carbazole (Cbz- $\pi$  (1)-(Bpin) $_2$ ).

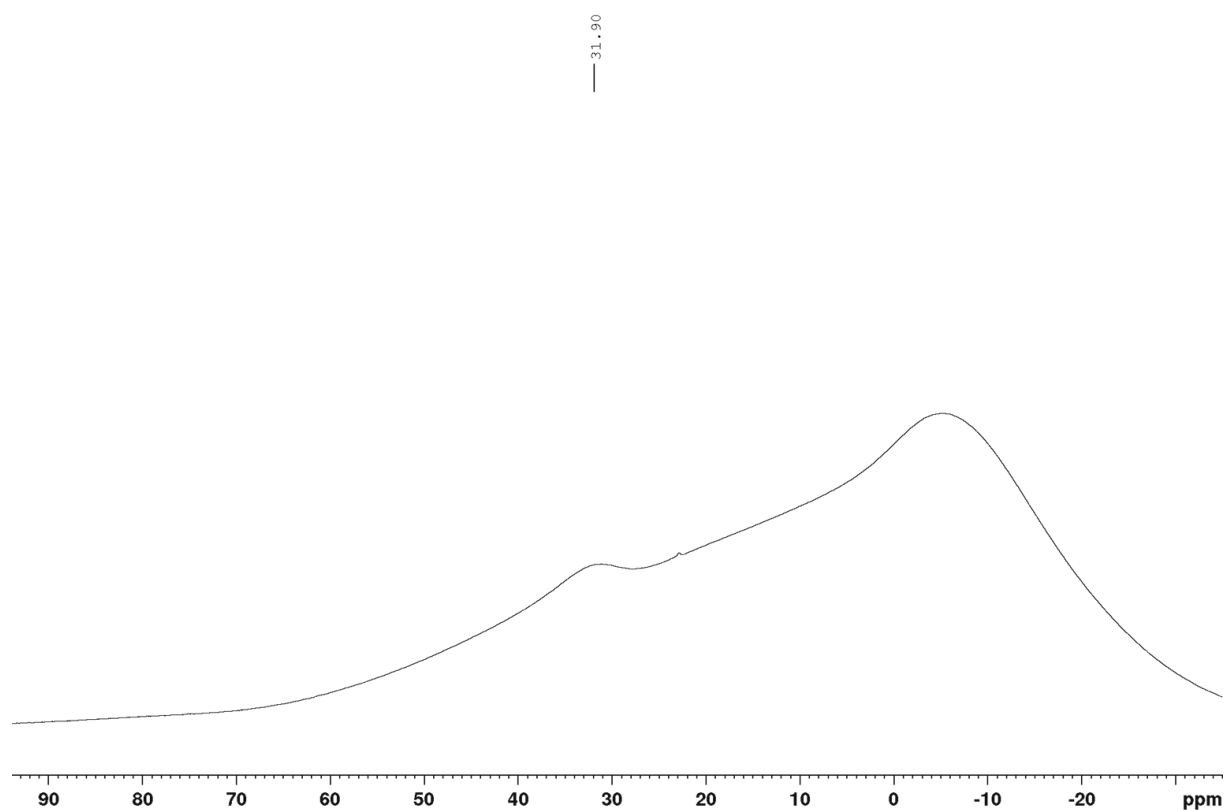


Figure 8.140:  $^{11}\text{B}$  NMR spectrum (160 MHz, 298 K,  $\text{C}_6\text{D}_6$ ) of 9-(4-(bis(4-(4,4,5,5-tetramethyl-1,3,2-dioxaborolan-2-yl)-2,6-bis(trifluoromethyl)phenyl)boryl)phenyl)-9H-carbazole (Cbz- $\pi$  (1)-(Bpin) $_2$ ).

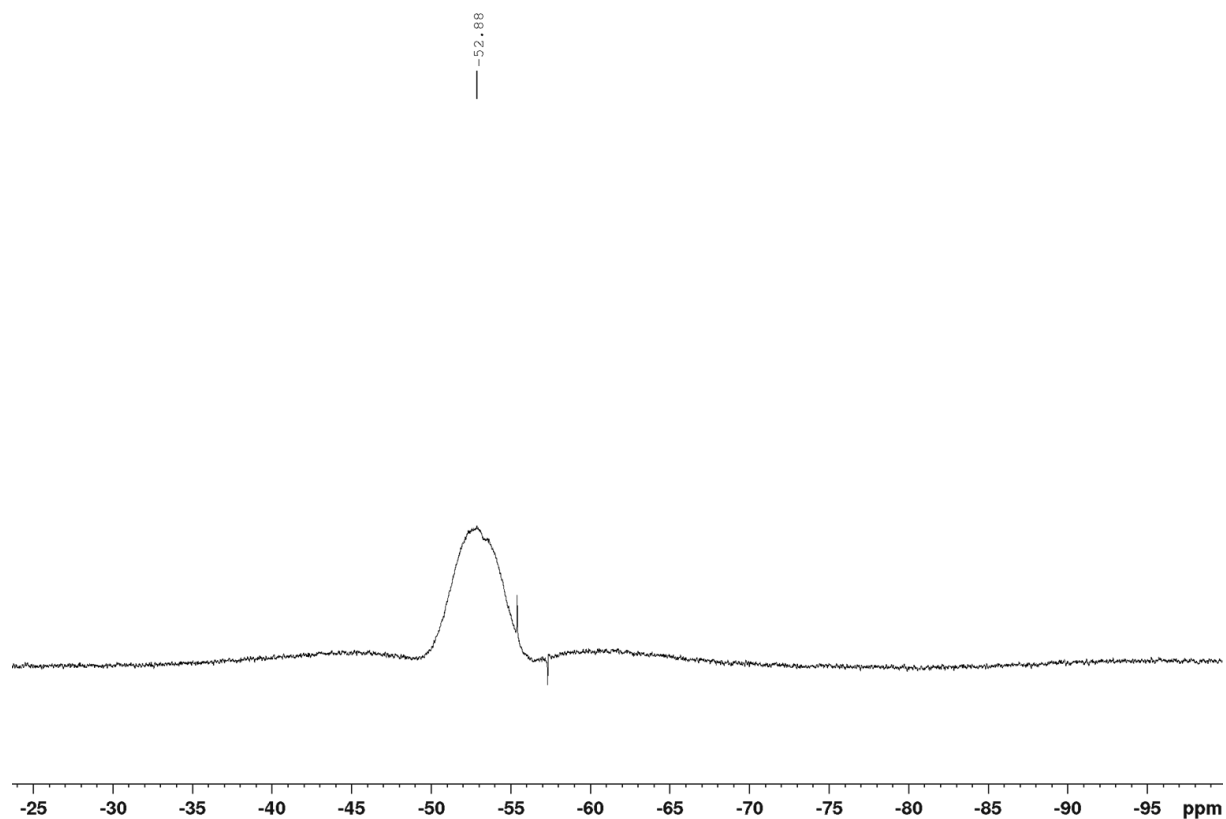


Figure 8.141:  $^{19}\text{F}$  NMR spectrum (471 Hz, 298 K,  $\text{C}_6\text{D}_6$ ) of 9-(4-(bis(4-(4,4,5,5-tetramethyl-1,3,2-dioxaborolan-2-yl)-2,6-bis(trifluoromethyl)phenyl)boryl)phenyl)-9H-carbazole (Cbz- $\pi$  (1)-(Bpin) $_2$ ).

## 8.2 XYZ Coordinates

### 8.2.1 Chapter 1

Cartesian coordinates (Å), energies ( $E$ , Hartree), and number of imaginary vibrational frequencies ( $N_{\text{imag}}$ ) of the optimized structures at ground singlet ( $S_0$ ) and triplet state ( $T_1$ ) calculated at DFT/TZ2P/ZORA-BLYP-D3(BJ)//U-DFT/TZ2P/ZORA-LC-BLYP\* for the benchmark molecules.

<b>B1</b>				C	-4.524698	-4.924442	-1.679159
$E = -16.399$				C	-5.707860	-5.119938	-2.404460
$N_{\text{imag}} = 0$				C	-5.750701	-5.927516	-3.545652
<b><math>S_0</math></b>				C	-4.568486	-6.569084	-3.937777
C	-2.149312	-7.176319	-3.707052	C	-3.375448	-6.424621	-3.220232
C	-1.468305	-3.948517	-0.997891	H	-4.339906	-2.997272	-0.692739
C	-0.651772	-3.658416	0.117424	H	-6.621733	-4.633320	-2.064396
C	-0.192584	-2.369860	0.375722	H	-2.299442	4.718316	-0.042669
C	-1.298130	-1.590082	-1.642468	H	0.145949	4.411458	0.311674
C	-1.785131	-2.875950	-1.860521	N	-0.020501	-0.015655	-0.271042
H	-0.390990	-4.461165	0.803236	C	2.452978	-0.484133	0.063109
H	0.400744	-2.158433	1.260387	C	3.679500	0.132128	0.327765
H	-1.820406	-7.919059	-2.972519	C	1.315888	0.328538	0.005960
H	-1.518404	-0.786985	-2.339546	C	3.775094	1.524079	0.525209
H	-2.410205	-3.065412	-2.730065	C	1.396948	1.740863	0.185694
C	-4.594370	-4.035800	-0.447430	C	2.639649	2.333433	0.450263
H	-5.607598	-4.039966	-0.031262	C	0.056552	2.268003	0.015229
H	-3.902835	-4.351822	0.338059	C	-2.172595	1.321019	-0.448479
H	-3.528361	-6.582753	0.921466	C	-2.691842	2.616183	-0.363439
H	-3.540252	-8.338879	1.141214	C	-0.794728	1.159749	-0.269087
H	-3.906471	-7.626372	-0.443194	C	-1.862536	3.724623	-0.100064
H	1.979164	-10.220529	0.210751	C	-0.490109	3.556457	0.095223
H	0.484816	-10.917251	0.877569	H	2.391666	-1.555617	-0.096716
H	1.448180	-9.794603	1.844450	H	4.577657	-0.478395	0.379128
H	1.376794	-4.965705	-1.318191	H	4.744785	1.970054	0.731166
C	-7.025857	-6.090462	-4.343468	H	2.717839	3.409082	0.589227
H	-4.579656	-7.208939	-4.819680	H	-2.821257	0.473111	-0.642589
H	0.313691	-5.332733	-2.668526	H	-3.759560	2.767755	-0.501461
H	1.782650	-6.291606	-2.417812				
H	-7.909813	-5.892231	-3.727681	<b>B1</b>			
H	-7.110382	-7.101585	-4.758046	$E = -23.480$			
H	-7.048110	-5.388742	-5.189175	$N_{\text{imag}} = 0$			
H	-1.300808	-6.504438	-3.879796	<b><math>T_1</math></b>			
H	-2.363046	-7.693556	-4.647851	C	-2.055328	-7.020079	-3.783855
C	-0.505270	-1.328285	-0.513113	C	-1.459339	-3.951050	-1.005301
C	-1.176619	-6.616921	-0.719469	C	-0.447353	-3.665966	-0.001218
C	-1.800518	-7.611609	0.084030	C	0.024247	-2.418335	0.227705
C	-1.052222	-8.687386	0.575667	C	-1.493630	-1.539596	-1.509312
C	0.306941	-8.843588	0.273442	C	-1.940852	-2.795103	-1.743980
C	0.910205	-7.878500	-0.539589	H	-0.089208	-4.492284	0.608157
C	0.202341	-6.769814	-1.023346	H	0.734922	-2.235737	1.028811
C	-3.273245	-7.536704	0.445834	H	-1.579846	-7.631158	-3.010520
H	-1.545204	-9.430747	1.201535	H	-1.832168	-0.709742	-2.123261
C	1.097276	-10.009737	0.825289	H	-2.663825	-2.964743	-2.538293
H	1.959299	-7.993961	-0.811027	C	-4.622183	-4.129761	-0.480415
C	0.953911	-5.788108	-1.908333	H	-5.669902	-3.961770	-0.211737
B	-1.995377	-5.392015	-1.266498	H	-4.120333	-4.603780	0.369032
C	-3.329030	-5.580180	-2.076152	H	-3.390091	-6.472913	1.194005

## Appendix

H	-3.592333	-8.230050	1.177748	N	-0.018266	-0.013068	-0.273869
H	-3.918717	-7.270141	-0.282918	C	0.982350	2.723936	0.225745
H	1.828010	-10.280517	0.296478	C	-0.386752	2.208253	0.691096
H	0.323936	-10.898466	1.009268	C	-0.831609	0.892611	0.431281
H	1.348987	-9.792141	1.925818	C	3.299951	-0.276447	-1.929462
H	1.148287	-4.954559	-1.437233	C	3.816944	1.005867	-1.722259
C	-6.930844	-6.132923	-4.433930	C	3.045420	1.940062	-1.028155
H	-4.458063	-7.157199	-4.902313	C	1.768475	1.643282	-0.530036
H	0.333569	-5.674242	-2.819354	C	1.256901	0.344461	-0.748364
H	1.861613	-6.364367	-2.236948	C	2.035440	-0.604987	-1.448281
H	-7.826250	-5.985110	-3.822459	C	-1.241787	3.064226	1.400300
H	-6.974342	-7.134102	-4.874310	C	-2.106934	0.483922	0.882912
H	-6.972424	-5.411649	-5.259278	H	3.878009	-1.025535	-2.465535
H	-1.317388	-6.271443	-4.096290	H	4.802419	1.275712	-2.092660
H	-2.271030	-7.654987	-4.648587	H	3.452065	2.934919	-0.868510
C	-0.486191	-1.300137	-0.514607	C	-2.501396	2.663809	1.850651
C	-1.190608	-6.604772	-0.678763	C	-2.930678	1.360153	1.584492
C	-1.821446	-7.540312	0.168250	H	-3.134093	3.357876	2.397587
C	-1.115425	-8.629401	0.669414	H	-3.907178	1.020129	1.921389
C	0.220056	-8.847575	0.354430	C	1.805287	3.169247	1.471671
C	0.839288	-7.936045	-0.489576	H	-0.913243	4.078832	1.608125
C	0.164700	-6.829363	-0.998953	H	-2.448002	-0.524711	0.681162
C	-3.258214	-7.374207	0.583367	H	1.642871	-1.601500	-1.613357
H	-1.629114	-9.333635	1.324144	C	0.768046	3.945840	-0.717148
C	0.969202	-10.018548	0.922002	H	1.280248	3.954327	2.024942
H	1.879907	-8.095761	-0.772293	H	2.783104	3.560293	1.173293
C	0.916332	-5.910269	-1.923326	H	1.963698	2.319591	2.144314
B	-1.980155	-5.364605	-1.265148	H	1.727506	4.350629	-1.054360
C	-3.300910	-5.564043	-2.114164	H	0.224674	4.744497	-0.202348
C	-4.519431	-4.969344	-1.724927	H	0.190214	3.647426	-1.598376
C	-5.677474	-5.172830	-2.471023	C	-0.506511	-1.346370	-0.518945
C	-5.681259	-5.948615	-3.622056	C	-1.206816	-6.624266	-0.671098
C	-4.482561	-6.536522	-4.006402	C	-1.873113	-7.610051	0.109131
C	-3.310454	-6.362729	-3.277163	C	-1.153176	-8.683621	0.645612
H	-4.150030	-3.149172	-0.618291	C	0.218397	-8.846551	0.410914
H	-6.609306	-4.719136	-2.133097	C	0.864274	-7.890030	-0.379453
H	-2.322890	4.649832	0.120742	C	0.185204	-6.783155	-0.905758
H	0.129269	4.369150	0.369073	C	-3.361770	-7.528928	0.397438
N	-0.019736	-0.024283	-0.276746	H	-1.678417	-9.420004	1.253133
C	2.455034	-0.458289	-0.072150	C	0.976979	-10.010456	1.009711
C	3.674115	0.161433	0.163547	H	1.924937	-8.011099	-0.597966
C	1.316615	0.336926	-0.039844	C	0.981733	-5.810520	-1.760828
C	3.756716	1.533924	0.397935	B	-1.993438	-5.402959	-1.265922
C	1.389788	1.727082	0.161268	C	-3.297298	-5.585448	-2.120968
C	2.616786	2.328557	0.385701	C	-4.494631	-4.899049	-1.784997
C	0.039696	2.243912	0.035885	C	-5.651126	-5.087456	-2.553240
C	-2.176340	1.280456	-0.318889	C	-5.663362	-5.916569	-3.679877
C	-2.701446	2.559519	-0.200399	C	-4.479081	-6.587420	-4.011965
C	-0.796951	1.144499	-0.227973	C	-3.313300	-6.451379	-3.249539
C	-1.879195	3.662907	0.027514	H	-4.286752	-2.961349	-0.825086
C	-0.504251	3.511334	0.160227	H	-6.568262	-4.577152	-2.260205
H	2.402810	-1.518879	-0.291557	C	-6.908037	-6.071180	-4.525774
H	4.581403	-0.435189	0.151402	H	-4.467164	-7.243565	-4.881742
H	4.727286	1.988593	0.573559	C	-2.083254	-7.235158	-3.671813
H	2.689171	3.402119	0.537499	C	-1.462266	-3.956659	-0.999354
H	-2.825205	0.422885	-0.457673	C	-0.733718	-3.648671	0.169513
H	-3.775929	2.698623	-0.273954	C	-0.273368	-2.356604	0.420229
				C	-1.211141	-1.623924	-1.695068
				C	-1.695697	-2.911932	-1.919200
				H	-0.532407	-4.437799	0.890334
				H	0.274460	-2.120154	1.328837
				H	-1.803328	-7.974881	-2.914265

### B2

$$E = -18.138$$

$$N_{\text{imag}} = 0$$

$$S_0$$

H	-1.380121	-0.825593	-2.413207
H	-2.262703	-3.120577	-2.823489
C	-4.594350	-3.984033	-0.574861
H	-5.627255	-3.941527	-0.213090
H	-3.958384	-4.311217	0.252264
H	-3.640601	-6.565739	0.839633
H	-3.661732	-8.316823	1.095637
H	-3.951052	-7.638675	-0.519162
H	1.888369	-10.227005	0.442128
H	0.360481	-10.916312	1.037039
H	1.276156	-9.788904	2.043844
H	1.355172	-4.970694	-1.162279
H	0.387389	-5.380311	-2.571587
H	1.847558	-6.313870	-2.204160
H	-7.811739	-5.838985	-3.952083
H	-6.998202	-7.089913	-4.919986
H	-6.879479	-5.389775	-5.387691
H	-1.213351	-6.584086	-3.815191
H	-2.266648	-7.760464	-4.614497

**B2** $E = -25.652$  $N_{\text{imag}} = 0$  $T_1$ 

N	-0.016649	-0.002687	-0.272022
C	0.988650	2.719592	0.231176
C	0.079391	1.961396	1.173651
C	-0.421463	0.680241	0.878420
C	2.139709	0.401166	-3.228245
C	2.548482	1.723033	-3.086161
C	2.149015	2.448450	-1.974987
C	1.315961	1.907074	-1.002751
C	0.858322	0.589506	-1.187178
C	1.314026	-0.167226	-2.283465
C	-0.332699	2.564337	2.356428
C	-1.375983	0.085014	1.725024
H	2.479479	-0.193390	-4.070923
H	3.200347	2.179316	-3.825485
H	2.509190	3.466286	-1.853636
C	-1.226637	1.951528	3.220032
C	-1.762096	0.711047	2.889672
H	-1.526144	2.453312	4.135577
H	-2.495961	0.237812	3.535067
C	2.303890	3.063558	0.959453
H	0.046664	3.551589	2.605128
H	-1.813485	-0.865082	1.443633
H	1.018563	-1.205811	-2.368910
C	0.285737	4.025900	-0.190349
H	2.100086	3.659728	1.853655
H	2.962757	3.643550	0.306904
H	2.830889	2.153607	1.262895
H	0.924135	4.601598	-0.866749
H	0.072087	4.645780	0.685072
H	-0.657847	3.813085	-0.702360
C	-0.499164	-1.311627	-0.513432
C	-1.433729	-6.575640	-0.397593
C	-2.304602	-7.396020	0.353397
C	-1.812678	-8.463068	1.099651
C	-0.457401	-8.772632	1.134477
C	0.401129	-7.976266	0.389508
C	-0.059125	-6.894397	-0.360990
C	-3.784212	-7.122921	0.397544

H	-2.513100	-9.075379	1.669109
C	0.056419	-9.917039	1.961479
H	1.466643	-8.209517	0.379245
C	0.956698	-6.107250	-1.145885
B	-1.983823	-5.361833	-1.262439
C	-3.067144	-5.610679	-2.397425
C	-4.322902	-4.966350	-2.375314
C	-5.267946	-5.214014	-3.370908
C	-5.017471	-6.084999	-4.422035
C	-3.782274	-6.723346	-4.446433
C	-2.821622	-6.504890	-3.463137
H	-4.255116	-3.027282	-1.419384
H	-6.237111	-4.716842	-3.312962
C	-6.033941	-6.319712	-5.503400
H	-3.559027	-7.419387	-5.256054
C	-1.504581	-7.223002	-3.587616
C	-1.469747	-3.955074	-1.002094
C	-0.681352	-3.621914	0.155030
C	-0.227779	-2.358410	0.404990
C	-1.259421	-1.594729	-1.677320
C	-1.733587	-2.856849	-1.894214
H	-0.446299	-4.414983	0.862154
H	0.374052	-2.147942	1.286982
H	-1.261201	-7.779542	-2.676761
H	-1.487730	-0.788080	-2.371307
H	-2.330534	-3.049242	-2.783533
C	-4.705380	-4.016803	-1.270919
H	-5.792475	-3.889871	-1.229634
H	-4.355085	-4.371363	-0.296752
H	-3.990911	-6.156009	0.872611
H	-4.306460	-7.896178	0.970302
H	-4.215994	-7.077963	-0.607525
H	1.038737	-10.249203	1.610596
H	-0.628390	-10.771114	1.927892
H	0.162366	-9.626796	3.014397
H	1.215153	-5.169132	-0.638807
H	0.574486	-5.828628	-2.132607
H	1.877864	-6.685489	-1.275120
H	-7.039763	-6.049013	-5.166595
H	-6.046263	-7.369060	-5.816880
H	-5.810000	-5.717562	-6.392987
H	-0.684362	-6.513329	-3.751529
H	-1.518802	-7.919666	-4.432109

**B3** $E = -16.605$  $N_{\text{imag}} = 0$  $S_0$ 

N	-2.537848	2.175404	-0.189336
O	-1.435728	4.745791	0.243775
C	-2.618155	4.358423	0.877355
C	-3.187811	3.085376	0.667255
C	0.753822	1.943998	-1.953434
C	1.268480	3.218428	-1.715028
C	0.517531	4.136354	-0.964921
C	-0.730588	3.776865	-0.472764
C	-1.265792	2.492889	-0.705085
C	-0.502404	1.580980	-1.449229
C	-3.226049	5.290903	1.708171
C	-4.396759	2.785441	1.312657
H	1.323077	1.220437	-2.531071
H	2.241914	3.505844	-2.102286

## Appendix

H	0.887906	5.137157	-0.758906
C	-4.435024	4.979324	2.348786
C	-5.015663	3.727252	2.145733
H	-4.909045	5.713515	2.994106
H	-5.953387	3.470795	2.631654
H	-0.897334	0.588118	-1.635769
H	-2.747654	6.257822	1.840207
H	-4.852617	1.813477	1.157760
C	-3.071140	0.851920	-0.369297
C	-3.876118	-4.408040	-0.367400
C	-4.509942	-5.366278	0.472079
C	-3.774835	-6.438108	0.990974
C	-2.421346	-6.626518	0.681845
C	-1.809256	-5.697986	-0.166653
C	-2.502453	-4.593062	-0.678338
C	-5.978252	-5.256818	0.843408
H	-4.273951	-7.152677	1.644781
C	-1.645695	-7.787758	1.263561
H	-0.764812	-5.839852	-0.443068
C	-1.744024	-3.651855	-1.600506
B	-4.678511	-3.187200	-0.941132
C	-6.032422	-3.367287	-1.713953
C	-7.197898	-2.654494	-1.325250
C	-8.401429	-2.846104	-2.016784
C	-8.493171	-3.704502	-3.117376
C	-7.339835	-4.400602	-3.502735
C	-6.128321	-4.261972	-2.816289
H	-6.895377	-0.698942	-0.428301
H	-9.292348	-2.315084	-1.682716
C	-9.789360	-3.865844	-3.880497
H	-7.389427	-5.079197	-4.353760
C	-4.937169	-5.075354	-3.291039
C	-4.108611	-1.744680	-0.735001
C	-3.310585	-1.428047	0.385416
C	-2.807977	-0.142502	0.580189
C	-3.846516	0.566072	-1.497623
C	-4.370278	-0.716098	-1.664582
H	-3.085816	-2.206065	1.111319
H	-2.204206	0.099788	1.451062
H	-4.628065	-5.805975	-2.535968
H	-4.037340	1.352549	-2.223299
H	-4.991078	-0.931627	-2.531107
C	-7.212072	-1.707530	-0.135965
H	-8.222855	-1.631603	0.278843
H	-6.540359	-2.029525	0.664668
H	-6.219178	-4.278812	1.275206
H	-6.246968	-6.022224	1.578339
H	-6.621065	-5.382079	-0.034444
H	-0.765673	-8.024222	0.655895
H	-2.269139	-8.686244	1.337652
H	-1.293934	-7.551250	2.277616
H	-1.325162	-2.804185	-1.044535
H	-2.378731	-3.231795	-2.385666
H	-0.912215	-4.177711	-2.081240
H	-10.650677	-3.574401	-3.270002
H	-9.931257	-4.901533	-4.210370
H	-9.792126	-3.234791	-4.780331
H	-4.065628	-4.443177	-3.495346
H	-5.182207	-5.614815	-4.211435

**B3**

$E = -23.878$

$N_{\text{imag}} = 0$

**T<sub>1</sub>**

N	-2.471005	2.154681	-0.099078
O	-1.424511	4.719765	0.300603
C	-2.236629	4.153458	1.231154
C	-2.785126	2.872767	1.041607
C	-0.409017	2.646443	-3.110405
C	0.060255	3.945564	-2.893665
C	-0.293749	4.631174	-1.749690
C	-1.129705	4.022634	-0.827793
C	-1.632246	2.726664	-1.039678
C	-1.240196	2.038752	-2.198265
C	-2.521659	4.899311	2.363190
C	-3.664141	2.371403	2.013867
H	-0.110817	2.105583	-4.002795
H	0.716157	4.414572	-3.620335
H	0.068842	5.633101	-1.541855
C	-3.370117	4.377254	3.317978
C	-3.945387	3.116022	3.135710
H	-3.600035	4.955899	4.207097
H	-4.627325	2.719839	3.881234
H	-1.602443	1.028278	-2.349832
H	-2.074085	5.883121	2.464788
H	-4.111653	1.396668	1.856151
C	-3.004094	0.845959	-0.302058
C	-4.038400	-4.389678	-0.115881
C	-4.851050	-5.190248	0.716665
C	-4.319270	-6.276578	1.403736
C	-2.977799	-6.626230	1.299514
C	-2.176817	-5.849517	0.476040
C	-2.678425	-4.749227	-0.219182
C	-6.309128	-4.873906	0.912113
H	-4.976391	-6.871821	2.038864
C	-2.418520	-7.792504	2.063578
H	-1.125085	-6.112857	0.357405
C	-1.721987	-3.986269	-1.096333
B	-4.640202	-3.153874	-0.916171
C	-5.839234	-3.375535	-1.937368
C	-7.074162	-2.710682	-1.787117
C	-8.119908	-2.937906	-2.681708
C	-7.994173	-3.808429	-3.753808
C	-6.779292	-4.466930	-3.905638
C	-5.720525	-4.267820	-3.025639
H	-6.913382	-0.763168	-0.862559
H	-9.068910	-2.423944	-2.524228
C	-9.119808	-4.023468	-4.725150
H	-6.651532	-5.162955	-4.735527
C	-4.435351	-5.005997	-3.285697
C	-4.071434	-1.764522	-0.703709
C	-3.150559	-1.461264	0.352937
C	-2.638190	-0.207421	0.558728
C	-3.899305	0.603783	-1.362398
C	-4.413439	-0.653255	-1.543112
H	-2.856973	-2.263743	1.026737
H	-1.940363	-0.019074	1.372846
H	-4.115578	-5.579074	-2.409627
H	-4.186212	1.421390	-2.021516
H	-5.104463	-0.822693	-2.366481
C	-7.327160	-1.756762	-0.650338
H	-8.401837	-1.644159	-0.472268
H	-6.847909	-2.096588	0.272123
H	-6.436826	-3.897860	1.395327



H	-6.790679	-5.627596	1.543343
H	-6.841730	-4.822296	-0.042773
H	-1.463804	-8.120653	1.640859
H	-3.108881	-8.642577	2.053997
H	-2.242758	-7.529422	3.113963
H	-1.362414	-3.076841	-0.599236
H	-2.202181	-3.658555	-2.022704
H	-0.851271	-4.601916	-1.345636
H	-10.076172	-3.705110	-4.298667
H	-9.204179	-5.077648	-5.009496
H	-8.961327	-3.450543	-5.647151
H	-3.622363	-4.307458	-3.517140
H	-4.542971	-5.690040	-4.133575

**B4**

$E = -19.861$

$N_{\text{imag}} = 0$

**S<sub>0</sub>**

N	-0.982465	1.488642	-0.352755
C	0.308458	4.105662	0.119417
C	-1.119179	3.933415	-0.418189
C	-1.702813	2.664882	-0.632565
C	2.283265	0.313953	0.981706
C	2.936811	1.526146	1.223512
C	2.271844	2.720086	0.936634
C	0.970375	2.752371	0.414910
C	0.322249	1.520446	0.174039
C	0.991253	0.309581	0.462408
C	-1.884323	5.069248	-0.720680
C	-3.021199	2.576710	-1.133523
H	2.775791	-0.631822	1.195137
H	3.945650	1.544067	1.627367
H	2.784667	3.659315	1.124535
C	-3.186934	4.987140	-1.217163
C	-3.753587	3.725400	-1.421964
H	-3.746809	5.891802	-1.439315
H	-4.766249	3.630023	-1.806755
C	0.258645	4.943288	1.432007
H	-1.448077	6.051966	-0.564319
H	-3.468581	1.603044	-1.296158
H	0.493305	-0.635045	0.277176
C	1.159860	4.861159	-0.944950
H	-0.191097	5.924538	1.251633
H	1.264926	5.101599	1.831992
H	-0.337066	4.424121	2.190373
H	2.182302	5.016411	-0.585984
H	0.724287	5.840587	-1.167140
H	1.203923	4.283627	-1.874539
H	-2.248104	-7.731621	1.026295
B	-3.519269	-3.650644	-1.243394
O	-1.947186	-2.210482	-3.234240
C	-2.119625	-1.657173	-1.983217
C	-2.865933	-2.287174	-0.963578
C	-3.539937	-5.873645	-4.422112
C	-2.762707	-5.086089	-5.294284
C	-2.241820	-3.866151	-4.874972
C	-2.503938	-3.433172	-3.566843
C	-3.277230	-4.190606	-2.660070
C	-3.787212	-5.426088	-3.131185
C	-1.495236	-0.415388	-1.794387
C	-2.962622	-1.605995	0.274172
H	-3.940443	-6.824720	-4.763758

H	-2.565240	-5.430939	-6.306398
H	-1.640643	-3.247369	-5.535555
C	-1.619202	0.213698	-0.561571
C	-2.354991	-0.376605	0.482849
H	-2.432425	0.141502	1.434391
H	-4.385278	-6.023576	-2.447036
H	-0.926569	0.043949	-2.597209
H	-3.533286	-2.075110	1.071717
C	-4.359269	-4.419799	-0.162924
C	-5.746658	-4.197400	-0.045237
C	-6.479516	-4.886403	0.931286
C	-5.868487	-5.795848	1.801469
C	-4.488783	-6.008193	1.674999
C	-3.731192	-5.335575	0.709801
H	-7.844317	-2.362183	0.474505
H	-7.551185	-4.715524	1.022857
H	-5.191274	-6.509451	4.457237
H	-3.995789	-6.711158	2.343368
H	-2.409906	-7.334883	-0.694682
C	-6.442190	-3.209585	-0.980128
H	-5.674444	-2.794085	-1.648253
C	-7.487630	-3.906761	-1.877020
H	-7.024639	-4.714844	-2.454652
H	-7.934059	-3.191791	-2.579097
H	-8.295148	-4.340379	-1.274945
C	-7.057073	-2.021946	-0.208878
H	-6.292836	-1.507605	0.384709
H	-7.500455	-1.297486	-0.903093
C	-6.686883	-6.531311	2.855743
H	-7.726540	-6.191398	2.750536
C	-6.670155	-8.059669	2.628329
H	-7.026577	-8.308850	1.622265
H	-7.312226	-8.566743	3.359190
H	-5.654805	-8.460519	2.735270
C	-6.223410	-6.179590	4.287275
H	-6.263393	-5.097374	4.456103
H	-6.861810	-6.670523	5.032210
C	-2.227387	-5.582707	0.599824
H	-1.851546	-4.961335	-0.225336
C	-1.479241	-5.137304	1.874826
H	-0.396880	-5.269933	1.755460
H	-1.799480	-5.725157	2.743407
H	-1.675836	-4.080990	2.090496
C	-1.909535	-7.049191	0.237498
H	-0.829517	-7.190565	0.107615

**B4**

$E = -28.518$

$N_{\text{imag}} = 0$

**T<sub>1</sub>**

N	-0.989585	1.484455	-0.297206
C	0.413936	4.031145	0.085381
C	-0.863300	3.878918	-0.706290
C	-1.524288	2.642221	-0.844765
C	1.876753	0.278379	1.651620
C	2.540854	1.474136	1.915803
C	2.045355	2.665139	1.412970
C	0.880329	2.713260	0.657862
C	0.196856	1.503317	0.428088
C	0.719634	0.287430	0.911014
C	-1.443003	4.991653	-1.300674
C	-2.757195	2.564054	-1.524186

## Appendix

H	2.272817	-0.662349	2.020537	C	-6.122869	-8.263632	2.747508
H	3.455099	1.474037	2.501446	H	-6.376763	-8.630092	1.747989
H	2.588549	3.584938	1.607289	H	-6.688075	-8.845557	3.484115
C	-2.637057	4.907806	-1.998274	H	-5.056412	-8.454912	2.913866
C	-3.299985	3.687336	-2.100522	C	-6.110840	-6.289759	4.297671
H	-3.061450	5.799429	-2.449703	H	-6.357821	-5.230399	4.418750
H	-4.248209	3.619654	-2.624093	H	-6.674686	-6.864465	5.040940
C	0.168231	5.025937	1.238948	C	-2.123228	-5.209497	0.766964
H	-0.953044	5.956339	-1.210452	H	-1.799578	-4.238008	0.372337
H	-3.266475	1.609840	-1.577826	C	-1.448359	-5.409148	2.119476
H	0.198503	-0.634742	0.685003	H	-0.363479	-5.297714	2.017317
C	1.516895	4.589512	-0.838072	H	-1.634259	-6.412071	2.521309
H	-0.139725	5.997475	0.844478	H	-1.800939	-4.679677	2.856036
H	1.083710	5.169066	1.818486	C	-1.659055	-6.283389	-0.219875
H	-0.613908	4.660188	1.910214	H	-0.566618	-6.281980	-0.313336
H	2.443125	4.738745	-0.277576				
H	1.211655	5.553073	-1.253882	<b>B5</b>			
H	1.718496	3.902870	-1.665114	$E = -20.465$			
H	-1.970526	-7.275658	0.129271	$N_{\text{imag}} = 0$			
B	-3.603435	-3.576190	-1.231554	$S_0$			
O	-2.230566	-2.033726	-3.261080	C	-4.554745	0.690536	2.911702
C	-2.292049	-1.546438	-1.979509	N	-5.169363	4.438521	1.121950
C	-2.945309	-2.256641	-0.937697	C	-6.453982	2.024555	-3.894532
C	-3.892153	-5.598929	-4.538705	C	-5.484669	2.625975	-0.249100
C	-3.203737	-4.766648	-5.417462	C	-4.376010	1.842283	3.713070
C	-2.658934	-3.574970	-4.954928	C	-4.545289	3.153881	3.251071
C	-2.808197	-3.231824	-3.618936	C	-4.910702	3.286436	1.893101
C	-3.491656	-4.038221	-2.697903	C	-5.105012	2.145640	1.061566
C	-4.028082	-5.233758	-3.208853	C	-4.925556	0.852530	1.577173
C	-1.676418	-0.329067	-1.797157	C	-4.342723	4.315648	4.202011
C	-2.911970	-1.621684	0.348146	C	-5.512137	4.049516	-0.189490
H	-4.320291	-6.531861	-4.896726	C	-5.828339	4.827294	-1.325052
H	-3.089527	-5.042272	-6.462353	C	-6.123521	4.112438	-2.493143
H	-2.116591	-2.904762	-5.616873	C	-6.115552	2.700796	-2.581514
C	-1.671234	0.241020	-0.501478	C	-5.790103	1.959483	-1.446005
C	-2.287018	-0.415296	0.564966	H	-5.768941	0.872323	-1.487362
H	-2.274770	0.036823	1.554265	C	-5.863181	6.341520	-1.343414
H	-4.567063	-5.883352	-2.520884	H	-6.371232	4.684646	-3.386412
H	-1.189172	0.165369	-2.632556	C	-4.346363	-0.685433	3.510861
H	-3.405002	-2.126154	1.175748	H	-4.094124	1.706853	4.756571
C	-4.355600	-4.429587	-0.130273	H	-5.076456	-0.016342	0.939732
C	-5.760336	-4.462705	-0.078247	H	-6.380776	0.935398	-3.808310
C	-6.409440	-5.219973	0.894984	H	-5.776093	2.347554	-4.695516
C	-5.704979	-5.955845	1.836834	H	-7.474358	2.270260	-4.217543
C	-4.316009	-5.918814	1.788329	H	-4.121328	3.939005	5.205179
C	-3.639413	-5.174402	0.827924	H	-5.232744	4.951188	4.265011
H	-7.284097	-2.210513	0.448509	H	-3.514462	4.961721	3.890667
H	-7.497482	-5.241202	0.928419	H	-5.009276	-0.850282	4.370424
H	-5.043709	-6.412535	4.516255	H	-4.917214	6.777967	-1.005424
H	-3.747292	-6.489071	2.520443	H	-6.647194	6.739179	-0.688721
H	-2.091119	-6.118918	-1.211974	H	-6.058793	6.695432	-2.360154
C	-6.565828	-3.611160	-1.042179	H	-3.316245	-0.811615	3.869769
H	-5.983943	-3.541965	-1.969711	H	-4.545554	-1.471185	2.774670
C	-7.931680	-4.188896	-1.396142	H	-1.947521	10.763673	7.042638
H	-7.851190	-5.220381	-1.754580	H	-3.321205	9.754190	7.531715
H	-8.400910	-3.588352	-2.182802	B	-4.578131	9.874172	3.024487
H	-8.609670	-4.182532	-0.534852	O	-7.107327	8.425650	2.908037
C	-6.715820	-2.191537	-0.489715	C	-5.954957	7.804435	2.476358
H	-5.736640	-1.744400	-0.290111	C	-4.693119	8.437495	2.489628
H	-7.251619	-1.551145	-1.200423	C	-7.261043	12.311580	4.405715
C	-6.429064	-6.772621	2.883278	C	-8.416914	11.513356	4.296972
H	-7.505037	-6.632037	2.712394	C	-8.340644	10.218961	3.792786

C	-7.091457	9.722018	3.392966	C	-5.239673	2.123735	1.085228
C	-5.908494	10.487956	3.483085	C	-5.215802	0.854166	1.600424
C	-6.034231	11.799802	4.004427	C	-4.573320	4.257168	4.242424
C	-6.125210	6.487153	2.028298	C	-5.354569	4.052454	-0.168408
C	-3.592801	7.684439	2.013097	C	-5.511012	4.886983	-1.290714
H	-7.335872	13.320850	4.802537	C	-5.755088	4.223000	-2.493616
H	-9.380533	11.908212	4.609689	C	-5.844258	2.837496	-2.610724
H	-9.222525	9.590427	3.703860	C	-5.685962	2.034407	-1.464561
C	-5.013581	5.787786	1.575719	H	-5.757368	0.952152	-1.545913
C	-3.738432	6.382315	1.560308	C	-5.438169	6.378493	-1.261315
H	-2.891656	5.808239	1.195436	H	-5.883842	4.827611	-3.388705
H	-5.133624	12.404280	4.083586	C	-4.953124	-0.691697	3.561464
H	-7.106023	6.022031	2.040245	H	-4.604715	1.655347	4.845197
H	-2.613797	8.156709	2.010822	H	-5.371657	-0.014894	0.965275
C	-3.204497	10.629769	3.103344	H	-5.291232	1.514009	-4.202789
C	-2.766867	11.436253	2.032944	H	-6.210969	2.938858	-4.728041
C	-1.527435	12.086395	2.115607	H	-7.023332	1.595296	-3.898917
C	-0.704002	11.955612	3.239186	H	-4.408877	3.878426	5.253723
C	-1.149559	11.150395	4.296578	H	-5.427868	4.941982	4.251292
C	-2.381877	10.489846	4.243286	H	-3.711521	4.861449	3.940523
H	-2.026059	11.479779	-0.695847	H	-4.771085	-0.668061	4.638162
H	-1.187797	12.708859	1.289035	H	-4.457542	6.726566	-0.919953
H	1.758856	11.113558	4.360297	H	-6.163784	6.801525	-0.558418
H	-0.522286	11.036221	5.178257	H	-5.630796	6.778211	-2.259461
H	-3.597921	11.257054	6.621886	H	-4.167884	-1.293746	3.090107
C	-3.636009	11.583661	0.785307	H	-5.902060	-1.209403	3.380983
H	-4.563162	11.020409	0.963248	H	-2.689457	10.824516	6.765847
C	-4.044012	13.050408	0.531589	H	-3.548261	9.300504	7.075612
H	-4.561500	13.465184	1.404022	B	-4.540106	9.805736	3.053556
H	-4.714501	13.120982	-0.333719	O	-7.037348	8.340851	2.987070
H	-3.165477	13.675021	0.330390	C	-5.890220	7.725924	2.549113
C	-2.961088	10.959567	-0.455552	C	-4.633501	8.386960	2.562336
H	-2.725308	9.904061	-0.278815	C	-7.267023	12.209824	4.438472
H	-3.620806	11.024270	-1.329641	C	-8.396916	11.399150	4.362312
C	0.638188	12.674125	3.305974	C	-8.282577	10.102560	3.869837
H	0.757766	13.220598	2.360190	C	-7.041461	9.635438	3.461809
C	0.672887	13.710570	4.451715	C	-5.875192	10.414462	3.522522
H	-0.145652	14.432394	4.350434	C	-6.037008	11.719569	4.025402
H	1.622342	14.260175	4.448067	C	-6.063761	6.432933	2.102326
H	0.570476	13.219194	5.426999	C	-3.531284	7.608960	2.083159
C	1.815424	11.680216	3.422925	H	-7.350861	13.224129	4.821599
H	1.805028	10.962827	2.594337	H	-9.366240	11.771338	4.683510
H	2.774245	12.213041	3.408176	H	-9.146123	9.445947	3.796625
C	-2.836055	9.607756	5.405682	C	-4.937115	5.726837	1.636018
H	-3.849912	9.252962	5.172468	C	-3.675286	6.314455	1.629393
C	-1.943318	8.356090	5.551772	H	-2.819135	5.749171	1.266329
H	-2.310286	7.709630	6.358512	H	-5.153560	12.353905	4.084558
H	-0.909639	8.638631	5.784910	H	-7.051341	5.979556	2.111490
H	-1.934290	7.775315	4.622793	H	-2.546406	8.071166	2.081303
C	-2.931433	10.393876	6.730410	C	-3.179320	10.616736	3.081582
<b>B5</b>				C	-2.902976	11.595610	2.109197
$E = -28.982$				C	-1.699598	12.299288	2.141911
$N_{\text{imag}} = 0$				C	-0.741256	12.061879	3.117848
$T_1$				C	-1.012360	11.090963	4.076436
C	-4.983657	0.684681	2.979019	C	-2.205221	10.374105	4.071860
N	-5.105590	4.392363	1.150267	H	-2.651753	10.986355	-0.584291
C	-6.106880	2.195263	-3.934816	H	-1.493614	13.056241	1.386445
C	-5.444522	2.641669	-0.260178	H	1.837977	11.210122	3.791858
C	-4.783425	1.805384	3.782711	H	-0.271622	10.890911	4.848865
C	-4.798042	3.116180	3.304930	H	-4.211736	10.476904	5.919596
C	-5.035176	3.246854	1.924082	C	-3.892265	11.831137	0.981709
				H	-4.891457	11.628321	1.387732

## Appendix

C	-3.893891	13.256429	0.438250
H	-4.026786	13.991813	1.238910
H	-4.709627	13.382839	-0.282118
H	-2.959345	13.491838	-0.084751
C	-3.648188	10.830274	-0.151773
H	-3.707445	9.800481	0.215968
H	-4.389953	10.957052	-0.949781
C	0.557376	12.837495	3.135523
H	0.530170	13.528730	2.281772
C	0.701397	13.670185	4.409713
H	-0.142822	14.356387	4.531212
H	1.626080	14.258259	4.388128
H	0.735549	13.020969	5.292640
C	1.767461	11.919903	2.959113
H	1.693944	11.342359	2.032007
H	2.696239	12.501274	2.933005
C	-2.492774	9.367253	5.171485
H	-3.132765	8.591759	4.731296
C	-1.250587	8.682335	5.732332
H	-1.542193	7.885521	6.425534
H	-0.618309	9.382570	6.291406
H	-0.641906	8.239852	4.936487
C	-3.287184	10.030769	6.300092

### B6

$E = -23.489$

$N_{\text{imag}} = 0$

$S_0$

N	0.427508	0.293120	0.311781
H	-0.978143	-1.084946	2.410255
C	-0.656018	-0.274275	-0.387784
C	-0.848665	-1.670530	-0.398305
C	3.524600	-2.078843	1.944245
C	3.637493	-0.683700	1.923186
C	2.618185	0.096553	1.383827
C	1.454956	-0.504538	0.853586
C	1.331802	-1.908465	0.881136
C	2.373876	-2.669580	1.423949
C	-1.567161	0.553213	-1.081151
C	-1.935498	-2.199359	-1.104737
H	4.316681	-2.693752	2.362906
H	4.523137	-0.197619	2.325520
H	2.719529	1.175552	1.368662
C	-2.642994	0.001589	-1.771741
C	-2.834777	-1.384961	-1.791630
H	-3.331023	0.659399	-2.297502
H	-3.672046	-1.822029	-2.328980
H	5.274890	8.327414	0.883961
H	-1.426298	1.627879	-1.077423
H	-2.076297	-3.277173	-1.107022
H	2.270613	-3.751485	1.440837
C	0.051653	-2.619639	0.410290
O	-0.605126	-5.453515	1.055210
C	0.093274	-5.135927	-0.100510
C	0.428596	-3.826914	-0.455652
C	-1.888114	-2.519696	3.728200
C	-2.151695	-3.878890	3.955649
C	-1.709782	-4.833672	3.043585
C	-1.002616	-4.428408	1.902590
C	-0.727122	-3.080318	1.654562
C	-1.184006	-2.136863	2.588853
C	0.450188	-6.227715	-0.906227

C	1.138605	-3.634082	-1.651207
H	-2.230384	-1.769078	4.435734
H	-2.699844	-4.192170	4.840548
H	-1.899375	-5.893367	3.192769
C	1.154137	-6.010136	-2.087194
C	1.502259	-4.703872	-2.464837
H	1.431213	-6.855194	-2.712379
H	2.051909	-4.527212	-3.385550
H	1.403896	-2.618764	-1.935523
H	0.167135	-7.227604	-0.588376
H	5.022317	7.373599	2.358585
B	1.022975	6.062632	0.378909
O	-0.374198	4.511747	2.416742
C	0.196454	3.858165	1.346853
C	0.888723	4.531755	0.317234
C	-0.258427	8.638838	2.979609
C	-0.904104	7.784374	3.894782
C	-0.929686	6.409408	3.685373
C	-0.300678	5.887768	2.545519
C	0.357487	6.707571	1.602776
C	0.358080	8.101613	1.857688
C	0.040142	2.463680	1.353523
C	1.424574	3.734766	-0.723630
H	-0.246631	9.711290	3.156669
H	-1.388745	8.199070	4.775381
H	-1.423142	5.736753	4.381525
C	0.584211	1.725137	0.310772
C	1.280917	2.355426	-0.737692
H	1.694033	1.749165	-1.538686
H	0.860504	8.748891	1.142575
H	-0.496864	1.974127	2.160131
H	1.960311	4.236607	-1.525557
C	1.780949	6.886148	-0.721630
C	1.092357	7.368829	-1.853434
C	1.787092	8.095110	-2.830566
C	3.156643	8.356415	-2.715213
C	3.830278	7.870722	-1.586182
C	3.163819	7.143272	-0.594007
H	-0.421080	6.771242	-4.174878
H	1.256210	8.468878	-3.704903
H	5.767281	8.018648	-3.759712
H	4.895855	8.063286	-1.479534
H	3.748941	8.469445	1.775994
C	-0.403240	7.099110	-2.008668
H	-0.723699	6.514648	-1.134444
C	-1.225602	8.405679	-2.000525
H	-1.036383	8.976341	-1.084378
H	-2.299338	8.188252	-2.056697
H	-0.962957	9.040488	-2.855215
C	-0.707358	6.243630	-3.257262
H	-0.153550	5.298539	-3.224375
H	-1.778327	6.014288	-3.318401
C	3.889227	9.147463	-3.792008
H	3.147091	9.410573	-4.558504
C	4.472576	10.465614	-3.235488
H	3.687529	11.077003	-2.776103
H	4.942895	11.049364	-4.036406
H	5.233961	10.265752	-2.471755
C	4.986287	8.301156	-4.476069
H	4.564850	7.380262	-4.895006
H	5.461059	8.866007	-5.287822
C	3.925901	6.620691	0.622884

H	3.201285	6.102157	1.266684
C	4.997284	5.582637	0.224713
H	5.495722	5.178692	1.114504
H	5.762851	6.034966	-0.416969
H	4.545031	4.749770	-0.325371
C	4.529457	7.767604	1.461310

**B6** $E = -33.400$  $N_{\text{imag}} = 0$ **T<sub>1</sub>**

N	0.410271	0.289944	0.199838
H	0.070896	-1.391166	2.933423
C	-0.843126	-0.264881	-0.044473
C	-1.073175	-1.643630	0.113573
C	3.741151	-2.084811	1.080889
C	3.860744	-0.697404	1.035713
C	2.759783	0.082321	0.762591
C	1.511171	-0.517249	0.508156
C	1.375353	-1.912168	0.602259
C	2.504061	-2.671866	0.879299
C	-1.885299	0.574010	-0.492460
C	-2.351122	-2.131191	-0.114247
H	4.607228	-2.703379	1.295736
H	4.818628	-0.223367	1.226224
H	2.841278	1.162093	0.748023
C	-3.144441	0.060178	-0.706542
C	-3.386511	-1.296341	-0.505179
H	-3.940049	0.714384	-1.049081
H	-4.376853	-1.707075	-0.676861
H	5.505675	8.157654	1.195977
H	-1.674797	1.619880	-0.679086
H	-2.537521	-3.195392	0.007581
H	2.399395	-3.751498	0.950572
C	0.032272	-2.611680	0.502031
O	-0.824320	-5.396467	0.936351
C	-0.333555	-5.006400	-0.284232
C	0.104119	-3.716035	-0.548709
C	-0.614551	-2.929900	4.253799
C	-1.034234	-4.254180	4.360165
C	-1.090143	-5.053806	3.234890
C	-0.730517	-4.529458	1.996376
C	-0.312299	-3.212061	1.865787
C	-0.259037	-2.424880	3.016735
C	-0.304738	-5.994815	-1.264701
C	0.578904	-3.435312	-1.830565
H	-0.566088	-2.296607	5.134319
H	-1.315235	-4.663835	5.326032
H	-1.407705	-6.091338	3.286896
C	0.165656	-5.692597	-2.527968
C	0.612872	-4.404509	-2.815829
H	0.187860	-6.463708	-3.292590
H	0.985263	-4.161076	-3.806207
H	0.927939	-2.428751	-2.051865
H	-0.654901	-6.990733	-1.008773
H	4.745361	7.871607	2.762109
B	0.979311	6.029936	0.236990
O	-0.706578	4.527103	2.051848
C	0.004306	3.855814	1.088885
C	0.848572	4.532302	0.169154
C	-0.714655	8.630602	2.575857
C	-1.490685	7.796196	3.378653

C	-1.467584	6.422665	3.174303
C	-0.666123	5.898644	2.168347
C	0.129160	6.698846	1.335487
C	0.074969	8.083909	1.577172
C	-0.172347	2.491597	1.090602
C	1.526008	3.688210	-0.781419
H	-0.731474	9.706052	2.734271
H	-2.114326	8.213591	4.164810
H	-2.061442	5.747655	3.785333
C	0.551061	1.704147	0.146672
C	1.396107	2.321794	-0.783967
H	1.924147	1.713974	-1.515233
H	0.682209	8.733322	0.948200
H	-0.820579	2.027361	1.828034
H	2.160060	4.169438	-1.522325
C	1.906963	6.860921	-0.738585
C	1.519687	7.114595	-2.066730
C	2.346559	7.857986	-2.908048
C	3.563067	8.366183	-2.473850
C	3.947146	8.110717	-1.161287
C	3.145027	7.371522	-0.297829
H	0.259386	7.167914	-4.675376
H	2.039281	8.053755	-3.934375
H	6.352718	8.411279	-2.701833
H	4.899243	8.499658	-0.804653
H	4.084082	9.104634	1.669479
C	0.167109	6.633915	-2.560703
H	-0.072380	5.723440	-1.995688
C	-0.912837	7.670670	-2.238574
H	-0.940509	7.889458	-1.166068
H	-1.902755	7.311519	-2.544506
H	-0.708930	8.606735	-2.773434
C	0.135921	6.279942	-4.044275
H	0.927261	5.568656	-4.303946
H	-0.828860	5.829883	-4.302989
C	4.442813	9.173516	-3.402427
H	3.920642	9.234554	-4.367259
C	4.649022	10.598434	-2.888150
H	3.691843	11.110135	-2.745581
H	5.252967	11.182191	-3.592137
H	5.171131	10.588983	-1.924063
C	5.790636	8.491837	-3.639772
H	5.658188	7.481127	-4.039024
H	6.398041	9.067406	-4.347532
C	3.628144	7.048824	1.104866
H	2.736583	6.973666	1.740820
C	4.319095	5.682040	1.122259
H	4.623019	5.411915	2.140716
H	5.217456	5.706859	0.492738
H	3.653964	4.900432	0.740118
C	4.539819	8.109780	1.712799

**B7** $E = -22.820$  $N_{\text{imag}} = 0$ **S<sub>0</sub>**

C	-1.094203	0.614809	-1.797016
C	-2.418876	0.263927	-1.514336
C	-2.876560	0.223013	-0.169486
C	-1.958220	0.534997	0.869247
C	-0.633455	0.864519	0.562355
C	-0.200727	0.910384	-0.764933

## Appendix

N	1.149921	1.255887	-1.064913	H	-4.844342	3.896475	-0.318323
B	-4.368677	-0.158830	0.162241	H	-7.717262	2.876613	4.727255
C	2.290797	0.637156	-0.529944	H	-7.147491	4.313328	3.845087
C	3.452323	1.268735	-1.065922	H	-8.598565	3.458993	3.308378
C	2.989549	2.313671	-1.958721	H	-6.545250	-1.831043	1.742073
C	1.562048	2.276316	-1.935946	H	-4.959968	-1.706032	2.487798
C	-5.217453	0.763936	1.106849	H	-6.411381	-1.463613	3.472201
C	-4.995477	-1.458421	-0.456230	H	-2.696150	-3.908246	0.374670
C	-5.959077	0.212668	2.187730	H	-2.156892	-2.383420	-0.351150
C	-6.691483	1.051722	3.036856	H	-2.910826	-2.377848	1.236720
C	-6.754079	2.435964	2.836997	H	-6.476258	0.701551	-1.562322
C	-6.033282	2.973952	1.763568	H	-7.909131	-0.279296	-1.907538
C	-5.260114	2.172679	0.915024	H	-7.493878	0.156102	-0.238891
C	-6.267388	-1.420947	-1.091914	H	-2.888342	-0.403843	2.602952
C	-6.799492	-2.581823	-1.666238	H	-1.470835	0.589807	2.973058
C	-6.132862	-3.811700	-1.604623	H	-3.025565	1.347545	2.575083
C	-4.887865	-3.848109	-0.965033	H	-2.845783	0.225012	-3.631472
C	-4.305791	-2.701235	-0.411320	H	-3.569842	-1.119482	-2.727159
C	2.392892	-0.447182	0.348840	H	-4.280407	0.484230	-2.627322
C	3.668766	-0.878605	0.709030	H	8.761950	-0.796756	0.099958
C	4.830317	-0.263707	0.188461	H	10.436793	0.842035	0.890306
C	4.723375	0.804060	-0.709196	H	9.733632	2.793250	2.280061
C	3.643782	3.270395	-2.748733	H	7.322524	3.070751	2.866645
C	2.879611	4.172001	-3.493251	H	5.650207	1.421357	2.086943
C	1.470256	4.129720	-3.448273	H	7.643421	-2.177565	2.268069
C	0.793001	3.186104	-2.670475	H	8.128227	-4.595760	2.101070
C	-4.508865	2.859826	-0.212611	H	7.163494	-5.950610	0.238670
C	-7.594345	3.319050	3.732767	H	5.708036	-4.835798	-1.456411
C	-5.967208	-1.276394	2.489281	H	5.238102	-2.411568	-1.298042
C	-2.945773	-2.849764	0.249317	H	-7.389847	-4.833806	-3.043443
C	-7.078527	-0.141527	-1.207848	H	-5.981759	-5.778042	-2.502356
C	-2.356342	0.514789	2.334332	H	-7.377280	-5.570683	-1.436404
C	-3.327752	-0.052124	-2.688826				
N	6.120940	-0.738269	0.588933	<b>B7</b>			
C	7.089743	0.192909	1.045787	<b>E</b> = -32.355			
C	8.449568	0.044369	0.711294	<b>N<sub>imag</sub></b> = 0			
C	9.391234	0.971774	1.160907	<b>T<sub>1</sub></b>			
C	8.998140	2.070274	1.936737		-1.040150	0.606054	-1.870380
C	7.644183	2.225898	2.261665	C	-2.346759	0.255642	-1.591282
C	6.697308	1.296465	1.827844	C	-2.840019	0.196037	-0.239258
C	6.412244	-2.122311	0.492123	C	-1.885914	0.519662	0.788496
C	7.227401	-2.757509	1.449903	C	-0.580129	0.850646	0.482818
C	7.498651	-4.122829	1.350588	C	-0.140962	0.898107	-0.842493
C	6.954372	-4.886276	0.308827	N	1.205606	1.233006	-1.136978
C	6.135205	-4.259395	-0.638747	B	-4.301847	-0.189409	0.086822
C	5.869072	-2.891102	-0.555831	C	2.306863	0.669883	-0.582158
C	-6.750394	-5.064987	-2.184383	C	3.481100	1.299021	-1.094579
H	-0.748064	0.642471	-2.826729	C	3.024265	2.303000	-2.036677
H	0.064799	1.104515	1.359746	C	1.619909	2.240078	-2.031836
H	-7.230402	0.612754	3.875896	C	-5.092555	0.485624	1.285303
H	-6.069095	4.048596	1.586956	C	-5.081902	-1.280285	-0.761184
H	-7.762150	-2.525858	-2.173541	C	-5.804123	-0.281552	2.236373
H	-4.352141	-4.794858	-0.902111	C	-6.533624	0.331997	3.251306
H	1.510542	-0.933144	0.752567	C	-6.609329	1.715739	3.371790
H	3.780327	-1.708382	1.400629	C	-5.906843	2.475588	2.445038
H	5.620725	1.262710	-1.114638	C	-5.159151	1.890432	1.424395
H	4.730164	3.312082	-2.777129	C	-6.383475	-1.045773	-1.262048
H	3.373019	4.918199	-4.110852	C	-7.072060	-2.034548	-1.959597
H	0.895447	4.846507	-4.029650	C	-6.526017	-3.293958	-2.185267
H	-0.291640	3.162677	-2.638189	C	-5.244787	-3.528765	-1.702770
H	-3.429353	2.869292	-0.026067	C	-4.525957	-2.555333	-1.010526
H	-4.657884	2.359528	-1.175155	C	2.394166	-0.398882	0.327349

C	3.635980	-0.809064	0.725748	H	8.457745	-1.231195	-0.255894
C	4.817811	-0.178841	0.242876	H	10.438741	0.253829	-0.302035
C	4.719618	0.885492	-0.686587	H	10.276173	2.569499	0.569663
C	3.670700	3.234716	-2.835106	H	8.127150	3.391662	1.494948
C	2.899021	4.088785	-3.614533	H	6.149965	1.902725	1.547823
C	1.505084	4.021236	-3.586793	H	7.344202	-1.273222	2.887078
C	0.839904	3.096861	-2.790000	H	7.711049	-3.571084	3.735286
C	-4.439071	2.805632	0.470707	H	6.824122	-5.515280	2.477572
C	-7.437558	2.360617	4.446978	H	5.576056	-5.153897	0.365525
C	-5.764839	-1.786895	2.211532	H	5.216113	-2.856132	-0.483985
C	-3.146225	-2.914948	-0.527951	H	-7.933480	-3.937529	-3.688556
C	-7.053919	0.292601	-1.096588	H	-6.634136	-5.100490	-3.358301
C	-2.246780	0.446596	2.246183	H	-7.963785	-4.903253	-2.212815
C	-3.251267	0.007661	-2.766119				
N	6.052599	-0.607950	0.670160				
C	7.185994	0.255515	0.633617	<b>B8</b>			
C	8.393371	-0.215518	0.123689	<i>E</i> = -17.776			
C	9.499374	0.619476	0.102202	<i>N</i> <sub>imag</sub> = 0			
C	9.406696	1.918929	0.587606	<b>S<sub>0</sub></b>			
C	8.201600	2.382054	1.101694	C	-1.804770	7.131518	3.496220
C	7.090300	1.553460	1.130989	C	-3.772889	12.259217	4.509351
C	6.247881	-1.932925	1.160496	C	-2.406609	10.940763	6.558737
C	6.958953	-2.129766	2.341325	C	3.548442	5.051195	9.866367
C	7.162893	-3.418060	2.810298	C	0.028346	8.741916	10.602797
C	6.662396	-4.507434	2.106569	C	-2.542848	10.310864	5.312109
C	5.958956	-4.305627	0.925243	C	-2.050511	6.567453	2.236856
C	5.752721	-3.021026	0.445968	B	0.769012	6.107874	9.258307
C	-7.301936	-4.362994	-2.901451	C	-2.741185	7.289064	1.262678
H	-0.704422	0.648925	-2.905123	C	-3.188335	8.587472	1.554150
H	0.116946	1.086422	1.285730	C	-2.939631	9.145691	2.801468
H	-7.054038	-0.292531	3.979115	C	-3.629069	12.879487	5.760470
H	-5.942588	3.563727	2.515971	C	-2.944844	12.215918	6.779436
H	-8.066621	-1.810767	-2.348600	C	0.017169	6.895196	8.116134
H	-4.787027	-4.505202	-1.868424	C	0.738417	7.716809	7.209016
H	1.496459	-0.873916	0.708541	C	2.246636	7.872242	7.281064
H	3.729547	-1.617869	1.441355	C	0.058402	8.402676	6.194583
H	5.621800	1.334605	-1.088879	C	-1.326959	8.309716	6.084239
H	4.755336	3.301844	-2.850480	C	-2.050148	7.518299	6.974486
H	3.385388	4.823615	-4.249186	C	-1.393929	6.797832	7.979897
H	0.925665	4.707635	-4.197313	C	-2.240285	5.946736	8.909164
H	-0.243593	3.048117	-2.756127	C	0.516103	4.569886	9.435000
H	-3.352117	2.768266	0.615312	C	0.235197	4.024324	10.718546
H	-4.611722	2.509528	-0.570608	C	-0.018208	2.654588	10.858090
H	-4.767182	3.841819	0.605372	C	-2.243769	8.429736	3.798330
H	-7.433898	1.763285	5.364862	C	0.028448	1.777252	9.768212
H	-7.067008	3.362327	4.687567	C	-0.261587	0.302660	9.939349
H	-8.483968	2.465875	4.133765	C	0.325680	2.314201	8.509891
H	-6.331790	-2.192481	1.366260	N	-2.012577	9.035518	5.046442
H	-4.738121	-2.153470	2.091352	C	0.547706	3.683652	8.323070
H	-6.178278	-2.200622	3.137351	C	0.169558	4.883482	11.969845
H	-2.968546	-3.990984	-0.628851	C	0.851054	4.162155	6.913469
H	-2.368685	-2.384177	-1.091474	C	1.758501	6.875085	10.203385
H	-3.004421	-2.626519	0.520178	C	3.056497	6.356370	10.468690
H	-6.372531	1.111027	-1.358836	C	3.940444	7.065368	11.290633
H	-7.943794	0.361202	-1.731091	O	-3.398268	10.447399	3.018152
H	-7.353581	0.469411	-0.057681	C	3.578497	8.271658	11.902012
H	-2.777254	-0.487879	2.467305	C	4.554137	9.027609	12.776387
H	-1.346736	0.501577	2.867793	C	2.293204	8.768689	11.655504
H	-2.926021	1.250940	2.549239	C	-3.234729	10.997308	4.291998
H	-2.767074	0.322145	-3.696704	C	1.393829	8.108899	10.809573
H	-3.532614	-1.046856	-2.861734	H	-1.268094	6.568174	4.251966
H	-4.194334	0.556287	-2.650727	H	-4.298261	12.747747	3.692770
				H	-1.876071	10.426852	7.353045

## Appendix

H	4.628259	4.947580	10.013728	C	0.110607	4.309835	10.982932
H	3.348068	4.987554	8.791786	C	-0.197600	2.999479	11.335686
H	3.056820	4.187779	10.327664	C	-1.866445	8.750388	3.691410
H	-0.130241	9.550757	11.323110	C	-0.316521	1.990045	10.387008
H	-0.787000	8.021302	10.723493	C	-0.670896	0.585589	10.784847
H	-0.067489	9.161601	9.595374	C	-0.121199	2.338418	9.057531
H	-1.697502	5.560934	2.027777	N	-2.094544	9.043731	5.023182
H	-2.935645	6.857819	0.284705	C	0.176733	3.644288	8.672533
H	-3.729085	9.177943	0.819031	C	0.194289	5.332580	12.084687
H	-4.049338	13.867704	5.924821	C	0.369391	3.913830	7.204434
H	-2.823544	12.682173	7.753764	C	1.950684	6.784740	9.988174
H	2.624673	8.359172	6.376764	C	3.170396	6.093373	10.159486
H	2.756627	6.908783	7.383318	C	4.210107	6.648618	10.899153
H	2.541315	8.476999	8.145474	O	-3.448263	10.438215	3.015813
H	0.605322	9.020101	5.485876	C	4.097805	7.893693	11.507671
H	-3.131792	7.463283	6.876096	C	5.238473	8.486146	12.284998
H	-2.089420	4.879242	8.715876	C	2.900497	8.577043	11.345126
H	-3.302431	6.173380	8.774219	C	-3.680856	10.717157	4.324240
H	-1.991491	6.113256	9.962383	C	1.845955	8.052137	10.600363
H	-0.251346	2.259424	11.846338	H	-0.481593	7.155297	4.062036
H	0.293545	-0.300068	9.212033	H	-5.101400	12.210785	3.783362
H	-1.330525	0.097050	9.786855	H	-2.705957	9.900969	7.469302
H	-0.003040	-0.040490	10.947138	H	4.458407	4.469623	9.579168
H	0.383407	1.648086	7.649628	H	3.097674	4.752571	8.469286
H	1.166054	5.218864	12.277273	H	2.808755	3.965266	10.006966
H	-0.269972	4.317221	12.797255	H	0.617402	9.718611	11.185820
H	-0.432388	5.786304	11.823129	H	-0.301372	8.273402	10.690029
H	1.722985	4.823290	6.877174	H	0.460250	9.274266	9.474115
H	0.009926	4.725520	6.494730	H	-0.111810	6.683278	1.660624
H	1.049162	3.310109	6.255494	H	-1.297836	8.009281	-0.068973
H	4.937148	6.661385	11.465289	H	-2.893600	9.798192	0.618512
H	5.262002	8.348203	13.263920	H	-5.561205	12.830202	6.154887
H	4.033533	9.603245	13.549659	H	-4.345061	11.681583	7.987515
H	5.141213	9.738683	12.178166	H	2.494300	8.548615	6.375470
H	1.983539	9.697532	12.133446	H	2.660242	7.051941	7.331658
<b>B8</b>				H	2.455098	8.581081	8.150899
$E = -25.543$				H	0.520123	9.148955	5.534487
$N_{\text{imag}} = 0$				H	-3.176351	7.360770	6.785441
$T_1$				H	-2.106990	4.838449	8.631436
C	-0.989030	7.729503	3.295394	H	-3.348781	6.108265	8.619676
C	-4.600441	11.714010	4.608096	H	-2.048739	6.097508	9.840959
C	-3.248076	10.408010	6.679395	H	-0.353040	2.758790	12.388192
C	3.401430	4.748750	9.522706	H	-0.357736	-0.133591	10.021700
C	0.591338	8.875682	10.487616	H	-1.753785	0.471733	10.917916
C	-3.000744	10.035790	5.349281	H	-0.198526	0.307940	11.732668
C	-0.791272	7.475073	1.958756	H	-0.196897	1.566086	8.291093
B	0.724671	6.143904	9.208605	H	1.224666	5.665441	12.249451
C	-1.462458	8.219959	0.982804	H	-0.193039	4.923697	13.023354
C	-2.345144	9.213660	1.350251	H	-0.379433	6.232414	11.833397
C	-2.548748	9.472519	2.696149	H	1.276146	4.501291	7.021858
C	-4.843748	12.049604	5.923291	H	-0.457897	4.503391	6.790592
C	-4.160183	11.398868	6.956314	H	0.434693	2.975632	6.643877
C	-0.021607	6.911090	8.099854	H	5.141694	6.090510	11.001767
C	0.654405	7.819020	7.207283	H	5.777940	7.718886	12.849703
C	2.143305	8.016816	7.265695	H	4.885837	9.246090	12.989136
C	-0.023754	8.491446	6.210918	H	5.964973	8.967984	11.619159
C	-1.400485	8.329165	6.052376	H	2.778378	9.551587	11.819466
C	-2.099067	7.469495	6.900779				
C	-1.440384	6.766905	7.889335				
C	-2.285705	5.907530	8.787247				
C	0.306931	4.671460	9.631714				



Cartesian coordinates (Å), energies ( $E$ , Hartree), and number of imaginary vibrational frequencies ( $N_{\text{imag}}$ ) of the optimized structures at ground singlet ( $S_0$ ) and triplet state ( $T_1$ ) calculated at DFT/TZ2P/ZORA-BLYP-D3(BJ)//U-DFT/TZ2P/ZORA-LC-BLYP\* for the model molecules.

**Cbz- $\pi$**  $E = -15.365$  $N_{\text{imag}} = 0$  $S_0$ 

F	-0.034527	4.651416	13.619790
F	1.040839	6.084230	12.372155
F	-1.143080	6.260277	12.618410
F	1.372889	4.524144	7.340666
F	-0.671549	4.078193	6.653008
F	0.706654	2.448947	7.162291
F	4.807846	4.131118	10.162418
F	2.685361	3.797484	9.776660
F	3.994085	4.537065	8.164025
F	-0.234066	8.082922	10.775062
F	0.982954	9.582444	11.800690
F	0.639487	9.756828	9.640915
N	-1.931992	8.918745	5.199941
C	0.076163	6.815289	8.297972
C	0.778362	7.644992	7.394518
H	1.854346	7.757017	7.494992
C	0.131390	8.323946	6.368976
H	0.690029	8.961260	5.690873
C	-1.262540	8.217262	6.232063
C	-1.989356	7.411422	7.124042
H	-3.063945	7.314417	7.005984
C	-1.323033	6.714903	8.124998
H	-1.901634	6.082022	8.792093
C	0.107116	4.704379	9.939225
C	-0.358592	4.447634	11.256944
C	-1.152780	3.330712	11.561955
H	-1.507340	3.190847	12.577092
C	-1.482997	2.401015	10.585024
H	-2.099733	1.541043	10.827888
C	-0.984087	2.574036	9.299026
H	-1.189783	1.832603	8.533775
C	-0.208476	3.694455	8.984407
C	-0.113061	5.363184	12.445662
C	0.301322	3.705432	7.550641
C	2.173868	6.697196	9.953338
C	3.459123	6.092345	9.910753
C	4.631443	6.813511	10.188283
H	5.592156	6.315861	10.116537
C	4.576514	8.150074	10.560109
H	5.487570	8.702003	10.770477
C	3.333686	8.759355	10.689506
H	3.267411	9.788349	11.027775
C	2.163382	8.052082	10.395972
C	3.714685	4.648619	9.507517
C	0.888736	8.846745	10.641336
C	-1.565511	8.928496	3.838836
C	-2.488498	9.745783	3.123781
C	-2.350388	9.893544	1.736753
H	-3.046985	10.513363	1.177426
C	-1.311478	9.226993	1.083901
H	-1.191471	9.333684	0.008844

C	-0.420160	8.406904	1.803409
H	0.373761	7.885873	1.274193
C	-0.535664	8.242764	3.186973
C	-3.078070	9.723607	5.360379
C	-3.444846	10.253610	4.089252
C	-4.547475	11.113417	3.990945
H	-4.839294	11.526099	3.028246
C	-5.259283	11.438236	5.147516
H	-6.117433	12.102551	5.085896
C	-4.870532	10.921418	6.399073
H	-5.429915	11.197541	7.289411
C	-3.775148	10.061847	6.524588
B	0.809880	6.047266	9.433822
H	0.149063	7.598366	3.728324
H	-3.477703	9.680292	7.495717

**Cbz- $\pi$**  $E = -22.626$  $N_{\text{imag}} = 0$  $T_1$ 

F	-0.238328	5.029402	13.631997
F	1.007467	6.236901	12.352026
F	-1.151952	6.477962	12.309030
F	1.172666	4.436375	7.279764
F	-0.902689	3.967282	6.852448
F	0.518542	2.382779	7.245700
F	4.759390	4.028355	9.752627
F	2.623935	3.750770	9.648121
F	3.686098	4.652535	7.980216
F	-0.130941	8.261241	10.683637
F	1.162604	9.643205	11.714636
F	0.949412	9.774707	9.564623
N	-1.918808	8.903163	5.218936
C	0.082881	6.804413	8.305180
C	0.766380	7.720970	7.429396
H	1.827442	7.895917	7.584630
C	0.134710	8.385178	6.426599
H	0.675183	9.104003	5.817734
C	-1.265316	8.216709	6.223995
C	-1.979079	7.328000	7.078678
H	-3.033896	7.147889	6.893080
C	-1.326900	6.646828	8.056562
H	-1.888842	5.948465	8.670625
C	0.107256	4.725056	9.977666
C	-0.296042	4.508565	11.314835
C	-0.957128	3.356703	11.728734
H	-1.246384	3.256003	12.769206
C	-1.253756	2.350508	10.831583
H	-1.769689	1.452623	11.156175
C	-0.870463	2.508471	9.515714
H	-1.072907	1.722857	8.794316
C	-0.204226	3.657385	9.103803
C	-0.155618	5.558863	12.385465
C	0.158910	3.633896	7.638417
C	2.188504	6.659251	9.938267
C	3.435472	5.994250	9.913351
C	4.623036	6.597621	10.314329

## Appendix

H	5.548177	6.033840	10.262769
C	4.636238	7.901551	10.766946
H	5.563701	8.370771	11.079002
C	3.442150	8.590243	10.823004
H	3.421629	9.609700	11.195692
C	2.254400	7.984715	10.427751
C	3.608908	4.614124	9.335149
C	1.053283	8.885058	10.591132
C	-1.435843	9.118302	3.919263
C	-2.385834	9.859716	3.193548
C	-2.148191	10.172444	1.868404
H	-2.873664	10.738832	1.291101
C	-0.964670	9.732677	1.282198
H	-0.761181	9.970472	0.242237
C	-0.047721	8.969644	2.002318
H	0.854774	8.614503	1.514322
C	-0.273915	8.636386	3.330949
C	-3.181005	9.507539	5.320622
C	-3.504432	10.104833	4.088778
C	-4.694505	10.793762	3.949626
H	-4.957477	11.266512	3.007432
C	-5.544535	10.883414	5.048353
H	-6.484258	11.420020	4.956432
C	-5.196464	10.316739	6.272810
H	-5.863476	10.424858	7.122616
C	-4.000723	9.630181	6.434839
B	0.803394	6.051918	9.422879
H	0.421647	8.006606	3.874185
H	-3.714810	9.228271	7.400367

### **Cbz-Me $\pi$**

$$E = -16.543$$

$$N_{\text{imag}} = 0$$

**S<sub>0</sub>**

F	-0.120267	3.979285	13.278245
F	0.782582	5.727717	12.333204
F	-1.409924	5.500298	12.359194
F	1.842698	4.924515	7.229704
F	-0.004829	4.219346	6.258517
F	1.596563	2.804070	6.753138
F	5.019828	4.761120	10.372932
F	3.039480	4.121791	9.712712
F	4.334356	5.274598	8.351145
F	-0.695534	7.671255	10.822734
F	0.115964	9.203979	12.155537
F	-0.046616	9.611842	10.006244
N	-1.961974	8.934193	5.232227
C	0.077751	6.816559	8.278912
C	0.704469	7.866511	7.577529
H	1.731242	8.131356	7.815728
C	0.059560	8.566488	6.556039
C	-1.272454	8.217823	6.260264
C	-1.949142	7.188777	6.943361
C	-1.249645	6.493370	7.931508
H	-1.762835	5.695676	8.462106
C	0.336102	4.544506	9.668981
C	-0.197340	4.044495	10.887390
C	-0.810018	2.783793	10.969806
H	-1.227653	2.455806	11.915235
C	-0.880629	1.950122	9.861793
H	-1.358105	0.977581	9.932880
C	-0.300764	2.368798	8.669563
H	-0.300374	1.710683	7.806651

C	0.292548	3.631544	8.575405
C	-0.224393	4.820245	12.195076
C	0.928029	3.911977	7.221591
C	1.990594	6.842092	10.148206
C	3.363535	6.478219	10.185343
C	4.351714	7.349581	10.670779
H	5.390391	7.038619	10.654229
C	4.016492	8.597804	11.178064
H	4.786526	9.266990	11.549668
C	2.675801	8.962035	11.231595
H	2.389411	9.912145	11.670944
C	1.688953	8.107161	10.730952
C	3.916217	5.163548	9.658017
C	0.271767	8.629473	10.914862
C	-2.192505	8.471510	3.931880
C	-2.912215	9.470979	3.209802
C	-3.253257	9.231627	1.870814
H	-3.799975	9.977769	1.298980
C	-2.878619	8.021627	1.280643
H	-3.137957	7.824582	0.243559
C	-2.163980	7.050412	2.011606
H	-1.881296	6.118666	1.527903
C	-1.808653	7.261738	3.347135
C	-2.518479	10.211371	5.364188
C	-3.120620	10.580264	4.123360
C	-3.753285	11.827203	4.016821
H	-4.220626	12.130673	3.082941
C	-3.776826	12.673733	5.128404
H	-4.263771	13.643022	5.057633
C	-3.179382	12.286855	6.345639
H	-3.214705	12.962536	7.196659
C	-2.543144	11.049465	6.482130
B	0.827449	6.040429	9.403950
H	-1.253517	6.516645	3.910363
H	-2.086782	10.747628	7.420837
C	-3.384558	6.853505	6.612415
H	-4.010730	7.752882	6.617173
H	-3.467756	6.412630	5.611500
H	-3.790140	6.140715	7.335803
C	0.760841	9.663829	5.790262
H	0.666941	9.512206	4.708986
H	0.323429	10.644573	6.013697
H	1.823029	9.695404	6.048394

### **Cbz-Me $\pi$**

$$E = -24.309$$

$$N_{\text{imag}} = 0$$

**T<sub>1</sub>**

F	-0.46591928	4.15350277	13.20735665
F	0.62001516	5.78472168	12.30726013
F	-1.51358253	5.57324261	11.95402590
F	1.83153000	4.90819527	7.13983130
F	-0.01133765	4.09664948	6.32865699
F	1.67328520	2.79813422	6.72794544
F	5.07152216	4.88219483	10.09593676
F	3.09059857	4.17564296	9.62037957
F	4.11724684	5.52764402	8.26383545
F	-0.75126042	7.77200816	10.74346921
F	0.03921832	9.21893694	12.13197735
F	0.07346225	9.64132794	10.00964564
N	-1.94888158	8.91539222	5.25126065
C	0.10022736	6.78996434	8.27520562
C	0.66430275	7.94909667	7.63936236

H	1.67345777	8.24824113	7.91426954	F	0.895659	5.928136	12.337845
C	0.02515604	8.66367253	6.67476372	F	-1.303323	5.858354	12.473622
C	-1.27048628	8.20930132	6.23263531	F	1.656173	4.697311	7.262080
C	-1.87017000	7.03192721	6.81374057	F	-0.260805	4.013187	6.420786
C	-1.19479996	6.38617137	7.80229480	F	1.283008	2.560097	6.984227
H	-1.68474532	5.54822777	8.29347217	F	4.974093	4.533428	10.247195
C	0.39692414	4.52292792	9.64686005	F	2.924502	3.989673	9.727391
C	-0.10971937	4.01229849	10.86295941	F	4.217211	4.966584	8.232076
C	-0.53294120	2.69571160	11.01306945	F	-0.516300	7.852849	10.745772
H	-0.91898388	2.36846721	11.97236903	F	0.455692	9.383185	11.970112
C	-0.47367306	1.80974352	9.95621263	F	0.233229	9.701128	9.810735
H	-0.80390432	0.78278780	10.07465769	N	-1.944355	8.925107	5.199875
C	0.02425773	2.25685787	8.74957430	C	0.087337	6.775836	8.243465
H	0.10107383	1.57420274	7.90896716	C	0.764789	7.736825	7.460895
C	0.45265922	3.57141321	8.60196984	C	-3.548504	10.190030	6.690333
C	-0.35065618	4.88203665	12.06877661	C	0.104882	8.418305	6.439753
C	0.99128131	3.86521167	7.22254767	C	-1.266074	8.157654	6.178366
C	1.95540991	6.84122596	10.18804489	C	-1.938142	7.178895	6.939422
C	3.31628222	6.47211606	10.28022919	C	-1.261023	6.505987	7.962028
C	4.26846954	7.24782033	10.93351860	C	-0.802866	8.121842	3.093074
H	5.29908461	6.91100218	10.96120624	C	0.248679	4.593647	9.788599
C	3.91694181	8.43860643	11.53663197	C	-0.262663	4.221361	11.061285
H	4.66073758	9.04290920	12.04584524	C	-0.958038	3.018120	11.260984
C	2.59689716	8.83682942	11.48652503	C	-2.981694	9.833280	5.465124
H	2.29035394	9.75797738	11.97247588	C	-1.137403	2.115603	10.221226
C	1.64442794	8.05823606	10.83837561	C	-3.425502	10.392400	4.230642
C	3.87928745	5.26626963	9.57469142	C	-0.582878	2.404481	8.979646
C	0.25449288	8.64224036	10.91957132	C	-4.463782	11.334653	4.241537
C	-2.36865070	8.41248703	4.01273784	C	0.093766	3.610084	8.768880
C	-3.02405129	9.43060475	3.29787710	C	-0.176124	5.086668	12.308776
C	-3.48648581	9.17707113	2.01775386	C	0.690384	3.740048	7.375084
H	-3.98868323	9.95078751	1.44362104	C	2.076249	6.795505	10.031181
C	-3.27921794	7.91431033	1.47282524	C	3.423190	6.343218	10.028699
H	-3.63681477	7.69831681	0.47043556	C	4.488761	7.174372	10.410338
C	-2.59626051	6.92610152	2.18294697	B	0.828169	6.027601	9.394260
H	-2.42506264	5.95761700	1.72307057	C	4.260664	8.471719	10.849457
C	-2.11620557	7.16446048	3.46220605	C	-5.037685	11.696227	5.463100
C	-2.34039618	10.25893464	5.32770711	C	2.950434	8.928225	10.939585
C	-3.01079058	10.61359775	4.14386897	C	-3.766031	6.664047	5.412044
C	-3.53532667	11.88809976	4.01187593	C	1.886793	8.112199	10.541894
H	-4.06451564	12.18189741	3.10959270	C	3.862187	4.964157	9.562539
C	-3.38675204	12.78179221	5.06721434	C	0.518053	8.741747	10.754018
H	-3.79109296	13.78586047	4.97967466	C	-1.711857	8.895654	3.817084
C	-2.74834894	12.40231857	6.24856679	C	-2.619094	9.792774	3.181459
H	-2.66963921	13.11183038	7.06658819	C	-2.592575	9.917118	1.784929
C	-2.22593350	11.12681452	6.40386005	C	-4.583683	11.129507	6.671339
B	0.82933183	6.03880409	9.38724679	C	-1.679148	9.153421	1.053824
H	-1.55415326	6.41127076	4.00662998	C	2.058526	9.717803	5.901342
H	-1.75828183	10.81440270	7.33318233	C	-0.797632	8.264775	1.702630
C	-3.27099262	6.62593975	6.46520546	O	-3.263306	6.855033	6.767163
H	-3.93821370	7.49343123	6.41188516	O	0.674313	9.385894	5.658731
H	-3.32739659	6.11908448	5.49709196	H	1.806068	7.950617	7.664949
H	-3.65618806	5.94252971	7.22522810	H	-3.200039	9.751834	7.620543
C	0.72602523	9.79101895	5.97702716	H	-1.815158	5.762793	8.525722
H	0.62419947	9.71273819	4.88885045	H	-0.122452	7.439134	3.593087
H	0.32943057	10.76902904	6.26608326	H	-1.355144	2.789769	12.243843
H	1.78968278	9.77312313	6.22483126	H	-1.679552	1.188851	10.382744
				H	-0.667629	1.688653	8.168310
				H	-4.816381	11.777808	3.313221
				H	5.502972	6.793131	10.366996
				H	5.089780	9.109095	11.141426
				H	-5.844478	12.424457	5.485264
				H	2.747638	9.921177	11.328083
<b>Cbz-MeO<math>\pi</math></b>							
$E = -16.969$							
$N_{\text{imag}} = 0$							
$S_0$							
F	-0.077226	4.317614	13.444876				

## Appendix

H	-2.973265	6.288745	4.757778
H	-4.174640	7.595140	5.011205
H	-4.559704	5.919059	5.500356
H	-3.276060	10.594428	1.278363
H	-5.046930	11.427190	7.608720
H	-1.648141	9.240389	-0.029339
H	2.296788	10.501836	5.181634
H	2.704469	8.847682	5.732345
H	2.197117	10.093078	6.922491
H	-0.098792	7.678365	1.111061

### **Cbz-MeO $\pi$**

$$E = -25.049$$

$$N_{\text{imag}} = 0$$

#### **T<sub>1</sub>**

F	-0.322825	4.863583	13.520855
F	0.933091	6.154396	12.336077
F	-1.229712	6.296414	12.176875
F	1.202786	4.618282	7.129801
F	-0.728077	3.726148	6.705509
F	0.982127	2.473298	7.153118
F	4.894927	4.274533	9.478057
F	2.778701	3.867155	9.424767
F	3.709086	4.996640	7.818125
F	-0.227117	8.218013	10.706279
F	0.978781	9.382777	12.060199
F	0.912446	9.907881	9.959424
N	-1.983883	8.917130	5.219486
C	0.085999	6.840219	8.315867
C	0.669747	7.933845	7.643083
C	-4.147171	9.469993	6.385046
C	0.000874	8.625204	6.659523
C	-1.329526	8.218992	6.211680
C	-1.930178	7.132268	6.903020
C	-1.263760	6.483012	7.892432
C	-0.284043	8.793880	3.362788
C	0.204155	4.673816	9.876750
C	-0.228527	4.392388	11.193412
C	-0.820167	3.187418	11.556758
C	-3.284713	9.443226	5.298787
C	-1.018987	2.188247	10.625187
C	-3.603216	10.061778	4.077952
C	-0.613486	2.412446	9.326942
C	-4.825222	10.699555	3.927583
C	-0.015789	3.616135	8.965674
C	-0.198500	5.422798	12.292033
C	0.375175	3.636304	7.507537
C	2.176756	6.718013	9.969621
C	3.457240	6.123434	9.881590
C	4.614053	6.741633	10.342753
B	0.827554	6.070789	9.398714
C	4.564118	7.996276	10.917335
C	-5.705204	10.712334	5.001328
C	3.339489	8.619873	11.025448
C	-3.207498	5.972396	5.307839
C	2.180588	7.997360	10.570275
C	3.694496	4.820307	9.163865
C	0.951511	8.839711	10.815116
C	-1.483370	9.192900	3.932932
C	-2.457057	9.893428	3.203617
C	-2.209543	10.242730	1.883869
C	-5.365009	10.110100	6.214114
C	-0.998658	9.876313	1.313544

C	1.681630	10.300554	6.553262
C	-0.052923	9.153741	2.044076
O	-3.181382	6.707405	6.537538
O	0.442741	9.744599	6.094751
H	1.669965	8.249760	7.914718
H	-3.884640	9.005209	7.328595
H	-1.763561	5.633643	8.348792
H	0.447722	8.219543	3.921582
H	-1.133990	3.038857	12.584033
H	-1.480707	1.248335	10.909594
H	-0.745614	1.638829	8.576185
H	-5.084571	11.188584	2.992479
H	5.565384	6.231301	10.240834
H	5.467271	8.477287	11.278660
H	-6.667503	11.206192	4.902197
H	3.269579	9.600930	11.486017
H	-2.551635	5.096518	5.379152
H	-2.895484	6.598833	4.462848
H	-4.239713	5.653459	5.160141
H	-2.954266	10.781567	1.304328
H	-6.065475	10.144032	7.043242
H	-0.787476	10.141202	0.281659
H	1.809502	11.227756	5.997062
H	2.506729	9.614181	6.338427
H	1.627727	10.499646	7.627774
H	0.879541	8.861013	1.570556

### **MeCbz- $\pi$**

$$E = -16.534$$

$$N_{\text{imag}} = 0$$

#### **S<sub>0</sub>**

F	-0.134317	5.180019	13.848851
F	1.035492	6.377274	12.447777
F	-1.111426	6.793973	12.726017
F	1.017371	4.367673	7.562266
F	-1.079610	4.016146	6.986881
F	0.192572	2.342866	7.614648
F	4.515821	3.858214	10.290626
F	2.356288	3.710745	10.007753
F	3.660342	4.189984	8.296015
F	-0.097990	8.336840	10.692131
F	1.287118	9.767087	11.597058
F	0.921232	9.830943	9.434966
N	-1.889390	8.847353	5.115813
C	0.004470	6.838066	8.347341
C	0.757862	7.518637	7.364797
H	1.841856	7.532129	7.433242
C	0.143461	8.164301	6.296727
H	0.729685	8.677713	5.539883
C	-1.252437	8.171432	6.202737
C	-2.027285	7.519649	7.168192
H	-3.109758	7.532521	7.078206
C	-1.402119	6.850536	8.215340
H	-2.014979	6.337109	8.950683
C	-0.112099	4.884168	10.175630
C	-0.553062	4.794768	11.523901
C	-1.438672	3.793240	11.952569
H	-1.768629	3.781186	12.985370
C	-1.890235	2.815504	11.076199
H	-2.576380	2.045338	11.415108
C	-1.423881	2.822137	9.766786
H	-1.725921	2.038253	9.079738
C	-0.557669	3.828693	9.328136

C	-0.180735	5.785763	12.615662
C	-0.102380	3.658523	7.886955
C	2.136625	6.652609	9.956981
C	3.354047	5.919633	9.929305
C	4.600114	6.538860	10.116109
H	5.504229	5.942959	10.059722
C	4.689768	7.899242	10.379312
H	5.657350	8.371075	10.520684
C	3.518274	8.639238	10.489377
H	3.564793	9.693354	10.743145
C	2.274973	8.032512	10.284572
C	3.451760	4.430825	9.635207
C	1.094880	8.969132	10.493360
C	-1.975332	8.364964	3.791524
C	-2.678508	9.335183	3.016671
C	-2.921458	9.114837	1.654007
H	-3.457323	9.852955	1.062359
C	-2.468594	7.928852	1.081501
H	-2.641976	7.729567	0.026874
C	-1.796950	6.971674	1.864558
H	-1.470557	6.044857	1.396984
C	-1.534456	7.145060	3.232132
C	-2.526492	10.104914	5.196708
C	-3.028499	10.425826	3.900081
C	-3.706781	11.632479	3.680106
H	-4.089750	11.878478	2.692754
C	-3.870299	12.507653	4.750936
H	-4.392008	13.451227	4.611352
C	-3.349303	12.186778	6.018234
H	-3.474279	12.896713	6.833421
C	-2.660094	10.994123	6.286195
B	0.699392	6.100302	9.532738
C	-0.833474	6.045528	4.001291
H	0.174933	6.339684	4.314196
H	-1.375676	5.766926	4.909739
H	-0.743858	5.154983	3.371915
C	-2.108007	10.748687	7.674345
H	-2.634870	9.937481	8.189828
H	-1.049321	10.473579	7.655094
H	-2.213157	11.654981	8.278319

**MeCbz- $\pi$** 

$E = -24.314$

$N_{\text{imag}} = 0$

**T<sub>1</sub>**

F	-0.546152	5.234226	13.599019
F	1.383245	5.619463	12.706976
F	-0.352058	6.777654	12.100833
F	0.789985	4.557811	7.122145
F	-1.255017	3.861802	6.934487
F	0.361471	2.451421	7.232152
F	4.562383	4.164068	9.952757
F	2.629237	3.785682	10.839535
F	2.783425	4.310802	8.737066
F	-0.333301	8.646587	10.325789
F	0.888191	9.906617	11.571955
F	1.072225	10.025315	9.417287
N	-1.899075	8.869111	5.090282
C	-0.014891	6.859660	8.310367
C	0.687666	7.765074	7.472705
H	1.747026	7.932504	7.650588
C	0.082656	8.430194	6.434378
H	0.647215	9.110669	5.800460

C	-1.269171	8.197116	6.166008
C	-2.003466	7.305343	6.953032
H	-3.060090	7.149612	6.745858
C	-1.387323	6.668364	8.002389
H	-1.978292	6.001480	8.625239
C	0.041006	4.770707	9.984973
C	-0.245494	4.514674	11.352835
C	-0.828541	3.340138	11.801726
H	-1.023748	3.211762	12.860879
C	-1.177946	2.341100	10.910084
H	-1.640147	1.423077	11.258464
C	-0.918131	2.536347	9.570113
H	-1.165605	1.756418	8.855889
C	-0.317362	3.709204	9.116742
C	0.060510	5.531445	12.420126
C	-0.084516	3.679365	7.624708
C	1.962688	6.779183	10.114601
C	3.167441	6.054361	10.319968
C	4.318682	6.623084	10.841643
H	5.205929	6.012180	10.968017
C	4.349776	7.963402	11.184877
H	5.251918	8.412364	11.587780
C	3.205478	8.712566	11.010448
H	3.201953	9.761286	11.292998
C	2.041207	8.140745	10.500959
C	3.274025	4.595600	9.963194
C	0.905795	9.135367	10.446909
C	-2.335084	8.264207	3.917136
C	-2.911715	9.261319	3.095982
C	-3.408185	8.947099	1.854835
H	-3.848080	9.705398	1.213717
C	-3.313485	7.617853	1.431877
H	-3.699910	7.336709	0.456626
C	-2.708381	6.655204	2.225129
H	-2.619872	5.639019	1.850420
C	-2.182438	6.931475	3.490469
C	-2.173437	10.231295	5.051627
C	-2.801945	10.518668	3.817351
C	-3.208805	11.795585	3.518034
H	-3.697242	12.026700	2.575914
C	-2.990582	12.790978	4.475311
H	-3.298144	13.811569	4.267279
C	-2.412705	12.492762	5.699703
H	-2.290329	13.283856	6.434593
C	-1.991228	11.206776	6.050004
B	0.667030	6.132328	9.476946
C	-1.493312	5.844693	4.249900
H	-0.558451	6.188565	4.703667
H	-2.104830	5.467747	5.075658
H	-1.278028	5.010189	3.578287
C	-1.434567	10.965765	7.415549
H	-1.837162	10.054702	7.869429
H	-0.347858	10.836401	7.400321
H	-1.666141	11.817495	8.059552

**MeCbz-Me $\pi$** 

$E = -17.717$

$N_{\text{imag}} = 0$

**S<sub>0</sub>**

F	-4.520129	1.348285	7.382748
F	-2.665940	1.678218	6.279227
F	-4.606655	2.099836	5.321814
F	-1.156504	-2.575493	3.512344

## Appendix

F	-2.890308	-3.299207	2.363674
F	-2.295806	-4.302074	4.222263
F	0.805367	-1.518050	7.381963
F	-1.049742	-1.849283	6.280369
F	0.890182	-2.271749	5.321737
F	-2.561865	2.400877	3.510107
F	-1.422309	4.128586	4.216937
F	-0.829194	3.123565	2.359069
N	-1.860643	-0.090418	-1.735620
C	-1.859344	-0.087814	2.501867
C	-0.660778	0.054469	1.772412
H	0.280353	0.163318	2.304727
C	-0.636246	0.044116	0.376737
C	0.654885	0.188862	-0.392776
C	-1.860208	-0.089540	-0.301460
C	-3.083749	-0.222361	0.377659
C	-4.375345	-0.368084	-0.390883
C	-3.058357	-0.230990	1.773332
H	-3.999166	-0.339168	2.306355
C	-3.089558	-0.821247	4.768067
C	-4.040839	-0.210732	5.630261
C	-5.209315	-0.873111	6.038638
H	-5.918733	-0.356550	6.675465
C	-5.464483	-2.180222	5.645743
H	-6.371253	-2.685207	5.964511
C	-4.523932	-2.839706	4.863425
H	-4.681075	-3.877153	4.585961
C	-3.367418	-2.178754	4.436609
C	-3.941321	1.217494	6.142540
C	-2.423757	-3.063047	3.636226
C	-0.627624	0.648554	4.766215
C	0.324451	0.039085	5.628255
C	1.493211	0.702032	6.034903
H	2.203212	0.186258	6.671721
C	1.747913	2.008727	5.640319
H	2.654908	2.514157	5.957741
C	0.806647	2.667240	4.858033
H	0.963463	3.704381	4.579240
C	-0.350159	2.005694	4.432954
C	0.225489	-1.388601	6.142119
C	-1.294610	2.888881	3.632298
C	-1.677927	-1.225213	-2.550580
C	-1.744975	-0.805935	-3.913087
C	-1.595522	-1.739482	-4.948312
H	-1.646362	-1.424699	-5.987763
C	-1.383070	-3.074841	-4.613979
H	-1.263081	-3.821186	-5.395390
C	-1.326053	-3.472145	-3.264474
H	-1.165071	-4.522829	-3.031373
C	-1.472068	-2.575919	-2.195063
C	-2.043800	1.043377	-2.551865
C	-1.977527	0.622435	-3.913897
C	-2.127573	1.554719	-4.950175
H	-2.077343	1.238667	-5.989272
C	-2.339809	2.890488	-4.617352
H	-2.460221	3.635884	-5.399605
C	-2.396057	3.289439	-3.268300
H	-2.556892	4.340409	-3.036390
C	-2.249454	2.394516	-2.197880
B	-1.858844	-0.086813	4.061334
C	-1.413395	-3.087299	-0.771434
H	-0.581950	-2.650831	-0.207486
H	-2.325400	-2.856533	-0.212695

H	-1.284582	-4.173762	-0.773599
C	-2.307355	2.907606	-0.774839
H	-3.138516	2.471850	-0.209918
H	-1.395061	2.677458	-0.216319
H	-2.436118	3.994072	-0.778228
H	1.501215	0.307952	0.289244
H	0.619838	1.058342	-1.060156
H	0.840697	-0.686167	-1.027114
H	-4.561430	0.506023	-1.026405
H	-5.221288	-0.486075	0.291809
H	-4.340782	-1.238559	-1.056994

### **MeCbz-Me $\pi$**

$E = -25.605$

$N_{\text{imag}} = 0$

**T<sub>1</sub>**

F	-4.681789	1.389005	7.024675
F	-2.528733	1.196107	7.021582
F	-3.567485	1.887700	5.241070
F	-1.287640	-2.688968	3.011625
F	-3.227681	-3.310760	2.261543
F	-2.274164	-4.397539	3.875814
F	0.949633	-1.557317	7.037056
F	-1.203578	-1.365968	7.025504
F	-0.157595	-2.059056	5.249853
F	-2.431953	2.511094	3.004152
F	-1.452096	4.222267	3.870819
F	-0.489378	3.134810	2.262419
N	-1.848521	-0.090392	-1.766987
C	-1.856657	-0.089077	2.460905
C	-0.690515	0.200764	1.714510
H	0.236795	0.408714	2.245778
C	-0.660499	0.217162	0.336614
C	0.606132	0.503204	-0.415266
C	-1.850246	-0.090580	-0.343265
C	-3.043201	-0.397812	0.331624
C	-4.306931	-0.684652	-0.424927
C	-3.019342	-0.379804	1.709557
H	-3.949134	-0.586721	2.236875
C	-2.953070	-0.950364	4.747339
C	-3.774678	-0.427996	5.784646
C	-4.763349	-1.165423	6.418361
H	-5.356906	-0.702341	7.199492
C	-5.010703	-2.477295	6.050345
H	-5.788343	-3.054386	6.540752
C	-4.240240	-3.035489	5.050925
H	-4.403677	-4.069831	4.761737
C	-3.233915	-2.303553	4.422452
C	-3.631172	0.995198	6.255068
C	-2.487607	-3.133088	3.404170
C	-0.772204	0.777642	4.750389
C	0.045920	0.257436	5.791350
C	1.031451	0.996687	6.427833
H	1.622574	0.535238	7.211771
C	1.278691	2.308360	6.059027
H	2.053825	2.886960	6.551619
C	0.511494	2.864435	5.055912
H	0.674957	3.898547	4.765910
C	-0.491558	2.130514	4.424532
C	-0.098351	-1.165285	6.262988
C	-1.234518	2.957567	3.401768
C	-1.800530	-1.224984	-2.563773
C	-1.823057	-0.817870	-3.919474

C	-1.760775	-1.749359	-4.927408
H	-1.770903	-1.453745	-5.972742
C	-1.669374	-3.098730	-4.566084
H	-1.621041	-3.857846	-5.341488
C	-1.620266	-3.485769	-3.234498
H	-1.526241	-4.540966	-2.991432
C	-1.675882	-2.573345	-2.176504
C	-1.901962	1.043957	-2.564226
C	-1.887779	0.635910	-3.919718
C	-1.959056	1.566452	-4.927955
H	-1.956129	1.269918	-5.973075
C	-2.051080	2.915899	-4.567121
H	-2.106731	3.674272	-5.342758
C	-2.092246	3.303755	-3.235566
H	-2.187520	4.358863	-2.992601
C	-2.027535	2.392219	-2.177209
B	-1.860757	-0.087501	3.998392
C	-1.587007	-3.061644	-0.767537
H	-0.859964	-2.490171	-0.179905
H	-2.540035	-2.962521	-0.235095
H	-1.301629	-4.116583	-0.761481
C	-2.109524	2.881477	-0.768164
H	-2.833464	2.310116	-0.176552
H	-1.153902	2.783181	-0.240349
H	-2.395379	3.936281	-0.761382
H	1.435523	0.642772	0.282063
H	0.524866	1.411620	-1.025881
H	0.869602	-0.315732	-1.096535
H	-4.566208	0.132039	-1.110495
H	-5.139544	-0.820117	0.269365
H	-4.224661	-1.595677	-1.031478

**Phox-Me $\pi$** 

$E = -16.752$

$N_{\text{imag}} = 0$

**S<sub>0</sub>**

F	-0.103865	3.949696	13.257065
F	0.782451	5.712838	12.323536
F	-1.408254	5.471017	12.359404
F	1.850126	4.942776	7.222398
F	-0.008846	4.278022	6.244122
F	1.576368	2.834797	6.707377
F	5.013406	4.791067	10.381974
F	3.039394	4.142521	9.711099
F	4.335210	5.303260	8.357296
F	-0.715432	7.655695	10.829521
F	0.077972	9.218913	12.137751
F	-0.092049	9.592114	9.983043
H	-4.042515	7.772735	6.759968
C	0.068524	6.824827	8.274100
C	0.704958	7.858040	7.557122
H	1.735190	8.115325	7.789054
C	0.059584	8.554592	6.533328
C	-1.278206	8.221600	6.254951
C	-1.963882	7.212521	6.954672
C	-1.266508	6.516255	7.943993
H	-1.782914	5.726049	8.482816
C	0.333887	4.548436	9.652404
C	-0.194664	4.036451	10.867699
C	-0.803977	2.773471	10.940436
H	-1.218091	2.435847	11.884043
C	-0.875471	1.949785	9.825115
H	-1.350347	0.975450	9.888675

C	-0.299565	2.380314	8.634971
H	-0.299547	1.729605	7.766533
C	0.290255	3.645185	8.550464
C	-0.219273	4.800151	12.182533
C	0.922814	3.941443	7.198458
C	1.974806	6.854908	10.146773
C	3.349563	6.499804	10.188050
C	4.330488	7.377570	10.676804
H	5.371259	7.073461	10.663572
C	3.985192	8.623404	11.183162
H	4.749540	9.297621	11.557396
C	2.641824	8.979042	11.232595
H	2.347953	9.927042	11.671462
C	1.662431	8.117902	10.728607
C	3.911369	5.188553	9.662067
C	0.240007	8.628007	10.906119
H	-3.504716	6.579126	5.578518
H	-3.777173	6.089750	7.265104
B	0.819237	6.047596	9.398210
H	0.236825	10.601976	5.865507
H	1.787900	9.765830	6.096111
C	-3.402421	6.892797	6.624398
C	0.756989	9.643125	5.752632
H	0.773297	9.410588	4.681167
H	-0.737066	6.727370	4.295081
N	-1.969968	8.938763	5.218211
O	-3.329940	10.352736	3.175989
C	-3.337023	10.812508	4.494596
C	-2.665873	10.121576	5.524362
C	-1.265404	6.848624	2.202396
C	-1.944441	7.569883	1.220265
C	-2.629293	8.743119	1.573150
C	-2.628245	9.179284	2.891823
C	-1.945922	8.461714	3.895721
C	-1.265266	7.290457	3.532351
C	-4.035863	11.984427	4.754020
C	-2.718941	10.646478	6.823915
H	-0.730714	5.938111	1.945350
H	-1.948481	7.233217	0.187418
H	-3.168508	9.328387	0.832954
C	-4.082970	12.500767	6.058321
C	-3.423680	11.828712	7.087687
H	-4.631133	13.417636	6.255768
H	-3.450416	12.215648	8.102855
H	-2.205731	10.125814	7.626007
H	-4.538116	12.482991	3.929181

**Phox-Me $\pi$** 

$E = -24.706$

$N_{\text{imag}} = 0$

**T<sub>1</sub>**

F	-0.458597	4.298177	13.168078
F	1.403975	5.183337	12.526562
F	-0.488611	6.080460	11.949914
F	1.379861	4.961017	6.810661
F	-0.470094	3.939227	6.326243
F	1.369158	2.822550	6.568827
F	4.965704	4.833316	9.895749
F	3.098672	3.954080	10.532308
F	3.274470	4.833577	8.553714
F	-0.746794	8.187202	10.488548
F	0.127158	9.438488	12.005903
F	0.396728	9.938292	9.916343

## Appendix

H	-4.019862	7.432000	6.414014
C	0.045190	6.854001	8.245544
C	0.590604	8.006401	7.638197
H	1.569654	8.358455	7.957104
C	-0.051398	8.713434	6.640957
C	-1.304404	8.249287	6.225097
C	-1.910339	7.116367	6.779662
C	-1.222701	6.448835	7.773680
H	-1.694712	5.572520	8.213509
C	0.423149	4.565138	9.590677
C	0.112899	4.035737	10.874507
C	-0.252622	2.715653	11.086232
H	-0.480909	2.379302	12.091497
C	-0.347513	1.830545	10.026121
H	-0.640850	0.798505	10.189028
C	-0.052279	2.289781	8.759587
H	-0.099154	1.606494	7.916782
C	0.332737	3.611285	8.543685
C	0.145513	4.898534	12.107480
C	0.662898	3.868677	7.092849
C	1.883936	6.848092	10.197942
C	3.196516	6.338976	10.404915
C	4.177372	7.023404	11.105261
H	5.159549	6.578783	11.221192
C	3.920955	8.274546	11.639299
H	4.690102	8.815175	12.181336
C	2.662296	8.813383	11.473060
H	2.433273	9.784069	11.902867
C	1.667426	8.121861	10.785199
C	3.617196	5.004964	9.848786
C	0.359939	8.877188	10.781743
H	-3.235214	6.359790	5.249849
H	-3.580569	5.783584	6.884974
B	0.788365	6.084617	9.352080
H	-0.041602	10.828028	6.197097
H	1.555772	10.111670	6.442795
C	-3.256454	6.651698	6.307147
C	0.565449	9.931725	6.019216
H	0.677594	9.825020	4.933327
H	-0.529731	6.944319	4.279033
N	-1.997516	8.965363	5.181818
O	-3.335158	10.347225	3.166733
C	-3.466282	10.727800	4.463472
C	-2.798942	10.041035	5.494420
C	-0.950555	7.136430	2.176396
C	-1.639619	7.852920	1.188949
C	-2.435572	8.925763	1.528875
C	-2.545342	9.285393	2.862966
C	-1.861359	8.576308	3.867537
C	-1.055205	7.488311	3.500269
C	-4.281660	11.815101	4.735702
C	-2.970393	10.472834	6.818278
H	-0.326894	6.294185	1.895336
H	-1.546818	7.562750	0.147342
H	-2.980045	9.499794	0.785981
C	-4.435945	12.224351	6.042909
C	-3.779546	11.551349	7.081881
H	-5.071919	13.074653	6.267123
H	-3.909896	11.883443	8.106595
H	-2.453098	9.939808	7.609981
H	-4.777942	12.316123	3.910754

$$E = -17.177$$

$$N_{\text{imag}} = 0$$

$S_0$

F	-0.077226	4.317614	13.444876
F	0.895659	5.928136	12.337845
F	-1.303323	5.858354	12.473622
F	1.656173	4.697311	7.262080
F	-0.260805	4.013187	6.420786
F	1.283008	2.560097	6.984227
F	4.974093	4.533428	10.247195
F	2.924502	3.989673	9.727391
F	4.217211	4.966584	8.232076
F	-0.516300	7.852849	10.745772
F	0.455692	9.383185	11.970112
F	0.233229	9.701128	9.810735
N	-1.944355	8.925107	5.199875
C	0.087337	6.775836	8.243465
C	0.764789	7.736825	7.460895
C	-3.548504	10.190030	6.690333
C	0.104882	8.418305	6.439753
C	-1.266074	8.157654	6.178366
C	-1.938142	7.178895	6.939422
C	-1.261023	6.505987	7.962028
C	-0.802866	8.121842	3.093074
C	0.248679	4.593647	9.788599
C	-0.262663	4.221361	11.061285
C	-0.958038	3.018120	11.260984
C	-2.981694	9.833280	5.465124
C	-1.137403	2.115603	10.221226
C	-3.425502	10.392400	4.230642
C	-0.582878	2.404481	8.979646
C	-4.463782	11.334653	4.241537
C	0.093766	3.610084	8.768880
C	-0.176124	5.086668	12.308776
C	0.690384	3.740048	7.375084
C	2.076249	6.795505	10.031181
C	3.423190	6.343218	10.028699
C	4.488761	7.174372	10.410338
B	0.828169	6.027601	9.394260
C	4.260664	8.471719	10.849457
C	-5.037685	11.696227	5.463100
C	2.950434	8.928225	10.939585
C	-3.766031	6.664047	5.412044
C	1.886793	8.112199	10.541894
C	3.862187	4.964157	9.562539
C	0.518053	8.741747	10.754018
C	-1.711857	8.895654	3.817084
C	-2.619094	9.792774	3.181459
C	-2.592575	9.917118	1.784929
C	-4.583683	11.129507	6.671339
C	-1.679148	9.153421	1.053824
C	2.058526	9.717803	5.901342
C	-0.797632	8.264775	1.702630
O	-3.263306	6.855033	6.767163
O	0.674313	9.385894	5.658731
H	1.806068	7.950617	7.664949
H	-3.200039	9.751834	7.620543
H	-1.815158	5.762793	8.525722
H	-0.122452	7.439134	3.593087
H	-1.355144	2.789769	12.243843
H	-1.679552	1.188851	10.382744
H	-0.667629	1.688653	8.168310
H	-4.816381	11.777808	3.313221

$\text{Phox-MeO}\pi$



H	5.502972	6.793131	10.366996
H	5.089780	9.109095	11.141426
H	-5.844478	12.424457	5.485264
H	2.747638	9.921177	11.328083
H	-2.973265	6.288745	4.757778
H	-4.174640	7.595140	5.011205
H	-4.559704	5.919059	5.500356
H	-3.276060	10.594428	1.278363
H	-5.046930	11.427190	7.608720
H	-1.648141	9.240389	-0.029339
H	2.296788	10.501836	5.181634
H	2.704469	8.847682	5.732345
H	2.197117	10.093078	6.922491
H	-0.098792	7.678365	1.111061

**Phox-MeO $\pi$**  $E = -25.096$  $N_{\text{imag}} = 0$ **T<sub>1</sub>**

F	-0.421493	4.623636	13.229316
F	1.472808	5.329360	12.463077
F	-0.375913	6.327871	11.902038
F	1.129650	4.798071	6.757985
F	-0.732186	3.733652	6.419991
F	1.120486	2.644275	6.707027
F	4.878991	4.553676	9.648234
F	2.991053	3.843865	10.425723
F	3.116896	4.625165	8.399984
F	-0.529056	8.375733	10.335763
F	0.478275	9.505093	11.869058
F	0.743417	10.046934	9.786439
H	-3.031231	9.384818	7.530342
C	0.037565	6.851957	8.160569
C	0.611785	7.983434	7.533836
H	1.599117	8.309869	7.840155
C	-0.056883	8.681879	6.551718
C	-1.327217	8.253331	6.131347
C	-1.915027	7.123941	6.725343
C	-1.248872	6.451738	7.727260
H	-1.716884	5.592008	8.193098
C	0.327790	4.609277	9.610245
C	0.036021	4.181767	10.936214
C	-0.403744	2.903636	11.246173
H	-0.611040	2.646496	12.279491
C	-0.596542	1.961551	10.249576
H	-0.946545	0.962499	10.489685
C	-0.323743	2.321356	8.946183
H	-0.445612	1.591636	8.150263
C	0.133939	3.600415	8.631752
C	0.179210	5.112938	12.110822
C	0.427443	3.733168	7.156302
C	1.971679	6.805051	10.025717
C	3.254053	6.207451	10.184774
C	4.319285	6.841239	10.806490
H	5.271124	6.327531	10.889635
C	4.184056	8.126363	11.304625
H	5.018712	8.626419	11.785818
C	2.960156	8.750680	11.182802
H	2.823836	9.749959	11.587386
C	1.881444	8.111096	10.573141
C	3.545641	4.824028	9.666762
C	0.635872	8.963500	10.624107

H	-6.177433	11.987229	6.185682
H	-4.993624	10.809711	8.023571
B	0.781738	6.086848	9.268901
H	-0.519606	8.677926	0.078447
H	-2.467531	10.093134	0.732198
H	-5.370353	11.749607	3.836851
C	-5.317525	11.362810	5.963500
C	-4.650560	10.696390	6.999971
H	0.002741	7.501779	4.180076
N	-2.018271	8.963496	5.106198
O	-3.370114	10.356097	3.099338
C	-3.781376	10.438627	4.391398
C	-3.108700	9.751163	5.417687
C	-0.140124	8.004933	2.094319
C	-0.829099	8.735913	1.117473
C	-1.906175	9.523141	1.466165
C	-2.292179	9.586664	2.797099
C	-1.603140	8.870786	3.792663
C	-0.518269	8.066841	3.414103
C	-4.882394	11.238324	4.660989
C	-3.560522	9.901933	6.736684
H	0.699465	7.379101	1.808448
O	0.412561	9.794284	5.922941
O	-3.138680	6.785843	6.233756
C	1.669065	10.302637	6.368006
C	-3.739641	5.604575	6.761821
H	1.848144	11.208221	5.787480
H	2.471427	9.578957	6.181963
H	1.633537	10.541885	7.437016
H	-3.090274	4.735819	6.603999
H	-4.675748	5.475946	6.217505
H	-3.946427	5.716514	7.832702

**Cbz-FMe $\pi$**  $E = -16.608$  $N_{\text{imag}} = 0$ **S<sub>0</sub>**

F	-0.062783	3.984874	13.304833
F	0.847122	5.721206	12.343431
F	-1.347427	5.528980	12.417803
F	1.792900	4.924535	7.248215
F	-0.106066	4.325728	6.302863
F	1.450084	2.832773	6.703054
F	5.010618	4.709698	10.348372
F	3.012119	4.093451	9.719782
F	4.304679	5.216825	8.331974
F	-0.647272	7.668443	10.836230
F	0.163462	9.267340	12.092551
F	-0.015007	9.574914	9.928219
N	-1.976450	8.945511	5.213158
C	0.071439	6.826543	8.293018
C	0.717119	7.823507	7.544385
H	1.755134	8.058437	7.747774
C	0.060144	8.514258	6.526568
C	-1.294231	8.241567	6.244690
C	-1.958209	7.255195	7.002440
C	-1.273864	6.556085	7.996313
H	-1.803084	5.793848	8.555753
C	0.316596	4.555071	9.687926
C	-0.192390	4.057878	10.917681
C	-0.817981	2.804383	11.007585
H	-1.216037	2.476179	11.961227
C	-0.925900	1.977521	9.897323

## Appendix

H	-1.413094	1.010569	9.976004
C	-0.372092	2.394357	8.691811
H	-0.400350	1.740428	7.826359
C	0.232664	3.650175	8.589660
C	-0.177994	4.830007	12.228788
C	0.839386	3.941946	7.226202
C	2.009930	6.832737	10.137207
C	3.376918	6.447629	10.168155
C	4.378557	7.309635	10.641623
H	5.412698	6.984362	10.622240
C	4.063135	8.566394	11.140929
H	4.844669	9.226884	11.503566
C	2.728368	8.952450	11.197554
H	2.457684	9.909690	11.631013
C	1.728383	8.108125	10.707445
C	3.905586	5.120562	9.644842
C	0.315679	8.641587	10.883626
C	-2.042482	8.552800	3.862857
C	-2.809805	9.518137	3.151393
C	-3.017970	9.341773	1.775799
H	-3.600354	10.064820	1.209940
C	-2.466688	8.224493	1.144280
H	-2.620938	8.076702	0.078506
C	-1.711260	7.282486	1.870981
H	-1.292812	6.420767	1.357179
C	-1.488331	7.433504	3.242434
C	-2.690743	10.147626	5.375191
C	-3.220592	10.529131	4.109950
C	-3.976631	11.706511	4.016145
H	-4.391805	12.019547	3.061262
C	-4.187875	12.470215	5.166433
H	-4.772263	13.384782	5.106707
C	-3.652554	12.071207	6.407557
H	-3.830579	12.682393	7.288678
C	-2.895214	10.902914	6.529553
B	0.831352	6.037605	9.421553
H	-0.906215	6.706105	3.800723
H	-2.483168	10.597610	7.486955
C	-3.419084	6.922231	6.736493
F	-4.238642	8.000922	6.920352
F	-3.621712	6.473101	5.460350
F	-3.872708	5.937648	7.573627
C	0.820880	9.572098	5.740499
F	0.884688	9.280418	4.406245
F	0.251694	10.810385	5.857152
F	2.113177	9.693591	6.177769

### **Cbz**<sup>-FMe</sup> $\pi$

$$E = -24.719$$

$$N_{\text{imag}} = 0$$

#### **T<sub>1</sub>**

F	-0.318615	4.384851	13.362934
F	0.768417	5.922559	12.312934
F	-1.400970	5.843546	12.187416
F	1.674225	4.698216	7.179546
F	-0.283318	4.096038	6.458774
F	1.240526	2.612727	6.857078
F	4.979022	4.569019	9.981457
F	2.930282	4.030880	9.579345
F	4.056236	5.192599	8.126541
F	-0.529970	7.913691	10.856553
F	0.479472	9.399803	12.045506
F	0.316080	9.672541	9.905534

N	-1.978966	8.953544	5.207993
C	0.088614	6.805832	8.293483
C	0.661285	7.925097	7.624684
H	1.661867	8.248163	7.895317
C	0.013750	8.613416	6.633550
C	-1.290010	8.237419	6.232833
C	-1.891697	7.131951	6.879207
C	-1.220123	6.450437	7.858964
H	-1.724207	5.611609	8.329132
C	0.275869	4.586885	9.744423
C	-0.214013	4.171304	11.001539
C	-0.767477	2.913378	11.220246
H	-1.136001	2.660308	12.208451
C	-0.854203	1.992485	10.196612
H	-1.288583	1.012766	10.367382
C	-0.360192	2.339294	8.955907
H	-0.389316	1.621858	8.141978
C	0.195889	3.595291	8.738562
C	-0.277114	5.082626	12.199270
C	0.714347	3.775069	7.330091
C	2.055381	6.789203	10.080934
C	3.389525	6.327541	10.096237
C	4.441442	7.069727	10.624646
H	5.446035	6.661897	10.595067
C	4.219658	8.313418	11.179078
H	5.041118	8.892797	11.588003
C	2.927509	8.795510	11.217914
H	2.722498	9.757717	11.676404
C	1.875916	8.052083	10.692979
C	3.818239	5.034404	9.453363
C	0.534521	8.727846	10.863422
C	-1.953798	8.646438	3.862560
C	-2.752897	9.575095	3.159556
C	-2.871429	9.459421	1.797078
H	-3.475553	10.152988	1.219843
C	-2.187249	8.413681	1.155800
H	-2.273285	8.311293	0.078145
C	-1.403091	7.506599	1.863724
H	-0.889774	6.711780	1.332927
C	-1.270665	7.607031	3.240115
C	-2.776494	10.063082	5.406041
C	-3.287284	10.495223	4.162250
C	-4.112622	11.591155	4.122083
H	-4.526547	11.954904	3.186371
C	-4.415558	12.240951	5.329940
H	-5.067193	13.109424	5.311397
C	-3.903764	11.801740	6.547985
H	-4.160459	12.329911	7.460192
C	-3.068776	10.696470	6.609091
B	0.814993	6.051960	9.385138
H	-0.666934	6.913184	3.817356
H	-2.654641	10.333001	7.544796
C	-3.267465	6.700498	6.487996
F	-4.179467	7.704231	6.624679
F	-3.332853	6.328070	5.178425
F	-3.722439	5.663339	7.206719
C	0.688237	9.773050	5.975992
F	0.785142	9.613519	4.625817
F	-0.003024	10.934183	6.154501
F	1.931319	9.990902	6.430483

### **MeO<sub>3</sub>Ph**<sup>-FMe</sup> $\pi$

$$E = -14.741$$

$N_{\text{imag}} = 0$  $S_0$ 

F	-0.035622	3.960144	13.298349
F	0.857466	5.711098	12.347748
F	-1.335354	5.505068	12.435178
F	1.779399	4.961809	7.234423
F	-0.117661	4.348259	6.295232
F	1.453322	2.868540	6.687061
F	5.019159	4.739187	10.305313
F	3.019137	4.119008	9.685737
F	4.294148	5.266095	8.300900
F	-0.652925	7.664890	10.869514
F	0.162703	9.242406	12.149579
F	-0.030026	9.588435	9.992085
F	0.203915	10.829738	5.853428
C	0.052005	6.845421	8.312918
C	0.682127	7.856291	7.570122
H	1.714864	8.108215	7.779865
C	0.017908	8.533064	6.547424
C	-1.333623	8.249507	6.240690
C	-1.972017	7.244918	7.004946
C	-1.286596	6.555680	8.004888
H	-1.806950	5.783382	8.558692
C	0.319965	4.565634	9.685466
C	-0.181646	4.055400	10.912822
C	-0.802674	2.799030	10.994806
H	-1.195487	2.461343	11.947339
C	-0.912899	1.981563	9.877907
H	-1.396996	1.012527	9.950010
C	-0.365100	2.410685	8.674020
H	-0.395040	1.764149	7.803066
C	0.235282	3.669414	8.580032
C	-0.163114	4.815244	12.230900
C	0.835510	3.971734	7.215774
C	2.004535	6.847531	10.144313
C	3.374012	6.469925	10.159014
C	4.375134	7.331613	10.634150
H	5.410827	7.012336	10.601926
C	4.057262	8.580626	11.151079
H	4.838313	9.241214	11.514657
C	2.720958	8.958264	11.223651
H	2.448539	9.909014	11.670172
C	1.721269	8.114014	10.732511
C	3.905712	5.152429	9.615771
C	0.307678	8.639414	10.926556
F	2.067488	9.734198	6.218303
B	0.822895	6.055156	9.429306
C	0.780908	9.593426	5.766459
F	0.871954	9.285128	4.432728
C	-3.421250	6.869687	6.730240
F	-4.279166	7.922352	6.881872
F	-3.593701	6.390619	5.455364
F	-3.862945	5.883617	7.573665
O	-1.391765	7.355865	3.462049
C	-2.054860	8.977744	5.152568
C	-2.760826	10.164781	5.429157
C	-3.438501	10.861714	4.428854
C	-3.411977	10.362770	3.121700
C	-2.724060	9.188704	2.808487
C	-2.051852	8.506800	3.827151
O	-2.744292	10.597991	6.734848
H	-3.980019	11.777367	4.651114
O	-4.095791	11.085402	2.165649

H	-2.700497	8.795547	1.795668
H	-0.962193	6.958276	4.241618
H	-3.261283	11.420720	6.803675
H	-4.003141	10.640935	1.303359

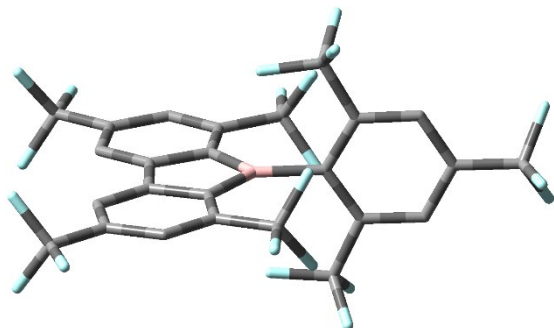
 $\text{MeO}_3\text{Ph-FMe}\pi$  $E = -22.725$  $N_{\text{imag}} = 0$  $T_1$ 

F	-0.323606	4.367504	13.350473
F	0.742211	5.921377	12.309054
F	-1.422577	5.812760	12.180279
F	1.689743	4.729391	7.185510
F	-0.242343	4.074868	6.453002
F	1.313144	2.634900	6.870412
F	4.987843	4.617780	9.969902
F	2.948851	4.065382	9.555125
F	4.068994	5.248011	8.119431
F	-0.551613	7.888235	10.860434
F	0.435554	9.355562	12.085567
F	0.284748	9.670560	9.953512
F	-0.086625	10.927899	6.193866
C	0.080840	6.804185	8.299151
C	0.632856	7.941141	7.643896
H	1.617172	8.293948	7.935327
C	-0.011136	8.603364	6.639210
C	-1.292909	8.193395	6.172537
C	-1.875902	7.086200	6.852103
C	-1.214007	6.424576	7.845728
H	-1.709877	5.577711	8.309651
C	0.286155	4.585034	9.742137
C	-0.211060	4.163662	10.991858
C	-0.753218	2.901049	11.202724
H	-1.128728	2.642598	12.186318
C	-0.818539	1.981584	10.178333
H	-1.243736	0.997385	10.343095
C	-0.315127	2.335035	8.944875
H	-0.327634	1.618999	8.129947
C	0.227725	3.596368	8.735237
C	-0.290428	5.069347	12.191908
C	0.754420	3.783367	7.331511
C	2.045619	6.801609	10.088966
C	3.383561	6.357818	10.094023
C	4.426125	7.107186	10.627093
H	5.435456	6.713357	10.589937
C	4.189524	8.339232	11.197322
H	5.003972	8.924310	11.610799
C	2.892390	8.802466	11.246140
H	2.675418	9.755868	11.716159
C	1.850864	8.052483	10.714715
C	3.827466	5.075862	9.441148
C	0.502721	8.711652	10.891079
F	1.870918	10.033294	6.445661
B	0.811068	6.057405	9.387990
C	0.632274	9.788926	6.002378
F	0.717701	9.648914	4.646497
C	-3.242271	6.642723	6.449740
F	-4.180566	7.605480	6.659697
F	-3.307272	6.371646	5.112760
F	-3.662475	5.544513	7.087841
O	-1.159008	7.624962	3.462570
C	-2.043195	8.979147	5.191815
C	-2.881858	10.075941	5.557297

## Appendix

C	-3.552991	10.773670	4.594858
C	-3.409808	10.397659	3.234368
C	-2.608720	9.336369	2.818656
C	-1.934914	8.637589	3.784339
O	-2.943745	10.340027	6.861384
H	-4.198614	11.613230	4.833557
O	-4.096793	11.131268	2.376380
H	-2.517411	9.070018	1.770699
H	-0.768695	7.260328	4.293973
H	-3.527088	11.096002	7.042798
H	-3.963271	10.830017	1.459199

## 8.2.2 Chapter 2

**<sup>F</sup>Mes<sup>F</sup>Bf**DFT B3LYP/6-31G+g(d), gas phase, S<sub>0</sub>Point group: C<sub>s</sub>Total energy: -1,931,585.71 kcal mol<sup>-1</sup>

Dipole moment: 0.97 D

Imaginary frequencies: 0

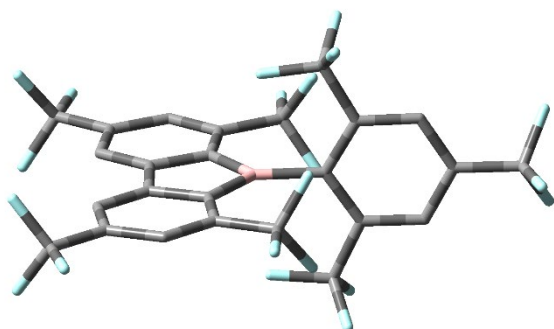
C	1.95932733	-3.48367691	0.00000000
C	3.24125601	-2.94041650	0.00000000
C	3.43542773	-1.55393774	0.00000000
C	2.32085175	-0.72748835	0.00000000
C	1.00315511	-1.24677972	0.00000000
C	0.84227238	-2.63626552	0.00000000
C	2.30925459	0.75377166	0.00000000
C	0.98358821	1.25229130	0.00000000
B	0.01666565	-0.00484050	0.00000000
C	3.41067163	1.59767629	0.00000000
C	3.19464035	2.98093856	0.00000000
C	1.90431100	3.50394216	0.00000000
C	0.80076593	2.63902953	0.00000000
C	-1.55619437	-0.01670955	0.00000000
C	-2.29787139	-0.02348364	-1.19397401
C	-3.69106341	-0.03646791	-1.20427300
C	-4.38994640	-0.04478603	0.00000000
C	-3.69106341	-0.03646791	1.20427300
C	-2.29787139	-0.02348364	1.19397401
C	-1.61001934	-0.01901545	2.53483798
F	-1.92143268	-1.10647906	3.27405300
F	-1.94041199	1.06167897	3.27595697
F	-0.25097833	-0.00690914	2.39855997
C	-1.61001934	-0.01901545	-2.53483798
F	-1.94041199	1.06167897	-3.27595697
F	-1.92143268	-1.10647906	-3.27405300
F	-0.25097833	-0.00690914	-2.39855997
C	-0.58298132	3.24718425	0.00000000
F	-0.55449464	4.59806621	0.00000000
F	-1.29673278	2.86934414	1.08982194
F	-1.29673278	2.86934414	-1.08982194
C	-0.53159540	-3.26635082	0.00000000
F	-0.48167007	-4.61664788	0.00000000
F	-1.25148996	-2.90000294	-1.08963899
F	-1.25148996	-2.90000294	1.08963899
C	4.45670190	-3.83344100	0.00000000
F	4.14009827	-5.14554461	0.00000000
F	5.23547619	-3.60407296	1.08774595

F	5.23547619	-3.60407296	-1.08774595
C	4.39586648	3.89300607	0.00000000
F	4.05864710	5.19995049	0.00000000
F	5.17967020	3.67420009	-1.08635914
F	5.17967020	3.67420009	1.08635914
C	-5.89654636	-0.01031816	0.00000000
F	-6.41511313	-0.61934253	-1.09132996
F	-6.36239378	1.26513242	0.00000000
F	-6.41511313	-0.61934253	1.09132996
H	1.82747000	-4.55756674	0.00000000
H	4.44243523	-1.14842099	0.00000000
H	4.42396015	1.20811204	0.00000000
H	1.75552433	4.57562135	0.00000000
H	-4.22684243	-0.04603226	-2.14749499
H	-4.22684243	-0.04603226	2.14749499

## Appendix

### **<sup>F</sup>Mes<sup>F</sup>Bf**

DFT RB3LYP/6-31G+G(d), gas phase, S<sub>1</sub>



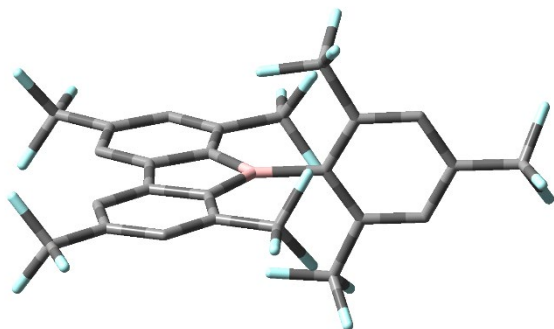
Point group: C<sub>1</sub>

Total energy: -1,931,575.25 kcal mol<sup>-1</sup>

Dipole moment: 2.07 D

C	1.98897900	-3.42531900	-0.00004700
C	3.30662700	-2.88946100	-0.00001300
C	3.50679400	-1.53623400	-0.00004800
C	2.37754800	-0.68840700	-0.00008800
C	1.00893900	-1.20420900	-0.00010300
C	0.87778900	-2.60937300	-0.00009700
C	2.36623700	0.71638900	-0.00008000
C	0.98947100	1.20999200	-0.00009500
B	0.04136900	-0.00484600	-0.00008500
C	3.48158300	1.58244200	-0.00002900
C	3.25942100	2.93221800	0.00002300
C	1.93324100	3.44665500	-0.00000200
C	0.83544600	2.61278600	-0.00007200
C	-1.54028700	-0.01687200	-0.00005700
C	-2.28849700	-0.02340500	-1.18862200
C	-3.67834800	-0.03568500	-1.19650500
C	-4.37600900	-0.04280500	-0.00002600
C	-3.67829400	-0.03572200	1.19646000
C	-2.28847800	-0.02343400	1.18855600
C	-1.66277400	-0.02071200	2.56135800
F	-2.03357500	-1.10776300	3.27007900
F	-2.05976900	1.05264000	3.27693500
F	-0.31634600	-0.00425400	2.55310900
C	-1.66284900	-0.02067200	-2.56144700
F	-2.05998600	1.05261300	-3.27704500
F	-2.03357100	-1.10779200	-3.27011200
F	-0.31642600	-0.00407700	-2.55325600
C	-0.53781600	3.23222100	-0.00011200
F	-0.48771800	4.57737200	-0.00010000
F	-1.24661500	2.86511600	1.08389300
F	-1.24653700	2.86513500	-1.08417800
C	-0.48513900	-3.25114100	-0.00015100
F	-0.41312200	-4.59534100	-0.00019300
F	-1.19986200	-2.89565800	-1.08413700
F	-1.19992200	-2.89573200	1.08381700
C	4.45741300	-3.85192900	0.00010000
F	4.42385200	-4.65596900	1.08187300
F	5.64513700	-3.22383600	-0.00004200
F	4.42378300	-4.65635400	-1.08136200
C	4.39441300	3.91328400	0.00008900
F	4.34774900	4.71690900	-1.08145100
F	5.59219800	3.30453600	0.00004600
F	4.34775100	4.71673000	1.08178500
C	-5.87713900	-0.00962100	0.00018300

F	-6.39330400	-0.61353100	-1.08661800
F	-6.34606000	1.25688100	0.00281700
F	-6.39299700	-0.61785000	1.08475100
H	1.86510800	-4.50239600	-0.00004600
H	4.51126000	-1.12883500	-0.00004500
H	4.49255500	1.19146400	-0.00002600
H	1.79188200	4.52158000	0.00002900
H	-4.21463100	-0.04570900	-2.13920400
H	-4.21456500	-0.04577800	2.13917500

**[<sup>F</sup>Mes<sup>F</sup>Bf]<sup>-</sup>**DFT UB3LYP/6-31G+G(d), gas phase, D<sub>1</sub>Point group: C<sub>1</sub>Total energy: -1,931,649.96 kcal mol<sup>-1</sup>

Dipole moment: 2.85 D

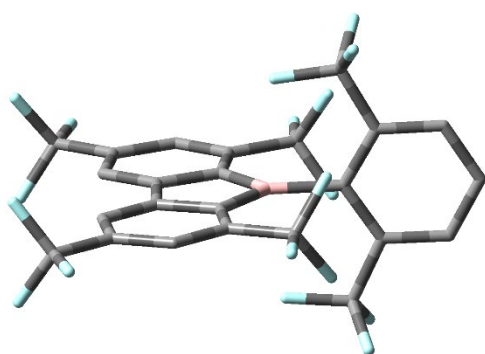
C	-5.88285900	-0.00903200	0.00003900
F	-6.41577000	-0.61702300	-1.09121300
F	-6.36900300	1.26571700	-0.00067300
F	-6.41577800	-0.61582900	1.09194200
H	1.84701100	-4.55305700	-0.00005000
H	4.47353400	-1.14529700	-0.00011700
H	4.45672900	1.20014300	-0.00019900
H	1.78115000	4.56955800	-0.00011100
H	-4.21558800	-0.04375900	-2.14317200
H	-4.21547800	-0.04344100	2.14325500

C	1.98287600	-3.47945700	-0.00006400
C	3.27855200	-2.94493100	-0.00007700
C	3.46606300	-1.55329700	-0.00009900
C	2.36093000	-0.71920600	-0.00009200
C	1.01343300	-1.22461400	-0.00006300
C	0.87239500	-2.63550900	-0.00004000
C	2.35045900	0.74350900	-0.00009300
C	0.99593300	1.22948800	-0.00006500
B	0.06102900	-0.00430700	-0.00006800
C	3.44344900	1.59350100	-0.00014500
C	3.23579300	2.98225700	-0.00018900
C	1.93253300	3.49803400	-0.00009100
C	0.83440000	2.63809000	-0.00006700
C	-1.52696200	-0.01534100	-0.00003000
C	-2.28557000	-0.02185200	-1.19246400
C	-3.68047200	-0.03485300	-1.19989200
C	-4.38377100	-0.04435700	0.00004800
C	-3.68041300	-0.03467500	1.19994700
C	-2.28550700	-0.02169300	1.19243900
C	-1.67084500	-0.01805700	2.57549700
F	-2.07022500	-1.11037900	3.29134700
F	-2.09570400	1.06182400	3.29594200
F	-0.32922400	-0.00224100	2.60545800
C	-1.67098600	-0.01821500	-2.57555800
F	-2.09544500	1.06196200	-3.29577700
F	-2.07085600	-1.11025100	-3.29158700
F	-0.32936000	-0.00295200	-2.60559600
C	-0.53664900	3.24653000	-0.00002600
F	-0.51905600	4.60901400	-0.00007600
F	-1.27263000	2.88381000	1.08853700
F	-1.27274600	2.88373100	-1.08848300
C	-0.48954900	-3.26396500	-0.00004300
F	-0.45206500	-4.62610800	0.00005000
F	-1.23091500	-2.91218100	-1.08855200
F	-1.23100100	-2.91203400	1.08835400
C	4.47669400	-3.83184700	-0.00022100
F	4.16765500	-5.15476700	0.00068100
F	5.28602200	-3.62618200	1.08522200
F	5.28486800	-3.62743600	-1.08678100
C	4.42100500	3.88641700	0.00036000
F	4.09287900	5.20471400	-0.00354500
F	5.23510300	3.69037900	-1.08325300
F	5.23012800	3.69577100	1.08874200

## Appendix

### **<sup>F</sup>Xyl<sup>F</sup>Bf**

DFT B3LYP/6-31G+g(d), gas phase, S<sub>0</sub>



F	2.39474200	-0.00000000	0.88863086
C	-2.53088200	-0.00000000	2.24932186
F	-3.27628600	1.08395000	2.56617986
F	-3.27628600	-1.08395000	2.56617986
F	-2.39474200	-0.00000000	0.88863086
H	0.00000000	4.56618600	-1.15640814
H	0.00000000	1.17551900	-3.79465214
H	0.00000000	-1.17551900	-3.79465214
H	0.00000000	-4.56618600	-1.15640814
H	2.14809900	-0.00000000	4.86683786
H	0.00000000	-0.00000000	6.12357786
H	-2.14809900	-0.00000000	4.86683786

Point group: C<sub>2v</sub>

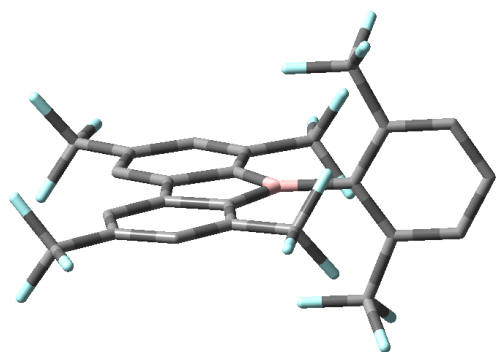
Total energy: -1,720,076.00 kcal mol<sup>-1</sup>

Dipole moment: 2.48 D

Imaginary frequencies: 0

C	0.00000000	2.63823700	-0.18434814
C	0.00000000	3.49330000	-1.29577314
C	0.00000000	2.95938500	-2.58154514
C	0.00000000	1.57439200	-2.78496614
C	0.00000000	0.74055600	-1.67576314
C	0.00000000	1.24974500	-0.35426814
C	0.00000000	-0.74055600	-1.67576314
C	0.00000000	-1.57439200	-2.78496614
C	0.00000000	-2.95938500	-2.58154514
C	0.00000000	-3.49330000	-1.29577314
C	0.00000000	-2.63823700	-0.18434814
C	0.00000000	-1.24974500	-0.35426814
B	0.00000000	-0.00000000	0.62624886
C	0.00000000	-0.00000000	2.19733786
C	1.19388500	-0.00000000	2.93948686
C	1.20145000	-0.00000000	4.33507786
C	0.00000000	-0.00000000	5.03842086
C	-1.20145000	-0.00000000	4.33507786
C	-1.19388500	-0.00000000	2.93948686
C	0.00000000	3.26107000	1.19312486
F	0.00000000	4.61330000	1.14806086
F	1.09010500	2.89416000	1.91070686
F	-1.09010500	2.89416000	1.91070686
C	0.00000000	3.86065100	-3.79025014
F	0.00000000	5.17103300	-3.46508014
F	-1.08822900	3.63824200	-4.57108414
F	1.08822900	3.63824200	-4.57108414
C	0.00000000	-3.26107000	1.19312486
F	0.00000000	-4.61330000	1.14806086
F	-1.09010500	-2.89416000	1.91070686
F	1.09010500	-2.89416000	1.91070686
C	0.00000000	-3.86065100	-3.79025014
F	0.00000000	-5.17103300	-3.46508014
F	1.08822900	-3.63824200	-4.57108414
F	-1.08822900	-3.63824200	-4.57108414
C	2.53088200	-0.00000000	2.24932186
F	3.27628600	-1.08395000	2.56617986
F	3.27628600	1.08395000	2.56617986



**<sup>F</sup>Xyl<sup>F</sup>Bf**DFT B3LYP/6-31G+g(d), gas phase, S<sub>1</sub>Point group: C<sub>1</sub>Total energy: -1, 720,013.49 kcal mol<sup>-1</sup>

Dipole moment: 0.96 D

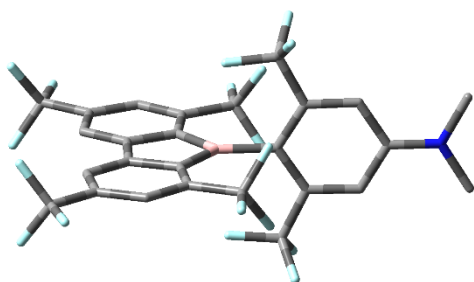
C	0.20467774	2.61737848	0.00033540
C	1.32386459	3.44869365	0.00044778
C	2.64220554	2.92520122	0.00038683
C	2.84500620	1.55834781	0.00020850
C	1.72197197	0.70652135	0.00009486
C	0.34067396	1.21433146	0.00015963
C	1.72196541	-0.70653626	-0.00009671
C	2.84499164	-1.55837328	-0.00021666
C	2.64217811	-2.92522481	-0.00039836
C	1.32383224	-3.44870487	-0.00045653
C	0.20465324	-2.61737913	-0.00033866
C	0.34066271	-1.21433346	-0.00015890
B	-0.62292180	0.00000337	0.00000449
C	-2.20078218	0.00001028	0.00000427
C	-2.95287330	-0.00027246	1.19407634
C	-4.35069064	-0.00027505	1.19818982
C	-5.05591982	0.00002129	0.00000222
C	-4.35068897	0.00031180	-1.19818439
C	-2.95287168	0.00029817	-1.19406867
C	-1.16181618	3.26244211	0.00039648
F	-1.08733526	4.61651342	0.00061558
F	-1.88224418	2.91032784	1.09041761
F	-1.88217549	2.91067944	-1.08978327
C	3.83620723	3.84224770	0.00048028
F	3.48565610	5.14593856	0.00087071
F	4.62238863	3.63340864	-1.08706959
F	4.62266536	3.63282544	1.08771563
C	-1.16184700	-3.26242940	-0.00039837
F	-1.08737951	-4.61650146	-0.00062295
F	-1.88227464	-2.91030361	-1.09041602
F	-1.88219975	-2.91066374	1.08978475
C	3.83617118	-3.84228251	-0.00048840
F	3.48560781	-5.14597004	-0.00096036
F	4.62230818	-3.63350748	1.08710625
F	4.62267763	-3.63281102	-1.08767893
C	-2.32361720	-0.00060340	2.56747692
F	-2.70630354	-1.08684985	3.29016508
F	-2.70648961	1.08517431	3.29077269
F	-0.96763219	-0.00048105	2.56234241
C	-2.32361257	0.00062255	-2.56746776
F	-2.70628861	1.08687124	-3.29015805
F	-2.70649166	-1.08515317	-3.29076301
F	-0.96762756	0.00048954	-2.56232963

H	1.19089832	4.52330627	0.00058170
H	3.85186862	1.15252442	0.00015793
H	3.85185786	-1.15255935	-0.00016988
H	1.19085586	-4.52331624	-0.00059364
H	-4.88369816	-0.00050115	2.14400550
H	-6.14128708	0.00002548	0.00000146
H	-4.88369509	0.00054164	-2.14400086

## Appendix

### *p*-NMe<sub>2</sub>-<sup>F</sup>Xyl<sup>F</sup>Bf

DFT B3LYP/6-31G+g(d), gas phase, S<sub>0</sub>



Point group: C<sub>2v</sub>

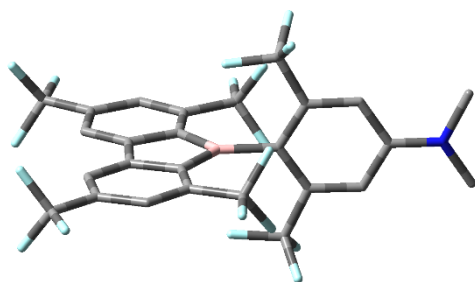
Total energy: -1,803,445.62 kcal mol<sup>-1</sup>

Dipole moment: 5.97 D

Imaginary frequencies: 1

C	1.20112308	0.00000000	-3.81673326
C	1.18370906	0.00000000	-2.42688726
C	0.00000000	0.00000000	-1.67009928
C	-1.18370906	0.00000000	-2.42688726
C	-1.20112308	0.00000000	-3.81673326
C	0.00000000	0.00000000	-4.55742728
N	0.00000000	0.00000000	-5.93371328
C	1.25449813	0.00000000	-6.65511526
C	-1.25449813	0.00000000	-6.65511526
B	0.00000000	0.00000000	-0.10525628
C	0.00000000	-1.25324200	0.86214066
C	0.00000000	-0.76422305	2.19100068
C	0.00000000	0.76422305	2.19100068
C	0.00000000	1.25324200	0.86214066
C	0.00000000	-2.63914799	0.67217861
C	0.00000000	-3.51052704	1.77114557
C	0.00000000	-2.99574209	3.06469259
C	0.00000000	-1.61387010	3.28827165
C	0.00000000	1.61387010	3.28827165
C	0.00000000	2.99574209	3.06469259
C	0.00000000	3.51052704	1.77114557
C	0.00000000	2.63914799	0.67217861
C	-2.52494395	0.00000000	-1.74389632
F	-3.27317297	1.11897607	-2.04530029
F	-2.39677198	0.00000000	-0.38250132
F	-3.27317297	-1.11897607	-2.04530029
C	2.52494395	0.00000000	-1.74389632
F	3.27317297	-1.11897607	-2.04530029
F	2.39677198	0.00000000	-0.38250132
F	3.27317297	1.11897607	-2.04530029
C	0.00000000	-3.24350793	-0.71386842
F	0.00000000	-4.59805993	-0.68439648
F	1.08917609	-2.87129488	-1.42708939
F	-1.08917609	-2.87129488	-1.42708939
C	0.00000000	-3.91447114	4.25948155
F	0.00000000	-5.22044713	3.91572850
F	-1.07885000	-3.69439919	5.05400254
F	1.07885000	-3.69439919	5.05400254
C	0.00000000	3.24350793	-0.71386842
F	0.00000000	4.59805993	-0.68439648
F	-1.08917609	2.87129488	-1.42708939
F	1.08917609	2.87129488	-1.42708939

C	0.00000000	3.91447114	4.25948155
F	0.00000000	5.22044713	3.91572850
F	1.07885000	3.69439919	5.05400254
F	-1.07885000	3.69439919	5.05400254
H	2.15867509	0.00000000	-4.32149625
H	-2.15867509	0.00000000	-4.32149625
H	1.95565911	0.77374634	-6.39097322
H	1.95565911	-0.77374634	-6.39097322
H	1.05865914	0.00000000	-7.72575626
H	-1.95565911	-0.77374634	-6.39097322
H	-1.95565911	0.77374634	-6.39097322
H	-1.05865914	0.00000000	-7.72575626
H	0.00000000	-4.58123803	1.61625252
H	0.00000000	-1.22968214	4.30369067
H	0.00000000	1.22968214	4.30369067
H	0.00000000	4.58123803	1.61625252

***p*-NMe<sub>2</sub>-<sup>F</sup>Xyl<sup>F</sup>Bf**DFT B3LYP/6-31G+g(d), gas phase, S<sub>0</sub>Point group: C<sub>1</sub>Total energy: -1,803,464.96 kcal mol<sup>-1</sup>

Dipole moment: 5.87 D

Imaginary frequencies: 0

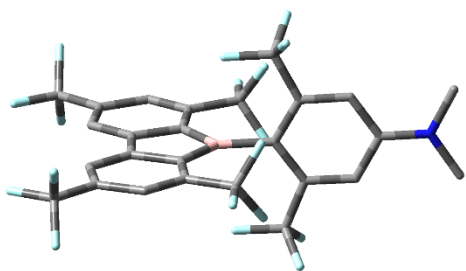
C	-3.84207727	-0.06005421	1.20112311
C	-2.45223116	-0.04258615	1.18370911
C	-1.69544310	-0.03433611	0.00000102
C	-2.45225516	-0.04322715	-1.18368807
C	-3.84210126	-0.06069021	-1.20106707
C	-4.58277132	-0.07935024	0.00004102
N	-5.95905743	-0.11886830	0.00006402
C	-6.68045948	0.02704768	1.25449811
C	-6.68048150	0.02638168	-1.25443308
B	-0.13059998	-0.01059804	-0.00001698
C	0.83679704	1.25324209	-0.00036998
C	2.16565716	0.76422311	-0.00026398
C	2.18757922	-0.71686800	0.00013302
C	0.87377615	-1.24493310	0.00029902
C	0.64683496	2.63914819	-0.00086498
C	1.74580201	3.51052730	-0.00122498
C	3.03934913	2.99574232	-0.00121698
C	3.26292821	1.61387022	-0.00067798
C	3.30941134	-1.53380102	0.00047902
C	3.12662439	-2.92167013	0.00101502
C	1.84880731	-3.47442322	0.00110202
C	0.72467219	-2.63581121	0.00079802
C	-1.76924011	-0.03088712	-2.52494418
F	-2.07064408	-1.11897621	-3.27317323
F	-0.40784500	-0.00987706	-2.39677217
F	-2.10467218	1.04844296	-3.27133123
C	-1.76919311	-0.02938712	2.52494621
F	-2.10441618	1.05056895	3.27053227
F	-0.40779500	-0.00870506	2.39674020
F	-2.07078508	-1.11685321	3.27399227
C	-0.73921217	3.24350818	-0.00113398
F	-0.70974022	4.59806028	-0.00142998
F	-1.45243321	2.87129512	1.08917610
F	-1.45222020	2.87081412	-1.09143207
C	4.23413819	3.91447144	0.00035002
F	3.89038510	5.22044752	-0.01458298
F	5.02865925	3.69439946	-1.07885007
F	5.00996125	3.71463546	1.09709510
C	-0.64320588	-3.28033432	0.00112202
F	-0.57418682	-4.63338941	0.00147102
F	-1.36670295	-2.92890032	-1.08926006

F	-1.36645896	-2.92832032	1.09149610
C	4.34801752	-3.80473714	-0.00034198
F	4.04298455	-5.12028726	0.01254402
F	5.13447057	-3.56268909	1.08008210
F	5.11885357	-3.58061610	-1.09590906
H	-4.34684030	-0.05871523	2.15867518
H	-4.34688230	-0.05986923	-2.15861014
H	-6.41631743	-0.77374637	1.95565917
H	-6.47993152	0.99440077	1.74003915
H	-7.75110058	-0.04388737	1.05865910
H	-6.47997253	0.99348276	-1.74047912
H	-6.41633542	-0.77477437	-1.95518213
H	-7.75112058	-0.04446137	-1.05854507
H	1.59090896	4.58123838	-0.00174498
H	4.27834730	1.22968224	-0.00078798
H	4.31307540	-1.11988694	0.00051202
H	1.72550135	-4.54923831	0.00161002

## Appendix

### *p*-NMe<sub>2</sub>-<sup>F</sup>Xyl<sup>F</sup>Bf

DFT UB3LYP/6-31G+g(d), gas phase, T<sub>1</sub>



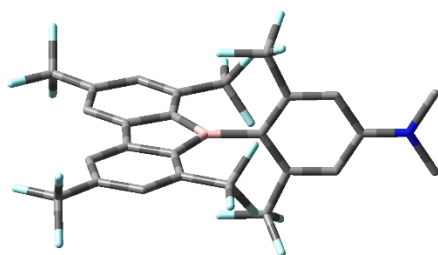
Point group: C<sub>1</sub>

Total energy: -1,804,106.70 kcal mol<sup>-1</sup>

Dipole moment: 7.93 D

C	-3.85183400	0.00044600	1.16148900
C	-2.46360700	0.00025800	1.18328700
C	-1.66794500	0.00003400	0.01575700
C	-2.39973300	0.00003400	-1.19334800
C	-3.78784400	0.00023000	-1.24286200
C	-4.55797900	0.00048000	-0.06060400
N	-5.93086900	0.00081300	-0.09674500
C	-6.69389100	-0.00035400	1.14274100
C	-6.62696900	-0.00076900	-1.37494100
B	-0.09296400	-0.00001300	0.06042100
C	0.86484900	1.21727500	0.03525700
C	2.23700500	0.70966000	0.00983200
C	2.23699800	-0.70969700	0.00990200
C	0.86486400	-1.21731000	0.03537000
C	0.71466300	2.62676400	0.02116300
C	1.81808600	3.46110300	0.01461400
C	3.14536800	2.93038000	0.00183700
C	3.35506900	1.57011000	-0.00106600
C	3.35504700	-1.57014800	-0.00096400
C	3.14529900	-2.93043600	0.00216100
C	1.81810900	-3.46111400	0.01512300
C	0.71464400	-2.62674200	0.02152300
C	-1.73870900	-0.00024500	-2.55573300
F	-2.10993900	-1.08660800	-3.28479500
F	-0.38885000	0.00016500	-2.51759000
F	-2.11056200	1.08542700	-3.28553400
C	-1.86617200	0.00029100	2.57379100
F	-2.26821300	1.08601400	3.28689200
F	-0.51525100	0.00047400	2.58973800
F	-2.26793600	-1.08554900	3.28684300
C	-0.65684400	3.25548500	0.03539400
F	-0.60830900	4.60985000	0.05336300
F	-1.37490000	2.87875800	1.12287300
F	-1.38439600	2.90919000	-1.05635600
C	4.28870600	3.90162700	-0.01110500
F	4.23854700	4.72024500	-1.09592300
F	5.49343900	3.28780000	-0.02901200
F	4.26792400	4.71424200	1.07915000
C	-0.65686200	-3.25544300	0.03595300
F	-0.60835900	-4.60980900	0.05414700
F	-1.38447700	-2.90929500	-1.05579600
F	-1.37484800	-2.87849000	1.12340900
C	4.28862200	-3.90175100	-0.01124300
F	4.26817000	-4.71447000	1.07891400
F	5.49344800	-3.28795700	-0.02946300

F	4.23808700	-4.72022600	-1.09603800
H	-4.38581500	0.00059000	2.10283100
H	-4.27198400	0.00023900	-2.21069200
H	-6.47600100	-0.89199800	1.74518400
H	-6.47529600	0.88982000	1.74703300
H	-7.75784500	0.00039400	0.90623600
H	-6.37650400	0.88929300	-1.96693400
H	-6.37692700	-0.89245400	-1.96472500

***p*-NMe<sub>2</sub>-<sup>F</sup>Xyl<sup>F</sup>Bf**DFT UCAAM-B3LYP/6-31G+g(d), hexane, T<sub>1</sub>Point group: C<sub>1</sub>Total energy: -1,803,470.87 kcal mol<sup>-1</sup>

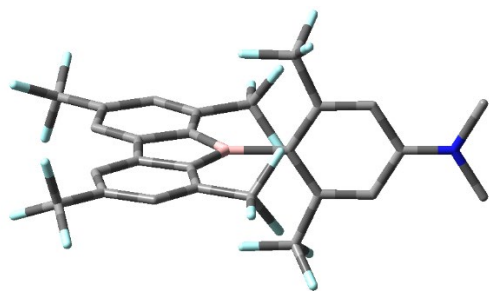
Dipole moment: 23.71 D

F	-4.24115735	4.73363537	-1.07878978
H	4.28426011	0.00016292	2.16536621
H	4.28422147	0.00047958	-2.16532183
H	6.35719621	0.89383472	1.84071995
H	6.35652204	-0.89157892	1.84179714
H	7.66084030	0.00010541	1.03766564
H	6.35634678	-0.89220266	-1.84151602
H	6.35730745	0.89321113	-1.84098739
H	7.66082241	-0.00046239	-1.03768142
H	-1.66067883	-4.55266420	-0.00024177
H	-4.32733155	-1.18856158	-0.00012188
H	-4.32767310	1.18749219	0.00007497
H	-1.66202296	4.55238028	-0.00016451
C	3.76660480	0.00019287	1.21556178
C	2.39662714	0.00013211	1.20051867
C	1.63182251	0.00027786	0.00004650
C	2.39660591	0.00043269	-1.20043549
C	3.76658341	0.00035773	-1.21550791
C	4.50216839	0.00023631	0.00002019
N	5.84779225	0.00022210	0.00000794
C	6.59688715	0.00067702	1.25848785
C	6.59686525	0.00019520	-1.25848504
B	0.05207328	0.00009301	0.00004629
C	-0.88163949	-1.22264183	-0.00001917
C	-2.22194334	-0.73049371	-0.00001727
C	-2.22215054	0.73004754	0.00000447
C	-0.88198593	1.22258700	-0.00003694
C	-0.71780386	-2.62552282	-0.00007470
C	-1.80812812	-3.47891721	-0.00016893
C	-3.10696883	-2.95724994	-0.00019439
C	-3.31596920	-1.58094883	-0.00009580
C	-3.31642758	1.58017909	0.00004258
C	-3.10783573	2.95653977	-0.00000433
C	-1.80915209	3.47858911	-0.00009574
C	-0.71857023	2.62552155	-0.00012493
C	1.77586238	0.00061326	-2.58656866
F	2.19562579	1.08134415	-3.28352425
F	0.44780659	0.00119007	-2.60906597
F	2.19469918	-1.08051398	-3.28343253
C	1.77592914	-0.00018181	2.58667488
F	2.19510220	-1.08138596	3.28323901
F	0.44787502	-0.00000103	2.60923252
F	2.19541573	1.08046717	3.28390101
C	0.65425168	-3.21591139	-0.00005796
F	0.66389497	-4.56200601	0.00001602
F	1.38594258	-2.83183437	1.08092008
F	1.38591633	-2.83196080	-1.08109738
C	-4.25361858	-3.91243828	-0.00010227
F	-4.23962883	-4.73461009	-1.07922720
F	-5.45150898	-3.29400030	-0.00164696
F	-4.24134400	-4.73239651	1.08075252
C	0.65328726	3.21636904	-0.00025627
F	0.66246667	4.56246465	-0.00047291
F	1.38507575	2.83244382	-1.08122608
F	1.38512638	2.83280131	1.08080279
C	-4.25476899	3.91138835	0.00028238
F	-4.24260073	4.73127808	1.08119027
F	-5.45247589	3.29259552	-0.00115309

## Appendix

### *p*-NMe<sub>2</sub>-<sup>F</sup>Xyl<sup>F</sup>Bf

DFT CAM-B3LYP/6-31G+g(d), hexane, S<sub>1</sub>



Point group: C<sub>1</sub>

Total energy: -1,803,461.12 kcal mol<sup>-1</sup>

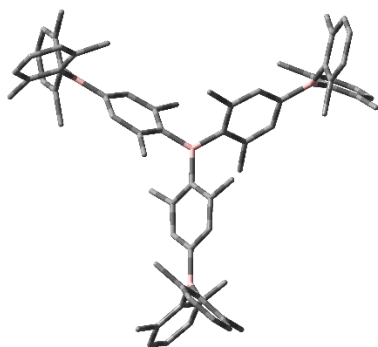
Dipole moment: 22.68 D

C	-3.76258331	0.00828866	-1.21833235
C	-2.39865521	0.00535924	-1.20470481
C	-1.62620314	0.00006400	-0.00000155
C	-2.39868428	-0.00518267	1.20468279
C	-3.76261265	-0.00811045	1.21827729
C	-4.50192576	0.00007279	-0.00003645
N	-5.83873920	0.00004455	-0.00005365
C	-6.58872872	0.04193054	-1.25666128
C	-6.58876121	-0.04188720	1.25653325
B	-0.06012645	0.00000820	0.00001422
C	0.87470590	-1.22407905	0.00411113
C	2.21542513	-0.73092709	0.00207032
C	2.21547965	0.73077464	-0.00206223
C	0.87480350	1.22402459	-0.00408349
C	0.70929148	-2.62439039	0.01846658
C	1.80164826	-3.47950857	0.02525225
C	3.09756432	-2.95960366	0.02155367
C	3.30636484	-1.58009134	0.00844141
C	3.30648878	1.57985871	-0.00844113
C	3.09778905	2.95938003	-0.02154289
C	1.80190627	3.47938234	-0.02522423
C	0.70948874	2.62434897	-0.01842849
C	-1.77815773	0.00323085	2.59247046
F	-2.14210175	1.12326838	3.25502837
F	-0.45197829	-0.06403051	2.61627466
F	-2.25087705	-1.03536461	3.31754077

C	-1.77809100	-0.00304040	-2.59247631
F	-2.14187199	-1.12314969	-3.25499829
F	-0.45191964	0.06439486	-2.61624936
F	-2.25092306	1.03546624	-3.31760356
C	-0.66207744	-3.21446030	0.03603450
F	-0.67164694	-4.56006441	0.03833449
F	-1.40699060	-2.83110493	-1.03580848
F	-1.38055924	-2.82842538	1.12577587
C	4.26071865	-3.89320476	-0.02711034
F	4.02570683	-5.04802779	0.63542980
F	5.37930089	-3.35474724	0.50465292
F	4.58549318	-4.25354523	-1.29658862
C	-0.66183945	3.21451721	-0.03597019
F	-0.67131400	4.56012128	-0.03827385
F	-1.40675449	2.83121729	1.03589048
F	-1.38037146	2.82852569	-1.12569375
C	4.26096192	3.89296032	0.02709639
F	4.02629220	5.04738745	-0.63627241
F	5.37977408	3.35415039	-0.50380270
F	4.58512252	4.25409828	1.29650398
H	-4.28298713	0.01077705	-2.16587383
H	-4.28303987	-0.01057644	2.16580621
H	-6.31357439	0.92598258	-1.83606041
H	-6.39592103	-0.85723354	-1.84745006
H	-7.65051494	0.09094412	-1.03138129
H	-6.31357963	-0.92593085	1.83593236
H	-6.39601454	0.85728116	1.84733527
H	-7.65053891	-0.09094908	1.03122353
H	1.65289693	-4.55211963	0.03963291
H	4.31821015	-1.18761225	0.00930261
H	4.31830311	1.18730463	-0.00931611
H	1.65323625	4.55200660	-0.03959564

## 8.2.3 Chapter 3

## BG1H

DFT B3LYP/6-31G, gas phase, S<sub>0</sub>Point group: C<sub>3</sub>

Total energy: -1,813,590.94

kcal mol<sup>-1</sup>

Dipole moment: 0.01 D

Imaginary frequencies: 0

C	-0.00021900	1.58674700	-0.00212200
C	-1.37405400	-0.79356300	-0.00212200
C	0.77748200	2.32342000	-0.94761800
C	0.73860800	3.72424700	-0.94648600
C	0.00011900	4.46410600	-0.00051800
C	-0.73859800	3.72335700	0.94456900
C	-0.77790100	2.32254500	0.94411400
C	-1.62243300	-1.83495500	0.94411400
C	-2.85522300	-2.50132400	0.94456900
C	-3.86608800	-2.23195000	-0.00051800
C	-3.59459700	-1.22247000	-0.94648600
C	-2.40088200	-0.48839000	-0.94761800
C	-1.64083300	1.64562200	1.99537500
C	-0.60473400	-2.24381400	1.99537500
C	-2.24666600	0.59672400	-1.99960200
C	1.64011100	1.64730700	-1.99960200
B	0.00000000	0.00000000	-0.00238600
C	1.37427300	-0.79318400	-0.00212200
C	1.62339900	-1.83502900	-0.94761800
C	2.85598900	-2.50177700	-0.94648600
C	3.86597000	-2.23215600	-0.00051800
C	3.59382100	-1.22203400	0.94456900
C	2.40033400	-0.48759100	0.94411400
C	2.24556700	0.59819200	1.99537500
C	0.60655400	-2.24403200	-1.99960200
B	0.00000000	6.03373200	0.00030300
B	5.22536500	-3.01686600	0.00030300
B	-5.22536500	-3.01686600	0.00030300
C	-6.02719000	-3.15645800	-1.36060600

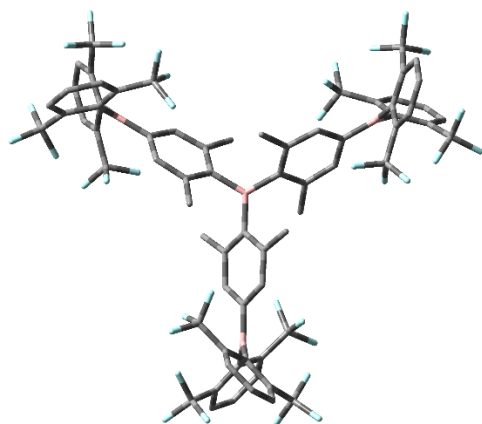
C	-5.74563800	-3.64100400	1.36197100
C	-0.28038300	6.79637100	1.36197100
C	0.28002200	6.79792900	-1.36060600
C	6.02602100	-3.15536700	1.36197100
C	5.74716800	-3.64147000	-1.36060600
C	-6.03352400	-5.03433400	1.47417900
C	-6.47138400	-5.56671300	2.69741300
C	-6.65725500	-4.75029900	3.81321300
C	-6.39410600	-3.38409700	3.71452300
C	-5.92932800	-2.82018500	2.51534100
C	-7.37829300	-2.71020900	-1.47196900
C	-8.05889400	-2.82375700	-2.69478300
C	-7.44501000	-3.39238200	-3.81100900
C	-6.12992700	-3.84666400	-3.71309100
C	-5.40855800	-3.72560200	-2.51430500
C	1.34203700	7.74489300	-1.47196900
C	1.58400100	8.39108600	-2.69478300
C	0.78461600	8.14375900	-3.81100900
C	-0.26634500	7.23200500	-3.71309100
C	-0.52218700	6.54675000	-2.51430500
C	-1.34309900	7.74235200	1.47417900
C	-1.58522300	8.38774000	2.69741300
C	-0.78525200	8.14050200	3.81321300
C	0.26633900	7.22950600	3.71452300
C	0.52231200	6.54504100	2.51534100
C	7.37662300	-2.70801800	1.47417900
C	8.05660700	-2.82102600	2.69741300
C	7.44250700	-3.39020300	3.81321300
C	6.12776700	-3.84541000	3.71452300
C	5.40701600	-3.72485600	2.51534100
C	6.03625600	-5.03468500	-1.47196900
C	6.47489300	-5.56732800	-2.69478300
C	6.66039400	-4.75137700	-3.81100900
C	6.39627200	-3.38534100	-3.71309100
C	5.93074500	-2.82114800	-2.51430500
C	-3.97852900	-4.24161900	-2.50547200
C	5.85178500	-5.99108600	-0.30848100
C	5.66261500	-1.32469800	-2.50547200
C	8.11277900	-2.06962400	0.31098900
C	3.97733000	-4.24170100	2.50520100
C	-2.26404300	8.06068500	0.31098900
C	-1.68408500	5.56631700	-2.50547200
C	2.26254000	8.06333800	-0.30848100
C	1.68475600	5.56532000	2.50520100
C	-5.84873600	-5.99106100	0.31098900
C	-8.11432500	-2.07225200	-0.30848100
C	-5.66208600	-1.32361900	2.50520100
H	1.31014800	4.26049400	-1.69938200
H	-1.30994000	4.25889000	1.69812100
H	-3.03333700	-3.26388600	1.69812100
H	-4.34477000	-0.99562500	-1.69938200
H	-1.99174100	2.38032300	2.72698400
H	-2.52143300	1.16847700	1.55216800
H	-1.10132500	0.86734600	2.54652500
H	-0.20048100	-1.38744800	2.54652500
H	-1.06555000	-2.91505900	2.72698400
H	0.24878600	-2.76786400	1.55216800
H	-2.27184200	1.59817200	-1.55686100
H	-1.30390600	0.51712800	-2.55225200
H	-3.05964100	0.53382200	-2.72986600
H	1.09979800	0.87065200	-2.55225200
H	1.99212400	2.38281600	-2.72986600

## Appendix

H	2.51997800	1.16838700	-1.55686100
H	3.03462200	-3.26486900	-1.69938200
H	4.34327700	-0.99500400	1.69812100
H	2.27264800	1.59938700	1.55216800
H	1.30180600	0.52010200	2.54652500
H	3.05729000	0.53473700	2.72698400
H	0.20410700	-1.38777900	-2.55225200
H	1.06751800	-2.91663800	-2.72986600
H	-0.24813600	-2.76655900	-1.55686100
H	-6.67457500	-6.63167900	2.76655800
H	-6.54965800	-2.73975400	4.57560500
H	-9.08311900	-2.46810500	-2.76329300
H	-5.64988600	-4.30326600	-4.57444300
H	2.40411800	9.10026500	-2.76329300
H	-0.90179500	7.04457800	-4.57444300
H	-2.40591500	9.09619100	2.76655800
H	0.90213200	7.04204800	4.57560500
H	9.08049000	-2.46451200	2.76655800
H	5.64752600	-4.30229300	4.57560500
H	6.67900100	-6.63216000	-2.76329300
H	6.55168100	-2.74131200	-4.57444300
H	-3.83737000	-4.98706000	-3.29541000
H	-3.25951000	-3.43247700	-2.68104500
H	-3.70138700	-4.70769500	-1.55581200
H	4.80111500	-6.05988000	0.00145600
H	6.17287100	-7.00011000	-0.58571400
H	6.42715600	-5.68253100	0.56932900
H	6.23760600	-0.82973000	-3.29541000
H	4.60236700	-1.10658000	-2.68104500
H	5.92767700	-0.85164800	-1.55581200
H	7.64472800	-1.12725700	-0.00132900
H	9.14602300	-1.83969900	0.58961500
H	8.13667000	-2.72353000	-0.56576600
H	3.83343800	-4.98080100	3.30054800
H	3.25713500	-3.43160000	2.67102300
H	3.70442800	-4.71580800	1.55820400
H	-1.70968900	8.40832800	-0.56576600
H	-2.84613000	7.18415700	-0.00132900
H	-2.97978600	8.84053800	0.58961500
H	-2.40023600	5.81679000	-3.29541000
H	-1.34285700	4.53905700	-2.68104500
H	-2.22629000	5.55934300	-1.55581200
H	1.70763900	8.40734600	0.56932900
H	2.84745200	7.18782700	0.00145600
H	2.97583800	8.84591800	-0.58571400
H	2.39678100	5.81025500	3.30054800
H	1.34328500	4.53656100	2.67102300
H	2.23179500	5.56603200	1.55820400
H	-4.79859700	-6.05690000	-0.00132900
H	-6.16623700	-7.00083900	0.58961500
H	-6.42698100	-5.68479800	-0.56576600
H	-7.64856700	-1.12794800	0.00145600
H	-9.14870900	-1.84580800	-0.58571400
H	-8.13479500	-2.72481500	0.56932900
H	-6.23021900	-0.82945400	3.30054800
H	-4.60042000	-1.10496100	2.67102300
H	-5.93622300	-0.85022500	1.55820400
H	-0.97561200	8.65785500	4.74877200
H	-7.01011700	-5.17383200	4.74877200
H	7.98572900	-3.48402300	4.74877200
H	0.97489400	8.66175000	-4.74623300
H	-7.98874300	-3.48659200	-4.74623300
H	7.01384900	-5.17515800	-4.74623300



## BFG1H

DFT B3LYP/6-31G, gas phase, S<sub>0</sub>Point group: C<sub>3</sub>Total energy: -4,054,541.64 kcal mol<sup>-1</sup>

Dipole moment: 0.01 D

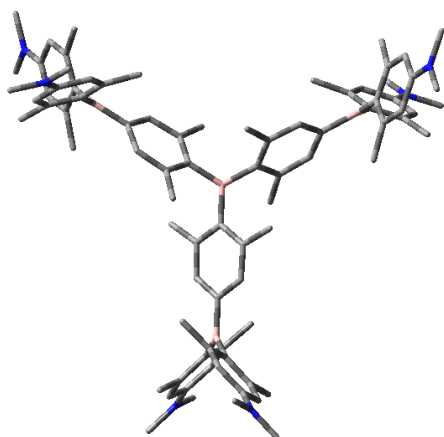
Imaginary frequencies: 0

C	-0.00204800	1.58214400	-0.01101900
C	-1.36915200	-0.79284600	-0.01101900
C	0.76812600	2.31373300	-0.96530500
C	0.72133000	3.71129300	-0.96763400
C	-0.00146900	4.44422000	-0.00502400
C	-0.72514200	3.70750400	0.95393900
C	-0.77280600	2.30996500	0.94570100
C	-1.61408600	-1.82425200	0.94570100
C	-2.84822200	-2.48174300	0.95393900
C	-3.84807300	-2.22338200	-0.00502400
C	-3.57473900	-1.23095600	-0.96763400
C	-2.38781400	-0.49165000	-0.96530500
C	-1.62599400	1.62941600	2.00188300
C	-0.59811900	-2.22286000	2.00188300
C	-2.22725300	0.58442600	-2.02486000
C	1.61975400	1.63664500	-2.02486000
B	0.00000000	0.00000000	-0.01200600
C	1.37120100	-0.78929800	-0.01101900
C	1.61968800	-1.82208300	-0.96530500
C	2.85340900	-2.48033600	-0.96763400
C	3.84954100	-2.22083800	-0.00502400
C	3.57336400	-1.22576100	0.95393900
C	2.38689100	-0.48571300	0.94570100
C	2.22411300	0.59344400	2.00188300
C	0.60749900	-2.22107000	-2.02486000
B	0.00000000	5.99245800	-0.00066900
B	5.18962100	-2.99622900	-0.00066900
B	-5.18962100	-2.99622900	-0.00066900
C	-5.91505100	-3.28571700	-1.40690400
C	-5.79667600	-3.47407100	1.41033400
C	-0.11029500	6.75710400	1.41033400
C	0.11201100	6.76544300	-1.40690400
C	5.90697200	-3.28303300	1.41033400
C	5.80304000	-3.47972500	-1.40690400
C	-6.21179800	-4.81416000	1.66462100
C	-6.70514000	-5.23073400	2.90664200

C	-6.81895500	-4.32617400	3.95670300
C	-6.43819300	-3.00625900	3.75295200
C	-5.93592600	-2.57939500	2.51183200
C	-7.28414300	-2.97400400	-1.65447500
C	-7.89873000	-3.19555100	-2.89251300
C	-7.17879700	-3.75017700	-3.94507500
C	-5.84466600	-4.08164900	-3.74779000
C	-5.21673700	-3.85767100	-2.51071100
C	1.06650900	7.79525500	-1.65447500
C	1.18193700	8.43827600	-2.89251300
C	0.34165000	8.09210800	-3.94507500
C	-0.61247900	7.10245400	-3.74779000
C	-0.73247300	6.44666200	-2.51071100
C	-1.06328600	7.78665500	1.66462100
C	-1.17737900	8.42218900	2.90664200
C	-0.33709900	8.06847500	3.95670300
C	0.61560000	7.07876900	3.75295200
C	0.73414200	6.43036100	2.51183200
C	7.27508400	-2.97249400	1.66462100
C	7.88251900	-3.19145500	2.90664200
C	7.15605400	-3.74230100	3.95670300
C	5.82259400	-4.07250900	3.75295200
C	5.20178500	-3.85096600	2.51183200
C	6.21763500	-4.82125100	-1.65447500
C	6.71679300	-5.24272500	-2.89251300
C	6.83714600	-4.34193200	-3.94507500
C	6.45714500	-3.02080500	-3.74779000
C	5.94921000	-2.58899100	-2.51071100
C	-3.75585800	-4.24735200	-2.52714500
C	6.17064000	-5.87713000	-0.58952400
C	5.55624400	-1.12899300	-2.52714500
C	8.17263800	-2.40804900	0.60305000
C	3.74028000	-4.23849800	2.52149800
C	-2.00088800	8.28173600	0.60305000
C	-1.80038600	5.37634500	-2.52714500
C	2.00442400	8.28249600	-0.58952400
C	1.80050700	5.35842700	2.52149800
C	-6.17175000	-5.87368800	0.60305000
C	-8.17506400	-2.40536600	-0.58952400
C	-5.54078700	-1.11992800	2.52149800
H	1.29071600	4.24313500	-1.72374000
H	-1.29428400	4.23644200	1.71227300
H	-3.02172400	-3.23910400	1.71227300
H	-4.32002100	-1.00377500	-1.72374000
H	-1.98556900	2.36483800	2.72824600
H	-2.50189800	1.13274000	1.57212100
H	-1.07165800	0.86759200	2.56104600
H	-0.21552800	-1.36187900	2.56104600
H	-1.05522500	-2.90197300	2.72824600
H	0.26996700	-2.73307700	1.57212100
H	-2.22659400	1.59230400	-1.59740900
H	-1.29481000	0.47853000	-2.59036500
H	-3.04924300	0.53074600	-2.74540300
H	1.06182400	0.88207300	-2.59036500
H	1.98426100	2.37534900	-2.74540300
H	2.49227300	1.13213500	-1.59740900
H	3.02930500	-3.23936000	-1.72374000
H	4.31600800	-0.99733800	1.71227300
H	2.23193000	1.60033700	1.57212100
H	1.28718600	0.49428700	2.56104600
H	3.04079500	0.53713400	2.72824600
H	0.23298600	-1.36060300	-2.59036500
H	1.06498200	-2.90609500	-2.74540300
H	-0.26567900	-2.72443900	-1.59740900
H	-6.99374700	-6.26402200	3.04500600
H	-6.53944800	-2.28810400	4.55634700
H	-8.93827700	-2.92782900	-3.02588200
H	-5.27841800	-4.53138400	-4.55311100
H	1.93356400	9.20468900	-3.02588200

## Appendix

H	-1.28508500	6.83693600	-4.55311100
H	-1.92792900	9.18877300	3.04500600
H	1.28816800	6.80738000	4.55634700
H	8.92167600	-2.92475100	3.04500600
H	5.25128000	-4.51927600	4.55634700
H	7.00471200	-6.27686000	-3.02588200
H	6.56350300	-2.30555200	-4.55311100
H	-0.42113300	8.56044200	4.91856500
H	-7.20299400	-4.64493300	4.91856500
H	7.62412700	-3.91550900	4.91856500
H	0.42676100	8.58982800	-4.90387700
H	-7.65239000	-3.92532800	-4.90387700
H	7.22562900	-4.66450000	-4.90387700
F	3.17080500	-4.54825200	1.30174600
F	2.35349900	5.02012300	1.30174600
F	-5.52430400	-0.47187200	1.30174600
F	2.94831700	-3.23123300	3.08950700
F	1.32417100	4.16893400	3.08950700
F	-4.27248800	-0.93770100	3.08950700
F	3.53260100	-5.36386500	3.32868600
F	2.87894300	5.74125500	3.32868600
F	-6.41154400	-0.37738900	3.32868600
F	8.58717800	-3.36034100	-0.33051200
F	-1.38344800	9.11688500	-0.33051200
F	-7.20373000	-5.75654400	-0.33051200
F	7.56589600	-1.38559800	-0.12309000
F	-2.58298500	7.24505700	-0.12309000
F	-4.98291100	-5.85946000	-0.12309000
F	9.34173900	-1.86404500	1.12960900
F	-3.05655900	9.02220600	1.12960900
F	-6.28518000	-7.15816100	1.12960900
F	4.97777900	-5.85924500	0.12994500
F	2.58536500	7.24050500	0.12994500
F	-7.56314400	-1.38126100	0.12994500
F	7.19754900	-5.75782900	0.34935800
F	1.38765200	9.11217500	0.34935800
F	-8.58520100	-3.35434600	0.34935800
F	6.28566400	-7.16351200	-1.11101300
F	3.06095200	9.02530100	-1.11101300
F	-9.34661600	-1.86178800	-1.11101300
F	4.29052200	-0.94688500	-3.10079500
F	-2.96528800	-3.24225900	-3.10079500
F	-1.32523500	4.18914400	-3.10079500
F	5.53599700	-0.47671100	-1.30971100
F	-3.18084200	-4.55595900	-1.30971100
F	-2.35515500	5.03267000	-1.30971100
F	6.43130900	-0.39057200	-3.33345600
F	-3.55390000	-5.37439100	-3.33345600
F	-2.87740900	5.76496300	-3.33345600

**BG1NMe<sub>2</sub>**DFT B3LYP/6-31G, gas phase, S<sub>0</sub>Point group: C<sub>3</sub>Total energy: -2,317,460.76 kcal mol<sup>-1</sup>

Dipole moment: 0.01 D

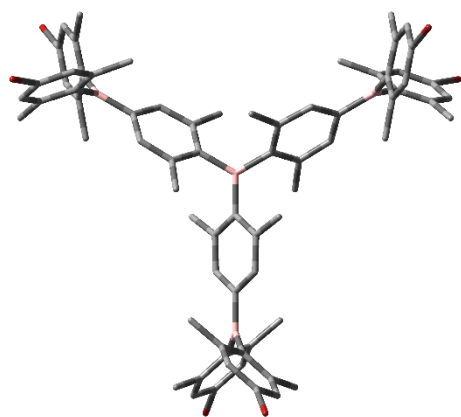
Imaginary frequencies: 0

C	-0.00040700	1.58632700	-0.00249300
C	-1.37359600	-0.79351600	-0.00249300
C	0.78137300	2.32495600	-0.94314800
C	0.74281000	3.72621400	-0.94165400
C	0.00009500	4.46734000	-0.00066200
C	-0.74290600	3.72530500	0.93937000
C	-0.78206500	2.32401400	0.93903000
C	-1.62162300	-1.83929600	0.93903000
C	-2.85475600	-2.50602900	0.93937000
C	-3.86887700	-2.23358800	-0.00066200
C	-3.59840100	-1.21981500	-0.94165400
C	-2.40415700	-0.48578900	-0.94314800
C	-1.64982900	1.64794700	1.98737300
C	-0.60224900	-2.25276800	1.98737300
C	-2.25313600	0.60290800	-1.99241900
C	1.64870200	1.64981900	-1.99241900
B	0.00000000	0.00000000	-0.00281500
C	1.37400300	-0.79281100	-0.00249300
C	1.62278500	-1.83916700	-0.94314800
C	2.85559100	-2.50639900	-0.94165400
C	3.86878300	-2.23375200	-0.00066200
C	3.59766200	-1.21927700	0.93937000
C	2.40368800	-0.48471900	0.93903000
C	2.25207900	0.60482000	1.98737300
C	0.60443400	-2.25272700	-1.99241900
B	0.00000000	6.04302000	0.00000800
B	5.23340900	-3.02151000	0.00000800
B	-5.23340900	-3.02151000	0.00000800
C	-5.97978900	-3.24721100	-1.37072800
C	-5.80081000	-3.55486000	1.37137700
C	-0.17819400	6.80107900	1.37137700
C	0.17772700	6.80225500	-1.37072800
C	5.97900400	-3.24621900	1.37137700
C	5.80206200	-3.55504400	-1.37072800

C	-6.18571300	-4.92066200	1.53602800
C	-6.65725900	-5.39754900	2.76296400
C	-6.80963900	-4.54964900	3.88224800
C	-6.45705600	-3.19246600	3.71734600
C	-5.95021700	-2.70424700	2.50859700
C	-7.35586700	-2.90013400	-1.53440900
C	-8.00520100	-3.07115400	-2.76084500
C	-7.34694000	-3.62594500	-3.88064600
C	-5.99463300	-3.99704200	-3.71665500
C	-5.31783300	-3.80102900	-2.50839200
C	1.16634400	7.82043500	-1.53440900
C	1.34290300	8.46828400	-2.76084500
C	0.53331000	8.17560900	-3.88064600
C	-0.46422300	7.19002600	-3.71665500
C	-0.63287100	6.50589300	-2.50839200
C	-1.16856200	7.81731600	1.53602800
C	-1.34578500	8.46413000	2.76296400
C	-0.53529200	8.17214500	3.88224800
C	0.46377100	7.18820700	3.71734600
C	0.63316200	6.50516200	2.50859700
C	7.35427500	-2.89665400	1.53602800
C	8.00304400	-3.06658100	2.76296400
C	7.34493100	-3.62249600	3.88224800
C	5.99328500	-3.99574100	3.71734600
C	5.31705400	-3.80091500	2.50859700
C	6.18952300	-4.92030100	-1.53440900
C	6.66229800	-5.39713000	-2.76084500
C	6.81363000	-4.54966500	-3.88064600
C	6.45885700	-3.19298400	-3.71665500
C	5.95070500	-2.70486400	-2.50839200
C	-3.86490300	-4.24954700	-2.46221300
C	6.07547500	-5.92700800	-0.40187900
C	5.61266700	-1.22233000	-2.46221300
C	8.16869300	-2.29288900	0.40405600
C	3.86485800	-4.25157500	2.46096000
C	-2.09864600	8.22074000	0.40405600
C	-1.74776500	5.47187800	-2.46221300
C	2.09520200	8.22502000	-0.40187900
C	1.74954300	5.47285200	2.46096000
C	-6.07004600	-5.92785100	0.40405600
C	-8.17067700	-2.29801200	-0.40187900
C	-5.61440100	-1.22127700	2.46096000
H	1.31717000	4.26324400	-1.69231100
H	-1.31700800	4.26158700	1.69075600
H	-3.03213900	-3.27135600	1.69075600
H	-4.35066300	-0.99091900	-1.69231100
H	-2.00339200	2.38403400	2.71670900
H	-2.52835000	1.16974800	1.54111200
H	-1.11264700	0.86955100	2.54089200
H	-0.19673000	-1.39835600	2.54089200
H	-1.06293800	-2.92700600	2.71670900
H	0.25114300	-2.77448900	1.54111200
H	-2.27841200	1.60323500	-1.54707600
H	-1.31055800	0.52656600	-2.54609700
H	-3.06756400	0.54022200	-2.72149100
H	1.11129800	0.87169300	-2.54609700
H	2.00162800	2.38647700	-2.72149100
H	2.52764800	1.17154600	-1.54707600
H	3.03349300	-3.27232500	-1.69231100
H	4.34914700	-0.99023100	1.69075600
H	2.27720600	1.60474100	1.54111200
H	1.30937700	0.52880500	2.54089200
H	3.06633000	0.54297100	2.71670900
H	0.19925900	-1.39825900	-2.54609700
H	1.06593600	-2.92669900	-2.72149100
H	-0.24923600	-2.77478000	-1.54707600
H	-6.90944100	-6.44808500	2.84049500
H	-6.58124200	-2.49653700	4.53830900
H	-9.04165300	-2.76603400	-2.83766300

## Appendix

H	-5.45390600	-4.45182500	-4.53794600	C	-0.13499600	8.50225500	-6.23877700
H	2.12537000	9.21331800	-2.83766300	H	-0.04239600	7.44303100	-6.51690800
H	-1.12844100	6.94913400	-4.53794600	H	-1.19746400	8.70606900	-6.04137700
H	-2.12948400	9.20779400	2.84049500	H	0.17015700	9.10408300	-7.09649800
H	1.12855600	6.94779100	4.53830900	C	-7.67939700	-6.43346700	5.22768300
H	9.03892600	-2.75970900	2.84049500	H	-8.48306700	-6.70418500	4.52821400
H	5.45268500	-4.45125400	4.53830900	H	-6.83255800	-7.11026300	5.04450600
H	6.91628200	-6.44728400	-2.83766300	H	-8.04043900	-6.61221900	6.24192800
H	6.58234700	-2.49730900	-4.53794600	C	9.41124500	-3.43382000	5.22768300
H	-3.66110100	-4.97230100	-3.25970000	H	10.04752800	-3.99446000	4.52821400
H	-3.17916000	-3.40484200	-2.59376400	H	9.57394800	-2.36203700	5.04450600
H	-3.60259100	-4.72014000	-1.51001100	H	9.74656900	-3.65711500	6.24192800
H	5.05850700	-5.97386600	0.00486600	C	-1.73184700	9.86728700	5.22768300
H	6.33629800	-6.93158400	-0.75114600	H	-1.56446100	10.69864400	4.52821400
H	6.73799100	-5.67454900	0.43178100	H	-2.74139000	9.47230000	5.04450600
H	6.13669000	-0.68445600	-3.25970000	H	-1.70613000	10.26933400	6.24192800
H	4.53825900	-1.05081300	-2.59376400	C	-7.42631600	-4.13376200	6.24043300
H	5.88905700	-0.75986500	-1.51001100	H	-6.46324600	-3.68273400	6.51785600
H	7.69859800	-1.39038600	-0.00382700	H	-8.13539200	-3.31673000	6.04293100
H	9.16785600	-2.01333600	0.75433400	H	-7.79367900	-4.69902800	7.09864200
H	8.28439100	-2.99306600	-0.42903200	C	7.29310100	-4.36449700	6.24043300
H	3.65969900	-4.97014200	3.26186500	H	6.42096400	-3.75596900	6.51785600
H	3.17760200	-3.40712100	2.58568200	H	6.94006800	-5.38709200	6.04293100
H	3.60603200	-4.72808900	1.51064600	H	7.96631700	-4.40001000	7.09864200
H	-1.55012400	8.67102600	-0.42903200	C	0.13321500	8.49825900	6.24043300
H	-2.64518900	7.36237500	-0.00382700	H	0.04228200	7.43870200	6.51785600
H	-2.84032800	8.94626500	0.75433400	H	1.19532400	8.70382100	6.04293100
H	-2.47558900	5.65675700	-3.25970000	H	-0.17263800	9.09903800	7.09864200
H	-1.35909900	4.45565400	-2.59376400	N	-0.71021100	8.83186800	5.09566500
H	-2.28646600	5.48000500	-1.51001100	N	-7.29351600	-5.03099400	5.09566500
H	1.54530800	8.67254600	0.43178100				
H	2.64426600	7.36772900	0.00486600				
H	2.83477900	8.95318700	-0.75114600				
H	2.47442000	5.65446400	3.26186500				
H	1.36185200	4.45544500	2.58568200				
H	2.29162900	5.48696000	1.51064600				
H	-5.05340900	-5.97198800	-0.00382700				
H	-6.32752900	-6.93292800	0.75433400				
H	-6.73426700	-5.67796000	-0.42903200				
H	-7.70277300	-1.39386300	0.00486600				
H	-9.17107600	-2.02160300	-0.75114600				
H	-8.28329900	-2.99799700	0.43178100				
H	-6.13411900	-0.68432200	3.26186500				
H	-4.53945400	-1.04832400	2.58568200				
H	-5.89766100	-0.75887100	1.51064600				
N	7.29864500	-5.03101600	-5.09358600				
N	8.00372700	-3.80087300	5.09566500				
N	0.70766500	8.83632000	-5.09358600				
N	-8.00631000	-3.80530400	-5.09358600				
C	-9.41455100	-3.44062700	-5.22456500				
H	10.04934200	-4.00224100	-4.52452700				
H	-9.57890300	-2.36909700	-5.04140600				
H	-9.75029200	-3.66460300	-6.23852400				
C	7.68694600	-6.43292700	-5.22456500				
H	8.49071300	-6.70186500	-4.52452700				
H	6.84115000	-7.11102500	-5.04140600				
H	8.04878500	-6.61169900	-6.23852400				
C	1.72760500	9.87355400	-5.22456500				
H	1.55862800	10.70410600	-4.52452700				
H	2.73775300	9.48012200	-5.04140600				
H	1.70150700	10.27630200	-6.23852400				
C	-7.29567100	-4.36803800	-6.23877700				
H	-6.42465600	-3.75823100	-6.51690800				
H	-6.94094500	-5.39006900	-6.04137700				
H	-7.96944500	-4.40468100	-7.09649800				
C	7.43066700	-4.13421700	-6.23877700				
H	6.46705200	-3.68480000	-6.51690800				
H	8.13840900	-3.31600000	-6.04137700				
H	7.79928900	-4.69940100	-7.09649800				

**BG1Br**DFT B3LYP/6-31G, gas phase, S<sub>0</sub>Point group: C<sub>3</sub>Total energy: - 11,493,076.47 kcal mol<sup>-1</sup>

Dipole moment: 0.01 D

Imaginary frequencies: 0

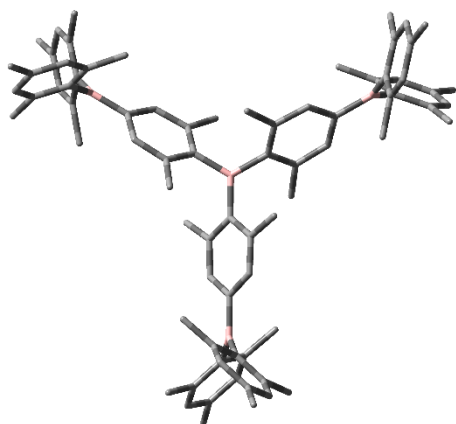
C	-0.00024900	-1.58702600	0.00245500
C	-1.37428100	0.79372900	0.00245500
C	0.77700600	-2.32330600	0.94866900
C	0.73838800	-3.72405600	0.94734700
C	0.00010100	-4.46382100	0.00075900
C	-0.73842300	-3.72311800	-0.94492600
C	-0.77749800	-2.32236100	-0.94458300
C	-1.62247400	1.83451400	-0.94458300
C	-2.85510300	2.50105200	-0.94492600
C	-3.86583300	2.23182200	0.00075900
C	-3.59432100	1.22256500	0.94734700
C	-2.40054500	0.48874600	0.94866900
C	-1.63996300	-1.64547100	-1.99605500
C	-0.60503800	2.24298500	-1.99605500
C	-2.24612300	-0.59594700	2.00083400
C	1.63916700	-1.64722600	2.00083400
B	0.00000000	0.00000000	0.00276300
C	1.37453000	0.79329700	0.00245500
C	1.62353900	1.83456000	0.94866900
C	2.85593300	2.50149100	0.94734700
C	3.86573100	2.23199800	0.00075900
C	3.59352600	1.22206600	-0.94492600
C	2.39997300	0.48784700	-0.94458300
C	2.24500100	-0.59751400	-1.99605500
C	0.60695600	2.24317300	2.00083400
B	0.00000000	-6.03143200	0.00000500
B	5.22337300	3.01571600	0.00000500
B	-5.22337300	3.01571600	0.00000500
C	-6.02702900	3.15730000	1.35911600
C	-5.74632000	3.64054300	-1.35981800
C	-0.27964300	-6.79673100	-1.35981800
C	0.27921200	-6.79821000	1.35911600
C	6.02596300	3.15618800	-1.35981800
C	5.74781700	3.64091000	1.35911600
C	-6.04245200	5.03211100	-1.46703500
C	-6.48148300	5.57196600	-2.68660600

C	-6.65143900	4.74400600	-3.78673800
C	-6.38959600	3.38387100	-3.71637100
C	-5.92390600	2.82314900	-2.51572000
C	-7.38058800	2.71865000	1.46582800
C	-8.06813500	2.82969300	2.68501500
C	-7.43629500	3.39078800	3.78533100
C	-6.12726900	3.84348000	3.71543300
C	-5.40829800	3.71988800	2.51513900
C	1.33587400	-7.75110100	1.46582800
C	1.58348100	-8.40205700	2.68501500
C	0.78163900	-8.13541500	3.78533100
C	-0.26491700	-7.22811000	3.71543300
C	-0.51736900	-6.54366800	2.51513900
C	-1.33671000	-7.74897200	-1.46703500
C	-1.58472300	-8.39911200	-2.68660600
C	-0.78271000	-8.13231900	-3.78673800
C	0.26428000	-7.22548800	-3.71637100
C	0.51703400	-6.54182800	-2.51572000
C	7.37916200	2.71686100	-1.46703500
C	8.06620600	2.82714600	-2.68660600
C	7.43415000	3.38831200	-3.78673800
C	6.12531600	3.84161700	-3.71637100
C	5.40687200	3.71867900	-2.51572000
C	6.04471300	5.03245200	1.46582800
C	6.48465400	5.57236300	2.68501500
C	6.65465600	4.74462700	3.78533100
C	6.39218500	3.38463000	3.71543300
C	5.92566700	2.82378000	2.51513900
C	-3.97678000	4.23038700	2.51638400
C	5.87198100	5.98848200	0.30075600
C	5.65201200	1.32879900	2.51638400
C	8.12105600	2.08982300	-0.30180900
C	3.97558200	4.22972800	-2.51572900
C	-2.25068900	-8.07795200	-0.30180900
C	-1.67523300	-5.55918600	2.51638400
C	2.25018700	-8.07952600	0.30075600
C	1.67526100	-5.55781900	-2.51572900
C	-5.87036700	5.98813000	-0.30180900
C	-8.12216800	2.09104400	0.30075600
C	-5.65084300	1.32809100	-2.51572900
H	1.31120500	-4.25949500	1.69978900
H	-1.31104400	-4.25782600	-1.69803300
H	-3.03186400	3.26431100	-1.69803300
H	-4.34443400	0.99421000	1.69978900
H	-1.98931800	-2.37924600	-2.72915300
H	-2.52178500	-1.17046800	-1.55296600
H	-1.10093600	-0.86601100	-2.54577200
H	-0.19951900	1.38644400	-2.54577200
H	-1.06582900	2.91242300	-2.72915300
H	0.24723800	2.76916400	-1.55296600
H	-2.27390700	-1.59737000	1.55819800
H	-1.30249800	-0.51743000	2.55195100
H	-3.05744400	-0.53211000	2.73267500
H	1.09935600	-0.86928100	2.55195100
H	1.98954300	-2.38176900	2.73267500
H	2.52031600	-1.17057600	1.55819800
H	3.03322800	3.26528500	1.69978900
H	4.34290800	0.99351600	-1.69803300
H	2.27454800	-1.59869600	-1.55296600
H	1.30045600	-0.52043300	-2.54577200
H	3.05514700	-0.53317600	-2.72915300
H	0.20314100	1.38671100	2.55195100
H	1.06790100	2.91387900	2.73267500
H	-0.24640900	2.76794600	1.55819800
H	-6.69291400	6.63184000	-2.76571000
H	-6.54384500	2.75471200	-4.58545200
H	-9.09195400	2.48343800	2.76373600
H	-5.65973500	4.29169600	4.58460900
H	2.39525700	-9.11558200	2.76373600

## Appendix

H	-0.88685000	-7.04732300	4.58460900
H	-2.39688500	-9.11215400	-2.76571000
H	0.88627200	-7.04449200	-4.58545200
H	9.08979900	2.48031300	-2.76571000
H	5.65757300	4.28978000	-4.58545200
H	6.69669800	6.63214400	2.76373600
H	6.54658500	2.75562700	4.58460900
H	-3.83881100	4.97969800	3.30252100
H	-3.26479000	3.41792300	2.70326800
H	-3.69078100	4.68799300	1.56569200
H	4.82850500	6.03834500	-0.03406300
H	6.16898300	7.00190900	0.58625000
H	6.47534100	5.69052700	-0.56175400
H	6.23195100	0.83465800	3.30252100
H	4.59240300	1.11842900	2.70326800
H	5.90531100	0.85231400	1.56569200
H	7.63912900	1.16477900	0.03785300
H	9.14525600	1.83457800	-0.58923400
H	8.17027400	2.76427100	0.55816700
H	3.83467700	4.97230400	-3.30766900
H	3.26248900	3.41599000	-2.69233200
H	3.69391600	4.69582400	-1.56776900
H	-1.69120900	-8.45780000	0.55816700
H	-2.81083600	-7.19806900	0.03785300
H	-2.98383600	-8.83731300	-0.58923400
H	-2.39314000	-5.81435700	3.30252100
H	-1.32761300	-4.53635300	2.70326800
H	-2.21453100	-5.54030600	1.56569200
H	1.69047000	-8.45307300	-0.56175400
H	2.81510800	-7.20078000	-0.03406300
H	2.97934000	-8.84345000	0.58625000
H	2.38880400	-5.80707900	-3.30766900
H	1.32709000	-4.53339300	-2.69233200
H	2.21974500	-5.54693700	-1.56776900
H	-4.82829300	6.03329000	0.03785300
H	-6.16141900	7.00273500	-0.58923400
H	-6.47906600	5.69353000	0.55816700
H	-7.64361300	1.16243500	-0.03406300
H	-9.14832200	1.84154100	0.58625000
H	-8.16581200	2.76254600	-0.56175400
H	-6.22348000	0.83477500	-3.30766900
H	-4.58957800	1.11740300	-2.69233200
H	-5.91366100	0.85111300	-1.56776900
Br	7.28443600	5.50869900	5.46372100
Br	8.41012700	3.55086600	-5.46559200
Br	1.12845500	-9.06285700	5.46372100
Br	-1.12992300	-9.05881700	-5.46559200
Br	-8.41289200	3.55415700	5.46372100
Br	-7.28020400	5.50795000	-5.46559200

## BG1Me

DFT B3LYP/6-31G, gas phase, S<sub>0</sub>Point group: C<sub>3</sub>Total energy: -1,961,212.46 kcal mol<sup>-1</sup>

Dipole moment: 0.004 D

Imaginary frequencies: 0

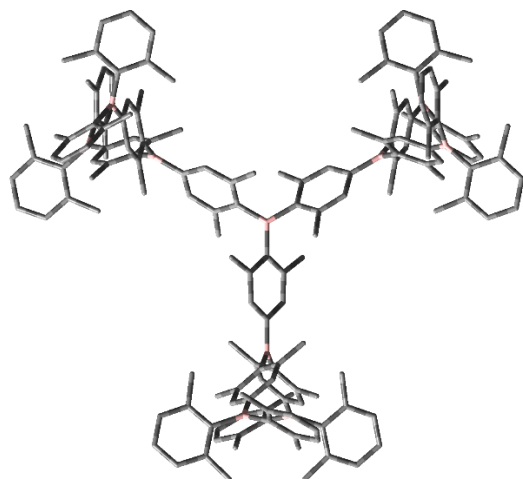
C	6.40856500	-3.35594100	-3.71353600
C	5.93637300	-2.80151000	-2.51447700
C	7.37288100	-2.74080800	1.48709200
C	8.04471900	-2.86584900	2.71174500
C	7.43774900	-3.43799000	3.83660200
C	6.11346000	-3.87405000	3.71206300
C	5.39629700	-3.74151800	2.51354400
C	-1.31283100	7.75550600	1.48709200
C	-1.54046200	8.39985600	2.71174500
C	-0.74148800	8.16027500	3.83660200
C	0.29829600	7.23143700	3.71206300
C	0.54210100	6.54409000	2.51354400
C	1.31348200	7.75323100	-1.48907900
C	1.54146300	8.39637300	-2.71439400
C	0.74234800	8.15623600	-3.83893200
C	-0.29795300	7.22795100	-3.71353600
C	-0.54200800	6.54180400	-2.51447700
C	-7.37123600	-2.73910700	-1.48907900
C	-8.04220400	-2.86324100	-2.71439400
C	-7.43468100	-3.43522600	-3.83893200
C	-6.11061300	-3.87201000	-3.71353600
C	-5.39436500	-3.74029500	-2.51447700
C	-6.06005000	-5.01469800	1.48709200
C	-6.50425800	-5.53400700	2.71174500
C	-6.69626100	-4.72228500	3.83660200
C	-6.41175600	-3.35738700	3.71206300
C	-5.93839800	-2.80257100	2.51354400
C	3.96225100	-4.24635600	2.50141800
C	-5.87924300	-5.98403800	0.33335300
C	-5.65857800	-1.30823100	2.50141800
C	-8.12107800	-2.09861600	-0.33540400
C	-3.96064300	-4.24594500	-2.50087000
C	2.24308500	8.08236800	-0.33540400
C	1.69632700	5.55458800	2.50141800
C	-2.24270700	8.08359300	0.33335300
C	-1.69677500	5.55299000	-2.50087000
C	5.87799300	-5.98375200	-0.33540400
C	8.12195100	-2.09955500	0.33335300
C	5.65741800	-1.30704500	-2.50087000
H	-1.31030300	4.26109300	1.69904200
H	1.31024900	4.25933800	-1.69733700
H	3.03357100	-3.26437800	-1.69733700
H	4.34536600	-0.99579100	1.69904200
H	1.99249400	2.38068100	-2.72591100
H	2.52236400	1.16891800	-1.55090400
H	1.10259100	0.86722700	-2.54536600
H	0.19974500	-1.38848500	-2.54536600
H	1.06548300	-2.91589100	-2.72591100
H	-0.24886900	-2.76889000	-1.55090400
H	2.27272600	1.59860100	1.55623800
H	1.30463200	0.51808400	2.55185200
H	3.06054500	0.53414200	2.72931400
H	-1.10099000	0.87080200	2.55185200
H	-1.99285300	2.38343900	2.72931400
H	-2.52079200	1.16893800	1.55623800
H	-3.03506300	-3.26530200	1.69904200
H	-4.34381900	-0.99496000	-1.69733700
H	-2.27349500	1.59997200	-1.55090400
H	-1.30233600	0.52125800	-2.54536600
H	-3.05797700	0.53521000	-2.72591100
H	-0.20364200	-1.38888600	2.55185200
H	-1.06769200	-2.91758100	2.72931400
H	0.24806600	-2.76753900	1.55623800
H	6.70695400	-6.59831100	-2.78843800
H	6.55694700	-2.70303400	-4.57078800
H	9.07056100	-2.51243100	2.78510600
H	5.62269900	-4.32914900	4.56951200
H	-2.35945200	9.11155100	2.78510600
H	0.93780400	7.03397500	4.56951200
C	0.00026800	1.58665800	0.00244500
C	1.37395200	-0.79356100	0.00244500
C	-0.77777700	2.32365300	0.94739500
C	-0.73880400	3.72455400	0.94623400
C	-0.00004800	4.46451600	0.00073100
C	0.73894200	3.72358600	-0.94382800
C	0.77832500	2.32269800	-0.94328600
C	1.62235300	-1.83539800	-0.94328600
C	2.85524900	-2.50173600	-0.94382800
C	3.86640800	-2.23221600	0.00073100
C	3.59496100	-1.22245400	0.94623400
C	2.40123100	-0.48825200	0.94739500
C	1.64172600	1.64584700	-1.99429800
C	0.60448200	-2.24469900	-1.99429800
C	2.24742600	0.59722300	1.99915500
C	-1.64092400	1.64771600	1.99915500
B	0.00000000	0.00000000	0.00273100
C	-1.37422000	-0.79309700	0.00244500
C	-1.62345400	-1.83540100	0.94739500
C	-2.85615700	-2.50210000	0.94623400
C	-3.86636000	-2.23230000	0.00073100
C	-3.59419100	-1.22185000	-0.94382800
C	-2.40067800	-0.48730000	-0.94328600
C	-2.24620800	0.59885300	-1.99429800
C	-0.60650200	-2.24494000	1.99915500
B	0.00000000	6.03514200	-0.00015100
B	-5.22658600	-3.01757100	-0.00015100
B	5.22658600	-3.01757100	-0.00015100
C	6.01890500	-3.17334200	1.36248700
C	5.75608900	-3.62532200	-1.36361300
C	0.26157600	6.79758000	-1.36361300
C	-0.26125700	6.79919600	1.36248700
C	-6.01766500	-3.17225800	-1.36361300
C	-5.75764700	-3.62585300	1.36248700
C	6.05775400	-5.01412400	-1.48907900
C	6.50074100	-5.53313300	-2.71439400
C	6.69233300	-4.72101000	-3.83893200

## Appendix

H	2.36082800	9.10754800	-2.78843800
H	-0.93757800	7.03000000	-4.57078800
H	-9.06778200	-2.50923700	-2.78843800
H	-5.61937000	-4.32696600	-4.57078800
H	-6.71110900	-6.59912100	2.78510600
H	-6.56050300	-2.70482600	4.56951200
H	3.80870600	-4.97924000	3.30069700
H	3.24791200	-3.42946400	2.65828300
H	3.69044200	-4.72411000	1.55574900
H	-4.83065000	-6.05144200	0.01639700
H	-6.19462900	-6.99121200	0.62377400
H	-6.46144500	-5.68646200	-0.54379900
H	-6.21650200	-0.80881600	3.30069700
H	-4.59395900	-1.09804300	2.65828300
H	-5.93642000	-0.83396100	1.55574900
H	-7.65216600	-1.16000200	-0.01357500
H	-9.14917500	-1.86288500	-0.62808200
H	-8.15985600	-2.75461000	0.53932700
H	-3.80461600	-4.97339900	-3.30458600
H	-3.24524500	-3.42843500	-2.64923900
H	-3.69274200	-4.73051800	-1.55748400
H	1.69436500	8.44394800	0.53932700
H	2.82149200	7.20697100	-0.01357500
H	2.96128200	8.85486100	-0.62808200
H	2.40779600	5.78805600	3.30069700
H	1.34604700	4.52750700	2.65828300
H	2.24597800	5.55807100	1.55574900
H	-1.69389800	8.43900600	-0.54379900
H	-2.82537700	7.20918700	0.01639700
H	-2.95725300	8.86031200	0.62377400
H	-2.40478200	5.78159300	-3.30458600
H	-1.34649000	4.52468200	-2.64923900
H	-2.25037800	5.56326700	-1.55748400
H	4.83067400	-6.04696900	-0.01357500
H	6.18789300	-6.99197600	-0.62808200
H	6.46549100	-5.68933700	0.53932700
H	7.65602700	-1.15774500	0.01639700
H	9.15188100	-1.86910000	0.62377400
H	8.15534300	-2.75254400	-0.54379900
H	6.20939800	-0.80819400	-3.30458600
H	4.59173400	-1.09624700	-2.64923900
H	5.94312000	-0.83274900	-1.55748400
C	7.21865800	-5.29422600	-5.13593700
H	8.31734900	-5.28703600	-5.15802800
H	6.89900500	-6.33295400	-5.27363900
H	6.87296200	-4.71521100	-5.99914300
C	-8.19426300	-3.60442800	-5.13593700
H	-8.73738200	-4.55951700	-5.15802800
H	-8.93400200	-2.80823600	-5.27363900
H	-7.51997400	-3.59455400	-5.99914300
C	0.97560600	8.89865400	-5.13593700
H	0.42003300	9.84655400	-5.15802800
H	2.03499700	9.14119000	-5.27363900
H	0.64701200	8.30976500	-5.99914300
C	-0.97473900	8.90406300	5.13282400
H	-0.43169400	9.85932900	5.14746500
H	-2.03620300	9.13323100	5.27771600
H	-0.63205800	8.32247600	5.99544200
C	-7.22377500	-5.29618000	5.13282400
H	-8.32258300	-5.30352300	5.14746500
H	-6.89150900	-6.33001900	5.27771600
H	-6.89144600	-4.70861600	5.99544200
C	8.19851400	-3.60788300	5.13282400
H	8.75427700	-4.55580700	5.14746500
H	8.92771200	-2.80321200	5.27771600
H	7.52350400	-3.61385900	5.99544200



## BG2H

DFT B3LYP/6-31G, gas phase, S<sub>0</sub>Point group: D<sub>3</sub>Total energy: -4,240,486.04 kcal mol<sup>-1</sup>

Dipole moment: 0 D

Imaginary frequencies: 0

C	0.0000000	1.58692600	0.00000000
C	1.37431800	-0.79346300	0.00000000
C	-0.77637300	2.32275000	0.94731000
C	-0.73694700	3.72342800	0.94718400
C	0.00000000	4.46336400	0.00000000
C	0.73694700	3.72342800	-0.94718400
C	0.77637300	2.32275000	-0.94731000
C	1.62337400	-1.83373300	-0.94731000
C	2.85611000	-2.49992800	-0.94718400
C	3.86538700	-2.23168200	0.00000000
C	3.59305700	-1.22350000	0.94718400
C	2.39974700	-0.48901700	0.94731000
C	1.63804000	1.64619600	-1.99962800
C	0.60662800	-2.24168200	-1.99962800
C	2.24466700	0.59548600	1.99962800
C	-1.63804000	1.64619600	1.99962800
B	0.00000000	0.00000000	0.00000000
C	-1.37431800	-0.79346300	0.00000000
C	-1.62337400	-1.83373300	0.94731000
C	-2.85611000	-2.49992800	0.94718400
C	-3.86538700	-2.23168200	0.00000000
C	-3.59305700	-1.22350000	-0.94718400
C	-2.39974700	-0.48901700	-0.94731000
C	-2.24466700	0.59548600	-1.99962800
C	-0.60662800	-2.24168200	1.99962800
B	0.00000000	6.03117400	0.00000000
B	-5.22315000	-3.01558700	0.00000000
B	5.22315000	-3.01558700	0.00000000
C	6.03365200	-3.14504200	1.35784000
C	5.74051300	-3.65277500	-1.35784000
C	0.29314000	6.79781700	-1.35784000
C	-0.29314000	6.79781700	1.35784000

C	-6.03365200	-3.14504200	-1.35784000
C	-5.74051300	-3.65277500	1.35784000
C	6.01255300	-5.04966700	-1.46833300
C	6.44232200	-5.58558600	-2.68972600
C	6.67452300	-4.78890200	-3.82974200
C	6.42544800	-3.40736100	-3.69762100
C	5.94268600	-2.83642300	-2.51239800
C	7.37941600	-2.68219000	1.46833300
C	8.05842000	-2.78642200	2.68972600
C	7.48457200	-3.38585600	3.82974200
C	6.16358500	-3.86092100	3.69762100
C	5.42775800	-3.72830600	2.51239800
C	-1.36686400	7.73185700	1.46833300
C	-1.61609800	8.37200700	2.68972600
C	-0.81004900	8.17475700	3.82974200
C	0.26186300	7.26828200	3.69762100
C	0.51492800	6.56472900	2.51239800
C	1.36686400	7.73185700	-1.46833300
C	1.61609800	8.37200700	-2.68972600
C	0.81004900	8.17475700	-3.82974200
C	-0.26186300	7.26828200	-3.69762100
C	-0.51492800	6.56472900	-2.51239800
C	-7.37941600	-2.68219000	-1.46833300
C	-8.05842000	-2.78642200	-2.68972600
C	-7.48457200	-3.38585600	-3.82974200
C	-6.16358500	-3.86092100	-3.69762100
C	-5.42775800	-3.72830600	-2.51239800
C	-6.01255300	-5.04966700	1.46833300
C	-6.44232200	-5.58558600	2.68972600
C	-6.67452300	-4.78890200	3.82974200
C	-6.42544800	-3.40736100	3.69762100
C	-5.94268600	-2.83642300	2.51239800
C	3.99947700	-4.24874300	2.51073800
C	-5.81177200	-6.00174300	0.30428300
C	-5.67925800	-1.33927700	2.51073800
C	-8.10354800	-2.03227100	-0.30428300
C	-3.99947700	-4.24874300	-2.51073800
C	2.29177600	8.03401400	-0.30428300
C	1.67978100	5.58802000	2.51073800
C	-2.29177600	8.03401400	0.30428300
C	-1.67978100	5.58802000	-2.51073800
C	5.81177200	-6.00174300	-0.30428300
C	8.10354800	-2.03227100	0.30428300
C	5.67925800	-1.33927700	-2.51073800
H	-1.30727600	4.25898500	1.70142400
H	1.30727600	4.25898500	-1.70142400
H	3.03475100	-3.26162700	-1.70142400
H	4.34202700	-0.99735800	1.70142400
H	1.98848300	2.38082100	-2.73142300
H	2.51911500	1.16908300	-1.55739300
H	1.09790900	0.86845100	-2.55076600
H	0.20314600	-1.38504300	-2.55076600
H	1.06761000	-2.91248700	-2.73142300
H	-0.24710200	-2.76615900	-1.55739300
H	2.27201300	1.59707600	1.55739300
H	1.30105600	0.51659100	2.55076600
H	3.05609300	0.53166600	2.73142300
H	-1.09790900	0.86845100	2.55076600
H	-1.98848300	2.38082100	2.73142300
H	-2.51911500	1.16908300	1.55739300
H	-3.03475100	-3.26162700	1.70142400
H	-4.34202700	-0.99735800	-1.70142400
H	-2.27201300	1.59707600	-1.55739300
H	-1.30105600	0.51659100	-2.55076600
H	-3.05609300	0.53166600	-2.73142300
H	-0.20314600	-1.38504300	2.55076600
H	-1.06761000	-2.91248700	2.73142300
H	0.24710200	-2.76615900	1.55739300
H	6.61643500	-6.65633300	-2.75461200

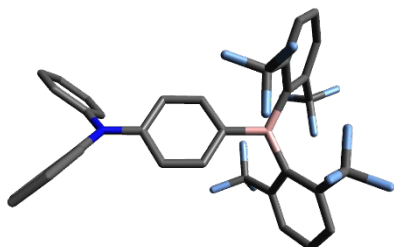
## Appendix

H	6.60913400	-2.75849800	-4.55011300	H	-1.81939000	9.62811000	-3.64704500
H	9.07277000	-2.40183400	2.75461200	H	-0.52024300	10.77950400	-3.91544000
H	5.69349700	-4.34442900	4.55011300	C	5.21103400	10.30036600	-6.02269900
H	-2.45633600	9.05816700	2.75461200	H	4.35034600	12.26511800	-6.20750100
H	0.91563700	7.10292700	4.55011300	H	0.94654600	11.61654200	-6.45869600
H	2.45633600	9.05816700	-2.75461200	H	1.29491400	11.97089400	-4.76702700
H	-0.91563700	7.10292700	-4.55011300	H	2.16352800	12.83174600	-6.03788400
H	-9.07277000	-2.40183400	-2.75461200	H	5.76660700	8.23336700	-5.79084300
H	-5.69349700	-4.34442900	-4.55011300	H	4.29180100	6.44783400	-5.66133600
H	-6.61643500	-6.65633300	2.75461200	H	3.45826100	6.80727600	-4.14292300
H	-6.60913400	-2.75849800	4.55011300	H	2.53378200	6.62632000	-5.62600700
H	3.85996700	-4.97881600	3.31480600	H	-3.12303100	9.76847800	-8.63538100
H	3.27787200	-3.43856600	2.66975400	H	6.22287200	10.63412200	-6.23237400
H	3.72509500	-4.73415100	1.56967100	B	7.19205200	-5.40721000	-5.17539400
H	-4.75998100	-6.05435500	-0.00473800	C	8.00613300	-4.48513600	-6.17686700
H	-6.11766600	-7.01538000	0.58098700	C	6.88237700	-6.93138800	-5.48616100
H	-6.39201000	-5.70175300	-0.57377600	C	7.57892100	-4.30097300	-7.52607100
H	-6.24176500	-0.85342100	3.31480600	C	9.18616700	-3.80745000	-5.74576800
H	-4.61682100	-1.11943700	2.66975400	C	7.93218600	-7.85843100	-5.76078600
H	-5.96244300	-0.85895100	1.56967100	C	5.53928800	-7.41499300	-5.48942900
H	-7.62321600	-1.09508700	0.00473800	C	8.30461900	-3.46171200	-8.38652600
H	-9.13433000	-1.79036400	-0.58098700	C	6.32643200	-4.96168800	-8.07124100
H	-8.13386800	-2.68476700	0.57377600	C	9.90054300	-2.99667300	-6.64281100
H	-3.85996700	-4.97881600	-3.31480600	C	9.73639100	-3.93920300	-4.33468100
H	-3.27787200	-3.43856600	-2.66975400	C	7.63323000	-9.20719000	-6.01164800
H	-3.72509500	-4.73415100	-1.56967100	C	9.39230500	-7.44560200	-5.75837100
H	1.74185800	8.38651900	0.57377600	C	5.27727800	-8.76573300	-5.77052800
H	2.86323500	7.14944200	0.00473800	C	4.34470200	-6.51439400	-5.21860700
H	3.01666400	8.80574400	-0.58098700	C	9.46243100	-2.81444900	-7.95436000
H	2.38179800	5.83223800	3.31480600	H	7.95752700	-3.32531700	-9.40691600
H	1.33894900	4.55800300	2.66975400	H	6.35736700	-6.04963800	-7.96065900
H	2.23734800	5.59310200	1.56967100	H	5.42224800	-4.61023500	-7.55771100
H	-1.74185800	8.38651900	-0.57377600	H	6.20285700	-4.73319600	-9.13456700
H	-2.86323500	7.14944200	-0.00473800	H	10.80918500	-2.50690800	-6.30311100
H	-3.01666400	8.80574400	0.58098700	H	10.80969800	-3.72124100	-4.32203900
H	-2.38179800	5.83223800	-3.31480600	H	9.24788300	-3.23841700	-3.64704500
H	-1.33894900	4.55800300	-2.66975400	H	9.59544600	-4.93920800	-3.91544000
H	-2.23734800	5.59310200	-1.56967100	C	6.31486100	-9.66307100	-6.02269900
H	4.75998100	-6.05435500	0.00473800	H	8.44673100	-9.90006900	-6.20750100
H	6.11766600	-7.01538000	-0.58098700	H	9.58694700	-6.62800400	-6.45869600
H	6.39201000	-5.70175300	0.57377600	H	9.71964100	-7.10687600	-4.76702700
H	7.62321600	-1.09508700	-0.00473800	H	10.03085400	-8.28954300	-6.03788400
H	9.13433000	-1.79036400	0.58098700	H	4.24700200	-9.11071200	-5.79084300
H	8.13386800	-2.68476700	-0.57377600	H	3.43808800	-6.94072600	-5.66133600
H	6.24176500	-0.85342100	-3.31480600	H	4.16614400	-6.39858000	-4.14292300
H	4.61682100	-1.11943700	-2.66975400	H	4.47167100	-5.50747900	-5.62600700
H	5.96244300	-0.85895100	-1.56967100	H	10.02150000	-2.17975000	-8.63538100
B	1.08675500	8.93210500	-5.17539400	H	6.09798400	-10.70622700	-6.23237400
C	-0.11882400	9.17608300	-6.17686700	B	-8.27880700	-3.52489500	-5.17539400
C	2.56156900	9.42600700	-5.48616100	C	-7.88730800	-4.69094600	-6.17686700
C	-0.06470900	8.71402500	-7.52607100	C	-9.44394600	-2.49461900	-5.48616100
C	-1.29573600	9.85917900	-5.74576800	C	-7.51421200	-4.41305200	-7.52607100
C	2.83950700	10.79869000	-5.76078600	C	-7.89043200	-6.05172900	-5.74576800
C	3.65192800	8.50466100	-5.48942900	C	10.77169300	-2.94025900	-5.76078600
C	-1.15437900	8.92286700	-8.38652600	C	-9.19121600	-1.08966800	-5.48942900
C	1.13373200	7.95969500	-8.07124100	C	-7.15024000	-5.46115500	-8.38652600
C	-2.35507700	10.07245800	-6.64281100	C	-7.46016400	-2.99800700	-8.07124100
C	-1.45674600	10.40156300	-4.33468100	C	-7.54546600	-7.07578500	-6.64281100
C	4.15704500	11.21416700	-6.01164800	C	-8.27964500	-6.46236100	-4.33468100
C	1.75192800	11.85677600	-5.75837100	C	11.79027600	-2.00697600	-6.01164800
C	4.95270900	8.95312300	-5.77052800	C	11.14423300	-4.41117300	-5.75837100
C	3.46927900	7.01981900	-5.21860700	C	10.22998600	-0.18739000	-5.77052800
C	-2.29383200	9.60193000	-7.95436000	C	-7.81398200	-0.50542600	-5.21860700
H	-1.09895400	8.55407900	-9.40691600	C	-7.16860000	-6.78748200	-7.95436000
H	2.06045700	8.53046100	-7.96065900	H	-6.85857300	-5.22876200	-9.40691600
H	1.28145700	7.00092200	-7.55771100	H	-8.41782400	-2.48082200	-7.96065900
H	0.99764000	7.73842900	-9.13456700	H	-6.70370500	-2.39068700	-7.55771100
H	-3.23354600	10.61448300	-6.30311100	H	-7.20049600	-3.00523300	-9.13456700
H	-2.18216000	11.22209300	-4.32203900	H	-7.57563900	-8.10757500	-6.30311100

H	-8.62753800	-7.50085200	-4.32203900	H	10.80918500	-2.50690800	6.30311100
H	-7.42849300	-6.38969300	-3.64704500	H	10.80969800	-3.72124100	4.32203900
H	-9.07520300	-5.84029600	-3.91544000	H	-9.24788300	-3.23841700	3.64704500
C	11.52589500	-0.63729500	-6.02269900	H	-9.59544600	-4.93920800	3.91544000
H	12.79707700	-2.36504900	-6.20750100	C	-6.31486100	-9.66307100	6.02269900
H	10.53349400	-4.98853800	-6.45869600	H	-8.44673100	-9.90006900	6.20750100
H	11.01455500	-4.86401800	-4.76702700	H	-9.58694700	-6.62800400	6.45869600
H	12.19438200	-4.54220300	-6.03788400	H	-9.71964100	-7.10687600	4.76702700
H	10.01360900	0.87734400	-5.79084300	H	10.03085400	-8.28954300	6.03788400
H	-7.72988900	0.49289200	-5.66133600	H	-4.24700200	-9.11071200	5.79084300
H	-7.62440500	-0.40869600	-4.14292300	H	-3.43808800	-6.94072600	5.66133600
H	-7.00545200	-1.11884100	-5.62600700	H	-4.16614400	-6.39858000	4.14292300
H	-6.89846900	-7.58899800	-8.63538100	H	-4.47167100	-5.50747900	5.62600700
H	12.32085600	0.07210500	-6.23237400	H	10.02150000	-2.17975000	8.63538100
B	-1.08675500	8.93210500	5.17539400	H	-6.09798400	-10.70622700	6.23237400
C	0.11882400	9.17608300	6.17686700	B	8.27880700	-3.52489500	5.17539400
C	-2.56156900	9.42600700	5.48616100	C	7.88730800	-4.69094600	6.17686700
C	0.06470900	8.71402500	7.52607100	C	9.44394600	-2.49461900	5.48616100
C	1.29573600	9.85917900	5.74576800	C	7.51421200	-4.41305200	7.52607100
C	-2.83950700	10.79869000	5.76078600	C	7.89043200	-6.05172900	5.74576800
C	-3.65192800	8.50466100	5.48942900	C	10.77169300	-2.94025900	5.76078600
C	1.15437900	8.92286700	8.38652600	C	9.19121600	-1.08966800	5.48942900
C	-1.13373200	7.95969500	8.07124100	C	7.15024000	-5.46115500	8.38652600
C	2.35507700	10.07245800	6.64281100	C	7.46016400	-2.99800700	8.07124100
C	1.45674600	10.40156300	4.33468100	C	7.54546600	-7.07578500	6.64281100
C	-4.15704500	11.21416700	6.01164800	C	8.27964500	-6.46236100	4.33468100
C	-1.75192800	11.85677600	5.75837100	C	11.79027600	-2.00697600	6.01164800
C	-4.95270900	8.95312300	5.77052800	C	11.14423300	-4.41117300	5.75837100
C	-3.46927900	7.01981900	5.21860700	C	10.22998600	-0.18739000	5.77052800
C	2.29383200	9.60193000	7.95436000	C	7.81398200	-0.50542600	5.21860700
H	1.09895400	8.55407900	9.40691600	C	7.16860000	-6.78748200	7.95436000
H	-2.06045700	8.53046100	7.96065900	H	6.85857300	-5.22876200	9.40691600
H	-1.28145700	7.00092200	7.55771100	H	8.41782400	-2.48082200	7.96065900
H	-0.99764000	7.73842900	9.13456700	H	6.70370500	-2.39068700	7.55771100
H	3.23354600	10.61448300	6.30311100	H	7.20049600	-3.00523300	9.13456700
H	2.18216000	11.22209300	4.32203900	H	7.57563900	-8.10757500	6.30311100
H	1.81939000	9.62811000	3.64704500	H	8.62753800	-7.50085200	4.32203900
H	0.52024300	10.77950400	3.91544000	H	7.42849300	-6.38969300	3.64704500
C	-5.21103400	10.30036600	6.02269900	H	9.07520300	-5.84029600	3.91544000
H	-4.35034600	12.26511800	6.20750100	C	11.52589500	-0.63729500	6.02269900
H	-0.94654600	11.61654200	6.45869600	H	12.79707700	-2.36504900	6.20750100
H	-1.29491400	11.97089400	4.76702700	H	10.53349400	-4.98853800	6.45869600
H	-2.16352800	12.83174600	6.03788400	H	11.01455500	-4.86401800	4.76702700
H	-5.76660700	8.23336700	5.79084300	H	12.19438200	-4.54220300	6.03788400
H	-4.29180100	6.44783400	5.66133600	H	10.01360900	0.87734400	5.79084300
H	-3.45826100	6.80727600	4.14292300	H	7.72988900	0.49289200	5.66133600
H	-2.53378200	6.62632000	5.62600700	H	7.62440500	-0.40869600	4.14292300
H	3.12303100	9.76874800	8.63538100	H	7.00545200	-1.11884100	5.62600700
H	-6.22287200	10.63412200	6.23237400	H	6.89846900	-7.58899800	8.63538100
B	-7.19205200	-5.40721000	5.17539400	H	12.32085600	0.07210500	6.23237400
C	-8.00613300	-4.48513600	6.17686700				
C	-6.88237700	-6.93138800	5.48616100				
C	-7.57892100	-4.30097300	7.52607100				
C	-9.18616700	-3.80745000	5.74576800				
C	-7.93218600	-7.85843100	5.76078600				
C	-5.53928800	-7.41499300	5.48942900				
C	-8.30461900	-3.46171200	8.38652600				
C	-6.32643200	-4.96168800	8.07124100				
C	-9.90054300	-2.99667300	6.64281100				
C	-9.73639100	-3.93920300	4.33468100				
C	-7.63323000	-9.20719000	6.01164800				
C	-9.39230500	-7.44560200	5.75837100				
C	-5.27727800	-8.76573300	5.77052800				
C	-4.34470200	-6.51439400	5.21860700				
C	-9.46243100	-2.81444900	7.95436000				
H	-7.95752700	-3.32531700	9.40691600				
H	-6.35736700	-6.04963800	7.96065900				
H	-5.42224800	-4.61023500	7.55771100				
H	-6.20285700	-4.73319600	9.13456700				

## 8.2.4 Chapter 4

## Compound 1

Point group:  $C_1$ 

Total energy: -1,622,547.83

kcal mol<sup>-1</sup>

Dipole moment: 2.35 D

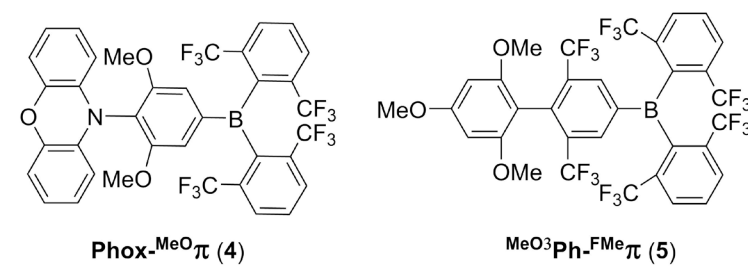
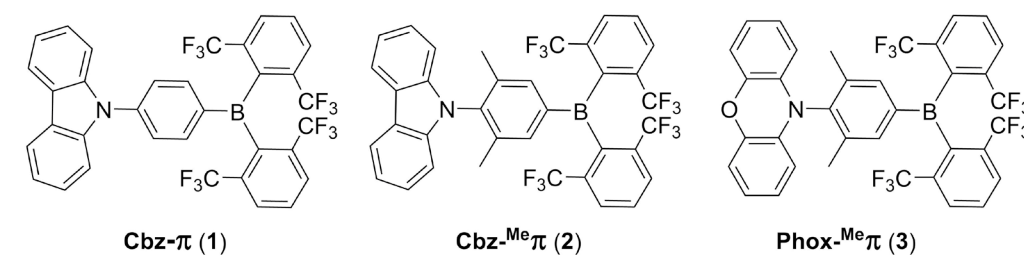
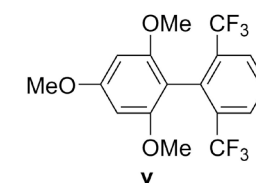
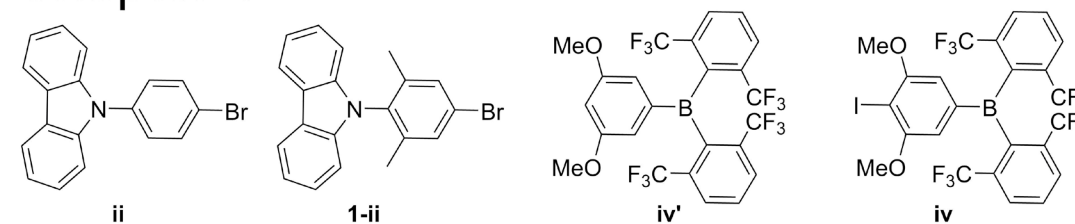
Imaginary frequencies: 0

C	2.05260400	0.97330700	-0.72247900
C	0.66742500	0.95301900	-0.73072600
C	-0.07592200	-0.00001800	0.00000300
C	0.66742700	-0.95300100	0.73081300
C	2.05260700	-0.97319600	0.72269300
C	2.77042800	0.00007000	0.00012200
N	4.17267200	0.00010100	0.00016900
B	-1.61903400	-0.00013400	-0.00006600
C	-2.33191400	-0.66952600	1.26750500
C	-2.33206100	0.66929600	-1.26751300
C	4.89691900	1.22123200	-0.09252900
C	4.89696700	-1.22100300	0.09287200
C	5.99789800	-1.32163700	0.95416400
C	6.71930600	-2.51306300	1.02923800
C	6.34359800	-3.61802900	0.25980200
C	5.24245900	-3.51740500	-0.59601200
C	4.52662600	-2.32427500	-0.68900100
C	5.99788800	1.32190000	-0.95376900
C	6.71924300	2.51335900	-1.02883100
C	6.34344700	3.61832300	-0.25943500
C	5.24226900	3.51766600	0.59632500
C	4.52648700	2.32450400	0.68930200
C	-3.19786700	-1.79093800	1.24526200
C	-3.63037800	-2.42318600	2.41877600
C	-3.24976200	-1.94732100	3.66546300
C	-2.45359400	-0.81107600	3.73245800
C	-2.00848400	-0.18757300	2.56436500
C	-3.19847100	1.79037700	-1.24507200
C	-3.63079400	2.42300700	-2.41846200
C	-3.24954300	1.94789100	-3.66523300
C	-2.45301700	0.81192000	-3.73246500
C	-2.00813100	0.18799300	-2.56450600
C	-1.18607500	1.06224100	2.81727300

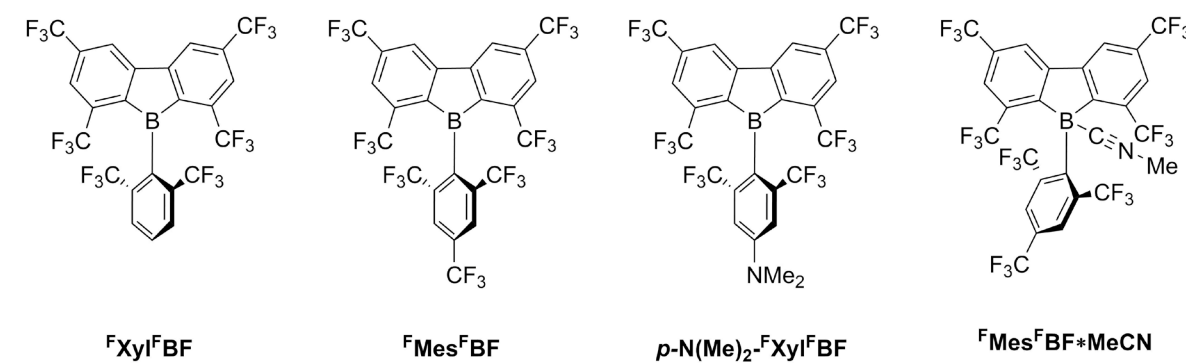
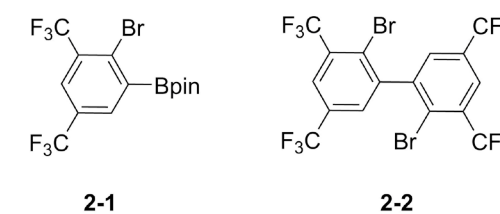
F	-1.12132800	1.90699800	1.76735600
F	0.09209300	0.77092700	3.17880400
F	-1.70765900	1.78220900	3.84823300
C	-3.68584600	-2.45892100	-0.02321800
F	-2.85551200	-3.45971300	-0.41665100
F	-3.82534900	-1.61625300	-1.06880800
F	-4.90592800	-3.03297100	0.15772000
C	-1.18548600	-1.06159000	-2.81793000
F	-1.12082400	-1.90698900	-1.76855800
F	0.09269600	-0.76987900	-3.17909900
F	-1.70683300	-1.78098300	-3.84940900
C	-3.68730500	2.45775700	0.02340700
F	-2.85781100	3.45909200	0.41724200
F	-3.82652300	1.61485300	1.06882900
F	-4.90776400	3.03092500	-0.15784700
H	2.59170000	1.72565900	-1.28798200
H	0.14341800	1.70203100	-1.31777900
H	0.14342900	-1.70201400	1.31786900
H	2.59171300	-1.72548900	1.28826500
H	6.28316300	-0.46434900	1.55588200
H	7.57127700	-2.58015700	1.70044500
H	6.90357500	-4.54651100	0.32468100
H	4.94569100	-4.36653300	-1.20570400
H	3.67895600	-2.24052300	-1.36204600
H	6.28322300	0.46461500	-1.55545700
H	7.57124500	2.58047800	-1.69999700
H	6.90338400	4.54683000	-0.32430500
H	4.94543200	4.36679200	1.20598600
H	3.67878700	2.24072500	1.36230600
H	-4.27561200	-3.29114700	2.34797900
H	-3.58699600	-2.44088700	4.57137200
H	-2.18050900	-0.39587800	4.69658100
H	-4.27638200	3.29069300	-2.34749500
H	-3.58656500	2.44179300	-4.57103700
H	-2.17946000	0.39726800	-4.69669000

## 9 List of Compounds

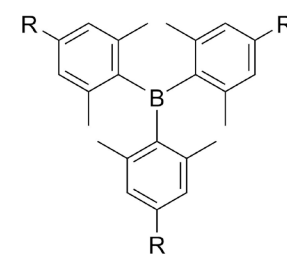
## Chapter 1



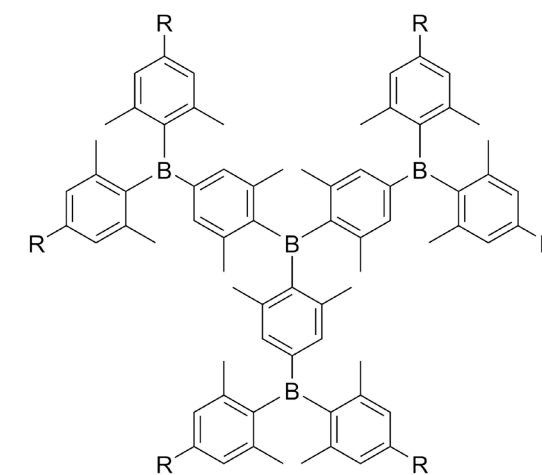
## Chapter 2



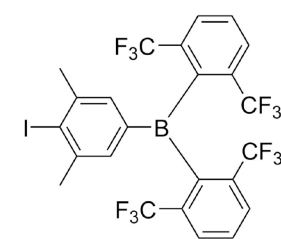
## Chapter 3



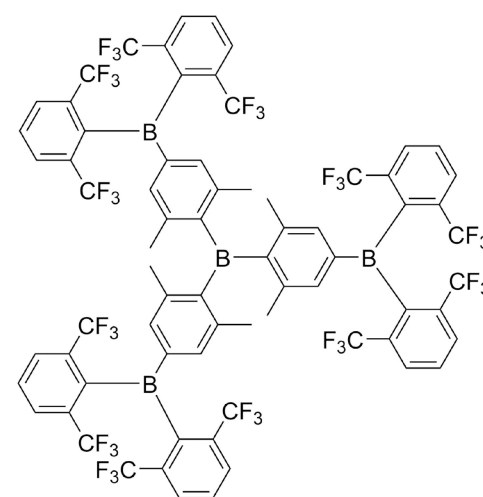
**BG0H:** R = H  
**BG0Bpin:** R = Bpin  
**BG0BF<sub>3</sub>K:** R = BF<sub>3</sub>K



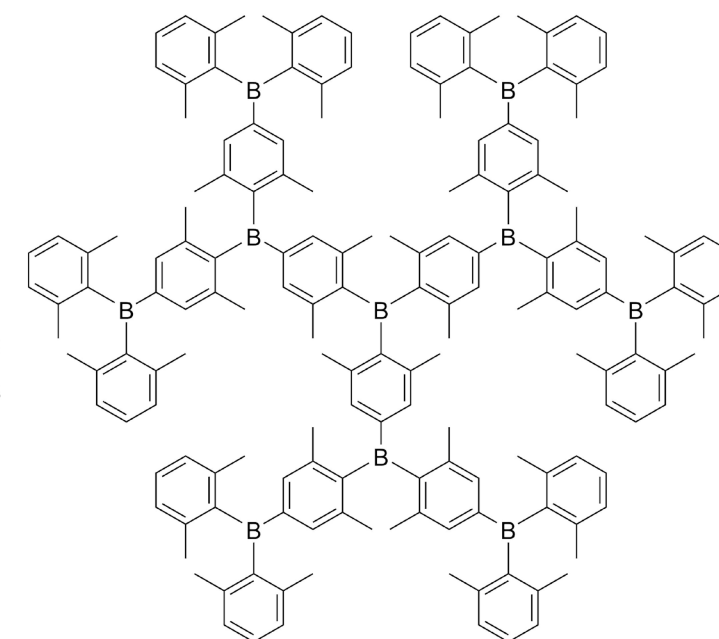
**BG1H:** R = H  
**BG1Me:** R = Me  
**BG1Br:** R = Br  
**BG1NMe<sub>2</sub>:** R = NMe<sub>2</sub>  
**BG1Bpin:** R = Bpin  
**BG1BF<sub>3</sub>(*n*Bu<sub>4</sub>N):** R = BF<sub>3</sub>(*n*Bu<sub>4</sub>N)



**BFD1H**



**BFG1H**



**BG2H**

## Chapter 4

